

The infra-red spectrum and molecular structure of poly(cyclohexane 1,4-dimethylene terephthalate)

T. R. MANLEY and D. A. WILLIAMS*

Films of poly(cyclohexane 1,4-dimethylene terephthalate) (PCHT) that had been drawn and crystallized in various ways were examined by normal and polarized infra-red radiation in the range 5000 cm^{-1} to 20 cm^{-1} . The *trans* PCHT isomer is centro symmetric in the crystalline phase. The space group of the monomeric unit is P_1 isomorphous with C_i symmetry. The *cis*-polymer is not centro symmetric, the space group is probably $P1$ isomorphous with C_1 symmetry. A number of model compounds were also studied. The terephthalate framework is expected to behave similarly to that in polyethylene terephthalate, the terephthalate conformation being more affected by changes in molecular orientation and crystallization than by those in the conformation of the diol fragment. In the same way the terephthalate framework is expected to be centro-symmetric and planar (symmetry $V_h \equiv D_{2h}$) only when highly crystallized and oriented. In amorphous regions, out of plane bending of C=O groups causes lowering to C_{2v} symmetry. The spectral changes in *cis* and *trans* PCHT, as would be expected from the above, are very similar to those of PET. There is little difference between *cis* and *trans* isomers in the same state, apart from a strong band at 630 cm^{-1} in both Raman and infra-red spectra of the *cis* isomer, that is practically absent in the *trans*. On change of state, however, *trans* substituted isomers do show significant intensity changes, in contrast to *cis* isomers.

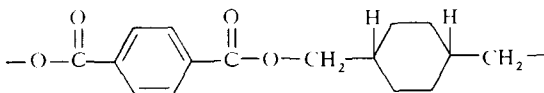
THERE IS little published work on the infra-red spectrum of poly(cyclohexane 1,4-dimethylene terephthalate), PCHT, and then only in the conventional region. Boye¹ has examined the *cis* and *trans* isomers of PCHT and a number of model compounds were studied in the region $5000\text{--}500\text{ cm}^{-1}$ and a number of tentative assignments made for some of the principal skeletal and C-H modes, by analogy with poly(ethylene terephthalate) PET. The crystal bands for *trans*-PCHT were very similar in behaviour to those observed in crystalline drawn PET, but *cis*-PCHT showed very little change in its spectrum upon change of phase. The same was found to be true of model compounds of PCHT and PET. The structure and properties of PCHT have been discussed by Martin *et al*² and by Devaney³.

STRUCTURE OF POLY(CYCLOHEXANE 1,4-DIMETHYLENE TEREPHTHALATE)

The PCHT structure differs from that of PET only by the presence of the cyclohexane ring between the two methylene groups of the latter. The repeating

*Present address: Commercial Plastics Ltd, Wallsend-on-Tyne, Northumberland, UK

unit of the polyester is



The number average molecular weight is about 10 000 indicating that the repeating unit occurs about 36 times in the molecule.

The structure determination of PCHT is complicated by the number of possible conformations that the 1,4-disubstituted cyclohexane ring can assume. Molecular models show that two forms of the cyclohexane ring are possible – the rigid chair form and the flexible boat form⁴. Crystallographic data⁵ indicate that the 1,4-disubstituted cyclohexane ring is in the chair form. In the latter the hydrogen atoms are either polar or equatorial thus giving rise to two possible *trans* isomers.

In one isomer each substituent group is polar and in the other, each group is equatorial. Only one form is possible for the chair *cis* isomer since one group is polar and the other is equatorial. However, the x-ray diffraction study of both *cis* and *trans* isomers⁶ indicates that the cyclohexane ring is substituted in equatorial positions in *trans*-PCHT.

The ethylene glycol fragment in PET assumes a *trans* configuration, as do the substituted equatorial atoms in the cyclohexane ring of PCHT. The latter is centro-symmetric, and has a centre of symmetry in the crystalline phase⁶. Consequently the space group of the monomeric unit is $P\bar{1}$, which is isomorphic to C_i symmetry.

Boye⁶ has shown from a study of classical molecular models that the repeating unit of the *cis* polymer is not potentially centro-symmetric, and the space group is probably $P1$, which is isomorphic to C_1^1 symmetry.

EXPERIMENTAL

The *cis* and *trans* isomers of PCHT were examined in thin films of the following forms:

- (1) doubly oriented, heat crystallized
- (2) doubly oriented, non-heat crystallized
- (3) uniaxially oriented heat crystallized
- (4) uniaxially oriented non-heat crystallized
- (5) amorphous

The films were in the range 20–100 μm , and were supplied by courtesy of Dr R. G. Devaney (Eastman Kodak Co.). Spectroscopically, the films and model compounds were examined in a similar manner to the PET specimens discussed in a previous paper⁷.

The polarized far infra-red spectra of uniaxially oriented, non-heat treated and uniaxially oriented heat-treated films of PCHT consisting of 70% *trans* and 30% *cis* stereoisomer are illustrated in *Figures 1* and *2* respectively. *Figure 3* shows the effect on the far infra-red spectrum of drawing and annealing at 180°C a similar film sample of amorphous PCHT. *Figure 4* shows the changes occurring in the far infra-red spectrum of amorphous PCHT, due to

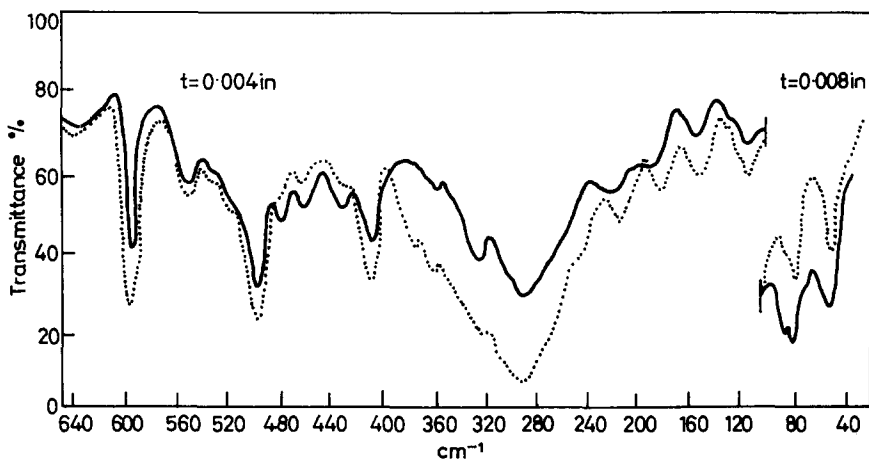


Figure 1 Polarized far infra-red spectra of uniaxially oriented (cold drawn) PCHT

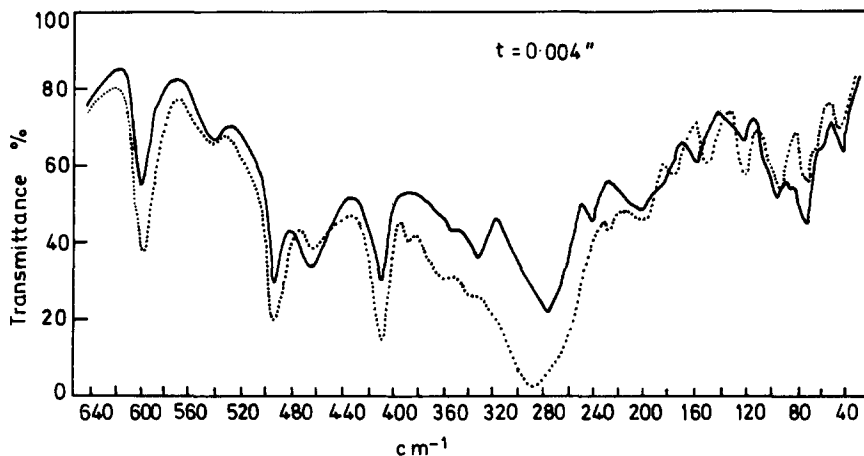


Figure 2 Polarized far infra-red spectra of uniaxially oriented, heat-treated PCHT

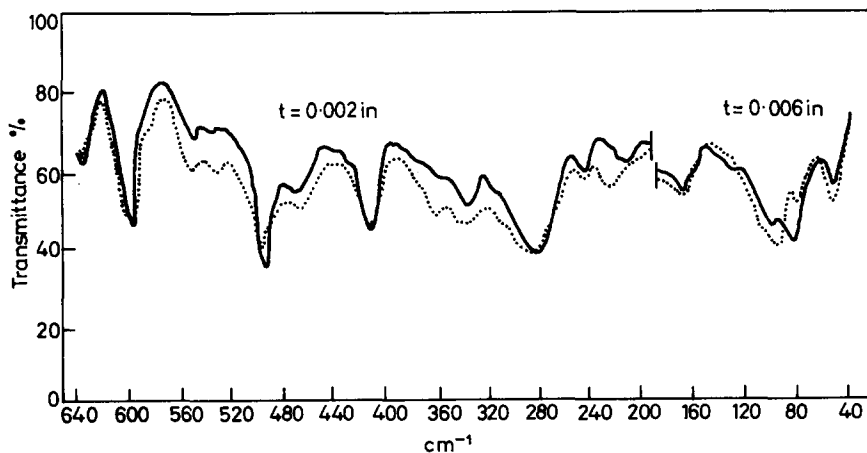


Figure 3 Effect of drawing and heat treatment on the far infra-red spectrum of amorphous PCHT

POLY(CYCLOHEXANE 1,4-DIMETHYLENE TEREPHTHALATE)

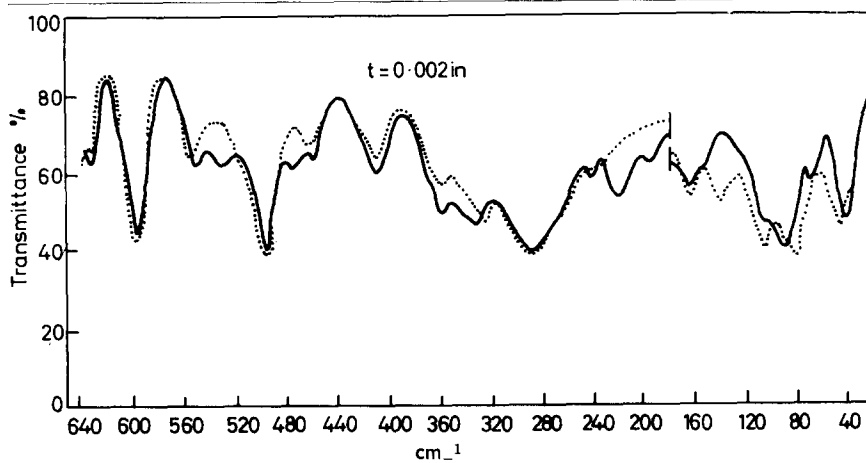


Figure 4 Effect of cold drawing on the far infra-red spectrum of amorphous PCHT

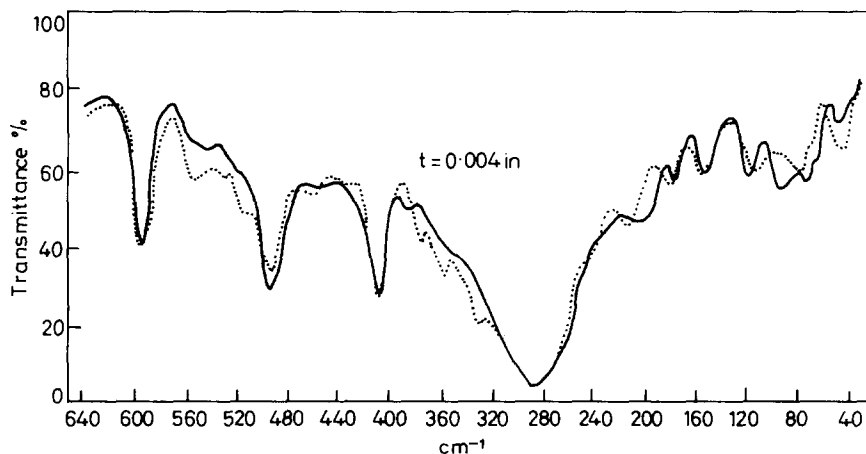


Figure 5 Effect of heat treatment on the far infra-red spectrum of uniaxially oriented (cold drawn) PCHT

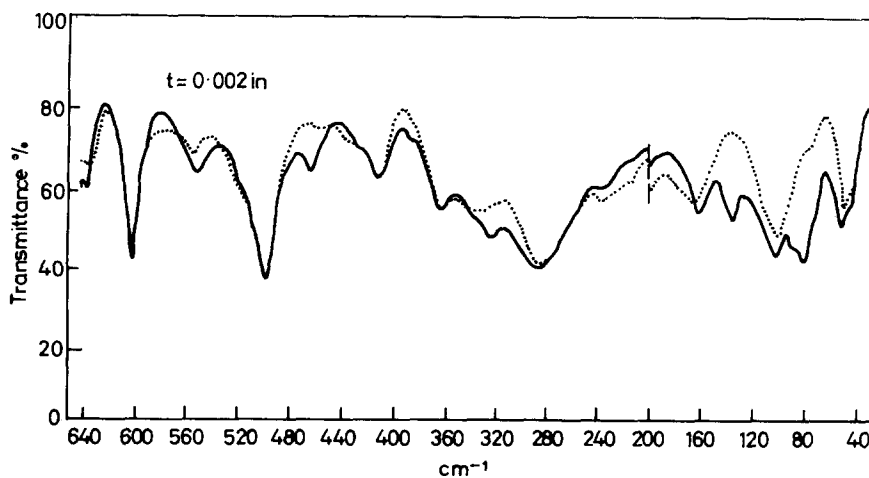


Figure 6 Far infra-red spectra of non-heat treated, uniaxially oriented and biaxially oriented PCHT

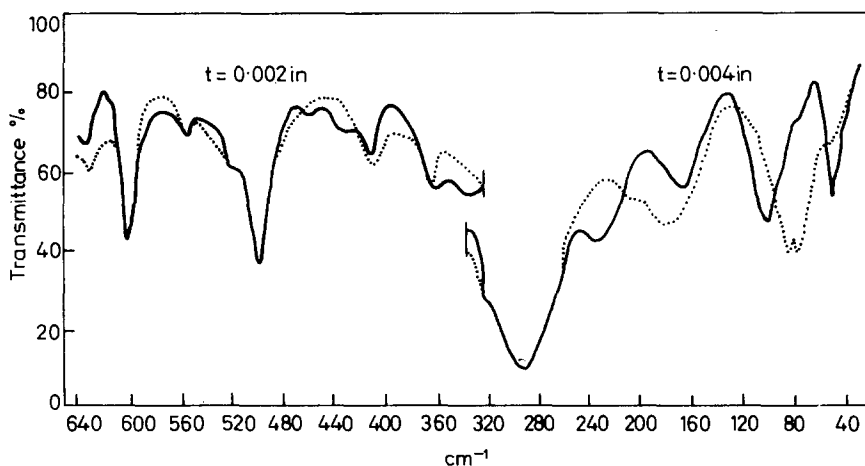


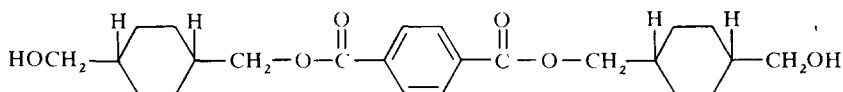
Figure 7 Effect of heat treatment on the far infra-red spectrum of biaxially oriented (cold drawn) PCHT

cold drawing alone. Figure 5 illustrates the subsequent spectral changes which occur in this sample upon annealing at 180°C. The changes incurred in the far infra-red spectrum of one-way cold drawn PCHT upon biaxial, plane orientation are shown in Figure 6 and the subsequent changes occurring in the latter upon annealing are illustrated in Figure 7. The results of the far infra-red studies on *cis* and *trans* PCHT are summarized in Table 1 and those of the conventional region (5000–640 cm^{-1}) in Table 2. Since the spectra of the *cis* and *trans* stereoisomers are very similar, it was found convenient to illustrate the spectra of the mixed *cis-trans* isomer samples of both PCHT and the model compounds. Bands peculiar to the *cis* or *trans* configurations are indicated in the figures.

Spectra were not obtained for *cis* and *trans*-PCHT in the molten state. These spectra are in direct correlation with those of the quenched film, the only difference being in bandwidths due to the different sample temperatures¹. Spectra of *cis* and *trans*-PCHT at -194°C differed from those at room temperature only in that some bands were sharpened. Cooling the amorphous *cis*-PCHT to -194°C produced virtually the same changes in the infra-red spectrum as did crystallization, but crystallization in the *trans* polymer produced more pronounced changes than cooling.

Model compounds

The model compounds examined included *cis* and *trans* cyclohexane-1,4-dimethanol,



cis and *trans* terephthalic acid-*bis*(cyclohexane-1,4-dimethanol)

Table 1 Far infra-red spectra of *cis* and *trans* poly(cyclohexane-1,4-dimethylene terephthalate)

Biaxially oriented crystallized	Uniaxially oriented crystallized		Biaxially oriented uncrystallized		Uniaxially oriented uncrystallized		Amorphous	P	O	I*	Assignment
	⊥	∥	⊥	∥	⊥	∥					
43 vvw	46 vw	41 vw	36 vvw	43 vw	41 vw	34 vvw	σ	a?			τ COCC τ COCC (B ₂₇) τ C ₆ H ₄ CO
74 w, b 94 vw	73 w 96 vw	68 w 94 vw	76 vw 96 m, b	51 sh 74 w 82 w	49 sh 72 w 82 w	43 vw 51 sh 74 w 82 w	σ	c	<i>trans</i>		
115 vvw	120 vw 128 vw 158 vw	119 vw 147 vw	111 w	116 vw 156 vw	114 vw 147 vw	112 160 vvw	π	π			ρ ⁹⁶ (B ₂) δ C-(C=O) + δCH ⊥ v ₃₄ (B ₁₀) δ COC
175 w, b 195 w 211 vw 237 vvw 278 m 288 m, b	184 203 211 vw 239 vw 278 m 293 m, b	173 200 vw 225 vw 245 vvw 277 292 m, b	166 w 220 vw 234 w 278 m 293 m, b	190 201 vw 224 260 284 m 294 m	184 vw 210 w 222 244 284 m 294 m	173 vw 222 w 240 vvw 282	π	π	<i>cis</i> <i>trans</i>		δ COC δ CCC ⊥ (v ₃₂ , B ₃₀) δ C-(C=O) ∥ (v ₃₃ , B ₃₃) 76 (A ₂) δ C-(C=O) ⊥ (v ₁₈ , B ₃₂) 102 (A ₁) 102 (A ₁) ρ CH ₂ ring (A ₁₉)?
320 w, b 360 w 365 w	329 vw 355 vw 370 vvw	335 vw 360 vw 373 vw	330 w, b 361 w, b 373 vw	326 w, b 360 w 373 vw	325 w 360 w 373 vw	332 w 359 m, b 372 w	σ	a	<i>cis</i> <i>trans</i>		δ COC δ CCC ⊥ (v ₃₂ , B ₃₀) δ CCC ∥ (v ₃₃ , B ₃₃) δ CCC ∥ (E ₂)? (v ₂₃ , B ₁₉)
394 vw, b 407 w 421 w 460 vwb	385 vw 407 w 462 w	388 vw 408 w 420 460 vw	409 w 430 vw 460 vvw	407 w 430 vw 459 w	409 w 423 vw 456 w	396 vvw 408 m, b 424 w 461 w, b	σ	a	<i>trans</i>		δ COC δ CCC ⊥ (v ₃₂ , B ₃₀) δ CCC ∥ (E ₂)? (v ₂₃ , B ₁₉)
475 vw 497 m 515 w, b 530 vwb 547 w 552 w	475 vw 498 m 530 vw	475 vw 497 m 530 vw	497 515 w, b 530 vwb	476 vw 499 m 516 w 530 vwb	476 vw 499 m 516 w 530 vw	468 w, b 476 vwb 499 vw 529 w, b	σ	a	<i>cis</i> <i>trans</i>		ω C=O (v ₃₂ , B ₃₀)? ρ C=O (v ₂₃ , B ₁₉)? ρ CH ₂ ring
598 m	598 w	598 m	598 m	594 w	594 m	598 m	π	π			δ CCC ⊥

*Isomer - *cis/trans*; bands not identified as being of *cis* or *trans* origin are common to both stereo-isomers

Table 2. Infra-red spectra of *cis* and *trans* poly(cyclohexane-1,4-dimethylene terephthalate)

Biaxially oriented crystallized	Uniaxially oriented crystallized	Biaxially oriented uncrystallized	Uniaxially oriented uncrystallized	Amorphous	P	O	I	Assignment
637 w	633 vw	633 vw	633 vw	634 vw	π		<i>cis</i>	ω C=O (ν_{135} , B_{30})
645 w	658 vvw	645 vwb	645 vwb	641 vwb	π ?		<i>cis</i>	ω C=O?
658 w	672 vvw	656 vw	656 vw	656 vw	π ?	a?		δ CCC \perp (ν_{145} , B_{32})
665 vvw		666 vvw	674 vvw	675 vvw	σ ?			
705 sh	711 sh	712 sh	711 sh	709 sh				δ CH + δ C(O) (E_u , 27)
725 s	727 s	722 s	726 s	729 s				δ C—(CO) + δ CH \perp (ν_{215} , B_{10})
770 vw	770 vw	770 vw	770 vw	772 vw		a?		δ CH \perp (ν_{145} , B_{32})
787 w	791 w	791 w	792 w	795 w		a?		ν CC (ν_{95} , A_g)
807 vvw	808 vw	802 vvw	808 vvw	802 vvw		a	<i>trans</i>	δ CCC \perp ring
850 vw	818 vwb	818 vwb	819 vvw	825 vvw	σ ?	c	<i>cis</i>	ρ CH ₂ (A_{1g})
867 w	847 w	853 vw	847 w	845 sh	σ	c		ρ CH ₂ (A)
882 vvw	872 w	873 w	871 w	874 w	σ	a?		ρ CH ₂ (A)
895 vvw	880 vvw	885 vvw	882 vvw	885 vvw	σ	a		ρ CH ₂ ring
920 sh	901 vw	898 vw	895 vvw	895 vvw	π	c		δ CH \perp (ν_{145} , B_{32})
951 m	925 sh	925 sh	926 sh	930 sh				ν CC ring
966 m	955 m	956 m	957 m	955 m	π			δ CCC \parallel (ν_{90} , B_{20})
	964 s	970 m	964 s	963 s	π			ρ CH ₂ ring (E_g)
	995 sh				π			δ CH \parallel (ν_{231} , B_{20})/vcc
1012 m	1015 m	1016 m	1015 m	1020 m	π	c?		ν CO
1037 vvw	1046 vvw	1045 vvw	1038 vvw	1047 vvw	π			ω CH ₂ (A_{32})
1107 vs	1105 vs	1110 vs	1105 vs	1107 vs	π	c		ν C—O
					π			ν_{93} C—O (A_{1g})
1147 w	1158 w	1149 w	1151 w	1153 w	π			ν_{93} C—O (A_{1g})
1161 w	1187 sh	1166 w	1177 w	1168 w				ν_{93} C—O (A_{1g})
1216 w			1198 w	1195 sh				ν CC ring?
			1224 w					ω CH ₂ ring (E_g)?
			1253 vs		π			ω CH ₂ ring
1263 vs	1274 vwb	1272 vs	1271 vs	1272 vs	π			ν C—O
1310 vw			1295 m		π			ν C(CO) (B)
1330 sh			1318 w			c?		δ CH ₂ (B_{10})?
1352 sh			1333 sh					ν C—(C=O) ν_{235} (B_{20})
1370 w	1355 vvw	1355 sh	1350 sh	1332 sh				ν CH ₂ ring
1385 w	1387	1374 w	1385	1370 m	π	a?		ν C—(C=O) (ν_{145} , A_g)
1402 m		1407 m	1400 m	1402 m	π			δ C—OH (end groups)
1445 m	1453 s	1447 m	1455 s	1422	π			δ CH ₂ ring? (E_g)
1456 m		1457 m		1456 m	σ			δ CH ₂ ring
				1466 m	σ			ν CC (ν_{95} , B_{30})
1499 m	1497 m	1506 m	1497 m	1475 m	σ			ν CC (ν_{95} , B_{30})
1520 vw	1518 vw	1525 vvw	1518 vw	1501 m	π			ν CC (ν_{95} , B_{30})
1556 sh	1539 vvw	1557 vvw	1538 vvw	1519 vvw	π ?			
1572 w	1565 sh	1575 sh	1555 sh	1540 vvw	π ?	c?		
1604 w	1578 w	1575 w	1571 w	1557 sh		a?		
1635 vvw	1610 w	1606 w	1604 w	1583 w				
1651 sh	1635 vvw	1637 vvw	1635 vvw	1616 w		a		
1675 w	1648 vvw	1646 vvw	1648 vvw	1637 vvw	π ?			ν CC (ν_{95} , A_g)?
	1680 sh	1676 w	1680 sh	1645 vvw	σ ?			ν C—O (ν_{95} , A_g)
				1676 sh		c		384 (R) + 1263 (I) = 1647
								426 (R) + 1263 (I) = 1689

Table 3 Infra-red spectra and frequency correlations of some model compounds of *cis* and *trans* poly(cyclohexane-1,4-dimethylene terephthalate)

Terephthalic acid	<i>cis/trans</i> 1,4-cyclohexane dimethanol	Terephthalic acid(bis CHD)	<i>cis/trans</i> 1,4-CHD hemi-ester	<i>cis/trans</i> 1,4-CHD dibenzoate	<i>cis/trans</i> poly CHD isophthalate	<i>cis/trans</i> CHDM oligomer	<i>cis/trans</i> PCHT	* I	Assignment
41 m	36 vvw	50 vvw	62 vvw	73 vvw	67 vw	49 vvw	43 vw	}	τ COCC
59 vw	48 vvw	63 vvw	75 vw	83 w	85 vw	72 vvw	50 sh		
89 vvw	70 m	75 vw	90 vw	100 w	100 vw	100 vw	66 vvw	}	τ COCC τ C ₆ H ₄ CO ρ CH + ρ C(CO) δ C-(CO) + δ CH \perp (v _{9a} , B _{1a})
110 w	87 vw	83 w	110 w	115 w	127 vvw	140 vw	88 m, b		
123 vvw	110 vw	125 w	122 w	134 w	140 vw	182 w, b	112		
	145 vw	141 vvw	141 vvw	153 vw	178 w	200 w	128 vw		
165 vvw	172 w	178 m	178 m	179 w	188 vw	216 vw	178 vw	}	δ COCC δ COC \parallel / δ CCC \perp δ C-(CO) \parallel / δ CCC \perp
200 vw	192 w	198 vw	198 vw	193 vw	232 w	244 w	202 w		
225 w	214 w	237 vw	241 m	241 vw	252 w	300 vw	222 w	}	δ C-(CO) \parallel (v _{9a} , B _{9a}) v _{9a} (A _g) δ C-(CO) \perp / δ CCO \perp (v _{18a} , B _{9a})
243 m	257 w	252 w	241 m	256 vvw	289 w	320 w	240 w		
263 vvw	280 vvw	280 vvw	298 w	272 w	316 vw	320 w	280 m	}	δ COC \perp (A') δ COC \parallel / δ COC \parallel ρ CH ₂ ring (A _{1g})
295 w	311 w	314 m	314 m	290 m	331 w?	369 w, b	292 m, b		
321 m	320 w	320 w	322 m	316 vvw	375 w, b	375 w, b	320 w	}	δ COC \perp (A') δ COC \parallel / δ COC \parallel ρ CH ₂ ring (A _{1g})
339 w	339 w	339 w	341 w	325 vw	405 w, b	441 w	328 w		
352 w	363 vw	360 w	360 w	360 w, b	445 vwb	460 w	359 w	}	δ COC \parallel / δ COC \parallel ρ CH ₂ ring (A _{1g})
409 vvw	392 w	386 vw	396 w, b	388 w	478 vw	510 vw	372 w		
447 m	443 w	446 w, b	446 w	422 vw	505 vw, b	557 w, b	389 vw	}	δ COC \perp (v ₇ , A _g) / δ COC \perp δ COC \parallel (E _g) δ COC \parallel ?
490 m	473 m	516 m, b	506 w	439 w, b	548 w	598 m	408 m, b		
525 m	526 w	562 w, b	527	582 vw, sh	565 vw	600 w	424 w	}	δ COC \parallel / δ COC \parallel ρ CH ₂ ring (A _{1g})
562 m	570 m	586 w	565	614 vw	596 vw	634 vw	468 w, b		
610 vw	612 m	640 w, b	631 w	614 vw	614 m	683 vw	476 vw	}	δ COC \parallel / δ COC \parallel ρ CH ₂ ring (A _{1g})
630 vvw	660 vw	685 vw	687 vw	654 vvw	687 vw	709 sh	499 m		
685 w	683 vw	685 vw	702 sh	705 m	687 vw	705 m	515 w, b	}	ω C=O ω C=O δ CCC \perp (v ₁₈ , B ₁₈) δ CH + δ C(CO) (E _g)
							530 vvw, b		

* isomer-*cis/trans*; bands not identified as being of *cis* or *trans* origin are common to both stereo-isomers in PCHT and model compounds

Table 3 (Cont.) Infra-red spectra and frequency correlations of some model compounds of *cis* and *trans* poly(cyclohexane-1,4-dimethylene terephthalate)

Terephthalic acid	<i>cis/trans</i> cyclohexane dimethanol	Terephthalic acid/bis CHD ester	<i>cis/trans</i> 1,4-CHD hemi-ester	<i>cis/trans</i> 1,4-CHD diben-zoate	<i>cis/trans</i> poly-CHD iso-phthalate	<i>cis/trans</i> CHDM oligomer	<i>cis/trans</i> PCHT	* I	Assignment
731 m	765 vvw	737 s	716 w		725 w	713 m	722 s	} δ C—CO \perp + δ CH \perp (ν_{21} , B_{10}) δ CH \perp (ν_{24} , B_{27}) ν CC ring (ν_6 , A_1)	
781 m		749 vvw	750 w		755 vvw	729 m	730 s		
		778 vvw	781 m		777 vvw	782 w	772 vw		
				803 vw			795 w		
833 vw	816 vw			820 vvw			802 vvw		
	822 vvw	829 vvw	825 vvw				806 vvw		
		866 vw	831 vw				842 w		
880 m	877 vw	873 vw	878 m	861 w			825 vvw		
	887 w						845 sh		
	894 vw						874 w		
935 s	917 vw			900 vw			885 vvw		
	943 vw	950 vvw	936 m, b	935 w			895 vw		
				957 m			930 sh		
980 vvw	960 vvw			969 w			955 m		
955 vvw	983 m						963 s		
	990 sh	1000 vw	985 vvw	1015 w			995 sh		
1017 w	1032 vs	1016 vvw	1002 vvw				1020 m		
1078 vw	1062 w	1048 vw	1018 m	1025 w			1047 vvw		
	1092 w	1103 vw	1065 s, b	1097 w					
1110 w	1112 w	1119 vw	1111 s	1112 m			1107 vs		
	1127 vw	1132 sh	1127 vvw				1119		
1134 w	1142 w	1178 vw	1134 w	1132 m			1136		
	1185 sh		1177 w	1150 vvw			1153 w		
1183 w	1193 w	1213 w	1176 w	1177 w			1168 w		
	1225 vvw	1252 vw	1215 s	1220 w			1195 sh		
	1266 w	1273 m	1254 w				1224 w		
1282 s	1284 w	1312 vw	1288 vs	1247 m			1253 vs		
	1305 vw		1316 sh	1263 s			1272 vs		
1320 sh	1330 vw			1290 sh			1295 vs		
	1345 vw			1315 m			1318 w		
				1350 sh			1332 sh		
1380 w	1371 w	1405 vw	1375 w	1375 w			1355 vvw		
	1405 sh		1390 m				1370 m		
1414 m		1432 w	1402 s	1404 sh			1387 vw		
			1425 s	1418 w			1402 m		
				1434 vvw			1422		

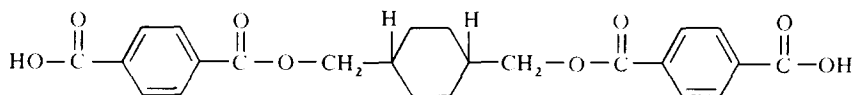
* isomer-*cis/trans*; bands not identified as being of *cis* or *trans* origin are common to both stereo-isomers in PCHT and model compounds

Table 3 (Cont.) Infra-red spectra and frequency correlations of some model compounds of *cis* and *trans* poly(cyclohexane-1,4-dimethylene terephthalate)

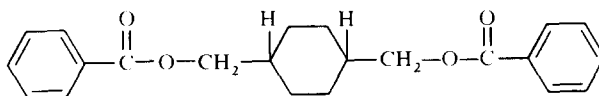
Terephthalic acid	<i>cis</i> / <i>trans</i> 1,4-cyclohexane dimethanol	Terephthalic acid-bis CHD ester	<i>cis</i> / <i>trans</i> 1,4-CHD hemi-zoate	<i>cis</i> / <i>trans</i> poly CHD iso-phthalate	<i>cis</i> / <i>trans</i> CHDM oligomer	<i>cis</i> / <i>trans</i> PCHT	*I	Assignment
1458 m	1444 w 1452 m		1450 m	1447 vvw 1455 vvw	1445 vw 1455 vvw	1447 m 1456 m 1466		δ CH ₂ ring δ CH ₂ /pCC (v ₂₈ , B ₃₀)
1511 w	1469 w 1504 vvw	1505 vw	1470 m 1490 w	1485 vvw	1498 sh 1506 w	1475 1501 m 1519 vw	<i>trans</i> <i>cis</i>	v CC (v ₂₇ , B ₂₉) v CC (v ₂₈ , B ₃₀)
1567 w 1613 w		1545 vw	1545 vvw	1540 vvw	1539 vvw 1557 vvw	1540 vvw 1557 sh	<i>trans</i>	v CC (v ₂₇ , B ₂₉) v CC (v ₂₈ , B ₃₀)
1672 s	1650 vvw 1682 vvw 1702 w 1711 w 1717 w	1571 vw 1575 m 1613 vw	1585 w 1602 w 1637 vvw 1655 vvw 1688 sh 1700 sh	1577 vvw 1608 vvw 1635 vvw 1652 vvw 1683 vs	1574 w 1616 w	1583 w 1574 w 1616 w 1645 sh 1676 sh 1701 vs	<i>trans</i> <i>trans</i>	v CC (v ₂₇ , A ₁) v ₂ C=O (v ₂₈ , A ₁) 384 + 1263 426 + 1263
1812 w		1717 m	1710 vs	1715 s 1730 s	1720 vs	1721 vs 1734 vs 1766 sh		v ₂₈ C=O (v ₂₈ , B ₃₀)
1898 vw	1890 vvw	1785 m	1772 vw 1792 vvw	1790 w	1889 vs	1826 w 1850 vw 1870 vw	<i>trans</i>	384 + 1456
1957 vw			1903 vvw, b		1956 vw, b	1915 sh 1931 vvw 1956 w	<i>trans</i>	1029 + 955
2860 s 2916 vs	2730 w 2845 s 2920 vs	2900 m	2860 w 2900 vvw	2880 w, b 2940 w	2847 m 2925 m	2750 vvw 2854 s 2914 s 2922 vs 2945 s		v ₂₈ CH ₂ ring v ₂ CH ₂ ring v ₂₈ CH ₂ ring
3058 m 3096 vw		3069 w 3098 vw	3040 w 3075 vvw 3100 vvw	3080 w 3120 vvw	3060 w 3103 vw	3078 w 3085 vvw 3115 vvw 3160 vvw		v CH (v ₂₈ , B ₃₀) v CH (v ₂₈ , B ₃₀)
3413 vvw		3413 w, b	3410 w 3480 w	3450 m, b	3440 w, b	3420 w		v ₂ O—H

* isomer-*cis*/*trans*; bands not identified as being of *cis* or *trans* origin are common to both stereo-isomers in PCHT and model compounds

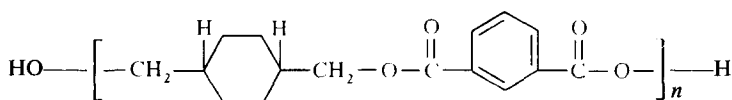
POLY(CYCLOHEXANE 1,4-DIMETHYLENE TEREPHTHALATE)



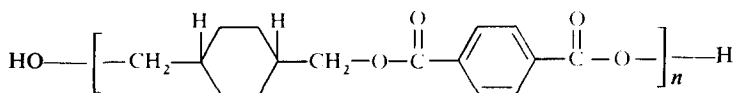
cis and *trans* cyclohexane-1,4-dimethanol-*bis*-terephthalate-hemi-ester



cis and *trans* cyclohexane-1,4-dimethanol dibenzoate



cis and *trans* poly(cyclohexane 1,4-dimethylene isophthalate)



cyclohexane 1,4-dimethanol terephthalate, both as oligomer

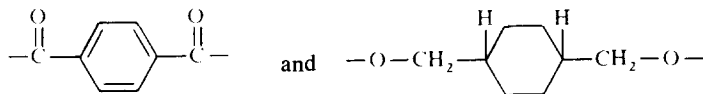
$n = 3$ and polymer $n = 36$;

and ethylene-glycol dibenzoate; and 1,6-hexanediol dibenzoate.

The infra-red spectra and band assignments of the model compounds are summarized in *Table 3*.

Predicted spectrum of poly(cyclohexane-1,4-dimethylene terephthalate)

As with PET⁷ the repeat unit of PCHT is broken down into the discrete fragments:



It is probable that the terephthalate framework will behave in a very similar 'spectral' manner in both PET and PCHT, its conformation being more affected by changes in molecular orientation and crystallization than by the influence of the different conformations of the cyclohexane-1,4-dimethanol fragment. It is therefore convenient to commence the analysis with the contribution of the vibrational modes of the terephthalate framework to the PCHT spectrum.

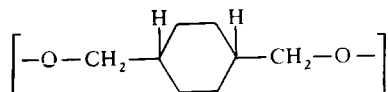
Normal modes of vibration of the $\left[\text{---}\overset{\text{O}}{\parallel}\text{C}\text{---C}_6\text{H}_4\text{---}\overset{\text{O}}{\parallel}\text{C}\text{---} \right]$ fragment in PCHT

By analogy with PET the terephthalate framework is expected to be centrosymmetric and planar (symmetry $V_h \equiv D_{2h}$) only in highly crystalline, oriented polymer. In amorphous regions the symmetry is likely to be lowered to C_{2v} due to out-of-plane bending of the C=O groups, as in PET⁷.

Similarly appreciable rotation of the cyclohexane 1,4-dimethanol fragment would be expected about the $\text{---O---CH}_2\text{---}$ linkage and about the $\text{---}\overset{\parallel}{\text{C}}\text{---O---}$ bond. Such rotation is not expected to affect the orientation of the terephthalate framework appreciably with respect to the drawing axis of a uniaxially oriented specimen. X-ray diffraction analysis of one-way drawn PCHT⁶ shows that although rotation about the $\text{---O---CH}_2\text{---}$ and $\text{---}\overset{\parallel}{\text{C}}\text{---O---}$ bonds almost certainly does occur, the plane of the benzene ring is parallel to the film plane and the uniaxial orientation at 200–300% extension is almost complete.

Spectral changes in *cis* and *trans* PCHT occurring upon crystallization and attributed to the terephthalate framework ought to be very similar to those in PET. Corresponding bands were observed in *cis* and *trans* PCHT and they exhibit similar polarization and intensity changes upon drawing and crystallization as those modes attributed to the framework in PET. The assignments of these modes in PCHT and PET are summarized elsewhere⁷.

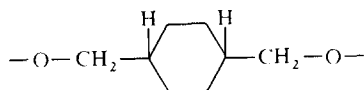
Normal modes of vibration of the fragment



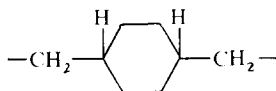
The fragment possesses 24 atoms and will therefore contribute $(3N-6)$ normal modes of vibration, as a discrete unit. These 66 normal vibrations may be broken down as follows. The cyclohexane skeleton will contribute 12 vibrations involving essentially 3 ring stretching modes and 3 ring breathing modes (ν_{CC}), 3 ring in-plane deformation modes ($\delta_{\text{CCC}} \parallel$) and 3 ring out-of-plane deformation modes ($\delta_{\text{CCC}} \perp$). The 4 ring methylene groups contribute 24 vibrations involving 4 CH_2 symmetric stretching ($\nu_{\text{s}}\text{CH}_2$), 4 CH_2 asymmetric stretching ($\nu_{\text{as}}\text{CH}_2$), 4 CH_2 deformation (δCH_2), 4 CH_2 twisting (τCH_2), 4 CH_2 wagging (ωCH_2) and 4 CH_2 rocking (ρCH_2) modes. The 1,4-dimethylene substituents will contribute 12 CH_2 vibrations, involving $\nu_{\text{s}}\text{CH}_2$ (2), $\nu_{\text{as}}\text{CH}_2$ (2), δCH_2 (2), τCH_2 (2), ωCH_2 (2) and ρCH_2 (2). The 1,4-dimethylene carbon substituents in the equatorial positions together with the 1,4-*trans* substituted hydrogen atoms in the polar positions contribute 12 vibrations. These are approximately equivalent to the 12 normal modes of the *trans* $X_2Y_2Z_2$ molecule [e.g. $\text{C}_2\text{H}_2\text{Cl}_2$]⁸. The remaining 6 vibrations of the fragment are contributed by motion of the two oxygen atoms attached to the 1,4-disubstituted methylene groups, about the x , y and z axes. The resulting modes are symmetric and asymmetric C–O bond stretching ($\nu_{\text{s}} \text{C---O}$, $\nu_{\text{as}} \text{C---O}$) and two in-plane CCO deformation modes ($\delta_{\text{CCO}} \parallel$) and two out-of-plane CCO deformation modes ($\delta_{\text{CCO}} \perp$).

'Trans' configuration

The PCHT repeat unit with the 1,4-substituents in the *trans* conformation is potentially centro-symmetric, since it has a centre of symmetry in the crystalline phase⁶, and the space group will then be $P\bar{1}$, which is isomorphic to the point group C_i . In the repeat period of the *trans*-PCHT unit, the cyclohexane ring in the chair configuration must be substituted in equatorial positions, since polar substitution would produce too much contraction from the extended form⁶. The fragment



of '*trans*' configuration will then also possess the space group $P\bar{1}$ ($\equiv C_i$). However, if the '*trans*' fragment



is considered neglecting the terminal oxygen atoms, the fragment will possess C_{2h} symmetry, which implies a two-fold rotation axis about the y (i.e. 1,4) axis, a centre of inversion and a reflection plane through the y axis. It is more convenient to classify the normal modes of the fragment under the four vibrational species of C_{2h} symmetry than under the two species of C_i symmetry. The infra-red selection rules for both symmetries are the same, the '*g*' modes being Raman active and the '*u*' modes infra-red active.

The 60 vibrations of the '*trans*' configuration (without terminal oxygen atoms) will transform under the characters for the irreducible representations

Table 4 Characters, selection rules and numbers of normal modes for the fragment ($-\text{O}-\text{CH}_2\text{C}_6\text{H}_{10}\text{CH}_2-\text{O}-$) of '*trans*' configuration in PCHT on basis of C_{2h} symmetry

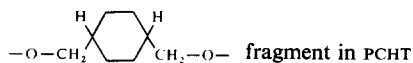
C_{2h}	E	$C_2(x)$	i	σ_h	n		
A_g	1	1	1	1	20	R_z	$\alpha_{xx}, \alpha_{yy}, \alpha_{zz}, \alpha_{xy}$
B_g	1	-1	1	-1	10	R_x, R_y	α_{yz}, α_{zx}
A_u	1	1	-1	-1	11	T_z	
B_u	1	-1	-1	1	19	T_x, T_y	

at the point group C_{2h} according to Table 4. The 60 normal vibrations are then found to divide as follows

$$20A_g + 10B_g + 11A_u + 19B_u$$

Since the fragment is centro-symmetric the mutual exclusion rule will apply and the A_g and B_g modes will be Raman active, and the A_u and B_u modes infra-red active. The normal modes of the fragment under C_{2h} symmetry are

Table 5 Assignments of the fundamental modes of vibration of the



<i>C_i-A_g species; Raman, P</i>		<i>Trans</i>		<i>C_s</i>	<i>Cis</i> (R, IR)		
<i>C_{2h}</i>	No.	ν_i^*	Approximate motion	<i>D_{3d}</i> †	ν_i	<i>P</i> ‡	
<i>A_g</i>	37	(2930)	ν_s CH ₂ ring	<i>A_{1g}</i> (1)	<i>A'</i>	σ	
	38	(2852)	ν_s CH ₂ ring	<i>A_{1g}</i> (2)		σ	
	39	(2897)	ν_s CH ring	<i>E_g</i> (17)		σ	
	40	—	ν_s CH ₂			σ	
	41	—	ν_{as} CH ₂			σ	
	42	—	<i>s</i> ν_s C(CO)	<i>E_g</i> (18)		1295	π
	43	(1465)	δ CH ₂ ring	<i>A_{1g}</i> (3)		1445	σ
	44	—	δ CH ₂ in-phase				σ
	45	—	δ CH + δ C(CO)	<i>E_g</i> (19)		630?	σ
	46	(1348)	τ CH ₂ ring	<i>E_g</i> (20)		1350	—
	47	—	τ CH ₂ in-phase				—
	48	(1267)	ω CH ₂ ring	<i>E_g</i> (21)		1220	π
	49	—	ω CH ₂ out-of-phase				π
	50	(384)	ρ CH ₂ ring	<i>A_{1g}</i> (6)		372	σ
	51	—	ρ CH ₂ in-phase			885	σ
	52	—	<i>s</i> ρ CH + ρ C(CO)	<i>E_g</i> (22)			σ
53	(1157)	<i>s</i> ν CC ring	<i>A_{1g}</i> (4)	1195			
54	?	<i>s</i> ν CC ring	<i>E_g</i> (23)				
55	(802)	<i>s</i> δ CCC \perp	<i>A_g</i> (5)	825	σ		
56	(426)	<i>s</i> δ CCC \parallel	<i>E_g</i> (24)		π		
<i>B_g</i>	57	?	ν_s CH ₂ ring	<i>E_g</i> (17)	<i>A''</i>	σ	
	58	(2871)	ν_s CH ₂	<i>E_g</i> (18)		σ	
	59	(1443)	δ CH ₂ ring	<i>E_g</i> (19)		1422	σ
	60	?	τ CH ₂ ring	<i>A_{2g}</i> (10)			—
	61	—	τ C(H + CO)	<i>E_g</i> (20)			—
	62	(1107)	ω CH ₂ ring	<i>A_{2g}</i> (11)			π
	63	—	<i>s</i> ω [CH + C(CO)]	<i>E_g</i> (21)			σ
	64	(1029)	ρ CH ₂ ring	<i>E_g</i> (22)		995	σ
	65	?	<i>s</i> ν CC ring	<i>E_g</i> (23)			π
	66	?	<i>s</i> δ CCC \parallel	<i>E_g</i> (24)			π
	67	—	<i>s</i> ν_s C—O			1043	π
	68	—	<i>s</i> δ CCO \parallel				π
	69	—	<i>s</i> δ CCO \perp				σ

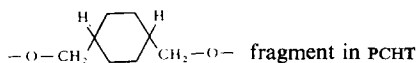
* () The frequencies in parentheses are the modes observed in cyclohexane, assigned by Miller and Golob

† Corresponding modes in cyclohexane. The frequency notation is due to Miller and Golob.

‡ Predicted infra-red dichroism in oriented polymer — applies to both *cis* and *trans* configuration

s Denotes 'skeletal' vibration

Table 5 (Continued) Assignments of the fundamental modes of vibration of the



<i>Trans</i>						<i>Cis</i>	
<i>C_t-A_u species; infra-red</i>						<i>C_s</i>	<i>(R, IR)</i>
<i>C_{2h}</i>	<i>No.</i>	<i>ν_i</i>	<i>P_‡[†]</i>	<i>Approximate motion</i>	<i>D_{3d}[†]</i>		<i>ν_i</i>
<i>A_u</i>	70		<i>σ</i>	<i>ν_{as}</i> CH ₂ ring	<i>E_u</i> (25)	<i>A''</i>	
	71	2850	<i>σ</i>	<i>ν_{as}</i> CH ₂ ring	<i>E_u</i> (26)		2850
	72	1445	<i>σ</i>	<i>δ</i> CH ₂ ring	<i>E_u</i> (27)		1445
	73		—	<i>τ</i> CH ₂ ring	<i>A_{1u}</i> (7)		
	74		—	<i>τ</i> C(H, CO)	<i>E_u</i> (28)		
	75	1136	<i>π</i>	<i>ω</i> CH ₂ ring	<i>A_{1u}</i> (8)		1136
	76	278	<i>σ</i>	<i>s</i> <i>ω</i> [CH + C(CO)]	<i>E_u</i> (29)		278
	77	872	<i>σ</i>	<i>s</i> <i>ρ</i> CH ₂ ring	<i>E_u</i> (31)		872
	78		<i>σ</i>	<i>s</i> <i>ν</i> CC ring	<i>A_{1u}</i> (9)		
	79		<i>σ</i>	<i>s</i> <i>ν</i> CC ring	<i>E_u</i> (30)		598?
80		<i>σ</i>	<i>s</i> <i>δ</i> CCC ⊥	<i>E_u</i> (32)			
<i>B_u</i>	81	2925	<i>π</i>	<i>ν_{as}</i> CH ₂ ring	<i>A_{2u}</i> (12)	<i>A'</i>	2925
	82	2750	<i>π</i>	<i>ν_{as}</i> CH ₂ ring	<i>A_{2u}</i> (13)		2750
	83		<i>σ</i>	<i>ν_{as}</i> CH ring	<i>E_u</i> (25)		
	84	2945	<i>σ</i>	<i>ν_{as}</i> CH ₂			
	85	2909	<i>σ</i>	<i>ν_s</i> CH ₂			
	86	1386	<i>π</i>	<i>ν_{as}</i> C(CO)	<i>E_u</i> (26)		1395
	87	1445	<i>π</i>	<i>δ</i> CH ₂ ring	<i>A_{2u}</i> (14)		
	88	1318?	<i>σ</i>	<i>δ</i> CH ₂ out-of-phase			
	89	710	<i>σ</i>	<i>δ</i> CH + <i>δ</i> C(CO)	<i>E_u</i> (27)		630?
	90	1355	—	<i>τ</i> CH ₂ ring	<i>E_u</i> (28)		1355
	91		—	<i>τ</i> CH ₂ out-of-phase			
	92	1253	<i>π</i>	<i>ω</i> CH ₂ ring	<i>E_u</i> (29)		1253
	93	1370?	<i>π</i>	<i>ω</i> CH ₂ in-phase			1374
	94	529	<i>π</i>	<i>ρ</i> CH ₂ ring	<i>A_{2u}</i> (16)		530?
	95	848	<i>σ</i>	<i>ρ</i> CH ₂ out-of-phase			825?
	96	128	<i>σ</i>	<i>s</i> <i>ρ</i> CH + <i>ρ</i> C(CO)	<i>E_u</i> (31)		128
	97	955	<i>π</i>	<i>s</i> <i>ν</i> CC ring	<i>E_u</i> (30)		950
	98	895	<i>π</i>	<i>s</i> <i>δ</i> CCC ⊥	<i>A_{2u}</i> (15)		898
	99	222	<i>σ</i>	<i>s</i> <i>δ</i> CCC ⊥	<i>E_u</i> (32)		202
	100	1152	<i>π</i>	<i>s</i> <i>ν_{as}</i> C—O			1150
101	335	<i>σ</i>	<i>s</i> <i>δ</i> CCO ⊥		320		
102	43	<i>σ</i>	<i>s</i> <i>δ</i> CCO ⊥ ≡ <i>τ</i> OCH ₂ C ₆ H ₁₀		43		

* () The frequencies in parentheses are the modes observed in cyclohexane, assigned by Miller and Golob.

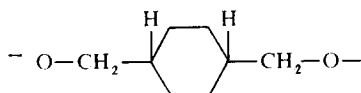
† Corresponding modes in cyclohexane. The frequency notation is due to Miller and Golob.

‡ Predicted infra-red dichroism in oriented polymer—applies to both *cis* and *trans* configurations

s Denotes 'skeletal' vibration

given in *Table 5*, together with an approximate description of the motions involved. The infra-red polarizations given in this table are those predicted for the dipole transitions with respect to the plane of the film. The compilation of *Table 5* was facilitated by correlating the relevant normal modes of the fragment under C_{2h} symmetry with the corresponding normal modes of cyclohexane, of D_{3d} symmetry. Those vibrations in which the (1,4-) substituents remain virtually stationary in PCHT will consequently occur at similar frequencies to the corresponding modes in cyclohexane. Each degenerate mode in cyclohexane gives rise to two vibrations in PCHT, one of which will correspond closely in frequency to the degenerate frequency (the 1,4-substituents being at rest) and the other will be significantly lower than the degenerate vibration due to vibrations involving the heavier 1,4-substituents.

Also given in *Table 5* are the normal modes of the fragment



which, taking the off-axis oxygen atoms into account, will possess the symmetry C_i . The 66 normal modes of the fragment, according to *Table 6* will then divide as follows

$$33 A_g + 33 A_u$$

Table 6 Characters and selection rules for the fragment ($-\text{O}-\text{CH}_2\text{C}_6\text{H}_{10}\text{CH}_2-\text{O}-$) of 'trans' configuration in PCHT on the basis of C_i symmetry

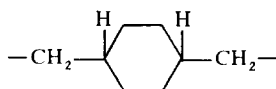
C_i	C_{2h}	E	i	n^*		
A_g	A_g, B_g	1	1	33	R	α
A_u	A_u, B_u	1	-1	33	T	

*Number of normal modes under each irreducible representation

the A_g modes being Raman active, and the A_u modes being infra-red active. The six 'additional' modes in this fragment will be due to motions of the terminal oxygen atoms about the $-\text{CH}_2-\text{C}_6\text{H}_{10}-\text{CH}_2-$ skeleton, resulting in three A_g modes involving $\nu_s \text{ C-O}$, $\delta\text{CCO}\parallel$ and $\delta\text{CCO}\perp$ and three A_u modes involving $\nu_{as} \text{ C-O}$, $\delta\text{CCO}\parallel$ and $\delta\text{CCO}\perp$.

'Cis' configuration

The repeating unit of the *cis* polymer is not centrosymmetric and the space group⁶ is probably $P1$, which is equivalent to the identity operation E . However, an examination of classical models of the polymer indicate that the *cis* fragment



will possess a reflection symmetry plane along the 1,4-axis and will therefore belong to the C_s point group. According to the characters and selection rules for the C_s point group in Table 7, the 60 normal modes of the fragment will divide as follows

$$39 A' + 21 A''$$

where both the A' and A'' vibrational species are Raman and infra-red active, the A' and A'' notations representing vibrations symmetric and antisymmetric with respect to the single reflection plane.

Table 7 Characters and selection rules for the fragment ($-\text{CH}_2-\text{C}_6\text{H}_{10}-\text{CH}_2-$) of 'cis' configuration on the basis of C_s symmetry.

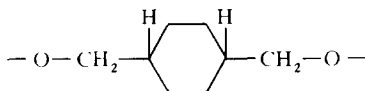
C_s	E	σ_h	n^*		
A'	1	1	39	T_x, T_y, R_z	$a_{zz}, a_{yy}, a_{xx}, a_{xy}$
A''	1	-1	21	T_z, R_x, R_y	a_{yz}, a_{zx}

*Number of normal modes under each irreducible representation.

The 6 modes involving the terminal oxygen atoms cannot be considered under the point group C_s , but under the space group $P1$, isomorphic to point group C_1 . Such a low symmetry implies both infra-red and Raman activity of all six skeletal modes.

For convenience the 66 normal modes of the *cis* fragment are also included in Table 5.

Assignment of the normal modes of the fragment



The infra-red spectra of the *cis* and *trans* isomers of 1,4-disubstituted cyclohexanedimethanol derivatives are very similar^{1, 9, 10}. There are few appreciable band shifts and intensity changes on going from pure *cis* to pure *trans* conformations for derivatives studied in the same state. However, upon change of state significant intensity changes do occur in many bands in *trans* substituted isomers, whilst the *cis* isomers show little spectral change as will be discussed later. The most important spectral difference between the two isomers is a strong infra-red and Raman band observed in the *cis* isomer at 630 cm^{-1} , which is very weak or totally absent in the *trans* isomer. It has been suggested^{9, 10} that this band is an indication of the axial substitution of cyclohexane.

Because of the over-all spectral similarity between the two stereoisomers it is evident that there are no significant shifts in frequency between the corresponding modes in the two isomers. Consequently the assignment of the

modes attributable to the two conformations will be discussed together. The assignments will be hampered by the low symmetry of the fragments, especially the *cis*-form, in which all of the normal vibrations are expected to be infra-red active, with some of the expected infra-red dichroisms in the extended polymer in some doubt.

A_g and B_g species

The modes of vibration of the *trans* stereoisomer belonging to the A_g and B_g species are inactive in the infra-red. The vibrational modes of the fragment in which the 1,4-substituents are essentially at rest are expected to occur at similar frequencies to those in cyclohexane,¹¹ which are given in parentheses under the A_g and B_g species in *Table 5*.

In *Table 5* the frequency notation is not in exact order of decreasing frequency due to the low symmetry of the fragment and the large number of vibrations involved under each symmetry species. The A' and A'' modes in the *cis*-stereoisomer corresponding to the inactive A_g and B_g modes of the *trans* isomer will be infra-red active. The assignment of these *cis* A' and A'' modes is somewhat arbitrary, since many of the frequencies will lie close to, or will be coincident with, their active counterparts corresponding to the infra-red active A_u and B_u modes of the *trans* configuration. This is seen on comparing the spectra of the *cis* and *trans* isomers of PCHT and the associated model compounds. These additional bands which are peculiar to the *cis*-stereo isomers and which are not attributed to the terephthalate framework are consequently assigned to the A' and A'' modes according to *Table 5*. In many cases the infra-red dichroism was very difficult to ascertain due to masking by more intense absorption, but the assignments for those modes of known polarization are consistent with the predicted polarizations. The assignments of these modes were made largely by analogy with the corresponding infra-red inactive Raman active modes of cyclohexane (*Table 5*).

We believe the infra-red absorption at ~ 630 cm^{-1} and characteristic of the *cis*-stereo isomer^{9, 10} is most probably due to the vibrations ν_{45} (A') or ν_{89} (A') which are mixed C-H and C-(CO) deformation modes, $\delta\text{CH} + \delta\text{C}(\text{CO})$. It is felt that this normal vibration will be more sensitive to *cis*-substitution at the 1,4-position than any of the other related vibrations involving the 1,4-substituents, expected to lie in this region.

The mixed CH_2 (ring) rocking mode (ν_{50}) is observed at 384 cm^{-1} in cyclohexane¹¹ and at 372 cm^{-1} in the Raman and infra-red spectrum of *cis*-cyclohexane 1,4-dimethanol, and in the Raman at 376 cm^{-1} for the *trans* isomer¹². The very weak band in the spectrum of the *cis*-polymer at 372 cm^{-1} is therefore assigned to this mode.

A_u and B_u species (*trans* configuration); A'' and A' species (*cis* configuration)

A_u/A'' species. The normal vibrations of both the *cis* and *trans* stereoisomers corresponding to the A_u and B_u species will be active in the infra-red

These modes are assigned to bands which are peculiar to PCHT which are absent in the PET spectrum, and which occur at similar frequencies in both the *cis* and *trans* isomers, in both PCHT and the associated model compounds. As with the A_g and B_g species the assignments of the A_u and B_u vibrational species was aided by the correlation with similar modes occurring in cyclohexane. Consequently, the bands occurring in both isomers at 2850, 1445 and 872 cm^{-1} and the π band at 1136 cm^{-1} are assigned to $\nu_{as}\text{CH}_2$, δCH_2 , ρCH_2 and ωCH_2 (all of the A_u symmetry species) respectively. All the bands display the polarizations predicted. In cyclohexane the corresponding $\nu_{as}\text{CH}_2$, δCH_2 and ρCH_2 modes occur at 2864, 1440 and 906 cm^{-1} respectively. The medium σ band at 278 cm^{-1} is assigned to the 'mixed' $\omega[\text{CH} + \text{C}(\text{CO})]$ mode, ν_{76} (A_u, A''). In the terephthalate ring framework the $\omega\text{C}(\text{CO})$ mode is assigned at $\sim 240\text{ cm}^{-1}$.

The medium π band common to both polymers at 598 cm^{-1} is believed to be due to one of the ring breathing modes, ν_{78}, ν_{79} . However, the observed dichroism of this band is not consistent with the σ polarization predicted, although the latter is itself in doubt due to ignorance of the exact spatial orientation of the cyclohexane ring with respect to the rolled film plane in a fully oriented specimen. The modes which remain unassigned in this group and which are expected to occur as weak infra-red bands are probably masked by other absorption.

B_u/A' species. The following assignments have been made for the B_u/A' vibrations in the *trans/cis* configurations of the fragment (the frequencies in square brackets are the corresponding values in cyclohexane): $\rho\nu_{as}\text{CH}_2$ (ring) 2925 (ν_{81}), 2750 (ν_{82}) [2935, 2801 cm^{-1}]; τCH_2 (ring) 1355 cm^{-1} (ν_{90}) [1355 cm^{-1}]; ωCH_2 (ring) 1253 cm^{-1} (ν_{92}) [1263 cm^{-1}]; ν_{CC} (ring)—950 cm^{-1} (ν_{27}) [1040 cm^{-1}]; $\delta\text{CCC}\parallel$ —898 cm^{-1} (ν_{98}) [862 cm^{-1}]; ρCH_2 (ring)—530 cm^{-1} (ν_{94}) [522 cm^{-1}]. The observed polarizations are in agreement with those predicted.

Cis-cyclohexane-1,4-dimethanol has infra-red and Raman bands at 127, 193 and 311 cm^{-1} due to a mixed skeletal C(CO) rocking mode, a ring out-of-plane deformation mode and a CCO bending vibration¹². Infra-red bands are observed in the *cis*-PCHT spectrum, and the spectra of the *cis* isomers of the associated model compounds, at 128, ~ 202 and $\sim 320\text{ cm}^{-1}$. These bands are consequently assigned to $\rho\text{CH} + \rho\text{C}(\text{CO})$ (A', ν_{96}), $\delta\text{CCC}\perp$ ($A' \nu_{99}$) and $\delta\text{CCO}\perp$ ($A' \nu_{102}$) in the *cis*-stereo isomers. The *trans* counterpart to ν_{99} is tentatively assigned to a weak band peculiar to the *trans* isomer at 222 cm^{-1} .

In *trans*-cyclohexane-1,4-dimethanol two bands at 337 and 127 cm^{-1} were found and assigned to $\delta\text{CCO}\perp$ and $\rho\text{CH} + \rho\text{C}(\text{CO})$, together with the band at 376 cm^{-1} (already assigned to ρCH_2 (A_g), in accordance with predicted values)¹³. *Trans*-PCHT and the *trans* stereo-isomers of the associated model compounds have absorptions at ~ 335 (σ) and $\sim 128\text{ cm}^{-1}$. These bands are therefore assigned to $\delta\text{CCO}\perp$ (ν_{102}, σ) and $\rho\text{CH} + \rho\text{C}(\text{CO})$ (ν_{96}, σ) respectively.

The π bands at 1386 cm^{-1} (*cis*) are attributed to the $\nu_{as}\text{C}-(\text{CO})$ mode (ν_{86}, π) in the two isomers. In the terephthalate framework the mode is believed to occur in the region $1330\text{--}1370\text{ cm}^{-1}$. The $\nu_{as}\text{ C-O}$ mode (ν_{100}, π)

occurs in polyesters at $\sim 1120 \text{ cm}^{-1}$ and is consequently assigned to the π band at $\sim 1150 \text{ cm}^{-1}$ in the two isomers.

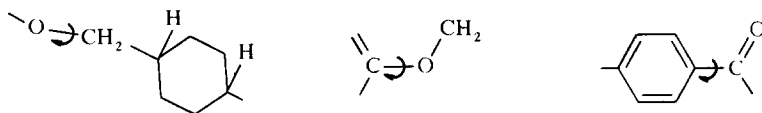
The modes associated with the CH_2 groups of the 1,4-ring substituents are less readily identified. However the π band at 1374 cm^{-1} (*cis* and *trans*) and the σ band at 848 (*trans*), 825 cm^{-1} (*cis*) are tentatively assigned to ωCH_2 (in-phase) (ν_{93} , π) and ρCH_2 out-of-phase (ν_{95} , σ) since similar absorption due to these modes is observed in $\text{DO-CH}_2\text{CH}_2\text{-OD}^{14}$.

A study of the molecular models of *cis* and *trans*-PCHT shows that the in-plane CCO deformation mode (ν_{102}) is equivalent to the torsion of the 1,4-disubstituted cyclohexane ring about the (1,4 -O- CH_2) substituents as axis. In *cis* and *trans* cyclohexane-1,4-dimethanol a weak-medium absorption band occurs in the far infra-red at 41 cm^{-1} , which is believed to be attributed to this mode. The torsional mode ν_{102} is therefore tentatively assigned to the weak infra-red absorption at 43 cm^{-1} in *cis*- and *trans*-PCHT.

No other modes associated with the cyclohexane dimethanol fragment can be accounted for with certainty. There is, of course, a strong likelihood that in such a complex spectrum, many of the weaker bands expected, but not detected, are masked by other absorption.

The 'internal' stretching, deformation and torsional modes of the PCHT chain skeleton

The eight 'internal' skeletal modes which are derived from the twelve 'null' modes of the discrete terephthalate and cyclohexane-1,4-dimethanol fragments on joining the two fragments to form the polymer repeat unit, are expected to be of a similar nature to those in PET⁷. They will involve essentially stretching of the $-\text{O}-\overset{\parallel}{\text{C}}-\text{O}-$ bond, $\nu(\text{O}-\overset{\parallel}{\text{C}}-\text{O})$, four in-plane and out-of-plane chain bending modes and three skeletal torsional vibrations. The latter will arise in PCHT due to restricted rotation about the three bonds



As in PET the symmetries of these internal skeletal vibrations must be considered under the appropriate factor group or unit cell group. For the *trans* configuration⁶ the unit cell group is equivalent to the point group C_i and these vibrations will then divide as in *trans* PET, namely

$$5A_g + 3A_u$$

Due to the low C_1 symmetry of the unit cell group of the *cis*-polymer, all eight skeletal modes are likely to be infra-red active.

A tentative assignment for the internal skeletal modes in the *cis* and *trans* isomers of PCHT is given in Table 8, together with approximate descriptions of the motions involved. The exact forms of these eight normal vibrations are not known. The assignments have been made chiefly by correlation with the skeletal modes in PET and the related model compounds.

Table 8 Assignment of the 'internal' skeletal modes in *cis* and *trans* poly(cyclohexane-1,4-dimethylene terephthalate)

Unit cell group C_i 'Trans'	No_i	ν_i	P	Unit cell group C_i 'Cis'	ν_i	P	Assignment
A_g	(103)	460	π	A	290	π	$\delta \overset{\parallel}{\text{C}}\overset{\parallel}{\text{C}}\text{O} \parallel$
A_g	(104)	174	π	A	190	π	$\delta \overset{\parallel}{\text{C}}\text{O}\overset{\parallel}{\text{C}} \parallel$
A_g	(105)	90	π	A	115	π	$\tau (\text{C}_6\text{H}_4) \overset{\parallel}{\text{C}}\text{O}$
A_g	(106)	72	σ	A	72	σ	$\tau \overset{\parallel}{\text{C}}\text{C}\text{O}\overset{\parallel}{\text{C}}$
A_g	(107)	50	σ	A	50/35	σ	$\tau \overset{\parallel}{\text{C}}\text{O}\overset{\parallel}{\text{C}}\overset{\parallel}{\text{C}}$
A_u	(108)	1272	π	A	1272	π	$\nu (-\overset{\parallel}{\text{C}}-\text{O}-)$
A_u	(109)	391	π	A	360	π	$\delta \overset{\parallel}{\text{C}}\text{O}\overset{\parallel}{\text{C}} \perp$
A_u	(110)		σ	A	270	σ	$\delta \overset{\parallel}{\text{C}}\overset{\parallel}{\text{C}}\text{O} \perp$

The intense π band at 1272 cm^{-1} in both isomers is assigned to the $\nu\overset{\parallel}{\text{C}}-\text{O}$ skeletal stretching mode. In *trans* PET the mode is assigned at 1266 cm^{-1} .

The $\overset{\parallel}{\text{C}}\text{C}\text{O}$ and $\overset{\parallel}{\text{C}}\text{O}\overset{\parallel}{\text{C}}$ skeletal modes in *trans* PCHT are not expected to differ significantly from those in *trans* PET. Consequently the weak bands common to both polymers at 460 (σ), 391 (crystal) and 174 (π , crystal) cm^{-1} are assigned to $\delta\overset{\parallel}{\text{C}}\overset{\parallel}{\text{C}}\text{O} \parallel$ (A_g, σ), $\delta\overset{\parallel}{\text{C}}\text{O}\overset{\parallel}{\text{C}} \perp$ (A_u, π) and $\delta\text{COC} \parallel$ (A_g, π) respectively.

Certain bands in the *cis* isomers of PCHT and model compounds are insensitive to phase changes. These are tentatively assigned as follows

$$290 (\pi) \delta \overset{\parallel}{\text{C}}\overset{\parallel}{\text{C}}\text{O} \parallel; 190 (\pi) \delta \overset{\parallel}{\text{C}}\text{O}\overset{\parallel}{\text{C}} \parallel$$

$$360 (\pi) \delta \overset{\parallel}{\text{C}}\text{O}\overset{\parallel}{\text{C}} \perp; 270 (\sigma) \delta \overset{\parallel}{\text{C}}\overset{\parallel}{\text{C}}\text{O} \perp$$

the polarizations observed agree with those predicted. The analogy here with the assignments for the skeletal modes of '*gauche*' PET is interesting in that although the two assignments are almost identical the bands in '*gauche*' PET are of definite amorphous origin.

This is most probably explained by the fact that whereas in amorphous PET the glycol fragment is predominantly *gauche* as a result of rotational isomerism, no such isomerism can occur in *cis*-PCHT and the bands associated with the skeletal modes in the latter are neither of crystalline nor amorphous origin.

Assignment of combination bands and overtones in PCHT

All the assignments attempted for combination bands in PCHT are for the *trans*-stereoisomer. A number of characteristic infra-red active combination tones are known to occur in cyclohexane¹¹. Since both cyclohexane and the 1,4-disubstituted cyclohexane fragment in *trans*-PCHT possess a centre of symmetry, combination tones will only be active in the infra-red for combinations of infra-red and Raman active fundamentals. Bands common to both

cyclohexane and *trans*-PCHT and assigned as combination tones occur at 2526, 2362, 2270, 2124, 2073, 1950, 1815, 1675 and 1651 cm^{-1} and their appearance as π bands in the *trans*-PCHT spectrum lends support to the assignments of the normal modes of vibration of the *trans*-1,4-disubstituted cyclohexane fragment summarized in Table 7.

Characteristic combination tones occurring in benzene¹⁵ and disubstituted benzene derivatives¹⁶ have not been observed in PCHT, this is probably due to masking.

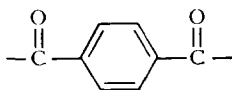
Many of these combination tones are however observed in the spectra of the model compounds given in Table 3 and ref. 7.

DISCUSSION

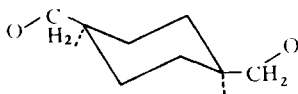
The most striking feature of the *cis*-PCHT infra-red spectrum is the apparent lack of sensitivity of the band intensities to change of phase. There appear to be no bands of definite amorphous or crystalline origin and there is no significant change in intensity, even in solution, of any of the bands which are phase-sensitive in the *trans* isomer. Those bands which show crystal or amorphous origin in the latter can be attributed almost entirely to the terephthalate framework, by analogy with the PET spectrum. The crystal bands are attributed to the planar conjugated terephthalate framework and these bands gradually decrease in intensity with increasing amorphous content, accompanied by a corresponding increase in intensity of certain other bands associated with a distorted terephthalate system. This signifies increasing distortion of the planar terephthalate skeleton from D_{2h} to C_{2v} symmetry, and also implies a sharp increase in the number of such distorted units.

Since *cis*-PCHT does not exhibit any significant changes in band intensity in the amorphous \rightarrow crystalline transition, it is concluded that the terephthalate framework remains distorted in the *cis*-stereoisomer, even in highly crystalline, oriented polymer and retains the over-all space group of the unit cell, namely P_1 .

It is concluded that the *cis*-cyclohexane-1,4-dimethanol fragment in PCHT and the *gauche* ethylene glycol residue in PET are associated with a distorted terephthalate skeleton. It is also probable that the *trans* ethylene glycol fragment in PET is associated with a planar conjugated terephthalate system which appears to be stable only in a strong crystal field. Orientation of an amorphous specimen alone does not significantly increase the degree of crystallinity, and hence many bands associated with amorphous regions of both PET and *trans* PCHT still persist strongly in the uniaxially non-heat crystallized specimens. With a relaxation in crystal field, rotation about the bond $-\text{CH}_2-\text{CH}_2-$ commences with the formation of the '*gauche*' rotational isomer with a corresponding distortion of the $-\text{C}-\text{O}-\text{CH}_2-$ bond, causing the



fragment to be non-planar. Since the orientation of the terminal groups of the



fragment in *cis*-PCHT will have a similar spatial orientation to the terminal groups of the ethylene glycol residue in 'gauche' PET¹ the strain induced about the $\text{--}\overset{\parallel}{\text{C}}\text{--O--CH}_2\text{--}$ bond in *cis*-PCHT will lead to similar distortion of the terephthalate skeleton, which cannot be relaxed by any change in phase, as in the case of PET, since *cis*→*trans* rotational isomerism cannot occur in the cyclohexane-1,4-dimethanol fragment in the linear polymer.

In *trans*-PCHT partial rotation about the $\text{--O--CH}_2\text{--CH--}$ bonds leads to a distortion of the terephthalate skeleton ($D_{2h} \rightarrow C_{2v}$) upon relaxation of the crystal field, although, the *trans* substitution of the cyclohexane-1,4-dimethanol fragment is completely unaffected by any change of phase in that *trans*→*cis* isomerism cannot occur, in contrast to the *trans*-gauche isomerism of PET. The *trans*-substituted CHDM fragment is therefore associated with a conjugated, planar terephthalate framework in a strong crystal field, with increasing distortion of the former occurring upon relaxation of the latter.

As in PET rotation about the $\text{--O--CH}_2\text{--}$ and $\text{--}\overset{\parallel}{\text{C}}\text{--O--}$ bonds occurs in the *cis* and *trans* isomers of PCHT, but the barriers to rotation appear to be very similar in the two isomers in both highly crystalline and amorphous specimens.

ACKNOWLEDGEMENTS

We thank Dr A. E. Martin (Grubb Parsons) for his interest and the provision of facilities and the Science Research Council for finance.

Newcastle upon Tyne Polytechnic,
Department of Materials Science,
Ellison Building,
Ellison Place,
Newcastle upon Tyne, NE1 8ST UK

(Received 15 June 1970)

REFERENCES

- 1 Boye, C. A. *J. Polym. Sci.* 1961, **55**, 263
- 2 Martin, E. V., and Busch, H. *Angew. chem.* 1962, **74**, 624; Martin, E. V. *Textile Res. J.* 1962, **32**, 619
- 3 Devaney, R. G. *Natl. Acad. Sci. Natl. Res. Council Publ. No. 1080*, 1963, p32
- 4 Hassel, O. *Quart. Rev. (London)* 1953, **7**, 221
- 5 Wyckoff, R. W. G., 'Crystal Structures', Vol. III, Interscience, New York - London 1953
- 6 Boye, C. A. *J. Polym. Sci.* 1961, **55**, 275
- 7 Manley, T. R. and Williams, D. A. *Polymer, Lond.* 1969, **10**, 339

- 8 Herzberg, G., 'Molecular Spectra and Molecular Structure, II Infra-red and Raman Spectra of Polyatomic Molecules', Van Nostrand, New York 1964, p 331
- 9 Zhizhin, G. N., Sterin, Kh. E., Aleksanyan, V. T., Bovrov, A. V., Vasina, T. V., Lerman, B. M., Tyun'kina, N. I., and Liberman, A. L. *Neftekhimiya* 1965, **5**, 461, 645
- 10 Zhizhin, G. N., Sterin, Kh. E., Aleksanyan, V. T. and Liberman, A. L. *Zh. Strukt, Khim.* 1965, **6**, 684
- 11 Miller, F. A. and Golob, H. R. *Spectrochim. Acta* 1964 **20**, 1517
- 12 Zirnit, M. A. and Suschinskii, M. M. *Optika i Spektroskopiya* 1963, **15**, 190
- 13 Kuznetsova, T. I. and Suschinskii, M. M., 'Optics and spectroscopy', Supplement 2, 'Molecular Spectroscopy', Acad. of Science of U.S.S.R. Press 1963, p 144
- 14 Sawodny, W., Niedenzu, K. and Dawson, J. W. *Spectrochim. Acta* 1967, **23A**, 799
- 15 Mair, R. D. and Hornig, D. F. *J. Chem. Phys* 1949, **17**, 1236
- 16 Whiffen, D. H. *Phil. Trans. Roy. Soc.* 1955, A **248**, 131

Morphology of bulk crystallized *trans*-1,4-polybutadiene

S. FERNÁNDEZ BERMÚDEZ, J. M^a G. FATOU and F. CATALINA

Replicas of fracture surfaces of fractions of *trans*-1,4-polybutadiene, over the molecular weight range from 2×10^4 to 3.1×10^5 , have been examined by electron microscopy. Striated, lamella type crystallites were observed and the sizes increased, slightly as the molecular weight increased, and they were very much smaller than the extended chain length. The crystallite interfacial free energy increased with molecular weight.

INTRODUCTION

THE EXAMINATION of surfaces or fracture surfaces of crystalline polymers by electron microscopy is a very interesting experimental technique which allows the analysis of the morphology in these systems and the direct measurement of the sizes of the crystallites formed from isothermally crystallized polymers from the melt. It has been established that under the proper conditions of crystallization, many polymers display lamellar structures¹⁻⁴. The step heights of these lamellae have been associated with the sizes of the crystallites.

Anderson⁵ observed in polyethylene crystallized from the melt three different types of lamellae: type I or regular lamellae, which are similar to solution grown lamellae, type II or narrow lamellae and type III lamellae which have step heights equal to fully extended chain lengths, with a crystallite structure similar to that reported by Bunn *et al*⁶ for polytetrafluoroethylene. Mandelkern *et al*⁷ have demonstrated that striated lamellae are observed in polyethylene for all molecular weights and, therefore, structures of this type are not indication that the crystallite sizes are comparable to the extended chain length.

In a recent study, crystallization kinetics from the melt and the melting and transition temperatures of molecular weight fractions of *trans*-1,4-polybutadiene have been analysed^{8,9}. Because of the importance of the relationship between these parameters and the morphology of isothermally bulk-crystallized samples, we decided to investigate the fracture-surfaces by electron microscopy. Moreover, there is no information about the crystallite sizes and their relation with molecular weight in bulk crystallized fractions of *trans*-1,4-polybutadiene. In this work, we report the results in a molecular range of 20 000-310 000.

EXPERIMENTAL

The molecular weight fractions utilized in this work were obtained from *trans*-1,4-polybutadiene, kindly supplied by Phillips Petroleum Co.

The method of fractionation and characterization has previously been described⁸. The viscosity average molecular weights of the fractions, were obtained from intrinsic viscosity measurements in benzene at 25°C and the molecular weight of the fractions selected for this work were 20 000, 129 000, 238 000 and 310 000.

The microstructure of these fractions was determined by infra-red in a Perkin Elmer 621 spectrophotometer, using the technique described by Silas *et al*¹⁰. The 1,4-*trans* content for the fraction of the lowest molecular weight was 92% and for the other fractions was 97%.

Samples for study were prepared by moulding films 1 mm thick in a small aluminium mould; these films were then recovered in aluminium foil and after being completely melted in vacuum sealed tubes, were isothermally crystallized at 86°C for a sufficient length of time so that no further crystallization would occur at these temperatures. The time required for this was predetermined through the dilatometric experiments⁸ and range from ten to twelve days, depending on the molecular weight of the fractions. After completion of the crystallization at 86°C, the tubes were cooled to room temperature over a period of 24 h.

In another set of experiments, the fractions were quenched at 0°C, from the melted state. The densities of the specimens crystallized in these two manners were determined in a gradient column. The crystallinity was calculated from the wide-angle x-ray diffraction patterns, which were obtained in a North American Phillips Co. spectrometer with Ni filtered Cu-K α radiation. *Table 1* summarizes these data.

Table 1

$M\eta$	$T_c = 86^\circ\text{C}$		$T_c = 0^\circ\text{C}$	
	Density (g/cm ³)	Crystallinity%	Density	Crystallinity%
20 000	0.9847	56.8	0.9760	47
129 000	0.9708	60.0	0.9535	54
238 000	0.9640	65.0	0.9522	52
310 000	0.9640	64.7	0.9512	55

The specimens thus prepared were fractured after storage in liquid nitrogen. The freshly fractured surfaces were fastened to a slide with double back Scotch tape and oriented parallel to each other.

A film (1 mm thick) of Triafol was deposited over the surfaces, with the contact face wetted with acetone. Following this operation, the polymer was removed and chromium was evaporated on the replica in high vacuum; the angle of shadow was 45°, and after the deposition of the metal, a carbon replica was made in the usual manner. Following the deposition of the thin metal-carbon film, the Triafol was removed with acetone.

The calibration was performed with polystyrene latex particles (Dow Chem. 586). The particle size was 2.200 Å.

The replicas were picked up on naked cooper grids and examined with a Siemens Elmiskop 1 A electron microscope. Micrographs were made on

Agfa-Gevaert, type Scientia 19D-50P plates, photographically enlarged as desired.

The micrographs of the fracture's surface was measured with an optical microscope.

RESULTS

The electron micrographs of the fracture surface replicas are similar to those reported for other crystalline polymers⁵⁻⁷. The striated, banded type lamellar crystallite is the predominant structural feature and these structures correspond to the type III lamella, reported by Anderson in polyethylene⁵.

Besides these striate structures, type I and II lamella are observed. (Figures 1-3).

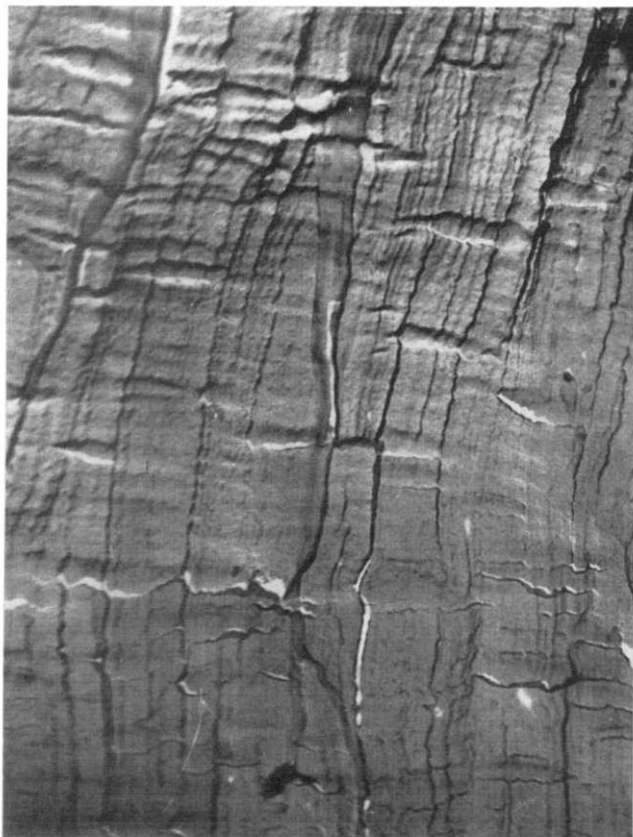


Figure 1. Micrograph of replica of fracture surface of 1,4-*trans*-polybutadiene. $M_{\eta} = 238\ 000$; $T_c = 86^{\circ}\text{C}$.



Figure 2. Micrograph of replica of fracture surface of 1,4-*trans*-polybutadiene. $M_{\eta} = 310\ 000$; $T_c = 0^{\circ}\text{C}$



Figure 3. Micrograph of replica of fracture surface of 1,4-*trans*-polybutadiene. $M\eta = 20\ 000$; $T_c = 0^\circ\text{C}$.

We have undertaken an analysis of the lamella thicknesses or step heights for the fracture surfaces of our samples crystallized at 0 and 86°C . More than twenty measurements were made on each fracture surface, and the results of these measurements are summarized in *Table 2*, where the average thicknesses are given.

Table 2

$M\eta$	$T_c = 86^\circ\text{C}$ (\AA)			$T_c = 0^\circ\text{C}$ (\AA)		
	<i>Min</i>	<i>Max</i>	<i>Average</i>	<i>Min</i>	<i>Max</i>	<i>Average</i>
20 000	130	540	341	112	505	278
129 000	168	562	355	100	900	290
238 000	188	560	392	112	1.070	364
310 000	135	630	369	112	1.123	350

A plot of the crystallite thickness as a function of molecular weight is

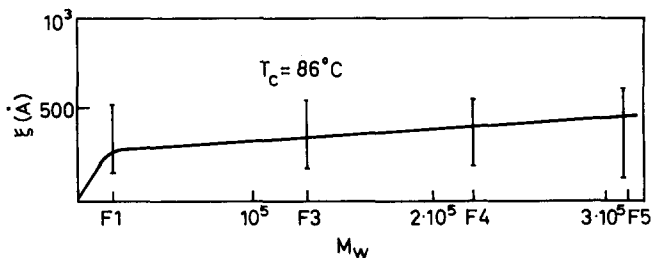


Figure 4. Crystallite size against molecular weight for 1,4-*trans*-polybutadiene fractions.

given in Figure 4 for the samples crystallized at 86°C. The range of sizes is indicated by the lines. From this figure, we conclude that in the molecular weight range studied here, the crystallite size increases only slightly with molecular weight either in the samples crystallized at 86°C or in the ones crystallized at 0°C. However, smaller lamellae are present in the last conditions.

In both cases the average lamella thickness is smaller compared to the extended chain length.

Therefore, the banded lamellae are characteristic over a very wide molecular weight range and their existence is not indication that the crystallite sizes are comparable to the extended chain length. This conclusion has been previously reached by Mandelkern *et al*⁷.

With the samples crystallized at 0°C, the predominant type is the thinner lamella. We can conclude that this occurs as a consequence of crystallization where the sizes of the crystallites are smaller. Similar results have been indicated by others^{5,7}.

Moreover, the crystallite sizes reported in this work are higher than those reported by Takayanagi *et al*^{11,12} in single crystals of *trans*-1,4 polybutadiene. This thickness corresponds to 100 Å. After heat treatment, there is a thickening of the lamella and they have suggested that the amorphous region, attached to the end surface of the crystal is dragged into the crystalline phase to form tight loops.

It is clear that in our molecular range, a significant portion of the chain units cannot be assigned to the interior of crystallites. They have to be assigned to the interfacial regions in the 001 face or to the interzonal regions. Therefore, it would be expected a relatively large value for the crystallite interfacial energies.

The melting temperature of a crystallite of finite thickness is given by^{13,14}

$$\frac{1}{T_m} - \frac{1}{T_m^\circ} = \frac{R}{\Delta H_u} \left[\frac{2\sigma_{ec}}{\xi RT_m} - \frac{1}{\xi} \ln \frac{(x - \zeta + 1)k}{x} \right] \quad (1)$$

In this equation, T_m° represents the equilibrium melting temperature; T_m is the observed melting temperature and σ_{ec} is the interfacial free energy per chain as it emerges from the 001 face of the crystallite.

When x is large, equation (1) reduces to

$$\frac{1}{T_m} - \frac{1}{T_m^\circ} = \frac{2\sigma_{ec}}{\xi\Delta Hu T_m} \quad (2)$$

The value of σ_{ec} can be calculated by means of equations (1) and (2). The quantities required must be known independently. The equilibrium melting temperature of the form I has been estimated to be 75°C.

The fusion enthalpy for the form I, was obtained for the relation between the apparent enthalpy, calorimetrically measured, and the crystallinity of the samples⁹. This heat of fusion corresponds to 28 ± 1 cal/g (1510 ± 54 cal/mol), for the form I, and 16 ± 1 cal/g (865 ± 54 cal/mol) for the form II.

The heat of fusion for the form I is smaller than the values reported by others¹⁵⁻¹⁷, which correspond to a range of 2400–3300 cal/mol.

The value for the form II, agrees with the values reported¹⁶, but there is not any explanation for the contradictory results in the form I.

However, Dainton *et al*¹⁸ by direct specific heat measurements estimated the heat for the transition I–II to be 830 cal/mol. It is quite clear that if the higher values of 2.400–3300 cal/mol were considered, this value corresponds to 2.200 cal/mole, which is too high.

For our values, ΔHu (I–II) corresponds to 645 cal/mol which agrees better with Dainton's results.

The values of σ_{ec} , calculated by means of equation (1) are tabulated in Table III. These values are given for both the average value and the largest value of ξ .

Table 3

$M\eta$	σ_{ec} (erg/cm ²)	
	Average ξ	Max ξ
20 000	134	212
129 000	140	222
238 000	153	240
310 000	159	271

As the molecular weight increases there is an increase on the crystallite interfacial free energy. For the three higher molecular weight fractions the relative change is not as great as for the lowest molecular weight fraction. In the higher molecular weight region the crystallite sizes represent only a very small portion of the extended molecular length, and the interfacial energies increase. These results agree with those reported for polyethylene⁷.

ACKNOWLEDGEMENT

We wish to acknowledge our gratitude to Dr Silas for sending us the details of his infra-red technique and the standards to be used.

*Sección de Química Física y de Polimeros,
Instituto de Plásticos y Caucho,
Juan de la Cierva 3,
Madrid 6,
Spain*

(Received 28 July 1970)

REFERENCES

- 1 Eppe, R., Fischer, E. W., and Stuart, H. A. *J. Polym. Sci.* 1959, **34**, 721
- 2 Keller, A. *Makromol. Chem.* 1959, **34**, 1
- 3 Geil, P. H. *J. Polym. Sci.* 1960, **44**, 449
- 4 Kampf, G. *Kolloid Z.* 1960, **172**, 507
- 5 Anderson, F. R. *J. Appl. Phys.* 1964, **35**, 64
- 6 Bunn, C. W., Cobbold, A. J. and Palmer, R. P. *J. Polym. Sci.* 1958 **38**, 365
- 7 Mandelkern, L., Price, J. M., Gopalan, M. and Fatou, J. G. *J. Polym. Sci. (A-2)* 1966, **4**, 385
- 8 Bermúdez, S. F., Fatou, J. G., and Royo, J. *Anal. Fis. Quim.* (in press)
- 9 Fatou, J. G. and Bermúdez, S. F. (unpublished results)
- 10 Silas, R. S., Yates, J. and Thornton, V. *Anal. Chem.* 1959 **31**, 529
- 11 Takayanagi, M., Imada, K., Nagai, A., Tatsumi, T. and Matsuo, T. *J. Polym. Sci., (C-1)* 1967, **6**, 867
- 12 Tatsumi, T., Fukushima, T., Imada, K. and Takayanagi, M. *J. Macromol. Sci. Phys. (B)* 1967, **1**, 459
- 13 Flory, P. J. *J. Chem. Phys.* 1949, **17**, 223
- 14 Fatou, J. G. and Mandelkern, L. *J. Phys. Chem.* 1965, **69**, 417
- 15 Natta, G., Corradini, P., Porri, L. and Morero, D. *Atti. Acad. Nazl. Lincei. Rend.* 1956, **20**, 728
- 16 Natta, G., Porri, L., Corradini, P. and Morero, D. *La Chimica e L'Industria* 1958, **40**, 362
- 17 Danusso, F. *Polymer, Lond.* 1967, **8**, 302
- 18 Dainton, F. S., Evans, D. M., Hoare, F. E. and Meliá, T. P. *Polymer, Lond.* 1962, **3**, 297

The structure of feather keratin

R. D. B. FRASER, T. P. MACRAE, D. A. D. PARRY* and E. SUZUKI

When feather rachis is pressed in steam the keratin molecules are partially denatured and the x-ray diffraction pattern, which is greatly simplified, indicates that the microfibrils have a helical structure with four units per turn. Quantitative infra-red and x-ray data have been collected which suggest that this simplified pattern originates from about one third of the material in the form of a central core or framework which is resistant to denaturing agents. A model for this core consisting of a helical array of β -crystallites is shown to give quantitative agreement with the observed x-ray pattern over a wide range of angles. Each crystallite contains two sheets symmetrically disposed about the fibre axis and the sheets are distorted to conform to a ruled surface of opposite sense to the primitive helix.

INTRODUCTION

KERATINS have been classified according to the type of wide angle x-ray diffraction pattern which they yield and two major groups have been recognized¹⁻³. Epidermis from all vertebrate classes yields an ' α -pattern' which is believed to be associated with a polypeptide chain conformation in which α -helices are coiled in pairs to form two-strand ropes^{4, 5}. In contrast the x-ray patterns obtained from the hard epidermal appendages of terrestrial vertebrates, for example claws, are of two distinct types. Those from the class Mammalia are typical α -patterns whilst those from Avia are of a quite different type which is conveniently referred to as the 'feather pattern'. This same pattern also occurs in a slightly modified form in the hard keratins from Chelonia (turtles and tortoises), Crocodylia (alligators and crocodiles), Squamata (snakes and lizards)³ and Rhinchocephalia (tuatara)⁶, the four main groups of the class Reptilia.

Various models have been proposed for the structure of feather keratin. Astbury and Marwick⁷ concluded that the polypeptide chain conformation resembled that present in β -keratin except that the chain was contracted so that the axial rise per residue was 3.1 Å rather than 3.34 Å. In support of their argument they quoted the observation that feather specimens could be stretched by up to 6% in steam before breaking and that the extension was accompanied by an increase in axial rise per residue to 3.3 Å. Later, specific models involving various types of chain folding were suggested^{8, 9} but a fresh approach to the problem followed the recognition by Schor and Krimm¹⁰ that the structure was most probably helical. These authors supposed that there were tubular assemblies of helical polypeptide chains with a conformation similar to that of the polar pleated sheet, whilst Ramchandran and Dweltz¹¹ claimed that the conformation resembled that found in collagen.

*Present address: Children's Cancer Research Foundation, Inc., 35 Binney St., Boston Mass., USA

Neither of these structures however appears to be capable of accounting for the rich diffraction pattern of feather keratin (*Figure 1a*).

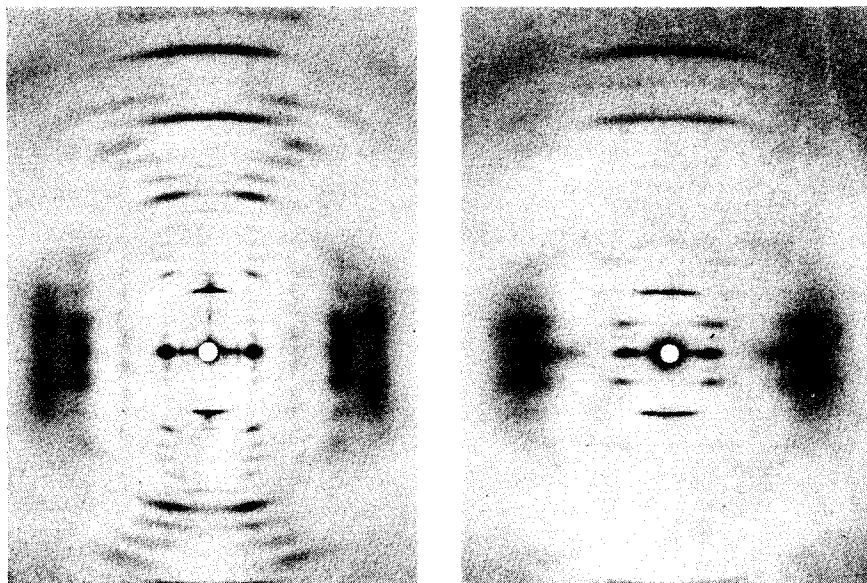


Figure 1 X-ray diffraction patterns of seagull feather rachis (a) native (b) simplified pattern obtained after pressing in steam

Although the degree of crystallinity is very high compared with other native fibrous proteins it is not sufficient for conventional crystallographic procedures to be used. On the other hand external interference is too great for the pattern to be treated as the cylindrically averaged intensity transform of a helix and analyzed accordingly.

Bear and Rugo¹² showed that the effect of external interference on the low-angle x-ray pattern could be reduced by certain denaturing treatments. Later¹³, specimens were prepared in which all traces of external interference were removed, yielding a simplified diffraction pattern (*Figure 1b*) which could readily be identified as the rotationally averaged intensity transform of a helix with four units per turn of pitch $\sim 95 \text{ \AA}$.

The present communication describes a further investigation of the structure of feather keratin in which quantitative x-ray diffraction and infra-red data were collected and analyzed with a view to determining the nature of the molecular framework responsible for the simplified diffraction pattern.

EXPERIMENTAL

Pieces of rachis from the feathers of the silver gull (*Larus novae-hollandiae*) were degreased by extraction with petroleum ether and ethanol and washed in distilled water. Specimens yielding the simplified diffraction pattern were prepared by subjecting flat strips of rachis to lateral pressure whilst they were

held under tension in steam. The required time of treatment was found to vary from specimen to specimen and so was monitored by taking x-ray patterns.

For x-ray examination the specimens were mounted with the fibre axis normal to the x-ray beam and then tilted through an angle appropriate to the region of the diffraction pattern to be recorded. Low-angle data was recorded with a 5cm specimen to film distance using either a lead glass capillary collimator camera or a focusing camera¹⁴; wide-angle data was collected using a toroidal focusing camera¹⁵. The texture of the pressed specimens was investigated by comparing photographs taken with the x-ray beam passing firstly parallel then perpendicular to the direction of pressing. No evidence of preferred orientation was found.

The optical density along layer lines was recorded with a Joyce Loebel microdensitometer either by direct recording or by the technique of isodensitracing¹⁶. The latter method was used over regions of the film in which the layer lines departed appreciably from straight lines. The actual path of a layer line through the isodensitracing was calculated and plotted automatically by a computer program. The optical densities from different films were scaled by standard procedures to put them on a common basis. The accuracy attainable in dealing with continuous layer line distributions in fibre-type patterns is inherently low and it was not considered worth-while applying corrections for absorption or polarization.

Specimens suitable for infra-red studies were prepared by cutting thin uniform sections about $2\mu\text{m}$ thick from the specimens used in the x-ray studies. The technique used for sectioning and mounting has been described elsewhere¹⁷, an additional precaution used in the present study was to wet the specimen with 1,3-dibromopropane in order to reduce reflection losses. A Beckman IR-9 prism/grating spectrophotometer equipped with twin refracting beam condensers and a selenium polarizer was used to measure spectra with the electric vector vibrating first parallel then perpendicular to the fibre axis. The spectra were analyzed using an iterative non-linear least squares procedure¹⁸ (Figure 2).

TREATMENT OF INFRA-RED DATA

In an earlier study of the infra-red spectrum of feather keratin¹⁹ it was shown that the Amide I vibration of the peptide groups had components *ca* 1635 and 1690cm^{-1} together with a broad underlying absorption. The frequencies, dichroisms and relative intensities of the first two components were close to those predicted²⁰ for the antiparallel chain pleated sheet conformation²¹ and it was concluded that this conformation was present in feather keratin. Since that time the technique of resolving overlapping bands has progressed to the stage where it is possible to attempt an analysis of the feather keratin spectrum with the aim of obtaining an approximate idea of the proportion of residues in the pleated sheet conformation.

The analysis is complicated by the presence of sidechain absorptions associated with glutamine and asparagine, arginine, glutamic and aspartic acids and tyrosine²². A study of the concentrations of these residues and the

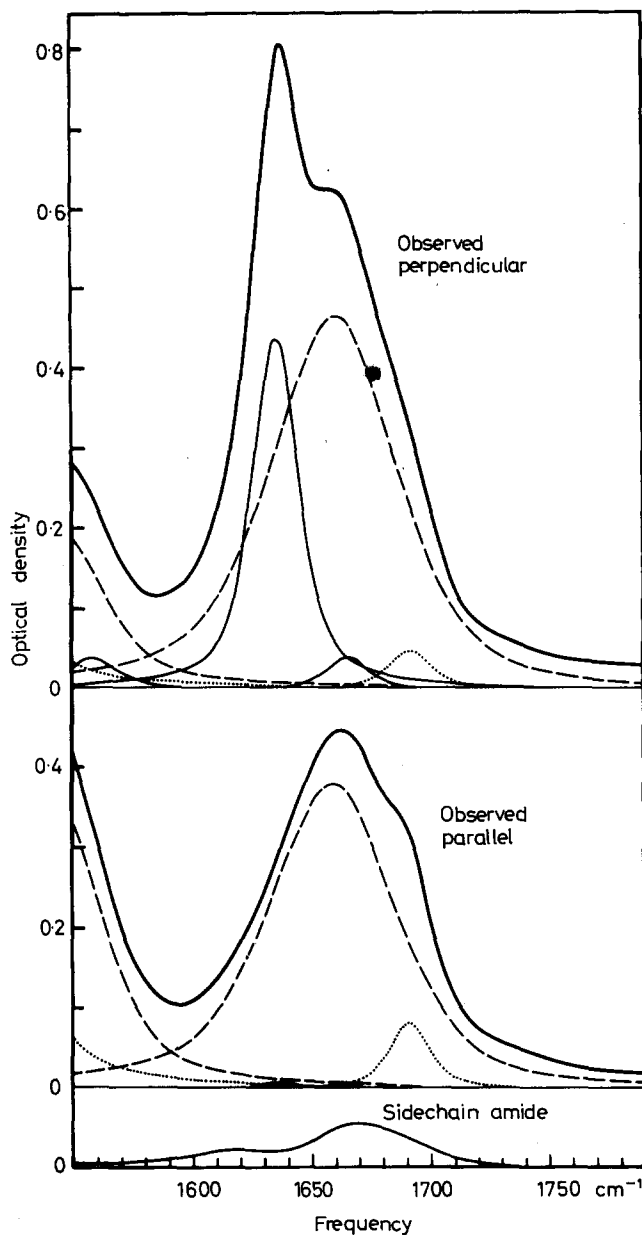


Figure 2 Infra-red spectra obtained from seagull feather rachis using polarized radiation. The observed spectra have been analyzed by a non-linear least squares procedure into component bands associated with the Amide I mode of the peptide linkage and bands associated with the sidechain amide groups. The $(\pi, 0)$ and (π, π) components of the antiparallel chain pleated sheet are shown as full line, the $(0, \pi)$ component is shown dotted. The broad asymmetric band which underlies these components is shown as a broken line

intensities of the associated bands showed that the only band likely to produce appreciable error if neglected was that due to the amide sidechains of glutamine and asparagine. A correction was applied by measuring this band in the spectrum of molten propionamide ($\text{CH}_3\text{CH}_2\text{CONH}_2$) and subtracting a similar band from the feather keratin spectrum. The amount of correction required was determined from the known ratio of $-\text{CONH}_2/-\text{CONH}-$ content²³ and a comparison of the spectrum of propionamide with that of molten N-methyl acetamide ($\text{CH}_3\text{CONHCH}_3$) measured in the same cell.

The band shapes of the Amide I and II components associated with the pleated sheet were represented by the symmetrical function

$$D/D_m = g \exp \left\{ -\ln 2 \left[(\nu - \nu_m) / \Delta\nu_{\frac{1}{2}} \right]^2 \right\} + (1 - g) / \left\{ 1 + \left[(\nu - \nu_m) / \Delta\nu_{\frac{1}{2}} \right]^2 \right\} \quad (1)$$

where D is the contribution of the band to the optical density at frequency ν , D_m and ν_m specify the maximum and its frequency and $\Delta\nu_{\frac{1}{2}}$ is the band width at $\frac{1}{2}D_m$. This function, which is a linear combination of Gauss and Cauchy shapes in the ratio g to $(1 - g)$, has been found to give a satisfactory representation of amide band shape in silk fibroin¹⁷ and in β -keratin²⁴. The broad underlying band in the Amide I region is asymmetric and the function in equation 1 was multiplied, in this case, by

$$1 + \tanh[2b(\nu - \nu_m) / \Delta\nu_{\frac{1}{2}}] \quad (2)$$

where b is an adjustable parameter. For $b = 0$ the factor reduces to unity and the band is symmetrical whilst negative values of b produce negative skew and vice versa.

In addition to analyzing the Amide I region it was also necessary to effect a partial analysis of the Amide II components in order to make allowance for their overlap in the Amide I region. The Amide I components are listed in Table 1 and an estimate of the fraction of residues in the antiparallel chain pleated sheet conformation was obtained from the expression

Table 1 Analysis of Amide I region of the spectrum of feather keratin

Component	ν_m (cm^{-1})	D_m	$\Delta\nu_{\frac{1}{2}}$ (cm^{-1})	Area (cm^{-1})
Parallel Spectrum				
$\nu(\pi, 0)$	1634.8	0.004	23.3	0.14
$\nu(\pi, \pi)$	1665.0	0.005	20.0	0.14
$\nu(0, \pi)$	1691.4	0.083	20.2	2.34
ν_a	1658.3	0.380	asymmetric	31.68
Perpendicular Spectrum				
$\nu(\pi, 0)$	1634.8	0.440	23.2	14.30
$\nu(\pi, \pi)$	1665.0	0.040	20.0	1.11
$\nu(0, \pi)$	1691.4	0.049	20.2	1.37
ν_a	1658.3	0.465	asymmetric	38.76

Goodness of Fit: The root mean square deviation between the observed spectra and the sum of the components listed above plus side chain amide and baseline corrections was 0.004 optical density units.

$$\frac{(\Sigma \text{ Areas of pleated sheet Amide I bands})_{\parallel} + 2(\Sigma \text{ Areas of pleated sheet Amide I bands})_{\perp}}{(\Sigma \text{ Area of all Amide I bands})_{\parallel} + 2(\Sigma \text{ Area of all Amide I bands})_{\perp}} \quad (3)$$

which yielded a value of 0.25. A correction is required for the contribution of non-keratinous proteins which constitute about 10% of the tissue. The corrected estimate is therefore 0.28.

THE NATURE OF THE FEATHER KERATIN MICROFIBRIL

About 90% of feather rachis can be extracted²⁵ in the form of soluble proteins of homogeneous molecular weight 10400 ± 300 . These proteins can be fractionated on the basis of chemical composition but no marked differences between fractions are found as is the case with mammalian keratins, where two distinct types of protein can be isolated²⁶.

The mean residue weight of the total extract from feather rachis is 99.5 so that the number of residues per molecule is $(10400 \pm 300)/99.5 = 104.5 \pm 3$. The analysis of the infra-red data indicates that on average about $104.5 \times 0.28 = 29.3$ of these are in the antiparallel pleated sheet conformation. This figure must necessarily be approximate as the corrections for side chain absorption and intercellular proteins are not known exactly.

Filshie and Rogers²⁷ showed that feather rachis contains a close packed arrangement of microfibrils which are revealed in cross section by the presence of approximately circular patches of lightly stained material surrounded by a densely stained matrix. In the case of α -keratin where a similar situation obtains²⁸, the lightly stained regions are believed to correspond to the site of the organized secondary structure (α -helix). By analogy we may suppose that the lightly stained regions in feather keratin correspond to the pleated sheet fraction. This leads to the concept of a microfibril in which the pleated sheet portions of the molecules form a central framework whilst the non-pleated sheet portions correspond to the osmiophilic matrix.

Bear and Rugo¹² observed that during a number of treatments in which the feather keratin structure was partially disrupted, certain near meridional reflections at moderate and wide angles were unaffected. The simplified pattern in *Figure 1b* is one such treatment. An explanation of these persistent reflections follows logically from the type of microfibril structure envisaged above as it may be supposed that the treatments used by Bear and Rugo resulted in the denaturation of the outer portions of the molecules, which are devoid of regular secondary structure, without significant disturbance of the central core consisting of the pleated sheet portions. The pleated sheet portions of the molecules would be expected to be more stable due to the regular two dimensional array of hydrogen bonds.

The simplified pattern in *Figure 1b* probably represents the stage where the non-pleated sheet portion of the microfibril is quantitatively disrupted and the remaining sections describe a test of this hypothesis. The number of parameters which needed to be chosen was very large and the search for an arrangement of pleated sheets which would account quantitatively for the observed pattern was necessarily protracted. Only the final solution will be discussed in detail.

DERIVATION OF TRIAL STRUCTURE

The diffraction pattern of native rachis (*Figure 1a*) is crossed by regularly spaced layer lines corresponding to an axial period of 94.6 \AA and row lines which indicate a layer structure of lateral period 33 \AA . The second lateral periodicity is not well developed¹² but does not appear from electron micrographs to be greatly different in value from the first²⁷. The internal arrangement of the microfibril¹³ is that of a helix with four units per turn of pitch 94.6 \AA and so the volume per unit is $\sim 33 \times 33 \times 94.6 \times \frac{1}{4} = 25750 \text{ \AA}^3$. The macroscopic density²⁹ is 1.27 gcm^{-3} which leads to a mass ~ 19700 dalton per unit or $19700/10400 \sim 1.9$ molecules per unit.

Earlier studies¹³ indicated that the line group of the helix was $s2(M = 4)$ and so the unit presumably consists of a pair of molecules, related by a diad perpendicular to the helix axis (*Figures 3 and 4*).

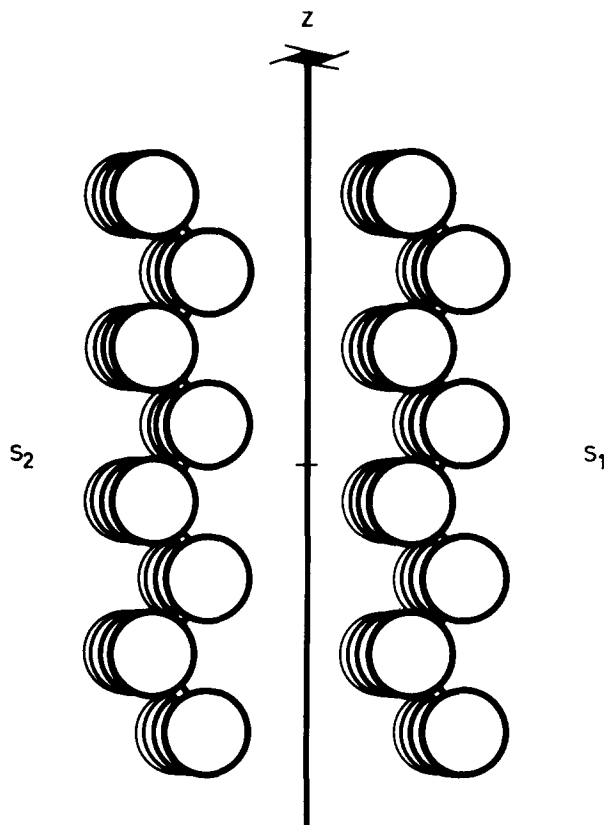


Figure 3 Trial structure for the pleated sheet framework of feather keratin. Each sheet contains four chains with eight residues per chain and pairs of sheets are related by a horizontal diad. In this low resolution model the residues are represented by Gaussian spheres of electron density. The asymmetric unit is a single sheet, all other sheets being generated by the line group symmetry $s2 (M = 4)$

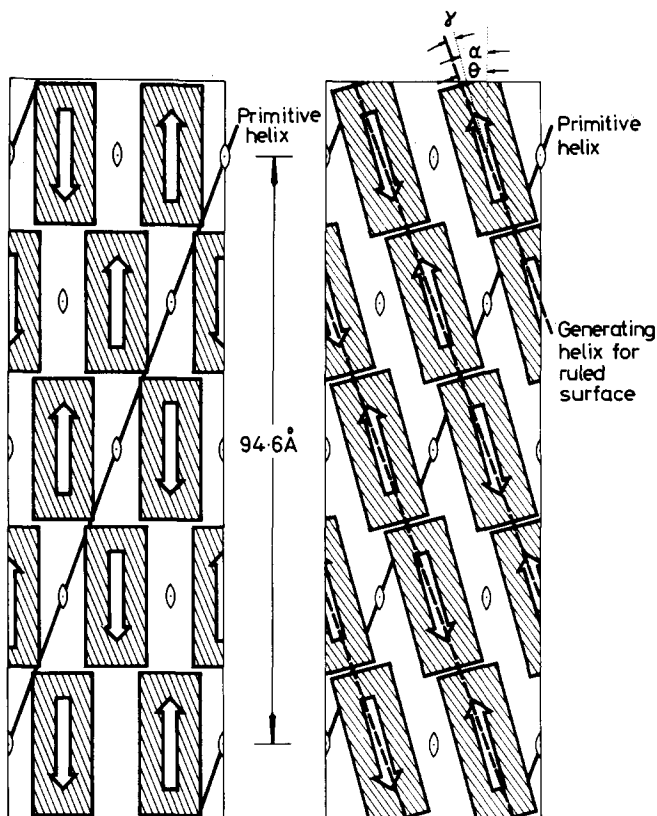


Figure 4 Diagrammatic radial projection representing the disposition of the crystallites (shown shaded) in (a) the trial structure and (b) the refined structure for the pleated-sheet framework of feather keratin

A striking feature of the data collected from the simplified pattern (*Figure 5*) is the way in which strong diffraction occurs on even layer lines in the equatorial and 3Å regions of the meridian and on odd layer lines in the 6Å region. It was found that this observation could be explained very simply by supposing that the microfibril contained a helical array of β -crystallites each with two sheets S_1 and S_2 , related by a diad perpendicular to the fibre axis Oz . Except for the residues at one end of each sheet there exists for each residue in S_1 a corresponding residue in S_2 which is related to it by a rotation of π around Oz and a displacement h parallel to Oz . Hence residues occur in pairs at (r, ϕ, z) and $(r, \phi + \pi, z + h)$.

The cylindrically averaged intensity transform of a helix with 4 units per turn is confined to layer lines with $\zeta = l/c$ where l is the layer line index, c is the axial repeat of structure which in this case is equal to the pitch of the helix. The intensity at a distance R from the ζ -axis is given³⁰ by

$$I(R, l/c) = \sum_n G_{n,l} G_{n,l}^* \quad (4)$$

where $G_{n,l}^*$ is the complex conjugate of $G_{n,l}$ and the summation extends

over values of n which satisfy the selection rule $l = n + 4m$ with $m = 0, \pm 1, \pm 2, \dots$ etc. Thus odd layer lines only contain terms with odd n and even layer lines terms with even n .

The value of the terms in equation 4 is given by,

$$G_{n,l} = \sum_j f_j J_n(2\pi R r_j) \exp [i(-n\phi_j + 2\pi l z_j/c)] \quad (5)$$

where f_j is the scattering factor of the atom with cylindrical polar coordinates r_j, ϕ_j, z_j ; $J_n(x)$ is a Bessel function of the first kind of order n , and the summation extends over the atoms of the repeating unit.

To the extent to which residues are similar, and neglecting one set of end residues in each sheet, the value of $G_{n,l}$ for the two sheet unit will be related to that of the single sheet S_1 by

$$G_{n,l} = G'_{n,l} \{1 + \exp [i(-n\pi + 2\pi h l/c)]\} \quad (6)$$

where $G'_{n,l}$ refers to a summation over S_1 .

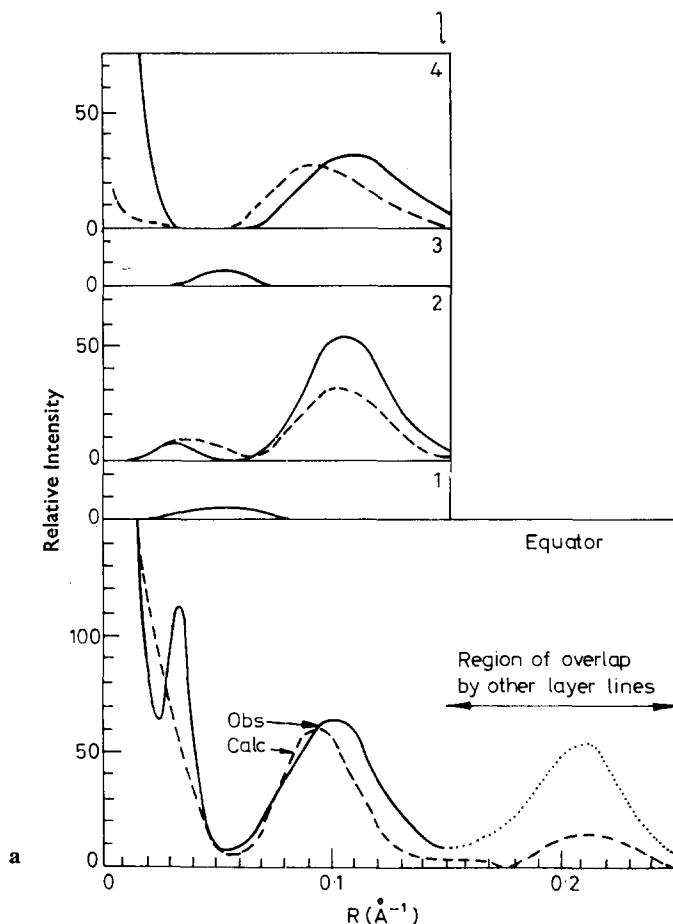


Figure 5a Comparison of observed intensity in the simplified x-ray pattern (full line) and that calculated for the refined model for the pleated sheet framework illustrated in Figure 6 (broken line)

When l/c is small (near-equatorial region), and when $l/c \sim \text{fig. } 1/h$ ($l \sim 30$)

$$G_{n,l} \simeq G'_{n,l} [1 + (-1)^n] \quad (7)$$

so that odd layer lines, on which n is always odd, are either weak or absent. When $l/c \sim 1/2h$ ($l \sim 15$)

$$G_{n,l} \simeq G'_n [1 - (-1)^n] \quad (8)$$

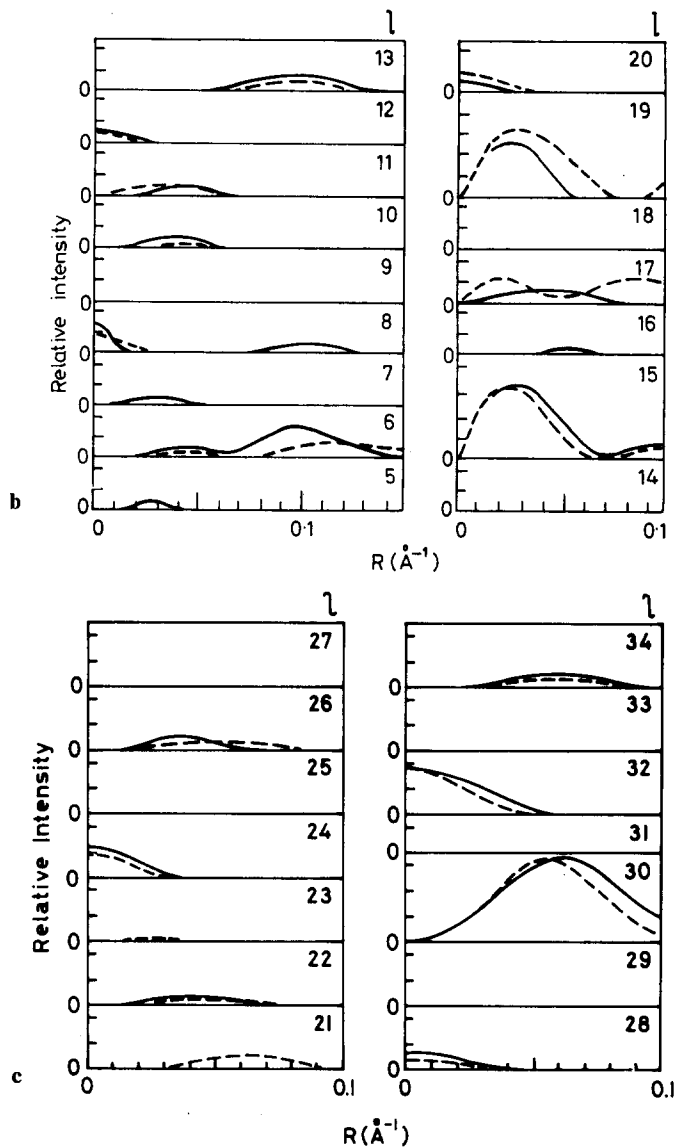


Figure 5 b and c Comparison of observed intensity in the simplified x-ray pattern (full line) and that calculated for the refined model for the pleated sheet framework illustrated in Figure 6 (broken line)

and so even layer lines, on which n is always even, will be weak or absent. The observed alternation of intensity between even and odd layer lines can thus be accounted for in a very simple way by supposing that two-sheet β -crystallites are symmetrically disposed about the fibre axis.

Earlier studies⁸ using the optical diffractometer suggested that the length of the β -crystallites was around one quarter of the axial period and using a value of 3.08 Å for the mean axial projection of the length of a residue³¹ we obtain an estimate for the pleated sheet dimensions of 23.6/3.08 \sim 7.7 residues per chain and from the number of pleated sheet residues per molecule 29.3/7.7 \sim 3.8 chains per sheet. The asymmetric unit of structure was therefore initially assumed to be a pleated sheet with an interchain spacing of 4.7 Å and an axial rise per residue of 3.1 Å, containing four chains each with eight residues. The sheet was oriented parallel to and distant 5 Å from the Oxz plane so that the operation of a diad along the x axis produced the second sheet of the crystallite (*Figures 3 and 4*).

REFINEMENT OF TRIAL STRUCTURE

The number of parameters required to specify the positions of all the atoms in the unit far exceeds the number of data available in the diffraction pattern and it is not possible to refine these parameters on the basis of the observed data. The problem of reducing the number of parameters to be refined has been discussed by Arnott and Wonacott³². In the present instance a low resolution model was used in which each residue was represented by a Gaussian 'blob' of electron density³³

$$d = d_0 \exp[-r^2/r_e^2] \quad (9)$$

where r_e is the radius at which the density drops to $1/e$ of its origin value. The normalized transform of the blob is

$$F = \exp[-\pi^2 r_e^2 (\zeta^2 + R^2)] \quad (10)$$

and an additional factor f equal to the scattering factor for a carbon atom³⁴ was also incorporated so that the normalized function for simulating residue scattering at low resolution became

$$F(R, \zeta) = \frac{f(R, \zeta)}{f(0, 0)} \exp[-\pi^2 r_e^2 (\zeta^2 + R^2)] \quad (11)$$

The unit of structure consists of two sheets related by a horizontal diad (*Figure 3*) and for each residue with coordinates r_j, ϕ_j, z_j there exists a corresponding residue with coordinates $r_j, -\phi_j, -z_j$. Thus the expression for $G_{n,l}$ becomes

$$G_{n,l} = 2 \sum_j F(R, l/c) J_n(2\pi R r_j) \cos(-n\phi_j + 2\pi l z_j / c) \quad (12)$$

where the summation extends over a single sheet, which is the asymmetric unit of the model. A correction factor to allow for the effects of disorientation in the specimen was applied to $I(R, l/c)$ to give a calculated intensity $I_c(R, l/c)$ which could be compared directly with the observed microdensitometer records. The derivation of this factor is described in *Appendix 1*.

The expression for $I_c(R, l/c)$ makes no allowance for any residual external interference between microfibrils. The only layer line showing evidence of

external interference is the equator where an interference maximum of spacing 33 Å is observed (*Figure 5*).

No contribution from the denatured non- β portions of the molecules has been included in $I_c(R, l/c)$. The main differences between the native and the simplified patterns occur on layer lines 0 to 10 and it is in this region that residual contribution from the globular portions might be expected. In particular the microfibrils will appear, in equatorial projection, to be embedded in a matrix of uniform electron density. An additional term was therefore included in $G_{0,0}$ to give

$$G_{0,0} = \sum_j F(R, 0) J_0(2\pi R r_j) - k[2J_1(2\pi R r_m)/(2\pi R r_m)] \quad (13)$$

where k and r_m are adjustable parameters. The additional term is the transform of a cylinder of radius r_m with the sign reversed, which by Babinet's principle should approximate the matrix scattering.

Preliminary calculations showed that the trial structure was unsatisfactory in that it produced very strong meridional diffraction on layer lines 28 and 32 whereas the observed intensity is mainly off-meridional. In addition the strong off-meridional maxima on $l = 15$ and 19 in the observed pattern were completely absent in the calculated pattern. No improvement could be obtained by varying axial rise per residue, intersheet distance or the disposition of the residues in the sheet.

Following the suggestion made in earlier studies⁸ various types of tilt were applied to the asymmetric unit and it was found that by tilting different portions of the sheet by different amounts a tolerable fit to the observed data could be obtained in the range $l = 28$ –32 but not elsewhere. It was noted that although the basic helix had been assumed, for convenience to be right-handed, the tilt was such as to direct the chains in the opposite sense. The structures were unsatisfactory as tilting the chains of a sheet by different amounts destroyed the hydrogen bonding.

A search was therefore made for a type of distortion which would allow the chain axes to be tilted without destroying the hydrogen bonding. A type of helical twist related to a ruled surface was found in which the interchain distance was preserved and corresponding points on neighbouring chains remained in exact lateral register thus preserving the hydrogen bond arrangement. This transformation is fully described in *Appendix 2* and illustrated in *Figure 6*. The calculated transform for this model showed immediate promise of providing an overall fit and the various parameters were refined by trial and error. The parameters investigated (see *Appendix 2*) were intersheet distance, tilt, sense of ruled surface (left- or right-handed), axial rise per residue, number of chains in a sheet, number of residues in a chain, v coordinate and r_e value of the simulated residue, and r_m and k values for the matrix correction term. The final values were

Primitive helix	right-handed	$\left\{ \begin{array}{l} v = 0.9v(C^\alpha) \\ r_e = 0.94 \text{ \AA} \\ h_0 = 2.96 \text{ \AA} \\ \gamma = 9.8^\circ \\ \alpha = 8.6^\circ \\ r_m = 11.2 \text{ \AA} \end{array} \right.$
Generating helix for ruled surface	left-handed	
Number of chains	4	
Number of residues/chain	8	
Intersheet distance	10 Å	
r_0	5 Å	

The optimum value of k in equation 13 corresponded to a matrix electron density equal to 0.9 times the mean value within the core. The assumption of a right-handed primitive helix is of course arbitrary. In the event that the actual primitive helix is left-handed, the ruled surface would be of opposite sense to that given above. The coordinates of the 32 residues in the asymmetric unit of structure are given in *Table 2*.

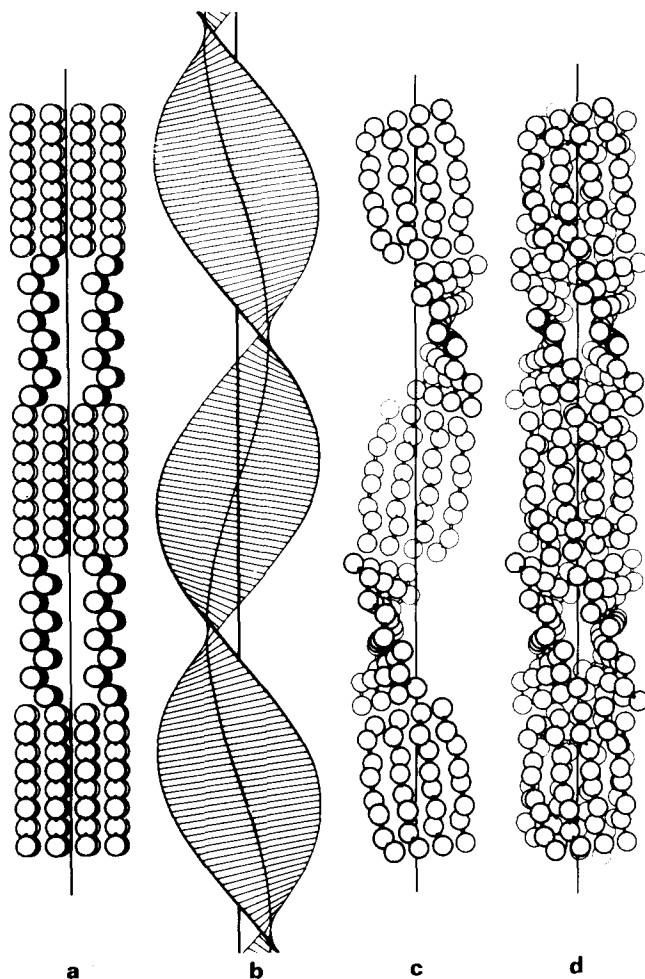


Figure 6 Stages in the development of a model for the structure of the pleated sheet framework of feather keratin. (a) Trial structure with pairs of pleated sheets at each level related by a horizontal diad. Pairs at different levels are related by a right-handed 4 fold screw axis; (b) left-hand ruled surface; (c) a strand of β -sheets distorted so as to conform to the ruled surface in (b); (d) complete model for the core of the feather keratin microfibril consisting of two strands of β -sheets

COMPARISON OF CALCULATED AND OBSERVED TRANSFORMS

The intensity transform calculated for the refined model is compared with the observed intensity transform in *Figure 5*. The concentration of intensity on

Table 2 Coordinates of the residues in the asymmetric pleated sheet unit of the core model. Equivalent positions (r, ϕ, z) , $(r, -\phi, -z)$

Chain 1 (up)			Chain 2 (down)		
r (Å)	ϕ (deg)	z (Å)	r (Å)	ϕ (deg)	z (Å)
7.92	169.5	-9.49	5.70	97.3	10.84
6.99	171.2	-5.94	7.01	94.0	7.44
8.58	153.1	-3.67	5.01	111.2	4.94
7.86	153.4	-0.05	6.57	107.9	1.64
9.30	136.0	2.15	4.45	122.9	-0.97
8.76	134.8	5.81	6.26	120.9	-4.14
10.07	118.3	7.99	4.07	132.1	-6.89
9.70	115.6	11.67	6.10	133.3	-9.93

Chain 3 (up)			Chain 4 (down)		
r (Å)	ϕ (deg)	z (Å)	r (Å)	ϕ (deg)	z (Å)
7.27	93.4	-10.34	6.57	0.3	8.88
5.35	75.5	-7.89	8.24	18.6	6.58
6.78	78.9	-4.54	7.42	17.6	2.99
4.71	62.7	-1.98	8.94	35.3	0.76
6.40	65.5	1.25	8.31	35.8	-2.88
4.23	52.2	3.93	9.68	52.8	-5.07
6.16	52.8	7.03	9.23	54.8	-8.74
3.97	44.0	9.85	10.46	70.8	-10.92

even layer lines in the range $l = 24$ to 34 is correctly reproduced and the agreement between the calculated and observed distributions is sufficiently good to justify the approximations used. Evidently the distribution of residues in the model must closely resemble that in the actual core of the microfibril. This portion of the observed diffraction pattern is very little changed in the transition from the native to the simplified pattern and so the contribution from the globular portions of the molecules must be very small.

The concentration of intensity on odd layer lines in the range $l = 13$ – 19 is correctly reproduced. The overall agreement in this region is again satisfactory apart from a discrepancy between the positions of the observed and calculated maxima on $l = 17$. The intensity in this region of the diffraction pattern stems from the fact that the residues project alternately above and below the plane of the sheet. Any discrepancy in this region will almost certainly stem from the fact that all residues were assumed to be equal. In the actual structure the scattering power of the residues will be variable and may be systematically displaced in alternate chains due to their antiparallel character. Assumptions about the likely effect of these parameters can be made but the present data were not considered to be sufficiently accurate or extensive to serve as a basis for such a further refinement.

The overall fit in the range $l = 0$ – 8 is again satisfactory and differences in detail may be attributed to small residual contributions from the denatured non- β portions of the molecule. This probably accounts for the weak streaks on $l = 1, 3$ and 5 not predicted by the model. The intense meridional reflection in the observed pattern is not predicted by the core model, however this reflection is almost certainly not associated with the core as it is highly variable

in intensity. In feather keratins it is generally very intense but in certain reptilian keratins it is weak^{3, 6} even though the remainder of the diffraction pattern is very similar. The oscillation in the observed equatorial curve *ca* 0.03 \AA^{-1} is due to residual external interference between microfibrils for which no allowance was made in the calculations.

The overall agreement between the observed and calculated pattern is surprisingly good in view of the very simple method of representing the scattering material of the core in which every residue was assumed to have the same *v* coordinate in the undistorted sheet and the same scattering power. The particular type of helical distortion used is also probably an oversimplification of the one actually present. In the event that more precise data can be collected these features may be further refined.

DISCUSSION

The inter-relationship of the sheets in the core is shown in the helical projection in *Figure 4* and the diagram in *Figure 6*. No information can be obtained from the present work on the course of the polypeptide chain of a molecule, but the simplest assumption is probably that each sheet corresponds to the β -portion of one molecule. If this is so there is a striking similarity between the form of the chain folding present in the core of the feather keratin microfibril and that believed to be present in the micelles of the egg-stalks of *Chrysopa* which have been studied by Geddes *et al*³⁶. In this material the polypeptide chains are regularly folded to give an antiparallel chain pleated sheet with each chain section containing eight residues.

If a similar type of folding is present in feather keratin it will be seen from *Figure 6* that the molecules aggregate end-to-end via the loops between chain segments and side-to-side via sidechain interactions between pairs of sheets.

In the coordinate transformation described in *Appendix 2* the hydrogen bonding in the sheet is preserved and the distortion is taken up by having a variable distance along the chain between successive residues. This distance varies from 2.96 to 3.39 \AA with a mean value of 3.18 \AA . The meshing of sidechains between the two sheets is good for the inner chains but less satisfactory for the outer chains. In the actual structure it is likely that the distortion is less idealized than envisaged in the model and that the *u* axis is in fact not exactly straight. The actual distortion probably does not involve such a wide range of distances between successive residues and gives better meshing of the outer chains.

Examples of small pleated sheet assemblies have been found in lysozyme³⁷ and in carboxypeptidase A³⁸. Although topologically similar these assemblies show appreciable departures from the idealized structure described by Pauling and Corey²¹. The assembly in carboxypeptidase A resembles that envisaged in the present model for the core of the feather keratin microfibril in that the sheet is twisted.

It is difficult to correlate the infra-red dichroism with the model in a quantitative way as the analysis of the pleated sheet vibrations given by Miyazawa³⁹ refers to an undistorted sheet of infinite dimensions and it is uncertain how the vibrational pattern would be affected by the limited size

and distortion present in the feather keratin molecules. The $\nu(\pi, 0)$ component of Amide I involves a collaborative build up of transition moment parallel to the u axis of the pleated sheet (*Appendix 2*) and as this axis is transformed without distortion the transition moment direction for $\nu(\pi, 0)$ might be expected to be inclined at an angle of $90 - \alpha = 81^\circ$ to the fibre axis. The value calculated from the observed dichroic ratio is 85° which is in reasonable agreement with the value calculated from the model. The $\nu(0, \pi)$ component of Amide I is much weaker than the $\nu(\pi, 0)$ component and has a low parallel dichroism (*Figure 2*). This component arises from a collaborative build up of transition moment between residues at consecutive axial levels. In the model each level of residues is rotated relative to the one above and below (*Figure 6*) and it is not clear what effect this is likely to have on the dichroic ratio of the associated band apart from the expectation that it will be lowered.

CONCLUDING REMARKS

The present model for the framework of the feather keratin microfibril is based on data collected from feather rachis but the 'persistent' reflections on layer lines 15, 19, 24, 30, 32 are also observed in reptilian keratins^{3, 6}, and it seems likely that a very similar framework is also present in these materials. The axial period in the claws of the lizard *Varanus niloticus*³ is somewhat greater than that in feather rachis indicating a slightly longer pitch of the helix.

Soluble extracts containing 80–90% of feather can be prepared by reducing the cystine residues and blocking the thiol groups to prevent reoxidation^{25, 40}. Films cast from these derived proteins yield x-ray diffraction patterns which contain the persistent reflections^{13, 41} and it may be concluded that the molecules repolymerize in such a manner that the core structure is regenerated. The films obtained from certain purified fractions²⁵ exhibit strong meridional diffraction at 4.8 and 2.4 Å suggesting a cross- β conformation⁴². It is possible that the pleated sheet portions aggregate side to side in these fractions rather than end-to-end as in the native material.

Various lines of evidence suggest that the non-core portion of the microfibril, which represents a little over two thirds of the keratin, is mainly responsible for the very rich low-angle pattern extending from $l = 0-12$ and laterally from $R = 0-0.06 \text{ \AA}^{-1}$ (*Figure 7*). Bear and Rugo¹² showed that the intensities of these reflections changed with water content and that they could be eliminated by treatment with denaturing agents. The simple 'net' pattern at low angles remaining after such treatments can be explained by supposing that the denatured portions of the molecules still retain an approximate helical symmetry by virtue of their attachment to the undisturbed framework.

Rudall³ showed that heavy atoms could be used as markers for studying feather keratins and an example of this is shown in *Figure 7*, which shows the pattern of feather rachis after treatment with uranyl acetate. The intensities of the reflections in the low-angle pattern are considerably modified without any appreciable changes in their positions. Other isomorphous replacements have been reported⁸ and there would seem to be a possibility of using either

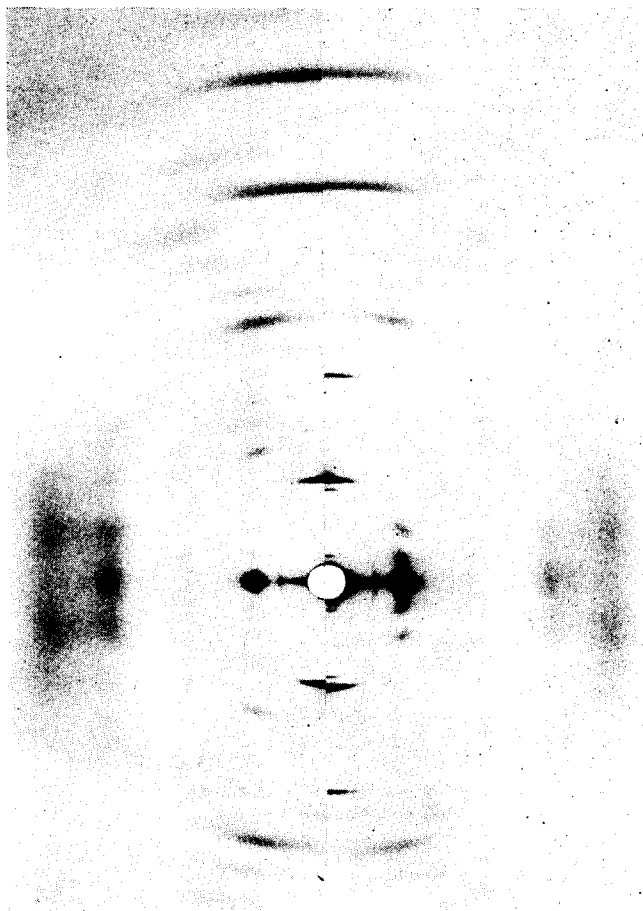


Figure 7 Comparison of x-ray diffraction patterns from (left) native feather rachis and (right) feather rachis treated with uranyl acetate showing changes in the relative intensities in the low-angle region

the heavy atom method or the method of multiple isomorphous replacement to learn more about the 'non-core' portion of the feather keratin microfibril.

*Division of Protein Chemistry, CSIRO,
343, Royal Parade,
Parkville, Victoria 3052,
Australia*

(Received 4 August 1970)

REFERENCES

- 1 Astbury, W. T. and Woods, H. J., *Phil. Trans. Roy. Soc. A* 1933, **232**, 333
- 2 Marwick, T. C. *J. Text. Sci.* 1931, **4**, 31

- 3 Rudall, K. M., *Biochim. Biophys. Acta* 1947, **1**, 549
- 4 Fraser, R. D. B., MacRae, T. P. and Miller, A., *J. Mol. Biol.* 1965, **14**, 432
- 5 Cohen, C. and Holmes, K. C., *J. Mol. Biol.* 1963, **6**, 423
- 6 Fraser, R. D. B., MacRae, T. P. and Rogers, G. E., 'Keratins', Charles C. Thomas (to be published)
- 7 Astbury, W. T. and Marwick, T. C., *Nature* 1932, **130**, 309
- 8 Fraser, R. D. B. and MacRae, T. P., *J. Mol. Biol.* 1959, **1**, 387
- 9 Astbury, W. T. and Beighton, E., *Nature* 1961, **191**, 171
- 10 Schor, R. and Krimm, S., *Biophys. J.* 1961, **1**, 467, 489
- 11 Ramachandran, G. N. and Dweltz, N. E. 'Collagen', (N. Ramanathan, Ed.), Interscience, 1962, p 147
- 12 Bear, R. S. and Rugo, H. J., *Ann. N.Y. Acad. Sci.* 1951, **53**, 627
- 13 Fraser, R. D. B. and MacRae, T. P., *J. Mol. Biol.* 1963, **7**, 272
- 14 Franks, A., *Proc. Phys. Soc.* 1955, **68**, 1054
- 15 Elliott, A., *J. Sci. Inst.* 1965, **42**, 312
- 16 Miller, C. S., Parsons, F. G. and Kofsky, I. L., *Nature* 1964, **202**, 1196
- 17 Suzuki, E., *Spectrochim. Acta* 1967, **23A**, 2303
- 18 Fraser, R. D. B. and Suzuki, E., *Analyt. Chem.* 1966, **38**, 1770
- 19 Fraser, R. D. B. and Suzuki, E., *J. Mol. Biol.* 1965, **14**, 279
- 20 Miyazawa, T. and Blout, E. R., *J. Amer. Chem. Soc.* 1961, **83**, 712
- 21 Pauling, L. and Corey, R. B., *Proc. Nat. Acad. Sci. USA* 1953, **39**, 253
- 22 Bendit, E. G. 'Symposium on Fibrous Proteins', (W. G. Crewther, Ed.), Butterworths, 1968, p 386
- 23 Harrap, B. S. and Woods, E. F., *Comp. Biochem. Physiol.* 1967, **20**, 449
- 24 Fraser, R. D. B., MacRae, T. P., Parry, D. A. D. and Suzuki, E. *Polymer, Lond.* 1969, **10**, 810
- 25 Harrap, B. S. and Woods, E. F., *Biochem. J.* 1964, **92**, 8, 19
- 26 Crewther, W. G., Fraser, R. D. B., Lindley, H. and Lennox, F. G., 'Advances in Protein Chemistry', Vol. 20 (C. B. Anfinsen, M. L. Anson, J. T. Edsall and F. M. Richards, Eds.), Academic Press, 1965, p 191
- 27 Filshie, B. K. and Rogers, G. E., *J. Cell Biol.* 1962, **13**, 1
- 28 Birbeck, M. S. C. and Mercer, E. H., *J. Biophys. Biochem. Cytol.* 1957, **3**, 203
- 29 Fraser, R. D. B. and MacRae, T. P., *Text. Res. J.* 1957, **27**, 384
- 30 Klug, A., Crick, F. H. C. and Wyckoff, H. W., *Acta Cryst.* 1958, **11**, 199
- 31 Astbury, W. T. and Bell, F. O., *Tabulae Biologica* 1939, **17**, 90
- 32 Arnott, S. and Wonacott, A. J., *Polymer, Lond.* 1966, **7**, 157
- 33 Caspar, D. L. D. and Holmes, K. C., *J. Mol. Biol.* 1969, **46**, 99
- 34 *International Tables for X-ray Crystallography*, Vol. III (K. Lonsdale, Ed.), Kynoch Press, 1962
- 35 Massey, H. S. W. and Kestelman, H., *Ancillary Mathematics*, Pitman, 1959
- 36 Geddes, A. J., Parker, K. D., Atkins, E. D. T. and Beighton, E. J., *J. Mol. Biol.* 1968, **32**, 343
- 37 Blake, C. C. F., Koenig, D. F., Mair, G. A., North, A. C. T., Phillips, D. C. and Sarma, V. R., *Nature* 1965, **206**, 757
- 38 Lipscomb, W. N., Hartsuck, J. A., Reeke, G. N., Quiocho, F. A., Bethge, P. H., Ludwig, M. L., Steitz, T. A., Muirhead, H. and Coppola, J. C., 'Brookhaven Symposia in Biology', No. 21, Vol. I, 1968, p 24
- 39 Miyazawa, T., *J. Chem. Phys.* 1960, **32**, 1647
- 40 Woodin, A. M., *Biochem. J.* 1954, **57**, 99
- 41 Rougvie, M. A. quoted by Woodin, A. M., *Biochem. J.* 1956, **63**, 576
- 42 Filshie, B. K., Fraser, R. D. B., MacRae, T. P. and Rogers, G. E., *Biochem. J.* 1964, **92**, 19
- 43 Franklin, R. E. and Gosling, R. G., *Acta Cryst.* 1953, **6**, 678
- 44 Arnott, S., *Polymer, Lond.* 1965, **6**, 478
- 45 Fraser, R. D. B., *J. Chem. Phys.* 1958, **28**, 1113
- 46 Trotter, I. F. and Brown, L. quoted from Bamford, Elliott and Hanby, 'Synthetic Polypeptides', Academic Press, 1956
- 47 Sandemann, I. and Keller, A., *J. Polym. Sci.* 1956, **19**, 401
- 48 Leach, S. J., Némethy, G. and Scheraga, H. A., *Biopolymers* 1966, **4**, 369

APPENDIX 1

Correction of observed intensities for disorientation and finite layer line thickness

Procedures for correcting lattice reflections for the effects of disorientation have been described^{43, 44} but in the present work where continuous distributions of intensity were measured a slightly different procedure is required.

The distribution of molecular directions in a fibrous specimen may be described conveniently (*Figure 8a*) by means of a probability density function

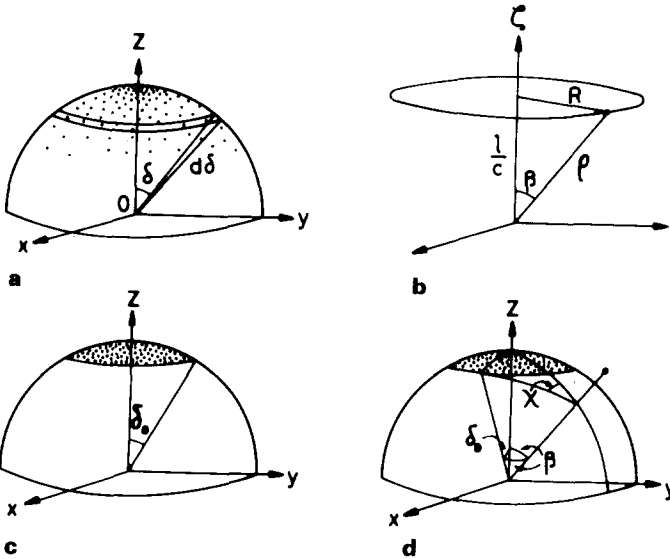


Figure 8

$G(\delta)$ such that the probability of finding a molecular axis inclined at an angle δ to the fibre axis is $2\pi G(\delta) \sin \delta d\delta$ ⁴⁵. If $I(R, \zeta)$ (*Figure 8b*) is the rotated intensity transform of a molecule with $\delta = 0$, the intensity transform for the fibre in the absence of external interference will be the convolution of $I(R, \zeta)$ with $G(\delta)$. A convenient representation of $G(\delta)$ for well oriented materials^{46, 47} is (*Figure 8c*)

$$G(\delta) = \frac{1}{2\pi(1 - \cos \delta_0)}, 0 \leq \delta \leq \delta_0 \quad (14a)$$

$$G(\delta) = 0 \quad \delta_0 < \delta \leq \pi/2 \quad (14b)$$

The rotated intensity transform $I(R, \zeta)$ consists of a series of thin layers spaced c^{-1} apart and $\Delta\zeta \sim L^{-1}$ thick where L is the coherent molecular length. If attention is restricted to points in the observed transform $I_0(R, l/c)$ in which layer line overlap does not occur the only molecules which contribute to the convolution are those with directions which make an angle $\beta = \tan^{-1}(Rc/l)$ with a line drawn from the origin to the point (*Figure 8d*) i.e. a fraction

$$\epsilon = 2X \sin \beta \cdot \Delta\beta \times \frac{1}{2\pi(1 - \cos \delta_0)}, \beta \geq \frac{\delta_0}{2} \quad (15a)$$

$$\epsilon = 2\pi \sin \beta \cdot \Delta\beta \times \frac{1}{2\pi(1 - \cos \delta_0)}, \beta < \frac{\delta_0}{2} \quad (15t)$$

From *Figure 8d*

$$\cos \delta_0 = \cos^2 \beta + \sin^2 \beta \cos \chi \quad (16)$$

and since $\zeta = \rho \cos \beta$

$$\Delta\beta = \frac{-\Delta\zeta}{\rho \sin \beta} = \frac{1}{\rho L \sin \beta},$$

hence

$$\epsilon = \frac{\cos^{-1} \left[\frac{\cos \delta_0 - \cos^2 \beta}{\sin^2 \beta} \right]}{\pi \rho L (1 - \cos \delta_0)}, \beta \geq \frac{\delta_0}{2} \quad (18a)$$

$$\epsilon = \frac{1}{\rho L (1 - \cos \delta_0)}, \quad \beta < \frac{\delta_0}{2} \quad (18b)$$

If, as in the present instance, relative rather than absolute intensities are being used the factor $[L(1 - \cos \delta_0)]^{-1}$ may be omitted from equation 18.

APPENDIX 2

Transformation to curvilinear coordinates on a left-handed helical ruled surfaces

Let S_{0uw} in *Figure 9* be the plane containing the chain axes of a pleated sheet with S_0w parallel to the chain axes. A helical distortion of this surface is required such that interchain distance and hydrogen bond register are maintained, that is, distances between points having the same w coordinate are unchanged and lines of constant u remain perpendicular to lines of constant w .

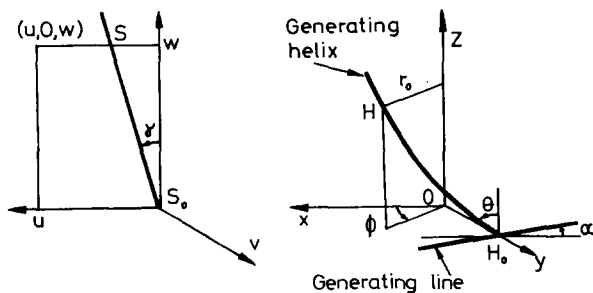


Figure 9

Consider the ruled surface³⁵ generated by a line drawn through a point H , inclined at an angle α to the Oxy plane and normal to the perpendicular from H to Oz , as H moves along a left-handed helical path of pitch P and radius

r_0 . If S_0 is brought into coincidence with H_0 and S_0u aligned with the generating line through H_0 the surface S_0uw may be distorted in such a way that S_0S lies on the generating helix H_0H and the line through S and the point (u, O, w) coincides with the generating line through H .

We may now regard u and w as curvilinear coordinates which specify position on the ruled surface such that a point at (u, O, w) in the undistorted sheet corresponds to a point $x(u, O, w), y(u, O, w), z(u, O, w)$ in the distorted sheet. Expressions for x, y and z may be derived as follows. The cylindrical polar coordinates of H are $r = r_0, \phi = \pi/2 + \Delta\phi, z = -P\Delta\phi/2\pi$; where $\Delta\phi = \phi_H - \phi_{H_0}$. Also

$$-\Delta\phi:2\pi::H_0H:P/\cos\theta \quad (19)$$

where

$$\tan\theta = 2\pi r_0/P,$$

and

$$H_0H = S_0S = w/\cos\gamma \quad (20)$$

hence

$$\Delta\phi = \frac{-2\pi w \cos\theta}{P \cos\gamma} \quad (21)$$

Since distances between points with the same w coordinate are preserved the transformed point (u, O, w) will lie on the generating line through H at a distance $u - w \tan\gamma$ from H . Thus

$$x(u, O, w) = (u - w \tan\gamma) \cos\alpha \times \cos\Delta\phi - r_0 \sin\Delta\phi \quad (22a)$$

$$y(u, O, w) = (u - w \tan\gamma) \cos\alpha \times \sin\Delta\phi + r_0 \cos\Delta\phi \quad (22b)$$

$$z(u, O, w) = (u - w \tan\gamma) \sin\alpha - P\Delta\phi/2\pi \quad (22c)$$

The condition that curves of constant u are orthogonal to curves of constant w on the ruled surface is that³⁵

$$x_u x_w + y_u y_w + z_u z_w = 0 \quad (23)$$

where $x_u = \partial x/\partial u, x_w = \partial x/\partial w$ etc. The solution of equation 23 leads to the condition

$$\alpha = \theta - \gamma \quad (24)$$

Substitution of this value for α in equation 22 provides all the information needed to effect the required transformation to curvilinear coordinates on the ruled surface. The 'out-of-plane' coordinate v in the original sheet is measured normal to the plane S_0uw and in the distorted sheet may be laid off along the normal to the ruled surface. The outward normal has direction cosines given³⁵ by:

$$\lambda = (y_w z_u - z_w y_u)/s \quad (25a)$$

$$\mu = (z_w x_u - x_w z_u)/s \quad (25b)$$

$$v = (x_w y_u - y_w x_u)/s \quad (25c)$$

where

$$s = [(y_v z_u - z_w y_u)^2 + (z_w x_u - x_w z_u)^2 + (x_w y_u - y_w x_u)^2]^{1/2} \quad (26)$$

In the pleated sheet the α -carbon atoms of successive residues are connected by peptide groups of length 3.8 \AA ⁴⁸. If the axial length per residue is h_0 it follows that the α -carbon atoms are distant $\frac{1}{2}(3.8^2 - h_0^2)^{1/2}$ from the axis. The orientation of the chain in known β -structures is such that the plane containing the α -carbon atoms is nearly normal to S_{0uv} and so the v coordinate of the α -carbon atom is approximately $\frac{1}{2}(3.8^2 - h_0^2)^{1/2}$. When the pleated sheet is distorted the change in the w coordinate between successive residues is increased from the value h_0 in the undistorted sheet to $h_0(x_v^2 + y_v^2 + z_v^2)^{1/2}$ and to retain a distance of 3.8 \AA between successive α -carbon atoms the magnitudes of the v coordinates must be reduced by a fraction

$$t = \left[\frac{3.8^2 - h_0^2(x_v^2 + y_v^2 + z_v^2)}{3.8^2 - h_0^2} \right]^{1/2} \quad (27)$$

Combining equations we obtained for the complete transformation to a left-handed helical ruled surface,

$$x(u, v, w) = (u - w \tan \gamma) \cos(\theta - \gamma) \cos \Delta\phi - r_0 \sin \Delta\phi + \lambda tv \quad (28a)$$

$$y(u, v, w) = (u - w \tan \gamma) \cos(\theta - \gamma) \sin \Delta\phi - r_0 \cos \Delta\phi + \mu tv \quad (28b)$$

$$z(u, v, w) = (u - w \tan \gamma) \sin(\theta - \gamma) - P\Delta\phi/2\pi + \nu tv \quad (28c)$$

This transformation has the following properties

- (1) distances between points having the same w coordinate are preserved exactly for $v = 0$ and approximately for v small.
- (2) curves of equal u and equal w are orthogonal for $v = 0$.
- (3) when applied to a pleated sheet the depth of the pleats varies in such fashion that the distance between successive α -carbon atoms is maintained very close to 3.8 \AA . Very slight departures occur due to the curvilinear nature of the transformation.

Statistics of randomly branched polycondensates: Part 2

The application of Lagrange's expansion method to homodisperse fractions

KANJI KAJIWARA*

The method of Lagrange's expansion is applied to the bivariate generating function ('trail-weighting generating function') previously introduced for combinatorial calculation in polymer science. The wide range of applicability of this method is illustrated by calculation of the moments of the molecular weight distribution function, the Stokes radius and the particle scattering factor of random f -functional branched molecules which are monodisperse (i.e. of fixed molecular weight). The branched molecules in our system are composed of the (random) isomeric mixtures of all possible monodisperse f -functional molecules. This is chemically more realistic than assuming a fixed number of branching units in a molecule, as in Zimm and Stockmayer's, or Kurata and Fukatsu's model. In our model, each branch unit is not necessarily f -functional but the maximum functionality of a branch unit is f , while in an extreme case, the molecule will be linear. Also, the route of the combinatorial calculation is more systematic and appreciably simpler, so that this work helps to clarify the competing effects of branching and polydispersity.

1. INTRODUCTION

SINCE GOOD has pointed out the applicability of the method of Lagrange's expansion to random branching processes,¹ this method has been adapted to the calculation of the molecular weight distribution and/or other statistical parameters of randomly branched polycondensates by Good² and Gordon and co-workers^{3, 4}. For example, the coefficient of θ^x in the weight fraction generating function

$$W(\theta) = \sum_{x=1}^{\infty} w_x \theta^x \quad (1)$$

gives the weight fraction of x -mers. Using Lagrange's expansion,^{1, 2} w_x for homopolycondensates is calculated as:

$$w_x = C(\theta^x) W(\theta) = \frac{(fx - x)! f}{(x - 1)! (fx - 2x + 2)!} \alpha^{x-1} (1 - \alpha)^{fx-2x+2} \quad (2)$$

because the weight fraction generating function for homopolycondensates is written as^{5, 6}:

$$W(\theta) = \theta(1 - \alpha + \alpha u)^f \quad (3)$$

*Present address: Institut für Makromolekulare Chemie der Universität Freiburg, Freiburg i. Br., Germany.

with the auxiliary variable

$$u = (1 - a + au)^{f-1} \quad (4)$$

Here $C(\theta^x)$ denotes 'the coefficient of θ^x in', f is the functionality of a monomer and a is the fraction of functionalities which have reacted.

The calculations of statistical parameters of polycondensates have been simplified by the introduction of the trail-weighting generating function^{7,8}. Since the trail-weighting generating function is defined as:

$$u_0(\{\theta\}) = \sum_{x,k} w_{xk} x^{-1} \theta_1^x \sum_{l=1}^x \theta_2^{\sum_{n=0}^{x-1} N_{lnxk}} \phi_n \quad (5)$$

the coefficient of θ_1^x in $[\partial u_0(\{\theta\}) / \partial \theta_2]_{\theta_2=1}$ will be

$$C(\theta_1^x) \left[\frac{\partial}{\partial \theta_2} [u_0(\{\theta\})] \right]_{\theta_2=1} = \sum_k w_{xk} \sum_{l=1}^x \sum_{n=0}^{x-1} N_{lnxk} \phi_n / x \quad (6)$$

which corresponds to the isomeric average of some statistical quantity ϕ_n of an x -mer in polycondensate mixture. Here $\{\theta\}$ denotes the set (θ_1, θ_2) , w_{xk} is the weight fraction of the k -th isomer among x -mers, N_{lnxk} the number of distinct paths ('trails') of n links starting at repeat unit l , and ϕ_n an arbitrary function of the trails of length n . In preceding papers,^{7,8} we have calculated several statistical quantities of random polycondensates, such as the angular distribution function of Rayleigh scattering, Stokes radii and so on. The purpose of this paper is to present a general method of calculating the isomeric average *over the x -mer fraction alone* of a statistical quantity, ϕ_n , so as to obtain an estimate of the effects of the molecular weight distribution. In this way one can clarify the relative contributions of branching and polydispersity of random polycondensates to their physical properties.

2. APPLICATION OF LAGRANGE'S EXPANSION TO THE TRAIL-WEIGHTING GENERATING FUNCTION

As the trail-weighting generating function $u_0(\{\theta\})$ for homo-polycondensates is written as⁸:

$$u_0(\{\theta\}) = \theta_1 \theta_2^{\phi_0} [1 - a + au_1(\{\theta\})]^f \quad (7)$$

with

$$u_n(\{\theta\}) = \theta_1 \theta_2^{\phi_n} [1 - a + au_{n+1}(\{\theta\})]^{f-1} \quad (n=1,2,\dots) \quad (8)$$

then $[\partial u_0(\{\theta\}) / \partial \theta_2]_{\theta_2=1}$ is calculated as:

$$H(u) = \left(\frac{\partial u_0}{\partial \theta_2} \right)_{\theta_2=1} = \phi_0 u (1 - a + au) + fau^2 \sum_{n=0}^{\infty} \left[\frac{(f-1)au}{1-a+au} \right]^n \phi_{n+1} \quad (9)$$

where

$$u(\theta_1) \equiv u_1(\theta_1, 1) = u_2(\theta_1, 1) = \dots = \theta_1 [1 - a + au(\theta_1)]^{f-1} \quad (10)$$

In most cases⁸, $\phi_0=0$, that is,

$$H(u) = fau^2 \sum_{n=0}^{\infty} \left[\frac{(f-1)au}{1-a+au} \right]^n \phi_{n+1} \quad (9')$$

Lagrange's expansion for $H(u)$ with the condition of equation (10) gives:

$$H(u) = \sum_{x=1}^{\infty} \frac{\theta_1^x}{x!} \frac{d^{x-1}}{du^{x-1}} \left[H'(u) (1 - \alpha + \alpha u)^{(f-1)x} \right]_{u=0} \quad (11)$$

Using equation (9')

$$H(u) = \sum_{x=1}^{\infty} \frac{\theta_1^x}{x!} \frac{d^{x-1}}{du^{x-1}} \left\{ f\alpha (1 - \alpha + \alpha u)^{(f-1)x} \sum_{n=0}^{\infty} \left[\frac{(f-1)\alpha u}{1 - \alpha + \alpha u} \right]^n \times \left[2u + \frac{n(1 - \alpha)u}{1 - \alpha + \alpha u} \right] \phi_{n+1} \right\} \quad (12)$$

so that

$$\sum_k w_{xk} \sum_{l=1}^x \sum_{n=1}^{x-1} N_{lnxk} \phi_n = \frac{1}{(x-1)!} \frac{d^{x-1}}{du^{x-1}} \left\{ f\alpha (1 - \alpha + \alpha u)^{(f-1)x} \times \sum_{n=0}^{\infty} \left[\frac{(f-1)\alpha u}{1 - \alpha + \alpha u} \right]^n \left[2u + \frac{n(1 - \alpha)u}{1 - \alpha + \alpha u} \right] \phi_{n+1} \right\}_{u=0} \quad (13)$$

The right side of equation (13) is calculated to be

$$\sum_k w_{xk} \sum_{l=1}^x \sum_{n=1}^{x-1} N_{lnxk} \phi_n = f\alpha^{x-1} (1 - \alpha)^{(f-2)x+2} \frac{x}{[(f-2)x + 2]!} \times \sum_{n=0}^{x-2} (f-1)^n \phi_{n+1} \frac{[(f-1)x - (n+1)]!}{(x-n-2)!} \{n(f-2) + 2(f-1)\} \quad (14)$$

Since⁷

$$\sum_{l=1}^x N_{lnxk} = 2N_{nxk} \quad (15)$$

$$N_{1xk} = x - 1 \quad (16)$$

where N_{nxk} is the number of distinct trails of length n in the k -th x -mer, we deduce from equation (14) as a check:

$$w_x \equiv \sum_k w_{xk} = \frac{[(f-1)x]! f}{(x-1)! [(f-2)x + 2]!} \alpha^{x-1} (1 - \alpha)^{fx-2x+2} \quad (17)$$

which coincides with equation (2), when we put

$$\phi_1 = 1, \phi_2 = \phi_3 = \phi_4 = \dots = 0.$$

Comparing the coefficients of ϕ_n on both sides of equation (14) and using equation (17) or equation (2), the average number of distinct trails of length n in the x -mers (averaged over the statistical mixture of isomers) is obtained as:

$$\langle N_{nx} \rangle_{\text{iso}} = \frac{x! [(f-1)x - n]!}{2 [(f-1)x]!} \frac{(f-1)^{n-1}}{(x-n-1)!} \{n(f-2) + f\} \quad (18)$$

where

$$\langle N_{nx} \rangle_{\text{iso}} \equiv \sum_k w_k N_{nxk} \quad (19)$$

Also, from equation (14):

$$\begin{aligned}
 \left\langle \sum_{l=1}^x \sum_{n=1}^{x-1} N_{lnxk} \phi_n \right\rangle_{\text{iso}} &\equiv \sum_k w_k \sum_{l=1}^x \sum_{n=1}^{x-1} N_{lnxk} \phi_n \\
 &= \frac{x!}{[(f-1)x]!} \sum_{n=0}^{x-2} (f-1)^n \phi_{n+1} \frac{[(f-1)x - (n+1)]!}{(x-n-2)!} \\
 &\quad \times \{n(f-2) + 2(f-1)\} \quad (20)
 \end{aligned}$$

3. UNPERTURBED DIMENSIONS

For a Gaussian chain, the m -th moment of the distribution function for the distance $|R_n|$ of the trails of length n is written as:

$$\langle R_n^m \rangle = A_m n^{m/2} \quad (21)$$

where

$$A_m = [(m+1)! / (\frac{1}{2}m)!] (\frac{1}{6}\sigma^2)^{m/2} \quad (22)$$

for $m = 0$ and positive even integers,

$$A_m = (2/\pi^{\frac{1}{2}}) [\frac{1}{2}(m+1)]! (\frac{2}{3}\sigma^2)^{m/2} \quad (23)$$

for $m = -1$ and positive odd integers, and σ is the effective unit length. Usually the summation of $\langle R_n^m \rangle$ over all the possible trails is required, so that, putting $\phi_n = A_m n^{m/2}$ in equation (20), we obtain:

$$\begin{aligned}
 \left\langle \sum_{\substack{\text{all possible} \\ \text{trails}}} \langle R_n^m \rangle \right\rangle_{\text{iso}} &= \left\langle A_m \sum_{l=1}^x \sum_{n=1}^{x-1} N_{lnxk} n^{m/2} \right\rangle_{\text{iso}} \\
 &= \frac{A_m x!}{[(f-1)x]!} \sum_{n=0}^{x-2} (f-1)^n \frac{[(f-1)x - (n+1)]!}{(x-n-2)!} \\
 &\quad \times \{n(f-2) + 2(f-1)\} (n+1)^{m/2} \quad (24)
 \end{aligned}$$

which is very similar to the results of Kurata and Fukatsu⁹ although they have derived their theory from a different model. When x is large, equation (24) is approximated with the aid of the Euler-Maclaurin's formula⁹ in terms of the gamma-function:

$$\begin{aligned}
 \langle \sum \langle R_n^m \rangle \rangle_{\text{iso}} &\simeq A_m x(x-1) \left\{ [2/(f-2)]^{m/4} \left[\Gamma\left(\frac{m}{4} + 1\right) \right] [(f-1)x]^{m/4} \right. \\
 &\quad \left. - \frac{1}{12} f [2/(f-2)]^{[(m/4)+\frac{1}{2}]} \left(\frac{m^2}{4} + \frac{7}{2}m\right) \right. \\
 &\quad \left. \times \Gamma\left(\frac{m}{4} + \frac{1}{2}\right) [(f-1)x]^{[(m/4)-\frac{1}{2}] + \dots} \right\} \quad (25)
 \end{aligned}$$

In the special case of $m = 2$, the isomeric average mean-square radius of

gyration is derived from equation (24) as:

$$\begin{aligned} \langle S^2 \rangle_b &= \frac{1}{2x^2} \langle \Sigma \langle R_n^2 \rangle \rangle_{\text{iso}} \\ &= \frac{\sigma^2}{2x} \frac{(x-1)!}{(f-1)x!} \sum_{n=0}^{x-2} (f-1)^n \frac{[(f-1)x - (n+1)]!}{(x-n-2)!} \\ &\quad \times \{n(f-2) + 2(f-1)\} (n+1) \end{aligned} \quad (26)$$

which is approximated for large x as:

$$\langle S^2 \rangle_b \simeq \frac{\sigma^2}{2} \left[\frac{\pi(f-1)x}{2(f-2)} \right]^{\frac{1}{2}} \quad (27)$$

and reduces to the classic result of Zimm and Stockmayer¹⁰ except for the difference in counting the number of units: a unit in our model contains f subchains in the zero-th generation (and $f-1$ subchains in the other generations) in Zimm and Stockmayer's sense. The branching factor g is defined as:

$$g = \langle S^2 \rangle_f / \langle S^2 \rangle_l = \langle S^2 \rangle_b / (\frac{1}{3}x\sigma^2) \quad (28)$$

Using equation (26)

$$\begin{aligned} g &= \frac{3}{x^2} \frac{(x-1)!}{[(f-1)x!]} \sum_{n=0}^{x-2} (f-1)^n \frac{[(f-1)x - (n+1)]!}{(x-n-2)!} \\ &\quad \times [n(f-2) + 2(f-1)] (n+1) \end{aligned} \quad (29)$$

or for large x ,

$$g \simeq 3 \left[\frac{\pi(f-1)}{2x(f-2)} \right]^{\frac{1}{2}} \quad (30)$$

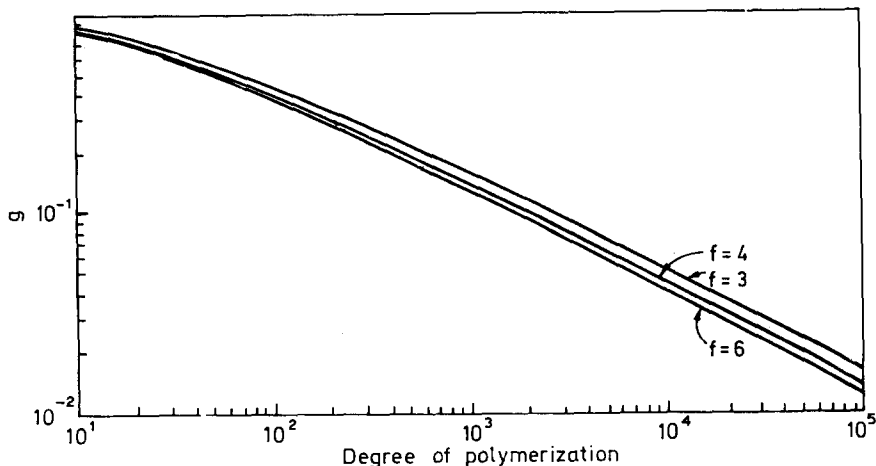


Figure 1 The g -factors (see equations 29 and 30) of 3, 4 and 6 functional branched molecules plotted against the degree of polymerization. The functionalities of the branching unit are shown

The results are shown in *Figure 1* which predict extremely small g -values because our model is one of highly-branched molecules.

4. EFFECTIVE HYDRODYNAMIC RADIUS

The effective hydrodynamic radius (the Stokes radius), R_{sb} , for branched molecules is written as:

$$R_{sb}^{-1} = 6\pi\eta_0\bar{\mathcal{E}}_b^{-1} = x^{-2} \sum_{\text{(all possible trails)}} \langle R_n^{-1} \rangle \quad (31)$$

from the non-draining limit of Kirkwood's formula¹¹ for the translational frictional constant:

$$\bar{\mathcal{E}}_b^{-1} = (x\zeta)^{-1} + (6\pi\eta_0x^2)^{-1} \sum_{\text{(all possible trails)}} \langle R_n^{-1} \rangle \quad (32)$$

where $\bar{\mathcal{E}}_b$ denotes the translational frictional constant of a branched molecule, ζ the frictional constant of a unit, η_0 the viscosity of the solvent, and the summation extends over all distinguishable trails in an unrooted tree. Putting $m = -1$ in equation (24), we obtain

$$R_{sb}^{-1} = \frac{1}{\sigma} \left(\frac{6}{\pi}\right)^{\frac{1}{2}} \frac{(x-1)!}{x[(f-1)x]!} \sum_{n=0}^{x-2} (f-1)^n \frac{[(f-1)x - (n+1)]!}{(x-n-2)!} \times \{n(f-2) + 2(f-1)\} (n+1)^{-\frac{1}{2}} \quad (33)$$

or, for large x

$$R_{sb}^{-1} \simeq \frac{1.42405}{\sigma} \left[\frac{(f-2)}{(f-1)x} \right]^{\frac{1}{2}} \quad (34)$$

Since the branching factor h is defined as the ratio of the Stokes radius of a branched molecule to that of a linear molecule¹²

$$h^{-1} = R_{sl}^{-1}/R_{sb}^{-1} = \frac{3}{8} \frac{(x-1)!}{x^{\frac{1}{2}}[(f-1)x]!} \sum_{n=0}^{x-2} (f-1)^n \frac{[(f-1)x - (n+1)]!}{(x-n-2)!} \times [n(f-2) + 2(f-1)] (n+1)^{-\frac{1}{2}} \quad (35)$$

or for large x

$$h^{-1} \simeq 0.3864 \left[\frac{(f-2)x}{(f-1)} \right]^{\frac{1}{2}} \quad (36)$$

Figure 2 shows the computed results of the branching factor h . The asymptotic value of the ratio $h/g^{\frac{1}{2}}$ in the limit of large x is

$$h/g^{\frac{1}{2}} = 1.3346 \quad (37)$$

and independent of the functionality f , which agrees closely with Kurata and Fukatsu's value⁹. The degree of polymerization dependence of the value of $h/g^{\frac{1}{2}}$ is shown in *Figure 3*.

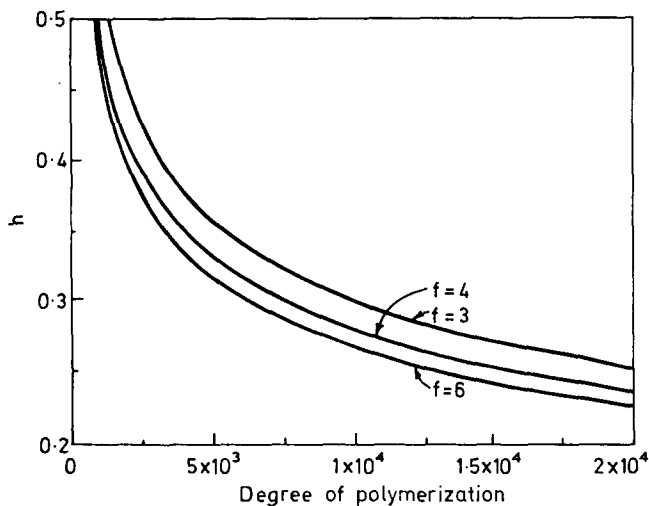


Figure 2 The h -factors (see equations 35 and 36) of 3, 4 and 6 functional branched molecules, plotted against the degree of polymerization. The functionalities of the branching unit are shown

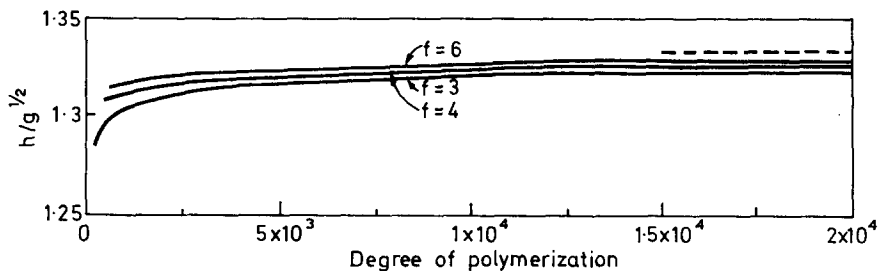


Figure 3 Values of $h/g^{1/2}$ for 3, 4 and 6 functional branched molecules, plotted against the degree of polymerization. The broken line shows the asymptotic value of $h/g^{1/2}$ in the limit of large degree of polymerization

5. ANGULAR DISTRIBUTION OF RAYLEIGH SCATTERING

The normalized angular intensity distribution of light scattered from a branched molecule is given by^{7, 13}

$$P(\vartheta) = \frac{1}{x^2} \sum_{\text{(all possible trails)}} \left\langle \frac{\sin(sr_n)}{sr_n} \right\rangle \quad (38)$$

with

$$s = \frac{4\pi \sin(\vartheta/2)}{\lambda} \quad (39)$$

where $\langle \rangle$ denotes the configurational average, ϑ is the scattering angle,

λ the wave length of the light in the solution, and r_n the distance between two ends of a trail of length n . Using Debye's approximation for Gaussian subchains¹⁴

$$\left\langle \frac{\sin(sr_n)}{sr_n} \right\rangle = \exp(-s^2 \langle r_n^2 \rangle / 6) \quad (40)$$

where $\langle r_n^2 \rangle$ is given by

$$\langle r_n^2 \rangle = n\sigma^2 \quad (41)$$

when we put

$$\phi_n = \exp(-s^2 \sigma^2 n / 6) \quad (42)$$

in equation (20), the angular distribution of Rayleigh scattering for the isomeric mixture of tree-like branched molecules whose degree of polymerization is x , will be obtained as:

$$P_{\text{iso}}(\vartheta) = \frac{(x-1)!}{x[(f-1)x]!} \sum_{n=0}^{x-2} [(f-1) \exp(-s^2 \sigma^2 / 6)]^n \exp(-s^2 \sigma^2 / 6) \\ \times \frac{[(f-1)x - (n+1)]!}{(x-n-2)!} \{n(f-2) + 2(f-1)\} \quad (43)$$

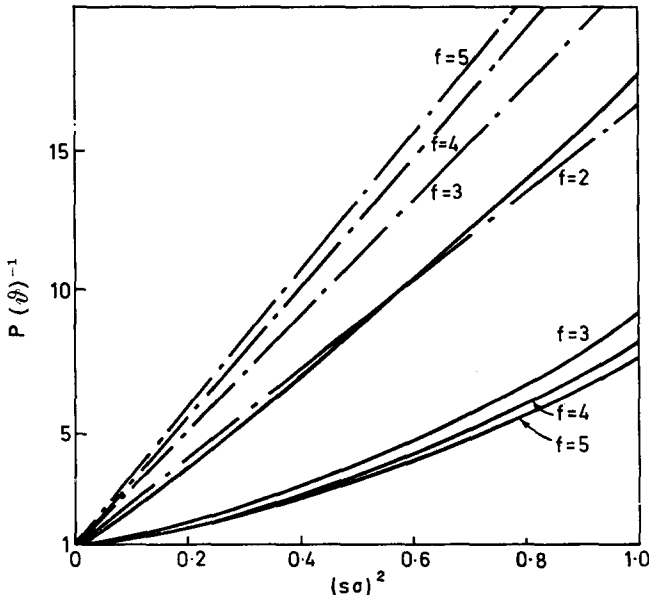


Figure 4 $P(\vartheta)^{-1}$, plotted against $(s\sigma)^2$ (Zimm-plot). Solid lines are for mono-disperse molecules whose degrees of polymerization are 187. Chain lines (see ref. 7) are for polydisperse molecules whose weight average degrees of polymerization are 187. For mono-disperse molecules, $P(\vartheta)^{-1}$ denote $\bar{P}_{180}(\vartheta)^{-1}$, and for polydisperse molecules, $P(\vartheta)^{-1}$ denote $\bar{P}_z(\vartheta)^{-1}$. The functionalities of the branching unit are shown

From equations (26) and (43) in the limit of $s^2\sigma^2 \rightarrow 0$, this reduces, as expected, to:

$$P_{\text{iso}}(\vartheta) \simeq 1 + \frac{16\pi^2 \langle S^2 \rangle_2}{3 \lambda^2} \sin^2(\vartheta/2) \quad (44)$$

The difference of the particle scattering functions between polydisperse and monodisperse branched molecules is remarkable as we see in *Figure 4*. As predicted in the case of cruciform molecules¹⁵, the curves of the reciprocal scattering factors versus $\sin(\vartheta/2)$ of monodisperse branched molecules show

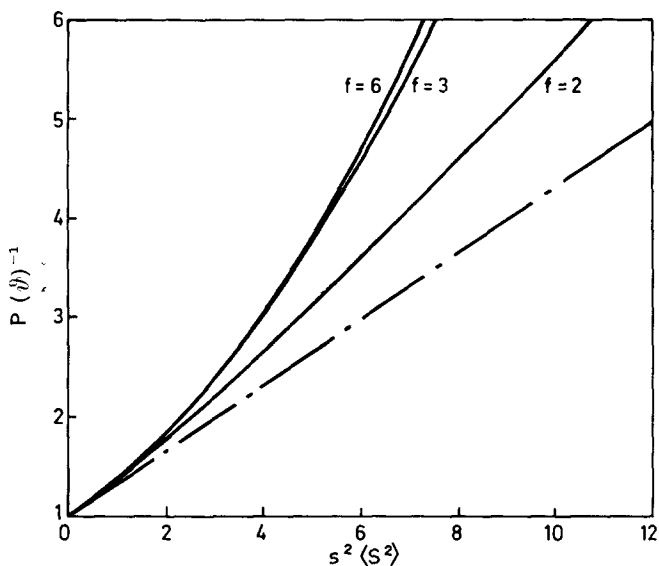


Figure 5 The effect of branching on the shape of the particle scattering factor of monodisperse molecules. Chain line shows the particle scattering factor of a polydisperse linear chain with $M_w/M_n=2$ (in this case, $P(\vartheta)^{-1}$ and $\langle S^2 \rangle$ denote $P_z(\vartheta)^{-1}$ and $\langle S^2 \rangle_z$ respectively)

a strong upturn due to the increase of the segment density, although those of polydisperse branched molecules show a slight downturn. *Figure 4* should be useful for assessing the efficiency of procedures for fractionating random polycondensates according to molecular weights. In either case, the initial slopes of the curves (see *Figure 5*) are determined by the mean-square radii of gyration (in the case of polydisperse branched molecules, the z-average mean-square radii of gyration), as we see from equation (44).

ACKNOWLEDGEMENT

The author is indebted to Professor M. Gordon for valuable discussions and comments. This work was carried out with the financial support of the Science Research Council.

*Department of Chemistry,
University of Essex,
Wivenhoe Park,
Colchester, Essex,
England*

(Received 12 May 1970)

REFERENCES

- 1 Good, I. J. *Proc. Camb. Phil. Soc.* 1960, **56**, 369
- 2 Good, I. J. *Proc. Roy. Soc.* 1963, **A292**, 54
- 3 Dobson, G. R., and Gordon, M. *J. Chem. Phys.* 1964, **41**, 2389
- 4 Gordon, M., Malcolm, G. N., and Butler, D. S. *Proc. Roy. Soc. (London)* 1966, **A295**, 29
- 5 Good, I. J. *Proc. Camb. Phil. Soc.* 1955, **51**, 240
- 6 Gordon, M. *Proc. Roy. Soc.* 1960, **268**, 240
- 7 Kajiwara, K., Burchard, W., and Gordon, M. *Brit. Polymer J.* 1970, **2**, 110
- 8 Kajiwara, K., *J. Chem. Phys.* (in press)
- 9 Kurata, M., and Fukatsu, M. *J. Chem. Phys.* 1964, **41**, 2934
- 10 Zimm, B. H., and Stockmayer, W. H. *J. Chem. Phys.* 1949, **17**, 1301
- 11 Kirkwood, J. G. *J. Polym. Sci.* 1953, **12**, 1
- 12 Stockmayer, W. H., and Fixman, M. *Ann. N.Y. Acad. Sci.* 1953, **57**, 334
- 13 Debye, P. *J. Phys. Chem.* 1947, **51**, 18
- 14 Debye, P., Technical Report N. 637 to Rubber Reserve Company (1945), (in 'Light Scattering from Dilute Polymer Solutions', (Ed. McIntyre, D., and Gormich, F.), Gordon and Beech, New York and London, 1964)
- 15 Benoit, H. *J. Polym. Sci.* 1953, **11**, 507

Book Reviews

Polyolefin plastics

by THEODORE O. J. KRESSER

Van Nostrand Co Ltd, London, 1970, 179 pp., £5 17s

The jacket describes this book as 'geared to the needs of people with little or no specialized training in the field' and hence the treatment is descriptive rather than mathematical and quantitative. However, the selection of material is curious for such readership—31 pages are devoted to the chemistry of polyolefines, including stereospecificity and branching, yet the effects of these on crystallinity and physical properties is dismissed in a few words. A section of 15 pages covers an admittedly simplified summary of extruder theory, yet the application of this to practical processing is hardly mentioned—a page and a half describe extruder drives but temperature control is not discussed, possibly because the author believes 'most modern extruders are operated essentially adiabatically' (p. 99). Why then all the attention by designers to barrel cooling systems, use of which is mentioned on the previous page? It may be argued that a description of rheological properties would be out of place in a 'Plastics Applications Series' volume—one must search for a mention of non-Newtonian behaviour—but then why for instance include three pages on molecular weight distribution and its measurement but only apply it to physical properties with the vague statement 'The physical properties (of a broad distribution) will not be quite as good as a material of . . . narrower distribution'? The imbalance between basic science and practical application is seen in that of 175 pages of text, the former occupies 55 pages, the latter, in the sense of end products, takes only 19 pages.

This book is also claimed to be 'easy-to-grasp in presentation' yet the description on p. 48 of carbon bond angles might be confusing to a student of solid geometry. On p. 90 the effect of speed ' N ' on extruder output is explained by ' N appears only in the drag flow, so if everything else is held constant, output is directly proportional to screw speed'; the equation is of the form $Q = AN - B$, so the approach to proportionality depends on the relative magnitudes of A and B rather than their constancy. In any event, B which includes the pressure drop in the die, is not normally independent of Q ; the explanation tends to confuse the known phenomena. The sections on finishing and compounding describe both the various mixers and blenders and the possible operational sequences, but without a single illustration or diagram, which could have saved space as well as promoting clarity.

The book conveys the impression that the author was restricted by considerations of space and commercial security and that both quantitative data and explanations of practical phenomena have suffered in consequence. However, the severest criticism is that, granting limitations necessitated by space and presentation, the jacket claims that 'encompassing the whole spectrum of polyolefin plastics, . . . this volume covers their processing . . . and applications', yet gives not a single reference to the vast literature.

M. J. STEVENS

Epoxy resins

(*Advances in Chemistry Series, 92*)

American Chemical Society, Washington, 1970, 230 pp., \$10.50

Division-sponsored symposia are important features of the American Chemical Society meetings and one looks to these for information on recent developments in particular fields of chemical science and technology. Some symposia papers appear as volumes of

preprints available to members but the practice of this Society subsequently to publish collected papers in their *Advances in Chemistry* series makes them available more widely. The present volume is one of this series and includes in revised form 15 papers from those given at a symposium organised by the Division of Organic Coatings and Plastics Chemistry for the 155th meeting in April 1968 (preprints Vol. 28, No. 1, pp. 375 *et seq.*). A further paper, not presented then, is included.

Of the 16 contributions, all of U.S. origin, 14 arise from industrial laboratories, one from the Jet Propulsion Laboratory (California Inst. of Technol.) and one from the U.S. Naval Laboratory. They cover a range of topics associated with epoxy resins and differ widely in subject matter. Work on new compositions includes thermosetting epoxy compounds based on pentaerythritol, on fluorine-containing intermediates and an alternative method of preparing glycidyl esters. A paper on work sponsored by U.S. Dental Research details an investigation on amine-cured epoxy resins for use in small areas. Attention is given to improved accelerators and hardeners, including the special effects of substituted phenols in amine-epoxy compositions; amino-siloxanes are shown to be effective hardeners, and co-ordinated silicate/amine derivatives are investigated as delayed action curing agents.

Studies on electro-deposition of surface coatings and on the mechanism of reaction between phosphorous amides and epoxy resins are reported, as are those on the kinetics of gelation in anhydride-activated systems and β -transition phenomena in relation to structure. Other papers deal with compositions for special applications, e.g. composites of higher strength and modulus, flexible compositions incorporating carboxy-terminated polyisobutene, formulations for maximum moisture resistance, and light-weight epoxy foams.

The book is by no means a text-book generally but records researches in specific areas. At the price quoted it is not cheap and the volume will be of most value to those concerned primarily with research and development in epoxy resins. Many non-specialists, however, will find in it much of considerable interest.

It is well produced with a high standard of print and presentation of the numerous tables and figures. Each paper provides a list of references and a summary. There is a good subject (but no author) index. It is substantially free from typographical error although one is surprised to see the name of Carothers misprinted (p. 179) and 'donnors' for donors (p. 31). Comparison with the original preprint shows that a line is omitted on p. 74, leading to an incorrect description of the epoxy novolac DEN 431 and no data at all on DEN 438. Other features are the widespread use of letters as abbreviations for intermediates, hardeners and catalysts (a standardised glossary would have been helpful) and (p. 174) the use of °C in the text but °F in figure 1.

R. J. W. REYNOLDS

Book Reviews

Polyolefin plastics

by THEODORE O. J. KRESSER

Van Nostrand Co Ltd, London, 1970, 179 pp., £5 17s

The jacket describes this book as 'geared to the needs of people with little or no specialized training in the field' and hence the treatment is descriptive rather than mathematical and quantitative. However, the selection of material is curious for such readership—31 pages are devoted to the chemistry of polyolefines, including stereospecificity and branching, yet the effects of these on crystallinity and physical properties is dismissed in a few words. A section of 15 pages covers an admittedly simplified summary of extruder theory, yet the application of this to practical processing is hardly mentioned—a page and a half describe extruder drives but temperature control is not discussed, possibly because the author believes 'most modern extruders are operated essentially adiabatically' (p. 99). Why then all the attention by designers to barrel cooling systems, use of which is mentioned on the previous page? It may be argued that a description of rheological properties would be out of place in a 'Plastics Applications Series' volume—one must search for a mention of non-Newtonian behaviour—but then why for instance include three pages on molecular weight distribution and its measurement but only apply it to physical properties with the vague statement 'The physical properties (of a broad distribution) will not be quite as good as a material of . . . narrower distribution'? The imbalance between basic science and practical application is seen in that of 175 pages of text, the former occupies 55 pages, the latter, in the sense of end products, takes only 19 pages.

This book is also claimed to be 'easy-to-grasp in presentation' yet the description on p. 48 of carbon bond angles might be confusing to a student of solid geometry. On p. 90 the effect of speed ' N ' on extruder output is explained by ' N appears only in the drag flow, so if everything else is held constant, output is directly proportional to screw speed'; the equation is of the form $Q = AN - B$, so the approach to proportionality depends on the relative magnitudes of A and B rather than their constancy. In any event, B which includes the pressure drop in the die, is not normally independent of Q ; the explanation tends to confuse the known phenomena. The sections on finishing and compounding describe both the various mixers and blenders and the possible operational sequences, but without a single illustration or diagram, which could have saved space as well as promoting clarity.

The book conveys the impression that the author was restricted by considerations of space and commercial security and that both quantitative data and explanations of practical phenomena have suffered in consequence. However, the severest criticism is that, granting limitations necessitated by space and presentation, the jacket claims that 'encompassing the whole spectrum of polyolefin plastics, . . . this volume covers their processing . . . and applications', yet gives not a single reference to the vast literature.

M. J. STEVENS

Epoxy resins

(*Advances in Chemistry Series, 92*)

American Chemical Society, Washington, 1970, 230 pp., \$10.50

Division-sponsored symposia are important features of the American Chemical Society meetings and one looks to these for information on recent developments in particular fields of chemical science and technology. Some symposia papers appear as volumes of

*Investigation of the sequence length distribution in ethylene-propylene copolymers by pyrolysis and reaction gas chromatography**

L. MICHAJLOV, H.-J. CANTOW and P. ZUGENMAIER

A series of copolymers in the composition range 5–70 mol-% propylene were prepared under kinetically controlled conditions. The copolymerization was carried out at constant monomer feed composition in a homogeneous reaction medium, using the soluble catalyst system vanadium oxytrichloride/ethylaluminium sesquichloride. From the kinetic data the distribution functions of the ethylene sequence lengths were calculated. These values were then correlated with the distribution of the fragment chain lengths obtained from the thermal degradation with subsequent reaction gas chromatography of the copolymers. Good agreement between the kinetic and the pyrolysis values of the ethylene sequence length distribution is observed in samples with up to 50 mol-% propylene.

INTRODUCTION

DEPENDING on the polymerization conditions, copolymers of ethylene and propylene of the same overall composition may exhibit differing distribution of the monomer units along the copolymer chain. Accordingly, these copolymers may exhibit a broad spectrum of physical and applicational properties ranging from tough, thermoplastic materials to amorphous, elastomeric gums. Therefore, it is of considerable scientific – as well as practical – interest to obtain information on the monomer sequence length distribution in ethylene-propylene copolymers, which strongly influence those properties.

Up to now, n.m.r. spectroscopy has been used, in addition to i.r. spectroscopy, predominantly for the determination of sequence length distribution in copolymers¹. However, the n.m.r. method only gives direct information about triade – eventually pentade – sequences being either homopolymeric or inter-sequential.

Thermal degradation provides the means of isolating and directly analysing even longer sequences. We therefore pyrolysed ethylene-propylene copolymers to derive sequence length from fragment length distributions. Pyrolysis coupled directly with reaction gas chromatography was used for this purpose.

In an earlier paper² we showed that the distribution of the copolymer chain fragments according to length may be correlated with the blockiness of the ethylene-propylene copolymers, as evidenced, for example, by x-ray measurements.

*L. Michajlov, Doktorarbeit, University of Freiburg

The results obtained during this first part of our investigations suggested that it may be possible to achieve a more quantitative correlation between the sequence length distribution (as predicted from kinetic data) and the fragment chain length distribution (as derived from the thermal degradation). Therefore, our next step was to prepare a series of ethylene-propylene copolymers under kinetically controlled conditions³.

In this paper we will be concerned with the copolymerization procedure and the fragmentation of the copolymers, as well as with the interpretation of the relation between fragment length and sequence length distribution.

EXPERIMENTAL

(a) Materials

Isopropylcyclohexane (IPCH) was purified in the usual way with sulphuric acid, dried with calcium chloride, calcium hydride and molecular sieve (4Å), fractionally distilled (b.p. 153.5–154.5°C) and stored over a molecular sieve under nitrogen. Before use it was finally distilled under a nitrogen atmosphere over sodium wire into a specially designed flask.

Nitrogen (Messer Griesheim, 99.99%) was purified by passing it consecutively through columns filled with potassium hydroxide, silica gel, phosphorus pentoxide and molecular sieve (4Å).

Ethylene (Messer Griesheim, 99.7%) and *propylene* (Messer Griesheim 99%) were purified in the same way as nitrogen and passed, to remove polar impurities, through a column filled with molecular sieve (4Å) impregnated with a 10% solution of triethylaluminium in IPCH.

The other chemicals: *ethylaluminiumsesquichloride*, *vanadium oxytrichloride* (KuK Laboratory, pure), *methanol* (Merck, p.a.), and *isopropanol* (Merck, p.a.), were used as received.

(b) Apparatus

The scheme of the polymerization apparatus is shown in *Figure 1*. Reactions were carried out in a jacketted 1.5 l vessel (11) equipped with a magnetic stirrer, a reflux condenser (12) in the gas outlet, a gas inlet tube fitted with a porous glass disc 2G and three inlet tubes for separate addition of both catalyst components and the solvent. The vessel was heated by an ultra-thermostat.

The solvent was stored in the flask (20), from which – after recycling through beds filled with molecular sieve (4Å) (16) – it was pumped into the vessels for polymerization or catalysts.

Monomers were purified in the columns (2, 3) metered through calibrated rotameters (6, 7), mixed in the gas mixing flask (8) and introduced finally into the reactor well below the liquid level. Two other flow meters placed in inlet and outlet lines were used to check the flow rate of the total gas stream.

The composition of the monomer feed in both inlet and outlet gas streams was analysed gas chromatographically using valves (22, 23) for sampling.

The catalyst solutions were prepared in two 500ml graduated cylindrical

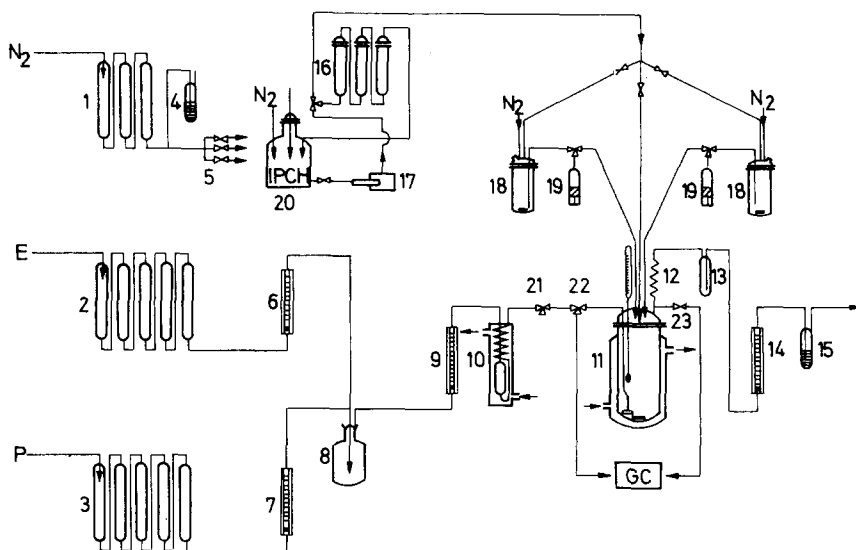


Figure 1 Scheme of the polymerization apparatus:

- | | | |
|---|---|--|
| 1, 2 and 3 purifying beds for nitrogen, ethylene and propylene | 9 inlet gas flow meter | 18 graduated vessels for catalyst solutions |
| 4 safety valve | 10 heat exchanger | 19 adjustable syringe |
| 5 manifold | 11 reaction vessel | 20 IPCH flask |
| 6 and 7 calibrated flow meters with valves for metering of ethylene and propylene | 12 reflux condenser | 21, 22, 23 valves for metering both catalyst components |
| 8 gas mixing vessel | 13 cooling vessel | GC gas chromatograph coupled with the inlet and outlet gas lines |
| | 14 outlet gas flow meter | |
| | 15 bubbler (vent) | |
| | 16 beds filled with molecular sieve (4 Å) | |
| | 17 pump | |

bottles (18) and transferred to the polymerization vessel through two motor syringes (19).

The apparatus was evacuated through the valve (21).

(c) Preparation of catalyst solutions

The catalysts were stored under nitrogen as 10% stock solutions in IPCH in a dry box. More dilute solutions were used in the polymerizations runs. They were prepared in the following way: dry IPCH was separately pumped under nitrogen into both bottles. The corresponding amounts of the stock catalyst solutions were injected by means of hypodermic syringes through serum caps. Mixing was carried out with a magnetic stirrer. The concentrations of ethylaluminiumsesquichloride and vanadium oxytrichloride were 0.2M and 0.013M, respectively.

(d) Copolymerization

All copolymerization runs were carried out at 40°C using 600ml of solvent. The polymerization apparatus was first alternately evacuated and

flushed several times with nitrogen. The solvent was then added and nitrogen bubbled through for one hour. The composition of the monomer feed in both inlet and outlet gas streams was analysed before and during the polymerization.

After equilibration of both feed components had been achieved, runs were started by adding the catalysts at the rate 1.1 ml/min for each solution. The copolymerization was stopped by adding methanol.

The copolymer was precipitated by pouring the reaction mixture into a stirred 1:1 mixture of methanol and *isopropanol*. The precipitated polymer was washed several times with precipitant mixture, dried in air at room temperature and then in vacuum at 50°C.

The overall composition of the copolymers was determined with a Perkin Elmer IR spectrometer 125 following the method proposed by Gössl⁴.

The ethylene-propylene copolymers prepared under the above conditions are given in *Table 1*.

Copolymerization runs were carried out over a broad range of monomer composition. The copolymerization diagram is given in *Figure 2*.

Table 1 Synthesized copolymer samples

Sample No.	Mol %P in feed	Mol %P in copolymer	X-ray crystallinity (%)
M 1	12.5	5*	—
M 2	35	16	~20
M 3	42	18	~10
M 4	44	25	~10
M 5	53	30	0
M 6	56	36	0
M 7	59	37	0
M 8	62	38	0
M 9	65	40	0
M 10	70	49	0
M 11	80	54	0
M 12	86	70	0

* Calculated on the basis of the copolymerization equation

The copolymerization reactivity ratios r_1 and r_2 ($1 = \text{ethylene}$) were determined by the Mayo-Lewis⁵ method as well as by that of Fineman and Ross⁶

$$\frac{F}{f} (f - 1) = r_1 \times \frac{F^2}{f} - r_2 \quad (1a)$$

$$\frac{f - 1}{F} = -r_2 \times \frac{f}{F^2} + r_1 \quad (1b)$$

$F = [M_1]/[M_2]$, molar feed composition in the gas or in the liquid phase

$f = [m_1]/[m_2]$, molar composition in the copolymer

Figure 3 shows the Mayo-Lewis plot, *Figure 4* the two equivalent Fineman-Ross plots. No significant deviation from a straight line has been observed for the latter plots indicating that no 'penultimate effects' in the chain growth could be detected.

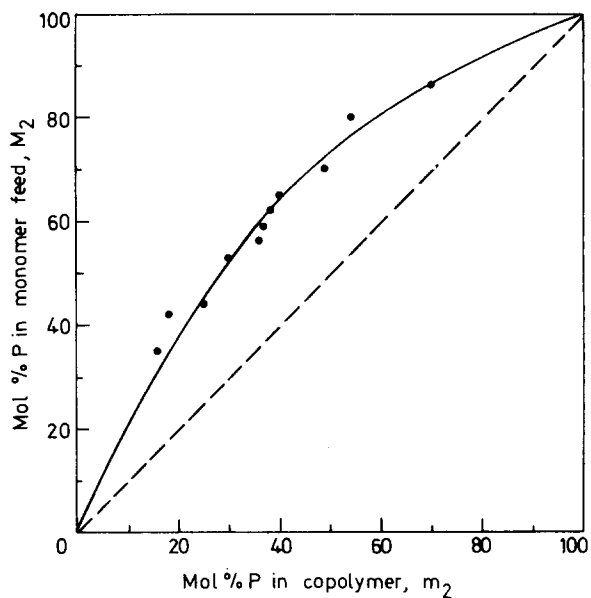


Figure 2 Copolymerization diagram of ethylene-propylene system (P = propylene)

From the plots it was realized, that within a mean deviation of 10% $r_1 = 2.5$ and $r_2 = 0.35$ ($r_1 r_2 = 0.87$).

The reactivity ratios in this paper have been obtained from feed ratio data in the gaseous phase. The differing solubility of both monomers

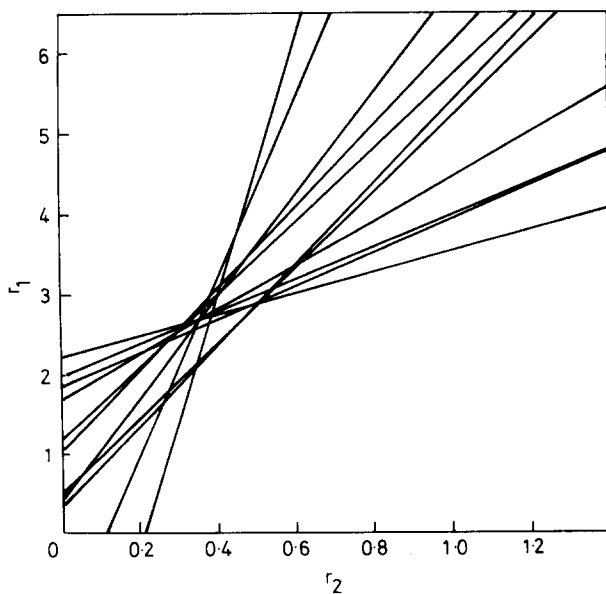


Figure 3 Treatment of copolymerization data according to Mayo-Lewis method; r_1 , r_2 are copolymerization parameters

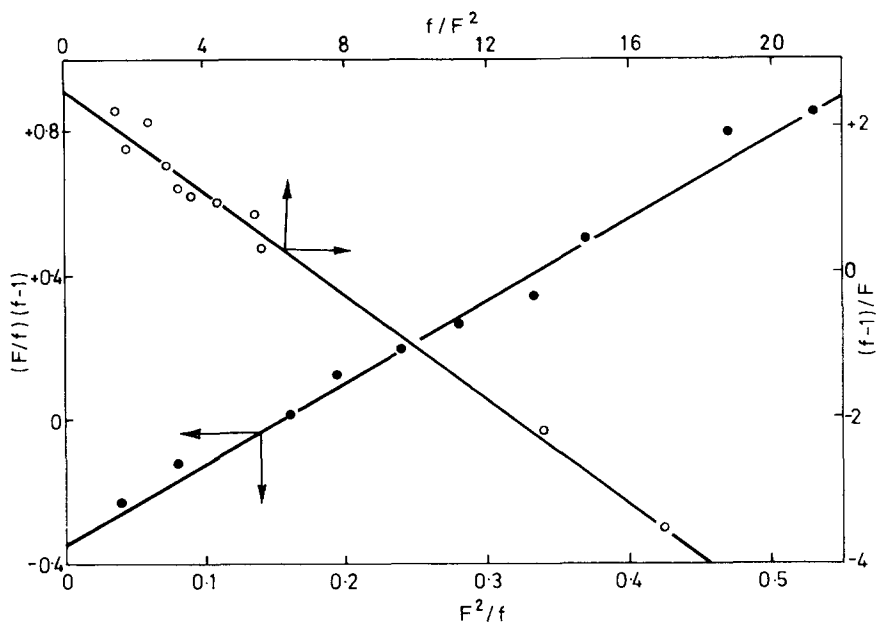


Figure 4 Treatment of copolymerization data according to Finemann-Ross method. Symbols are explained in the text

makes these reactivity ratios different from those measured directly in the solution, but this fact is irrelevant with respect to the calculation of sequence length distributions from kinetic parameters. For this calculation r_1F and r_1/F only are included, these being independent of the differing solubilities of the monomer components.

Reaction gas chromatography

Flash pyrolysis coupled with on line hydrogenation and gas chromatographic separation of the polymer chain fragments was used throughout this work. The experimental technique has been discussed elsewhere².

Results and Discussion

Polymer fragmentation. First we would like to discuss the fragmentation of polymers for extreme examples as in our previous paper².

Figure 5 represents the pyrograms of linear polyethylene and of isotactic polypropylene respectively. Besides minor-branched fragments polyethylene yields *n*-alkanes, indicated by their C-number in the figure. Polypropylene on the other hand decomposes into monomer and oligomer fragments, shown as I to IX in the pyrogram. A physical mixture of equal parts of both gives the pyrogram in the upper part of Figure 6, which is purely a superposition of those of polyethylene and of polypropylene. Pyrolysing a statistical copolymer with equal parts of both monomers produces new peak

groups which appear essentially between odd and even C-number straight chain fragments, shown by circles with arrows in *Figure 6*. These peaks correspond to hetero-sequences with ethylene and propylene. Their concentration increases with decreasing average sequence length. Consequently the concentration of long chain fragments decreases in the same way.

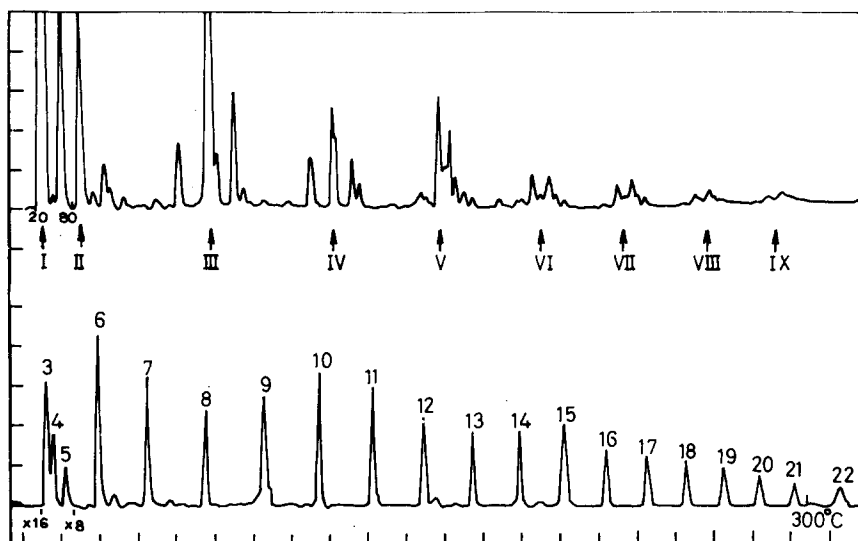


Figure 5 Pyrograms of linear polyethylene (below) and isotactic polypropylene (above)

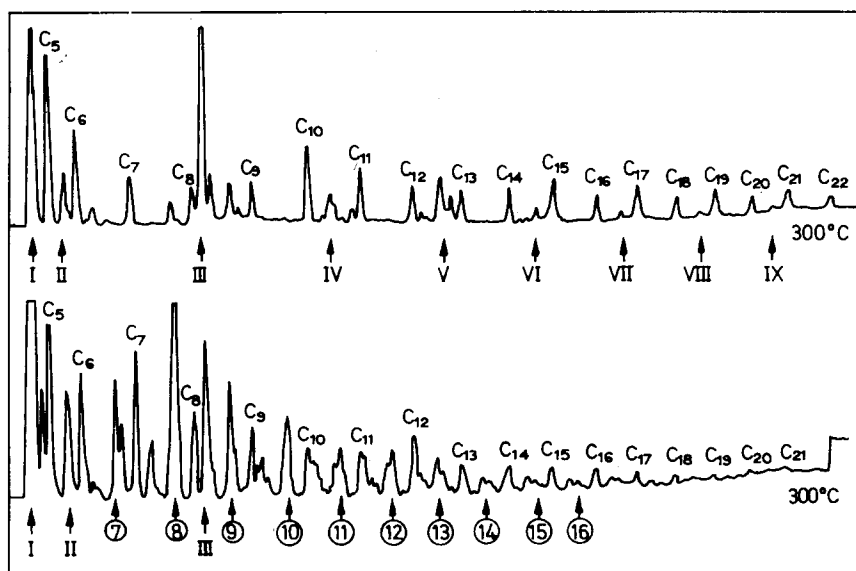


Figure 6 Pyrograms of a mixture of polyethylene and polypropylene (above) and a statistical copolymer of ethylene and propylene (below). Both have equal parts of ethylene and propylene

In the following an attempt is made to analyse these effects more quantitatively, i.e. to correlate the fragmentation products distribution with that of the sequence lengths as derived from copolymerization kinetics.

Sequence length distribution from kinetic data

Using the usual equation for copolymerization the expressions for the probabilities of sequences of ethylene (*E*) and propylene (*P*) of length *n* are derived as follows⁷

$$P_{n(E)} = \left(\frac{1}{1 + (1/r_1 F)} \right)^{n-1} \times \frac{1}{1 + r_1 F}$$

$$P_{n(P)} = \left(\frac{1}{1 + (F/r_2)} \right)^{n-1} \times \frac{1}{1 + (r_2/F)}$$

To convert frequency into mass distributions, the probabilities have to be multiplied by the respective chain lengths⁸

$$M_{n(E)} = n \times P_{n(E)}$$

Figure 7 represents the differential mass distributions of the ethylene sequences (calculated from the kinetics) for the copolymers under discussion (compare Table 1). The shift of the distribution maximum with increasing ethylene content towards higher sequence lengths is evident in this figure.

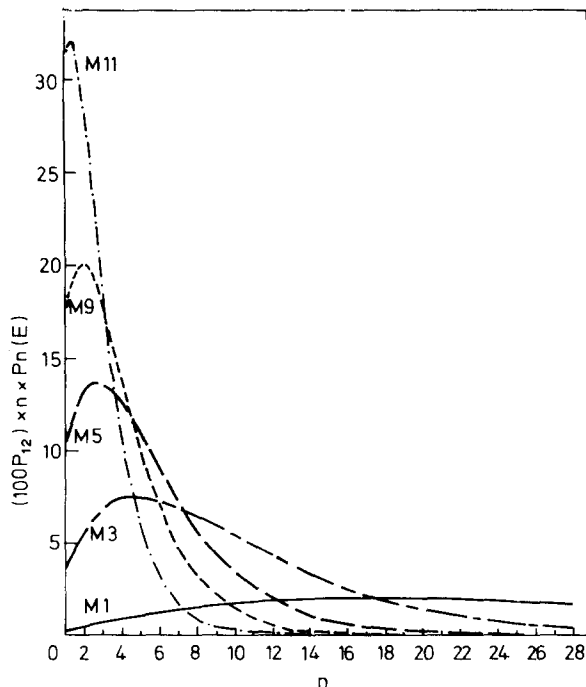


Figure 7 Differential mass distribution of the ethylene sequences of some copolymers calculated from kinetics data (compare Table 1)

In the following we will discuss the pyrolysis results of some of our samples as stated in *Table 1*.

Interpretation of the fragmentation of copolymers

Looking at the pyrograms of our copolymers (*Figure 8*), which are synthesized under kinetically controlled conditions, one finds a similarity in average sequence and average fragment lengths respectively.

Neighbourhood odd and even C-number fragments are present in essentially identical concentrations.

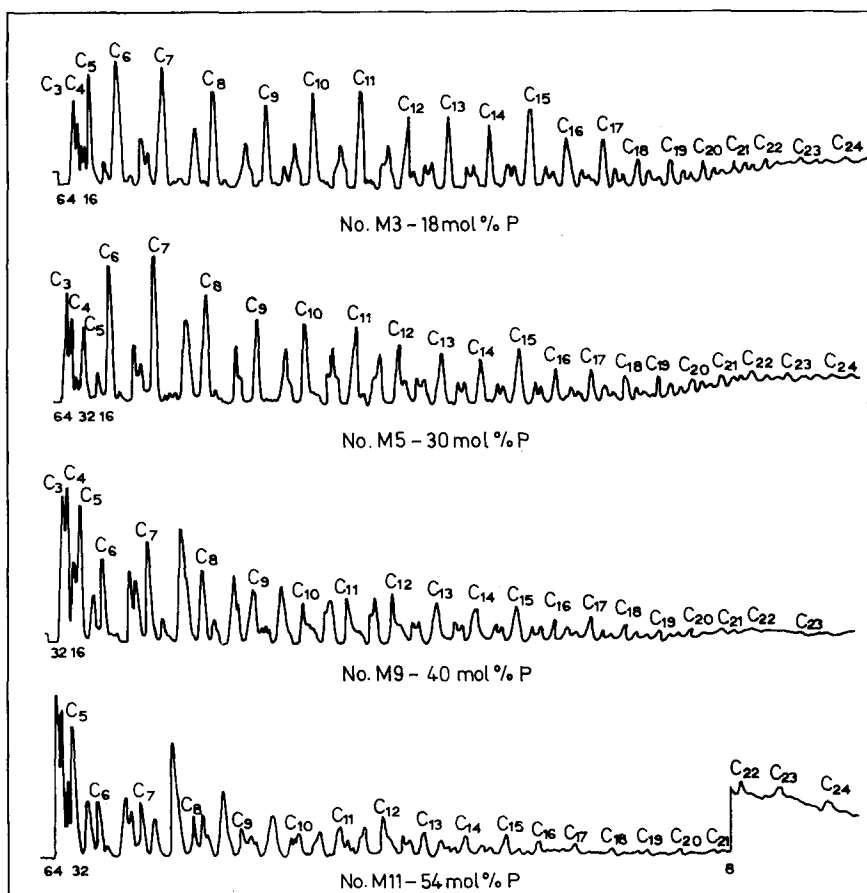


Figure 8 Pyrograms of some copolymers samples (compare *Table 1*)

For a more quantitative discussion of the fragmentation of ethylene-propylene copolymers by thermal degradation we have to consider several types of scission:

- (1) Preferential scission at the tertiary C-atoms. The scission probability is higher here in the chain backbone than at the methyl side group.

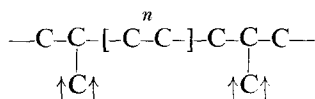
(2) Statistical scission within the ethylene sequences.

Furthermore secondary reactions may influence the fragment length distribution as well as apparatus effects, i.e. absorption of longer fragments in colder parts of the equipment etc.

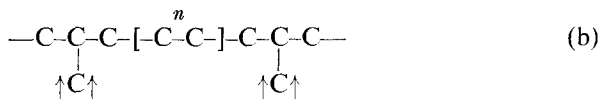
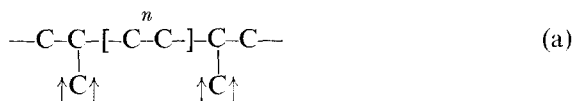
First we will consider the preferential scission in the polymer backbone at the tertiary C-atoms.

Two types of propylene addition in the growing chain are to be considered

(1) The 'normal' head-to-tail arrangement within the propylene sequence



(2) The 'abnormal' head-to-head or tail-to-tail arrangement



Only odd C-number fragments should be obtained for the 'normal' arrangement, if only backbone scission is considered at the tertiary C-atoms. The chain lengths of such fragments would then be $n + 0.5$, $n + 1.5$ and $n + 2.5$ ethylene sequences ($n = 1, 2 \dots$ etc). For example for a ethylene sequence of 4 units, fragments with C_9 , C_{11} and C_{13} will appear.

Even C-number fragments should however appear for both the types of 'abnormal' arrangement, again if only propylene backbone scission is considered. The corresponding lengths will be for (a) n , $n + 1$ and $n + 2$ for head-head addition and for (b) $n - 1$, $n + 2$ and $n + 3$ for tail-tail addition respectively.

The fact that identical concentrations of neighbored odd and even C-number fragments have been found experimentally would lead to the conclusion that both types of arrangement in the chain are exhibiting the same frequency. Tosi *et al.*⁹ have effectively shown by IR-spectroscopy that their atactic polypropylene and ethylene-propylene copolymers have up to 30% 'abnormal' arrangement.

As discussed before there are other scission types forming additional even C-number fragments arising from ethylene sequences flanked by normally arranged propylene units: preferential scission of CH_3 -side groups at the tertiary C-atom and statistical scission in the ethylene sequences. Whereas the former case, as well as secondary reactions, will not be discussed more quantitatively in this paper, the influence of the statistical ethylene sequence scission will be considered later on.

In the discussion of the preferential intrachain scission at the tertiary C-atoms we may assume firstly, that the tertiary C-C bonds along the chain are equivalent. Then for the 'normally' arranged sequences the frequency of formation of odd C-number fragments of the length $n + 1.5$ will be twice that of fragments with $n + 0.5$ or $n + 2.5$.

For evaluation of our experiments now we are not interested primarily in the fragments built up from sequences of a fixed length. We have to analyse the frequency of the fragments, $P_{C_{n+0.5}}$ of a fixed C-number with regard to their formation from corresponding sequences. The frequency of formation of fragments with odd C-numbers $n + 0.5$ ($P_{C_{n+0.5}}$) turns out to be proportional to the sum of the probabilities of the sequence length distribution of ethylene, P_{n-2} , P_{n-1} and P_n , with the corresponding weights 1:2:1. Applying now the equation for the expression for the ethylene sequence distribution one can easily see that for head tail flanked sequences this sum is proportional to the probability of the sequence length distribution of ethylene $p_{n(E)}$

$$P_{C_{n+0.5}} \propto P_{n-2} + 2P_{n-1} + P_n \propto P_{n(E)}$$

For head-head and tail-tail arrangement however the corresponding even C-number fragments correlate with the ethylene sequence distribution in the following way: the frequency of the formation of fragments with the length n is proportional to the probability for the corresponding ethylene sequences for both types of 'abnormal' arrangement

$$P_{C_n} \propto P_n + 2P_{n+1} + P_{n+2} \propto P_{n(E)} \quad (a)$$

$$P_{C_n} \propto P_{n+1} + 2P_{n+2} + P_{n+3} \propto P_{n(E)} \quad (b)$$

It is evident, that because of the proportionality of fragment and sequence probabilities for both 'abnormal' types of addition expressions (a), (b), respectively hold for any arbitrary a-b type ratio.

Let us consider finally the overlapping of the preferential intra-chain scission at the tertiary C-atoms with the statistical scission within the ethylene sequences. The probability of the latter may be obtained from the pyrogram of linear polyethylene. By folding both dominant scission at the tertiary C-atoms and statistical ethylene scission an appropriate first approximation model of the copolymer fragmentation may be established. As a consequence of the competition of both scission types some even C-number fragments are formed from 'normally' arranged propylene units too and vice versa.

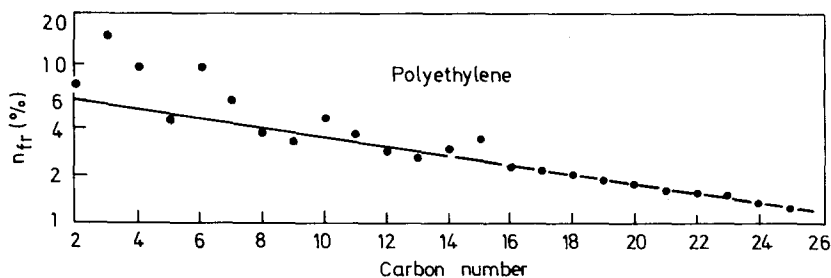


Figure 9 Frequency distribution of the fragments from the pyrolysis of linear polyethylene

In Figure 9 the frequency distribution derived from the polyethylene pyrogram is plotted versus the C-number of the fragments. Starting from about C₇ the relation is a linear one in the semi-logarithmic plot.

Besides the statistical scission within the ethylene sequences the slope of this straight line is influenced somewhat by apparatus effects too, e.g. absorption in the injector block. It has been proved however, by Exner and Seeger¹⁰, that these effects do not interfere with the sequence length distributions obtained by folding the preferential with the statistical scission plot. This has been established by carrying out the respective measurements at different pyrolysis temperatures and at different injector block temperatures, so influencing the degree of apparatus effects. Irrespective of changing conditions the sequence length distribution curves derived from the folding operations remained identical within experimental error.

The deviation of the plot from a straight line below C_7 seems to be caused also by secondary reactions as shown by measurements of the temperature dependence of pyrolysis. Therefore, in the following discussion of evaluations those fragments lower than C_7 are omitted.

In the present state it does not seem to be reasonable to derive distributions of the propylene sequence lengths from the fragmentation data. The analytical information arising from the *iso*-alkane peaks in the pyrograms does not seem to be effective enough for that purpose. However, experiments are in progress in our laboratory with labelled propylene units in copolymers to evaluate the *iso*-fragments for the propylene sequences. It should be possible to study the scission of the methyl side groups at the tertiary C-atoms, discussed before, more quantitatively.

Correlation between sequence and fragment distribution

In *Figure 10* the results on the ethylene-propylene copolymers described earlier are evaluated. Here the frequency distributions, n_{fr} , of the fragments found experimentally from the pyrograms (points and unbroken lines) as well as those calculated under the assumptions cited above from the kinetic data (dotted lines) are plotted. In every case the upper dotted line corresponds to the even number fragments and the lower to the odd number fragments. Because pyrolysis as well as kinetic data have been normalized, for comparison of both types of data the slope of the diagram is relevant. To give an idea of their difference, the sequence length distribution function $P_{n(E)}$ as derived from kinetics is given (upper abscissa = monomer units) as well as n_{fr} .

In the diagram the propylene content of the model copolymers increases from M3 to M11. For the high ethylene copolymers the agreement between pyrolysis data and data derived from copolymerization parameters seems to be very satisfactory. For the samples with more propylene in the copolymer chain the pyrolysis points are scattering more because the separation of *n*-alkane and *iso*-alkane peaks tends to be inferior as demonstrated in the pyrogram of the M11 sample (*Figure 8*).

Improved analysis should be possible here by copolymerization with labelled propylene followed by pyrolysis and radio-gas chromatography.

In this and our earlier paper² we hope we have shown that pyrolysis gas chromatography may be developed into a method giving more than qualitative information on the sequence microstructure of copolymers even if no kinetic information concerning their synthesis is given.

First measurements on ethylene-propylene terpolymers with a third component added for vulcanizability show that sequence analysis concerning ethylene is also possible if the third component is either built-in in monomer steps only, or if it decomposes to monomer. This has been performed particularly for amorphous rubbers with dicyclopentadiene as the third component.

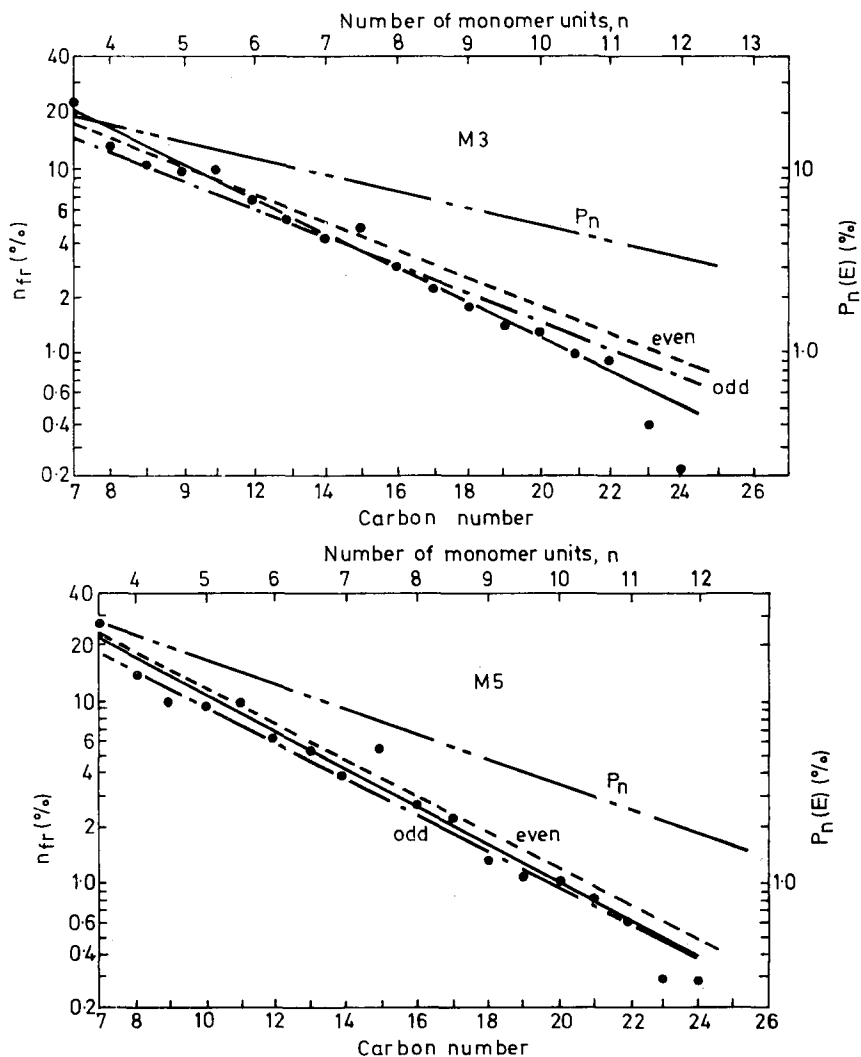


Figure 10a Frequency distribution of the fragments of the samples of Figure 8: points and continuous lines are the experimental results; dotted lines are the calculated curves for odd and even fragments from the copolymerization data

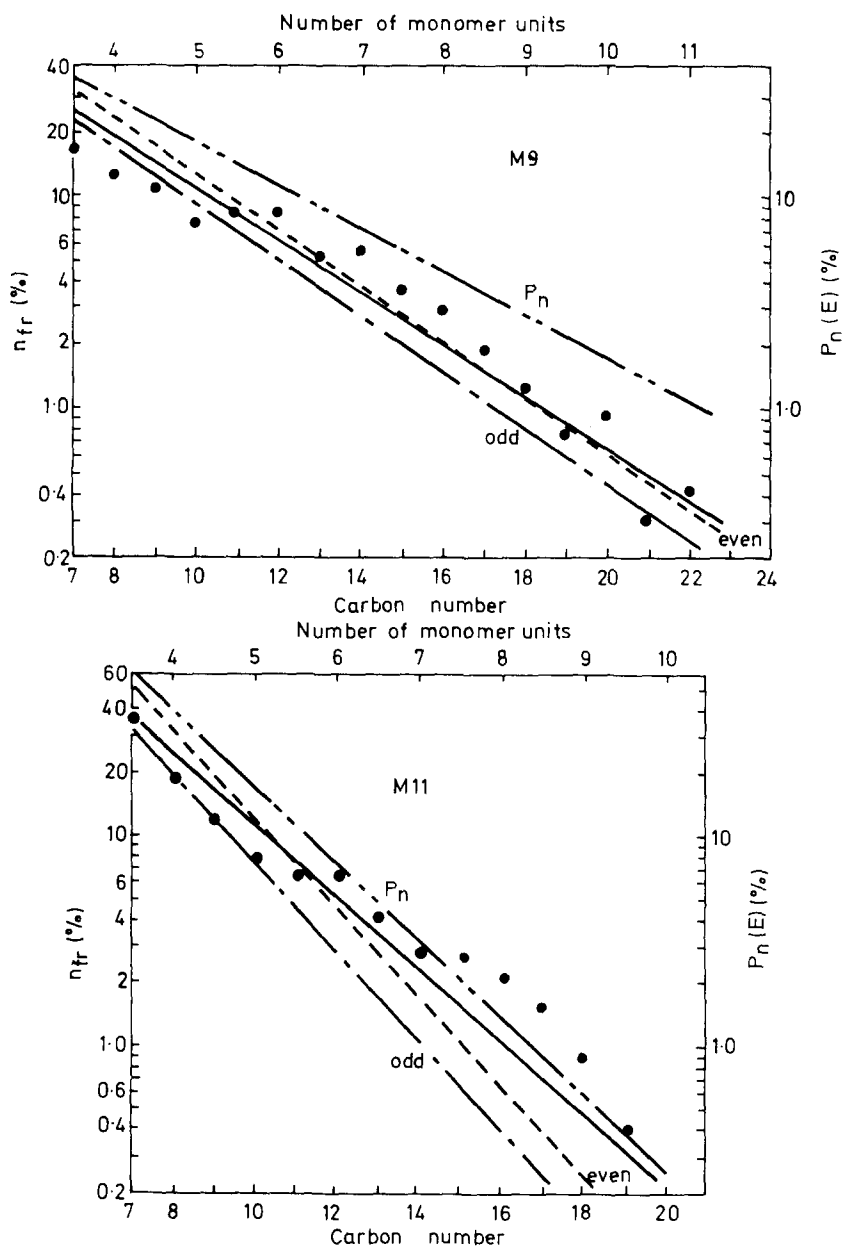


Figure 10b Frequency distribution of the fragments of the samples of Figure 8: points and continuous lines are the experimental results; dotted lines are the calculated curves for odd and even fragments from the copolymerization data

ACKNOWLEDGMENT

We have to thank Dr Josef Exner and Dipl.-Phys. Michael Seeger for fruitful discussions and additional measurements. The grateful financial assistance of Deutsche Forschungsgemeinschaft is acknowledged with thanks. Furthermore we have to thank Chemische Werke Hüls AG., Marl, for valuable reagents.

*Institute of Macromolecular Chemistry,
University of Freiburg,
Freiburg 78, Germany*

(Received 1 June 1970)

REFERENCES

- 1 Harwood, H. J. *Angew. Chemie* 1965, **77**, 405, 1124
- 2 Michajlov, L., Cantow, H.-J. and Zugenmaier, P. *Polymer, Lond.* 1968, **9**, 325
- 3 Mayo, R. F., Bunsen-Diskussionstagung, Ludwigshafen, 1965
- 4 Gössl, T., *Makromol. Chem.* 1960, **42**, 1
- 5 Mayo, F. R. and Lewis, F. M. *J. Amer. Chem. Soc.* 1944, **66**, 1594
- 6 Finemann, M. and Ross, S. D. *J. Polym. Sci.* 1950, **2**, 259
- 7 Alfrey, T. and Goldfinger, G. *J. Chem. Phys.* 1944, **12**, 205
- 8 Natta, G. A., Mazzanti, G., Valvassori, A., Sartori, G. and Morero, D., *Chim. Ind., Milan* 1960, **42**, 125
- 9 Tosi, C., Valvassori, A. and Ciampelli, F. *Europ. Polym. J.* 1959, **5**, 575
- 10 Exner, J. and Seeger, M. (Private communication)

Relaxation phenomena in some aromatic polymers: effect of water content on the low temperature relaxation

G. ALLEN, J. MCAINSH and G. M. JEFFS

Relaxation studies have been carried out on polysulphone, polycarbonate, poly(2,6-dimethylphenylene oxide) and polysulphone A using the dielectric relaxation technique as the primary method of monitoring motional effects. In certain instances this technique has been supplemented by low frequency dynamic mechanical and broad-line nuclear magnetic resonance studies. It was found that the α -relaxation for these amorphous polymers could not be completely resolved owing to the temperature limitations of the apparatus. However the β -relaxations in all four polymers were clearly resolved. The amplitude and the activation energy of these β -relaxations were found to be dependent on the water content of the samples. In addition the amount of water absorbed depended on the polarity of the molecule under consideration. These results indicate that the absorbed water hydrogen bonds to polar groups along the polymer chain and, as such, takes part in the molecular process which gives rise to the β -relaxation.

INTRODUCTION

BACCAREDDA *et al*¹ have reported the results of audio frequency dynamic mechanical investigations on Union Carbide polysulphone. They found two relaxation regions, one associated with glass transition, and the other, at low temperatures, was unassigned, but was found to be dependent on the water content of the sample.

Dielectric relaxation studies on polycarbonate have been reported by Ishida and Matsuoka². Again two relaxation regions are observed; one at high temperature associated with the glass transition and a low temperature region. It is not reported if the low temperature is dependent on the water content of the sample.

In this paper we report the results of a relaxation study of these polymers and of two similar polymers i.e. poly(2,6-dimethylphenylene oxide) and polysulphone A, using primarily the dielectric relaxation technique. In certain instances this method has been supplemented by low frequency dynamic mechanical and broadline nuclear magnetic resonance studies.

EXPERIMENTAL

Samples

The four polymers studied were polysulphone, polycarbonate, poly(2,6-dimethylphenylene oxide) (hereafter denoted PMPO) and polysulphone A. The structures of these polymers are given in *Table 1*.

Table 1 The polymer structures

Polymer	Structure
Polysulphone	
Polycarbonate	
PMPO	
Polysulphone A	

Commercial samples of polysulphone, polycarbonate and PMPO were obtained from Union Carbide, Bayer and AKU respectively. The sample of polysulphone A was prepared by condensing 4,4'-dichlorodiphenyl sulphone and 4,4'-dihydroxy diphenyl sulphone³. The molecular weights and the heterogeneity indices for the samples are shown in *Table 2*.

Table 2 Glass transition temperatures and molecular weight data

Polymer	T_g (dilatometry) [°C]*	T_g (DTA) [°C]†	\bar{M}_w	(\bar{M}_w/\bar{M}_n) GPC
Polysulphone	176	179	40 000	2.35
Polycarbonate	145	—	34 900	2.17
PMPO	209	—	112 000	>2
Polysulphone A	—	214	32 000	2.40

* In the region of T_g the rate of heating was 2° an hour

† On extrapolation to zero rate of heating over the range 40°C/min–20°C/min

Thermal Properties

The glass temperature for each of the four polymers was determined by dilatometry and differential thermal analysis (DTA). The results are given in *Table 2*, along with the rates of heating.

Crystallinity

All four polymers were analysed for crystallinity using x-ray crystallography. The diffraction patterns indicated that all the polymers possessed little or no crystallinity.

Physical Measurements

Dielectric. The samples for dielectric measurements were moulded into the form of discs 5 cm in diameter and 0.16 cm thick. Dimensional details and the moulding temperatures and pressures are given in *Table 3*. To ensure a good electrical contact metal foil electrodes were attached to the sample by a thin layer of silicone grease.

The measurements were made in a dielectric cell in which the electrodes were in a three terminal arrangement. A General Radio Transformer ratio-arm bridge Type 1615A was used over the frequency range $60 \rightarrow 5 \times 10^4$ Hz. The generator used over the frequency range $60 \rightarrow 10^4$ Hz was the General

Table 3 Moulding details for the dielectric discs

<i>Polymer</i>	<i>Diameter [cm]</i>	<i>Thickness [cm]</i>	<i>T [°C]</i>	<i>P [psi]</i>
Polysulphone	5.05	0.165	260	4800
Polycarbonate	5.5	0.155	240	4800
PMPO	5.5	0.165	290	6100
Polysulphone A	5.5	0.163	320	6100

Radio Audio Oscillator Type 1317A. Over the range $10^4 \rightarrow 5 \times 10^4$ Hz an Advance Audio Oscillator was used. The detector employed throughout was the General Radio Tuned Amplifier and Null detector Type 1232A. The temperature of the cell was thermostatically controlled to $\pm 0.25^\circ\text{C}$ in a liquid bath over the temperature range -196°C to $+180^\circ\text{C}$.

The permittivity (ϵ'), dielectric loss tangent ($\tan \delta$) and the dielectric loss factor (ϵ'') were measured at all temperatures. These quantities are related by

$$\epsilon^* = \epsilon' - i\epsilon''$$

and

$$\tan \delta = \epsilon''/\epsilon'$$

Dynamic mechanical. The samples for the study of the dynamic mechanical properties were moulded into the form of a bar. The dimensions of each bar are given in *Table 4*. The moulding conditions were the same as for the dielectric discs.

The dynamic mechanical measurements were made using a low frequency (~ 1 Hz) torsion pendulum. The sample was enclosed in an environmental chamber which was thermostatically controlled to $\pm 0.1^\circ\text{C}$ over the temperature range -130°C to $+180^\circ\text{C}$.

The dynamic shear modulus, G' , was calculated from the period τ of the torsion pendulum, its moment of inertia, I , and the sample dimensions according to the relationship:

$$G' = \frac{64\pi^2 Il}{cd^3\mu\tau^2}$$

where l , c and d are the length, breadth and thickness respectively of the sample and μ is a shape factor⁴. The mechanical loss tangent Q^{-1} , was calculated from $\log(\text{decrement})/\pi$.

Table 4 Dimensions of the samples for the dynamic-mechanical measurements

Polymer	Length [cm]	Width [cm]	Thickness [cm]
Polysulphone	5.95	0.965	0.338
Polycarbonate	5.95	0.640	0.168
PMPO	5.95	0.650	0.178

Broad line nuclear magnetic resonance. The sample for n.m.r. measurements were prepared by heating and compressing the polymer granules in a glass tube which was then sealed. The spectrometer used was built to a design by Robinson⁵ and the resonant frequency, for protons, was 24.5 MHz. The modulation frequency was 90 Hz and the field sweep available was equivalent to 200 kHz. The probe was placed in a glass dewar between the pole pieces of a permanent magnet. The temperature of the sample could be held to $\pm 0.25^\circ\text{C}$ over the range -160°C to $+240^\circ\text{C}$. The line width values were derived from the first derivative of the proton resonance lines.

RESULTS

(1) The water treatment of the polymer samples

The dielectric discs, as prepared by compression moulding, contained various amounts of water, e.g. a freshly moulded polysulphone disc contained 0.22% w/w of water. 'Dry' samples were prepared by treatment in vacuum at 120°C for at least 60 hours. Longer periods of heating showed no measurable decrease in weight. These 'dry' samples were then immersed in water at room temperature and the percentage of water absorbed determined by weighing. *Figure 1* shows the results obtained for a series of immersion experiments. The weight of water absorbed (expressed as a percentage) is plotted as a function of time. The time taken to reach equilibrium absorption was roughly proportional to the percentage of water in the equilibrium condition. The behaviour of the samples soaked in deuterium oxide and methanol was similar.

(2) Polysulphone

Dielectric. The temperature dependence of the dielectric loss tangent for polysulphone is shown in *Figure 2* for a sample containing 0.22% w/w of water at frequencies of 1 and 10 kHz. At the higher temperatures the increase in $\tan \delta$ is indicative of the relaxation process associated with the glass-rubber transition (the α -relaxation). The contour of this peak was not com-

pletely defined because of the temperature limitations of the apparatus. At the lower temperatures a broad relaxation region is observed (the β -relaxation). The amplitude of the peak increases as the temperature and frequency are decreased.

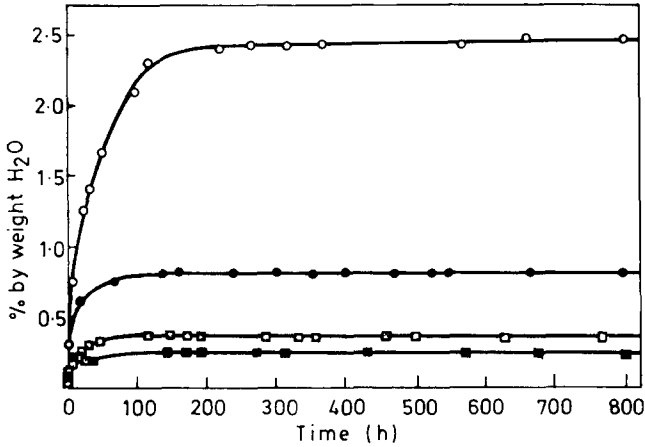


Figure 1 Weight percentage of absorbed water for the indicated polymers as a function of time:

●, polysulphone; □, polycarbonate; ■, PMPO; ○, polysulphone A

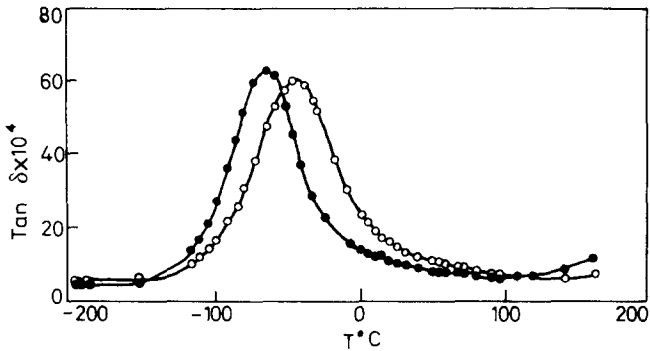


Figure 2 Loss tangent as a function of temperature for polysulphone (H₂O content = 0.22%) ○ 10 kHz ● 1 kHz

Figure 3 illustrates the frequency dependence of the dielectric loss factor in the β -relaxation over the temperature range from -80.5°C to -49.3°C for a sample containing 0.22% of water. As the temperature is lowered the broad peak moves to lower frequencies and increases in amplitude.

Figure 4 illustrates the effect of water content on the amplitude and frequency/temperature behaviour of the β -relaxation. $\text{Tan } \delta$ values are illustrated at 1 and 10 kHz for samples containing up to 0.79% w/w of water. The temperature of the maximum in $\text{tan } \delta$, at a given frequency, is constant until the water content tends to zero. The peak temperatures observed in the wet samples are -66.7°C and -45.5°C for 1 and 10 kHz respectively. The

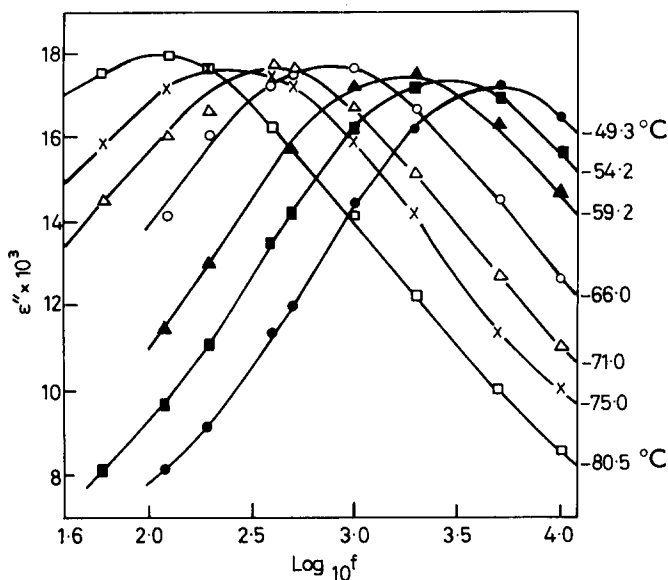


Figure 3 ϵ'' as a function of $\log_{10} f$ for polysulphone at the indicated temperatures (H_2O content = 0.22%)

small amplitude peak temperatures ('dry' samples) are -53.0°C and -38.5°C for 1 and 10 kHz respectively. The behaviour of the sample containing 0.90% w/w of deuterium oxide is similar to that of a sample containing 0.79% w/w of water.

Dynamic-mechanical. The temperature dependence of the mechanical loss tangent is illustrated in Figure 5. Two mechanical absorptions are observed over the accessible experimental temperature range. At the higher temperatures the increase in Q^{-1} is indicative of the glass-rubber transition, T_g . At the lower temperatures the β -relaxation is observed.

The shear modulus decreases with increasing temperature and shows a marked decrease around T_g .

The β -relaxation differs in amplitude for the samples containing 0.073% w/w and 0.31% w/w of water. It was found that the samples could not be maintained in a 'dry' state for the duration of the experiment due to the design of the environmental chamber.

Broad line n.m.r. The variation of the proton line width with temperature for samples of polysulphone is shown in Figure 6. The first sample was 'dry' and the second (denoted 'wet') contained 0.79% w/w of water.

The 'dry' sample shows a large decrease in line width at 210°C . This is associated with the T_g of polysulphone. There is a moderate narrowing of the line width at about -60°C and this effect is slightly more pronounced in the wet sample.

The derivative of the absorption signals obtained for the 'dry' sample are superimposed in Figure 7. The decrease in line width over the experimental temperature range is illustrated. The vertical scale has been changed (from spectrum to spectrum) for convenience in drawing.

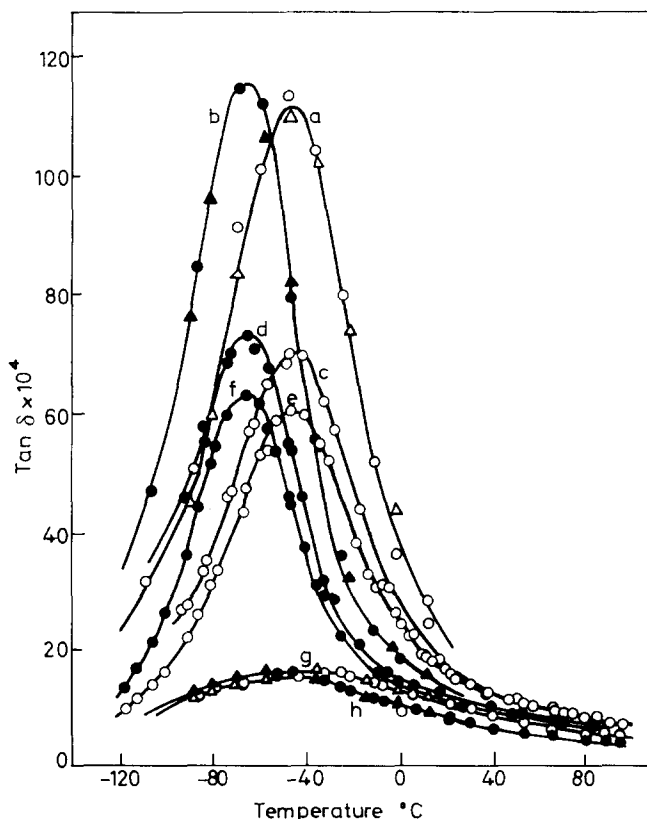


Figure 4 The effect of H₂O and D₂O on the low temperature transition in polysulphone

○ H₂O 10kHz ● H₂O 1kHz
 △ D₂O 10kHz ▲ D₂O 1kHz

(a) } 0.79% H₂O (c) } 0.39% H₂O
 (b) } 0.90% D₂O (d) }
 (e) } 0.22% H₂O (g) } ~0.0% H₂O
 (f) } (h) } ~0.0% D₂O

(3) Polycarbonate

Dielectric. Ishida and Matsuoka² have made an extensive dielectric study on polycarbonate over a wide temperature range, including the α -relaxation associated with T_g . In this work, attention is confined to the β -relaxation.

Figure 8 illustrates the variation of the dielectric loss tangent with temperature in the range from -100°C to 20°C for samples containing $<0.02\%$, 0.20% and 0.37% w/w of water. Measurements were made at 1, 5 and 10 kHz. The broad peak, corresponding to the β -relaxation, moves to lower frequencies and decreases in amplitude as the temperature decreases. Again the temperature of the maximum in $\tan \delta$, at a given frequency, is constant until the water content tends to zero. The peak temperatures observed for 1, 5 and

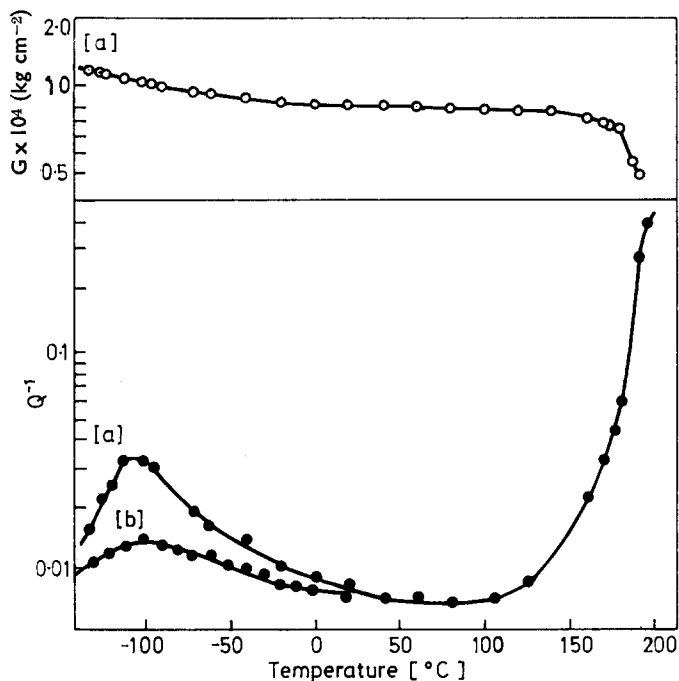


Figure 5 Shear modulus and loss factor as a function of temperature for polysulphone (a) 0.31% H₂O (b) 0.07% H₂O

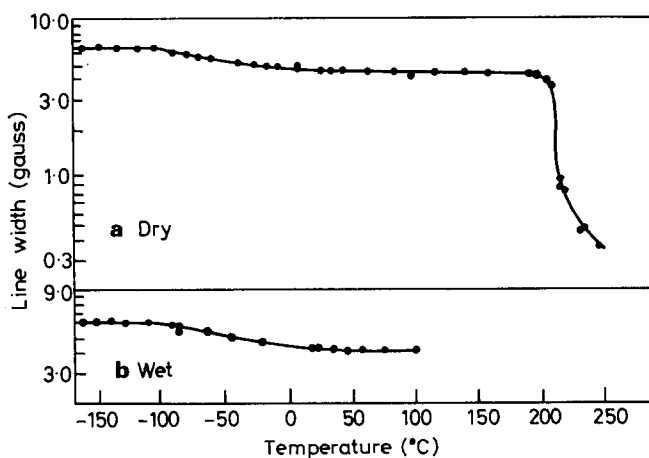


Figure 6 Line width as a function of temperature for dry and wet polysulphone

10 kHz are -62.5°C , -50.0°C and -43.0°C respectively for the wet sample and -71.5°C , -55.6°C and 48.0°C for the dry samples.

Dynamic-mechanical. The temperature dependence of the mechanical loss tangent is illustrated in Figure 9. At the higher temperatures the increase in

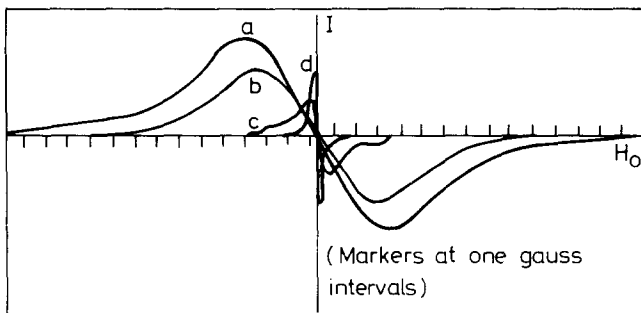


Figure 7 Variation of the derivative of the absorption signal with temperature for polysulphone (dry)
 (a) -162.5°C (c) 215.0°C
 (b) -10.6°C (d) 245.8°C

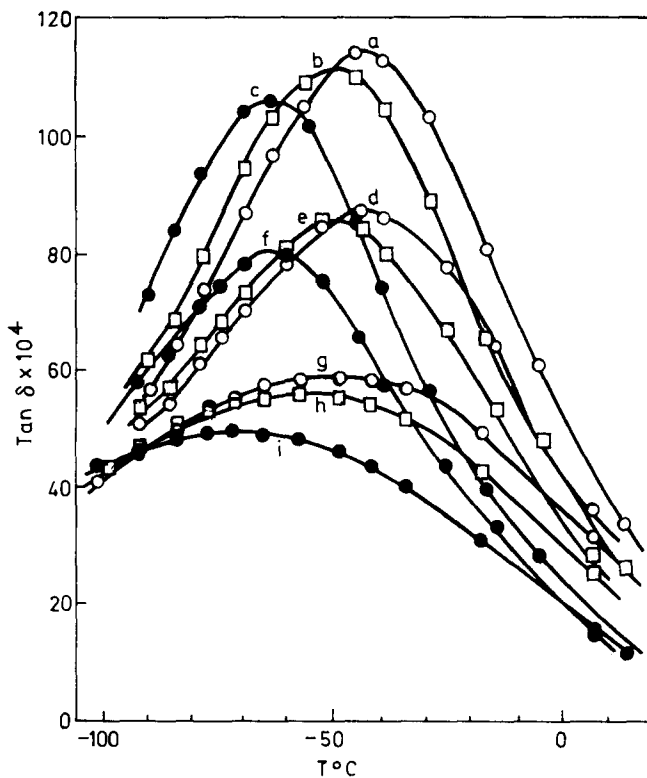


Figure 8 The water dependence of the low temperature transition in polycarbonate

(a), (b), (c) 0.37% H_2O
 (d), (e), (f) 0.20% H_2O
 (g), (h), (i) 0.0% H_2O
 ○ 10 kHz □ 5 kHz ● 1 kHz

Q^{-1} is indicative of the glass-rubber transition and at the lower temperatures the β -relaxation is observed.

As in the case of polysulphone the shear modulus decreases with increasing temperature and shows a marked decrease around T_g . The β -relaxation varies in amplitude depending upon the water content of the samples (increasing as the water content increases).

(4) Poly(2,6-dimethylphenylene oxide)

Dielectric. The temperature and water dependence of the dielectric loss tangent for PMPO is shown in Figure 10. The temperature range covered is from -100°C to 140°C at 1, 5 and 10 kHz for water contents of 0.02%, 0.207% and 0.252% w/w.

At the higher temperatures the increase in $\tan \delta$ is indicative of the relaxation process associated with the glass-rubber transition. The contour of this peak was not completely defined because of the temperature limitations of the apparatus. At the lower temperatures a broad relaxation region is observed and is denoted the β -relaxation. The amplitude and the frequency/temperature behaviour of this peak are dependent upon the water content of the

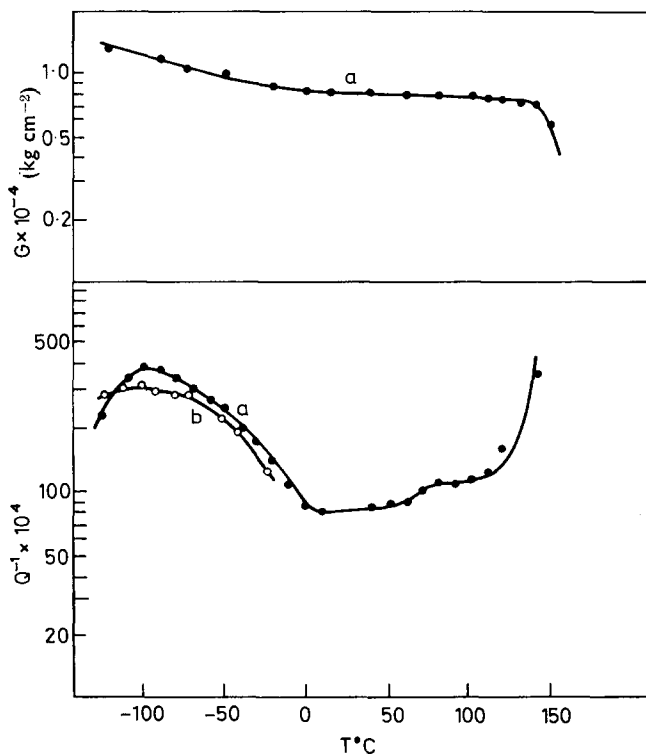


Figure 9 Shear modulus and loss factor as a function of temperature for polycarbonate
(a) 0.37% H_2O (b) 0.15% H_2O

sample. For the 'dry' sample the maxima in $\tan \delta$ occur at -68.0°C , -54.8°C and 148.0°C for 1, 5 and 10kHz respectively. The peak temperatures observed in the samples containing 0.252% water are -85.0°C , -71.5°C and -65.0°C for the frequencies 1, 5 and 10kHz. It is also apparent that as the frequency is lowered the peaks move to lower temperatures and decrease in amplitude. *Figure 10* also illustrates a peak in the temperature range 20 – 100°C . Although of low amplitude this peak is quite pronounced in the wet samples. In the dry sample the effect is much less significant and appears merely as a shoulder on the increase in $\tan \delta$ associated with the T_g .

Dynamic-Mechanical. The temperature dependence of the mechanical loss tangent and its variation with water content are illustrated in *Figure 11*. Only one mechanical absorption is observed over the experimental temperature range. At the higher temperatures the increase in Q^{-1} is indicative of the T_g .

(5) Polysulphone A

Figure 12 illustrates the variation of the dielectric loss tangent with temperature and water content at 1, 10 and 50kHz. The temperature range covered

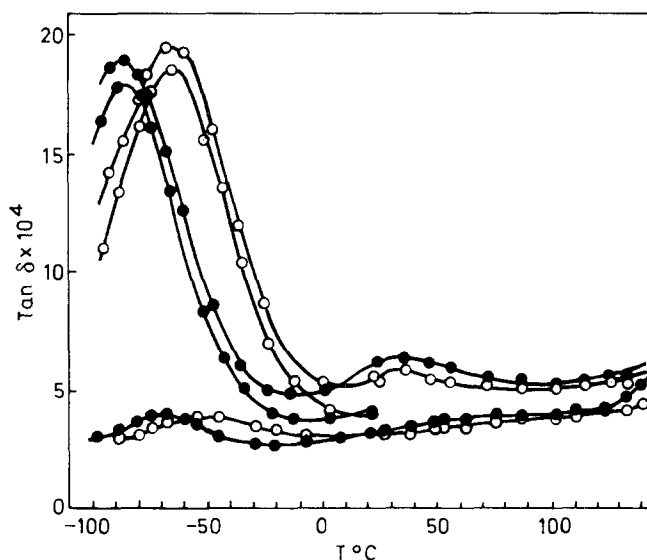


Figure 10 The water dependence of the low temperature transition in poly(2,6-dimethyl-phenylene-oxide)

Top two curves, 0.252% H_2O ; middle two curves, 0.207% H_2O ;
bottom two curves, $\sim 0.0\%$ H_2O
○ 10kHz ● 1kHz

was from -140°C to 160°C (measurements were also made at 5 and 20 kHz).

The increase in $\tan \delta$ at the higher temperatures is indicative of the α -relaxation associated with T_g . As before the contour of this peak was not completely defined because of the temperature limitations of the apparatus. The dry sample shows a broad absorption region amplitude between

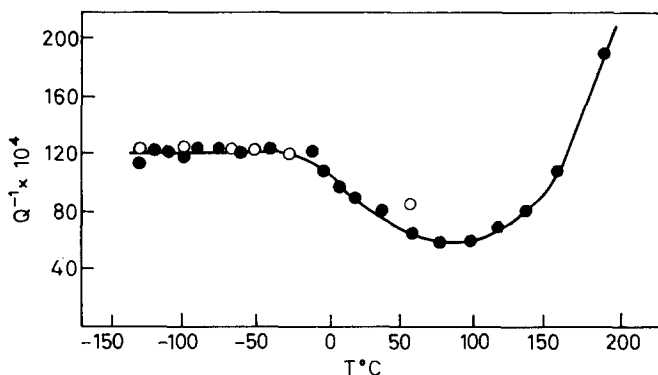


Figure 11 Loss factor as a function of temperature and water content for poly(2,6 dimethyl phenylene oxide)
 ○ 'Dry' ● 0.25% H₂O

−100°C and 20°C. The maxima in $\tan \delta$ occur at −47.0°C, −35.5°C and −26.0°C for 1, 5 and 10 kHz respectively. The sample of intermediate wetness (0.70% w/w of water) shows a stronger absorption at low temperatures. The frequency/temperature behaviour of this sample differs from that of the dry sample. In this case the maxima in $\tan \delta$ occur at −64°C and −42.0°C for 1 and 10 kHz respectively.

The low temperature variation of $\tan \delta$ for samples of maximum wetness (2.48% w/w of water) differs greatly from the above. The curves for these exhibit a large amplitude, narrow peak centred at −95.0°C, −90.0°C, −88.0°C, −81.5°C and −78.5°C at 1, 5, 10, 20 and 50 kHz respectively. A large shoulder appears on the high temperature side of this narrow peak. The frequency/temperature behaviour of this shoulder is significantly the same as that for the sample of intermediate wetness.

DISCUSSION

The α -relaxation

In our work the temperature limitations of the dielectric and mechanical apparatus prohibited the observation of the complete α -relaxation region. It is quite clear, however, from other investigations that this is the glass-rubber transition involving the onset of long-range thermal motions of the main chain.

We were unable to investigate the influence of moisture content on the α -relaxation, despite the fact that this is of interest⁶⁻¹⁸. Jackson¹⁹ for example has suggested that in polyamides⁹ with $T_g \sim 120^\circ\text{C}$ water is not a plasticizer because T_g is above its boiling point. Presumably if this argument is valid it should hold for the four polymers studied in this work.

The β -relaxation

The activation energy for each β -process was calculated from the frequency dependence of the temperature of maximum dielectric loss. In every case the plots were linear and for polysulphone and polycarbonate mechanical

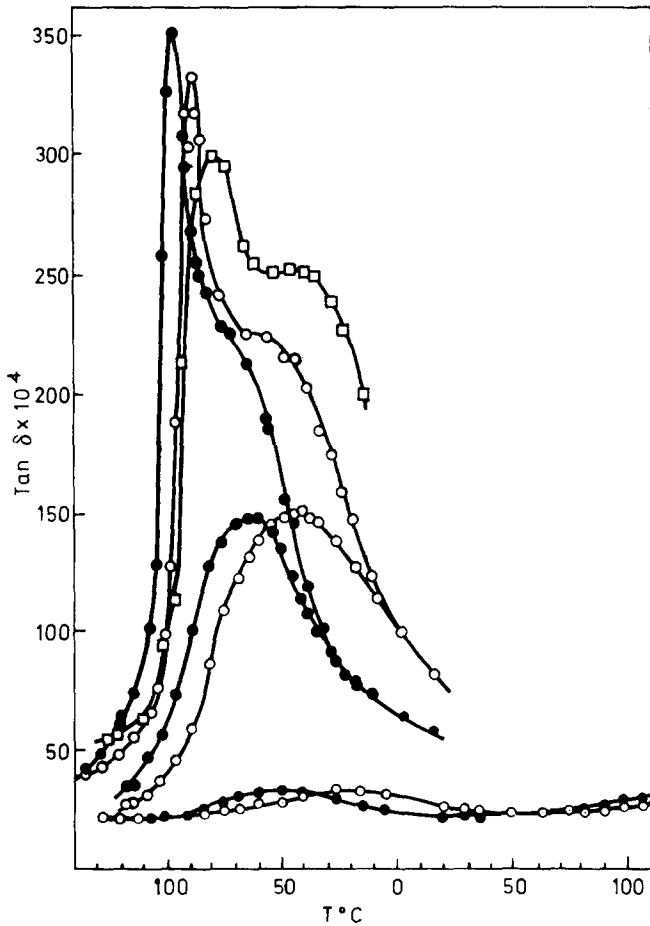


Figure 12 The water dependence of the low temperature transition in polysulphone A.

□ 50kHz ○ 10kHz ● 1kHz
 Top three curves: 2.480% H₂O
 Middle two curves: 0.700% H₂O
 Bottom two curves: 0.202% H₂O

Table 5 The activation energies in kcal/mol for the indicated polymers

Polymer	ΔH^* ('dry')	ΔH^* ('wet')
Polysulphone	16.6	11.2
Polycarbonate	8.7	12.4
PMPO	10.4	9.2
Polysulphone A	13.1	10.2

loss data were also included. The results for 'dry' and 'wet' samples are summarized in *Table 5*.

The behaviour of the β -relaxation peaks show well defined trends with water content of the sample which gives some insight into the origins of these peaks:

- (1) In each polymer the amplitude of the loss peak increases with increasing water content of the sample.
- (2) The temperature of maximum loss in the wet samples is independent of the water content yet it is different from the temperature of maximum loss in the dry sample, which may represent some unmeasurably low water content.
- (3) The activation energy for wet samples is also independent of water content yet the value is substantially different from the activation energy for the dry sample.
- (4) In no case was the temperature of maximum loss or the activation energy identical for wet and dry samples.
There is, however, one important aspect in which polycarbonate differs from the other three polymers, with respect to the influence of moisture:
- (5) The activation energy and temperature of maximum loss is lower for the dry sample than for the wet sample of polycarbonate. For poly-(2,6-dimethylphenylene oxide), for polysulphone and for polysulphone A the reverse holds.

The effect of the increase in the β -relaxation amplitude with water content has been reported in other polar polymers (e.g. polyoxymethylene²⁰, polyethylene terephthalate²¹, various nylons^{6,22,23}, and polymethylmethacrylate²⁴). Previous studies^{2,25,26} of essentially 'dry' polycarbonate have concluded that the weak β -relaxation process is due to a combined motion of the carbonate residue and the phenylene rings. If we assume that in the 'wet' samples the water molecules form hydrogen bonds with the carbonate residue, the polar water molecules would be involved in the molecular process and this could account for the observation that the strength of the loss increases with increasing water content. Further the 'dry' state of the sample could represent a water content so low that hydrogen bonding ceases to be effective and in this state only the polar polymer group contributes to the observed loss.

Similar explanations are plausible for the three other polymers and the plausibility is enhanced by the observation that if the four 'wet' polymers are compared, the strength of the loss is in accord with the relative affinities of the polymers for moisture. For example, the amplitude of the β -peak in PMPO is increased by water to a much lower level than in the other polymers.

Figure 1 shows that for PMPO the equilibrium water absorption is low presumably because the ether linkage is the only hydrogen bonding site available. In the cases of polycarbonate, polysulphone and PMPO it is possible that methyl group motions are responsible for the β -relaxations. This explanation is discounted for three reasons. It is unlikely that a $-\text{CH}_3$ group rotation would give rise to a detectable dielectric loss. Secondly spin lattice n.m.r. relaxation studies on other polymers indicate that methyl group motions relax at much lower temperatures^{2,27}. Furthermore the n.m.r. line width of 6.5 gauss measured for polysulphone between -150 and -100°C indicates that some motional narrowing has already occurred at these temperatures and one can conclude that the narrowing observed at -60°C is more likely to be due to phenyl group motion. Broad line n.m.r. studies on PMPO²⁴ indicate that the methyl groups are already in motion at -180°C .

Another feature of our results which requires comment is item (5) above. If our explanation holds for the influence of water on the relaxation behaviour of all four polymers it is surprising that water should 'plasticize' the β -relaxation in polysulphone, polysulphone A and PMPO and yet act as an 'antiplasticizer' in polycarbonate. A possible explanation is that water absorption 'tightens' the polycarbonate structure, possibly by increasing its density whereas in the other three polymers a less densely packed structure results. A preliminary study of density revealed no detectable trends and a very precise, extensive study of the influence of water on the density of these materials would be required to further this hypothesis.

Finally, it will be seen in *Figure 12* that the β loss in polysulphone A becomes a doublet at water contents in excess of 0.70%. The process at the higher temperature is assigned to the mechanism described above and is observed in all wet samples. The secondary peak which appears at high water content may be related to the presence of unbounded water which may be present in microvoids arising from a rather unsatisfactory sample preparation. The absorption experiments (*Figure 1*) show that this sample absorbed rather more water than might be expected and did not reach equilibrium. The narrowness of the peak suggests that it arises from local aggregates of water molecules in the voids.

CONCLUSION

The dielectric and mechanical loss of polar polymers containing *para* phenylene linkages are affected by the presence of water. The evidence suggests that the absorbed water molecules hydrogen bond to the polar groups in the polymer chain and influence the β -relaxations of these polymers. Water is a 'plasticizer' for the β -relaxation of PMPO, polysulphone and polysulphone A and it is an 'antiplasticizer' for polycarbonate. Polymer samples which we have termed 'dry' were dried for more than 60 hours in vacuum at 120°C . Although these samples were dried to constant weight this does not preclude the possibility that some water molecules still remain in the samples. Certainly the temperature of maximum loss, and activation energy for the β -process differed from those for 'wet' samples but whether or not these residual water

molecules are responsible for the very low amplitude relaxation observed in the 'dry' samples is debatable.

*Department of Chemistry,
University of Manchester, UK*

G. Allen

*I.C.I. Ltd,
Petrochemical and Polymer Laboratory,
The Heath,
Runcorn,
Cheshire, UK*

J. McAinsh

G. M. Jeffs

(Received 26 June, 1970)

REFERENCES

- 1 Baccaredda, M., Butta, E., Frosini, V. and Petris, S. *J. Polym. Sci.*, (A-2) 1967, **5**, 1296
- 2 Matsuoka, S. and Ishida, Y. *J. Polym. Sci.*, (C) 1966, **14**, 247
- 3 Union Carbide Corporation, Dutch Patent 640 8130 (1964)
- 4 American Society for Testing and Materials, Method P2236-67T, Philadelphia (1967)
- 5 Robinson, F.N.H. *J. Sci. Insts.* 1959 **36**, 481
- 6 Illers, K. H. *Die Makromolek. Chemie* 1960, **38**, 168
- 7 Woodward, A. E., Crissman, J. M. and Sauer, J. A. *J. Polym. Sci.* 1960, **44**, 23
- 8 Boyd, R. H. *J. Chem. Phys.* 1959, **30**, 1276
- 9 McLoughlin, J. R. and Tobolsky, A. V. *J. Col. Sci.* 1952, **7**, 555
- 10 Jacobs, J. and Jenckel, E. *Die Makromolek. Chemie* 1961, **47**, 72
- 11 Takayanagi, M. *Mem. Fac. Eng., Kyushu Univ.* 1963, **23**, 1
- 12 Illers, K. H. and Breuer, H. *J. Col. Sci.* 1963, **18**, 1
- 13 Illers, K. H. and Jacobs, H., *Die Makromolek. Chemie* 1960, **39**, 234
- 14 Broens, O. and Müller, F. H. *Kolloid Zeit.* 1955, **140**, 121
- 15 Würstlin, F. *Kolloid Zeit.* 1953, **134**, 135
- 16 Fuoss, R. M. *J. Amer. Chem. Soc.* 1941, **63**, 369
- 17 Würstlin, F. *Kolloid Zeit.* 1943, **105**, 9
- 18 Würstlin, F. *Kolloid Zeit* 1949, **113**, 18
- 19 Jackson, J. B. *Polymer, Lond.* 1969, **10**, 159
- 20 McCrum, N. G. *J. Polym. Sci.* 1961, **54**, 561
- 21 Reddish, W. *Trans. Farad. Soc* 1950, **46**, 459
- 22 Curtis, A. J. *J. Res. Nat. Bur. Stds.* 1961, **65A**, 185
- 23 Baker, W. O. and Yager, W. A. *J. Am. Chem. Soc.* 1942, **64**, 2171
- 24 Gall, W. G. and McCrum, N. G. *J. Polym. Sci.* 1961, **50**, 489
- 25 Nielson, L. E., 'Mechanical Properties of Polymers', Reinhold, New York (1965)
- 26 Illers, K. H., Kilian, H. G. and Kosfeld, R. *Ann. Rev. Phys. Chem.* 1961, **12**, 49
- 27 Mattes, R. and Rochow, E. G., *J. Polym. Sci. (A-2)* 1966, **4**, 375

The effect of hydrostatic pressure on the visco-elastic properties of polymers

P. R. BILLINGHURST and D. TABOR

This paper describes an experimental study of the effect of hydrostatic pressure on the visco-elastic properties of some common thermoplastic polymers, and natural rubber. A torsion pendulum was constructed to operate inside a thick walled cylindrical pressure vessel. The pressure could be varied from atmospheric to 1500 atmospheres and the temperature from -20°C to 120°C . The pressure medium was nitrogen gas but in some cases the polymer specimen was surrounded with a hydrocarbon oil to prevent the nitrogen from coming into contact with the polymer. The results obtained show that the glass transition temperatures of rigid polymers and rubber, are raised with pressure by amounts which vary between 15 and 30°C per thousand atmospheres depending upon the material. The values of this shift, for individual polymers, are in agreement with quasi-theoretical predictions based on the 'Free-Volume' theory of the glass transition temperature; they also agree with experimental studies of a related nature, by other workers. The experiments have also revealed a new phenomenon with PTFE: this polymer is rapidly plasticized by nitrogen at pressures of a few hundred atmospheres.

INTRODUCTION

VISCO-ELASTIC losses, relaxation times and phase changes in thermoplastics and elastomers are generally associated, like the viscosity of liquids, with a free volume; this provides room for appropriate movement of chain segments. It is clear therefore that hydrostatic pressure must play a very direct part in these phenomena and provide some insight into their mechanism. For some reason, no direct studies of this type, apart from those of Zösel¹ have been carried out. This paper describes a study which we began in this field before we were aware of Zösel's work.

FREE VOLUME - THE EFFECT OF PRESSURE

The free volume in the liquid phase has been defined by Doolittle² as 'that space seemingly arising from the total thermal expansion of the liquid without phase change'. It implies that all the increase in volume, on heating goes into an increase in free volume. Other definitions have been discussed by Bondi³ but it is quite adequate for our purpose if in dealing with solid polymers we slightly modify the Doolittle definition and assume that the increase in free volume with temperature is a constant fraction of the total increase in volume of the specimen with temperature.

The free volume is, of course, influenced by pressure as well as by temperature. To derive a relation for the effect of these parameters on the free volume we need two quantities: α_f the coefficient of volume expansion, and β_f the compressibility, of the free volume itself. Then if v_f is the free volume

at temperature T_0 and pressure P_0 , and v'_f the free volume at temperature T and pressure P , we have

$$v'_f = v_f [1 + \alpha_f (T - T_0) - \beta_f (P - P_0)]$$

so that there is no change in free volume, i.e., $v'_f = v_f$ when

$$\frac{T - T_0}{P - P_0} = \beta_f / \alpha_f$$

For any given polymer the glass transition temperature T_g may, as a first approximation, be considered as a position of constant free volume. Thus if (cf. Zösel) α_f and β_f are the values observed as the polymer is taken through the glass transition at atmospheric pressure the shift of T_g with pressure is at once given as

$$\frac{\partial T_g}{\partial P} = \left(\frac{\beta_f}{\alpha_f} \right)_{T_g}$$

Most workers, e.g. Zösel¹, take α_f , β_f to be the changes in expansion and compressibility as the polymer is taken through T_g , at which point, these parameters show marked discontinuities. If these quantities are known it is possible to calculate the change in T_g to be expected and to compare the prediction with direct observation of the effect of pressure on the visco-elastic properties of the polymer.

In our experiments we have determined the variation of shear modulus with temperature at various hydrostatic pressures, and have identified the glass-transition temperature as occurring at the point of inflexion in the modulus-temperature curve. Although this is an arbitrary choice it does not involve serious error.

APPARATUS

The requirements for the design of the apparatus were in principle very simple. The equipment was required to measure the dynamic mechanical properties of polymers and rubbers (1) over a hydrostatic pressure range from atmospheric up to 2000 atmospheres and (2) over a temperature range sufficient to cover the more marked transitions displayed by a number of common polymeric materials.

The main components of the instrument are shown schematically in *Figure 1*. The readings are taken by observing the free vibration of the torsion pendulum system which comprises a tungsten alloy inertia member, a piano wire upon which the weight of the rotor hangs, and the specimen.

A gaseous pressure medium, nitrogen, was chosen to minimize viscous drag, since the annular gap between the curved surface of the rotor and the inside wall of the pressure vessel was required to be kept as small as possible. In addition to this, no suitable liquid appeared to be available which was guaranteed to have no effect on the polymer samples, particularly under the temperatures and pressures to be encountered.

Using a proprietary two stage boosting system we were able to reach a maximum pressure of 1700 atmospheres.

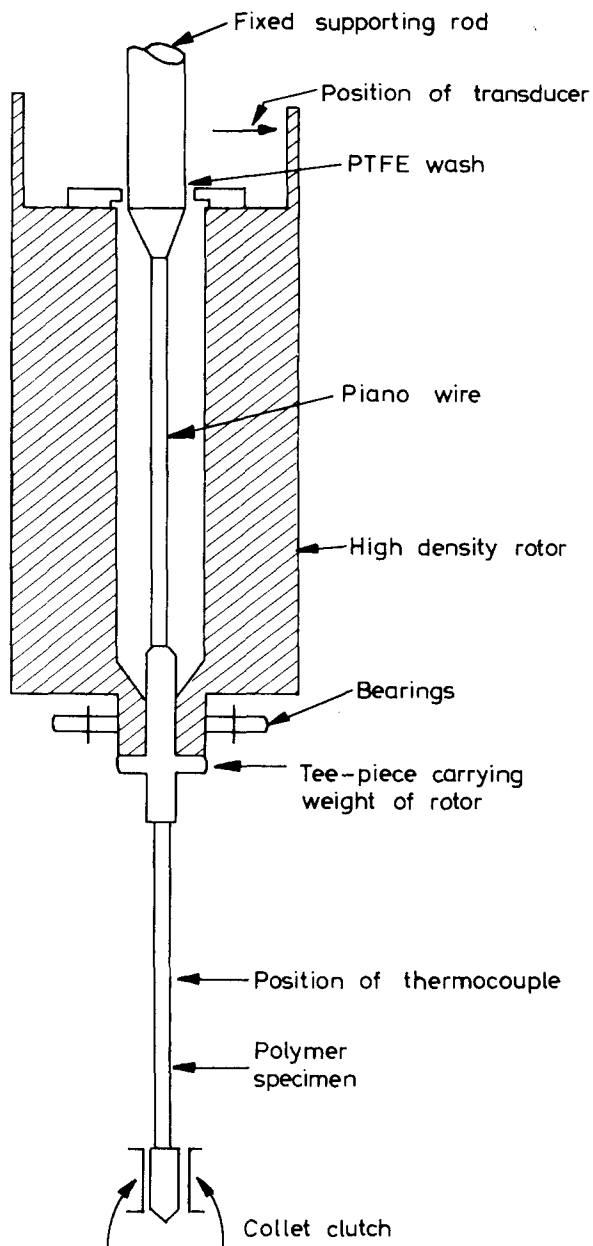


Figure 1 Arrangement of oscillating system

The temperature of the specimen is controlled by having the entire pressure vessel mounted inside a heat exchanger equipped with heating coils, and also a liquid nitrogen cooling coil. A stainless steel sheathed thermocouple is employed to measure the temperature of the polymer itself, and it is placed in close proximity to the specimen.

The interior of the pressure vessel is constructed so that the polymer specimen can be removed very readily, without having to remove the cylinder end caps. This has proved valuable in saving time during experiments. The oscillations of the torsion pendulum are started mechanically by a shaft running through the pressure vessel, with suitable sealing, and the resulting oscillations are observed with a miniature inductive transducer, the positive lead of which is taken out of the high pressure area via a tapered, insulated, plug. The body of the vessel carries the return lead.

Finally, a clutch is employed in the rotating system so that free vibration decay traces can be obtained with or without the polymer specimen being subjected to strain. In the latter case, the torsional stiffness for the system is supplied only by the piano wire. The purpose of this arrangement is to enable an estimate to be made of the extraneous energy losses in the system when calculating the damping due to the specimen alone.

In practice, due to extraneous energy losses we have been unable to measure polymer damping when it is very low. Consequently it has not yet proved possible to study the smaller visco-elastic peaks. However, the apparatus has proved completely satisfactory for a study of the main glass-transition temperatures.

EXPERIMENTAL PROCEDURE

The polymer torsion specimens were all cut from 1/16in sheet, to be approximately 3in long and 3/32in wide. The experiments were performed by allowing the oscillating system to undergo free vibration with, or without, the specimen being subjected to strain. In the former case, the damped sinusoid yielded a certain frequency ($f_{(w+s)}$) and a certain attenuation constant (a_t). In the latter case, the frequency of vibration (f_w) is reduced by comparison with $f_{(w+s)}$ and also the damping will be lower, giving a value for the attenuation constant (a_b).

From the theory of the oscillating system, the rigidity modulus, G , of the polymer is calculated from the equation:—

$$4 \pi^2 I (f_{w+s}^2 - f_w^2) = \frac{JG}{l}$$

where J , the section constant, = $\frac{\mu AB^3}{16}$

A = width of specimen

B = thickness of specimen

μ = shape factor and is a function of A/B

l = length of specimen

I = moment of Inertia of the Rotor

The damping is calculated using the equation:

$$a_{\text{specimen}} = a_{\text{total}} - a_{\text{background}}$$

or

$$a_s = a_t - a_b$$

and

$$a_s = \pi \tan \delta \left(\frac{f_{(w+s)}^2 - f_w^2}{f_{(w+s)}} \right)$$

In most cases, two measurements of damping were calculated: one, $\tan \delta$, being the measurement of the specimen damping at the particular temperature and pressure being investigated and the other, Δ , being the logarithmic decrement ($\ln \theta_n/\theta_{n+1}$) for the case where both the piano wire and specimen are being strained. In practice it was found that both the background damping and the frequency of oscillation, without the specimen, remained substantially unchanged over wide temperature and pressure variations so that standardized values for these two quantities could be used.

As mentioned in the previous section, the equipment was designed so that the specimen could be changed with the minimum amount of disturbance which saved considerable time during experiments. The large thermal inertia of the pressure vessel caused some delay during high temperature runs and so experiments were often programmed to take readings on different samples of polymer once the required temperature had been reached. A certain amount of leakage at high pressures also restricted the length of such tests, but not to any serious extent.

Measurements of the frequency of oscillation, from which the rigidity modulus, G , is calculated were very reproducible; the main error arose from the non-uniformity of the width and thickness of the polymer specimens. The overall error in the absolute value of G is estimated to be of the order of $\pm 8\%$. For this reason no attempt was made to allow for the effect of temperature and pressure on the dimensions of the specimen. Such a correction could contribute not more than an additional error of $\pm 1\%$ to the absolute value of G . For values of the logarithmic decrement greater than 0.2 the reproducibility was about $\pm 5\%$; for values of $\tan \delta$ greater than 0.05 the reproducibility was of the order of $\pm 20\%$. The reliability of these damping measurements diminished as the value for the damping itself became smaller because of the increasingly important part played by the background damping. For this reason, very low damping measurements have not been recorded in the results.

The torsional amplitude was kept as small as was consistent with practical measurements of the decrement. The maximum strain imposed on the specimens was of the order of 1%.

RESULTS

The glass transition region

Preliminary quantitative experiments were performed on a sample of plasticized PVC, an amorphous polymer. The plasticizer in the sample was dioctyl phthalate present as 0.125 volume fraction.

The results for shear modulus and $\tan \delta$ for this polymer are shown in *Figure 2* for two independent tests, one at atmospheric, and the other at 1000 atmospheres. The bottom set of curves gives the corresponding values for the logarithmic decrement. The short vertical line AB at 22°C joining the

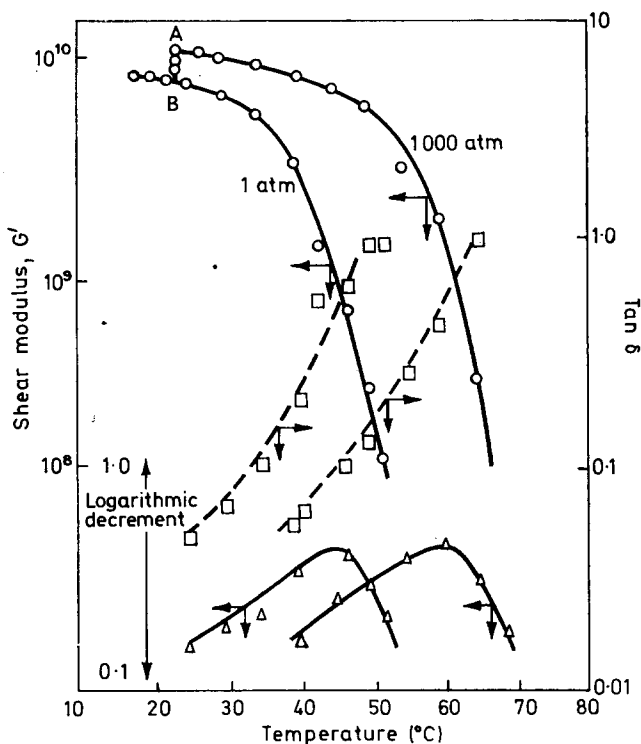


Figure 2 Plasticized PVC, dynamic mechanical properties
 —○— Shear modulus G' , —□— $\tan \delta$, —△— logarithmic decrement

two shear modulus-temperature curves shows the effect of pressure on the modulus at constant temperature. Figure 3 shows the effect on modulus of applying the pressure at P after the polymer has reached the rubbery state. It is seen that an application of 1000 atmospheres at 53°C is sufficient to return the modulus almost to the glassy value (point Q).

Figure 4 shows similar results for a sample of unplasticized PVC. Analysis of detailed results shows that within the range of experimental error, the shift of the glass transition temperature is linear with pressure over the pressure ranges studied. Further, the amount of the shift per 1000 atmospheres is the same as for the plasticized sample. Comparison of Figures 2 and 3 with Figure 4 also shows the well known phenomenon of the broadening of the transition region by the plasticizer.

Similar curves are shown in Figure 5 for a sample of natural rubber. The behaviour at atmospheric pressure was explored over the whole length of the curve, but only selected points were measured at elevated pressures. Nevertheless, the shift appears to be linear with pressure as for PVC, but with a slightly larger value per 1000 atmospheres. Similar tests were also performed on polystyrene, but the samples appeared to suffer from severe penetration by the nitrogen gas. The recorded results also showed that the polymer had undergone a shift in glass transition with pressure of a much smaller amount than would have been expected. The damping of the polymer specimen was

also greatly reduced under pressure. When the pressure was released and the specimen removed its appearance was found to represent more that of expanded polystyrene and so great was this effect that it had concertinad into a shape reminiscent of a helical spring in order to accommodate an increase in length of approximately $1\frac{1}{2}$ times the original.

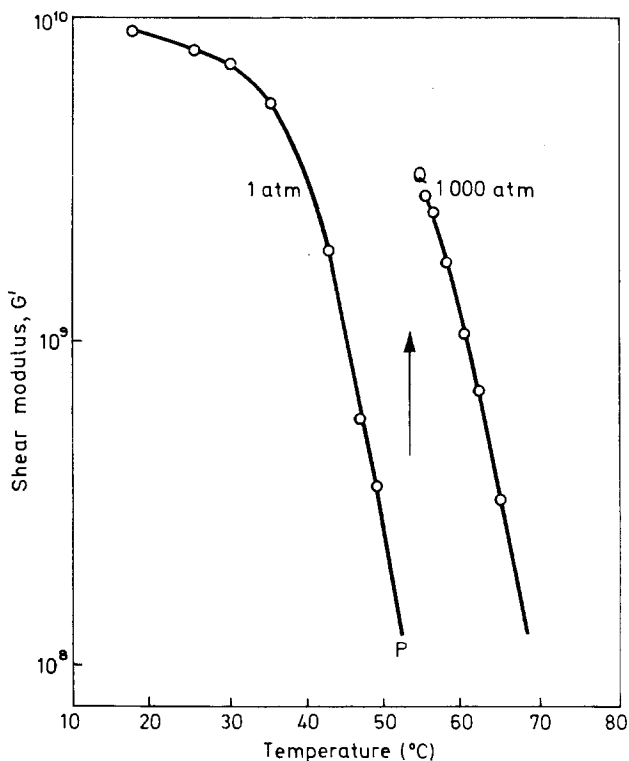


Figure 3 Plasticized PVC; modulus against temperature and pressure

For subsequent tests on polystyrene, therefore, the lower portion of the pressure vessel was filled with hydrocarbon oil of sufficient quantity to cover the specimens. The same precaution was also taken with the PMMA specimens, and with some of the PTFE samples. The presence of the oil appeared to have no effect on the polymers. *Figures 6 and 7* show the results for polystyrene and PMMA performed in this manner.

The phenomenon of gas penetration into the PTFE samples was studied in detail as described below.

Regions remote from the T_g

The glass transition temperature of PTFE is 126°C , which is outside the range of operation of the apparatus. There is however, a marked transition of a different kind which normally occurs at about 19°C . This corresponds to the uncoiling of the chains in the crystal from 13 to 15 CF_2 units per helical

revolution. The effect of pressure on this transition was studied for samples of two different crystallinities. As mentioned above, nitrogen at a few hundred atmospheres of pressure can plasticize the PTFE specimens. For this reason the polymer was immersed in hydrocarbon oil, as with polystyrene and PMMA. As shown in *Figures 8 and 9* this transition is affected by pressure in a

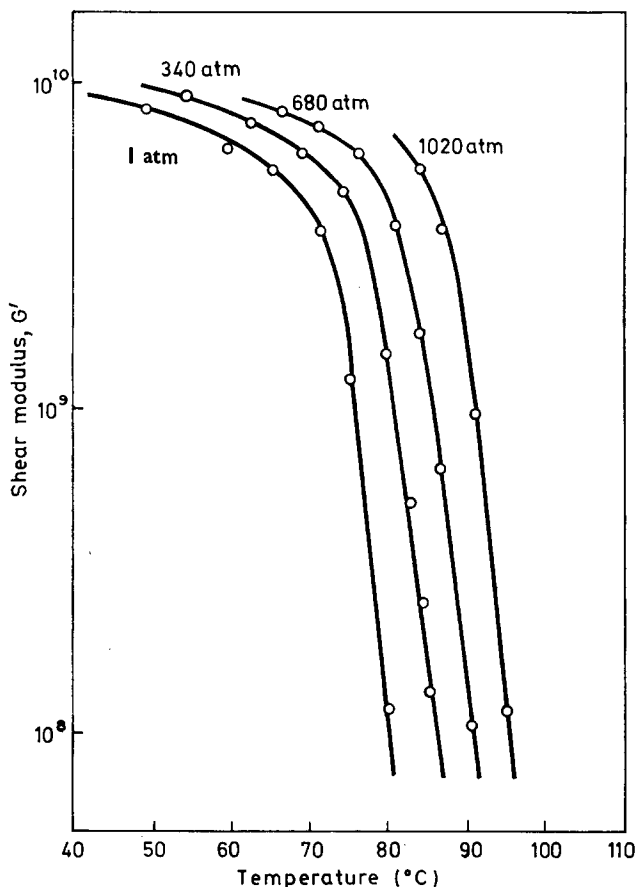


Figure 4 Unplasticized PVC; modulus against temperature and pressure

way which resembles the effect of pressure on the glass transitions of the other polymers. A notable difference, however, is that the modulus/temperature curve is not shifted bodily sideways; the shift varies as the transition is traversed. Comparison of *Figures 8 and 9* shows that the effect of pressure is more marked on the specimen of lower crystallinity. This is discussed later.

Polymethylmethacrylate also exhibits a secondary transition which, at atmospheric pressure, occurs around 40°C. This transition is very weak but its presence is reflected in the form of the modulus/temperature curve in this region. Portion AB in *Figure 10* shows that there is a steeper fall-off in modulus than would normally be expected for an amorphous polymer in

the glassy state. Furthermore, in these portions of the curves the sideways displacement of the curves when pressure is applied is not constant.

Experiments were also carried out on a series of polyethylene samples of varying crystallinity and molecular weight. The effect of pressure on samples of three different crystallinities is shown in *Figure 11*. It is seen that although the

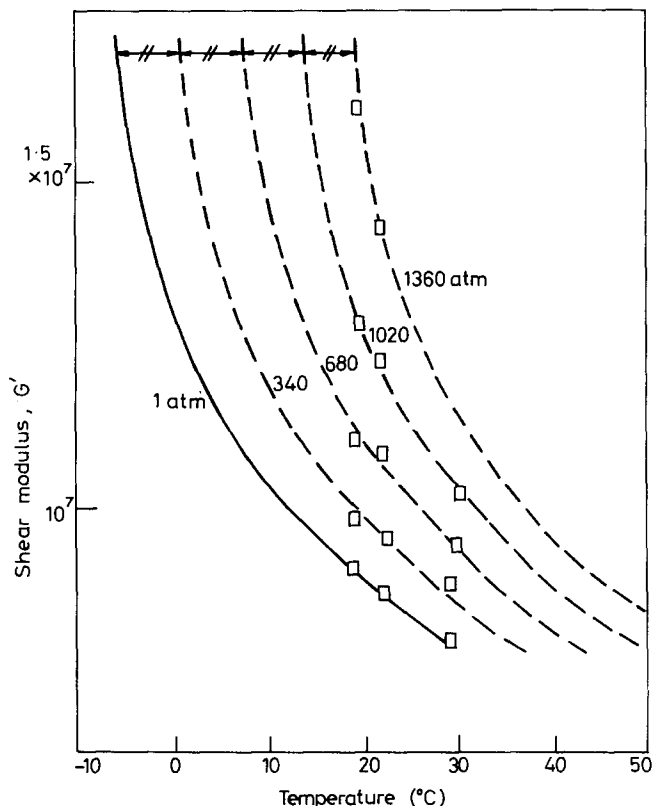


Figure 5 Rubber; modulus against temperature and pressure

absolute values of the modulus depend on crystallinity the horizontal shift produced by pressure is practically independent of crystallinity. Similar experiments show that the shift is also little affected by the molecular weight of the polymer.

Plasticization of PTFE

If the PTFE specimens were not immersed in oil and the nitrogen gas was allowed to come into direct contact with the surface of the polymer a very marked softening of the polymer occurred. The softening or plasticization grew more pronounced with time, the rate being strongly dependent on the sample of polymer used, the temperature of the test and, to a lesser extent, the pressure. The softening is most conveniently shown as a decrease in the shear modulus. Typical results for specimens of 68%, 65% and 60% crystal-

linity are plotted in *Figure 12* as $G'(t)/G'(0)$ vs. time. It is seen that the modulus of the sample of lowest crystallinity falls to as little as 20% of its normal value, under a nitrogen gas pressure of 340 atmospheres at 80°C, after 45 minutes. The specimen possessing 8% more crystallinity behaves in a similar way qualitatively but the effect is very much less marked. It is clear that a small drop in crystallinity produces a very large increase in the rate of softening.

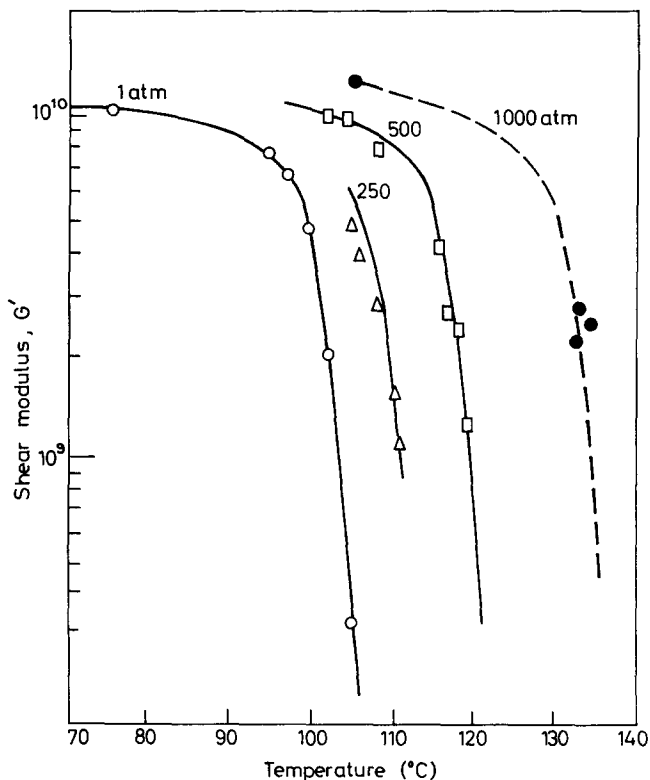


Figure 6 Polystyrene; modulus against temperature and pressure

The small increase in modulus at very short times shown in the curves at 17°C is due to the normal effect of an increase in modulus with pressure: at 80°C however, the plasticization takes place so much more quickly that this initial rise is obscured.

Figure 13 shows the effect of gas pressure on this phenomenon. There are two main points. First the softening is quite marked even at relatively low pressures. The main effect of increasing the gas pressure is to increase the rate at which the softening occurs. Secondly there is, superposed on the softening, an increase in modulus due to pressure itself. This is seen by comparing the results observed at pressures of 510 and 340 atmospheres. The greater initial rise in modulus at 510 atmospheres over-compensates for the increased rate of plasticization at this pressure. Consequently the modulus

after 45 minutes is actually higher than at the lower pressure of 340 atmospheres.

The results in *Figure 14* show that the softening phenomenon does not occur when helium is used as the pressure medium.

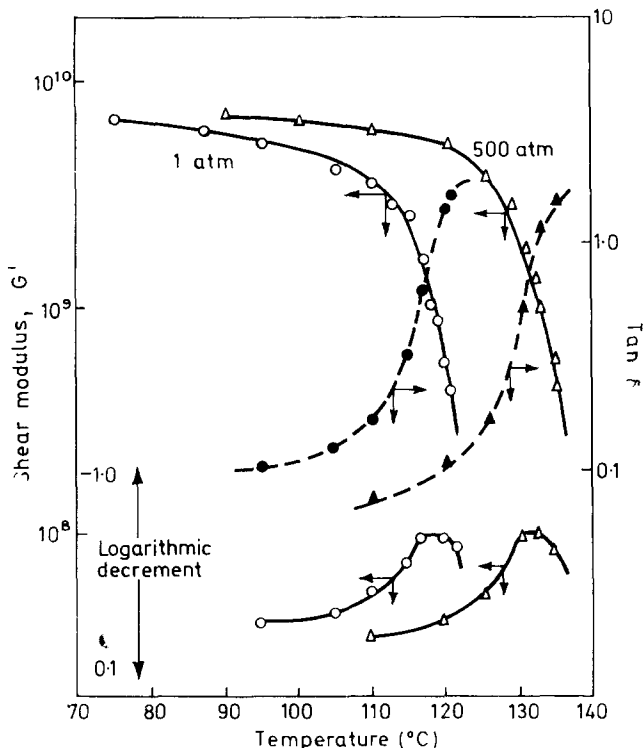


Figure 7 Polymethyl methacrylate, specimen immersed in oil
 Upper curves: continuous lines, shear modulus G' ; broken lines, $\tan \delta$. Lower curves: continuous lines, logarithmic decrement

DISCUSSION

The shift of the glass transition with pressure

The results of this work show that the glass transitions of amorphous thermo-softening polymers are shifted upwards in temperature by the application of an imposed external hydrostatic pressure. The shift varies for individual polymers and the values of the shifts for the polymers studied are in agreement with those of other workers.

	PVC	PS	PMMA
This paper	16	32	29
Zösel	17	—	24
Hellevege	13.5	30	23
$\Delta\beta/\Delta\alpha$	32	61	65

(all values in $^{\circ}\text{C}/1000 \text{ atm}$)

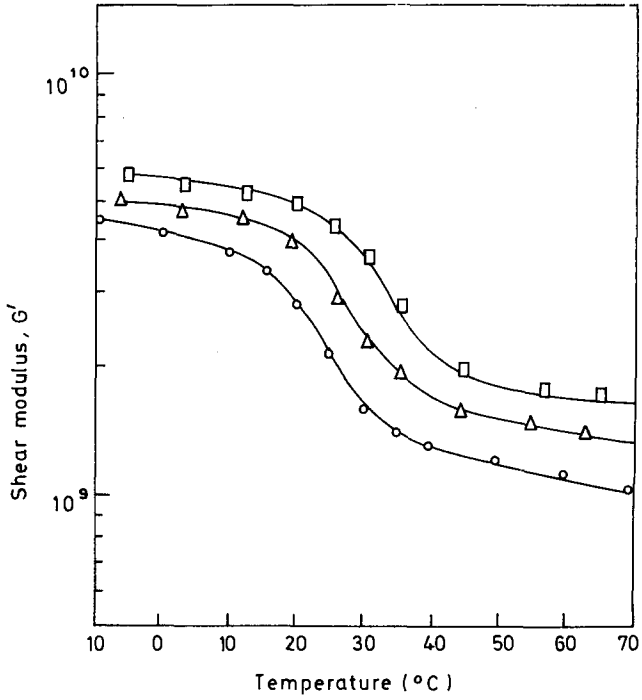


Figure 8 PTFE, specimen immersed in oil, medium crystallinity 65%
 —○— 1 atm, —△— 500 atm, —□— 1000 atm

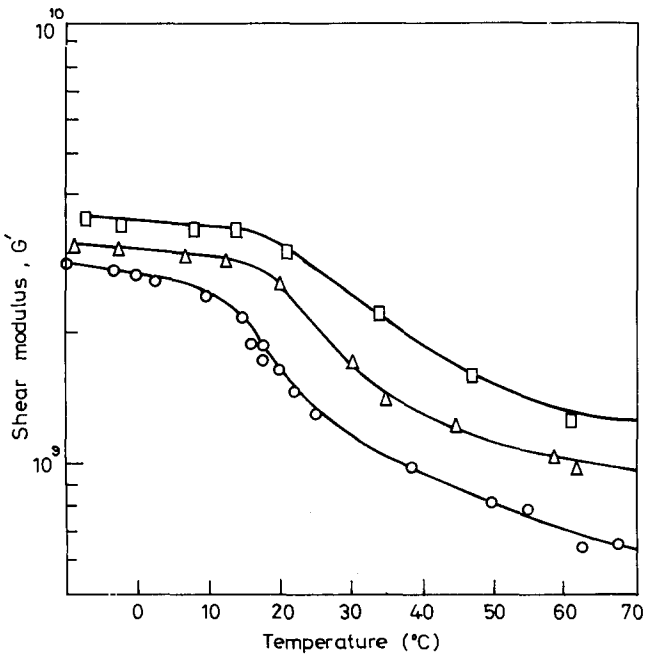


Figure 9 PTFE, specimen immersed in oil, medium crystallinity 54%
 —○— 1 atm, —△— 500 atm, —□— 1000 atm

The table compares the authors' results with those of Zösel¹ who performed similar experiments using a torsion pendulum, while the results of Hellevege⁴ were obtained in dilatometric experiments.

The values for $\Delta\beta/\Delta\alpha$ are quoted from work of Bianchi^{5,6}. Hellevege also gives values for these quantities, which are in fact in much better agreement

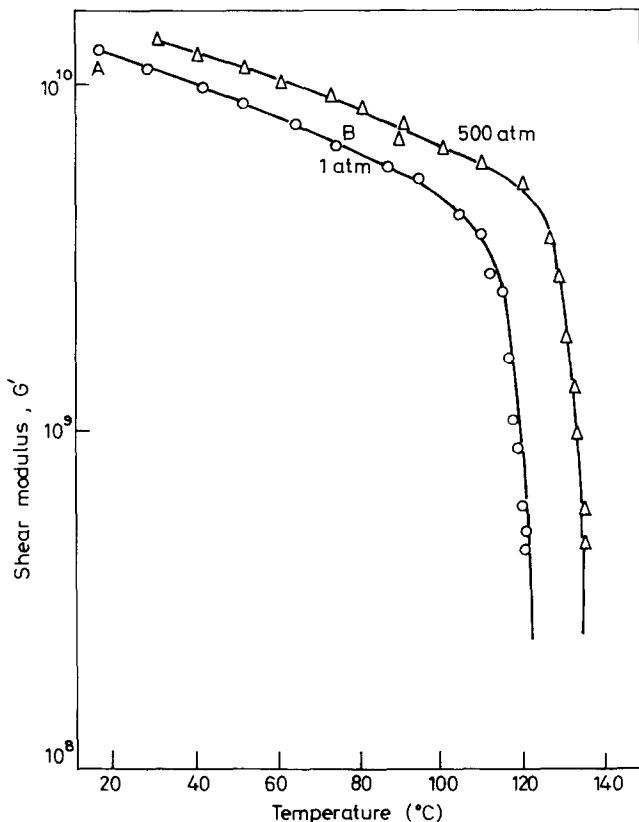


Figure 10 Polymethyl methacrylate, specimen immersed in oil

with the shifts, but are considered by Goldstein⁷ to be inaccurate since the values chosen for the glassy compressibilities are rather high. In fact, since the compressibility of a polymer changes with pressure in the regions surrounding the T_g it is possible to choose suitable values to get $\Delta\beta/\Delta\alpha$ very close to $\partial T_g/\partial P$. Using the present data, however, it is reasonable to investigate the lack of agreement between Bianchi^{5,6} and Hellevege⁴.

Bianchi⁶ raises the point that the value of the temperature shift of the glass-transition under pressure depends on the route taken: that is, upon whether, in the high pressure test, the readings are taken with the temperature increasing or decreasing. He reports, in dilatometric experiments, a maximum possible value of $\partial T_g/\partial P$ of $38^\circ\text{C}/1000$ atmospheres for PVC but this value appears to be obtained from the data by extrapolation and in any case the path taken for this reading is that of increasing temperature; the

same as was used in the authors' own experiments. It seems doubtful whether the lack of agreement between $\partial T_g/\partial P$ and $\Delta\beta/\Delta\alpha$ depends upon inaccuracies in the measurement of the former quantity.

Bianchi explains his results in terms of a densification process such that if the polymer is exposed to pressure while in the rubbery state at a certain

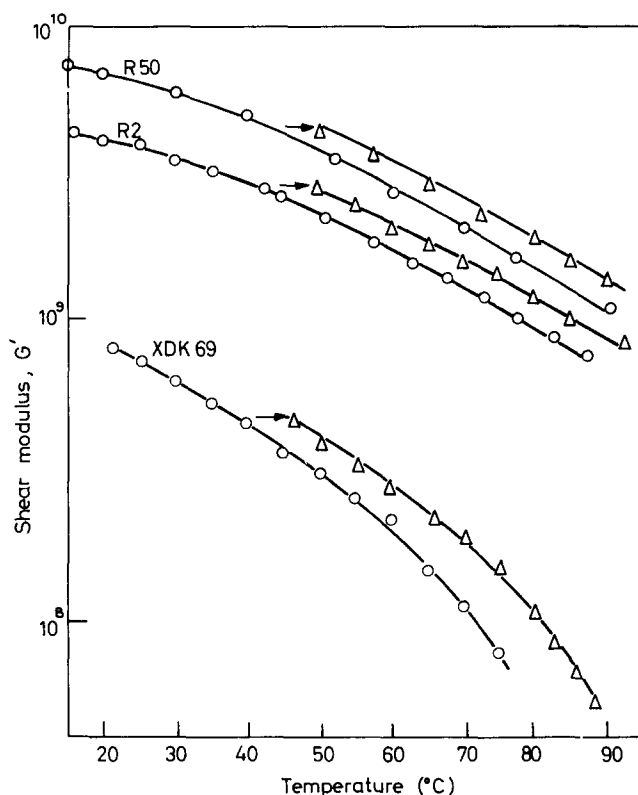


Figure 11 Polyethylene, samples of varying crystallinity

Samples	Density	M.F.I.
Alkathene XDK 69	0.92	0.2
Rigidex 2	0.95	0.2
Rigidex 50	0.96	0.5

—○— 1 atm —△— 500 atm

temperature it will compress to a smaller volume than if it is pressurized below the T_g and then heated to that temperature. If this is the case it is possible to show, very simply, that $\partial T_g/\partial P$ is always less than $\Delta\beta/\Delta\alpha$, but it is difficult to make an estimate of the inequality.

Cross-linked polymers might be expected to show a considerably reduced amount of densification, comparable to their reduced ability to exhibit plastic deformation, when compared with thermo-softening polymers, so that they might, in consequence give closer agreement between $\partial T_g/\partial P$ and $\Delta\beta/\Delta\alpha$. In fact, this better agreement has been obtained by McKinney, Belcher and

Marvin⁸ who, for natural rubber, observed a $\partial T_g/\partial P$ of $24^\circ\text{C}/1000$ atmospheres and $\Delta\beta/\Delta\alpha$ of 27°C while in similar measurements on poly-(vinyl acetate) they found $\Delta\beta/\Delta\alpha$ to be almost twice $\partial T_g/\partial P$.

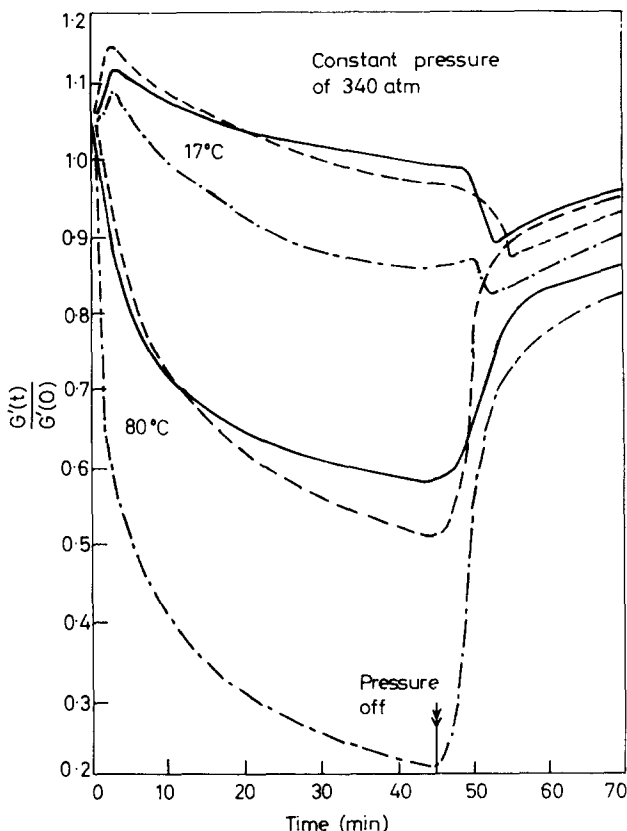


Figure 12 PTFE; plasticization curves.

— 68% crystallinity, - - - 65% crystallinity, - · - · - 60% crystallinity

Temperature shift of secondary transitions

Dealing firstly with PMMA, it is seen that in Figure 10, the modulus/temperature curve over the portion AB falls more steeply than it would if due to thermal softening alone. This is due to the well known secondary transition in this polymer.

Thus we can put an estimate on the effective shift of the secondary transition with pressure by observing the temperature shift at constant modulus in the region, near 20°C , at which this transition occurs. As can be seen in Figure 10, this is of the order of $50^\circ\text{C}/1000$ atmospheres. In our measurements we were unable to observe the damping peak because it was too small. However, Zösel was able to determine the position of the peak and he found a negligible shift with pressure. It is hoped that improvements now being made to our instrument will enable us to resolve this difference.

Figures 8 and 9 show the effect of pressure on the secondary transition in PTFE. As with PMMA, the damping peak due to this transition is both broad

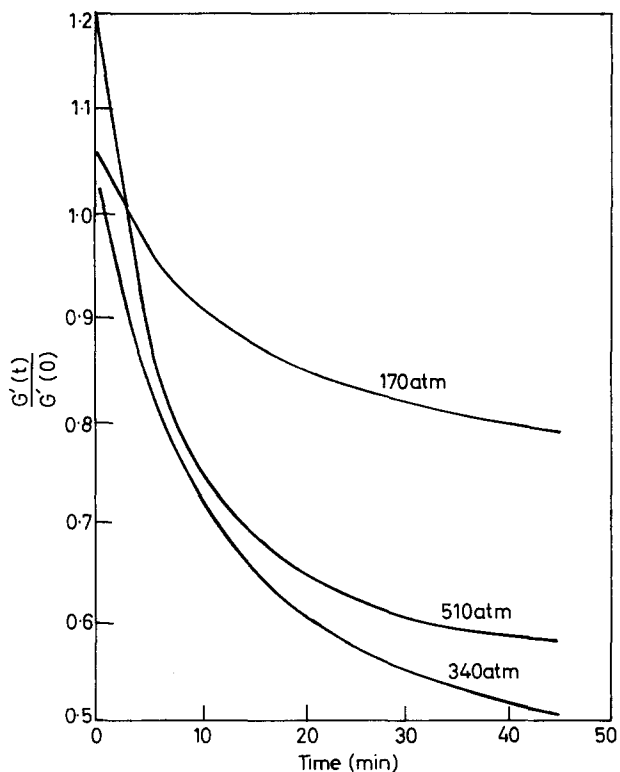


Figure 13 Plasticization-effect of pressure in a medium crystallinity sample of PTFE at constant temperature, $83^{\circ}\text{C} (\pm 3^{\circ}\text{C})$

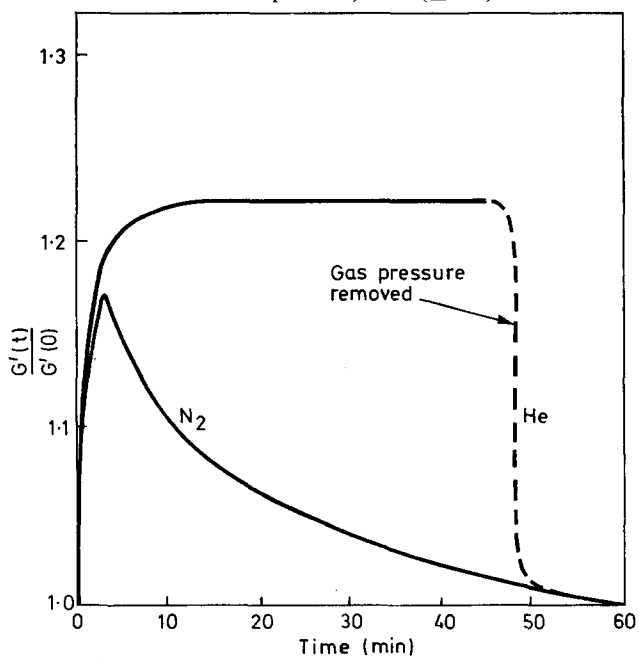


Figure 14 Softening of PTFE, crystallinity 61%: pressure medium helium, 20°C

and low and its position not definable with the present equipment. However, the relatively sharp inflexions of modulus with temperature enable a reasonably accurate estimate to be made of transition temperatures. Comparison with other work suggests that the behaviour is associated with a crystalline transition in which the helix lengthens from 13 to 15 carbon links per turn. The response to pressure and temperature is a consequence of the amorphous-crystalline nature of the specimens. The effect of pressure is to increase the modulus, presumably of the amorphous phase. Indeed, if the modulus is plotted as a function of temperature on a linear scale the results show that there is almost a constant vertical shift of shear modulus with pressure. This is of order 10^9 dyn/cm² ($\pm 30\%$) per 1000 atmospheres for both specimens. On the other hand the pressure restricts the transition in the crystalline phase, causing it to occur at a higher temperature. The curves show that a pressure of 1000 atmospheres shifts the transition by 14 to 20°C depending on crystallinity. These figures agree well with those of other workers for example Yasuda and Araki⁹ and Weir¹⁰.

It is appropriate to deal here with the polyethylene results since the polymer is in a semi-crystalline state and the results bear some resemblance to those for PTFE. In general, the various samples give horizontal shifts of 15°C/1000 atmospheres, but for the lowest crystallinity sample the shift is greatly increased at higher temperatures. This is considered to be due to the onset of melting, and the corresponding effect of pressure on the melting point. Maxwell and Matsuoka¹¹ have performed tests on this effect and for a typical sample the melting temperature is raised by 30°C/1000 atmospheres. Thus the effect is quite pronounced and at temperatures near the melting point would swamp the pressure effect on the amorphous regions. Consequently in this temperature range, no differences are apparent between samples of varying crystallinity.

The plasticization of PTFE by high pressure nitrogen gas

The plasticization of PTFE by nitrogen gas was completely different in nature from that observed on polystyrene. The results suggest that the gas is able to penetrate between the individual grains from which the sintered polymer specimen is prepared. The gas then diffuses into the grains and plasticizes them.

Further experimentation is being carried out to determine more exactly the nature of this effect, but because of the specificity of the gas it would appear to be a solubility effect. Nitrogen is very much more soluble in fluorinated hydrocarbons than, for instance, helium.

ACKNOWLEDGEMENTS

We wish to express our thanks to the Science Research Council for a research grant and to the Ministry of Technology for financial support; to Mr P. W. Turner and Mr C. King, of the Cambridge University Engineering Department, for their help in designing the apparatus, and to Dr P. B. Bowden, Dr G. R. Davies and Mr E. Jones Parry for their helpful discussions.

*Surface Physics,
Cavendish Laboratory,
Cambridge, CB2 3RQ, UK*

(Received 3 August 1970)

REFERENCES

- 1 Zösel, A. *Kolloid-Zeit* 1964, **199**, 113
- 2 Doolittle, A. K. *J. Appl. Phys.* 1951, **22**, 1471
- 3 Bondi, A. *J. Phys. Chem.* 1954, **58**, 929
- 4 Hellevege, K. H., Knappe, W. and Lehman, P. *Kolloid-Zeit* 1963, **183**, 110
- 5 Bianchi, U. *J. Phys. Chem.* 1965, **69**, 1497
- 6 Bianchi, U. *J. Phys. Chem.* 1967, **71**, 3555
- 7 Goldstein, M., 'Modern aspects of the vitreous state', (ed. Mackenzie, J. D.), Butterworths, London, 1964
- 8 McKinney, J., Belcher, H. and Marvin, R. S. *Trans. Rheo. Soc.* 1960, **4**, 347
- 9 Yasida, T. and Araki, Y. *J. Appl. Poly. Soc.* 1961, **5**, 331
- 10 Weir, C. E. *J. Res. Nat. Bur. Stan.* 1953, **50**, 95
- 11 Maxwell, B. and Matsuoka, S. *J. Polym. Sci.* 1958, **32**, 131

Reactivity and mechanism in the cationic polymerization of isobutyl vinyl ether

C. E. H. BAWN, C. FITZSIMMONS, A. LEDWITH, J. PENFOLD,
D. C. SHERRINGTON, and J. A. WEIGHTMAN

The cationic polymerization of *isobutyl vinyl ether* initiated by triphenyl methyl and tropylium hexachloroantimonates, and by triphenyl methyl tetrafluoroborate, has been studied in detail. Initiation was rapid and complete, termination was shown to be insignificant, polymerization half lives were of the order of 5–10 s and reaction rates were measured by an adiabatic calorimetric technique. Catalyst concentrations employed were sufficiently low that essentially complete dissociation into free ions is indicated by ion-pair dissociation constants, and this permits estimation of the rate coefficient for propagation by free cations (k_p). At 0°C in methylene dichloride $k_p \sim 5 \times 10^3 \text{ M}^{-1} \text{ s}^{-1}$, in substantial agreement with values obtained by radiation induced polymerization of bulk monomer. Molecular weights of the poly(*isobutyl vinyl ether*) samples fell in the range 2000–5000 on account of monomer transfer processes. Detailed mechanisms for initiation, propagation, transfer and termination reactions are considered.

ALKYL VINYL ETHERS have long been known to polymerize readily under the influence of Lewis acids and protic acids^{1,2}. Polymerizations initiated by iodine^{3–5} or boron trifluoride solvates^{6–11} have been most commonly used for kinetic studies and there is considerable variation in reported values for absolute reactivity in these systems^{2,12}. Most of the difficulties encountered in analysing kinetic data arise from ambiguity as to the nature and rate of formation of active catalyst species. In addition recent work has shown¹⁴ that steric strain in the ground states of alkyl vinyl ethers causes apparent inconsistencies in reactivity sequences, and this factor could be equally important in determining some of the reported solvent and structural effects on polymerization reactivity.

At the start of this research programme it seemed clear that a real understanding of absolute reactivity in cationic polymerization would result only if the nature and concentration of propagating units were easily determined or were known unambiguously from the components of reaction systems. The most obvious way of initiating cationic polymerization is to use a preformed, stable carbonium salt and, given that the latter reacts rapidly and completely with polymerizable olefin, then a quantitative estimate of the initial number of active sites is available. Furthermore, if termination can be shown to be kinetically unimportant, then this technique gives an estimate of propagation rate coefficients directly. Stable carbonium ion salts such as triphenyl methyl and tropylium derivatives were found^{15–17} to be very efficient initiators for reactive olefins, such as *isobutyl vinyl ether* and N-vinylcarbazole, and detailed kinetic studies have now been completed. Many years ago triphenyl methyl cation, formed *in situ* by dissociation of triphenyl methyl chloride,

had been shown¹⁸ to initiate polymerization of 2-ethyl-hexyl vinyl ether in *m*-cresol but the complexities of ionization-dissociation equilibria precluded evaluation of absolute rate coefficients.

In the present work it was found most convenient to use carbonium ions in the form of hexachloroantimonate salts (e.g. $\text{Ph}_3\text{C}^+\text{SbCl}_6^-$, $\text{C}_7\text{H}_7^+\text{SbCl}_6^-$) providing well characterized and thermally stable initiating systems¹⁷.

A proper analysis of any ionic polymerization must take account of ion pair dissociation equilibria for both initiating and propagating intermediates^{12,19,20}. Data for the initiating systems used in this work has been obtained experimentally^{17,21,22} and permits the conclusion that free cations are the dominant reacting species.

Reaction rates were measured by an adiabatic calorimetric technique originally devised by Plesch and Biddulph²³. However, it should be noted that reproducibility of reaction rates was obtained only by following the laborious, but rigorous, solvent and monomer drying procedures, described in the experimental section.

EXPERIMENTAL

Materials

Methylene chloride (5 litre) was stirred for two hours with concentrated sulphuric acid (100ml/l) to remove unsaturated compounds. The solvent was decanted from the acidic lower layer and washed with water ($3 \times 250\text{ml}$), 5% sodium bicarbonate solution (300 ml) and once again with water ($2 \times 250\text{ml}$). At each stage the acidity was checked, and after all the washings, was found to be the same as that of deionized water. After bulk drying overnight using anhydrous calcium chloride the solvent was refluxed for 24 hours over freshly crushed calcium hydride and then fractionated. A middle fraction of ~ 3 litre was collected (b.p. 40.0°C at 760mmHg). This was further refluxed over calcium hydride for 12 hours before being poured into a 3 litre storage vessel containing freshly crushed calcium hydride and a magnetic stirrer. The flask was closed with a greased stopper and mercury seal and the methylene dichloride degassed. By means of a condenser the solvent could be made to reflux or distil into a 100ml burette. From this, known volumes could be run through a Biddulph-Plesch metal tap into a 'scavenge' vessel containing triphenylmethyl hexachloroantimonate. The purified solvent was then distilled into the required reaction vessel. *Isobutyl vinyl ether* (IBVE) (Eastman Kodak Limited) was washed with water ($5 \times 100\text{ml}$) the pH of which had been adjusted so that it was just alkaline to litmus. After standing over potassium hydroxide pellets for 24 hours and then over a repeat, fresh sample for a further 12 hours it was fractionally distilled. A middle fraction (250ml) was collected (b.p. 83.0°C at 766mmHg). This was then left for 12 hours over calcium chloride (25g) which had previously been heated to 150°C for 4 hours under vacuum. The solution was filtered then refluxed with barium oxide, in a flask constructed with a break-seal in a side arm and a constricted neck. After refluxing for 12 hours the condenser was removed and an air tight stopper fitted in its place. The flask was cooled in liquid nitrogen and sealed off at the constriction. It was then glass-blown onto the vacuum

line and the vinyl ether distilled via the break-seal into a storage flask containing fresh barium oxide. The original flask was then sealed off and discarded. To prevent contamination from grease a Biddulph-Plesch metal tap was used.

Triphenyl methyl hexachloroantimonate. This was prepared as described previously²⁴. Final purification was effected by recrystallization from hot methylene dichloride to give orange-yellow crystals (96% yield) of $\text{Ph}_3\text{C}^+\text{SbCl}_6^-$, m.p. $230^\circ\text{C}(\text{d})$. Required C, 39.50, H, 2.62; found, C, 39.87, H, 2.63.

Tropylium hexachloroantimonate. This was prepared as described previously²⁴ and purified by dissolving in hot methylene dichloride, followed by cooling in ice with addition of carbon tetrachloride to precipitate white crystalline $\text{C}_7\text{H}_7^+\text{SbCl}_6^-$, m.p. $284^\circ\text{C}(\text{d})$ (84% yield) Required, C, 19.74, H, 1.66; Found, C, 19.98, H, 1.70. The product was stored *in vacuo*.

Adiabatic calorimeter

The vessel was based on an early design described by Biddulph and Plesch²³ and consisted of two parts (*Figure 1*). Both of these employed large ground flanges (QQ, FG 75), the lower half being in the form of a double wall vessel, which could be evacuated when required to minimize heat exchanges with the atmosphere. The top section was fitted with a stirrer system, S, a glass phial breaking arrangement, B, operated magnetically and a platinum resistance thermometer, P, along with its compensator in a glass sheath (not shown in diagram). Taps T_1 and T_2 enabled the vessel to be evacuated and solvent and monomer to be distilled in. The stirrer was driven by a powerful electric motor and was mounted in two Teflon bearings, TB, for smooth stirring at high speeds, during kinetic runs. The resistance thermometer was wound on a glass former using 0.08 mm platinum wire, resistance ~ 14 ohm at room temperature. The thermometer leads and compensator were made from 0.3 mm platinum wire welded to tungsten terminals, and were identical.

Phials of initiator solution were held in position in the phial holder by means of movable glass ring wedges, and it was possible to hold two phials simultaneously. By means of magnetic stops S_1 and S_2 it was possible to break the two phials separately, when required. The temperature measuring circuit consisted of a Wheatstone Bridge with a Sefram Gravispot recorder (Type GRVAC), used in place of a simple galvanometer to record off balance potentials arising from changes in the resistance of the platinum wire in the calorimeter. (The recorder trace was calibrated in ohm by changing one of the resistances in the bridge circuit by 0.1Ω and noting the rise on the recorder). Determination of the resistance of the thermometer at the freezing points of the pure solvents, benzene, water, carbon tetrachloride, acetonitrile and chloroform allowed calibration of the temperature coefficient of the platinum wire, over the range $+10$ to -60°C . The compensator resistance (r), was measured over the temperature range $+20$ to -80°C . H , the total heat capacity of the vessel and contents, as used in a kinetic run, was determined over the temperature range $+25$ to -55°C , by using the resistance wire both as a temperature measuring device and an electrical heating element. A measured electrical energy input was supplied by two 2 volt accumulators,

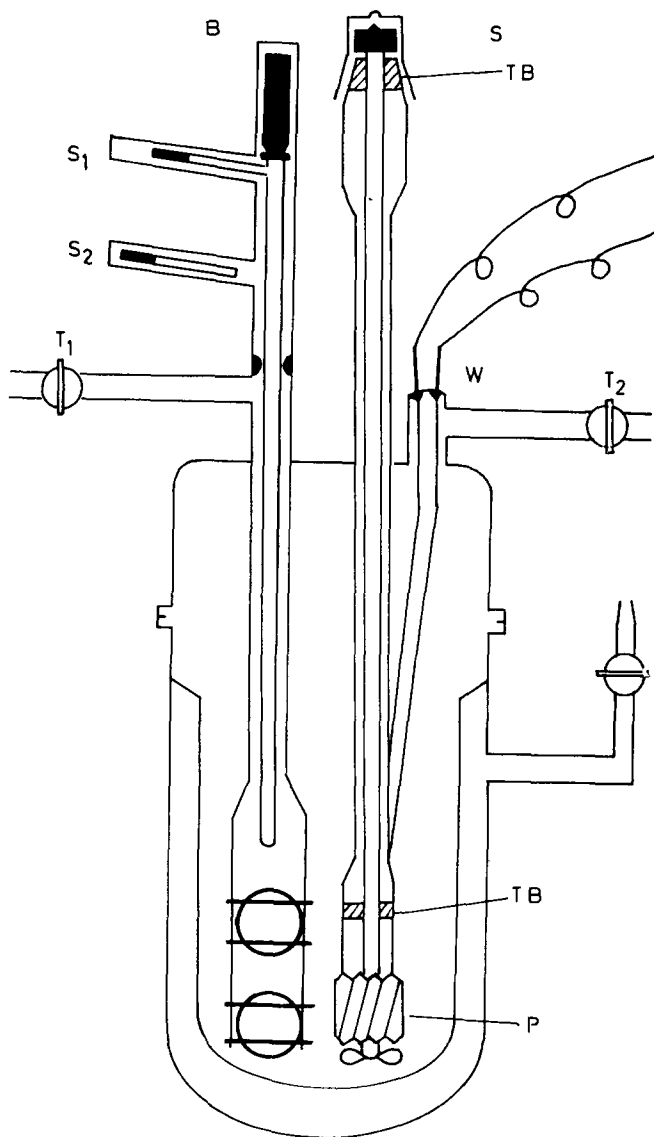


Figure 1 Adiabatic calorimeter for polymerization rate measurements

the actual potential applied being recorded across a 1:11 potential divider (Test Equipment Repair Company Ltd), using a sensitive potentiometer (Tinsley Company Limited, Type 4025). A temperature rise of $\sim 1.5^{\circ}\text{C}$ was obtained over a period of 8 min.

It was found necessary to make corrections due to heat losses in spite of the calorimeter vacuum jacket. H was determined as follows:

- if T is the total temperature rise ($^{\circ}\text{C}$) allowing for heat losses
 t , the duration of heating (s),
 E , the average E.M.F. (volt) recorded on the potentiometer during time, t ,
 n , the ratio of the potential divider,
 R , the mean resistance (ohm) of the platinum wire during time, t ,
 r , the compensator leads resistance (ohm),
 V , the average E.M.F. (volt) across the platinum resistance wire only
 J , the joules/calories conversion factor,

then from Ohm's Law, the power input is given by n^2V^2/R . It can readily be shown that $V = ER/R + r$, so that the power input becomes $E^2R/(R + r)^2$. The total energy input is therefore $E^2Rt/(R + r)^2J \text{ cal} = HT$.

Thus

$$H = E^2Rt/(R + r)^2JT \text{ cal deg}^{-1}$$

The temperature at which a heat capacity was determined was taken as the mean temperature over the time, t , i.e. the temperature corresponding to the resistance, R .

Procedure for a kinetic run

Initiator phials were first prepared under vacuum. These consisted of thin glass bubbles blown from 4mm tubing, and were filled with known volumes (0.25 – 2.00ml) of a methylene dichloride solution of initiator using a vacuum burette arrangement. At the start of a run an initiator phial was placed in the lower position in the phial holder and a vacuum tight seal made between the two halves of the calorimeter, using a 'worm' of Apiezon Q compound, previously extruded from a sodium press. The whole calorimeter was then evacuated at 10^{-6} mmHg for 3 hours; isolated from the pumps and solvent and monomer distilled in. It was arranged that the total volume of liquid in the calorimeter was always 100ml. The Bridge circuit was connected, the reaction mixture stirred, and the whole calorimeter kept at constant temperature by means of a large Dewar containing cooled methanol. When a steady recorder trace was obtained at the required temperature, the outer jacket of the calorimeter was evacuated and the phial breaker released by drawing back both magnetic stops. The recorder trace rose sharply and levelled out again giving a steady reading corresponding to complete polymerization. The recorder chart was immediately calibrated by changing one of the bridge resistances by 0.1Ω and noting the rise. The Bridge circuit was then broken, the stirrer stopped, and air admitted to the outer jacket and calorimeter proper. A razor blade was used to break the Q compound seal and the reaction mixture quenched by addition of methanol (2ml).

The calorimeter and its contents were washed with methylene dichloride to remove traces of polymer and the washings added to the polymerization solution. All solvent was removed on a water pump and the tacky polymer dissolved in a minimum volume of benzene. This solution was filtered into a weighed flask, freeze-dried and the yield of polymer determined. Molecular

weights of samples were always low and were conveniently determined on a Mechrolab vapour pressure osmometer.

Successive polymerization technique

If no termination occurs then addition of more monomer should result in further polymerization and heat evolution. To test this idea the calorimeter was set up with an initiator phial in the upper position in the phial holder and a phial of monomer in the lower position. The normal kinetic procedure was then followed until the breaker was released. This time the initiator phial only was first broken by drawing back stop S_1 leaving S_2 in position. When polymerization was almost complete the monomer phial was broken by releasing the breaker again, this time with both stops S_1 and S_2 withdrawn. The normal procedure was then adopted for the isolation and molecular weight determination of the polymer.

RESULTS

Calibration of calorimeter

The resistance of the platinum resistance thermometer, R_T , at a series of known temperatures, T , is listed in *Table 1*. A plot of R_T against T gives a straight line the gradient of which is the temperature coefficient of resistance.

Table 1 Resistance of platinum wire thermometer

<i>Solvent</i>	<i>Temperature</i> (T°C)	<i>Resistance</i> R_T (ohm)
C_6H_6	+5.53	14.392
H_2O	0.00	14.099
CCl_4	-22.80	12.848
CH_3CN	-43.72	11.690
$CHCl_3$	-63.55	10.608

Temperature coefficient of resistance (θ) = 0.0527 ohm deg⁻¹

The resistance of the compensator leads at various temperatures is shown in *Table 2*. From a straight line plot of these values the corresponding resistance at other temperatures could readily be obtained.

The total heat capacity, H , of the calorimeter and contents, as set up for a kinetic run, over a range of temperatures, T , is shown in *Table 3*. From a least mean squares calculation a best straight line plot of H against T was constructed giving values of $H = 69.5$ cal deg⁻¹ at 0°C and 66.4 cal deg⁻¹ at -25°C.

It was observed that a small temperature rise occurred when the phial breaker was operated under the conditions of a kinetic run even when no initiator was present in the phial. This rise was recorded at -25°C and 0°C and corresponding allowances made in the calculations. At 0°C the total rise was 0.133°C and at -25°C, 0.290°C.

Polymerization of isobutyl vinyl ether (IBVE)

On account of the exothermicity of polymerization of IBVE and the very rapid reaction rates obtained using $\text{Ph}_3\text{C}^+\text{SbCl}_6^-$ and $\text{C}_7\text{H}_7^+\text{SbCl}_6^-$ as initiators it was necessary to work in the concentration ranges 3.5 – 12 ($\times 10^{-2}$) M for [IBVE] and 2.5 – 11.0 ($\times 10^{-5}$)M for the catalysts, [Co].

A typical recorder trace was similar in shape to that of the log plot (Figure 2) and gave some evidence for a relatively 'slow' initiation reaction followed by rapid propagation. Introduction of a second sample of monomer after *ca* 90% conversion of the first sample showed that the initial 'slow' reaction was now absent and the estimated rates (see below) of first and second polymerizations were almost identical, providing clear evidence for the absence of a significant termination process during the kinetic lifetimes.

Table 2 Resistance of compensator circuit

Temperature (°C)	Resistance <i>r</i> (ohms)
+3.5	0.430
-23.0	0.425
-45.0	0.422
-58.0	0.418
-77.0	0.415

Table 3 Heat capacity of calorimeter

Temperature (°C)	Heat capacity (cal deg ⁻¹)	Temperature (°C)	Heat capacity (cal deg ⁻¹)
+19.5	70.8	-4.0	72.2
+19.0	73.5	-9.0	71.3
+18.5	72.3	-10.0	68.9
+18.0	71.2	-13.0	65.8
+5.5	70.3	-21.5	67.8
+4.0	74.0	-24.0	64.5
+2.5	73.6	-40.0	66.3
+1.0	71.0	-42.0	64.2
+0.5	68.0	-44.0	66.0
-2.5	64.5	-47.5	64.1

After correcting for the small heat rise due to the glass breaker, the total heat rise indicated by the trace was equated with the yield of polymer (always >90%). In this way the monomer consumed at time *t* was readily calculated from the appropriate position in the trace. For each kinetic run plots of $\log_{10} [\text{IBVE}]_t$ versus time were constructed (Figure 2) and values of $-k_p[\text{Co}]/2.303$ calculated from the maximum gradients (see Kinetic Appendix).

The molar heat of polymerization (ΔH_p) was calculated from the total corrected trace rise, converted to ohms by means of the 0.1 ohm calibration peaks, using the following relationship:

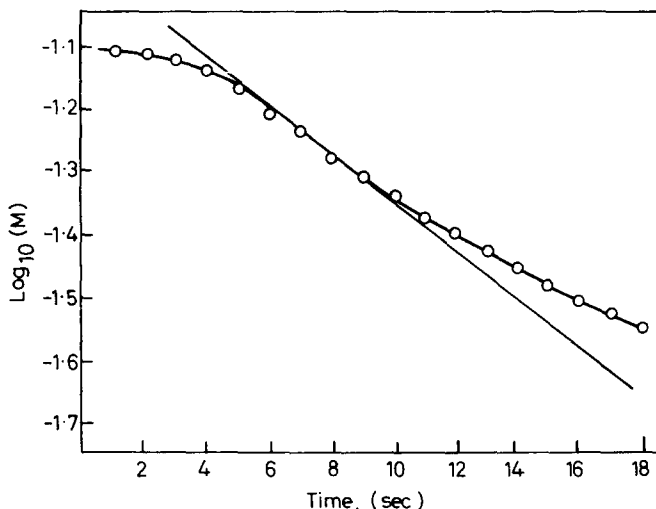


Figure 2 Typical plot used for evaluation of propagation rate coefficient

$$\Delta H_p = \frac{RH}{1000 \theta Y} \text{ kcal mol}^{-1}$$

where R = rise of trace (ohm)

H = heat capacity at the temperature of the run (cal deg⁻¹)

θ = temperature coefficient of resistance of the platinum wire (ohm deg⁻¹)

Y = yield of polymer (mol)

A representative analysis of a typical kinetic run is shown in *Table 4* for: $[\text{Co}] = 8.01 \times 10^{-5}\text{M}$, $[\text{IBVE}]_0 = 7.88 \times 10^{-2}\text{M}$.

Yield of polymer = 97%. Total trace rise corrected for breaker rise = 11.50 chart divisions. Hence 11.50 chart divisions $\equiv 7.88 \times 10^{-2} \times 97/100\text{M}$.

Maximum slope of plot of $\log_{10} [\text{IBVE}]_t$ against t (*Figure 2*)

was $-7.10 \times 10^{-2} = -k_p [\text{Co}]/2.303$;

hence $k_p = 2.04 \times 10^3 \text{ M}^{-1} \text{ s}^{-1}$

Since $0.1\Omega \equiv 7.53$ chart divisions, the heat of polymerization (ΔH_p) is calculated to be 25.1 kcal mol⁻¹.

Summaries of the results obtained with $\text{C}_7\text{H}_7^+\text{SbCl}_6^-$ and $\text{Ph}_3\text{C}^+\text{SbCl}_6^-$ as initiators are given in *Table 5* and *Table 6* respectively.

Successive polymerization experiments

In order to demonstrate the absence of significant termination, experiments were performed in which a second equivalent sample of monomer was introduced after approximately 90% conversion of the first sample. Analysis of the two recorder traces gave the data in *Table 7*.

CATIONIC POLYMERIZATION OF *is*BUTYL VINYL ETHER

 Table 4 Typical kinetic run for polymerization of [IBVE] in CH₂Cl₂ by C₇H₇⁺SbCl₆⁻ at -25°C

Time (s)	Rise (chart divisions)	Rise due to breaker alone (chart divisions)	Corrected rise (chart divisions)	[IBVE] (chart divisions)	[IBVE] × 10 ⁻² (mol litre ⁻¹)	log ₁₀ [IBVE]
0	0·00	0·00	0·00	11·50	7·88	-1·1035
1	0·37	0·20	0·17	11·32	7·76	-1·1100
2	0·90	0·40	0·50	11·00	7·54	-1·1228
3	1·50	0·55	0·95	10·55	7·23	-1·1409
4	2·50	0·70	1·80	9·70	6·64	-1·1774
5	3·70	0·80	2·90	8·60	5·89	-1·2297
6	5·10	0·85	4·25	7·25	5·00	-1·3039
7	6·20	0·90	5·30	6·20	4·25	-1·3718
8	7·20	0·93	6·27	5·23	3·58	-1·4461
9	7·92	0·95	6·97	4·53	3·11	-1·5086
10	8·55	0·97	7·58	3·92	2·69	-1·5703
11	9·15	1·00	8·15	3·35	2·29	-1·6392
12	9·50	1·01	8·49	3·01	2·06	-1·6856
13	9·95	1·02	8·93	2·57	1·76	-1·7543
14	10·20	1·03	9·17	2·33	1·60	-1·7968
15	10·47	1·03	9·44	2·02	1·39	-1·8577
16	10·62	1·04	9·58	1·91	1·31	-1·8821
17	10·82	1·04	9·78	1·71	1·18	-1·9300
18	11·10	1·05	10·05	1·45	0·994	-2·0028
19	11·22	1·05	10·17	1·32	0·908	-2·0420
20	11·32	1·06	10·26	1·23	0·845	-2·0726

 Table 5 Polymerization of IBVE by C₇H₇⁺SbCl₆⁻ in CH₂Cl₂

Temp (°C)	[Co] × 10 ⁺⁵ (M)	[IBVE] × 10 ⁺ (M)	k _p × 10 ⁻³ (M ⁻¹ s ⁻¹)	ΔH _p (kcal mol ⁻¹)	Molecular Wt
0	2·53	7·88	7·36	21·3	2985
0	5·05	7·88	7·14	21·8	2440
0	5·74	7·88	6·60	21·5	2288
0	5·82	7·88	7·17	21·4	2403
0	6·31	7·88	8·29	21·8	2440
0	7·58	7·88	9·15	22·5	2653
0	7·58	3·94	3·90	24·2	1542
0	7·58	4·73	5·40	22·1	1782
0	7·58	5·52	5·37	23·6	2010
0	7·58	6·30	5·74	21·8	1862
0	7·58	7·09	8·17	23·4	2370
		average	6·8	22·3	
-25	4·00	7·88	2·16	24·7	3452
-25	6·01	7·88	2·26	24·1	3372
-25	7·01	7·88	2·17	25·1	4042
-25	8·01	7·88	2·04	25·1	3131
-25	10·20	7·88	2·06	25·0	3294
-25	8·01	4·73	1·49	27·6	2992
-25	8·01	6·30	1·94	25·0	3529
-25	8·01	7·09	1·91	27·3	3506
-25	8·01	8·67	2·16	25·6	4374
		average	2·0	25·5	

Table 6 Polymerization of IBVE by $\text{Ph}_3\text{C}^+\text{SbCl}_6^-$ in CH_2Cl_2

Temp (°C)	$[\text{Co}] \times 10^{+5}$ (M)	$[\text{IBVE}] \times 10^{+2}$ (M)	$k_p \times 10^{-3}$ ($\text{M}^{-1} \text{s}^{-1}$)	ΔH_p (kcal mol $^{-1}$)	Molecular Wt
0	7.20	3.94	2.55	21.5	1850
0	7.20	5.91	3.38	21.2	2150
0	7.20	6.85	4.29	22.2	2335
0	7.20	7.88	3.60	22.2	2804
0	7.20	9.85	5.22	21.6	2970
0	2.00	7.88	3.92	21.0	—
0	3.00	7.88	4.40	20.3	—
0	3.98	7.88	4.43	22.5	—
		average	4.0	21.5	
-25	8.80	3.98	0.91	24.1	2720
-25	8.80	5.91	1.02	25.0	2960
-25	8.80	7.88	1.26	22.2	3660
-25	8.80	9.85	1.69	23.5	4750
-25	8.80	11.82	2.56	22.1	4800
-25	2.23	7.88	1.82	21.0	4140
-25	6.61	7.88	1.46	22.3	3570
-25	11.02	7.88	1.44	23.2	3630
		average	1.5	23.0	

Table 7 Successive polymerizations of IBVE by $\text{C}_7\text{H}_7^+\text{SbCl}_6^-$ in CH_2Cl_2 at -25°C

$[\text{Co}] \times 10^{+5}$ (M)	$[\text{IBVE}]_0 \times 10^{+2}$ (M)	$k_p \times 10^{-3}$ ($\text{M}^{-1} \text{s}^{-1}$)	Molecular weight
7.57	5.52	2.22	3200†
		2.25*	3160‡
8.58	5.52	2.37	3100†
		2.22*	3300‡

*Value obtained after adding a second sample of monomer so that IBVE was the same as in the initial run.

†Molecular weight of a sample prepared independently under identical conditions

‡Molecular weight of total polymer yield from the successive polymerisations

Polymerization with triphenylmethyl tetrafluoroborate

$\text{Ph}_3\text{C}^+\text{BF}_4^-$ was hydrolytically much less stable in the solid and in solution, than the corresponding SbCl_6^- salt. Consequently considerable difficulty was encountered when preparing catalyst stock solutions of reproducible activity. As a result the polymerization data obtained with this catalyst (Table 8) was not so extensive as that shown in Table 6, and is not quite as reliable.

Table 8 Polymerization of IBVE by $\text{Ph}_3\text{C}^+\text{BF}_4^-$ in CH_2Cl_2 at 0°C

$[\text{Co}] \times 10^{+5}$ (M)	$[\text{IBVE}]_0 \times 10^{+2}$ (M)	$k_p \times 10^{-3}$ ($\text{M}^{-1} \text{s}^{-1}$)	ΔH_p (kcal mol $^{-1}$)
2.98	11.62	2.7	21.9
7.39	12.61	2.7	20.5
6.50	11.87	2.3	20.1
3.69	12.40	2.9	21.5

Identification of initiator residues

A special polymerization mixture was made up, *in vacuo*, containing $\text{Ph}_3\text{C}^+\text{SbCl}_6^-$ (0.32 g) and IBVE (10 ml) in 24 ml CH_2Cl_2 . After rapid polymerization at 0°C the reaction was quenched in the usual way and all volatiles removed by evacuation. The residue was chromatographed on neutral alumina, with elution by $60\text{--}80^\circ\text{C}$ petrol followed by benzene. Only the first three fractions eluted with $60\text{--}80^\circ\text{C}$ petrol gave polymeric material containing Ph_3C -groups (monosubstituted benzene ring absorption in the i.r. spectra at $705, 765\text{cm}^{-1}$). The remaining fractions contained polymer but gave no evidence for aryl groups in the i.r. spectra. Independent g.l.c. analysis of the original polymerization product, and of the fractions containing aryl groups, established that Ph_3CH was not present.

Absorption spectra of reaction mixtures

It was observed during the kinetic runs that the polymerization mixtures were colourless but that a blue colour began to build up at the end of the reaction. This blue colour was independent of whether C_7H_7^+ or Ph_3C^+ salts were used and by low temperature visible spectroscopy was shown to consist of two bands at 440 and 670 nm, respectively (Figure 3). At -25° the blue

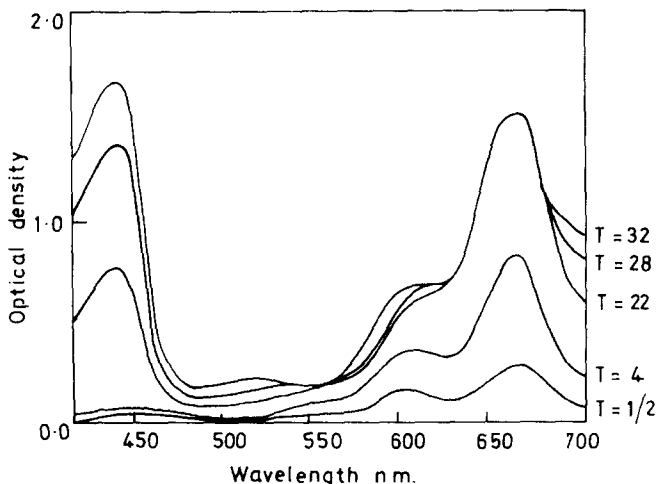


Figure 3 Absorption spectra of reaction mixture. Values of T shown on the right represent time intervals (minutes) after complete consumption of monomer

colour was fairly stable but at 0°C it rapidly decayed through a series of green and violet shades. All the colours were instantaneously removed when the reactions were quenched with methanol, leaving solutions with multiple absorption maxima in the region $325\text{--}450\text{ nm}$ (Figure 4).

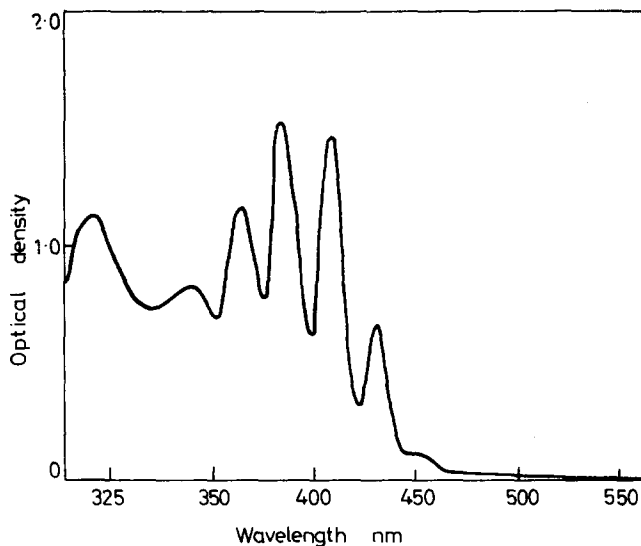


Figure 4 Absorption spectrum of reaction mixture, quenched by methanol, approximately 30 minutes after complete polymerization

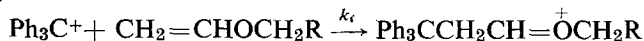
DISCUSSION

Polymerizations of *isobutyl* vinyl ether initiated by tropylium and triphenyl methyl hexachloroantimonates showed very similar features. For both catalysts there was a comparatively slow initiation process followed by very rapid propagation. Experiments with $C_7H_7^+SbCl_6^-$ established that termination was not significant during the kinetic lifetimes. Molecular weights of poly(*isobutyl* vinyl ether) were always in the range 2000–5000 providing clear evidence of dominant transfer reactions, as observed for other homogeneous cationic polymerizations of this and related monomers^{1,12}. Mechanistic features of the initiation, propagation, and transfer processes will now be considered in detail.

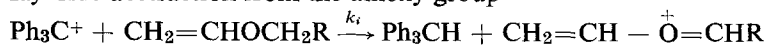
Initiation

There are at least three different mechanisms whereby stable organic cations may initiate cationic polymerization of alkyl vinyl ethers, e.g. for triphenylmethyl cation

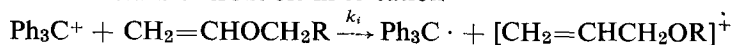
- (1) Direct addition of cation to the olefin



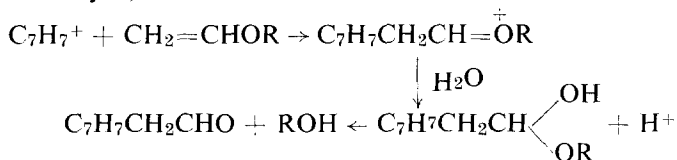
- (2) Hydride abstraction from the alkoxy group



- (3) Electron transfer from olefin to cation

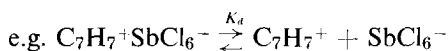


Reaction (3) was originally suggested^{15,16} to explain the reactivity of tropylium ions towards very nucleophilic olefins but Russian workers have demonstrated^{25,26} that simple addition (i.e. reaction 1) of tropylium ion to alkyl vinyl ethers may be used as a convenient synthetic route to cycloheptatrienyl acetaldehyde, viz:



In the present work it was not possible to detect cycloheptatrienyl end groups in the polymer chains but column chromatographic analysis of the polymers prepared by triphenylmethyl salt initiation, gave some fractions showing (i.r. analysis) clear evidence of aryl end groups. Reaction (2) is the most common mechanism for initiation of cyclic ether polymerization by carbonium ion salts^{27,28} and yields either triphenyl methane or cycloheptatriene, respectively. These hydrocarbons are readily detected by g.l.c. analysis in polymerizing mixtures formed from cyclic ethers but could not be detected in the present work. It seems reasonable to conclude therefore that initiation of polymerization of alkyl vinyl ethers by triphenylmethyl and cycloheptatrienyl salts, involves primary addition of the cation to a monomer olefinic linkage (reaction 1).

The ion pair dissociation equilibria for tropylium and triphenylmethyl salts have been determined from conductance measurements in the solvent CH_2Cl_2 ^{17,21}



For $\text{C}_7\text{H}_7^+\text{SbCl}_6^-$ and $\text{Ph}_3\text{C}^+\text{SbCl}_6^-$ the values of K_d were $0.3 \times 10^{-4}\text{M}$ and $3.1 \times 10^{-4}\text{M}$ respectively at 0°C . It follows that for the catalyst concentrations employed in the present work, the initiating salt will be predominantly dissociated into its free ions. Initiation therefore involves reaction of mainly free organic cation with polymerizable olefin.

It is apparent from the slight 'S' shape of the adiabatic calorimetric reaction curves (e.g. *Figure 2*) that initiation is a somewhat slower reaction than propagation. This effect being most marked at the lower polymerizing temperature (-25°C), indicates that initiation has a slightly higher activation energy than propagation. However it is also clear from the kinetic curves, and the kinetic analysis, that the initiator was completely consumed after approximately 10–20% reaction.

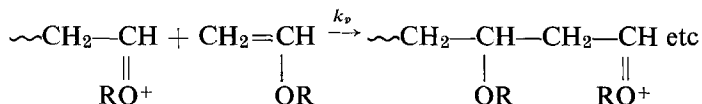
Carboxonium ions such as $\text{CH}_3\text{CH}=\overset{+}{\text{O}}\text{CH}_2\text{CH}_3$ ²⁹ and $\text{CH}_3\overset{+}{\text{O}}=\text{CH}_2$ ³⁰ are known to have a greater thermodynamic stability than e.g. PH_3C^+ , hence k_i would not be expected to be significantly less than k_p .

Propagation and transfer reactions

Homogeneous cationic polymerization of alkyl vinyl ethers normally leads to low molecular weight semi-liquid polymers as a result of highly efficient

transfer reactions¹. Since similar molecular weights result from polymerizations in a wide variety of solvents, the transfer process is generally assumed to involve reaction of the growing chain with monomer, as in the case of most other cationic polymerizations¹². In fact the only known conditions leading to formation of higher molecular weight poly(alkyl vinyl ethers) involve heterogeneous catalysis—conditions which also favour formation of isotactic polymers³¹.

In the present work all polymerizations were truly homogeneous and the propagation reaction may be represented



Since the initiating salt was shown to be present predominantly in the form of free ions, it may be assumed that the propagating species will be similarly dissociated. This follows since the charge density on the propagating cation will be less than that of the initiating tropylium or triphenylmethyl cations and the counter ion is common to all (SbCl_6^-). For sodium derivatives of condensed aromatic hydrocarbons, Slates and Szwarc have shown³² that ion pair dissociation constants increase markedly with increasing size of the anion, i.e. with the increasingly diffuse character of the anionic charge cloud.

Accordingly the values of k_p obtained by kinetic analysis of the reaction curves (see Kinetic Appendix) represent estimates of the rate coefficient for reaction of free propagating cation with monomer. Combined average data from *Tables 5–8* are summarized in *Table 9*.

Table 9 Polymerization of *isobutyl vinyl ether* in CH_2Cl_2

<i>Initiator</i>	<i>Temp</i> (°C)	ΔH_p (kcal mol ⁻¹)	$10^3 k_p$ (M ⁻¹ s ⁻¹)
$\text{C}_7\text{H}_7^+\text{SbCl}_6^-$	0	22.3	6.8
$\text{Ph}_3\text{C}^+\text{SbCl}_6^-$	0	21.5	4.0
$\text{Ph}_3\text{C}^+\text{BF}_4^-$	0	21.0	2.8
$\text{C}_7\text{H}_7^+\text{SbCl}_6^-$	-25	25.5	2.0
$\text{Ph}_3\text{C}^+\text{SbCl}_6^-$	-25	23.0	1.5

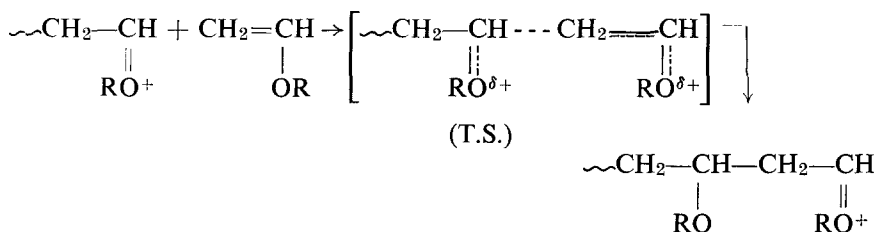
Within the experimental limitations of the fast reaction technique employed, these data provide adequate confirmation of the assumptions made above. Thus complete consumption of initiator is indicated by the close agreement of values for k_p from initiation by different cations, while the assumption regarding free cations as propagating species is fully justified by the correspondence between data from initiators having different counter ions i.e. $\text{Ph}_3\text{C}^+\text{BF}_4^-$ and $\text{Ph}_3\text{C}^+\text{SbCl}_6^-$. In fact it is highly likely that the observed small differences in values of k_p obtained with the three salts results entirely from very slight decomposition of the salts by adventitious impurities in the solvent or on the surface of the glass apparatus. The initiating salts show stability which falls in the sequence:

$C_7H_7^+SbCl_6^- \rightarrow Ph_3C^+SbCl_6^- \gg Ph_3C^+BF_4^-$, and the experimental values of k_p apparently decrease slightly in the same sequence.

From Table 9 the activation energy for free cation propagation of *isobutyl vinyl ether* may be estimated to be 6 kcal mol⁻¹, with an average rate coefficient of $\sim 5 \times 10^3 \text{ M}^{-1}\text{s}^{-2}$ at 0°C.

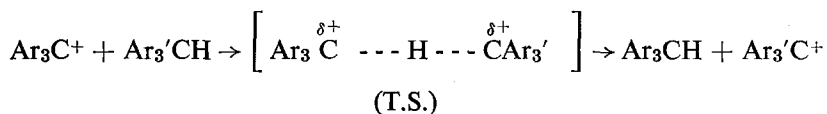
Independent support for the conclusions drawn above comes from a comparison of values of k_p with those obtained from studies of radiation induced polymerization of *isobutyl vinyl ether*^{33,34}. In the present work free ions are assumed to be the propagating entities from known ion-pair dissociation behaviour of the initiating salts and because the polymerization technique is sufficiently sophisticated to permit the use of very low concentrations of initiator ($< 10^{-4}\text{M}$). Radiation induced polymerization on the other hand, necessitates the use of extreme drying procedures because even lower concentrations of propagating species ($< 10^{-7}\text{M}$) are involved. In addition the counter-ions will be either solvated electrons or solvated anions formed by reaction of solvated electron with monomer, solvent or adventitious impurity. From studies of this type, William *et al*³³ estimate that $k_p = 3 \times 10^5 \text{ M}^{-1} \text{ s}^{-1}$, for free ion propagation of *isobutyl vinyl ether* in bulk at 30°C, with an activation energy of 6.6 kcal mol⁻¹. Extrapolation of the data obtained in the present work gives an estimate of $2 \times 10^4 \text{ M}^{-1} \text{ s}^{-1}$ for k_p at 30°C in CH_2Cl_2 , apparently one order of magnitude less than that from the radiation induced polymerization. However agreement between the two sets of data is seen to be much closer after taking into account the effect of solvent.

A probable transition state for free ion propagation of alkyl vinyl ether polymerization must involve some charge dispersion with respect to reactants i.e.



The general theory of solvent effects on ionic organic reactions predicts³⁵ that such processes will be retarded by increasing polarity of the reaction medium because the reactant cation will be more solvated (i.e. more stabilized) than the transition state. Specific solvating characteristics of organic molecules are difficult to assess but for the type of solvent used in cationic polymerizations, solvent dielectric may be used as a rough indication of the ability to solvate a cation. It follows therefore that in vinyl polymerization propagation reactions of free cations will be retarded by increasing solvent dielectric. Quite different effects may be observed for initiation and termination processes. For polymerization of *isobutyl vinyl ether* values of k_p (free ion at 30°C) were estimated as $2 \times 10^4 \text{ M}^{-1} \text{ s}^{-1}$ in CH_2Cl_2 (dielectric constant ~ 9) and $3 \times 10^5 \text{ M}^{-1} \text{ s}^{-1}$ in bulk (dielectric constant ~ 3). At present

there is no means of estimating the retarding effect on k_p of a change in solvent from bulk monomer to CH_2Cl_2 , however hydride ion transfer between two stable organic cations would be anticipated to show the same rate retarding effect of increasing solvent polarity because the transition state will involve similar charge dispersal e.g.

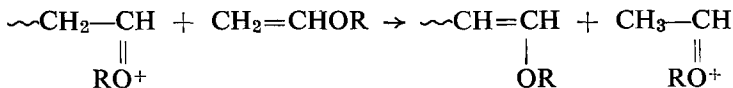


Solvent effects on the rate of hydride ion transfer between (free) triphenylmethyl cation and a dicarbazolymethane derivative have been studied from this viewpoint and do show the anticipated order²⁴. Increasing the dielectric constant of reaction mixtures by a factor of approximately 3 (corresponding to that for the two polymerizing systems) lowered the rate of hydride transfer by a factor of approximately 4.

Taking into account the probable effect of changing solvent on k_p it can be seen therefore that the values obtained in the present work are in quite good agreement with the value obtained by radiation introduced polymerization. Considering the vastly different techniques employed and the probable experimental errors for both techniques, this measure of agreement is quite remarkable and provides ample justification for the assumptions involved in estimating rate coefficients. It now appears likely that the much lower values of k_p previously reported for isobutyl vinyl ether polymerization²⁻⁵, represent either ion pair propagation reactions, or else result from incorrect analysis of the number of active centres.

Tables 5 and 6 show that molecular weights of poly(isobutyl vinyl ether) obtained in the present work are only slightly increased by lowering reaction temperatures. Changing from 0°C to -25°C increased average molecular weights by less than a factor of two. In addition the fact that polymers were isolated only after 100% conversion of monomer diminished any possibility of recognising or analysing a dependence of molecular weight on either [catalyst] or [monomer]. Average degrees of polymerization fall in the range 20-40 whereas the theoretical maximum should be somewhere between 1000-1500. It follows therefore that propagation is only 30-50 times faster than transfer, both processes having rather similar activation energies.

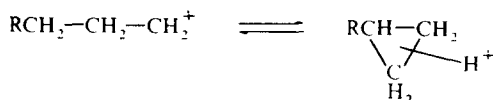
Monomer transfer in cationic polymerization is widely assumed^{1,12} to involve simple proton transfer between growing chain and monomer, e.g. for alkyl vinyl ethers



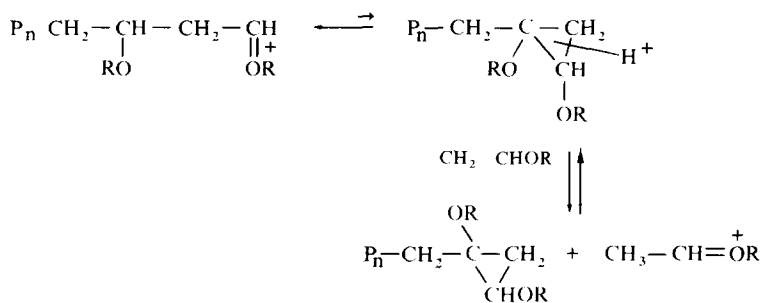
Proton equilibria such as this no doubt play a role, but the tremendous efficiency of monomer transfer, especially in vinyl ether polymerization, suggests that other forms of monomer transfer may be operative.

In essence the proton transfer equilibrium shown above represents the relative basicities of a vinyl alkyl ether monomer and the corresponding alkenyl alkyl ether, formed as a terminal unit. Studies of the mechanism of acid catalysed hydrolysis of unsaturated ethers^{36,37} indicate that propenyl alkyl ethers may be very much more reactive (i.e. more basic) than corresponding vinyl alkyl ethers, arguing against the proposed proton transfer, except at very high monomer concentrations. There are at least two alternative reactions which may explain the ease of monomer transfer in cationic polymerization of alkyl vinyl ethers.

Recent studies of carbonium ion behaviour have established beyond doubt that protonated cyclopropanes constitute active intermediates in many reactions of simple alkyl cations³⁸. There is still some uncertainty regarding the exact structure of protonated cyclopropanes, i.e. as to whether the ring is 'face protonated', 'edge protonated', or 'corner protonated', but a primary alkyl cation may be represented as an equilibrium between classical and non-classical structures

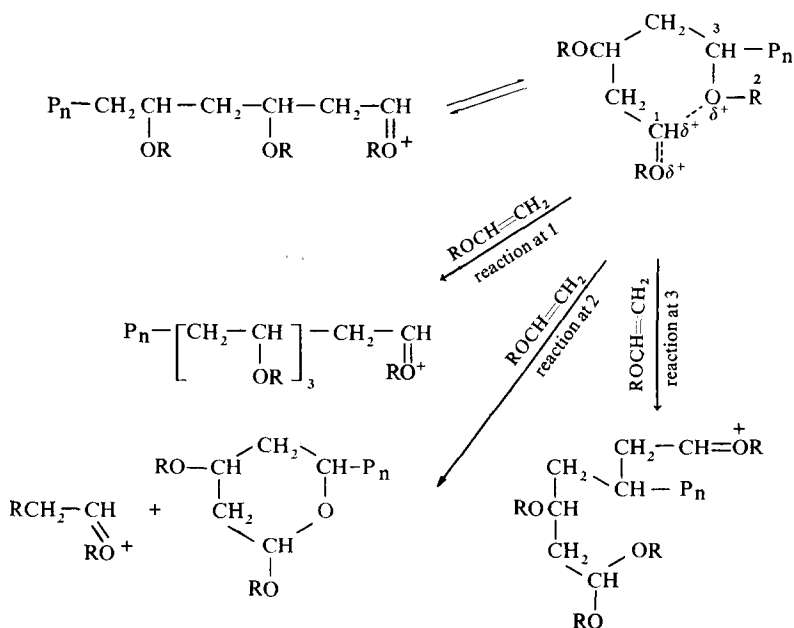


For a simple alkane structure the order of carbonium ion stabilities falls in the sequence tert>sec>protonated-cyclopropyl>primary. However for substituted derivatives, the free energy differences between protonated cyclopropyl and secondary or tertiary classical structures are not very great³⁹⁻⁴³. It is plausible therefore to suggest that the propagating classical cation in vinyl ether polymerization is in equilibrium with a very small concentration of the non-classical protonated cyclopropyl derivative, e.g.



For the particular example considered the presence of stabilizing alkoxy groups would overwhelmingly favour the open chain classical structure, but cyclopropanes are much less basic than similarly substituted olefins, providing a simple explanation for the facile monomer transfer reaction.

A second alternative monomer transfer process would be possible if the propagating carboxonium ion derived any stabilization by neighbouring group effects of monomer segments in the same chain, e.g.



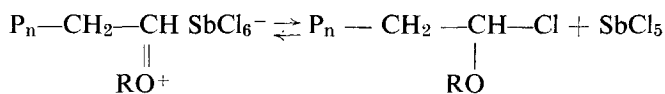
The cyclic oxonium ion formed by intramolecular stabilization would have electrophilic reactivity at positions 1, 2, and 3, according to the nature of the substituents, but here again reactivity at position 1 would be heavily favoured by the alkoxy substituent. Reaction at position 1 leads to propagation and would be expected to dominate, reaction at position 2 constitutes a monomer transfer reaction in which an alkyl group has been transferred, and reaction at position 3 results in propagation with branching. A similar cyclic oxonium ion was proposed some years ago⁴⁴ to explain the stereoregular nature of vinyl ether polymerizations with heterogeneous catalysts.

Characterisation of cyclopropyl or acetal end groups formed by any of the suggested monomer transfer processes is almost impossible because of anticipated reactivity towards the electrophilic species remaining at the completion of polymerization. It is perhaps worth noting however that the semi-liquid nature of homogeneously polymerized poly(alkyl vinyl ethers) may indicate a degree of branching, as well as low molecular weights, both of which would be expected following internal cyclic oxonium ion formation.

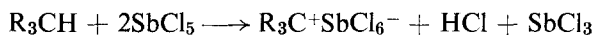
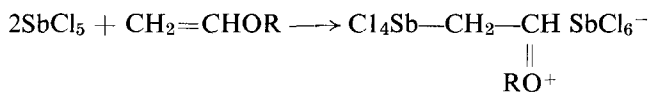
Termination reactions

For many cationic polymerizations it is almost impossible to envisage a true, spontaneous termination process. In the present work the rate studies suggest that termination is not significant during kinetic lifetimes but that there must be some termination (i.e. destruction of active centres) when the reaction mixtures are allowed to stand before work up, or when working at temperatures above 0°C.

A most probable termination process involves dissociation of the counterion, e.g.

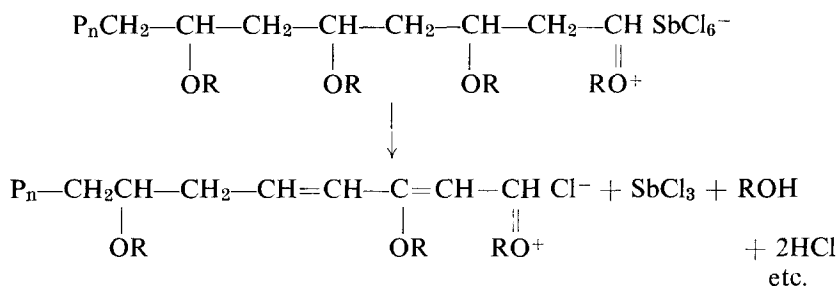


Antimony pentachloride is itself a good initiator for polymerization of alkyl vinyl ethers¹ and cyclic ethers^{27,28}, and for oxidation and chlorination of reactive C-H bonds^{24,45-47}. In all these reactions however there is a net loss of SbCl_5 species consequent upon generation of a catalyst site, e.g.



Whilst the exact nature of the side reactions occurring in the poly(*isobutyl* vinyl ether)- SbCl_5 systems remain obscure, it is evident that both olefinic and highly reactive acetal and ether functions may contribute to the slow overall consumption of SbCl_5 .

Further evidence regarding the complex nature of termination in these systems is provided by the spectra shown in *Figures 3* and *4*. The strong colours developed subsequent to monomer consumption indicate some kind of conjugated cationic species (*Figure 3*). This is confirmed by the quenching effect of methanol leading to absorption spectra resembling those of conjugated polyenes⁴⁸ (*Figure 4*). It is suggested therefore that solutions of poly-(alkyl vinyl ethers) readily undergo elimination reactions similar to those encountered in degradation of poly(vinyl chloride)^{49,50} e.g.



The resulting conjugated cations would give rise to absorption spectra in the visible region and on quenching with methanol, would yield neutral polyenes of varying chain length, as indicated by the multiple absorbance maxima in *Figure 4*.

ACKNOWLEDGEMENT

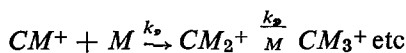
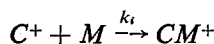
We wish to acknowledge the valuable help given by Dr H. Block in kinetic analysis, and the award of S.R.C. Studentships to D.S.C. and J.A.W.

*Donnan Laboratories,
University of Liverpool, UK*

(Received 7 August 1970)

KINETIC APPENDIX

Assuming absence of termination reactions, then let $[C_0]$ = concentration of catalyst (C^+) added, $[M]$ = concentration of monomer and $[CM^+]$ = concentration of propagating species, where reactivities of CM^+ , CM_1^+ , CM_2^+ etc are assumed constant.



$$\therefore \frac{d[CM^+]}{dt} = k_i[C^+][M] \quad (1)$$

and
$$\frac{-d[C^+]}{dt} = k_i[C^+][M] \quad (2)$$

now
$$\frac{-d[M]}{dt} = k_i[C^+][M] + k_p[CM^+][M] \quad (3)$$

$$\text{and } [C^+] + [CM^+] = [C_0]$$

$$\begin{aligned} \therefore \frac{-d[M]}{dt} &= \{k_i[C^+] + k_p([C_0] - [C^+])\}[M] \\ &= (k_i - k_p)[C^+][M] + k_p[C_0][M] \end{aligned} \quad (4)$$

from (3)
$$\frac{-d \ln[M]}{dt} = (k_i - k_p)[C^+] + k_p[C_0]$$

or
$$[C^+] = 1/k_i - k_p \left\{ k_p [C_0] + \frac{d \ln[M]}{dt} \right\} \quad (5)$$

from (4)
$$\frac{-d[C^+]}{dt} = \frac{1}{k_i - k_p} \frac{d^2 \ln[M]}{dt^2} \quad (6)$$

Substituting (4) and (5) into (2)

$$\frac{1}{k_i - k_p} \frac{d^2 \ln[M]}{dt^2} + \frac{k_i}{k_i - k_p} \left\{ k_p [C_0] + \frac{d \ln[M]}{dt} \right\} [M] = 0$$

$$\therefore \frac{d^2 \ln[M]}{dt^2} + k_i \frac{[M]d\ln[M]}{dt} + k_i k_p [C_0] [M] = 0 \quad (7)$$

If $\ln[M]$ is plotted against t , then $\frac{d^2 \ln[M]}{dt^2}$ vanishes at the point of maximum slope hence k_p may be evaluated from the simple relationship

$$\left[\frac{-d \ln[M]}{dt} \right]_{\max} = k_p [C_0] \quad (8)$$

REFERENCES

- 1 Eley, D. D., 'The Chemistry of Cationic Polymerisation', (P. H. Plesch, Ed.), Pergamon, Oxford, 1963, p 375
- 2 Higashimura, T., 'Structure and Mechanism in Vinyl Polymerisation', (T. Tsuruta and K. F. O'Driscoll, Eds.), Dekker, New York, 1969, p 313
- 3 Eley, D. D., Isack, F. L. and Rochester, C. H. *J. Chem. Soc. (A)* 1968, p 872
- 4 Eley, D. D. and Saunders, J. *J. Chem. Soc.* 1954, p 1677
- 5 Okamura, S., Kanoh, N. and Higashimura, T., *Makromol. Chem.*, 1961, **47**, 19, 35; 1962, **56**, 65
- 6 Okamura, S., Higashimura, T. and Yamanoto, H. *J. Polym. Sci.* 1958, **33**, 510
- 7 Fishbein, L. and Crowe, B. F. *Makromol. Chem.* 1961, **48**, 221
- 8 Eley, D. D. and Seabrooke, A. *J. Chem. Soc.* 1964, p 2226
- 9 Coombes, J. D. and Eley, D. D. *J. Chem. Soc.* 1952, p 4167
- 10 Eley, D. D. and Johnson, A. F. *J. Chem. Soc.* 1964, p 2238
- 11 Blake, G. J. and Eley, D. D. *J. Chem. Soc.* 1965, p 7405, p 7412
- 12 Plesch, P. H. *Progress in High Polymers* 1968, **2**, 137
- 13 Zlamal, Z. in 'Vinyl Polymerisation', Vol 1, Pt 11, Ham, G., Ed., Dekker, New York, 1970, p 231
- 14 Ledwith, A. and Woods, H. J. *J. Chem. Soc. (B)* 1970, p 310
- 15 Bawn, C. E. H., Fitzsimmons, C. and Ledwith, A. *Proc. Chem. Soc.* 1964, p 391
- 16 Ledwith, A. *J. Appl. Chem.* 1967, **17**, 344
- 17 Ledwith, A. *A.C.S. Advances in Chemistry Series* 1969, No. 91, 317
- 18 Eley, D. D. and Richards, A. W. *Trans. Faraday Soc.* 1949, **45**, 436
- 19 Szwarc, M. 'Carbanions, Living Polymers and Electron Transfer Processes', Interscience, New York, 1968
- 20 Szwarc, M. *Accounts of Chem. Research* 1969, **2**, 87
- 21 Bowyer, P., Ledwith, A. and Sherrington, D. C. *J. Chem. Soc. (B)* 1971, in press
- 22 Kalfoglu, N. and Szwarc, M. *J. Phys. Chem.* 1968, **72**, 2233
- 23 Biddulph, R. and Plesch, P. H. *Chem. and Ind.* 1959, p 1482
- 24 Cowell, G. W., Ledwith, A., White, A. C. and Woods, H. J. *J. Chem. Soc. (B)* 1970, p 227
- 25 Kursanov, D. N., Vol'pin, M. E. and Akhrem, I. S. *Dokl. Akad. Nauk. USSR* 1958, **120**, 531
- 26 Vol'pin, M. E., Akhrem, I. S. and Kursanov, D. N. *Zhur. Obshchei Khim.* 1960, **30**, 159
- 27 Ledwith, A. and Fitzsimmonds, C., 'Polymer Chemistry of Synthetic Elastomers', (Kennedy, J. P., Tornqvist, E. G. M., Eds.) Interscience, New York, 1968, p 377
- 28 Dreyfuss, M. P. and Dreyfuss, P. *Adv. Polymer Sci.* 1967, **4**, 528
- 29 Deno, N., Saines, G. and Spangler, M. *J. Amer. Chem. Soc.* 1962, **84**, 3295
- 30 Briggs, P. R. and Shannon, T. W. *J. Amer. Chem. Soc.* 1969, **91**, 4307
- 31 For reviews see Lal, J. in Ref. 27, p 331, and Saegusa, T. in Ref. 2, p 283
- 32 Slaters, R. V. and Szwarc, M. *J. Phys. Chem.* 1965, **69**, 4124
- 33 Williams, F., Hayashi, K., Ueno, K., Hayashi, K. and Okamura, S. *Trans. Faraday Soc.* 1967, **63**, 1501
- 34 Ueno, K., Hayashi, K. and Okamura, S. *J. Macromol. Sci.* 1968, **2**, 209

- 35 Ingold, C. K., 'Structure and mechanism in organic chemistry', Cornell Univ. Press, New York, 1953, p 345
- 36 Ledwith, A. and Woods, H. J. *J. Chem. Soc. (B)* 1966, p 753
- 37 Jones, D. M. and Wood, N. F. *J. Chem. Soc. (B)* 1964, p 5400
- 38 Lee, C. C. *Prog. in Phys. Org. Chem.* 1970, 7, 129
- 39 Deno, N. C., Billups, W. E., La Vietes, D., Scholl, P. C. and Schneider, S. *J. Amer. Chem. Soc.* 1970, **92**, 3700
- 40 Karabatsos, G. J., Orzech, C. E., Fry, J. L. and Meyerson, S. *J. Amer. Chem. Soc.* 1970, **92**, 606
- 41 Karabatsos, G. J., Fry and Meyerson, S. *J. Amer. Chem. Soc.* 1970, **92**, 614
- 42 Karabatsos, G. J., Hsi, N. and Meyerson, S. *J. Amer. Chem. Soc.* 1970, **92**, 621
- 43 Saunders, M. and Rosenfeld, J. *J. Amer. Chem. Soc.* 1969, **91**, 7756
- 44 Bawn, C. E. H. and Ledwith, A. *Quart. Revs.* 1962, **16**, 362
- 45 Holmes, J. and Pettit, R. *J. Org. Chem.* 1963, **28**, 1695
- 46 Fleischpresser, B. E., Cheng, W. J., Pearson, J. M. and Szwarc, M. *J. Amer. Chem. Soc.* 1968, **90**, 2172
- 47 Szwarc, M., Bracke, W., Cheng, W. J. and Pearson, J. M. *J. Amer. Chem. Soc.* 1969, **91**, 203
- 48 Hausser, W. W., Kuhn, R. *Z Physik, Chem. (B)* 29 1935, pp 363, 373, 378, 384, 391
- 49 Braun, D., Thallmaier, *Makromol. Chem.* 1966, **99**, 59
- 50 Klemchuk, P. P. *A.C.S. Advances in Chemistry Series* 1968, No. 85, p 1

Notes to the Editor

Amylose: a non-helical biopolymer in aqueous solution

W. BANKS and C. T. GREENWOOD

THE HELICAL macromolecule is now a firmly established concept in the protein and nucleic acid fields, but it is often overlooked that this model was first applied over 30 years ago to the amylose component of starch. In 1937, Hanes¹ suggested that the characteristic blue colour produced on the addition of iodine to an amylose solution resulted from a complex formed by the iodine entering the helical cavity of the polysaccharide. Frendenberg *et al*², independently advanced the same model. The correctness of this model for the *solid* amylose-iodine complex was confirmed by the x-ray diffraction methods of Rundle and French³, who showed that the structure corresponded to one iodine atom per six glucose residues.

In contrast, the conformation of amylose in neutral, aqueous solution still appears to be a matter of some controversy, notwithstanding the large amount of published work on this aspect of starch chemistry. This diversity is perhaps unexpected, and is certainly disturbing. We wish to outline the nature of the problem, and to present evidence to show – simply and unambiguously – that amylose in water is not in the form of a helix.

The three extreme model conformations which have been considered for amylose are shown in *Figure 1*. *Figure 1a* shows the amylose chain in the form of a tight helix, the helix itself taking up the overall form of a random coil. The interrupted helix of Holló⁴ is given in *Figure 1b*, and here the molecule is considered to be composed of long helical sections (each containing about 100 anhydroglucose units) with portions of random coil between, the latter conferring flexibility on the molecule as a whole. In both of these models, the helical portions are thought to be stabilized by intra-molecular hydrogen bonds, so that the dimensions are little different from those of amylose in the crystalline state, i.e. the helix has a pitch of about 8 Å and contains 6 glucose units per turn. *Figure 1c* shows the random coil model for amylose – any helical character is merely a reflection of the nature of the α -1:4 inter-unit bonding between the monomer units.

Szejtli and Augustat⁵ have summarized the indirect evidence which favours the concept that amylose in solution behaves as a molecule with helical character. Later evidence purporting to substantiate this concept has also been presented by Erlander^{3,7}.

Recently⁸⁻¹⁰, we have investigated the hydrodynamic behaviour of amylose in both neutral and alkaline aqueous solvents by viscosity, light scattering and sedimentation measurements. These studies show that:

- (1) in neutral aqueous potassium chloride solution, the amylose macromolecule behaves as a random coil at its θ -point, and
- (2) in formamide, dimethylsulphoxide and 0.15 M potassium hydroxide, the amylose undergoes coil expansion as a result of solvent-solute interaction (the classical model of Flory).

However, in all the solvents the skeletal structure of the polymer backbone remains the same. Obviously, the extensive hydrogen-bonding necessary to stabilize a helix cannot exist in dimethylsulphoxide or in 0.15 M potassium hydroxide. The fact that the skeletal structure in these two solvents is the same as that in neutral aqueous salt solution then requires that in this medium also, the helical structure must be absent.

The above argument depends on the interpretation of hydrodynamic

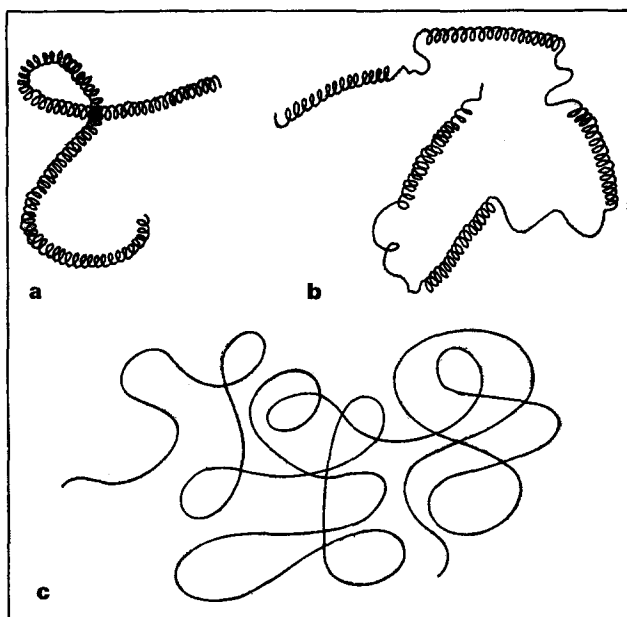


Figure 1 Models proposed for the amylose molecule in aqueous solution.

- a random helical coil (6 glucose units per turn)
- b interrupted helix (sections of 6-unit helical coil about 100 glucose units in length)
- c random coil (no helical character)

theory, which is far from rigorous. Thus Burchard¹¹ has interpreted results similar to our own to show that the skeletal structure of amylose is a function of the solvent system, and that this is reflected by varying degrees of partial free-draining in these solvents.

We therefore decided to investigate the changes, if any, which occur in the hydrodynamic volume of the macromolecule on the addition of complexing agents such as iodine and butan-1-ol. If the molecule is as in *Figure 1a* or *b*, the complexing agent would be expected to enter immediately the pre-formed helix – as it does in the solid state – and this process would occur with little, or no, change in the volume of the complexed molecule. On the other hand, the addition of a complexing agent to the random coil form of *Figure 1c* would necessitate some co-operative phenomenon occurring: the molecule

would have to be forced into a helix, which would then be stabilized by intramolecular bonding along the helix, and hydrophobic bonding between the complexing agent and the helical cavity in the polysaccharide. More importantly, the molecule would necessarily have to decrease in size through helical complex formation, and its hydrodynamic volume would *decrease*. Conformational changes of this type in amylose can be easily followed by

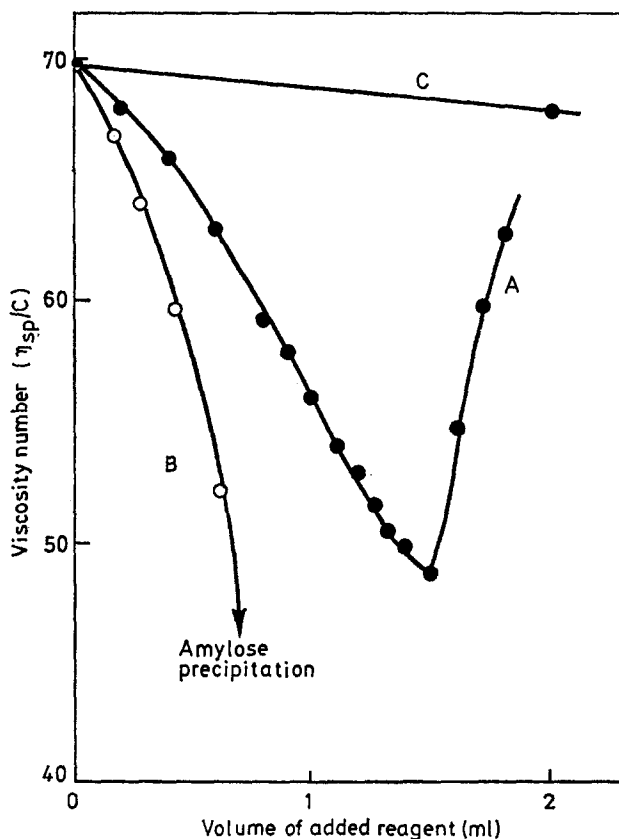


Figure 2 Changes in viscosity number of wheat amylose in aqueous solution (initial concentration = 10^{-3} g ml $^{-1}$, initial volume = 10 ml)
 A Amylose in 0.015 M potassium iodide + iodine (0.005 M in 0.015 M in iodide)
 B Amylose in water + butan-1-ol
 C Amylose in water + water (control)

measuring the viscosity of the system, as was first appreciated by Holló⁴.

Figure 2 shows the changes in viscosity number which occur when iodine and butan-1-ol are added to amylose in neutral, aqueous solution to form the appropriate complexes. It can be seen that complex-formation is associated

with a large decrease in viscosity number, i.e. a decrease in hydrodynamic volume. In the case of iodine, the minimum in the graph of viscosity number as a function of iodine concentration occurs when the expected stoichiometric amount of reagent necessary to form the complex has been added, i.e. at 19 mg of iodine per 100 mg of amylose. The subsequent increase in viscosity number is due to aggregation and after a period of several hours, a visible precipitate is formed.

The amylose-iodine complex in solution, as in the solid state, has been shown¹² to be helical in nature. The only conclusion to be drawn from the above work is that the helical conformation is forced upon amylose by the addition of the complexing agent. Thus, in neutral aqueous salt solution the amylose molecule possesses no pronounced helical character, in agreement with our earlier interpretation of hydrodynamic theory.

It should be noted that Holló⁴ reported *no change* in the viscosity of amylose solutions on adding iodine. This result was due, we believe, to a combination of two circumstances – the experiments were performed in such a manner that the ionic strength of the solution was varied in addition to the iodine concentration, and, more importantly, the *relative* viscosity was graphed. As the latter quantity contains the contribution of the solvent, it would effectively disguise the change in hydrodynamic volume of the amylose.

We conclude that amylose, the first biopolymer for which a helical structure was suggested, thus differs from nucleic acids and proteins in that the helical conformation of its crystalline state is not retained in solution. However, this behaviour is not unique – in the field of synthetic polymers, those which are isotactic prefer a helical crystalline structure, but conform to the random coil model in solution. Amylose is, of course, an isotactic polymer, the stereoregularity of which is much higher than that of the more conventional synthetic macromolecules. There has existed a tendency to separate the hydrodynamic behaviour of synthetic polymers from that of biopolymers. It is therefore satisfying to record that those theories which have been applied successfully to describe the solution properties of synthetic macromolecules are equally applicable to amylose.

*Department of Chemistry,
The University of Edinburgh,
Edinburgh, EH9 3JJ,
Scotland, UK*

(Received 13 November 1970)

REFERENCES

- 1 Hanes, C. S. *New Phytologist* 1937, **36**, 189
- 2 Frendenberg, K., Schaaf, E., Dumpert, G. and Ploetz, T. *Naturwissenschaften* 1939, **27**, 850
- 3 Rundle, R. E. and French, D. J. *Amer. Chem. Soc.* 1943, **65**, 558
- 4 Holló, J. and Szejtli, J. *Stärke* 1958, **10**, 49
- 5 Szejtli, J. and Augustat, S. *Stärke* 1966, **18**, 38
- 6 Erlander, S. R. and Griffen, H. L. *Stärke* 1967, **19**, 139
- 7 Erlander, S. R. and Purves, R. M. *Stärke* 1968, **20**, 37

- 8 Banks, W. and Greenwood, C. T. *Carbohydrate Res.* 1968, **7**, 349
 9 Banks, W. and Greenwood, C. T. *Carbohydrate Res.* 1968, **7**, 414
 10 Banks, W. and Greenwood, C. T. *European Polymer J.* 1969, **5**, 649
 11 Burchard, W. *Makromol. Chem.* 1963, **64**, 110
 12 Rundle, R. E. and Baldwin, R. R. *J. Amer. Chem. Soc.* 1943, **65**, 554

On the measurement of thermal diffusivity

D. HANDS and F. HORSFALL

IN A NOTE¹ to *Polymer* 'On a common misunderstanding in the measurement of thermal diffusivity' Martin shows that the heat equation used in diffusivity experiments on polymers is frequently incorrectly derived. While we agree with this observation we do not agree with various conclusions that he makes.

Using nearly the same notation as Martin (ρ density; c_p specific heat at constant pressure; T temperature; t time; k thermal conductivity; α thermal diffusivity) the heat equation in one dimension is

$$\rho c_p \frac{\partial T}{\partial t} = \frac{\partial}{\partial x} \left(k \frac{\partial T}{\partial x} \right) \quad (1)$$

Martin points out that the equation used in measurements of thermal diffusivity

$$\frac{\partial T}{\partial t} = \frac{k}{\rho c_p} \frac{\partial^2 T}{\partial x^2} \quad (2)$$

is incorrect since, for the materials under consideration, the thermal conductivity is a function of temperature and therefore of position. From this he draws two main conclusions:

- (1) The thermal diffusivity

$$\alpha = \frac{k}{\rho c_p}$$

is meaningless if the thermal conductivity varies with temperature because it cannot be used in the heat equation.

- (2) Shoulberg² and other workers did not measure diffusivity since they used equation (2).

If we differentiate equation (1) and re-arrange the terms we get

$$\frac{1}{\alpha} \frac{\partial T}{\partial t} = \frac{\partial^2 T}{\partial x^2} + \frac{1}{k} \frac{dk}{dT} \left(\frac{\partial T}{\partial x} \right)^2 \quad (3)$$

Hence if the thermal conductivity varies with temperature two parameters

- 8 Banks, W. and Greenwood, C. T. *Carbohydrate Res.* 1968, **7**, 349
 9 Banks, W. and Greenwood, C. T. *Carbohydrate Res.* 1968, **7**, 414
 10 Banks, W. and Greenwood, C. T. *European Polymer J.* 1969, **5**, 649
 11 Burchard, W. *Makromol. Chem.* 1963, **64**, 110
 12 Rundle, R. E. and Baldwin, R. R. *J. Amer. Chem. Soc.* 1943, **65**, 554

On the measurement of thermal diffusivity

D. HANDS and F. HORSFALL

IN A NOTE¹ to *Polymer* 'On a common misunderstanding in the measurement of thermal diffusivity' Martin shows that the heat equation used in diffusivity experiments on polymers is frequently incorrectly derived. While we agree with this observation we do not agree with various conclusions that he makes.

Using nearly the same notation as Martin (ρ density; c_p specific heat at constant pressure; T temperature; t time; k thermal conductivity; α thermal diffusivity) the heat equation in one dimension is

$$\rho c_p \frac{\partial T}{\partial t} = \frac{\partial}{\partial x} \left(k \frac{\partial T}{\partial x} \right) \quad (1)$$

Martin points out that the equation used in measurements of thermal diffusivity

$$\frac{\partial T}{\partial t} = \frac{k}{\rho c_p} \frac{\partial^2 T}{\partial x^2} \quad (2)$$

is incorrect since, for the materials under consideration, the thermal conductivity is a function of temperature and therefore of position. From this he draws two main conclusions:

- (1) The thermal diffusivity

$$\alpha = \frac{k}{\rho c_p}$$

is meaningless if the thermal conductivity varies with temperature because it cannot be used in the heat equation.

- (2) Shoulberg² and other workers did not measure diffusivity since they used equation (2).

If we differentiate equation (1) and re-arrange the terms we get

$$\frac{1}{\alpha} \frac{\partial T}{\partial t} = \frac{\partial^2 T}{\partial x^2} + \frac{1}{k} \frac{dk}{dT} \left(\frac{\partial T}{\partial x} \right)^2 \quad (3)$$

Hence if the thermal conductivity varies with temperature two parameters

govern the temperature distribution, thermal diffusivity α , and $(1/k)(dk/dT)$. Thermal diffusivity is therefore still an essential part of the heat equation.

We have developed a computer programme for simulating diffusivity experiments using equation (3). Using data for k^3 , ρ^4 and c_p^5 for polystyrene the programme predicts that to detect the effect of neglecting $(1/k)(dk/dT)(\partial T/\partial x)^2$ Shoulberg would have needed thermocouples sensitive to about 0.002°C. The sensitivity of the system he used was at least an order of magnitude worse than this. Thus in his case equation (2) was quite adequate. Since the thermal properties of polymers all appear to be of the same order of magnitude we expect similar results for other polymers.

Hence diffusivity not only arises in the heat equation but in general it is the dominant parameter. If under circumstances different from the ones considered above the term $(1/k)(dk/dT)(\partial T/\partial x)^2$ becomes significant it can be taken into account using, for instance, data from conductivity measurements.

*Rubber and Plastics Research Association,
Shawbury,
Shrewsbury, SY4 4NR, UK*

(Received 14 September 1970)

REFERENCES

- 1 Martin, B. *Polymer, Lond.* 1970, **11**, 287
- 2 Shoulberg, R. H. *J. appl. Polym. Sci.* 1963, **7**, 1597
- 3 Lohe, P. *Kolloid Z.* 1965, **203**, 115
- 4 Brandrup, J. and Immergut, E. H., 'Polymer Handbook', Wiley, 1966
- 5 Abu-Isa, I. and Dole, M. *J. Phys. Chem.* 1965, **69**, 2668

On the temperature dependence of the thermal diffusivity

A. W. RIDDIFORD

MARTIN recently stated¹ that knowledge of the temperature dependence of the diffusive conductivity $\kappa(T)$ is of no value, and that separate measurements of the density ρ , specific heat per unit mass at constant pressure c_p , and thermal conductivity k as functions of temperature should be made.

It is the intent of this note to show that only the diffusive conductivity $\kappa(T) = k/(\rho c_p)$ and the thermal conductivity $k(T)$ are needed.

Following Martin's derivation: in one-dimension the defining relation for thermal conductivity k in an isotropic material is

$$q_x = -k \frac{\partial T}{\partial x} \quad (1)$$

where q_x is the local heat flux and $\partial T/\partial x$ the temperature gradient. Sub-

govern the temperature distribution, thermal diffusivity α , and $(1/k)(dk/dT)$. Thermal diffusivity is therefore still an essential part of the heat equation.

We have developed a computer programme for simulating diffusivity experiments using equation (3). Using data for k^3 , ρ^4 and c_p^5 for polystyrene the programme predicts that to detect the effect of neglecting $(1/k)(dk/dT)(\partial T/\partial x)^2$ Shoulberg would have needed thermocouples sensitive to about 0.002°C. The sensitivity of the system he used was at least an order of magnitude worse than this. Thus in his case equation (2) was quite adequate. Since the thermal properties of polymers all appear to be of the same order of magnitude we expect similar results for other polymers.

Hence diffusivity not only arises in the heat equation but in general it is the dominant parameter. If under circumstances different from the ones considered above the term $(1/k)(dk/dT)(\partial T/\partial x)^2$ becomes significant it can be taken into account using, for instance, data from conductivity measurements.

*Rubber and Plastics Research Association,
Shawbury,
Shrewsbury, SY4 4NR, UK*

(Received 14 September 1970)

REFERENCES

- 1 Martin, B. *Polymer, Lond.* 1970, **11**, 287
- 2 Shoulberg, R. H. *J. appl. Polym. Sci.* 1963, **7**, 1597
- 3 Lohe, P. *Kolloid Z.* 1965, **203**, 115
- 4 Brandrup, J. and Immergut, E. H., 'Polymer Handbook', Wiley, 1966
- 5 Abu-Isa, I. and Dole, M. *J. Phys. Chem.* 1965, **69**, 2668

On the temperature dependence of the thermal diffusivity

A. W. RIDDIFORD

MARTIN recently stated¹ that knowledge of the temperature dependence of the diffusive conductivity $\kappa(T)$ is of no value, and that separate measurements of the density ρ , specific heat per unit mass at constant pressure c_p , and thermal conductivity k as functions of temperature should be made.

It is the intent of this note to show that only the diffusive conductivity $\kappa(T) = k/(\rho c_p)$ and the thermal conductivity $k(T)$ are needed.

Following Martin's derivation: in one-dimension the defining relation for thermal conductivity k in an isotropic material is

$$q_x = -k \frac{\partial T}{\partial x} \quad (1)$$

where q_x is the local heat flux and $\partial T/\partial x$ the temperature gradient. Sub-

stituting equation (1) into the differential equation governing non-steady heat flow in one dimension

$$\rho c_p \frac{\partial T}{\partial t} = - \frac{\partial q_x}{\partial x} \quad (2)$$

gives

$$\rho c_p \frac{\partial T}{\partial t} = \frac{\partial}{\partial x} \left(k \frac{\partial T}{\partial x} \right) \quad (3)$$

where t denotes time.

Introducing

$$w(T) \equiv \int_0^T \kappa(T) dT, \quad (4)$$

the heat equation (3) becomes

$$\frac{\partial w}{\partial t} = \kappa(T) \frac{\partial^2 w}{\partial x^2} \quad (5)$$

where $\kappa(T)$ is the diffusive conductivity. Boundary conditions involving w or $\partial w / \partial x$ can be stated in terms of T or $\partial T / \partial x$ by using equation (4) or (taking the gradient of equation 4)

$$\frac{\partial w}{\partial x} = \kappa(T) \frac{\partial T}{\partial x}. \quad (6)$$

The equation (5) is not linear because of the temperature dependence of the diffusive conductivity $\kappa(T)$. But numerical calculations can be made with it using the known temperature profile at the beginning of each time step to define $\kappa(T)$ for each node. For the geometry and initial conditions that we have used, the solution becomes independent of time step when the time step is shortened to make $Dx^2/Dt = \min(\kappa(T))$, where Dx is the node spacing and Dt the time step.

It must be pointed out that at the end of each time step the temperature profile $T(x)$ must be found from $w(x)$, so a simple analytic form of the inverse of equation (4) must be known. In our experience $k(T)$ was approximated by straight lines making the inverse function involve square roots.

Meaningful calculations require only the knowledge of the diffusive conductivity $\kappa(T)$ and the thermal conductivity $k(T)$. The essential idea of the above method can be found on p. 209 of Crank's book.²

Continental Can Company, Inc.
7622 South Racine Avenue
Chicago, Illinois 60620, USA

(Received 30 October 1970)

REFERENCES

- 1 Martin, B. *Polymer, Lond.* 1970, **11**, 287
- 2 Crank, J. 'The Mathematics of Diffusion', Oxford Univ. Press, 1956

Kinetics of non-isothermal crystallization

T. OZAWA

Non-isothermal kinetics of the process of nucleation and its growth are derived by extending Avrami's equation. Kinetic analysis of the thermo-analytical data of the process is also described and applied to DSC curves of crystallization obtained by cooling poly(ethylene terephthalate) at constant rates. Crystallization is thought to proceed by nuclei being formed randomly and growing in three-dimensions.

INTRODUCTION

ALTHOUGH THE kinetics of isothermal process have been thoroughly studied, few attempts to elucidate the kinetics of dynamic, non-isothermal processes have been made. Recently Flynn¹ proposed non-isothermal kinetics for simple homogeneous chemical reactions and the present author also published papers on the subject^{2,3}. Practical processes such as industrial synthesis proceed under dynamic, non-isothermal conditions and not under isothermal conditions. It is necessary to extend the isothermal kinetics to non-isothermal dynamic kinetics for various types of processes.

One of the kinetic studies of importance is the process of growth and nucleation; crystallization is a typical part of nucleation and growth. Avrami's equation is proposed for these processes⁴⁻⁷, and many processes such as tinning and galvanizing were found to follow Avrami's kinetic equation. Crystallization of high polymers also follows Avrami's equation⁸, and in practical processes including melt-spinning of synthetic fibres and fabrication of crystalline polymers crystallization of the polymer occurs under non-isothermal conditions. However there have been no kinetic investigations of these processes.

Kinetic investigations have been carried out isothermally, since isothermal kinetics are simpler than non-isothermal kinetics, but isothermal measurement is only possible when the thermal response time of the measured system is small compared with the rate of the process. Otherwise the process begins to occur before the system reaches the desired temperature. In this case, one should use a thermoanalytical method in which observations of the sample are made under a constant rate of heating or cooling. Such a situation seems to be encountered in crystallization under high pressure. For these cases the method of kinetic analysis of thermoanalytical data should be developed.

In this paper, non-isothermal kinetics of the process of nucleation and growth are investigated theoretically, extending Avrami's equation to the non-isothermal situation, and a method of kinetic analysis of thermoanalytical data of the process is derived from the theory. The theory and the method obtained have been applied to the thermoanalytical data of the crystallization of poly(ethylene terephthalate).

THEORY

In the theoretical treatment of the kinetics of the process it has been assumed that the substance is heated or cooled at a constant rate and the mathematical derivation made by Evans⁷ has been extended. We should first calculate the expectancy of circular waves on a pond caused by raindrops passing over a representative point, P. A nucleus and a front of its growth are compared with the raindrop and the wave, respectively. Up to time t , P is passed over by waves caused by the raindrops falling until the time τ and within the distance which the wave traverses from τ to t . The expectancy, E is equal to the number of such raindrops, and the probability that i waves pass over P is equal to $\exp(-E)E^i/i!$ according to Poisson's formula. In the actual process under consideration, a point once passed over by the growing front is not passed over by other fronts. Then, the only valid probability is that of $i = 0$ for the actual process, and it is equal to the fraction not converted.

When we expand the above treatment to the case of the substance being cooled at a constant rate, a , the distance r which the front of the growth traverses from the time τ to t is given by

$$r = \int_{\tau}^t v(T) dt \quad (1)$$

where $v(T)$ is the linear growth rate as a function of the temperature T , and integration gives

$$r = \frac{1}{a} [R_c(T) - R_c(\theta)] \quad (2)$$

where $R_c(T)$ equals to $\int_{T_m}^T v(T) dT$, and T , θ and T_m are respectively the temperature at t , that at τ and the temperature above which the process cannot proceed. The number j of the nuclei per unit volume or area which form from T_m to θ is given by

$$j = \int_{T_m}^{\theta} v(T) dt \quad (3)$$

$$= \frac{1}{a} \int_{T_m}^{\theta} v(T) dT \quad (4)$$

$$= N_c(\theta)/a \quad (5)$$

where $\nu(T)$ is the nucleation rate as a function of T and $N(\theta)$ equals $\int_{T_m}^{\theta} \nu(T) dT$.

The expectancy, $E(T)$, that the number of the waves pass over P from T_m to T is then as follows

$$E(T) = g \int_{T_m}^T jr^m dr \quad (6)$$

$$= (g/a^{m+2}) \int_{T_m}^T N_c(\theta) [R_c(T) - R_c(\theta)]^m v(\theta) d\theta \quad (7)$$

where m and g depend on the dimension of the growth as follows;

dimension of growth	m	g
one dimensional growth	0	area of nucleus
two dimensional growth	1	2π
three dimensional growth	2	π

As the integration of equation (7) depends only on T

$$E(T) = \chi_c(T)/a^n \tag{8}$$

where n equals to $m + 2$ and $\chi_c(T)$ is $g \int_{T_m}^T N_c(\theta)[R_c(T) - R_c(\theta)]^m v(\theta) d\theta$, and it should be called the cooling function of the process.

Thus, the conversion C at temperature T and cooling rate a is given by

$$1 - C(T) = \exp [-\chi_c(T)/a^n] \tag{9}$$

When the substance is heated at a rate, a , from the temperature at which the process scarcely occurs, the following similar equation holds

$$1 - C(T) = \exp [-\chi_h(T)/a^n] \tag{10}$$

where

$$\chi_h(T) = g \int_0^T N_h(\theta)[R_h(T) - R_h(\theta)]v(\theta) d\theta \tag{11}$$

and

$$R_h(\theta) = \int_0^\theta v(T) dT \tag{12}$$

$$N_h(\theta) = \int_0^\theta \nu(T) dT \tag{13}$$

The equations for the rate of the process are given as follows

$$dC(T)/dt = [1 - C(T)]\chi'_c(T)/a^{n-1} \tag{14}$$

and

$$dC(T)/dt = [1 - C(T)]\chi'_h(T)/a^{n-1} \tag{15}$$

where

$$\chi'_c(T) = d\chi_c(T)/dT \tag{16}$$

and

$$\chi'_h(T) = d\chi_h(T)/dT \tag{17}$$

If the pre-determined nuclei exist before cooling, the number of nuclei becomes constant and equals the density ω of the nuclei. Then, on cooling

$$E(T) = g\omega \int_{T_m}^T r^m dr \tag{18}$$

$$= (g\omega/a^{m+1}) \int_{T_m}^T [R_c(T) - R_c(\theta)]^m v(\theta) d\theta \tag{19}$$

$$= \chi_c(T)/a^n \tag{20}$$

where

$$\chi_c(T) = g\omega \int_{T_m}^T [R_c(T) - R_c(\theta)]^m v(\theta) d\theta \quad (21)$$

and equations (9) and (14) hold for this case, but n equals $m + 1$. Similar equations are also derived in the case of heating, where

$$\chi_h(T) = g\omega \int_0^T [R_h(T) - R_h(\theta)]^m v(\theta) d\theta \quad (22)$$

and n also equals $m + 1$.

If we now observe the process at different rates of cooling or heating, the kinetic parameter mentioned above can be obtained, since from equations (9) or (10)

$$\log \{-\ln \{1 - C(T)\}\} = \log \chi(T) - n \log a \quad (23)$$

If we plot $\log \{-\ln [1 - C(T)]\}$ against $\log a$ at a given temperature, a straight line can be obtained, and n and $\chi(T)$ can be estimated from the slope and the intercept of the line. $\chi(T)$ is obtained as a function of the temperature from the plots at different temperatures. A similar procedure is also applied to the rate according to equations (14) or (15).

If the cooling or heating rate is changed during the process, the kinetic equation can be obtained according to the additivity of the expectancy. For instance, when the substance is cooled from T_m to T_1 at a_1 , from T_1 to T_2 at a_2 , from T_2 to T_3 at a_3 and so on.

$$\begin{aligned} -\ln \{1 - C(T)\} = & \chi_c(T_1)/a_1^n \\ & + [\chi_c(T_2) - \chi_c(T_1)]/a_2^n \\ & + [\chi_c(T_3) - \chi_c(T_2)]/a_3^n \\ & + \dots \end{aligned} \quad (24)$$

EXPERIMENTAL

The sample of poly(ethylene terephthalate), kindly supplied by Toray Industries Ltd, was dissolved in a mixture of phenol and *sym*-tetrachloroethane (1:1 by volume), reprecipitated by methanol, and dried under vacuum. The molecular weight was obtained by measuring the viscosity of the solution of the same mixed solvent at 25°C⁹: it was estimated to be 20 300.

Both the isothermal and dynamic (cooling) crystallizations of the sample were observed with a Perkin-Elmer differential scanning calorimeter, since differential thermal analysis is not suitable for kinetic analysis³. The sample was heated from 480 K to 550 K at the rate of 16 K/min and cooled at the rate of 1.2 or 4 K/min, immediately after the sample reached 550 K. The isotherms were obtained by heating the sample from 480 K to 550 K at 16 K/min and immediately cooling it to the desired temperature by manual operation of the temperature-dial. Both operations were carried out under nitrogen.

RESULTS AND DISCUSSION

Typical DSC curves obtained in the dynamic cooling crystallization are shown in *Figure 1*. The curves were analysed according to equation (23) at a few

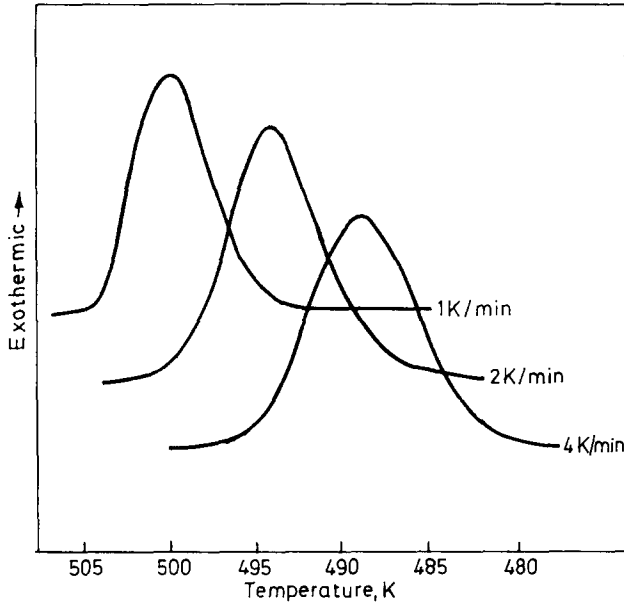


Figure 1 Typical DSC thermograms of the dynamic cooling crystallization of poly(ethylene terephthalate).

temperatures, the results are shown in *Figure 2* where the straight lines of the slope of four are drawn. *Figure 2* shows the clear linear dependence of $\log \{-\ln [1 - C(T)]\}$ upon $\log a$ and the slopes of the lines suggest that the nuclei of crystallization of poly(ethylene terephthalate) are randomly formed during crystallization and that the crystallites grow three-dimensionally in the temperature ranges. From the intercepts of the lines at 1 K/min, we obtained the cooling crystallization function of the polymer, which is shown in *Figure 3*.

The DSC curves of the isothermal crystallization were also analysed by the ordinary procedure¹⁰, and the results are shown in *Figure 4*. The slopes of the lines are estimated by the method of least squares, to be 3.4, 3.6 and 3.6 at 493 K, 495 K and 500 K, respectively.

The agreement between the results of the isothermal and cooling crystallization is satisfactory. Rybnikar¹¹ reported $n = 4$ above 217°C for the samples heat-treated for 15 min at 265°C from their isotherms of the crystallization of the polymer and found $n = 3$ in the temperature range between 160°C and 240°C, when the sample is maintained at 290°C for 15 min. Morgan *et al*¹² reported $n = 4$ above 235°C and $n = 3$ between 170°C and 220°C for the sample melted at 294°C for 15 min, but $n = 4$ at 250°C and $n = 3$

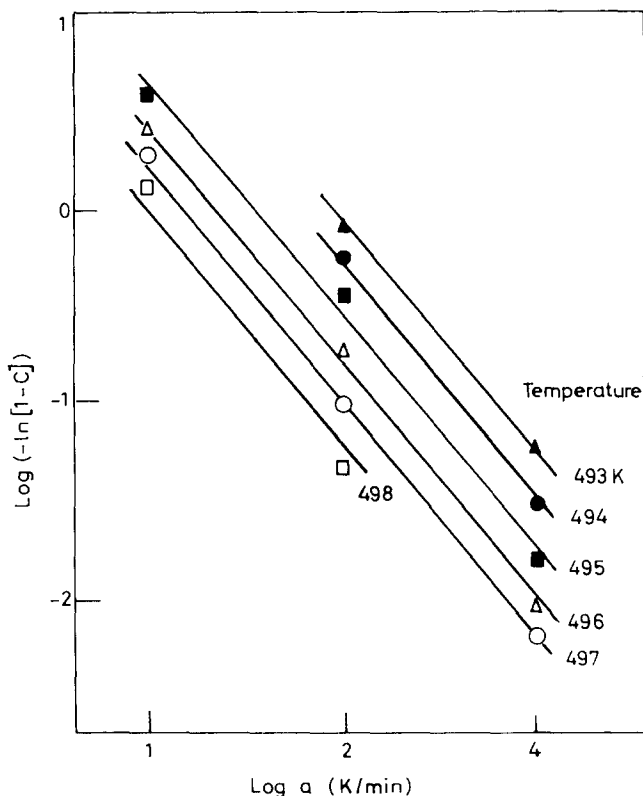


Figure 2 The plots of $\log[-\ln(1-C)]$ versus $\log a$ for the dynamic cooling crystallization of poly(ethylene terephthalate).

between 106°C and 249°C, when they melted the sample at 268°C for 15 min. Cobbs and Burton¹³ reported smaller values for n in the same temperature range. Our results are in good agreement with the results of isothermal observations at the higher temperature reported by Rybnikar and Morgan *et al.* It is interesting to note that there is agreement between the isothermal crystallization at the higher temperature and the dynamic crystallization carried out in the sample cooled from the higher temperature.

The results mentioned above suggest that the kinetic formulae derived in this paper for the dynamic, non-isothermal process of nucleation and growth is applicable, and that the mathematical treatment described can be used to predict the actual and non-isothermal processes.

For the dynamic crystallization of polymers, the fold-length of the polymer chain should be taken into account, since the fold-lengths crystallized isothermally are different at different temperatures. If the changes in fold-length depend upon the temperature during the dynamic crystallization, $v(T)$ is not the rate of linear growth but the product of the rate and the fold-length. Otherwise, $v(T)$ is the rate of linear growth. Another point to be taken account of is the variation of n with the crystallization temperature. Unless

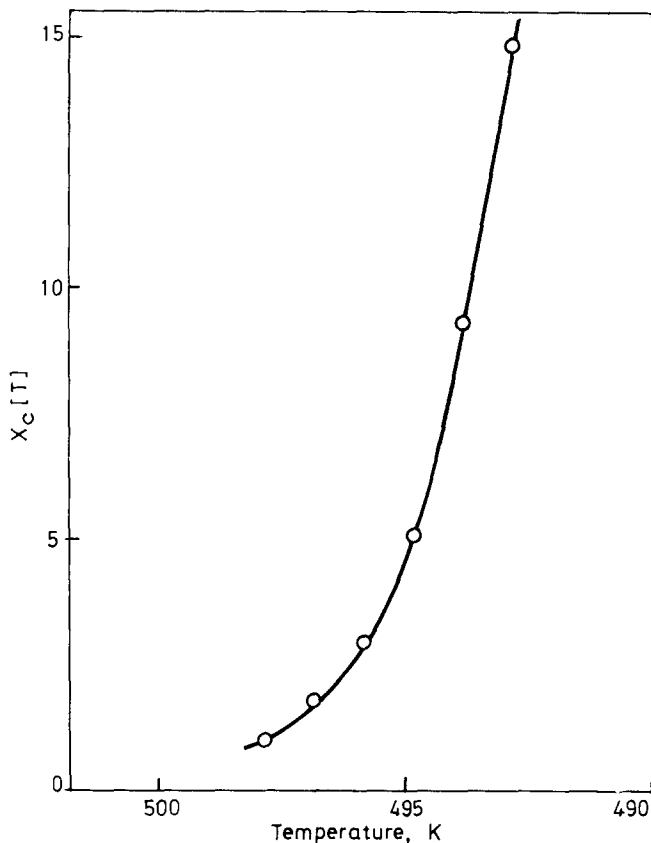


Figure 3 The cooling crystallization function of poly(ethylene terephthalate). The dimensions are degree and minute.

the mechanism of variation is elucidated, the equation modified by taking the variation into account cannot be derived.

Furthermore, the crystallization of polymers consists of two processes – the ‘primary’ (Avrami) crystallization followed by the slow ‘secondary’ (post-Avrami) crystallization. The theory and method of analysing thermoanalytical curves for the process of nucleation and growth described in this paper neglect the secondary crystallization. A more exact theory might be derived by expanding the theory of isothermal crystallization of polymers derived by Gordon and Hillier¹⁴. As pointed out by Hillier¹⁵, a false value of n might be obtained if the slow secondary crystallization is neglected in an isotherm. However, this effect is not so serious in dynamic, non-isothermal observations as in the isothermal ones, since the slow secondary crystallization following the primary one becomes slower at the lower temperature and the rate is recorded in the dynamic DSC curve. The discrepancy between the value of n obtained by dynamic observations and those obtained isothermally seems to be caused by this effect.

KINETICS OF NON-ISOTHERMAL CRYSTALLIZATION

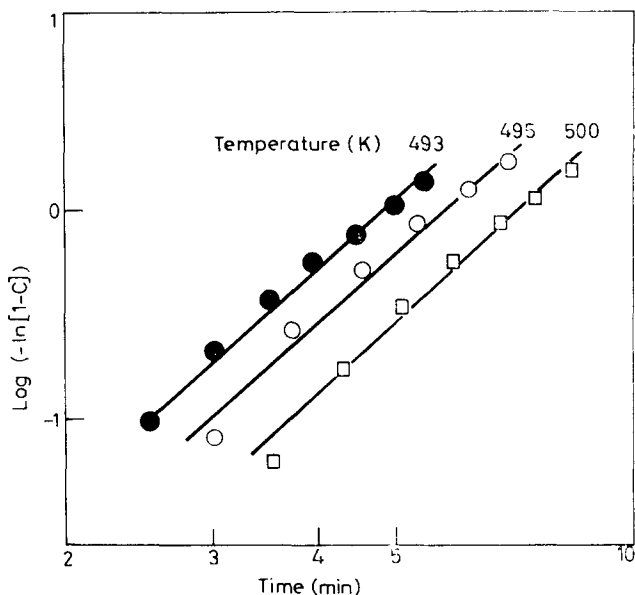


Figure 4 The analysis of isotherms of the crystallization of poly(ethylene terephthalate).

The experimental master curve can be drawn, since the plots of $\log \{-\ln [1 - C(T)]\}$ against the temperature at different cooling rates are superimposed on each other by longitudinal shifts, and the length of the shift is equal to $n \log a$. If there is appreciable secondary crystallization, the superposition cannot be made, especially in the latter part of the master curve. Thus the effect might be detected in the experimental master curve.

Among the processes of nucleation and growth are solid heterogeneous reactions such as thermal decomposition of inorganic hydrates^{16, 17}, where nucleation occurs on the surface of the crystallite. However, the analysis of thermoanalytical curves of these processes has been made on the basis of the conventional kinetics of homogeneous reactions¹⁸ or the phenomenological equations¹⁹. The analysis should be made on the basis of the kinetic formulae derived from the actual model of the nucleation and growth. The formulae would be derived by modification of the derivation described in this paper.

*Electrotechnical Laboratory,
Tanashi, Tokyo,
Japan*

(Received 22 May 1970)
(Revised 2 September 1970)

REFERENCES

- 1 Flynn, J. H., 'Thermal analysis', Vol 2, p 1111 (Eds. R. F. Schwenker, Jr. and P. D. Garn) Academic Press, New York, 1969
- 2 Ozawa, T. *Bull. Chem. Soc. Japan* 1965, **38**, 1881
- 3 Ozawa, T. *J. Thermal Analysis* to be published
- 4 Avrami, M. *J. Chem. Phys.* 1939, **7**, 1103; *ibid* 1940, **8**, 212; *ibid* 1941, **9**, 177
- 5 von Goler, F. and Sachs, G. *Z. Physik* 1932, **77**, 281

- 6 Johnson, W. A. and Mehl, R. F. *Trans. Amer. Inst. Mining Met. Engrs.* 1939, **135**, 416
- 7 Evans, U. R. *Trans. Faraday Soc.* 1945, **41**, 365
- 8 Mandelkern, L., 'Crystallization of polymers', McGraw-Hill, New York, 1964
- 9 Gaylord, N. G. and Rosenbaum, S. *J. Polym. Sci.* 1959, **39**, 545
- 10 For example, Booth, A. and Hay, J. N. *Polymer, Lond.* 1969, **10**, 95
- 11 Rybnikar, F. *Coll. Czech. Chem. Comm.* 1960, **25**, 1529; *ibid.* 1960, **25**, 1540
- 12 Keller, A., Lester, G. R. and Morgan, L. B. *Phil. Trans. Roy. Soc., Lond.* 1954, **A247**, 1; Hartley, F. D., Lord, F. W. and Morgan, L. B. *ibid.* 1954, **A247**, 24
- 13 Cobbs, W. H. and Burton, R. L. *J. Polym. Sci.* 1953, **10**, 275
- 14 Gordon, M. and Hillier, I. H. *Trans. Faraday Soc.* 1964, **60**, 763
- 15 Hillier, I. H. *J. Polym. Sci. (A)* 1965, **3**, 3067
- 16 Clarke, T. A. and Thomas, J. M. *Nature* 1968, **219**, 1149
- 17 Heide, K. *J. Thermal Analysis* 1969, **1**, 183
- 18 For example, Freeman, E. S. and Carroll, B. *J. Phys. Chem.* 1958, **62**, 394
- 19 For example, Sharp, J. H. and Wentworth, S. A. *Anal. Chem.* 1969, **41**, 2060

Low frequency dielectric behaviour of polyamides

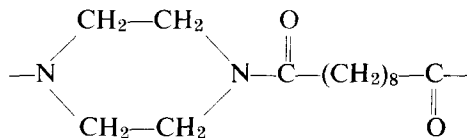
M. E. BAIRD, G. T. GOLDSWORTHY and C. J. CREASEY

At low audio frequencies and at temperatures above the glass transition a large relaxation occurs in polyamides. Both this low frequency relaxation and the relatively high d.c. conductivity of polyamides have been attributed by several workers to the movement of amide protons. A comparison of the dielectric behaviour of a normal polyamide (6,10 and 6,6) with poly(sebacyl piperazine), prepared from the secondary diamine piperazine, in which no N-H groups are present in the repeat unit is described. D.C. step response measurements were used (as well as normal a.c. measurements) in order to separate the components of loss due to relaxation and conduction. The data showed that amide protons are not the main cause of this low frequency relaxation and on the basis of all existing information they do not make any significant contribution until temperatures over 110°C are reached. The main relaxation observed arises from interfacial polarization throughout the bulk of the polymer, almost certainly due to trapping of electrons at the boundaries between crystalline and amorphous regions. Possible mechanisms are discussed. The d.c. step response measurements showed that the dielectric behaviour at low frequencies is quite complicated and that almost certainly a second mode or relaxation occurs at still lower frequencies. Since the retardation times involved in this second mode are extremely long this behaviour requires further study with very long charging times.

INTRODUCTION

VARIOUS relaxations have been observed in polyamides, forming a complicated spectrum. At low frequencies and at temperatures above the glass transition, T_g , a large relaxation process occurs. Both this relaxation and the relatively high d.c. conductivity of polyamides have been attributed¹⁻⁵ to the movement of protons originating in the hydrogen bonds which are traditionally thought to occur between polyamide molecules. Loss peaks in this region have been studied by Hirota *et al*⁶. In a previous publication⁷ certain data which were not consistent with this postulate of proton movement were listed together with the work of Cannon⁸⁻¹¹ who discussed the role of quantum mechanical hydrogen bonding and forces between dipoles in controlling the packing and configuration of the polyamide molecules in the solid state. These facts cast some doubt on the importance of amide protons in the conduction and relaxation processes. Previous work on the d.c. conductivity of polyamides¹²⁻¹⁴ 6,6 and 6,10 also showed that amide protons did not play a significant part until temperatures over about 110°C were reached. In this publication⁷ a brief summary of results was given showing that this low frequency dielectric behaviour occurred to a similar extent in poly(sebacyl piperazine), a polyamide prepared from the secondary diamine, piperazine, in which no N-H groups were present and no hydrogen bonding could occur. This indicated that amide protons could not be the main cause of this

low frequency relaxation in polyamides. A full account of the dielectric behaviour of normal and piperazine-polyamide is now given and the nature of the mechanism of this low frequency relaxation is discussed. The repeat unit of poly(sebacyl piperazine) is shown below



EXPERIMENTAL

Polymers

The infra-red spectrum of the Pip-10 polyamide closely matched one published¹⁵ and showed the complete absence of the strong N-H stretching absorption at 3300cm^{-1} found in ordinary polyamides.

The general properties of the 6,10 and Pip-10 polyamides used are now given in *Table 1*.

The 6,10 polymer had impurities not exceeding 0.003% (as given by the supplier, ICI Ltd, Plastics Division) and the Pip-10 polymer was purified by

Table 1 General properties of the 6,10 and Pip-10 polyamides used

<i>Polyamide</i>	<i>Melting Pt.</i> (°C)	<i>Glass Transition</i> (°C, dry)	<i>Approx.,</i> <i>Molecular Wt</i>	<i>Density</i> (g/ml) (room temp.)	<i>% Crystallinity</i>
6,10	220	50	20000 (weight average) 15000 (number average)	1.09	40
Pip-10	160	80*	33000 (solution viscosity average) 16000 (number average)	1.15	medium†

* Undefined transition as observed in dilatometry experiments

† Obtained from x-ray powder photographs and infra-red spectroscopy. Unfortunately the assessment is not as reliable as for a normal polyamide because of a lack of background experience and no actual figure can be given

re-precipitation from benzyl alcohol and subsequent thorough washing with acetone.

Some measurements were also made with 6,6 polyamide which had a melting point of about 260°C , a number average molecular weight of about 17000, a density of $1.14 \pm 0.01\text{g/ml}$ at room temperature and crystallinity probably in the region of 35%. It contained no filler or other additives.

Disc specimens with thicknesses in the range 0.04–0.52cm were moulded, coated with aluminium electrodes by vacuum deposition, dried* and examined

* The specimens were heated for a total of about 5 hours at 120°C in dry nitrogen and stored over phosphorus pentoxide to constant weight before use. The data obtained were reproducible after further heating

in a three-terminal shielded electrode assembly immersed in a temperature controlled oil bath, as described in a previous paper⁷. Dry nitrogen was passed through the assembly to keep the specimens dry. The polymers were examined over the audio-frequency range 50–10⁵ Hz using a GR 1615-A capacitance bridge and at low frequencies about 10⁻⁵ Hz to 10⁻² Hz, using the d.c. transient technique (d.c. step response¹⁶ measurements). A Keithley 610-B electrometer was used to measure the direct currents, the circuit being as in figure 6 of reference 15. The emf used was 125 ± 2 volts.

Results presented later show that the low frequency relaxation and d.c. conductivity are representative of the bulk polymer and a direct comparison of the properties of normal and Pip-10 polyamides is now given.

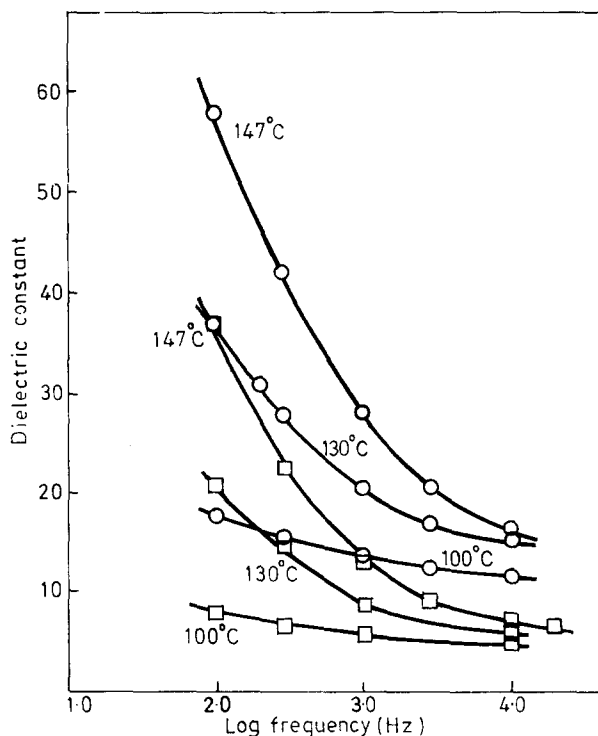


Figure 1 Plots of dielectric constant against log frequency for dry polyamides
 ○ 6,10 □ Pip-10

A.C. data

The behaviour of the dielectric constant ϵ' of both polyamides is shown in Figure 1 as functions of frequency at various temperatures. This behaviour of the 6,10 polymer is typical of results obtained in previous studies and shows the large magnitude of this low frequency relaxation occurring at temperatures above T_g . The behaviour of the Pip-10 polyamide is similar to that of the 6,10 polymer. Clearly this low frequency relaxation is also present in the Pip-10 polyamide. In order to assess whether this relaxation is of

comparable magnitude in the Pip-10 polyamide, it is probably better to compare values of dielectric constant since the loss factor contains an appreciable component arising from d.c. conductivity. There is considerable variation between specimens and between batches. Including data from reference 4, the dielectric constant for 6,10 and 6,6 polyamides at 100Hz and about 145°C ranged from 38 to 65 and at 100Hz and about 125°C from 29 to 41. The corresponding ranges for Pip-10 polyamide from our work were 16 to 46 and 14 to 30 respectively.

At the same temperature the values for the Pip-10 polymer are lower on the whole than for the 6,10 polymer but some of the Pip-10 specimens show

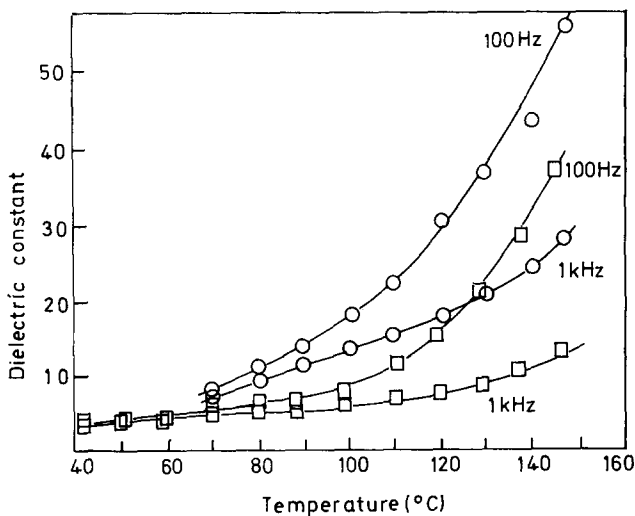


Figure 2 Variation of dielectric constant with temperature for dry polyamides
○ 6,10 □ Pip-10

dielectric constants as large as for the 6,10 and 6,6 polyamides. Moreover the glass transition for the Pip-10 polyamide is probably in the region of 80°C whilst that for the 6,10 polymer is about 50°C, so that there is very little difference between the dielectric constants for the two polymers at the same increment above T_g . This is further illustrated in Figure 2 where the dielectric constant is plotted against temperature at fixed frequency for the polymers described in Table 1. The curves for a frequency of 1kHz show a point of inflection due to the presence of the α -relaxation as well as the low frequency relaxation. It is interesting to note that in the region 70–110°C similar values are observed at 100Hz for the two polymers at temperatures about 20–30°C apart, although above 110°C the values for Pip-10 approach those for 6,10 at the same temperature. Although firm conclusions cannot be made because the dielectric constant is still rising and the dielectric increment cannot be evaluated at these temperatures, these results definitely suggest that there is not a great difference between this low frequency relaxation in normal and piperazine polyamides.

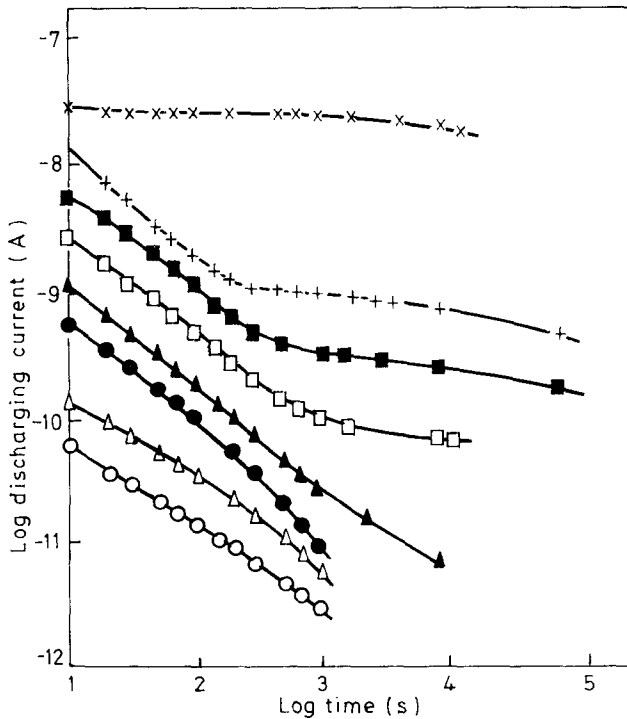


Figure 3 Double log plots of discharging current against time for dry 6.6 polyamide
 ○ 49.5°C △ 54.6°C ● 64.5°C ▲ 70°C □ 79.9°C
 ■ 84.5°C; + 89.4°C; × 113.7°C

D.C. data

Further information was obtained from d.c. step response (charge-discharge) measurements. This technique has the advantage of separating the components¹⁶ of loss factor ϵ'' from relaxation and d.c. conductivity and the discharging currents may be transformed to yield the loss factor for relaxation alone. Small currents were observed before the specimens were put on charge, these being traced to small voltages (~ 0.3 volts) exhibited by the polymer, probably from thermoelectric, piezo-electric or electrochemical phenomena. The specimens were charged for a minimum period of three hours. The discharging currents were corrected to allow for these small currents. Typical behaviour of the discharging currents is shown in the double log plots in Figure 3 for nylon 6,6. Similar behaviour was observed with pip-10 polyamide. The behaviour to be expected has been discussed in a previous paper¹⁶ for materials which conform to a Cole-Cole^{17,18} distribution of relaxation times. The displacement or reversible transient current for these materials for unit applied voltage and unit vacuum capacitance is given by the formula

$$i(t) = \left(\frac{\epsilon_s - \epsilon_\infty}{\tau_0} \right) (1 - \alpha) \left(\frac{t}{\tau_0} \right)^{-\alpha} \sum_{n=1}^{\infty} \frac{(-1)^{n-1} n}{\Gamma(1 + n(1 - \alpha))} \left(\frac{t}{\tau_0} \right)^{(n-1)(1-\alpha)} \quad (1)$$

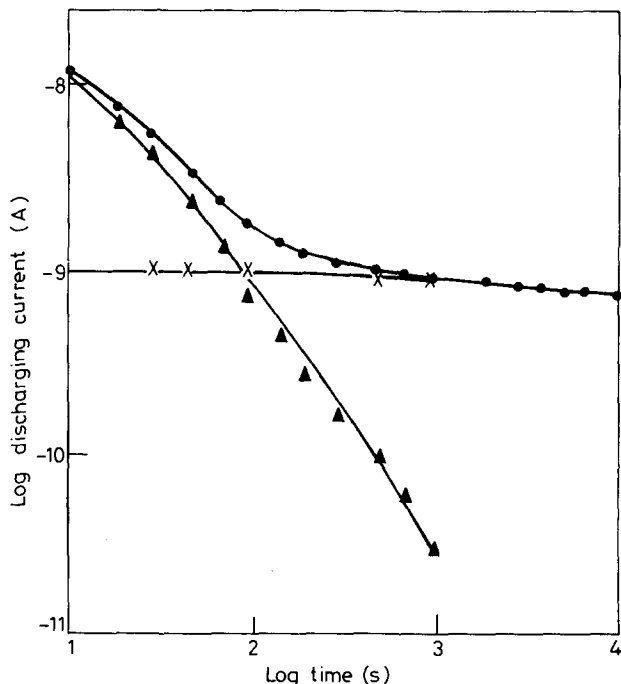


Figure 4 Resolution of observed discharging current into its two components for dry polyamide 6,6 at 89.4°C;
 ● observed current; ▲ 1st component; × 2nd component

where $\epsilon_s - \epsilon_\infty$ is the dielectric (constant) increment, t is the time, α is the parameter determining the width of the Cole-Cole distribution and τ_0 is the most probable relaxation time. The double log plot of current against time shows, with slight exceptions, a continuously increasing negative slope in the dispersion region. This slope passes through the value -1 in the region $t \simeq \tau_0$ and approaches a value of $-(2 - \alpha)$ when $t \gg \tau_0$. When $t \ll \tau_0$ the slope is $-\alpha$. This type of behaviour was shown at lower temperatures by all the polyamides, e.g. nylon 6,6 in the range 50–65°C and pip-10 (Batch B) in the range 35 to about 50°C. The increase of current at short times as the temperature was raised is readily explained by an increase in $\epsilon_s - \epsilon_\infty$ and a reduction in τ_0 . However at higher temperatures the behaviour obviously becomes more complicated as shown in Figure 3. The total discharging current would appear to be the sum of two components as illustrated in Figure 4. The first component is a normal (relaxation) transient current but the other is a nearly constant current which could arise from a bi-modal distribution of relaxation times, the second mode consisting of a fairly narrow distribution of very long retardation times. This mode would give a fairly constant current for times $t \ll \tau_0$, the most probable retardation time for the second mode, but the current would begin to fall as t approaches τ_0 . The possibility of assigning one mode to electrons and the other to amide protons is ruled out because the phenomenon is exhibited by pip-10 polyamide as well as the normal polyamide.

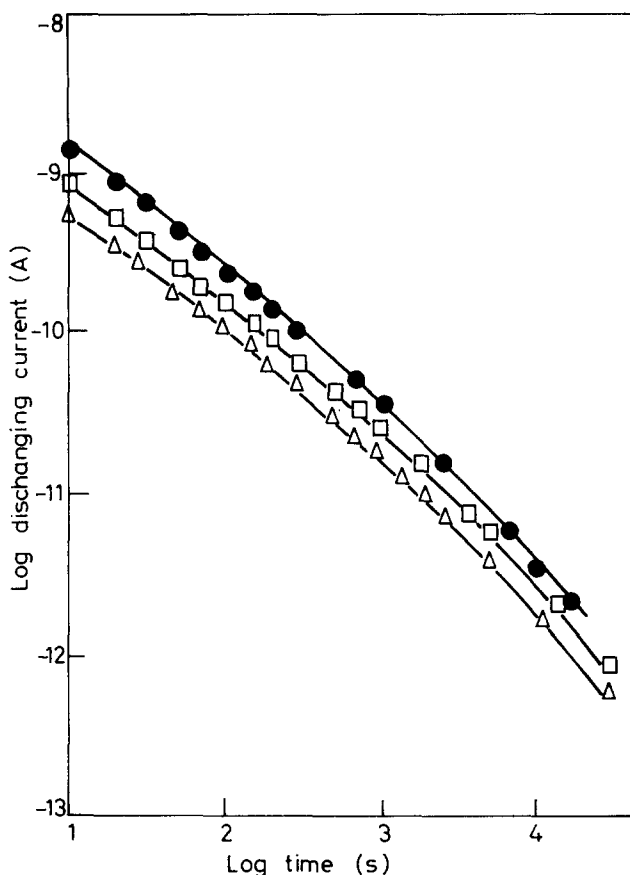


Figure 5 Double log plots of discharging current against time for dry 6,10 polyamide
 △ 57°C □ 60°C ● 64.4°C

A second explanation may be considered in terms of a distribution discussed by Macdonald¹⁹, in which both the pre-exponential factor and the activation energy in the expression for a single relaxation time are distributed each depending on a structure factor S . A two parameter, generalized, truncated exponential probability density function is chosen for the distribution of S , giving a power law distribution for $G(\tau)$, the overall relaxation time distribution function. Asymmetry in the distribution can be introduced by a suitable choice of parameters. The transient current response $i(t)$ to a step voltage which is constant for measuring times less than the shortest relaxation, time of the material, then exhibits one or two regions where $i(t) \propto t^{(1+\rho)}$, where ρ is a parameter of the material (usually $|\rho| \ll 1$) and finally decreases very rapidly when the measuring time exceeds the longest relaxation time of the material. It is possible for ρ_1 to be greater than ρ_2 so that the behaviour in Figure 3 might be explained in terms of Macdonald's distribution, although dielectric retardation data would usually be expected to give

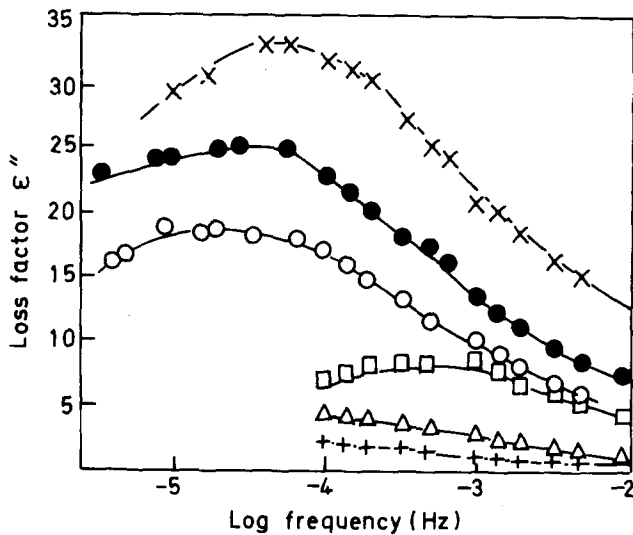


Figure 6 Plots of loss factor for relaxation alone against log frequency for dry 6,10 and 6,6 polyamides
 + 6,6, 49.5°C \triangle 6,6, 54.6°C \square 6,6, 64.5°C \circ 6,10, 57°C
 \bullet 6,10, 60.3°C \times 6,10, 64.4°C

$\rho_1 \leq \rho_2$. The general increase of current as the temperature is raised is also readily explicable in terms of Macdonald's theory. These results are important because the distribution is physically realizable at all reasonable temperatures.

However a second component of current exists in addition to a transient for a Cole-Cole distribution and this almost certainly represents a second mode rather than a feature of McDonald's distribution.

Unfortunately the behaviour of the 'tail' in Figure 3 obviously corresponds to a system of very long retardation times and the specimens were put on charge for a minimum period of 3 hours at each temperature in order to evaluate the transient currents accurately in the region 10–1000 seconds¹⁶. Mechanisms with retardation times much larger than 1000 seconds at the relevant temperatures will not have been charged for a sufficiently long time^{16,19} and so the 'tail' is probably subject to inaccuracies and should be studied with much longer charging times. Moreover an adequate comparison of the behaviour of 6,10 and Pip-10 polyamides is available in the lower temperature region with d.c. measurements where no tail is detectable and at higher temperatures by dielectric constant measurements. Thus a discussion of the 'tail' or levelling off of the double log plots of discharging current against time is deferred for a further separate study.

A detailed study of the lower temperature region where the double log plots of discharging current against time behave as for a Cole-Cole distribution is shown in Figures 5 and 6 for 6,10 polyamide (Figure 6 also includes data for 6,6 nylon obtained from the currents shown in Figure 3) and in Figures 7 and 8 for Pip-10 (Batch A) polyamide. The loss factor ϵ'' obtained from these currents is that for relaxation alone and does not contain any

component arising from d.c. conductivity. It was determined using the Hamon²⁰ approximation, which is valid over the ranges of temperature used.

$$\epsilon''(\omega) = \frac{i(t)}{\omega C_a V} \tag{2}$$

and

$$t = \frac{0.63}{\omega} = \frac{0.1}{f} \tag{3}$$

where ω is the angular frequency ($=2\pi \times$ frequency f), t the time, C_a capacitance with a vacuum replacing the material, and V the direct voltage applied. Similarly the behaviour of the loss factor for relaxation alone for Pip-10 (batch B) polyamide over the limited temperature range 40–53°C is shown in Figure 9.

The loss peaks are all fairly broad corresponding roughly with Cole-Cole¹⁷ α values in the range 0.37–0.50. Accurate values of α cannot be assigned to the individual curves because the full extent of the peaks is not available and there are sometimes indications of asymmetry.

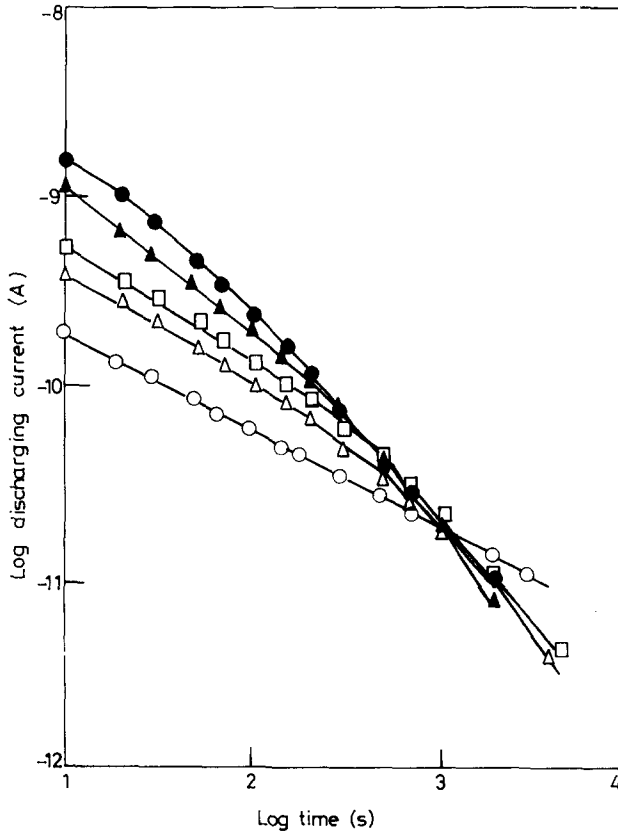


Figure 7 Double log plots of discharging current against time for dry Pip-10 (Batch A) polyamide;

○ 37°C; △ 45°C; □ 49°C; ▲ 51.2°C; ● 54.2°C

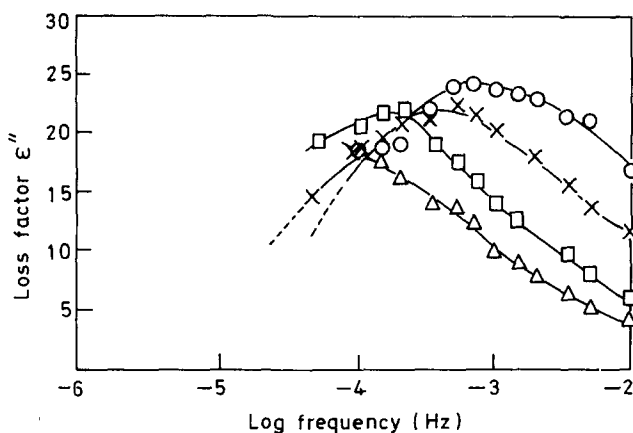


Figure 8 Plots of loss factor for relaxation alone against log frequency for dry Pip-10 (Batch A) polyamide;
 \triangle 45°C; \square 49°C; \times 51.2°C; \circ 54.2°C

A comparison of the magnitude of this relaxation for normal and Pip-10 polyamides was shown in a previous paper (Reference 7, figure 2) and this is extended in Table 2 to give the values of maximum ϵ'' and dielectric increment $\epsilon_s - \epsilon_\infty$ for the various polyamides at different temperatures and also the

Table 2 Parameters of the low frequency relaxation

Polyamide (dry specimens)	Temperature (°C)	ϵ''_{\max}	Dielectric increment $\Delta\epsilon = \epsilon_s - \epsilon_\infty$	Frequency of maximum loss f_m (Hz)
6,10	57	19	110	2.4×10^{-5}
	60	25	130	4.0×10^{-5}
	64	33	180	4.5×10^{-5}
6,6	55	4	19	1.0×10^{-4}
	65	8	34	6.8×10^{-4}
(6 Hirota <i>et al</i> ⁶) Pip-10, Batch A	72	7.2	39	3.1×10^{-3}
	49	22	90	1.4×10^{-4}
	51	23	110	4.5×10^{-4}
Pip-10, Batch B	54	25	110	7.0×10^{-4}
	40	4.8	22	6.8×10^{-5}
	46	6.0	25	2.7×10^{-4}
	50	6.6	30	5.0×10^{-4}
	53	6.7	31	1.4×10^{-3}

positions of the loss peaks. The values for $\epsilon_s - \epsilon_\infty$ were obtained from the well known relation²¹

$$\epsilon_s - \epsilon_\infty = \frac{2}{\pi} \int_{-\infty}^{\infty} \epsilon'' d(\ln\omega) \quad (4)$$

and were evaluated from the areas under the curves of loss factor ϵ'' against log frequency. The values for $\epsilon_s - \epsilon_\infty$ are only estimates, because of the difficulties described previously.

A considerable variation exists between the values of dielectric (constant) increment for the different batches of Pip-10 polyamide and also between the various types of normal polyamide and in general the magnitude of the relaxation increases as the temperature increases. However at comparable temperatures the values for maximum ϵ'' and dielectric increment $\epsilon_s - \epsilon_\infty$ for the Pip-10 (Batch A) and 6,10 polyamides are similar whilst the values for

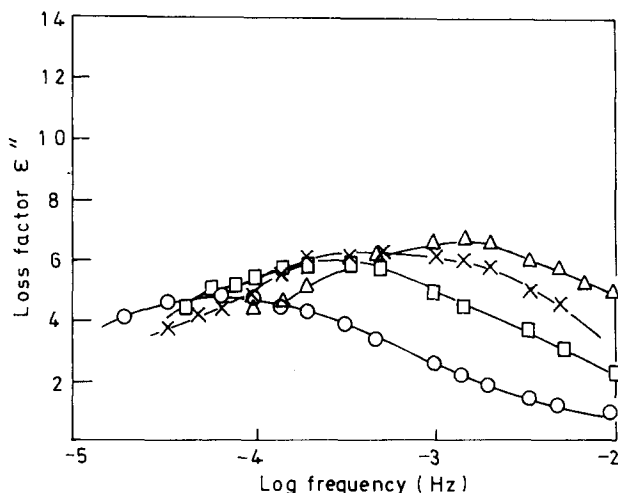


Figure 9 Plots of loss factor for relaxation alone against log frequency for dry Pip-10 (Batch B) polyamide
 ○ 40°C □ 45.5°C × 49.5°C △ 53°C

Pip-10 Batch B are similar to those for polyamide 6 (Hirota⁶), although the highest temperature for Pip-10 (Batch B) is lower than that for polyamide 6, and rather more than for polyamide 6,6. Thus this unusual low frequency dielectric behaviour observed in polyamides as the temperature is raised, occurs to much the same extent in the Pip-polyamide in which no N-H groups are present and no hydrogen bonding can occur.

Locus of low frequency relaxation

The plots of log frequency of maximum loss against 1000/T K fall in the regions associated with the loci for nylons 6 and 12⁶. The activation energies for the various polymers are listed in Table 3.

The values for polyamides 6,6 and Pip-10 (Batches A and B) are similar to those for polyamide 12 (data from Hirota⁶) with the value for 6,10 somewhat lower.

Table 3 Activation energies of polymers used

Polyamide (dry specimens)	Activation energy (10^5 J/mol)
6,10	1.5
6,6 (estimate)	1.8
Pip-10 Batch A	2.1
Pip-10 Batch B	1.8
6 Hirota ⁶	2.5
12 Hirota ⁶	2.1

Location of polarization

Since the dielectric constant (at fixed frequency) rises continuously as the temperature is raised^{1,2,4} without passing through a peak value and falling off as expected for dipolar polarization, and no corresponding low frequency relaxation is observed in the dynamic mechanical behaviour of polyamides^{6,22}, this low frequency dielectric relaxation is almost certainly caused by a space charge (interfacial) polarization. In view of the fact that it has been attributed to amide protons, it is important to distinguish between bulk and electrode polarization effects. This was achieved by making measurements on a series of 6, 10 polyamide discs of widely varying thickness (approximately 0.05–0.50 cm) at a fixed temperature (128°C) and a fixed frequency (100 Hz or 1 kHz). The product of capacitance increase due to the low frequency relaxation positions ΔC and thickness showed some fluctuation but the product was constant within experimental error showing that ΔC is nearly proportional to (thickness)⁻¹ and that the polarization is mainly a bulk rather than an electrode phenomenon.

If electrode polarization^{23–26} were predominant the increase in capacitance ΔC should be approximately proportional to (thickness)⁻² provided that the peak voltage applied to the specimen $V \ll kT/e$ where k is Boltzmann's constant and e is the electronic charge. The measured capacitance was found to be virtually independent of V down to values less than kT/e . Furthermore similar results for capacitance (at 100 Hz and 130°C) and d.c. conduction current (at 63°C) under fixed conditions were obtained for 6,10 and Pip-10 polyamides with different types of electrode (vacuum deposited aluminium, silverpaint and even aluminium foil and silicone grease). The d.c. conduction current for 6,10 polyamide at 63°C and a given applied voltage was also approximately inversely proportional to the thickness of the specimen. These effects confirm that the measured phenomena arose from the bulk of the polymer and were not associated with the electrodes.

Effects of polarization with constant voltage on a.c. results

The polarization of a specimen by the continued application of direct voltage was found to reduce the (a.c.) dielectric constant appreciably. This was found with 6,10 and Pip-10 polyamides but the capacitance recovered considerably and sometimes completely after discharging for a sufficient time at elevated temperatures, as shown in *Figure 10*.

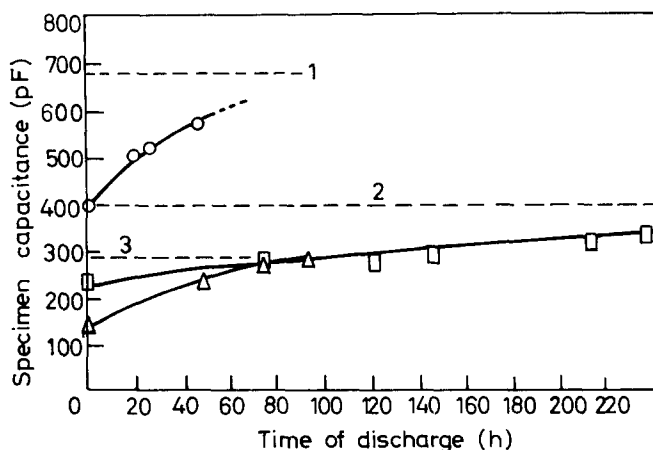


Figure 10 Recovery of specimen capacitance of dry polyamides at approximately 150°C on discharging at the same temperature after being subjected to a steady field;

- 6,10: field 2000 volts/cm for about 50 hours at 150°C, original value of capacitance given by dotted line 1
- △ Pip-10 Batch B: field \approx 1500 volts/cm for about 50 hours at 150°C, original value of capacitance given by dotted line 3
- Pip-10 Batch C (cast disc): field \approx 3300 volts/cm for about 370 hours at 150°C, original value given by dotted line 2

DISCUSSION

In a previous publication¹⁴ it was shown that the conduction in the pure Pip-10 polyamide was almost certainly electronic, any contribution from terminal protons to the conductivity at 150°C probably being about 3 orders lower than observed. Similar conclusions apply at lower temperatures, e.g. 60°C. These calculations were made assuming Frenkel defects for the protons and using the relationship $n = \sqrt{NN_i}e^{-(U/2kT)}$ where n is the number of mobile protons per cm³, N is the number of ends per cm³ and N_i is the number of interstitial sites for protons per cm³. U is the energy required to liberate the proton and a minimum value of U as twice the lowest observed activation energy from the plot of log conductivity against $1/T$ K was used. The value used for the mobility of the proton of 10^{-8} cm² sec⁻¹ volt⁻¹ was realistic because the terminal protons in the Pip-10 polyamide were on average about 22 Å apart with no possibility of forming a chain of hydrogen bonds and because of the low mobilities found in polymers. Since the low frequency relaxation is caused by a space charge mechanism closely associated with the d.c. conductivity (see Figure 11) it is almost certain that the same charge carrier is responsible for both phenomena. Thus the contribution of terminal protons to the low frequency relaxation in Pip-10 polyamide is almost certainly negligible.

Comparison of the experimental results given here for normal and Pip-10 polyamides shows that amide protons cannot be the major cause of this low frequency relaxation in normal polyamides, although some contribution

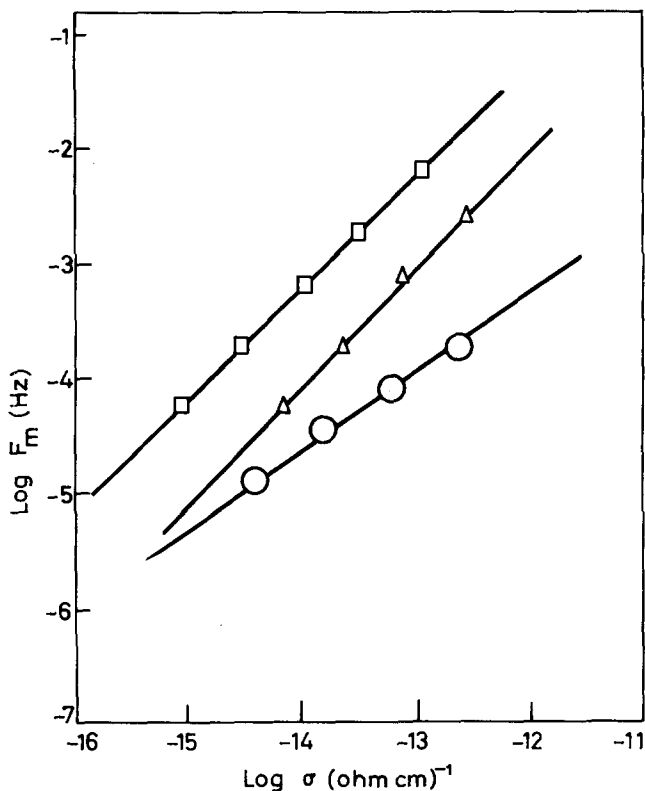


Figure 11 Relationships between the frequency of maximum loss (F_m) and d.c. conductivity (σ) for dry polyamides;
 \circ 610; \triangle Pip-10 Batch A; \square Pip-10 Batch B

from them cannot be ruled out. However, when taken in conjunction with the results of earlier work on the d.c. conductivity of polyamides¹²⁻¹⁴, the data indicate that amide protons probably do not make a significant contribution except at temperatures over about 110°C. The space charge must arise mainly from electrons which are trapped at the boundaries between crystalline and amorphous regions.

It is interesting to note that a similar low frequency relaxation has been observed in proteins²⁷ where the conductivity is electronic²⁸. Obviously the parameters of the relaxation will then depend markedly on the morphology of the specimen being examined. In view of the spherulitic nature of polyamides it seems likely that charge could build up at the surface of spherulites. The theory of interfacial polarization has been developed by Maxwell²⁹ for a two layer capacitor and by Wagner³⁰ and Sillars³¹ for spheres and particles of various shapes in a different surrounding medium. A considerable rise in dielectric constant can occur, when the particles possess a different dielectric constant and d.c. conductivity from those of the surrounding medium and needle shaped particles lying along the direction of the field can cause marked effects. When conducting spheres³⁰ are dispersed in a relatively

non-conducting medium a simple proportional relationship exists between the frequency of maximum loss and the d.c. conductivity of the spheres, and the two parameters will possess the same activation energy. A linear relationship between the frequency of maximum loss and conductivity of the bulk polyamide has been observed by Hirota *et al*⁶, and similar activation energies were obtained for both quantities. However it is not clear whether this has any connection with the relationship found by Wagner³⁰. In the present work the double log plots of frequency of maximum loss against d.c. conductivity¹⁴ of the bulk polymer were found to be linear (*Figure 11*) with slopes near unity for the Pip-10 polyamide specimens, but the slope deviated from unity for the 6,10 polymer indicating a non-proportional relationship. Small differences between the corresponding activation energies for the low frequency relaxation and d.c. conductivity were also observed for the 6,10 polymer but the values for both batches of the Pip-10 polymer were similar. The frequency of maximum loss is obviously strongly related to the d.c. conductivity.

Unfortunately these theories hold only for low concentrations of dispersed particles. At higher concentrations the theory becomes more complicated³², although formulae have been obtained for spheres dispersed in a surrounding medium³³, as follows

$$\epsilon_s \left[\frac{3}{\sigma - \sigma_2} - \frac{1}{\sigma} \right] = 3 \left[\frac{\epsilon_2 - \epsilon_1}{\sigma_2 - \sigma_2} + \frac{\epsilon_2}{\sigma - \sigma_2} \right] - \frac{\epsilon_1}{\sigma_1} \quad (5)$$

and

$$\left(\frac{\sigma - \sigma_2}{\sigma_1 - \sigma_2} \right) \left(\frac{\sigma_1}{\sigma} \right)^{1/3} = 1 - v_2 \quad (6)$$

where v_2 is the volume fraction of the dispersed spheres, ϵ_2 and σ_2 are the dielectric constant and conductivity of the spheres, ϵ_1 and σ_1 are the corresponding properties for the surrounding medium and ϵ_s and σ are the static dielectric constant and conductivity of the whole assembly. The high frequency dielectric constant ϵ_∞ of the whole assembly is given by

$$\frac{\epsilon_\infty - \epsilon_2}{\epsilon_1 - \epsilon_2} \left(\frac{\epsilon_1}{\epsilon_\infty} \right)^{1/3} = 1 - v_2 \quad (7)$$

This theory has been used with reasonable success to explain the dielectric behaviour of nitrobenzene/water emulsions³⁴. The main difficulty in applying these formulae lies in a lack of knowledge of the individual d.c. conductivities of the crystalline and amorphous regions of the polymer. However it is quite likely that the conductivity σ_2 of the crystalline regions will be much less than that of the amorphous regions σ_1 and also quite possible that the conductivity σ of the bulk polymer will not be much different from that of the amorphous regions i.e., $\sigma_2 \ll \sigma_1$ and $\sigma_2 \ll \sigma$.

With $v_2 = 0.5$ equations (5) and (6) then become³³:

$$\epsilon_s = 0.970 \epsilon_2 + 0.354 \epsilon_1 \quad (8)$$

and

$$\sigma = \frac{\sigma_1}{\sqrt{2}} = 0.354 \sigma_1 \quad (9)$$

Typical values for the dielectric constants of amorphous (ϵ_1) and crystalline (ϵ_2) regions for polyamides in the region 100 — 150°C may be taken from figure 3 of Reference 1 as

- $\epsilon_1 \simeq 20$ (static dielectric constant of amorphous regions with regard to α -relaxation allowing for the semi-crystalline nature of the bulk polymer).
 $\epsilon_2 \simeq 3$ (High frequency dielectric constant of bulk polymer with regard to α -relaxation, allowing only electronic and atomic polarizations).

Using these values in equation (8) gives a value for the static dielectric constant ϵ_s of about 10. At these temperatures ϵ_s for the bulk polyamide must be well in excess of 100 and so this large low frequency relaxation cannot be explained by Hanai's theory³³. (For the case $\sigma_1 \ll \sigma_2$ and $\sigma \ll \sigma_2$ equation 5 reduces to $\epsilon_s = \epsilon_1/(1 - v_2)^3$ and this could explain the large dielectric constants observed in the high temperature regions. However, it seems hardly likely that the crystalline regions could have a much higher conductivity than that of the amorphous regions). Thus given the validity of the assumptions made above, it seems unlikely that the build up of charge at the surfaces of spherulites would be sufficient to explain the large dielectric constants observed at elevated temperatures.

The spherulites in moulded polyamide samples may be of a fibrillar or lamellar³⁵⁻³⁹ character and the accumulation of charge at the surfaces of lamellae or elongated crystallites lying along the direction of the field could obviously lead to much larger values for the static dielectric constant. Owing to the complex nature of spherulites no existing theory is applicable and no further analysis is attempted here. The development of such a theory would form a complex and separate study but observations of the sites where concentrations of space charge build up, if possible, could help in the development of such a theory. A bi-modal distribution of retardation times can be readily explained by assigning the shorter retardation time mode to the build up of space charge at the surfaces of spherulites and the longer time mode to the build up of charge at crystallite boundaries inside spherulites, but the former then seems unlikely to explain the large dielectric constants observed, as mentioned earlier.

Future work should include a study of the effect of morphology on the dielectric behaviour of suitable specimens by correlating the spherulitic behaviour seen between crossed polars with dielectric properties.

At lower temperatures the second mode might well consist of extremely long retardation times so that its effect is not noticed on the double log plots of discharging current against time. As the temperature is raised it produces the observed effects on the current curves in the experimental time range. At much higher temperatures (as used for the a.c. data) the second mode will now play an important part in the dielectric behaviour and the lack of a point of inflection in the plots of dielectric constant against log frequency could be explained by the retardation times still being comparatively very long for this second mode. As the temperature is raised both the d.c. conductivity and the magnitude of the space charge polarization increase. The variation of the latter is illustrated in the behaviour of the (a.c.) dielectric constant in *Figures 1* and *2*. The appreciable fall in dielectric constant observed for specimens which had been subjected to a d.c. field for some length of time is

interesting and readily explained by the loss of electrons able to respond to the a.c. field, due to large numbers being trapped during the application of the d.c. field. Discharging the specimen removes the polarization by de-trapping the electrons and the measured dielectric constant increases.

Michel and co-workers⁴⁰ found that the superposition of a continuous voltage caused a marked reduction in the dielectric constant of dry polyamide 6.6 at low frequencies and elevated temperatures, owing to a similar effect.

*Department of Applied Physics,
University of Wales Institute of Science
and Technology,
Cardiff, S. Wales*

(Received 13 July 1970)

(Revised 20 October 1970)

REFERENCES

- 1 Baker, W. O. and Yager, W. A. *J. Amer. Chem. Soc.* 1942, **64**, 2171
- 2 McCall, D. W. and Anderson, E. W. *J. Chem. Phys.* 1960, **32**, 237
- 3 Rushton, E. and Russell, G., E.R.A. Report, L/T 355-2, Sept. 1956
- 4 Curtis, A. J. *J. Res. Nat. Bur. Stand.* 1961, **65A**, No. 3, 185
- 5 Eley, D. D. and Spivey, D. I. *Trans. Faraday Soc.* 1961, **57**, 2280
- 6 Hirota, S., Saito, S. and Nakajima, T. *Kolloid-Z* 1966, **213**, 109
- 7 Baird, M. E., Goldsworthy, G. T. and Creasey, C. J. *J. Polym. Sci. (B)* 1968, **6**, 737
- 8 Cannon, C. G. *J. Chem. Phys.* 1956, **24**, 491
- 9 Cannon, C. G. *Disc. Faraday Soc.* 1958, **25**, 59
- 10 Cannon, C. G. *Spectrochim. Acta* 1958, **10**, 341; 1960, **16**, 302
- 11 Arridge, R. G. C. and Cannon, C. G. *Proc. Roy. Soc. (Lond.)*, Ser. A, 1964, **278**, 91
- 12 Seanor, D. A. *J. Polym. Sci. (C)* 1967, **17**, 195
- 13 Seanor, D. A. *J. Polym. Sci. (A-2)* 1968, **6**, 463
- 14 Baird, M. E. *J. Polym. Sci. (A-2)* 1970, **8**, 739
- 15 Cannon, C. G., *Documentation of Molecular Spectra*, 1957, Spectrum No. 2568 (Butterworths, London)
- 16 Baird, M. E. *Revs. Mod. Phys.* 1968, **40**, 219
- 17 Cole, K. S. and Cole, R. H. *J. Chem. Phys.* 1941, **9**, 341
- 18 Cole, K. S. and Cole, R. H. *J. Chem. Phys.* 1942, **10**, 98
- 19 MacDonald, J. R. *J. Appl. Phys.* 1963, **34**, 538
- 20 Hamon, B. V. *Proc. Inst. Elec. Engrs. (Lond)* 1952, **99**, 115
- 21 Böttcher, C. J. F., 'Theory of Electric Polarisation', Elsevier, 1952, Chapter 10
- 22 Takayanagi, M. *Mem. Fac. Eng., Kyushu Univ.* 1963, **23**, No. 1., 41
- 23 Jaffe, G. *Am. Physik* 1933, **16**, 217 and 249
- 24 MacDonald, J. R. *Phys. Rev.* 1953, **92**, 4
- 25 Friauf, R. J. *J. Chem. Phys.* 1954, **22**, 1329
- 26 Jacobs, P. W. M. and Maycock, J. N. *J. Chem. Phys.* 1963, **39**, 757
- 27 Algie, J. E. *Kolloid-Z* 1968, **223**, 13
- 28 Eley, D. D. and Spivey, D. I. *Trans. Faraday Soc.* 1960, **56**, 1432
- 29 Maxwell, J. C., 'Electricity and Magnetism', Clarendon, Oxford, 1892, **1**, 452
- 30 Wagner, K. W. *Arch. Elektrotech.* 1914, **2**, 371
- 31 Sillars, R. W. *J. Inst. Elec. Engrs.* 1937, **80**, 378
- 32 Beek, L. K. H. Van, 'Progress in Dielectrics', (Ed. Birks, J. B.) Iliffe, 1967, **7**, 69
- 33 Hanai, T. *Bull. Inst. Chem. Res., Kyoto Univ.* 1961, **39**, 341
- 34 Hanai, T., Koizumi, N. and Gotoh, R. *Bull. Inst. Chem. Res., Kyoto Univ.* 1962, **40**, 240
- 35 Keller, A. *J. Polym. Sci.* 1955, **17**, 291 and 351
- 36 Keller, A. and Waring, J. R. S. *J. Polym. Sci.* 1955, **17**, 447
- 37 Khoury, F. *J. Polym. Sci.* 1958, **33**, 389
- 38 Keller, A., 'Fibre Structure' (Eds. Hearle, J. W. S. and Peters, R. H.), Butterworths and Textile Institute, 1963, p 332
- 39 Geil, P. H., 'Polymer Single Crystals', Interscience, 1963, Chapter 4
- 40 Michel, R., Asch, G. and Matriot, M. *Acad. Sci., Paris (Ser. B)* 1970, **270**, 1644

The effects of varying peroxide concentration in crosslinked linear polyethylene

T. R. MANLEY and M. M. QAYYUM

We have investigated certain physical and mechanical properties of linear polyethylene that had been crosslinked under high pressure with various amounts of di-tertiary butyl peroxide. Good correlation was obtained between the amount of peroxide used and the density of the crosslinked polymer. The shear modulus also gave good correlation at temperatures below the crystalline melting point, but not at higher temperatures. The gel content (by Soxhlet extraction) using tetralin showed a complex relationship. Toluene, white spirit, and xylene were unsatisfactory solvents for this work. Little relationship was observed between the amount of peroxide used and the tensile strength or elongation at break of the crosslinked polymer.

INTRODUCTION

POLYETHYLENE is one of the most important thermoplastics but its use is restricted in certain applications by its low melting point, solubility in hydrocarbons and a tendency to crack when stressed. In an effort to mitigate these disadvantages, there has been considerable work on the crosslinking of polyethylene.

High energy radiation has been extensively used to crosslink polyethylene¹⁻³ and a commercial polymer (Irrathene) was made by electron beam radiation. The use of high energy radiation to crosslink polymers requires high capital expenditure and is limited to articles of thin cross section. Most commercial material is crosslinked chemically using peroxide initiators. To obtain uniform crosslinked polyethylene, the peroxide must be evenly dispersed in the polymer. Care must be taken that peroxide does not react during mixing. The peroxide-containing polyethylene is then extruded or moulded^{4,5}. Several grades of crosslinkable polyethylene are at present marketed. These are mainly used in the pipe, wire and cable manufacturing industries.

Kados and others⁶ studied the effect of high pressure on the molecular structure of polyethylene under cooled conditions in the absence of crosslinking agent and observed the rise in density and variation in the polymer structure even at 500 atm. The effect of pressure on different grades of polyethylene is shown in *Table 1*.

In 1967 a new process of crosslinking polyethylene, introduced by Engel,⁷ gave a material with considerably higher molecular weight than that obtained with other crosslinking techniques. In this process the polyethylene is fed from a hopper into a mixing chamber where the peroxide is injected. The mixture is then taken to a heated pressure chamber by a screw conveyor. The peroxide diffuses completely into the plastic under the action of the high pressure.

PEROXIDE CROSSLINKED POLYETHYLENE

Table 1 Effects of high pressure on crystallization of polyethylenes

<i>Type of plastic</i>	<i>Crystallization pressure atmospheres</i>	<i>Density (gm/cc 23°C)</i>	<i>% Crystallization based on density</i>
Medium density polyethylene	1	0.9513	69
	2500	0.9576	71
	3000	0.9665	77
	5000	0.9737	82
High density polyethylene	1	0.9692	79
	3000	0.9818	87
	5000	0.9893	92
Polymethylene	4760	0.995 (25°C)	96

Because of the intimate mixing of the peroxide and polymer, very small amounts of peroxide are necessary. The high pressure softens and shapes the polymer, forcing it through a heated die to complete the crosslinking process. The rate of crosslinking may be varied by changing the pressure, the temperature, amount of peroxide and the rate of extrusion.

The Engel process has considerable commercial attractions and, therefore, a fundamental study of the operating conditions was commenced.

EXPERIMENTAL

Materials

The high density polyethylene used was Lupolen 5261Z (BASF). This has a density between 0.950 and 0.953 with a melt flow index of 1.7–2.3. Trigonox B (Di-tertiary butyl peroxide) was supplied by Novadel Limited in 95% purity. Special Boiling Point Spirit No. 4; (Aniline Point 58.5°C) (Shell-Mex and BP) and silicone Fluid MS 550 (Midland Silicones Ltd) were used as a solvent for the Trigonox B and as a lubricant respectively; 100 parts of peroxide, 100 parts of solvent and 40 parts of lubricant were used to assist dispersion.

Crosslinked polyethylene pipes were extruded using the Engel process⁷. The temperatures of the pressure chamber, pin and die were 130°C, 110°C and 200–210°C respectively. The design pressure of the chamber was 150 000 lbft/cm²*. Different rates of extrusion were used.

Density

The method given in BS 2782 509A was used at 23°C. Isopropyl alcohol and water, which give better wetting of polyethylene, were used as the density gradient liquids. The work was performed by courtesy of Mr. W. J. Allwood, Plastics Division, British Petroleum Ltd.

*1lbft/cm² = 6.895kN/m²

Gel content

The percentage gel was determined as the percent of the original weight (0.2 to 0.5 g) remaining after Soxhlet extraction for 24 hours. Toluene (110°C), Xylene (137–140°C), white spirit and tetrahydronaphthalene (203–209°C) were studied.

Shear modulus

Dynamic modulus was measured at room temperature at a constant frequency of 0.5Hz and from 20°C–175°C \pm 1 at 0.25Hz on a Nonious Torsional Pendulum.

Tensile strength and elongation

Tensile strength and elongation were measured on a Hounsfield Tensometer. The specimens were 3/16 in. wide and 3 in. long (gauge length 1.1/8 in.)*. At 100°C and 140°C the rate of strain was 5 in. per minute; at room temperature rates of 2, 5, 12 and 20 in. per minute were employed. The results which are given in *Tables 5–8* are the means of 10 readings in the former instances and five readings for *Tables 7 and 8*.

RESULTS

Density

In the Engel process the crosslinking takes place in the amorphous polymer as there is insufficient time for the polythene to crystallize. A significant amount of crosslinking makes it more difficult for the molecules to orient themselves relative to one another within crystallites hence the amount of

Table 2 Density of crosslinked polyethylene at 23°C

No.	1	2	3	4	5	6	7	8	9	10
% Peroxide	Nil	0.140	0.223	0.263	0.266	0.393	0.436	0.543	0.585	0.693
Density g/cc	0.953	0.940	0.938	0.936	0.936	0.938	0.936	0.934	0.933	0.932

crystallinity in ultra-high pressure crosslinked polyethylene is very low. This reflects in the low density of the polymer shown in *Table 2*. These results show that density decreases with increasing the peroxide concentration in chemically crosslinked polythene.

Gel content

Four solvents, toluene, xylene, white spirit and tetralin were used. Results are shown in *Table 3*. Samples were taken from different places along the

*1in. = 2.54 cm

PEROXIDE CROSSLINKED POLYETHYLENE

crosslinked polyethylene pipe in order to measure the variation in cross-linking throughout the pipe.

The toluene figures are unsatisfactory; this is attributed to the high softening point of the original polymer (150°C). Tetralin gives good correlation but its boiling point is very high, (203–209°C) so xylene was investigated. This gives reasonable figures, higher than tetralin, as would be expected, but the figure of 26% gel in the raw material makes xylene unsatisfactory.

Table 3 Gel content of crosslinked polyethylene

No.	% Peroxide	% Gel content			
		Toluene (110°C)	Xylene (137–140°C)	White Spirit	Tetraline (203–209°C)
1	Nil	93.04	26.1	Nil	Nil
2	0.140	97.84	52.08	59.18	45.84
3	0.223	94.77	71.10	31.44	67.74
4	0.263	90.86	75.60	86.96	68.06
5	0.266	*	90.2	75.82	69.25
6	0.393	*	76.5	44.62	67.84
7	0.436	94.60	94.6	65.42	70.12
8	0.543	*	*	78.04	71.05
9	0.585	94.17	83.7	83.54	73.81
10	0.693	*	*	90.11	75.69

* Not determined

Results with white spirit were very scattered which may be due to its composition and the low boiling point fractions present. From the gel content figures it is clear that different values for crosslinking are obtained using different solvents. Baskett⁸ obtained similar results using Benzene (78°C), toluene (110°C) and xylene (137–140°C) with low density polyethylene.

Tetralin appears to be a satisfactory solvent but because of its high boiling point, some error may result. Therefore, other solvents having lower boiling points, e.g. mesitylene, decalin or other cheap hydrocarbons such as Shell No. 4 will be investigated.

Shear modulus—the torsional pendulum technique

Many experimental methods exist for the determination of the dynamic modulus of a plastic^{9,10}. The torsional pendulum method was chosen as it provides reliable information on samples that are conveniently prepared. A uniform rectangular bar of the material under investigation is clamped rigidly at one end while the upper end is clamped in a movable member of known moment of inertia. The time required for one complete oscillation, *P* is measured. The modulus is calculated from the specimen dimensions, moment of inertia of the movable member and the period of the movement.

The shear modulus is calculated from

$$G = \frac{KLI}{WT^3\sigma P^2}$$

where K = a constant which is 38.54 when G is in dyn/cm²

L = length of the specimen in inches

W = width of the specimen in inches

T = thickness of the specimen in inches

I = moment of inertia in g/cm²

P = period of oscillation in seconds

δ = a shape factor depending upon the ratio of the width to thickness of the specimen

(1 dyn/cm² = 0.1N/m²)

The modulus at temperatures below the crystalline melting point varies with the amount of crystallinity and the concentration of crosslinks. From *Table 4* it is clear that as the amount of peroxide increases, shear modulus decreases. One cannot, however, extrapolate from these results to higher temperatures because crosslinking becomes increasingly important above the

Table 4 Shear modulus of crosslinked polyethylene at 0.5 Hz, 20°C

No.	1	2	3	4	5	6	7	8	9	10
% Peroxide	Nil	0.140	0.223	0.263	0.266	0.393	0.436	0.543	0.585	0.693
$G \times 10^{-9}$ dyn/cm ² *	4.90	3.86	3.37	3.33	3.41	3.35	2.76	2.70	2.75	2.30

* 1 dyn/cm² = 0.1 N/m²

crystalline melting point. A graph of shear modulus versus temperature is shown in *Figure 1*. The shear modulus of polythene, both uncrosslinked and crosslinked, falls slowly but above the crystalline melting point there is a sharp decrease in the shear modulus of uncrosslinked material only.

Above the crystalline melting point no correlation was obtained between the amount of peroxide and the shear modulus.

Tensile strength and elongation

Tensile strength and elongation at break with different rates of a strain at room temperature are shown in *Table 5* and *6*. *Table 7* and *8* give tensile strength and elongation at higher temperatures.

At room temperature tensile strength falls slowly as the peroxide concentration increases and with a further increase it goes down sharply. This is shown in *Figure 2* for the results at a strain of 5 in./min.* The crosslinked

*1in/min = 2.54cm/min

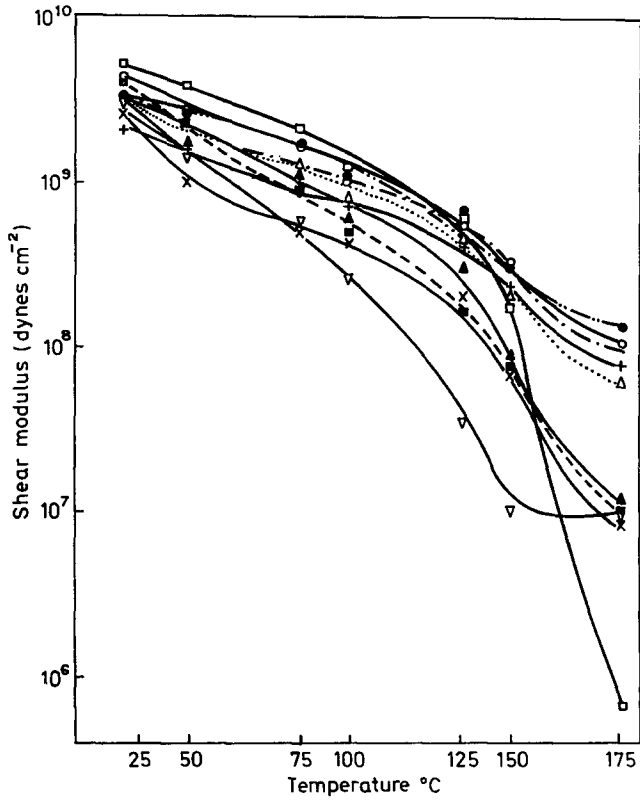


Figure 1 Shear modulus of crosslinked linear polyethylene at different temperatures. Percentage peroxide in polymer: \square Nil, \circ 0.140, \bullet 0.223, \blacktriangle 0.263, \triangle 0.266, \blacksquare 0.393, ∇ 0.436, \times 0.543, $-\cdot-\cdot-$ 0.585, $+$ 0.693

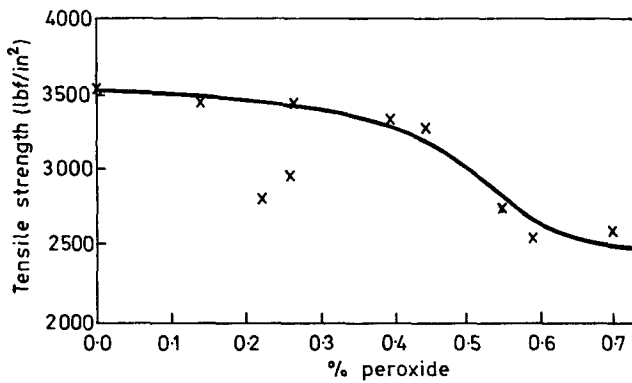


Figure 2 Tensile strength of crosslinked polyethylene. Straining rate 5 in./min ($11\text{bf/in}^2 = 6.895\text{ kN/m}^2$)

Table 5 Tensile strength of crosslinked linear polyethylene. P.S.I. at 19°C (BS 2782). Mean of 10 results

Sample No.	Peroxide content Extrusion rate f_i/h^*	Rate of strain in./min†	Tensile strength (P.S.I.)										
			Nil	0-140	0-223	0-263	0-266	0-393	0-436	0-543	0-585	0-693	
			171	180	195	171	195	157	210	157	160	150	
1	2		(510)	(693)	(327)	(407)	(326)	(235)	(480)	(118)	(255)	(121)	
			3590	4014	3438	3053	3389	2479	2871	2820	2587	2541	
2	5		(605)	(444)	(659)	(197)	(410)	(286)	(456)	(108)	(238)	(125)	
			3551	3480	2827	2967	3449	3393	3285	2743	2549	2608	
3	12		(689)	(446)	(434)	(334)	(328)	(255)	(205)	(146)	(282)	(145)	
			3702	3284	2678	2708	3452	3373	3059	2868	2568	2734	
4	20		(641)	(488)	(501)	(320)	(320)	(350)	(445)	(165)	(322)	(175)	
			3978	3240	2535	3475	3423	3346	3217	3090	2712	2827	

Standard Deviation is given in brackets

* 1 ft/h = 0.305 m/h

† 1 in./min = 0.0253 m/min

PEROXIDE CROSSLINKED POLYETHYLENE

Table 6 Percentage elongation at break of crosslinked linear polyethylene at 19°C (BS 2784). Mean of 10 results

Sample No.	Peroxide content Extrusion rate ft./h*	Rate of strain in./min†	0.140	0.223	0.263	0.266	0.393	0.436	0.543	0.585	0.693
1	Nil		180	195	171	195	157	210	157	160	150
	638	(75.7)	492	490	462	462	462	462	462	462	462
2			(124.8)	(140.1)	(103.2)	(46.8)	(72.0)	(49.6)	(36.5)	(50)	(31.1)
	462	(253.6)	370	334	438	137	180	159	138	168	127
3			(148.6)	(139.1)	(98.2)	(34.5)	(39.0)	(60.1)	(39.3)	(33.5)	(50.5)
	100	(12.2)	244	258	259	157	137	159	214	115	153
4			(38.1)	(70.3)	(84.0)	(44.7)	(37.0)	(56.7)	(72.6)	(43.3)	(33.7)
	98	(26.4)	179	219	268	177	161	161	189	143	149

Standard Deviation is given in brackets

* 1 ft/h = 0.305 m/h

† 1 in/min = 0.0254 m/min

Table 7 Tensile strength of crosslinked polyethylene at different temperatures. Strain rate 5in./min

Temp (°C)	% of peroxide				
	0.263	0.393	0.543	0.585	0.693
19	2967	3393	2743	2549	2608
100	1645	2130	1490	1340	1845
140	1275	1260	1155	1175	1295

Results are in lbf/in². (1 lbf/in² = 6.895 kN²)

Table 8. Elongation of crosslinked polyethylene at different temperatures. Strain rate 5in./min

Temp (°C)	% peroxide				
	0.263	0.393	0.543	0.585	0.693
19	438	180	138	168	127
100	360	300	90	100	220
140	360	320	115	155	175

Results are in lbf/in². (1 lbf/in² = 6.895 KN²)

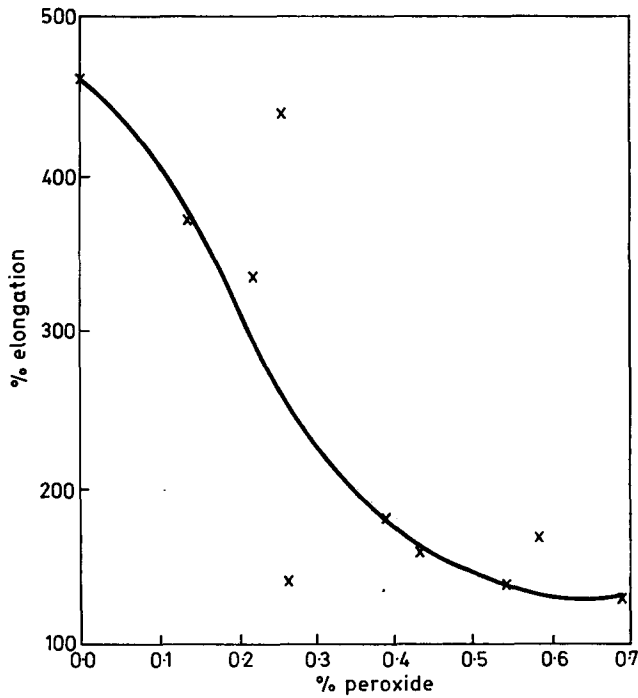


Figure 3 Elongation of crosslinked polyethylene. Straining rate 5in./min

polyethylene tubes were extruded in presence of air, thus peroxide compounds are probably formed. Such structures are the main cause of reduction in tensile strength.

The graph of elongation at break against the amount of peroxide shows an initial rapid decrease in elongation but this later flattens out. This is illustrated, again for the results at a strain rate of 5 in./min in *Figure 3*.

In most cases tensile strength increases and elongation decreases as the rate of straining increases. It is not possible to draw general conclusions from these results because pipes from which the samples were taken were extruded at different rates.

DISCUSSION OF RESULTS

The degree of crosslinking is affected by the amount of peroxide, the base polymer and the processing conditions. The presence of other ingredients, e.g. solvent and lubricant, makes it difficult to obtain a clear picture of peroxide effect of crosslinking. One obtains a good correlation between amount of peroxide and density measurement. The density falls with peroxide content in agreement with Danneberg⁴ and Narkis *et al*¹¹ who used x-rays to study crystallinity.

The gel content, as measured in tetralin, increases with the amount of peroxide used. Initially, this increase is rapid but it slows down until a gel content of 70% is reached after which it again tends to increase.

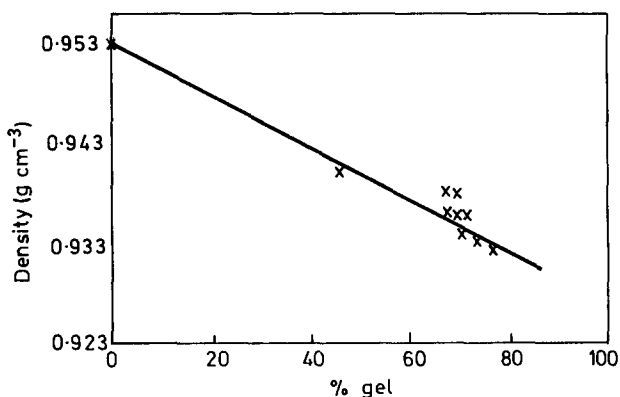


Figure 4 Densities of crosslinked polyethylene against gel content in tetralin

A comparison of density measurements (*Table 2*) and gel content (tetralin) indicates that crosslinking occurs more readily in amorphous polythene since the gel content rises with decreasing crystallites (*Figure 4*).

The relationship with peroxide content is not so clear. The initial rapid rise in gel content (*Figure 5*) is readily explained as each link formed will contribute to a gel. After a while, however, a number of redundant links may be formed between two molecules that are already linked and the net increase in gel content will be less. There will also be some reduction in gel content

because of degradation and thus the rate of gelation will tend to flatten out. This reduction in gel content because of degradation is not likely to be great as the polymer used contains very few branches. Considerably more degradation would be expected in low density polyethylene.

Finally when all the readily broken branches are degraded the gel content will again rise (*Table 3*).

There is good correlation between the shear modulus at room temperature and the amount of peroxide used (*Table 4*). Above the crystalline melting

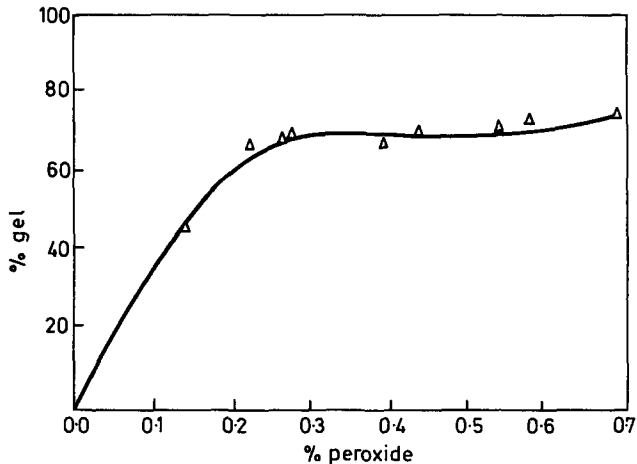


Figure 5 Gel content against peroxide content of crosslinked polyethylene

point of the polymer, however, apart from the fact that modulus of the crosslinked polymer is higher than that of the original material, little correlation may be observed. Some of this discrepancy may be introduced by the variations in the rates of heating employed in measurement of the shear modulus. Another factor may be that both degradation and crosslinking are occurring in the polymer at elevated temperatures.

All measurements were made in a normal atmosphere; the results obtained are shown in *Figure 1*. The inflexions in the curves in this figure give the temperature of the crystalline melting point. The amount of peroxide used has a clear relationship to the crystalline melting point (*Figure 6*).

The tensile strength of crosslinked polyethylene falls with the increase of peroxide but the relationship is poor. At high temperatures it has the same trend but gives a better correlation with peroxide content except for one sample (0.393% peroxide) which has high value. If density, which is a measure of crystallinity, is compared with tensile strength (*Tables 2 and 7*) it seems to indicate that the tensile strength is dependent to a greater extent of the crystallinity than the crosslinking caused by the peroxide.

The elongation at high temperature (*Table 8*) has no relation to the temperature. This is thought to be due to the non-homogeneity of the pipe and the small number of samples measured. This probably also applies to the high temperature tensile measurements to a lesser degree.

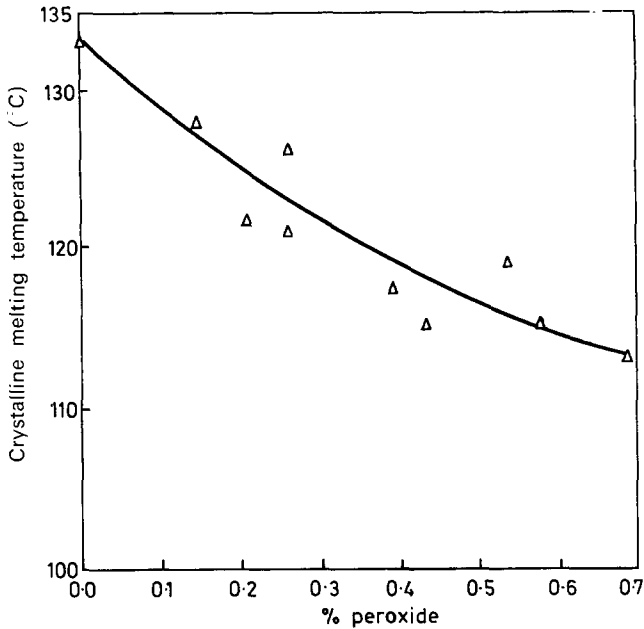


Figure 6 Temperature of the crystalline melting point against peroxide content, of crosslinked polyethylene.

Similarly, the elongation at high temperature has very little correlation with the peroxide content although the general trend is that it falls with percent peroxide as is shown with the room temperature measurements.

CONCLUSIONS

Although variations in the amount of peroxide used play the major role in the determination of the mechanical properties of crosslinked polyethylene, they cannot be used in isolation to prognosticate the properties of finished materials. Further study of the effects of operating conditions is required and is being undertaken.

The most reliable techniques for monitoring the quality of finished articles are at present density and shear modulus at room temperature.

ACKNOWLEDGEMENTS

We thank Mr C. W. Evans for his encouragement and interest in this work, Mr J. Hood for helpful discussions, and the Dunlop Company Ltd for permission to publish.

*Department of Materials Science,
Newcastle upon Tyne Polytechnic,
Ellison Place,
Newcastle upon Tyne NE1 8ST, UK*

(Received 10 October 1970)

REFERENCES

- 1 Dole, M., Killing, C. D. and Rose, D. G. *J. Am. Chem. Soc.* 1954, **76** (17), 4304
- 2 Manley, T. R. *Research* 1959, 42
- 3 Charlesby, A. and Hancock, N. H. *Proc. Roy. Soc.* 1953, **A218**, 245
- 4 Dannenberg, E. N., Jordon, M. E. and Cole, H. M. *J. Poly. Sci.* 1958, **31**, 127
- 5 Narkis, M. and Tobolsky, A. V. *J. Appl. Polymer Sci.* 1969, **13**, 2257
- 6 Kados, J. L., Baer, E., Gail, P. H. and Koeing, J. L. *Kolloid-Z* 1965, **204**, 1
- 7 Engel, T. *Plastics and Polymers* 1970, **38**, 174
- 8 Baskett, A.C., 'Proceedings of the Symposium on Macromolecular Chem. Milan', 1954, Sept 26–October 2
- 9 Nielsen, L. E. *Rev. Sci. Instr.* 1951, **22**, 690
- 10 Karas, G. C. and Warburton, B. *British Plastics* 1961, **34**, 189 and 131
- 11 Narkis, M. and Miltz, J. *Israel Chem.* 1970, **8**, 7

The relationship between volume and elasticity in polymer glasses

R. N. HAWARD and J. R. MACCALLUM

It is proposed that the adiabatic bulk modulus of a polymeric glass is determined by interchain forces which obey conventional intermolecular force relationships. Based on the Lennard-Jones expression for the intermolecular forces in liquids an equation is derived relating the bulk modulus and the volume of the polymer glass relative to its volume at the condition of zero expansion volume. The relationship deduced is tested on data available for poly(methyl methacrylate), polystyrene, polyethylene, and poly(vinyl chloride).

SOME YEARS ago it was suggested that the adiabatic bulk modulus of an organic glass (generally of the order of $2-5 \times 10^4$ bar*) was determined by the deformation of carbon-carbon bonds¹. More recently calculations have shown that the modulus associated with bond distortion is some two orders of magnitude higher than the Young's or adiabatic bulk modulus^{2,3}. Just prior to Tuckett's postulate Muller had measured the bulk modulus of hydrocarbon crystals both along and perpendicular to the axis of the molecular chain, obtaining values of 3.3×10^6 bar and $3.3 - 0.8 \times 10^5$ bar respectively⁴. Measurements of a similar nature have been made on oriented crystals of macromolecules. Thus a value of 2.4×10^6 bar has been obtained for the modulus due to bond extension for polyethylene⁵ which compares well with the figure reported for the low molecular weight analogues⁴. Robertson and Wilson examined a sample of polycarbonate and obtained a value of about 1.7×10^5 bar for the elastic modulus along the polymer chains⁶. They found that this longitudinal modulus showed little variation with temperature, whereas the temperature dependence of the transverse modulus was considerable. These authors concluded that the modulus for a sample of unoriented polycarbonate was almost totally due to the interchain modulus.

In view of these observations it is now proposed that the adiabatic bulk modulus of an isotropic organic glass, in which the molecular chains are randomly oriented, is largely determined by the interchain modulus. This being so it is to be expected that the interchain forces follow conventional inter-molecular force relationships.

The concept that the modulus is determined by intermolecular forces is not universally accepted and recently it has been suggested that bond rotations are involved⁶. This view was supported by arguments based on the relation between volume and elasticity. In this paper an accepted model for describing intermolecular forces is used to relate volume and elasticity, and some experimental data examined in the light of the derived relationship.

* 1 bar = 10^5Nm^{-2}

Intermolecular forces

The most commonly used expression which describes the intermolecular forces in a non-polar liquid is that of Lennard-Jones⁸. It can be written in the form

$$U = \frac{A}{V^{n/3}} - \frac{B}{V^{m/3}} \quad (1)$$

in which U is the intermolecular potential for the system of molar volume V , A , B , n , and m are constants. (n and m usually have values of 9 and 6, or 12 and 6 respectively). Equation (1) can be rewritten thus

$$U = K \left\{ \left(\frac{V_0}{V} \right)^{n/3} - \frac{n}{m} \left(\frac{V_0}{V} \right)^{m/3} \right\} \quad (2)$$

in which K is a constant and V_0 is the molar volume of the system for the condition that $(dU/dV)_{V=V_0} = 0$. V_0 can be considered as the molar volume when the expansion volume is zero⁹.

Since the adiabatic bulk modulus, B , equals $-V(d^2U/dV^2)_s$, equation (2) can be used to derive the following relationship between B and V .

$$B = \frac{B_0}{(n-m)} \left\{ (n+3) \left(\frac{V_0}{V} \right)^{\frac{n+3}{3}} - (m+3) \left(\frac{V_0}{V} \right)^{\frac{m+3}{3}} \right\} \quad (3)$$

B_0 is the modulus corresponding to the volume V_0 .

Recently, Haward has discussed the methods available for estimating V_0 for liquids and polymers⁹. The validity of equation (3) can be verified for various combinations of n and m using a computed value for V_0 , and measured values for B and V . Although the Lennard-Jones type potential was originally derived for liquids it should also be applicable to non-polar polymeric glasses in which thermal fluctuation of the molecular segments are minimal and inter-chain forces are of the van der Waals type. Some applications of equation (3) are described below.

Poly (methyl methacrylate)

Equation (3) can be applied to data obtained by Asay, Lamberson and Guenther¹⁰. *Figure 1* shows a plot of B against V for a 12:6 potential. V_0 was calculated by assuming $V_0/V = 0.87$ at T_g , with $V_g = 87.0 \text{ cm}^3 \text{ mol}^{-1}$, resulting in $V_0 = 75.7 \text{ cm}^3 \text{ mol}^{-1}$ ¹¹. An alternative method for estimating V_0 is the bond additive values derived by Biltz and by Sugden which yield values of 78.7 and 78.9 $\text{cm}^3 \text{ mol}^{-1}$ respectively⁹. Using these values makes little difference to the linearity of the plot which, however, can be marginally improved by using a 9:6 potential. For the purposes of this paper, however, it is adequate to consider only the more generally used 12:6 potential.

An alternative procedure can be employed for estimating B_0 . Ramon Rao compiled a set of atomic increments whereby the velocity of sound through a liquid can be calculated for a given density¹². The applicability of this technique has been confirmed for a series of hydrocarbons¹³. Thus it is possible to estimate B_0 for a polymeric glass using equations (4) and (5).

$$S_0^{1/3} = k \rho_0 \quad (4)$$

S_0 is the longitudinal velocity of sound, k is a constant which can be calculated using tabulated values for constituent atoms, and ρ_0 is the density when the expansion volume is zero. Using conventional equations for S_0 and for the relations between elastic constants, it follows that

$$S_0^2 = \frac{3B_0(1-\sigma)}{\rho_0(1+\sigma)} \quad (5)$$

where σ is Poisson's ratio and is assumed to be 0.33 for a polymeric glass¹⁴.

The application of equation 4 and 5 to poly(methyl methacrylate) results in a value of 5.90×10^4 for B . From Figure 1 B_0 is calculated to be 14×10^4 .

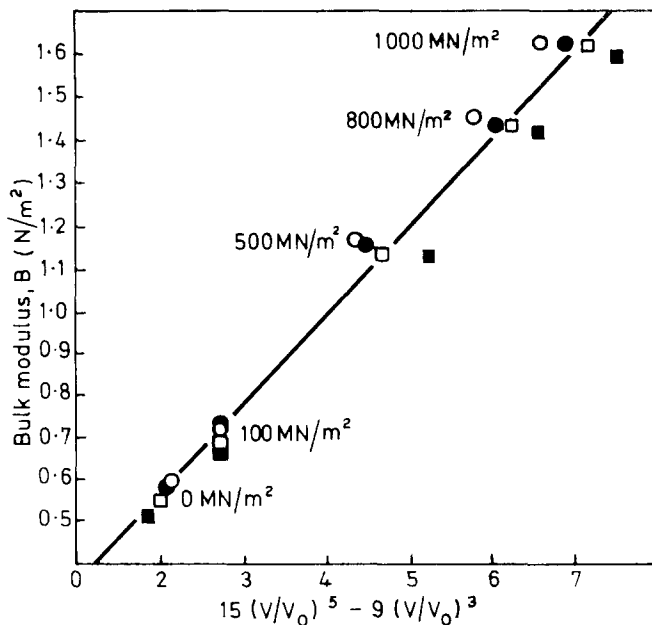


Figure 1 A plot of B , the adiabatic bulk modulus, versus $15(V/V_0)^5 - 9(V/V_0)^3$ for data on poly(methyl methacrylate)¹⁰. The values were obtained at different temperatures, ○ 25°C, ● 40°C, □ 55°C, ■ 75°C, and at the pressures indicated alongside the points

The two quantities are of the right magnitude which suggests that equations 4 and 5 provide a useful means of estimating the approximate value of B_0 for a given polymer glass.

Polystyrene

Haward has proposed a modified van der Waals equation which makes it possible to estimate the isothermal compressibility at the volume V_0 , and by applying this equation to data available for polystyrene he estimated a value of $8.0 \times 10^{-6} \text{ bar}^{-1}$ for this parameter¹⁵. It is very reasonable to assume that the isothermal and adiabatic bulk moduli are equal under the conditions of

zero expansion volume and therefore a value of 12.5×10^4 bar is obtained for B_0 . This is very close to the measured B_0 for poly(methyl methacrylate). Using this value for B_0 and equation (3) it is possible to compare calculated and observed data on the bulk modulus. Gee has proposed a value of 3.0×10^4 bar for the experimentally determined isothermal bulk modulus at the T_g ¹⁶ and, assuming the difference between the isothermal and adiabatic moduli is small in the glassy state, this can be taken as B . It has been shown that at T_g $V_0/V = 0.87$ ¹⁷, and substituting this value with the computed value of B_0 in equation 3 results in a calculated B of 3.2×10^4 bar. Warfield *et al* measured B at room temperature to be 5.4×10^4 bar¹⁸, taking the density of polystyrene at this room temperature as 1.051 g cm^{-3} ,¹⁹ and using Breuer, Haward and Rehage's value for ρ_0 ¹⁷ we calculate B to be equal to 4.2×10^4 bar. In both examples the agreement between calculated and observed modulus is good.

Using Rao's approach, i.e. equations (4) and (5), B_0 is calculated to be 4.5×10^4 bar which, as for poly(methyl methacrylate), is between one half and one third of the measured value.

Polyethylene

Using Doolittle's value for ρ_0 , 1 g cm^{-3} ²⁰, and equation (4) and (5) a value of 4.5×10^4 bar is obtained for B_0 . Thus from equation (3) B is calculated to equal 0.8×10^4 bar for amorphous polyethylene with $\rho = 0.85 \text{ g cm}^{-3}$. Data for experimentally determined values of Young's modulus, determined from sound velocity measurements at a frequency of 2m cycle/s, which with $\sigma = 0.33$ is almost equal to B , are somewhat scattered, but a value of $B = 2 \times 10^4$ bar can be deduced for amorphous polyethylene²¹. The difference between observed and calculated values is most likely to be due to the uncertainty in evaluating B_0 by Rao's method.

Poly(vinyl chloride)

ρ_0 calculated from Sugden's atomic increment values²² is 1.0502 g cm^{-3} and ρ at T_g was estimated from published data¹⁹. B_0 equal to 8.7×10^4 bar was calculated as previously, and thus, from equation (3), B is found to be 1.7×10^4 bar. The experimentally determined modulus with which this value can be compared is the isothermal bulk modulus which is equal to 3.3×10^4 bar at T_g ¹⁶. Assuming the adiabatic and isothermal bulk moduli are almost equal for a glass then the measured modulus is almost twice that calculated using B_0 estimated by Rao's method. This difference is similar to that noted previously and indicates that Rao's method gives a useful, but rather low, guide to the approximate value of B_0 .

DISCUSSION

The variation of bulk modulus with volume for poly(methyl methacrylate) can be satisfactorily accounted for using a Lennard-Jones type expression for the inter-molecular forces. Indeed the bulk moduli for the few polymers for

which data are available appear to depend on inter-molecular forces. Previous work has been concerned with crystalline polymers rather than glasses. It is of interest to note that the modulus for deformation of a C-C bond in an oriented crystallite is of the order of the modulus for diamond.

Graphite which may be considered as a macromolecule of a rather special type has been examined by Girifalco and Lad²³, who used the Lennard-Jones approach to calculate the inter-planar modulus and obtained good agreement between this value (3.15×10^5 bar) and that measured experimentally (3.37×10^5 bar). They concluded that the decrease in volume with increasing pressure was due to compression of inter-layer spacing.

It would seem to be reasonable to conclude that the bulk modulus of a polymeric material, crystalline or glassy, especially when measured at high frequencies, is determined by inter-chain forces and is not dependent on the bonding along the macromolecule. However, where there is an appreciable dependence of modulus on frequency²⁴ and, especially at long times under tension as in a creep experiment, local molecular adjustment including bond rotations will of course take place leading to a decrease in modulus at long times. The dependence of the thermal expansion of polymeric materials on inter rather than intra-chain forces has also been noted²⁵.

*University of Manchester Institute of
Science and Technology,
Sackville Street,
Manchester 1, UK*

R. N. Haward

*Department of Chemistry,
The University,
St. Andrews, Scotland*

*J. R. MacCallum
(Received 7 September 1970)*

REFERENCES

- 1 Tuckett, R. F. *Chem. and Ind.* 1943, **62**, 430
- 2 Treloar, L. R. G. *Polymer, Lond.* 1960, **1**, 95
- 3 Asahini, M., Enomoto, S. and Shimanouchi, T. *J. Polymer Sci.* 1962, **59**, 93
- 4 Muller, A. *Proc. Roy. Soc.* **178A**, 1941, 227
- 5 Sakurada, I., Ito, T. and Nakamae, K. *Makromol. Chem.* 1964, **75**, 1
- 6 Robertson, R. E. and Wilson, C. M. *Polymer Letters*, 1965, **3**, 427
- 7 Bowden, P. B. *Polymer, Lond.* 1968, **9**, 449
- 8 Lennard-Jones, J. E. *Proc. Roy. Soc. (A196)* 1924, 463
- 9 Haward, R. N. *Reviews Macromol. Chem. (C4)* 1970, 45
- 10 Asay, J. R., Lamberson, D. L. and Guenther, A. H. *J. Appl. Phys.* 1969, **40**, 1768
- 11 Bondi, A. *J. Polymer Sci. (A2)* 1964, 3159
- 12 Rao Raman, M. *J. Chem. Phys.* 1941, **9**, 682
- 13 Bakhshi, N. N. and Parthasawathy, S. *J. Phys. Chem.* 1953, **57**, 453
- 14 Neilson, L. E., 'The Mechanical Properties of Polymers', Rheinhold, New York, 1962
- 15 Haward, R. N. *J. Polymer Sci. (A2)* 1969, **7**, 219
- 16 Gee, G. *Polymer, Lond.* 1966, **7**, 177
- 17 Breuer, J., Haward, R. N. and Rehage, G. *Polymer Letters* 1966, **4**, 375
- 18 Barnet, F. R., Cuevas, J. E. and Warfield, R. W. *J. Appl. Polymer Sci.* 1968, **12**, 1147

- 19 Lewis, O. C., 'Physical Constants of Linear Homopolymers', Springer, Berlin, 1968
- 20 Doolittle, A. K. *J. Appl. Phys.* 1951, **22**, 1471
- 21 Schuyer, J. J. *Polymer Sci* 1959, **36**, 475
- 22 Sugden, S. J. *Chem. Soc.* 1927, 1786
- 23 Girifalco, L. A. and Lad, R. A. *J. Chem. Phys.* 1956, **25**, 693
- 24 Turner, S., 'Testing of Polymers', (Ed. W. E. Brown), Vol. 4., Interscience, 1969, pp 1,
73
- 25 Swan, P. R. *J. Polymer Sci.* 1962, **56**, 403

The melting behaviour of heat crystallized poly(ethylene terephthalate)

P. J. HOLDSWORTH and A. TURNER-JONES

The crystallization of amorphous poly(ethylene terephthalate) has been investigated using differential scanning calorimetry (DSC) and x-ray techniques. In particular, the occurrence of double melting peaks in the DSC thermograms has been examined. It is shown that the high temperature peak is due to a recrystallization and melting process taking place while the material is being scanned. Hence the DSC peaks are not a direct reflection of the state of the material at room temperature prior to the scan. As a result, some proposals in the literature for the structural changes accompanying the crystallization of poly(ethylene terephthalate) must be re-examined. Some interesting differences between the effect of temperature and time on the crystallization of poly(ethylene terephthalate) are also reported.

INTRODUCTION

POLY(ETHYLENE TEREPHTHALATE) (PET) can be quenched from the melt to produce material which is amorphous at room temperature. This amorphous PET can be crystallized by heating to above its glass transition temperature. The structural changes accompanying this crystallization process have often been investigated using differential scanning calorimetry (DSC), or the similar technique of differential thermal analysis. It has been found that PET which has been crystallized under a wide range of conditions frequently exhibits two endothermic fusion peaks¹⁻⁶. One of these peaks, peak I, remains at a constant temperature. The second peak, peak II, is only observed after heat treatment above a certain temperature. Initially peak II is small and occurs at much lower temperatures than peak I. However, with increasing crystallization temperature, or crystallization time, peak II increases in size and moves to higher temperatures. At the same time peak I decreases in size and eventually disappears completely.

At present there are conflicting views about the origin of these peaks. Bell and Murayama⁵ have proposed that peak I is associated with chain folded crystals and peak II with crystals containing partially extended chains. Roberts⁶, on the other hand, has interpreted peak I as being due to bundle-like crystals and peak II to chain folded crystals. Both authors tacitly assumed that no structural changes took place during scanning in the DSC. On this basis, the melting peaks were assumed to be directly related to the structure of the material at room temperature prior to the scan. It is our contention that these assumptions are incorrect.

The isothermal crystallization of amorphous PET has been examined in detail by various authors⁷⁻¹⁰. Zachmann and Stuart¹⁰ found, in particular, that only imperfect crystallites were formed at low crystallization temperatures. Upon heating to higher temperatures, the perfection of the crystallites

increased, often within very short times. They concluded that this was due to partial melting and recrystallization.

Hughes and Sheldon¹¹ carried out a DTA study of amorphous PET. They found that the apparent area under the melting peak was significantly larger than the apparent area under the crystallization peak. They suggested that the crystallization peak was followed by a continuous crystallization process which was not detectable in the thermogram baseline.

Bair¹² *et al* have shown conclusively that multiple melting peaks observed in DSC thermograms of polyethylene single crystals are the result of annealing during scanning.

Considering the above results, and many of our own unpublished results, we were lead to the following working hypothesis:

When PET is scanned on a DSC, crystallites formed at low temperatures undergo a continuous perfection process as a result of partial melting and recrystallization during the scan. This leads to an increase in the overall crystallinity.

We would like to present experimental evidence to show that this is a reasonable hypothesis. This is based on complementary DSC and x-ray studies of heat crystallized PET.

We will show that on the basis of this hypothesis we can readily account for the occurrence of double endotherm peaks in DSC scans of PET.

Some interesting differences between the temperature and time dependence of the crystallization process will also be reported.

EXPERIMENTAL

The starting material was a 0.25 mm thick cast film of PET. The polymer was made from dimethyl terephthalate and ethylene glycol by an ester interchange reaction. It contained less than 2% copolymerized diethylene glycol.

Samples of film were heat crystallized by heating in a Perkin Elmer DSC-1 calorimeter from room temperature to the required temperature, holding at this temperature for a given time, and then cooling to room temperature. In all cases heating and cooling rates of 16°C/min were used. X-ray, DSC and density measurements were carried out on the resulting samples.

The melting behaviour of the samples was examined on the DSC using 10 mg of sample and at a scanning rate of 16°C/min. Scale readings were calibrated by scanning standard melting point substances at the same rate.

Wide angle x-ray patterns of the materials were recorded in transmission using a Philips Diffractometer equipped with a proportional counter and pulse height analyser. Cu-K α radiation was used.

Density measurements were made at 23°C using a density gradient column made up from a calcium nitrate-water mixture. From the measured density values (ρ), values of the volume crystalline fraction of the materials were calculated using the relation

$$W_v = \frac{\rho - \rho_a}{\rho_c - \rho_a} \quad (1)$$

It was assumed that $\rho_c = 1.455 \text{ g/cm}^3$ (ref. 13). The measured density of the cast amorphous film was 1.338 g/cm^3 . This was assumed as the value of ρ_a . These crystallinity values should not be regarded as absolute. However, particularly since all the materials used in this study were unoriented it is thought that the use of equation (1) will give a good guide to relative changes in crystallinity.

The spherulitic texture of some samples was investigated by observing thin microtomed sections between crossed polars.

RESULTS

Figure 1 shows DSC traces of amorphous samples which had first been heated in the DSC to various temperatures and cooled immediately. A scan of the

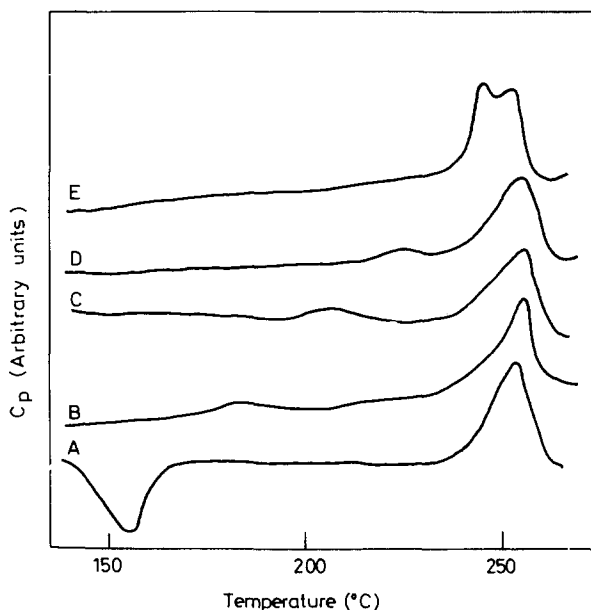


Figure 1 DSC traces of samples of originally amorphous PET which had been heated to various temperatures and cooled immediately: (A) amorphous, (B) 177.5°C , (C) 201°C , (D) 220°C , (E) 240°C

original amorphous film is also included. Figure 2 shows x-ray scans of the principal reflections of these materials. The intensity scale should be regarded as arbitrary since no attempt was made to standardize the volume of material irradiated. Density crystallinity values are shown in Figure 3.

The samples prepared in the above manner were at elevated temperatures for different times, that is the total time spent in the DSC during heating and cooling. Taking an arbitrary highest temperature of 248.5°C , a second series of samples was prepared by heating the amorphous film to a given temperature, and then holding for a time, $t = (2/16)(248.5 - T)$ min. In this way all samples were treated in the DSC for equal times. They will be referred to as

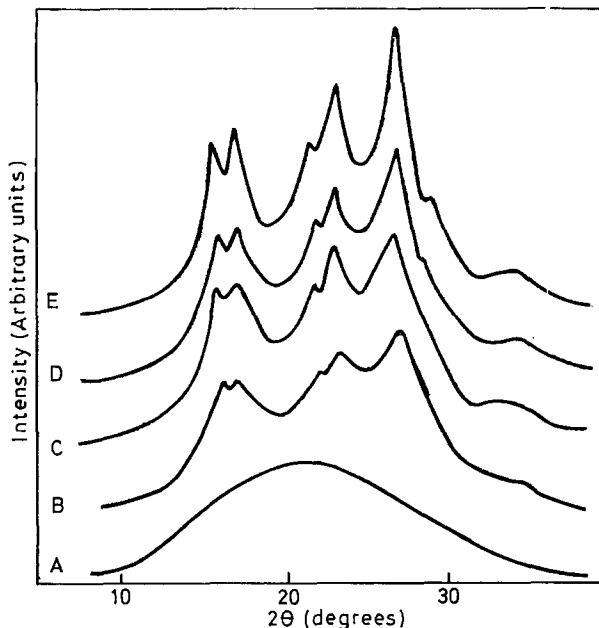


Figure 2 X-ray diffractometer scans of PET samples which had been crystallized at various temperatures: (A) amorphous, (B) 177.5°C, (C) 201°C, (D) 220°C, (E) 240°C

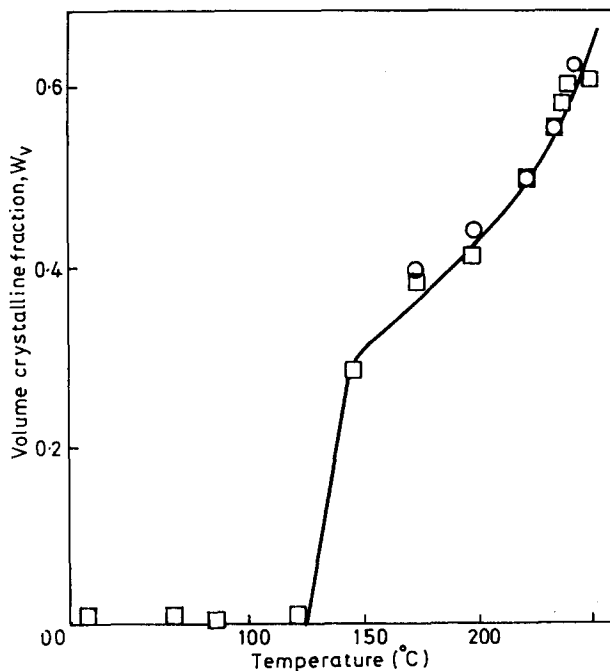


Figure 3 Variation of the volume crystalline fraction (W_v) with crystallization temperature of originally amorphous PET samples
 □ immediately cooled series; ○ isochronous series

an isochronous series. Their density crystallinity values are shown in *Figure 3*. The x-ray patterns of the samples were indistinguishable from those of the materials cooled immediately from the same temperatures.

DSC traces of a third series of samples, originally amorphous, which had been heated to temperatures close to the original melting point of the material, and then cooled immediately, are shown in *Figure 4*. Also shown is the scan of a sample which had been heated to 280°C, which is well above the melting point, and then cooled immediately to room temperature at 16°C/min.

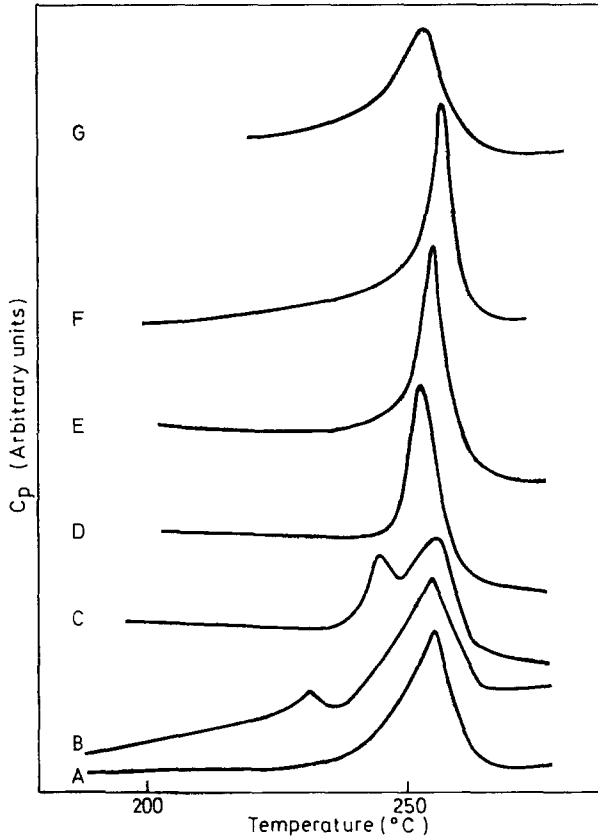


Figure 4 DSC traces of originally amorphous PET which had been heated to the following temperatures (and cooled immediately) (A) amorphous, (B) 224°C, (C) 236°C, (D) 244.5°C, (E) 248.5°C, (F) 252°C, (G) 280°C

The effect of different holding times was also investigated. Amorphous samples were heated to 220°C or 240°C and then either cooled immediately (holding time 0 min) or held for 5, 30 or 960 min before cooling. The resulting DSC scans and some of the x-ray traces are shown in *Figures 5* and *6* respectively. Density and density crystallinity values for these samples are given in *Table 1*.

Table 1 Density and crystallinity values of PET following crystallization at 220°C and 240°C

Temperature (°C)	Time (min)	ρ (g/cm ³)	W_v
220	0	1.396	0.50
	5	1.397	0.505
	30	1.399	0.52
	960	1.404	0.56
240	0	1.406	0.58
	5	1.407	0.59
	30	1.408	0.60
	960	1.409	0.61

One amorphous sample was heated to 220°C, held for 5 min and then scanned to higher temperatures. The same procedure was also carried out using a holding temperature of 240°C. The resulting scans are shown in *Figure 7*. Also shown for comparison are scans of samples which had been similarly prepared but cooled to room temperature prior to scanning.

Four amorphous samples were heat crystallized at 240°C for 5 min. They were subsequently scanned at 2°, 4°, 8° and 16°C/min respectively. The results are shown in *Figure 8*.

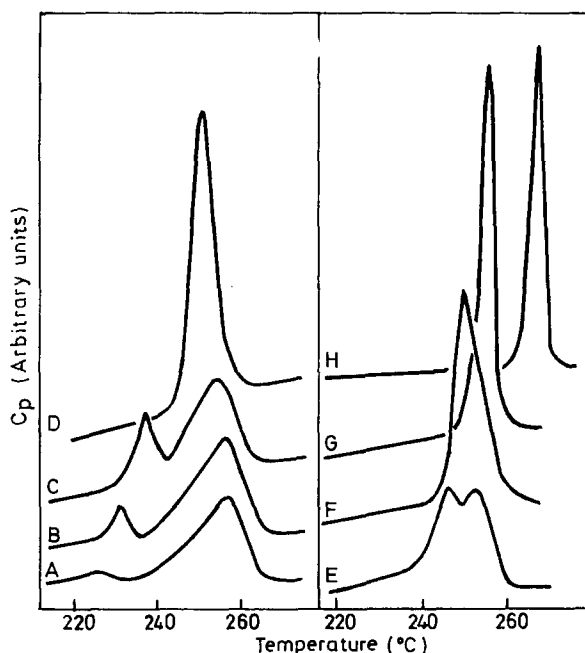


Figure 5 DSC traces of PET samples crystallized at 220°C for: (A) 0 min, (B) 5 min, (C) 30 min, (D) 960 min, and at 240°C for (E) 0 min, (F) 5 min, (G) 30 min, (H) 960 min

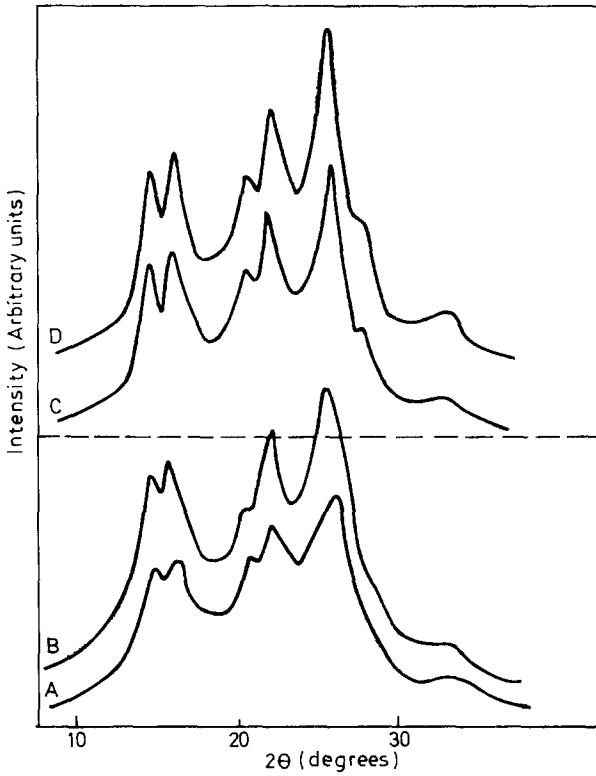


Figure 6 X-ray diffractometer scans of PET crystallized at 220°C for: (A) 0 min, (B) 960 min, and at 240°C for (C) 0 min, (D) 960 min

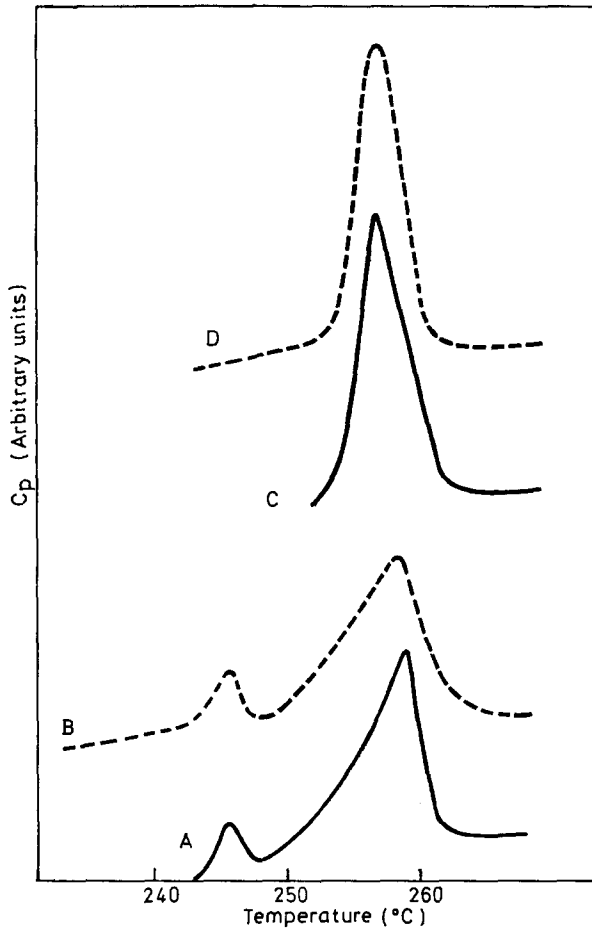


Figure 7 DSC traces of materials crystallized for 5 min at (A) (B) 220°C (C) (D) 240°C. (A) and (C) were recorded without cooling to room temperature, (B) and (D) were recorded after cooling

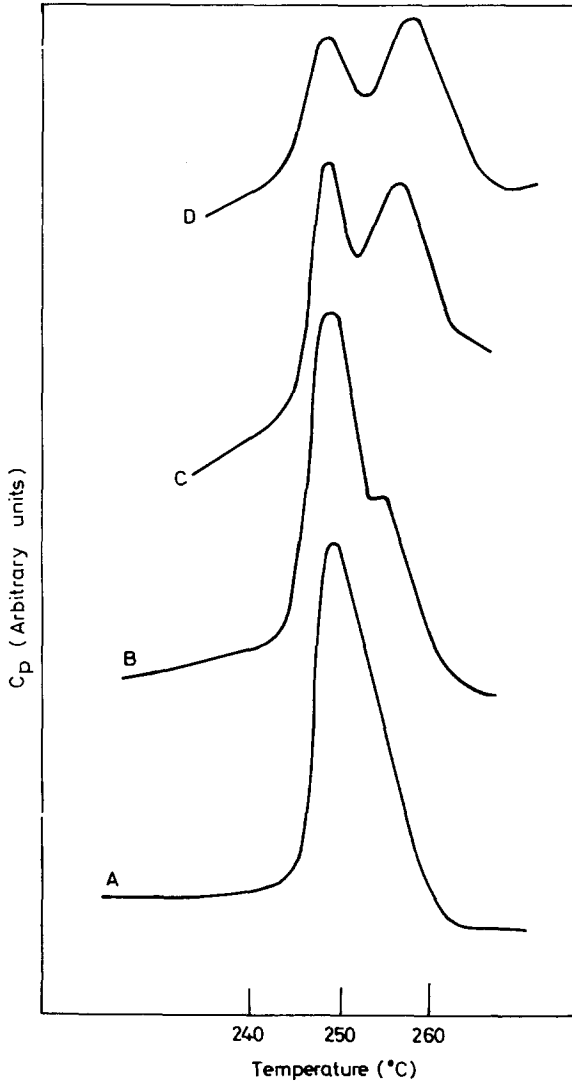


Figure 8 DSC traces of PET which had been crystallized at 240°C for 5 min and recorded at heating rates of (A) 16°C/min, (B) 8°C/min, (C) 4°C/min, (D) 2°C/min

DISCUSSION

The DSC scan of amorphous PET shows a 'cold' crystallization peak and a melting peak (*Figure 1*). Between these peaks there is a wide intermediate temperature range over which nothing appears to happen. From measurements made on several samples, however, we found that the area under the crystallization peak was only about 70–80% of the area under the melting peak. Similar differences have been reported previously^{4,11}. The simplest explanation is that there is a continuous increase in crystallinity during the intermediate temperature range which is not detectable in the DSC baseline. The results in *Figure 3* confirm that there is an increase in crystallinity in the intermediate temperature range.

Points from the isochronous and the immediately cooled series fall on roughly the same curve in *Figure 3*. Hence the increase in crystallinity is not merely because samples which had been treated at higher temperatures had also been in the calorimeter for longer times. The correspondence between the x-ray traces of these two series supports this conclusion.

All samples which had been heated to temperatures in the intermediate temperature range showed the same, space-filling, spherulitic texture, irrespective of the holding temperature, or time. Hence, crystallinity changes within this range must occur within the spherulites. This is in agreement with the work of Zachmann and Stuart¹⁰.

The increase in crystallinity might occur in two ways. Either the total number of crystallites or the average perfection of the existing crystallites, may increase. The x-ray scans in *Figure 2* suggest strongly that the second alternative is more important. As the temperature of treatment increases, there is a continuous increase in the sharpness and degree of resolution of the reflections. The broadening of x-ray reflections is usually attributed to two effects¹⁴. If the crystal size is small in a direction perpendicular to a set of planes, the x-ray reflection from those planes will be broadened. Broadening will also result if a lattice is strained. With polymers it is very difficult to separate size and strain effects¹⁵. We have made no attempt to do so and will use the general term 'perfection' to cover both effects. On this basis, the x-ray results show that the overall perfection of the crystallites increases continuously in the DSC over the intermediate temperature range.

An indication of the nature of the perfection process is given by the work of Zachmann and Stuart¹⁰. They isothermally crystallized samples of amorphous PET as fully as possible, raised the temperature, and then quenched after different times. They found that the density initially decreased, but then increased to exceed the starting value. They concluded that upon raising the temperature more perfect crystals are produced as a result of partial melting followed by recrystallization. These results applied to isothermal experiments. In a DSC scan the temperature is changing continuously. It is reasonable to suppose, therefore, that the increase in perfection of the crystallites occurring during a DSC run is the result of a continuous melting and recrystallization process. On this basis, consider what is happening at any particular temperature in the intermediate range during a scan. The least perfect crystals will be melting. These will recrystallize to form more perfect crystals at some higher temperature (i.e. later in the scan). Crystals which had

previously melted will be recrystallizing. Some crystals will be stable and will not melt until a higher temperature is reached. The net result is a small increase in the average perfection of the crystals. When we talk about the 'melting of crystals' in the present context, we do not wish to imply that the crystals necessarily melt completely. It could be that only partial melting takes place before recrystallization.

On the basis of the foregoing considerations, the thermograms of amorphous PET can now be interpreted as follows

- (1) When amorphous PET is heated in a scanning calorimeter, there is a crystallization process which converts the material into an assembly of imperfect crystallites. This is revealed by a large exothermic peak. The peak width suggests that crystallites with differing degrees of perfection are formed.
- (2) In the intermediate temperature range there is a continuous increase in crystallinity. This is due, at least primarily, to an increase in the average perfection of the crystallites by a continuous melting and recrystallization process. This produces a gradual increase in crystallinity which takes place over a wide temperature range and, therefore, is not detectable in the DSC baseline.
- (3) When the temperature is sufficiently high, crystallites which are melting, can no longer recrystallize. The result is a broad endothermic melting peak.

Consider now the origin of double melting peaks. If we stop scanning at some temperature above the crystallization peak, the continuous melting and recrystallization process will be interrupted, producing a crystallite perfection distribution characteristic of the holding temperature. Upon rescanning we can await an associated melting process at some temperature above the holding temperature. If the holding temperature were low enough, we could expect the original continuous melting and recrystallization process to be completely re-established, as scanning proceeds. The complete thermogram should then display a melting process corresponding to the holding temperature and a main melting peak indistinguishable from that given by amorphous PET. This is in complete agreement with the present experimental results (see *Figure 1*) and those of the literature¹⁻⁶. If a high holding temperature is used, the crystals attain a high perfection and hence a high stability. The associated melting process may then occur at such high temperatures that the continuous melting and recrystallization process is only partially re-established or not at all. This is because melted crystals are unable to recrystallize before they are scanned to temperatures so high that recrystallization is no longer possible. As the holding temperature is raised, the melting peak arising from the continuous melting and recrystallization process should diminish and finally vanish altogether, leaving only a melting peak characteristic of the original crystallization conditions. This is in complete agreement with the present experimental results (*Figures 1 and 4*) and with those in the literature¹⁻⁶.

Consider now the effect of scanning rate on thermograms of material which had been crystallized at 240°C for 5 min (*Figure 8*). At a rate of 16°C/min, only one melting peak is evident but as the rate is reduced, a second peak appears at higher temperature and grows in size. This effect is perfectly explicable on the basis of the foregoing arguments. The peak in the 16°C/min run is associated with the holding temperature. Because the scanning rate is fast there is no chance for recrystallization to occur. As the scanning rate is reduced however, there will be increasing recrystallization, producing material which melts at a higher temperature.

As the holding time is increased at any particular temperature the crystallite perfection distribution should become more characteristic of the holding temperature and the associated melting process greater in magnitude. This is in agreement with present results (see *Figure 5*) and those in the literature¹⁻⁶. An increase in temperature is also observed.

Some of the foregoing effects might occur because material remains molten at the holding temperature and then recrystallizes upon subsequent cooling. Two sets of results speak against this. Firstly, none of the subsequent DSC traces resembles that of material which had definitely been melted by heating to 280°C prior to cooling (see *Figure 4*). Secondly, essentially identical thermograms are observed irrespective of whether or not the materials are cooled to room temperature prior to scanning (see *Figure 8*). From the results of similar experiments Bell and Murayama⁵ also concluded that the observed effects were not the results of recrystallization during cooling.

In the foregoing paragraphs we have shown that a continuous perfection process can take place during scanning of PET in a scanning calorimeter. We have shown further that when account is taken of this process the occurrence of double melting peaks in heat crystallized PET can be easily explained. It should be noticed that it has not been necessary to postulate that the peaks represent crystallites with basically distinct morphologies. Neither do we have to postulate that crystals of high melting point are converted into crystals with initially lower melting points (which would seem to be very unlikely on thermodynamic grounds). Previous explanations of the effect^{5,6} contained both postulates.

Similar double melting peak thermograms have been observed in nylon 66¹⁶, polystyrene¹⁶, and drawn PET¹⁷. In these cases too continuous melting and recrystallization during scanning with the DSC may provide the correct explanation.

To conclude, we wish briefly to point out some interesting differences between the effect of time and temperature upon the crystallization of amorphous PET.

The breadths of the x-ray reflections of PET samples, and hence their x-ray perfections, are highly dependent upon crystallization temperature, but relatively insensitive to time (see *Figures 2 and 6*). Similar results can be found in the literature¹⁷⁻¹⁹. The density crystallinity values show a similar trend (see *Table 1*). Contrary to this, the melting behaviour is highly sensitive to crystallization time (see *Figure 5*). With increasing time the melting peaks associated with the holding temperatures of 220°C or 240°C become more pronounced and move to higher temperatures. This must be due to structural changes which have little or no effect upon the x-ray perfection or the density.

The simplest expression for the melting point of a polymer is

$$T_m = T_m^\infty \left(1 - \frac{2\sigma_e}{\Delta H_f L} \right) \quad (2)$$

Where T_m^∞ is the melting point of an infinite perfect crystal, σ_e is the surface energy of the crystals, ΔH_f their heat of fusion and L their thickness.

The x-ray long period of most materials increases with holding time at a given crystallization (annealing) temperature. It is generally thought that this is due, at least partly, to an increase in the thickness of the crystalline regions. As can be seen from equation (2), such an increase would produce an increase in melting point. Zachmann and Schmidt¹⁹ have reported however, that the long period of PET decreases with holding time. It seems very unlikely that the crystalline regions would decrease in thickness, but if this happened the melting point would be reduced and not increased. The increase in melting point is also unlikely to be due entirely to an increase in ΔH_f since this would mean a reduction in lattice strain and hence an increase in x-ray perfection. As mentioned previously, no appreciable increase in x-ray perfection is observed. The melting point would increase if σ_e were reduced. This would happen if the surfaces became smoother in the course of time.

Very tentatively, it is possible to suggest one process that might produce a more regular surface at the same time as thinner crystals. Suppose the original crystals have irregular surfaces through which the molecules pass roughly at right angles and suppose that with increasing time the surface tries to regularize in such a way that the crystals become bounded by a crystallographic plane. If this were a plane such as (001), which is not perpendicular to the molecular axis, a reduction in crystal thickness would result.

It is clear that more work is required before the differing effects of time and temperature on the crystallization of PET can be properly understood.

CONCLUSIONS

When heat crystallized PET is run on a DSC, two melting peaks are often observed. Whilst the peak at the lower temperature is associated with the crystallization conditions, the peak at the higher temperature is the result of a melting and recrystallization process which takes place during the scan. Consequently, the DSC scans are not a direct reflection of the state of the material at room temperature prior to the scan.

There are significant differences between the effects of temperature and time on the crystallization process. When the temperature is increased there is an increase in x-ray perfection. At a given temperature, further structural changes take place in the course of time which result in an increased melting point but no large change in x-ray perfection.

The present work also illustrates the pitfalls which can be awaited if DSC is used for morphological studies in isolation from other techniques.

ACKNOWLEDGEMENTS

The authors would like to thank W. J. Price for carrying out much of the practical work, and D. A. Hemsley for making the optical examination of the materials.

*ICI Plastics Division,
Welwyn Garden City,
England*

(Received 11 September 1970)

REFERENCES

- 1 Kanetsuna, H. and Maeda, K. *Kogyo Kagaku Zasshi* 1966, **69**, 1784
- 2 Mitsubishi, Y. and Ikeda, M. *Kobunshi Kagaku* 1966, **23**, 319
- 3 Mitsubishi, Y. and Ikeda, M. *Kobunshi Kagaku* 1966, **23**, 310
- 4 Lawton, E. L. and Cates, D. M. *Amer. Chem. Soc. Reprints*, San Francisco Meeting, 1968, p 851
- 5 Bell, J. P. and Murayama, T. *J. Polym. Sci. (A-2)* 1969, **7**, 1059
- 6 Roberts, R. C. *Polymer, Lond.* 1969, **10**, 117
- 7 Keller, A., Lester, G. and Morgan, L. B. *Phil. Trans. Roy. Soc.* 1954, **A247**, 23
- 8 Cobbs, W. H. and Burton, R. L. *J. Polym. Sci.* 1953, **10**, 275
- 9 Zachmann, H. G. and Stuart, H. A. *Makromol. Chem.* 1960, **41**, 131
- 10 Zachmann, H. G. and Stuart, H. A. *Makromol. Chem.* 1960, **41**, 148
- 11 Hughes, M. A. and Sheldon, R. P. *J. appl Polym. Sci.* 1964, **8**, 1541
- 12 Bair, H. E., Salovey, R. and Huseby, T. W. *Polymer, Lond.* 1967, **8**, 9
- 13 Daubeny, R. De P., Bunn, C. W. and Brown, C. J. *Proc. Roy. Soc. (A)* 1954, **226**, 531
- 14 Klugg, H. P. and Alexander, L. E., 'X-ray diffraction procedures', John Wiley, New York, 1954, Chapter 9
- 15 Buchanan, D. R., McCullough, R. L. and Miller, R. L. *Acta cryst.* 1966, **20**, 922
- 16 Bell, J. P. and Dumbleton, J. H. *J. Polym. Sci. (A-2)* 1969, **7**, 1033
- 17 Yabayashi, T., Orito, Y. and Yamada, N. *Kogyo Kagaku Zasshi*, 1966, **69**, 9
- 18 Kilian, H. G., Halboth, H. and Jenckel, E. *Kolloid Z.* 1960, **172**, 166
- 19 Zachmann, H. G. and Schmidt, G. F. *Makromol. Chem.* 1962, **52**, 23

Polymerization and 2+2 cycloaddition in the system N-vinylcarbazole- tetracyanoethylene

C. E. H. BAWN, A. LEDWITH and M. SAMBHI

N-Vinylcarbazole reacts with tetracyanoethylene in a variety of solvents to give mixtures of the 2 + 2 cycloadduct 1-(*N*-carbazolyl)-2,2,3,3-tetracyano-cyclobutane V; a product VI formed by elimination of hydrogen cyanide – 1-(*N*-carbazolyl)-3,4,4-tricyano-1,3-butadiene and poly(*N*-vinylcarbazole). Cationic polymerization of NVC may be initiated by TCNE or by the cyclobutane V, which exists in equilibrium with its components. ESR experiments show that (TCNE⁻) is the gegen-ion during polymerization and mechanisms for all these processes are discussed. It is concluded that a charge transfer complex is a common primary intermediate for both cycloaddition and polymerization, with subsequent electron transfer from NVC to TCNE.

N-VINYL CARBAZOLE (NVC) (I) is a very reactive vinyl monomer undergoing polymerization by both cationic and free radical processes and, like all carbazole derivatives, readily oxidised by a wide variety of reagents. These two characteristics were first combined by Ellinger¹ and by Scott *et al*², who independently showed that NVC may be polymerized by a series of organic electron acceptors. Since the majority of neutral organic acceptors employed gave rise to coloured solutions (charge transfer spectra) when mixed with NVC, the role of so called charge transfer complexes in polymerization has been studied extensively, and the topic has been reviewed by Ellinger³. For NVC polymerization the only detailed kinetic studies reported are those of Pac and Plesch⁴, and Szwarc *et al*⁵ both using tetranitromethane as initiator. Tetracyanoethylene (TCNE) (II) is one of the best known organic electron acceptors, readily exhibiting charge transfer spectra when mixed with molecules possessing π - electrons or groups having atoms with unshared electron pairs^{6,7}, and a particular feature of the interaction between TCNE and olefins is the ready formation of corresponding cyclobutanes by 2 + 2 cycloaddition⁷.

As part of a continuing interest in the relationship between charge transfer spectra and reaction intermediates⁸, we have investigated the reactions between TCNE and NVC under conditions which lead to both polymerization and 2 + 2 cycloaddition. Preliminary reports of this work have been published⁹⁻¹¹ since its completion¹² and Barrales-Rienda, Brown and Pepper¹³ have demonstrated, by copolymerization with *p*-methoxy styrene, that interaction of NVC and TCNE leads to cationic polymerization. Very recently Nakamura, Soma, Onishi and Tamaru¹⁴ have published results from a study similar to that now reported, and whilst there are many common features there are major apparent discrepancies between the two studies.

EXPERIMENTAL

Materials

Acetonitrile was dried first by passing down a column of activated alumina and then by refluxing with calcium hydride (10 g per litre) for at least 72 hours. Fractional distillation using a 2ft (0.305 m) Vigreux column gave a middle fraction, b.p. 81–82°.

Methylene chloride was similarly purified except that the alumina column treatment was omitted, b.p. 39.5–40.5°.

Methanol (A.R.) was fractionated through a short Vigreux column to give a middle fraction, b.p. 64.5–65°.

N-Vinylcarbazole. Commercial material was re-crystallized three times from methanol and stored in the dark in a vacuum desiccator over calcium chloride, m.p. 64–65°.

Tetracyanoethylene. Commercial grade reagent was recrystallized twice from dry methylene chloride and finally sublimed under high vacuum. The white solid obtained had m.p. 198–200°.

Hexamethyl benzene. Commercial grade reagent was twice recrystallized from ethanol to give white plates, m.p. 165°C.

Kinetic measurements

Polymerization rates. Reactions were followed by conventional dilatometric techniques under high vacuum. The dilatometers were attached to two separate vessels in which CH₂Cl₂ solution of TCNE and NVC were out-gassed, and allowed to reach temperature equilibrium, before mixing.

Rates of polymerization (R_p) were estimated from the expression

$$R_p = \frac{\pi r^2 R_c [\text{NVC}] \gamma}{V.v}$$

where R_c = rate of contraction (cm min⁻¹)

γ = contraction conversion factor = $d_p/d_p - d_m$

d_p = density of polymer, d_m = density of monomer in CH₂Cl₂ at the appropriate temperature

r = radius of capillary stem of dilatometer (cm)

V = volume of dilatometer (ml)

v = volume fraction of monomer in solution.

In order to use the rate expression it was necessary to determine the values of d_m and d_p , the latter being assumed independent of molecular weight. Density values for both monomer and polymer were determined dilatometrically and are shown in *Table 1*.

Table 1 Densities of NVC and poly(NVC) in methylene chloride

Temp. (°C)	d_m (gram/ml)	d_p (gram/ml)
25	1.096	1.231
30	1.088	1.225
35	1.081	1.219

Dissociation of cyclobutane. Reaction rates were followed by spectrophotometric techniques. The apparatus and procedure were as described for dilatometry, with the dilatometer replaced by a standard path length spectrophotometer cell. Ultra-violet and visible spectra were then measured on Unicam SP 500 or SP 800 spectrophotometers.

Molecular weight determinations

After completion of each polymerization (approximately 20% conversion) the mixture was poured into ice-cold methanol, and the precipitated poly(NVC) filtered, washed with methanol and dried in a vacuum oven at 40°C.

Intrinsic viscosities (η) were measured in benzene at 25°C and average molecular weights (M_v) calculated from the relationship of Ueberreiter and Springer¹⁵

$$[\eta] = 3.35 \times 10^{-4} M_v^{0.58} \text{ dl/g}$$

RESULTS

Reactions of NVC with TCNE in benzene

A solution of NVC in benzene immediately turned purple on addition of TCNE. White crystals precipitated and the reaction was complete after about 10 minutes at 30°C. The purple colour changed eventually to the characteristic green colour of benzene-TCNE solutions. In a typical preparation 25 ml of a benzene solution, $6.3 \times 10^{-2}M$ in both TCNE and NVC, yielded an initial precipitate, 0.4 g (90% recovery). After washing with benzene and drying, the white crystals, m.p. 130–131°C, had C, 75.1; H, 3.9; N, 21.2%; required for $C_{20}H_{11}N_5$, C, 74.8, H, 3.4, N, 21.8%. Infra-red analysis showed a $C\equiv N$ stretching at 2250 cm^{-1} and the characteristic carbazole aromatic vibrations between $700\text{--}800 \text{ cm}^{-1}$. The compound was thus identified as 1-(*N*-carbazolyl)-2,2,3,3-tetracyanocyclobutane (V), the anticipated⁷ 2+2 adduct of NVC and TCNE.

Reaction of TCNE with excess NVC in benzene similarly gave high yields of V (based on TCNE) with very slow subsequent polymerization of residual NVC.

Reaction of NVC with TCNE in Methanol

Addition of TCNE to a solution of NVC in methanol produced an immediate blue colour which faded after approximately one minute at 30°C, the solution then becoming yellow. Typically 25 ml of a solution of $2.1 \times 10^{-2}M$ reagents yielded, after refluxing for two hours, 0.14 g (82%) of a red crystalline product (VI) with the solution remaining having a very strong smell of hydrogen cyanide. After recrystallization from acetonitrile the red crystals, m.p. 271–272°, had infra-red absorptions at 2250 cm^{-1} ($C\equiv N$), 1613 cm^{-1} (conjugated $C=C$) and characteristic carbazole bands between $700\text{--}800 \text{ cm}^{-1}$. Found C, 77.4; H, 3.7; N, 18.9%; required for $C_{19}H_{10}N_4$, C, 77.5; H, 3.4; N, 19.0%. The visible absorption spectrum of VI in CH_2Cl_2 had

λ_{\max} 474nm (ϵ_{\max} $4.4 \times 10^4 \text{ M}^{-1} \text{ cm}^{-1}$). In acetonitrile and methanol λ_{\max} values were 466 and 464 nm respectively. Compound VI is thus identified as 1-(N-carbazolyl)-3,4,4-tricyano-1,3-butadiene⁷. Significantly there was no evidence whatever for polymer formation in methanol.

Dissociation of (1-N-carbazolyl)-2,2,3,3-tetracyanocyclobutane(V)

One of the most notable characteristics of V was the formation of intensely coloured solutions when it was dissolved in aromatic solvents. The absorption spectra of these solutions corresponded exactly with the charge transfer spectra of TCNE with the same solvent¹⁶. In non aromatic solvents the dissociation of V into its components was readily demonstrated by addition of hexamethyl benzene (HMB), a good donor molecule, to the solutions. In all cases the characteristic colour of the HMB-TCNE complex was observed. (See Table 2).

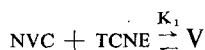
Table 2 Absorption spectra of solutions of V and TCNE

Solvent	Solute	Added donor	λ_{\max} (nm)
Benzene	V		385
Benzene	TCNE		384
Toluene	V		405
Toluene	TCNE		406
Anisole	V		505
Anisole	TCNE		506
CH ₂ Cl ₂	V	HMB	546
CH ₃ CN	V	HMB	545
CH ₃ OH	V	HMB	544
HMB	TCNE		545

In the more polar solvents solutions of V gradually became yellow in colour with λ_{\max} corresponding to that of the butadiene VI.

Quite obviously the cycloadduct V was dissociating back into its component olefins and a dynamic equilibrium was established for solutions in methylene dichloride, as indicated below.

Assuming that the equilibrium between TCNE, NVC and V may be represented as

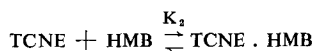


then the overall equilibrium constant K_1 may be expressed as

$$K_1 = \frac{[\text{V}]_e}{[\text{NVC}]_e [\text{TCNE}]_e}$$

although there may be several intermediate equilibrium steps.

If hexamethyl benzene (HMB) is added to the reaction mixture, a 1:1 complex TCNE . HMB is formed in a second equilibrium



$$\therefore K_2 = \frac{[\text{TCNE} \cdot \text{HMB}]_e}{[\text{TCNE}]_e [\text{HMB}]_e}$$

This equilibrium has been studied previously¹⁶ and in methylene dichloride at 22°C, $K_2 = 17.1 \text{ M}^{-1}$ with $\lambda_{\text{max}} = 546 \text{ nm}$ and $\epsilon_{\text{max}} = 4390 \text{ M}^{-1} \text{ cm}^{-1}$.

Various solutions containing NVC, TCNE and HMB were prepared and the absorbance at 546 nm determined at 25°C. If the total concentration of intermediates is much less than equilibrium concentrations of TCNE, NVC and V and assuming ϵ_{max} (and hence K_2) change only slightly over a small temperature range $[\text{TCNE} \cdot \text{HMB}]_e$ may be calculated and K_1 estimated from the following expression:

$$K_1 = \frac{[\text{TCNE}]_0 - [\text{TCNE}]_e - [\text{TCNE} \cdot \text{HMB}]_e}{([\text{NVC}]_0 - [\text{V}]_e) [\text{TCNE}]_e}$$

where

$$[\text{TCNE}]_0 - [\text{TCNE}]_e - [\text{TCNE} \cdot \text{HMB}]_e = [\text{V}]_e$$

Experimental data are shown in *Table 3* and a plot of $[\text{V}]_e$ against $([\text{NVC}]_0 - [\text{V}]_e) [\text{TCNE}]_e$ gave a straight line of slope $K_1 = 582 \text{ M}^{-1}$. Using a similar treatment but starting with V, the calculated value of K_1 was 588 M^{-1} in excellent agreement with the value based on the forward equilibrium.

Table 3. Competing equilibria between TCNE, NVC and HMB in methylene dichloride at 25°C

10^3 [HMB] ₀	10^3 [NVC] ₀	10^3 [TCNE] ₀	O.D. (564 nm)	10^4 [HMB.TCNE] _e	10^3 [TCNE] _e	10^3 [V] _e	10^6 [TCNE] _e / ([NVC] ₀ [V] _e)
3.59	1.43	1.90	0.32	0.73	1.21	0.62	0.98
4.12	2.62	2.86	0.45	1.03	1.50	1.26	2.04
5.10	2.75	3.18	0.63	1.44	1.70	1.34	2.40
4.93	2.63	3.67	0.75	1.71	2.10	1.40	2.58

Formation of 1-(N-carbazolyl)-3,4,4-tricyano-1,3-butadiene (VI) from cycloadduct (V)

When NVC and TCNE were allowed to react in polar solvents formation of the butadiene VI was always observed, as noted previously for the reactions in methanol. Qualitatively it was apparent that the rate of formation of VI was faster the more polar the solvent. A further complication was concurrent polymerization of NVC (see later) whenever [NVC] was in excess of [TCNE].

Similarly it was observed that V decomposed in polar solvents to give VI plus some polymer. Once again the rate of formation of VI was more rapid the more polar the solvent and a simple kinetic study was made using solutions of V in methylene chloride.

The reaction rates were followed by monitoring the absorbance at 474 nm due to VI, and complete reproducibility was obtained only when the reactions were carried out *in vacuo*.

Table 4 Formation of VI in methylene chloride

$10^3 [V]_0$ (M)	$10^8 \times \text{Initial rate of formation of VI}$ (M min ⁻¹)
3.9	4.4
6.4	6.7
9.4	10.5
12.5	13.8

Typical data are shown in Table 4 and a plot of initial rate of formation VI against initial concentration of V was linear indicating that formation of VI was a reaction first order in [V] i.e.

$$\frac{d[VI]}{dt} = k'[V]$$

where

$$k' = 2 \times 10^{-7} \text{ s}^{-1} \text{ at } 25^\circ \text{ in methylene chloride}$$

Reactions of NVC and TCNE in methylene chloride

Addition of excess TCNE to a solution of NVC in methylene chloride at 30°C resulted in immediate formation of the blue NVC-TCNE charge transfer complex. The colour faded first to pink, becoming colourless after 3–4 minutes, and white crystals of V separated. If the process was carried out such that [NVC] was in excess of [TCNE], similar reactions occurred together with slow polymerization of NVC and the solution finally became yellow due to formation of VI.

Polymerization of NVC by TCNE in methylene chloride

Polymerization of NVC initiated by TCNE was faster in acetonitrile than in methylene chloride but for both solvents, reaction rates were higher *in vacuo* than in air, and final polymer yields were in the range 30–50%. Accordingly polymerizations in methylene chloride were followed dilatometrically *in vacuo*, and the results, based on initial rates, are summarized in Table 5.

Table 5 Polymerization of NVC by TCNE in methylene chloride at 30°C

$10 [NVC]$ (M)	$10^3 [TCNE]$ (M)	$10^3 R_p$ (Initial) (M min ⁻¹)	10^{-4} molecular weight
1.66	9.51	1.23	8.80
2.52	5.51	1.82	9.40
3.01	9.51	2.2	9.42
3.93	9.51	3.00	—
5.83	9.51	4.40	9.44
3.01	1.63	2.27	8.70
3.01	4.01	2.10	9.04
3.01	5.39	2.05	9.42

From the data in *Table 5* it is clear that the initial rate of polymerization is dependent on $[NVC]$ but apparently independent of $[TCNE]$. A plot of R_p versus initial $[NVC]$ was linear with a slope of $1.3 \times 10^{-4} \text{ s}^{-1}$ and first order dependence on $[NVC]$ was confirmed by the linearity of plots of $\log_{10} [NVC]$ versus time, for individual kinetic runs. Similar rate data obtained at 25° and 35°C yielded an estimate for the overall activation energy of $\sim 20 \text{ kcal mol}^{-1}$, although this value may be seriously in error because of the narrow temperature range employed.

Samples of poly(*N*-vinylcarbazole) taken at different % conversions during a kinetic run did not show significant change in molecular weights as determined by measurement of intrinsic viscosities, and the molecular weights did not vary significantly with changing $[NVC]$ or $[TCNE]$ (at 20% conversion) see *Table 5*. Temperature affected viscosity average molecular weights as indicated by the representative values 107000 (25°C), 90000 (30°C) and 78000 (35°C).

ESR spectrum of polymerizing solutions

ESR examination of polymerizing mixtures showed an eleven line spectrum with a spacing of 1.60 G, identical with that of the anion radical ($TCNE^{\cdot -}$) formed by addition of one electron to $TCNE$ ¹⁷. It was further noted that the intensity of the e.s.r. signal due to $TCNE^{\cdot -}$ increased if additional NVC was added to the solution, and decreased steadily during polymerization.

Absolute concentrations of $TCNE^{\cdot -}$ were estimated by calibration of the e.s.r. signals with those from *aa'*-diphenyl- β -picryl hydrazyl. Instantaneous values of R_p and $[NVC]$ were calculated from tangential slopes of dilatometric contraction curves and data from a representative run are shown in *Table 6*.

Table 6. Decrease in $[TCNE^{\cdot -}]$ during polymerization of NVC by $TCNE$ in methylene dichloride at 30°

<i>Time (t)</i> (min)	$10^3 [NVC]_t$ (M)	$10^5 [TCNE^{\cdot -}]_t$ (M)	$10^6 [NVC]_t [TCNE^{\cdot -}]_t$ (M ²)	$10^3 (R_p)_t$ (M min ⁻¹)
0	3.01	1.37	4.12	2.20
5	2.90	1.18	3.42	1.95
15	2.68	0.84	2.25	1.36
25	2.51	0.56	1.41	1.13

It is clear that $[TCNE^{\cdot -}]$ decreases rapidly during polymerization and plots of $\log[TCNE^{\cdot -}]$ versus time were linear showing the decay to be a first order process in $[TCNE^{\cdot -}]$. In addition *Table 6*, and *Figure 1* show that $(R_p)_t$ is directly proportional to the product $[NVC]_t [TCNE^{\cdot -}]_t$. The fact that the best line through the points in *Figure 1* does not pass through the origin can almost certainly be ascribed to the errors involved in estimating $[TCNE^{\cdot -}]$.

DISCUSSION

Tetracyanoethylene ($TCNE$) is perhaps the most widely used neutral organic acceptor molecule for the study of charge transfer spectra^{6,18}. The latter may

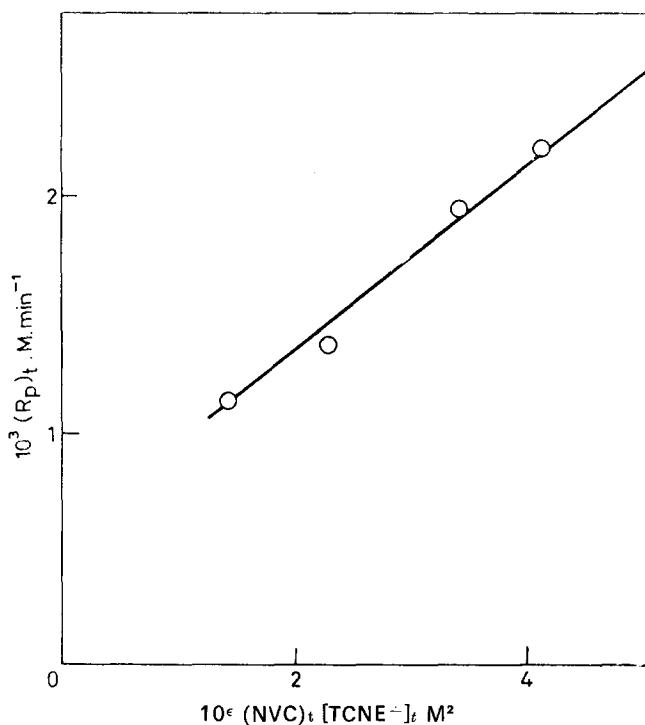


Figure 1 Polymerization of NVC in methylene chloride

arise either as major contributions to the total binding energy of intermolecular complexes with suitable donor molecules, or may be the result of purely incidental orbital overlap in such complexes. It is now common to describe charge transfer spectra as arising from 'charge transfer complexes' although this expression may be quite misleading. In recent years there has been a considerable interest in the nature and significance of charge transfer complexes¹⁸ with special reference to their role as reaction intermediates¹⁹.

Kosower¹⁹ has fully reviewed the types of reaction where charge transfer complexes may be involved, but it needs to be stressed that for many reported experimental examples, there is still no proof that the charge transfer spectra represent actual reaction intermediates. Reactions of TCNE with olefins commonly lead to corresponding 2 + 2 cycloadducts⁷ and are thought to involve polar intermediates, largely because of a pronounced rate acceleration in more polar solvents²⁰. These reactions are characterised by the formation of coloured solutions and, for the case of alkyl vinyl ethers (and presumably for other electron rich olefins) it has been shown convincingly^{8b} that the charge transfer spectra represent intermediates on the reaction pathway leading to cycloaddition.

The reactions of NVC with TCNE are somewhat more complex than those of other olefins which have been studied, largely because of competing, concurrent polymerization. In the present study it was shown that TCNE reacts with NVC to form the 2 + 2 cycloadduct V, the butadiene VI, and poly-

(*N*-vinylcarbazole). In most solvents all three products are formed simultaneously although at quite different rates, all reactions being accelerated by increasing solvent polarity. Arguing along the lines of the previous discussion, it seems reasonable to conclude that the charge transfer spectra observed in all cases, represent common primary reaction intermediates. Polymerization of *NVC* could be initiated either by *TCNE* or by the cycloadduct *V* and, in the absence of polymerizable monomer, the latter compound apparently undergoes a first order decay process to give *VI*.

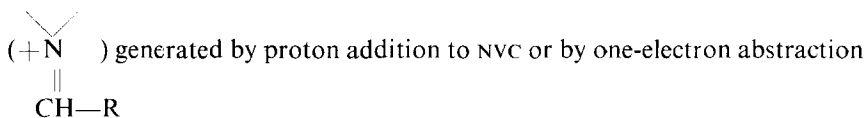
An important feature of all these reactions was the dynamic equilibrium established between *NVC*, *TCNE* and cycloadduct *V*.

Reversible 2+2 cycloaddition of TCNE and NVC

2 + 2 Cycloaddition of *TCNE* and *NVC* occurs readily in almost all solvents. In benzene the adduct *V* was difficultly soluble permitting ready isolation and characterization, although its formation and presumed structure had been reported previously^{7,14}.

When *V* was dissolved in other aromatic solvents the characteristic colours of solvent/*TCNE* complexes were observed. By studying competing equilibria between *NVC/TCNE* and *TCNE/hexamethyl benzene* it was possible to show that the values of the equilibrium constant (K_1) for adduct formation was 582 M^{-1} in methylene chloride at 25°C . The dynamic equilibrium between *TCNE*, *NVC*, and *V* has important consequences for interpretation of the mechanism of cycloadditions of *TCNE* and provides a simple explanation for the apparent activity of *V* in initiating polymerization of *NVC* (see below).

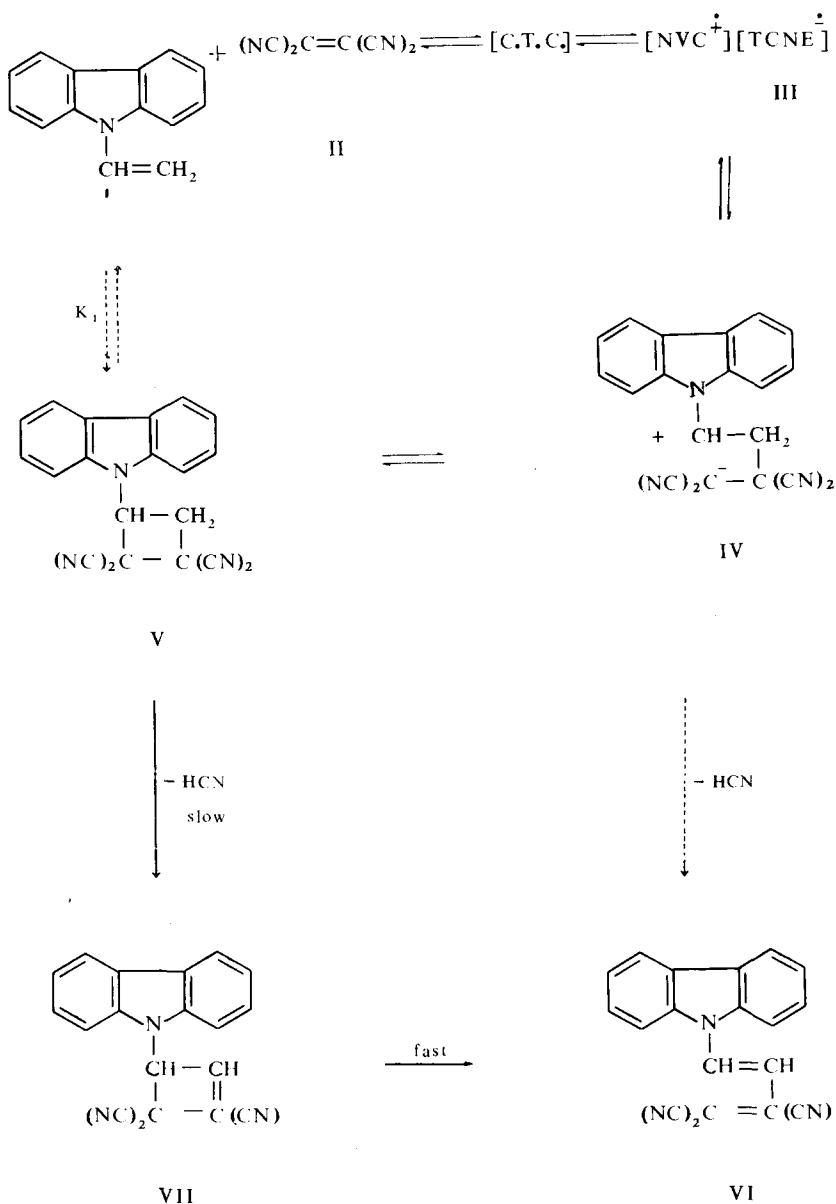
Of particular mechanistic significance is formation of the butadiene *VI* with elimination of hydrogen cyanide, notably the reactions in methanol producing *VI*, to the exclusion of polymer or methanolysis products. The latter are readily formed by rapid solvolysis of *N*-carbazolyl substituted carbonium ions



from *NVC*²¹, and it seems unlikely that elimination of *HCN* from, e.g. *IV* would be more rapid than methanolysis. On the other hand, rapid ring closure of *IV* might be expected to compete favourably with methanolysis. The conclusion must be that formation of butadiene *VI* does not involve *III* or *IV* but represents a completely separate mode of reaction for cyclobutane *V*. A plausible reaction sequence accounting for most of the experimental results is shown below.

Molecular models indicate that relief of strain in *V* may be obtained either by ring opening to re-form *IV* or by loss of $-\text{CN}$ *cis*- to the 1-(*N*-carbazolyl) substituent at positions 2 or 3. The constitution of *VI* demands that loss of $-\text{CN}$ should be from position 3 and hence intermediate formation of cyclobutene *VII* is a possible alternative to re-formation of *IV*. Symmetry allowed²² electrocyclic rearrangement of *VII* to the butadiene *VI* would be expected to be extremely rapid, and the overall conversion $\textit{V} \rightarrow \textit{VII} \rightarrow \textit{VI}$ would accord with the experimentally observed first order dependence of reaction rate on

[V], and with the comparatively low rate coefficient ($\sim 10^{-7} \text{ s}^{-1}$ at 25° in methylene dichloride).



Reaction Scheme 1

Mechanism of the polymerization of NVC initiated by TCNE

The salient features of this polymerization are as follows

(1) Polymerization may be initiated by TCNE or by cyclobutane V.

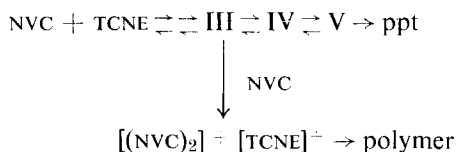
- (2) Rates of polymerization are first order in [NVC] but, for the concentration range employed, are apparently independent of [TCNE].
- (3) Dissolved air or oxygen has a pronounced retarding effect.
- (4) (TCNE⁺) was detected by e.s.r. spectroscopy at a concentration proportional to the instantaneous rate of polymerization.
- (5) Attempts to form copolymers of NVC with free radically susceptible monomers such as methyl methacrylate, by initiation with TCNE, yielded only homopolymers of NVC.
- (6) Formation of poly(*N*-vinylcarbazole), cycloadduct V, and butadiene VI were concurrent processes.
- (7) Molecular weights of polymers showed little variation with changing [TCNE] or [NVC] but were slightly increased by lowering the reaction temperature.

Undoubtedly the most notable of these is the apparent relationship between [TCNE⁺] and the rate of polymerization. In fact *Figure 1* shows that

$$R_p = \frac{-d[\text{NVC}]}{dt} = k [\text{NVC}] [\text{TCNE}^+]$$

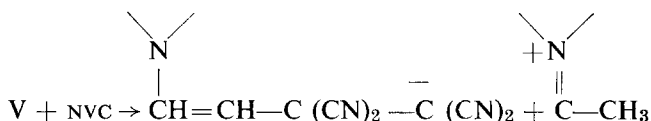
from which the formal rate coefficient for polymerization (k) is evaluated as $13 \text{ M}^{-1} \text{ s}^{-1}$ at 30°C . The present results, and those of other workers, confirm the cationic nature of TCNE initiated polymerization of NVC and it is interesting that the value of k from the present work compares very well with those of Pac and Plesch⁴ ($11 \text{ M}^{-1} \text{ s}^{-1}$ at 34°C) and Szwarc *et al*⁵ ($4.3 \text{ M}^{-1} \text{ s}^{-1}$ at 10°C), for initiation by tetranitromethane in nitrobenzene solvent. If the polymerization is cationic then it follows that the gegenion, in the present work, is TCNE⁻ and the concentration of active centres (cationic) is being estimated by e.s.r. measurement of gegenion concentration. However it is known that the rate coefficient for free cation propagation of NVC is $> 10^6 \text{ M}^{-1} \text{ s}^{-1}$ at 30°C and hence the value of k now reported must relate to some type of ion pair species²³.

The apparent independence of polymerization rate on [TCNE] remains enigmatic although it is significant that other workers report a similar result, over a particular concentration range, for the polymerization in benzene. Probably the explanation lies in the very low solubility of V e.g.,



From the value of K_1 it may be estimated that, at the higher concentrations of I and II employed for polymerization, the equilibrium concentration of V is in excess of its (very low) solubility, and hence the equilibrium concentrations of III, IV and V will be independent of [TCNE]₀. E.s.r. spectroscopy suggests that each (TCNE)⁺ is associated with one growing polymer chain, and it is reasonable to suggest therefore that initiation of polymerization involves interception of III by excess NVC, as indicated above. For the concentration of TCNE employed the rate of initiation, and hence polymerization, would be governed by [NVC]₀ and by (constant) [III]_e, as observed experimentally.

Nakamura, Soma, Onishi and Tamaru¹⁴ have also suggested that the apparent independence of R_p on $[\text{TCNE}]_0$ results from insolubility of V, but that initiation involves a bimolecular reaction between V and NVC viz:



Such a process would lead to the same kinetic consequences as reported in the present work but would not accord with the e.s.r. data. The Japanese workers used benzene as solvent (vs methylene chloride in the present work) and report that e.s.r. signals could not be detected during polymerization, but, in agreement with the present observations, oxygen had a retarding effect. The latter is easily understood if (TCNE^-) is the gegenion because of its known sensitivity towards dissolved oxygen. Furthermore the demonstration of a dynamic equilibrium between I, II and V provides a simple explanation for the catalytic activity of V, observed in the present study and by the Japanese workers.

ACKNOWLEDGEMENT

The authors are indebted to Dr. H. Block for many useful discussions.

REFERENCES

- 1 Ellinger, L. P. *Chem. and Ind.* 1963, 1982; *Polymer, Lond.* 1964, **5**, 559; 1965, **6**, 549
- 2 Scott, H., Miller, G. A. and Labes, M. M. *Tetrahedron Letters*, 1963, 1073; Scott, H., Konen, T. P. and Labes, M. M. *J. Polymer Sci., (B2)* 1964, 689
- 3 Ellinger, L. P. *Adv. in Makromol. Chem.* 1968, **1**, 169
- 4 Pac, J. and Plesch, P. H. *Polymer, Lond.* 1967, **8**, 237
- 5 Gumbs, R., Penczek, S., Jagur-Grodzinski, J. and Szwarc, M. *Macromolecules*, 1969 **2**, 77
- 6 Vasudevan, K. and Ramakrishnan, V. *Rev. Pure and Appl. Chem.* 1967, **17**, 95
- 7 Williams, J. K., Wiley, D. W. and McKusick, B. C. *J. Amer. Chem. Soc.* 1962, **84**, 2210
- 8 (a) This paper should be regarded as Part V of a series 'Charge Transfer Spectra and Reaction Intermediates'; (b) Part IV, Ledwith, A. and Woods, H. J. *J. Chem. Soc. (B)* 1970, 310; (c) Part III, Iles, D. H. and Ledwith, A. *Chem. Comm.*, 1969, 364; (d) Part II, Ledwith, A. and Woods, H. J. *J. Chem. Soc., (C)* 1970, 1422
- 9 Ledwith, A. *J. Appl. Chem.* 1967, **17**, 344
- 10 Bawn, C. E. H. *Pure and Appl. Chem.* 1968, **16**, 285
- 11 Ledwith, A. *Ann. N.Y. Acad. Sci.* 1969, **155**, 385
- 12 Sambhi, M. Ph.D. Thesis, University of Liverpool, 1966
- 13 Barrales-Rienda, J. M., Brown, G. R. and Pepper, D. C. *Polymer, Lond.* 1969, **10**, 327
- 14 Nakamura, T., Soma, M., Onishi T. and Tamura, K. *Die Makromol. Chem.* 1970, **135**, 341
- 15 Ueberreiter, K. and Springer, J. *Z. Phys. Chem.* 1963, **36**, 299
- 16 Merrifield R. E. and Phillips, W. D. *J. Amer. Chem. Soc.* 1958, **80**, 2778
- 17 Phillips W. D., Rowell, J. C. and Weissman, S. J. *J. Chem. Phys.* 1960, **33**, 626
- 18 Foster, R. 'Organic Charge Transfer Complexes', Academic Press, London, 1969
- 19 Kosower, E. M. *Prog. Phys. Org. Chem.* 1965, **3**, 81
- 20 Ledwith, A. *Ann. Rep. Chem. Soc., (B)* 1968, **65**, 143
- 21 Bell, F. A., Crellin, R. A., Fujii, H. and Ledwith, A. *Chem. Comm.* 1969, 251; Bawn, C. E. H., Ledwith, A. and Yang Shih Lin *Chem. and Ind.* 1965, 769
- 22 Woodward, R. B. and Hoffman, R. 'The Conservation of Orbital Symmetry', Academic Press, London, 1970
- 23 Ledwith, A. *A.C.S. Advances in Chemistry Series*, 1969, **91**, 317

The birefringence and mechanical properties of a 'single crystal' from a three-block copolymer

M. J. FOLKES and A. KELLER

The birefringence and mechanical properties of macroscopic single crystals of a three-block copolymer (styrene-butadiene-styrene) are described. The samples investigated were extruded plugs previously shown to consist of a hexagonal array of styrene cylinders embedded in the butadiene matrix with the cylinder axes along the extrusion direction. The birefringence is shown in this paper to be entirely due to form-birefringence and the dispersed styrene phase to consist of randomly oriented chains. The Young's modulus is highly anisotropic. It is found that this anisotropy as well as the absolute values of the moduli can be fully accounted for by the simplest model based on the previously established morphology of the samples.

(1) INTRODUCTION

RECENTLY, a considerable amount of attention has been given to the relationship between the morphology and macroscopic properties of the new class of materials known as thermoplastic elastomers¹. These materials are usually three-block copolymers consisting of chains of the form styrene-butadiene-styrene (SBS) or styrene-isoprene-styrene (SIS). The polystyrene exists as a dispersed phase, which is glass-like at ambient temperatures and can be regarded as acting as crosslinks for the rubberlike polybutadiene matrix.

The dispersed styrene phase can be in the form of spheres, cylinders or lamellae. Past electron microscopic and low angle x-ray studies performed on solvent cast films have shown that these entities can form ordered structures locally. Quite recently it was found in these laboratories that in certain extruded samples the dispersed particles can give rise to a practically perfect lattice extending over large regions of the sample. In particular low angle x-ray studies^{2,3} followed by electron microscopy⁴ revealed that macroscopic portions of such extruded plugs were in fact 'single crystals' composed of a hexagonal array of styrene cylinders embedded in the butadiene matrix, with the cylinder axes along the extrusion direction.

Material exhibiting such a single crystal nature provides a unique opportunity for studying macroscopic properties and correlating them with the morphology. The polymer can be expected to be very highly anisotropic with particular reference to optical and mechanical properties. The material is of special interest with regard to mechanical properties since it can be regarded as a very highly perfect composite in which the embedded rods are molecularly bonded to the rubber matrix. This overcomes many of the problems associated with conventional fibre-resin composites.

In this paper measurements of the birefringence and mechanical properties of an SBS 'single-crystal' copolymer will be described and the results interpreted in terms of the physical properties and morphology of the styrene and butadiene phases.

(2) SAMPLE PREPARATION AND CHARACTERIZATION

The material used in these investigations was a commercial sbs polymer containing 25% weight fraction of polystyrene and manufactured by Shell Chemical Company under the trade name Kraton 102. The molecular weight of the styrene block is 10^4 and the butadiene block 5.5×10^4 (ref. 5). The 'single-crystal' samples were prepared and characterized in a manner similar to that previously reported³. The 'as-received' commercial material was extruded at 100°C to form a rod, of typical diameter 9 mm, and was then annealed for 2 h at 150°C .

Samples cut from the rod were first examined by low angle x-ray diffraction by means of a Franks camera. It was found that in general the outer annulus had a different structure from that of the core and was the sample portion of greatest interest to us. With the beam parallel to the extrusion direction this annular region showed an unusually sharp single crystal diffraction pattern of hexagonal symmetry – see *Figure 1*. The same sample portion with

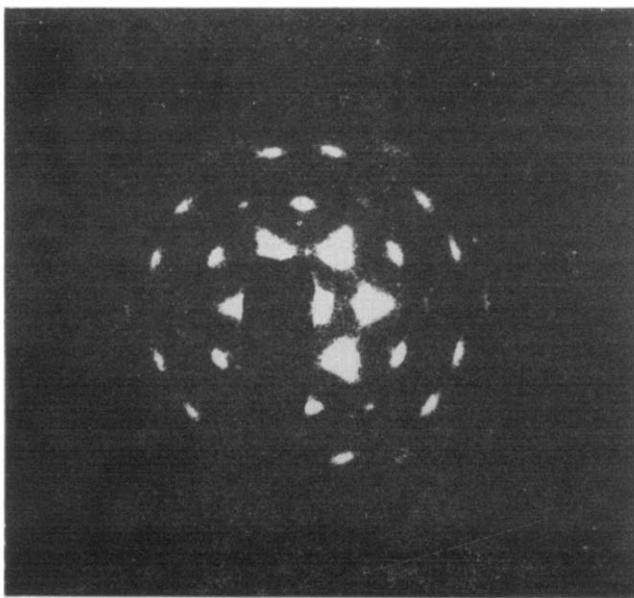


Figure 1 Low angle x-ray diffraction pattern from an annealed sample of extruded sbs copolymer (Kraton 102) with the beam parallel to the extrusion direction. (One of the six strongest reflections obscured by beamstop)

the beam perpendicular to the extrusion direction gave reflections only along the zero layer line. All this confirms the single crystal nature of the samples in accord with the previous findings where these diffraction effects were attributed to polystyrene cylinders of 150 \AA (15 nm) diameter forming a hexagonal lattice with a lattice parameter of 300 \AA .

All the measurements reported in this paper were performed only on samples possessing a single crystal nature as cut from the outer edge of the

plug. This ensured optimum correlation between the observed macroscopic properties and morphology.

Samples for birefringence and mechanical measurements must be uniform rectangular blocks with the styrene in a known accurate orientation with respect to the long edge of the sample. This presents certain problems in cutting since the original material is in the form of a rod and only material from the outer annulus of the rod is required. Two methods in principle are available, the first is to reduce the temperature of the Kraton and cut with a diamond saw and the second to use a thin, very sharp blade at room temperature and hold the sample in a small jig into which the blade can be inserted. The latter method was eventually chosen and found to work quite satisfactorily considering the softness of the polymer.

Typical sample dimensions were 5 mm \times 2 mm \times 1 mm and each dimension was accurate to about $\pm 5\%$. The clamping of the samples by the jaws of the tensometer presented difficulties owing to slippage taking place during the measurements. These problems were overcome very successfully by first gluing the ends of the Kraton to Tufnol blocks and then holding the Tufnol blocks in the tensometer jaws.

(3) THE BIREFRINGENCE

(3. 1) *Measurements*

All of the optical studies were carried out using a Carl Zeiss Ultraphot I polarizing microscope. Quantitative measurements of the birefringence were made with an Ehringhaus quartz compensator.

(3. 2) *Results*

When rotating a small sample between crossed polars a very sharp extinction was observed when the extrusion direction was either parallel or perpendicular to the plane of polarization of the incident light. Using a quartz wedge it was found that the sample exhibited a positive birefringence with respect to the extrusion direction.

With the incident light along the extrusion direction the material appeared non-birefringent showing that we have transverse isotropy about the extrusion direction.

Using a uniform cross-section sample a value for the birefringence was obtained and found to be $(4.92 \pm 1.0) \times 10^{-4}$.

The effect of stress applied along and perpendicular to the extrusion direction was also investigated. Here, in addition to the above annealed sample, unannealed samples were also used. The unannealed samples did not show such a sharply defined extinction throughout but nevertheless they displayed positive birefringence of magnitude close to that of the annealed samples. However, the unannealed samples could be stretched much further along the extrusion direction and hence extended the range of measurement.

Figure 2 shows the birefringence as a function of strain. With the stress applied perpendicular to the extrusion direction the birefringence decreased

monotonically until at about 10% strain the sample ceased to be birefringent. Further increase in the strain resulted in negative birefringence (as referred to the extrusion direction). As seen there was no difference between annealed and unannealed samples.

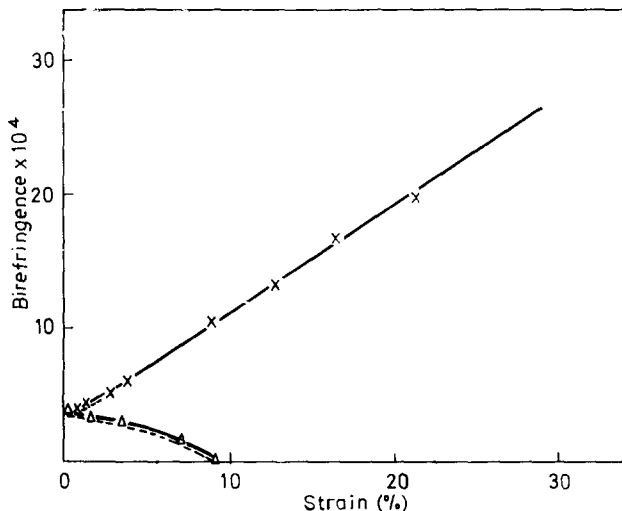


Figure 2 Birefringence versus strain for some extruded samples of an sbs copolymer: unbroken line, unannealed samples; broken line, annealed samples (macroscopic single crystal); \times , stress applied parallel to extrusion direction; \triangle , stress applied perpendicular to extrusion direction

With the stress applied along the extrusion direction the birefringence increased with strain. The maximum strain induced in the annealed samples was 1–2% but the unannealed material allowed measurements to be made to beyond 20% (the reason for this difference will be apparent from the mechanical behaviour later). We see that the birefringence increases linearly.

(3. 3) Discussion

With a hexagonal single crystal we may expect optical anisotropy. The resulting birefringence could be of two kinds. Firstly, if the molecules are oriented in any one or both of the phases we would have the usual molecular birefringence. It is to be recalled that in polybutadiene the greatest polarizability is along while in polystyrene it is perpendicular to the chain direction. Accordingly the birefringence as referred to the extended molecule will be positive for polybutadiene and negative for polystyrene. If there is molecular orientation within the Kraton sample it will be the resultant of the two.

Secondly a parallel array of cylinders embedded in a matrix of differing refractive index should give rise to positive form-birefringence. Our samples should in fact be model substances for this often quoted, but elusive effect. This form-birefringence should contribute to the total birefringence. Con-

versely, if its contribution can be determined the contribution of the molecular birefringence, hence the molecular orientation within the individual phases, should become accessible. This we shall proceed to do.

As the form-birefringence is determined only by the volume fraction of the dispersed phase and by the refractive indices of the two phases, its value for our samples can be calculated from the data available.

For an assembly of parallel cylinders (not necessarily arranged regularly) composed of isotropic material with refractive index n_1 embedded in an isotropic matrix of refractive index n_2 the form birefringence is given by $n_a - n_0$ where $n_a^2 = v_1 n_1^2 + v_2 n_2^2$

and

$$n_0^2 = n_2^2 \left[\frac{(v_1 + 1)n_1^2 + v_2 n_2^2}{(v_1 + 1)n_2^2 + v_2 n_1^2} \right]$$

and v_1 and v_2 are the volume fractions of phases 1 and 2 respectively⁶. This model gives a positive birefringence with respect to the cylinder axes.

$$\text{For Kraton 102:} \quad \begin{array}{ll} v_1 = 0.2 & v_2 = 0.8 \\ n_1 = 1.59 & n_2 = 1.52 \end{array}$$

where we have taken bulk values for the refractive indices. Computing n_a and n_0 separately showed them to be very close. The birefringence can be evaluated to a greater degree of accuracy by writing:

$$n_a^2 - n_0^2 = (n_a - n_0)(n_a + n_0) \approx 2n_a(n_a - n_0) = \frac{v_1 v_2 (n_1^2 - n_2^2)^2}{(v_1 + 1)n_2^2 + v_2 n_1^2}$$

$$\text{or} \quad n_a - n_0 = \frac{v_1 v_2 (n_1^2 - n_2^2)^2}{2n_a [(v_1 + 1)n_2^2 + v_2 n_1^2]} = 5.15 \times 10^{-4}$$

This theoretical value is almost identical with the measured value of $(4.92 \pm 1.0) \times 10^{-4}$ and considering we are not certain of the values of n_1 and n_2 pertaining within the material, the agreement is excellent.

We see then, that the expected form birefringence fully accounts for the birefringence actually measured. It follows that there is no contribution from the molecules as such and consequently there is no appreciable molecular orientation within any of the phases which indicates that they are made up of random chains. Another possibility, which is unlikely but cannot be excluded a priori, is the small chance that any molecular birefringence within the separate phases would exactly cancel in the aggregate (which incidently would require identical direction of chain orientation within both phases in view of the opposite signs of birefringence of the respective molecules).

Stress is expected to orient the polybutadiene chains (see also later). This should produce a molecular birefringence with maximum polarizability along the stress direction. With the stress along the extrusion direction it will reinforce the form-birefringence and with the stress perpendicular to the extrusion direction it will reduce and eventually cancel the form-birefringence, which is the effect observed.

(4) MECHANICAL PROPERTIES

(4. 1) *Measurements*

The Young's modulus was measured using a simple dead-loading tensometer. Loads were applied by means of a scale pan and weights. Extensions and sample dimensions were measured to an accuracy of 10^{-4} cm by means of a travelling microscope. Within the range of loads applied no significant creep was observed during the time scale required for performing a measurement. However, for complete reversibility after each successive measurement of extension a few minutes were allowed for the sample to relax in the unstressed state. All measurements were performed at room temperature (23°C).

At the start of the series of measurements a check was made of the uniformity of strain across the width of the sample. This was carried out by first printing a grid pattern on the surface of the sample by evaporating aluminium either through an electron microscope grid or through a specially prepared mask. It was found that strains measured using the grid network did not differ significantly from those obtained by directly recording the extension of the complete sample length.

Modulus measurements were carried out on samples cut with their long axes at 0° , 33° , 45° , 55° and 90° with respect to the extrusion direction. The samples were examined on a polarizing microscope to confirm that the angles were accurate. The dimensions of the samples were determined using a travelling microscope.

(4. 2) *Results*

Figure 3 shows stress-strain plots for the three orientations $\theta = 0^{\circ}$, 55° and 90° of the long axes of the sample with respect to the extrusion direction. (The corresponding results for 33° and 45° are not included in this figure to avoid excessive crowding of points but the values of Young's modulus at these angles are given in a later plot). Over the range of strains considered the plots are linear and the anisotropy of the mechanical properties is very striking. The Kraton exhibited glass-like behaviour for $\theta = 0^{\circ}$ and was rubber-like at $\theta = 55^{\circ}$ and 90° .

The results illustrated were very reproducible and represent the maximum anisotropy obtainable from the particular morphology. Further annealing of the samples had no effect on the anisotropy. Unannealed samples are not shown in Figure 3 for two reasons. First, the results varied considerably from sample to sample and second, the anisotropy was greatly reduced due to a large reduction in the modulus for $\theta = 0^{\circ}$, compared with annealed samples.

(4. 3) *Discussion*

An evaluation of the elastic constants of the annealed Kraton can, at least in principle, be carried out in a similar manner to Eshelby's⁷ calculation of the effect of inclusions in an elastic matrix. Essentially the problem is one of calculating the elastic stored energy due to the presence of inclusions and interpreting the result in terms of an effective Young's modulus. This calculation will be the subject of a future publication.

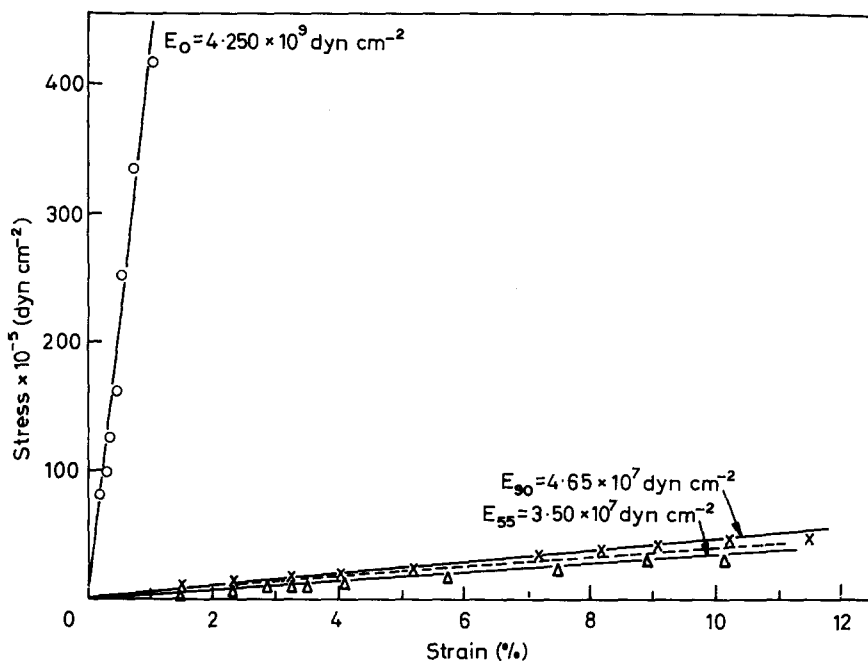


Figure 3 Stress-strain curves for some samples of a macroscopic single crystal of an SBS copolymer. ($1 \text{ dyn cm}^{-2} \equiv 0.1 \text{ N m}^{-2}$): \circ , stress parallel to extrusion direction; \triangle , stress at 55° to extrusion direction; \times , stress perpendicular to extrusion direction; the broken line represents the theoretical plot of $f = G [(i + \epsilon) - 1/(i + \epsilon)^3]$ fitted to E_{90} at infinitesimal strains

We shall nevertheless attempt to account for the modulus E_θ as measured along the different directions specified by θ . In the first place we consider E_0 and E_{90} for which, from Figure 3, we have the experimental values of $4.250 \times 10^9 \text{ dyn cm}^{-2}$ and $4.650 \times 10^7 \text{ dyn cm}^{-2}$ * respectively. We will interpret these two results in terms of a simple model for a two phase polymer

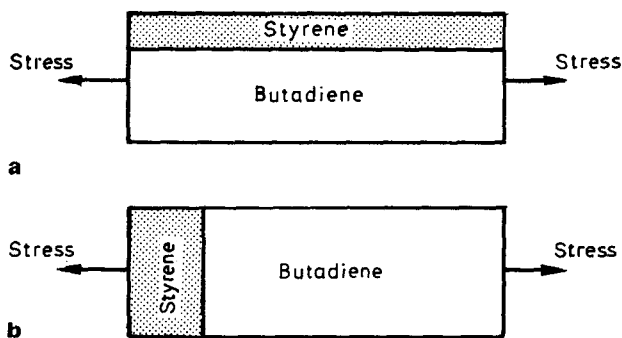


Figure 4 Models used in the evaluation of E_0 and E_{90} using the Takayanagi method (a) Parallel coupling (b) Series coupling

* $1 \text{ dyn cm}^{-2} \equiv 0.1 \text{ N m}^{-2}$

due to Takayanagi⁸. On the basis of this model E_0 is evaluated by considering a hypothetical solid depicted in *Figure 4a* in which the styrene and butadiene exist as distinct regions labelled S and B, the size of these blocks being proportional to their respective volume fractions. A stress applied in the direction shown produces an equal strain in each component phase while the stress is divided unequally between the phases – this is referred to as *parallel coupling*. It is easy to show that the combined modulus is given by:

$$E_0 = v_s E_s + (1 - v_s) E_b \quad \text{where } v_s = \text{volume fraction of styrene}$$

$$E_s = \text{Young's modulus of styrene}$$

$$E_b = \text{Young's modulus of butadiene}$$

If we take bulk values for the respective moduli

$$E_s = 2 \times 10^{10} \text{ dyn cm}^{-2} \quad \text{and} \quad v_s = 0.2$$

$$E_b = 1 \times 10^7 \text{ dyn cm}^{-2}$$

we calculate $E_0 = 4.0 \times 10^9 \text{ dyn cm}^{-2}$ which in fact is very close to the measured value of $4.250 \times 10^9 \text{ dyn cm}^{-2}$. In actual fact the value used for E_b is relatively unimportant in this calculation since the styrene will support practically all the applied stress due to its very much larger modulus compared with butadiene. Our result therefore represents a verification of the assumption that the bulk modulus of polystyrene also pertains to the dispersed state in our specimens.

This simple law of mixtures is actually a theoretical lower bound for E_0 since the actual energy of deformation will be greater than the sum of that due to the styrene and butadiene separately imagined free of any mutual constraint. It has been shown by many workers (e.g. Heaton⁹) that the predicted Young's modulus based on an exact treatment nevertheless agrees to within 1% with the value calculated by weighting the fibre and matrix Young's moduli according to their respective volume fractions.

The agreement between theory and experiment again indicates that the morphology of the annealed samples is in complete agreement with the model proposed by Keller *et al*² and that the styrene rods can be regarded as infinitely long at least from a mechanical viewpoint.

The value of E_{90} corresponds to Young's modulus measured under pure shear conditions. This arises because when a stress is applied perpendicular to the extrusion direction the transverse contraction of the sample that occurs can only take place along one dimension, the other contraction being prevented due to the presence of the constraining styrene cylinders.

We can use the Takayanagi model to evaluate the combined modulus (E'_{90}) for the usual situation in which both transverse dimensions are unconstrained while a uniaxial stress is applied. It is then necessary to relate this to the practical situation of pure shear to obtain E_{90} .

The model depicted in *Figure 4b* corresponds to the situation in which we have 20% by volume of styrene in *series coupling* with 80% butadiene. In this case the applied stress is supported by both component phases S and B but the total strain is the sum of the strains in each separate phase. Hence the compliances are additive to give for the combined modulus:

$$E'_{90} = 1 / \left(\frac{v_s}{E_s} + \frac{1 - v_s}{E_b} \right)$$

It can be seen that the butadiene will have practically the full amount of the total strain since $E_b \ll E_s$ and in fact we can write

$$E'_{90} = \frac{E_b}{1 - v_s} \quad (1)$$

This is the value of the combined modulus that would be measured if both transverse dimensions were unconstrained.

We can now relate the modulus measured under practical conditions to the value computed above. For this purpose we will use some results from the kinetic theory of rubber elasticity¹⁰ but it should be emphasized that the relationship to be derived is a completely general one and could also be developed from simple ideas of small strain elasticity applicable to any solid.

For a rubber in simple uniaxial tension, the relationship between the force per unit area of the undeformed cross-section and extension is given by:

$$f = G \left[(1 + \epsilon) - \frac{1}{(1 + \epsilon)^2} \right]$$

where ϵ is the strain and G is the shear modulus.

Thus for vanishingly small strains we have:

$$\text{Young's modulus} = \left(\frac{df}{d\epsilon} \right)_{\epsilon \rightarrow 0} = G \left[1 + \frac{2}{(1 + \epsilon)^3} \right]_{\epsilon \rightarrow 0} = 3G$$

which is the well known result for any incompressible solid.

For a rubber under pure shear conditions, that is, stretched uniaxially but with one transverse dimension constrained we have:

$$f = G \left[(1 + \epsilon) - \frac{1}{(1 + \epsilon)^3} \right]$$

$$\text{Modulus} = \left(\frac{df}{d\epsilon} \right)_{\epsilon \rightarrow 0} = G \left[1 + \frac{3}{(1 + \epsilon)^4} \right]_{\epsilon \rightarrow 0} = 4G$$

Thus the observed modulus measured under pure shear conditions (E_{90}) will be a factor 4/3 times larger than E'_{90} calculated on the basis of the simple series model with each phase in simple uniaxial tension. Hence we may write:

$$E_{90} = \frac{4}{3} E'_{90} = \frac{4}{3} \times \frac{E_b}{1 - v_s} \quad (2)$$

The value of E_{90} was found to be 4.65×10^7 dyn cm⁻² and for $v_s = 0.2$ we find a value for $E_b = 2.79 \times 10^7$ dyn cm⁻². Values quoted for the bulk polymer are in the range 10^7 – 10^8 dyn cm⁻², dependant on crosslinking. Since we have no knowledge of the number of network junctions, which in our case will be entanglement, the above result is very reasonable.

It is of interest to plot the function $G \left[(1 + \epsilon) - \frac{1}{(1 + \epsilon)^3} \right]$ over the experimental range of strains. This is also shown in *Figure 3* and it is seen that over the range of strains considered there is no significant disagreement with the predictions of rubber elasticity theory.

It has been pointed out to us by Professor F. C. Frank that we are probably overestimating the value of E_b using the Takayanagi model because a dispersion of cylindrical glassy rods embedded in a rubber matrix will produce a greater strain energy than considered as two discrete blocks. It can be shown that in general:

$$E_{90} = \frac{4}{3} (1 + av_s) E_b$$

where $a > 1$ can be evaluated using a method similar to Eshelby's⁷. Our simple treatment here gives a value of $a = 1.25$.

The observed value of 3.50×10^7 dyn cm⁻² for E_{55} as derived from *Figure 3* is lower than E_{90} and in fact represents the minimum value measured. This is entirely in accord with the model; in fact the measurement of E_{55} was undertaken to test this expectation.

It can be shown from the general considerations presented in Appendix I that the dimension of the sample inclined at $54^\circ 44'$ to the tensile axis does not change for small extensions provided the transverse contraction is isotropic. As it can be demonstrated that for the S cylinders at $54^\circ 44'$ to the tensile axis the transverse contraction is isotropic (see end of Appendix II) it follows that S cylinders at this angle will not constrain the lateral contraction of the B matrix for strains small enough for the following two conditions to hold: (1) the approximation in the derivation of Appendix I remains valid; (2) the rotations involved are sufficiently slight not to remove the cylinder axes so far from the $54^\circ 44'$ direction that the constraints imposed by the cylinders at the altered angles should become noticeable within the accuracy of our measurements. Under these conditions for stress at $54^\circ 44'$ to the cylinder axes the modulus will be as for simple uniaxial tension under the condition of series coupling. Thus when $E_b \ll E_s$ by equations (1) and (2)

$$E_{55} = E_b / (1 - v_s) = \frac{3}{4} E_{90} \quad (3)$$

This should clearly be a minimum for the system as at any other angle the modulus will be raised by the constraints imposed by the S cylinders. This minimum is reflected by our experiment. Further, the relation between E_{55} and E_{90} can be specifically tested. For $E_{90} = 4.65 \times 10^7$ a value for $E_{55} = 3.48 \times 10^7$ is expected by equation (3) in practically complete agreement with the experimental value of 3.50×10^7 dyn cm⁻².

Measurements were also performed on samples at $\theta = 33^\circ$ and 45° and this justified a more complete examination of the angular dependence of the Young's modulus. The experimental values of Young's modulus at these angles together with those already discussed are shown in *Figure 5*. A theoretical relationship is derived in Appendix II for the angular dependence of the Young's modulus and can be expressed as:

$$\frac{1}{E_\theta} = \frac{1}{E_{90}} (\sin^4 \theta + 4 \sin^2 \theta \cos^2 \theta)$$

A plot of E_θ versus θ is also shown in *Figure 5* and it can be seen that for the limited number of measurements made, agreement between theory and experiment is excellent. Verification of the theory particularly for values of $\theta < 30^\circ$ will form the subject of a future publication. The theory correctly predicts the minimum Young's modulus at $\theta = 54^\circ 44'$ but because we have

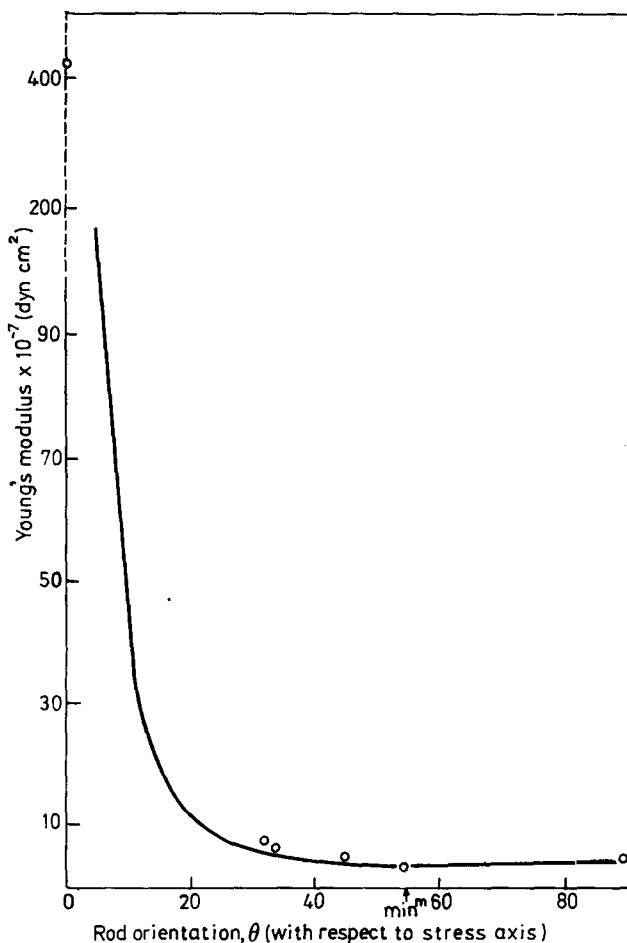


Figure 5 Variation of Young's modulus with orientation angle θ ($1 \text{ dyn cm}^{-2} \equiv 0.1 \text{ N m}^{-2}$). The curve is the theoretical plot and the points (O) are experimental results for extruded samples of Kraton

102

assumed rigid styrene planes it predicts an infinite Young's modulus for $\theta = 0^\circ$. The rapid decrease in Young's modulus over the range $0 \leq \theta \leq 20^\circ$ is also shown in previous work on fibre-resin composites but for these materials the minimum value of Young's modulus occurs closer to $\theta = 45^\circ$ rather than $\theta = 54^\circ 44'$.*

* We are currently involved, with R. G. C. Arridge, in testing established theories of fibre reinforcement on the presently used samples. It is apparent even at the present initial stage that by using such theories, a virtually perfect agreement with experiment is obtained for the variation of Young's modulus with rod orientation, i.e. even the very slight discrepancies in Figure 5 are removed. A full account of this extension of the work will be published separately. The present remark is merely included here to indicate that, even if the simple treatment in itself is sufficient to bring us very close to complete agreement, further improvements can still be obtained. At the same time it should dispel possible doubts that the close agreement between such a simple treatment and observation may be accidental.

The large difference in behaviour of annealed and unannealed Kraton when a stress is applied along the extrusion direction is related to the presence of defects which have been observed using electron microscopy⁴. Simple breaks in the styrene cylinders will not have a marked effect on the mechanical properties, but defect planes perpendicular to the cylinder axes have been observed in which a complete group of cylinders end and another group begin. These large scale faults will have a significant effect on the mechanical properties. The defect density has been found to decrease on annealing which will manifest itself as an increase in E_0 .

(5) CONCLUDING REMARKS

The birefringence and mechanical properties measured are entirely consistent with the previously reported morphology of these extruded Kraton samples. In particular, the birefringence was shown to be due only to the form contribution, thus both the dispersed styrene phase and the butadiene matrix consist of random chains. The mechanical anisotropy is very marked and can be quantitatively predicted in terms of a model composite based on the previously established morphology. All this relates to the special single crystal type sample examined here. It will be obvious that in the case of a more general sample the knowledge of the anisotropic properties of the basic constituent (in the present case the hexagonal lattice of cylinders) will be a prerequisite for any further evaluation. Such an evaluation will then have to account for the aggregate effect of these constituents in the texture pattern pertaining to the samples which are under examination.

ACKNOWLEDGEMENTS

The authors would like to thank Dr F. Scalisi for providing the extruded samples of copolymer and Professor F. C. Frank for very valuable discussions. This work originated from part of the research activity of Dr E. Pedemonte (Istituto di Chimica Industriale, Università, Genova, Italy) to whom we are greatly indebted.

*H. H. Wills Physics Laboratory,
University of Bristol,
Royal Fort,
Tyndall Avenue,
Bristol BS8 1TL, UK*

(Received 9 October 1970)

REFERENCES

- 1 Symposium on Block Copolymers *J. Polym. Sci. (C)* 1969, vol. 26
- 2 Keller, A., Pedemonte, E. and Willmouth, F. M. *Nature* 1970, **225**, 538
- 3 Keller, A., Pedemonte, E. and Willmouth, F. M. *Kolloid Z.* 1970, **238**, 385
- 4 Dlugosz, J., Keller, A. and Pedemonte, E. *Kolloid Z.* in press
- 5 Bianchi, V., Pedemonte, E. and Turturro, A. *Polymer, Lond.* 1970, **11**, 268

- 6 Ambronn, H. and Frey, A. *Das Polarisationsmikroskop (Leipzig)* 1926, p 114
- 7 Eshelby, J. D. *Proc. Roy. Soc. (Lond.)* 1957, **A241**, 376
- 8 Takayanagi, M. *Mem. Fac. Eng. Kyushu Univ.* 1963, **23**, 50
- 9 Heaton, M. D. *Brit. J. Appl. Phys.* 1968, **1**, 1039
- 10 Treloar, L. R. G., 'Physics of Rubber Elasticity', Oxford University Press, 1958, p 85

APPENDIX I

Evaluation of θ corresponding to the minimum value of Young's modulus

We will consider the deformation of a specimen of rubber subjected to a simple uniaxial stress. It is well known that the subsequent strain in any direction within the sample can be evaluated by considering the deformation of a unit sphere composed of this rubber (see *Figure 6*). The application of a

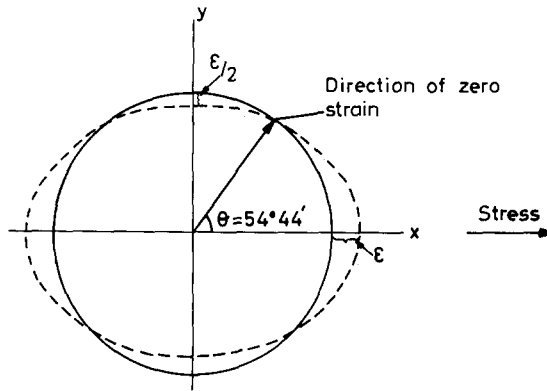


Figure 6 The deformation of a unit sphere in simple uniaxial extension

stress along the x direction will produce a corresponding strain ϵ together with a transverse contraction of $\frac{1}{2}\epsilon$ along y and z providing the strain is small and the rubber incompressible. The sphere deforms to an ellipsoid of revolution about the x axis. It will be shown that a direction exists along which the strain is zero.

The parametric equations for the strain ellipse (because of rotational symmetry about x we need only consider the cross-section of the ellipsoid through $z = 0$) are given by:

$$x = (1 + \epsilon) \cos\theta; \quad y = (1 - \frac{1}{2}\epsilon) \sin\theta$$

where θ is the angle between any direction and the x axis. The direction of zero strain is given by the value of θ corresponding to the intersection of the strain ellipse and unit circle:

$$(1 + \epsilon)^2 \cos^2\theta + (1 - \frac{1}{2}\epsilon)^2 \sin^2\theta = 1$$

Ignoring second order terms in ϵ we have:

$$(1 + 2\epsilon) \cos^2\theta + (1 - \epsilon) \sin^2\theta = 1$$

$$\therefore \tan\theta = \sqrt{2}, \quad \theta = 54^\circ 44'$$

APPENDIX II

Angular dependence of Young's modulus

The dependence of Young's modulus on the angle θ can be computed with the aid of a model shown schematically in *Figure 7*. The Kraton sample can be regarded as composed of alternate layers of rubber and 'planes' of styrene and rubber. It is assumed that these planes are infinitely rigid and if a uniaxial stress σ is applied to such a sample containing planes oriented at an angle θ

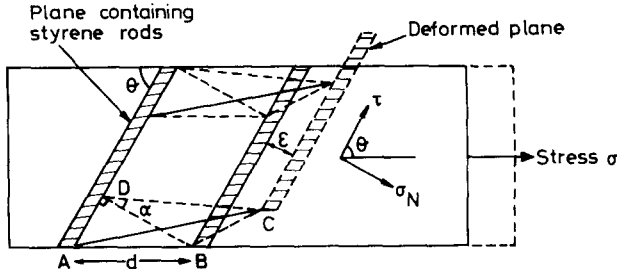


Figure 7 The deformation of a single 'plane' of styrene rods under simple uniaxial extension

to the stress direction, the rubber contained between 'planes of rods' will suffer two simultaneous deformations – a simple extension perpendicular to the planes and simple shear parallel to the planes. This will cause a point B to move to C and we must calculate the resultant extension BC and hence the strain due to these two mechanisms.

The applied stress σ can be resolved into two components:

- (1) A stress normal to the rods $\sigma_N = \sigma \sin^2\theta$
- (2) A shear stress parallel to the rods $\tau = \sigma \sin\theta \cos\theta$

Let us suppose σ_N produces a strain ϵ normal to the rods, while τ produces a shear strain α . We require $BC \approx AC - AB$ for small strains. Let $AB = d$.

Now $AD = d \cos\theta$ $DC \approx DB(1 + \epsilon) = d \sin\theta(1 + \epsilon)$,
 $\angle CDA = 90 + \alpha$

$$\begin{aligned} \therefore AC^2 &= d^2[\cos^2\theta + \sin^2\theta(1 + \epsilon)^2 + 2 \sin\theta \cos\theta(1 + \epsilon) \sin\alpha] \\ &\approx d^2[\cos^2\theta + \sin^2\theta + 2\epsilon \sin^2\theta + 2\alpha(1 + \epsilon) \sin\theta \cos\theta] \\ &\approx d^2[1 + 2\epsilon \sin^2\theta + 2\alpha \sin\theta \cos\theta] \end{aligned}$$

$$\therefore AC \approx d[1 + \epsilon \sin^2\theta + \alpha \sin\theta \cos\theta]$$

$$\therefore \text{Resultant strain} = (AC - AB)/AB = \epsilon \sin^2\theta + \alpha \sin\theta \cos\theta$$

But $\epsilon = \frac{\sigma_N}{E_{90}}$ and $\alpha = \frac{\tau}{G}$; $E_{90} = 4G$

$$\therefore \epsilon = \frac{\sigma_N}{4G} ; \quad \alpha = \frac{\tau}{G}$$

$$\therefore \text{Resultant strain} = \frac{\sigma_N}{4G} \sin^2\theta + \frac{\tau}{G} \sin\theta \cos\theta$$

$$= \frac{\sigma}{4G} \sin^4\theta + \frac{\sigma}{G} \sin^2\theta \cos^2\theta$$

$$\therefore \frac{1}{E_\theta} = \frac{1}{E_{90}} [\sin^4\theta + 4 \sin^2\theta \cos^2\theta]$$

The variation of E_θ with orientation angle θ is shown plotted in *Figure 5*.

The following special cases are of interest:

$$E_{35} \left(\text{corresponding to } \tan\theta = \frac{1}{\sqrt{2}} \right) = E_{90} = 4.65 \times 10^7 \text{ dyn cm}^{-2}$$

$$E_{45} \text{ (corresponding to } \tan\theta = 1) = \frac{4}{3}E_{90} = 3.72 \times 10^7 \text{ dyn cm}^{-2}$$

$$E_{55} \text{ (corresponding to } \tan\theta = \sqrt{2}) = \frac{3}{4}E_{90} = 3.48 \times 10^7 \text{ dyn cm}^{-2}$$

$$E_{90} = 4.65 \times 10^7 \text{ dyn cm}^{-2}$$

The equality of E_{35} and E_{90} justifies our application of simple ideas of rubber elasticity to establish the value of θ corresponding to minimum Young's modulus. The value of $\theta = 54^\circ 44'$ calculated in Appendix I depends on equal deformations occurring along y and z when a stress is applied along x (see *Figure 6*). These deformations for the special case of $\theta = 54^\circ 44'$ will be primarily dependent on the Young's moduli E_{35} and E_{90} along y and z respectively. In view of the equality of these two moduli our assumption of transverse isotropy about the stress direction for this sample is valid. Also note the relation between E_{55} and E_{90} which is identical to equation (3) in the text, derived on the basis of rubber elasticity theory.

Electron microscopy of crazes in polystyrene and rubber modified polystyrene: use of iodine-sulphur eutectic as a craze reinforcing impregnant

R. P. KAMBOUR AND R. R. RUSSELL

Iodine-sulphur eutectic has been impregnated into crazes in polystyrene and rubber-modified polystyrene to act as a reinforcing agent during microtomy. Craze filaments and holes are much larger than in sulphur-reinforced poly(dimethyl phenylene oxide) crazes due to a physical aging process involving polymer flow. In polycarbonate crazes impregnated with sulphur similar effects are observed due to plasticization by the sulphur. Reinforcing impregnation and rubber-staining are complementary tools in studying crazing in rubber-modified polystyrene.

DURING the ultramicrotoming of sections of glassy polymers thin enough to be used for transmission electron microscopy, pre-existing crazes tend to collapse, distort, and rip apart under the high stress occurring at the knife tip. A previous study¹ demonstrated the utility of a suitable impregnant in reinforcing and protecting craze structure during microtomy. In that study solvent-crazed bars of poly(2,6-dimethyl-1,4-phenylene oxide) were immersed in liquid sulphur at 125°C, long enough for the sulphur to replace the organic liquid in the craze. After quenching to solidify the sulphur, polymer sections were microtomed, coated with carbon for dimensional stability, and examined by transmission electron microscopy. Sulphur-free crazes were observed, the sulphur having sublimed away in the vacuum of the carbon deposition chamber. A craze structure resembling an irregular, open-celled foam was observed. The filaments and holes of the structure tended to be roughly 200 Å in diameter.

Because of the importance of craze formation and breakdown to the strength and toughness of glassy polymer systems² it is desirable to be able to investigate craze structure in other materials beside poly(dimethyl phenylene oxide). However, the usefulness of pure sulphur as a reinforcing agent is limited to nonpolar resins of high glass temperature. Sulphur³ has a solubility parameter δ of 12.5 and we find that it tends to plasticize polar resins like polycarbonate or polysulphone, lowering their T_g 's and the mechanical stability of their crazes. Neither is sulphur useful with polystyrene since T_m for sulphur is 120°C and T_g for polystyrene is 90°C; the infusion process would thus have to take place 30° above T_g ; i.e. 30° above the maximum temperature of craze stability.

Iodine and sulphur at a 1:1 mole ratio, however, form a simple eutectic melting at 65°C³ and we have found this mixture useful in providing a degree of stability to crazes in homopolystyrene and in rubber-modified poly-

styrene. However, as will become apparent, this reinforcing agent is not as ideal for polystyrene as sulphur appears to be for the polyarylene oxide.

EXPERIMENTAL

The homopolystyrene used was Dylene 8 (Kopper Co.), a resin of $\bar{M}_n = 125\,000$ and $\bar{M}_w = 390\,000$. The rubber-modified polystyrene was Lustrex HT 91, a product of the Monsanto Co. containing an estimated 5% rubber in the form of discrete particles containing polystyrene inclusions that presumably result from the mode of polymerization used. Both materials were used in the form of moulded bars.

The bars were strapped down on elliptical strain jigs and immersed at once in the iodine sulphur eutectic bath at about 70°C. Immersion times varied from 10 minutes to several hours. Crazeing begins immediately upon bending in the high strain region and after immersion continues to develop both here and more slowly in the regions of lower strain. The clarity of homopolystyrene allows the crazes to be seen if the bar is removed after a short time. The crazes appear light red due to the infused iodine but otherwise have the usual appearance of crazes. If left immersed for several hours, the bar surfaces become a deep, opaque red from iodine absorption and the crazes can no longer be easily seen. Upon removal of the jigs, they were quenched in water briefly and the bars immediately removed and dried to prevent water from affecting the iodine in the crazes.

Microtomy was carried out, as before, with a diamond knife in a Porter Blum ultramicrotome set nominally to cut 750 Å slices. The slices were lifted off the surface of the water in the microtome trough with microscope grids. The grids were blotted dry in the conventional manner and placed in the evaporator for carbon deposition. They were subsequently examined in a Philips EM-100B electron microscope. As with the poly(arylene oxide) no evidence of residual impregnant was ever seen. This, of course, is to be expected in that iodine is more volatile than sulphur. Some slices from the rubber-modified polystyrene were exposed to osmium tetroxide vapour after carbon deposition in order to stain the rubber particles for better viewing⁴.

RESULTS

Homopolystyrene

Figure 1 shows the right-hand half of a single craze. Two overlapping micrographs were taken of the half-craze. Each micrograph was cropped and cut in half. The four micrograph sections are displayed in order in *Figure 1*. The centre of the craze is just to the left of the left-hand edge of the top photograph and the right-hand craze tip is at the right side of the bottom photograph. Thus, the sections of micrograph are 'read' from left to right and top to bottom, as with a printed page.

The symmetry of the whole craze in respect to variations in thickness and average hole size with distance from the geometric centre suggests that the craze initiated at its centre and grew to the right and the left with equal

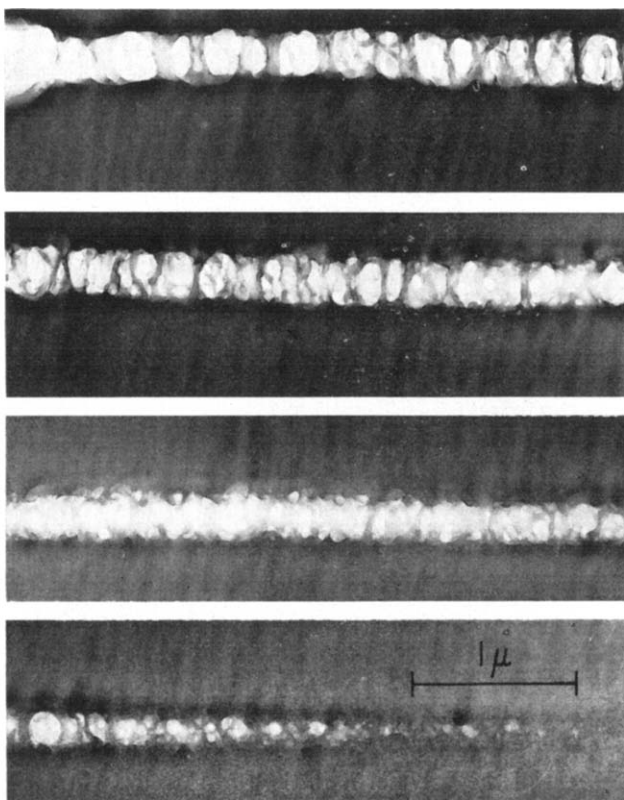


Figure 1 One-half of a craze in homopolystyrene impregnated with iodine-sulphur eutectic. Initiation thought to have occurred to the left of left edge of top photograph. Craze propagated left to right and top to bottom. Note progressive coarsening of structure.

velocities. Thus, the hole at the centre, about 40% of which is seen at the left-hand edge of the top photograph, is in the oldest part of the craze. The craze tip is the youngest part, by the same line of reasoning. Thus, the size of the holes in a given section of craze tends to increase steadily as time goes on (or alternatively as the craze tip gets farther and farther away). The holes at the tip in *Figure 1* are 400–1000 Å in diameter while those near the centre are as large as the craze is thick, 3000 Å. The hole at the centre is about 10 000 Å long. From craze tip to craze centre the filaments appear to get steadily larger also. In short, craze structure becomes noticeably coarser with age. We are led to imagine that the region at the left-hand edge of the top photograph resembles the true tip of a crack propagating slowly to the right.

Figure 2 shows a section of a thicker craze found in the same microtomed polymer section. This section of craze is more typical of what is usually seen in these polymer sections. The craze tip is presumably some distance away. When account is taken of the 4× greater magnification, it is clear that craze structure is approximately the same as that in the older parts of the craze

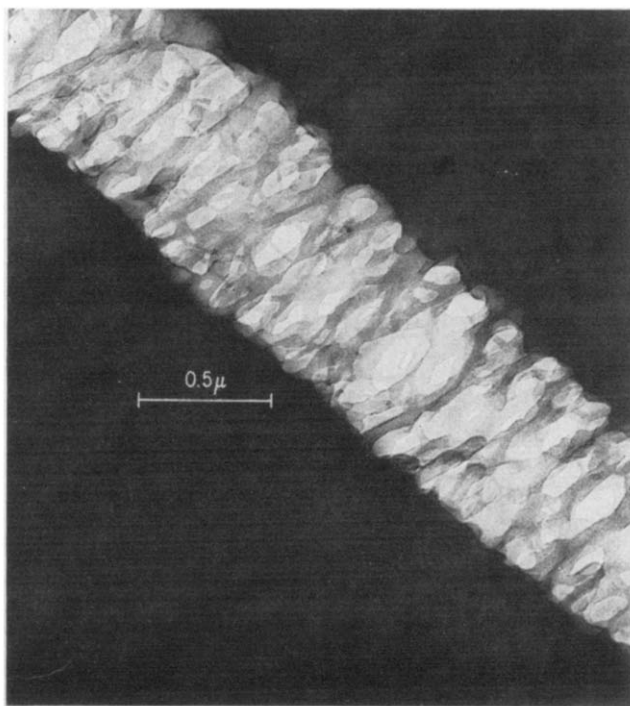


Figure 2 Thicker craze in homopolystyrene impregnated with iodine-sulphur eutectic.

in Figure 1. Most of the polymer is in the form of filaments 300 to 1000 Å thick in both crazes. However, several filaments of a much smaller size—perhaps 80 to 200 Å—can be seen. This broad dispersity in filament diameter is typical of polystyrene crazes prepared and treated as reported here.

Figure 3 shows a section of craze in homopolystyrene which had been immersed for only 10 minutes in the eutectic bath before removal and quenching. Craze structure has a coarser appearance than in the preceding figures. The smallest filaments are again less than 100 Å thick but a very large fraction of the polymer is in filaments 600 to 5000 Å thick. The most interesting feature of this craze is the large number of dark spots distributed over the large filaments. Each spot is a region of greater thickness and, hence, greater electron scattering power. Upon careful inspection a few of these lumps or nodules can be seen in profile on the sides of the large filaments. A few of the very thin filaments are seen to be attached at their ends to nodules on the thick filaments.

It seems likely that the nodules are the residues of filaments that grew thinner and finally snapped under the action of surface tension. Each end of such a broken filament then rapidly retracts into its base leaving a bump on the thick base filament as evidence of the previous existence of the thin filament. In time the nodule itself would disappear completely into the base filament. We have occasionally seen events like this occur while studying a particular section of a craze in the microscope: the heat generated in the

polymer section by the electron beam can cause a substantial increase in temperature and consequent softening of the filaments.

Although structural details vary from one craze to the next, it is clear that in each case the craze shows evidence of a physical aging process. The aging is facilitated by the unavoidable proximity of the temperature of the eutectic

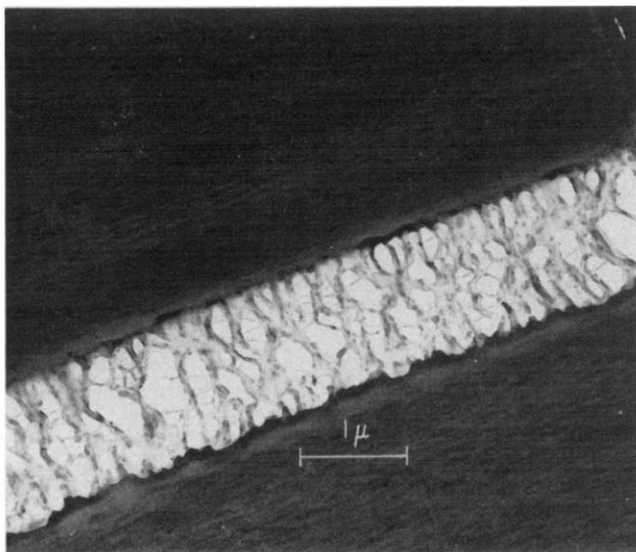


Figure 3 Homopolystyrene craze showing marked thermal aging. Nodules appear to be stumps of broken filaments.

bath to the glass temperature of polystyrene. Moreover, iodine at least dissolves in polystyrene to a limited degree, eventually turning the polymer a deep red. Whether sulphur is somewhat soluble also is not known. In any case, polystyrene films immersed in the eutectic bath for several hours are subsequently found by differential scanning calorimetry to have T_g 's reduced by 10°C at least. Thus the bath temperature and the T_g of the eutectic-plasticized filaments of the craze nearly coincide. Marked evidence of physical deterioration in the craze structure is thus not surprising.

Poly(bisphenol-A carbonate) crazed in liquid sulphur at 125°C yields microtomed sections showing even more markedly aged crazes (Figure 4). The T_g of polymer films soaked in liquid sulphur is reduced 20° through plasticization by the sulphur. Thus the filaments of the craze have T_g 's equal to the bath temperature which accounts for the marked deterioration. (The polymer actually dissolves in the iodine-sulphur eutectic precluding its use as a reinforcing impregnant.)

The gradual coarsening (and presumably weakening) of craze structure seen in Figures 1 to 4 appears then to take place by a breaking of the thinner filaments followed by their retraction and coalescence with thicker filaments. As this process continues, the holes get larger and fewer in number and the surviving filaments grow thicker. In the process the strength of the craze

probably deteriorates also so that these structural changes may be considered part of a high-temperature static fatigue process wherein crazes gradually transform into cracks. The same kind of process probably takes place in so-called solvent-cracking of glassy polymers whenever the organic fluid is absorbed sufficiently to lower T_g to about ambient temperature⁵.

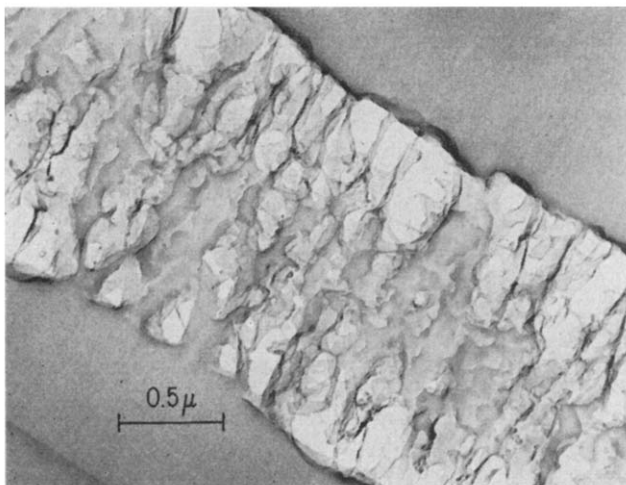


Figure 4 Craze in poly(bisphenol-A carbonate) produced in liquid sulphur at 125°C. Craze structure markedly deteriorated through sulphur plasticization.

Certainly the structures seen here are much coarser than those observed in poly(dimethyl phenylene oxide) crazes reinforced with sulphur. In that resin, craze infusion can be effected 85° below T_g of the polymer. Furthermore, the T_g is unchanged by long-time immersion in liquid sulphur, indicating a negligible degree of plasticization. Filament retraction and void coalescence occur at a much lower rate, if at all, and the characteristic dimensions of mature craze structure remain in the 200 Å range indefinitely.

Rubber-modified polystyrene

Since the discovery of the role of crazing in the deformation of rubber-modified polystyrene and similar composite polymer systems^{6,7}, interest in their morphology and behaviour under stress has increased markedly. Much of the advance in understanding of these systems has come from optical and electron microscopic studies. The latter have depended largely on the use of osmium tetroxide to stain selectively the rubber. The agent attaches to residual double bonds and thus shows the morphology of the rubber particle and its inclusions. Happily osmium tetroxide also seems to react somehow with craze material sufficiently to leave a general indication of the number and spatial disposition of the crazes. However, the staining does not protect

craze structure during microtomy. Thus the knowledge of craze structures is restricted.

It appears that suitable impregnants can be useful in preserving craze structure in rubber-modified systems during microtomy. We report here preliminary results obtained using iodine-sulphur eutectic as a reinforcing impregnant with rubber-modified polystyrene. For the same temperature limitations previously mentioned in connection with homopolystyrene this impregnant is not an ideal one for studying 'unaged' crazes in rubber-modified polystyrene. Results suggest, however, that proper impregnation will become a very useful tool that complements rubber staining.

Figure 5 shows a microtomed section of Styron 453 (Dow Chemical Co.) rubber-modified polystyrene that had been crazed by straining in the eutectic bath for 10 minutes at 70°C, removed, and quenched. The section was backed with carbon as before and examined without further treatment. The oval shape in the centre is a rubber particle, originally a sphere 3.5 μm in

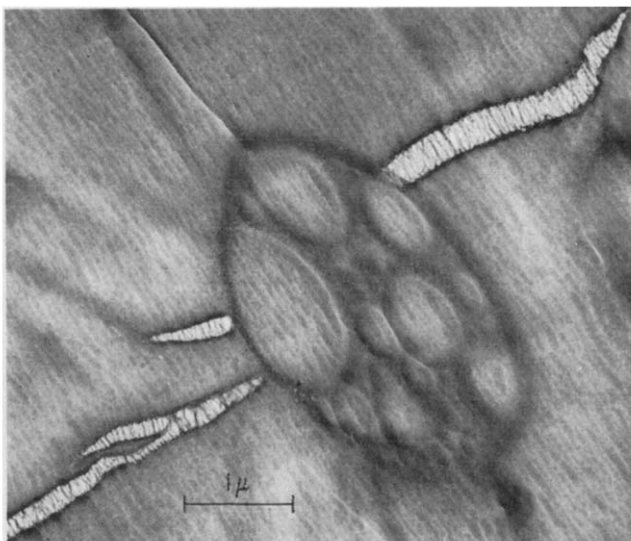


Figure 5 Rubber-modified polystyrene crazed in iodine-sulphur eutectic. Rubber particle visible because of difference in cutting characteristics of rubber and polystyrene. No staining.

diameter. As is usually the case, microtomy has produced a compression of the slice of about 40% in the cutting direction (top left, bottom right) and the rubber particle shape is consequently distorted. Three crazes are seen that interact with the rubber particle. Not surprisingly, their structure is similar to that seen in *Figure 2*. On the basis of change of thickness with distance, two of the crazes appear to have initiated at or near the edge of the rubber particle. The initiation site of the third craze is by no means evident. When it is borne in mind, however, that this is just one section in a body containing rubber particles distributed in three dimensions, it is evident that the third craze may have initiated either on the same rubber particle at a greater or

lesser depth or on another rubber particle no part of which is located in this section.

The rubber particle is visible here apparently because the rubber has different cutting characteristics from the polystyrene. In some sections the rubber appears darker and hence is thicker; in others the rubber appears lighter and is thinner. The tendency of one material to deform out of the way of the knife more than another is well known to microtomists. If more polystyrene than rubber is cut off in one slice, rubber must tend to protrude above the polystyrene surface on the cut face of the block. The protrusion would then be present on the surface of the next slice making the rubber in the second slice thicker by the same amount that it was thinner in the first; hence the alternation in contrast between styrene and rubber from slice to slice.

The different cutting characteristics do not delineate as sharply or as certainly the morphology of the rubber particle as does staining. We have, therefore, treated microtomed sections with osmium tetroxide subsequent to carbon deposition. *Figure 6* shows a section of crazed Lustrex HT91 resin (Monsanto Co.) in which the crazes were impregnated with iodine-sulphur eutectic and the rubber subsequently stained lightly. After carbon evaporation the microscope grids holding the sections were turned upside down on a glass slide and the slide placed in a closed chamber containing an open ampoule of osmium tetroxide solid for one hour. Staining, of course, results from the osmium tetroxide vapour. The rubber boundaries and the polystyrene inclusions are more sharply delineated than in *Figure 5*.

Examination of impregnated and stained sections like that in *Figure 6* suggests that in most cases the craze edge is coincident with the rubber particle boundary to within 200 Å or so. Not infrequently, however, the craze edge is separated from the rubber particle by a gap of non-voided polystyrene. Less frequently the craze edge penetrates through the rubber skin into the first included particle of polystyrene and occasionally the penetration goes deep into the rubber particle. Since serial sections have not been examined, we do not know how far the gap or the limited penetration extend above and below the plane of the section.

Another feature of *Figure 6* should be mentioned. The random clustering of rubber particles that frequently is seen changes the pattern of craze development. With an isolated rubber particle crazes initiate preferentially in the equatorial zones (defining the poles as the direction of stress) since the stress concentration factor is greatest there. In clusters the stress fields of the individual particles may interact sufficiently to allow crazes to run from the pole region of one particle to that of the next. The pattern of the particular cluster may even allow crazes to run at angles of as little as 45° from the applied stress direction (*Figure 6*). These complexities are not surprising, of course, but are worthy of notice by those engaged in stress analysis of these systems.

CONCLUSIONS

The work reported here demonstrates a limited utility of iodine-sulphur eutectic in reinforcing crazes in polystyrene. In the most general context the attendant physical deterioration of the craze is undesirable in that 'undamaged' craze structure cannot be studied. The coarsening of structure that

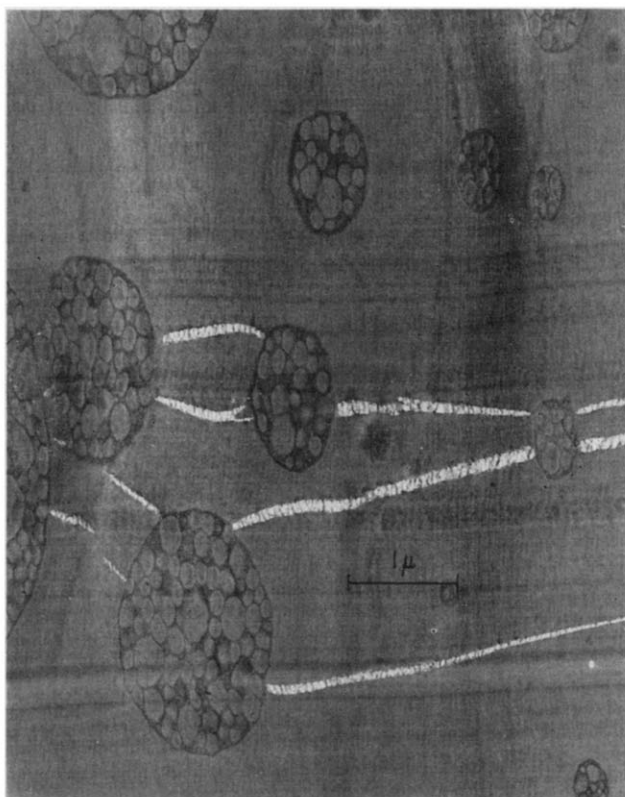


Figure 6 Rubber-modified polystyrene crazed in iodine-sulphur eutectic. Microtomed sections stained with osmium tetroxide.

occurs during impregnation suggests how crazes may age under stress at temperatures approaching T_g . A similar process probably occurs in many environmental stress cracking events taking place in environments that swell the polymer and lower T_g of the craze filaments substantially.

It also seems clear that optimum craze impregnation will be a very useful tool, complementary to rubber-staining, in studying deformation mechanisms in rubber-modified polystyrene. The optimum impregnant will be one that wets polystyrene without plasticizing it, that melts only 10 or 20°C above ambient temperature, and that is hard in the solid state, fluid in the liquid state, insoluble in water, and sublimable.

ACKNOWLEDGMENT

We are grateful to Professor B. Wunderlich for bringing to our attention the low melting point of the sulphur-iodine eutectic.

*General Electric Research and Development Centre,
Schenectady,
New York, 12301, USA*

(Received 30 October 1970)

REFERENCES

- 1 Kambour, R. P. and Holik, A. S. *J. Polym. Sci. (A-2)* 1969, **7**, 1393
- 2 Kambour, R. P., *J. Appl. Polym. Sci., Applied Polymer Symposia* 1968, **7**, 215
- 3 'Elemental Sulfur,' Ed., Meyer, B. Interscience Publishers, New York, 1965
- 4 Kato, K. *J. Electron Microscopy* 1965, **14**, 220
- 5 Bernier, G. A. and Kambour, R. P. *Macromolecules* 1968, **1**, 393
- 6 Bucknall, C. B. and Smith, R. R. *Polymer, Lond.*, 1965, **6**, 437
- 7 Matsuo, M. *Polymer, Lond.* 1966, **7**, 421

Network properties: (1) Multiple glass transitions

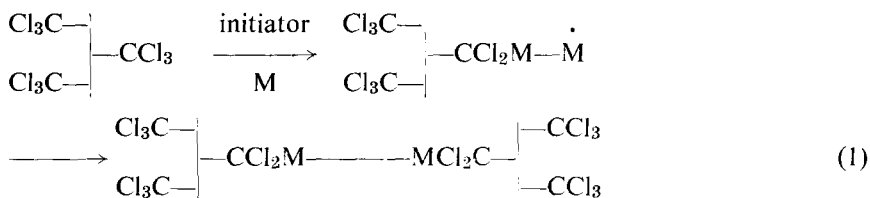
C. H. BAMFORD, G. C. EASTMOND and D. WHITTLE

Networks composed of polyvinyl trichloroacetate (PVTCA) cross-linked by polymethyl methacrylate or polystyrene were prepared from mixtures of PVTCA and the appropriate monomer by thermal initiation with molybdenum carbonyl at 80°C or photoinitiation with manganese carbonyl at 25°C. From details of the syntheses the following properties of the networks were calculable: (1) the mean numbers of cross-linked units per weight average PVTCA chain, (2) the mean degree of polymerization of the cross-links and (3) the ratio (number of branches)/(number of cross-links). Dilatometric observations showed that normally the networks have two glass temperatures and are two-phase systems. The slopes of the volume-temperature curves between the transition points were higher than expected, markedly so with copolymers containing methyl methacrylate and to a much smaller extent with those containing styrene. It is concluded that in the former systems the PVTCA-rich phase contains considerable proportions of polymethyl methacrylate while in the latter there is only a small degree of incorporation of styrene into the PVTCA-rich phase. In agreement with these conclusions is the observation that for the polymethyl methacrylate systems the lower glass temperature is appreciably higher than the glass temperature of PVTCA. With the systems containing styrene this difference is not found. The influence of structural characteristics of the networks, particularly the branch/cross-link ratio and the length of the cross-links, on the compositions of the two phases is discussed.

GREAT INTEREST¹ has recently been shown in properties of block copolymers of the types AB, ABA in which A and B represent glassy and rubbery polymer segments, respectively. It has been shown that, at least over certain ranges of composition, the different components often form two separate phases in the solid state, one component existing in the form of domains in a matrix of the other. Evidence for two-phase behaviour is provided by electron microscopy²⁻⁶, low-angle x-ray scattering^{7, 8}, dilatometry^{9, 10}, differential thermal analysis^{3, 11}, and mechanical relaxation phenomena^{12, 13}. Electron-microscopy shows the coexistence of two phases directly, while the second technique allows an evaluation of inter-domain distances. The other techniques show the existence of two glass transition temperatures, which may approximate to those of the pure components. In these systems polymer molecules in the domains are effectively cross-linked by physical forces.

We have recently¹⁴⁻¹⁷ described general methods of synthesizing networks composed of chains of different components, the nature of which is variable over a wide range. These materials may be prepared by cross-linking a prepolymer with chains of a vinyl polymer. Cross-linking involves free radical generation by reaction of suitable halogen-containing groups in the prepolymer with an organometallic derivative in the presence of a vinyl monomer

M as shown below



Repetition of this process ultimately leads to a three-dimensional network. The cross-link density and length are statistically controllable as already described. If the termination reaction occurs partly by disproportionation the prepolymer molecules will carry branches as well as cross-links.

We have embarked on a programme designed to investigate the properties of such networks with predetermined structures. The polymers will be characterized by tensile and torsion measurements, dilatometry, nuclear magnetic resonance, electron microscopy and swelling behaviour. In this paper we report the results of dilatometric studies on networks consisting of polyvinyl trichloroacetate cross-linked with methyl methacrylate and styrene.

EXPERIMENTAL

Materials

Methyl methacrylate, styrene, molybdenum and manganese carbonyls were purified as previously described¹⁸. The prepolymer (PVTCA) was prepared by trichloroacetylation of polyvinyl alcohol as in earlier work¹⁴. Networks containing PVTCA cross-linked by polymethyl methacrylate and polystyrene were prepared¹⁴⁻¹⁷ from mixtures of PVTCA and the appropriate monomer by initiation with molybdenum carbonyl at 80°C or photoinitiation ($\lambda = 4358 \text{ \AA}^*$) with manganese carbonyl at 25°C. Excess monomer was removed under vacuum for 15 h, approximately, and the resulting networks were then weighed. All reactions were carried out under vacuum in a laboratory illuminated with sodium light.

Techniques

Dilatometry. Measurements of glass-transition temperatures and coefficients of cubical expansion were carried out in conventional pyrex dilatometers with mercury as the confining liquid. Polymers were annealed by immersing the dilatometer bulb containing a weighed quantity of polymer in a water bath and heating to 100°C under high vacuum. After cooling, a weighed amount of degassed mercury was transferred to the dilatometer and the bulb was agitated by an electric vibrator to remove voids between mercury and the polymer. The dilatometer was then opened to the atmosphere. This annealing process removes excessive free volume which may be present in the polymer films and eliminates contraction-effects¹⁰ which may occur during a heating-cooling cycle.

* $1 \text{ \AA} = 0.1 \text{ nm}$

MULTIPLE GLASS TRANSITIONS

A dummy dilatometer was prepared containing only a known weight of mercury. The two dilatometers were clamped together and suspended vertically in a thermostat. Simultaneous observations of the meniscus levels were made at 3–5°C intervals over a temperature range 20–130°C with a cathetometer. A plot of the difference between the two volumes ΔV against temperature allowed glass-transition temperatures and cubical expansion coefficients to be evaluated, the former to $\pm 3^\circ\text{C}$.

Care was taken to ensure that thermal equilibrium, indicated by a steady cathetometer reading, had been achieved at each temperature. This usually required 15–30 min. Some samples were kept at temperatures $< 100^\circ\text{C}$ for several hours without further variation in ΔV (see *Figure 3*). At temperatures $> 115^\circ\text{C}$, decomposition of PVTCA occurred and constant readings could not be obtained; this effect was greatest for networks having a high PVTCA content.

Polymer densities. These were determined by a flotation method¹⁹.

Gel times. These were measured in vacuum viscometers as described in an earlier publication¹⁴.

RESULTS AND DISCUSSION

(1) *Network synthesis and characterization*

The prepolymer contained 53% chlorine, corresponding to 60.4% trichloroacetylation of the parent polyvinyl alcohol. The effective \bar{P}_w of the trichloroacetate residues was 2600. Preparative details and structural characteristics of the networks are given in *Table 1*. Gel-times quoted are corrected for transfer to monomer¹⁵. Initial rates of initiation \mathcal{J}_0 were derived from observed rates of polymerization of the vinyl monomer under comparable conditions but with ethyl trichloroacetate as halide instead of PVTCA; in this way effects of variations in the termination coefficient arising from attachment of growing chains to prepolymer molecules and gelation are avoided. This method of determining \mathcal{J}_0 is described in more detail in reference 17. Carbonyl consumption is small in polymerizations I and VII–IX and no allowance for consumption¹⁵ in VII–IX is necessary. The kinetics of initiation by manganese carbonyl when consumption is appreciable are insufficiently understood at present to permit a precise correction and only limiting values can be estimated. The resulting uncertainties in the calculated mean number of cross-linked units per weight-average prepolymer chain and the length of cross-links are apparent from columns 8 and 9 of *Table 1*. Recent investigations²⁰ on initiation by molybdenum carbonyl suggest that under our conditions no consumption correction should be made. Estimation of mean cross-link lengths from conventional kinetic parameters is unreliable on account of the incidence of the gel effect, which was particularly pronounced in polymerizations VII–IX involving styrene. These quantities were therefore calculated from the total number of cross-linked units and the conversion of the vinyl monomer. Branch:cross-link ratios were obtained from available information on the nature of the termination reaction^{16, 17}; a small correction for chain transfer to methyl methacrylate at 80°C has been made¹⁵.

Table 1 Network preparation and parameters

Polymerization	Vinyl monomer	Polymerization temperature (°C)	Corrected gel time (min.)	Reaction time (min.)	Weight of gel (gl ⁻¹)	$10^7 \int_0^{\infty} (\text{mol l}^{-1} \text{s}^{-1})$	Mean no. of cross-linked units per prepolymer chain	\bar{P}_n cross-links	No. of branches/ no. of cross-links
I	methyl methacrylate	25	4.8	16	23.2	0.85	3	4560-4740	4
II	methyl methacrylate	25	4.8	48	62.4	0.85	9	5060-5440	4
III	methyl methacrylate	25	4.8	96	150.4	0.85	16-18	6900-8000	4
IV	methyl methacrylate	80	6.0	7	23.6	0.75	1	11 820	10
V	methyl methacrylate	80	6.0	21	64.9	0.75	3.5	12 700	10
VI	methyl methacrylate	80	6.0	42	163.2	0.75	7	16 760	10
VII	styrene	25	3.7	3.7	6.5	0.46	1	2880	~ 0
VIII	styrene	25	3.7	11.1	12.4	0.46	3	4750	~ 0
IX	styrene	25	3.7	22.2	23.1	0.46	6	5800	~ 0

[Mn₂(CO)₁₀]: I-III 7.71 × 10⁻⁴ mol l⁻¹VII-IX 5.14 × 10⁻⁴ mol l⁻¹[Mo(CO)₆]: IV-VI 6.98 × 10⁻⁴ mol l⁻¹[prepolymer] = 5 gl⁻¹

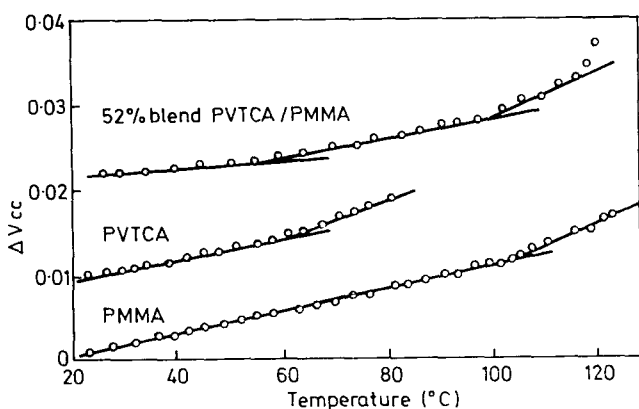


Figure 1 Dilatometric data for polyvinyl trichloracetate (PVTCA), polymethyl methacrylate (PMMA) and a blend containing 52% w/w PVTCA

(2) Dilatometric data

(2.1) *PVTCA—polymethyl methacrylate system.* Figure 1 gives dilatometric data from which the glass transition temperatures of PVTCA and polymethyl methacrylate are seen to be 59°C and 103°C, respectively. The coefficients of cubical expansion below and above T_g are

$$\left. \begin{array}{l} \alpha_{gpp} = 2.8 \times 10^{-4} \text{ per K} \\ \alpha_{lpp} = 6.6 \times 10^{-4} \text{ per K} \end{array} \right\} \text{ for prepolymer}$$

$$\left. \begin{array}{l} \alpha_{gpm} = 2.1 \times 10^{-4} \text{ per K} \\ \alpha_{lpm} = 5.4 \times 10^{-4} \text{ per K} \end{array} \right\} \text{ for polymethyl methacrylate} \quad (2)$$

Dilatometric data for the samples I–VI are presented in Figures 2 and 3. In samples I–V two transitions T_{g1} , T_{g2} are observed, the former somewhat higher than that of the pure prepolymer and the latter close to that of polymethyl methacrylate. A blend of the homopolymers containing 52% w/w PVTCA showed two glass transition temperatures close to those of the homopolymers (Figure 1).

The existence of two transition temperatures indicates the presence of two phases, which would result from limited compatibility of the two components. This type of behaviour has been reported for block copolymers of the type AB, ABA^{1, 12} and also for polymer blends^{21, 22}; in these systems independent evidence^{2–6} has often indicated the formation of discrete domains containing a preponderance of one component.

We define S_1 , S_3 as the slopes of the volume-temperature curves below T_{g1} and above T_{g2} , respectively, and S_2 as that in the intermediate region. Values of S_1 , S_3 have been calculated on the assumption that the coefficients of expansion of the two components are additive, in which case equation (3) is applicable.

$$S_1 = \alpha_{gpp}V_{gpp} + \alpha_{gpm}V_{gpm} + \alpha_{Hg} \Delta V_{Hg} \quad (3)$$

$$S_3 = \alpha_{lpp}V_{lpp} + \alpha_{lpm}V_{lpm} + \alpha_{Hg} \Delta V_{Hg}$$

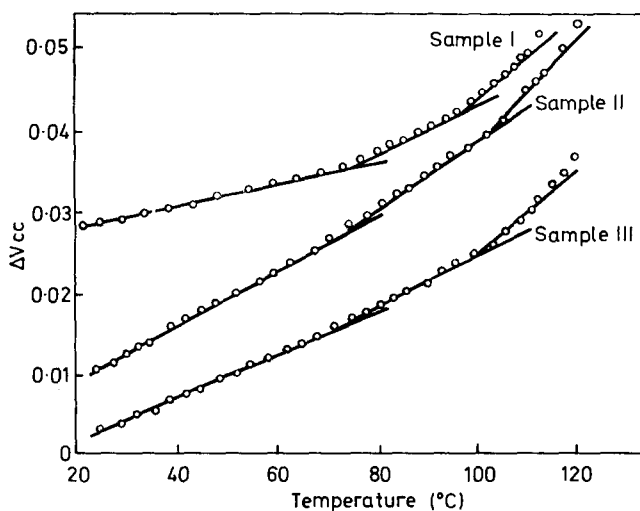


Figure 2 Dilatometric data for networks I, II, III showing two glass transition temperatures T_{g1} (lower), T_{g2}
 ○ represent experimental data
 Curves below T_{g1} and above T_{g2} calculated from equation (3)

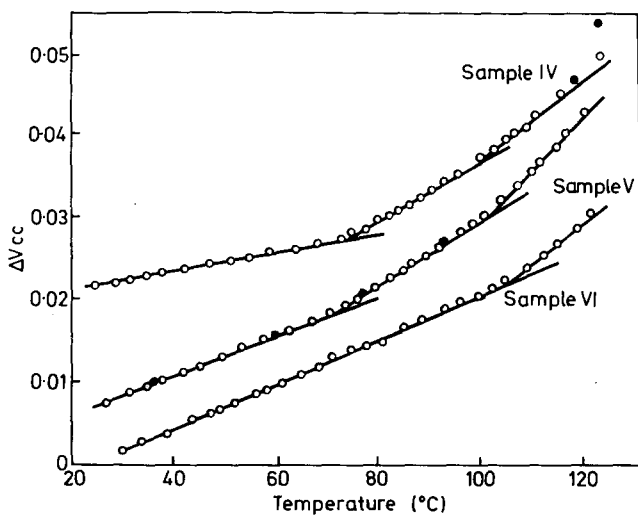


Figure 3 Dilatometric data for networks IV, V, VI showing the presence of two glass-transition temperatures (except for sample VI)
 ○ represent experimental data; ● represent experimental data for network V obtained after holding a specimen at the indicated temperature for several hours
 Curves below T_{g1} and above T_{g2} calculated from equation (3)

MULTIPLE GLASS TRANSITIONS

Here the α 's are the coefficients of cubical expansion and the V 's the respective volumes of the components at the appropriate temperature, and in the appropriate states denoted by the subscripts g (below glass transition) and l (above glass transition). Subscripts pp , pm refer to PVTCA and polymethyl methacrylate, respectively, and ΔV_{Hg} represents the difference between the volumes of mercury in the dilatometer containing the sample and the dummy dilatometer. Lines with the calculated slopes are superimposed on the experimental points in *Figures 2 and 3*; in all cases the calculated slopes S_1 are in excellent agreement with observations. The experimental points in the region just above T_{g2} appear to agree with the calculated slopes, but diverge at temperatures above 110°C , especially for materials containing significant proportions of PVTCA. The divergence is attributable to thermal decomposition of the prepolymer; independent observations on pure PVTCA have shown that decomposition sets in above 110°C .

Values of S_2 were calculated from equation (4)

$$S_2 = \alpha_{lpp}V_{lpp} + \alpha_{gpm}V_{gpm} + \alpha_{Hg}\Delta V_{Hg} \quad (4)$$

and are compared with experimental slopes in *Table 2*. The observed values are appreciably and consistently higher than those calculated (except for VI). We interpret these results to mean that the assumption of independent

Table 2

Sample	$10^4 S_2$ (mlK ⁻¹)		α	W	PVTCA in network (% w/w)	T_{g1} (°C)	T_{g2} (°C)
	observed	calculated					
I	3.75	2.64	0.326	1.2	21.5	74	97.5
II	5.23	4.66	0.15	1.7	8	71	102
III	3.83	3.57	0.071	2.1	3.5	69	101
IV	4.78	2.34	0.87	2.8	21	74	99
V	5.06	3.42	0.37	4.4	7.5	71	102
VI	3.41	3.51	—	—	3	—	103
VII	3.03	2.89	0.57	0.17	77	55	97
VIII	3.64	3.52	0.083	0.12	40.5	60	97
IX	4.00	3.85	0.061	0.22	21.5	60	100
PVTCA						59	
polystyrene							100
polymethyl methacrylate							103

behaviour of the two components, which is the basis of equation (4), is not valid for the networks. Independent experiments have established that equation (4) holds much more closely for a 1:1 w/w blend of PVTCA and polymethyl methacrylate, the calculated and observed values of S_2 agreeing within 4%. It is necessary to assume that in the networks the phase which is relatively rich in PVTCA (phase 1) also contains polymethyl methacrylate, which can partake in the transition at the lower T_g . To facilitate analysis of

the data we shall assume that all the PVTCA is in this phase, together with a weight fraction a of the polymethyl methacrylate component. Phase 2 is supposed to consist of pure polymethyl methacrylate. On this basis we derive the modified equation (5)

$$S_2 = \alpha_{lpp}V_{lpp} + a\alpha_{lpm}V_{lpm} + (1-a)\alpha_{gpm}V_{gpm} + \alpha_{Hg} \Delta V_{Hg} \quad (5)$$

By equating S_2 to the measured slope, values of a have been calculated from equation (5) and are shown in Table 2. The weights of polymethyl methacrylate W associated with unit weight of PVTCA in phase 1 have been computed from values of a and the data in Table 1, and are also presented in Table 2.

From these results it appears that phase 1 contains large amounts of polymethyl methacrylate, especially when the proportion of the latter in the network is high. If phase 2 is not pure polymethyl methacrylate, but contains some PVTCA which does not participate in the lower glass transition, our method of calculation would lead to underestimates of W .

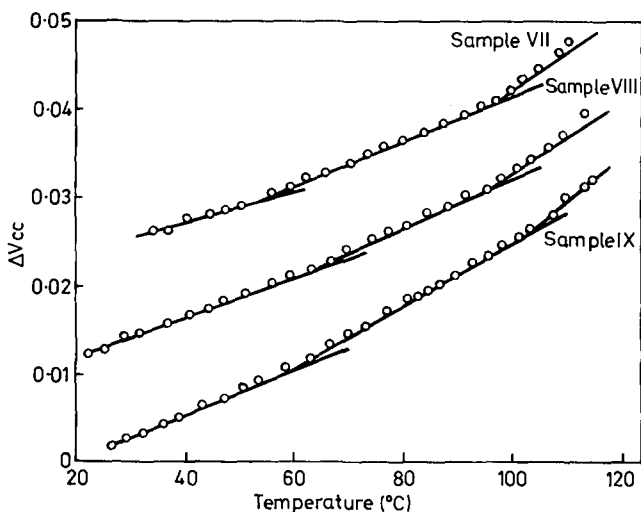


Figure 4 Dilatometric data for networks VII, VIII and IX showing the presence of two glass-transition temperatures T_{g1} (lower) and T_{g2}
 ○ represent experimental data
 Curves below T_{g1} and above T_{g2} calculated from equation (3)

(2.2) *PVTCA—polystyrene system.* Data for this system (samples VII–IX) are shown in Figure 4. Again two transitions occur, T_{g1} , T_{g2} being close to the transition temperatures of the two components. Values of S_1 , S_3 were calculated from equation (3) with the appropriate parameters for polystyrene (α_{gps} , V_{ps} etc.). The coefficients of expansion are given in equation (6)

$$\alpha_{gps} = 1.9 \times 10^{-4}, \quad \alpha_{lps} = 5.5 \times 10^{-4} \text{ per K} \quad (6)$$

Both calculated slopes are in satisfactory agreement with experiment, provided the temperature is not high enough to cause thermal decomposition

of the prepolymer. Values of S_2 calculated from the equation analogous to equation (4) are again lower than those observed (*Table 2*), although the differences are smaller than in the methyl methacrylate system. Analysis of the results by an equation of the type (5) allows a and W to be calculated, with results presented in *Table 2*. Both quantities are considerably smaller than for polymers I-V, indicating that only small amounts of polystyrene are incorporated into phase 1.

(3) Texture of the networks

Figure 5a is a schematic representation of a portion of a network of the type used in these studies, in which polymer chains B are cross-linked by chains A and which also contains branches of A and loose-ends of B. As a basis for discussion we consider an idealised model containing discrete and

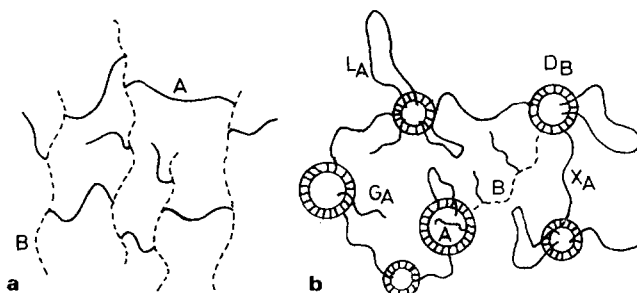


Figure 5

- (a) Portion of a network composed of polymer chains B (broken lines) cross-linked by chains of A (continuous lines)
 (b) Schematic representation of an idealized structure consisting of discrete phases of B + A in a matrix of A. (See text for explanation of symbols)

continuous phases and we first assume that the former consist mainly of B. Typical structural features are shown in *Figure 5a*, D_B is a domain of collapsed and aggregated molecules B; such regions are cross-linked by A-chains X_A . Loops L_A are A-chains connecting molecules B in a single domain. Branches G_A of A may protrude from the domains. A single molecule of B such as that shown may be unable to aggregate with like molecules and will be trapped in a region mainly composed of A. Similarly a chain of A (e.g. a branch) may be trapped in a domain containing B.

If the two polymers were completely incompatible, the maximum degree of phase separation consistent with the geometry would be expected, the cross-linked units of B being near the surface of the discrete domains. Geometric constraints would necessitate the trapping of some chains of A in the domains and the exclusion of some chains of B from the domains. With partially compatible polymers, the junction points will be more deeply embedded in the domains, thus incorporating a larger proportion of A in B. For reasons of geometry, such incorporation might be expected to occur more

readily with branches or loops of A than with cross-links between different domains. The domain composition probably varies radially, with higher local concentrations of A near the surface, giving rise to a diffuse boundary of the type already proposed¹ for block and graft copolymers. These boundaries are represented by the hatched rings in *Figure 5b*. With partially compatible polymers a greater proportion of B chains in the phase rich in A would also be expected.

In general, the detailed morphology of the solid network must be influenced by the relative solvent powers for the separate homopolymers of the liquid from which the network is isolated⁵; a non-solvent for A could lead to discrete domains of A within a continuous phase of B. In the present work the solid networks were prepared by removal of monomers, which are solvents for both homopolymers A and B. This type of situation could lead to the most intimate mixture of A and B consistent with the compatibility of the polymers and the geometry of the networks.

The low values of W in the networks containing styrene (*Table 2*) indicate that polystyrene and PVTCa are effectively incompatible and mainly coexist as separate phases. This is not surprising since the homopolymers are undoubtedly incompatible. The appearance of a small proportion of polystyrene in the regions mainly composed of PVTCa (phase 1) is a result of the chemical attachment of the homopolymers, and the trapping of portions of polystyrene chains near junction-points and short cross-links in these regions. The marked phase separation in these systems is consistent with the observation that T_{g1} and T_{g2} are close to those of the homopolymers (*Table 2*).

Polymethyl methacrylate and PVTCa are essentially incompatible as shown by the existence of two glass transitions in blends of the two polymers, at temperatures characteristic of the homopolymers (*Figure 1*). Although in the network two phases exist (as shown by two glass transitions) large proportions of polymethyl methacrylate are incorporated in regions containing PVTCa (phase 1). The glass transition corresponding to these regions occurs at a perceptibly higher temperature than that of PVTCa (*Table 2*). On the other hand, T_{g2} differs little from T_g for polymethyl methacrylate (*Table 2*), suggesting that phase 2 consists essentially of this polymer.

During the isolation of the network unrestricted coagulation of the PVTCa as a pure phase is impossible, so that formation of regions relatively rich in PVTCa would be expected. Such regions (phase 1) must be connected by cross-links of polymethyl methacrylate which are necessarily excluded from phase 1. However, polymethyl methacrylate branches will not be under such constraints, and these, together with the remaining cross-links, may become incorporated into this phase. The view that branches are more readily included than cross-links in phase 1 is consistent with the higher values of W for networks prepared at 80°C (*Table 2*), i.e. under conditions more favourable to termination by disproportionation, and consequent branch formation. The longer cross-links in samples IV–VI would also favour high values of W . Since according to our model, a considerable amount of polymethyl methacrylate is located in phase 1, further phase separation in these regions would be anticipated; however, the observation of a well-defined glass transition temperature T_{g1} higher than the glass temperature of PVTCa suggests that the two components are finely dispersed.

Further work on the factors influencing the morphology of these networks is in progress.

*Donnan Laboratories,
Department of Inorganic, Physical
and Industrial Chemistry,
University of Liverpool, UK*

(Received 15 October 1970)

REFERENCES

- 1 IUPAC Symposium *J. Polym. Sci. (C)* 1969, **26**. See particularly: Fetters, L. J. p 1; Holden, G., Bishop, E. T. and Legge, N. P. p 37; Meier, D. J. p 81
- 2 Bradford, E. B. and Vanzo, E. *J. Polym. Sci. (A-1)* 1968, **6**, 1661
- 3 Beecher, J. F., Marker, L., Bradford, R. D. and Aggarwal, S. L. *J. Polym. Sci. (C)* 1969, **26**, 117
- 4 Matsuo, M., Nozaki, C., Jyo, Y. *Polymer Eng. and Sci.* 1969, **9**, 197
- 5 Inoue, T., Soen, T., Hashimoto, T. and Kawai, H. *Macromolecules* 1970, **3**, 87
- 6 Saam, J. C., Gordon, D. J. and Lindsey, S. *Macromolecules* 1970, **3**, 1
- 7 Legrand, D. G. *J. Polym. Sci. (C)* 1969, **26**, 117
- 8 McIntyre, D. and Campos-Lopez, E. *Macromolecules* 1970, **3**, 322
- 9 Lewis, P. R. *J. Int. R. Inst.* 1968, Oct., 217
- 10 Holt, T. and Edwards, D. *J. Appl. Chem.* 1965, **15**, 223
- 11 Chandler, L. A. and Collins, E. A. *J. Appl. Polym. Sci.* 1969, **13**, 1585
- 12 Angelo, R. J., Ikeda, R. M. and Wallach, M. L. *Polymer, Lond.* 1965, **6**, 141
- 13 Cooper, S. L. and Tobolsky, A. V. *J. Appl. Polym. Sci.* 1966, **10**, 1837
- 14 Bamford, C. H., Dyson, R. W. and Eastmond, G. C. *J. Polym. Sci. (C)* 1967, **16**, 2425
- 15 Bamford, C. H., Dyson, R. W., Eastmond, G. C. and Whittle, D. *Polymer, Lond.* 1969, **10**, 759
- 16 Bamford, C. H., Eastmond, G. C. and Whittle, D. *Polymer, Lond.* 1969, **10**, 771
- 17 Bamford, C. H., Dyson, R. W. and Eastmond, G. C. *Polymer, Lond.* 1969, **10**, 885
- 18 Bamford, C. H., Eastmond, G. C. and Robinson, V. J. *Trans. Faraday Soc.* 1964, **60**, 751
- 19 Millar, J. R. *J. Chem. Soc.* 1960, p 1311
- 20 Bamford, C. H., Eastwood, G. C. and Fildes, F. J. T., in course of publication
- 21 Hughes, L. J. and Brown, G. L. *J. Appl. Polym. Sci.* 1961, **5**, 580
- 22 Sperling, L. H. and Friedman, D. W. *J. Polym. Sci. (A-2)* 1969, **7**, 425

The morphology of $(\text{styrene})_x(\text{butadiene})_y(\text{styrene})_x$ block copolymers

P. R. LEWIS and C. PRICE

A study has been made of the domain morphologies of two block copolymers of the type, $(\text{styrene})_x(\text{butadiene})_y(\text{styrene})_x$; for the first sample the weight-average molecular weights of the styrene and butadiene blocks were 13 300 and 75 000 respectively, whilst for the second sample they were 10 300 and 71 000 respectively. The morphologies of films cast at different rates of evaporation from benzene solution were investigated by electron microscopy. With the exception of those prepared at very high rates of evaporation, the films formed highly regular domain structures, which were subdivided into grains. Low-angle x-ray studies were made on both solvent cast and compression moulded test pieces. It was found that at the tertiary level the latter consisted of an hexagonal lattice of glassy cylinders embedded in a rubbery matrix. The solvent cast test pieces also formed a regular domain structure, but for these it was not possible to make a definite structural assignment. Finally an attempt was made to trace the interrelationship between the force-extension behaviour of the samples and the morphology.

INTRODUCTION

A COMPREHENSIVE study of the mechanical properties of a range of styrene/butadiene block copolymers has been reported by Holden, Bishop and Legge¹. The stress-strain behaviour and tensile strength of triplex polymers of the type $(\text{styrene})_x(\text{butadiene})_y(\text{styrene})_x$ were found to be very dependent on the percentage styrene content. At 13% styrene content the polymer was found to behave like an under-cured vulcanizate, at 27.5% styrene content the behaviour was close to that of a conventional vulcanizate, whilst between 30 and 53% styrene contents the polymer exhibited yield point followed by drawing and then an elastic extension. In an attempt to explain the properties of those copolymers having properties similar to conventional vulcanizates Aoiden *et al* proposed a two phase model in which the polystyrene end blocks formed spherical aggregates or domains (there being 600 or so blocks in each aggregate) within a matrix composed predominantly of the polybutadiene centre blocks. Thus, the model consisted essentially of a random array of hard spherical particles, which could act both as multi-functional crosslinks and as reinforcing filler, embedded in a rubbery matrix. The overall rubbery nature of the two phase system was accounted for by the fact that the rubbery components form the continuous phase. Supporting evidence for the occurrence of distinct microphase separation in styrene/butadiene block copolymers has been obtained by electron microscopy²⁻⁵.

At the start of the present investigation we carried out some preliminary measurements on $(\text{styrene})_x(\text{butadiene})_y(\text{styrene})_x$ copolymers having styrene contents of $\sim 25\%$. Whilst the results broadly confirmed the findings outlined above, we observed in addition a number of characteristics which did

not appear to be accounted for by the simple model. It was found that the mechanical behaviour of test pieces was strongly influenced by the manner in which they had been moulded. Thus, the elastic modulus, and the presence or absence of a yield point was dependent on the physical history of the test piece as well as the chain geometry and percentage styrene content. Furthermore many test pieces were found to be markedly anisotropic. To gain a clearer understanding of the interrelation between the mechanical properties of the styrene/butadiene copolymers and chain geometry we have carried out a detailed programme of structural characterization. We have already presented two preliminary reports of this work^{6,7}. At the present time we report more detailed results and attempt to explain some of the anomalies mentioned above.

EXPERIMENTAL

Materials

Two samples of copolymer of the type (styrene)_x(butadiene)_y(styrene)_x were studied both of which had been synthesized anionically using secondary butyl lithium as initiator. The first sample, *S*₁, had a real weight-average molecular weight (M_w) of 102 000 (as determined using Benoit's light scattering method⁸), and a number-average molecular weight of 84 000. A combination of u.v. and i.r. spectroscopic analyses showed the chains were composed of 34% *cis*-, 34% *trans*-, and 6% *vinyl*-polybutadiene, and a residue of 26% polystyrene. Thus for *S*₁ the weight-average molecular weights of the styrene and butadiene blocks were estimated to be 75 000 and 13 300 respectively. The light scattering data indicated that its compositional heterogeneity⁸ was relatively small and this result was confirmed by analysing a series of fractions isolated by liquid-liquid phase separation. A less detailed study of the second sample, *S*₂, gave the weight and number average molecular weights of the polymer to be 91 000 and 75 000 respectively. The weight average molecular weights of the polybutadiene and polystyrene blocks were estimated to be 71 000 and 10 000 respectively.

Preparation of test pieces

Samples were prepared in sheet form (~0.25 cm thick) either by solution-casting or compression moulding. In the casting technique a solution of the polymer was slowly evaporated on a clean mercury surface. Benzene was used as solvent for this purpose. Visual examination of the cast samples placed between crossed polaroids showed them to be optically isotropic. In the compression-moulding process the polymer in crumb form was positioned centrally in a mould, which was then inserted in a hot press thermostating at $152 \pm 2^\circ\text{C}$. After the system had reached thermal equilibrium, a nominal hydrostatic pressure of 15 MN m^{-2} was applied for ten minutes. The press was then cooled to room temperature, and the sample was stripped slowly from the mould. A severe adhesion problem initially encountered was circumvented by covering the mould with aluminium foil thinly layered with cellophane sheeting. Examination of the moulded samples using crossed

polaroids revealed a partially formed Maltese cross pattern indicating the sample was oriented having a centre of symmetry near the centre of the mould (i.e. near the position from which melt flow was initiated).

Low-angle x-ray diffraction

Initial, exploratory studies of the compression-moulded samples were carried out using a pinhole box-camera. More extensive studies of both solvent-cast (*B*) and compression-moulded (*CM*) samples, S_1 and S_2 , were carried out using a Rigaku-Denki slit-collimated low-angle camera. Copper K_α radiation ($\lambda = 0.1542$ nm) was generated by a Philips 'fine focus' tube operated at 36 kV and 20 mA; a nickel filter was used to remove K_β radiation. The main beam was collimated by means of three slits, the first two defining the overall size of the beam while the third was used to control parasitic scattering. The slit widths were 0.02, 0.01 and 0.015 cm taken in order from source to sample. The calculated beam size, 3.3×0.03 cm correlated well with that determined experimentally. The instrument was standardized with a finely powdered sample of calcium stearate, the low-angle spacing of which matched that determined previously in a wide-angle diffraction experiment. Automatic count scanning was used to check the main beam profile prior to each experiment; it was found that readjustment of the slit system was necessary at fairly frequent intervals.

Long periods were studied by two different methods. The first method involved timing a fixed number of counts over a narrow range of angles necessary to define the long period under investigation. A typical experiment entailed recording the times for a fixed count of 8000 at 30 seconds of angle intervals. In the second method the diffraction pattern was recorded on a 5 cm square of Ilford industrial 'G' film. A sample to camera distance of 25.5 cm was used. Exposure time varied from 30 minutes to 24 hours depending on which part of the diffraction pattern was being examined. Following exposure, the film was developed, washed and then air-dried for several hours. Spacings were measured directly from the negative using a Joyce-Loeble mark IIIC recording microdensitometer. Film shrinkage was found to be negligible. Of the two methods the second provided far greater freedom than the first without any significant loss in accuracy. The effect of slit smearing on the scattering curves was assessed using an infinite slit correction. A check on the correction, which lay between 3 and 10%, was afforded by comparison with the positions of diffraction peaks (maximum of 2) observed using pin-hole collimation.

Electron microscopy

Electron micrographs of ultra-thin films were obtained using an AEI EM6G electron microscope. The instrument was operated at an accelerating voltage of 100 kV, under which conditions the stated resolution was better than 1 nm. (An objective lens aperture of $50 \mu\text{m}$ was used to enhance contrast in the sample.) The instrument was calibrated at various currents and nominal magnifications using a ruled diffraction grating. The ultra-thin films were prepared by evaporating solutions of the polymer on a clean mercury surface. The concentration of the solutions used was calculated to give a film thickness

of 50 nm. Films were scooped up onto 300 mesh grids by drawing the latter slowly up through the surface using needle point tweezers. The films were stained in an identical manner by exposing the mounted grids to osmium tetroxide vapour. A glass slide covered with ten grids was suspended in a deep, closed crystallizing dish, containing a 1% aqueous suspension of osmium tetroxide. The films were stained for half an hour at room temperature and then stored in cellulose capsules. Each mounted grid was examined in the electron microscope in the following way. A scan was first made at very low magnification ($\times 500$) to check whether the film was adequately supported by the grid; it was found that film adhesion was considerably better with the shiny rather than the matt surface of the copper grids. The films were then studied at progressively higher magnifications and micrographs taken at suitable intervals. All the micrographs were obtained as glass mounted negatives. Positive prints were taken by contact to minimise distortion and magnification errors.

Tensile tests

Stress-strain experiments were carried out using a Hounsfield type E tensile testing machine fitted with an environmental chamber. The instrument consists of a straining unit coupled to a control console containing an automatic chart recorder. The test sample is held vertically in between a fixed lower grip and a mobile upper grip. The latter grip is connected to a load cell mounted on a mechanized drive cross-head bar. Simple screw-tightened clamps were used in the majority of experiments, adhesion being enhanced by applying a smear of Eastman Kodak 910 adhesive. Two load cells covering the ranges 0–10 kg and 0–100 kg were used in the investigation; the cells were calibrated before and immediately after a test had been made simply by suspending known weights from the upper tensile grip. Owing to the temperature sensitivity of the load cell it was necessary to thermostat the upper section of the straining unit to $\pm 0.1^\circ\text{C}$.

RESULTS AND DISCUSSION

Electron microscopy

Figures 1, 2 and 3 show micrographs of films prepared at increasing rates of evaporation from benzene solution. Since the osmium tetroxide preferentially stains polybutadiene due to the formation of an addition compound with olefinic bonds, dark regions are indicative of polybutadiene and light regions of polystyrene. Films prepared at both low and intermediate rates of evaporation from benzene solution showed a distinct two phase structure. At low rates of evaporation (~ 24 h) the domain morphology, i.e. the tertiary structure, obtained is a highly ordered array of uniform glassy domains embedded in a rubbery matrix. Whether these domains are spheres, prolate ellipsoids or cylinders (viewed end-on) cannot be decided from the limited two dimensional information provided by the electron micrographs. Examination of micrographs at lower magnification (see Figure 4) reveals that the films have a grain texture which constitutes a quaternary structure. The grains vary in size from about 0.07 to 5 μm . The grain boundaries are defined

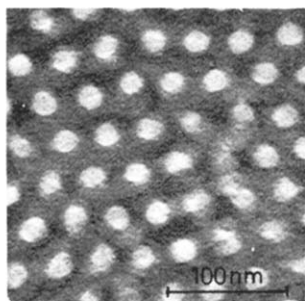


Figure 1

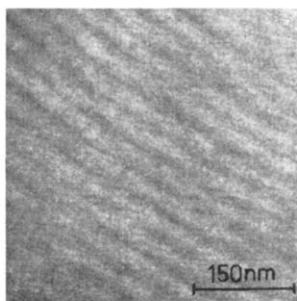


Figure 2

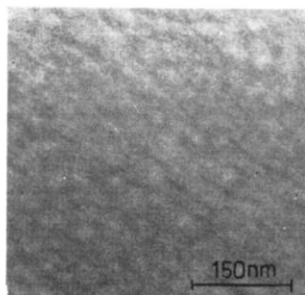


Figure 3

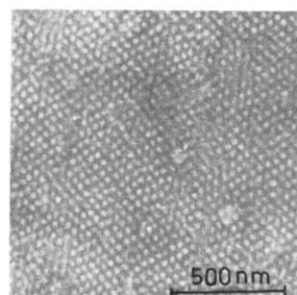


Figure 4

Figure 1 Film of sample 1 prepared at low rate of evaporation

Figure 2 Film of sample 1 prepared at intermediate rate of evaporation

Figure 3 Film of sample 1 prepared at high rate of evaporation

Figure 4 Film of sample 1 (prepared at low rate of evaporation) showing grain structure

by two types of defect; classical line defects similar to those associated with crystalline lattices and regions of incomplete phase separation.

For films isolated at intermediate rates of evaporation (~ 4 h) the morphology consists of a parallel array of cylinders or alternatively lamellae viewed end-on embedded in a rubbery matrix. It is interesting to note that because of the continuity of the glassy phase these films prove much easier to mount and were far less sensitive to stray vibrations in the microscope than those obtained at low rates of evaporation. With films prepared at high rates of evaporation (flash drying conditions) phase separation is far from complete and one is just able to discern a rather disorganised mixture of domains of various shapes and sizes. After lengthy storage at ambient temperatures these films showed no enhancement of phase separation.

In the context of the present study we feel the electron microscopy of thin films serves three main purposes:

(1) It reveals the possibility of a tertiary structure having long-range order and also the existence of a quaternary structure.

(2) It suggests a number of morphological units which are likely to occur in the bulk state, e.g. sphere, cylinder.

(3) It emphasizes that with this class of material, as is the case with crystalline polymers, the physical history plays a controlling role in determining the higher levels of structural organization.

However, in order to obtain more direct information about the state of the bulk polymer we turn to low-angle x-ray diffraction.

Low-angle x-ray diffraction and mechanical properties

The observed intensity of scatter at a given angle, 2θ , from the incident beam, will be proportional to the product $a(h)F^2(h)$, where $a(h)$ is an inter-particle interference function, $F^2(h)$ is a function which depends on the structure of the individual particles (i.e. whether cylinder, sphere etc.), and $h = 4\pi/\lambda \times \sin \theta$, where λ is the wavelength of the radiation in the medium. For a solid sphere^{9,10} of radius R ,

$$F(h) = \left[\frac{9\pi}{2} \left(\frac{J_{3/2}(hR)}{(hR)^{3/2}} \right) \right]^{1/2} \quad (1)$$

whilst for a solid cylinder^{11,12} of radius R ,

$$F(h) = \frac{2J_1(hR)}{hR} \quad (2)$$

where $J_{3/2}$ and J_1 are Bessel functions of order 3/2 and 1 respectively. Plots of $F^2(h)$ against h for both cases give rapidly damped oscillating curves; the first two minima occur at 4.43 and 7.73 for function 1 and at 3.83 and 7.02 for function 2. If the particles form a highly ordered array, the function $a(h)$ will consist of a series of sharp maxima whose positions are governed by the Bragg equation ($n\lambda = 2d \sin \theta$). For such a case sharp diffraction maxima would be observed at values of h corresponding to maxima in $a(h)$. The function $F^2(h)$ would have very little influence on these positions and would affect only the intensity of the peaks. However, if the particles form a disordered array, the maxima in $a(h)$ and hence in $i(h)$ would be diffuse and their positions would no longer coincide, because of the influence of $F^2(h)$; for the latter case the Bragg equation would no longer be directly applicable.

Compression moulded samples

Long periods are given in the first two rows of *Table 1* for the compression moulded sheets of samples 1 and 2; the values are all expressed relative to the first observed long period, d_1 , in each case. For both S_1/CM and S_2/CM , the first peak was by far the most intense and the fourth peak appeared as a shoulder on the third (see *Figure 5*). However, the third peak was slightly more intense than the second for S_1/CM , but less intense than the second for S_2/CM . The fifth peak, which was observed only for S_1/CM , was extremely weak and only just detectable.

The long period ratios, d_i/d_1 for both compression moulded samples are consistent within experimental error, with the theoretical ratios d_{hk}/d_{10} , given in *Table 2*, for a lattice composed of hexagonally packed cylinders (h.p.c.). The inter-axial distances calculated for this model are given in column

8, *Table 1* and the radii of the cylinders obtained from a knowledge of the percentage styrene content and assuming complete separation of components are given in column 10, *Table 1*. If the structural assignment is correct there are a number of diffraction peaks which are apparently missing. It seems likely that the influence of the particle scattering function $F^2(h)$ is responsible for these absences. Similar absences were studied in the work of Skoulios and colleagues for the case of ethylene oxide-polystyrene block copolymers¹³. In

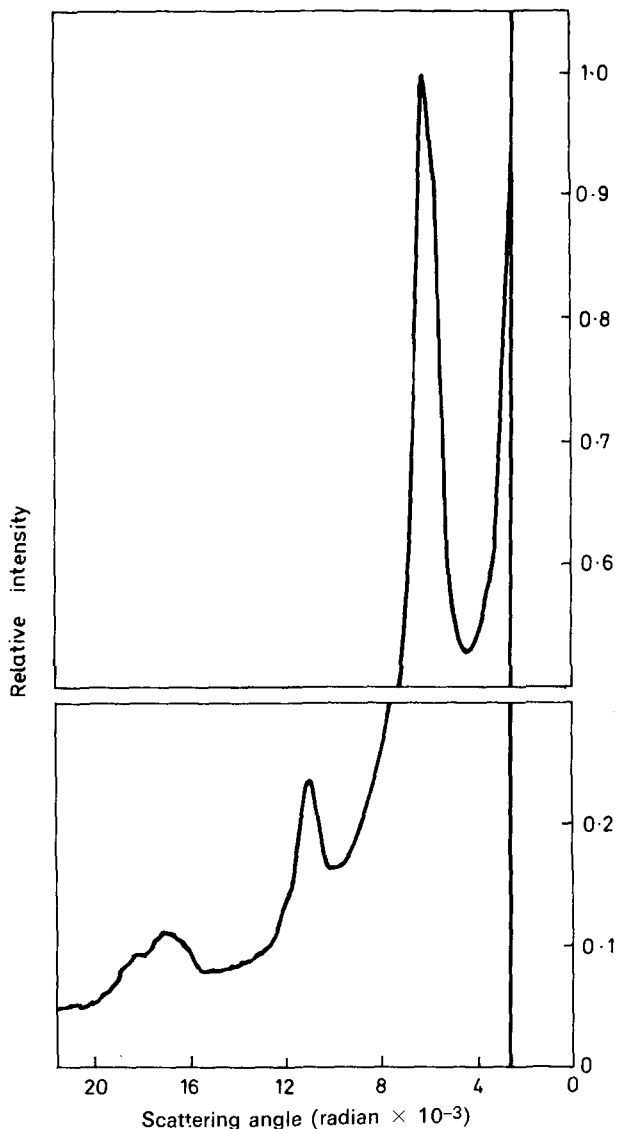


Figure 5 Plot of intensity against scattering angle for S_2/CM . The intensity of the first long-period has been set equal to unity for reference

(STYRENE)_x(BUTADIENE)_y(STYRENE)_x BLOCK COPOLYMERS

Table 1 Low angle x-ray and electron microscopy data for compression (CM) and solvent cast (B) test pieces

Sample	d_1/d_1	d_2/d_1	d_3/d_1	d_4/d_1	d_5/d_1	Assignment	$d_{int}(\text{nm})$ (x-ray)	$d_{int}(\text{nm})$ (EM)	$R(\text{nm})$ (calc)
S_1/CM	1	0.579	0.360	0.330	0.231	h.p.c.	37.5	37.0	9.5
S_2/CM	1	0.560	0.368	0.338	—	h.p.c.	28.0	33.0	6.5
S_1/B	1	0.615	0.381	—	—	f.c.c.s.(?)	40.0	43.0	13.5
S_2/B	1	0.608	0.396	—	—	f.c.c.s.(?)	31.0	34.5	10.0

Table 2 Characteristic ratios for two-dimensional lattice of hexagonally packed cylinder (h.p.c.)

d_{hk}/d_{10}	1	0.577	0.500	0.378	0.333	0.289	0.270	0.250
hk	10	11	20	21	30	22	31	40
$*d_{min}/d_{10}; S_1/CM$				0.48				0.26
$d_{min}/d_{10}; S_2/CM$				0.44				0.24

* Values represent ratios at which $F^2(h)$ would be a minimum for the calculated radii of the cylinders.

$$d_{hk}/d_{10} = [3/(h^2 + hk + k^2)]^{1/2}$$

Table 2 are given positions of the first two minima (d_{min}/d_{10}) in $F^2(h)$, calculated for the case of cylindrical units with sharp phase boundaries. Because of the simplicity of the assumed model we would not expect exact agreement between the experimental and calculated values of d_{min}/d_{10} ; from the data it appears that the latter are a little too low. However it is encouraging to find that the predicted minima all occur in the vicinity of positions for which absences have been noted. Since the d_{min}/d_{10} are somewhat higher for S_1/CM than S_2/CM it is also possible to explain why the second peak is weaker for the former sample than the latter.

That relatively few diffraction peaks are observed is accounted for by the rapid damping of the structure factor. Thus for a solid sphere the normalized intensity is reduced to one half at $hR = 1.76$ and for a solid cylinder at $hR = 1.61$, whereas for an atom of mercury the half intensity is not reached until $hR_a = 6.0$ where $R_a = 0.15$ is the apparent radius of the mercury atom.

In column 9, Table 1 are given inter-particle distances obtained from electron micrographs of thin films having morphologies of the type shown in Figure 2. The very good agreement between these values and those in column 8 is encouraging, but perhaps somewhat fortuitous in view of the fairly large calibration errors associated with the electron microscopy values ($\pm 5\%$) and the fact that the x-ray data relates to the average state in the bulk polymer, whilst the electron microscopy data relates to the state of the system at or near a surface.

A variation of diffraction intensity occurred when the compression moulded samples were rotated in a plane perpendicular to the incident beam (see Figure 6). As mentioned in our preliminary communication⁷ analysis of the behaviour indicated that grains of the tertiary lattice structure were oriented so that the axes of the cylindrical units were preferentially aligned in the direction of melt flow. A similar (but more distinct) orientation effect together with the presence of a cylindrical morphology has been reported recently by Keller for extruded samples¹⁴. The moulding technique described earlier gave sheets in which flow lines radiated out from the centre of the

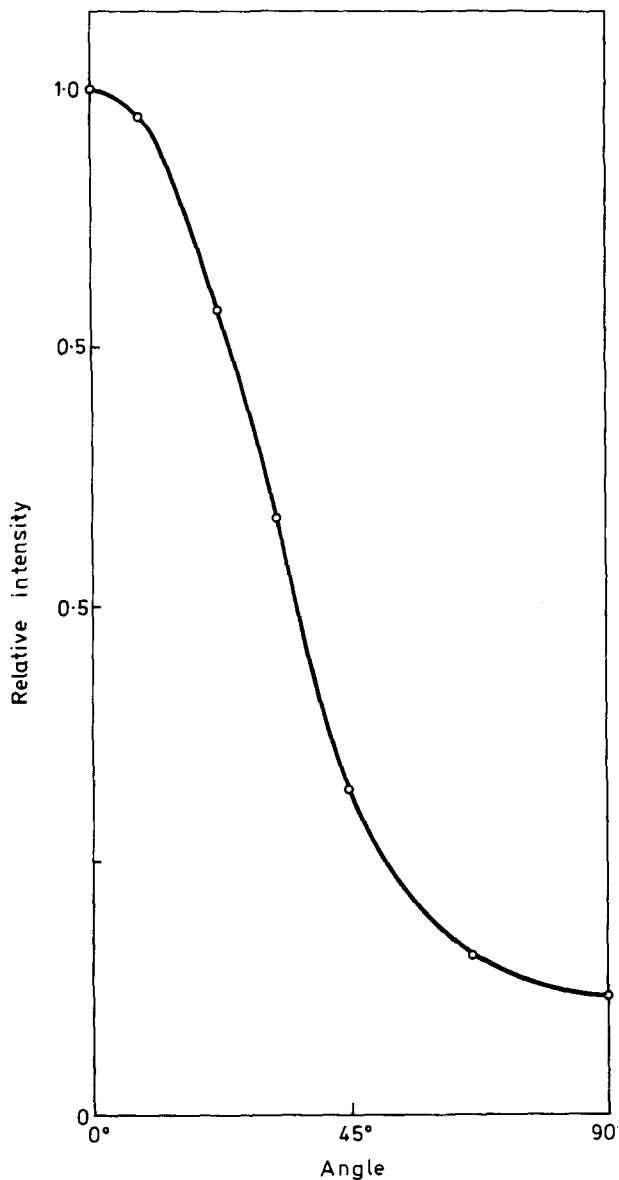


Figure 6 Variation of intensity of the first long-period on rotation of the sample in the plane perpendicular to the incident beam. The direction of melt flow corresponds to the 90° angle

mould. The degree of orientation was found to be a sensitive function of the temperature and moulding pressure. However, because of the complexity of the factors involved no attempt was made to study the orientation effect in a quantitative manner. The anisotropy of the samples was also reflected in the mechanical properties. In *Figure 7* are shown stress-strain curves for simple

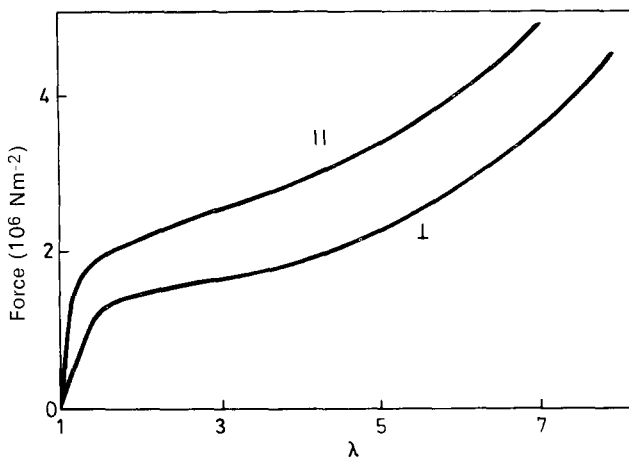


Figure 7 Force-extension curves for a compression moulded test piece of sample 2. || and ⊥ indicate extensions parallel and perpendicular to the flow lines respectively

extension taken parallel and perpendicular to flow lines in test piece *A* of sample 1. The two curves are well separated over the complete range of study; the initial moduli are 7.6 ± 0.5 and 3.6 ± 0.2 MN m⁻² respectively. Some test pieces showed a much higher degree of structural orientation than *A*. For one such sample a modulus of 210 MN m⁻² and a yield point of 3 MN m⁻² were recorded in a direction parallel to the flow lines. The mechanical properties of the compression moulded samples can be fully accounted for at least qualitatively in terms of the model assigned earlier. If we consider a single grain only, then if the strain is applied parallel to the orientation of the cylindrical units the response of the system will be dominated by the high elastic modulus of the glassy phase. For the latter case the equilibrium modulus for a polymer having 25% styrene content would be 10³ MN m⁻². At fairly low strains however, the grains would begin to respond irreversibly either by fracturing or as is more likely for the present situation by yielding and then drawing. For the case of a stress applied perpendicular to the axes of the cylindrical units the response would be characteristic of the rubbery matrix. It is important to remember that a lattice composed of glassy spherical domains embedded in a rubbery matrix would never exhibit behaviour characteristic of the domains simply because whatever strain axis was chosen would by necessity repeatedly cross from one phase to the other. Electron microscopy revealed that at the quaternary level (styrene)_x-(butadiene)_y(styrene)_x polymers consist of a neatly fitting assembly of grains. The overall properties of a given sample will therefore be influenced by the detailed structure of this mosaic, and in particular by the average orientation of the grains.

Solvent cast samples

The data for these materials were treated in a manner similar to that described in the previous section. In *Table 1* long-period ratios are recorded

for solvent cast sheets of both samples. In each case the first diffraction peak was much more intense than the other two. The third peak was rather broad and was possibly a convolution of two peaks. The long-period ratios showed small but experimentally significant differences from those observed for compression moulded samples indicating some change in the domain morphology.

From a comparison of the values of d_1/d_1 in *Table 1* with those of $d_{h,k,l}/d_{111}$ in *Table 3* it is tempting to assume that the domain morphology for both

Table 3 Characteristic ratios for a face-centred cubic lattice of spheres

d_{hkl}/d_{111}	1	0.866	0.613	0.521	0.500	0.434	0.379	0.387
hkl	111	200	220	311	222	400	331	420
$*d_{\min}/d_{111}; S_1/B$			0.59				0.34	
$d_{\min}/d_{111}; S_2/B$			0.56				0.32	

* Values represent ratios at which $F^2(h)$ would be a minimum for the calculated radii of the spheres

S_1/B and S_2/B is that of a face centred cubic lattice of spheres (f.c.c.s.). Indeed the f.c.c.s. assignment would be in keeping with the most obvious interpretation of the electron micrographs shown in *Figures 1* and *4*. The inter-domain distances, d_{int} and domain radii, R , given in columns 8 and 10 respectively of *Table 1*, have been calculated on the basis of the f.c.c.s. assignment making the same assumptions as those for the h.p.c. morphology. However, for the f.c.c.s. structure there are a number of absent reflections which we have, as yet, not been able to adequately explain and which could not simply be put down to the influence of the $F^2(h)$ function. The predicted locations of minima in $F^2(h)$ for spherical particles are given in *Table 3*. It is clearly not possible on the basis of the simple f.c.c.s. model to explain:

(1) the absence of the 200 peak which should be well removed from the first minimum in $F^2(h)$

(2) the presence of the 220 peak which might have been expected to be absent because of its proximity to the first minimum in $F^2(h)$.

Further studies are currently being carried out in an attempt to clarify the situation. For the time being however we are not able to come to any clear decision with regards to the domain morphology of the solvent cast samples.

Recent work by McIntyre and Campos-Lopez¹⁵ on a (styrene)_x(butadiene)_y-(styrene)_x polymer provides more definite low-angle x-ray evidence for spherical domains. Their structural assignment was that of a face-centred orthorhombic lattice. The copolymer investigated by them however contained a higher styrene content (36%) than those used in the present study.

The intensities of the low-angle x-ray diffraction peaks for the solvent cast sheets in contrast to the compression moulded sheets were found to be independent of the angle of rotation within the plane of the sheet. Similarly the elastic properties were found to be angularly isotropic; the initial elastic moduli for S_1/B and S_2/B were 8.4 ± 1.0 MN m⁻² and 11.3 ± 1.0 MN m⁻². On no occasion was a yield point observed for such samples; a typical force-extension curve is shown in *Figure 8*. The mechanical properties were therefore consistent with a model in which there are discrete hard domains of limited dimensions in a rubbery matrix. The isotropy of the solvent cast

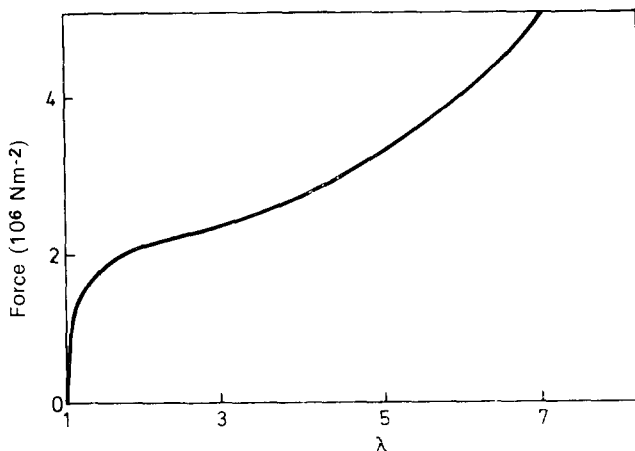


Figure 8 Force-extension curve for a solvent cast test piece of sample 2

sheets, however, indicates the existence of a randomly oriented grain structure, which is in accord with the micrograph shown in *Figure 4*. Thus on the basis of the mechanical properties it is not readily possible for this case to distinguish between a morphology based on spheres and a morphology based on cylinders.

ACKNOWLEDGEMENTS

We wish to express our gratitude to Dr J. A. Chapman and Mr S. M. W. Grunday (Dept. of Rheumatology, University of Manchester) and Dr G. W. Lorimer (Dept. of Metallurgy, University of Manchester) for the assistance they gave us with the electron microscopy, and to Dr J. Waring and Mr R. R. Sharpe (ICI Blackley) for numerous discussions and help with the low-angle x-ray scattering. We also thank the Shell Chemical Company for the supply of samples 1 and 2 (trade designations K1101 and K1102).

*Department of Chemistry,
University of Manchester,
Manchester M13 9PL, UK*

(Received 10 November 1970)

REFERENCES

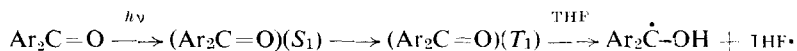
- 1 Holden, G., Bishop, E. T. and Legge, N. R. *J. Polym. Sci. (C)* 1969, **26**, 37
- 2 Hendus, H., Illers, K. and Ropte, E. *Kolloid-Z* 1967, **216**, 110
- 3 Fischer, E. *J. Macromol. Sci. (A)* 1968, **2**, 1285
- 4 Matsuo, M. *Japan. Plastic* 1968, **19**, 6
- 5 Beecher, J. F., Marker, L., Bradford, R. D. and Aggarwal, S. L. *J. Polym. Sci. (C)* 1969, **26**, 117
- 6 Lewis, P. R. and Price, C. *Nature* 1969, **223**, 494

- 7 Price, C. and Lewis, P. R. *Lab. Practice* 1970, **19**, 599
- 8 Bushuk, N. and Benoit, H. *Canad. J. Chem.* 1958, **36**, 1616
- 9 Oster, G. and Riley, D. P. *Acta Cryst.* 1952, **5**, 1
- 10 Rayleigh, Proc. Roy. Soc., 1914, **A90**, 219
- 11 Oster, G. and Riley, D. P. *Acta Cryst.* 1952, **5**, 272
- 12 Guinier, A. *Ann. Phys., Paris* 1939, **12**, 161
- 13 Skoulios, A. *Adv. Colloid Interface Sci.* 1967, **1**, 3
- 14 Keller, A., Pedemonte, E. and Willmouth, F. M. *Nature* 1970, **225**, 538
- 15 McIntyre, D. and Campos-Lopez, E. *Macromolecules* 1970, **3**, 321

Polymerization of methyl methacrylate photosensitized by benzophenones

H. BLOCK, A. LEDWITH and A. R. TAYLOR

Polymerization of methyl methacrylate (MMA) in tetrahydrofuran (THF) may be photosensitized with benzophenone, 3,3',4,4'-benzophenone tetracarboxylic dianhydride (BTDA) and 3,3',4,4'-tetramethoxy carbonyl benzophenone (TMCB) with an efficiency comparable to that of azodiisobutyronitrile as a photosensitizer. The reactions show conventional chain kinetics for radical polymerizations in which initiation involves hydrogen abstraction from THF by triplet excited sensitizer, i.e.



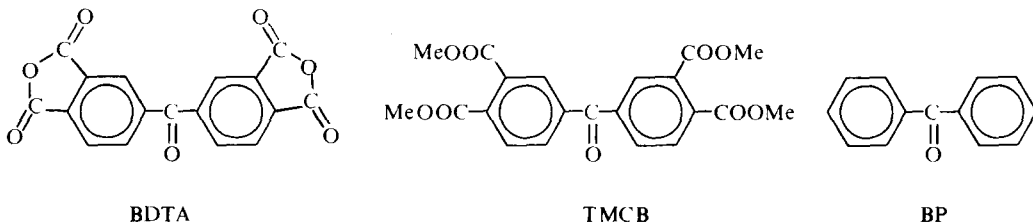
The semipinacol radicals $\text{Ar}_2\dot{\text{C}}-\text{OH}$ do not initiate (at 30°C) but act as terminating agents with an apparent efficiency increasing in the series $\text{BTDA} < \text{TMCB} \ll \text{Ph}_2\text{C}=\text{O}$. However, a detailed kinetic analysis suggests that this order results from decreasing rates (in the given order) of self dimerization of the semipinacol radicals.

THE EXPRESSION 'photosensitized polymerization' is normally taken to imply initiation of a chain polymerization process through primary absorption of light by the sensitizer rather than the monomer. Photosensitization can occur either by direct energy transfer to monomer, or by chemical reaction of photo-excited sensitizer with solvent, monomer, or other additive, to produce the initiating species. In order to describe fully the mechanism of any photosensitized chemical reaction it is necessary to have a knowledge of a number of processes. These are, the initial effect of the absorption of a quantum of light on the sensitizer molecule, the subsequent fate of the excited sensitizer molecule, the nature of the unstable intermediates formed by reaction of the excited sensitizer molecule, and finally, the sequence of molecular rearrangements caused by chemically reactive collisions of the unstable intermediates.

Benzophenone and its derivatives have become the most widely used sensitizers for organic photochemistry and both photochemical and photo-physical characteristics have been studied extensively¹. It is quite surprising therefore that benzophenones have not previously found favour as photo-initiators for free radical vinyl polymerization since both energy transfer and free radical forming, hydrogen abstraction processes are possible.

Previously we have shown² that free radical polymerization of methyl methacrylate (MMA) may be induced by sensitization via the charge transfer transitions of tetrahydrofuran/maleic anhydride complexes. The sensitization is general for ethers and unsaturated anhydrides³ and in an attempt to improve the initiating efficiency we have studied sensitization of MMA polymerization in tetrahydrofuran (THF) by the commercially important 3,3',4,4'-benzophenone tetracarboxylic dianhydride (BTDA). This compound has both an anhydride function for possible complexing, and a carbonyl group for

sensitization. However since the anhydride has rather limited solubility in most organic solvents it was convenient to study also the related ester 3,3',4,4'-tetramethoxycarbonylbenzophenone (TMCB) and for comparison purposes, benzophenone (BP).



MATERIALS

(1) Monomers

(1.1) Methyl methacrylate (MMA)

Methyl methacrylate (Hopkin and Williams, stabilized monomer) was washed 5 times with 10% v/v portions of 20% aqueous sodium hydroxide to remove the inhibitor and then with deionized water to constant pH. The monomer was dried over anhydrous calcium chloride for 1 hour then decanted onto a fresh sample of anhydrous calcium chloride and stored overnight in a stoppered flask. The dry monomer was then fractionated under reduced pressure, with a dry air bleed, through a 2.5 ft* column packed with Fenske helices. The middle fraction, boiling at 45°C under 95 mmHg was collected at a reflux ratio of 2:1.

The fractionation procedure was repeated with the middle fraction and the purified monomer was stored over molecular sieve pellets (British Drug Houses, BDH, Type 4A) at -5°C in the dark.

(1.2) Methyl acrylate (MA)

Methyl acrylate (BDH) was washed 5 times with 10% v/v portions of 10% aqueous sodium hydroxide to remove the inhibitor and then with deionized water to constant pH. The monomer was dried over anhydrous calcium chloride for 1 hour then decanted onto a fresh sample of anhydrous calcium chloride and stored overnight in a stoppered flask. The dry monomer was then fractionated under reduced pressure, with a dry air bleed, through a 2.5 ft vigreux column. The middle fraction, boiling at 47°C under 250 mmHg, was collected at a reflux ratio of 5:1. The purified monomer was stored over molecular sieve pellets (BDH Type 4A) at -5°C, in the dark.

(1.3) Styrene

Styrene (Hopkin and Williams, stabilized monomer) was washed 5 times with 10% v/v portions of 20% aqueous sodium hydroxide to remove the inhibitor and then with deionized water to constant pH. The monomer was

*1 ft = 0.3048 m

dried over anhydrous calcium chloride for 12 hours and then over calcium hydride for a further 24 hours. During the drying process, the monomer was kept under a nitrogen atmosphere to reduce oxidation by atmospheric oxygen. The dry monomer was then fractionated under reduced pressure, with a nitrogen bleed, through a 2.5 ft vigreux column. The middle fraction, boiling at 57°C under 30 mmHg was collected at a reflux ratio of 3:1. The purified monomer was stored, under vacuum, over calcium hydride at -5°C in the dark.

(1.4) *Vinyl acetate*

Vinyl acetate (Hopkin and Williams, stabilized monomer) was washed 5 times with 10% v/v portions of 2% aqueous sodium hydroxide to remove the inhibitor and then with deionized water to constant pH. The monomer was dried over anhydrous calcium chloride for 1 hour and then over calcium hydride and sodium metabisulphite for 48 hours. The dry monomer was then fractionated, with a nitrogen bleed, through a 2.5 ft column packed with Fenske helices. A good middle fraction, boiling at 73.5°C at 760 mmHg, was collected at a reflux ratio of 8:1, after discarding the first 25% of the distillate. The purified monomer was stored over calcium hydride and sodium metabisulphite at -5°C in the dark.

(1.5) *Acrylonitrile*

Acrylonitrile (Hopkin and Williams) was dried over calcium chloride for 24 hours. The monomer was then fractionated, with a nitrogen bleed, through a 2.5 ft column packed with Fenske helices. The middle fraction, boiling at 76°C at 760 mmHg, was collected at a reflux ratio of 3:1. The purified monomer was stored over molecular sieve pellets (BDH Type 4A) at -5°C in the dark.

(2) *Solvents*

(2.1) *Tetrahydrofuran (THF)*

Tetrahydrofuran (BDH stabilized with 0.1% hydroquinone) was refluxed for 24 hours over freshly ground calcium hydride. The dry THF was then fractionated through a 2.5 ft column packed with Fenske helices, the middle fraction boiling at 66.5°C was collected at a reflux ratio of 3:1. Sodium wire was added from a press and the THF was allowed to stand overnight in a stoppered flask. Fresh sodium wire was then added and the THF allowed to stand for a further 2-3 hours. The flask was connected to the vacuum line and after degassing, the THF was vacuum distilled into a storage vessel on the vacuum line. The storage vessel contained a number of small pieces of sodium and sufficient anthracene to form a 0.1% w/v solution. The THF was stored under vacuum at room temperature in this manner and a sample freshly distilled from the storage vessel gave a negative test for peroxide with ferrous thiocyanate.

(2.2) *Ethanol*

Dry magnesium turnings (2.5 g) and sublimed iodine (0.25 g) were placed in a 1 litre round bottomed flask fitted with a reflux condenser and silica gel drying tube. 50 cm³ of commercial absolute ethanol were added and the

mixture heated until all the iodine had disappeared. Heating was continued until all the magnesium had dissolved to form the magnesium ethanolate and then a further 500 cm³ of ethanol were added. The mixture was refluxed for 1 hour. The dry solvent was then fractionated through a 2.5 ft vigreux column. The middle fraction, boiling at 78°C was collected at a reflux ratio of 3:1.

(2.3) *Isopropanol*

Isopropanol (Hopkin and Williams, 'Analar' grade) was refluxed for 24 hours over freshly ground calcium hydride. The dry solvent was fractionated through a 2.5 ft vigreux column and the middle fraction, boiling at 82°C, was collected at a reflux ratio of 3:1. A small amount of sodium wire was added from a press. The solvent was stored over sodium wire and redistilled under reduced pressure immediately before use.

(2.4–2.6) *Benzene, toluene and chlorobenzene*

These were dried by refluxing over calcium hydride following by fractionation. Middle fractions collected had boiling points of 80.0, 110, and 130°C respectively.

(3) *Sensitizers*

(3.1) *Benzophenone*

Benzophenone (BDH Laboratory reagent) was recrystallized twice from 40–60°C petroleum ether to yield white crystals, m.p. 48°C (lit. 48°C).

(3.2) *3,3',4,4'-Benzophenonetetracarboxylic dianhydride*

3,3',4,4'-Benzophenonetetracarboxylic dianhydride (Aldrich Chemicals) was recrystallized twice from acetone, and dried under vacuum at 110°C to yield white crystals, m.p. 225–6°C (lit. 225–6.5°C).

(3.3) *Benzhydrol*

Benzhydrol (Hopkin and Williams) was recrystallized from petroleum ether (60–80°C b.p.) to yield white needles, m.p. 68°C (lit. 68°C).

(3.4) *Azodiisobutyronitrile*

Azodiisobutyronitrile (AIBN) (Eastman Kodak) was recrystallized 3 times from absolute ethanol by dissolving the solid at 30°C and cooling to 0°C. The resulting white crystals, m.p. 102°C (lit. 103°C) were dried at room temperature on the vacuum line and stored in an air tight jar at –5°C in the dark.

(3.5) *Benzopinacol*

Benzophenone (2 g) was added to isopropanol (50 cm³) in a large pyrex tube and the mixture shaken to dissolve all the benzophenone. The tube was stoppered and irradiated by means of a 250 watt medium pressure mercury vapour lamp for 12 hours. After a short induction period the pinacol began to precipitate. The benzopinacol was filtered off and recrystallized from absolute ethanol to yield white crystals, m.p. 186°C (lit. 170–180°C).

(3.6) 3,3',4,4'-Tetramethoxycarbonyl benzophenone

3,3',4,4'-Benzophenonetetracarboxylic dianhydride (24 g) was refluxed with methanol (200 cm³) until all the anhydride had dissolved. Anhydrous hydrogen chloride was bubbled through the solution for 3 minutes and reflux continued for a further 4 hours. The cooled solution was poured into an excess of 5% aqueous sodium bicarbonate solution, when the product separated as a sticky white solid. The product was extracted with 2 × 1 litre portions of 60% ether/40% ethyl acetate and the extracts washed with two 200 cm³ portions of deionized water. The extracts were dried over sodium sulphate and the solvent removed on a rotatory evaporator. The product was recrystallized from aqueous ethanol to yield white needles (52%), m.p. 91–92°C (lit. 91.6–93.5°C). Required for C₂₁H₁₈O₉, C, 60.6, H, 4.34%; found C, 60.4, H, 4.43%.

METHODS

Rates of polymerization

Polymerization rates were followed by conventional dilatometric techniques, the dilatometer being constructed by attaching a capillary stem to a 'lollipop' shaped reaction vessel. High vacuum techniques were used throughout; THF solvent was distilled directly from sodium/anthracene solution and MMA monomer was prepolymerized (5% conversion) by exposure to a 250 watt medium pressure mercury lamp, before final distillation. After filling and sealing, the dilatometer was placed in a constant temperature bath with transparent windows on an optical bench. Irradiation was by means of a 250 watt medium pressure mercury lamp operated from a stabilized d.c. power supply. Light from the lamp was passed through a collimator having a 5 cm diameter plano-convex lens ($f = 15$ cm), mounted with the source at its focus so as to produce a parallel beam. Short wavelength u.v. light was removed by placing a $\frac{1}{2}$ in* Pyrex glass filter in the path of the beam. The constant temperature housing and dilatometer were completely covered with a black cloth to prevent the incidence of stray light on the flat side of the polymerization vessel.

Rates of polymerization (R_p) were calculated from the standard expression

$$R_p = \frac{\pi r^2 h}{FVf} \times \frac{100}{t} \text{ (MMA) } \text{ M s}^{-1}$$

where h = fall in height of meniscus (cm) in time t (s)

r = radius of capillary (cm)

V = volume of solution (ml) in the dilatometer

f = volume fraction of monomer in the solution

F = volume contraction = $(\rho_p - \rho_m)/\rho_p \times 100$

ρ_p and ρ_m are the densities of polymer and monomer in solution, respectively and were assumed equal to those reported by Matheson *et al*⁴ for bulk monomer/polymer.

* 1 in = 25.4 mm

At 30°C F has the value 23.3% and for the polymer samples isolated from kinetic runs, the actual yield was, on average, 97.6% that calculated using this value of F . This correspondence shows that the errors involved in taking bulk values of ρ_p and ρ_m , rather than corresponding values in THF, are not significant.

Calibration of light source

The intensity of the light given out by the u.v. lamp was found to decrease with the time of running of the lamp. The lamp was calibrated, using standard samples of azodiisobutyronitrile, in 1:1 v/v mixtures of methyl methacrylate and tetrahydrofuran. The rate of polymerization was determined for three of these standard samples, at three times during the lifetime of each lamp used. The procedure adopted was the same as that used in the determination of rates of photosensitized polymerization.

Since the rate of polymerization of methyl methacrylate photosensitized by azodiisobutyronitrile is proportional to the square-root of the intensity, the square of the observed rate of polymerization is a measure of the intensity of the lamp. A plot of (rate of polymerization)² against time was constructed and the best straight line drawn. From this graph the intensity of the lamp at any time, as a function of the initial intensity, could be read off. The rates of all photosensitized polymerizations were corrected to allow for the decay of the intensity of the lamp, assuming in all cases a square-root dependence on the intensity.

Molecular weights

Molecular weights were estimated by measuring the intrinsic viscosity of polymer samples in benzene at 30°C. Values for \bar{M}_v were then calculated from the expression derived by Fox, Mason, and Cohn-Ginsberg⁵

$$\log \bar{M}_v = (\log[\eta] + 4.28)/0.76$$

Spectra

UV and visible spectra were recorded (qualitatively) by means of a Unicam SP800 spectrophotometer, and quantitatively by a Unicam SP500 spectrophotometer.

RESULTS

All three benzophenones were found to be effective photosensitizers for polymerization of MMA in THF at 30°C. Initial rates of polymerization (R_p) were determined for each sensitizer as a function of [sensitizer] and [MMA], the data being corrected for rate of polymerization in the absence of sensitizer, and for ageing of the light source. The data are summarized in *Figures 1* and *2*.

The effect of light intensity on polymerization rates was studied by interposing a series of gauze filters between the light source and the dilatometer, and data for the three sensitizers is summarized graphically in *Figure 3*.

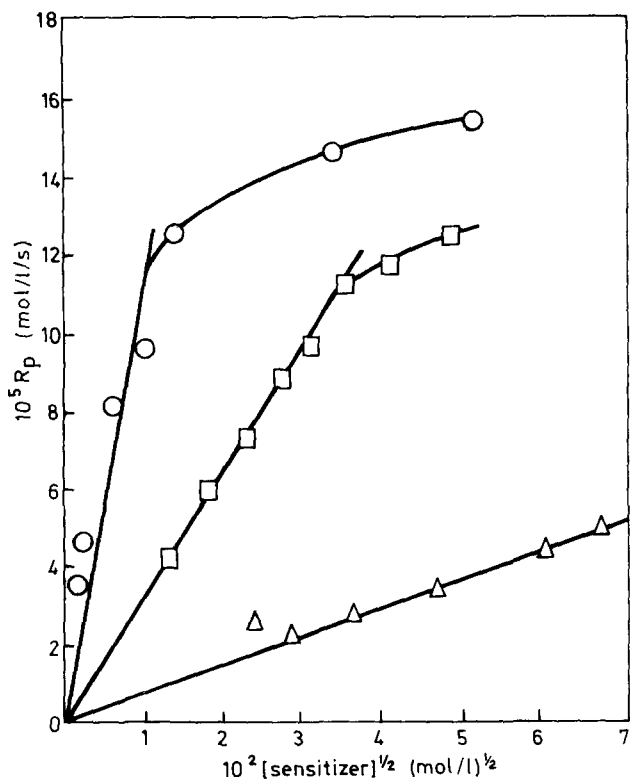


Figure 1 Polymerization of MMA in THF, sensitized by benzophenones at 30.0°C ([MMA] = 4.68 mol/l)

△ BP ○ BTDA □ TMCB

Analysis of the rate data (Figures 1-3) led to the following rate expressions

$$\frac{-dM}{dt} = K_1[\text{MMA}]^{1.02} [\text{BTDA}]^{0.49} I_0^{0.49}$$

$$\frac{-dM}{dt} = K_2[\text{MMA}]^{0.98} [\text{TMCB}]^{0.50} I_0^{0.50}$$

$$\frac{-dM}{dt} = K_3[\text{MMA}]^{0.84} [\text{Ph}_2\text{C}=\text{O}]^{0.50} I_0^{0.30}$$

During polymerization, the instantaneous rate decreased steadily as the sensitizer was consumed. Accordingly for correlations of rate with molecular weight, it was more appropriate to use average rates of polymerization rather than initial rates. The former being the numerical average of R_p over the time required for approximately 10% conversion. Data for the three benzophenones, and for AIBN are represented graphically in Figure 4, as a plot of reciprocal viscosity average molecular weight against average rate of polymerization.

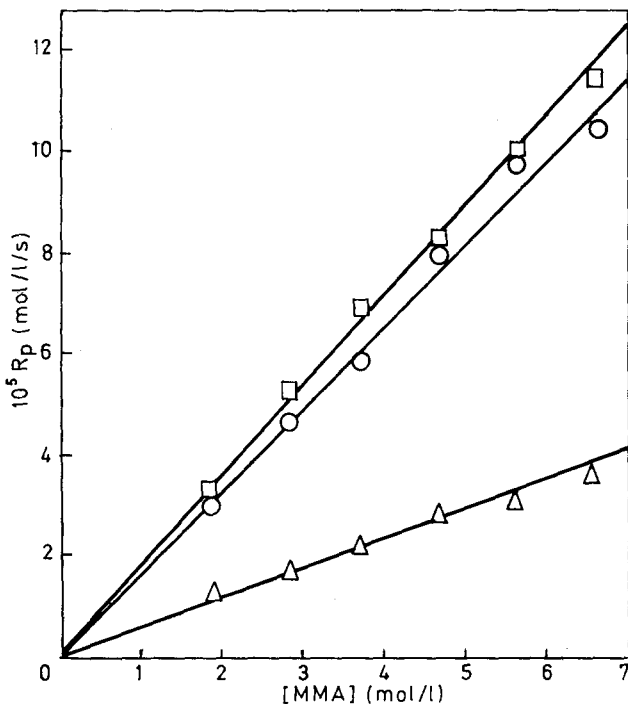


Figure 2 Polymerization of MMA sensitized by benzophenones in THF at 30.0°C [BP] = 1.32×10^{-3} mol/l, [TMCB] = 7.76×10^{-4} mol/l, [BDTA] = 6.67×10^{-4} mol/l
 \triangle BP \circ BTDA \square TMCB

From Figure 4 the straight line correlations, obtained by the method of least squares, gave rise to the following relationships:

$$\text{benzophenone, } 1/\bar{M}_v = 0.2552\bar{R}_p + (0.0481 \times 10^{-5})$$

$$\text{BTDA, } 1/\bar{M}_v = 0.0766\bar{R}_p + (0.1829 \times 10^{-5})$$

$$\text{TMBP, } 1/\bar{M}_v = 0.1465\bar{R}_p + (0.1173 \times 10^{-5})$$

Molecular weights of polymethylmethacrylate (<10% conversion) varied in an essentially linear manner with monomer concentration for all three benzophenones. Representative data are shown in Table 1.

Effect of additives on polymerization of methyl methacrylate

The gradients of the plots of reciprocal of viscosity average molecular weight against average rate of polymerization, for all the benzophenones studied, were found to be greater than that for azodiisobutyronitrile. Thus, it appears that some extra mode of termination, other than mutual termination of growing polymer radicals, is operative when benzophenones are used as photosensitizers, the effect being most pronounced in the case of benzophenone.

POLYMERIZATION OF METHYL METHACRYLATE

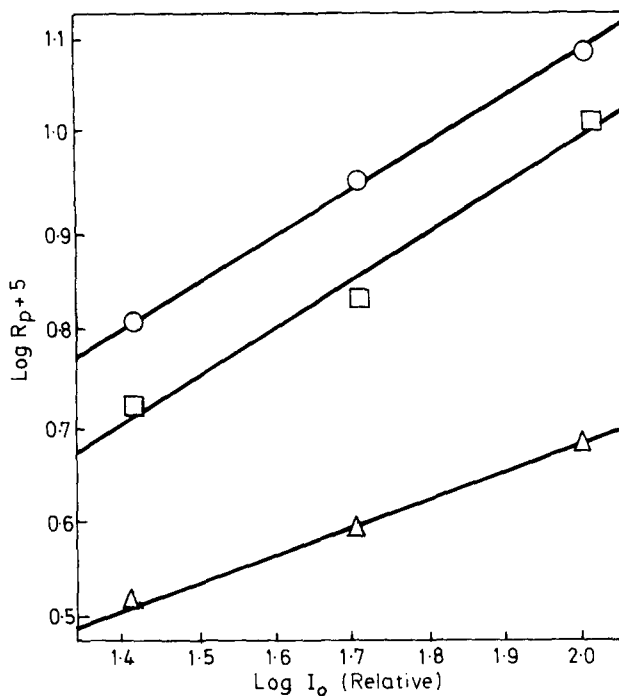


Figure 3 Effect of light intensity (I_0) on rates of polymerization of MMA in THF, sensitized by benzophenones at 30.0°C. [MMA] = 4.68 mol/l, [BP] = 1.32×10^{-3} mol/l, [BDTA] = 7.14×10^{-4} mol/l, [TMCB] = 7.36×10^{-4} mol/l
 \triangle BP \circ BTDA \square TMCB

Table 1 Photopolymerization of MMA by benzophenones at 30°C

Sensitizer	[Sensitizer] (10 ³ M)	[MMA] (M)	$[\eta]$ dl/g benzene, 30°C	$10^{-5} \bar{M}_v$
Benzophenone	1.32	6.55	0.535	1.88
		5.62	0.424	1.38
		4.68	0.348	1.07
		3.74	0.287	0.83
		2.81	0.207	0.54
		1.87	0.220	0.58
TMCB	0.74	6.55	0.441	1.46
		5.62	0.378	1.19
		4.68	0.229	0.62
		3.74	0.292	0.85
		2.81	0.239	0.65
		1.87	0.220	0.58
BDTA	0.67	6.55	0.444	1.47
		5.62	0.404	1.30
		4.68	0.332	1.00
		3.74	0.302	0.89
		2.81	0.243	0.67
		1.87	0.207	0.52

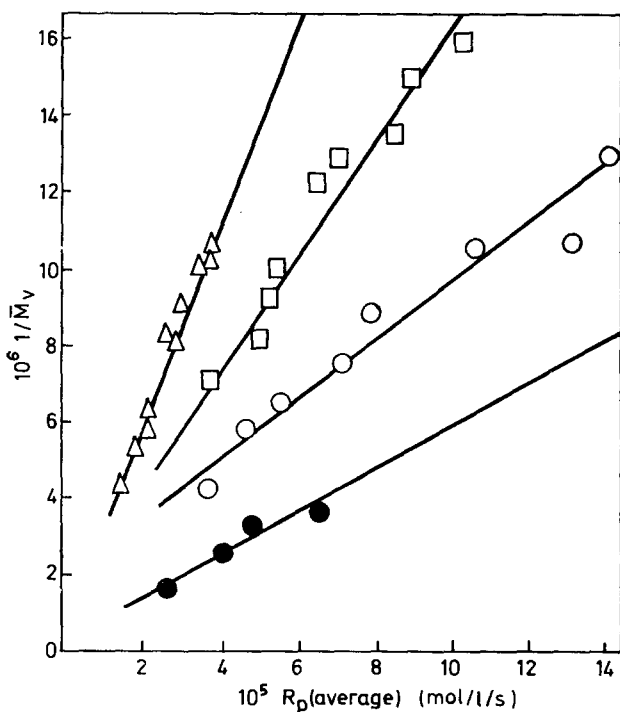


Figure 4 Variation of molecular weight with rate of polymerization of MMA in THF, sensitized by benzophenones at 30.0°C. ([MMA] = 4.68 mol/l)

△ BP ○ BTDA □ TMCB ● AIBN

A series of thermal polymerizations were carried out, at 50.0°C, using azodiisobutyronitrile as initiator, at a methyl methacrylate concentration of 4.68 mol/l. Duplicate experiments were carried out with no additive present, together with experiments in the presence of two concentrations of each of benzophenone, benzhydrol, and benzopinacol. Molecular weights of the polymers formed were determined by viscometry in benzene at 25°C, and are summarized in *Table 2*.

Table 2 Effect of additives on the free radical polymerization of MMA* in THF initiated thermally by AIBN at 50°C

Additive	[Additive] (10 ³ M)	R_p (10 ⁵ M s ⁻¹)	$[\eta]$ dl/g benzene, 25°C	\bar{M}_v × 10 ⁻⁵
none	—	5.32	1.26	5.47
none	—	5.65	1.25	5.41
benzophenone	1.79	5.54	1.25	5.41
benzophenone	7.42	5.48	1.28	5.57
benzhydrol	1.33	5.39	1.28	5.57
benzhydrol	5.54	5.65	1.23	5.33
benzopinacol	0.81	5.49	1.33	5.88
benzopinacol	4.18	5.39	1.23	5.33

* [MMA] = 4.68M

POLYMERIZATION OF METHYL METHACRYLATE

There was no appreciable reduction in either the rates of polymerization or the molecular weights of the polymers formed in the presence of any of the additives.

A further series of experiments was carried out to test the effect of different hydrogen donor solvents (*Table 3*) for benzophenone and TMCB. In each case it is apparent that a suitable hydrogen donor solvent is required for efficient photosensitization although there is some evidence for slight catalytic activity even in pure benzene solvent.

Table 3 Effect of solvents on photopolymerization of MMA* at 30.0°C

Sensitizer†	Solvent	$10^3 R_p$ ($M s^{-1}$)
Benzophenone	Benzene	0.57
	Benzene	0.51‡
Benzophenone	Benzene + Toluene§	0.80
Benzophenone	Benzene + THF§	2.00
Benzophenone	Benzene + Isopropanol§	1.57
TMCB	Benzene	1.17
	Benzene	0.51‡
TMCB	Benzene + Toluene§	2.34
TMCB	Benzene + THF§	4.11
TMCB	Benzene + Isopropanol§	4.39

* [MMA] = 4.68M

† [Sensitizer] = 8.0×10^{-4} M

‡ Reference run without sensitizer

§ Solvent additive present at a concentration of 2.0M

Polymerization of other monomers

Polymerization of styrene, acrylonitrile and vinyl acetate were attempted by photosensitization with benzophenone and TMCB. The results are summarized in *Table 4*.

Table 4 Polymerizations photo-initiated by benzophenones at 48°C

Sensitizer*	Monomer†	Solvent	$10^3 R_p$ (Initial) ($M s^{-1}$)
Benzophenone	Styrene	THF	0.61
TMCB	Styrene	THF	0.82
None	Styrene	THF	0.43
Benzophenone	Acrylonitrile	THF	13.18
TMCB	Acrylonitrile	THF	8.49
None	Acrylonitrile	THF	0.08
Benzophenone	Vinyl acetate	THF	7.82
TMCB	Vinyl acetate	THF	9.29
None	Vinyl acetate	THF	12.05
Benzophenone	Vinyl acetate	Toluene	2.30
TMCB	Vinyl acetate	Toluene	1.66
None	Vinyl acetate	Toluene	0.23

* [Sensitizer] = 8.0×10^{-4} M

† Monomers present as 50% v/v solutions

The two ketones photosensitized the polymerization of styrene and acrylonitrile in THF, and of vinyl acetate in toluene. Both appeared to retard the polymerization of vinyl acetate in THF, although in this case the rates of polymerization appeared to be unusually high.

Effect of light wavelength

A series of three filter experiments were carried out with BTDA at a sensitizer concentration of 6.67×10^{-4} mol/l, a monomer concentration of 4.68 mol/l, and a temperature of 30.0°C. Initial rates of polymerization were determined in the presence of two gauze filters (26% transmittance), a 312 nm interference filter (26% transmittance), or a blue-glass filter which transmitted between 350 nm and 420 nm. The conditions used were otherwise identical with those used for a study of variation of rate of polymerization with [monomer] for BTDA, and the results obtained are summarized in Table 5.

Table 5 Polymerization of MMA by BTDA in THF at 30°C

Filter	Transmittance (Relative, %)	10^5 Initial rate of polymerization (M s ⁻¹)
None	100	9.07
2 Gauzes	26	4.99
Interference	26 { (312 nm)	0.63
Blue Glass	~60 { (350-420 nm)	4.29

[MMA] = 4.68M [BTDA] = 6.67×10^{-4} M

Appreciable polymerization occurred with the 365 nm line of the mercury vapour lamp isolated, but the amount of polymerization with the 313 nm line isolated was small. Allowing for the fact that the transmittance at this wavelength was only 26%, the rate of polymerization was of the same order as the rate of polymerization in the absence of sensitizer. The result of the experiment with two gauze filters gave an intensity exponent of 0.44, in reasonable agreement with the value of 0.49 obtained from Figure 3.

UV absorption spectra of benzophenones

UV absorption spectra of benzophenone, BDTA and TMCB in the region 300-450 nm, are shown in Figure 5 for solutions in THF. There are only minor variations in absorbance for the three sensitizers in the readily accessible photoactive area centred around 366 nm. The anhydride has an additional band centred around 310 nm but this does not appear to be photochemically active (see Table 4). Solvent effects in the absorbance maxima were very similar (Table 6) indicating that the long wavelength transitions were of the $\pi^* \leftarrow n$ type in all cases.

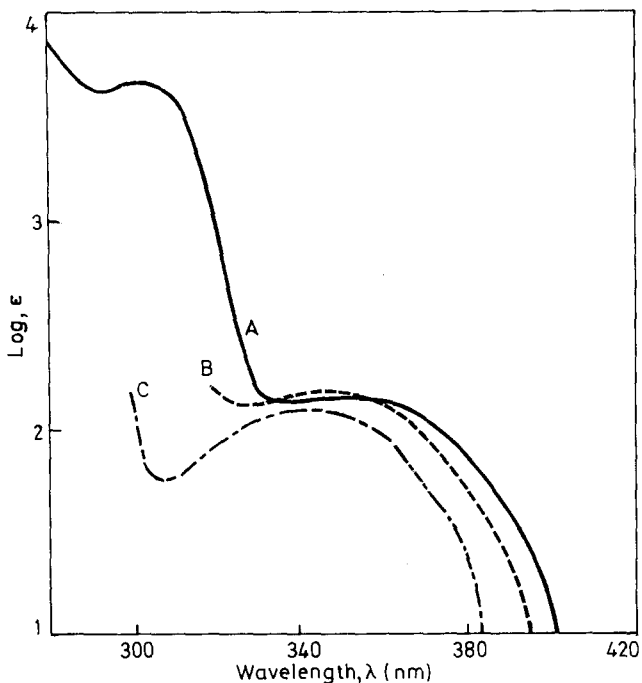


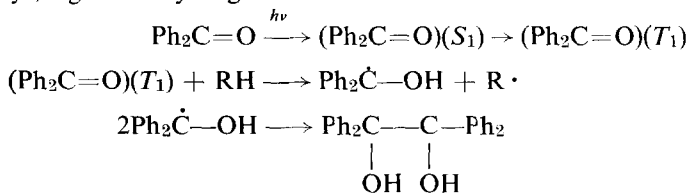
Figure 5 Absorption spectra of benzophenone in THF at 30.0°C
A Benzophenone B BTDA C TMCB

Table 6 Absorption spectra of benzophenones

Solvent	Carbonyl compound		
	Ph ₂ C=O	BTDA	TMCB
CH ₃ OH	λ _{max} (nm)	331	341
	ε(M ⁻¹ cm ⁻¹)	154	150
THF	λ _{max} (nm)	344	301; 350
	ε(M ⁻¹ cm ⁻¹)	132	4630; 143
CH ₂ Cl ₂	λ _{max} (nm)	339	302; 353
	ε(M ⁻¹ cm ⁻¹)	143	5200; 170

DISCUSSION

Benzophenone has a lowest energy electronic transition of π*←n character and yields the lowest energy triplet excited state (T₁) with unit quantum efficiency¹, e.g. for a hydrogen donor solvent:



The precise fate of the radicals $\text{Ph}_2\dot{\text{C}}-\text{OH}$ and $\text{R}\cdot$ depends upon the particular reaction conditions, but in all cases benzpinacol [$\text{Ph}_2\text{C}(\text{OH})\text{C}(\text{OH})\text{Ph}_2$] is a major reaction product.

Hydrogen donor solvents useful in this type of photo-oxidation include alcohols and ethers, for which the quantum yields for photopinacolization are essentially unity. Efficient photo-reduction by alcohols and ethers appears to require $\pi^*\leftarrow n$ character of the reacting triplet excited carbonyl compound and, from the data in *Table 6*, this would be anticipated for the sensitizers used in the present work.

In THF all three carbonyl compounds photosensitized the free radical polymerization of MMA and experiments with filtered light (*Table 5*) established that initiation was most efficient when exciting via the $\pi^*\leftarrow n$ band of the ketone (366 nm irradiation). The additional (carbonyl) chromophore at ~ 300 nm, present in BTDA and TMCB, was apparently unimportant. Polymerizations were studied in conventional dilatometers with vacuum outgassing; rates of polymerization were reproducible to within 10% and the presence of air or oxygen had a retarding effect.

For benzophenone, BTDA and TMCB, linear plots for rate of polymerization against $[\text{sensitizer}]^{1/2}$ were obtained. In the case of BTDA and TMCB, the plots were linear up to a limiting sensitizer concentration, after which the rate of polymerization became less dependent on sensitizer concentration (*Figure 1*), possibly due to self quenching. BTDA and TMCB would be expected to have lower triplet state energies than benzophenone and this might account for the more efficient self quenching process observed for the former compounds.

It can be seen that the rates of polymerization obtained at the same concentration of each sensitizer differ considerably. Relative rates of polymerization for each photosensitizer were determined from the least squares plots for rate of polymerization against $[\text{sensitizer}]^{1/2}$ and are summarized in *Table 7*.

Table 7 Photopolymerization of MMA in THF at 30°C by benzophenones

Sensitizer	Rel. rate	$k_p/k_t^{1/2}(1 + \alpha)^{1/2}$ ($\text{M}^{-1/2} \text{s}^{-1/2}$)	ϵ_{366} (THF) ($\text{M}^{-1} \text{cm}^{-1}$)	$\alpha = k_t'/(k_t k_c)^{1/2}$
Benzophenone	1.00	0.0306	72	3.62
TMCB	4.44	0.0404	112	1.65
BTDA	7.24	0.0559	122	0.39
(AIBN)		(0.0658)		(0)

Molecular weights of polymers formed using benzophenones as photosensitizers were much less than the molecular weights of polymers formed at comparable rates of polymerization using azodiisobutyronitrile as photosensitizer. For all photosensitizers, linear plots of $1/\bar{M}_v$ against average rate of polymerization, \bar{R}_p , were obtained (*Figure 4*). From the gradients of these plots, apparent values of $k_p/k_t^{1/2}$ were calculated and were observed to parallel corresponding relative rates, as summarized in *Table 7*.

For experiments in which the monomer concentration was varied, the time of polymerization for each sensitizer was kept constant at each monomer concentration. This procedure was adopted to ensure that the decay of

sensitizer, and hence of rate of initiation, was constant throughout each series of experiments. Reasonable linear plots of \bar{M}_v against monomer concentration could be obtained for each sensitizer from the data in *Table 1*, the scatter of experimental points being somewhat greater in the case of benzophenone and TMCB than for BTDA.

The pattern of rates of polymerization and molecular weights obtained is characteristic of a free-radical polymerization reaction, although some additional complicating reactions appear to occur. Data in *Table 2* show that benzophenone, benzhydrol, and benzopinacol had no effect on the rate of thermal initiated free radical polymerization, or the molecular weight of the polymers formed, suggesting that the reduction in molecular weight is caused by an intermediate formed in the initiation reaction.

For all three benzophenones, the rate of polymerization decreased rapidly with time as the sensitizer was consumed, and conversion against time data for all benzophenones gave a reasonable fit with an expression of the form

$$\frac{[\text{MMA}]_0 - [\text{MMA}]_t}{[\text{MMA}]_0} - C_1 t = C_2(1 - e^{-C_3 t})$$

where C_1 , C_2 , and C_3 are constants. C_3 is an apparent first order rate coefficient for loss of sensitizer and values of $10^2 C_3$ for BP, BTDA, and TMCB were 0.80, 1.7, and 1.9 min^{-1} respectively.

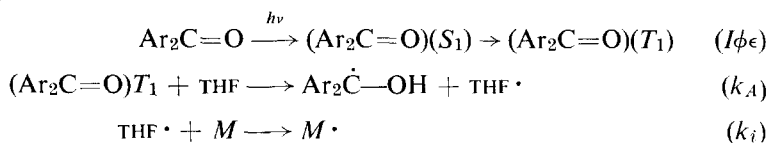
Several series of experiments were carried out to show that photosensitization by benzophenones occurred in solvents other than tetrahydrofuran and with monomers other than methyl methacrylate.

Polymerizations carried out in 2 mol/l solutions of toluene, tetrahydrofuran, and isopropanol, in benzene using benzophenone and TMCB (*Table 3*) as photosensitizers showed that photosensitization also occurred in these solvents. It would appear that the solvent must have an abstractable hydrogen atom for effective photosensitization to occur, as indicated by the very poor activity in pure benzene.

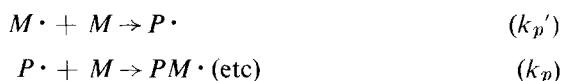
Both benzophenone and TMCB were shown to photosensitize the polymerization of acrylonitrile and styrene in tetrahydrofuran (*Table 4*). With vinyl acetate large amounts of polymer were formed in tetrahydrofuran but no photosensitization took place. However photosensitization was observed in toluene solvent.

A mechanism consistent with most of the experimental observations is shown below

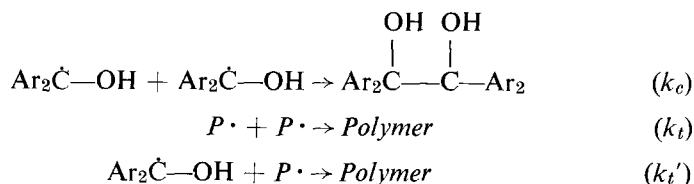
Initiation



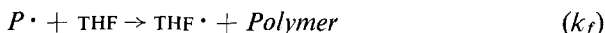
Propagation



Termination



Transfer



Initiation by semipinacol radicals $\text{Ar}_2\dot{\text{C}}-\text{OH}$ appears to be unimportant except possibly at higher temperatures⁶ and termination or transfer involving the benzophenone or benzopinacol are not considered because, at least for benzophenone itself, these species have no effect on rate of polymerization or the molecular weight of polymers formed (*Table 2*).

Applying conventional steady state kinetic treatment, assuming $k_p' = k_p$, and solving for $[P\cdot]$ it may be shown that

$$[P\cdot] = \frac{(I_0\phi\epsilon)^{1/2}[\text{Ar}_2\text{C}=\text{O}]^{1/2}}{k_t^{1/2}(1 + \alpha)^{1/2}}$$

where I_0 = intensity of incident irradiation

ϕ = quantum yield for production of radicals

ϵ = molar extinction coefficient of sensitizer at the wavelength employed

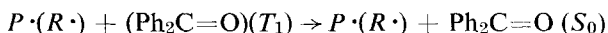
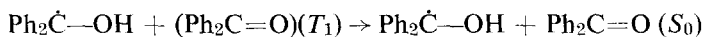
$$\alpha = k_t'/(k_t k_c)^{1/2}$$

Monomer is consumed mainly in the propagation reaction

$$\begin{aligned} \therefore \frac{-d[M]}{dt} &= k_p[M][P\cdot] \quad \text{and substituting for } [P\cdot] \\ \frac{-d[M]}{dt} &= \frac{k_p}{k_t^{1/2}(1 + \alpha)^{1/2}} (I_0\phi\epsilon)^{1/2}[M][\text{Ar}_2\text{C}=\text{O}]^{1/2} \end{aligned}$$

The derived kinetic equation is in good agreement with the experimentally determined relationships for BTDA and TMCB. For benzophenone the monomer exponent of 0.84 is almost within experimental error of the predicted value of 1.0, and a linear plot of rate against concentration of monomer can be obtained within the 10% error limit for each rate determination. The intensity exponent of 0.30 is outside the probability range of experimental error and indicates that the above reaction scheme does not completely describe the mechanism of polymerization, at least in the case of benzophenone.

Testa⁷ and Yang and Murov⁸ have observed that the quantum yield of benzophenone reduction in isopropanol decreases with increasing light intensity. The latter workers explained this observation by postulating the quenching of the triplet state of benzophenone by paramagnetic radical intermediates in the reaction, e.g.



Inclusion of reactions such as these in the reaction scheme could explain the low intensity dependence found for benzophenone although it is not clear why the benzophenone triplet and/or its semipinacol radical are so much more reactive in this sense, than the corresponding derivatives of BTDA and TMCB. A further complication arises from the possibility that termination may involve hydrogen transfer rather than the direct combination shown above, e.g.

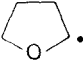


It is not yet possible to estimate the significance of this process for the three carbonyl sensitizers, but regeneration of sensitizers via termination reactions would increase the complexity of reaction mechanisms. In this way it is possible to understand the apparent differences in rates of consumption of sensitizer reflected in values of C_3 quoted above.

Undoubtedly the most striking feature of the polymerizations was the great difference in relative rates and molecular weights observed for the different carbonyl sensitizers (*Table 7*). For benzophenone ϕ is unity¹ hence the increased rates with BTDA and TMCB must be due to other factors. Some of the rate differential may be ascribed to differences in light absorption characteristics (ϵ), but it is apparent that the various semipinacol radicals show markedly different rates of either self combination (k_c), or combination with growing polymer radicals (k_t'). Independent photo-initiated polymerizations with AIBN under identical conditions yielded a value for $k_p/k_t^{1/2} = 0.0658$, in good agreement with other values in the literature⁹, and it can be seen (from *Table 7*) that only the anhydride gives molecular weights approaching these to be expected from a typical free radical polymerization.

Both rates and molecular weights are inversely proportional to a which in turn reflects the ratio k_t'/k_c . It does not seem reasonable that the various semipinacol radicals ($\text{Ar}_2\dot{\text{C}}\text{—OH}$) should show marked differences in their rates of combination with growing polymer radicals and hence there would appear to be some special factors facilitating self combination of semipinacol radicals in the case of BTDA and TMCB. Conceivably hydrogen bonding between the semipinacol radicals of BTDA and TMCB could promote more rapid self dimerization. This would not be possible for benzophenone and apparently enhanced termination by $\text{Ph}_2\dot{\text{C}}\text{—OH}$ would result, as observed experimentally. Alternatively more efficient hydrogen transfer from $\text{Ph}_2\dot{\text{C}}\text{—OH}$ could explain the results (see discussion above).

It is interesting that polymerization of vinyl acetate was not photosensitized by the benzophenone/THF systems. In all cases the proposed

mechanism involves initiation by reaction of the  radical with polymerizable monomer. This species is very similar to a typical α -alkoxy carbon radical formed during free radical polymerization of alkyl vinyl ethers (i.e. $\text{RCH}_2\text{—}\dot{\text{C}}\text{HOR}'$), and free radical copolymerization of vinyl acetate and alkyl vinyl ethers does not occur to any detectable extent,

indicating that α -alkoxy carbon radicals do not add at a significant rate to vinyl acetate monomer. The present observations on initiation of vinyl acetate polymerization are entirely consistent with this result and confirmation is provided by the observed photosensitization when toluene was used as solvent and hydrogen donor. In this case the initiating radicals would be benzyl radicals ($\text{PhCH}_2\cdot$) similar to those formed during free radical polymerization of styrene, a monomer readily copolymerized with vinyl acetate. The data of *Table 4* show that benzophenone is apparently a better photo-initiator for acrylonitrile polymerization than is TMCB, in marked contrast to the behaviour with methyl methacrylate. It is conceivable that this results from additional activity involving direct triplet state energy transfer from benzophenone to acrylonitrile¹⁰; as noted earlier, the lowest triplet level of TMCB would be expected to be lower than that for benzophenone and the polymerizing monomers.

In conclusion, it may be stated that benzophenones may be used as photo-initiators for the polymerization of MMA in hydrogen donor solvents with initiator efficiencies comparable to that of AIBN. However, depending on the substituents present in the aryl groups, the semipinacol radicals formed in the initiation processes, may act as efficient terminating species.

ACKNOWLEDGEMENT

The authors are indebted to S.R.C. for a Research Studentship (A.R.T.).

*Donnan Laboratories,
Department of Inorganic, Physical
and Industrial Chemistry,
University of Liverpool, UK*

(Received 3 November 1970)

REFERENCES

- 1 Turro, N. J., 'Molecular Photochemistry', Benjamin, New York, 1965; Neckars, D. C., 'Mechanistic Organic Photochemistry', Reinhold, New York, 1967
- 2 Bawn, C. E. H., Ledwith, A. and Parry, A. *Chem. Comm.* 1965, p 490; Ledwith, A. and Sambhi, M. *J. Chem. Soc. (B)* 1966, p 670
- 3 Ledwith, A., Parry, A. and Sambhi, M. (paper submitted to *Polymer*)
- 4 Matheson, M. S., Aner, E. E., Bevilacqua, E. B. and Hart, E. J. *J. Amer. Chem. Soc.* 1949, **71**, 500
- 5 Cohn-Ginsberg, E., Fox, T. G. and Mason, H. F. *Polymer, Lond.* 1962, **3**, 97
- 6 Braun, von D. and Becker, K. H. *Angew. Makromol. Chemie*, 1969, **6**, 186
- 7 Testa, A. C. *J. Phys. Chem.*, 1963, **67**, 1341; see also Rubin, M. B. *Tetrahedron Letters*, 1969, p 3931
- 8 Yang, N. C. and Murov, S. *J. Amer. Chem. Soc.* 1966, **88**, 2852
- 9 Bamford, C. H., Barb, W. G., Jenkins, A. D. and Onyon, P. F., 'The kinetics of vinyl polymerization by radical mechanisms', Butterworth, London, 1958
- 10 Hosaka, S. and Wakamatsu, S. *Tetrahedron Letters*, 1968, p 219

Statistical thermodynamics of solutions of polymers in mixed solvents

MISAZO YAMAMOTO*, JAMES L. WHITE† and DONALD L. MACLEAN

An improved statistical thermodynamic theory of polymers dissolved in mixed solvents has been devised. In particular a rather general lattice formulation of the partition function has been used to take into account: (1) preferential gathering of the good solvent about the polymer chains and (2) incorporation of volume effects, allowing consideration of the variation of specific volume with temperature, pressure and mixing conditions. The former effect is analysed by two methods: (a) consideration of a good solvent monolayer forming about the polymer chains and (b) quasi-chemical method. The first approach is developed in some detail. The volume effect is accounted for through lattice vacancies.

INTRODUCTION

THE THERMODYNAMIC characteristics of solutions of polymers in mixed solvents and the nature of phase equilibrium in such systems is of great interest to polymer physical chemists who must frequently rely on such properties to fractionate polydisperse materials. Indeed the important fractionation methods of fractional precipitation¹ and Baker-Williams precipitation chromatography^{2,3} are based upon phase equilibrium in such multi-component systems.

The basic method of evaluating the thermodynamic properties of polymer solutions has been through the generalization of the lattice method to long chain molecules, a development which may be progressively seen in the papers of Fowler and Rushbrooke⁴, Meyer⁵, Huggins⁶, Flory⁷⁻¹⁰, Scott and Magat^{11,12} and Gee^{13,14}. It was Flory⁸ and Scott and Magat who first considered polydisperse polymers and Gee and Scott and Magat who explicitly developed expressions, based upon the lattice theory, for the thermodynamic properties of a polymer dissolved in a mixture of two solvents. Gee and Scott and Magat not only developed expressions for the free energy of mixing but treated various thermodynamic characteristics of such solutions, with Scott¹² analysing phase equilibria in some detail. A basic assumption of the lattice theories of polymer solutions is the random arrangement of the molecules of the constituents on the lattice with the sole restriction that the various segments of the polymer molecules are tied together to form linear chains. For mixed solvents, the lattice theory analyses (i.e. those of Gee and Scott and Magat) are based upon this type of model and the sea beyond the individual polymer chains stretching from their nearest neighbours to the furthest molecule is presumed to consist of a uniform random mixture. In

*Permanent address: Department of Physics, Tokyo Metropolitan University, Setagaya-ku, Tokyo, Japan

†To whom all correspondence should be addressed

addition to the random mixing assumption, these lattice models are also limited in that they do not allow for variations in volume due to mixing effects and changes in external pressure.

The success or failure of a theory of polymer solutions depends upon how well the model of the theory represents reality and whether the mode of analysis is sufficiently sophisticated to give results within the degree of approximation desired. The study of polymers in mixed solvents began in the last century with the development of collodion – a solution of cellulose nitrate in an alcohol–ether mixture. (This polymer would not dissolve in either pure alcohol or pure ether). In 1896, H. Kneebone Tompkins presented a dissertation in which he studied the swelling of vulcanized rubber in a solution of carbon disulphide and acetone and found that the composition of the solvent mixture within the rubber was different from that in the external liquid, the former being richer in carbon disulphide, the better solvent. More extensive observations of this phenomenon in other vulcanizate–solvent systems have been made by Krigbaum and Carpenter¹⁶ and Bristow¹⁷. If this preferential absorption occurs within vulcanizates, it should similarly occur around isolated macromolecules in solution. This has been pointed out by Ewart and his colleagues^{18,19} who have noted that this gathering of good solvent causes complications in the analysis of light scattering experiments, and they have suggested means of remedying such difficulties. The various theories of polymers dissolved in mixed solvents described in the previous paragraph are not able to deal with the Tompkins Effect. Papers by Krigbaum and Carpenter¹⁶ and Shultz and Flory²⁰ have however considered the Tompkins Effect for swollen vulcanizates and isolated polymer chains. However, the methods of these papers cannot deal with the concentrated solution case.

In this paper we will derive a new and more general theory of polymer solutions in mixed solvents. The analysis will be based upon a lattice formulation and a constant pressure ensemble. Utility of such an ensemble readily allows consideration of holes in the lattice and their variation with pressure and temperature; therefore, volume effects may be considered. In the following section, we will develop a general lattice formulation of this problem. We will then consider special cases. First we will treat a model consisting of a random distribution of solvent molecules, holes, and a polydisperse polymer in the lattice. In succeeding sections, we will consider the ordering phenomenon which leads to the Tompkins Effect. A companion paper treats the excluded volume effect in dilute polymer solutions with mixed solvents²¹.

GENERAL FORMULATION

Our basic approach consists of computing the constant pressure ensemble partition function Z for a lattice model containing N_0 sites of which $N_p \bar{M}$ are of polymer, N_1 are of solvent 1, N_2 are of solvent 2, and N_h are lattice vacancies or holes. Each of the solvent molecules is taken to occupy a single lattice site while the polymer chains will occupy a series of adjacent sites. The polymer is considered to be polydisperse so that the N_p molecules consist of a mixture of species with varying numbers of segments. We may

summarize this by

$$N_p = \sum_{M=1}^{\infty} N_{pM}; \quad N_p \bar{M} = \sum_{M=1}^{\infty} N_{pM} M \quad (1)$$

where \bar{M} is the number average number of segments or degree of polymerization. The lattice has a coordination number z , while the polymer molecules restricted by the tetrahedral nature of the carbon-carbon bonds in the polymer backbone occupy a sub-lattice with coordination number $z_p \sim 4 < z$. The backbone bonds have the choice of either *gauche* (g^+ or g^-) or *trans* conformations. We shall assume as in Flory's 1956 treatment of lattices of semi-flexible chains¹⁰ and Oka's model of isolated chains^{22,23} that the bond rotation potential of each carbon-carbon bond is independent of that of any other bond. Thus restricted conformations such as the g^+g^- pentane effect²³ are not excluded from our model. We shall further presume, at least at this point, that each bond potential function in the polymer is symmetric about the *trans* form and further that all such bond potential functions are identical. This essentially restricts our treatment to polyethylene or polyethylene-like molecules for if we take a symmetric bond potential function with two equal *gauche* positions (with energy ϵ_G) and a lower energy *trans* conformation (with energy $\epsilon_T < \epsilon_G$), the polymer will tend to crystallize into an all *trans* zig-zag structure. Isotactic polymers on the other hand crystallize into helical forms; and form a *gttgt* structure. It follows that the bond rotational energy function varies from bond to bond in this type of polymer, but the bond rotation function for alternate bonds is essentially the same. It will be shown, however, that the above restrictions on flexibility while affecting the general partition function do not affect the free energy of mixing of amorphous polymers.

With the above remarks in mind, we are now in a position to evaluate the partition function, which is defined by

$$\begin{aligned} Z &= \sum_{N_h} \exp(-pv_0 N_0/kT) Q(N_p, N_1, N_2, N_h, T) \\ &= \sum_{N_h} \sum_j \Omega_j(N_p, N_1, N_2, N_h, E_j) \exp(-pv_0 N_0/kT) \exp(-E_j/kT) \end{aligned} \quad (2a)$$

and

$$G = U + pV - TS = -kT \ln Z \quad (2b)$$

where p is the pressure and Ω_j is the total number of configurations available to the system compatible with fixed values of N_p, N_1, N_2, N_h , and E_j . Here E_j is the total energy of the system which may be expressed (compare White and Yamamoto²⁴) as

$$\begin{aligned} E_j &= N_p \bar{M} \epsilon_p^i + N_1 \epsilon_1^i + N_2 \epsilon_2^i + E_{\text{sol}} \\ &+ \sum_M \sum_f N_{pMf} [f \epsilon_G + (1-f) \epsilon_T] (M-1) \end{aligned} \quad (3)$$

where the last term on the right hand side represents the bond rotation or 'flex' energy, E_{sol} is the energy of solution, f represents the fraction of the bonds in a particular chain in the *gauche* conformation, and N_{pMf} represents the number of such chains with M segments or units.

Following the methods of White and Yamamoto²⁴ and placing one polymer chain at a time into the lattice, followed by the N_1 solvent 1 molecules and the N_2 solvent 2 molecules, the partition function Z may be expressed

$$\begin{aligned} Z &= q_1^{N_1} q_2^{N_2} q_p^{N_p \bar{M}} \sum_{N_h} \exp(-pv_0 N_0/kT) \Omega_{\text{sol}} \prod_{M=1}^{\infty} \prod_{f=0}^{M-1} \frac{1}{N_{pMf}!} \\ &\times \prod_{a=1}^{N_{pMf}} \frac{(M-1)!}{2[f(M-1)]![(1-f)(M-1)]!} \nu_{Mfa} \exp(-E_{\text{sol}}/kT) \\ &\times \exp\{-(M-1)[f\epsilon_G + (1-f)\epsilon_T]/kT\} \end{aligned} \quad (4)$$

where q_1 , q_2 , and q_p are the internal partition functions of molecules of solvent 1, solvent 2, and polymer segments, Ω_{sol} is the number of possible arrangements of solvent molecules once the polymer chains are in the lattice, N_{pMf} is the number of polymer chains with M units and f flexed bonds, and ν_{Mfa} is the number of possible lattice conformations for the a th chain with M units and f flexed bonds. The quantity ν_{Mfa} will be

$$\nu_{Mfa} = (N_0 - \sum_M N_{pM} M) z (z_p - 2)^f (M-2) \prod_{s=2}^M (1 - \delta_{as}) \quad (5)$$

with δ_{as} being the probability that the s th lattice site in a chain is occupied. Substitution of equation (5) into equation (4) yields

$$\begin{aligned} Z &= q_1^{N_1} q_2^{N_2} q_p^{N_p \bar{M}} \{1 + (z_p - 2) \exp[-(\epsilon_G - \epsilon_T)/kT N_p (\bar{M}-1)]\} \\ &\times \exp[-N_p (\bar{M} - 1) \epsilon_T/kT] \frac{(z/2)^{N_p}}{\prod_M N_{pM}!} \sum_{N_h} \exp(-pv_0 N_0/kT) \\ &\times \sum_j g(N_1, N_2, N_{pM}, N_h, E_{\text{sol}}) \exp(-E_{\text{sol},j}/kT) \end{aligned} \quad (6)$$

where

$$g = \Omega_{\text{sol}} \prod_{a=1}^{\infty} \prod_{M=1}^{N_{pMf}} (N_0 - \sum_M N_{pM} M) \prod_{s=2}^M (1 - \delta_{as}) \quad (7)$$

The basic problem of computing the partition function Z is the determination of the factors δ_{as} , Ω_{sol} , and E_{sol} .

RANDOM POLYMER SOLUTION

The simplest model of polymer solutions involves presuming a completely random structure. We hypothesize then (1) equal probability of occupancy of lattice sites available to polymer segments and thus no gathering of polymer and (2) random occurrence of '1' and '2' molecules and holes in the remainder of the lattice and thus no gathering of solvent. It follows that

$$\delta_{as}(\text{independent of } s) = \sum N_{pM} M / N_0 \quad (8a)$$

and

$$\Omega_{\text{sol}} = \frac{[N_1 + N_2 + N_h]!}{N_1! N_2! N_h!} \quad (8b)$$

and the energy of solution may be expressed*

$$E_{\text{sol}} = (z - 2)N_p\bar{M}\phi W_{pp} + 2(z - 1)N_p\bar{M}[\phi_1 W_{1p} + \phi_2 W_{2p}] \\ + z[N_1\phi_1 W_{11} + N_2\phi_2 W_{22} + 2N_1\phi_2 W_{12}] \quad (8c)$$

where $2W_{ij}$ is the energy per inter-unit nearest neighbour interaction. Equations (8a) and (8b) lead to

$$g = (1/N_0^{N_p(\bar{M}-1)})(N_0!/N_1!N_2!N_h!) \quad (8d)$$

The partition function Z , equation (6), becomes

$$Z = q_1^{N_1} q_2^{N_2} q_p^{N_p\bar{M}} \sum_{N_h} \frac{[N_1 + N_2 + N_h]!}{N_1!N_2!N_h!} \exp(-pv_0 N_0/kT) \\ \times \exp(-E_{\text{sol}}/kT) Q_p(N_h, T) \quad (9)$$

where

$$Q_p = \left\{ \frac{z \exp[-(\bar{M} - 1)\epsilon_T/kT]}{2N_0^{\bar{M}-1}} \right\}^{N_p} \frac{N_0!}{\prod_M N_{pM}! [N_1 + N_2 + N_h]!} \\ \times \{1 + (z_p - 2) \exp[-(\epsilon_G - \epsilon_T)/kT]\}^{N_p(M-1)} \quad (10)$$

The number of holes N_h may be computed by the maximum term method and shown to be

$$\ln \phi_h = -\{\phi_p(1 - 1/\bar{M}) + pv_0/kT \\ + \phi_p[(z - 2)(-W_{pp}/kT)\phi_p + 2(z - 1)(-W_{1p}/kT)\phi_1 \\ + 2(z - 1)(-W_{2p}/kT)\phi_2] + z[(-W_{11}/kT)\phi_1^2 \\ + (-W_{22}/kT)\phi_2^2 + 2(-W_{12}/kT)\phi_1\phi_2]\} \quad (11)$$

where ϕ_j is the volume fraction of component j , i.e., N_j/N_0 for solvent and holes and $N_p\bar{M}/N_0$ for the polymer. Equation (11) is a generalization of an expression given by White and Yamamoto²⁴ for the fractional free volume of an amorphous polymer.

From equations (2), (9), and (10), the Gibbs free energy may be expressed

$$G_{\text{sol}} = N_p(\bar{M} - 1)\epsilon_T - N_p(\bar{M} - 1)kT \ln \{1 + (z_p - 2) \exp[-(\epsilon_G - \epsilon_T)/kT]\} \\ + N_p\bar{M}[(z - 2)\phi_p W_{pp} + 2(z - 1)\phi_1 W_{1p} + 2(z - 1)\phi_2 W_{2p}] \\ + z[N_1\phi_1 W_{11} + N_2\phi_2 W_{22} + 2N_1\phi_2 W_{12}] \\ + pv_0(N_1 + N_2 + N_h + N_p\bar{M}) + kT[N_1 \ln \phi_1 + N_2 \ln \phi_2 \\ + N_h \ln \phi_h + \sum_M N_{pM} \ln \phi_{pM}] - kT \sum_M N_{pM} \ln \left(\frac{zM}{2}\right) \\ + kTN_p(\bar{M} - 1) - kT[N_p\bar{M} \ln q_p + N_1 \ln q_1 + N_2 \ln q_2] \quad (12)$$

*This expression should be seen to be somewhat different from that used by Flory⁷⁻⁹, Scott and Magat^{11,12}, and Gee^{13,14}. Essentially this is due to different approximate treatments relating to the number of contacts between polymer and solvent

The free energy of mixing is given by

$$\Delta G_m = G_{\text{sol}} - [G_p + G_1 + G_2] \quad (13)$$

where G_p is the free energy of the polymer and G_1 and G_2 are the free energies of the two solvents. Each of these may be obtained by suitably simplifying equation (12), with the quantity G_p being equivalent to the free energy of the amorphous polymer in the paper of White and Yamamoto²⁴. The free energy of solvent 1 is simply

$$G_1 = zN_1\phi_1^0 W_{11} + pv_0(N_1 + N_{h1}) + kT[N_1 \ln \phi_1^0 + N_{h1} \ln \phi_{h1}] - kTN_1 \ln q_1 \quad (14a)$$

with

$$\ln \phi_{h1} = -[z(-W_{11}/kT)(\phi_1^0)^2 + pv_0/kT] \quad (14b)$$

Here ϕ_{h1} is the volume fraction of holes in liquid 1, and ϕ_1^0 is simply $(1 - \phi_{h1})$. An identical expression holds for solvent 2, except for an interchange of subscripts (compare the theory of Bresler and Frenkel as described by Frenkel²⁵).

Equation (12) may be rewritten (for large M) as

$$\begin{aligned} \Delta G_m = & kT[\chi_{1p}N_1\phi_p + \chi_{2p}N_2\phi_p + \chi_{12}N_1\phi_2] \\ & + z[N_1(\phi_{h1} - \phi_h)W_{11} + N_2(\phi_{h2} - \phi_h)W_{22}] \\ & + [(z-2)/z]N_p\bar{M}(\phi_{hp} - \phi_h)W_{pp}] + pv_0[N_h - N_{h1} - N_{h2} - N_{hp}] \\ & + kT[N_1 \ln (\phi_1/\phi_1^0) + N_2 \ln (\phi_2/\phi_2^0) + \sum_M N_{pM} \ln (\phi_{pM}/\phi_{pM}^0) \\ & + \ln \phi_h^{N_h}/\phi_{h1}^{N_{h1}}\phi_{h2}^{N_{h2}}\phi_{hp}^{N_{hp}}] \end{aligned} \quad (15)$$

where

$$\chi_{1p} = \frac{(z-1)}{kT} \left[2W_{1p} - \frac{(z-2)}{(z-1)} W_{pp} - \frac{z}{(z-1)} W_{11} \right] \quad (16a)$$

and

$$\chi_{2p} = \frac{(z-1)}{kT} \left[2W_{2p} - \frac{(z-2)}{(z-1)} W_{pp} - \frac{z}{(z-1)} W_{22} \right] \quad (16b)$$

and

$$\chi_{12} = \frac{z}{kT} [2W_{12} - W_{11} - W_{22}] \quad (16c)$$

The above theory is awkward in computing the variation of the free energy of mixing with temperature and pressure, for one must be concerned with changes in both the solution and the pure constituents. The situation may be improved if one chooses some appropriate standard state (i.e. a standard temperature and pressure) for the pure constituents. The most useful choice for the latter variable is infinite pressure. This allows us to write

$$\begin{aligned} \Delta G_m = & kT[\chi_{1p}N_1\phi_p + \chi_{2p}N_2\phi_p + \chi_{12}N_1\phi_2] \\ & - z\phi_h[N_1W_{11} - N_2W_{22} - N_p\bar{M}W_{pp}(z-2)/z] + pv_0N_h \\ & + kT[N_1 \ln \phi_1 + N_2 \ln \phi_2 + \sum_M N_{pM} \ln \phi_{pM} + N_h \ln \phi_h] \end{aligned} \quad (17)$$

It is also worth observing that the particular form of the potential energy barriers do not come into play in the free energy of mixing, as we assume that the variations in solvent environment (and hole concentrations) have no effect on the intramolecular character of the polymer chains.

GATHERING EFFECT - 1

The above analysis is probably reasonably valid for a system such as polystyrene dissolved in a mixture of xylene isomers or benzene and toluene. However, difficulties arise in solvent mixtures wherein the two solvent molecules are unlike. The solution is no longer random, and one of the solvent molecules preferentially gathers about the polymer chains. This is the Tompkins Effect.

We shall now attempt to compute the constant pressure ensemble partition function and Gibbs free energy for such a solution. As a first step in this direction we propose the following model. The polymer molecules are presumed to lie at random positions in the lattice, while the solvent is allowed to divide itself into two quasi-phases; one consisting of N' sites is adjacent to the surfaces of the individual macro-molecules and a second consisting of N'' sites is a 'sea' beyond the three-dimensional monolayer. The concentrations of 1 and 2 molecules in the monolayer and the sea will in general be different and we may write

$$N' + N'' = N_1 + N_2 + N_h$$

and

$$N' = N_1' + N_2' + N_h'$$

and

$$N'' = N_1'' + N_2'' + N_h''$$

where N_j' and N_j'' are the quantities of species j in the monolayer and sea. It will be presumed that solvent molecules 1, 2, and holes within each of two regions may occur randomly. This is equivalent to accepting the validity of equation (8a) but proposing in place of equation (8b)

$$\Omega_{\text{sol}} = \frac{N'!}{N_1'!N_2'!N_h'!} \frac{N''!}{N_1''!N_2''!N_h''!} \quad (18a)$$

and yielding for g ,

$$g = \frac{1}{N_0^{N_p(\bar{M}-1)}} \times \frac{N_0!}{[N' + N'']!} \times \frac{N'!}{N_1'!N_2'!N_h'!} \times \frac{N''!}{N_1''!N_2''!N_h''!} \quad (18b)$$

The energy of solution is

$$\begin{aligned} E_{\text{sol}} = & (z - 2)N_p\bar{M}\phi_p W_{pp} + \sum_{j=1,2,h} (z - 2)N_p\bar{M}(1 - \phi_p)\phi_j'(2W_{jp}) \\ & + \sum_{j=1,2,h} [z'N_j'(1 - \phi_p)\phi_j' + 2z''N_j''(1 - \phi_p)\phi_j''] \\ & + \{zN_j'' - z''N'(1 - \phi_p)\phi_j''\}\phi_j''W_{jj} \\ & + \sum_{i < j=1,2,h} [z'N_i'(1 - \phi_p)\phi_j' + z''(1 - \phi_p)(N_i''\phi_j'' + N_j''\phi_i'')] \\ & + \{zN_i'' - z''N'(1 - \phi_p)\phi_i''\}\phi_j''(2W_{ij}) \end{aligned} \quad (18c)$$

or

$$\begin{aligned}
 E_{\text{sol}} = & (z - 2)N_p \bar{M} W_{pp} + z \sum_{j=1,2,h} N_j W_{jj} \\
 & + \{1 + (z - 1)\phi_p\} \sum_{j=1,2,h} N_j' \Delta W_{jp} \\
 & + \sum_{i < j=1,2,h} \left\{ (1 - \phi_p) \left[z' \frac{N_i' N_j'}{N'} + z'' \left(\frac{N_i' N_j''}{N''} + \frac{N_i'' N_j'}{N''} \right. \right. \right. \\
 & \quad \left. \left. \left. - \frac{N_i' N_i'' N_j''}{N''^2} \right) \right] + \frac{z N_i'' N_j''}{N''} \right\} \Delta W_{ij} \quad (18d)
 \end{aligned}$$

where the hole is considered as a 'solvent' with zero pair-wise interaction energies, $W_{ih} = 0$ ($i = 1, 2, h$ and p), for the convenience of symmetrical treatments. The volume fractions ϕ_j' and ϕ_j'' refer to the volume fractions of solvent species and holes in the (polymer lacking) monolayer and sea, i.e.

$$\sum_{j=1,2,h} \phi_j' = \sum_{j=1,2,h} \phi_j'' = 1 \quad (19)$$

while the coordination number between the monolayer and sea is defined by

$$z'' = z - z' - 1 \quad (20)$$

Also we have used the abbreviations

$$\Delta W_{ij} = 2W_{ij} - (W_{ii} + W_{jj}) \quad (i, j = 1, 2, h, p) \quad (21)$$

The total partition function Z for this model is

$$\begin{aligned}
 Z = & q_1^{N_1} q_2^{N_2} q_p^{N_p} \bar{M} \{1 + (z_p - 2) \exp [-(\epsilon_G - \epsilon_T)/kT]\}^{N_p (\bar{M} - 1)} \\
 & \times \exp [-N_p (\bar{M} - 1) \epsilon_T / kT] \sum_{N_1'} \sum_{N_2'} \sum_{N_1''} \sum_{N_2''} \frac{N'!}{N_1'! N_2'! N_h'!} \\
 & \times \frac{N''!}{N_1''! N_2''! N_h''!} \times \frac{N_0!}{M N_{pM}! [N' + N'']!} \\
 & \times [z/2 N_0^{\bar{M} - 1}]^{N_p} \exp (-p v_0 N_0 / kT) \exp (-E_{\text{sol}} / kT) \quad (22)
 \end{aligned}$$

where E_{sol} is given by equation (18d). From equation (2) we may calculate the free energy of the solution to be

$$\begin{aligned}
 G_{\text{sol}} = & N_p (\bar{M} - 1) \epsilon_T - N_p (\bar{M} - 1) kT \ln [1 + (z_p - 2) \exp \{-(\epsilon_G - \epsilon_T / kT)\}] \\
 & + E_{\text{sol}} + p v_0 [N_1 + N_2 + N_h + N_p \bar{M}] \\
 & + kT [N_1' \ln \phi_1' + N_1'' \ln \phi_1'' + N_2' \ln \phi_2' \\
 & + N_2'' \ln \phi_2'' + N_h' \ln \phi_h' + N_h'' \ln \phi_h'' + \sum_M N_{pM} \ln \phi_{pM}] \\
 & + (N' + N'') \ln \frac{N' + N''}{N_0} + N_p (\bar{M} - 1) \\
 & - kT [\sum_M N_{pM} \ln \frac{1}{2} z M + N_p \bar{M} \ln q_p \\
 & + N_1 \ln q_1 + N_2 \ln q_2] \quad (23)
 \end{aligned}$$

where we have utilized the maximum term for each of the series. The free energy of mixing can be obtained in the same manner as in the previous section by using equation (13) with the same values for G_1 , G_2 , and G_p but using equation (23) for G_{sol} instead of equation (12).

In order to utilize equation (23) we must know the total number N' of molecules in the monolayer, the compositions of the solvents in each of the quasi-phases, and the number of holes in each quasi-phase. The quantity n_p represents the total number of polymer-monomer contacts, i.e., the contacts between the N_p polymer chains and the N' monolayer sites. We may write

$$n_p = (1 - \phi_p) \sum N_{pM} [(z - 2)M + 2] \quad (24a)$$

and

$$N' = \sum_{j=1}^z n_j \quad (24b)$$

where n_j is the number of solvent molecules and lattice vacancies with j (greater than zero) polymer contacts. The value of n_j is

$$n_j = \frac{(z - 1)!}{(j - 1)!(z - j)!} \phi^{j-1} (1 - \phi_p)^{z-j} N' \quad (24c)$$

which satisfies equation (24b). Carrying out the summation of equation (24a) yields

$$n_p = N' [1 + (z - 1)\phi_p] = (1 - \phi_p) \sum N_{pM} [(z - 2)M + 2] \quad (25)$$

Equation (25) yields the value of N' ; N'' is the difference between N_0 and $(N' + N_p \bar{M})$.

The composition of the solvent in the monolayer (and also in the sea) is found by determining the maximum term of the N' series in the partition function, equation (22), or equivalently by minimizing the free energy G of equation (23). The maximization is to be carried out at constant N_1 , N_2 and N_p so that it consists of mutually interchanging 1 and 2 molecules (or holes) between solvent monolayer and sea. Such a procedure yields three equations for the pairs (i, j) of $(1, h)$, $(2, h)$ and $(1, 2)$; however, only two equations are independent. The solution is simplified somewhat by using a separation constant K ; for example, the equation for solvent 1 is given by

$$\begin{aligned} kT \ln (\phi'_1 / \phi''_1) = & -[1 + (z - 1)\phi_p](\Delta W_{1p} + \Delta W_{2h}) \\ & + \{(1 - \phi_p)[z'\phi'_1 + (z''/\theta'')(\phi''_1 - \theta'\phi'_1)] - z\phi''_1\}(\Delta W_{1h} + \Delta W_{12} - \Delta W_{2h}) \\ & + K \end{aligned} \quad (26)$$

where

$$\theta' = \frac{N'}{N' + N''} \quad (27a)$$

and

$$\theta'' = \frac{N''}{N' + N''} \quad (27b)$$

The equations for solvent 2 and the holes are given by cyclic permutations of the subscripts 1, 2, and h . The separation constant K is determined by the normalization condition, equation (19).

In addition to these equations, we have to determine the overall concentration of holes. This is again carried out by the maximum term method, i.e. by the condition

$$\left(\frac{\partial G}{\partial N_h}\right)_{N_1, N_2, N_p} = 0 \quad (28)$$

Making use of equation (23), we have

$$\begin{aligned} \frac{1}{kT} \left(\frac{\partial G}{\partial N_h}\right) &= -\ln q_h + \ln(1 - \phi_p) + \phi_p(1 - 1/\bar{M}) \\ &+ \ln \phi_h'' + \ln \left(\frac{\phi_h'}{\phi_h''}\right) \frac{\partial N'}{\partial N_h} \\ &+ \ln \left(\frac{\phi_1' \phi_h''}{\phi_h' \phi_1'}\right) \frac{\partial N_1'}{\partial N_h} + \ln \left(\frac{\phi_2' \phi_h''}{\phi_h' \phi_2'}\right) \frac{\partial N_2'}{\partial N_h} \\ &+ \frac{1}{kT} \frac{\partial E_{sol}}{\partial N_h} + \frac{pv_0}{kT} \end{aligned} \quad (29)$$

with $\ln q_h = 0$. The expression for $\partial E_{sol}/\partial N_h$ is rather complicated

$$\begin{aligned} \frac{\partial E_{sol}}{\partial N_h} &= zW_{hh} - A \Delta W_{12} + B_1 \Delta W_{1h} + B_2 \Delta W_{2h} \\ &+ [(A - A') \Delta W_{12} - (B_1 - D_1) \Delta W_{1h} - (B_2 - D_2) \Delta W_{2h}] \frac{\partial N'}{\partial N_h} \\ &+ [C_2(\Delta W_{12} - \Delta W_{2h}) + (C_h - C_1) \Delta W_{1h}] \frac{\partial N_1'}{\partial N_h} \\ &+ [C_1(\Delta W_{12} - \Delta W_{1h}) + (C_h - C_2) \Delta W_{2h}] \frac{\partial N_2'}{\partial N_h} \end{aligned} \quad (30)$$

where

$$A = (1 - \phi_p) z'' \frac{\theta'}{\theta''} (\phi_1' \phi_2'' + \phi_2' \phi_1'' - 2\phi_1'' \phi_2'') + z \phi_1'' \phi_2'' \quad (31a)$$

$$A' = (1 - \phi_p) \left(z' \phi_1' \phi_2' + z'' \frac{2\theta' - \theta''}{\theta''} \phi_1'' \phi_2'' \right) \quad (31b)$$

$$\begin{aligned} B_j &= (1 - \phi_p) z'' \frac{\theta'}{\theta''} [(\phi_1'' + \phi_2'')(\phi_j' - \phi_j'') - \phi_j''(\phi_h' - \phi_h'')] \\ &+ z(\phi_1'' + \phi_2'') \phi_j'' \quad (j = 1, 2) \end{aligned} \quad (31c)$$

$$C_j = (1 - \phi_p) \left[z' \phi_j' - z'' \frac{\theta'}{\theta''} \left(\phi_j' - \frac{1}{\theta'} \phi_j'' \right) \right] - 2\phi_j'' \quad (j = 1, 2, h) \quad (31d)$$

$$D_j = (1 - \phi_p) z' (\phi_1' + \phi_2') \phi_j' + z'' (\phi_1'' + \phi_2'') \phi_j'' \quad (j = 1, 2, h) \quad (31e)$$

Furthermore, from equation (25) we have

$$\frac{\partial N'}{\partial N_h} = \frac{z(z-2)\phi_p^2}{[1 + (z-1)\phi_p]^2} \quad (32)$$

The values of $\partial N'_1/\partial N_h$ and $\partial N'_2/\partial N_h$ can be determined by differentiation of equation (26) with respect to N_h . This gives three simultaneous equations

$$\frac{kT\phi_j}{\phi'_j\phi''_j\theta'\theta''(1-\phi_p)} \frac{\partial N'_j}{\partial N_h} = (z-1)\phi_p(\Delta W_{jp} + \Delta W_{3-j,h}) + \left[P_j - R_j \frac{\partial N'}{\partial N_h} + U \frac{\partial N'_j}{\partial N_h} \right] [\Delta W_{12} - (-1)^j(\Delta W_{1h} - \Delta W_{2h})] + N_0 \frac{\partial K}{\partial N_h} \quad (j = 1, 2) \quad (33a)$$

$$\frac{kT\phi_h}{\phi'_h\phi''_h\theta'\theta''(1-\phi_p)} \left[\left(\frac{\partial N'_1}{\partial N_h} + \frac{\partial N'_2}{\partial N_h} \right) - \frac{\partial N'}{\partial N_h} \right] = - \frac{kT}{\phi''_h\theta''(1-\phi_p)} - (z-1)\phi_p(\Delta W_{hp} + \Delta W_{12}) - \left[P_h + \frac{z''}{\theta''^2} - \frac{z}{\theta''(1-\phi_p)} - (R_h - U) \frac{\partial N'}{\partial N_h} - U \left(\frac{\partial N'_1}{\partial N_h} + \frac{\partial N'_2}{\partial N_h} \right) \right] \times (\Delta W_{12} - \Delta W_{1h} - \Delta W_{2h}) - N_0 \frac{\partial K}{\partial N_h} \quad (33b)$$

where

$$P_j = z'\phi_p\phi'_j + \frac{z''}{\theta''^2} [(1-\phi_p\theta'')(\theta'\phi'_j - \phi'_j) - \theta'\phi''_j] + \frac{z'\theta''_j}{\theta''(1-\phi_p)} \quad (34a)$$

$$R_j = \frac{z'\phi'_j}{\theta'} - \frac{z''}{\theta''^2} (2\phi''_j - \theta'\phi'_j) + \frac{z\phi''_j}{\theta''(1-\phi_p)} \quad (34b)$$

$$U = \frac{z'}{\theta'} - z'' \frac{1+\theta''}{\theta''^2} + z \frac{1}{\theta''(1-\phi_p)} \quad (34c)$$

Although equation (33) seems at first separable, it is in reality not because of the term $N_0(\partial K/\partial N_h)$. The three equations must be solved simultaneously for $\partial N'_1/\partial N_h$, $\partial N'_2/\partial N_h$ and $\partial K/\partial N_h$.

Some simplification of the above analysis can be made if lattice vacancies are neglected. The free energy of the solution becomes

$$G_{\text{sol}} = N_p(\bar{M}-1)\epsilon_T - N_p(\bar{M}-1)kT \ln \{1 + (z_p-2) \exp [-(\epsilon_G - \epsilon_T/kT)]\} + E_{\text{sol}} + kT \left\{ N'_1 \ln \phi'_1 + N''_1 \ln \phi''_1 + N'_2 \ln \phi'_2 + N''_2 \ln \phi''_2 + \sum N_{pM} \phi_{pM} + (N' + N'') \ln \frac{N' + N''}{N_0} + N_p(\bar{M}-1) \right\} - kT \left[\sum N_{pM} \ln \frac{z'M}{2} + N_p\bar{M} \ln q_p + N_1 \ln q_1 + N_2 \ln q_2 \right] \quad (35)$$

$$\begin{aligned}
 \text{with } E_{\text{sol}} = & (z - 2)N_p \bar{M} W_{pp} + z(N_1 W_{11} + N_2 W_{22}) \\
 & + [1 + (z - 1)\phi_p](N_1' \Delta W_{1p} + N_2' \Delta W_{2p}) \\
 & + \left\{ (1 - \phi_p) \left[\frac{z' N_1' N_2'}{N'} + z'' \left(\frac{N_1' N_2'' + N_2' N_1''}{N''} \right. \right. \right. \\
 & \left. \left. \left. - \frac{N' N_1'' N_2''}{N''^2} \right) \right] + \frac{z N_1'' N_2''}{N''} \right\} \Delta W_{12} \quad (36)
 \end{aligned}$$

The composition of the monolayer (N_1') is found by minimizing equation (35) with respect to N_1' and results in

$$\begin{aligned}
 \ln \left(\frac{\phi_1' \phi_2''}{\phi_1'' \phi_2'} \right) + \frac{(z - 2)N_p \bar{M} (1 - \phi_p)}{N'} \left[\frac{\Delta W_{2p}}{kT} - \frac{\Delta W_{1p}}{kT} \right] \\
 + \left[z'(1 - \phi_p)(1 - 2\phi_1') + z''(1 - \phi_p) \left(1 - \frac{2N_1}{N''} + \frac{2N'}{N''} \phi_1' \right) \right. \\
 + z''(1 - \phi_p) \left(\frac{2N_1'}{N''} - \frac{2N_1 N'}{N''^2} + \frac{2N''^2}{N''^2} \phi_1' \right) \\
 \left. - z \left(1 - \frac{2N_1'}{N''} \right) \right] \frac{\Delta W_{12}}{kT} = 0 \quad (37)
 \end{aligned}$$

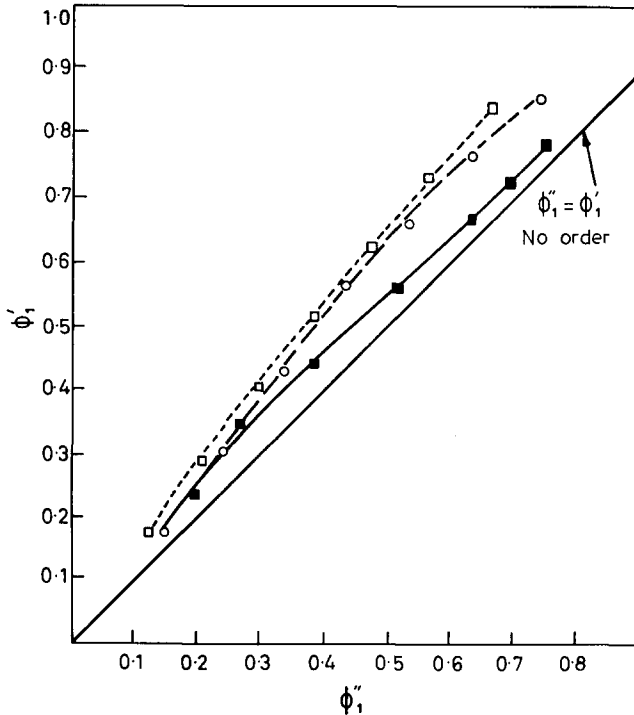


Figure 1 Ordering effect for natural rubber/benzene-ethyl acetate
 ■ Bristow's data¹⁷ (experiment for vulcanizate)
 ○ Authors' data (calculation for solution) $\phi_p = 0.01$
 □ Authors' data (calculation for solution) $\phi_p = 0.10$

Equation (37) can be used to calculate the magnitude of the Tompkins Effect. Unfortunately, however, the equation is transcendental, and the series expansion about $\phi_1' = \phi_1$ is slowly convergent. One is then forced to evaluate the effect numerically.

Calculations of the magnitude of the ordering effect have been made using equation (37) for the systems natural rubber in benzene-ethyl acetate mixtures and in benzene-acetone mixtures for $z = 10$ and 12 and $z' = 6$ to

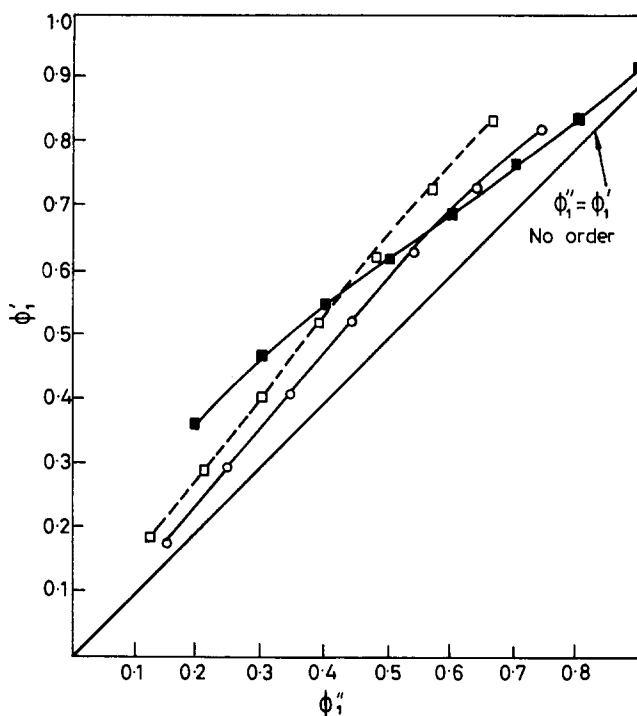


Figure 2 Ordering effect for natural rubber/benzene-acetone

- Bristow's data¹⁷ (experiment for vulcanizate)
- Authors' data (calculation for solution) $\phi_p = 0.01$
- Authors' data (calculation for solution) $\phi_p = 0.10$

($z - 2$). The ΔW were calculated using the particular homomorph method of Blanks and Prausnitz²⁶ without adding the entropy correction term. The ordering effect was rather insensitive to the value of the lattice parameters within the above ranges. Figures 1 and 2 show a comparison between these calculations and calculations based on the experimentally measured ordering phenomenon by Bristow¹⁷ on vulcanizates, which is the closest one may approach the concentrated solution problem with existing data in the literature. The major difference in the theoretical calculations on polymer solutions, and the experimental data on osmotic equilibrium in vulcanizates in mixed solvents is that the difference ($\phi_1' - \phi_1''$) does not decrease rapidly enough at high concentrations of good solvent.

GATHERING EFFECT - 2

Other procedures, perhaps less open to criticism, exist for consideration of the gathering effect. One of these is the so-called quasi-chemical approximation, as formulated by Guggenheim, Fowler, and Rushbrooke²⁷⁻³². Guggenheim^{31,32} has discussed its application to polymer solutions. Fowler and Guggenheim³⁰⁻³² have indicated two distinct methods of formulating the quasi-chemical approximation, one related to expressing a chemical equilibrium relationship between like and unlike pairs and the other to developing an expression for the combinatorial factor (essentially g). Referring first to the chemical equilibrium method one may consider the pair equilibria

$$(1 - 1) + (P - P) \rightleftharpoons 2(1 - P)$$

$$(2 - 2) + (P - P) \rightleftharpoons 2(2 - P)$$

$$(1 - 1) + (2 - 2) \rightleftharpoons 2(1 - 2)$$

In the above expressions we did not consider the presence of holes; if we had there would be three more equations. For arbitrary equilibria between i and j we may write for the number of contacts X_{ij}

$$\frac{X_{ij}^2}{4X_{ii}X_{jj}} = \exp(-\Delta W_{ij}/kT) \quad (38)$$

Three (six if holes are considered) equations of the form of equation (38) exist. The quantities X_{ii} may be expressed

$$X_{11} = zN_1 - X_{12} - X_{1p}(-X_{1h}) \quad (39a)$$

$$X_{22} = zN_2 - X_{12} - X_{1p}(-X_{2h}) \quad (39b)$$

$$X_{pp} = (z - 2)N_p\bar{M} - X_{1p}(-X_{hp}) - X_{2p} \quad (39c)$$

One can see after substitution of equations (39) into equation (38) that one must solve three (six if holes are considered) simultaneous quadratic equations which would prove rather difficult. When ΔW_{ij} is zero the solution to equation (38) and (39) including holes should lead to the expressions developed in our random solution approximation. For positive ΔW_{ij} the same situation is approached for $T \rightarrow \infty$. At moderate temperatures, however, the exponential on the right hand side of equation (38) is less than unity, and X_{ij} is appropriately smaller. Indeed the larger ΔW_{ij} the smaller will be X_{ij} . For a solution involving a polymer and two solvents for which $W_{1p} \sim W_{pp} \sim W_{11}$ and $W_{2p} \gg W_{pp}$ and W_{1p} , it will be seen that

$$X_{1p} \text{ (actual)} \sim X_{1p} \text{ (random)} \quad (40a)$$

and

$$X_{2p} \text{ (actual)} \ll X_{2p} \text{ (random)} \quad (40b)$$

and

$$X_{pp} \text{ (actual)} > X_{pp} \text{ (random)} \quad (40c)$$

The quasi-chemical approximation will then predict the Tompkins gathering effect. It also indicates as should have been expected that the polymer molecules themselves cluster together to a greater extent than in a random

solution, the extent of clustering depending upon the quantity of bad solvent.

Consistent with the above arguments are that W_{12} is greatly different from W_{11} and W_{22} and thus (assuming $\Delta W_{12} > 0$)

$$X_{12} \text{ (actual)} \ll X_{12} \text{ (random)} \quad (40d)$$

$$X_{11}, X_{22} \text{ (actual)} \gg X_{11}, X_{22} \text{ (random)} \quad (40e)$$

Equations (40) clearly indicate the solvent dividing into two regions, one rich in polymer and solvent 1 and the other rich in solvent 2. This largely corresponds to the model of the previous section.

It remains to place these remarks in quantitative form in terms of the partition function. We may again use equations (6) and (7) as a starting point, choosing the maximum terms in the summations and formulating g in terms of the number of possible arrangements of contacts as suggested by Fowler and Guggenheim. In particular we write

$$\begin{aligned} Z &= q_1^{N_1} q_2^{N_2} q_p^{N_p} \bar{M} \{1 + (z_p - 2) \exp [-(\epsilon_G - \epsilon_T/kT)]\}^{N_p \bar{M}} \\ &\times \left\{ \frac{\exp [-(\bar{M} - 1)\epsilon_T/kT]}{2} \right\}^{N_p} \exp \{-pv_0 N_0/kT\} \\ &\times g'(N_1, N_2, N_{pM}, N_h, E_{sol}) \exp \{-E_{sol}/kT\} \end{aligned} \quad (41)$$

Here g' is the number of possible configurations of polymer chains, solvent molecules, and holes in the lattice. If the contacts are presumed independent and distinguishable

$$g' = h \times \frac{\psi!}{X_{11}! X_{22}! X_{pp}! X_{hh}! (X_{12}!)^2 (X_{1p}!)^2 (X_{2p}!)^2 (X_{1h}!)^2 \dots} \quad (42a)$$

with

$$\psi = X_{11} + X_{22} + X_{pp} + X_{hh} + X_{12} + X_{1p} + X_{2p} + X_{1h} + \dots \quad (42b)$$

where the X_{ij} are given by equations (39), and h is a normalization factor independent of the X_{ij} , for g' is only an approximate quantity as the pairs interfere with one another and summing up equation (42a) over all possible configurations does not give the correct answer. The quantity E_{sol} is given by

$$\begin{aligned} E_{sol} &= X_{11}W_{11} + X_{22}W_{22} + X_{pp}W_{pp} \\ &\quad + 2X_{1p}W_{1p} + 2X_{12}W_{12} + 2X_{2p}W_{2p} \end{aligned} \quad (42c)$$

The values of X_{ij} are determined by maximization of Z .

CHEMICAL POTENTIALS AND APPLICATIONS

The equilibrium characteristics of a polymer solution may be determined from its free energy G , especially through the calculation of the partial model free energies or chemical potentials μ_i

$$\mu_i = \left(\frac{\partial G}{\partial n_i} \right)_{T,p,n} \quad (43)$$

Different expressions for μ_i are obtained for the two models presented in this paper. For the uniform random polymer-solvent mixture, the free energy G is given by equation (12). The chemical potential of solvent species 1 is

$$\begin{aligned} \mu_1 = & \mu_1^0 + kT \left[(\chi_{1p}\phi_p + \chi_{12}\phi_2)(1 - \phi_1) - \chi_{2p}\phi_2\phi_p \right. \\ & \left. + \ln \phi_1 + \sum \left(1 - \frac{1}{M} \right) \phi_{pM} \right] \\ & + [-z(1 - \phi_1)W_{11} + z\phi_2W_{22} + (z - 2)\phi_pW_{pp}]\phi_h \end{aligned} \quad (44)$$

where

$$\mu_1^0 = zW_{11} + pv_0 - kT \ln q_1 \quad (45)$$

The last term in equation (43) represents the contribution of the presence of holes upon the chemical potential. The chemical potential of species 2 may be obtained by interchanging subscripts. In the same way chemical potential of polymer species with degree of polymerization of M is found.

$$\begin{aligned} \mu_m = & \mu_m^0 + MkT [(\phi_1\chi_{1p} + \phi_2\chi_{2p})(1 - \phi_p) - \phi_1\phi_2\chi_{12}] \\ & + M(z - 2)(-\phi_h)(1 - \phi_p)W_{pp} + Mz\phi_1\phi_hW_{11} \\ & + Mz\phi_2\phi_hW_{22} + kT \left[\ln \phi_{pm} - (M - 1) + \phi_pM \left(1 - \frac{1}{M} \right) \right] \\ & + M[(z - 2)\phi_pW_{pp} + z\phi_1W_{1h} + z\phi_2W_{2h}]\phi_h \end{aligned} \quad (46)$$

where μ_M^0 is the chemical potential of a pure polymer species. For a polyethylene-like polymer, this is

$$\begin{aligned} \mu_M^0 = & (z - 2)MW_{pp} + (M - 1)\epsilon_T \\ & - (M - 1)kT \ln \{ 1 + (z_p - 2) \exp [-(\epsilon_G - \epsilon_T)/kT] \} \\ & + Mpv_0 - kT [\ln (zM/2) - (M - 1)] - MkT \ln q_p \end{aligned} \quad (47)$$

The chemical potentials of the second model may also be determined. However the situation is trickier because of the apparent two phase nature of the system. The values of μ_1 and μ_2 may be directly determined from equation (29) by cyclic interchange of the subscripts: h , 1 and 2. The value of μ_M is

$$\begin{aligned} \mu_M = & \mu_M^0 + \frac{\partial E_{sol}}{\partial N_{pM}} + kT \left[\ln \phi_{pM} - (M - 1) + \phi_{pM}M \left(1 - \frac{1}{M} \right) \right. \\ & \left. + \ln \left(\frac{\phi'_h}{\phi''_h} \right) \frac{\partial N'}{\partial N_{pM}} + \ln \left(\frac{\phi'_1\phi''_h}{\phi'_h\phi''_1} \right) \frac{\partial N'_1}{\partial N_{pM}} + \ln \left(\frac{\phi'_2\phi''_h}{\phi'_h\phi''_2} \right) \frac{\partial N'_2}{\partial N_{pM}} \right] \end{aligned} \quad (48)$$

where

$$\begin{aligned} \frac{\partial E_{sol}}{\partial N_{pM}} = & (z - 1)(1 - \phi_p)^2 M \theta' \sum_{j=1,2,h} \phi'_j \Delta W_{jp} \\ & - (1 - \phi_p)^2 M \theta' \sum_{j < k} \sum_{k=1,2,h} D_{jk} \Delta W_{jk} \\ & + \left[\sum_{j < k} \sum_{k=1,2,j} E_{jk} \Delta W_{jp} + C_1 \Delta W_{1h} + C_2 \Delta W_{2h} \right] \frac{\partial N'}{\partial N_{pM}} \end{aligned}$$

$$\begin{aligned}
& + [C_2 \Delta W_{12} - C_1 \Delta W_{1h} + C_h \Delta W_{1h}] \frac{\partial N'_1}{\partial N_{pM}} \\
& + [C_1 \Delta W_{12} - C_2 \Delta W_{1h} + C_h \Delta W_{2h}] \frac{\partial N'_2}{\partial N_{pM}} \quad (49)
\end{aligned}$$

Here the C_j are given by equation (31) and

$$D_{jk} = z' \phi_j \phi'_k + z'' (\phi_j \phi''_k + \phi''_j \phi'_k - \phi''_j \phi''_k) \quad (50a)$$

$$\begin{aligned}
E_{jk} = -(1 - \phi_p) \left\{ z' \phi'_j \phi'_k - z \frac{\theta'}{\theta''} \left[\phi_j \phi''_k + \phi''_j \phi'_k \right. \right. \\
\left. \left. - \left(\frac{1 + \theta'}{\theta'} \right) \phi''_j \phi'_k \right] \right\} - z \phi''_j \phi''_k \quad (50b)
\end{aligned}$$

and by equation (25), we have

$$\frac{\partial N'}{\partial N_{pM}} = M(1 - \phi_p)^2 \left[\frac{(z - 2) + (z - 1)\theta'}{1 + (z - 1)\phi_p} \right] \quad (51)$$

and the $\partial N'_j / \partial N_{pM}$ may be determined from equation (26) in the same manner as was used to obtain equation (33). These are

$$\begin{aligned}
\frac{kT\phi_2}{\phi'_j \phi''_j \theta' \theta'' (1 - \phi_p)} \frac{\partial N'_j}{\partial N_{pM}} = -(z - 1)(1 - \phi_p) M (\Delta W_{jp} + \Delta W_{3-j,h}) \\
+ \left[Q_j - R_j \frac{\partial N'}{\partial N_{pM}} + U \frac{\partial N'_j}{\partial N_{pM}} \right] [\Delta W_{12} - (-1)^j (\Delta W_{1h} - \Delta W_{2h})] \\
+ N_0 \frac{\partial K}{\partial N_{pM}} \quad (j = 1, 2) \quad (52a)
\end{aligned}$$

and

$$\begin{aligned}
\frac{kT\phi_h}{\phi'_h \phi''_h \theta' \theta'' (1 - \phi_p)} \frac{\partial N'_h}{\partial N_{pM}} = -(z - 1)(1 - \phi_p) M (\Delta W_{hp} + \Delta W_{12}) \\
+ \left[Q_h - (R_h - U) \frac{\partial N'}{\partial N_{pM}} - U \left(\frac{\partial N'_1}{\partial N_{pM}} + \frac{\partial N'_2}{\partial N_{pM}} \right) \right] [\Delta W_{1h} + \Delta W_{2h} - \Delta W_{12}] \\
+ N_0 \frac{\partial K}{\partial N_h} \quad (52b)
\end{aligned}$$

where R_j and U are given by equation (34) and

$$Q_j = -(1 - \phi_p) M [z' \phi'_j + (z'' / \theta'') (\phi''_j - \theta' \phi'_j)] \quad (52c)$$

Osmotic pressure measurements using a semi-permeable membrane, which is permeable to solvent 1 (and perhaps solvent 2) but not to the polymer, may be utilized to test the expressions for μ_1 (and μ_2) cited in this section. Frequently a situation arises when a non-solvent is added to a solution of a polymer in a single solvent. Beyond a certain concentration of the poor solvent, phase separation will occur. The criterion of physical equilibrium between two phases is equality of the chemical potentials for each of the species in the two phases, i.e.,

$$\mu_M^{(I)} = \mu_M^{(II)}; \quad \mu_1^{(I)} = \mu_1^{(II)}; \quad \mu_2^{(I)} = \mu_2^{(II)} \quad (53)$$

The values μ_j used in this section may be used to compute the relative concentrations in the two phases.

DISCUSSION AND CONCLUSIONS

A rather general lattice formulation has been utilized to develop a theory of solutions of polydisperse polymers in mixed solvents. The main feature of the theory is that it involves presumption of a monolayer of solvent mixture, rich in the good solvent, about the polymer molecules and a sea beyond this monolayer which is richer in the poorer solvent. This is in reality a rather good and not extreme model, for the polymer chains will not be too many lattice sites away at the moderate and high concentration levels of interest. The monolayer concept encompasses the idea of a region of good solvent about polymer chains which decays away with increasing distance. An attempt was made to carry out a similar development utilizing the quasi-chemical approximation of Guggenheim and his colleagues²⁷⁻³². This was however found to be intractable compared with the monolayer theory. We have tried elsewhere to apply the monolayer idea to dilute solutions²¹ where at least superficially its use is not as justified. However, arguments can be made even in this case for its application.

A second feature of our analysis is the inclusion of holes in the lattice theory. This was suggested to us by various discussions throughout Frenkel's 'Kinetic Theory of Liquids'²⁵ especially the Bresler-Frenkel theory of melting (p 106 ff). We have previously applied the idea of a lattice containing macromolecules and holes to the melting of polyethylene²⁴ where it is found that consideration of the volumetric expansion during melting was necessary in order to obtain reasonable predictions of the melting temperature. The use of holes in lattice theories of polymer solutions should give this approach new life as it will enable one to consider volume changes in mixing, coefficients of thermal expansion, and effects of pressure. We are in the process of considering a number of these phenomena at the present time. It would be of interest to contrast lattice theories of polymer solutions with holes to the cell theories of solutions^{33, 34}.

ACKNOWLEDGEMENT

The authors wish to acknowledge with thanks the partial support of this research under National Science Foundation Grant GK 11035.

*Dept of Chemical and
Metallurgical Engineering,
University of Tennessee,
Knoxville, Tennessee, USA*

(Received 30 September 1970)

(Revised 30 December 1970)

REFERENCES

- 1 Kotera, A., 'Fractional Precipitation' in 'Polymer Fractionation', (Ed., M. J. R. Cantow) Academic Press, New York, 1967

- 2 Baker, C. A. and Williams, R. J. P. *J. Chem. Soc.* 1956, p 2352
- 3 Porter, R. S. and Johnson, J. E., 'Polymer Fractionation' (Ed., M. J. R. Cantow) Academic Press, New York, 1967
- 4 Fower, R. H. and Rushbrooke, G. S. *Trans. Faraday Soc.* 1937, **33**, 1272
- 5 Meyer, K. H. *Z. Physik Chem.* 1939, **B44**, 383
- 6 Huggins, M. L. *J. Phys. Chem.* 1942, **46**, 151
- 7 Flory, P. J. *J. Chem. Phys.* 1942, **10**, 51
- 8 Flory, P. J. *J. Chem. Phys.* 1944, **12**, 425
- 9 Flory, P. J., 'Principles of Polymer Chemistry,' Cornell University Press, 1953
- 10 Flory, P. J. *Proc. Roy. Soc.* 1956, **A234**, 60
- 11 Scott, R. L. and Magat, M. *J. Chem. Phys.* 1945, **13**, 172
- 12 Scott, R. L. *J. Chem. Phys.* 1949, **17**, 268
- 13 Gee, G. *Trans. Faraday Soc.* 1944, **40**, 463
- 14 Gee, G. *Trans. Faraday Soc.* 1944, **40**, 468
- 15 Tompkins, H. K., 'The physics and chemistry of colloids,' Appendix II Report of a General Discussion held jointly by the Faraday Society and the Physical Society of London, His Majesty's Stationery Office, London, 1921; *Trans. Faraday Soc.* 1921, **16**, appendix
- 16 Krigbaum, W. R. and Carpenter, D. K. *J. Polym. Sci.* 1954, **14**, 241
- 17 Bristow, G. M. *Trans. Faraday Soc.* 1959, **55**, 1246
- 18 Ewart, R. H., 'Advances in Colloid Science,' Vol. 2, Academic Press, New York, 1946, and personal communication, 1964
- 19 Ewart, R. H., Roe, C. P., Debye, P., and McCartney, J. R. *J. Chem. Phys.* 1946, **14**, 687
- 20 Shultz, A. R. and Flory, P. J. *J. Polym. Sci.* 1955, **15**, 231
- 21 Yamamoto, M. and White, J. L. (manuscript submitted for publication).
- 22 Oka, S. *Proc. Phys. Math. Soc. Japan* 1942, **24**, 657
- 23 Flory, P. J., 'Statistical Mechanics of Chain Molecules,' Interscience, New York, 1969
- 24 White, J. L. and Yamamoto, M. *J. Phys. Soc. Japan* 1970, **24**, 891
- 25 Frenkel, J., 'Kinetic Theory of Liquids,' translated from the 1946 Russian edition, Dover, New York
- 26 Blanks, R. F. and Prausnitz, J. M. *I E C Fund* 1964, **3**, 1
- 27 Guggenheim, E. A. *Proc. Roy. Soc.* 1935, **A148**, 304
- 28 Rushbrooke, G. A. *Proc. Roy. Soc.* 1938, **A166**, 296
- 29 Fowler, R. H. and Guggenheim, E. A., 'Statistical Thermodynamics,' Cambridge, 1939
- 30 Fowler, R. H. and Guggenheim, E. A. *Proc. Roy. Soc.* 1940, **A174**, 189
- 31 Guggenheim, E. A. *Proc. Roy. Soc.* 1944, **A183**, 213
- 32 Guggenheim, E. A., 'Mixtures' Oxford, 1952
- 33 Prigogine, I., 'Molecular Theory of Solutions', North Holland, Amsterdam, 1957
- 34 Patterson, D. *Rubber Chem. and Tech.* 1967, **40**, 1

Thermodynamics of mixtures of poly(ethylene oxide) and benzene

C. BOOTH and C. J. DEVOY*

Specific volumes and vapour pressures of poly(ethylene oxide)-benzene mixtures have been measured at several temperatures. The thermodynamic dilution quantities calculated from these data are compared with the theory of Flory. Deviations from theory are entropic in origin and are ascribed to specific charge-transfer interactions in the mixture.

CONVENTIONAL theories of solution comprise an entropy of random mixing of the components on a rigid lattice and an energy of mixing arising from interchange of symmetrical interactions. Such are the regular solution theory¹ for small molecules and the Flory-Huggins theory² for chain molecules. The regular solution theory has enjoyed success and is a useful guide to the properties of mixtures of compact non-polar molecules. The Flory-Huggins theory, while accounting for the gross deviations from ideality which result from the chain nature of the polymer molecules, has proved comparatively unsuccessful in quantitative applications.

Recently attention has been drawn to those theories of solution³⁻⁶ which take proper account of the liquid nature of the pure components and the mixture (rather than treating them as quasi-solids) and particularly^{7,8} to the importance of these considerations when the components have such disparate properties as do polymeric and low molecular weight liquids. The application of these theories to polymer solutions has been reviewed recently by Patterson⁷. It is clear, from existing studies, that it is more rewarding to describe the properties of non-polar polymer solutions in terms of deviations from these theories than from the Flory-Huggins theory. It is some advantage, in terms of the initial information required, to use those theories which assume a simple analytical form for the equation of state of the liquids. Accordingly in this work we apply the theoretical equations of Flory *et al*⁸, which are based upon an equation of state of the van der Waals type, to new experimental data for solutions of poly(ethylene oxide) in benzene.

EXPERIMENTAL

'AnalaR' grade benzene was successively treated with concentrated sulphuric acid, washed, dried, fractionally crystallized five times, refluxed over sodium wire and finally distilled through a one metre column of Dixon rings, maintained at 79°C, at a reflux ratio of 12:1. The centre cut had vapour pressures within 0.2% of published values⁹, over the temperature range 45-70°C.

* Present address: Department of Chemistry, University of Essex, Colchester

Poly(ethylene oxide) samples were prepared from poly(ethylene glycol) 6000 (Shell Chemical Company) and Polyox WSR-205 (Union Carbide, Chemicals Division). Both were fractionated by adding isooctane to a dilute solution (0.5 wt%) of the polymer in benzene at 30°C¹⁰. The first fractions, some 30 wt% of the original polymers, were collected; the fraction of Polyox WSR-205 was reprecipitated under similar conditions. Fraction 6000F had viscosity⁻¹¹ and number-average molecular weights¹² of 6100 and 5700 respectively. Fraction 205F had a viscosity-average molecular weight¹³ of 8×10^5 . We assume, on the basis of previous work^{10,14}, that the number-average molecular weight of 205F was 6×10^5 .

Vapour pressures were usually measured by means of a differential manometer similar to those described earlier^{15,16}. Some measurements were made by the method of McGlashan and Williamson¹⁷, in which concentrations were determined by distilling known weights of solvent onto a known weight of polymer rather than by distilling known volumes of solvent. We found no systematic differences between the two methods. Construction and conditions were such that pressures could be measured to ± 0.01 cmHg* and weights of benzene transferred to ± 1 mg (± 0.5 mg in the case of the direct weight method). Precautions were taken to avoid fractionation of benzene during transfer; the vapour pressure did not change by more than 0.05% during an experiment. Vapour space corrections were made. Polymer samples were exhaustively outgassed; the residual pressure after equilibration for two days was never greater than 0.005 cmHg.

Densities of poly(ethylene glycol) 6000, and its solutions in AnalaR benzene, were measured by use of a pycnometer. It was not thought necessary to use the purified materials for these measurements.

RESULTS

Specific volumes of poly(ethylene glycol) 6000 and AnalaR benzene and their mixtures, are given in *Table 1*. The specific volumes of the pure components agree well with published values^{18-21,26}. The quantity $\Delta v/v_0$, where Δv is the volume change on mixing one gram of mixture and v_0 is the corresponding unmixed volume, is plotted against weight fraction in *Figure 1*. The volumes are defined by the equations

$$\Delta v = v_{sp} - v_0$$

$$v_0 = w_1 v_{sp,1} + w_2 v_{sp,2}$$

where v_{sp} , $v_{sp,1}$ and $v_{sp,2}$ are the specific volumes of the mixture and of pure liquids 1 and 2 respectively (see *Table 5*) and w_1 and w_2 are the weight fractions of 1 and 2 in the mixture.

The activity of benzene in the solution can be defined as

$$a_1 = (p_1/p_1^0) \exp[-B/RT(p_1^0 - p_1)]$$

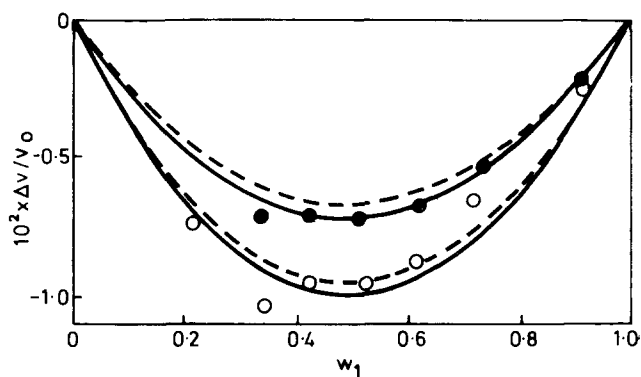
where p_1 and p_1^0 are the vapour pressures of benzene over the solution and over pure benzene respectively and B is the second virial coefficient of

* 1 cmHg = 1333 N m⁻²

THERMODYNAMICS OF MIXTURES OF POLY(ETHYLENE OXIDE) AND BENZENE

 Table 1 Weight fraction of benzene (w_1) and specific volumes of solutions of poly(ethylene glycol) 6000

(70.0°C)		(45.8°C)	
w_1	Specific volume ($\text{cm}^3 \text{g}^{-1}$)	w_1	Specific volume ($\text{cm}^3 \text{g}^{-1}$)
1.0000	1.2127	1.0000	1.1749
0.9035	1.1817	0.9019	1.1460
0.7129	1.1221	0.7308	1.0965
0.6124	1.0904	0.6186	1.0649
0.5227	1.0638	0.5100	1.0353
0.4208	1.0346	0.4201	1.0113
0.3138	1.0028	0.3303	0.9873
0.2105	0.9759		
0.0000	0.9218		


 Figure 1 Reduced volume change on mixing ($\Delta v/v_0$) against weight fraction of benzene (w_1) for mixtures with poly(ethylene glycol) 6000
 ○ at 70.0°C and ● at 45.8°C

 Theoretical curves are for $X_{12} = -4 \text{ cal cm}^{-3}$ (unbroken line) and $X_{12} = -3 \text{ cal cm}^{-3}$ (broken line)

 Table 2 Weight fraction (w_1) and activity (a_1) of benzene in solutions of poly(ethylene oxide) fraction 6000F

70.0°C		45.8°C	
w_1	a_1	w_1	a_1
0.0290	0.1091	0.3211	0.7348
0.0926	0.3104	0.4005	0.8188
0.1572	0.4718	0.4893	0.8853
0.2410	0.6321	0.6049	0.9438
0.3188	0.7409	0.7389	0.9806
0.3982	0.8239		
0.4875	0.8906		
0.6032	0.9467		
0.7385	0.9840		

benzene vapour over the appropriate pressure range. We have used values of B recommended by Allen, Everett and Penny²² i.e.

$$B = [70 - (13.2 \times 10^7)/T^2] \text{ cm}^3 \text{ mol}^{-1},$$

where T is the absolute temperature. Values of a_1 and w_1 are given in *Tables 2 and 3*.

In order to calculate the entropy and heat of dilution we have calculated the quantity

$$\chi' = \frac{\ln a_1 - \ln(1 - w_2) - (1 - 1/x_n)w_2}{w_2^2}$$

where x_n is the ratio of the number average molecular weight of the polymer to that of the solvent. The parameter χ' has values in the range 0.3–0.4 and is a slowly changing function of w_2 . Smoothed values of χ' were used to calculate the free energies of dilution at the two temperatures, and at given values of w_2 , and from these data entropies and heats of dilution, listed in *Table 4*, were calculated the usual way¹⁶.

Table 3 Weight fraction (w_1) and activity (a_1) of benzene in solutions of poly(ethylene oxide) fraction 205F

70.0°C		50.3°C	
w_1	a_1	w_1	a_1
0.0967	0.3145	0.3314	0.7474
0.1839	0.5232	0.4229	0.8390
0.2479	0.6392	0.4867	0.8865
0.3300	0.7544	0.5839	0.9363
0.4150	0.8387	0.7412	0.9822
0.4740	0.8831		
0.5802	0.9387		
0.7242	0.9797		

Table 4 Thermodynamic dilution quantities for poly(ethylene oxide) and benzene

Weight fraction benzene	Δh_1 (cal mol ⁻¹)	Δs_1 (cal deg ⁻¹ mol ⁻¹)	χ
6000F at 57.9°C			
0.3	-115	0.325	0.219
0.4	-82.7	0.140	0.228
0.5	-55.4	0.052	0.243
0.6	-33.9	0.0126	0.262
205F at 60.15°C			
0.3	-130	0.285	0.192
0.4	-93.9	0.106	0.204
0.5	-63.6	0.026	0.215
0.6	-40.3	-0.0073	0.223

Errors in χ' arising from instrumental limitations were estimated to be ± 0.003 . The scatter of experimental results, and the results of replicate determinations (not given in *Tables 2 and 3*) are consistent with this figure.

THEORY

The theory of Flory *et al*^{6,8,23} is based upon a model of molecules which consist of r segments of characteristic (hard core, i.e. 0 K) volume v^* , having s contact sites per segment, and having $3c$ external degrees of freedom per segment. The intermolecular potential energy has the van der Waals form, i.e. $E = -a/v$, where a is proportional to the number of contacts, each contact contributing intermolecular energy $-\eta/v$.

The partition function for N_1 molecules of a pure component 1 is written

$$Z_1 = \text{constant}[v_1^*(\bar{v}^{1/3} - 1)^3]^{N_1 r_1 c_1} \times \exp(a/v_1 kT)$$

where the constant contains numerical factors, and \bar{v} is the reduced volume v/v^* .

The corresponding partition function for a mixture of $N_1 + N_2$ ($= N$) molecules is written

$$Z = \text{constant} \times Z_{comb}[v^*(\bar{v}^{1/3} - 1)^3]^{Nrc} \times \exp(a/vkT)$$

where v^* , r , c and a are suitably averaged quantities for the mixture. The averages are as follows

$$v^* = v_1^*$$

$$r = r_1 x_1 + r_2 x_2 \quad (x = \text{mol fraction})$$

$$c = c_1 \phi_1 + c_2 \phi_2 \quad (\phi = \text{segment fraction})$$

$$a = a_1 \theta_1 + a_2 \theta_2 - \Delta a \theta_1 \theta_2 \quad (\theta = \text{site fraction})$$

and

$$\phi_1 = w_1 \bar{v}_{sp,1}^* / (w_1 \bar{v}_{sp,1}^* + w_2 \bar{v}_{sp,2}^*)$$

where \bar{v}_{sp}^* is the characteristic volume per gram

$$\theta_1 = s_1 r_1 N_1 / (s_1 r_1 N_1 + s_2 r_2 N_2)$$

and

$$\Delta a = a_1 + a_2 - 2a_{12}$$

The combinatory factor, Z_{comb} , is taken as that due to Flory²⁴ for random mixing of the two components.

Conventional treatment of the partition function leads to a reduced equation of state of the van der Waals type

$$(\bar{p} + 1/\bar{v}^2)(\bar{v} - \bar{v}^{2/3}) = \bar{T}$$

where the characteristic parameters

$$p^* = p/\bar{p}, \quad v^* = v/\bar{v}, \quad T^* = T/\bar{T}$$

are related to measurable quantities by the equations

$$v^* = v/[1 + \alpha T/3(1 + \alpha T)]^3$$

$$T^* = T\tilde{v}^{4/3}/(\tilde{v}^{1/3} - 1)$$

$$p^* = \gamma T\tilde{v}^2$$

where α is the coefficient of expansion, $(1/v)(\partial v/\partial T)_P$ and γ is the thermal pressure coefficient, $(\partial P/\partial T)_v$.

For the mixture

$$v^* = v_1^* = v_2^*$$

$$p^* = \phi_1 p_1^* + \phi_2 p_2^* - \phi_1 \theta_2 X_{12}$$

$$1/T^* = (\phi_1 p_1^*/T_1^* + \phi_2 p_2^*/T_2^*)/p^*$$

where the energy parameter $X_{12} = s_1 \Delta\eta/2v^{*2}$, where $\Delta\eta = 2 \Delta a/srN$.

The following measurable thermodynamic quantities are obtained from the partition function in the usual way

$$\Delta v/v_0 = \frac{\tilde{v} - \tilde{v}_0}{\tilde{v}_0}$$

where $\tilde{v}_0 = \phi_1 \tilde{v}_1 + \phi_2 \tilde{v}_2$

$$\Delta h_1 = p_1^* V_1^* \left[\left(\frac{1}{\tilde{v}_1} - \frac{1}{\tilde{v}} \right) + \frac{\alpha T(\tilde{T}_1 - \tilde{T})}{\tilde{v}\tilde{T}} + \frac{X_{12}(1 - \alpha T)\theta_2^2}{p_1^* \tilde{v}} \right]$$

$$\Delta s_1 = -R[\ln \phi_1 + (1 - 1/r_2)\phi_2]$$

$$- \frac{p_1^* V_1^*}{R} \left[3\tilde{T}_1 \ln \frac{(\tilde{v}_1^{1/3} - 1)}{(\tilde{v}^{1/3} - 1)} - \frac{\alpha T(\tilde{T}_1 - \tilde{T})}{\tilde{v}\tilde{T}} - \frac{\alpha T X_{12} \theta_2^2}{p_1^* \tilde{v}} \right]$$

$$\Delta \mu_1 = \Delta h_1 - T \Delta s_1$$

$$\chi = \frac{1}{\phi_2^2} \left[\frac{\Delta \mu_1}{RT} - \ln \phi_1 - (1 - 1/r_2)\phi_2 \right]$$

In these equations V_1^* is the molar characteristic volume of component 1 and

$$\alpha = \frac{3(\tilde{v}^{1/3} - 1)}{T(4 - 3\tilde{v}^{1/3})}$$

The data required in order to calculate the thermodynamic quantities are the molecular weights (number-average molecular weight for a polymer), the specific volumes and the coefficients of expansion and thermal pressure of the two components. The energy parameter X_{12} is an adjustable parameter. The surface ratio, s_2/s_1 , can be estimated from known molecular parameters.

COMPARISON OF EXPERIMENT WITH THEORY

The surface ratio (s_2/s_1) was calculated on the assumption that the benzene molecule is a sphere of radius $(3v_1^*/4\pi)^{1/3}$ and poly(ethylene oxide) a cylinder

of volume v_1^* and radius $(v_m^*/L\pi)^{1/2}$, where v_m^* is the molecular volume of a monomer unit in the polymer chain, and L is the distance per monomer unit in the C direction in the unit cell (repeat distance of 19.5 Å, 1.95 nm, for 7 monomer units²⁵). In this way we find values of s_2/s_1 in the region of 0.80.

The number of segments per polymer molecule, given $r_1 = 1$, is given by

$$r_2 = \frac{M_2 v_{sp,2}^*}{M_1 v_{sp,1}^*}$$

where M_1 and M_2 are the appropriate molecular weights. Values of r_2 are about 60 for 6000F and about 6500 for 205F.

We have made calculations for the temperatures 70.0, 60.15, 57.9 and 45.8°C. The values of specific volume, coefficient of expansion and thermal pressure coefficient which we have used are listed in *Table 5*. The characteristic parameters calculated from the data vary slightly with temperature. Values for $T = 57.9^\circ\text{C}$ are listed in *Table 6*.

A comparison of the volume change on mixing parameters $[(\bar{v} - \bar{v}_0)/\bar{v}_0]$ with the experimental values $(\Delta v/v_0)$ for poly(ethylene glycol) 6000 serves to

Table 5 Coefficients of expansion (α) and thermal pressure (γ), and specific volumes (v_{sp})
Table 5a Benzene

$T(^{\circ}\text{C})$	$\alpha_1(\text{deg}^{-1})^{26}$	$\gamma_1(\text{cal cm}^{-3} \text{ deg}^{-1})^{27}$	$v_{sp,1}(\text{cm}^3 \text{ g}^{-1})^{26}$
70.0	1.346×10^{-3}	0.230	1.2123
60.15	1.313×10^{-3}	0.245	1.1964
57.9	1.306×10^{-3}	0.249	1.1930
45.8	1.271×10^{-3}	0.269	1.1745

Table 5b Poly(ethylene oxide)

$T(^{\circ}\text{C})$	$\alpha_2(\text{deg}^{-1})^*$	$\gamma_2(\text{cal cm}^{-3} \text{ deg}^{-1})^\dagger$	$v_{sp,2}(\text{cm}^3 \text{ g}^{-1})^\S$
70.0	0.753×10^{-3}	0.317	0.9218
60.15	0.749×10^{-3}	0.328	0.9144
57.9	0.748×10^{-3}	0.330	0.9127
45.8	0.742×10^{-3}	0.344	0.9037

* Estimated from data of Hoechst Chemicals²⁸ for low molecular weight polyglycols

† For poly(ethylene glycol) 5000²⁹

‡ Calculated from value at 70.0°C, and values of α

Table 6 Parameters for benzene and poly(ethylene oxide) 6000F at 57.9°C

	Benzene	Poly(ethylene oxide)
$p^*(\text{cal cm}^{-3})$	146.6	160.5
$v_{sp}^*(\text{cm}^3 \text{ g}^{-1})$	0.8948	0.7532
$T^*(\text{K})$	4829	6469
r	1	61.5
$s_2/s_1 = 0.802$		

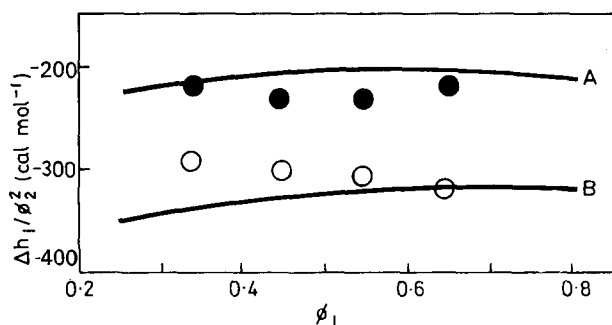


Figure 2 Reduced heat of dilution ($\Delta h_1/\phi_2^2$) against segment fraction of benzene (ϕ_1): ● with poly(ethylene oxide) 6000F at 57.9°C and ○ with poly(ethylene oxide) 205F at 60.2°C. Theoretical curves are for 6000F at 57.9°C. A, $X_{12} = -3 \text{ cal cm}^{-3}$ and B, $X_{12} = -4 \text{ cal cm}^{-3}$

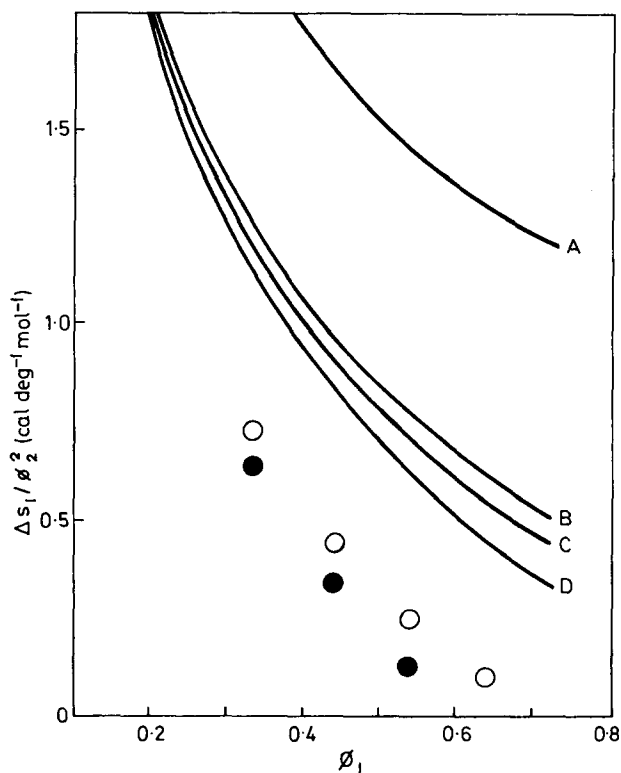


Figure 3 Reduced entropy of dilution ($\Delta s_1/\phi_2^2$) against segment fraction of benzene (ϕ_1): ○ with poly(ethylene oxide) 6000F at 57.9°C and ● with poly(ethylene oxide) 205F at 60.2°C. Curves are, A the Flory combinatorial entropy for 205F; B the theoretical values for 6000F at 57.9°C with $X_{12} = -3 \text{ cal cm}^{-3}$; C the theoretical values for 6000F at 57.9°C with $X_{12} = -4 \text{ cal cm}^{-3}$; D theoretical values for 205F at 60.2°C with $X_{12} = -4 \text{ cal cm}^{-3}$

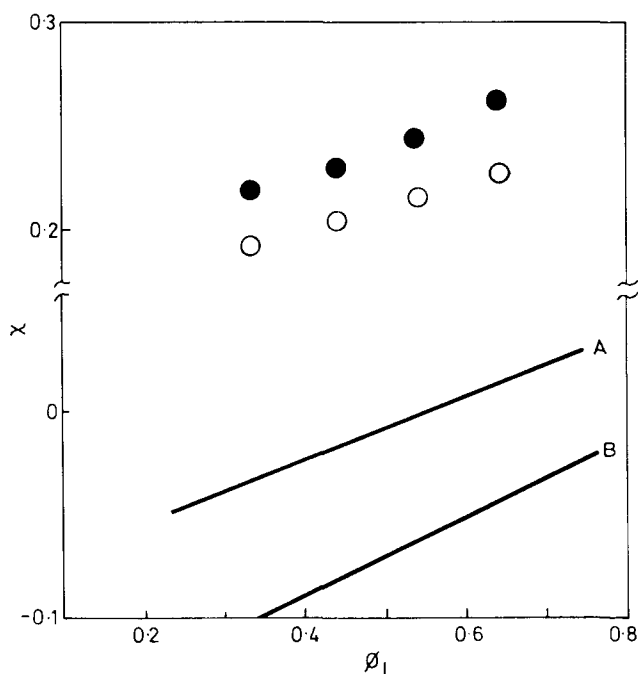


Figure 4 Parameter χ against segment fraction of benzene (ϕ_1): ● for mixtures with poly(ethylene oxide) 6000F at 57.9°C and ○ for mixtures with poly(ethylene oxide) 205F at 60.2°C. Theoretical curves are for 6000F at 57.9°C. A, $X_{12} = -3 \text{ cal cm}^{-3}$ and B, $X_{12} = -4 \text{ cal cm}^{-3}$

define the energy parameter X_{12} . Best agreement between experiment and theory is found for X_{12} between -3 and -4 cal cm^{-3} *. The comparison is illustrated in Figure 1.

Calculated values of the reduced entropies and heats of dilution, i.e. $\Delta s_1/\phi_2^2$ and $\Delta h_1/\phi_2^2$ respectively, and of the parameter χ are compared with experiment in Figures 2-4. The variation of the theoretical quantities with temperature is slight; compared with the values at 57.9°C the values of χ at 60.15°C are about 0.004 higher, and the values of $\Delta h_1/\phi_2^2$ about 3 cal mol⁻¹ lower. The estimated precision of the experimental values is $\Delta s_1/\phi_2^2$ to $\pm 0.12 \text{ cal deg}^{-1} \text{ mol}^{-1}$; $\Delta h_1/\phi_2^2$ to $\pm 40 \text{ cal mol}^{-1}$; χ to ± 0.003 .

DISCUSSION

It is clear, from Figures 2-4, that the theory accounts reasonably well for the thermodynamic properties of the benzene-poly(ethylene oxide) system. The major discrepancy between theory and experiment is in the entropy of dilution, where the experimental value of $\Delta s_1/\phi_2^2$ is about 0.5 cal deg⁻¹ mol⁻¹ lower than the theoretical value. This discrepancy corresponds to an entropy

* 1 cal = 4.186 J

parameter [$\chi_s = \Delta(\Delta s_1)/R\phi_2^2$] of 0.25. The discrepancy between the experimental and theoretical values of χ (of about 0.25) is mainly entropic in origin.

The assumption that Z_{comb} is given by the expression of Flory² leads to the combinatory term in the entropy of dilution

$$\Delta s_{1comb} = -R(\ln\phi_1 + (1 - 1/r_2)\phi_2)$$

An alternative approximation for Z_{comb} ³⁰ leads to the expression

$$\Delta s_{1comb} = -R(\ln\phi_1 + (1 - 1/r_2)\phi_2 + \chi_s\phi_2^2)$$

where $\chi_s = (1 - 1/r_2)^2/z + 4(1 - 1/r_2)^3\phi_2/3z$

In the concentration range (ϕ_2) 0.3–0.6, this equation yields values of $\chi_s \simeq 0.25$, when the liquid lattice co-ordination number (z) is taken to be 5. However, values of Δs_1 for non-polar polymer-liquid systems³¹ are not, in general, markedly lower than those predicted by the Flory approximation. For this reason a combination of the higher approximation for Z_{comb} with the equation of state terms etc., although providing a consistent explanation of our data, is not tenable in the wider context.

The large negative value of the energy interaction parameter ($X_{12} \simeq -4$ cal cm⁻³) indicates a specific interaction between benzene and poly(ethylene oxide) whereas the theory assumes spherically symmetrical force fields about each molecule or segment. Agreement between theory and experiment cannot be expected if no account is taken of this effect, which will lead to low values of the entropy of dilution. The specific interaction presumably originates in charge transfer between the benzene (donor) and ether oxygen (acceptor). If we ascribe to each non-complexing unlike contact in the mixture an interchange energy of about 10–20 cal mol⁻¹ (corresponding to $X_{12} \simeq +1$ cal cm⁻³ for a non-complexing mixture) then we find an interchange energy for complex formation somewhat greater than 0.5 kcal mol⁻¹, a value in keeping with those usually assigned to charge transfer interactions in the liquid state.

It is of interest that the energies of dilution at constant volume, calculated for a process of mixing at constant partial specific volume from the heats of dilution at constant pressure, are almost zero. Such results imply an average interchange energy per contact near zero, and this is less realistic than the result obtained from the Flory theory. The entropies of dilution at constant volume are lower than the Flory²⁴ entropies of dilution by amounts which correspond to an entropy parameter (χ_s) of about 0.25.

The differences between the dilution properties of samples 6000F and 205F are consistent with the differences in molecular weight. The differences in entropy of dilution are explained entirely by the end effect, i.e. by the term $R\phi_2/r_2$ of the Flory equation. The differences in heat of dilution are probably due to hydrogen bonds involving the hydroxyl groups which terminate the molecules in both samples. The severance of these bonds, on dilution with benzene, will result in a substantial positive contribution to Δh_1 for the low molecular weight sample 6000F, but a negligible contribution to Δh_1 for the high molecular weight sample 205F. More direct confirmation of hydrogen bonding in poly(ethylene glycol)–benzene systems comes from n.m.r. measurements³⁹.

ACKNOWLEDGEMENTS

We thank Mr J. M. B. Herbert for helpful discussions. C.J.D. acknowledges receipt of a Science Research Council Studentship.

*Department of Chemistry,
University of Manchester,
Manchester M13 9PL, UK*

(Received 5 November 1970)

REFERENCES

- 1 Hildebrand, J. H. and Scott, R. L., 'Regular Solutions', Prentice Hall, Englewood Cliffs, New Jersey, 1962
- 2 Flory, P. J., 'Principles of Polymer Chemistry', Cornell University Press, Ithaca, New York, 1953
- 3 Prigogine, I., Bellemans, A. and Mathot, V., 'The Molecular Theory of Solutions', North Holland Publishing Company, Amsterdam, 1957
- 4 Scott, R. L. *J. Chem. Phys.* 1956, **25**, 193
- 5 Brown, W. B. *Phil. Trans. Roy. Soc., London* 1957, **A250**, 157
- 6 Flory, P. J. *J. Amer. Chem. Soc.* 1965, **87**, 1833
- 7 Patterson, D. *Rubber Chem. and Tech.* 1967, **40**, 1
- 8 Eichinger, B. E. and Flory, P. J. *Trans. Faraday Soc.* 1968, **64**, 2035, 2053, 2061, 2066
- 9 Smith, E. R. *J. Res. Nat. Bur. Standards* 1941, **26**, 129
- 10 Booth, C. and Price, C. *Polymer, Lond.* 1966, **7**, 85
- 11 Sadron, C. and Rempp, P. *J. Polym. Sci.* 1958, **29**, 127
- 12 Vapour Pressure Osmometer, Mecrolab Inc., Mountain View, California
- 13 Allen, G., Booth, C., Hurst, S. J., Jones, M. N. and Price, C. *Polymer, Lond.* 1967, **8**, 391
- 14 Beech, D. R. and Booth, C. *J. Polym. Sci. (A-2)* 1969, **7**, 575
- 15 Gee, G. and Treloar, L. R. G. *Trans. Faraday Soc.* 1942, **38**, 147
- 16 Booth, C., Gee, G., Holden, G. and Williamson, G. R. *Polymer, Lond.* 1964, **5**, 343
- 17 McGlashan, M. L. and Williamson, A. G. *Trans. Faraday Soc.* 1961, **57**, 588
- 18 International Critical Tables, McGraw-Hill, New York, 1926
- 19 Research Project 44, American Petroleum Institute, Carnegie Press, New York, 1953
- 20 Ingham, J. D. and Lawson, D. D. *J. Polym. Sci. (A)* 1965, **3**, 2707
- 21 Simon, F. T. and Rutherford Jr., J. M. *J. Appl. Phys* 1964, **35**, 82
- 22 Allen, P. W., Everett, D. H. and Penney, M. F. *Proc. Roy. Soc.(A)* 1952, **212**, 149
- 23 Flory, P. J., Orwell, R. A. and Vrij, A. *J. Amer. Chem. Soc.* 1964, **86**, 3507, 3515
- 24 Flory, P. J. *J. Chem. Phys.* 1942, **10**, 51
- 25 'Polymer Handbook', Interscience Publishers, New York, 1966
- 26 Wood, S. E. and Brussie, J. P. *J. Amer. Chem. Soc.* 1943, **65**, 1891
- 27 Holder, G. A. and Whalley, E. *Trans. Faraday Soc.* 1962, **58**, 2095
- 28 Technical Literature, Hoechst Chemicals, Brentford, 1969
- 29 Malcolm, G. N. and Ritchie, G. L. D. *J. Phys. Chem.* 1962, **66**, 852
- 30 Huggins, M. L. *Ann. N. Y. Acad. Sci.* 1942, **41**, 1; Guggenheim, E. A. *Proc. Roy. Soc.(A)* 1944, **183**, 203
- 31 Booth, C., Gee, G., Jones, M. N. and Taylor, W. D. *Polymer, Lond.* 1964, **5**, 353
- 32 Liu, Kang-Jen and Parsons, S. L. *Macromolecules* 1969, **2**, 529

Thermodynamics of mixtures of poly(propylene oxide) and benzene

C. BOOTH and C. J. DEVOY*

Vapour pressures of mixtures of poly(propylene oxide) and benzene have been measured at temperatures between 47°C and 75°C. No differences are detected between the results for polymer samples of differing microstructure. The thermodynamic dilution quantities calculated from the results are compared with the theory of Flory. The discrepancies between theory and experiment are similar to those found for mixtures of poly(ethylene oxide) and benzene, and are attributed to the occurrence of specific (charge-transfer) bonding in the mixture.

IN THE preceding paper¹ we have discussed the thermodynamic properties of mixtures of poly(ethylene oxide) and benzene. It proved possible to rationalize the solution properties, in a semi-quantitative way, in terms of the Flory theory². Poly(propylene oxide) differs from poly(ethylene oxide) in its solution properties being, for example, less soluble in polar solvents (e.g. water, methanol) and more soluble in paraffin hydrocarbons. It is of interest to compare the solution properties of the two polymers in a common solvent to determine, in a particular case, whether the difference is due principally to differences in the properties of the polymers (equation of state terms) or to differences in the solvent-polymer interaction.

EXPERIMENTAL

Benzene was purified by methods described elsewhere¹. In the temperature range 40–70°C it had vapour pressures within 0.2% of published values³.

High molecular weight poly(propylene oxide), used in the vapour pressure measurements, was prepared by means of the zinc diethyl and water catalyst system and fractionated, on the basis of crystallizability, by cooling a dilute solution of the polymer in isooctane. Details of this preparation and fractionation, together with the fractionation data, have been published elsewhere⁴. In this work we have used fractions 1 and 5, which have identical viscosity-average molecular weights (1.5×10^6). We have reason to assume⁵ that these fractions have identical molecular weight distributions ($M_w/M_n \sim 3$), and we take the number-average molecular weights to be about 0.5×10^6 . The two fractions differ considerably in microstructure. From a study⁴ of the multiple melting transitions of fraction 1 we have estimated that this fraction has a number-average sequence length of isotactic placements near 55. Fraction 5 is not crystallizable at room temperature and presumably has much shorter isotactic sequence lengths.

Vapour pressures were measured by means of the differential manometer described earlier¹.

* Present address: Department of Chemistry, University of Essex, Colchester

RESULTS

The activities of benzene (a_1) in solutions of the poly(propylene oxide) fractions at several temperatures are given in *Table 1*. These values were calculated by use of the value of the second virial coefficient (B) of benzene

Table 1 Weight fraction (w_1) and activity (a_1) of benzene in solutions of poly(propylene oxide)

w_1	a_1	w_1	a_1
<i>Fraction 1 (74.7°C)</i>		<i>Fraction 1 (47.2°C)</i>	
0.0884	0.2536	0.3739	0.7532
0.1902	0.4833	0.4306	0.8112
0.2570	0.6026	0.5160	0.8814
0.3160	0.6895	0.6361	0.9463
0.3691	0.7556	0.6868	0.9649
0.4609	0.8451		
0.5952	0.9309		
0.6791	0.9633		
<i>Fraction 1 (69.9°C)</i>		<i>Fraction 5 (74.7°C)</i>	
0.0910	0.2601	0.1143	0.3190
0.1992	0.4993	0.2075	0.5172
0.2715	0.6244	0.3639	0.7500
0.3293	0.7060	0.4685	0.8512
0.3837	0.7705	0.5800	0.9232
0.4856	0.8636	0.6573	0.9562
<i>Fraction 1 (60.2°C)</i>		<i>Fraction 5 (47.2°C)</i>	
0.2101	0.5168	0.1305	0.3494
0.2947	0.6555	0.2449	0.5741
0.3568	0.7368	0.4177	0.8006
0.4122	0.7972	0.5184	0.8839
0.5014	0.8734	0.6177	0.9389
0.6230	0.9427	0.6845	0.9652
0.6848	0.9650		

recommended by Allen *et al*⁶, and the relation

$$a_1 = \frac{p_1}{p_1^0} \exp \left[\frac{-B}{RT} (p_1^0 - p_1) \right]$$

where p_1 and p_1^0 are the vapour pressures of benzene over, respectively, solution and pure solvent.

Inspection of *Table 1* reveals that the activities of benzene are unaffected by the nature of the polymer. This is in keeping with what is known of the dilute solution properties of fractions of poly(propylene oxide) of this type⁷. Accordingly we have analysed the data for both fractions together.

In order to calculate the entropy and heat of dilution we have calculated the quantity

$$\chi' = \frac{\ln a_1 - \ln(1 - w_2) - (1 - 1/x_n)w_2}{w_2^2}$$

Table 2 Thermodynamic dilution quantities for poly(propylene oxide) and benzene at 61.0°C

Weight fraction benzene	Δh_1 (cal mol ⁻¹)	Δs_1 (cal deg ⁻¹ mol ⁻¹)	χ
0.2	-144	0.952	0.119
0.3	-104	0.505	0.137
0.4	-71.3	0.266	0.156
0.5	-43.3	0.141	0.180
0.6	-21.9	0.075	0.208

where w_2 is the weight fraction of polymer and x_n the ratio of the number-average molecular weights of polymer and solvent. This parameter has values in the range 0.15–0.30, and is a slowly changing function of polymer concentration. Smoothed values of χ' were used to calculate the free energies of dilution at the given temperatures and at several values of w_2 , and from these data entropies and heats of dilution were calculated in the usual way⁸. Values are quoted in Table 2, and plotted in Figures 1 and 2.

COMPARISON OF EXPERIMENT WITH THEORY

The theory of Flory *et al*², has been described briefly in the preceding paper¹.

In order to calculate the thermodynamic dilution quantities from this theory it is necessary to know specific volumes (v_{sp}), coefficients of expansion (α) and thermal pressure coefficients (γ) for the two components. Values of these quantities are available^{9,10} for poly(propylene oxide) of molecular weights near 2000. There is some evidence¹⁰ that α is not much influenced by molecular weight, though the nature of the end groups is important. In Table 3 we present our own measurements of the specific volume of poly(propylene glycol) 2000 (Shell Chemical Company, number-average molecular

Table 3 Specific volumes of poly(propylene glycol) 2000

Temperature (°C)	Specific volume (cm ³ g ⁻¹)
74.7	1.0399
70.0	1.0359
60.2	1.0282
47.2	1.0179
20.0	0.9965

weight 1900), which are in substantial agreement with earlier measurements^{9,10}. The surface ratio, s_2/s_1 , was calculated on the assumption that the benzene molecule is a sphere of radius $(3v_1^*/4\pi)^{1/3}$ and that the poly(propylene oxide) unit in the chain is a cylinder of volume v_1^* and radius $(v_m^*/L\pi)^{1/2}$, where v_m^* is the characteristic volume of a monomer unit in the chain, and L is the distance per monomer unit in the C direction in the unit cell (repeat distance

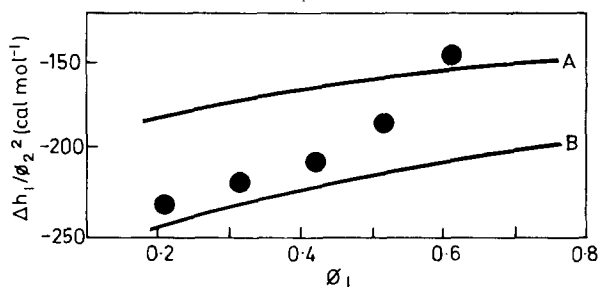


Figure 1 Reduced heat of dilution ($\Delta h_1/\phi_2^2$) against segment fraction of benzene (ϕ_1) for poly(propylene oxide) at 61.0°C. Theoretical curves are A, $X_{12} = -2 \text{ cal cm}^{-3}$ and B, $X_{12} = -3 \text{ cal cm}^{-3}$

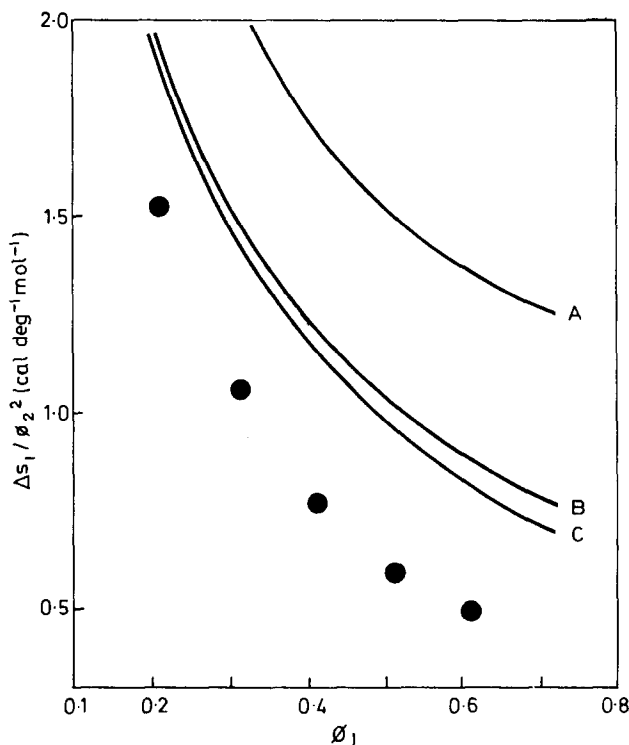


Figure 2 Reduced entropy of dilution ($\Delta s_1/\phi_2^2$) against segment fraction of benzene (ϕ_1) for poly(propylene oxide) at 61.0°C. Curves are A, the Flory combinatorial entropy; B, $X_{12} = -2 \text{ cal cm}^{-3}$; and C, $X_{12} = -3 \text{ cal cm}^{-3}$

$\sim 7 \text{ \AA}$, 0.7 nm, for 2 monomer units¹¹). We have made calculations for the temperature 61.0°C. Values of the initial data and the characteristic parameters are given in Table 4.

Comparison of the calculated and experimental heats of dilution serves to define the energy parameter X_{12} . Fair agreement between theory and experiment is found for X_{12} between -2 and -3 cal cm^{-3} : the comparison is illustrated in Figure 1. Calculated values of the reduced entropies of dilution and of the free energy parameter χ for $X_{12} = -2$ and -3 cal cm^{-3} are

compared with experimental values in *Figures 2* and *3*. The estimated precision of the experimental values is $-\Delta h_1/\phi_2^2$ to ± 25 cal mol $^{-1}$; $\Delta s_1/\phi_2^2$ to ± 0.08 cal deg $^{-1}$ mol $^{-1}$; χ to ± 0.003 . ϕ is the segment fraction.

Table 4 Parameters for the calculation of thermodynamic dilution quantities at 61.0°C

	Benzene	Poly(propylene oxide)†
α (deg $^{-1}$)	1.316×10^{-3} ¹²	0.780×10^{-3} §
γ (cal cm $^{-3}$ deg $^{-1}$)	0.244 ¹³	0.239 ⁹
v_{sp} (cm 3 g $^{-1}$)	1.1977 ¹²	1.0288§
p^* (cal cm $^{-3}$)	145.9	119.1
v_{sp}^* (cm 3 g $^{-1}$)	0.8954	0.8424
T^* (K)	4837	6330
r	1	6030
$s_2/s_1 = 0.742$		

† Low molecular weight polymer

§ From data of *Table 3*

1 cal \equiv 4.187J

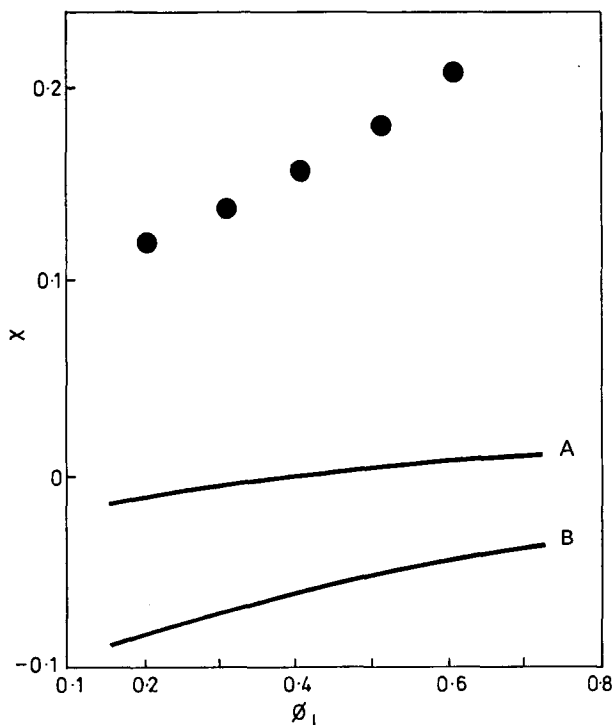


Figure 3 Parameter χ against segment fraction of benzene (ϕ_1) for poly(propylene oxide) at 61.0°C. Theoretical curves are A, $X_{12} = -2$ cal cm $^{-3}$ and B, $X_{12} = -3$ cal cm $^{-3}$

DISCUSSION

In general the results for poly(propylene oxide) and benzene are similar to those for poly(ethylene oxide) and benzene¹. The theory predicts higher values of Δh_1 and Δs_1 for poly(propylene oxide) than for poly(ethylene oxide) in agreement with experiment, even when the interaction parameter X_{12} is taken to be the same in both cases. This is due to the unusually large molecular cohesion in poly(ethylene oxide)⁹, as is evident from the high thermal pressure coefficient and high density of this polymer; $0.33 \text{ cal cm}^{-3} \text{ deg}^{-1}$ and 1.095 g cm^{-3} respectively¹ at 60°C . Poly(propylene oxide) has more typical values of $0.24 \text{ cal cm}^{-3} \text{ deg}^{-1}$ and 0.973 g cm^{-3} for these parameters at 60°C .

The discrepancy between theoretical and experimental values of the entropy of dilution for poly(propylene oxide) and benzene corresponds to an entropy parameter [$\chi_s = \Delta(\Delta s_1)/R\phi_2^2$] of about 0.15 for X_{12} between -2 and -3 cal cm^{-3} . The discrepancy between the theoretical and experimental values of χ (of 0.1 to 0.2) is mainly entropic in origin. We have suggested, in the case of poly(ethylene oxide) and benzene for which we find a similar discrepancy ($\chi_s = 0.25$), that this is due to the formation of a donor-acceptor complex between benzene and ether oxygen. The large negative value of X_{12} of between -2 and -3 cal cm^{-3} , compared with X_{12} near -4 cal cm^{-3} for high molecular weight poly(ethylene oxide) and benzene, is consistent with this explanation. It is of interest that the discrepancies between theory and experiment, as measured by χ_s , differ by about a factor of two between the poly(propylene oxide) and the poly(ethylene oxide) solutions. We would expect that errors introduced through approximations in the theory would be unimportant when comparing similar polymers. We conclude that a major contribution to the solution properties in these systems arises from specific intermolecular interactions which are weaker in the poly(propylene oxide)-benzene system than in the poly(ethylene oxide)-benzene system.

ACKNOWLEDGEMENTS

We thank Mr J. B. M. Herbert for helpful discussions. C.J.D. acknowledges receipt of a Science Research Council Studentship.

*Department of Chemistry,
University of Manchester,
Manchester M13 9PL, UK*

(Received 5 November 1970)

REFERENCES

- 1 Booth, C. and Devoy, C. J. *Polymer, Lond.* 1971, **12**, 309
- 2 Flory, P. J. *J. Amer. Chem. Soc.* 1965, **87**, 1833; Eichinger, B. E. and Flory, P. J. *Trans. Faraday Soc.* 1968, **64**, 2035, 2053, 2061, 2066
- 3 Smith, E. R. *J. Res. Nat. Bur. Standards* 1941, **26**, 129
- 4 Booth, C., Devoy, C. J., Dodgson, D. V. and Hillier, I. H. *J. Polym. Sci. (A-2)* 1970, **8**, 519

- 5 Booth, C., Higginson, W. C. E. and Powell, E. *Polymer, Lond.* 1964, **5**, 479
- 6 Allen, P. W., Everett, D. H. and Penney, M. F. *Proc. Roy. Soc. (A)* 1952, **12**, 149
- 7 Allen, G., Booth, C. and Price, C. *Polymer, Lond.* 1966, **7**, 167
- 8 Booth, C., Gee, G., Holden, G. and Williamson, G. R. *Polymer, Lond.* 1964, **5**, 343
- 9 Allen, G., Gee, G., Mangaraj, D., Sims, D. and Wilson, G. *Polymer, Lond.* 1960, **1**, 467
- 10 Allen, G., Booth, C., Jones, M. N., Marks, D. and Taylor, W. D. *Polymer, Lond.* 1964, **5**, 547
- 11 'Polymer Handbook', Interscience Publishers, New York, 1966
- 12 Wood, S. E. and Brussie, J. P. *J. Amer. Chem. Soc.* 1943, **65**, 1891
- 13 Holder, G. A. and Whalley, E. *Trans. Faraday Soc.* 1962, **58**, 2095

Heat of fusion of isotactic poly(propylene oxide)

C. BOOTH, C. J. DEVOY* and G. GEE

The melting points of mixtures of a crystallizable sample of poly(propylene oxide) and benzene have been determined by measuring their vapour pressures as a function of temperature. The activities of benzene in mixtures with poly(propylene oxide) have been reported earlier for a wide range of temperatures and compositions. By combining these sets of results the heat of fusion of isotactic poly(propylene oxide) is calculated to be 2.0 kcal† (mol of repeat units)⁻¹.

IN THE course of measurements of the thermodynamic properties of mixtures of poly(propylene oxide) and benzene¹, we have measured the melting points of mixtures of benzene with the crystallizable fraction of the polymer. These measurements enable us to determine the heat and entropy of fusion of isotactic poly(propylene oxide).

With the assumption that the heat of fusion of solute (Δh) is independent of temperature and that the system is in thermodynamic equilibrium, the relation between the chemical potential of the solute in the mixture (μ_2) and the melting point of the mixture (T_m^s) is

$$\mu_2^0 - \mu_2 = \Delta h(1 - T_m^s/T_m) \quad (1)$$

where μ_2^0 and T_m are respectively the chemical potential and the melting point of pure solute.

The chemical potential of the solute can be written in the Flory-Huggins² formulation as

$$\mu_2^0 - \mu_2 = RT_m^s r(\phi_1 - \chi\phi_1^2) \quad (2)$$

where ϕ_1 is the volume fraction of solvent, χ is the Flory-Huggins parameter, and r is the ratio of the molar volumes of polymer and solvent. In writing equation (2) it is assumed that r is very large. Substitution of equation (2) in equation (1) leads to the relation

$$1/\phi_1(1/T_m^s - 1/T_m) = Rr/(1 - \chi\phi_1) \Delta h \quad (3)$$

If χ is independent of concentration and proportional to T^{-1} , a plot of $1/\phi_1(1/T_m^s - 1/T_m)$ against ϕ_1/T_m^s will be linear with intercept $Rr/\Delta h$.² However, it is known from our earlier investigations¹ that for poly(propylene oxide) and benzene χ is concentration dependent and also contains contributions originating in the entropy of mixing (i.e. not proportional to T^{-1}). Here we present, without recourse to theory, an alternative method of evaluating Δh .

* Present address: Department of Chemistry, University of Essex, Colchester

† 1 cal = 4.187 J

The quantity $(\mu_2^0 - \mu_2)$ can be evaluated from measurements of the activity of the solvent in the solution (a_1) by use of the Gibbs-Duhem relationship, i.e. through the equation

$$\mu_2^0 - \mu_2 = RT \int_0^{n_1} \frac{n_1}{n_2} \left(\frac{\partial \ln a_1}{\partial n_1} \right)_{T, p} dn_1 \quad (4)$$

where the quantities n are the number of moles of solvent (1) and solute (2). For our purposes this equation is best expressed as

$$\mu_2^0 - \mu_2 = \frac{RTM_2}{M_1} \int_0^{w_1} \frac{w_1}{w_2} \left(\frac{\partial \ln a_1}{\partial w_1} \right)_{T, p} dw_1 \quad (5)$$

where M and w are respectively molecular weights and weight fractions. The activity of solvent in solutions in which w_1 approaches zero cannot be measured directly because the solute will crystallize. Here we make use of determinations of the activity of benzene in solutions covering a wide range of temperatures and concentrations, as well as measurements on solutions of a non-crystallizable poly(propylene oxide) fraction, to guide our extrapolation to $w_1 = 0$.

EXPERIMENTAL AND RESULTS

Benzene was purified by methods described in a preceding paper³. Poly(propylene oxide) was prepared by means of the zinc diethyl and water catalyst system and fractionated, on the basis of crystallizability, by cooling a dilute solution of the polymer in isooctane. Details of this preparation and fractionation have been published elsewhere⁴. Fractions had number-average molecular weights of about 5×10^5 .

Vapour pressures of benzene over mixtures with a crystallizable fraction 1 and a non-crystallizable fraction 5 were measured by means of a differential manometer³. Pressures were measured to ± 0.01 cmHg* and weights of the components of the mixtures to ± 1 mg. Vapour space corrections were made.

Melting points of mixtures of fraction 1 and benzene were determined as follows. Mixtures were held for 15 minutes at temperatures some 10°C above their melting points, and then crystallized at temperatures some 20°C below their melting points. Vapour pressures of benzene over the mixtures (p_1) were then measured from temperatures 10°C below the melting points at increments of 1°C or less, allowing at least one day for equilibration at each temperature. The concentration was maintained at a constant value by adjusting the vapour space volume. Vapour pressure ratios (p_1/p_1^0), where p_1^0 is the vapour pressure of the pure benzene, are plotted against temperature in *Figure 1*. These curves are of the form predicted⁵ for copolymers and differ from the corresponding curves for homopolymers (see for example *Figure 5*) in the persistence of small levels of crystallinity over a range of

* 1 cmHg = 1333 N m^{-2}

HEAT OF FUSION OF ISOTACTIC POLY(PROPYLENE OXIDE)

temperatures below the melting point. Consequently melting points were defined by the point of departure of the vapour pressure curves from the straight lines established at high temperatures where the mixture is homogeneous. These melting points are listed in *Table 1*.

We have studied⁴ the melting of fraction 1 in the absence of solvent, and

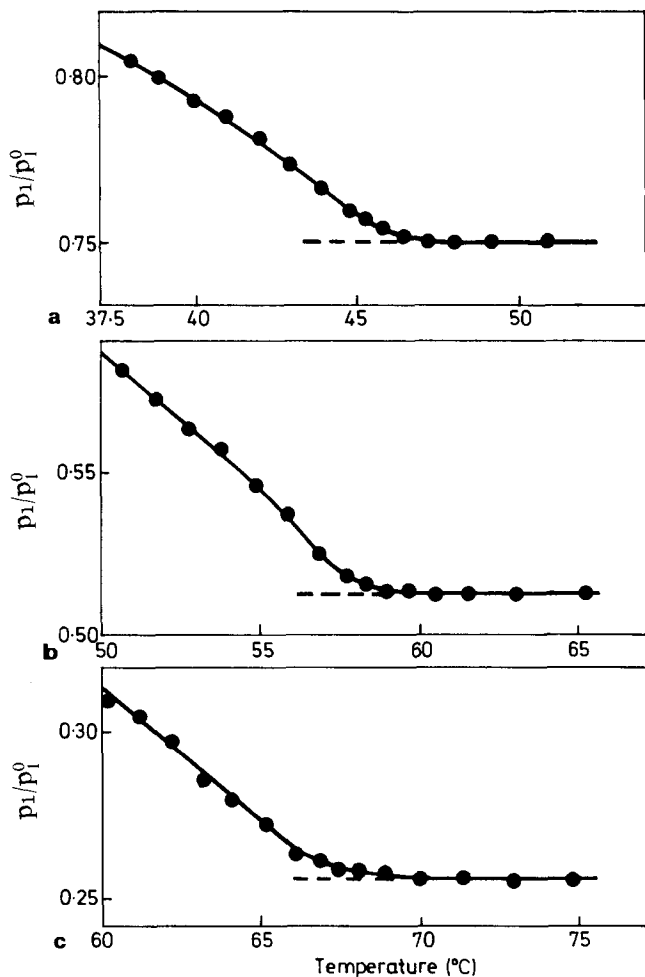


Figure 1 Vapour pressure ratio (p_1/p_1^0) against temperature for mixtures of poly(propylene oxide) fraction 1 and benzene. Weight fractions of benzene and crystallization temperatures are (a) 0.3740 and 30.0 $^{\circ}\text{C}$, (b) 0.2101 and 40.1 $^{\circ}\text{C}$ and (c) 0.0910 and 50.2 $^{\circ}\text{C}$

detected three melting points. Two of these are dependent upon the crystallization temperature and are ascribed to the melting of crystallites with thicknesses determined by nucleation processes. The third is largely independent of crystallization temperature and is ascribed to the melting of crystallites with thickness determined by the sequence lengths of isotactic placements in

the partially isotactic polymer. Analysis⁴ of these melting points, in terms of Flory's theory⁶ of the crystallization of copolymers, leads to the conclusion that fraction 1 has an equilibrium melting point of 80°C and a number-average sequence length of isotactic placements of 55. In this work we detect single melting points for the mixtures, and find no dependence of melting

Table 1 Melting points and chemical potentials for mixtures of poly(propylene oxide) and benzene

Weight fraction of benzene (w_1)	Melting point of mixture (T_m^s , °C)	Chemical potential difference $\mu_2^0 - \mu_2$ [cal (mol of repeat units) ⁻¹]
0.3740	47.2	169.5
0.2101	60.2	101.1
0.0910	69.9	45.7

point on crystallization temperature. This is as expected since ample time was allowed at temperatures immediately below the melting point for recrystallization and crystallite perfecting.

The activities of benzene (a_1) in homogeneous mixtures with fraction 1 and 5 at several temperatures, including those listed in Table 1, have been published in the preceding paper¹. The extrapolation of these activities to zero weight fraction of solvent is most easily achieved by extrapolating the quantity

$$\chi' = [\ln a_1 - \ln w_1 - (1 - 1/x_n)w_2]/w_2^2 \quad (6)$$

which is a slowly changing function of solvent concentration. x_n is the ratio of polymer number-average molecular weight to that of solvent. Plots of χ' against w_1 are shown in Figure 2. Curves through the data for fraction 1 at 69.9, 60.2 and 47.2°C, drawn by taking into account all the data, were expressed as polynomials in solvent concentration (w_1), and subsequent solution of equations (5) and (6) gave the values of $(\mu_2^0 - \mu_2)$ quoted in Table 1.

According to equation (1) a plot of $(\mu_2^0 - \mu_2)$ against T_m^s should be a straight line of intercept T_m and slope $-\Delta h/T_m$. This plot is shown in Figure 3, and yields values of $T_m = 78.2^\circ\text{C}$ and $\Delta h = 1.9$ kcal (mol of repeat units)⁻¹. If we take into account the variation of the heat of fusion with temperature, through the revised equation

$$\mu_2^0 - \mu_2 + \int_{T_m^s}^{T_m} \Delta C_p dT - T_m^s \int_{T_m^s}^{T_m} \frac{\Delta C_p}{T} dT = \Delta h(T_m) \left(1 - \frac{T_m^s}{T_m}\right) \quad (7)$$

together with $\Delta C_p = 7.25$ cal deg⁻¹ (mol of repeat units)⁻¹⁷ and $T_m = 78.2^\circ\text{C}$, we obtain a better value of $\Delta h(T_m)$ of 2.0 kcal (mol of repeat units)⁻¹. We estimate a precision of ± 0.1 kcal mol⁻¹. The corresponding value of the entropy of fusion, $\Delta s(T_m)$, is 5.7 ± 0.3 cal deg⁻¹ (mol of repeat units)⁻¹.

HEAT OF FUSION OF ISOTACTIC POLY(PROPYLENE OXIDE)

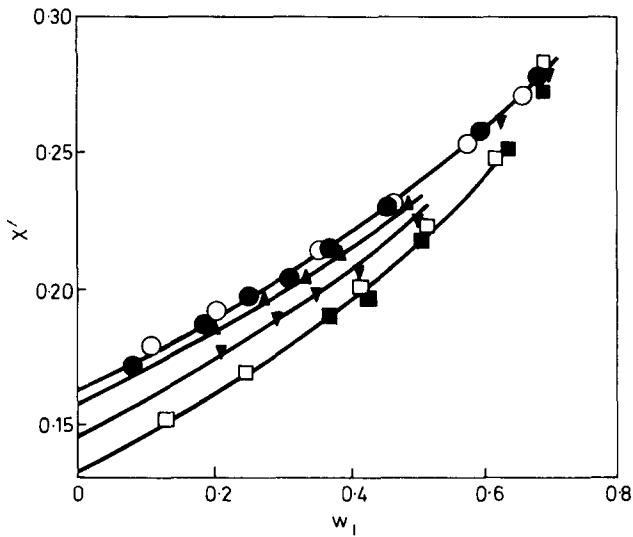


Figure 2 Parameter χ' against weight fraction of solvent (w_1) for poly(propylene oxide) and benzene. Points are for fraction 1 at \bullet 74.7°C , \blacktriangle 69.9°C , \blacktriangledown 60.2°C and \blacksquare 47.2°C , and for fraction 5 \circ at 74.7°C and \square 47.2°C . Curves are those used in the determination of $(\mu_2^0 - \mu_2)$

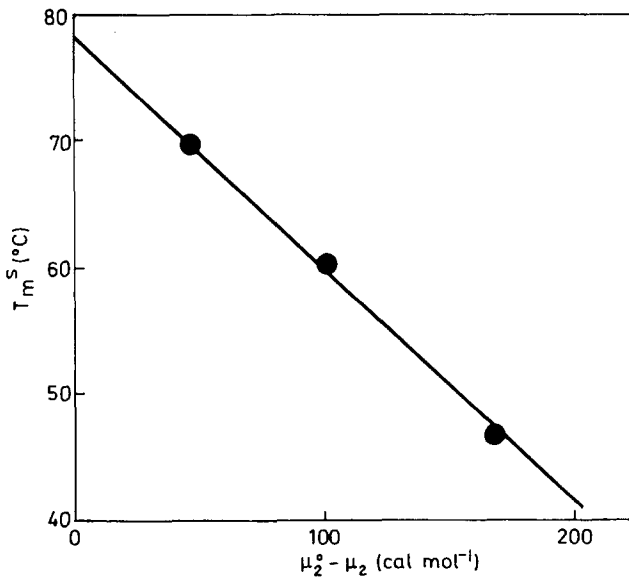


Figure 3 Melting point (T_m^s) against $(\mu_2^0 - \mu_2)$ for mixtures of poly(propylene oxide) fraction 1 and benzene

DISCUSSION

The only other determination of the heat of fusion of isotactic poly(propylene oxide) is that of Beaumont *et al*⁷, which is based upon calorimetric measurements. They conclude that Δh is not less than 1.8 kcal (mol of repeat units)⁻¹. The values quoted in the 'Polymer Handbook'⁸ of 2.0 and 1.3 kcal (mol of repeat units)⁻¹ are respectively a guess and a misplaced density.

Conventional treatment of the data of *Table 1*, by equation (3), yields a value of $\Delta h(T_m)$ near 1.8 kcal (mol of repeat units)⁻¹. The discrepancy between this value and 2.0 kcal mol⁻¹ reflects the deviation of the poly(propylene oxide)/benzene system from the Flory-Huggins ideal. The requirement that the polymer solution approximates a Flory-Huggins solution may well be a greater restriction upon the use of the conventional method of determining Δh than is generally realized.

The value of T_m of 78°C is higher than values which have been measured, by similar methods of slow heating, for bulk poly(propylene oxide). Most investigators⁸ place T_m for fractions of poly(propylene oxide) of high degree of crystallinity in the temperature range 73–75°C. The value of the melting point found here, by extrapolation of measurements of the melting points of polymer-solvent mixtures, is in fair agreement with the equilibrium melting point (80°C) calculated⁴ from the equilibrium melting-point (82°C) of high molecular weight isotactic poly(propylene oxide) and the number-average sequence length of isotactic placements (55) of fraction 1. The equilibrium melting point is that of crystallites composed of the largest sequence lengths in the polymer sample⁶. The fact that we obtain a higher melting point by extrapolation of the melting points of polymer-solvent mixtures than by direct measurements on bulk polymer is consistent with a greater ease of fractionation during crystallization and recrystallization in solution than in bulk.

ACKNOWLEDGEMENTS

We thank Mr J. B. M. Herbert for helpful discussions. C.J.D. acknowledges receipt of a Science Research Council Studentship.

REFERENCES

- 1 Booth, C. and Devoy, C. J. *Polymer, Lond.* 1971, **12**, 320
- 2 Flory, P. J., 'Principles of Polymer Chemistry', Cornell University Press, Ithaca, New York, 1953
- 3 Booth, C. and Devoy, C. J. *Polymer, Lond.* 1971, **12**, 309
- 4 Booth, C., Devoy, C. J., Dodgson, D. V. and Hillier, I. H. *J. Polym. Sci. (A-2)* 1970, **8**, 519
- 5 Flory, P. J. *Trans. Faraday Soc.* 1955, **51**, 848
- 6 Flory, P. J. *J. Chem. Physics* 1949, **17**, 223
- 7 Beaumont, R. H., Clegg, B., Gee, G., Herbert, J. B. M., Marks, D. J., Roberts, R. C. and Sims, D. *Polymer, Lond.* 1966, **7**, 401
- 8 'Polymer Handbook', Interscience Publishers, New York, 1966
- 9 Braun, W., Hellwege, K. H. and Knappe, W. *Kolloid-Z* 1967, **215**, 10
- 10 Beech, D. R., Ph.D. Thesis, University of Manchester, 1970

APPENDIX:

HEAT OF FUSION OF POLY(ETHYLENE OXIDE)

Measurements of the heat of fusion of low molecular weight poly(ethylene oxide) by calorimetry^{7,9} have yielded values near 2.0 kcal (mol of repeat units)⁻¹. Consequently it is possible to test a new method of determination of the heat of fusion of a polymer, such as that used here for poly(propylene oxide), by trial experiments with poly(ethylene oxide). In this work we used a poly(ethylene glycol) fraction 6000F³ which has a narrow molecular weight distribution and a number-average molecular weight of 5700.

The bulk melting point was measured dilatometrically, with a heating rate of 1 deg day⁻¹. Plots of dilatometer height against temperature (*Figure 4*)

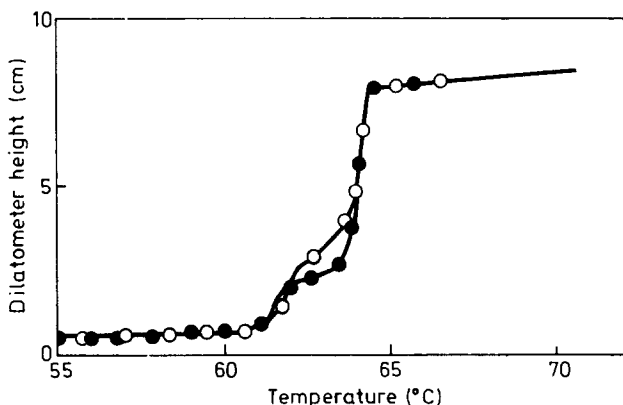


Figure 4 Height of mercury column in dilatometer versus temperature for poly(ethylene oxide) 6000F crystallized at ○ 41.0°C and ● 50.6°C

show two melting transitions. Subsequent work¹⁰ has shown that these are attributable to extended chain crystals (high melting) and once-folded chain crystals (low melting). The higher melting temperature was 64.4°C.

The melting point of a mixture of 6000F and benzene (weight fraction benzene = 0.3211) was measured by the vapour pressure method. Plots of vapour pressure ratio (p_1/p_1^0) against temperature (*Figure 5*) show one melting transition. This is in keeping with the greater chain mobility and ease of recrystallization expected in solution. We assume that the melting point of the mixture (45.8°C) is that of extended chain crystals.

The chemical potential difference ($\mu_2^0 - \mu_2$) for 6000F in the mixture at the melting point was found to be 101.8 cal (mol of repeat units)⁻¹. In this calculation we made use of equations (5) and (6) and measurements, already reported³, of activities of benzene in a number of mixtures with 6000F. Insertion of this value of $\mu_2^0 - \mu_2$, together with $T_m = 64.4^\circ\text{C}$ and $T_m^s = 45.8^\circ\text{C}$, into equation (1) yields a heat of fusion $\Delta h = 1.85$ kcal (mol of repeat units)⁻¹. Correction for the temperature dependence of Δh , by use of equation

(7) with $\Delta C_p = 13.0 - 0.0167T$ cal deg⁻¹ (mol of repeat units)⁻¹ ⁷, leads to a value of $\Delta h = 1.9_2$ cal (mol of repeat units)⁻¹.

This value is in good agreement with that of 2.0 kcal (mol of repeat units)⁻¹ found^{7,9} by calorimetry for poly(ethylene oxide) of molecular weight in the range 2000 to 4000. Close comparison of these values is not called for since they apply to lamellar crystals of limited thickness and may contain an appreciable contribution from the heat of formation of the end interface.

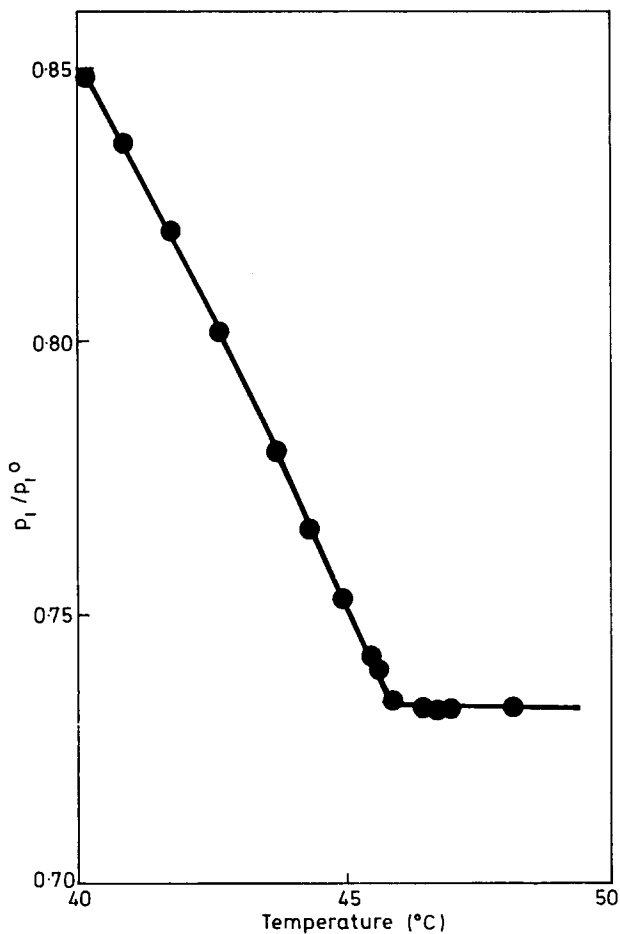


Figure 5 Vapour pressure ratio (p_1/p_1^0) against temperature for poly(ethylene oxide) 6000F mixed with benzene; weight fraction benzene = 0.3211; crystallization temperature = 30.0°C

*Kinetics of epoxy cure: (1) The system bisphenol-A diglycidyl ether/*m*-phenylene diamine*

M. A. ACITELLI, R. B. PRIME and E. SACHER

The cure of the system bisphenol-A diglycidyl ether/*m*-phenylene diamine has been monitored by several methods in the range 23–157°C. The methods give identical results and show that the same process occurs over the complete cure reaction in the temperature range studied: the kinetically indistinguishable network extension by both primary and secondary amines. The maximum extent of cure is governed by network rigidity, in not allowing reactants into proximity for reaction. The kinetics suggest the reaction itself is diffusion controlled.

INTRODUCTION

IN ORDER to make optimum use of epoxies as structural materials, it is important to know what the curing process is, to what extent it proceeds, the structure of the cured material and how these are influenced by temperature. The curing process, the subject of this paper, has been monitored by several techniques, among them d.c. conductivity¹, infra-red absorption² (IR), and differential scanning calorimetry³ (DSC), which are the methods used in the present study.

Both DSC, which measures the rate of heat production, and IR, which measures intensity changes in absorption bands, are more sensitive to the early stages of the process, where the rate of chemical reaction is highest. The d.c. conductivity suffers a small diminution in magnitude prior to the gel point because of increased viscosity; the large change subsequent to the gel point is due to the inhibition that the growing 3-dimensional network offers migrating charge carriers.

Thus, DSC and IR monitor the chemical reaction, while d.c. conductivity monitors the secondary process of inhibition to charge carrier migration. Although DSC and IR are expected to follow the same kinetics, no *a priori* reason exists for the d.c. conductivity to do so; if it did, the data would be complementary, covering the complete process.

The present study, one part of an investigation on the curing and physical properties of various epoxide/hardener systems, considers the cure of the system bisphenol-A diglycidyl ether/*m*-phenylene diamine, which is exemplary of the epoxide/amine system.

EXPERIMENTAL

Materials

Both the bisphenol-A diglycidyl ether (Dow DER 332) and the *m*-phenylene diamine (Aldrich, purissimus grade) were used without further purification.

although the diamine was stored at -20°C to prevent degradation. The comonomer mixture was prepared in the following way: 10 g of epoxide and 2 g of diamine (33% excess) were separately dissolved in minimal amounts of methylene dichloride, chilled in ice water, mixed and freeze dried, after which the mixture was stored at -20°C . In spite of this, some reaction was detectable after two weeks of storage, so a fresh sample was prepared at the beginning of each week, and the unused portion was discarded at the end.

DSC data

The experiments were carried out on a Perkin-Elmer DSC-1 differential scanning calorimeter. Sample size was 10–20 mg. The large temperature range covered, 23– 157°C , necessitated the use of two isothermal methods to accumulate data. In method 1, used between 115 and 157°C , samples were heated in the calorimeter as quickly as possible to temperature. Equilibrium was established in less than two minutes, after which the rate of enthalpy production at that temperature was followed with time^{4, 5}.

Below 100°C , method 1 proved insensitive, so method 2 was employed. Samples were cured outside the calorimeter at a given temperature. After various times, the residual cure was measured by DSC at a heating rate of $10^{\circ}\text{C}/\text{min}$. For both methods, α , the fraction reacted, was calculated as that fraction of the total possible enthalpy of reaction. Data were typically evaluated for $\alpha < 0.7$. Above 0.7, diminished rates gave poorer sensitivity, and these data were not used.

IR data

Infra-red spectra, as a function of time, were obtained on a Perkin-Elmer 521 grating spectrophotometer. Constant temperatures in the range 25– 75°C were obtained by holding half mil* samples between salt flats in a Research and Industrial Instruments Company VLT-2 variable temperature unit controlled with a TEM-1 automatic temperature controller. The extent of reaction, α , was obtained as that fraction of the change in the optical density of the oxirane ring at $10.95\ \mu\text{m}$, *Figure 1*, using baseline techniques; the optical density at infinite time was obtained after a postcure at 120°C for several hours. As with the DSC experiments, data were typically obtained for $\alpha < 0.7$.

DC conductivity data

Cells were specially moulded of DuPont Teflon FEP 110, having a 10 mil gap and containing guarded electrodes; they were allowed to reach thermal equilibrium at various constant temperatures in the range 23– 88°C before being loaded. These constant temperatures were maintained by suspending the cells in an air bath warmed by various refluxing liquids. Voltages in the range 0–200V were supplied by heavy duty batteries, and currents were measured with a Keithley 419 picoammeter, with display on a Leeds and Northrup Speedomax W AZAR strip chart recorder.

Conductivity, σ , was calculated as

$$\sigma = J/E \quad (1)$$

* 1 mil = $25.4\ \mu\text{m}$

where J is the current density flowing under the electric field, E . Behaviour was ohmic, in that conductivity-time plots were superimposable at any constant temperature over the entire voltage range. A typical log-log plot is seen in *Figure 2*, which indicates little change prior to the gel point. Subsequent to the gel point, there is a change in the conductivity over several

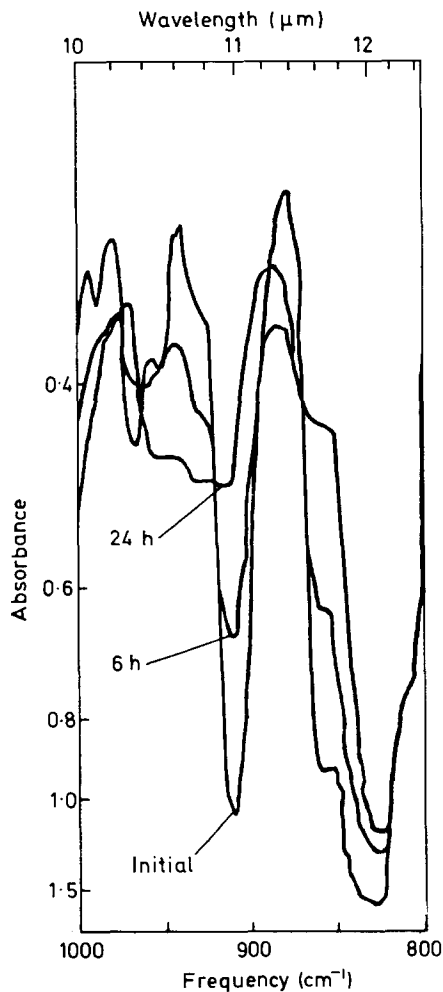


Figure 1 Infra-red absorption of the oxirane group during cure at 50°C

orders of magnitude before levelling out. The fraction reacted, α , was determined along the linear portion of plots such as *Figure 2*, subsequent to the gel point, using the fraction reacted at some point on the line as obtained from DSC data and the previously established¹ proportionality between $d \ln \sigma / dt$ and $d\alpha / dt$. Data were typically obtained for $\alpha > 0.7$.

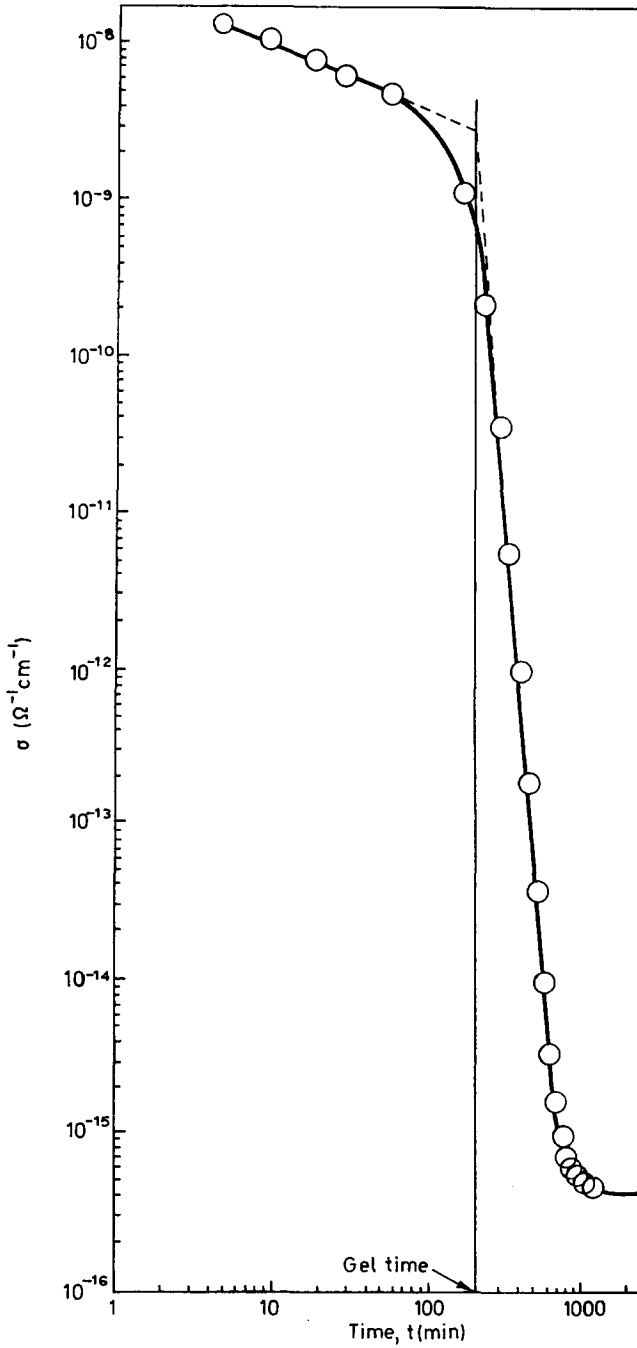


Figure 2 A conductivity-time plot during cure at 52°C

Treatment of data

With the exception of DSC method 1, which gave both $\alpha(t)$ and da/dt directly, the other methods gave only $\alpha(t)$, where t is time. Values of da/dt for these latter methods were obtained numerically on a computer. The various data were then fitted to the equation⁶

$$\frac{da}{dt} = k(1 - \alpha)^n \quad (2)$$

where k is the overall rate constant, and n is the overall reaction order.

The equation precludes an induction time since, at $\alpha = 0$, da/dt is finite. In the DSC and IR data near room temperature, there appeared to be small induction times; whether they were in fact induction times or were due to the inherent difficulties involved in obtaining very small values of α is not clear. In any case, in order to use equation (2), $\alpha(t)$ was extrapolated back to zero, and that time was defined as time zero. In the case of an unambiguous induction time, equation (2) would be replaced by one in which $da/dt = 0$ at $\alpha = 0^5, 6$.

Table 1 Rate constants and reaction orders for the cure of bisphenol-A diglycidyl ether/*m*-phenylene diamine

Temperature (°C)	DSC method 1		DSC method 2		IR		Conductivity	
	k(s ⁻¹)	<i>n</i>	k(s ⁻¹)	<i>n</i>	k(s ⁻¹)	<i>n</i>	k(s ⁻¹)	<i>n</i>
23			3.0 × 10 ⁻⁵ 2.3				1.3 × 10 ⁻⁵ 0.47	
25					1.8 × 10 ⁻⁵ 1.1			
35					3.0 × 10 ⁻⁵ 0.87			
50					9.6 × 10 ⁻⁵ 0.65			
52.5							7.1 × 10 ⁻⁵ 0.69	
56			3.4 × 10 ⁻⁴ 1.7					
60					2.2 × 10 ⁻⁴ 0.72			
72.5							1.3 × 10 ⁻⁴ 0.50	
75			3.8 × 10 ⁻⁴ 1.3		4.4 × 10 ⁻⁴ 0.50			
87.6							5.3 × 10 ⁻⁴ 0.79	
115	2.7 × 10 ⁻³ 1.1							
129	4.6 × 10 ⁻³ 1.0							
143	9.1 × 10 ⁻³ 1.0							
157	1.3 × 10 ⁻² 1.0							

RESULTS

The DSC, IR, and conductivity data were analysed according to equation (2). Values of rate constants and reaction orders are found in Table 1.

An Arrhenius plot of the data, Figure 3, fits the equation

$$k(\text{s}^{-1}) = 2.12 \times 10^4 \exp(-12.3 \text{ kcal mol}^{-1}/RT)^* \quad (3)$$

The points were found to fit this line with a correlation coefficient of 0.964,

* 1 kcal mol⁻¹ = 4.1868 kJ mol⁻¹

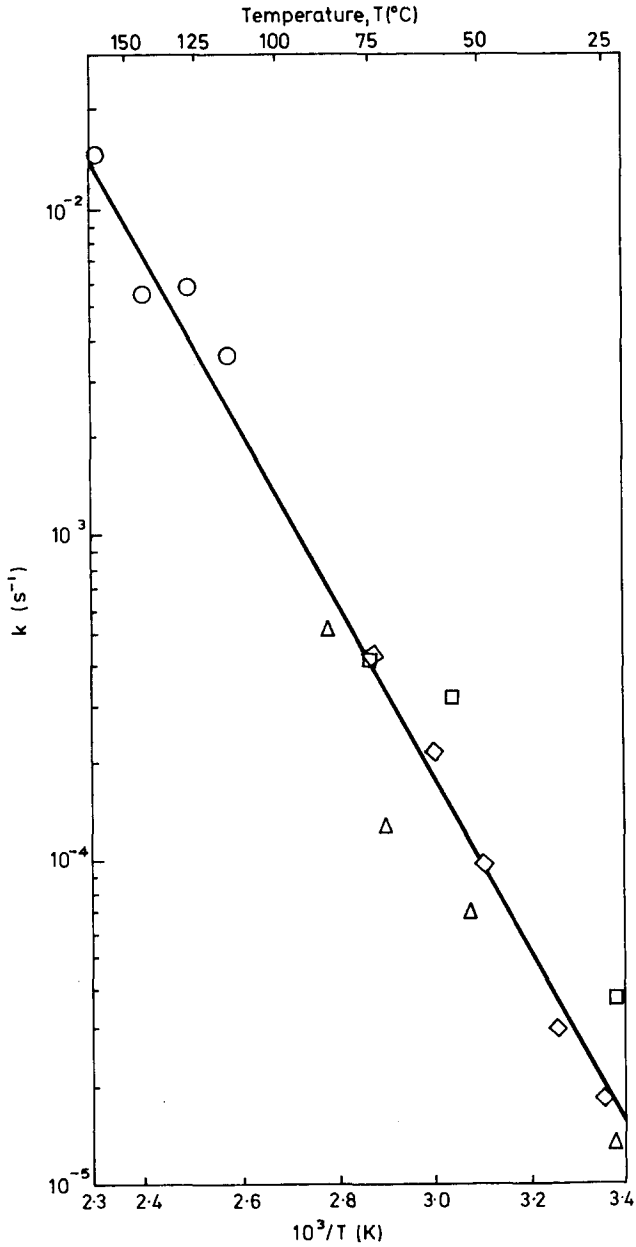


Figure 3 An Arrhenius plot of the cure data

- DSC method 1
- DSC method 2
- ◇ IR
- △ conductivity

a high positive correlation, indicating that the various methods all monitor the same phenomenon. An *F* test indicated that equation (3) represented the data with a probability of 0.9995.

DISCUSSION

On the basis of several model epoxide/amine reactions⁷⁻⁹, which indicated that the ratio of rate constants for primary:secondary amine reaction was 2:1, it was suggested¹⁰ that all of the primary amines react first to extend the chains; subsequent to this, secondary amines produced in the first step react to form cross-links. However, it can easily be demonstrated that reactions whose rate constants differ by a factor of 2 will occur essentially simultaneously, making the above scheme impossible.

Moreover, the present results indicate that identical kinetics hold over the entire reaction, in the temperature range studied. Since the concentrations of both primary and secondary amines change continuously during the cure process, this means that the rate constants for both primary and secondary amine reactions, as well as their temperature dependences, are indistinguishable⁵. To illustrate this point more clearly, the Arrhenius plot was submitted to a regression analysis using a confidence level of 95% (two standard deviations). The analysis showed that the pre-exponential in equation (3) was within ± 2.2 natural logarithmic units (i.e., between 2.25×10^3 and $2.0 \times 10^3 \text{ s}^{-1}$), and the activation energy was within $\pm 1.5 \text{ kcal mol}^{-1}$. Rate constants differing by a factor of 2 can easily be accommodated within these limits. The data suggest that one should consider the overall reaction as network extension, whether by primary or secondary amine. This is in general agreement with previous results for several other systems⁵.

The correlation of the conductivity data with those from DSC and IR indicates that the d.c. charge carriers experience the same energy barrier that the curing process does. This means the charge carriers are hindered by the process, itself. Since the overall curing process is one of network extension, the charge carriers must be too large to fit through the network voids. Thus, they must be ions, which may be impurities initially present or amine degradation products.

The gel point was determined, as in *Figure 2*, by the intersection of the tangent to the initial portion of the curve with the extension of the linear portion. A comparison with the DSC data indicated that the extent of reaction at the gel point was temperature independent, occurring in the range 67–70% of total possible cure; using the heat of reaction of the model system phenyl glycidyl ether/*n*-butylamine⁵, the total possible cure was estimated at 100% of epoxide present, due to the excess amine used in the present case.

The ultimate cure, the maximum extent of cure at any given temperature, was determined, as in *Figure 2*, as the extent of reaction at the final, abrupt levelling off of the conductivity. A comparison with the DSC data indicated that this ranged from 74% at 23°C to 90% at 88°C. When the system was permitted to cure at any constant temperature below the T_g of the totally cured system (130°C), the DSC trace seen on raising the temperature showed a glass transition prior to any further reaction. This has previously been seen

with an epoxide/anhydride system⁴ and means that network extension is limited by the rigidity of the network itself. The cure at any temperature below 130°C proceeds until the rigidity of the network prevents reactants from coming into proximity and reacting further, as in several other systems^{4, 5, 11}.

The fact that the same reaction occurs both prior to the gel point (DSC and IR) and subsequent to it (d.c. conductivity) means that the same kinetics exist in both viscous liquid and gel. This constancy of kinetics implies that the forming network has little effect on the rate. The activation energy for the cure of the present system, 12.3 kcal/mol, equation (3), agrees well with previously published values^{12, 13}. The activation energies of many epoxide/hardener systems fall generally near this value, exclusive of whether one deals with model systems^{5, 14} or with actual polymeric systems^{5, 11, 13-15}. This indicates that here too the structure of the forming network has little effect on the activation energy for reaction of chain ends on its periphery. Since the values are similar to those for the activation energy for the self-diffusion of polymers¹⁶, this suggests that the reactions may be diffusion controlled. In comparison, the activation energy for network motion (glass transition) of several epoxide/anhydride systems¹⁷ lies in the range 51-59 kcal/mol.

CONCLUSIONS

The cure kinetics of the system bisphenol-A diglycidyl ether/*m*-phenylene diamine indicate that only one reaction occurs over the complete cure, in the temperature range 23-157°C, i.e. network extension, whether by primary or secondary amine. Kinetic data indicate the reaction to be diffusion controlled. The final extent of cure is limited by the rigidity of the forming network, which prevents reactants from coming into proximity to react further.

ACKNOWLEDGMENTS

The authors wish to thank C. E. Diener, W. C. Hamm, R. C. Lasky, D. G. Sedor and F. J. Strock for obtaining most of the experimental data reported herein. Thanks are also due to C. Pettus for performing the statistical analyses.

*IBM Systems Development Division,
P.O. Box 6,
Endicott, N.Y. 13760,
USA*

(Received 8 December 1970)

REFERENCES

- 1 Warfield, R. W., 'Testing of Polymers', Volume 1, (Ed., J. V. Schmitz) Interscience, New York, 1965, p 271
- 2 Dannenburg, H. and Harp, W. R. *Anal. Chem.* 1960, **32**, 365
- 3 Prime, R. B., 'Analytical Calorimetry', Volume 2, (Eds., R. S. Porter and J. F. Johnson) Plenum Press, New York, 1970, p 201

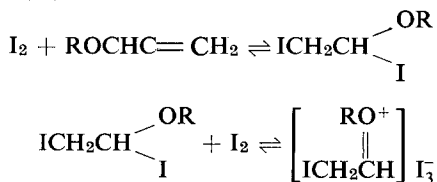
KINETICS OF EPOXY CURE (I)

- 4 Fava, R. A. *Polymer, Lond.* 1968, **9**, 137
- 5 Horie, K., Hiura, H., Sawada, M., Mita, I. and Kamke, H. *J. Polym. Sci. (A-1)* 1970, **8**, 1357
- 6 Piloyan, G. O., Ryabchikov, I. D. and Novikova, O. S. *Nature* 1966, **212**, 1229
- 7 Schechter, L., Wynstra, J. and Kurkcy, R. P. *Ind. Eng. Chem.* 1956, **48**, 94
- 8 Kakurai, T. and Noguchi, T. *Kogyo Kagaku Zasshi* 1961, **664**, 398
- 9 Harrod, J. F. *J. Appl. Polym. Sci.* 1962, **6**, S63
- 10 Kreaehling, R. P. and Kline, D. E. *J. Appl. Polym. Sci.* 1969, **13**, 2441
- 11 French, D. M., Strecker, R. A. H. and Tompa, A. S. *J. Appl. Polym. Sci.* 1970, **14**, 599
- 12 Warfield, R. W. and Petrie, M. C., paper presented at the 136th Meeting of the American Chemical Society, Atlantic City, New Jersey, September, 1959
- 13 Jenkins, R. and Karre, L. *J. Appl. Polym. Sci.* 1966, **10**, 303
- 14 Sokolnikova, I. N., Gurman, I. M., Sivergin, Yu. M. and Akutin, M. S. *Plast. Massy* 1967, **9**, 32
- 15 Gough, L. J. and Smith, I. T. *J. Appl. Polym. Sci.* 1960, **3**, 362
- 16 Rogers, C. E., 'Physics and Chemistry of the Organic Solid State', Volume II (Eds. D. Fox, M. M. Labes and A. Weissberger) Interscience, New York, 1965, p 509
- 17 Shito, N. *J. Polym. Sci. (C)* 1968, **23**, 569

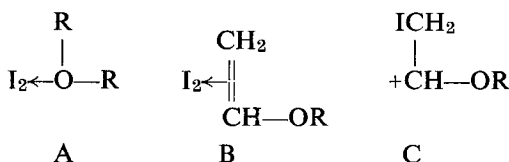
The mechanism of initiation of cationic polymerization of alkyl vinyl ethers by molecular iodine

A. LEDWITH and D. C. SHERRINGTON

Contrary to widely held beliefs, interaction of molecular iodine with alkyl vinyl ethers in methylene dichloride leads initially to equilibrium formation of appropriately substituted 1,2-di-iodoethanes. The reactions were studied spectrophotometrically at -40°C , to minimize polymerization, and it has been shown that with isobutyl vinyl ether (IBVE), the appropriate adduct was formed rapidly and completely when the mole ratio $[\text{IBVE}] / [\text{I}_2] \simeq 70$. Molecular iodine was shown to be an effective catalyst for carbon-iodine bond heterolysis in 2-iodopropane and hence it is suggested that the important primary processes in iodine initiated polymerization of alkyl vinyl ethers involve the reactions



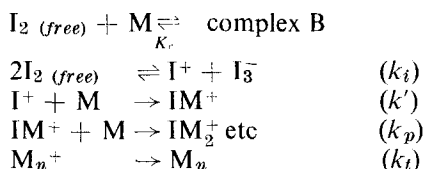
MOLECULAR IODINE was first used as early as 1878 to initiate polymerization of alkyl vinyl ethers¹ but it was not until 1949 that kinetic studies by Eley and Richards² provided the first real insight into the reaction mechanism. These workers showed conclusively that solvents of high dielectric constant increased the overall rate of polymerization and hence that ions, not free radicals as proposed earlier³, were the active intermediates. More detailed investigations⁴, using diethyl ether as solvent to minimize changes in the dielectric constant during polymerization, showed that there existed a definite monomer concentration at which the reaction velocity reached a maximum value for a given initial concentration of iodine. To explain this observation, it was proposed that several distinct 'complexes' between alkyl vinyl ethers and molecular iodine existed simultaneously, i.e.,



Complex A could be neglected since all molecules present in solution contained ethereal oxygen atoms (assumed equivalent in donor character) which could coordinate with iodine. Complex B was envisaged as a charge

transfer complex formed by overlap of the filled π -orbitals of the double bond of the alkyl vinyl ether with appropriate vacant orbitals in molecular iodine. Complex C was seen as an adduct of the iodonium ion, (I^+) from an initiation pre-equilibrium, with the double bond of the ether. Iodine in complex B was assumed to be inactive as an initiator leading to the following mechanistic scheme

(M = alkyl vinyl ether monomer)



Assuming a stationary state of active centres then it could be shown that the rate of polymerization, $-d[M]/dt$, approximates to

$$\frac{k_i k_p [I_2]^2 \text{ initial } [M] \text{ initial}}{k_t (1 + K_c [M] \text{ initial})^2}$$

Hence a plot of rate versus $[M] \text{ initial}$ should pass through a maximum as had been observed experimentally.

The first detailed ultraviolet(u.v.)/visible absorption spectrophotometric studies of these reactions were reported almost simultaneously by Higashimura *et al*⁵ and by Eley and Seabrooke⁶. Both groups of workers attributed the broad absorption ~ 295 nm to the complex B proposed earlier by Eley, and in fact the Japanese workers distinguished between a π (olefinic electron) and an oxygen (n -electron) complex with iodine. Kinetic studies based on the disappearance of the u.v. band were shown to be in agreement with earlier results obtained by different techniques.

More recently Eley's group⁷ have used infra-red (i.r.) and conductance studies to further clarify the nature of polymerizing and initiating intermediates. Similar rate expressions were obtained, and more evidence for a 1:1 I_2 /monomer complex was found and its corresponding stability constant determined. Rather disturbingly however the theoretically predicted absorption maxima of the ether/ I_2 π - and n -complexes showed poor agreement with the experimentally observed values. Experimental data for interaction of iodine with a wide range of π - and n -donor molecules is readily available⁸ and the above discrepancy between theory and experiment appeared to indicate a possible flaw in the band assignments.

The object of the present work was to reinvestigate the u.v./visible absorption spectra of iodine/alkyl vinyl ether systems; employing a low temperature technique, so that initiation and complexation phenomena could be investigated without the complications of significant polymerization.

EXPERIMENTAL

Materials

Methylene dichloride was dried and purified by fractionation from calcium hydride.

Isobutyl vinyl ether was washed with water (just alkaline to litmus) then dried by standing over KOH pellets for 24 hours. It was then fractionally distilled from a fresh sample of pellets.

Methyl isopropenyl ether (ICI Mond Division) was fractionated from sodium under a nitrogen atmosphere.

Methyl vinyl ether was used directly from a gas cylinder (Coleman-Mathe-son Company) while the other ethers were simply fractionated from calcium hydride using a micro-apparatus.

2-iodopropane was shaken with mercury to remove molecular iodine⁹, dried over P₂O₅ and fractionated. A middle fraction (b.p. 89.5°C) was retained and stored in a dark bottle. No discoloration was observed over a period of one month.

Iodine (Analar grade) was resublimed and stored in a dark glass stoppered bottle.

Apparatus and technique for low temperature spectroscopy

The main difficulty encountered in recording u.v./visible spectra at low temperatures is the misting of optical cells due to condensation of atmospheric moisture, a thin film of water droplets being sufficient to blank out the whole u.v. region. To overcome this a cell housing was designed (*Figure 1*) so

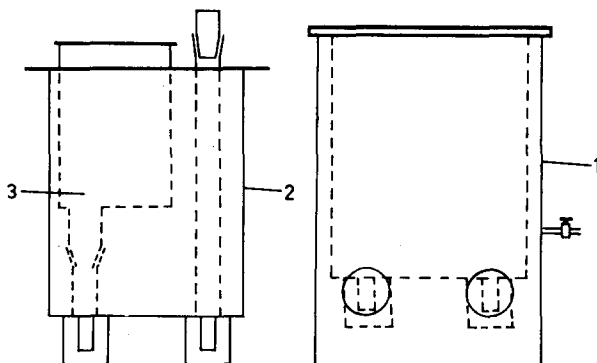


Figure 1. Cell housing for low temperature spectrophotometry: (1) outer casing; (2) inner housing; (3) third section

that the cells were in an evacuated environment. The housing consisted of three sections all of which were made of heavy gauge brass sheeting to give good thermal conductivity. The outer casing (1) was fitted with four silica optical windows seated against rubber O-rings to form vacuum tight seals. The exterior surfaces of these windows were at the temperature of the spectrophotometer (Unicam SP 800) whilst a spectrum was being run. The inner housing (2) had two heavy brass blocks designed to accommodate a matched pair of 1 cm optical cells in the paths of the light beams of the spectrophotometer. Housing (2) was held in position inside (1) by a series of bolts through top flanges, separated by a Perspex gasket, in order to form a seal and minimize heat conduction to the outer casing. The final seal around

these flanges was made with Apiezon Q compound. The space between (1) and (2) could be evacuated via the tap, and (2) also held the chilled methanol used as a coolant. The third section, (3), fitted into (2) by means of a brass cone socket arrangement and the top was ground flat so that a vacuum tight seal (silicone greased) could be made with a heavy brass plate, similarly ground, placed on top. Constructed in this manner the apparatus was evacuated completely by a single operation at the tap.

The cells containing reaction mixtures and solvent reference had dimensions carefully chosen to fit neatly into the respective cell compartments. A typical reaction mixture was set up by placing a sealed glass phial, containing a known volume of alkyl vinyl ether, into the reaction vessel (*Figure 2*). A

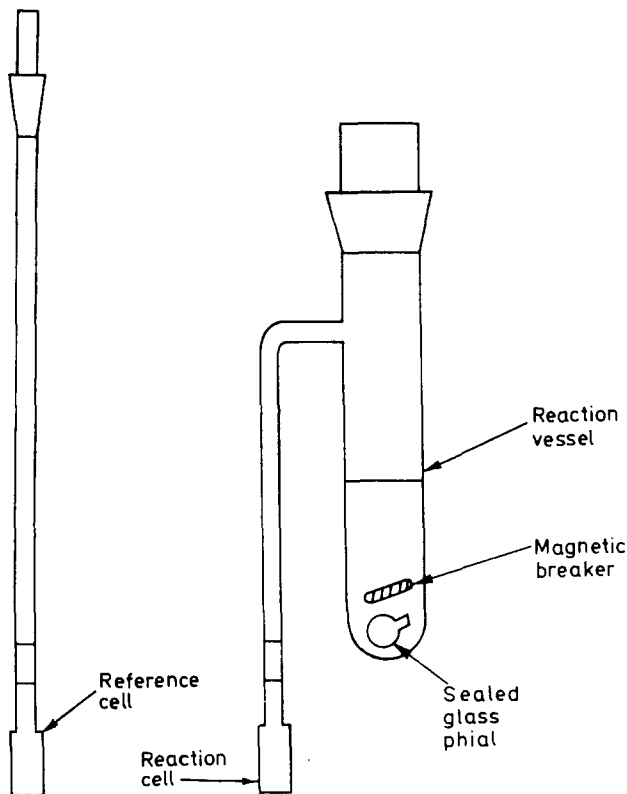


Figure 2 Reaction vessel and absorption cells for low temperature spectrophotometry

magnetic breaker was then introduced together with a measured volume of iodine/methylene dichloride solution. The vessel was then sealed with a greased stopper and the reference cell was made up to contain an equal concentration of alkyl vinyl ether in methylene dichloride.

After placing reaction vessel and reference cell in position in the spectrophotometer, the housing was sealed and evacuated. Chilled methanol was poured into the appropriate section and the whole apparatus kept at the

required temperature (usually -40°C) for about $1\frac{1}{2}$ hours to ensure thermal equilibrium of the reactants. Air was admitted and the reaction vessel quickly removed so that the phial containing monomer could be broken. The cell faces were then washed with acetone, the vessel rapidly replaced in the housing, and the latter immediately sealed and evacuated. Spectra were then recorded rapidly over the range 700–250 nm.

Kinetic measurements

The iodine catalysed methanolysis of 2-iodopropane was studied kinetically by following the rate of appearance of hydriodic acid. Freshly prepared solutions containing appropriate concentrations of iodine and 2-iodopropane in methanol were allowed to react at 50°C ; aliquot portions were periodically removed, quenched by additions of sodium thiosulphate solution, and titrated against standard methanolic sodium hydroxide solution. Phenolphthalein was used as indicator and carbon dioxide was eliminated by bubbling nitrogen throughout the titrations. Uncatalysed methanolysis of 2-iodopropane was followed in a similar manner except that quenching by sodium thiosulphate was not necessary.

RESULTS

Low temperature spectrophotometry

UV/visible absorption spectra of solutions of iodine (I_2) and isobutyl vinyl ether (IBVE) in methylene dichloride were recorded at -40°C with various concentrations of I_2 and IBVE, (Figure 3). IBVE concentrations in the range

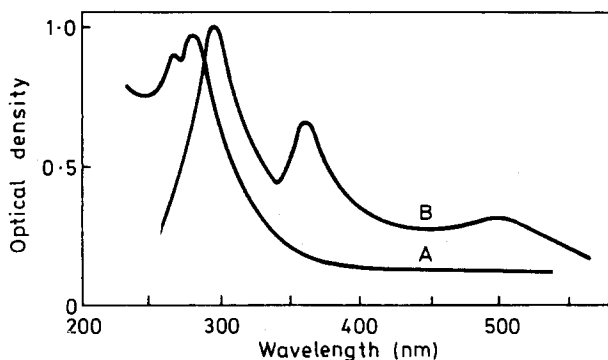


Figure 3 Absorption spectra of intermediates formed by reactions of isobutyl vinyl ether and iodine in methylene dichloride at -40°C
A, $[\text{IBVE}] / [\text{I}_2] > 70$; B, $[\text{IBVE}] / [\text{I}_2] \sim 70$

3.6×10^{-3} to 0.4M were examined, the corresponding I_2 concentrations being limited to the range 2.8×10^{-4} to $5.8 \times 10^{-4}\text{M}$. A broad asymmetric absorption, possibly consisting of two bands, was found in the u.v. region with $\lambda_{\text{max}} \sim 280\text{nm}$ for all solutions where the ratio $[\text{IBVE}]/[\text{I}_2]$ was $\sim 70/1$ or larger. Any combination of concentrations below this ratio resulted in the formation of tri-iodine (I_3^-) ions, (characterized by absorption maxima at 353

and 288nm in aqueous solution¹⁰, shifted to 356 and 294nm in methylene dichloride) and no absorption in the region of 280nm. When absorption at ~ 280 nm occurred no band was detectable at ~ 500 nm, i.e. in the region where free I_2 absorbs^{11,12}, while those concentration ratios giving solution with I_3^- bands also produced some absorption at ~ 500 nm. The formation of I_3^- was taken as an indication of the formation of propagating polymeric species (see Discussion). To check that initiation was a thermal—rather than a photochemical—reaction, a spectrum of a solution with concentration ratio $< 70/1$ was run at -40°C with the reactants mixed in the absence of light. I_3^- absorption was found as before showing the reaction to be purely thermal in origin. Mixing of reactants at 0°C when the concentration ratio was $> 70/1$ again yielded a broad absorption at ~ 280 nm with none in the 500nm region. On standing, however, I_3^- was slowly generated and irradiation by u.v. light of a reaction mixture giving a 280nm band (at -40°C) also resulted in the production of I_3^- .

Since whenever absorption at ~ 280 nm occurred free I_2 could not be detected spectroscopically, the concentration of the chromophore producing the absorption was assumed to be equal to the initial concentration of I_2 . A plot of optical density at ~ 280 nm against concentration of absorbing species (Figure 4) showed a Beer's Law dependence over the short range

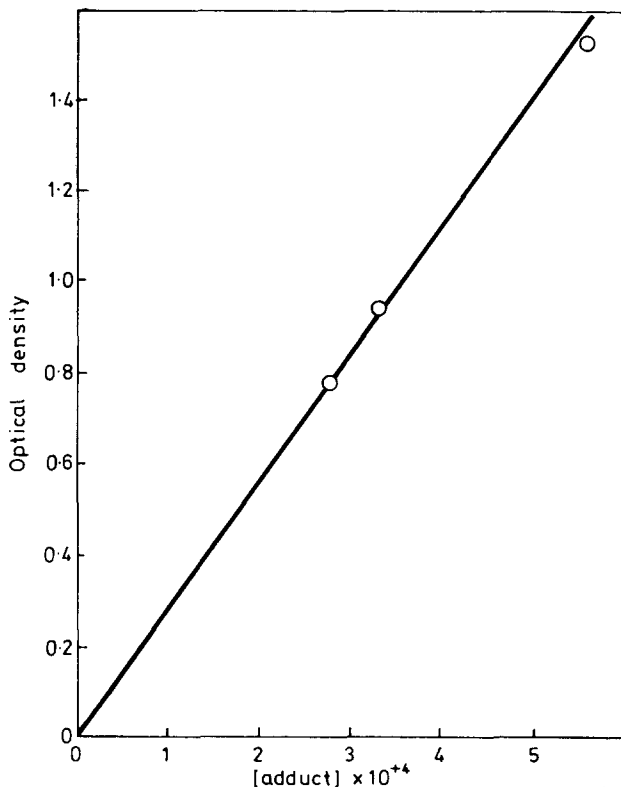
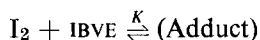


Figure 4 Beer's Law plot for adduct formation from isobutyl vinyl ether and iodine in methylene dichloride

studied, giving a molar extinction coefficient, $\epsilon = 2780 \text{ M}^{-1} \text{ cm}^{-1}$. It follows also that the equilibrium constant (K) for adduct formation between iodine and isobutyl vinyl ether must be greater than $\sim 10^3 \text{ M}^{-1}$ at -40°C . i.e.



Other vinyl ethers studied behave similarly although concentration ratios required to produce the species giving the u.v. absorptions varied slightly as did the approximate absorption maxima. A summary of the results obtained is shown in *Table 1*.

Table 1 Absorption maxima of adducts formed from I_2 and $\text{ROCH}=\text{CH}_2$ in methylene dichloride at -40°C

R-	$[\text{ROCH}=\text{CH}_2]$ (M)	$10^4 [\text{I}_2]$ (M)	λ_{max} (approx) (nm)
CH_3-	2.10	4.0	275
CH_3CH_2-	0.50	4.6	280
$(\text{CH}_3)_2\text{CH}-$	1.30	6.9	275
$(\text{CH}_3)_3\text{C}-$	1.00	4.2	265
$(\text{CH}_3)_2\text{CHCH}_2-$	0.41	5.6	280
$\text{ClCH}_2\text{CH}_2-$	0.47	4.6	283
$\text{CH}_2=\text{C}(\text{CH}_3)\text{OCH}_3$	0.67	4.5	285

Most of the vinyl ethers gave rise to transient yellow or brown colours when first mixed with an iodine solution, but even the most stable of these (formed by methyl isopropenyl ether) was too short lived to permit recording of its absorption spectrum.

The experimental results provide powerful arguments (see later) for concluding that the various u.v. chromophores, formed by reactions of iodine with alkyl vinyl ethers, are not charge transfer spectra but represent chemical adducts. Excess (i.e. free) iodine undoubtedly causes more rapid polymerization possibly due to iodine catalysed carbon-iodine bond heterolysis.

Electrophilic catalysis of carbon-halogen bond heterolysis is a common phenomenon¹³ but there does not appear to be any recorded instance of the use of molecular iodine for this purpose. Consequently the catalytic activity

Table 2 Methanolysis of 2-iodopropane* catalysed by I_2 at 50°C

$[(\text{CH}_3)_2\text{CHI}]$ (M)	$[\text{I}_2]$ (M)	$10^5 R_{\text{HI}} \dagger$ (M s^{-1})	$10^4 k_2 \ddagger$ ($\text{M}^{-1} \text{ s}^{-1}$)
0.200	0.201	1.34	3.34
0.200	0.152	1.17	3.85
0.200	0.104	0.72	3.47

* Reaction rates in the absence of I_2 were several orders of magnitude less than catalysed processes

† R_{HI} = initial rate of formation of HI

‡ k_2 calculated from the rate equation

$$\frac{d[\text{HI}]}{dt} = k_2 [(\text{CH}_3)_2\text{CHI}] \times [\text{I}_2]$$

of iodine was demonstrated by studying the methanolysis of 2-iodopropane. Solutions of 2-iodopropane in methanol containing I_2 were allowed to react at 50°C and the formation of methyl isopropyl ether readily confirmed by g.l.c. analysis (Carbowax 400 at 100°C). Rates of methanolysis were followed as described in the Experimental section, and the representative data shown in *Table 2* clearly indicate catalysis by, or participation of, I_2 in the rate determining process.

DISCUSSION

Reactions between iodine and alkyl vinyl ethers in methylene dichloride at -40°C were found to be extremely rapid and essentially uncomplicated by polymerization of the monomers. If the molar ratio [isobutyl vinyl ether]/ $[I_2]$ was maintained at a value in excess of 70 then all the iodine was immediately consumed with formation of a species absorbing in the region of 280 nm ($\epsilon_{\text{max}} = 2780 \text{ M}^{-1}\text{cm}^{-1}$). Values of λ_{max} observed in the present work are substantially in agreement with those of other groups of workers obtained in different solvents and at higher temperatures^{5, 6}. Transient brown and yellow colours however were also observed before the formation of the above species, similar to the colours obtained when I_2 is dissolved in 'oxygen-containing' solvents¹². The broad u.v. bands ($\lambda_{\text{max}} \sim 280\text{nm}$) have previously been assigned^{5, 6} to charge transfer transitions but, if this is the case, then absorption by the acceptor (I_2) in the visible region should be observed, as found for I_2 /aromatic charge transfer interactions^{8, 14} and analogous interactions of I_2 in such solvents as diethyl ether^{8, 15}. No such residual visible absorption was found in solutions giving the 280 nm absorption, as noted previously by Okamura *et al*¹⁶. Furthermore correlation of λ_{max} values for charge transfer spectra in methylene dichloride of I_2 /mesitylene, tetracyanoethylene (TCNE)/mesitylene, and TCNE/ethyl vinyl ether systems, gives an estimated value for that of I_2 /ethyl vinyl ether of $\sim 315\text{nm}$.

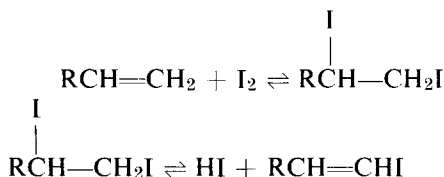
Eley *et al*⁷ have also noted a discrepancy between the predicted λ_{max} of such complexes and the experimentally observed values. Normally it is found^{8, 18-20} that a linear relationship exists between values of λ_{max} for charge transfer spectra of a series of related donor molecules with a common acceptor molecule, and the ionization potentials of the donors. The alkyl vinyl ethers used in the present work have significantly different ionization potentials yielding appropriate values of λ_{max} for charge transfer spectra with TCNE¹⁷. No such correlation is observed, however, for the interactions with iodine.

It seems reasonable to conclude therefore, that the u.v. absorption bands formed on mixing alkyl vinyl ethers and molecular iodine are not charge transfer spectra, but represent 1,2-di-iodoethanes formed by chemical reaction of iodine with the ethylenic bands. 1,2-Di-iodoethanes of the type suggested have not previously been reported and would no doubt be highly reactive and unstable. However spectroscopic data is available for some α, ω -di-iodoalkanes²¹⁻²³ and for $\text{ICH}_2\text{CH}_2\text{I}$ in petroleum ether solution ($\lambda_{\text{max}} = 261\text{nm}$ with $\epsilon_{\text{max}} 1900 \text{ M}^{-1}\text{cm}^{-1}$). These data are very similar to the corresponding values now reported for alkyl vinyl ether adducts and in fact

carbon-iodine bond heterolysis and, since $k_i' \lll k_i$, the rate expression would reduce to one similar to those found experimentally⁴⁻⁷. However if the initial ratio [monomer]/[I₂] is so large that all the I₂ is consumed by addition to the monomer double bond, then only a comparatively slow polymerization results following unimolecular heterolysis of the iodine adduct.

Obviously the overall rate of polymerization would appear to pass through a maximum value as the mole ratio (monomer)/(I₂) is progressively increased. Experimentally it was found⁴ that for isobutyl vinyl ether, maximum rate of polymerization occurred at [IBVE]/[I₂] ~ 100 which is in quite good agreement with observations made in the present work, showing that free iodine is reduced to an insignificant amount at mole ratios in excess of ~70.

The mechanism now proposed for iodine catalysed polymerization of alkyl vinyl ethers differs from those originally proposed^{4-6, 25} in that pre-equilibrium 'complex' formation is replaced by a chemical addition reaction and the formation of active cationic sites arises from I₂ catalysed bond heterolysis, rather than from bimolecular self ionization of molecular iodine. Eley, Isack and Rochester⁷ have previously noted that, at least for reactions in carbon tetrachloride, bimolecular auto-ionization of molecular iodine is not consistent with observed reaction kinetics and spectra. The same workers also suggested that chemical addition of molecular iodine may be a primary reaction process, drawing attention to related mechanisms established by Giusti *et al*²⁶ for iodine-catalysed polymerization of styrene, and acenaphthylene. For the latter monomers Giusti *et al*²⁶ concluded that initiation equilibria involved addition of iodine and subsequent elimination of hydriodic acid, i.e.



Elimination of HI provides a useful co-catalyst for generation of active cationic sites and similar reactions cannot be ruled out in the present case. However it is equally possible that active sites in the iodine-catalysed polymerization of styrene and acenaphthylene are generated by iodine-catalysed bond heterolysis, as now suggested for alkyl vinyl ether polymerization.

It should be noted however that these new initiation processes do not seriously conflict with previously reported rate equations⁴⁻⁷, but throw considerable doubt on the validity of the spectrophotometric technique for evaluating k_p in such systems²⁵. Values of k_p obtained by the spectrophotometric technique²⁵ are several orders of magnitude less than corresponding values obtained by other methods, as noted previously²⁷.

ACKNOWLEDGEMENT

The authors are indebted to SRC for a maintenance award to D.C.S.

Donnan Laboratories,
University of Liverpool, PO Box 147
Liverpool L69 3BX, UK

(Received 11 December 1970)

REFERENCES

- 1 Wislicenus, J. *Ann.* 1878, **92**, 106.
- 2 Eley, D. D. and Richards, A. W. *Trans. Faraday Soc.* 1949, **45**, 425.
- 3 Chalmers, W. *Can. J. Res.* 1936, **7**, 464, and 472.
- 4 Eley, D. D. and Saunders, J. J. *Chem. Soc.* 1952, p 4167
- 5 Higashimura, T., Kanoh, N. and Okamura, S. *Die Makromol. Chem.* 1961, **47**, 35
- 6 Eley, D. D. and Seabrooke, A. J. *Chem. Soc.* 1964, p 2226
- 7 Eley, D. D., Isack, F. L. and Rochester, C. H. *J. Chem. Soc. (A)* 1968, pp 872 and 1651
- 8 Foster, R. 'Organic Charge Transfer Complexes', Academic Press, London, 1969
- 9 Hughes, E. D. and Shapiro, U. G. *J. Chem. Soc.* 1937, p 1177
- 10 Awtrey, A. D. and Connick, R. E. *J. Amer. Chem. Soc.* 1951, **73**, 1842
- 11 Kleinberg, J. and Davidson, A. W. *Chem. Reviews* 1948, **42**, 601
- 12 Voigt, E. M. *J. Phys. Chem.* 1968, **72**, 3300
- 13 Streitwieser, A. *Chem. Rev.*, 1956, **56**, 751; Bethell, D. and Gold, D. 'Carbonium Ions', Academic Press, London, 1967
- 14 Benesi, H. A. and Hildebrand, J. H. *J. Amer. Chem. Soc.* 1949, **71**, 2703
- 15 de Maine, P. A. D. *J. Chem. Phys.* 1957, **26**, 1192
- 16 Higashimura, T., Kanoh, N., Yonezawa, T., Fukui, K. and Okamura, S. *Nippon Kagaku Zasshi* 1960, **8**, 550
- 17 Ledwith, A. and Woods, H. J. *J. Chem. Soc.* 1970, p 310
- 18 Kosower, E. M., 'Progress in Physical Organic Chemistry', 1965, **3**, 81
- 19 Mason, S. G. *Quart. Reviews* 1961, **15**, 287
- 20 Briegleb, G., 'Elektron-Donator-Acceptor-Komplexe', Springer-Verlag, Berlin, 1961
- 21 Kimura, K. and Nagakura, S. *Spectrochim. Acta.* 1961, **17**, 166
- 22 Ito, M., Hiang, P. C. and Kosower, E. M. *Trans Faraday Soc.* 1961, **57**, 1662
- 23 Hazeldine, R. N. *J. Chem. Soc.* 1953, p 1764
- 24 Muizebelt, W. J. and Noyes, R. M. *J. Amer. Chem. Soc.* 1970, **92**, 6012
- 25 Higashimura, T., 'Structure and Mechanism in Vinyl Polymerisation', (Eds., T. Tsuruta and K. F. O'Driscoll) Dekker, New York, 1969, p 313
- 26 Giusti, P. *Chimica e Industria* 1966, **48**, 435; Giusti, P. and Andruzzi, F. *ibid.*, 1966, **48**, 442 and 1079; Giusti, P., Puce, G., and Andruzzi, F. *Makromol. Chem.* 1966, **98**, 170
- 27 Bawn, C. E. H., Fitzsimmonds, C., Ledwith, A., Penfold, J., Sherrington, D. C. and Weightman, J. A. *Polymer, Lond.* 1971, **12**, 119

Book Reviews

Treatise on coatings, Vol. II

Characterization of coatings: physical techniques, Part 1

Edited by R. R. MYERS and J. S. LONG

Marcel Dekker, New York, 1969, 669 pp, £18-90, \$39-75

This volume comprises contributions from fifteen authors in thirteen chapters relating to techniques for identifying and characterizing coatings. The book is intended to establish the relevance of advanced analytical and specialized instrumental techniques, familiar in the high polymer field, to coatings. In this it succeeds admirably, though inevitably the different authors vary in the treatment of their subjects; some contributions stand out in such matters as detailed accounts of instruments and persuasive handling of material and argument. Most authors base their discussion specifically on coatings and not simply high polymers in general. The first chapter is something of an exception (A. R. H. Tawn on Intrinsic Properties), but it serves as a general introduction, and is concise and useful for reference. D. M. Gans has a good account of definitions of surface area and the ambiguities attached thereto and prints a useful table of results for surface areas by different methods. Lewis and Forrestal emphasise the significance of film shrinkage during formation and its probable effect on adhesion. The two chapters on mechanical properties (Pierce and Evans) are particularly well done, especially Evans' account of the distinction between free and attached films. Haken's chapter is very detailed and good on instrumentation and analysis. Garn deals with differential thermal analysis, particularly analytical and identification aspects, but does not mention the (almost universal?) use of DTA for measuring glass transition temperatures; he offers the interesting suggestion that DTA might be used to measure energies of attachment to a surface. The remaining chapters on microscopy, radioactive isotopes (activation analysis and labelled compounds—an excellent introduction), spectroscopy (comprehensive) and photoelastic coatings (optical birefringence under stress), are of the same high standard. In the chapter on colorimetry, colour physics is dealt with adequately, but the remainder of the material (colourants and colour styling) seems oddly out of place.

Allowing for the fact that the book was published in 1969 and that articles have to be written well in advance it is a little disappointing that the overwhelming bulk of the references (in some chapters very comprehensive) are for the early 60's and before.

Apart from the minor blemishes mentioned, the book is an excellent one, and will serve, for the technologist and research scientist in the coatings industry, as an authoritative work of reference, although at the price quoted, unfortunately, few copies are likely to be bought by individuals.

J. L. PROSSER

Vinyl polymerization

Vol. 1, Part II

Kinetics and mechanisms of polymerization

Edited by G. E. HAM

Marcel Dekker, New York, 1969, 416 pp, £10-70, \$25-75

The growth in publications over the past few years has meant that research scientists rely increasingly on review articles written by specialists. Such a review may be a comprehensive summary of work to date or a progress report on more recent developments. In Part II

of '*Vinyl polymerization*' both types of article are included in seven chapters which are classified according to polymerization process, namely emulsion, stereospecific, anionic, cationic and radiation-induced. The reviews on stereospecific (Chapter 4) and anionic polymerization (Chapter 5) are confined to particular aspects—the Ziegler-Natta catalyst for the polymerization of propylene and polymerizations initiated with organolithium compounds respectively. Few references to papers published after 1965 are quoted in these two contributions, and because of the time interval between writing and publication active workers in stereospecific and anionic polymerization may find little of interest. However, the two chapters are a useful starting point for newcomers to these two types of polymerization.

The current status of emulsion polymerization is covered thoroughly in three chapters which constitute almost half the book. In Chapter 1 the reader is led through the different mechanisms proposed for emulsion polymerization and then shown how these compare with extensive experimental data for eleven different monomer systems. It is readily apparent that a mechanism applicable to all monomers, initiators, surfactants and reaction conditions in emulsion polymerization is not available. Attempts to explain the mechanism of emulsion copolymerization (Chapter 2) and of the emulsion polymerization of ethylene at high pressures (Chapter 3) are shown to require further theoretical developments. These three chapters highlight the thesis in Part I that polymerization behaviour is dependent on monomer type and structure. This is also brought out in Chapter 6 in a review of cationic polymerization. Emphasis here is placed on how changes in monomer, catalyst, solvent and reaction conditions alter considerably the kinetics and mechanism of polymerization. Radiation-induced polymerization in the solid state or a range of monomer systems is described in Chapter 7. The reviews of radiation-induced polymerization in the vapour and liquid states are less detailed, attention being paid to the dependence of the polymerization process (radical, cationic or anionic) on reaction conditions.

This book is an adequate follow-up to Part I and achieves its objective of the right balance between theory and experiment. Part II should be bought by polymer libraries and will prove very useful to academic and industrial workers in emulsion polymerization, both as an introductory text and as a reference work. Bench workers will find the section on experimental methods in Chapter 1 of great value. Volume I is an adequate reference work on the radical polymerization of vinyl monomers to which a large proportion of Parts I and II is devoted. In view of this bias those involved in polymerization by non-radical processes are unlikely to purchase Part II for their personal libraries.

J. V. DAWKINS

Book Reviews

Treatise on coatings, Vol. II

Characterization of coatings: physical techniques, Part 1

Edited by R. R. MYERS and J. S. LONG

Marcel Dekker, New York, 1969, 669 pp, £18-90, \$39-75

This volume comprises contributions from fifteen authors in thirteen chapters relating to techniques for identifying and characterizing coatings. The book is intended to establish the relevance of advanced analytical and specialized instrumental techniques, familiar in the high polymer field, to coatings. In this it succeeds admirably, though inevitably the different authors vary in the treatment of their subjects; some contributions stand out in such matters as detailed accounts of instruments and persuasive handling of material and argument. Most authors base their discussion specifically on coatings and not simply high polymers in general. The first chapter is something of an exception (A. R. H. Tawn on Intrinsic Properties), but it serves as a general introduction, and is concise and useful for reference. D. M. Gans has a good account of definitions of surface area and the ambiguities attached thereto and prints a useful table of results for surface areas by different methods. Lewis and Forrestal emphasise the significance of film shrinkage during formation and its probable effect on adhesion. The two chapters on mechanical properties (Pierce and Evans) are particularly well done, especially Evans' account of the distinction between free and attached films. Haken's chapter is very detailed and good on instrumentation and analysis. Garn deals with differential thermal analysis, particularly analytical and identification aspects, but does not mention the (almost universal?) use of DTA for measuring glass transition temperatures; he offers the interesting suggestion that DTA might be used to measure energies of attachment to a surface. The remaining chapters on microscopy, radioactive isotopes (activation analysis and labelled compounds—an excellent introduction), spectroscopy (comprehensive) and photoelastic coatings (optical birefringence under stress), are of the same high standard. In the chapter on colorimetry, colour physics is dealt with adequately, but the remainder of the material (colourants and colour styling) seems oddly out of place.

Allowing for the fact that the book was published in 1969 and that articles have to be written well in advance it is a little disappointing that the overwhelming bulk of the references (in some chapters very comprehensive) are for the early 60's and before.

Apart from the minor blemishes mentioned, the book is an excellent one, and will serve, for the technologist and research scientist in the coatings industry, as an authoritative work of reference, although at the price quoted, unfortunately, few copies are likely to be bought by individuals.

J. L. PROSSER

Vinyl polymerization

Vol. 1, Part II

Kinetics and mechanisms of polymerization

Edited by G. E. HAM

Marcel Dekker, New York, 1969, 416 pp, £10-70, \$25-75

The growth in publications over the past few years has meant that research scientists rely increasingly on review articles written by specialists. Such a review may be a comprehensive summary of work to date or a progress report on more recent developments. In Part II

Studies on the copolymerization of trioxan with 1,3-dioxolan

CH. KONSTANTINOV AND V. KABAIVANOV

We have studied the block copolymerization of trioxan with 1,3-dioxolan by means of adiabatic calorimetry. Complexes with $(C_2H_5)_3Al$ have been found to be more active than those with $(iso-C_4H_9)_3Al$, and complexes based on BF_3 more active than those from $TiCl_4$. These results can probably be explained by the difference in the electron density of the central atom of the corresponding gegen-ions. The higher activity of the complexes based on $(C_2H_5)_3Al$ compared with those of $(iso-C_4H_9)_3Al$ cannot be explained on this theory, and it may be due to differences in mobility and to the effect of steric factors. The rate of copolymerization decreases in proportion to the concentration of 1,3-dioxolan in the monomer mixture, and on the basis of this result a kinetic equation is proposed in which the power index of the concentration of 1,3-dioxolan should have a negative sign.

THE COPOLYMERIZATION of trioxan (TO) with 1,3-dioxolan (DO) has been extensively studied¹⁻⁵. The great interest shown in this copolymerization has arisen because of the good thermal stability of the polymer and because of some anomalies in the copolymerization process. Moreover, no satisfactory explanation has yet been put forward for a number of findings, such as the higher rate of consumption of DO in its copolymerization with TO, in spite of the fact that the rate of homopolymerization of TO is higher than the corresponding rate for DO. No quantitative study of the effect of DO on the rate of copolymerization has been carried out.

We have studied the block copolymerization of TO and DO using adiabatic calorimetry. Complexes, based on the organoaluminium compounds of the type $(C_2H_5)_3Al$, $(iso-C_4H_9)_3Al$ and on some halides (BF_3 , $TiCl_4$), were used as catalytic initiators. The catalytic activity of this type of complex in the copolymerization of TO has already been demonstrated⁶, and the difference in activity of complexes of this type on the homopolymerization of TO has also been studied⁷. In our investigation of the catalytic activity of different complexes on the copolymerization of TO and DO we have established that the complexes with $(C_2H_5)_3Al$ are more active than those of $(iso-C_4H_9)_3Al$, and that the complexes based on BF_3 are more active than those from $TiCl_4$. The results are in agreement with the data obtained in a study of the activity of these complexes in the homopolymerization of TO⁷.

By varying the amount of DO in relation to that of TO we have found that the rate of reaction decreases in proportion to the concentration of DO in the monomer mixture, that is, DO appears to inhibit the polymerization process in some way. On the basis of these findings a kinetic equation is proposed in which the power index of the concentration of DO should have a negative sign.

METHODS AND MATERIALS

Purification and preparation of the starting materials

TO was prepared by vacuum distillation of a 60% aqueous solution of formaldehyde in the presence of sulphuric acid⁸. The crude TO was dehydrated by refluxing over metallic sodium, and immediately before use it was distilled over potassium-sodium alloy in the presence of anthracene. The purity of TO was checked by gas chromatography and the water content was determined by the method of K. Fischer.

DO was prepared by a previously published method⁹ and dried and checked for purity as for TO.

The toluene used as a solvent for the initiator components was freed from thiophene and unsaturated compounds by the usual methods and then dried like TO and DO.

In all the experiments the water content of TO, DO and toluene was below 0.002% w/w.

$\text{BF}_3 \cdot \text{C}(\text{C}_2\text{H}_5)_2$, supplied by British Drug Houses (England), was used after vacuum distillation.

$(\text{C}_2\text{H}_5)_3\text{Al}$, $(\text{iso-C}_4\text{H}_9)_3\text{Al}$, supplied by Fluka (Switzerland), and TiCl_4 , supplied by Dr Theodor Schuchardt (FDR) were used without additional treatment.

Equipment and procedure

The copolymerization was carried out in a glass calorimeter, provided with a mechanical stirrer, an inlet for the thermocouple and an inlet for the addition of reagents and for purging the system with nitrogen. The calorimeter was a cylindrical Dewar vessel with an inner diameter of 34 mm and a capacity of about 100 ml. The calorimeter had three jackets for good thermal insulation. Liquid paraffin was circulated in the outer jacket at a temperature 1.5°C. above that necessary for the reaction. The temperature changes during the polymerization process were measured by means of a copper-constantan thermocouple, calibrated in advance, and connected to a galvanometer (Goertz-Austria) with a sensitivity of 7.11×10^{-9} amp.

The calorimeter was cleaned before use with chromic acid, hot water and flushed with dry nitrogen (99.999% purity) after drying at 150°C. The purified monomers and the solutions of the initiator components were equilibrated in advance in a thermostat to a temperature 1.5°C higher than that necessary for the reaction. TO (15 ml) was first poured into the calorimeter, followed by the required amount of DO. The mixture was stirred constantly until it reached thermal equilibrium when the temperature changes were within $\pm 0.01^\circ\text{C}/\text{min}$. At this point the initiator complex, prepared and equilibrated in a thermostat in advance, was introduced by means of micro-syringe provided with a long needle. The initiator complexes were prepared by mixing equimolar amounts of the individual components in the form of toluene solutions of concentrations of about 1.5% v/v. They were kept under nitrogen in sealed injection vials.

After a rise of 5°C the polymerization process was stopped by injecting 20 ml of a 3% solution of ammonia in methanol. The separated polymer

was filtered off, and after extraction with methanol and hot water, dried to a constant weight in a vacuum oven at 35°C. By a series of gravimetric determinations made in advance the amount of copolymer corresponding to a 1°C rise in the temperature was found. This value was used for checking the results obtained by calculation. In the thermochemical calculations some previously published data¹⁰ were used, and the thermal capacities of TO and DO were determined electrically. In plotting the yield of polymer against time the following relationship was considered:

$$V = W Q = c \frac{d(\Delta T)}{dt} \quad (1)$$

where V = rate of heat release
 W = rate of polymerization
 c = thermal capacity of the reaction system
 ΔT = temperature difference
 t = time
 Q = heat of polymerization

Equation (1) after transformation and integration reduces to

$$P = \frac{c}{Q} \Delta T \quad (2)$$

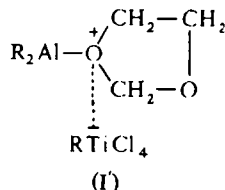
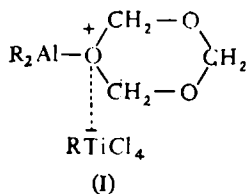
where P = degree of conversion of the monomer mixture.

RESULTS AND DISCUSSION

Although the polymerization process studied takes place essentially in the absence of solvent, the curves for temperature plotted against time showed the same well-defined sectors (athermal, endothermal and exothermal) which had been observed by Leese and Baumber during the polymerization of the TO in solution¹⁰. This is because the chemical structures of TO and DO are very similar and the mechanisms of polymerization of both monomers are also similar.

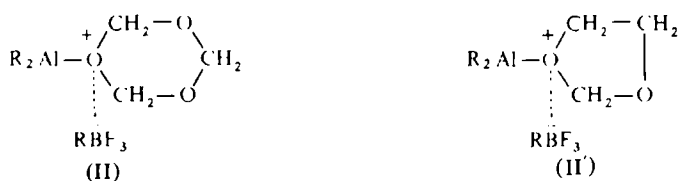
Initiation of the polymerization process with the complexes used results in the formation of the following active centres:

(I) In the complexes prepared from an organoaluminium compound and titanium(IV)chloride:



(II) In complexes obtained from an organoaluminium compound and boron trifluoride. (In the present experiments we used $\text{BF}_3 \cdot \text{O}(\text{C}_2\text{H}_5)_2$. The release of $(\text{C}_2\text{H}_5)_2\text{O}$ in the process of formation of the complex has been demonstrated by gas chromatography in one of our earlier papers¹¹):

COPOLYMERIZATION OF TRIOXAN WITH 1,3-DIOXOLAN



We have established in our experiments that the complexes I, I' differ considerably from the complexes II, II' in their polymerization activity. This difference in activity is clearly demonstrated in *Figure 1*. The figure

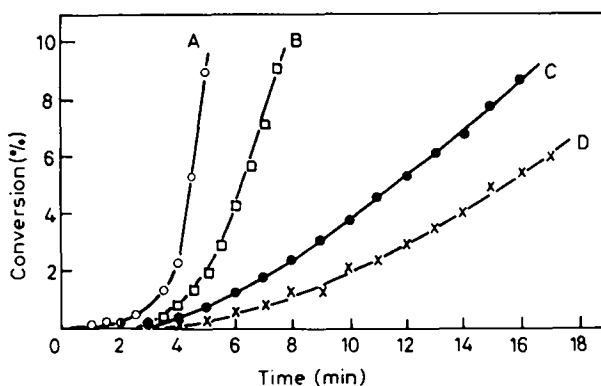


Figure 1 Block copolymerization of TO and DO at 70°C, TO: DO = 95:5 (mol-%), under the action of the following initiator complexes:
 (A) $\text{BF}_3 \cdot (\text{C}_2\text{H}_5)_3\text{Al} - 2 \times 10^{-4}$ mol/mol-TO;
 (B) $\text{BF}_3 \cdot (\text{iso-C}_4\text{H}_9)_3\text{Al} - 2 \times 10^{-4}$ mol/mol-TO;
 (C) $\text{TiCl}_4 \cdot (\text{C}_2\text{H}_5)_3\text{Al} - 20 \times 10^{-4}$ mol/mol-TO;
 (D) $\text{TiCl}_4 \cdot (\text{iso-C}_4\text{H}_9)_3\text{Al} - 20 \times 10^{-4}$ mol/mol-TO

shows that in order to obtain comparable results the complexes of the titanium(IV)chloride series should be used at substantially higher concentrations than the complexes based on boron trifluoride. Since the cation structure of both types of complexes is the same, it follows that the difference in activity can only be related to the corresponding gegen-ion. The charge density of the boron atom in $[\text{C}_2\text{H}_5\text{BF}_3]^-$ is +0.629 and that of titanium in $[\text{C}_2\text{H}_5\text{TiCl}_4]^-$ is +0.521, as calculated from the equation of L. Pauling:

$$\delta = 1 - \exp \left[-\frac{1}{4} (X_a - X_b)^2 \right] \quad (3)$$

where δ = electron density of the central atom

X_a, X_b = electronegativity of the corresponding atoms

By comparing the charge densities of both types of gegen-ions it can be seen that the gegen-ion $[\text{C}_2\text{H}_5\text{BF}_3]^-$ is an acid in relation to the gegen-ion $[\text{C}_2\text{H}_5\text{TiCl}_4]^-$. Therefore the former will have a smaller effect on splitting the polymer chain, as a result of which the polymerization rate is higher.

The higher activity of the complexes based on $(C_2H_5)_3Al$ in comparison with that of the $(iso-C_4H_9)_3Al$ complexes may be due to differences in mobility and to the effect of steric factors. Equation (3) cannot be used to determine the effect of the type of alkyl group on the charge density of the central atom, because in calculating the aluminium-carbon bond this relationship does not account for the structure and the type of the hydrocarbon radical.

In the very first stages of the polymerization process active centres of the type I' and II' will prevail in the system. This is easily explained when the higher kinetic activity of DO in relation to TO in the process of their copolymerization is taken into account⁵.

An important point of the kinetics of the process under study is the effect of the monomers ratio on the polymerization rate. We can find no references to the investigation of this problem. Such a study is seriously hampered by the difficulty of preparing the two monomers with the same water content in order to eliminate its effect on the polymerization process. Figure 2 shows

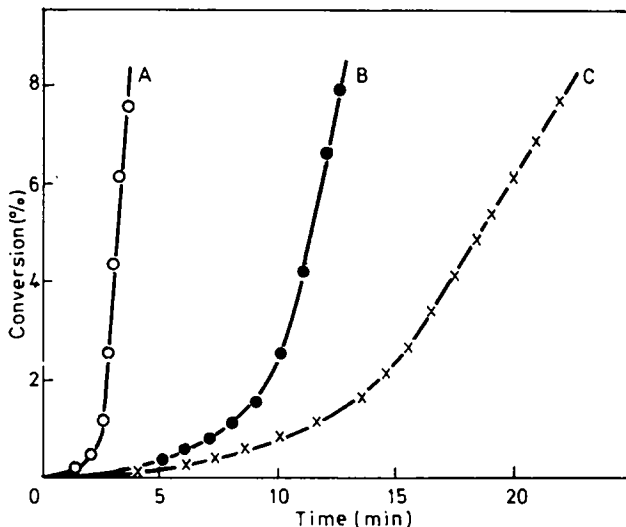


Figure 2 Effect of the concentration of DO on the copolymerization of TO and DO at 70°C, concentration of initiator complex $BF_3 + (C_2H_5)_3Al - 5 \times 10^{-5}$ mol/mol-TO; initial concentration of DO - (A) 0.0246 mol/mol-TO; (B) 0.0398 mol/mol-TO; (C) 0.0525 mol/mol-TO

the results of the investigation of the effect of the DO to TO ratio on the copolymerization. Only the ratios which have a practical importance for the synthesis of the thermostable polymer have been included. The data have been used to plot the maximum polymerization rate against the initial concentration of DO in the monomer mixture (Figure 3). The relationship obtained for the TO to DO ratios studied by us can be expressed by the following kinetic equation:

$$\frac{dP}{dt} = k(C_0) \frac{(T_0)}{(D_0)^n} \quad (4)$$

COPOLYMERIZATION OF TRIOXAN WITH 1,3-DIOXOLAN

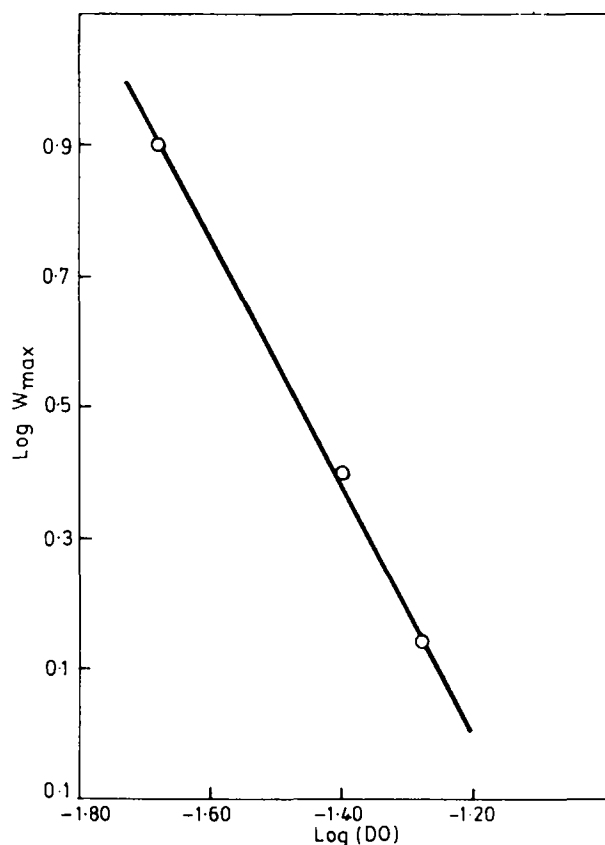


Figure 3 Dependence of the copolymerization rate on the amount of DO in the monomer mixture at 70°C and concentration of initiator complex $\text{BF}_3 \cdot (\text{C}_2\text{H}_5)_3\text{Al} = 5 \cdot 10^{-5}$ mol/mol-TO

where P — amount of polymer obtained
 C_0 — initial concentration of the initiator complex
 k — rate constant
 T_0, D_0 — initial concentrations of TO and DO

The aim of our study was to determine the power index n , which defines the order of the reaction in relation to the initial concentration of DO. The power index n was calculated from the slope of the straight line in Figure 3. For the range of DO concentrations covered by the present study the value for n is approximately equal to 2. The meaning of the negative sign in the order of the reaction can be explained by the fact that DO to some extent inhibits the polymerization process.

Technology of Plastics Department
 Higher Institute of Chemical Technology
 Sofia 56, Bulgaria

(Received 4 August 1970)
 (Revised 24 November 1970)

REFERENCES

- 1 Kučera, M. and Pichler, J. *Polymer, Lond.* 1964, **5**, 371
- 2 Weissermel, K. *et al Kunststoffe* 1964, **54**, 410
- 3 Irzhak, V. I. *et al Vysokomol. Soedineniya* 1966, **8**, 1481
- 4 Jaacks, V. *Makromol. Chem.* 1967, **101**, 33
- 5 Yamashita, Y. *et al Makromol. Chem.* 1969, **129**, 1
- 6 Kabaivanov, V. *et al Bulg. Patent No 10552/14.01.1966*
- 7 Mateva, R. *et al J. Polym. Sci. (A-1)* 1970, **8**, 3563
- 8 Natov, M. *et al Bulgarian Patent No 10563/9. 07.1962*
- 9 Clarce, J. *J. Chem. Soc.* 1912, **101**, 1788
- 10 Leese, L. and Baumber, M. W. *Polymer, Lond.* 1965, **6**, 269
- 11 Konstantinov, H. and Kabaivanov, V. *Compt. rendus de l'Academ. Bulg. des Sci.* 1971 **24**, 239

The kinetics of crystallization of polyethylene

A. BOOTH* and J. N. HAY†

Crystallization isotherms of polyethylene samples are analysed by modified Avrami equations which correct for secondary crystallization. While the isotherms are described more accurately by two processes rather than a single process, systematic deviations still exist which cannot be eliminated by assuming further complex modes of crystallizing. However, best fit values of the Avrami exponent, n , when used as an adjustable parameter, varied markedly from sample to sample and were significantly different from the integer values required by theory for spherulitic crystallization. These values were not significantly different to those determined by the analytical procedure adopted by Banks *et al* to suggest that both were identical and that the two crystallization processes were consecutive. Both analytical procedures cast doubt on the validity of the primary crystallization exhibiting the time dependence of the Avrami equation.

INTRODUCTION

ATTEMPTS to elucidate the details of the mechanism of polyethylene crystallization by analyses of the isotherms have not been particularly successful¹⁻⁴. This has generally been attributed to the presence of either an induction period or secondary crystallization, by which crystallinity increases logarithmically in time beyond the end of the primary process. It has been concluded⁵ that difficulties in resolving these two effects alone complicate the analysis of the isotherms and so cast doubts on the interpretation of crystallization isotherms in terms of the Avrami equation.

It would seem more likely that since the morphology of bulk crystallized polymer is complex, a two parameter equation cannot adequately describe the total crystallization. Attempts have been made to derive more complicated expressions based on the known morphology of crystalline polymers—a 'single crystal' model⁶ with non-constant lamellar growth and a spherulitic model^{7, 8} in which further crystallization proceeds within the spherulite boundary. Since the former deals with the growth of a fixed number of single crystals and does not allow for branching, the model cannot be applied to spherulitic crystallization, and only the second model is appropriate to polyethylene crystallization.

The present report discusses the success of this modified Avrami expression in describing the total crystallization isotherms of polyethylene samples. The same degree of rigour has been applied to the application of these equations as has been used formerly to the Avrami equations^{2, 9}.

EXPERIMENTAL

Materials

Samples of polyethylene (Marlex 60) were kindly supplied by the Phillips

* Present address: Revertex Co. Ltd, Harlow, Essex, UK

† To whom all communications should be addressed

Petroleum Chemical Company Ltd, and their characteristics as supplied are listed in Table 1. Other samples were prepared either by degradation *in vacuo*

Table 1 Sample characteristics

Serial number	Description	Inherent viscosity* (dm ³ /g)	Molecular weights		
			M_v^\dagger ($\times 10^3$)	M_w^\ddagger ($\times 10^3$)	M_n^\ddagger ($\times 10^3$)
A	Bulk	0.206	130.0	142.0	19.0
B	Fraction 3	0.083	29.0	41.0	25.2
C	Fraction 2	0.180	85.0	98.9	32.2
D	Fraction 1	0.247	150.0	165.4	78.1
E	A degraded 300°C, $\frac{1}{2}$ h	—	—	103.7	20.2
F	A degraded 350°C, $\frac{1}{2}$ h	—	—	48.0	8.9
G	Blend 75%E/25%D	—	—	119.9	25.0
H	Blend 75%D/25%E	—	—	150.8	46.5

* Measured in dekalin at 1.00 g/dm³

† From the relationship: $M_w = 5.10 \times 10^{-4} M_v^{0.78}$

‡ g.p.c. measurements — *o*-dichlorobenzene at 130°C

or by blending. The samples were further characterized by g.p.c. analysis using *o*-dichlorobenzene at 130°C¹⁰⁻¹¹

Apparatus and techniques

Conventional mercury filled dilatometers^{2,3} were employed having a measuring capillary of 0.60 mm internal diameter and containing 200 mg cylinders of polymer. Samples were pre-heated at 160°C for 15–30 min prior to re-crystallization. No abnormal dependence of the subsequent crystallization rate on temperature or duration of the pre-heating was observed.

RESULTS

Two stage crystallization rate equation

The dilatometric isotherms were analysed by the rate expression developed by Hillier⁸ for a spherulite growth mechanism in which further crystallinity ($x_{s,\infty}$) develops within the boundaries of the spherulites, for which the total crystallinity at time t is:

$$x_{c,t} = x_{a,\infty} [1 - \exp(-Z_1 t^n)] + x_{s,\infty} Z_2 \int_0^t \{1 - \exp(-Z_1 \theta^n)\} \times \{\exp[-Z_2(t-\theta)]\} d\theta \quad (1)$$

where $x_{a,\infty}$, Z_1 and n refer to the final degree of crystallinity, rate constant and Avrami exponent of the primary spherulitic growth, respectively, and $x_{s,\infty}$ and Z_2 the final increased degree of crystallinity and first order rate constant of the secondary process, respectively.

Analyses of the crystallization isotherms were carried out to determine the best fit values of $x_{a,\infty}$, $x_{s,\infty}$, Z_1 and Z_2 using $n = 3.0$ and 4.0 by a Newton-Raphson iterative procedure which determined these parameters to within 0.1%. Estimate of the fit of the equation was measured from the percentage error in the computed degree of crystallinity from the observed $x_{c,t}$ (%E).

KINETICS OF CRYSTALLIZATION OF POLYETHYLENE

Using these procedures fits of the crystallization isotherms of less than 5% could only be observed in all the samples after an initial period of 10–15% crystallinity. At higher crystallinities the apparent fit varied widely from sample to sample in that the best were observed with the isotherms of sample D, see *Figure 1*, and the worse (wide oscillation over the total isotherm from

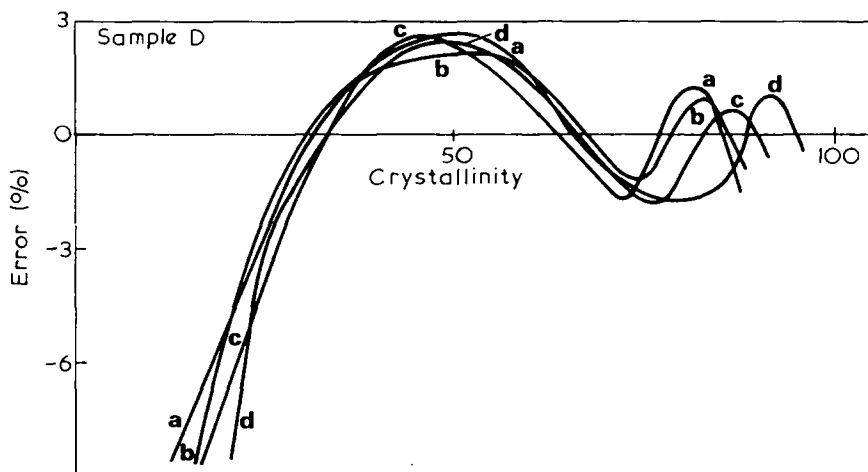


Figure 1 Degree of fit of equation (1). Sample D — a. 130.2 C; b. 128.7 C; c. 127.0 C; d. 129.5 C

10 to –6%) with those of F. The variations in %E with conversion were systematic rather than random in all the isotherms and the few turning points suggested that equation (1) was a crude fit of the isotherms. Indeed averaging the primary process over the initial portion of the curve and the second term in the equation over the final stages would alone account for the observed variation of %E with crystallinity. The accuracy of equation (1) in describing the isotherms of the various samples can be gauged from the sums of the squares of the residuals, σ , listed in *Table 2* along with the primary and secondary rate parameters.

Table 2 Rate parameters

Sample	Temp. Range (°C)	Z_1 (min ⁻³)	Z_2 (min ⁻¹)	A value	σ (10 ⁻³)
A	126.3–128.8	4×10^{-5} – 6×10^{-9}	2×10^{-3} – 7×10^3	0.82–0.66	0.3–3.0
B	127.0–129.2	6×10^{-4} – 8×10^{-8}	7×10^3 – 2×10^2	0.68–0.59	3.0–20.0
C	127.0–128.8	6×10^{-5} – 1×10^{-6}	1×10^2 – 5×10^2	0.71–0.62	0.7–8.8
D	127.0–130.2	1×10^{-4} – 2×10^{-8}	2×10^{-3} – 6×10^3	0.81–0.73	2.0–3.0
E	125.6–126.5	2×10^{-5} – 6×10^{-7}	2×10^3 – 4×10^3	0.57–0.48	10.8–37.3
F	120.3–121.3	3×10^{-5} – 2×10^{-6}	3×10^3 – 2×10^3	0.44–0.14	10.0–19.0
G	126.2–127.8	3×10^{-5} – 4×10^{-7}	2×10^3 – 4×10^3	0.68–0.57	3.5–16.4
H	127.5–129.0			0.71–0.67	

The coefficient, $A = (x_{a,\alpha}/x_{c,t})$ for most of the samples except E, F and G lay within the range 0.6–0.8 and there was no clear dependence on either the

molecular weight or the dispersities of the samples, see *Table 1*. Only the highly degraded samples, F, exhibited anomalously low values of A.

Variations were made to the basic crystallization growth mechanism in order to modify equation (1) and try to improve the overall fit of the dilatometric isotherms. These modifications introduced:

- (1) a variable induction period, τ_1
- (2) sporadic nucleation—such that the number of nuclei, N_t , increased by a first order rate process

$$\text{i.e. } N_t = N_0 [1 - \exp(-kt)]$$

- (3) a correction for initial periods of non-spherical growth—this corrected for the crystallinity which developed up to a variable time, τ_2 , at which all the growing entities had assumed spherical contours

$$\text{i.e. } x_{a,t} = 1 - \exp[-Z_1(t^3 - \tau_2^3)]$$

However, only the isotherms of samples A and D could be more accurately described by these modified equations but the additional parameters evaluated, i.e. τ_1 , τ_2 and k , had little or no theoretical significance. The equations did not substantially improve the fit of the isotherms of the remaining samples and the modifications were not considered to be generally applicable (*Table 3*).

Table 3 Degree of fit of modified model

<i>Model</i>	<i>Sample D</i> (129.53°C) ($\times 10^3$)	<i>Sample C</i> (128.75°C) ($\times 10^3$)
Unmodified	3.97	3.048
Induction period	1.381	2.845
Nucleation	1.229	2.851
Changing geometry	1.407	2.831
Fractional n values	1.884	0.5777

Non-integer value of the Avrami exponent, n

Banks *et al*² have approached the analysis of polyethylene crystallization isotherms in terms of two consecutive stages which could be separated on a time scale.

The primary process obeyed the general Avrami equation, which for dilatometry was

$$(h_t - h_\infty)/(h_0 - h_\infty) = \exp(-Z_1 t^n) \quad (2)$$

where h_0 , h_t and h_∞ are the initial, at time t , and dilatometric readings at end of the primary process. The analysis then consisted of determining the value of h_∞ which gave a constant value of n over the primary process, as determined by

$$n = -t \frac{dh_t}{dt} \{h_t - h_\infty\} \ln[h_0 - h_\infty] / [h_t - h_\infty]^{-1} \quad (3)$$

This procedure, however, invariably gave fractional values of n which had no mechanistic significance within the assumptions used in the derivation of the Avrami equation^{12, 13}. From the point of view of this approach, it is significant that the life time of the secondary process (determined from Z_2 of equation 1)

KINETICS OF CRYSTALLIZATION OF POLYETHYLENE

was much longer than that of the primary. Indeed, when the contributions from each to the total were analysed, then although the processes were simultaneous, the effective contribution of the secondary process was not significant (less than 10% of the total) until 40–60% crystallinity had developed. (see *Figure 2*). To a first approximation the assumptions inherent

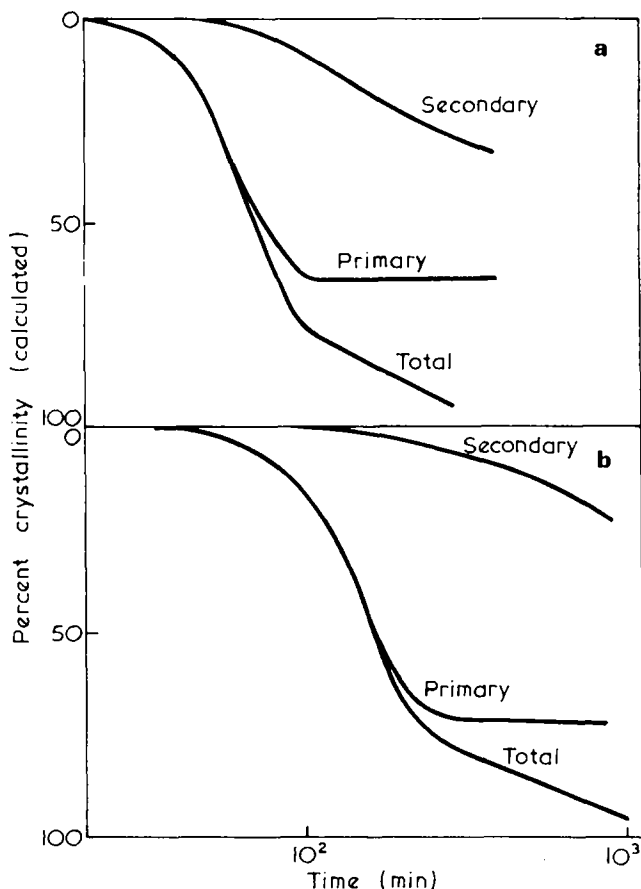


Figure 2 Resolution of primary and secondary processes: (a) sample A, 127.3 C; (b) sample D, 129.5 C

in the analysis adopted by Banks *et al*² would appear to be justified and their conclusions that the n value was non-integer worthy of further consideration. Accordingly equation (1) was fitted using n as a variable, adopting an iterative procedure varying n in units of 0.10. Error plots were determined but these exhibited the same oscillations as before, but showed a minimum at a single value of n . This improvement in the degree of fit can be seen from the sum of the squares of the residuals, σ , which exhibited a minimum at a single non-integer value of n , (see *Figure 3*). These values corresponded closely with those determined by the analytical procedure of Banks *et al*

(see Table 4). The differences observed in the values of n lay well within the scatter in the analytical procedure of equation (3) normally observed.

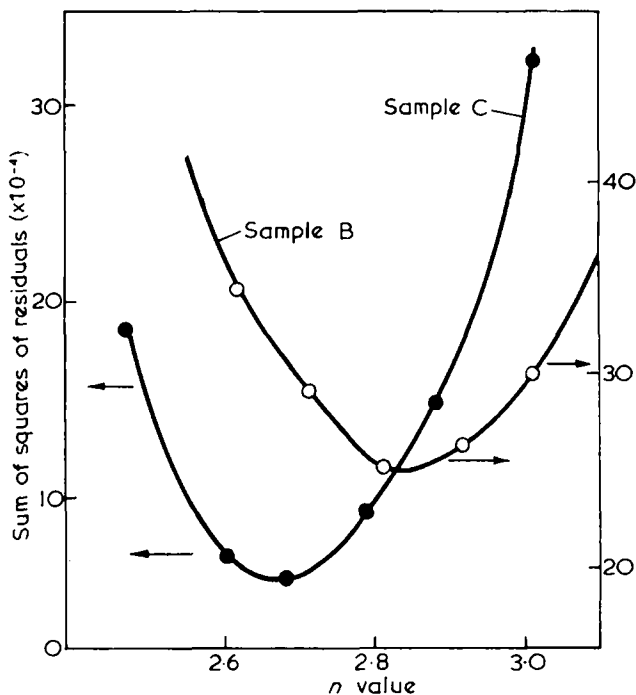


Figure 3 Best fit values of n . Samples B and C

Table 4 Fraction exponent values

Sample	n value equation (3)	n value variation of h_{∞}
A	3.55 ± 0.05	3.30 ± 0.10
B	2.85 ± 0.05	3.00 ± 0.20
C	2.70 ± 0.05	2.80 ± 0.10
D	3.20 ± 0.05	3.30 ± 0.10

DISCUSSION

Although large and systematic errors occur in analysing the crystallization isotherms with the two stage kinetic equation, it must be accepted that the approach represents a more satisfactory description of spherulitic crystallization than that of the single Avrami equation for growth of spheres. The model, however, can only predict the development of crystallinity in the polyethylene samples with an accuracy of no more than 3–4% of the total crystallinity. Minor modifications of the model to allow for the presence of an induction period, for changing nucleation characteristics and for non-

spherical growth in the initial regions of spherulite development, have no effect on its general fit, although with individual samples it was possible to account for the deviations.

The isotherms can in general more adequately be described by an Avrami equation with fractional exponents for the primary process followed by a secondary process: conclusions originally asserted by Banks *et al.*²

Reasons for these fractional values for the exponent must be sought in the basic model of spherulitic crystallization, in the detailed morphology of branching and lateral aggregation of the fibrillar sub-units^{14, 15}, and also in the detailed mechanism of fibril growth and thickening. Spherulites are accepted as a form in which multi-component systems containing species of different crystallizabilities can crystallize, and where preferential fractionation can occur during the course of the conversion. In the case of polydisperse polymers this will lead to fractionation by molecular weight, with the lower molecular weight material preferentially rejected and concentrated into interstitial regions, but subsequently crystallizing. It would then seem too limiting to assume that two rate constants, Z_1 and Z_2 , alone could describe the course of fibrillar and inter-fibrillar crystallization in polydisperse polymers. It may be more realistic to limit the application of the two stage crystallization model to monodispersed samples alone.

CONCLUSIONS

The assumption of a two stage crystallization rate equation does not remove the embarrassment of fractional values of the Avrami exponent, n , at least in the case of isotherms of polydisperse polyethylene.

ACKNOWLEDGEMENTS

One of the authors (A.B.) is indebted to the SRC for the award of a research studentship during the period of this work.

We are pleased to acknowledge the assistance of Dr T. Williams, University of Bristol, in the characterization of the polyethylene samples and in supplying calibration for the chromatograms.

*Chemistry Department,
University of Birmingham,
Birmingham, B15 2TT, UK*

*(Received 11 September 1970)
(Revised 11 March 1971)*

REFERENCES

- 1 Mandelkern, L. and Quinn, F. A., *Abstr. Amer. Chem. Soc.* 1958, **134**, 202
- 2 Banks, W., Gordon, M., Roc, R. J., and Sharples, A. *Polymer, Lond.* 1963, **4**, 61
- 3 Buchdahl, R., Miller, R. L. and Newman, S. *J. Polym. Sci.* 1959, **36**, 215
- 4 Rabesiaka, J. and Kovacs, A. J. *J. Appl. Phys.* 1961, **32**, 2314
- 5 Meares, P., 'Polymer Structure and Bulk Properties', Chapter 5, Van Nostrand, London, 1964
- 6 Gordon, M. and Hillier, I. H. *Trans. Faraday Soc.* 1964, **60**, 763

- 7 Price, F. P. *J. Polym. Sci. (A)* 1965, **3**, 3079
- 8 Hillier, I. H. *J. Polym. Sci. (A)* 1965, **3**, 3067
- 9 Hay, J. N., Sabir, M. and Stevens, R. L. T. *Polymer, Lond.* 1969, **10**, 187
- 10 Frank, F. C., Ward, I. M. and Williams, T. J. *J. Polym. Sci. (A-2)* 1968, **6**, 1357
- 11 Ward, I. M., and Williams, T. J. *J. Polym. Sci. (B)* 1968, **6**, 621
- 12 Avrami, M. *J. Chem. Phys.* 1939, **7**, 1103; 1940, **8**, 212; 1941 **9**, 177
- 13 Mandelkern, L. *Chem. Rev.* 1956, **56**, 903
- 14 Keith, H. D. and Padden, F. J. *Jnr. J. Appl. Phys.* 1963, **34**, 2409
- 15 Keith, H. D. and Padden, F. J. *Jnr. J. Appl. Phys.* 1964, **35**, 1270

Equilibrium ring concentrations and the statistical conformations of polymer chains: Part 5. Stereoisomeric cyclics in poly(phenylmethylsiloxane) equilibrates

M. S. BEEVERS and J. A. SEMLYEN

The molar cyclization equilibrium constants K_x for cyclic phenylmethylsiloxanes, $[\text{C}_6\text{H}_5(\text{CH}_3)\text{SiO}]_x$ ($x = 3-50$), have been measured in the undiluted polymer at different temperatures and in solution in toluene. The K_x values for $[\text{C}_6\text{H}_5(\text{CH}_3)\text{SiO}]_x$ in the bulk polymer at 383 K are the same, within experimental error, as those found previously for the corresponding cyclics $[\text{CH}_3\text{CH}_2(\text{CH}_3)\text{SiO}]_x$ and it is concluded that phenyl and ethyl groups have similar influences on the statistical conformations of siloxane chains. The weight fraction of cyclics in a high molecular weight undiluted phenylmethylsiloxane equilibrate at 383 K is 0.30 and this weight fraction increases to 0.90 when equilibration is carried out in the presence of 47% by volume of toluene. The K_x values for the cyclic tetramer and pentamer in the latter equilibrate are nearly twice as large as their values in the former, whereas the K_x values for the large cyclic phenylmethylsiloxanes are the same in both. The configurational isomers of the cyclic trimer, tetramer and pentamer were separated completely by gas-liquid chromatography. They were found to be present in the equilibrates in proportions close to those expected from the random cyclization of an atactic polymer. The configurational isomers of $[\text{C}_6\text{H}_5(\text{CH}_3)\text{SiO}]_3$ and the isomer of $[\text{C}_6\text{H}_5(\text{CH}_3)\text{SiO}]_4$ with all its phenyl groups in *cis* positions were the only stereoisomers that were found to be strained relative to the open siloxane chains.

INTRODUCTION

RECENT EXPERIMENTAL and theoretical studies have illustrated how a knowledge of cyclic concentrations in polymer equilibrates can provide detailed information about the statistical conformations of the corresponding chain molecules in solutions and in the bulk polymers¹⁻⁵. In this paper, we report the results of an investigation into the concentrations of cyclics in undiluted and solution equilibrates of the commercially-important silicone poly(phenylmethylsiloxane), which has the repeat unit $\text{C}_6\text{H}_5(\text{CH}_3)\text{SiO}$. In previous studies of ring-chain equilibria in unsymmetrically substituted polysiloxanes, cyclics $[\text{RR}'\text{SiO}]_x$ were treated as single compounds and individual stereoisomers were not considered separately^{4,6}. In the poly(phenylmethylsiloxane) system, all the configurational isomers of the cyclic trimer, tetramer and pentamer can be separated completely by gas-liquid chromatography. Hence, in addition to measuring the concentrations of each of the cyclics $[\text{C}_6\text{H}_5(\text{CH}_3)\text{SiO}]_x$ in poly(phenylmethylsiloxane) equilibrates, we have been able to determine the relative amounts of the stereoisomers of the cyclics with $x = 3, 4$ and 5 .

EXPERIMENTAL

Equilibrations

A mixture of cyclic phenylmethylsiloxanes $[\text{C}_6\text{H}_5(\text{CH}_3)\text{SiO}]_x$ ($x = 3-5$) was given to us by the Research Department of Midland Silicones Limited. The cyclics were purified by fractional distillation. 10-100g quantities were equilibrated in the bulk and in toluene solution using potassium hydroxide. Diethylene glycol dimethylether was added as a promoter to all the equilibrates except those carried out in the bulk at 438 and 478 K. Gas-liquid chromatography and gel permeation chromatography were used to follow the reactions and to establish that equilibrium had been attained. The equilibria were quenched by the addition of a small quantity of glacial acetic acid. The densities of the mixtures were determined separately.

Analysis of equilibrates

Toluene was added to the quenched undiluted and concentrated solution equilibrates so as to reduce the linear polymer concentration below 10% by weight. The solutions were washed with a solution of sodium hydrogen carbonate and then with distilled water. They were dried over anhydrous sodium sulphate. Cyclics were separated from linear polymers by several fractional precipitations using methanol. The cyclic trimer, tetramer, pentamer and some of the hexamer were distilled from the combined cyclic fractions at a pressure of 10^{-2} mmHg using a molecular still. Distillates containing these cyclics were analysed by gas-liquid chromatography. Gel permeation chromatographic tracings of the cyclic residues showed that they consisted almost entirely of cyclics $[\text{C}_6\text{H}_5(\text{CH}_3)\text{SiO}]_x$ with $x \geq 6$. The molecular weights of the linear polymer fractions of the equilibrates were determined either by viscometric measurements in toluene at 298 K using the empirical Mark-Houwink equation reported by Buch, Klimisch and Johanson⁷ or by gel permeation chromatography. The number average molecular weights of cyclic fractions were measured by means of a Mechrolab 301A vapour pressure osmometer.

Chromatographic methods

Cyclics $[\text{C}_6\text{H}_5(\text{CH}_3)\text{SiO}]_x$ with $x = 3-6$ were separated using a Pye 104 gas-liquid chromatograph fitted with a heated katharometer detector. An 8ft column was used. It was packed with Embacel, coated with 7% by weight of a methyl silicone gum (E30 supplied by W. G. Pye and Co. Ltd.). The gas-liquid chromatograph was calibrated for its response both to the cyclics with $x = 3-6$ and to individual stereoisomers of the cyclics with $x = 3, 4$.

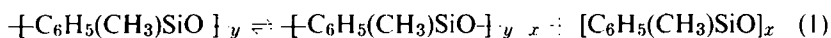
A gel permeation chromatograph was used to analyse total equilibrates as well as cyclic and linear fractions. The instrument was fitted with a Waters R4 differential refractometer detector, which was calibrated for its response to cyclic and linear phenylmethylsiloxanes. Crosslinked polystyrene gel columns were obtained from Waters Associates Limited. Cyclics were analysed on a system employing columns with gel of the following average porosities: 250, 1000, 3000, 3000, 3000 Å. The column system was calibrated as elution volume versus molecular weight for phenylmethylsiloxanes using calibration plots obtained previously for cyclic and linear dimethylsiloxanes⁸

by employing the universal calibration procedures recommended by Dawkins and others⁹⁻¹¹.

RESULTS AND DISCUSSION

Effect of phenyl groups on the conformations of siloxane chains

In the presence of catalytic amounts of potassium hydroxide and diethylene glycol dimethylether, a thermodynamic equilibrium can be set up between cyclic and linear phenylmethylsiloxanes. This equilibrium may be represented as follows



Assuming a most probable distribution of chain lengths, the equilibrium constants K_x for process (1) are given by

$$K_x = \{[\text{C}_6\text{H}_5(\text{CH}_3)\text{SiO}]_x\} / p^x \quad (2)$$

where p , the extent of reaction of functional groups in the chain fraction, can be calculated from the weight average molecular weight of the linear polymer by the methods of Flory¹².

Experimental molar cyclization equilibrium constants measured for an undiluted phenylmethylsiloxane equilibrate at 383 K are shown in *Figure 1*. The values of K_3 , K_4 and K_5 were determined by gas-liquid chromatographic analysis of fractions obtained by vacuum distillation. They are believed to be accurate to within $\pm 10\%$. Values for the larger cyclics were derived from gel permeation chromatographic tracings alone and they are probably subject to somewhat greater uncertainty. For values of $x > \text{ca } 20$, the plot of $\log K_x$ against $\log x$ shown in *Figure 1* exhibits the limiting slope of -2.5 predicted for unstrained macrocyclics by the Jacobson and Stockmayer¹³ theory. Evidently, phenylmethylsiloxane chains with more than 40 skeletal bonds are of sufficient length and flexibility to obey the Gaussian relationship for the density $W_x(\mathbf{0})$ of their end-to-end vectors \mathbf{r} in the region $\mathbf{r} \approx \mathbf{0}$. The average dimensions of such chains can be estimated by using the following expression for the molar cyclization equilibrium constants^{1,13}

$$K_x = \{3/2\pi \langle r_x^2 \rangle\}^{3/2} (1/2 N_A x) \quad (3)$$

where $\langle r_x^2 \rangle$ is the mean-square end-to-end distance of a chain containing x monomeric units and N_A is the Avogadro constant. Application of equation (3) to the experimental values shown in *Figure 1* yields a value of 10.7 for the ratio $\langle r_{50}^2 \rangle / 100l^2$ of phenylmethylsiloxane chains with 100 skeletal bonds (each of length $l = 1.64 \text{ \AA}$) in an undiluted equilibrate at 383 K. This value may be compared with the ratio of 7.0 found for dimethylsiloxane chains of the same length also in an undiluted equilibrate at 383 K^{2,8}.

The K_x values shown in *Figure 1* are close to the corresponding values found previously for cyclics in an undiluted ethylmethylsiloxane equilibrate at 383 K^{4,8}. In *Table 1*, K_4 and K_5 for phenylmethylsiloxanes are compared with those for some alkylmethylsiloxanes. The close agreement between the K_x values of phenylmethylsiloxanes and ethylmethylsiloxanes shows that phenyl and ethyl groups exert similar influences on the statistical conformations of

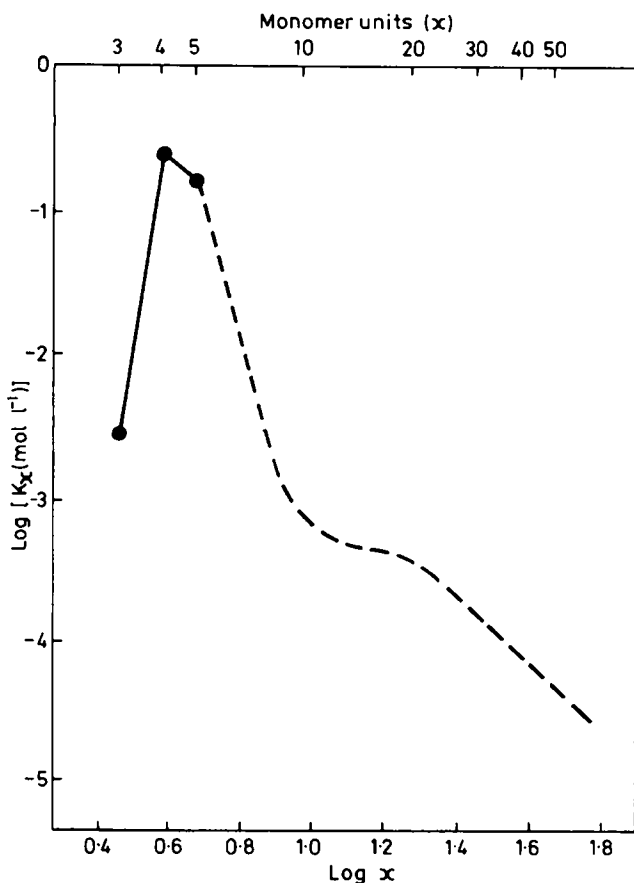


Figure 1 Experimental molar cyclization equilibrium constants K_x for cyclics $[\text{C}_6\text{H}_5(\text{CH}_3)\text{SiO}]_x$ in an undiluted equilibrated at 383 K

Table 1 K_x values for cyclic tetramers and pentamers in undiluted polysiloxane equilibrates at 383K

Substituent group R of unit $\text{R}(\text{CH}_3)\text{SiO}$	K_4 for $[\text{R}(\text{CH}_3)\text{SiO}]_4$ (mol l ⁻¹)	K_5 for $[\text{R}(\text{CH}_3)\text{SiO}]_5$ (mol l ⁻¹)
CH_3	0.19	0.09
CH_3CH_2	0.25	0.16
C_6H_5	0.25	0.16
$\text{CH}_3\text{CH}_2\text{CH}_2$	0.37	0.19

siloxane chains (see ref. 14 for a comparison of the effect of phenyl and ethyl groups on the conformations of $[-\text{CH}_2\text{CHR}-]_x$ chains).

Effect of dilution on cyclic content of phenylmethylsiloxane equilibrates

If phenylmethylsiloxanes are equilibrated in solution in toluene, the fraction of siloxane in the form of cyclics is found to increase with dilution as predicted

by the Jacobson and Stockmayer theory. In *Figure 2*, the total weight fraction of cyclics in solution equilibrates of phenylmethylsiloxanes is plotted as a function of solvent dilution and compared with results found previously for some alkylmethylsiloxanes^{2,4}. Extrapolation of the plot for phenylmethylsiloxanes to unit weight fraction of cyclics yields an experimental critical dilution point¹³ of 52% by volume of siloxane in toluene at 383 K. This critical dilution point may be compared with the value of ca 70% by volume of siloxane in toluene which would have been observed if the molar cyclization equilibrium constants for all the cyclic phenylmethylsiloxanes had remained constant with dilution. In fact, K_4 and K_5 each increase by nearly 100% over

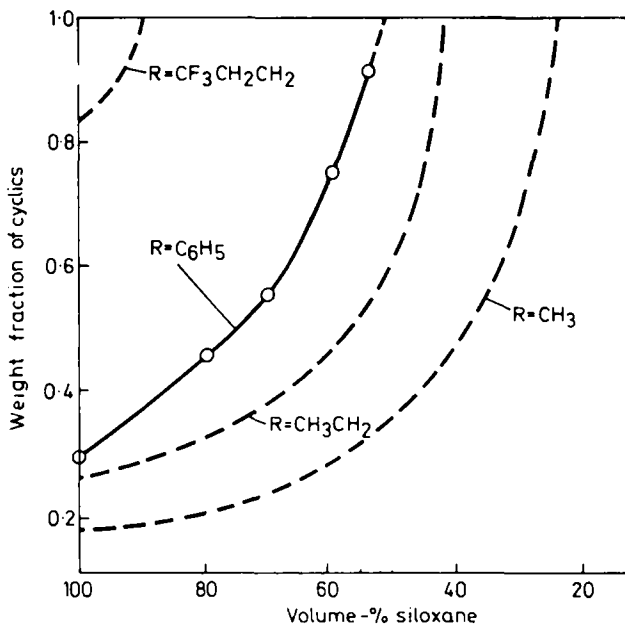


Figure 2 Weight fraction of cyclics $[R(CH_3)_2SiO]_x$ in high molecular weight ($p \cong 1$) polysiloxane equilibrates at 383 K as a function of volume per cent siloxane in toluene ($R = C_6H_5, CH_3CH_2, CH_3$) and cyclohexanone ($R = CF_3CH_2CH_2$)

the dilution range shown in *Figure 2*. These increases are similar in magnitude to those found for the cyclic tetramers and pentamers in the hydrogenmethylsiloxane⁴, dimethylsiloxane² and ethylmethylsiloxane⁴ systems. They can be interpreted⁸ in terms of polymer-solution thermodynamics by the methods applied by Ivin, Leonard^{15,16} and others^{17,18} to equilibria between other monomers and polymers in solution.

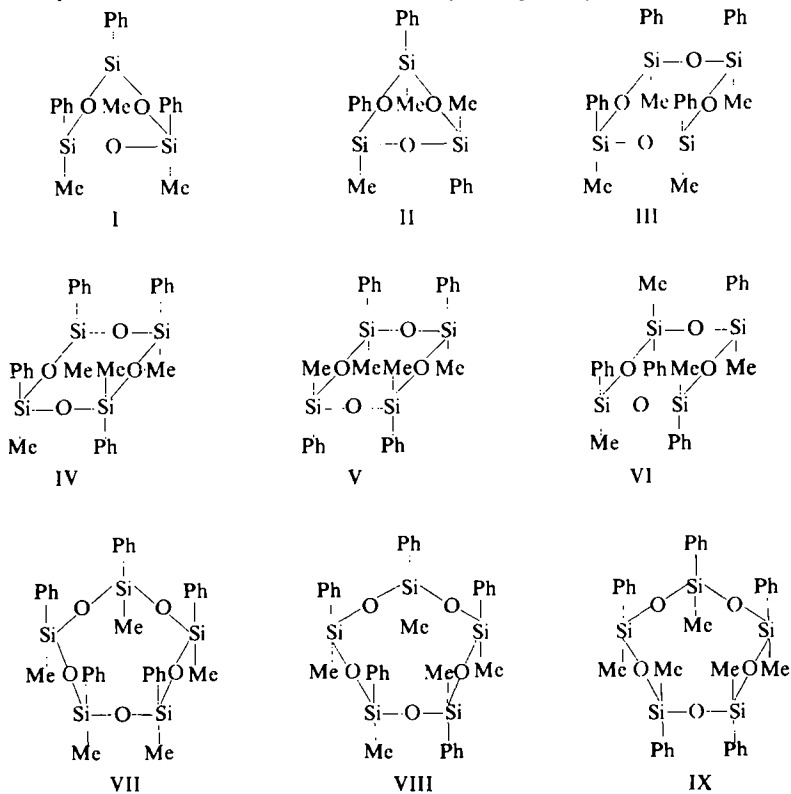
As in the alkylmethylsiloxane systems, the molar cyclization equilibrium constants of the larger cyclic phenylmethylsiloxanes do not change appreciably with solvent dilution, and the ratio $\langle r_{50}^2 \rangle / 100^2$ is found to be 10.4 for phenylmethylsiloxane chains in a solution equilibrate at 383 K containing less than 5% by weight of linear polymer. This ratio is in close agreement with the

value of 10.7 found for chains in the bulk polymer at the same temperature (see above).

Separation of configurational isomers of cyclic phenylmethylsiloxanes

Although all cyclic and linear oligomers of unsymmetrically substituted siloxanes consist of a mixture of configurational isomers^{19,20}, very few individual stereoisomers have been separated and identified up to the present time. However, the configurational isomers of the cyclics $[\text{C}_6\text{H}_5(\text{CH}_3)\text{SiO}]_3$ and $[\text{C}_6\text{H}_5(\text{CH}_3)\text{SiO}]_4$ have been found to be separable^{19,21-23}, and Hickton, Holt, Homer and Jarvie²² were able to characterize all the six stereoisomers.

Both Moore and Dewhurst²³ and Hickton and his coworkers²² reported the complete resolution of the cyclic trimer isomers by gas-liquid chromatography, but only a partial resolution of three of the isomers of the cyclic tetramer. We have found that all the isomers of the cyclic tetramer can be resolved completely on an 8ft gas-liquid chromatographic column packed with Embacel coated with 7% by weight of a methyl silicone gum, if the column temperature is maintained constant at 503 K. Furthermore, under these conditions, the cyclic pentamer $[\text{C}_6\text{H}_5(\text{CH}_3)\text{SiO}]_5$ can also be resolved into four separate components. We have tentatively assigned these to the four stereoisomers of the cyclic pentamer by assuming an analogous order of elution to that observed for the cyclic trimer and tetramer isomers (see *Figure 3*).



CYCLIC PHENYLMETHYLSILOXANES

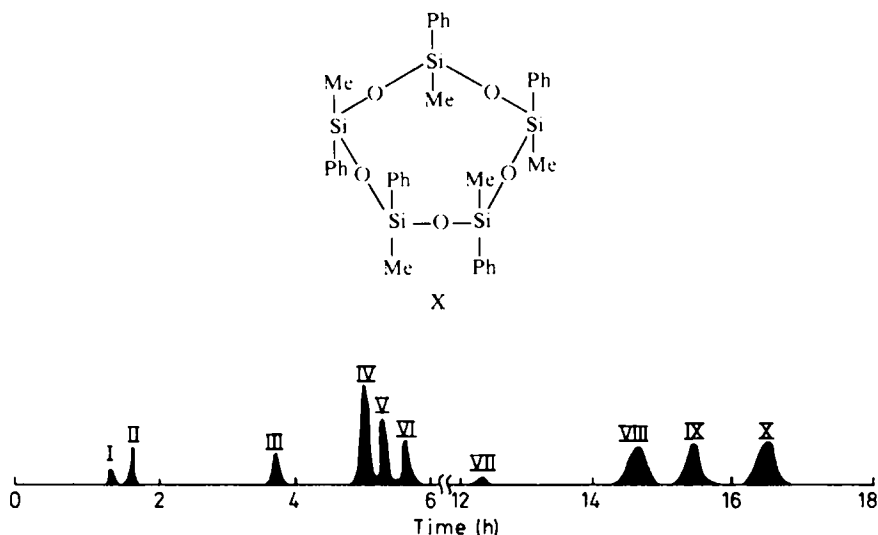


Figure 3 Gas-liquid chromatogram of a distillate obtained from the cyclic portion of an undiluted phenylmethylsiloxane equilbrates showing the separation of the configurational isomers of $[\text{C}_6\text{H}_5(\text{CH}_3)\text{SiO}]_x$ ($x = 3-5$)

Relative amounts of configurational isomers in phenylmethylsiloxane equilbrates

Equal weights of the two configurational isomers of $[\text{C}_6\text{H}_5(\text{CH}_3)\text{SiO}]_3$, which were prepared by methods described in the literature^{21,22}, were found to produce peaks of equal area on the gas-liquid chromatograph within the experimental uncertainty of ca. 5% which arises from the measurement of peak areas. Similarly, the katharometer detector was found to respond equally to equal weights of the configurational isomers of the cyclic tetramer, which were also prepared by published methods²¹. Hence identical response factors were assumed for the four stereoisomers of the cyclic pentamer.

The relative amounts of the configurational isomers of cyclic phenylmethylsiloxanes $[\text{C}_6\text{H}_5(\text{CH}_3)\text{SiO}]_x$ ($x = 3-5$) were determined for undiluted and solution equilbrates by gas-liquid chromatography. The results are presented in Table 2. The configurational isomers were found to be present in proportions close to those predicted to result from the random cyclization of an atactic polysiloxane. The corresponding results for stereoisomeric cyclics produced by non-equilibrium hydrolysis and pyrolysis reactions are also given in Table 2.

Enthalpy changes in the formation of small cyclic phenylmethylsiloxanes

The standard state enthalpy changes ΔH_x^0 for process (1) must be zero for the very large cyclics. However, ΔH_3^0 would not be expected to be zero, as the corresponding cyclic trimer in the dimethylsiloxane system is known to be strained by ca 15 kJ mol⁻¹ (see ref. 24). The strain in $[(\text{CH}_3)_2\text{SiO}]_3$ is thought to arise largely from bond angle deformations. The bond angles in the cyclic

Table 2 Weight fractions of configurational isomers of cyclic phenylmethylsiloxanes

Stereoisomers defined in Figure 3	Weight fraction of cyclic present as a particular isomer in different mixtures (see below)				
	(A)	(B)	(C)	(D)	(E)
Trimer I	0.25	0.22	0.24	0.26	0.28
Trimer II	0.75	0.78	0.76	0.74	0.72
Tetramer III	0.125	0.08	0.10	0.16	0.16
Tetramer IV	0.500	0.49	0.49	0.49	0.51
Tetramer V	0.250	0.25	0.23	0.20	0.24
Tetramer VI	0.125	0.18	0.18	0.16	0.10
Pentamer VII	0.0625	0.06	0.05	0.10	0.09
Pentamer VIII*	0.3125	0.30	0.62*	0.60*	0.62*
Pentamer IX*	0.3125	0.30			
Pentamer X	0.3125	0.34	0.33	0.30	0.29

*Temperature programming was used for determining some of the isomer ratios of the cyclic pentamer. Under these conditions isomers VIII and IX were not completely resolved.

- (A) This is the isomer ratio that would result from the random cyclization of an atactic polymer
 (B) Undiluted equilibrate at 383 K
 (C) Solution equilibrate at 383 K containing 47% by volume toluene. Linear polymer is present at concentration of less than 5% by weight
 (D) Cyclics prepared by hydrolysing phenylmethylchlorosilane by the method of Young *et al*²¹
 (E) Cyclics prepared by the pyrolysis of poly(phenylmethylsiloxane). High molecular weight polymer was chain stopped by trimethylchlorosilane. The polymer suffered a loss in weight of only 0.3% after 12 h at 513 K under 0.05mmHg. It decomposed at 668 K under 3×10^{-3} mmHg to give a distillate consisting of 37% trimer, 56% tetramer and 7% pentamer. The residue represented 28.6% by weight of the starting material

tetramer $[(\text{CH}_3)_2\text{SiO}]_4$ can adopt their normal values, and this cyclic and larger cyclic dimethylsiloxanes are unstrained².

We have measured the enthalpy changes ΔH_x^0 for the configurational isomers of $[\text{C}_6\text{H}_5(\text{CH}_3)\text{SiO}]_x$ ($x = 3-5$) by determining K_x values at different temperatures. All the ΔH_x^0 values were assumed to be independent of temperature over the range 383–478 K and the integrated form of the van't Hoff isochore was applied. Plots of $\log K_x$ against $1/T$ are shown in Figure 4 and ΔH_x^0 values were obtained from the slopes. The stereoisomers I and II of the cyclic trimer have ΔH_3^0 values of 27 and 22 kJ mol⁻¹ respectively. The cyclic tetramer isomer III (with $\Delta H_4^0 = 8$ kJ mol⁻¹) appears to be slightly strained, possibly as the result of steric crowding of the phenyl groups. The remaining isomers of the tetramer (plotted together in Figure 4), and all the isomers of the cyclic pentamer, were found to be strain free.

ACKNOWLEDGEMENTS

We are indebted to the Science Research Council for a Research Grant (for M.S.B.) and to Midland Silicones Limited for the gift of phenylmethylsiloxanes. We thank Dr W. G. Davies of the Research Department, Midland Silicones Limited for his continuing advice and encouragement.

Department of Chemistry,
University of York, York, UK

(Received 19 January 1971)

CYCLIC PHENYLMETHYLSILOXANES

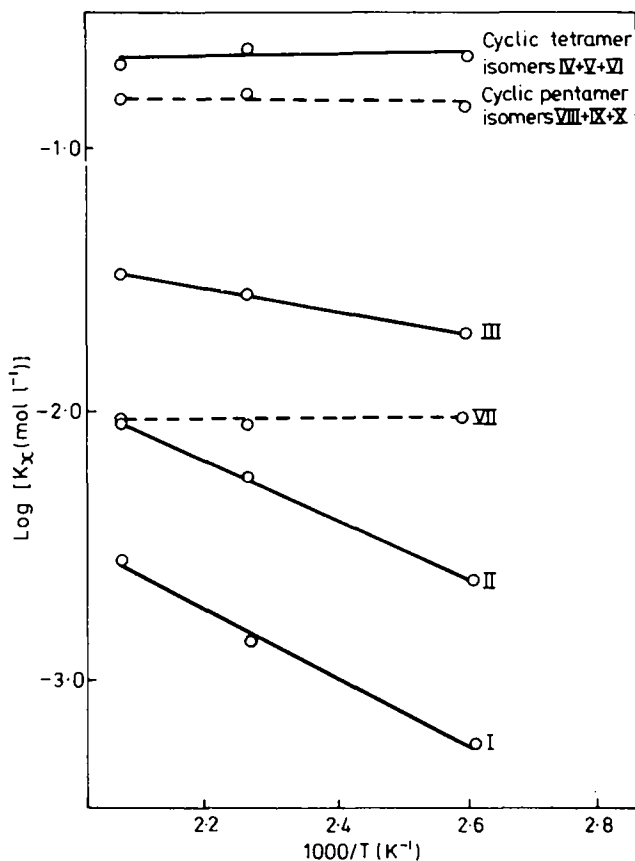


Figure 4 Plot of $\log K_T$ against $1/T$ for stereoisomeric cyclic phenylmethylsiloxanes

REFERENCES

- 1 Flory, P. J. and Semlyen, J. A. *J. Amer. Chem. Soc.* 1966, **88**, 3209
- 2 Semlyen, J. A. and Wright, P. V. *Polymer, Lond.* 1969, **10**, 543
- 3 Semlyen, J. A. and Walker, G. R. *Polymer, Lond.* 1969, **10**, 597
- 4 Wright, P. V. and Semlyen, J. A. *Polymer, Lond.* 1970, **11**, 462
- 5 Walker, G. R. and Semlyen, J. A. *Polymer, Lond.* 1970, **11**, 472
- 6 Brown, E. D. and Carmichael, J. B. *J. Polym. Sci. (B)* 1965, **3**, 473
- 7 Buch, R. R., Klimisch, H. M. and Johannson, O. K. *J. Polym. Sci. (A-2)* 1970, **8**, 541
- 8 Wright, P. V., D. Phil. thesis, University of York, 1970
- 9 Dawkins, J. V. *J. Macromol. Sci. (B)* 1968, **2**, 623
- 10 Boni, K. A., Sliemers, F. A. and Stickney, P. B. *J. Polym. Sci. (A-2)* 1968, **6**, 1567
- 11 Dawkins, J. V. Maddock, J. W. and Coupe, D. *J. Polym. Sci. (A-2)* 1970, **8**, 1803
- 12 Flory, P. J. 'Principles of Polymer Chemistry', Cornell University Press, New York, 1953
- 13 Jacobson, H. and Stockmayer, W. H. *J. chem. Phys.* 1950, **18**, 1600
- 14 Utracki, L. A. and Simha, R. *Makromol. Chem.* 1968, **117**, 94
- 15 Ivin, K. J. and Leonard, J. *European Polym. J.* 1970, **6**, 331
- 16 Leonard, J. *Macromolecules* 1969, **2**, 661
- 17 Bywater, S. *Trans. Faraday Soc.* 1955, **51**, 1267
- 18 Scott, R. L. *J. Phys. Chem.* 1965, **69**, 261
- 19 Lewis, R. N. *J. Amer. Chem. Soc.* 1948, **70**, 1115

- 20 Daudt, W. H. and Hyde, J. F. *J. Amer. Chem. Soc.* 1952, **74**, 386
- 21 Young, C. W., Servais, P. C., Currie, C. C. and Hunter, M. J. *J. Amer. Chem. Soc.* 1948, **70**, 3758
- 22 Hickton, H. J., Holt, A., Homer, J. and Jarvie, A. W. *J. Chem. Soc. (C)* 1966, p149
- 23 Moore, C. B. and Dewhurst, H. A. *J. Org. Chem.* 1962, **27**, 693
- 24 Piccoli, W. A., Haberland, G. G. and Merker, R. L. *J. Amer. Chem. Soc.* 1960, **82**, 1883

Equilibrium ring concentrations and the statistical conformations of polymer chains: Part 6. Freezing point of liquid sulphur

J. A. SEMLYEN

The freezing point of liquid sulphur is known to be lower than the melting point of monoclinic sulphur because of the presence of the molecular species S_n in the equilibrated melt. In a previous publication, S_n was identified as a mixture of large sulphur cyclics S_x with $x > 8$. Here, the concentrations of these cyclics are calculated by the Jacobson-Stockmayer cyclization theory at temperatures below the critical polymerization temperature, using Gee's analysis of ring-chain equilibria in liquid sulphur to estimate the number average molecular weights of the sulphur chains. The depressions in the freezing point of pure liquid cyclo-octasulphur calculated to result from the presence of large sulphur cyclics are in close agreement with published experimental values.

INTRODUCTION

NEARLY one hundred years have elapsed since the discovery by Gernez¹ that the freezing point of liquid sulphur is lower than the melting point of monoclinic sulphur, yet a satisfactory explanation of this phenomenon still remains to be found. There have been several experimental investigations of the freezing point of liquid sulphur²⁻⁵, the most recent being by Wiewiorowski, Parthasarathy and Slaten⁶. These authors found that liquid sulphur equilibrated at 403, 413 and 423 K had freezing points that were lower than the melting points of monoclinic sulphur by 4.9, 5.9 and 7.6 K respectively.

Aten⁷ associated the depression in the freezing point of liquid sulphur with the formation of a molecular species S_n , which he distinguished from S_8 (cyclo-octasulphur), which is present in liquid sulphur at all temperatures, and S_n (polycatenasulphur), which is formed in appreciable concentrations only above a critical polymerization temperature of 432 K⁸⁻¹². Aten assumed that S_n in liquid sulphur has the same formula and constitution as the molecular species obtained, with cyclo-octasulphur, when quenched samples of liquid sulphur are extracted with carbon disulphide. Furthermore, he identified the bright yellow species formed when cyclo-octasulphur is heated with sulphur chloride^{13, 14}, carbon disulphide¹⁵ or toluene¹⁵ as S_n .*

There have been many suggestions as to the nature of the molecular

*The results of more recent work¹⁶⁻¹⁸ suggest that the species formed when S_8 is heated with S_2Cl_2 consists of a mixture of polysulphur chlorides $Cl-S_n-Cl$.

species S_n in liquid sulphur. In 1914, Aten⁷ proposed a formula S_4 for S_n . Over forty years later, H. Krebs¹⁹ suggested that S_n might be a mixture of low molecular weight cyclics and J. Schenk^{20, 21} tentatively identified S_n as a mixture of small, unstable molecules possibly including cyclohexasulphur. Following some experimental studies, P. W. Schenk and Thümmel^{22, 23} proposed that S_n consists of octa-atomic diradical chains, and Wiewiorowski and Tuoro²⁴ modified this proposal by postulating complex formation between molecules of catena-octasulphur and cyclo-octasulphur. In 1967, K. Krebs and Beine²⁵ concluded that S_n is a mixture of cyclics S_6, S_8, S_9, S_{10} and S_{23-33} . In the most recent publication on the subject, Harris²⁶ has suggested that the major components of S_n at 393 K are the cyclics S_7 and S_9 , with smaller amounts of S_{10} and S_6 and less than 1% by weight of cyclics with more than ten sulphur atoms.

Most of these proposals as to the nature of S_n in liquid sulphur were based on the results of experimental investigations of the material obtained by extracting quenched sulphur melts with carbon disulphide and cooling to low temperatures to precipitate cyclo-octasulphur. Invariably, it was assumed that the bright yellow solutions contained a molecular species identical to that responsible for the depression in the freezing point of liquid sulphur. This questionable assumption has never been verified experimentally. Sulphur allotropes and polysulphur molecules are notoriously unstable and readily convert to other forms^{27, 28}. Thus, if unstable sulphur molecules are present in liquid sulphur at equilibrium, some at least would not be expected to survive the quenching and leaching processes unchanged.

Three years ago, the present author²⁹ proposed that the molecular species S_n formed in liquid sulphur consists of a mixture of large sulphur cyclics S_x with $x > 8$. This proposal followed a calculation of the cyclic content of liquid sulphur at a temperature just above the critical polymerization temperature, where the average lengths of the sulphur chains are very long. The calculation was carried out using the Jacobson and Stockmayer³⁰ equilibrium theory of cyclization, and it was based on an analysis of the conformational statistics of sulphur chains^{29, 31} using the rotational isomeric state model of polycatenasulphur³². Liquid sulphur at 433 K was estimated to contain cyclics S_x with $x > 8$ in concentrations of more than 30% by weight²⁹.

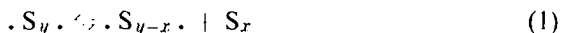
The proposal that large sulphur cyclics are present in liquid sulphur at all temperatures²⁹ has received some support from Schmidt and Block's³³ observation that the comparatively stable cyclic S_{12} can be isolated from rapidly quenched samples of liquid sulphur. Schmidt and his coworkers³⁴⁻³⁷ have synthesized and identified the sulphur cyclics $S_6, S_7, S_9, S_{10}, S_{12}$ and S_{18} (see also refs. 38 and 39). The most stable of these cyclics is S_{12} , and the isolation of other individual large sulphur cyclics from quenched samples of liquid sulphur would be expected to be a more difficult task.

In this paper, the proposal that S_n in liquid sulphur consists of cyclics S_x with $x > 8$ is tested by comparing the predicted depression in the freezing point of liquid sulphur resulting from their presence, with the experimental results of Wiewiorowski, Parthasarathy and Slaten⁶. The average lengths of sulphur chains at different temperatures are required for this calculation. They are estimated by using Gee's^{8, 10} thermodynamic analysis of the equilibrium between cyclo-octasulphur and polycatenasulphur.

FREEZING POINT OF LIQUID SULPHUR

CYCLIC CONTENT OF LIQUID SULPHUR BELOW THE CRITICAL
POLYMERIZATION TEMPERATURE

The equilibrium between ring molecules and diradical chains in liquid sulphur may be represented as follows



so that the molar cyclization equilibrium constants K_x for cyclics S_x are given by

$$K_x = \frac{[S_x] [\cdot S_{y-x} \cdot]}{[\cdot S_y \cdot]} \quad (2)$$

Assuming a most probable distribution of chain lengths for the linear diradicals⁸

$$K_x = [S_x] / (1 - 1/\bar{v})^x \quad (3)$$

where \bar{v} is the average number of sulphur atoms in the chain molecules.

The molar cyclization equilibrium constants K_x are related to the corresponding standard state entropy changes ΔS_x^0 and enthalpy changes ΔH_x^0 for process (1) by

$$K_x = \exp(\Delta S_x^0/R) \exp(-\Delta H_x^0/RT) \quad (4)$$

where R is the gas constant and T is the temperature.

Mass spectroscopic investigations⁴⁰⁻⁴² of the equilibria between cyclic molecules in sulphur vapour have established that cyclics with $x < 8$ are strained, and they have been predicted to be present in liquid sulphur in negligible amounts²⁹. This prediction is supported by Berkowitz and Chupka's⁴¹ experimental estimate that the concentration of cyclohexasulphur in liquid sulphur is only ca 10^{-3} that of cyclo-octasulphur. Hence, for present purposes, cyclics in liquid sulphur with $x < 8$ will be neglected.

Cyclo-octasulphur is energetically stable relative to open sulphur chains, so that ΔH_8^0 is negative for the forward step of process (1) when $x = 8$. The most reliable values for ΔH_8^0 have been obtained from the difference in the heat capacity of liquid sulphur just above and just below the critical polymerization temperature T_ϕ by the procedure described by Fairbrother, Gee and Merrill¹⁰. The most recent studies of the heat capacity of liquid sulphur as a function of temperature by West³⁴ and by Yoshioka⁴⁴ yield values of -13.4 ± 0.8 kJ mol⁻¹ and -14.2 ± 1.2 kJ mol⁻¹ respectively⁴⁵. We shall use the average value of -13.8 kJ mol⁻¹ for ΔH_8^0 in the calculations to follow, noting that this is close to the value of -13.3 kJ mol⁻¹ derived by Tobolsky and Eisenberg¹², from estimates of the S_8 content and average lengths of sulphur chains above T_ϕ , and by Fairbrother, Gee and Merrill¹⁰, from the heat capacity data of Braune and Möller⁴⁶. For cyclics with $x > 8$, the standard state enthalpy changes ΔH_x^0 are taken to be zero²⁹.

The entropy changes ΔS_x^0 have been estimated²⁹ using the Jacobson and Stockmayer³⁰ theory together with the rotational isomeric state model of

polycatenasulphur³². In this model, every bond in a sulphur chain is considered to lie in one of two rotational isomeric states at $\phi = +90^\circ$ and $\phi = -90^\circ$ (where ϕ is the internal rotation angle measured relative to the *trans* $\phi = 0^\circ$ position) and the interdependence of bond rotational states is taken into account. Analysis of the conformational statistics of sulphur chains unperturbed by excluded volume effects has shown that for chains $\cdot S_x \cdot$ with eight or more chemical bonds:

(I) Densities $W_x(\mathbf{0})$ of end-to-end vectors \mathbf{r} in the region $\mathbf{r} = \mathbf{0}$ are given approximately by the Gaussian expression

$$W_x(\mathbf{0}) = (3/2\pi \langle r_x^2 \rangle_0)^{3/2}$$

(II) Mean-square end-to-end distances $\langle r_x^2 \rangle_0$ are approximately proportional to x .

Assuming (I) and (II), the Jacobson and Stockmayer³⁰ expression for the entropy change of process (1) relative to a standard state in which the ring molecules are at unit concentration in mol l⁻¹ is as follows²⁹

$$\exp(\Delta S_x^0/\mathbf{R}) = (3/2\pi \langle r_x^2 \rangle_0)^{3/2} (1/N_A x) \quad (5)$$

where N_A is Avogadro's constant.

Combination of equations (3)–(5) yields the following expression for the ratio of the weight fractions of cyclics with x atoms and eight atoms

$$(w_x/w_8) = (8^{3/2}/x^{3/2}) \exp(-\Delta H_8^0/\mathbf{R}T)(1 - 1/\bar{y})^{x-8} \quad (6)$$

Gee⁸ has derived an approximate expression for the average number of sulphur atoms \bar{y} in chains in liquid sulphur below the critical polymerization temperature, T_ϕ . If cyclics other than cyclo-octasulphur are neglected, the equilibrium in the melt may be represented



and the molar cyclization equilibrium constant K_8 for cyclo-octasulphur

$$K_8 = [S_8]/(1 - 1/\bar{y})^8 \quad (8)$$

Chain molecules are present in negligible amounts when $T < T_\phi$, so the molar concentration of S_8 can be taken to be unity; furthermore, \bar{y} is very large at $T = T_\phi$ and, using the van't Hoff isochore, Gee⁸ has shown that

$$\bar{y} \cong 8\mathbf{R}/\Delta H_8^0(1/T - 1/T_\phi) \quad (9)$$

FREEZING POINT DEPRESSION OF LIQUID CYCLO-OCTASULPHUR

The depressions in the freezing point of pure liquid cyclo-octasulphur resulting from the presence of large ring molecules were calculated at different temperatures below T_ϕ using the formula

$$T_\lambda - T_f = \frac{\mathbf{R}T_\lambda T_f}{-\Delta H_f} \ln x_\lambda \quad (10)$$

FREEZING POINT OF LIQUID SULPHUR

where ΔH_f is the molar heat of fusion of S_λ , T_λ is the freezing point of pure S_λ , T_f is the freezing point of the equilibrated solution and x_λ is the mole fraction of cyclo-octasulphur in the solution. Values of x_λ were obtained by calculating the concentrations of large ring molecules S_x (with $x = 9-\infty$) in liquid sulphur at equilibrium by means of equations (6) and (9) with $\Delta H_8^0 = -13.8 \text{ kJ mol}^{-1}$. A value of $\Delta H_f = 13.74 \text{ kJ mol}^{-1}$ obtained by West¹³ was used for the calculations, together with the value of $T_\lambda = 392.0 \text{ K}$ reported by Wiewiorowski and his coworkers⁶.

The freezing point depressions of pure liquid cyclo-octasulphur, calculated to result when liquid sulphur is equilibrated at 403, 413 and 423 K are compared with the experimental values⁶ in Table 1. Agreement between theory and experiment is very satisfactory. Below T_ϕ it is believed that large sulphur cyclics S_x with $x > 8$ are effectively the only species responsible for the depressions in the freezing point of liquid sulphur.

Table 1 Calculated and experimental freezing point depressions

Equilibration temperature $T(\text{K})$	Wt. % cyclics with $x > 8$ [calc. by eqn. (6),(9)]	Ave. no. of atoms in cyclics	T_λ [calc. by eqn (10)]	$T_f(\text{K})$	$T_\lambda - T_f(\text{K})$ (exp.—ref.6)
393	8.2	13.8	4.6	—	—
403	10.6	14.6	5.7	4.9	4.9
413	13.7	15.7	7.1	5.9	5.9
423	18.8	17.6	9.1	7.6	7.6

ACKNOWLEDGEMENTS

The author gratefully acknowledges computational facilities at the University of York.

Department of Chemistry,
University of York, York, UK

(Received 19 January 1971)

REFERENCES

- 1 Gernez, M. D. *Compt. rend.* 1876, **82**, 115
- 2 Schaum, K. *Ann.* 1899, **308**, 18
- 3 Smith, A. and Holmes, W. B. *J. Amer. Chem. Soc.* 1905, **27**, 979
- 4 Smith, A. and Carson, C. M. *Z. physik. Chem.* 1907, **57**, 685
- 5 Beckmann, E., Paul, R. and Liesche, O. *Z. anorg. allgem. Chem.* 1918, **103**, 189
- 6 Wiewiorowski, T. K., Parthasarathy, A. and Slaten, B. L. *J. Phys. Chem.* 1968, **72**, 1890
- 7 Aten, A. H. W. *Z. physik. Chem.* 1914, **88**, 321
- 8 Gee, G. *Trans. Faraday Soc.* 1952, **48**, 515
- 9 Gee, G. *Sci. Prog.* 1955, **170**, 193
- 10 Fairbrother, F., Gee, G. and Merrill, G. T. *J. Polym. Sci.* 1955, **16**, 459
- 11 Tobolsky, A. V. and Eisenberg, A. *J. Amer. Chem. Soc.* 1959, **81**, 780
- 12 Tobolsky, A. V. and MacKnight, W. J. 'Polymeric sulphur and related polymers', Interscience, New York, 1965
- 13 Aten, A. H. W. *Z. physik. Chem.* 1913, **81**, 257
- 14 Aten, A. H. W. *Z. physik. Chem.* 1913, **83**, 442

- 15 Aten, A. H. W. *Verlag Akad. Wetenschappen Amsterdam* 1918, **26**, 813
- 16 Bruni, G. and Amadori, M. *J. Chem. Soc.* 1919, **116**(II), 281
- 17 Ruff, O. and Golla, H. *Z. anorg. Chem.* 1924, **138**, 33
- 18 Hammick, D. Ll. and Zvegintzov, M. *J. Chem. Soc.* 1928, p 1785
- 19 Krebs, H. *Z. Naturforsch.* 1957, **12**, 785
- 20 Schenk, J. *Physica* 1957, **23**, 325
- 21 Schenk, J. *Physica* 1957, **23**, 546
- 22 Schenk, P. W. and Thümmeler, U. *Z. Electrochem., Ber. Bunsenges. physik. Chem.* 1959, **63**, 1002
- 23 Schenk, P. W. and Thümmeler, U. *Z. anorg. allgem. Chem.* 1962, **315**, 271
- 24 Wiewiorowski, T. K. and Touro, F. J. *J. Phys. Chem.* 1966, **70**, 3528
- 25 Krebs, K. and Beine, H. *Z. anorg. allgem. Chem.* 1967, **355**, 113
- 26 Harris, R. E. *J. Phys. Chem.* 1970, **74**, 3102
- 27 Meyer, B. *Chem. Rev.* 1964, **64**, 429
- 28 Meyer, B. (ed.) 'Elemental sulphur', Interscience, New York, 1965
- 29 Semlyen, J. A. *Trans. Faraday Soc.* 1968, **64**, 1396
- 30 Jacobson, H. and Stockmayer, W. H. *J. Chem. Phys.* 1950, **18**, 1600
- 31 Semlyen, J. A. *Trans. Faraday Soc.* 1967, **63**, 2342
- 32 Semlyen, J. A. *Trans. Faraday Soc.* 1967, **63**, 743
- 33 Schmidt, M. and Block, H. D. *Angew. Chem.* 1967, **79**, 944
- 34 Schmidt, M. and Wilhelm, E. *Inorg. Nucl. Chem. Letters* 1965, **1**, 39
- 35 Schmidt, M. and Wilhelm, E. *Angew. Chem. (Internat. edit.)* 1966, **5**, 964
- 36 Schmidt, M., Block, B., Block, H. D., Kopf, H. and Wilhelm, E. *Angew. Chem. (Internat. edit.)* 1968, **7**, 632
- 37 Schmidt, M. and Wilhelm, E. *Chem. Comm.* 1970, p 1111
- 38 Kawada, I. and Hellner, E. *Angew. Chem. (Internat. edit.)* 1968, **7**, 379
- 39 Kutoglu, A. and Hellner, E. *Angew. Chem. (Internat. edit.)* 1966, **5**, 965
- 40 Berkowitz, J. and Marquart, J. R. *J. Chem. Phys.* 1963, **39**, 275
- 41 Berkowitz, J. and Chupka, W. A. *J. Chem. Phys.* 1964, **40**, 287
- 42 Berkowitz, J. in 'Elemental sulphur', (Ed. Meyer, B.) Interscience, New York, 1965
- 43 West, E. D. *J. Amer. Chem. Soc.* 1959, **81**, 29
- 44 Yoshioka, T. *Sci. Reports Tohoku Univ., First Ser.* 1960, **44**, 135
- 45 Poulis, J. A. and Massen, C. H. in 'Elemental sulphur' (Ed. Meyer, B.) Interscience, New York, 1965
- 46 Braune, H. and Möller, O. *Z. Naturforsch.* 1954, **9A**, 210

*The thermodynamic properties of liquids, including solutions: Part 2. Polymer solutions considered as ditonic systems**

MAURICE L. HUGGINS

The author's new theory of the thermodynamic properties of solutions is outlined. Theoretical equations are presented for applying it to polymer solutions. These equations are tested by applying them to poly(propylene oxide) + carbon tetrachloride and rubber + benzene solutions. The results are gratifying.

INTRODUCTION

THIS PAPER is concerned with a theory of the thermodynamic properties of solutions, and especially with applications of this theory to polymer solutions. The theory is based on concepts that I have used for a long time, but the quantitative aspects are new. The assumptions and basic equations have been presented in previous papers^{1,2}, with applications to the heats of mixing of a number of solutions of low-molecular-weight compounds for which precise data are available in the literature. The theoretical curves agree with the data within the probable error of the latter.

In this paper I briefly review the fundamentals of the theory, with regard to energy and enthalpy parameters, and show how the same fundamentals can be applied to volume and entropy properties. I then show some of the results recently obtained in applying the theory to polymer solutions. Detailed discussion of these results will be left for future papers.

FUNDAMENTAL IDEAS AND EQUATIONS

I use a model in which each molecule has a surface, with the surfaces of neighbouring molecules in mutual contact. If the molecules contain segments that are chemically different, I deal separately with the segment surfaces of each type and their contacts. For simplicity I first consider only systems having two kinds of segment.

Considering first the energies associated with the contacts between segments, I assume that for each segment type the average contacting segment surface area is constant at a given temperature, regardless of variations in the types and numbers of other segments, also that for each kind of segment-segment contact, the average contact energy per unit area of contact is

* Presented at the International Symposium on Macromolecular Chemistry, Leiden, September 1970, under the title 'Polymer solution thermodynamics'

constant at a given temperature, regardless of variations in the types and areas of other contacts. In order to minimize the free energy, I assume that the relative contact areas for the three types are governed by an equilibrium constant. (If there are more than two segment types, additional equilibrium constants must be used.)

These assumptions lead unequivocally to equations that can be tested experimentally, for example, by data on heats of mixing.

With regard to entropies, it is customary to use a Raoult's law type of relationship, if the molecular sizes do not differ greatly, or the Flory-Huggins relation, which allows for differences in size. Both involve the assumption of random mixing of the molecules (and so of the contacts between them). I believe that this leads to serious error if the energy per unit area for contacts between unlike segments differs much from the average energy per unit area for contacts between like segments - i.e., if the equilibrium constant differs much from unity. I have developed a theory, to be described in a later paper³, to correct the combinatorial entropy for departures from perfect randomness of contact distribution. This theory relates these departures to the magnitude of the equilibrium constant. As will be shown, the theoretical relationship appears satisfactory in the one case in which it has been tested: the rubber + benzene system.

Another important contribution to the entropy dependence on concentration, when one of the solution components is a flexible polymer molecule, results from the change in average randomness of orientation of a segment in the polymer chain, relative to the adjacent segments, as the concentration (hence the environment of each segment) changes. Both of these two entropy effects combine to give χ_s , the entropy part of the interaction parameter.

Volumes can usually be treated like energies or enthalpies. Different constants must of course be used for the volume contributions of the three kinds of contact, but the same equilibrium constant applies.

For a ditonic system (one having only two types of segments) the areas of the three kinds of contacts ($\sigma_{\alpha\beta}$, $\sigma_{\alpha\alpha}$, $\sigma_{\beta\beta}$) are related to the contacting areas of the two kinds of segments (σ_α , σ_β) and to the equilibrium constant (K) by the equations

$$\sigma_{\alpha\beta} = -2F; \quad \sigma_{\alpha\alpha} = \frac{1}{2}\sigma_\alpha + F; \quad \sigma_{\beta\beta} = \frac{1}{2}\sigma_\beta + F \quad (1)$$

where

$$F = (\sigma_\alpha \div \sigma_\beta)[1 - (1 + K'z_\alpha z_\beta)^{1/2}]/K' \quad (2)$$

$$K' = 4 \left(\frac{1}{K} - 1 \right) \quad K = \frac{\sigma_{\alpha\beta}^2}{4\sigma_{\alpha\alpha}\sigma_{\beta\beta}} \quad (3)$$

Here z_α and z_β are the contacting surface fractions:

$$z_\alpha = \frac{\sigma_\alpha}{\sigma_\alpha + \sigma_\beta} \quad z_\beta = \frac{\sigma_\beta}{\sigma_\alpha + \sigma_\beta} \quad (4)$$

For complete randomness of contacts:

$$K = 1 \quad \text{and} \quad F = -\sigma_\alpha z_\beta / 2 \quad (5)$$

σ_α and σ_β are products of the numbers of α and β segments in the system being considered, times the contacting surface areas per segment (σ_α^0 , σ_β^0).

The molar interaction enthalpy for a ditonic system is related to the contact energies per unit area ($\epsilon_{\alpha\alpha}$, $\epsilon_{\beta\beta}$, $\epsilon_{\alpha\beta}$) by the equation

$$H = \frac{1}{2}\sigma_{\alpha}\epsilon_{\alpha\alpha} + \frac{1}{2}\sigma_{\beta}\epsilon_{\beta\beta} - F\Delta\epsilon \quad (6)$$

with

$$\Delta\epsilon = 2\epsilon_{\alpha\beta} - \epsilon_{\alpha\alpha} - \epsilon_{\beta\beta} \quad (7)$$

A similar relationship, with each ϵ replaced by v , applies to the volume.

APPLICATION TO POLYMER SOLUTIONS

In my first applications of the theory to polymer solutions, I have made the simplifying assumption that each solvent molecule can be considered as constituting a single segment (of type α) and that each mer of the polymer can be treated as a single segment (of type β). For many polymer + solvent systems this simplification may be unjustifiable. Also, it will often be impossible or inadvisable to use it if the parameters to be used are determined from measurements on systems containing only compounds of low molecular weight.

Theory and experiment are to be compared for the following properties, each as a function of concentration:

\tilde{H}^E , the excess enthalpy or heat of mixing, per mole of mixture.

\tilde{V}^E , the excess volume of mixing, per mole of mixture.

χ_h , the enthalpy contribution to the interaction parameter.

χ , the total interaction parameter.

We shall also use theoretical curves for χ_s , the entropy contribution to the interaction parameter, to add to the theoretical curves for χ_h to obtain theoretical curves for the total χ .

The equation for the excess enthalpy, based on the theory outlined above, is

$$\tilde{H}^E = \epsilon_A x_1 z_{\beta} g_K \quad (8)$$

with

$$\epsilon_A = \sigma_{\alpha}^0 \Delta\epsilon / 2 \quad (9)$$

$$x_2 = 1 - x_1 = \frac{\phi_2}{(nr_v)\phi_1 + \phi_2} \quad (10)$$

$$z_{\beta} = 1 - z_{\alpha} = \frac{nr_{\sigma}x_2}{1 + (nr_{\sigma} - 1)x_2} = \frac{r_{\sigma/v}\phi_2}{1 + (r_{\sigma/v} - 1)\phi_2} \quad (11)$$

$$r_{\sigma/v} = r_{\sigma}/r_v \quad r_v = v_{\beta}^0/v_{\alpha}^0 \quad r_x = \sigma_{\beta}^0/\sigma_{\alpha}^0 \quad (12)$$

$$g_K = \frac{-2}{z_{\alpha}z_{\beta}K'} [1 - (1 + K'z_{\alpha}z_{\beta})^{1/2}] \quad (13)$$

For the excess volume:

$$\tilde{V}^E = v_A x_1 z_{\beta} g_K \quad (14)$$

with

$$v_A = \sigma_{\alpha}^0 \Delta v / 2 \quad (15)$$

For the enthalpy part of the interaction parameter:

$$\chi_h = \frac{\epsilon_A z_\beta}{RT\phi_2^2} \left(\frac{1 - z_\alpha g_K}{1 + z_\alpha z_\beta K' g_K / 2} \right) \quad (16)$$

For the segment orientation entropy part of the interaction parameter:

$$\chi_{s,or} = \frac{-k_s z_\beta}{r_\sigma \phi_2^2 [1 - k_s (1 - z_\alpha g_K)]} \left[\frac{z_\beta - z_\alpha}{(1 + z_\alpha z_\beta K')^{1/2}} + z_\alpha g_K \right] \quad (17)$$

For the combinatorial entropy correction contribution to the interaction parameter:

$$\chi_{s,cc} = \frac{-\sigma_a^2}{4\phi_2^2} \left[\ln \left(\frac{1 - z_\beta g_K}{z_\alpha} \right) + \left(\frac{z_\beta - 2z_\beta^2}{1 + K' z_\alpha z_\beta g_K / 2} - z_\alpha z_\beta g_K \right) \times \ln \left(1 + \frac{1 - g_K}{z_\alpha z_\beta g_K^2} \right) \right] \quad (18)$$

It may be noted that the assumption of volume additivity, implied in equation (10) for the relationship between the mole fractions and the volume fractions, introduces no significant error.

Equations (8), (14), (17), and (18), for \tilde{H}^E , \tilde{V}^E , $\chi_{s,or}$, and $\chi_{s,cc}$, respectively, each involve just three unknown parameters: one (ϵ_A , v_A , k_s , or σ_a^0) that determines the scale and two (r_σ and K') which determine the shape of the concentration dependence curve. These two are the same for all, so if their magnitudes can be determined from one property, e.g., V^E , they can be used for the others. Equation (16) for χ_h involves no parameters other than those in equation (8) for \tilde{H}^E . If the two parameters r_σ and K' are accurately known, the scaling parameter required for each property can be determined from a single measurement of that property, at any concentration (assuming the theory to hold).

I do not believe that the scaling parameters for \tilde{H}^E , $\chi_{s,or}$ and $\chi_{s,cc}$ are quantitatively related in any general way, nor do I believe that the number of parameters required to account for the concentration dependence of χ , for example, can be reduced below the number used in these equations – except in special cases, as when there is complete randomness of mixing of contact types. For this special case:

$$K' = 0 \quad K = 1 \quad g_K = 1 \quad (19)$$

Equations (8), (14), (16), (17), and (18) then reduce to the following:

$$\tilde{H}^E = \epsilon_A x_1 z_\beta \quad (20)$$

$$\tilde{V}^E = v_A x_1 z_\beta \quad (21)$$

$$\chi_h = \frac{\epsilon_A z_\beta^2}{RT\phi_2^2} \quad (22)$$

$$\chi_s = \chi_{s,or} = \frac{-k_s z_\beta^2}{r_\sigma \phi_2^2 (1 - k_s z_\beta)} \quad (23)$$

$$\chi_{s,cc} = 0 \quad (24)$$

THERMODYNAMIC PROPERTIES OF LIQUIDS (2)

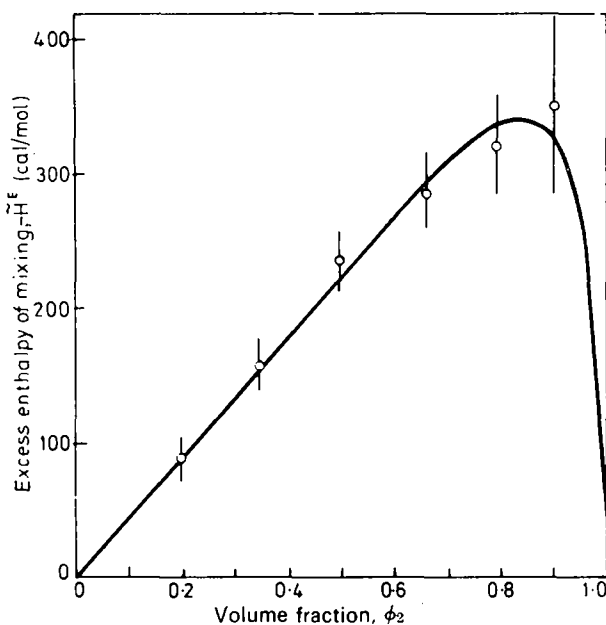


Figure 1 The excess enthalpy of mixing, in calories per mole of solution, vs. volume fraction, for solutions of poly(propylene oxide) + CCl₄ at 5.53°C. Data from Kershaw and Malcolm⁴. The vertical lines show their estimates of total experimental error. The curve is theoretical. (1 cal = 4.187 J)

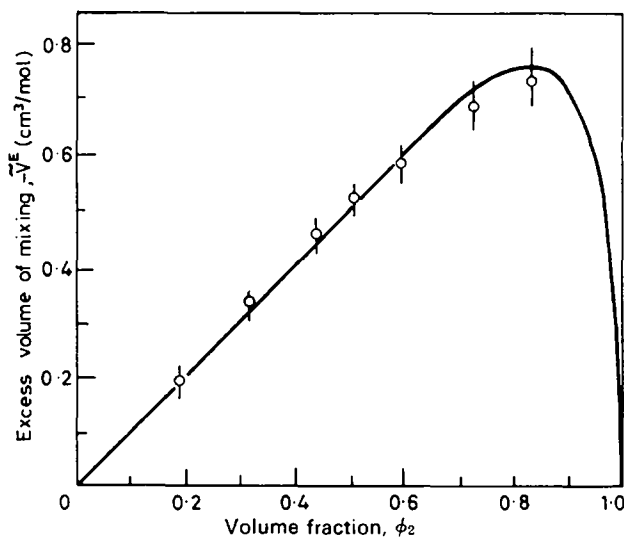


Figure 2 Excess volume of mixing, in cm³ per mole of solution, vs. volume fraction, for solutions of poly(propylene oxide) + CCl₄ at 5.53°C. Data from Kershaw and Malcolm⁴. The vertical lines indicate their estimates of maximum errors. The curve is theoretical

Poly(propylene oxide) + carbon tetrachloride

Kershaw and Malcolm⁴ have made precise measurements of heats and volumes of mixing and of vapour pressures for this system.

Their heat and volume of mixing data are in good agreement with the theoretical curves (*Figures 1 and 2*), with $K = 1$ (hence, random mixing), $r_\sigma = 0.48$, $\epsilon_d = -530$, and $v_d = -1.17$.

The χ_h curve, using the first three of these parameters, is shown in *Figure 3*, together with a curve for χ , passing through the experimental points for volume fractions less than 0.6 and using the same K and r_σ parameters. The

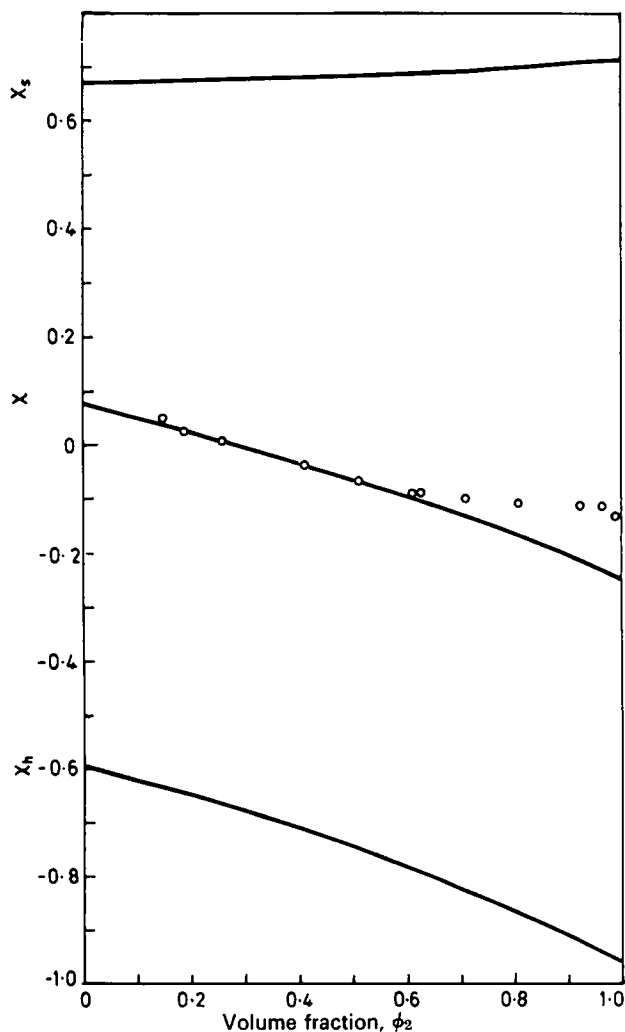


Figure 3 Theoretical curves for the interaction parameter X and its components X_h and X_s , for poly(propylene oxide) + CCl_4 . Experimental points by Kershaw and Malcolm⁴

χ_s curve, also using these parameters and obtained by subtracting χ_h from χ , is shown at the top of the graph. For this, $k_s = -0.519$.

The disagreement between the experimental points and the theoretical curve for χ at higher concentrations may be related to a tendency of the polymer molecules to associate at these concentrations, to a concentration dependence of the amount of intramolecular contacting between segments, to my tentative assumption that each mer can be treated as a single segment, or to other factors. A relatively small change in either of the theoretical curves, χ_s or χ_h , at the higher concentrations would suffice to give quantitative agreement for the χ curve over the whole range.

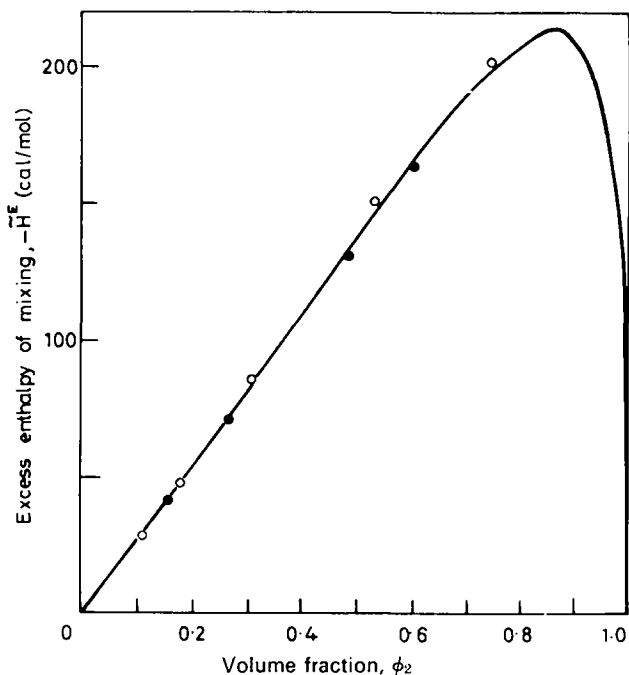


Figure 4 Excess enthalpy of mixing, in calories per mole of solution, for polyisoprene : benzene solutions at 16°C, vs. volume fraction. Data by Gee and Orr⁶. The curve is theoretical. (1 cal = 4.187 J)

Rubber + benzene

For testing the theory with this system I have used very old data by Gee and Treloar⁵ and Gee and Orr⁶, and new data by Eichinger and Flory⁷.

Heat of mixing data at 16°C by Gee and Orr and volume of mixing data at 25°C by Eichinger and Flory both agree (except for one point in the latter case) with theoretical curves drawn for $r_\sigma = K = 0.74$. (See Figures 4 and 5.) The scaling parameters are $\epsilon_d = 2.68$ and $v_d = 0.308$.

The heat of mixing data used were for solutions of a polyisoprene, not a natural rubber. Apparently neither the chemical and structural differences

between this and natural rubber nor the 9°C difference in temperature affect the parameters greatly.

The χ_h curve, assuming the parameters from the heat of mixing and volume of mixing curves, is compared with the data obtained by Gee and coworkers by four different techniques in *Figure 6*. Considering the scattering of the data points, the agreement is not bad.

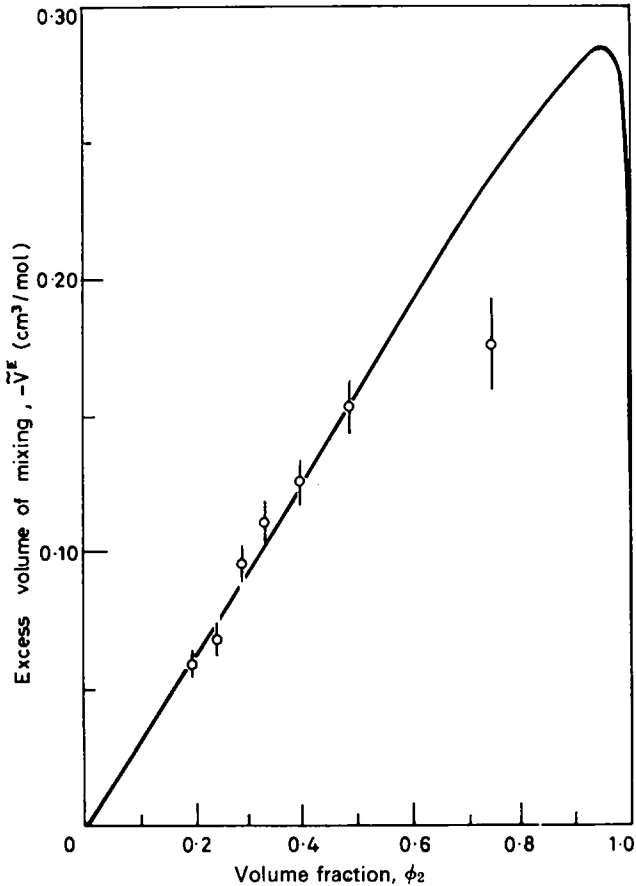


Figure 5 Excess volume of mixing, in cm³ per mole of solution, for rubber + benzene solutions at 25°C, vs. volume fraction. The circles are data points by Eichinger and Flory⁷. The vertical lines show their estimates of the experimental precision. The curve is theoretical

Using the same r_σ and K values, the scaling constants k_s and σ_a^0 , for the $\chi_{s,or}$ and $\chi_{s,cc}$ curves were adjusted to give reasonable agreement, when both are added to the χ_h curve, with Eichinger and Flory's χ data. (See *Figure 7*.) The curves for χ and its components, arrived at in this way, are collected in *Figure 8*.

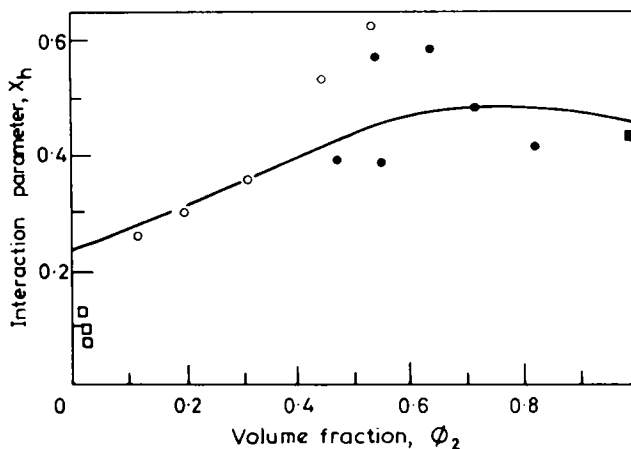


Figure 6 The enthalpy parameter, X_h , plotted vs. volume fraction, for rubber + benzene solutions at 25°C. ○●, data by Gee and Orr⁶; ■, data by Gee and Treloar⁵. The curve is theoretical

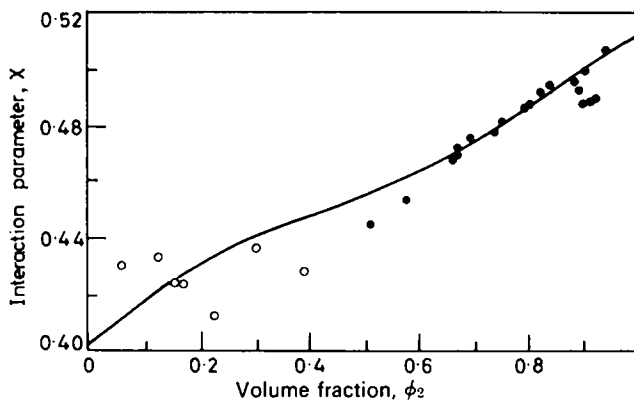


Figure 7 The interaction parameter, X , vs. volume fraction, for rubber + benzene solutions at 25°C. Data by Eichinger and Flory⁷. The curve is theoretical

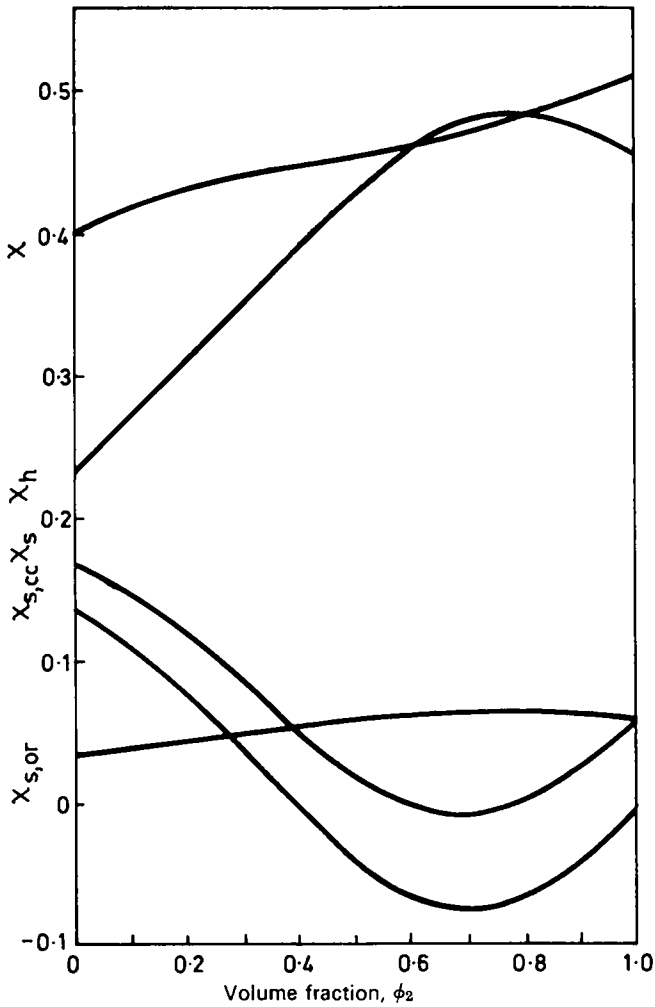


Figure 8 Theoretical curves for X and its components, for rubber-benzene solutions at 25°C

CONCLUSION

Considering the assumptions and approximations that have been made, the agreement for both systems is indeed satisfying. One must be careful, of course, about generalizing until other systems have been studied. This will be done.

The theory appears to afford a means for determining the parameters for polymer solutions from data on mixtures of compounds of low molecular weight. This, also, has not been done, but will be done.

It is also planned to test the new equation, relating the departures from the classical combinatorial entropy equations to the equilibrium constant of this theory, on various low-molecular weight systems.

*Arcadia Institute for Scientific Research,
135 Northridge Lane, Woodside,
California 94062, USA*

(Received 17 September 1970)

REFERENCES

- 1 Huggins, M. L. *J. Paint Technol.* 1969, **41**, 509
- 2 Huggins, M. L. *J. Phys. Chem.* 1970, **74**, 371
- 3 Huggins, M. L. *J. Phys. Chem.* 1971 (April)
- 4 Kershaw, R. W. and Malcolm, G. N. *Trans. Faraday Soc.* 1968, **64**, 323
- 5 Gee, G. and Treloar, L. R. G. *Trans. Faraday Soc.* 1942, **38**, 147
- 6 Gee, G. and Orr, W. J. C. *Trans. Faraday Soc.* 1946, **42**, 507
- 7 Eichinger, B. E. and Flory, P. J. *Trans. Faraday Soc.* 1968, **64**, 2035

Studies of heterocyclic polymers: Part 1. The synthesis and structure of macrocyclic polymers

R. J. GAYMANS, K. A. HODD and W. A. HOLMES-WALKER

Pyromellitic tetranitrile and 4,4'-diaminodiphenyl ether have been reacted in solution and in the solid state, and the macrocyclic polymer produced by each method of reaction has been shown to be structurally identical. Other macrocyclic polymers have been prepared by the solid state reactions of a number of aromatic diamines and pyromellitic tetranitrile. The diamines were selected to provide variations in the size of the macrocycle and in the level of strain within the ring. Preliminary studies suggest that these variations have an observable effect upon the ease of macrocyclization, but no marked influence upon the thermal stability of the polymers.

INTRODUCTION

THE PREPARATION, thermal stability and electrical properties of macrocyclic polymers have been reported by Packham and co-workers¹⁻³ and by Manecke and co-workers⁴. Both Packham² and the authors⁵ have made detailed studies of the macrocyclic polymer derived from pyromellitic tetranitrile and 4,4'-diaminodiphenyl ether.

This paper reports the results of synthetic studies made in an attempt to establish a link between ease of formation of the macrocycle, ring strain and the thermal stability of the polymer. To this end a number of macrocyclic polymers were prepared from pyromellitic tetranitrile and a series of aromatic diamines. The diamines were chosen to provide a range of ring sizes and ring strains.

EXPERIMENTAL

Materials

Pyromellitic tetranitrile was prepared from pyromellitic tetramide by modification⁶ of the method of Lawton and McRitchie⁷. The product was recrystallized three times under dry nitrogen from methyl ethyl ketone, m.p. 271-272°C (lit. 263°C)⁷. The i.r. absorption spectrum exhibited a strong band attributable to $C \equiv N$ at 2250 cm^{-1} but none attributable to $C=O$ (1720 cm^{-1}).

4,4'-Diaminodiphenyl ether (Sumitomo) was recrystallized with charcoal under dry nitrogen from methyl ethyl ketone, m.p. 193-193.5°C (lit. 192°C).

4,4'-Diaminodiphenyl methane (British Drug Houses, BDH) was recrystallized with charcoal under dry nitrogen from methyl ethyl ketone, m.p. 93.0-93.5°C (lit. 93°C).

m-Phenylene diamine (BDH) was recrystallized with charcoal under nitrogen from toluene, m.p. 62.0-62.5°C (lit. 62.8°C).

HETEROCYCLIC POLYMERS (I)

2,4-Diaminotoluene (BDH) was recrystallized with charcoal under dry nitrogen from methyl ethyl ketone, m.p. 99.0–99.5°C (lit. 99°C).

2,6-Diaminotoluene (BDH) was recrystallized with charcoal under dry nitrogen from methyl ethyl ketone, m.p. 104.5–105.0°C (lit. 105°C).

p-Phenylene diamine (BDH) was recrystallized with charcoal under dry nitrogen from toluene, m.p. 140.0–140.5°C (lit. 139.7°C).

2-Methoxyethanol (Shell) was dried over 5A molecular sieves and then fractionally distilled, b.p. 124°C (lit. 124°C).

Preparation of macrocyclic polymer

Solution polymerization. Macrocyclic polymer was prepared after the method of Packham and Rackley¹ from pyromellitic tetranitrile (8.9 g, 0.05 mol) and 4,4'-diaminodiphenyl ether (20.0 g, 0.1 mol) by reaction in 2-methoxyethanol solution under dry nitrogen, with sodium 2-methoxyethoxide (0.04 g) for catalyst. The polymer which was obtained in 85% yield was extracted with boiling 2-methoxyethanol to remove unreacted monomer, and dried *in vacuo* at 100°C. Table 1 summarizes the analytical data obtained for this polymer.

Table 1 Collected analytical data on macrocyclic polymers

Macrocyclic polymer diamine constituent	Elemental analyses						Salient infra-red bands		TGA 10% wt. loss temp. in air (°C)	DTA temp of degrada- tion exotherm in air (°C)
	Experimental			Theoretical			C	N		
	C	H	N	C	H	N	2250 cm ⁻¹	1720 cm ⁻¹		
4,4'- diamino- diphenyl ether.	(a)68.5	4.79	14.7	75.0	3.68	15.4	absent	absent	480	250
	(b)72.3	3.61	15.5	75.0	3.68	15.4	absent	absent	500	215
4,4'- diamino- diphenyl methane	74.8	4.48	15.6	85.3	4.53	15.83	absent	absent	525	170
<i>m</i> -phenylene diamine	65.4	3.02	22.7	73.4	3.3	23.3	absent	absent	540	200
2,4- diamino- toluene	69.7	4.15	21.0	74.2	4.12	21.6	absent	absent	505	150
2,6- diamino- toluene	72.8	4.31	21.7	74.2	4.12	21.6	absent	absent	490	150
<i>p</i> -phenylene diamine	66.7	3.79	22.5	73.4	3.3	23.3	absent	absent	475	150

(a) from solution polymerization; (b) from solid state polymerization

Solid state polymerization. Pyromellitic tetranitrile and 4,4'-diaminodiphenyl ether were mixed in a molar ratio of 1:2 and the mixture finely ground under dry nitrogen. About 20 g of the ground mixture was weighed accurately into a pyrex glass reaction tube. The reaction tube was heated in an aluminium block the temperature of which was raised from ambient to 330°C at a rate of 0.5°C/min by means of a Stanton-Redcroft Variable Rate Linear Programmer LVP/CA10. Dry nitrogen was passed through the reaction tube during the reaction and the ammonia evolved absorbed in 2% boric acid and estimated with 0.1N hydrochloric acid using screened methyl orange as an indicator.

Heating was stopped at 350°C and the polymer allowed to cool under nitrogen. The polymer was extracted with boiling dimethylformamide to remove unreacted monomers and other low molecular weight species.

This procedure was repeated for a series of preparations using a mixture of pyromellitic tetranitrile and each of the diamines listed below in turn:

4,4'-diaminodiphenyl methane
m-phenylene diamine
p-phenylene diamine
 2,4-diaminotoluene
 2,6-diaminotoluene

In each case, during the course of the heating programme the reactants were observed to melt and at this point ammonia was evolved rapidly. Within about 10°C the mixture resolidified and the reaction continued in the solid state.

Figure 1 and Table 2 give the amounts of ammonia evolved during the reactions and the yields of insoluble polymer.

Table 2 The preparation of macrocyclic polymer: the ammonia evolved and the yield

Macrocyclic polymer diamine constituent	Yield of insoluble polymer (%)	Moles of ammonia evolved per mole of polymer
4,4'-diaminodiphenyl ether	(a) 85 (b) 95	— 1.52
4,4'-diaminodiphenyl methane	95	1.58
<i>m</i> -phenylene diamine	95	1.30
2,4-diaminotoluene	90	1.36
2,6-diaminotoluene	95	1.28
<i>p</i> -phenylene diamine	30	1.10

(a) from solution polymerization; (b) from solid state polymerization

Thermogravimetric analysis (TGA)

Each of the polymers was analysed thermogravimetrically on the Stanton Thermobalance TR01 using a 60 mg 100 mesh powder sample and heating in air at 4°C/min. The temperature at which 10% weight loss was observed is reported in Table 1. The results have been corrected for buoyancy variations.

HETEROCYCLIC POLYMERS (I)

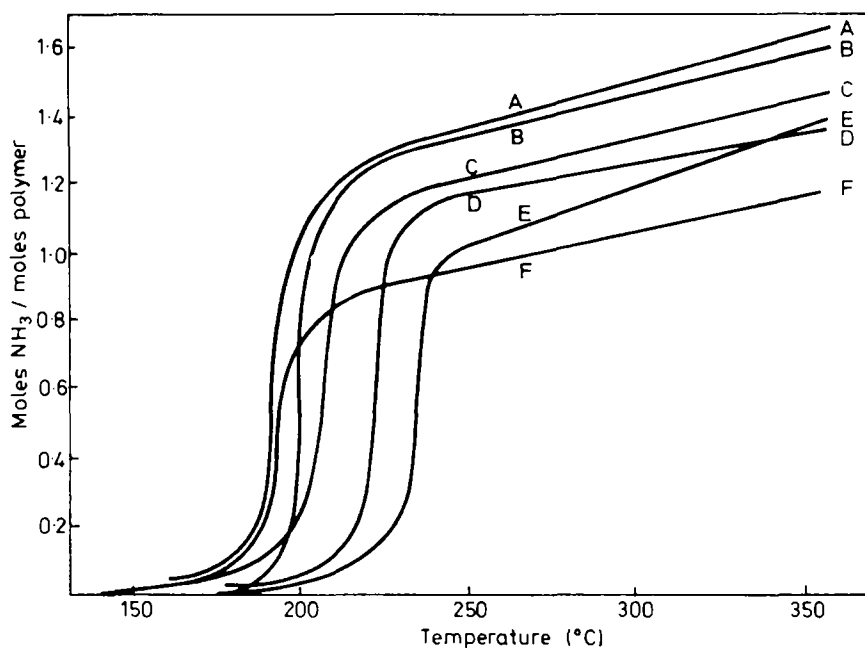


Figure 1 The ammonia evolved during the formation of macrocyclic polymer from: A, 4,4'-diaminophenyl ether; B, 4,4'-diaminophenyl methane; C, 2,4-diaminotoluene; D, *m*-phenylene diamine; E, 2,6-diaminotoluene; F, *p*-phenylene diamine

Differential thermal analysis (DTA)

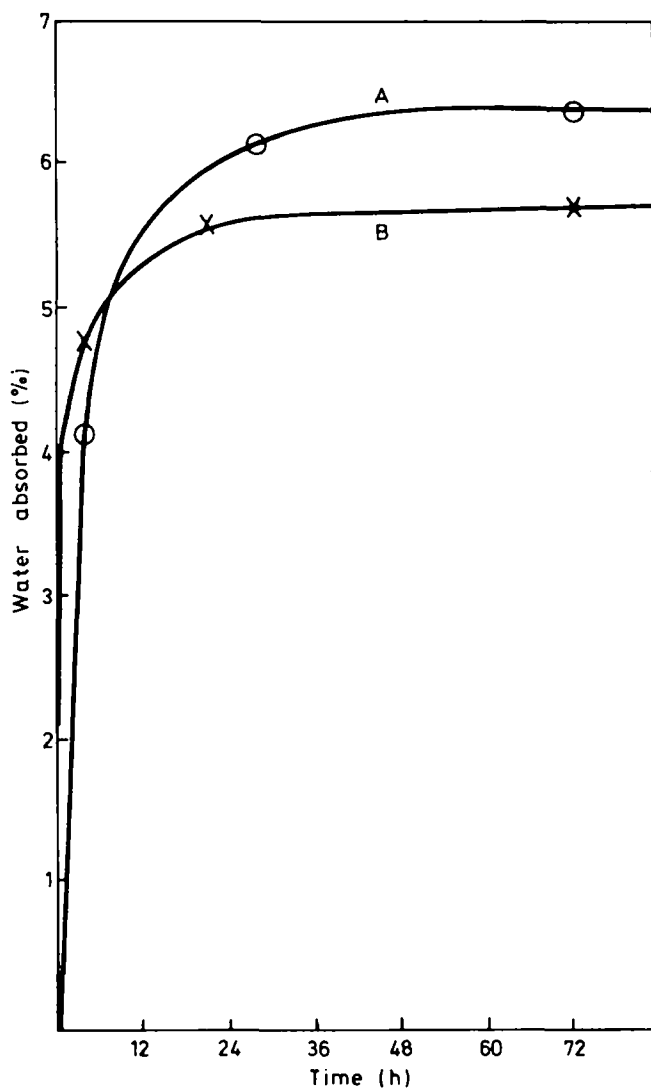
Differential thermal analyses were made with a Stanton LDTA using 100 mesh powder samples and heating in air at 10°C/min. The temperature reported in Table 1 for each polymer is the point at which the exotherm attributable to the thermo-oxidative breakdown of the polymer⁵ begins.

Infra-red spectra

All i.r. spectra were obtained using potassium bromide discs in a Hilger and Watts Infragraph.

Water absorption

Macrocyclic polymer derived from pyromellitic tetranitrile and 4,4'-diaminodiphenyl ether (5 g, 100 mesh powder) was dried to constant weight. The sample was exposed to air at 23°C and 60% relative humidity and weighed at intervals. The rate of water absorption is depicted in Figure 2, which also shows the curve obtained in the same way for the macrocyclic polymer prepared from pyromellitic tetranitrile and 4,4'-diaminodiphenyl methane.



[Figure 2 The water absorption of macrocyclic polymer from: A, 4,4'-diaminodiphenyl methane; and B, 4,4'-diaminodiphenyl ether]

DISCUSSION AND RESULTS

Macrocyclic polymers are produced by a two stage process involving reaction of diamine and tetranitrile (Figure 3). In the first stage the chain structure of the polymer is established by a proton transfer process and

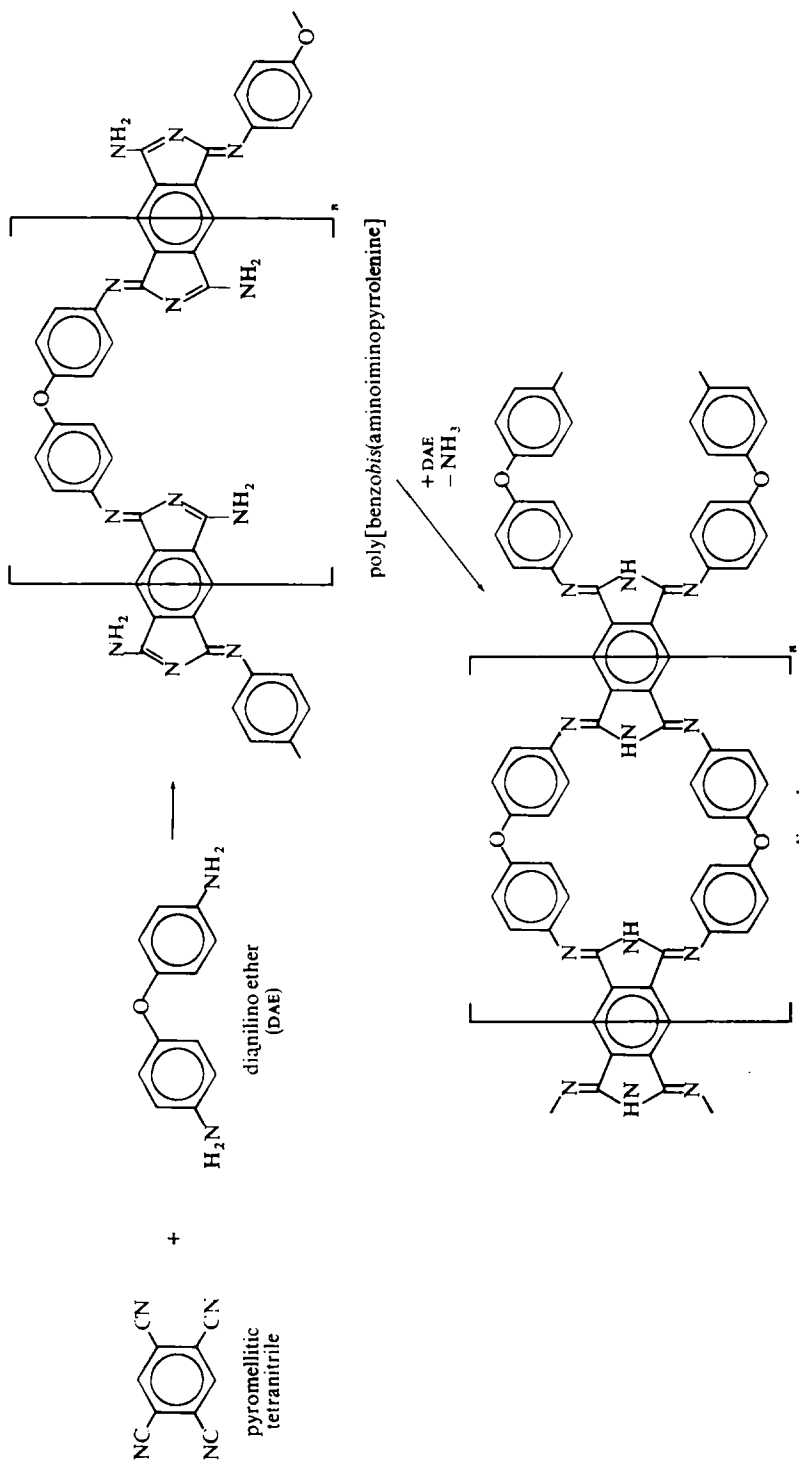


Figure 3 The formation of poly[benzobis(aminoiminopyrrolenine)] and macrocyclic polymer

concomitant cyclization. The second stage involves two condensation reactions which produce the macrocyclic structure.

Packham and Rackley¹ have reported that the reaction of pyromellitic tetranitrile and 4,4'-diaminodiphenyl ether proceeds rapidly through the first stage in 2-methoxyethanol solution. Our studies⁸ show that, whilst the solution polymerization is effective in the case of 4,4'-diaminodiphenyl ether, the first stage reaction of pyromellitic tetranitrile and some other aromatic diamines in solution is incomplete. In these cases the i.r. spectra of the fully extracted polymers exhibit nitrile absorption bands at 2250 cm^{-1} . This limitation was overcome by preparing the polymers from solid state reaction of the monomers. The products of these reactions did not exhibit nitrile absorption in the i.r. spectra (*Table 1*).

As may be seen from the photographs of the molecular models (*Figure 4*) all the diamines studied can be expected to form polymers involving macrocycles.

4,4'-Diaminodiphenyl ether (*Figure 4a*) and 4,4'-diaminodiphenyl methane (*Figure 4b*) yield open macrocycles with little or no ring strain. These macrocycles are large enough to accommodate molecules of water (shown in *Figures 4a* and *b*) and absorb atmospheric moisture as shown in *Figure 2*.

With *m*-phenylene diamine (*Figure 4c*) and 2,4-diaminotoluene (*Figure 4d*) the amino groups are ideally disposed (at 90° one to another) for ring formation so that although the macrocycle is reduced in size all the benzene rings are coplanar or very nearly so and ring strain is low. The macrocycles in these cases are too small to accommodate water molecules and these polymers are not hygroscopic.

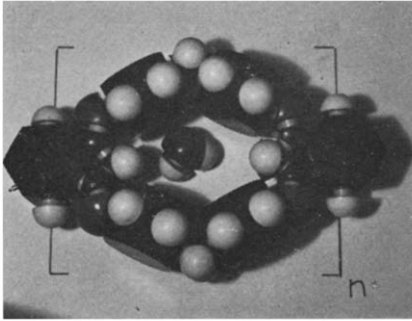
In the case of 2,6-diaminotoluene (*Figure 4e*) whilst the amino groups are ideally disposed the presence of the methyl group prevents the formation of a planar macrocycle and the ring strain is greater.

p-Phenylene diamine also forms a highly strained non-planar macrocycle (*Figure 4f*).

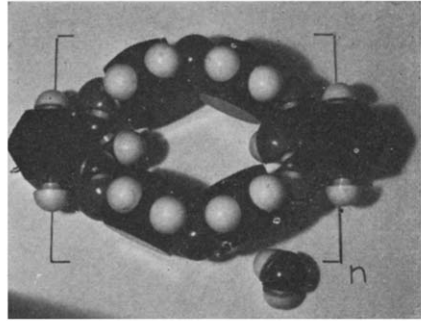
The ease of ring formation, predicted from model structures is borne out by the experimental evidence presented for the completeness of macrocyclization. The macrocyclization step is a two stage process (*Figure 3*) and at each stage ammonia is evolved. *Figure 1* shows that these two stages are identifiable from the evolution of ammonia curves, for these curves exhibit two distinct parts. The first part relates to an extremely rapid rate of evolution of ammonia from the molten monomers and inflects at near to 1 mole of ammonia to a slower rate of evolution from the solid phase. It is likely that the rate of ammonia evolution subsequent to the knee is related to the strain in the macrocycle for the amount of ammonia evolved during the formation of each polymer (*Table 2*) follows the trend predicted from the molecular models. Thus the diamines which form the largest macrocycles, e.g. 4,4'-diaminodiphenyl ether, react most completely whilst *p*-phenylene diamine, which yields a highly strained macrocycle, reacts most slowly. *Meta*-substituted diamines exhibit an intermediate reactivity.

The 10% weight loss temperatures for these polymers are all near to 500°C in air and the temperatures at which their degradation exotherms start in air lie between 150 and 250°C (*Table 1*). These results suggest that the thermal stability of macrocyclic polymer is independent of ring size and strain.

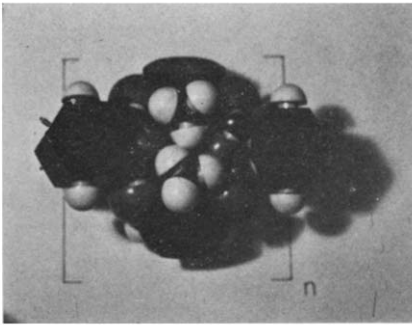
HETEROCYCLIC POLYMERS (I)



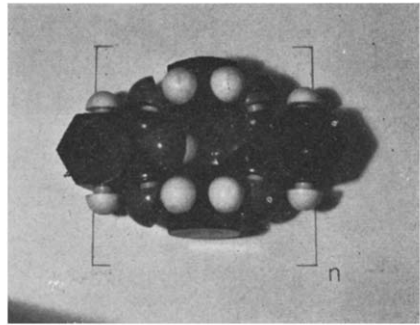
(a) 4,4'-diaminodiphenyl ether



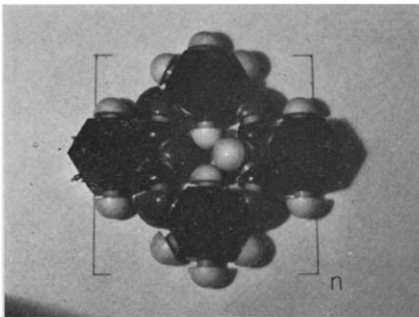
(b) 4,4'-diaminodiphenyl methane



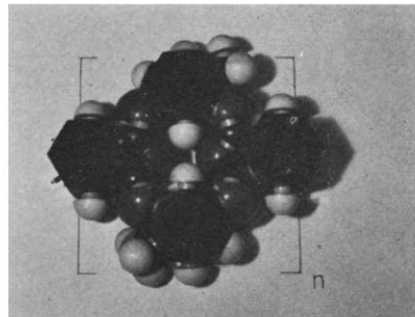
(c) *m*-phenylenediamine



(d) 2,4-diaminotoluene



(e) 2,6-diaminotoluene



(f) *p*-phenylenediamine

Figure 4 The model structure of macrocyclic polymer derived from the aromatic diamine shown

CONCLUSIONS

The results demonstrate that the solid state preparation of macrocyclic polymers is applicable to a number of aromatic diamines and pyromellitic tetranitrile and that the reaction is more complete than can be achieved from solution polymerization.

The completeness of macrocyclization increases in the order anticipated from the ring strain, i.e., in order of decreasing ease of reaction—4,4'-diaminodiphenyl ether; 4,4'-diaminodiphenyl methane >*m*-phenylenediamine; 2,4-diaminotoluene; 2, 6-diaminotoluene >*p*-phenylenediamine.

ACKNOWLEDGEMENTS

One of us (R.J.G.) acknowledges with thanks the financial support provided by the NRDC.

Dr D. Packham (NPL) gave us helpful advice upon the synthesis of pyromellitic tetranitrile and upon the solution preparation of macrocyclic polymer.

*Department of Polymer Science and Technology,
Brunel University,
Woodlands Avenue, London W3 9BX*

(Received 30 December 1970)

REFERENCES

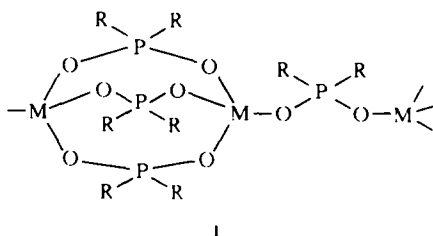
- 1 Packham, D. I., and Rackley, F. A. *Chem. and Ind.* 1969, p 1255
- 2 Packham, D. I., and Rackley, F. A. *Polymer, Lond.* 1969, **10**, 559
- 3 Graham, G., and Packham, D. I. *Polymer, Lond.* 1969, **10**, 645
- 4 Manecke, G., Wohrle, D. and Kossmehl, G. *J. Polym. Sci. (C)* 1968, **22**, 463
- 5 Gaymans, R. J., Hodd, K. A. and Holmes-Walker, W. A., Parts 2 and 3 submitted to *Polymer*
- 6 Packham, D. I., personal communication
- 7 Lawton, E. A. and McRitchie, D. D. *J. Org. Chem.* 1959, **24**, 26
- 8 Gaymans, R. J., Hodd, K. A. and Holmes-Walker, W. A., unpublished results
- 9 Packham, D. I., Davies, J. P. and Paisley, H. M. *Polymer, Lond.* 1970, **10**, 923
- 10 Manecke, G. and Wohrle, D. *Macromol. Chem.* 1968, **120**, 192

Solid state transitions in zinc(II) di-*n*-alkylphosphinate polymers

V. GIANCOTTI, A. RIPAMONTI AND P. A. TEMUSSI

A study has been made of the reversible solid state transitions in a series of eleven zinc(II) di-*n*-alkylphosphinate polymers, $[\text{Zn}(\text{R}_2\text{PO}_2)_2]_n$, with R from C_4 to C_{18} , by means of differential scanning calorimetry and x-ray analysis. Wide line n.m.r. measurements have been also made for some compounds. The existence of two crystal forms, denoted α and β , has been established for the compounds examined. The results indicate that the $\alpha \rightarrow \beta$ polymorphic transition is associated with disordering of the hydrocarbon side chains.

THE STRUCTURE of coordination polymers containing three-atom bridging phosphinate groups between tetrahedral metal atoms consists of linear chains (structure I), as established by x-ray structural investigations¹⁻³.



Since in zinc(II) and cobalt(II) di-*n*-alkylphosphinates^{1,2} the triple-bridged units of the chain backbone (I) have the top triplet of the oxygen atoms rotated with respect to the bottom triplet, two enantiomorphous triple-bridged units are possible. A random distribution of these two enantiomorphous cages has been found in the crystals of the copolymer $\{\text{Zn}[(n\text{-C}_4\text{H}_9)_2\text{PO}_2][(n\text{-C}_6\text{H}_{13})_2\text{PO}_2]\}_n$ (ref. 2) and in the crystalline form of $\{\text{Zn}[(n\text{-C}_4\text{H}_9)_2\text{PO}_2]_2\}_n$, stable at room temperature¹. Below room temperature $\{\text{Zn}[(n\text{-C}_4\text{H}_9)_2\text{PO}_2]_2\}_n$ undergoes a solid state transition.

The existence of two crystal forms, denoted α and β , has also been established for the di-*n*-hexyl and di-*n*-decyl analogues². Assuming for the α -form an ordered backbone structure, in which all the triple-bridged cages have the same conformation, the $\alpha \rightarrow \beta$ polymorphic transition has been associated with the onset of disorder along the inorganic main chains as a result of loosening of contacts between alkyl side groups.

In order to obtain more complete information on the solid state transition in zinc(II) di-*n*-alkylphosphinate polymers we have studied a series of eleven compounds with alkyl groups from C_4 to C_{18} , using differential scanning calorimetry and x-ray powder diffraction analysis. The transition was also followed in the case of the C_5 and C_{14} compounds, by means of wide line n.m.r. measurements.

EXPERIMENTAL

All di-*n*-alkylphosphinic acids were prepared as described by Kosolapoff⁴ and re-crystallized from *n*-hexane, ethanol and benzene.

Zn[(*n*-C₅H₁₁)₂PO₂]₂ was prepared by the method previously described for Zn(*n*-Bu₂PO₂)₂ and Zn[(*n*-C₆H₁₃)₂PO₂]₂ (ref. 5). All the other zinc di-*n*-alkylphosphinates were prepared by the method previously described for Zn[(*n*-C₁₀H₂₁)₂PO₂]₂ (ref. 5). Analytical data are listed in *Table 1*. Thermo-

Table 1 Analytical data for [Zn(R₂PO₂)₂]_{*n*}

R	Found (%)			Calculated (%)			Yield (%)
	C	H	Zn	C	H	Zn	
<i>n</i> -C ₄ H ₉	46.29	8.76	16.50	45.77	8.64	15.57	70
<i>n</i> -C ₅ H ₁₁	51.04	9.29	13.43	50.47	9.31	13.73	87
<i>n</i> -C ₆ H ₁₃	55.02	9.76	11.93	54.18	9.85	12.28	60
<i>n</i> -C ₈ H ₁₇	60.29	10.53	9.96	59.65	10.63	10.14	92
<i>n</i> -C ₉ H ₁₉	61.72	10.77	9.14	61.73	10.93	9.33	84
<i>n</i> -C ₁₀ H ₂₁	63.54	11.27	8.59	63.50	11.19	8.64	91
<i>n</i> -C ₁₂ H ₂₅	66.55	11.87	7.29	66.36	11.60	7.52	77
<i>n</i> -C ₁₄ H ₂₉	69.59	11.73	6.58	68.56	11.92	6.64	91
<i>n</i> -C ₁₅ H ₃₁	68.88	12.12	6.69	69.49	12.05	6.30	60
<i>n</i> -C ₁₆ H ₃₃	70.31	12.25	5.59	70.31	12.17	5.98	94
<i>n</i> -C ₁₈ H ₃₇	71.35	12.45	5.97	71.74	12.37	5.42	73

grams were obtained using a Perkin-Elmer DSC-1 differential scanning calorimeter. The temperature scale was calibrated using the melting temperature of standard compounds⁶. A sample of high purity indium was used as standard for calculation of the transition energies. Peak areas were measured with a planimeter. Sample weights of the order of 3-7mg gave adequate peak areas for solid state transitions. Larger samples (10-20mg) were used to measure the heat of fusion. A standard scan rate of 16°C/min. was used for heating and cooling runs.

X-ray powder photographs were recorded at different temperatures with a flat camera and Cu-K_α radiation.

All n.m.r. measurements were made on polycrystalline samples pressed in 10mm external diameter sample tubes, using a Varian 16 MHz broad-line spectrometer equipped with a V-4540 variable temperature accessory, over the temperature range 23-120°C. The temperature of the sample was measured by calibrating the dial setting temperatures by means of a copper-constantan thermocouple, the junction of which was positioned inside the sample. The estimated uncertainty of temperature measurement is ±3°C.

RESULTS

The thermograms of zinc(II) di-*n*-alkylphosphinates show endothermic peaks corresponding to solid state transitions. Some transitions are composite transitions in which two or more closely spaced peaks are observed in the

ZINC(II) DI-*n*-ALKYLPHOSPHINATE POLYMERS

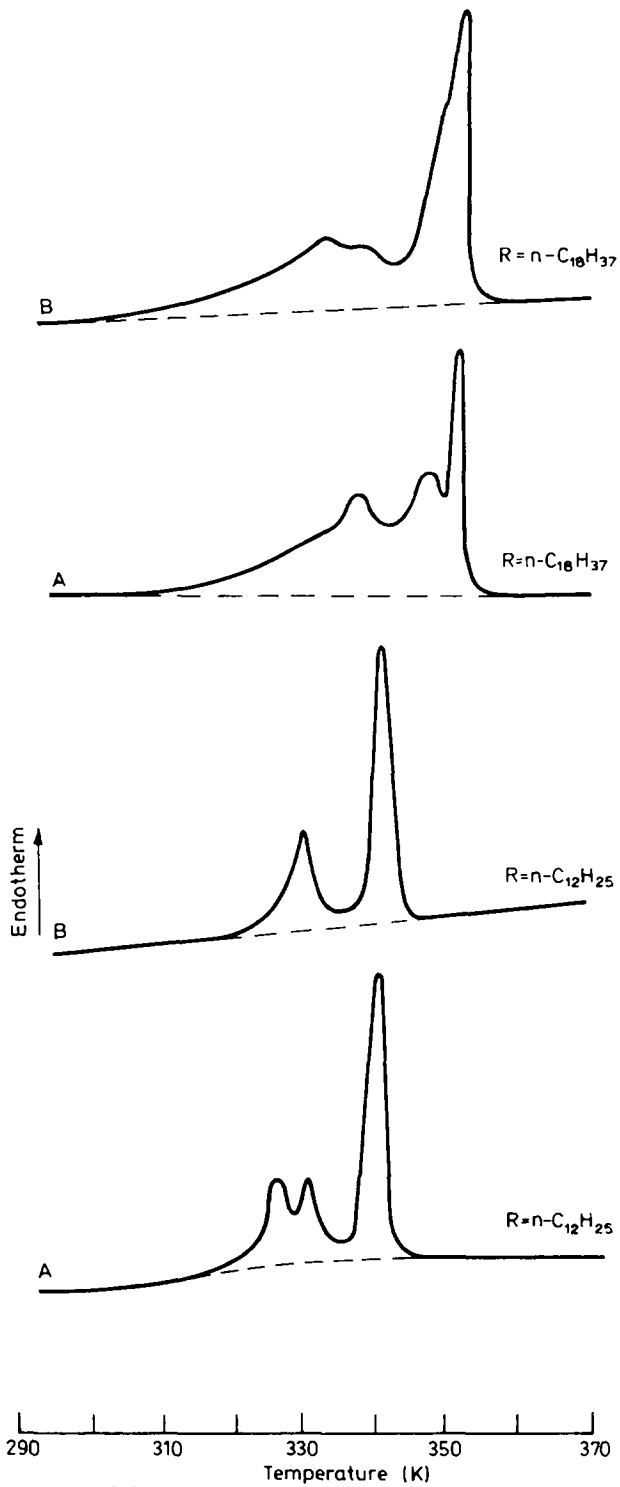


Figure 1 Thermograms of zinc (II) di-*n*-dodecyl- and di-*n*-octadecylphosphate polymer: A, first heating; B, heating after several thermal cycles

thermograms. The peak shape and resolution are influenced by the heating rate and sample size, but the value of the transition energies are well within estimated experimental error ($\pm 10\%$). The samples, with the exception of di-*n*-dodecyl and di-*n*-octadecyl derivatives, could be cycled through the solid state transitions with the same thermal behaviour. The thermograms of di-*n*-dodecyl and di-*n*-octadecyl-phosphinates obtained on first heating and after several thermal cycles are shown in *Figure 1*. The transitions were reversible although supercooling of transitions was observed for all compounds. Furthermore once having passed the melting temperature the crystalline phase is not rapidly reformed on cooling.

The temperatures corresponding to the peaks and the transition energies for samples scanned only once are given in *Table 2* for both increasing and decreasing directions of temperature scan. The different entries for a given compound correspond to the different peaks observed. The temperatures of the onset of the melting according to the endotherms are also given in *Table 2*

Table 2 Temperatures and enthalpies of melting and transition for $[\text{Zn}(\text{R}_2\text{PO}_2)_2]_n$

R	Heating		Cooling		M.p.(K)	ΔH fusion*	
	Transition (K)	ΔH^*	Transition (K)	ΔH^*			
<i>n</i> -C ₄ H ₉	273	1.5	264	1.5	443	3.3	
	281		270				
<i>n</i> -C ₅ H ₁₁	334	2.8	307	3.0	421	3.5	
<i>n</i> -C ₆ H ₁₃	332	3.6	310	3.7	422	3.1	
<i>n</i> -C ₈ H ₁₇	272	2.6	249	1.7	418	3.0	
	337	3.5	320	3.7			
<i>n</i> -C ₉ H ₁₉	338	3.9	325	3.6	405	3.0	
<i>n</i> -C ₁₀ H ₂₁	330	8.2	314	7.7	408	3.0	
	337		318				
	341		328				
<i>n</i> -C ₁₂ H ₂₅	343	8.8	310	8.3	406	2.6	
	327						330
	332						332
<i>n</i> -C ₁₄ H ₂₉	342	13.5	304	15.3	404	2.8	
	328						323
	339						333
<i>n</i> -C ₁₅ H ₃₁	347	17.1	316	16.7	407	2.4	
	341						334
7-C ₁₆ H ₃₃	348	21.1	324	22.2	401	3.1	
	347						337
	351						323
<i>n</i> -C ₁₈ H ₃₇	340	24.0	330	21.9	383	1.6	
	349						336
	353						339

*Units: kcal/formula unit (1 cal = 4.187 J)

ZINC(II) DI-*n*-ALKYLPHOSPHINATE POLYMERS

together with the corresponding energies. It must be noted that the small endothermic peaks at about 353K and 393K previously reported² for $\{\text{Zn}[(n\text{-C}_4\text{H}_9)_2\text{PO}_2]_2\}_n$ could not be observed although samples from several preparations were used.

The x-ray powder spectra recorded below and above the absorption of heat indicate the existence of two crystal forms, denoted by α and β respectively. A further crystal form was observed for the compound with $\text{R} = n\text{-C}_8\text{H}_{17}$ below 272K. The spacings and the intensities of x-ray powder spectra of the α - and β -form are listed in Table 3.

Figures 2 and 3 depict actual wideline nmr spectra of $\{\text{Zn}[(n\text{-C}_5\text{H}_{11})_2\text{PO}_2]_2\}_n$ and of $\{\text{Zn}[(n\text{-C}_{14}\text{H}_{29})_2\text{PO}_2]_2\}_n$ respectively. A single broad component can be observed in the ambient temperature spectrum of the compound with

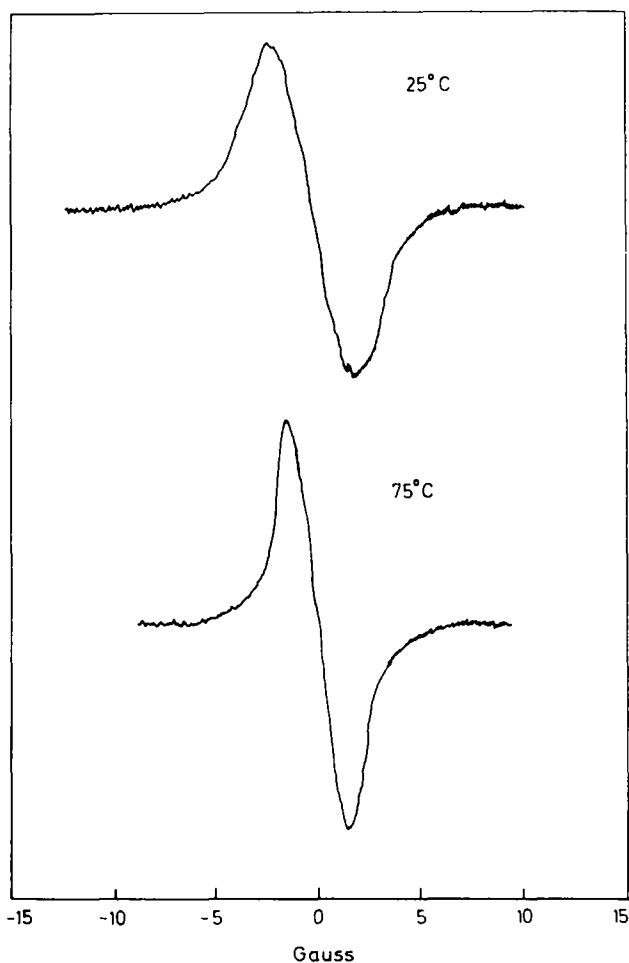


Figure 2 Typical wideline n.m.r. spectra of $\{\text{Zn}[(n\text{-C}_5\text{H}_{11})_2\text{PO}_2]_2\}_n$ below and above the transition temperature. The amplitudes are not on the same scale

Table 3 Intensities* and interplanar spacings (*d*) for [Zn(R₂PO₃)₂]_n (α- and β-forms)

R = n-C ₄ H ₉		R = n-C ₅ H ₁₁		R = n-C ₆ H ₁₃		R = n-C ₈ H ₁₇		R = n-C ₉ H ₁₉		R = n-C ₁₀ H ₂₁	
α-form	β-form	α-form	β-form	α-form	β-form	α-form	β-form	α-form	β-form	α-form	β-form
<i>d</i> (Å)	<i>d</i> (Å)	<i>d</i> (Å)	<i>d</i> (Å)	<i>d</i> (Å)	<i>d</i> (Å)	<i>d</i> (Å)	<i>d</i> (Å)	<i>d</i> (Å)	<i>d</i> (Å)	<i>d</i> (Å)	<i>d</i> (Å)
15-9s	17-5w	16-8vs	17-4s	18-6vs	19-8vs	18-9vs	21-2vs	20-4vs	24-8vs	21-2vs	
12-4vvs	13-9vvs	14-2vvs	15-7vs	15-9vvs	16-3vs	10-6s	17-8vs	11-4w	18-7vs	12-3w	
8-5vs	12-6vvs	10-4m	15-5vvs	10-7m	12-6vvs	8-8w	12-6vvs	10-3vw	13-1vw	10-6vw	
7-8s	9-4s	9-1w	12-2vw	10-2s	10-0w	8-3s	10-7vw	8-9vw	9-6m	9-0vw	
6-9w	8-4vs	8-4w	11-0s	7-7w	8-9w	6-9w	8-9s	7-9w	8-6vw	8-1vvs	
6-3s	7-0vw	7-6vw	8-7w	7-0m	8-0s	4-9s	8-1vw	7-1vw	7-5vw	7-3vw	
5-7w	6-3w	7-2vw	7-7w	5-9m	7-1w	4-3vw	7-4vw	6-1vvs	6-5vw	6-2vw	
5-3vw	5-8w	6-8vw	6-7s	4-9m	6-3w	4-1vw	5-9vvs	4-9m	6-1vw	4-9s	
4-9s	4-9s	6-4w	4-9m	4-7w	5-7vvs	3-7vw	5-4vw	3-8vw	5-4vw	3-9vvs	
4-6vw	4-5w	5-5vw	5-2w	4-3vw	4-9m	3-4vw	4-9m	3-2vvs	4-9s	3-4vvs	
4-3vs	4-2vs	4-9s	4-9s	4-0vw	4-5vw		4-3s		4-3s		
3-9m	3-9w	4-6vvs	4-4w	3-8vw	4-2m		3-9vw		4-0vw		
3-7m	3-7w	4-1vw	4-0w	3-6vw	4-0vw		3-5vw		3-8vw		
3-6m	3-4vw	3-9w	3-8vw	3-2vw	3-8vw		3-3vvs		3-5vvs		
3-4w	3-2vw	3-6vw	3-5vw	3-6vw	3-6vw		3-3vw		3-2vvs		
3-2vs	3-1vw	3-5vvs	3-2vw	3-0vw	3-2vw		3-2vw		3-0vw		
3-0w	2-9vvs	3-2vw	3-0vvs	3-1vw	3-0vvs		4-3s		3-2vvs		
2-9w	2-7vw	3-1vw	3-0vvs	3-0vw	3-0vw		3-9vw		4-0vw		
2-8m	2-2vw	3-1vw	2-8vvs	2-8vvs	2-8vvs		3-5vw		3-8vw		
2-7w	2-0vw	2-8vvs	2-7vvs	2-7vvs	2-7vvs		3-3vvs		3-5vvs		
2-6w									3-0vw		
2-5w									2-9vvs		
2-4vvs											
2-3vvs											

*vvs = very very strong; vs ... very strong; s = strong; w = weak; vw = very weak; vvw = very very weak

ZINC(II) DI-*n*-ALKYLPHOSPHINATE POLYMERS

Table 3 (continued) Intensities* and interplanar spacings (*d*) for [Zn(R₂PO₂)₂]_n (α- and β-forms)

R = <i>n</i> -C ₁₂ H ₂₅		R = <i>n</i> -C ₁₁ H ₂₃		R = <i>n</i> -C ₁₃ H ₂₇		R = <i>n</i> -C ₁₆ H ₃₃		R = <i>n</i> -C ₁₈ H ₃₇	
α-form	β-form	α-form	β-form	α-form	β-form	α-form	β-form	α-form	β-form
<i>d</i> (Å)	<i>d</i> (Å)	<i>d</i> (Å)	<i>d</i> (Å)	<i>d</i> (Å)	<i>d</i> (Å)	<i>d</i> (Å)	<i>d</i> (Å)	<i>d</i> (Å)	<i>d</i> (Å)
27-0vs	20-7vvs	24-3vvs	24-8vvs	24-5vvs	26-0vvs	25-5vvs	26-2vvs	26-0vvs	27-6vvs
20-7vvs	13-6w	13-3w	14-6w	13-9s	15-2w	14-6s	15-6m	15-4m	16-8m
14-5vw	12-0vvw	11-1w	12-6vw	11-8w	12-8vw	12-3m	13-3w	13-7w	14-0w
10-9s	9-0vw	9-6vw	4-9s	9-8vw	4-9m	9-7w	4-9s	10-0w	4-9m
9-2w	4-9s	8-3vw		8-6vw		8-3w		8-9w	
7-3vw	3-2vvw	7-3vw		7-8vw		7-2w		7-6vw	
4-9m		6-1vvw		7-1vw		6-3vw		6-8vw	
4-3s		4-9vw		6-3vvw		5-6vw		4-9vw	
3-9vw		4-5vvw		5-8vvw		4-9vvw		4-3s	
3-4vvw		4-3s		5-4vvw		4-5vvw		4-1vw	
3-1vvw		3-9vvw		4-9vw		4-3s		3-9vvw	
		3-7vvw		4-5vw		4-1w		3-7vvw	
		3-5vvw		4-3s		3-9vw			
				4-1vw		3-7vw			
				3-8vw		3-6vw			
				4-6vvw		3-2vvw			
				3-1vvw		3-1vvw			
						2-9vvw			

*vvs very very strong; vs very strong; s strong; w weak; vw very weak; vvw very very weak

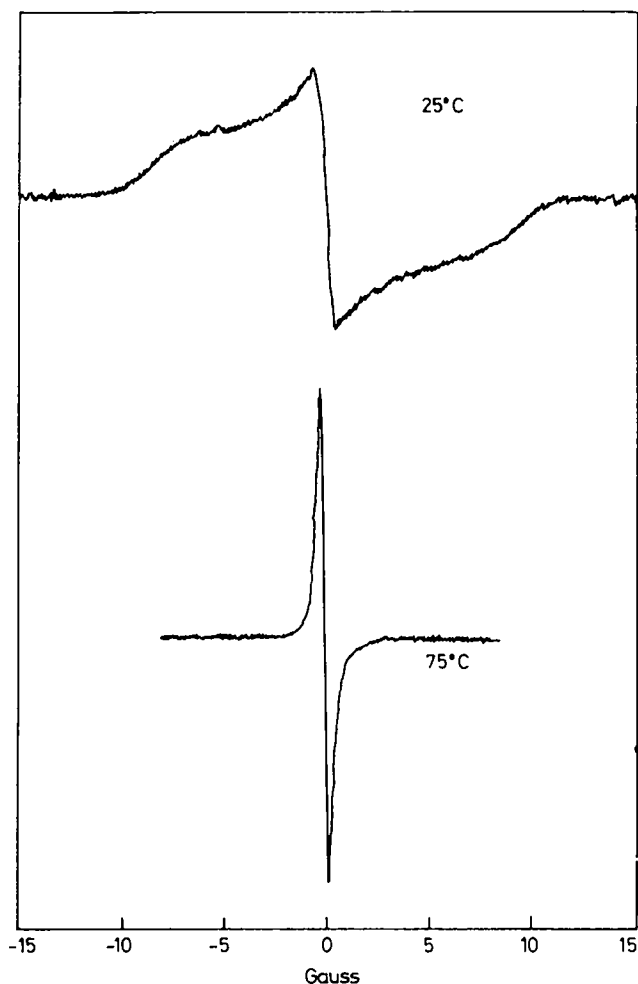


Figure 3 Typical wide-line n.m.r. spectra of $\{Zn[(n-C_{14}H_{29})_2PO_2]_2\}_n$ below and above the transition temperature. The amplitudes are not on the same scale

C_5 . The order of magnitude of the linewidth (~ 4 Gauss) indicates that even at this temperature considerable molecular motion is present. By raising the temperature, further line-narrowing can be observed. The temperature dependence of the linewidth and of the peak amplitude (registered in the same conditions throughout) gives sigmoid-type curves from which a transition temperature of 326K can be measured, as taken at the inflection point of the curves.

Two components can be observed in the ambient-temperature spectrum of the compound with C_{14} . The broader one has a linewidth of about 8 Gauss, the sharper one of about 1 Gauss. At higher temperatures the broad component gradually disappears, merging into the sharp line. The disappearance is complete between 333K and 343K. The temperature dependence of the linewidth and of the peak amplitude of the sharp component allowed the

identification of two transition temperatures respectively at 328K and at 350 K.

DISCUSSION

The x-ray fibre photographs of the α -forms of $[\text{Zn}(\text{R}_2\text{PO}_2)_2]_n$ with R = $n\text{-C}_4\text{H}_9$, $n\text{-C}_6\text{H}_{13}$ or $n\text{-C}_{10}\text{H}_{21}$ show an identity period of 9.9\AA (0.99nm) and a strong meridional reflection on the second layer^{2,5}. The x-ray structural investigation of the copolymer $\{\text{Zn}[(n\text{-C}_4\text{H}_9)_2\text{PO}_2][(n\text{-C}_6\text{H}_{13})_2\text{PO}_2]\}_n$ (ref. 2) and of the β -form of $\{\text{Zn}[(n\text{-C}_4\text{H}_9)_2\text{PO}_2]_2\}_n$ (ref. 1) indicate that these features are characteristic of a chain structure (I) with aligned tetrahedral metal atoms bounded by alternate single and triple bridging phosphinate groups. A strong reflection at about 4.9\AA (0.49nm), which corresponds to the separation between the planes passing through the phosphorus atoms of the chain structure (I), is common to the x-ray powder spectra of di-*n*-alkylphosphinates examined. This substantiates the previous conclusion that the backbone structure is not influenced by the length of the alkyl side groups².

On the basis of the characteristic features of the x-ray fibre photographs of the di-*n*-butyl, di-*n*-hexyl and di-*n*-decyl derivatives in the α -form it was postulated that the type of chain (I) with aligned zinc atoms is common to the polymorphs α and β (ref. 2). Thus it is reasonable to generalize and assume that the $\alpha \rightarrow \beta$ polymorphic transition does not imply a variation of the basic backbone structure. It must be noted that, when the hydrocarbon chain length increases, the intensity of the reflection at about 4.9\AA decreases. This may be indicative of an ordered packing of the organic side groups in the α -form. In fact the D_3 symmetry of the triple-bridged cage is such that the side chains in the extended zig-zag conformation are directed away from the planes normal to the chain axis and passing through the phosphorus atoms. Therefore, when the length of the alkyl chains increases, a greater number of carbon atoms is opposite in phase to the phosphorus atoms with a consequent weakness in the reflection at 4.9\AA . On the other hand the different trend of the intensity of this reflection in the x-ray spectra of the β -form may indicate that the hydrocarbon chains are flexing and twisting above the transition temperature. This view receives support from the increase of the transition energies with increase in the hydrocarbon chain length. Furthermore supercooling of transitions suggests that the hydrocarbon chains remain in a disordered condition for some time. Freezing-in of disorder could also explain the differences sometimes observed between the first and subsequent thermograms.

The narrowing of the wide-line n.m.r. spectra above the transition temperature gives direct support to the view that the hydrocarbon chains undergo molecular motions comparable to those of a liquid. A marked supercooling of the transitions of compounds with C_5 and C_{14} was observed also with the n.m.r. measurements on following the temperature dependence of the linewidths from high to low temperatures. As previously suggested², at the transition temperature the loosening of contacts between hydrocarbon chains may be responsible for the change of the inorganic main chains from a structure with the triple-bridged cages constrained to a definite conformation

to a structure with a random distribution of the two enantiomorphous cages.

The interpretation that a large amount of flexing and twisting motion of the side groups takes place above the transition temperature leads one to consider the conformation of the hydrocarbon chains as being similar to that of the *n*-alkanes in the liquid state, despite their being fixed at one end. The packing of the inorganic main chains then retains the crystalline character of the β -form. Since on the basis of this model the shielding of the interactions between the inorganic main chains is a function of the number of carbon atoms in the side groups, a regular trend of the heat of fusion might be expected in the homologous series of di-*n*-alkylphosphinates. However the steric hindrance of the alkyl groups in a disordered conformation may strongly influence the rigidity and the packing of the inorganic main chain. In this respect it is interesting to examine in greater detail the variation of the x-ray powder spectra of the β -form with increase in hydrocarbon chain length.

The crystal structures of the copolymer $\{\text{Zn}[(n\text{-C}_4\text{H}_9)_2\text{PO}_2][\text{C}_6\text{H}_{13}]_2\text{PO}_2\}_n$ (ref. 2) and of the β -form of $\{\text{Zn}[(n\text{-C}_4\text{H}_9)_2\text{PO}_2]_2\}_n$ (ref. 7) are characterized by pairs of closely interlocked parallel chains. In fact they are packed so that the triple-bridged cages of one chain fall midway between those of the other chain. The length of the alkyl groups in the extended zig-zag conformation does not influence this type of packing. However the bulkiness of the alkyl groups in a disordered conformation increases with increase in the number of carbon atoms. Thus above a certain number of carbon atoms the side groups may form a uniform shell around the polymeric chains, which can be considered cylindrical in shape. This behaviour is substantiated by the x-ray spectra. The x-ray diffraction patterns of the β -form of the compounds with alkyl groups from C₁₄ to C₁₈ are very similar and show only four reflections. The first three reflections may be easily indexed as reflections of the zero layer of a hexagonal lattice and the fourth reflection at 4.9 Å is related to the periodic crowding of atoms along the axis of the polymeric chains. Furthermore the variation of the spacings corresponding to the first three reflections is in agreement with the packing of cylinders whose radius increases with increasing number of carbon atoms.

ACKNOWLEDGEMENTS

We acknowledge financial assistance from the Consiglio Nazionale delle Ricerche, Roma, Italy. We gratefully acknowledge the help of Dr Andersson of Varian AG, Zurich, for recording the n.m.r. spectra.

*Istituto di Chimica,
Università di Trieste,
Trieste, Italy*

V. Giancotti

*Istituto Chimica,
Università di Napoli,
Via Mezzocannone, 4
80134 Napoli, Italy*

*A. Ripamonti and P. A. Temussi
(Received 19 January 1971)*

ZINC(II) DI-*n*-ALKYLPHOSPHINATE POLYMERS

REFERENCES

- 1 Giordano, F., Randaccio, L. and Ripamonti, A. *Chem. Comm.* 1967, p 19
- 2 Giacotti, V., Giordano, F., Randaccio, L. and Ripamonti, A. *J. Chem. Soc. (A)* 1968, p 757
- 3 Giordano, F. Randaccio, L. and Ripamonti, A. *Chem. Comm.* 1967, p 1239
- 4 Kosolapoff, G. M. *J. Amer. Chem. Soc.* 1950, **72**, 5508
- 5 Giacotti, V. and Ripamonti, A. *Chimica e Industria* 1966, **48**, 1065
- 6 Giacotti, V. and Ripamonti, A. *J. Chem. Soc. (A)*, 1969, p 706
- 7 Giordano, F. Randaccio, L. and Ripamonti, A., to be published

ERRATA

“The infra-red spectrum and molecular structure of poly(cyclohexane 1,4-dimethylene terephthalate)”, by T. R. Manley and D. A. Williams, *Polymer* 1971, **12**, 2-26.

The captions for figures 1-7 (pages 4, 5, 6) should read as follows:

Figure 1 Polarized far infra-red spectra of uniaxially oriented (cold drawn) PCHT, ——— electric vector perpendicular to stretching direction; electric vector parallel to stretching direction.

Figure 2 Polarized far infra-red spectra of uniaxially oriented, heat treated PCHT, ——— electric vector perpendicular to stretching direction; electric vector parallel to stretching direction.

Figure 3 Effect of drawing and heat treatment on the far infra-red spectrum of amorphous PCHT. (..... amorphous; ——— 1-way drawn and heat treated).

Figure 4 Effect of cold drawing on the far infra-red spectrum of amorphous PCHT. (—— amorphous; 1-way drawn).

Figure 5 Effect of heat treatment on the far infra-red spectrum of uniaxially oriented (cold drawn) PCHT. (..... 1-way drawn, non-heat treated; ——— 1-way drawn heat treated).

Figure 6 Far infra-red spectra of non-heat treated, uniaxially oriented and biaxially oriented PCHT. (—— 1-way drawn; 2-way drawn).

Figure 7 Effect of heat treatment on the far infra-red spectrum of biaxially oriented (cold drawn) PCHT. (—— cold drawn; heat treated).

We apologize for the omissions from the captions which appeared in the article.

‘Low frequency dielectric behaviour of polyamides’ by M. E. Baird, G. T. Goldsworthy and C. J. Creasey, *Polymer* 1971, **12**, 159-175

The following corrections should be made to this paper:

In *Table 1* (page 160) the crystallinity for Pip-10 polyamide should read ‘medium-high’.

Equations (5) and (9) on page 173 should read:

$$\epsilon_s \left[\frac{3}{\sigma - \sigma_2} - \frac{1}{\sigma} \right] = 3 \left[\frac{\epsilon_2 - \epsilon_1}{\sigma_2 - \sigma_1} + \frac{\epsilon_2}{\sigma - \sigma_2} \right] - \frac{\epsilon_1}{\sigma_1} \quad (5)$$

$$\sigma = \frac{\sigma_1}{2\sqrt{2}} = 0.354\sigma_1 \quad (9)$$

We apologize for these errors.

Polymerization of methyl methacrylate by metallocenes

KYOJI KAERIYAMA

Attempts at polymerizing methacrylate using metallocenes are reported. Polymerization is successful using ferrocene in a ketone solution, but not in benzene or without a solvent. Ketones are effective in the order: methyl ethyl ketone < cyclohexanone < cycloheptanone. Carbon tetrachloride has an accelerative effect on the polymerization in benzene and methyl ethyl ketone solutions, but no effect in cyclohexanone solution. Some binary systems, which consist of ferrocene and higher valence compounds such as cobalt trisacetylacetonate, are effective redox initiators. Cobaltocene polymerizes methyl methacrylate in the presence of carbon tetrachloride; zirconocene dichloride induces polymerization of methyl methacrylate in a cyclohexanone solution; whereas neither nickelocene nor titanocene dichloride are effective. Styrene and acrylonitrile were not polymerized by the metallocenes examined.

INTRODUCTION

MANY studies have been made on metallocenes since the discovery of ferrocene (Cp_2Fe , where Cp represents the cyclopentadienyl group). Cp_2TiCl_2 has been thoroughly studied as a catalyst for vinyl polymerization and, because it is soluble in organic solvents, it is used as a component of a modified Ziegler-Natta catalyst. A few workers have attempted to use ferrocene as an initiator for vinyl-polymerization. Furukawa and Tsuruta² reported that Cp_2Fe did not induce bulk polymerization of methyl methacrylate (MMA) and styrene. Kern, Achon-Samblancat and Schulz³ also showed that Cp_2Fe did not initiate polymerization of styrene in a benzene solution, but that a redox system, which consisted of benzoyl peroxide, benzoin and Cp_2Fe , had a higher activity than benzoyl peroxide. Bamford and Finch⁴ reported that Cp_2Fe , Cp_2VCl_2 and Cp_2TiCl_2 did not polymerize MMA in bulk, but that they were an initiator for MMA in the presence of carbon tetrachloride and carbon tetrabromide. Polymerization which proceeds via a radical intermediate is described in the present paper.

EXPERIMENTAL

Material

Commercially available metallocenes were used. Ferrocene was sublimed onto a cold finger and zirconocene dichloride was recrystallized from a toluene solution. The other metallocenes were used without further purification. Cobaltocene was obtained as a solution in a hydrocarbon which was used in an atmosphere of nitrogen. Metal acetylacetonates were of commercial origine (Dotite Reagent), and were used without further purification. Monomers, benzene, cyclohexanone, carbon tetrachloride and pyridine, were dried over molecular sieves (3A) and distilled just before use.

Procedure

The polymerizing mixture (10ml) was placed in a glass tube (volume 25 ml). After the tube had been degassed by repeated freezing, evacuating and thawing, it was sealed off. Polymerization was then carried out in the dark with gentle shaking. The polymer produced was precipitated in methyl alcohol containing a small amount of hydroquinone, collected on a sintered filter and dried *in vacuo* to a constant weight.

RESULTS

Polymerization of MMA by Cp₂Fe

Polymerization was carried out in a variety of solvents. The results are shown in *Table 1* and *Figure 1*. The solvent has a great effect on the polymer-

Table 1 Effect of solvents on the polymerization by Cp₂Fe (MMA, 3.0ml; Cp₂Fe, 50mg; solvent 7.0ml at 60°C for 20h)

Solvent	Conversion (%)
cyclohexanone	15.5
pyridine	3.97
benzene	0
ethyl alcohol	0
caproic aldehyde	16.9
ethyl acetate	4.26
cycloheptanone	45.7
acetic anhydride	3.42
benzene + acetic acid*	9.12
MMA	0.71
cyclohexanone†	0
cyclohexanone‡	0

*6.0ml benzene + 1.0ml acetic acid

†100mg of DPPH was added

‡100mg of benzoquinone was added

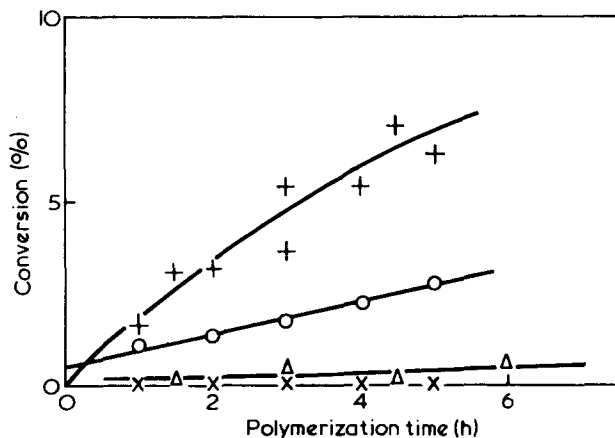


Figure 1 Effect of solvents on polymerization of MMA by Cp₂Fe. Cp₂Fe = 50mg; MMA = 3.0ml; solvent = 7.0ml; 60°C. +, cyclohexanone; O, methyl ethyl ketone; Δ, MMA; x, benzene

ization and conversion was found to be high with ketones, cyclanones being particularly good. The effectiveness of ketones increases in the following order: methyl ethyl ketone < cyclohexanone < cycloheptanone. The same order was also observed in polymerization by manganese *tris*acetylacetonate⁵. The absorption spectra of the chelate in cyclohexanone and benzene were identical. Coordination of the carbonyl group to the metal of the chelate in an activated state is probably important, however, since the order of effectiveness of ketones is the same as the order observed for the shift in the O—D stretching vibration of monodeuterated methanol in solutions of the ketones. The interpretation can also be true in the case of Cp₂Fe. Although absorption spectra of Cp₂Fe in cyclohexanone were identical with those in benzene, the carbonyl group of cyclanones coordinates to the central metal atom of Cp₂Fe in an activated state which leads to the generation of initiating radical.

Dutt and Palit⁶ have stated that a combination of ketone and zinc chloride in a 1:1 molar ratio is an initiator of polymerization and that the initiating power is more pronounced with the higher members of the series. The behaviour of the ZnCl₂-ketone system is similar to that of the Cp₂Fe-ketone system, but ZnCl₂ differs from Cp₂Fe in that the complex of ZnCl₂ with a carbonyl compound can be isolated and characterized.

The base pyridine, which has a large effect on the polymerization by manganese *tris*acetylacetonate, shows a small effect with Cp₂Fe. Acetic acid has an appreciable effect. Although Cp₂Fe is stable, a small amount of Cp₂Fe may be decomposed by the acid to form an initiating radical—probably cyclopentadienyl radical. It is noticeable that polymerization is not induced either in a benzene solution or in the absence of solvent. N,N-Diphenyl-N-picryl hydrazyl and benzoquinone inhibit the polymerization, which must therefore, proceed via a radical intermediate.

Carbon tetrachloride is known to have a large effect on polymerization by metallic compounds. In many cases, trichloromethyl radical is assumed to be an initiating radical. Bamford and Finch⁴ have reported that CCl₄ accelerates bulk polymerization of MMA by Cp₂Fe. Table 2 shows the result of polymerization in a benzene solution. The carbon tetrachloride-Cp₂Fe system initiates the polymerization of MMA. The addition of a small amount of cyclohexanone increases the effect of carbon tetrachloride.

Table 2 Effect of CCl₄ on polymerization by Cp₂Fe (50mg Cp₂Fe at 60°C for 20h)

MMA (ml)	CCl ₄ (ml)	Benzene (ml)	Cyclohexanone (ml)	Conversion (%)
3.0	—	7.0		0
3.0	0.7	6.3		5.08
5.0	—	5.0	0.5	5.17
5.0	0.5	5.0		6.62
5.0	0.5	5.0	0.5	18.7
4.0	0.03	6.0		0.59
4.0	0.1	5.9		1.18
4.0	0.3	5.7		13.3
4.0	0.8	5.2		13.6
4.0	1.4	4.6		2.24

Figure 2 shows the effect of CCl_4 in ketone solutions. It has no effect on polymerization in cyclohexanone solution; the time-conversion curves for polymerization in the presence and absence of CCl_4 coincide. The result is quite different from that obtained for a benzene solution. Addition of carbon tetrachloride to the methyl ethyl ketone solution, on the other hand, produces a marked acceleration in the polymerization by Cp_2Fe . The behaviour of CCl_4 can be interpreted in terms of strong nucleophilicity of cyclohexanone. The O—D stretching vibration of a solution of CH_3OD in cyclohexanone is shifted by 99cm^{-1} to a lower wave number compared with a solution in carbon

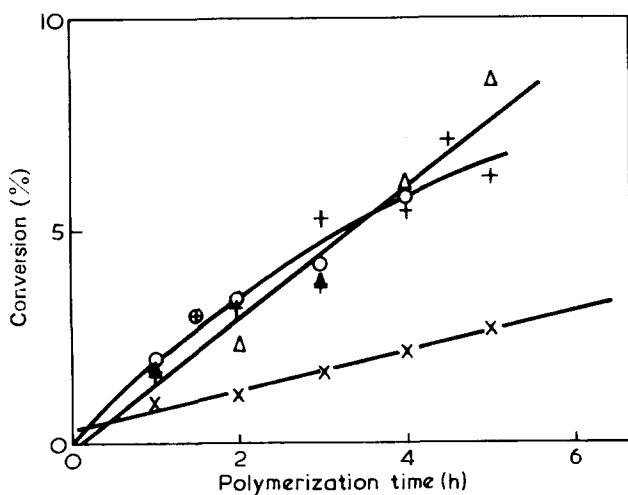


Figure 2 Effect of CCl_4 on polymerization of MMA by Cp_2Fe . Cp_2Fe = 50mg; MMA = 3.0ml; 60°C . +, cyclohexanone; O, cyclohexanone (6.3ml) + CCl_4 (0.7ml); x, methyl ethyl ketone; Δ, methyl ethyl ketone (6.3ml) + CCl_4 (0.7ml)

tetrachloride⁷. In the presence of a large amount of such a strong nucleophile as cyclohexanone, the weak nucleophile, carbon tetrachloride, cannot interact with Cp_2Fe in an activated state. This is the reason why CCl_4 has no effect on polymerization in a cyclohexanone solution.

MMA is polymerized by binary systems, which are composed of Cp_2Fe and other compounds with a higher valence. Some of them are effective additives for ferrocene. Some results are shown in Table 3. Aromatic nitro-compounds, which are known as π -acceptors, have no activity for polymerization in benzene, although some of them form complexes with Cp_2Fe as shown by a colour change of solutions. Aromatic nitro-compounds have been shown to retard polymerization of styrene⁸, but to have little effect on MMA⁹. Pyromellitic anhydride has no appreciable effect in a dimethyl sulphoxide solution. Although ceric ammonium nitrate initiates the polymerization, ceric sulphate does not produce poly(MMA). It is clear that both of them oxidize Cp_2Fe , because the blue colour of ferricinium cation appears on the

Table 3 Polymerization by Cp₂Fe and additives (MMA, 3.0ml; additive, 50mg; benzene, 7.0ml at 60°C for 3.0h)

Cp ₂ Fe (mg)	Additive	Conversion (%)
50	—	0
—	Coacac ₃ *	1.42
50	Coacac ₃	2.70
—	TiOacac ₂	1.93
50	TiOacac ₂	3.11
—	CAN†	0
50	CAN†	3.15
—	Feacac ₃	0
50	Feacac ₃	1.25

*acac = acetylacetyl ligand
 †Ceric ammonium nitrate (131 mg)

surface of the solid salts. It must be important for additives to liberate an initiating radical on reduction. Molybdenum (VI) dioxy-bisacetylacetonate does not polymerize MMA even in the presence of Cp₂Fe.

Polymerization by various metallocenes

Table 4 shows the results of polymerizing MMA using metallocenes other than Cp₂Fe. Titanocene dichloride, which is used as one component of a

Table 4 Polymerization of MMA by metallocenes other than Cp₂Fe (MMA, 3.0m at 60°C for 20h)

Metallocene		Solvent		Additive		Conversion (%)
type	wt (mg)	type	vol (ml)	type	vol (ml)	
Cp ₂ TiCl ₂	50	C ₆ H ₆	7.0			3.13
Cp ₂ TiCl ₂	50	C ₆ H ₆	6.5	CCl ₄	0.5	3.11
Cp ₂ TiCl ₂	50	C ₆ H ₁₀ O	7.0			3.50
Cp ₂ TiCl ₂	50	C ₆ H ₆	6.5	pyridine	0.5	2.40
Cp ₂ Co	28	C ₆ H ₆ *	7.0			0
Cp ₂ Co	28	C ₆ H ₆ *	6.5	CCl ₄	0.5	39.8
Cp ₂ Co	28	C ₆ H ₁₀ O	5.0	C ₆ H ₆ *	2.0	0
Cp ₂ Ni	50	C ₆ H ₆	7.0			0
Cp ₂ Ni	50	C ₆ H ₆	6.3	CCl ₄	0.7	0
Cp ₂ Ni	50	C ₆ H ₁₀ O	7.0			0
Cp ₂ ZrCl ₂	50	C ₆ H ₆	7.0			1.73
Cp ₂ ZrCl ₂	50	C ₆ H ₆	6.3	CCl ₄	0.7	0.20
Cp ₂ ZrCl ₂	50	C ₆ H ₁₀ O	7.0			13.1
Cp ₂ ZrCl ₂	50	C ₆ H ₆	6.5	pyridine	0.5	1.95

C₆H₆ = benzene; C₆H₁₀O = cyclohexanone

*Containing a small amount of hydrocarbon

modified Ziegler-Natta catalyst, shows little activity in the polymerization of MMA. Cobaltocene does not induce polymerization in cyclohexanone and benzene solutions, but it does initiate the polymerization of MMA in the presence of carbon tetrachloride. Cobaltocene is more active than Cp₂Fe. The high activity of Cp₂Co is explained in terms of the 18 electron rule, as

POLYMERIZATION OF MMA BY METALLOCENES

described later. Nickelocene produces no polymer at all. Furukawa and Tsuruta² showed that Cp₂Ni inhibited polymerization of MMA and styrene. Zirconocene dichloride does not induce polymerization of MMA in a benzene solution and in the presence of carbon tetrachloride, but it initiates polymerization of MMA in a cyclohexanone solution. Zirconocene dichloride has an interesting effect on cationic polymerization.

Binary mixtures, which consisted of equimolar mixtures of Cp₂Fe and Cp₂TiCl₂ or Cp₂ZrCl₂, were examined for polymerizing MMA in cyclohexanone and benzene solutions and styrene in a benzene solution. Conversions of monomers by binary mixtures are lower than those by a single metallocene.

Attempts were made to polymerize styrene using various metallocenes but conversion of styrene was found to be much lower than that of MMA. Because styrene polymerization is not terminated by Cp₂Fe as described later, the

Table 5 Polymerization of styrene (5.0 ml styrene at 60°C for 20h)

Metallocene type wt (mg)		Solvent type vol (ml)		Additive type vol (ml)		Conversion (%)
Cp ₂ Fe	50	C ₆ H ₆	5.0			0.37
Cp ₂ Fe	50	C ₆ H ₁₀ O	5.0			1.59
Cp ₂ Fe	50	C ₆ H ₆	4.5	CCl ₄	0.5	0.26
Cp ₂ ZrCl ₂	50	C ₆ H ₆	5.0			0
Cp ₂ ZrCl ₂	50	C ₆ H ₁₀ O	5.0			0.16
Cp ₂ ZrCl ₂	50	C ₆ H ₆	4.5	pyridine	0.5	1.89
Cp ₂ TiCl ₂	50	C ₆ H ₆	5.0			0.53
Cp ₂ TiCl ₂	50	C ₆ H ₁₀ O	5.0			0.94
Cp ₂ TiCl ₂	50	C ₆ H ₆	4.5	pyridine	0.5	3.05
Cp ₂ Co	20	C ₆ H ₆ *	4.5			0
Cp ₂ Co	20	C ₆ H ₁₀ O	3.0	C ₆ H ₆ *	1.5	0

C₆H₆ = benzene; C₆H₁₀O = cyclohexanone

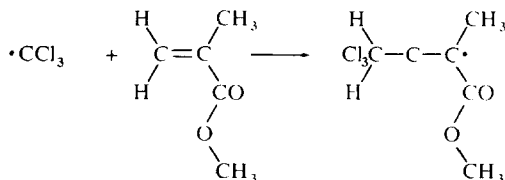
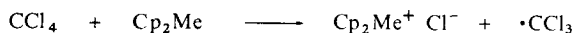
*Containing a small amount of hydrocarbon

initiation reaction does not take place. Styrene is not polymerized by either the Cp₂Fe/cyclohexanone or Cp₂ZrCl₂/cyclohexanone systems, which do polymerize MMA. Styrene is also not polymerized by Cp₂Fe/carbon-tetrachloride. Some systems, which contain carbon tetrachloride as a component, polymerize MMA, but do not initiate polymerization of styrene. The carbon-tetrachloride/acetamide system¹⁰, for example, polymerizes MMA and methyl acrylate to conversions of 32.8% and 61.2%, respectively. Conversion of styrene is 3.5% under the same conditions. Pyridine has a small effect on Cp₂TiCl₂ and Cp₂ZrCl₂.

Polymerization of acrylonitrile is not induced by Cp₂Fe/cyclohexanone or Cp₂ZrCl₂/cyclohexanone and Cp₂Fe/CCl₄ systems. Titanocene dichloride has a very low activity for acrylonitrile in cyclohexanone. The inactivity of metallocenes for acrylonitrile is unexpected, because, like MMA, acrylonitrile is polymerized by metal-containing initiators. Manganese trisacetylacetonate, in the presence of a suitable electron donor, polymerizes acrylonitrile better than it polymerizes MMA¹¹. The manganese-trisacetylacetonate/cyclohexanone system⁵ and the zinc-chloride/dihydrocivetone system⁶ polymerize acrylonitrile as well as MMA.

DISCUSSION

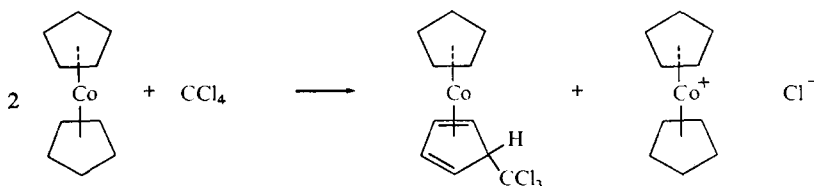
Cp_2Fe and Cp_2Co initiate the polymerization of MMA in the presence of carbon tetrachloride. This can be interpreted as follows:



Cp_2Me reacts with carbon tetrachloride to produce trichloromethyl radical, which in turn initiates polymerization of MMA. Bamford and Finch⁴ have also suggested the same reactions.

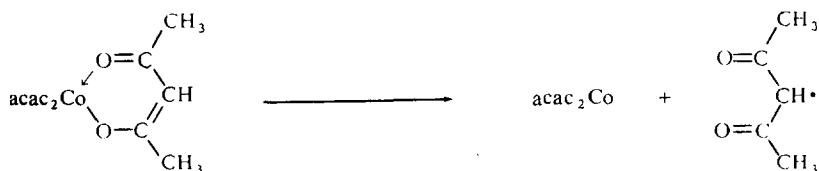
The ferrocene/carbon-tetrachloride system polymerizes MMA, but does not induce polymerization of styrene and acrylonitrile. Because carbon tetrachloride is a chain transfer agent for styrene and acrylonitrile as well as for MMA, the trichloromethyl radical can be assumed to initiate the polymerization of MMA and also styrene and acrylonitrile, if the radical is actually produced. This means that the initiation reaction does not consist of two separate reactions as in the above equations, but that it is a one step reaction involving Cp_2Fe , carbon tetrachloride and the monomer.

High reactivity of cobaltocene in the presence of carbon tetrachloride can also be explained by the above equations. The cobaltocenium cation (Cp_2Co^+) produced fits the 18 electron rule and is stable. This promotes the initiation reaction. The following reaction has been studied^{13, 14}.



Both products have been isolated. In the presence of MMA, trichloromethyl radical reacts with the monomer instead of Cp_2Co .

In the case of metal acetylacetonate, the central metal ion is reduced to liberate the acetylacetonyl radical, which in turn initiates polymerization. Cobalt *tris*acetylacetonate, for example, produce an initiating radical as in the following reaction scheme:



POLYMERIZATION OF MMA BY METALLOCENES

It is reasonable to suppose that the reductant Cp_2Fe accelerates the reaction. Additives to Cp_2Fe must have an appropriate oxidizing power, and must not react with Cp_2Fe too quickly. Furukawa and Tsuruta² have shown that the Cp_2Fe /benzoyl-peroxide system gives lower conversions than benzoyl peroxide alone, because the peroxide reacts with Cp_2Fe too quickly to supply radicals for initiation of polymerization. Ceric ammonium nitrite is a very strong oxidant, but because it does not dissolve in benzene and reaction takes place only on the surface of the solid salt, it can be an effective additive. The inner part of the complex salt remains yellow during reaction, although the blue ferricinium cation forms on the surface.

In a previous paper, it was shown that the ceric ion terminates polymerization of styrene in a benzene solution, but not in the presence of cyclohexanone¹². Ferrocene does not polymerize either MMA or styrene in benzene. To see whether Cp_2Fe terminates polymerization, its effect on polymerization by azo-bisisobutyronitrile has been studied. The results given in Table 6 show no effect. Obviously Cp_2Fe does not terminate the

Table 6 Effect of Cp_2Fe on the polymerization by azo-bisisobutyronitrile (AIBN) (styrene³ 5.0 ml; MMA, 3.0 ml; monomer + solvent, 10 ml at 60°C.

Monomer	Solvent	AIBN (mg)	Cp_2Fe (mg)	Polym. time (h)	Conversion (%)
styrene	C_6H_6	37.8	50	5.0	17.0
styrene	C_6H_6	37.8	—	5.0	16.9
styrene	$\text{C}_6\text{H}_{10}\text{O}$	41.3	50	5.0	20.2
styrene	$\text{C}_6\text{H}_{10}\text{O}$	41.3	—	5.0	20.2
MMA	C_6H_6	35.0	50	3.0	38.9
MMA	C_6H_6	35.0	—	3.0	39.1

C_6H_6 = benzene; $\text{C}_6\text{H}_{10}\text{O}$ = cyclohexanone

polymerization of MMA and styrene, which implies that Cp_2Fe does not initiate the polymerization of MMA in benzene, and styrene in benzene and cyclohexanone, and that the $\text{Cp}_2\text{Fe}/\text{CCl}_4$ system does not induce polymerization of styrene.

In the case of polymerization in a ketone solution, coordination of the carbonyl group to the central metal is important, but at present the reaction is not fully understood.

ACKNOWLEDGEMENT

The author is grateful to Dr M. Suzuki, Dr A. Okada and Mr Y. Shimura for his interest and encouragement during this work.

Research Institute for Polymers and Textiles,
Sawatari, Kanagawaku,
Yokohama, Japan

(Received 21 July 1970)
(Revised 13 April 1971)

REFERENCES

- 1 For example:
 Breslow, D. S. and Newburg, N. R. *J. Amer. Chem. Soc.* 1959, **81**, 81
 Olive, G. H. and Olive, S. *Makromol. Chem.* 1969, **121**, 70
 Reichert, K. H. and Berthold, J. *Makromol. Chem.* 1969, **124**, 103
- 2 Furukawa, J. and Tsuruta, T. *Kogyo Kagaku Zasshi* 1957, **60**, 802
- 3 Kern, W. Achon-Samblancat, M.-A. and Schulz, R. C. *Monatsh.* 1957, **88**, 763
- 4 Bamford, C. H. and Finch, C. A. *Z. Naturforsch* 1962, **176**, 500
- 5 Kaeriyama, K. *Bull. Chem. Soc. Japan* 1970, **43**, 1511
- 6 Dutt, P. K. and Palit, S. R. *J. Polym. Sci. (A-1)* 1970, **8**, 15
- 7 Tamres, M. and Searles, S. J. *Amer. Chem. Soc.* 1959, **81**, 2100
- 8 Price, C. C. and Durham, P. A. *J. Amer. Chem. Soc.* 1943, **65**, 757
- 9 Kice, K. J. *J. Amer. Chem. Soc.* 1954, **76**, 6274
- 10 Kaeriyama, K. *Bull. Chem. Soc. Japan* 1969, **42**, 3602
- 11 Bamford, C. H. and Ferrar, A. N. *Chem. Comm.* 1970, p 315
- 12 Kaeriyama, K. *Polymer, Lond.* 1969, **10**, 11
- 13 Katz, S. Weiher, J. F. and Voigt, A. F. *J. Amer. Chem. Soc.* 1958, **80**, 6459
- 14 Green, N. L. H. Pratt, L. and Wilkinson, G. J. *Chem. Soc.* 1959, p 3753

The electroinitiated polymerization of styrene: Part 1

B. M. TIDSWELL and A. G. DOUGHTY*

Electrolysis of a solution of styrene and sodium borofluoride in sulpholane gives rise to low molecular weight polystyrene at the anode. The polymerization occurs by a cationic mechanism initiated by electrolytically produced boron trifluoride co-catalysed by either hydrogen fluoride and/or water. Kinetics in a single compartment cell and a divided compartment cell show differences. Acceleration occurs in the anode compartment of the divided cell with current efficiencies higher than those observed in the single cell. This is ascribed to the presence of an electrolytic termination reaction occurring in the single cell.

THE PASSAGE of an electric current through a conducting solution containing an electrolyte and monomer in order to produce polymer has been the subject of several papers over the last few years most of which have been reviewed extensively¹⁻⁴. From this work it is obvious that transient species generated at the electrodes initiate polymerization which may be ionic or radical in character or possibly a mixture of both.

The aim of the present study was to use an electrolyte capable of producing different species which were able to initiate polymerization by either cationic or anionic mechanisms depending on the supporting solvent. For this purpose sodium borofluoride was used, which by virtue of the BF_4^- ions discharged at the anode could possibly give rise to cationic polymerization. Funt and Gray⁵ have postulated that discharge of the BF_4^- ion during the electrolysis of tetrabutyl ammonium borofluoride initiates cationic polymerization as a result of the formation of BF_3 . On the other hand, Na^+ ions discharged at the cathode could give rise to anionic polymerization by direct or indirect electron transfer through the formation of a radical anion⁴.

This paper describes the cationic polymerization of styrene whilst Part 2 will describe anionic polymerization.

EXPERIMENTAL

The solvents used were N,N-dimethyl formamide, DMF, (British Drug Houses Ltd), N,N-dimethyl acetamide, DMA, (BDH Ltd), dimethyl sulphoxide, DMSO, (Koch-Light Ltd) and sulpholane, tetrahydrothiophene-1,1-dioxide (Koch-Light Ltd). Sulpholane was stirred over sodium hydroxide pellets until no colour developed with concentrated sulphuric acid. Otherwise all solvents were then purified by refluxing over calcium hydride for six hours under an atmosphere of argon. Benzene (10% volume), previously rigorously dried, was used to azeotrope residual moisture. The remaining

* Present address ISR Ltd. Southampton, UK

benzene was then distilled off under argon at atmospheric pressure, and a middle fraction of solvent collected under argon at reduced pressure.

The electrolyte, sodium borofluoride (Hopkin and Williams Ltd), was recrystallized from distilled water, filtered and dried under vacuum at 200°C.

Argon was purified according to the method described by Funt⁶.

Monomers – styrene (BDH Ltd), acrylonitrile (BDH Ltd) and 2-chloroethylvinylether (Koch Light Ltd) were purified according to standard techniques⁷.

Apparatus and techniques

Electrolysis was carried out at constant temperature and under an inert atmosphere by bubbling purified argon through the reaction mixture using both single and divided cells. In the latter the anode and cathode compartments were separated by a sintered glass filter as described previously⁸. The electrodes in all cases were platinum foil (area 1 cm²), and a constant current (1–50 mA) was supplied from a type 1D 50/500 constant current unit (Sandmar Electronic Products Ltd, Manchester). In all cases the initial concentration of NaBF₄ was 0.05 M. Because of gaseous products evolved at the electrodes dilatometric techniques could not be used and, instead, the polymers produced were precipitated into ice cold methanol, filtered, washed and dried under vacuum to constant weight.

Molecular weights were determined using a Mechrolab vapour pressure osmometer at 37°C with benzene as solvent.

RESULTS AND DISCUSSION

Preliminary experiments showed that, in the divided cell, polymerization of styrene occurs in the cathode compartment when using DMA and to a lesser extent when using DMSO and DMF. On the other hand, with sulpholane as solvent, polymerization occurs almost entirely in the anode compartment. Pre-electrolysis prior to addition of monomer does not alter the position except for a slight increase in yield in the anode compartment when using sulpholane.

In view of the different paths of polymerization in DMA and sulpholane copolymerization studies were carried out in these solvents in an attempt to elucidate the general mechanism of polymerization and the results analysed according to the method of Finemann and Ross⁹.

Comparison, where possible, was made with literature values (*Table 1*). From this it is reasonable to assume that in sulpholane the reaction proceeds via a cationic mechanism, whilst in DMA the reaction is anionic.

The remainder of this paper will be entirely concerned with the polymerization of styrene in sulpholane.

The use of discriminant additives to substantiate the cationic mechanism leaves much to be desired. *p*-Benzoquinone has little effect on the system initially suggesting the absence of a free radical component. The use of diphenyl dipicryl hydrazyl (DPPH) produces some very interesting results. Electrolysis in the presence of styrene and DPPH gives rise to a decrease in yield, the magnitude of which depends on the concentration of DPPH, but

ELECTROINITIATED POLYMERIZATION OF STYRENE

no inhibition period is observed. Electrolysis in the absence of monomer shows a decoloration of the DPPH which may be followed quantitatively as a decrease in the 528 m μ absorption peak with time. These results suggest radical activity between possibly BF₄[•] or F[•] radicals with the DPPH.

Table I Copolymerization studies

Monomers: styrene (M_1) 2-chloroethylvinylether (M_2) Electrolysis 10 mA at 30°C in sulpholane $r_1 = 0.9$ $r_2 = 35$ Catalyst: BF ₃ (C ₂ H ₅) ₂ O 25°C in pyridine $r_1 = 0.11$ $r_2 = 24$ (Brown and Pepper) ¹⁰	Monomers: styrene (M_1) acrylonitrile (M_2) Electrolysis 40 mA at 25°C in N,N-dimethyl acetamide $r_1 = 0.4$ $r_2 = 14.2$ Catalyst: <i>n</i> -butyl lithium, -12°C in iso-octane $r_1 = 0.2$ $r_2 = 14$ (Zutty and Welch) ¹¹
--	--

However, if BF₃ gas is bubbled into sulpholane a definite 1:1 complex is produced in the form of a white crystalline solid which is relatively hydroscopic and unstable. A solution of this complex in sulpholane, giving a concentration of BF₃ similar to that obtained on electrolysis, produces a similar decoloration of the DPPH which cannot be related to free radical reactivity. In fact BF₃(C₂H₅)₂O complex in 1,2-dichloroethane behaves similarly, suggesting that DPPH must be used with care when used as a discriminator for cationic mechanisms. All the systems mentioned were examined by e.s.r., the spectra in all cases showed complete quenching of the radical signal of the DPPH.

From these results it is apparent that a complex system develops during electrolysis as detailed in Figure 1. Elemental analysis of the polymer produced allows certain alternatives to be eliminated. No boron or fluorine is found in combination with the polymer, eliminating the possible initiation by BF₄[•] and F[•] radicals. However, mass spectroscopic studies of the solvent following electrolysis indicate a parent peak at $M/e = 138$ which corresponds to a monofluorinated sulpholane.

Qualitative tests using turmeric¹² carried out on the anolyte, in the absence of monomer, following electrolysis showed the presence of BF₃. Both calcium chloride gelation¹³ and the decoloration of zirconium alizarinate complex¹⁴ indicate the presence of HF.

Analysis of the reaction mixture using the Karl Fisher technique indicated the presence of up to 2mmol/l moisture which could result in the formation of the BF₃(H₂O)₂ complex. Addition of further moisture in the range 1–50 mmol/l causes a progressive decrease in the initial rate of polymerization. Application of vacuum techniques similar to those developed by Funt⁶, in an attempt to eliminate moisture also causes a decrease in the initial rate of polymerization. Similar results were obtained by Clark¹⁵ in the polymerization of styrene using BF₃(H₂O)₂ complex as catalyst but in this case the polymerization was completely arrested on drying. In the present work HF produced during the reaction may also be acting as co-catalyst.

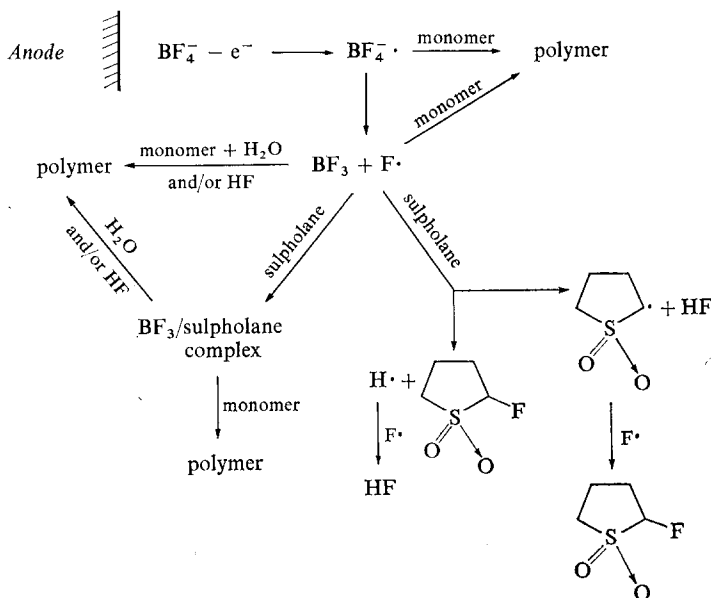


Figure 1 Possible reaction scheme as a result of the anodic discharge of the borofluoride ion.

It is interesting to note that electrolysis in the absence of monomer followed by subsequent addition of the anolyte to styrene initiates the polymerization several weeks after the electrolysis was performed suggesting the production of BF_3 or a complex of BF_3 . Table 2 illustrates the similarity of the poly-

Table 2 Polystyrene formed by various methods in sulfolane at 30°C

Method	DP_n	Conversion (%)
Electrolysis for 1 hour at 30 mA in divided cell (anode) together with 2M styrene/ NaBF_4 /sulfolane	24	88.1
Electrolysis for 1 hour at 30 mA NaBF_4 /sulfolane. Anolyte added to 2M styrene in sulfolane	26	77.4
BF_3 /sulfolane complex (0.2102 g) added to 2M styrene in sulfolane, (50 ml)	29	67.3

merization by three methods: electrolysis in the presence of styrene, electrolysis in the absence of monomer followed by subsequent addition of the anolyte to monomer, and finally polymerization using the BF_3 /sulfolane complex dissolved in sulfolane.

These results demonstrate that on electrolysis of a sulfolane/ NaBF_4 /styrene solution, the styrene polymerizes cationically as a result of the formation of BF_3 , the reaction being catalysed by H_2O and/or HF .

Figure 2 shows conversion/time curves obtained at several currents using a single cell. Values of the initial slopes of these curves, expressed as initial rate plotted against current, show a linear relationship with a slope of unity

ELECTROINITIATED POLYMERIZATION OF STYRENE

indicating a first order dependence on current (*Figure 3*). At the lower currents slight inhibition is evident which may be due to the electrolysis of impurities. *Figure 4*, illustrates conversion/time curves over a ten fold range of monomer concentration whilst maintaining the current constant at 10 mA.

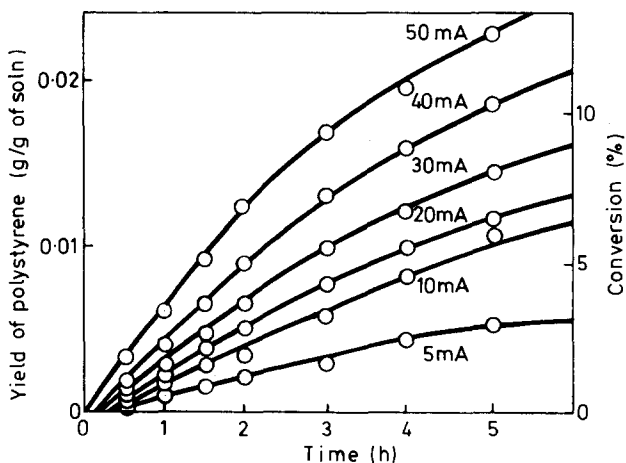


Figure 2 The formation of polystyrene with time at various currents for 2M styrene in sulpholane/ NaBF_4 in the single cell

Slight upward curvature of the plots is evident at the higher concentrations indicating possible slight acceleration of the reaction. The initial slopes of these curves again expressed as initial rates plotted against the square of the monomer concentration give a linear relationship as shown in *Figure 5*, indicating a second order dependence on monomer concentration. Kinetic analysis of data obtained from protracted electrolysis to higher conversions substantiated this hypothesis.

When using the divided cell with systems otherwise identical to those used previously much higher conversions are observed together with considerable acceleration at all currents increasing with increasing current (*Figure 6*). However, taking the initial slopes of these curves as being representative of a steady state condition, when plotted against current give a linear first order relationship (*Figure 3*). Again when the monomer concentration is varied, at a constant current, acceleration occurs and increases with increasing monomer concentration (*Figure 7*). The initial slopes of these curves are proportional to the square of the monomer concentration as in the case of the single cell (*Figure 5*).

In the case of the divided cell post-polymerization effects are observed, polymerization continuing after cessation of electrolysis. The magnitude of the effect depending not only on the quantity of current passed but on the rate of electrolysis. The effect is greater, for example, after passing 30 mA for one hour than 10 mA for 3 hours (*Figure 8*).

From these results it would appear that in the anode compartment of the divided cell there is a continuous production of active catalyst which gives rise to an acceleration of the rate of polymerization and which is capable of

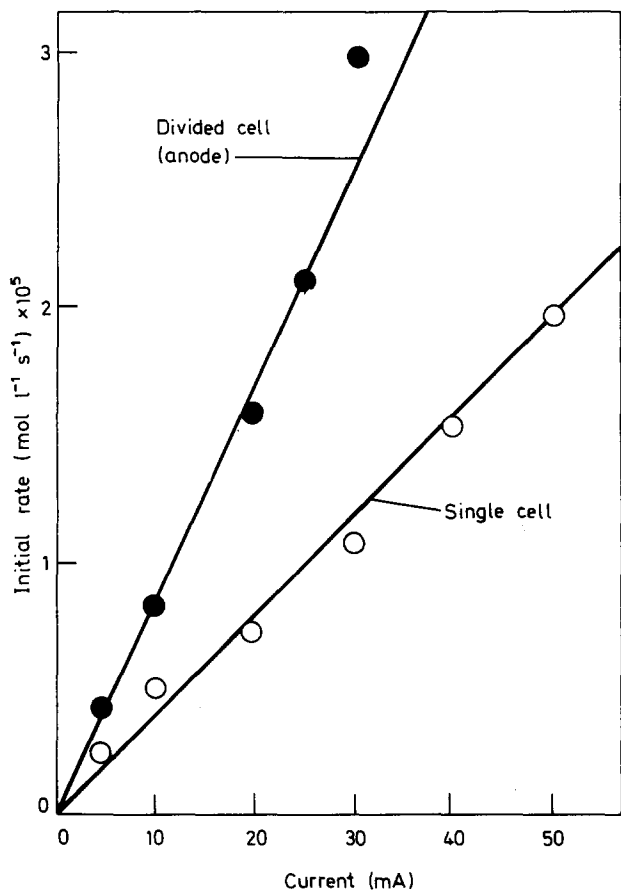


Figure 3 Dependence of initial rate of electropolymerization on the current for 2M styrene in sulpholane/NaBF₄

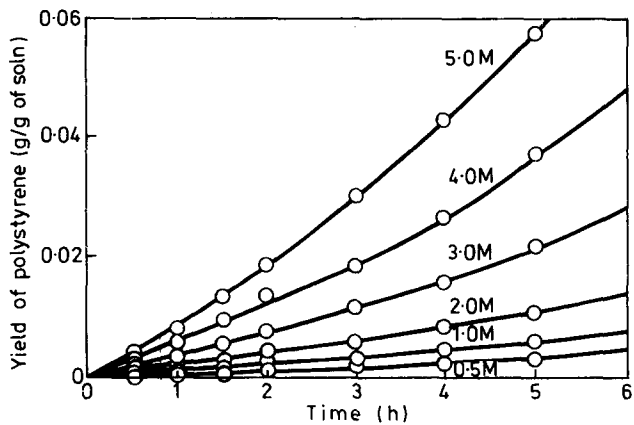


Figure 4 The formation of polystyrene with time at various initial monomer concentrations at 10 mA in sulpholane/NaBF₄ in the single cell

some further initiation after electrolysis has ceased. On the other hand, in the single cell, destruction of a similar catalyst is brought about by the presence in the same compartment of either the cathode or cathodically produced products.

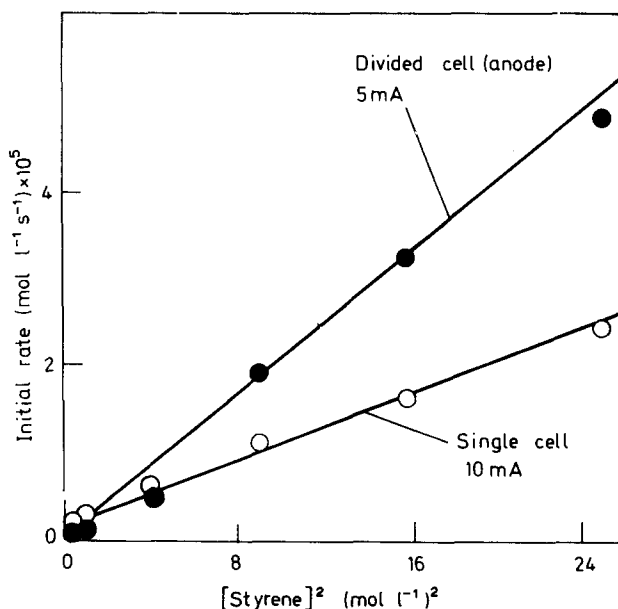


Figure 5 Dependence of initial rate of electropolymerization of styrene on the square of the initial monomer concentration in sulpholane/ NaBF_4

The degree of polymerization of the polymers produced at low conversions is relatively low even over a tenfold change in monomer concentration:

single cell 0.5–5.0 M styrene, $DP_n = 13-9$

anode compartment

divided cell 0.5–5.0 M styrene, $DP_n = 20-25$

It would appear therefore that considerable chain transfer to monomer is taking place as is indicated by the presence, in the i.r. spectra of the polymer, of the weak absorption band at 965 cm^{-1} which has been assigned to an out of plane deformation of a *trans* double bond at the end of a polymer chain¹⁶. Application of the Mayo equation¹⁷ to results shows a linear relationship between $1/DP_n$ and $1/(\text{monomer})$ in the case of the divided cell from which values of $k_m/k_p = 0.034$ and $k_t/k_p = 0.0175$ are obtained (k_m , k_p , k_t being the rate constants for transfer to monomer, propagation and spontaneous

termination, respectively). These are similar to other values reported for styrene.¹⁸

In the case of the single cell the variation of molecular weight with monomer concentration is difficult to interpret. This may be due to the presence of

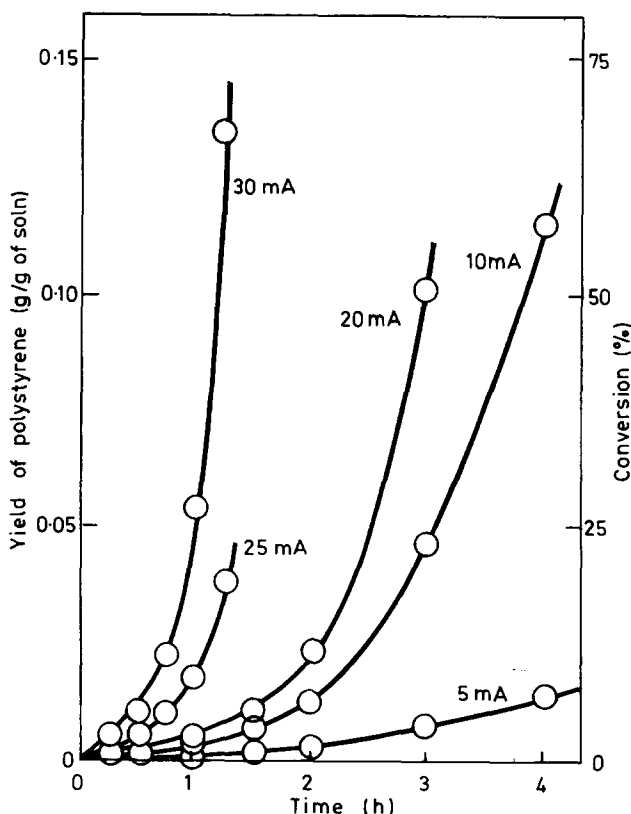


Figure 6 The formation of polystyrene with time at various currents for 2M styrene in sulpholane/ NaBF_4 at the anode of the divided cell

important termination mechanisms other than transfer to monomer. Figure 9 shows how, after prolonged electrolysis, the percentage conversion is quite low in the case of the single cell whilst in the divided cell the conversion calculated for the half cell is quite high, and approaches 100% at the higher monomer concentrations.

From a knowledge of the yield of polymer and the number of Faradays passed the current efficiency (CE), the number of moles of monomer polymerized per Faraday, can be calculated. Again in the case of the single cell the efficiency is low whilst in the case of the divided cell the efficiency approaches the theoretical, especially at higher monomer concentration.

By dividing the current efficiency by the average degree of polymerization of the polymer the number of molecules of polymer produced per electrical

ELECTROINITIATED POLYMERIZATION OF STYRENE

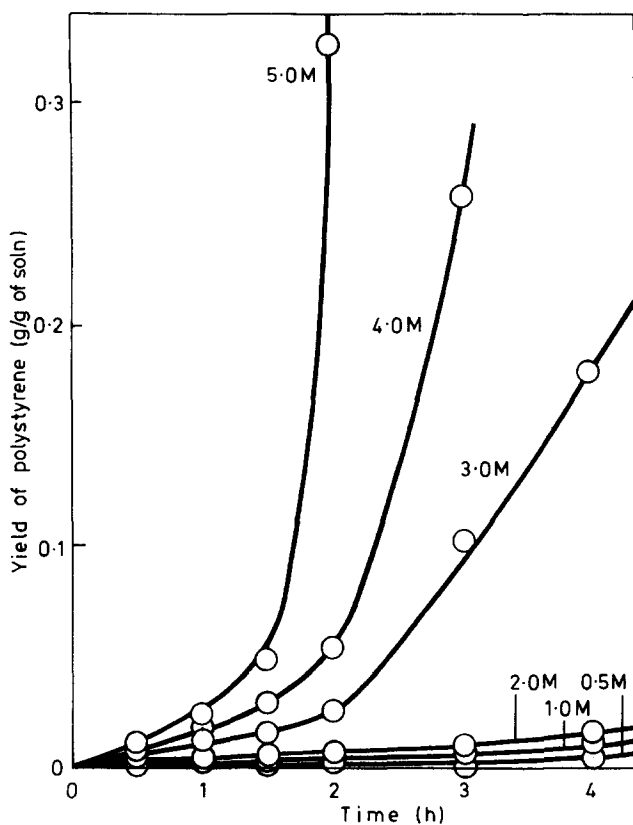


Figure 7 The formation of polystyrene with time at various initial monomer concentrations at 5 mA in sulpholane/NaBF₄ at the anode of the divided cell.

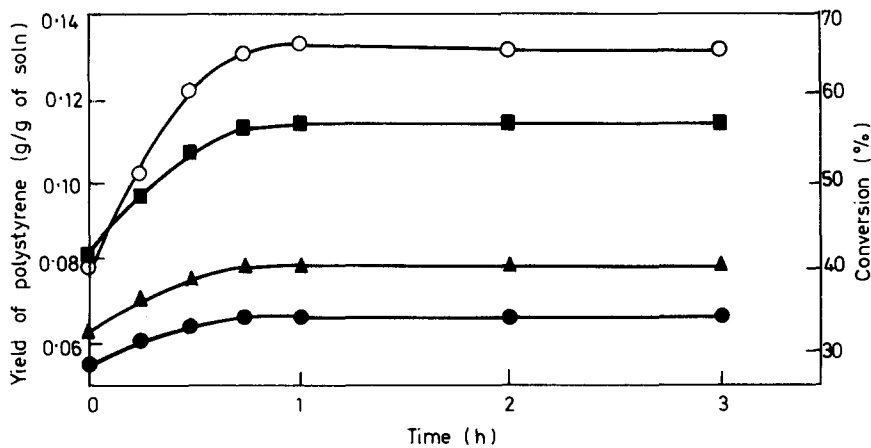


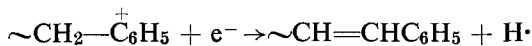
Figure 8 Post-polymerization at the anode of the divided cell for 2M styrene in sulpholane/NaBF₄: ○, 30mA for 1.0h; ■, 25mA for 1.5h; ▲, 20mA for 2.5h; ●, 10mA for 3.0h

Table 3 Electropolymerization of styrene sulpholane/ NaBF_4

Styrene (mol)	Yield (g)	Conversion (%)	Current efficiency (mol/Farad)	Molecules polymer/ electrical event
<i>Single cell (7h, 50 mA, $\overline{DP}_n = 12$)</i>				
0.5	0.0531	1.02	0.04	0.003
1.0	0.4441	4.3	0.3	0.03
2.0	2.4535	11.8	1.8	0.1
3.0	9.6443	30.9	7.1	0.6
4.0	18.1608	43.6	13.4	1.1
5.0	25.7524	49.5	18.9	1.6
<i>Divided cell (anode compartment) (1h, 30 mA, $\overline{DP}_n = 25$)</i>				
0.5	1.3002	49.9	11.0	0.4
1.0	3.4566	66.4	29.7	1.2
2.0	9.1731	88.1	78.7	3.2
3.0	14.2106	91.0	121.9	4.9
4.0	19.3545	93.0	166.1	6.6
5.0	25.4001	97.3	218.1	8.7

event is obtained. As can be seen in Table 3, in the case of the divided cell at the highest concentration some eight polymer molecules are produced for each individual electrical event indicating considerable chain transfer. At the lowest concentration, there appears to be no transfer, the initiation is apparently quite efficient, approaching 50%. In the case of the single cell, at the lowest concentration, the value is extremely low increasing to 1.58 at the highest concentration. In view of the low value at the low concentration it would appear that at the highest concentration there could be some chain transfers taking place.

The lower yield, current efficiencies and molecular weights of the polymers produced in the single cell may be due to the presence of additional termination steps which are absent in the divided cell. The presence of the cathode in the single cell could either remove growing carbonium ions by electrolysis or produce negatively charged species capable of reaction with the propagating carbonium ions. In the former case proton expulsion from the chain may occur:



In the latter case reaction of cathodically discharged sodium with the sulpholane may lead to products capable of chain termination. Analysis for sulphur in the polymer indicates that at the most only one sulphur atom per 12 polymer chains is available.

It is apparent from these results that some type of electrolytic termination process is active in the single cell. Thus \overline{DP}_n may be expressed as:

$$\overline{DP}_n = R_p / (R_m + R_t + R_e) \quad (1)$$

where R_p , R_m , R_t and R_e are the rates of propagation, transfer to monomer, spontaneous termination and electrolyte termination, respectively;

ELECTROINITIATED POLYMERIZATION OF STYRENE

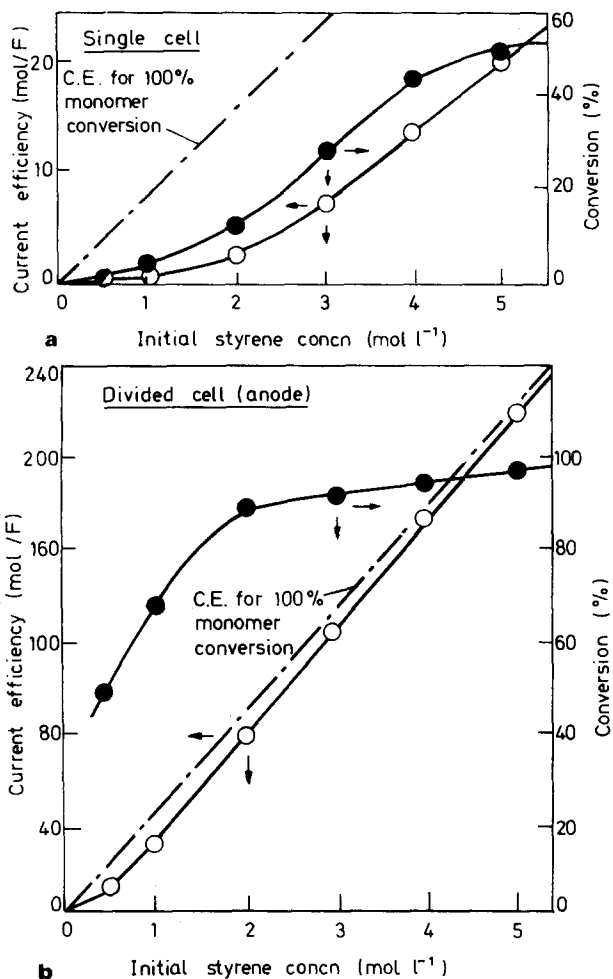


Figure 9 Variation in current efficiency and percentage conversion with initial monomer concentration in sulpholane/NaBF₄

$$\text{where } R_p = k_p[Mn^+] \cdot [M] \quad (2)$$

$$R_m = k_m[Mn^+] \cdot [M] \quad (3)$$

$$R_t = k_t[Mn^+] \quad (4)$$

$$R_e = k_e[Mn^+] \cdot [I] \quad (5)$$

where $[M]$ = concentration of monomer

$[I]$ = current expressed as Faraday per litre

$$\text{thus } \frac{1}{\overline{DP}_n} = \frac{k_m}{k_p} + \frac{k_t}{k_p[M]} + \frac{k_e[I]}{k_p[M]}$$

Thus a linear relationship should exist between $1/\overline{DP}_n$ and $[I]$ from the slope of which k_e/k_p may be evaluated. In order to substantiate this the total

amount of polymer produced, during electrolysis, of 2M styrene solutions at 30°C and at various currents, was isolated and the value of $1/\overline{DP}_n$ plotted against $[I]$ (Figure 10). In the single cell $1/\overline{DP}_n$ can be seen to increase with increasing current giving a value of k_e/k_p of 130×10^{-2} indicating consider-

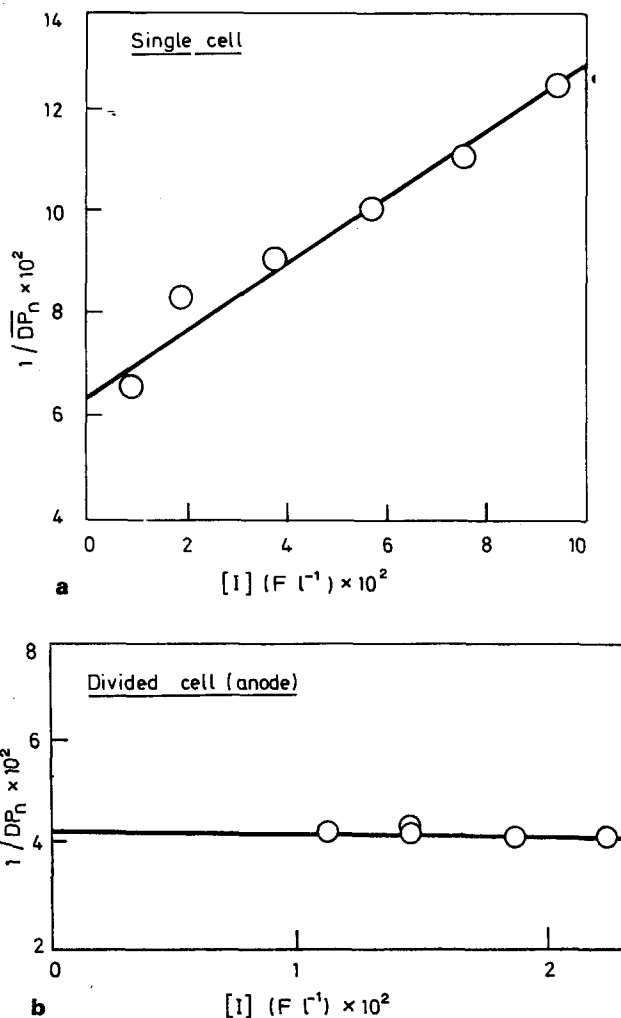


Figure 10 Effect of current on molecular weight of polystyrene formed during the electrolysis of sulpholane/ NaBF_4

able electrolytic termination. In the case of the divided cell $1/\overline{DP}_n$ is independent of current indicating the apparent absence of electrolytic termination in this case as expected.

It would appear from this evidence that polymerization is catalysed by anodically generated boron trifluoride and co-catalysed by either water or hydrogen fluoride (Figure 1) and that the concentration of the active catalyst is proportional to the quantity of current passed.

If one assumes that steady state conditions apply during the initial stages of polymerization then, for the single cell, the rate equation may be written as

$$R_p = \frac{k_p k_i [M]^2 [I]}{k_t + k_m [M] + k_e [I]} \quad (7)$$

whilst in the divided cell at the anode under similar conditions:

$$R_p = \frac{k_p k_i [M]^2 [I]}{k_t + k_m [M]}$$

The main difference being that in the single cell there is a considerable electrolytic termination step which limits the molecular weight and the percentage conversions. It is difficult to understand the reason why separation of the two electrodes by a single glass filter is sufficient to cause such a considerable effect and further work is in progress in an attempt to explain this phenomena.

ACKNOWLEDGEMENT

The authors wish to acknowledge with gratitude the grant of a University of Bradford research scholarship to one of them (A.G.D.).

*School of Polymer Science,
The University,
Bradford 7, Yorkshire, UK*

(Received 16 November 1970)

REFERENCES

- 1 Tidswell, B. M. *Rep. Prog. Appl. Chem.* 1968, **53**, 516
- 2 Funt, B. L. *Macromolecular Rev.* 1966, **1**, 35
- 3 Asahara, T. and Sen, M. J. *Synth. Org. Chem., Japan* 1967, **25**, 719
- 4 Yamazaki, N. *Adv. in Polym. Sci.* 1969, **6**, 377
- 5 Funt, B. L. and Gray, D. G. *J. Macromol. Chem.* 1966, **4**, 1
- 6 Funt, B. L. Bhadani, S. and Richardson, D. *Can. J. Chem.* 1966, **44**, 711
- 7 Elliott, V. R. in *Macromolecular Synthesis* 1966, **2**, 30 and 86, Wiley, New York, 1966
- 8 Tidswell, B. M. *S.C.I. Monograph* 1966, **20**, 129
- 9 Finemann, M. and Ross, S. D. *J. Polym. Sci.* 1950, **5**, 269
- 10 Brown, G. R. and Pepper, D. C. *J. Chem. Soc.* 1963, p 5930
- 11 Zutty, N. L. and Welch, F. T. *J. Polym. Sci.* 1960, **43**, 445
- 12 Kolthoff, I. M. and Elving, P. J. 'Treatise on Analytical Chemistry: Part 2. Analytical Chemistry of the Elements,' vol 7, p 290, Interscience, New York, 1961
- 13 Simons, J. H., 'Fluorine Chemistry,' vol 2, p 62, Academic Press, New York, 1954
- 14 Kline, G. M., 'Analytical Chemistry of Polymers: Part 3. Identification and Chemical Analysis,' p 61, Interscience, New York, 1962
- 15 Clark, D. in 'Cationic Polymerisation and Related Complexes' (Editor Plesch, P. H.) p 69, Heffer, Cambridge, 1953
- 16 Rao, C. N. R., 'Chemical Applications of Infra-red Spectroscopy', p 147, Academic Press, New York, 1963
- 17 Allen, P. E. M., in 'The Chemistry of Cationic Polymerisation' (Editor, Plesch, P. H.), p 122, Pergamon, Oxford, 1963
- 18 Mathieson, A. R., in 'The Chemistry of Cationic Polymerisation' (Editor, Plesch, P. H.), p 286, Pergamon, Oxford, 1963

Cationic polymerization of indene

A. D. ECKARD, A. LEDWITH and D. C. SHERRINGTON

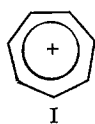
Cationic polymerization of indene in methylene dichloride was effected by two stable carbonium ion salt initiators, tropylium hexachloroantimonate and xanthylum perchlorate, the former being more efficient. Very high conversions of monomer to polyindene were obtained with catalyst concentrations $\sim 10^{-2}$ M. Molecular weights were approximately 10 000 and it is concluded that whilst initiation is fairly rapid and complete, active centres are lost by creation of more stable cationic species from polyindene chains. Mechanisms are proposed to account for the formation, during polymerization, of characteristically coloured species.

INTRODUCTION

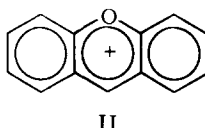
INDENE WAS first shown to be a polymerizable olefin in 1890¹. Polymerizations were achieved using various catalysts such as sulphuric acid, heat, antimony pentachloride and stannic chloride², although the polymers produced in all early work were of low molecular weight only. Typical samples consisted of oligomeric species containing up to ten or twelve indene residues, and in some cases separate fractions, each with a sharp melting point, were obtained². No details of mechanism were established although a stepwise process involving the 'wandering of a hydrogen atom' was envisaged.

Much more recently the susceptibility of indene to attack, particularly from cationic reagents, has been recognised³, and polymerization of indene and its derivatives⁴ has been studied by more sophisticated means⁵. The list of Lewis acids used as initiators has been extended to include boron trifluoride and titanium tetrachloride. Low temperature experiments using these two catalysts^{6,7} with and without co-catalysts such as water and hydrogen chloride have produced high polymers with intrinsic viscosities (benzene solvent) of up to 2 corresponding to a molecular weight⁸ of $\sim 2 \times 10^6$.

A growing number of stable carbonium ion salts have been shown to be very efficient initiators of cationic polymerization of certain electron-rich olefins and, unlike more conventional catalysts, allow for complete characterization of the initiating species⁹. In principle such salts should readily function as initiators of the polymerization of indene¹⁰ and it was with this in mind that the present work was undertaken. The salts investigated were tropylium hexachloroantimonate (I) and xanthylum perchlorate (II) both of which have previously been shown to be very reactive towards alkyl vinyl ethers and N-vinylcarbazole^{9,11}, olefins which are similar to indene in their reactivity towards electrophiles.



SbCl_6^-



ClO_4^-

EXPERIMENTAL

Indene (Hopkin and Williams) was purified according to the method of Russell¹². The pure liquid was placed in a flask fitted with a greaseless Teflon tap and degassed on the vacuum line. The flask was opened in an atmosphere of dry nitrogen and all polymerizations were subsequently carried out under these conditions. The methylene dichloride used was dried by refluxing over calcium hydride and purified by fractionation. Tropylium hexachloroantimonate (I) and xanthylium perchlorate (II) were prepared and purified as described previously^{10,11}.

Attempts to handle indene quantitatively on the vacuum line failed because of its high boiling point (182°C/760 mmHg) and so all reactions were carried out under dry nitrogen. Polymerizations were achieved by introducing known amounts of catalyst solution into samples of indene also in methylene dichloride. A spring loaded syringe (Becton, Dickinson and Company) was used to effect rapid addition and efficient mixing. Reactions were stopped and polymers precipitated by addition of excess methanol.

Polymerization of indene by tropylium hexachloroantimonate
($C_7H_7^+SbCl_6^-$)

Preliminary experiments (*Table 1*) showed that for initial catalyst concentrations, $[C]_0 > 10^{-2}$ M conversion to 100% polymer was almost instantane-

Table 1 Polymerization of indene in methylene dichloride at 22°C by tropylium hexachloroantimonate

$[C]_0$ (M)	$[M]_0$ (M)	Polymer yield (%)	Duration of polymerization (min)	Colour of reaction mixture
2.3×10^{-4}	1.60	2.5	~1	yellow
2.3×10^{-4}	0.78	30.0	15	yellow→red
2.2×10^{-3}	0.78	44.7	~1	yellow
2.3×10^{-3}	0.78	33.2	~1	yellow
2.3×10^{-3}	0.78	97.0	15	yellow→red
1.9×10^{-2}	0.78	96.0	~1	yellow→red

ous. Polymer yields in a given time were found to fall with decreasing $[C]_0$. From these results it seemed that a kinetic study based on conversion/time data was feasible using $[C]_0$ values $\sim 5 \times 10^{-4}$ M and polymerization times up to 1 hour. *Table 2* shows the data obtained.

Table 2 Conversion/time data for polymerization of indene in methylene dichloride by tropylium hexachloroantimonate at 22°C

$[C]_0$ (M)	$[M]_0$ (M)	Polymer yield (%)	Duration of polymerization (min)
4.2×10^{-4}	0.78	15.9	10
4.2×10^{-4}	0.78	15.3	20
4.2×10^{-4}	0.78	19.0	60
1.1×10^{-3}	0.78	57.9	10
1.1×10^{-3}	0.78	59.2	30

Since the yield for a given $[C]_0$ and $[M]_0$ did not increase appreciably with time it seemed that tropylium ion initiated polymerization fairly rapidly but some dominant termination reaction quickly ensued. Termination may be due to trace impurities, but in view of the purification techniques employed and the extent of active centre destruction it is more likely to be inherent in the polyindene molecules themselves. This view was supported to some extent by experiments (see later) in which stable cationic species were produced in terminated polyindene chains. Intrinsic viscosities and corresponding experimental molecular weights⁸ for three polymers prepared using $[C]_0$ values such that high conversion was obtained are shown in *Table 3*.

Table 3 Molecular weights of polyindenes prepared by tropylium hexachloroantimonate catalysis in methylene dichloride at 22°C

$[C]_0$ (M)	$[M]_0$ (M)	% yield	$[\eta]$	Experimental molecular wt.	Theoretical molecular wt.
3.8×10^{-3}	0.78	96.0	0.135	1.9×10^4	2.4×10^4
7.0×10^{-3}	0.71	96.2	0.119	1.5×10^4	1.2×10^4
2.2×10^{-2}	0.78	91.6	0.0886	9.0×10^3	4.1×10^3

As expected, molecular weights decreased with increase in $[C]_0$ but unexpectedly close agreement emerged between the experimental values and the theoretical values calculated from the ratio $[M]_0/[C]_0$. Superficially this could be interpreted as a lack of monomer transfer in the system, but this is very unlikely for a cationic polymerization. Catalyst, and active centres, are consumed by competing side reactions (see below) and it is highly likely that the observed molecular weights result from a fortuitous combination of these processes.

Visible spectra of polymerization solutions

Invariably polymerizations were accompanied by characteristic colours. Normally a yellow solution was formed initially and, if sufficient catalyst was present, reaction mixtures gradually became cherry red and finally after some hours a darker red with evidence of some fluorescence. Visible spectra were recorded on a Unicam SP 800 spectrophotometer in order to try and interpret the colour changes.

Mixing tropylium hexachloroantimonate and indene solutions in methylene dichloride at $\sim -20^\circ\text{C}$ gave a yellow solution, and a spectrum run before the solution warmed up showed a broad band (A in *Figure 1*) $\lambda_{\text{max}} \sim 435$ nm, merging into the intense u.v. aromatic absorption of indene. Addition of methanol to this solution destroyed the colour and yielded no polymer. This broad band was thought therefore to be due to a charge transfer (c.t.) phenomenon. When a similar solution was allowed to warm up to room temperature the broad c.t. band was replaced by a sharper band (B), λ_{max} 440 nm, the solution remaining yellow in colour. If left to react for 24 hours such a solution gradually became colourless. Addition of methanol any time after the collapse of the c.t. band resulted in loss of colour and precipitation of varying amounts of polymer. It is difficult to specify the exact nature of

CATIONIC POLYMERIZATION OF INDENE

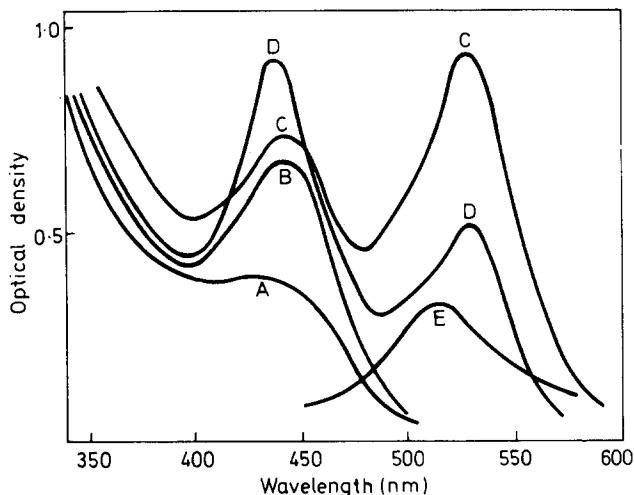


Figure 1 Visible absorption spectra of polymerizing solutions (solvent methylene dichloride) at 25°C

- A Indene (1.60 M) and tropylium hexachloroantimonate (2.3×10^{-4} M) immediately after mixing
- B Same solution as A after 5 min
- C Indene (0.78 M) and tropylium hexachloroantimonate (1.9×10^{-2} M) after 1 hour
- D Same solution as C after 4 hours
- E Polyindene plus $\text{BF}_3 \cdot \text{Et}_2\text{O}$

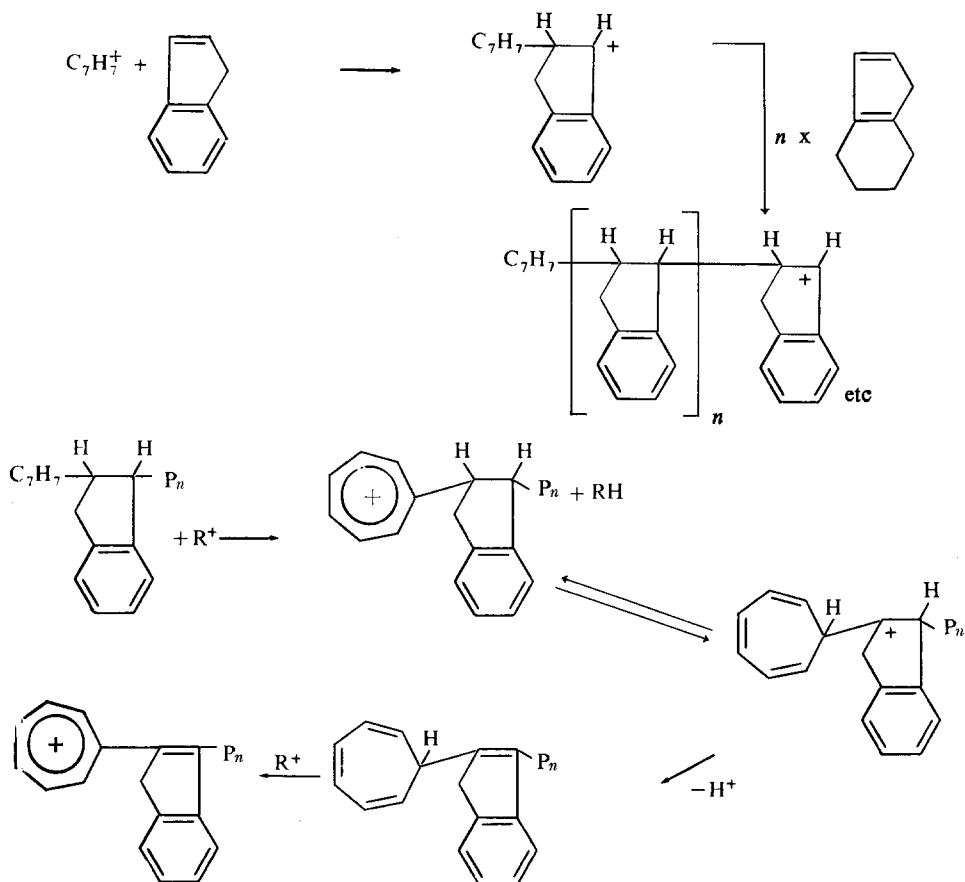
the chromophore responsible for the 440 nm band but in view of its similarity with the c.t. band and the failure to produce a similar absorption from terminated polyindene alone (see later), it seems reasonable to assume that the chromophore in question is one arising from a combination of tropylium and indene moieties.

When the concentration of tropylium ions was in excess of the minimum required to produce polymer at room temperature, the 435 nm band was quickly replaced by the 440 nm absorption as before. However an additional band (C), λ_{max} 525 nm, appeared and the solution gradually became cherry red in colour. This band after ~ 1 hour became the dominant feature of the visible spectrum. When left for some hours such a solution became darker red in colour and slightly fluorescent. A visible spectrum (D) at this time showed the 440 nm band once again to be more intense than the 525 nm absorption (now shifted slightly to higher wavelengths). As before some polymer could be precipitated by addition of methanol any time after the collapse of the initial c.t. band.

From these observations it appeared that the 525 nm absorption occurred only when both polyindene and excess tropylium ions were present, and was ascribable to a post-polymerization reaction. To test if polyindene units, or a tropylium ion derivative, or a combination of both was responsible for this absorption, a sample of preformed polyindene was dissolved in methylene dichloride and a $\text{BF}_3/\text{CH}_2\text{Cl}_2$ solution added. The mixture became red in colour and the visible spectrum consisted of only one peak (E), $\lambda_{\text{max}} \sim 520$

nm. Similar red colours with polyindenes have been observed before⁷ and it is clear that these result from 'acid' catalysed oxidation processes involving polyindene.

Formation of cationic species absorbing around 440 nm (e.g. B in Figure 1) is commonly encountered in cationic polymerizations of styrene¹³ and is usually ascribed to oxidative cyclization reactions leading to substituted indane-like carbonium ions. It is not surprising therefore that similar chromophores should be observed during cationic polymerization of indene. However the final colours developed (D) clearly result from reactions involving both tropylium ion and indane units in the polymeric molecules, and a possible reaction scheme is indicated below (SbCl_6^- counter-ions are omitted for clarity, $\text{R}^+ = \text{C}_7\text{H}_7^+$ or a growing polyindene cation):



Aryl substituted tropylium ions¹⁴ are known to absorb in the range 400–500 nm supporting the proposed mechanism, but the precise nature of the red chromophore formed by the action of Lewis acids on polyindene remains unknown.

Reactivity and copolymer formation

Although indene is clearly a relatively reactive olefin towards cationic centres these results show conclusively that its overall reaction with tropylium ion is inefficient because of accompanying side reactions. This is not true of other active monomers such as N-vinylcarbazole (NVC) which give 100% conversion to polymer almost instantaneously with $[C]_0$ values down to 10^{-5} M. It is not surprising therefore to find that attempts to form simple copolymers of these two monomers failed, presumably because of the large differences in reactivity of their corresponding cations. The copolymers which have been reported previously¹⁵ were prepared under very different and more drastic conditions, using radiation techniques, and possibly involving free radical growth mechanisms. In the present work with $[C]_0 \sim 10^{-3}$ M only a homopolymer of NVC was formed. Increasing $[C]_0$ to $\sim 10^{-2}$ M in an attempt to polymerize indene as well resulted only in the formation of crosslinked poly-N-vinylcarbazole in a manner similar to that observed previously when using high catalyst concentrations in methylene dichloride. Yields showed that some indene was indeed consumed but attempts to detect its residues in the product failed, probably because such units were incorporated deep in the crosslinked network of poly (NVC) chains.

Polymerization of indene by xanthylium perchlorate

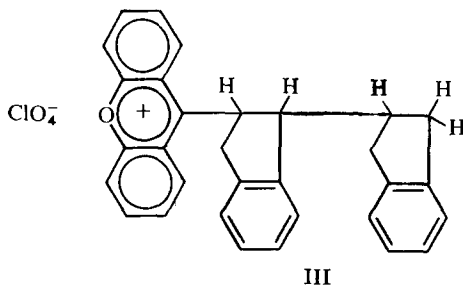
Again working under dry nitrogen a parallel study to tropylium ion initiation was carried out using xanthylium perchlorate (II). Initiation with xanthylium cation is slower than with tropylium ion and hence all reactions were allowed to proceed for approximately four hours before work up. Results obtained are shown in *Table 4*.

Table 4 Polymerization of indene in methylene dichloride by xanthylium perchlorate at 22°C

$[C]_0$ (M)	$[M]_0$ (M)	Yield (%)
1.3×10^{-4}	0.48	~8
3.0×10^{-4}	0.48	34.5
4.6×10^{-4}	0.48	10
5.4×10^{-4}	0.16	~10
1.4×10^{-3}	0.78	50.5
1.9×10^{-2}	5.7	69.0
3.8×10^{-2}	5.7	80.0

Even with catalyst concentrations up to 10^{-2} M yields were invariably less than 100% and the xanthylium cation must therefore be regarded as a much less efficient initiator than tropylium ion, in agreement with results found with other active olefins. Molecular weights were also found to be lower showing that transfer and other side reactions predominate. In a typical polymerization, after addition of catalyst solution to monomer solution, the yellow-orange colour characteristic of the initiator was rapidly replaced by a red colour, similar to that found with tropylium ion. Precipitation of polymer by addition of methanol was often accompanied by traces of a red compound.

Indeed at elevated temperatures using ethylene dichloride as solvent and very high $[C]_0$ values such that catalyst and monomer were present in almost equimolar quantities, it was possible to isolate only red products of low molecular weight, and no polymer. For example when 3.372 g of xanthylium perchlorate and 1.6 ml of indene were refluxed together for 30 minutes in ethylene dichloride and dry ether added to the cooled solution, a red-brown product was formed. This was collected, redissolved in acetonitrile, and reprecipitated by addition of ether. Analysis: found, C, 74.22; H, 4.31%; calculated for compound (III); C, 72.7; H, 4.88%.



An i.r. spectrum confirmed the product to be a perchlorate derivative and a visible spectrum showed two sharp bands, λ_{\max} 432 nm and 488 nm. The latter had a prominent shoulder at 520 nm probably arising from the same chromophore as described earlier. The two sharp bands are typical of xanthylium cations and were almost certainly characteristic of species such as III, although it is very unlikely that the product isolated was a single pure compound. More probably III was contaminated with traces of polyindene oligomers and corresponding 1:1 and 1:3 xanthylium:indene adducts. Indeed other preparations yielded products having similar spectra, but gave analytical data which varied as anticipated on this basis. Formation of III, and possibly unsaturated analogues, may occur readily following successive hydride abstraction processes similar to those described earlier for the tropylium ion adducts.

CONCLUSIONS

Both carbonium ion salts employed initiate the polymerization of indene, tropylium ion being more efficient than xanthylium ion. A polymer yield of ~60% within ten minutes of the addition of catalyst (10^{-3} M tropylium hexachloroantimonate) compares favourably with results of all previously reported polymerizations. As found by other workers¹⁶ relatively high catalyst concentrations (in this work $\sim 10^{-2}$ M) are required to produce 100% conversion. The initiation process itself seems to be efficient and rapid, however, it appears that as soon as polyindene chains are formed active centres are lost by the generation of stable positive charges on the polyindene backbone. The spectrophotometric evidence appears to confirm both of these observations. In view of this inherent side reaction it seems unlikely that indene will ever prove to be a useful monomer in the elucidation of detailed

reaction mechanism and the determination of absolute reactivity in cationic propagation.

The experiments with xanthylium ion however do give some insight into the initiation mechanism. The isolation of various red complexes shows clearly that the process involved is the addition of the primary stable carbonium ion to an indene molecule. By analogy the same mechanism can be envisaged as operating in the case of tropylium ion initiation, the addition going via the charge transfer complex detected in the spectrophotometric investigation.

*Donnan Laboratories,
University of Liverpool, UK*

(Received 11 December 1971)

REFERENCES

- 1 Kramer and Spilker *Ber.* 1890, **23**, 3276
- 2 Whitby, G. S. and Katz, M. *J. Amer. Chem. Soc.* 1928, **50**, 1160
- 3 Sigwalt, P. *J. Polym. Sci.* 1961, **52**, 15
- 4 Marechal, E., Basselier, J. and Sigwalt, P. *Bull. Soc. Chim. France* 1964, p 1740
- 5 Mizote, A., Tanaka, T. and Higashimura, T. *Kobunshi Kagaku* 1966, **23**, 78; *Chem. Absts.* 1966, **64**, 17722c
- 6 Cheradame, H. and Sigwalt, P. *Compt. Rend.* 1965, **260**, 159
- 7 Polton, A. and Sigwalt, P. *Compt. Rend.* 1967, **265C**, 1303
- 8 Bkouche-Waksman, Mme. Itka and Sigwalt, P. *Compt. Rend.* 1962, **255**, 680
- 9 Bawn, C. E. H., Fitzsimmons, C. and Ledwith, A. *Proc. Chem. Soc.* 1964, p 391
- 10 Bawn, C. E. H., Fitzsimmons, C., Ledwith, A., Penfold, J., Sherrington, D. C. and Weightman, J. A. *Polymer, Lond.* 1971, **12**, 119
- 11 Sauvet, G., Vairon, J. P. and Sigwalt, P. *Compt. Rend.* 1967, **265C**, 1090
- 12 Ledwith, A. *Amer. Chem. Soc. Advances in Chemistry Series* 1969, **91**, 317
- 13 Ledwith, A. *J. Appl. Chem.* 1967, **17**, 344
- 14 Russell, G. A. *J. Amer. Chem. Soc.* 1956, **78**, 1041
- 15 Plesch, P. H., 'Progress in High Polymers', (Eds. J. C. Robb and F. W. Peaker) Iliffe, London, 1968, Vol. II, p 137
- 16 Jutz, C. *Chem. Ber.* 1964, **97**, 2050, and other papers in this series
- 17 *British Patent*, No. 1,004, 074, September 8th, 1965
- 18 Cheradame, H., Vairon, J. P. and Sigwalt, P. *European Polymer J.* 1968, **4**, 13

*Amylose in aqueous solution— a viscometric study**

W. BANKS, C. T. GREENWOOD, D. J. HOURSTON and A. R. PROCTER

A detailed investigation of the viscometric behaviour of amylose in aqueous solution has been made. The effect of pH, and of different alkalis and salts on the molecular conformation of the polysaccharide has been studied. It has been found that the limiting viscosity number $[\eta]$ of amylose is constant up to pH 11 and thereafter increases rapidly, rising to a maximum in 0.15 M alkali. In the case of the inorganic alkalis, $[\eta]$ subsequently decreases with increasing pH, but in tetramethylammonium hydroxide, a further slow increase in $[\eta]$ occurs. In the presence of salts, this behaviour is completely modified, and a minimum in $[\eta]$ is then found at pH 12. It is shown that the nature of the anion of the supporting salt greatly influences the conformation of the polysaccharide in both neutral and alkaline solution. The changes in $[\eta]$ are related to changes in the shape of the dissolved macromolecule, and the manner in which the structure of the solvent water influences these changes is discussed.

THE MODEL of the helical macromolecule in solution is now widely accepted in the protein and nucleic acid fields. However, it is often overlooked that the concept was first applied to explain the amylose-iodine interaction^{1,2}, and that the first experimental verification of the existence of the helix was also for this system³. Whilst it is accepted that amylose in the solid state may exist in a helical conformation, the shape taken up by the molecule in solution has been the subject of some dispute.

Rao and Foster⁴ reported that when the pH of an aqueous amylose solution was altered, the limiting viscosity number $[\eta]$ went through a minimum at pH 12. These authors suggested that this behaviour could be due to a helix to coil transformation, the former existing in neutral aqueous solution, and the latter at pH 12. Our own hydrodynamic measurements⁵⁻⁷ are at variance with this model and show that the helical content of amylose in neutral solution is negligibly small. In view of this discrepancy, we report here detailed investigations of the viscometric behaviour of amylose in neutral and alkaline solution.

EXPERIMENTAL

The amylose samples used in this work were isolated from a number of starches—potato, rye, wheat, barley and tapioca. All of these samples were shown, by differential potentiometric iodine titration⁸ and enzymic assay⁹, to be free from the branched component, amylopectin. The behaviour reported herein was found to be independent of the source of the amylose samples.

* This is Part 59 in the series 'Physicochemical Studies on Starches'; Part 58 has been submitted to *Carbohydrate Research*.

In most instances, the amylose was used as the butan-1-ol complex, but control experiments were also carried out using solid amylose.

Amylopectin was isolated from waxy maize starch as previously described¹⁰ as the freeze-dried solid.

All viscosity measurements were carried out at 25°C, using modified Ubbelohde viscometers, having a negligible kinetic energy correction, and an average shear rate of 1200 s⁻¹. We have shown¹¹ that the limiting viscosity number $[\eta]$ of amylose is independent of the shear rate, at least up to this value.

In many experiments, the limiting viscosity number of amylose was measured for the various solvent systems. However, we found that essentially the same result was obtained from determinations of the viscosity number (η_{sp}/c), whilst progressively changing the solvent medium. To determine the viscosity-number/pH profile, it was necessary only to add the desired aliquots of alkali to an aqueous solution of amylose in the viscometer. Four concentrated alkali solutions (10⁻² M; 10⁻¹ M; 1 M; and 5 M) were used for this purpose. When investigating the effect of various salts on this profile, the amylose was dissolved in a 0.25 M aqueous solution of the salt, and the various alkali solutions were also 0.25 M with respect to the salt. In this procedure, the conditions were such that all measurements were performed whilst changing the volume of the solution from 10 ml to 15 ml.

Reagent grade chemicals were used in the preparation of solutions.

The concentrations of the amylose solutions were determined by either (1) hydrolysis to glucose in 1.5 N sulphuric acid at 100°C for 2 h, and estimation of the reducing power using the alkaline ferricyanide technique¹², or (2) hydrolysis by means of amyloglucosidase, and estimation of the glucose using the coupled enzyme system glucose oxidase/peroxidase¹³.

RESULTS

(1). *The degradation of amylose in alkali*

It is known that in alkaline solution, polysaccharides may undergo two types of degradative reaction¹⁴, (a) a 'zipping' process from the reducing end-group, with the liberation of isosaccharinic acids, and (b) a random hydrolytic scission of glycosidic bonds. The latter process is of more concern in viscosity measurements, because the random cleavage of one bond per molecule will reduce the molecular weight of the polysaccharide by a factor of two. For linear polymers, $[\eta]$ varies, in the extreme, as $M^{\frac{1}{2}}$ or M , hence degradation to a very limited extent (0.1%) will cause a 40–100% variation in $[\eta]$ when the initial degree of polymerization is 1000. Whistler and Johnson¹⁴ suggested that this type of degradation can be avoided with alkaline solutions of amylose, by rigorously excluding oxygen from the system. Wolff *et al*¹⁵ found only very slight decreases in the relative viscosity on storing alkaline amylose solutions at 0°C for periods of up to 24 h, and that this degradation was independent of whether the atmosphere did, or did not, contain oxygen. Bottle *et al*¹⁶ reported pronounced degradation of amylose in 0.5 M alkali at 100°C, but confirmed that it could be virtually eliminated by means of an inert atmosphere.

Figure 1 shows a graph of the number of bonds broken (N) per original molecule of amylose at 25°C for three concentrations of alkali, N being defined by

$$N = (\overline{DP}_0 / \overline{DP}_t) - 1$$

where \overline{DP}_0 and \overline{DP}_t are the average degrees of polymerization at times 0 and t , respectively. For this experiment, the amylose solutions were stored at 25°C for the requisite period, cooled to 0°C and complexed with butan-1-ol.

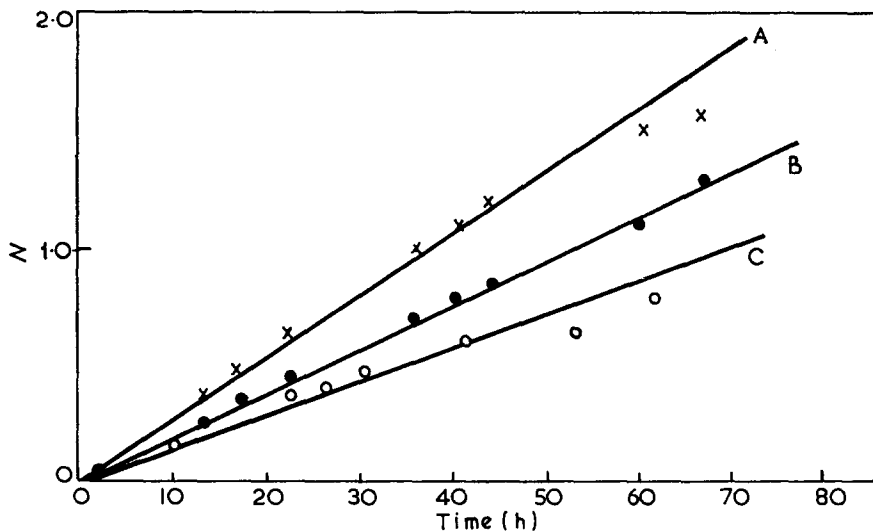


Figure 1 N , the number of bonds broken/original amylose molecule as a function of time at 25°C in (A) 1.0 M KOH, (B) 0.15 M KOH, and (C) 0.01 M KOH

The complex was removed, dissolved in 0.15 M KOH, and $[\eta]$ measured immediately. This was then converted into \overline{DP}_n , using the relation of Banks and Greenwood¹⁷.

It is obvious that the number of bonds broken increases with increasing concentration of alkali. However, the rate of hydrolytic scission is in all cases so low that any of these solvents can be employed routinely for the visometric characterization of amylose.

On repeating the above experiments in the presence of an inert atmosphere (nitrogen), the rate of degradation was found to be considerably reduced. Similarly, at lower temperatures (1°C), the degradative reaction was much slower—even in the presence of oxygen, only 0.05–0.08 bonds (depending on the concentration of the alkali) were broken in 50 h. Thus, our standard technique of dissolving amylose in alkali at low temperature prior to carrying out measurements at 25°C should lead to no serious error as a result of degradation. Consequently, the viscosity phenomena to be examined in detail in the following sections cannot result from degradative effects.

(2) *The variation of $[\eta]$ with alkali concentration*

(a) *In KOH solution.* Figure 2 shows a graph (solid line) of $[\eta]$ for amylose in solutions of various concentrations of alkali (KOH). In changing from neutral to alkaline solution, the $[\eta]$ is constant until the pH reaches about 11, when there is a rapid increase until a maximum is reached, corresponding to 0.15 M KOH, after which $[\eta]$ decreases.

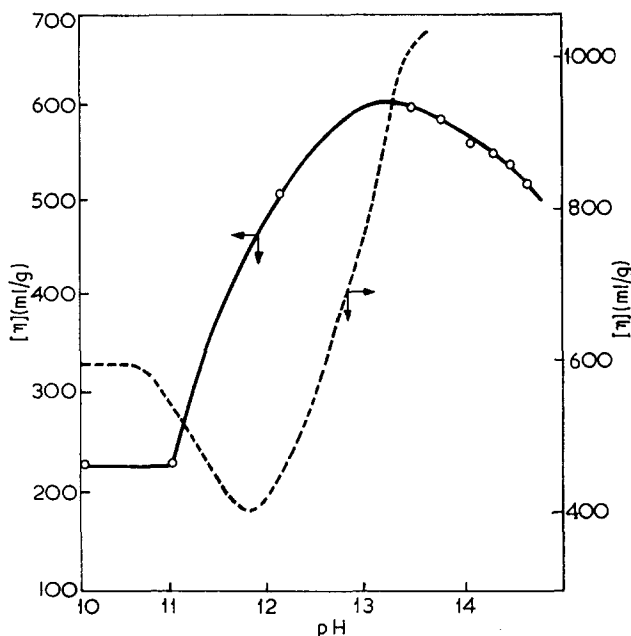


Figure 2 $[\eta]$, the limiting viscosity number of amylose, as a function of pH in KOH (solid line), and KOH + KCl (broken line, redrawn from results of Rao and Foster⁴)

Also shown in Figure 2 are the results obtained by Rao and Foster⁴ for $[\eta]$ as a function of pH (broken line). The form of the curve is completely different from that obtained in the present work, having a minimum rather than a maximum. However, these workers dissolved the amylose in 0.5 M KOH, and obtained the required pH by the addition of acid (1 N HCl). Thus, in addition to alkali they had present a variable amount of KCl, and therefore because the ionic strength was varying continuously their results are not directly comparable with those recorded in Figure 2.

(b) *In other alkalis.* Figure 3 shows a graph of η_{sp}/c for amylose as a function of pH for various alkalis. This procedure of measuring η_{sp}/c rather than $[\eta]$ is very much more rapid, but yields comparable results, as may be seen from a comparison of the graph for KOH in Figure 3 with that in Figure 2. For the inorganic alkalis, each pH value was obtained in a comparable manner, and hence at a given pH the concentration of amylose is identical in all cases. The tetramethylammonium hydroxide (TMAH), however,

was supplied in the form of a 25% aqueous solution, therefore in order to achieve the higher pH values it was necessary to add a greater amount of liquid to the viscometer. As a consequence, the latter points for TMAH are not strictly comparable with those for the inorganic alkalis since they refer to a lower concentration of amylose; but the difference is small.

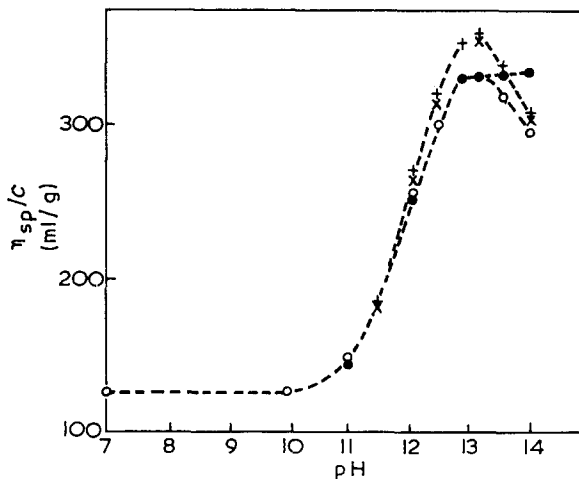


Figure 3 η_{sp}/c , the viscosity number of amylose, as a function of pH in LiOH (\times), NaOH ($+$), KOH (\circ) and TMAH (\bullet)

From Figure 3, it can be seen that the three inorganic alkalis behave similarly in that they give an apparent maximum in molecular extension, corresponding to an alkali concentration of approximately 0.15 M. However, the curves differ in detail—those for LiOH and NaOH are virtually identical but that for KOH shows a lower maximum. The graph for TMAH is the same as that for KOH, within experimental error, up to pH 13, but instead of subsequently decreasing, it appears to reach a limiting value.

The results in section (1) indicate that alkaline degradation of the amylose does not play any part in the viscometric measurements shown in Figures 2 and 3. This conclusion was further substantiated by measuring $[\eta]$ in 0.15 M KOH (found, $[\eta] = 455$ ml/g), complexing the polysaccharide with butan-1-ol, and determining $[\eta]$ in 1 M KOH (found, $[\eta] = 425$ ml/g), repeating the complexing, and measuring $[\eta]$ in 0.15 M KOH (found, $[\eta] = 455$ ml/g).

(3). The variation of $[\eta]$ with pH in the presence of salt

We have noted already the profound difference between the present results for the behaviour of amylose in alkali, and those reported by Rao and Foster⁴, and we have ascribed the difference to the varying ionic strength in the solutions used by these authors. To confirm this assumption, we measured $[\eta]$ as a function of KCl concentration for various molarities of alkali.

AMYLOSE IN AQUEOUS SOLUTION

The results are shown in *Figure 4* and it can be seen that in neutral solution, $[\eta]$ is independent of the KCl concentration, in alkaline solution the addition of KCl leads to a decrease in $[\eta]$, and in 1.5×10^{-1} M, 10^{-2} M, and 10^{-3} M KOH, the addition of KCl causes $[\eta]$ to decrease to a value lower than that observed in neutral KCl solution. This last phenomenon is, however, depen-

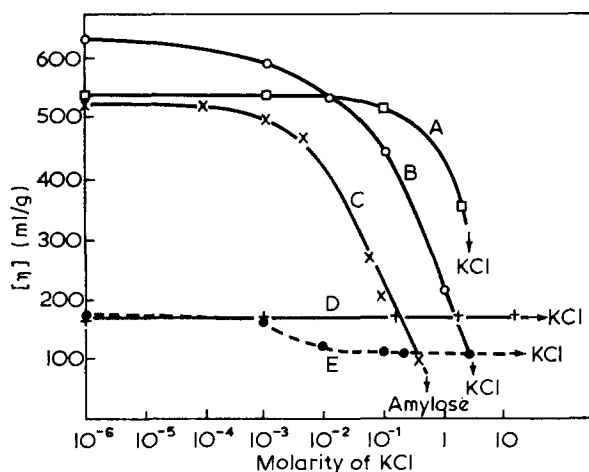


Figure 4 $[\eta]$, the limiting viscosity number of amylose, as a function of the concentration of KCl in (A) 1.0 M KOH, (B) 0.15 M KOH, (C) 0.01 M KOH, (D) water, and (E) 0.001 M KOH. The arrows indicate that precipitation of the named component occurred

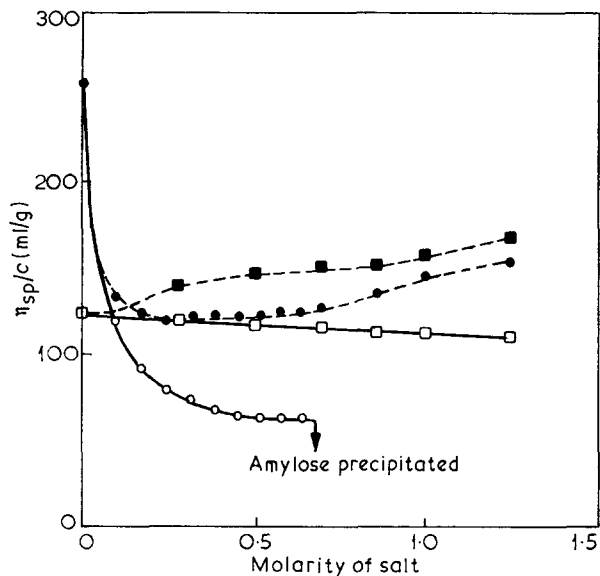


Figure 5 η_{sp}/c , the viscosity number of amylose as a function of salt concentrations in 0.01 M KOH + KCl (○), 0.01 M KOH + KI (●), water + KCl (□), and water + KI (■)

dent on the nature of the salt added, as shown in *Figure 5*, where aliquots of concentrated solutions of KCl and KI, and these salts in 0.01 M KOH, have been added successively to amylose in water, and amylose in 0.01 M KOH, respectively.

In the case of amylose in water, the addition of KCl solution causes a slight decrease in η_{sp}/c , due to the dilution effect, whereas that of KI solution leads to an increase in η_{sp}/c . In alkali, the addition of either salt causes a rapid diminution of η_{sp}/c , but with KI, the value never falls below that observed for amylose in water, as it does in the case of KCl. In view of the profound differences observed with these two salts, the effect of varying the cation and anion was investigated in more detail.

This effect was achieved by dissolving the amylose in a series of lithium, sodium and potassium salts (0.25 M) and varying the pH, whilst maintaining the salt concentration constant. In each case, the alkali added has a cation in common with the salt present. The resultant graphs are shown in *Figure 6* for lithium, sodium and potassium salts, respectively.

The graphs for the various salts are similar in form. It can be seen that (i) in each case, there is a minimum in η_{sp}/c of amylose at pH 12; (ii) in neutral solution, η_{sp}/c is greater in LiI, LiBr, NaI and KI than it is in water; (iii) in those salts which increase η_{sp}/c at neutral pH, the minimum at pH 12 is little different from the value in water, allowing for the dilution effect; (iv) in neutral solution, the presence of 0.25 M LiCl, NaF, NaCl, KF or KCl does not effect η_{sp}/c of amylose, whilst at pH 12, these salts cause η_{sp}/c to fall to values markedly lower than that observed in neutral solution; and (v) as the alkalinity is increased to values greater than pH 12, η_{sp}/c increases in all cases, and moreover, at this high pH, η_{sp}/c does not appear to be greatly affected by the nature of the anion.

DISCUSSION

We are concerned with two complex phenomena—the physical structures of the amylose solute and the water solvent—and the interrelation between them.

As stated earlier, our interpretation of hydrodynamic measurements is that in neutral, aqueous KCl solution, amylose is a random coil, effectively at its θ -temperature^{5,6}. In solvents such as formamide, dimethylsulphoxide and 0.15 M KOH, this random coil undergoes solvent expansion¹⁷, but maintains the same basic backbone structure, i.e. long-range interactions increase, but the short-range forces do not change. This model effectively precludes the so-called 'interrupted helix' advanced by Holló *et al*¹⁸, and by Rao and Foster⁴, in which the molecule is composed of long helical segments with short intermediate regions of random coil, the latter conferring on the macromolecule the flexibility necessary for it to conform to the Gaussian model. We have recently presented evidence¹⁹ to show that the addition of complexing agents such as butan-1-ol or iodine to an aqueous solution of amylose causes profound decrease in η_{sp}/c . This viscosity decrease is, in fact, to be expected, on the basis of theoretical calculations quoted by Brant and Min²⁰, when a molecule changes from a coiled to a helical conformation.

AMYLOSE IN AQUEOUS SOLUTION

Amylose in neutral aqueous solution might be expected to be helical for the macromolecule is highly stereospecific, and in poor solvents such polymers tend to assume the conformation of their crystalline state. In this case, a helical structure might be expected, therefore, because water is a thermodynamically ideal solvent for amylose. That this conformation is not adopted

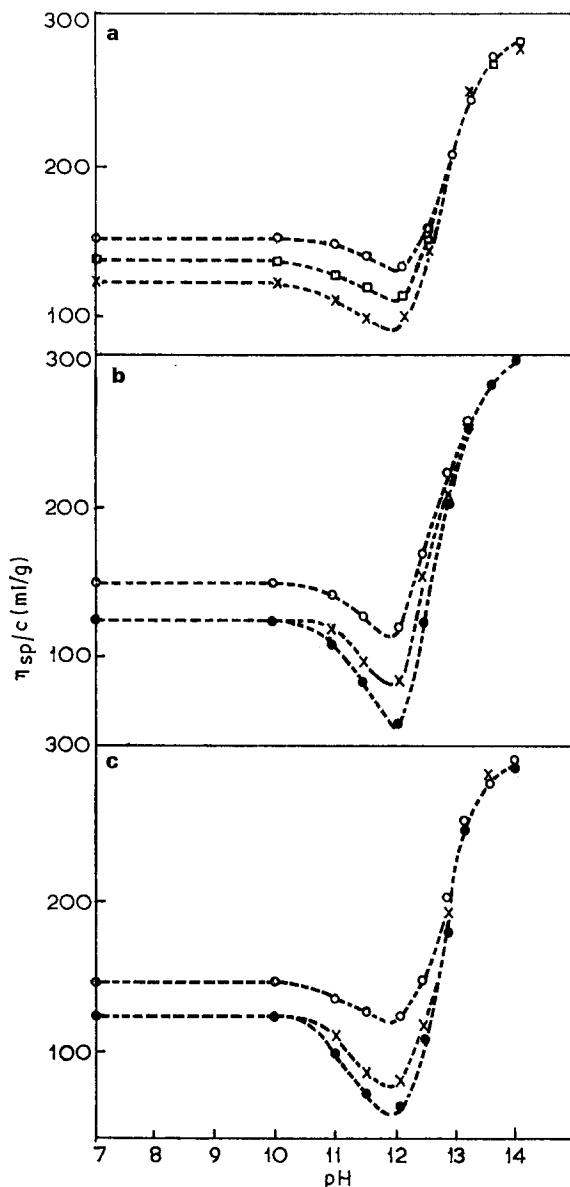


Figure 6 η_{sp}/c , the viscosity number of amylose, as a function of pH in (a) LiOH + 0.25 M lithium salts, (b) NaOH + 0.25 M sodium salts, and (c) KOH + 0.25 M potassium salts. The anions are F⁻ (●), Cl⁻ (×), Br⁻ (□), and I⁻ (○)

is due, we believe, to the properties of the core of the molecule when it takes up a helical form.

With the glucose units in the Cl conformation²¹, the amylose helix has all the hydroxyl groups on its external surface; the internal surface of the cavity is lined with CH-groups, and glycosidic oxygen atoms. We suggest that water cannot maintain its usual structure within the helix, and that to avoid a situation which is energetically unfavourable, amylose retains a random conformation. Support for this view has recently been supplied by Rees²² in a study relating the optical rotation of small sugars to their absolute conformation. His calculations show that on dissolving cyclohexa-amylose in water, the molecule adopts a strained conformation which is relaxed on the addition of a complexing agent to occupy the central cavity. One can readily imagine a similar phenomenon occurring in amylose, but in this case the increased flexibility of the linear molecule relative to the cyclic dextrin enables the polysaccharide to avoid the helical form.

The second complex phenomenon with which we must deal is that of the structure of water. Current thinking²³ appears to favour the mixture models, in which there may be water molecules involved in 4, 3, 2, 1, or 0 hydrogen bonds²⁴. Hydrogen bonding is thought to be a co-operative process²⁵ so that once two molecules associate in this fashion, the formation of large hydrogen-bonded clusters which are in dynamic equilibrium with monomeric water, is favoured. The equilibrium of this flickering cluster can be upset by the addition of solutes, some of which destroy the cluster (structure breakers), whilst others stabilize the clusters (structure makers). We suggest that the observed viscometric behaviour of amylose can be explained on the basis of alterations in the conformation of the polysaccharide as a result of the changes in the structure of its environment, water.

(1) *In neutral solution*

The interaction between amylose and water is most probably due to hydration of the -OH groups of the polysaccharide with free water molecules. Goring²⁶ has suggested that polysaccharides may be regarded as structure breakers, because the nature of the repeat unit is such as to exclude it from water clusters. If salts are added to the amylose solution, they will compete with the polysaccharide for the available water. As *Figure 4* shows, amylose must be regarded as having a higher affinity for water than does KCl, because $[\eta]$ remains constant over the entire solubility range of the salt. *Figures 5* and *6* show that, at a molarity of 0.25, none of the salts investigated is able to lower the η_{sp}/c of amylose relative to the value observed in water. However, as noted above, some salts are able to *increase* the value of η_{sp}/c relative to that in water, i.e. the salt medium is a better solvent for amylose than is water. This is particularly true when the iodide ion is present; η_{sp}/c in LiI, NaI and KI is about 150 ml/g, the value for water being 124 ml/g. We suggest that the explanation for this behaviour is that the iodide ion, because of its size, has the smallest charge/unit surface area of anions examined, and hence has the least effect in orienting the water molecules in its immediate vicinity. As a result, the -OH groups of the amylose can enter the hydration shell of the iodide ion, so that the solution behaviour of an

amylose-iodide complex is effectively being examined. The Br^- ion is capable of the same type of behaviour, but to a smaller degree (see *Figure 6a*). The charge/unit surface area is greater in this case, hence the degree of orientation required of the $-\text{OH}$ group if it is to enter the hydration shell is obviously greater. The $-\text{OH}$ group is attached to a rather bulky unit (the glucose residue) and therefore will find some difficulty in accommodating itself if a pronounced alignment is preferred. As the interaction between the anion and water molecules becomes more pronounced the necessary alignment becomes more difficult for the $-\text{OH}$ groups of the amylose. Thus one would expect that small anions such as F^- and Cl^- would be unable to share their hydration shells with the $-\text{OH}$ groups of amylose and would therefore not swell the polysaccharide molecule. This behaviour is observed (see *Figures 6a, 6b and 6c*).

We have stated earlier our belief that the nature of the helical cavity of amylose precludes its existence in water. Erlander²⁷ has shown that the presence of salts *reduces* the solubility of benzene in water, i.e. the solvent is less able to tolerate hydrophobic groups. Therefore, there is no reason to suppose that a helix should exist in any of the above salt solutions for no stabilizing influence has been introduced.

(2) *In alkaline solution*

The basic similarity of the curves in *Figure 3* shows that in alkaline solution the main contribution to the observed behaviour is made by the OH^- ion with superimposed minor differences which are attributable to the cation.

Although the dependence of $[\eta]$ of amylaceous polysaccharides on the concentration of alkali has long been known²⁸, the present work was the first detailed study* of the viscometric behaviour of amylose in alkali. It has long been recognised that, as the pH is increased amylose will act as a weak acid by virtue of its $-\text{OH}$ groups ionizing³². Reeves³³ postulated that the ionization was accompanied by a change in the conformation of the constituent anhydroglucose monomer units. Holló *et al*³⁴ whilst rejecting the possibility of dissociation of the hydroxyl groups of amylose did suggest that conformational changes occurred within the glucose ring as a result of the interaction with OH^- ions. Calculations by Burchard³⁵ have shown that the dimensions of the amylose molecule are grossly dependent on the conformation of the individual glucose units, hence this could provide an explanation for the change in $[\eta]$ or $[\eta]_{sp}/c$ with pH. However, n.m.r. studies^{36,37} have failed to detect any change in the conformation of the glucose residues with change in alkali concentration. The change in hydrodynamic volume of amylose with pH cannot therefore be due to conformational changes in the monomer units.

The most probable explanation for the increase in viscosity with pH is coulombic repulsion³⁸—the alkali induces charges on the polysaccharide by ionizing the hydroxyl groups³⁹, and these charges are mutually repulsive.

* This work has been presented at a number of conferences^{29,30}, and discussed briefly earlier³¹

The tendency of the charged groups to maintain a maximum separation from each other will deny the macromolecule its more compact conformations, and hence $[\eta]$ or η_{sp}/c will increase.

It is to be expected that as the concentration of gegen ion is increased, a masking effect will occur, and the polyelectrolyte structure will tend to collapse. In the case of amylose, this effect becomes important at an alkali concentration of 0.15 M (at which a maximum in viscosity is observed).

The above explanation satisfies the general shape of the graphs of η_{sp}/c as a function of pH for the various alkalis (*Figure 3*). It is now necessary to explain why the effect of KOH differs from that of LiOH and NaOH. As noted above, we are dealing with a reaction of the type



The RO^- anion will be able to form salts with the cation. However, assuming that the solubility of $\text{RO}^- \text{A}^+$, where A^+ is Li^+ , Na^+ or K^+ , is in the same order as the corresponding hydroxides, the viscosity would be expected to decrease in the order $\text{K}^+ > \text{Na}^+ > \text{Li}^+$, i.e. the lowest viscosity at a given concentration of alkali should occur in LiOH, which has the lowest solubility. Also, since the solubilities (molar) of LiOH:NaOH:KOH are approximately in the ratio of 1:3:4, NaOH and KOH should lead to similar viscosity behaviour of the amylose. This, in fact, is not the case.

Since the variations in behaviour cannot be due to the formation of a polyelectrolyte salt, it is highly likely that the explanation is to be found in the changing nature of the solvent with increasing alkali concentration. *Figure 7* shows the graph of a viscosity function of the solvent related to the pH of the medium. Variations in flow time first become apparent at pH 11–12; both

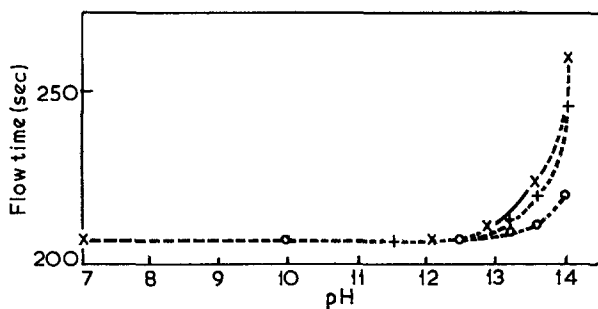


Figure 7 Solvent flow times as a function of pH for LiOH (\times), NaOH ($+$) and KOH (\circ)

LiOH and NaOH are much more effective in increasing the viscosity of water than is KOH. On the basis of the general rule that 'like dissolves like', it is not surprising that the viscosity of the amylose polyelectrolyte should be greater in a solvent medium which has more pronounced polyelectrolyte character of its own.

The behaviour of amylose in TMAH, in which there is a fairly rapid increase in viscosity between 10^{-4} and 0.15 M TMAH with a subsequent slow increase suggests that the cation masking effect is not so pronounced in this solvent i.e. the positive charges are not localized to the same extent as with the

inorganic alkalis at the site of the induced charge on amylose. This is probably due to the nature of the cation — the tetramethylammonium ion should be capable of hydrophobic bonding.

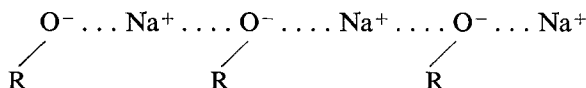
(3) *Alkaline solution in the presence of salt*

As noted above, in the presence of salt, a minimum in the viscosity is observed at pH 12. The salts may be divided into two groups, (a) those which reduce the viscosity to that observed in water, and (b) those which reduce it to appreciably lower values. The latter present a particularly perplexing problem.

The phenomenon was first reported by Rao and Foster⁴ and explained by them as a result of a helix to random coil conversion. Later, it was shown²⁹⁻³¹ that this behaviour did not arise as the result of the alkali *per se*, but rather as a consequence of the adventitious presence of KCl. Erlander and Purvinas⁴⁰ confirmed that supporting electrolyte was necessary for the decrease in viscosity to occur, but only slightly modified the explanation of Rao and Foster by suggesting that the OH⁻ ions served two functions, namely to break the hydrogen bonds between the C₂-C'₃ hydroxyl groups⁴¹ (which are supposed to stabilize the helix), so causing the molecule to contract, and as ionizing hydroxyl groups with subsequent molecular expansion due to coulombic repulsion. The latter cannot occur in the presence of supporting electrolyte, hence we observe only the change due to the destruction of hydrogen bonding and the subsequent disappearance of the helical structure. However, this explanation is based on the assumptions that amylose in water is in the helical state, that helicity results from hydrogen bondings, and that the dimension of the random coil are less than those of the helix. We have provided strong experimental evidence^{6,19,42,43} to show that all three assumptions are wrong.

The addition of complexing agents such as iodine or butan-1-ol to amylose in water leads to a decrease in viscosity¹⁹; a similar effect is achieved on adding butan-1-ol to amylose in alkali. We therefore conclude that when the viscosity of amylose falls significantly below that observed for water, the polysaccharide has adopted a helical conformation. Therefore, at pH 12 in the presence of LiCl, NaF, NaCl, KF and KCl, the macromolecule favours the helical state. The minimum value of η_{sp}/c varies somewhat depending on the nature of the salt, showing that different degrees of helicity must be present.

The stabilization of the helix is, we believe, due to ionic bonding. Doppert and Staverman³⁹ have shown that the pK value for the ionization of the hydroxyl groups is 12.7. Thus at pH 12, approximately one anhydroglucose unit in every five or six is ionized, i.e. one monomer unit per helical turn. We suggest that the ionic bonding takes the form



thus tending to stabilize a regular structure. (The groups R are in the same macromolecule and adjacent in space when amylose is helical). As already indicated, the conformation of minimum energy for amylose is the

helix, and the reason that it does not assume this state in water is that the hollow core cannot be accepted into the solvent structure. This type of ionic bonding would obviously provide an additional stabilizing force for the helix. Also, the structure of the solvent is different in this region from that found in water — the flickering clusters must now accommodate the negatively charged hydroxyl groups. The latter have a fairly small crystal radius, and hence there is a high degree of orientation of water molecules at their surfaces. This, of course, is equally true of other small anions such as F^- , but in the case of OH^- there is the additional factor that the negative charge is practically unlocalized within the primary hydration sphere. Thus it is possible that the changing nature of the solvent also contributes to the stabilization of the helix.

There are differences in the minimum values of η_{sp}/c , depending on the nature of the supporting electrolyte. For a series of salts having as a common anion Cl^- , the minimum values of η_{sp}/c are found to be in the order $Li^+ > Na^+ > K^+$. One would expect the postulated co-operative ionic bonding to be reduced if there is a pronounced tendency for the cation to be localized. We have already suggested that the most stable salt would be expected to be $ROLi$ (on the basis of the solubility of the hydroxide series), then $RONa$ and finally ROK , with quite small differences between the last two. This, in fact, is the order observed experimentally.

The nature of the anion also considerably influences the conformation of the amylose. For a series of sodium salts, the minimum value of η_{sp}/c is observed with NaF . This supports our view that the structure of the solvent is also important in stabilizing the helix—the F^- ion with its strongly oriented monolayer of hydration (A-region) will exert little effect on the structure of the solvent, whereas the larger anions, which have only B-regions (or negatively hydrated water), will tend to destroy solvent structure. Thus one may account qualitatively for the decrease in the viscosity of amylose to values lower than that observed in water.

The effect of those salts which do not decrease the viscosity of amylose to values lower than that in water will now be considered, i.e. $LiBr$, LiI , NaI and KI . Whilst all these salts give minimal viscosities at pH 12, the absolute values show some variation, e.g. from 134 ml/g for LiI to about 115 ml/g for $LiBr$, NaI , and KI ; the initial value of η_{sp}/c for this amylose in water is 124 ml/g, but carrying out a dilution analogous to that required in obtaining pH 12 yields a value of 116 ml/g. We have suggested earlier that I^- (or Br^-) might share its hydration shell with the hydroxyl groups of amylose. This, however, will not be possible once the polymer starts to ionize—the ionized OH^- groups on the polysaccharide will repel the negatively charged I^- ions. Hence the viscosity of the amylose falls in the presence of the salt and the hydroxyl ion at pH 12. In the case of LiI , the formation of $ROLi$ rather than $RO^- Li^+$ sufficiently reduces the negative charge on the polymer for the I^- ion to again act as a 'solvent'. The net charge on the polymer in the case of NaI and KI is sufficiently large to prevent this type of solvation, hence the viscosity falls to the value observed for water. The other effect of the I^- ion is to alter the structure of the solvent by virtue of its mono-molecular B-region. This change in solvent structure again forces the amylose to adopt a non-helical character.

As the pH is increased beyond 12, the nature of the supporting electrolyte plays progressively less part in determining η_{sp}/c . Thus, the important factor is the concentration of alkali. Whilst η_{sp}/c increases consistently in the region of pH 12–14, it is always less than the corresponding value in the absence of salt. Moreover, increasing the concentration of salt decreases η_{sp}/c . In this region of increasing viscosity, the nature of both the amylose and the solvent is changing, both becoming more polyelectrolyte in character. These changes are such as to favour the extended conformation rather than the helix.

Our view of amylose in aqueous solution as a non-helical polymer is confirmed by the work of Maywald *et al*⁴⁴ and of Dintzis and Tobin⁴⁵. The former carried out a viscosity study of amylose, amylopectin and glycogen in aqueous solution, over a wide temperature range, and could find no evidence of a helix–coil transition, which might be expected if the polymer were helical in water at room temperature. These workers also confirmed the form of the viscosity–pH graphs in the absence and presence of supporting electrolyte. However, for pH 12 in the presence of KCl they suggest only that the polysaccharide has undergone molecular aggregation. Dintzis and Tobin⁴⁵ measured the optical rotation of amylose in water, over a wide temperature range, and also failed to detect any helix–coil transformation.

The concept of the dissolved amylose macromolecule presented in this work is capable, we believe, of explaining its solution behaviour in a variety of solvents.

*Department of Chemistry,
University of Edinburgh,
Edinburgh, EH9 3JJ, UK*

W. Banks, D. J. Hourston and A. R. Procter

*Flour Milling & Baking Research Association,
Chorleywood, Rickmansworth,
Hertfordshire, WD3 5SH, UK*

*C. T. Greenwood
(Received 1 March 1971)
(Revised 6 May 1971)*

REFERENCES

- 1 Hanes, C. S. *New Phytologist* 1937, **36**, 189
- 2 Freudenberg, K., Schaaf, E., Dumpert, G. and Ploetz, T. *Naturwissenschaften* 1939, **27**, 850
- 3 Rundle, R. E. and French, D. J. *Amer. Chem. Soc.* 1943, **65**, 558
- 4 Rao, V. S. R. and Foster, J. F. *Biopolymers* 1963, **1**, 527
- 5 Banks, W. and Greenwood, C. T. *Makromol. Chem.* 1963, **67**, 49
- 6 Banks, W. and Greenwood, C. T. *Carbohydrate Res.* 1968, **7**, 349
- 7 Banks, W. and Greenwood, C. T. *European Polymer J.* 1969, **5**, 649
- 8 Banks, W., Greenwood, C. T. and Muir, D. D. *Stärke* 1971, **23**, 118
- 9 Banks, W. and Greenwood, C. T. *Stärke* 1967, **19**, 197
- 10 Banks, W., Greenwood, C. T. and Khan, K. M. *Stärke* 1970, **22**, 292
- 11 Greenwood, C. T., Hourston, D. J. and Procter, A. R. *European Polymer J.* 1970, **6**, 293
- 12 Adkins, G. K., Banks, W., Greenwood, C. T. and MacGregor, A. W. *Stärke* 1969, **21**, 57
- 13 Banks, W., Greenwood, C. T. and Khan, K. M. *Carbohydrate Res.* 1970, **12**, 79
- 14 Whistler, R. L. and Johnson, C. *Cereal Chem.* 1948, **25**, 418

- 15 Wolff, I. A., Gundrum, L. J. and Rist, C. E. *J. Amer. Chem. Soc.* 1950, **72**, 518
- 16 Bottle, R. T., Gilbert, G. A., Greenwood, C. T. and Saad, K. H. *Chem. and Ind.* 1953, p 541
- 17 Banks, W. and Greenwood, C. T. *Carbohydr. Res.* 1968, **7**, 414
- 18 Holló, J. and Szejtli, J. *Stärke* 1958, **10**, 49
- 19 Banks, W. and Greenwood, C. T. *Polymer, Lond.* 1971, **12**, 141
- 20 Brant, D. A. and Min, B. K. *Macromolecules* 1969, **2**, 1
- 21 Greenwood, C. T. and Rossotti, H. J. *Polym. Sci.* 1958, **27**, 481
- 22 Rees, D. A. *J. Chem. Soc. (B)* 1970, p 877
- 23 Blandamer, M. J. *Quart. Rev.* 1970, **24**, 169
- 24 Nemethy, G. and Scheraga, H. A. *J. Chem. Phys.* 1967, **36**, 3382
- 25 Frank, H. S. and Wen, W. Y. *Discuss. Faraday Soc.* 1957, **24**, 133
- 26 Goring, D. A. I. *Pulp Paper Mag. Canada* 1966, **67**, T 519
- 27 Erlander, S. R. and McGuire, J. P. *J. Macromol. Sci.* 1968, **A2**, 859
- 28 Koets, P. and Kruyt, H. R. *Kolloid Chem. Beih.* 1937, **47**, 100
- 29 Geddes, R., Greenwood, C. T. and Procter, A. R. *Abstr. International Symposium on Carbohydrate Chem.*, Munster, 1964, p 26
- 30 Geddes, R., Greenwood, C. T. and Procter, A. R. *Abstr. 13th Canadian High Polymer Forum*, Ottawa, 1965, p 17
- 31 Banks, W. and Greenwood, C. T., 'Conformation of Biopolymers' (Ed., G. N. Ramachandran) Academic Press, 1967, p 739
- 32 Saric, S. P. and Schofield, R. K. *Proc. Roy. Soc. (A)* 1946, **185**, 431
- 33 Reeves, R. E. *J. Amer. Chem. Soc.* 1954, **76**, 4595
- 34 Holló, J., Szejtli, J. and Toth, J. *Stärke* 1961, **13**, 222
- 35 Burchard, W. *Makromol. Chem.* 1960, **42**, 151
- 36 Rao, V. S. R. and Foster, J. F. *J. Phys. Chem.* 1965, **69**, 636, 656
- 37 Geddes, R., PhD Thesis, Edinburgh, 1965
- 38 Overbeek, J. Th. G. and De Jong, H. G. B., 'Colloid Science' Elsevier, 1949, Vol 2, p 209
- 39 Doppert, H. L. and Staverman, A. J. *J. Polym. Sci. (A-1)* 1966, **4**, 2367
- 40 Erlander, S. R. and Purvinas, R. M. *Stärke* 1968, **20**, 37
- 41 Casu, B., Reggiani, N., Gallo, G. G. and Vigevani, A. *Tetrahedron* 1966, **22**, 3061
- 42 Banks, W. and Greenwood, C. T. *Carbohydrate Res.* submitted for publication
- 43 Banks, W. and Greenwood, C. T. *Biopolymers* in press
- 44 Maywald, E. C., Leach, H. W. and Schoch, T. J. *Stärke* 1968, **20**, 189
- 45 Dintzis, F. R. and Tobin, R. *Biopolymers* 1969, **7**, 581

Polymer chain extension produced by impinging jets and its effect on polyethylene solution

F. C. FRANK, A. KELLER and M. R. MACKLEY

Longitudinal velocity gradients in a flowing system have a powerful, molecular weight dependent orienting influence on macromolecules. A system of impinging jets has been constructed for the in situ observation of this phenomenon in two simple, analysable flow patterns, corresponding to uniaxial extension and compression. The system studied was polyethylene in a solution of xylene. Up to a limiting temperature (108–112°C dependent on the molecular weight) fibrous crystallization was observed in a predictable manner. Above this temperature strong transient birefringence was seen in the regions of extensional flow which disappeared when the flow ceased, the phenomenon persisting up to 200°C the highest temperature examined. There is a sharp lower concentration limit for this effect indicative of a cooperation between molecules. Implications of these observations for chain extension, crystallization, technical flow processes and for molecular entanglements in solution are indicated.

THE IMPORTANCE of purely extensional flow for the achievement of large extensions of polymer chains has been pointed out by Ziabicki¹, Peterlin², Pennings³ and Frank⁴. The extension achieved with a strain rate $\dot{\epsilon}(t)$ is essentially

$$\int_0^{\infty} \dot{\epsilon}(t - \tau) \exp(-\tau/\tau_1) d\tau$$

where τ_1 is the gravest mode relaxation time for recovery of random coil configuration. In simple shear processes, as in any ordinary viscometer, any fluid element rotates relative to the axes of strain, with a rotation rate ω equal to the strain rate $\dot{\epsilon}$: hence the strain rate in the fluid element changes sign before a large elongation has been achieved—the integral can approach but cannot exceed unity. Large extension of the chain molecules from the random coil configuration can only be attained in strain processes free from this rotation. Extensional flow of this kind occurs in fibre spinning, but the strain rate is not large, and generally of the order 10 s^{-1} (whereas viscometers attain simple shear strain rates exceeding 10^4 s^{-1}).

A way of achieving a large strain rate free from rotation is to let two opposed fluid jets meet as shown in *Figure 1*. If the two jets have velocity V and diameter d , the velocity on the axis falls from V to zero in a distance of about $d/2$, making a strain rate $\dot{\epsilon}$ of about $-2V/d$ e.g. $8 \times 10^3 \text{ s}^{-1}$ for $V = 2 \text{ m s}^{-1}$, $d = 0.5 \text{ mm}$. High strain rates of this order occur on and near the axis of symmetry and the plane of symmetry of the system. On the axis and plane of symmetry the rotation rate is zero. The time of passage t_p through the region of high strain rate decreases with distance from the axis, becoming of order d/V , giving a product $\dot{\epsilon}t_p$ limited to the order of magnitude unity; but the

time of passage for an axial fluid element becomes in principle infinite because there is a point of zero velocity at the centre of symmetry of the system, so that for fluid elements entering along the axis there is no limit to this product, and molecules in the axial stream become highly extended provided only that $V\tau_1/d$ is large. The same considerations apply to the reverse flow obtainable by

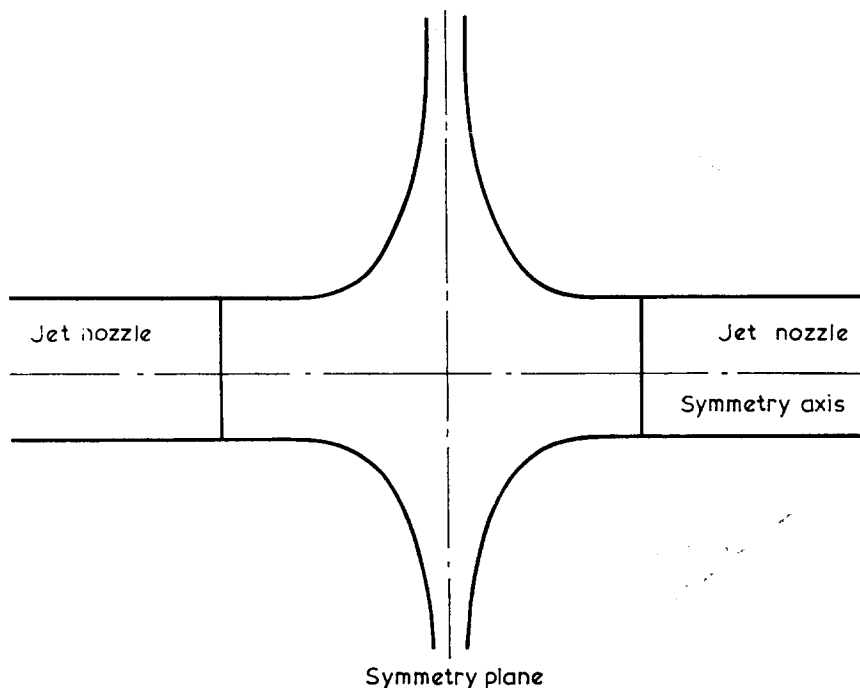


Figure 1 Line drawing of flow produced by impinging jets

sucking on the two jets immersed in a body of fluid. In the case first described (case 1) the extension produced at the symmetry point of the system is biaxial in the symmetry plane: in the reverse case (case 2) it is uniaxial, along the symmetry axis.

Exact analysis of such a flow system cannot be easy, particularly because flow will necessarily be non-Newtonian as soon as appreciable molecular extension occurs: however for the essential validity of the arguments we require only that the flow system retains its symmetry properties, which is a reasonable anticipation in such a highly symmetrical system.

Experiments have been conducted using the apparatus shown in *Figure 2*. The reflux bath with two optically flat observation windows recessed into the walls and the two tubes holding each jet were made from glass. The jets themselves were stainless steel hypodermic needles bent in the form shown in the diagram. Jets of internal diameter varying from 0.5 mm to 1.0 mm were used with a jet separation of between 0.5 mm and 3.0 mm. Alignment of the jets was found to be very critical, particularly in case 1, and very careful adjustment of the jet tubes was necessary to obtain a symmetrical flow

POLYMER CHAIN EXTENSION PRODUCED BY IMPINGING JETS

pattern. The system was kept at any required temperature by refluxing an appropriate fluid at atmospheric or reduced pressure in the outside jacket of the apparatus. Optical observations were made using a polarizing microscope with the polarizer and analyser generally crossed at 45° to the symmetry axis between the jets.

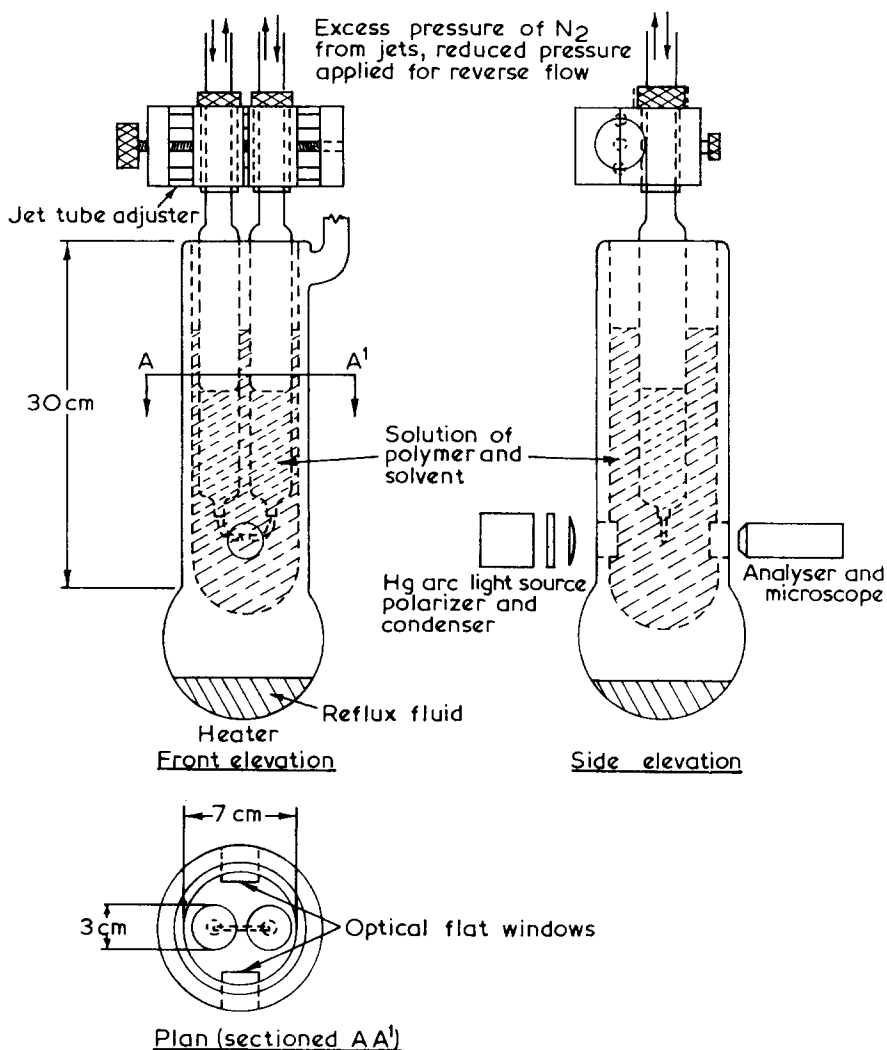


Figure 2 Diagram of apparatus

For case 1, where the two opposed fluid jets meet, an excess pressure of nitrogen was applied to the two jet tubes. For the reverse situation, case 2, where fluid is sucked into the jets from the surrounding medium, a reduced pressure was applied to the tubes. In either case the volumetric flow rate out of or into the jets could be calculated from the observed rate of change of the fluid level in the tubes.

Experiments were conducted using high density linear polyethylene: Rigidex type 2, $\bar{M}_n = 27500$, $\bar{M}_w = 202000$. Concentrations of 0.5–5% g/ml were used with xylene or diphenyl ether as solvent.

Fibrous crystallization was readily observed up to temperatures of 108°C in a xylene solution of 5% concentration. The upper temperature limit was not established conclusively. Amongst other factors, this was found to depend on the time the solution was kept at the elevated temperature: a feature which is indicative of the effect of degradation, which in turn underlines the role played by the longest molecules in the molecular weight distribution. From preliminary observations it has also been found that the upper temperature limit can be increased to 112°C by using a high molecular weight polyethylene: Hostalen GUR, $\bar{M}_w = 1.5 \times 10^6$.

The amount of crystallization at any given temperature increased with increasing applied strain rate. Optically detectable deposits of fibrous material could be seen for strain rates in excess of 2000 s^{-1} . For case 1, crystallization appeared along a sharply defined line of 3 mm length on the symmetry plane of the system with indications that what was observed was a disc seen in edge-on view; when the flow terminated the disc collapsed. For case 2, crystallization appeared along the symmetry axis: in this instance, when flow terminated, the fibres remained bridges between the jet nozzles as shown in *Figure 3*. The fibres themselves were observed to be birefringent along this

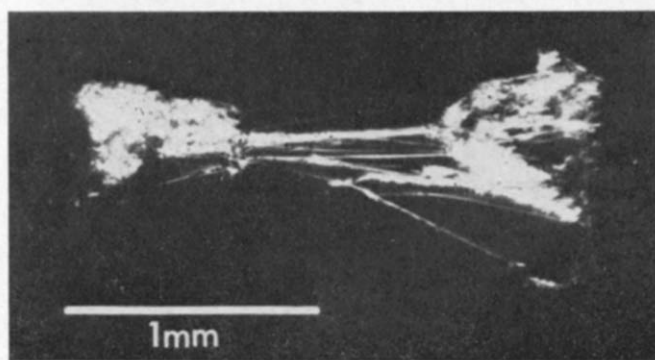


Figure 3 Photograph with polaroids crossed at 45° to the symmetry axis, of fibres remaining bridged between the jets after crystallization at 108°C from a 5% polyethylene solution

axis. A detailed study of these fibrous structures will be given in a later communication.

For each respective flow system crystallization was observed to take place in areas of rotation free longitudinal elongation and this may be taken as direct confirmation of Pennings³ conclusions that extensional flow is the essential cause of fibrous crystallization.

In addition: above the temperature where crystallization was seen to be stable a birefringence was observed when the fluid in the system was in motion. The effect was transient and disappeared on the cessation of flow. The birefringence appeared as a disc in the symmetry plane in case 1 and as a cylinder along the symmetry axis in case 2, as shown in *Figures 4* and *5*

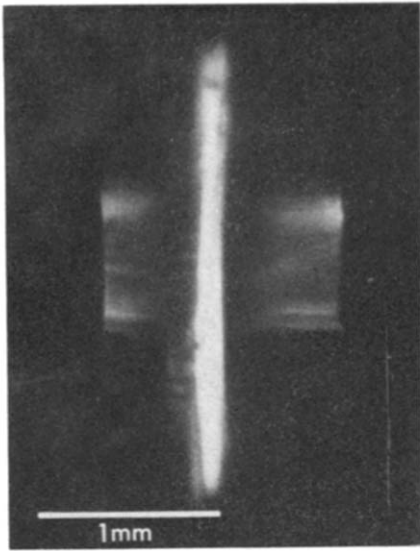


Figure 4 Birefringence observed with polaroids crossed at 45° to the symmetry axis for case 1 where the jets of fluid impinge. Photograph taken at 124°C for a 5% polyethylene solution

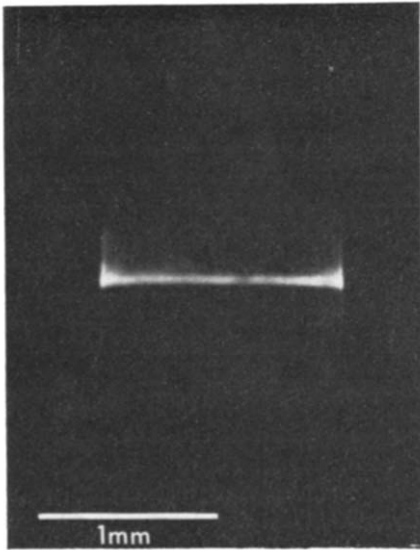


Figure 5 Birefringence observed with polaroids crossed at 45° to the symmetry axis for case 2, where the fluid is sucked into the jets. Photograph taken at 124°C for a 5% polyethylene solution

respectively. This birefringence was observed to persist at all temperatures tested; up to 200°C in a diphenyl ether solution. The same features, namely a disc on the symmetry plane in case 1 and an axial line in case 2, could be seen when either one or both polaroids were removed. (*Figure 6* where the disc

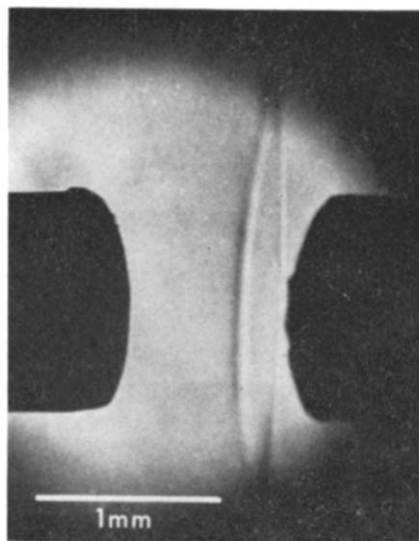


Figure 6 Oblique view of bright field contrast observed for case 1, at 124°C for a 5% polyethylene solution. No polaroids

shape is apparent from the off-axial view, and *Figure 7*). Here the visibility appears to be due to a difference in refractive index between the distinct regions and their surroundings. The observed birefringence is unambiguously associated with the localized alignment of the macromolecules. This will also account for the bright field contrast, which is observed to decay in just about the same time as the birefringence if the flow is stopped. Care has to be taken here to limit observations to the time in which less than half of the content of the reservoir tubes of the jets has been expelled. If more than half has been expelled, the bright field contrast is more persistent. Tests with a drop of dye confirm that, when half is expelled, liquid initially at the top of the tube emerges from the bottom: such liquid can become more concentrated by evaporation.

The induced birefringence has a marked solution concentration dependence. No birefringence is seen for a solution of 1% concentration whereas it is clearly seen for a concentration of 2%. This cut off is much more definite than a mere reduction of intensity of birefringence by a factor of two. This suggests that we are not strongly aligning many single molecules in these conditions but rather entangled aggregates. Concerning this subject, further work on high molecular weight material appears desirable and is intended.

In conclusion it can be seen from the observations reported that the proposed flow system produced by two opposing jets gives a new and efficient

POLYMER CHAIN EXTENSION PRODUCED BY IMPINGING JETS

mechanism for aligning polymer chains. It induces a fibrous type of crystallization which is similar to that obtained in Pennings' stirrer experiment except that here it is achieved in a comparatively simple and thus analysable flow system. At higher temperatures pronounced transient chain orientation is

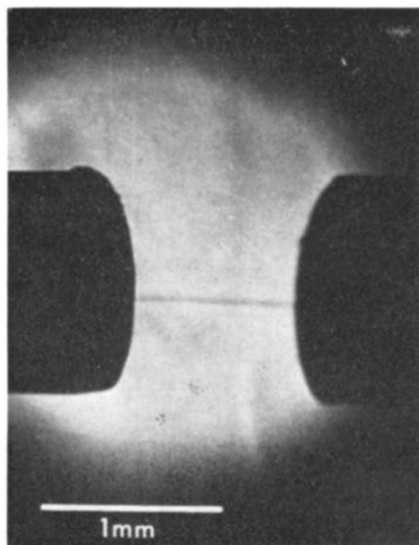


Figure 7. Oblique view of bright field contrast observed for case 2, at 124°C for a 5% polyethylene solution. No polaroids

observed which under our experimental conditions is readily observable owing to the localization of the elongational flow field.

Furthermore this method promises to give information on molecular entanglements and on the thermal degradation involving the longest molecules in a rather unconventional manner. Thus, in addition to any technological significance the system may have, it provides a new approach to the study of a number of fundamental aspects of macromolecules.

*H. H. Wills Physics Laboratory,
University of Bristol, Bristol, UK*

(Received 15 March 1971)

REFERENCES

- 1 Ziabicki, A. *J. Appl. Polym. Sci.* 1959, **2**, 14, 24
- 2 Peterlin, A. *J. Polym. Sci. (B)* 1966, **4**, 287
- 3 Pennings, A. J., Van der Mark, J.M.A.A. and Booij, H.C. *Kolloid Z.u.Z. für Polymer* 1970, **236**, 99
- 4 Frank, F. C. *Proc. Roy. Soc., Lond.* 1970, **A319**, 127

Book Reviews

Industrial Rheology

by PHILLIP SHERMAN

Academic Press, London and New York, 1970, 423 pp, £7

This book is intended as a practical introduction to industrial rheology including recent advances, both pure and applied. It is written with the rheological problems of the food, pharmaceutical and cosmetic industries especially in mind. Since no single individual can be expert in all these areas the treatment of the subject necessarily has to be selective.

The book is aimed at workers in industry having no previous knowledge of rheology or its mathematical bases. Some parts of the book are more advanced mathematically than appears to the author. Chapters 1 and 2 cover nomenclature and general theory, and methods, respectively, and provide a compact and effective introduction to the whole subject. The other four chapters deal with dispersed systems, foodstuffs, pharmaceuticals and cosmetics, and the correlation between rheological and sensory assessments of consistency. Throughout the book there are many highly informative tables which summarize various topics. Examples include the principles underlying different types of viscometers, and the logical bases of two forms of texture profile. Copious and effective use is made of illustrations of the various specialised rheological instruments and the type of data obtained with these instruments are presented graphically.

The contents are set out in considerable detail. Extensive author and subject indexes provide a means of tracing most special topics.

The bibliographies at the end of each chapter would have been much more helpful if they had included full titles of the journal articles referred to instead of using the abbreviated form, omitting titles, common in many journals. A glossary of nomenclature nearly 14 pages in length is included at the end of the book.

The author's professional interests are especially oriented towards analysis and measurement. The correlation between rheological measurements and related forms of sensory evaluation is discussed mainly in terms of his special interests. Particular attention is devoted to a system of texture profiles proposed by Dr A. S. Szczesniak and the author's proposed modification of the system. The treatment of particular commodities also varies in length and depth. 'Industrial rheology' by Dr Philip Sherman provides a valuable addition to the literature. It will be much used as a source of reference and, depending upon the user's interests, sections of the book will be used as a text book. The book is well written and well produced. At £7 it may be too expensive for some individual readers who are interested, but the price is comparable with that of other contemporary texts similar in scope and form of presentation.

ROLAND HARPER

Techniques and methods of polymer evaluation, Vol. 2

Thermal characterization

Edited by P. E. SLADE, JR. and L. T. JENKINS

Marcel Dekker, New York, 1970, 371 pp, £8-90, \$21-25

This volume reviews six areas in which the response of polymers to temperature change can be used to provide information about them. Each review is complete in itself, so that the volume is subject to the common criticism of review publications, i.e. that in order to acquire one essay which is particularly desired, it is necessary to pay also for several others. The six chapters of this book are in fact more closely related than is often the case. All are written from a practical viewpoint, presenting only the necessary theoretical background before dealing with experimental problems and results.

Five chapters are concerned essentially with physical properties. There is a particularly valuable review of stress-strain-temperature behaviour, covering both equilibrium and

time-dependent measurements: the introductory section on the relationships among the various quantities will be a great help to the uninitiated. Shorter chapters deal with differential scanning calorimetry, thermal conductivity and the effect of temperature on electrical conductivity. Another short chapter is devoted to the use of torsional braids as support for polymers which are not readily obtained in suitable form for physical testing. The remaining chapter is the second largest, and gives a detailed account of polymer identification by pyrolytic techniques incorporating gas chromatographic analysis of the products. This chapter, like the one on stress-strain behaviour, reports extensively on results obtained.

This volume deserves a place in any polymer library, but will be of greatest use in the laboratory.

G. GEE

Peptides: chemistry and biochemistry

Edited by BORIS WEINSTEIN and SAUL LAUDE

Marcel Dekker, New York, 1970, 538 pp, £9.30, \$19.50

This volume constitutes the proceedings of the First American Peptide Symposium, held at Yale University in August 1968. European peptide chemists have met regularly since 1958 and the proceedings of their symposia have, since 1962, also been published in book form, unfortunately under the very similar title of 'Peptides', a circumstance which seems likely to lead to considerable confusion in the literature and which ought to have been avoided. The European Peptide Symposia and the published proceedings have, without doubt, done much to stimulate research in the peptide field and the same will certainly be equally true of the American Symposia. Both groups invite a small number of their Transatlantic colleagues, a practice which serves to minimize what might otherwise become an unfortunate division.

The present volume, like its European predecessors, is valuable in bringing a collection of papers by leading workers before a wider audience than that provided by those actually attending the Symposium. It is divided into four sections, there being eight papers on peptide synthesis, nine on the relationships between structure and biological activity in peptides, six on racemization in peptide chemistry and nine on special problems in synthesis and analysis. Inevitably the nature, and to some extent the quality, of the contributions vary but all are worth reading and all bring something new to the subject. This book is a notable addition to the literature of peptide chemistry. It is primarily for experts and will be essential reading for them. The proceedings of the 1970 American Symposium will be awaited with interest.

H. N. RYDON

Biologische Zerstörung der makromolekularen Werkstoffe

by HANS H. M. HALDENWANGER

Springer-Verlag, Berlin, Heidelberg, New York, 1970, 283 pp, DM58, \$16

The aim of this work is to summarize the literature relating to biological attack on polymeric materials, for the benefit of chemists and technologists in the rubber, plastics and allied industries. The available information is scattered in books and the journals of several disciplines, and to bring this material together in one place should serve a useful purpose.

Book Reviews

Industrial Rheology

by PHILLIP SHERMAN

Academic Press, London and New York, 1970, 423 pp, £7

This book is intended as a practical introduction to industrial rheology including recent advances, both pure and applied. It is written with the rheological problems of the food, pharmaceutical and cosmetic industries especially in mind. Since no single individual can be expert in all these areas the treatment of the subject necessarily has to be selective.

The book is aimed at workers in industry having no previous knowledge of rheology or its mathematical bases. Some parts of the book are more advanced mathematically than appears to the author. Chapters 1 and 2 cover nomenclature and general theory, and methods, respectively, and provide a compact and effective introduction to the whole subject. The other four chapters deal with dispersed systems, foodstuffs, pharmaceuticals and cosmetics, and the correlation between rheological and sensory assessments of consistency. Throughout the book there are many highly informative tables which summarize various topics. Examples include the principles underlying different types of viscometers, and the logical bases of two forms of texture profile. Copious and effective use is made of illustrations of the various specialised rheological instruments and the type of data obtained with these instruments are presented graphically.

The contents are set out in considerable detail. Extensive author and subject indexes provide a means of tracing most special topics.

The bibliographies at the end of each chapter would have been much more helpful if they had included full titles of the journal articles referred to instead of using the abbreviated form, omitting titles, common in many journals. A glossary of nomenclature nearly 14 pages in length is included at the end of the book.

The author's professional interests are especially oriented towards analysis and measurement. The correlation between rheological measurements and related forms of sensory evaluation is discussed mainly in terms of his special interests. Particular attention is devoted to a system of texture profiles proposed by Dr A. S. Szczesniak and the author's proposed modification of the system. The treatment of particular commodities also varies in length and depth. 'Industrial rheology' by Dr Philip Sherman provides a valuable addition to the literature. It will be much used as a source of reference and, depending upon the user's interests, sections of the book will be used as a text book. The book is well written and well produced. At £7 it may be too expensive for some individual readers who are interested, but the price is comparable with that of other contemporary texts similar in scope and form of presentation.

ROLAND HARPER

Techniques and methods of polymer evaluation, Vol. 2

Thermal characterization

Edited by P. E. SLADE, JR. and L. T. JENKINS

Marcel Dekker, New York, 1970, 371 pp, £8-90, \$21-25

This volume reviews six areas in which the response of polymers to temperature change can be used to provide information about them. Each review is complete in itself, so that the volume is subject to the common criticism of review publications, i.e. that in order to acquire one essay which is particularly desired, it is necessary to pay also for several others. The six chapters of this book are in fact more closely related than is often the case. All are written from a practical viewpoint, presenting only the necessary theoretical background before dealing with experimental problems and results.

Five chapters are concerned essentially with physical properties. There is a particularly valuable review of stress-strain-temperature behaviour, covering both equilibrium and

time-dependent measurements: the introductory section on the relationships among the various quantities will be a great help to the uninitiated. Shorter chapters deal with differential scanning calorimetry, thermal conductivity and the effect of temperature on electrical conductivity. Another short chapter is devoted to the use of torsional braids as support for polymers which are not readily obtained in suitable form for physical testing. The remaining chapter is the second largest, and gives a detailed account of polymer identification by pyrolytic techniques incorporating gas chromatographic analysis of the products. This chapter, like the one on stress-strain behaviour, reports extensively on results obtained.

This volume deserves a place in any polymer library, but will be of greatest use in the laboratory.

G. GEE

Peptides: chemistry and biochemistry

Edited by BORIS WEINSTEIN and SAUL LAUDE

Marcel Dekker, New York, 1970, 538 pp, £9.30, \$19.50

This volume constitutes the proceedings of the First American Peptide Symposium, held at Yale University in August 1968. European peptide chemists have met regularly since 1958 and the proceedings of their symposia have, since 1962, also been published in book form, unfortunately under the very similar title of 'Peptides', a circumstance which seems likely to lead to considerable confusion in the literature and which ought to have been avoided. The European Peptide Symposia and the published proceedings have, without doubt, done much to stimulate research in the peptide field and the same will certainly be equally true of the American Symposia. Both groups invite a small number of their Transatlantic colleagues, a practice which serves to minimize what might otherwise become an unfortunate division.

The present volume, like its European predecessors, is valuable in bringing a collection of papers by leading workers before a wider audience than that provided by those actually attending the Symposium. It is divided into four sections, there being eight papers on peptide synthesis, nine on the relationships between structure and biological activity in peptides, six on racemization in peptide chemistry and nine on special problems in synthesis and analysis. Inevitably the nature, and to some extent the quality, of the contributions vary but all are worth reading and all bring something new to the subject. This book is a notable addition to the literature of peptide chemistry. It is primarily for experts and will be essential reading for them. The proceedings of the 1970 American Symposium will be awaited with interest.

H. N. RYDON

Biologische Zerstörung der makromolekularen Werkstoffe

by HANS H. M. HALDENWANGER

Springer-Verlag, Berlin, Heidelberg, New York, 1970, 283 pp, DM58, \$16

The aim of this work is to summarize the literature relating to biological attack on polymeric materials, for the benefit of chemists and technologists in the rubber, plastics and allied industries. The available information is scattered in books and the journals of several disciplines, and to bring this material together in one place should serve a useful purpose.

BOOK REVIEWS

Problems of biological attack have existed longer for natural polymers such as cellulose, rubber, wool and leather than for the newer synthetic materials, and are also likely to be intrinsically more severe for the former. It is therefore natural that a large part of the material relates to natural polymers and their derivatives; the relatively small amount of information specific to fully synthetic polymers is presented against this background.

The variety of the organisms that attack polymers in various environments is remarkable. Bacteria and fungi are omnipresent; in the sea, molluscs bore and barnacles encrust; on land, insects of many species ranging from earwigs to termites and wasps chew, and rodents gnaw. Tests must be carried out with many kinds of organism, especially micro-organisms, and standard methods of testing are tabulated and described in some detail, together with recipes for culture media. The value of some of this detail is questionable, for surely anyone proposing to test according to a standard would consult the authoritative specification, rather than a secondary document.

There is much information about the susceptibility of polymeric materials including films and fibres to attack, and the effectiveness of protective agents; this is perhaps the most useful feature of the book. The full synthetic polymers are in general very resistant to microbial attack, and the author considers that effective disposal of plastics litter by trained bacteria is unlikely. But insects will bore through packaging films, not only of cellulose but also polyolefins, and even polystyrene and PVC.

This book is reasonably easy to read; the print is clear and I found the author's German easier to follow than some. The index is rather cursory.

The book was completed in 1967, and only 5 out of the 384 references date from that year. It is a pity that it has taken three years to get the book out; the half-life of the value of a literature survey cannot much exceed five years.

This is nevertheless a work that most technical libraries concerned with polymers, natural or synthetic, will need to possess. Few private purchasers would find it worth nearly £7.

P. A. SMALL

time-dependent measurements: the introductory section on the relationships among the various quantities will be a great help to the uninitiated. Shorter chapters deal with differential scanning calorimetry, thermal conductivity and the effect of temperature on electrical conductivity. Another short chapter is devoted to the use of torsional braids as support for polymers which are not readily obtained in suitable form for physical testing. The remaining chapter is the second largest, and gives a detailed account of polymer identification by pyrolytic techniques incorporating gas chromatographic analysis of the products. This chapter, like the one on stress-strain behaviour, reports extensively on results obtained.

This volume deserves a place in any polymer library, but will be of greatest use in the laboratory.

G. GEE

Peptides: chemistry and biochemistry

Edited by BORIS WEINSTEIN and SAUL LAUDE

Marcel Dekker, New York, 1970, 538 pp, £9.30, \$19.50

This volume constitutes the proceedings of the First American Peptide Symposium, held at Yale University in August 1968. European peptide chemists have met regularly since 1958 and the proceedings of their symposia have, since 1962, also been published in book form, unfortunately under the very similar title of 'Peptides', a circumstance which seems likely to lead to considerable confusion in the literature and which ought to have been avoided. The European Peptide Symposia and the published proceedings have, without doubt, done much to stimulate research in the peptide field and the same will certainly be equally true of the American Symposia. Both groups invite a small number of their Transatlantic colleagues, a practice which serves to minimize what might otherwise become an unfortunate division.

The present volume, like its European predecessors, is valuable in bringing a collection of papers by leading workers before a wider audience than that provided by those actually attending the Symposium. It is divided into four sections, there being eight papers on peptide synthesis, nine on the relationships between structure and biological activity in peptides, six on racemization in peptide chemistry and nine on special problems in synthesis and analysis. Inevitably the nature, and to some extent the quality, of the contributions vary but all are worth reading and all bring something new to the subject. This book is a notable addition to the literature of peptide chemistry. It is primarily for experts and will be essential reading for them. The proceedings of the 1970 American Symposium will be awaited with interest.

H. N. RYDON

Biologische Zerstörung der makromolekularen Werkstoffe

by HANS H. M. HALDENWANGER

Springer-Verlag, Berlin, Heidelberg, New York, 1970, 283 pp, DM58, \$16

The aim of this work is to summarize the literature relating to biological attack on polymeric materials, for the benefit of chemists and technologists in the rubber, plastics and allied industries. The available information is scattered in books and the journals of several disciplines, and to bring this material together in one place should serve a useful purpose.

An electron microscope study of the microstructure of some rubber-reinforced polystyrenes

J. D. MOORE

Rubber-reinforced polystyrenes were prepared by graft copolymerization using various butadiene polymers and copolymers. Electron microscopy showed that variations in the pre-polymerization temperature, composition of the rubber, and molecular weight of the rubber influenced the size and structure of the dispersed rubber particles. Microstructures and impact strengths comparable to those of commercial materials were obtained from a limited range of conditions. Solution styrene-butadiene copolymers and a polybutadiene of low molecular weight gave unusual microstructures although polystyrenes of inferior impact strength were obtained. A particle size of 2 μm or greater was required to obtain reasonable improvements in impact strength. The particle size increased with an increase in the initial viscosity of the rubber in styrene solution provided that rubber type and concentration, and pre-polymerization temperature were constant. The effects of these three variables on particle size could not be related to viscosity changes.

INTRODUCTION

GRAFT copolymerization in bulk of a minor proportion of an elastomer usually polybutadiene, with styrene leads to a two phase system with improved impact resistance (HIPS). Some variations in polymerization conditions are permitted although frequently the limitations of existing plant may impose some restrictions on this parameter. For example the preparation of so called 'concentrates', which are suitable for subsequent blending with crystal polystyrene, may be restricted if high viscosities are involved. It is therefore of interest to examine the behaviour of elastomers with varying molecular weight and chemical composition in this process, especially with regard to the concentration of the rubber and the pre-polymerization temperature. In addition since the measurement of the viscosity of a 5% wt/wt solution of the elastomer in styrene is a widely used quality control test for elastomer selection, the significance of the initial solution viscosity is examined.

EXPERIMENTAL

Materials

Commercially available and experimental grades of low *cis* polybutadienes, and copolymers of styrene and butadiene containing 24% bound styrene, were used as the elastomeric phase (*Table 1*). The polybutadiene component has a chain configuration of approximately: *cis*-1,4, 44%; *trans*-1,4, 48%; vinyl-1,2, 8%. Number average molecular weights (\bar{M}_n) were determined on a Mechrolab 501 membrane osmometer. Styrene, a technical grade sup-

Table 1 Molecular weight data for elastomers examined

<i>Elastomer (Polybutadiene)</i>	\bar{M}_n	<i>Elastomer</i>	\bar{M}_n
Intene* 35 SA	110 000	Polybutadiene A	70 000
Intene 35 NFA	120 000	Polybutadiene B	210 000
Intene 45 NFA	140 000	Duradene† SBR	130 000
Intene 55 NFA	170 000	Solution SBR B	220 000

*Trademark of The International Synthetic Rubber Company Ltd

†Trademark of the Firestone Synthetic Rubber and Latex Company

plied by Forth Chemicals, was used as received. Tertiary-dodecyl mercaptan was supplied by Honeywell and Stein and ditertiary-butyl peroxide and tertiary-butyl hydroperoxide by Laporte.

Copolymerization procedure

Bulk inter-polymerizations were carried out in one litre flanged reaction flasks, fitted with water condensers, nitrogen inlets and anchor stirrers, and contained in thermostatically controlled water baths. The rubbers were first dissolved in styrene, at room temperature, using concentrations of 5–15% wt/wt, and polymerized in bulk using a two stage process. Stage 1 involved a stirred pre-polymerization at 150 rev/min of 300 g of rubber in styrene solution, 0.3 g of tertiary-dodecyl mercaptan as chain transfer agent and, for pre-polymerization at 100°C, 0.45 g of ditertiary-butyl peroxide, and additionally 0.45 g tertiary-butyl hydroperoxide for pre-polymerization at 60°C. Pre-polymerization was continued to 35–40% monomer conversion rather than a constant pre-polymerization time. Stage 2 involved a static bulk polymerization of the above prepolymer, which was first transferred to 16 oz jars, using a temperature programme of 16 h at 70°C, 3 h at 120°C and 3 h at 150°C. After polymerization the blocks of material were granulated prior to injection moulding.

Solution viscosity

Solutions of the elastomers in styrene were prepared at the concentrations subsequently used for polymerization (5–15% wt/wt). The viscosities of these solutions were determined using Ostwald viscometers, in each case measurements being made at the temperature used for pre-polymerization (Table 2).

Measurement of impact strength

Test specimens of dimensions $2\frac{1}{2} \times \frac{1}{2} \times \frac{1}{4}$ in ($63.5 \times 12.7 \times 6.35$ mm) were prepared by injection moulding using a $\frac{1}{2}$ oz (~14 g) ram injection moulding machine with a barrel temperature of 200°C. The specimens were notched to a depth of 0.1 in using a milling cutter of root radius 0.01 in, aged for 16 h at 23°C and 50% humidity and the impact strength determined using an Avery Izod impact test machine. ASTM D-256 allows the use of injection moulded test pieces although it is evident from electron micrographs that some moulding anisotropy is present. The assumption that the

energy to break is proportional to the depth of the sample from the base of the notch was made in order to calculate the impact strength in J cm^{-2} .

Table 2 Analysis of rubber-reinforced polystyrenes

<i>Elastomer</i>	<i>Conc.</i> (% wt/wt)	<i>Pre-polym.</i> <i>temp.</i> (°C)	<i>Initial soln.</i> <i>viscosity, η</i> <i>at pre-polym</i> <i>temp.</i> (mN m^{-2})	<i>Impact</i> <i>strength</i> (J cm^{-2})	<i>Estimate of</i> <i>Particle</i> <i>Size</i> (μm)
Intene 35 SA	5	60	71	0.52	≤ 2
Intene 35 NFA	5	60	60	0.63	≤ 3
Intene 45 NFA	5	60	89	0.68	≤ 3
Intene 55 NFA	5	60	112	0.68	5-6
Intene 35 SA	5	100	45	0.21	0.1-0.3
Intene 55 NFA	10	100	1110	1.4	≤ 6.0
Intene 55 NFA	10	60	2090	0.47	≥ 10
Polybutadiene A	5	60	37	0.31	0.2-1.0
Polybutadiene A	7	60	93	0.37	0.2-0.8
Polybutadiene A	15	60	2130	0.37	0.2-0.8
Polybutadiene B	5	60	370	0.47	≤ 6.0
Duradene SBR	5	60	47	0.21	0.2-0.6
Solution SBR B	5	60	372	0.31	0.2-1.0

Electron microscopy

The microstructures of the polystyrenes were examined by electron microscopy of thin ultra-microtomed sections using the method of Kato¹ in which osmium tetroxide is used as the fixing medium. Estimates of particle size were made from several electron micrographs for each polystyrene, although the accuracy of the method is limited since not all the particles in the section are cut through their centres. The magnification on all electron micrographs is $\times 6860$.

SUMMARY OF RESULTS

The initial viscosity of the rubber solution at the pre-polymerization temperature, the impact strength of the composition, and the estimated particle size by electron microscopy are shown in Table 2. It is apparent that the rubber type, molecular weight of the rubber and the pre-polymerization temperature have marked effects on both the particle size of the disperse phase and the impact strength. The effect of concentration is less significant since, in general, elastomers that resulted in a low impact strength at low concentrations gave a similar result at higher concentrations, in spite of large differences in solution viscosity.

DISCUSSION

General

The work of Dobry and Boyer-Kawenoki² showed that a solution of two different polymers in a mutual solvent generally separates into two phases.

Phase equilibrium data for a system of natural rubber and polystyrene in benzene, one closely resembling that examined here, showed that at quite small concentrations of either phase one becomes a solution of the other in benzene due to their immiscibility. The phase separation occurring in the preparation of high impact polystyrene has also been described, notably by Bender³ and Molau⁴. Briefly the single phase present initially of rubber in styrene becomes a continuous phase containing a disperse phase of polystyrene in styrene at an early stage of the polymerization. At about 10% monomer conversion a phase inversion occurs resulting in a disperse phase of rubber in styrene within a continuous phase of polystyrene in styrene. The final structure is largely controlled by the phase inversion step. Grafting by transfer also occurs during the polymerization and this also has an important influence on the size of the dispersed rubber particles. The evidence for the occurrence of grafting in HIPS has been summarized by Angier and Fettes⁵.

The microstructure of typical commercial HIPS prepared using 5–6% wt/wt of low *cis* polybutadiene as the reinforcing rubber are shown in Figures 1 and 2. The notched Izod impact strengths of these materials were

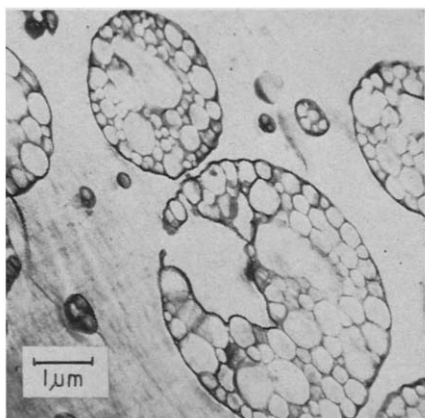


Figure 1 Commercial HIPS B

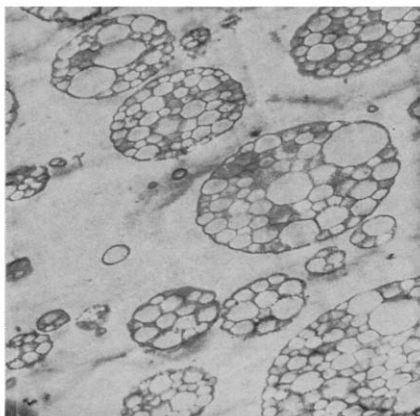


Figure 2 Commercial HIPS A

0.63 and 0.42 J/cm² respectively. An estimation of the particle size shows particles up to 3–4 μm. As can be clearly seen, the interior of the particles contains inclusions of polystyrene. This has been noted by, amongst others, Keskkula⁶ and Seward⁷. The proportion of styrene contained in the gel phase may be determined by an extraction method such as that described by Galenko *et al*^{8,9} using dimethyl formamide. Analysis carried out by this method showed that the dispersed gel phase contains 75–80% of polystyrene which agrees with the published figures of Galenko.

Molecular weight of rubber

The microstructures of impact polystyrenes obtained from 5% wt/wt

solutions of low *cis* polybutadiene with \bar{M}_n in the range 110 000–170 000, and a catalysed pre-polymerization at 60°C, closely resembled those of commercial materials, the particle size increasing from about 2 μm to 6 μm , with increasing molecular weight (*Figures 3–6*). A reduction in molecular

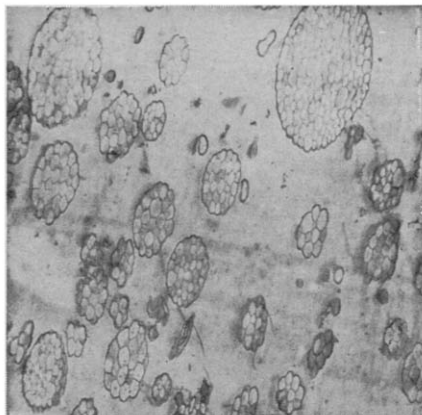


Figure 3 5% Intene 35SA, 60°C.

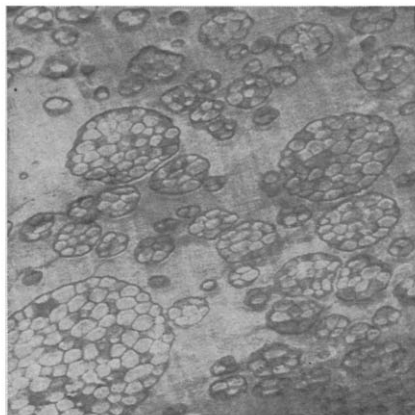


Figure 4 5% Intene 35NFA, 60°C.

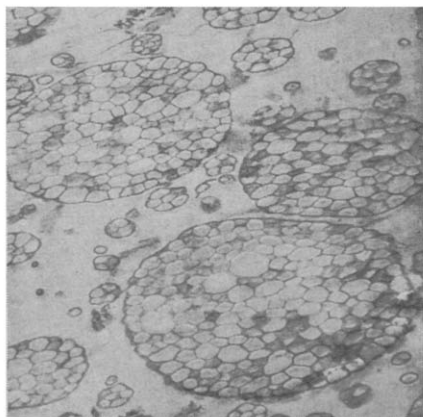


Figure 5 5% Intene 45NFA, 60°C.

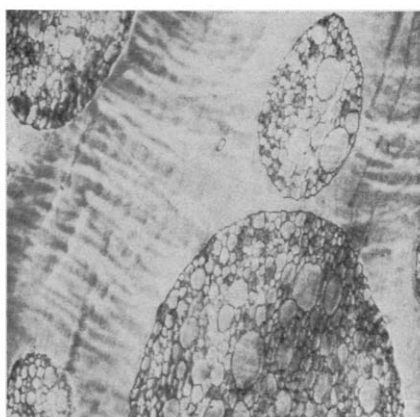


Figure 6 5% Intene 55NFA, 60°C.

(All micrographs have the magnification $\times 6860$)

weight of the rubber to 70 000 \bar{M}_n gave smaller particles (0.2–1.0 μm) that contained few inclusions, some of which consisted of a single particle surrounded by a thin rubber membrane (*Figure 7*). It was observed that the volume fraction of the occluded polystyrene could be larger than that of the inclusions normally found in these materials, indicating that they were unlikely to occur purely from a breakdown of larger particles. On the other hand an increase in molecular weight, \bar{M}_n to 210 000 resulted in particles of about 6 μm , (*Figure 8*) slightly in excess of commercial materials (*Figures 1–2*). Since particle size increased with \bar{M}_n the change could be related to the increase in the initial solution viscosity, at a constant pre-polymerization temperature and rubber type.

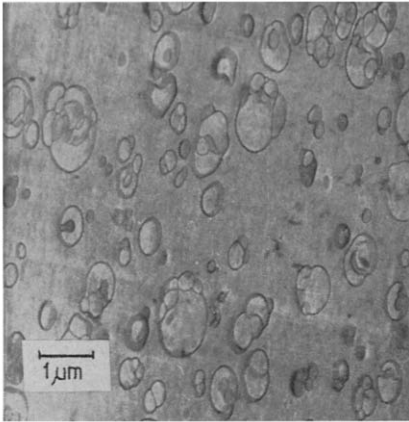


Figure 7 5% polybutadiene A, 60°C.

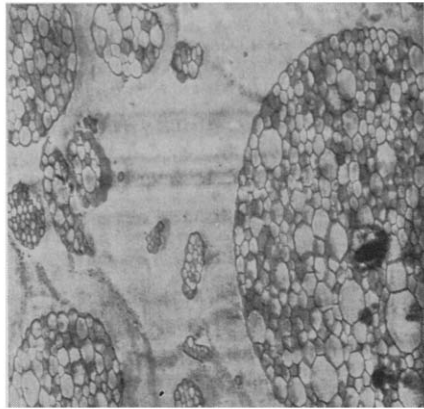


Figure 8 5% polybutadiene B, 60°C.

Rubber concentration

The microstructure obtained by increasing the concentration of Intene 55NFA low *cis* polybutadiene, \bar{M}_n 170 000, from 5% to 10% wt/wt, at a pre-polymerization temperature of 60°C, consisted of very large composite particles, well in excess of 10 μm (Figure 9). However 10% wt/wt of this polybutadiene with a pre-polymerization at 100°C (Figure 10) resulted in particles that were similar in size and structure to those from 5% of the rubber at a 60°C pre-polymerization (Figure 6), although the initial solution viscosity was higher.

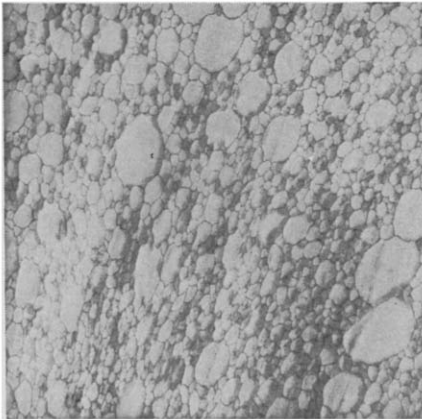


Figure 9 10% Intene 55NFA, 60°C.

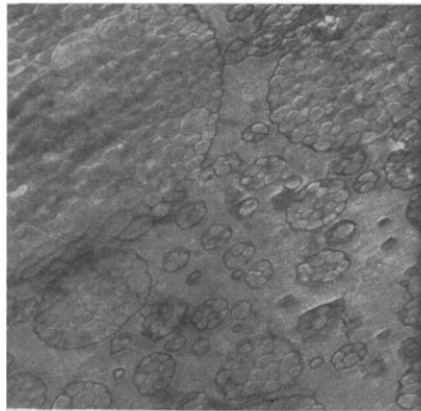


Figure 10 10% Intene 55NFA, 100°C.

(All micrographs have the magnification $\times 6860$)

The change in particle size obtained from an increase in the concentration of polybutadiene A, \bar{M}_n 70 000, was slight, in spite of a large increase in solution viscosity, although differences in the structure of the particles were observed (Figures 11–12). At 15% wt/wt the number of inclusions was similar to that from Intene low *cis* polybutadiene of \bar{M}_n 110 000–170 000 used at 5% wt/wt.

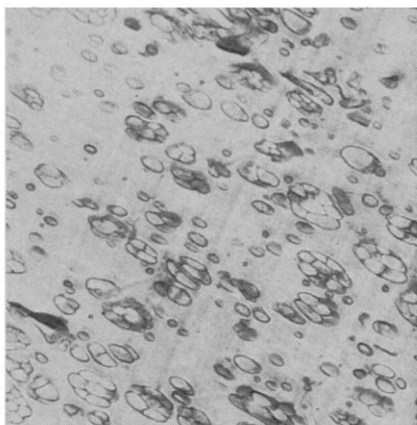


Figure 11 7% polybutadiene A, 60°C.

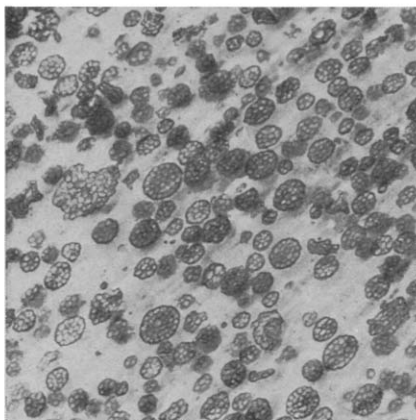


Figure 12 15% polybutadiene A, 60°C.

Rubber type

The microstructure from 5% wt/wt of a commercially available SBR (Duradene) resembled that from 5–10% wt/wt of low molecular weight polybutadiene although the particles, often consisting of a single inclusion surrounded by a rubber membrane, were even smaller (Figure 13). The

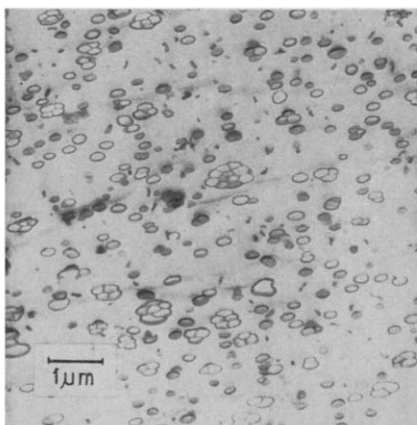


Figure 13 5% Duradene SBR, 60°C.

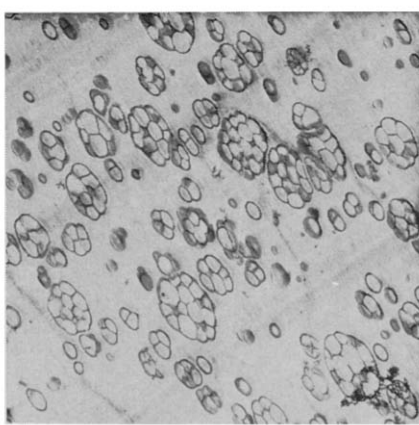


Figure 14 5% solution SBR B, 60°C.

(All micrographs have the magnification $\times 6860$)

microstructure from the higher molecular weight SBR ($\bar{M}_n = 220\,000$) (Figure 14) was closer to that obtained from high molecular weight polybutadiene, a larger number of inclusions being present. It was observed that the initial solution viscosity of the SBR of $\bar{M}_n 220\,000$ was higher than the low *cis* polybutadienes at the same concentration.

Inversion conditions

Inversion conditions were varied by increasing the temperature of pre-polymerization. The higher temperature should lead to increased graft polymerization of styrene to polybutadiene therefore affecting the formation of the dispersed rubber phase. The microstructure obtained from an increase in pre-polymerization temperature from 60°C to 100°C with 5% wt/wt of low *cis* polybutadienes, \bar{M}_n 110 000, consisted of very small particles with few inclusions; some particles had circular rubber membranes within them (Figure 15), whereas at 60°C the particles were larger and contained many small inclusions. The microstructure from 10% wt/wt of polybutadiene,

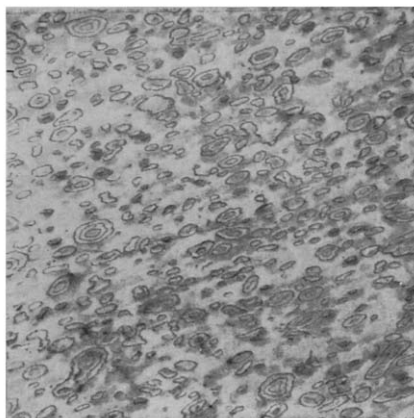


Figure 15 5% Intene 35 SA, 100°C. (\times 6860)

\bar{M}_n 170 000, pre-polymerized at 100°C (Figure 10) was similar to that of 5% wt/wt of the rubber pre-polymerized at 60°C (Figure 6). It was noted that the initial solution viscosity was much higher in the former case although a similar particle size was obtained.

Impact strength

It has been reported that it is necessary to have a dispersed rubber phase with a certain minimum particle size in HIPS to obtain adequate reinforcement³. It is considered that the incorporation of low modulus spheres into a rigid matrix leads to a lowering of the craze initiation stress¹⁰. The reason for a necessary minimum particle size is most likely due to the inability of small particles to terminate crazes. Too large particles will affect the surface finish although it is not clear whether there is an upper limit to the particle size required for reinforcement. This work has shown that particles of 2.5–5 μm are adequate for reinforcement of HIPS obtained by this method. This size is obtained from low *cis* polybutadienes of molecular weight in the range 110 000–170 000 \bar{M}_n except when high temperatures are used in

combination with low concentrations of the lower molecular weight polybutadienes. It should be stressed that the stirring conditions are also extremely important in modifying particle size so that valid comparisons may only be made under standard conditions of reactor size and stirring rate.

Low molecular weight polybutadienes and solution SBR copolymers generally gave particles of the order 0.2–1.0 μm and these gave only minimal reinforcement of the polystyrene matrix. In the case of the solution SBR copolymers small particles were obtained even when the molecular weight was in excess of 200 000 \bar{M}_n .

CONCLUSION

In the preparation of HIPS by bulk inter-polymerization the particle size of the dispersed rubber phase increases with an increase in the molecular weight of the polybutadiene rubber. To obtain significant reinforcement of the polystyrene matrix requires a particle size of $\geq 2\mu\text{m}$ this being obtained with a polybutadiene of molecular weight $\geq 110\,000 \bar{M}_n$. Provided that comparisons are made at a constant elastomer concentration, type of rubber, and pre-polymerization temperature the increase in particle size correlates with an increase in the initial solution viscosity. However, the composition of the rubber and the pre-polymerization temperature influence the particle size and type of structure independently of the initial viscosity. These effects indicate the importance of the phase inversion step and the formation of a stabilizing graft copolymer during the early stages of the pre-polymerization. This is supported by the previously reported occurrence of grafting in HIPS.

A study of the composition of the dispersed rubber phase will be the subject of a future paper.

*The International Synthetic Rubber Co. Ltd,
Brunswick House, Brunswick Place,
Southampton, SO9 3AT, UK*

*(Received 1 December 1970)
(Revised 16 March 1971)*

REFERENCES

- 1 Kato, K. *Polym. Eng. Sci.* 1967, **7**, 38
- 2 Dobry, A. and Boyer-Kawenoki, F. *J. Polym. Sci.* 1947, **2**, 90
- 3 Bender, B. W. *J. Appl. Polym. Sci.*, 1965, **9**, 2887
- 4 Molau, G. E. and Keskkula, H. *J. Polym. Sci. (A-1)*, 1966, **4**, 1595
- 5 Angier, D. J. and Fettes, E. M. *Rubb. Chem. Tech.* 1965, **38**, 1164
- 6 Keskkula, H. and Traylor, P. A. *J. Appl. Polym. Sci.* 1967, **11**, 2301
- 7 Seward, R. J. *J. Appl. Polym. Sci.* 1970, **14**, 852
- 8 Galenko, N. V. and Komashko, A. M. *Zorina V. B. Plast. Massy.* 1966, **12**, 66
- 9 Komashko, A. M. and Galenko, N. V. *Plast. Massy.* 1967, **2**, 64
- 10 Bucknall, C. B. *Brit. Plast.* 1967, **40**, 11

Development of the γ -crystal form in random copolymers of propylene and their analysis by DSC and x-ray methods

A. TURNER-JONES

Random copolymers of propylene with minor proportions of ethylene, butene and other comonomers develop γ -form crystallinity, mixed with α -form, on crystallisation from near the melting point. The proportion of γ -form increases with comonomer content. γ -form determinations, together with measurement of degrees of crystallinity by x-rays and melting point distributions by differential scanning calorimetry (DSC), after carefully controlled thermal treatment, can be used to characterize the chain distribution present. The effect of thermal history on the melt distribution observed by DSC and the α/γ ratio has been investigated in detail for one copolymer containing 6.5mol% ethylene, and the crystal morphology developed in this copolymer and fractions obtained by solvent extraction is discussed.

INTRODUCTION

IN AN EARLIER paper by the author¹ it was shown that stereoblock fractions obtained by solvent extraction of normal commercial polypropylene cooled from above their melting points gave γ -form crystallinity as well as normal α -form. The low temperature fractions, obtained over the approximate range 35–70°C using petroleum ether or xylene as solvents, were of high molecular weight and crystallized entirely in the γ -form. The development of γ -form was ascribed to discontinuities in the isotactic sequences in the chains. These discontinuities were caused either by short atactic sequences of propylene units or by simple switches (one heterotactic unit) from an isotactic sequence where the methyl groups are all on one side of the main C—C backbone (regarded as a linear zig-zag) to an isotactic sequence where they are all on the opposite side.

Since then highly isotactic polypropylene, as opposed to stereoblock polymer has been obtained in the γ -form free of α -form by crystallization under very high pressure by Kardos² and Pae³ and also independently in these laboratories. Very low molecular weight isotactic polymer has also been shown to crystallize in the γ -form by melt crystallization⁴ and from certain solvents⁴⁻⁶.

In this paper it is shown that random copolymerization of small amounts of various comonomers with propylene using stereospecific catalysts, gives copolymers which, on slow cooling from the melt, yield mixed α/γ crystallinity with a high proportion in the γ -form. This supports the thesis that development of the γ -form is due to interruptions in the isotactic propylene sequences, in this case due to comonomer units. As with the stereoblock fractions the copolymers as originally made, before they are melted, show

α -form of relatively low crystallinity. The two comonomers showing this effect that have been investigated in most detail are ethylene and butene, but 3-methylbutene and octene and other randomly polymerized comonomers have also been shown to increase the proportion of γ on crystallization from the melt. Neither of these two comonomers co-crystallizes with polypropylene although low levels of randomly distributed butene units may enter the polypropylene lattice to a limited extent, reducing, but not disrupting crystallinity. This is shown by the expansion of the polypropylene crystal lattice^{7,8}. Random copolymers of propylene and ethylene in roughly comparable proportions are, as is well known, amorphous.

This paper discusses the effect of the proportion of comonomer and the thermal history on the amount of γ -form produced in mixed α/γ crystallinity and on the melting point distribution observed by differential scanning calorimetry (DSC). It describes how these parameters can be used to analyse qualitatively the chain distribution in propylene copolymers containing small amounts of ethylene and butene distributed randomly, or as block copolymers, and mixtures of polypropylene with small amounts of polyethylene. The methods differ from those of Barrall *et al.*⁹ previously reported.

One copolymer containing 6.5 mol% ethylene was selected for more detailed investigation and for fractionation studies.

EXPERIMENTAL

Preparation of copolymers

All the copolymers were made with $\text{TiCl}_3/\text{AlEt}_2\text{Cl}$ catalysts in a high boiling aliphatic hydrocarbon at 60°C. The rates of feeding propylene and ethylene (or butene) were adjusted so as to obtain random copolymers. The molecular weights were controlled by hydrogen modification to approximately $M_w = 300\,000$. The polymer was isolated by filtration at 60°C and the soluble portion discarded.

Five random copolymers were examined containing between 3 and 17 mol% butene (B_1 – B_5 , see *Table 1*) and two random copolymers E_1 and E_2 containing 3 mol% and 6.5 mol% ethylene respectively. Three other copolymers with ethylene were examined. These were made by first polymerizing propylene to homopolymer before introducing the ethylene to make random copolymer during the subsequent polymerization. The initial polypropylene portion amounted to 15% or 30% by weight of the final polymer. The data on the copolymers E_1 – E_5 are also included in *Table 1*.

In the butene series of copolymers a very small amount of homopolymer (1.5% by weight of the total polymer) was polymerized before the butene was introduced. Four of these copolymers, all except B_4 , contained a nucleating agent. None of the copolymers with ethylene contained a nucleating agent.

Unfortunately no directly comparable homopolymer was made at the same time under identical conditions but a typical commercial polypropylene (PP) has been included for comparison, and also a blend of the same propylene homopolymer with 4% of high density polyethylene (PP/E) made by mixing the homopolymers as powders and milling into a crêpe.

Determination of comonomer content

The proportion of comonomer present in the samples was determined by M. E. A. Cudby of these laboratories by infra-red methods which will be published separately. It was shown that the ethylene was present mainly as $-(CH_2)_n-$ sequences where $n = 5$ or 7 . The average length of the butene sequences is not certain.

Table 1 Degrees of crystallinity and percent γ developed on slow cooling

Sample	Comonomer		Cryst. % (cooled from 160°C at 6C°/h)	γ %*	Cryst. % (cooled from 190°C at 6C°/h)	γ %*
	(Wt%)	(Mol%)				
PP	—	—	70	0	69	7
PP/E	ethylene	4	6	70	0	62.5
B ₁	blend					0
	butene (random)	4	3	60.5	20	
B ₂		7	5.5	58.5	32	
B ₃		10	8	52.5	39	
B ₄		12	10	50	48	
B ₅		20.5	17	40	?	
E ₁	ethylene (random)	2	3	60	22	59
E ₂		4.5	6.5	57.5	46	53
E ₃	(15% PP)†	3	4.5	57.5	24	55
E ₄	(15% PP)†	4.5	7	53	34	52
E ₅	(30% PP)†	5	7.5	57.5	31	50.5

* % of total crystallinity ($\alpha + \gamma$) not of whole sample

† Proportion polymerized as propylene homopolymer before ethylene is fed to give random copolymer

Crystallinity determinations

These were carried out by methods basically similar to that of Natta¹⁰. x-ray diffraction scans were obtained with a Philips PW 1010 diffractometer with Cu-K α radiation and pulse height discrimination and working in transmission. A straight background was drawn in between 4° and 16° of θ and the diffraction scans were then divided into areas attributable to diffuse scatter from the amorphous regions (*A*) and to sharp diffraction peaks from the crystalline regions (*C*) as shown by the dotted lines of *Figures 1a* and *1b*. The crystallinity was calculated as $C/(C + A)$ with no corrections. The object was to place samples in order of crystallinity and show trends in crystallinity. Naturally the method is not claimed to be absolute. No polymer in any case is a simple two phase system of crystalline and amorphous regions and the determinations are further complicated by the presence of two crystal forms. Close comparisons are not valid when different proportions of the two forms are present.

Determination of α - and γ -forms

The x-ray diffraction patterns of the α - and γ -forms were described in

reference 1. They are similar in many respects but the third strong reflection at d -spacing 4.77 \AA (0.477 nm) of the α -form (α_3) is absent in the γ -form and is replaced by a line at 4.42 \AA (γ_3). The relative proportions of α and γ of the total crystallinity (not of the total sample) which are quoted are based on the relative intensities of these two lines. The x-ray diffractometer scans of the two samples, one wholly α -form and the other wholly γ -form and both with overall crystallinity 60%, were normalized to constant area (crystalline + amorphous) above background between 4° and 16° of θ (see *Figures 1a* and *1e*

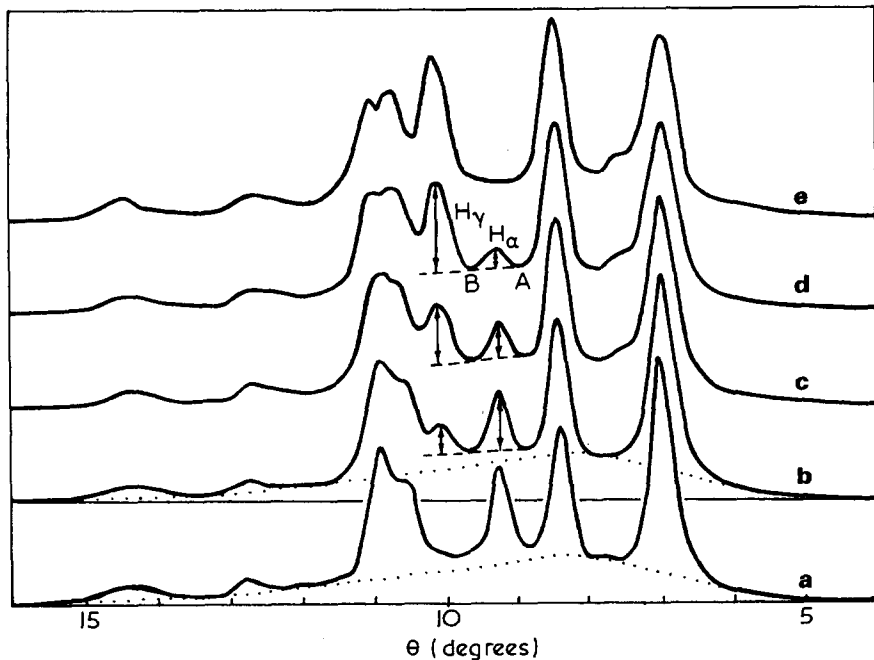


Figure 1 x-ray diffraction scans of propylene homopolymer: (a) α -form; (e) γ -form; (b), (c), (d) α/γ ratios of 75:25, 50:50, 25:75, respectively, derived graphically from (a) and (e)

respectively). The scan attributable to a polymer of 60% crystallinity with α/γ ratio 50:50 was obtained by adding graphically one half of the intensity above background of the γ -form scan to half of the intensity of the α -form scan at suitable intervals of θ . The resulting scan is shown in *Figure 1c*. Similar scans were obtained for α/γ ratios of 25:75 and 75:25 (see *Figures 1b* and *1d*). The heights H_α and H_γ of the α and γ peaks were measured as shown in *Figure 1* and the quantity $H_\gamma/(H_\alpha + H_\gamma)$ plotted against the percent γ crystallinity (*Figure 2*).

From the graph the proportion of γ -form could be obtained in experimental specimens by measuring H_γ and H_α in the same way. (The extrapolation of the line AB was used as a base line in determining H_γ because γ_3 is not always well resolved from the strong reflections at $\theta = 10.5\text{--}11^\circ$, particularly in poorly crystalline specimens.) Confirmation of the validity of the method

was obtained by mixing together the finely divided all- γ and all- α polymers in the proportions 50:50 and 40:60 and 60:40. γ -form determinations from the X-ray scans of these mixtures are marked with crosses in *Figure 2* and fall close to the line obtained graphically.

This method differs slightly from that used by K. D. Pae¹¹ who, in the investigation of γ to α conversion in high pressure crystallized polypropylene,

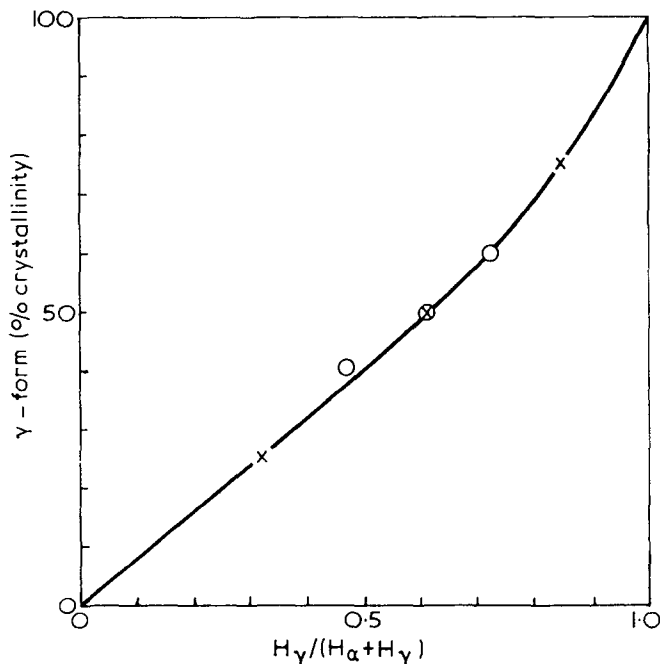


Figure 2 Percent of total crystallinity in γ -form vs. $H_\gamma / (H_\alpha + H_\gamma)$ (see *Figure 1*)

took the proportions of α and γ equal when the height of the α and γ peaks were equal and from that of Morrow and Newman⁴ who regarded them as equal when the height of the γ peak was twice that of α .

Preparation of DSC and X-ray specimens

Specimens for DSC examination (10 mg) were cut from thin films to fit the standard aluminium pans ($\frac{1}{4}$ in diameter). The films were obtained by pressing, at 210°C, the powders as originally made and cooling at a moderate rate.

In some of the experiments the specimens were first slowly cooled at 6°C/h from 160°C or 190°C. Specimens of the polymers to be compared were placed in their aluminium pans in cavities of suitable size cut in a brass block sealed by a thick brass lid. The whole was placed in an oil bath heated to the temperature from which cooling was to start. The mass of metal reduced the temperature of the bath and slow heating was continued until the desired

starting temperature was again reached as measured by a thermocouple placed inside the metal block. Cooling was then started immediately. The final heating process took some 15 min and the starting temperature was thus reached asymptotically, the last ten degrees taking about 10 min. This thermal history before cooling was started is important and, in comparing different batches of samples, it is necessary to carry out the procedure consistently and not to exceed the starting temperature for reasons which become clear later. The high thermal conductivity and heat capacity of the metal block ensured that all the samples at different parts of the block were given the same thermal treatment and helped to smooth out the temperature fluctuations of the oil bath. The block itself showed cyclic temperature fluctuation of $\pm 1^\circ\text{C}$. When required, extra specimens of each polymer were included for x-ray crystallinity determinations to ensure that DSC and x-ray specimens had received identical thermal treatment. These were subsequently chopped finely and placed in thin walled PANTAK glass tubes of 2 mm diameter for x-ray examination.

Differential scanning calorimetry

Differential scanning calorimetry was carried out with a Perkin-Elmer DSC-1 instrument using 10 mg samples. Calibration for heating runs was carried out by observing the onset of melting of standard indium samples. This takes account of both the temperature scale error and the lag in recording which arises from the relative positions of the temperature sensors and the base of the sample pan; this lag varies with heating rate. No correction has been made for thermal lag through the sample which only amounts to $\sim 1^\circ\text{C}$. Owing to the particular characteristics of the Perkin-Elmer instrument the corrections to the temperature scale are not constant over the whole temperature range. All the DSC heating curves shown in the diagrams were obtained at a heating rate of $16^\circ\text{C}/\text{min}$. Investigations using slower and faster rates showed that no significant recrystallization occurred during scanning. The approximate correction was -4°C at the melting point of indium (156.5°C) and the temperature scales shown are correct at this temperature. The main object has been to present an entirely consistent series of scans. To facilitate comparison between different DSC curves all the scans have been normalized to a horizontal background. The position of the background could not always be clearly determined, especially at low temperatures when melting started gradually. Hence too much reliance should not be placed on small differences in these low temperature regions.

RESULTS AND DISCUSSION

X-RAY AND DSC ANALYSIS OF COPOLYMERS OF PROPYLENE WITH ETHYLENE AND BUTENE

The degrees of crystallinity and the proportions of γ -form developed in the butene and ethylene copolymers after prior cooling at $6^\circ\text{C}/\text{h}$ from 160°C or 190°C are given in *Table 1*. The DSC scans of samples similarly slow cooled are shown in *Figures 3* and *4*. The scans shown by dotted lines in these figures

were obtained after continuing heating to 230°C, holding for 5 min, cooling at 16°C/min to room temperature and then reheating. Details of the crystallization exotherms recorded during cooling are given in *Table 2*.

The similarity in crystallization and melting behaviour between these copolymers and the stereoblock fractions obtained from homopolymers by

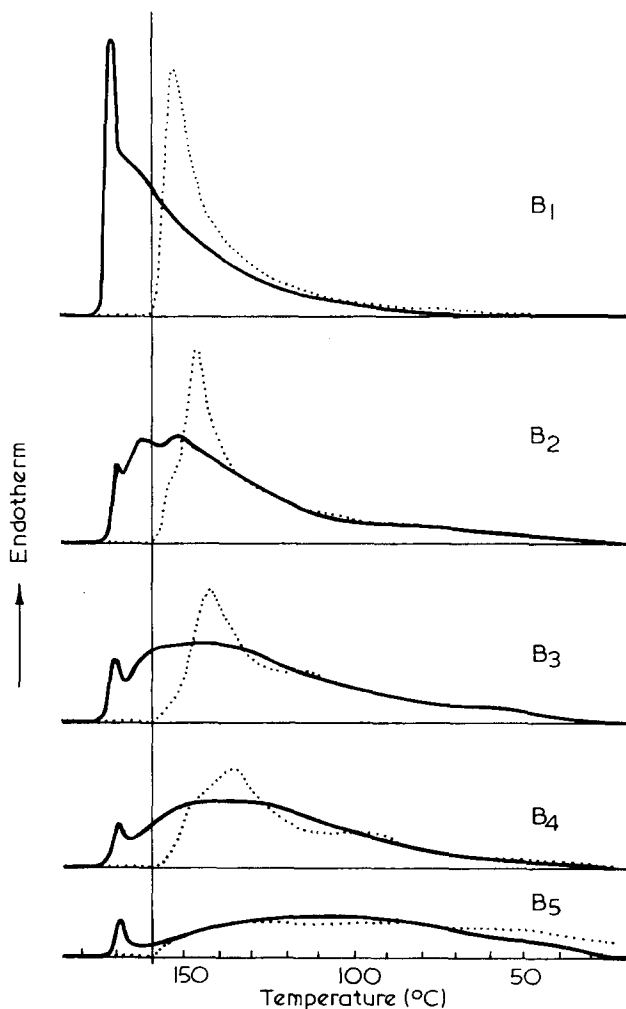


Figure 3 DSC reheat endotherms of random copolymers of propylene with butene (B_1 – B_5 , see *Table 1*) after cooling at 6°C/h from 160°C (thick lines); from 230°C at 16°C/min (dotted lines)

solvent fractionation¹ lends support to the hypothesis that the development of the γ -form is due to interruptions in the polypropylene isotactic sequences. In the copolymers these interruptions are now the comonomer units. When the interruptions are more frequent a higher proportion of γ -form is developed.

The wide melting ranges observed after slow cooling from 160°C show

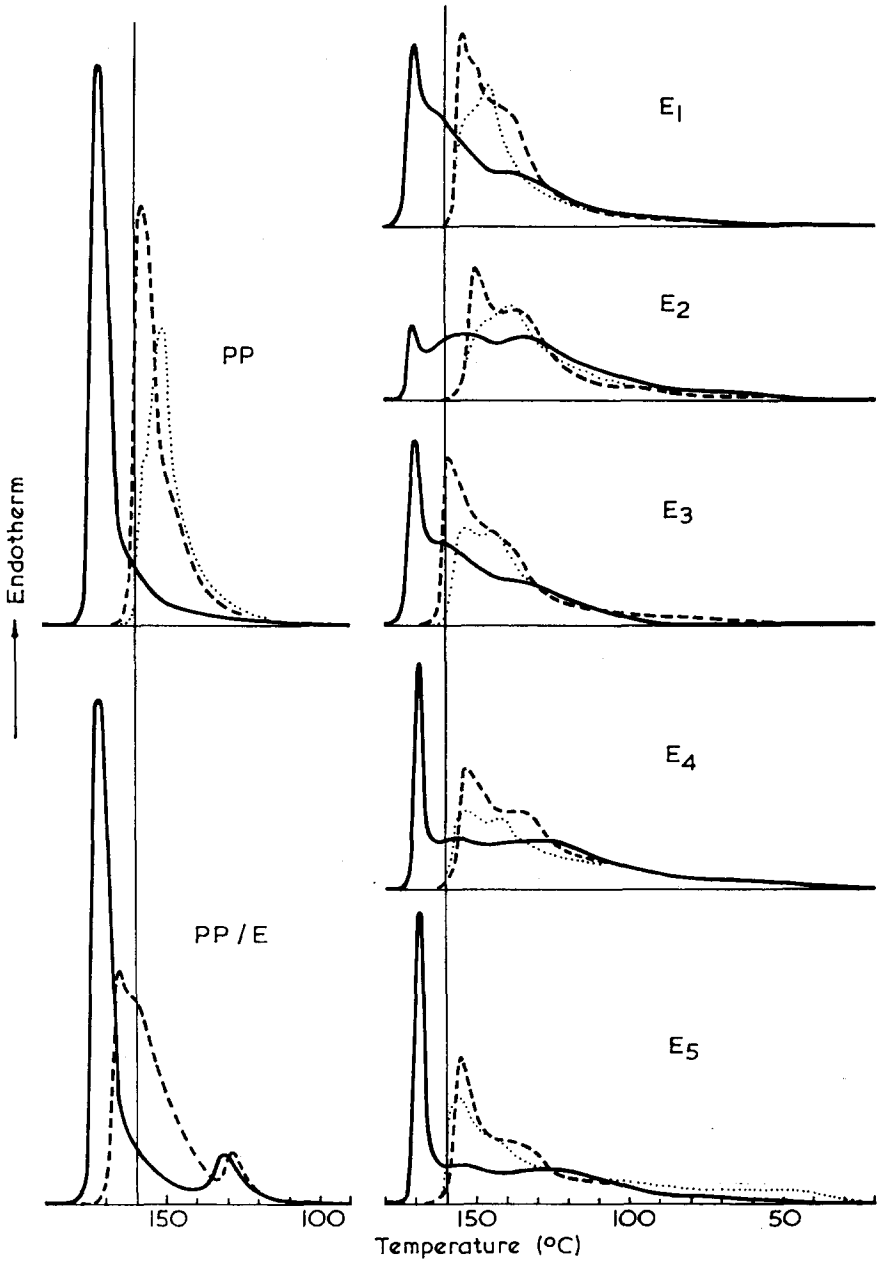


Figure 4 DSC reheat endotherms of propylene homopolymer (PP), blend with polyethylene (PP/E) and copolymers with ethylene (E_1 - E_5 , see Table I), after first cooling at $6^\circ\text{C}/\text{h}$ from 160°C (thick lines) and from 190°C (dashed lines); from 230°C at $16^\circ\text{C}/\text{min}$ (dotted lines)

that the polymerization method adopted has resulted in copolymer chains with a wide distribution of isotactic polypropylene sequence lengths which, on slow cooling, crystallize at different temperatures to give crystallites of different thicknesses and perfection and hence different melting points. The high melting peaks at $\sim 170^\circ\text{C}$ show that some chains of very long isotactic sequences (either similar to those in normal propylene homopolymer or containing very few interruptions by comonomer units) are present in all

Table 2 DSC exotherms on cooling from 230°C at $16\text{C}/\text{min}$

Polymer	$T_s(^{\circ}\text{C})$	$T_c(^{\circ}\text{C})$	Peak height [†]	Peak width [‡]
PP	117	112	7.3	3.2
B ₁ *	120	113	6.3	4.0
B ₂ *	118	111	5.4	4.5
B ₃ *	115	107	4.2	4.6
B ₄	103	85	2.8	7.7
B ₅ *	112	102	1.1	v. wide
E ₁	108	96	3.6	7.5
E ₂	106	90	2.6	10

T_s start of exotherm as defined by clear departure from base line; T_c peak of exotherm

* contains a nucleating agent

[†] in arbitrary units

[‡] in $^\circ\text{C}$ on DSC trace, at half height

polymers but, as expected, are much fewer in the copolymers with the highest comonomer content. The very small peak at 168°C present in the most highly modified copolymer B₅ is due, at least in part, to the 1.5% of homopolymer present, as already mentioned.

As comonomer content increases the proportion of polymer melting at progressively lower temperatures increases. This is accompanied by increasing amounts of γ -form which must have developed from chains of progressively shorter, but still crystallizable, polypropylene sequences. The proportion of γ -form developed in B₅, the copolymer containing the highest proportion of butene (17 mol%), could not be determined because of the changes in the polypropylene x-ray spacings due to lattice expansion and to the presence of some polybutene type crystallinity. The development of polypropylene and polybutene phases during copolymerization with highly stereospecific catalysts when the butene content exceeds about 20% by weight has been described previously by the author⁷ and also by Coover *et al*.⁸

The object of starting the slow cooling process from 160°C , that is from below the maximum melting point of polypropylene, was to prevent complete melting and so leave some nuclei or crystallites on which crystallization could start immediately on cooling. The chains with the longest isotactic polypropylene sequences would then be expected to crystallize first, then, as the temperature drops, those with progressively shorter sequences thus effecting a fractionation on a chain structure basis which is reflected in the melt distribution on reheating.

Lower final melting points and therefore much narrower melt distributions are obtained by cooling from 190°C , even in the homopolymer and blend. At this time and temperature in the melt, nuclei are evidently effectively destroyed

and crystallization starts after the considerable supercooling normally observed in un-nucleated polypropylene¹². As a result the final melting points are not much higher than those observed in the same samples cooled much faster at 16C°/min from 230°C, at which temperature nuclei are known to be destroyed¹³. It appears that both the long sequence chains and shorter sequence chains now crystallize simultaneously to give crystallites of similar melting point. Hence these conditions are much less effective in producing a melt distribution characteristic of the chain distribution present. The advantage

Table 3 Crystallinity and % γ developed in E₂ under various thermal treatments in DSC

Heat- ing rate (C°/min)	Hold- ing temp. (°C)	Holding time	Cool- ing rate/ min	T _s (°C)	T _c (°C)	Cryst. %	% γ	DSC reheat figure no.			
16	160	0	0.5	immed.		54	55.5	5b			
			16	123	110	49	44	5b (dashed)			
			64	103	89	48	16				
		10 min	0.5	16				57	52.5	5c	
								48	45	5c (dashed)	
								55	31	5d	
		16 h	0.5	16		immed.		50	19	5d (dashed)	
						121	104				
		230	5 min	0.5		121	112	55	42	5e	
						16	106	90	48	7	5e (dashed)
						64	90	74	45	0	
4 0.5*	160	10 min	0.5	immed.				6a			
			0.5	immed.		58	41	6b			
			64	immed.				6b (dotted)			
	160	1 h	0.5		immed.				6c		
					immed.				6d		
					immed.				6e		
	162.5	0	16 h		immed.				6f		
					immed.		57.5	63.5	6f		
					immed.				6f (dashed)		
	170	0			~135	124	55	45.5	6g		

T_s start of exotherm as defined by clear departure from baseline; T_c peak of exotherm

*Heated 16C°/min to 140°C then at 0.5 C°/min

of cooling from 160°C instead of 190°C is evident from Figure 4. The melt distributions observed in copolymers E₂ and E₄ after cooling from 190°C would suggest that they had similar chain structure distributions. The differences are brought out by cooling from 160°C.

The usefulness of the method is further illustrated by the melt distributions of E₃, E₄ and E₅. The endotherms accurately reflect the composition of the copolymers. The size of the sharp endothermic peak at ~170°C characteristic of homopolymer is larger in E₅ which contained 30% homopolymer than in E₃ and E₄ (15% homopolymer). The size and melt distribution shown by the very broad low melting endotherms appropriately reflect the proportion and degree of modification of the random copolymer present. In making the comparison it must be noted that the ethylene contents of the random

copolymer portions are higher than the overall contents given in *Table 1*. The 7.5 mol% ethylene in E₅ is equivalent to about 9.5 mol% in the random copolymer portion.

Where high density polyethylene is present as a separate phase as in the blend PP/E it is shown as a distinct endothermic peak at $\sim 130^\circ\text{C}$. Low density polyethylene is shown as a peak at $\sim 110^\circ\text{C}$. Slow cooling from 160°C effects

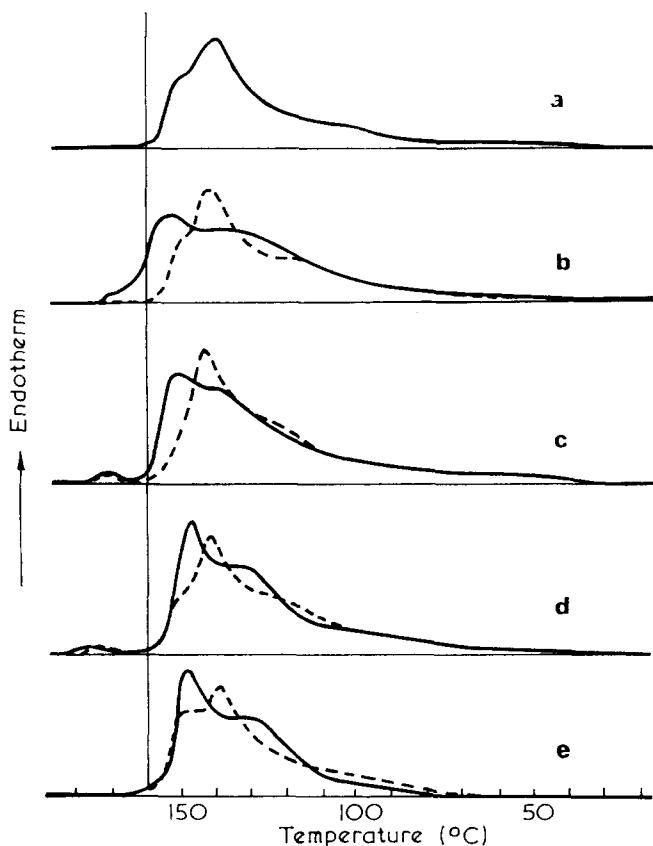


Figure 5 dsc heating curves of E₂ samples: (a) pressed sheet, no heat treatment; (b)–(e) prior thermal treatment as in *Table 3*, involving $16^\circ\text{C}/\text{min}$ approach to maximum temperature and cooling rate $0.5^\circ\text{C}/\text{min}$ (thick lines), $16^\circ\text{C}/\text{min}$ (dashed lines)

the best resolution of the polypropylene and polyethylene melting peaks and hence facilitates quantitative estimation of the proportion of crystalline polyethylene present. This may most readily be carried out by comparing the areas of the polyethylene endotherms with those obtained from a series of calibration blends slow cooled under the same conditions.

EFFECT OF THERMAL HISTORY ON MELTING POINT DISTRIBUTION
AND DEVELOPMENT OF γ -FORM

The results given in *Table 1* for the E series of copolymers show that the relative proportions of α - and γ -forms developed in each copolymer varied with the temperature from which slow cooling was started. Since the overall degrees of crystallinity are not very different it is clear that some chains can crystallize in either the α - or γ -forms. Copolymer E₂ was therefore selected for

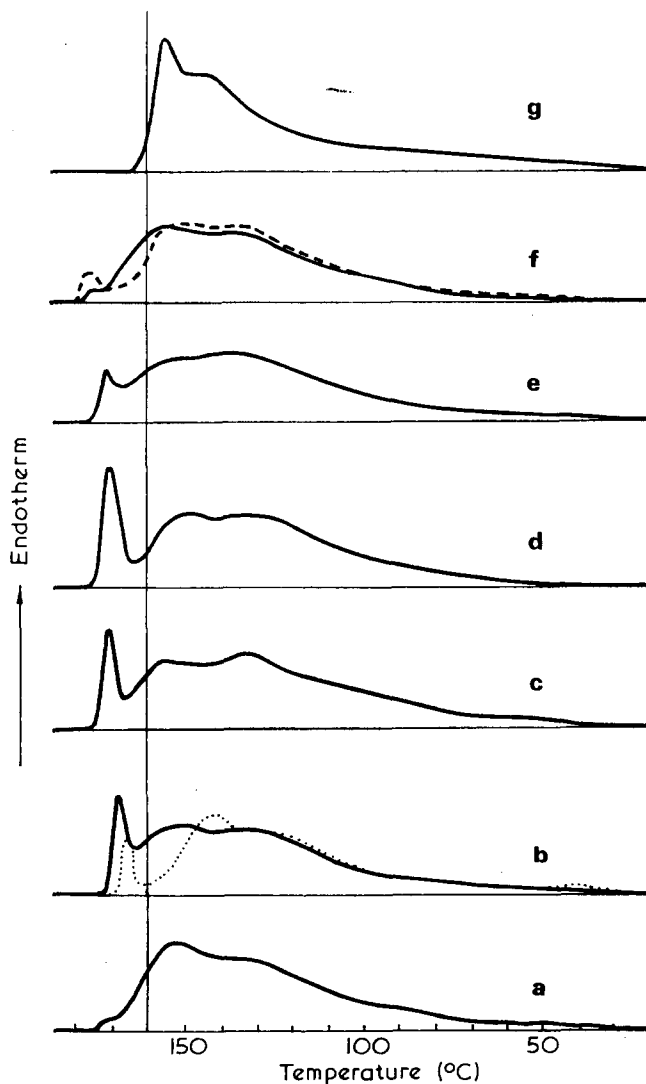


Figure 6 DSC heating curves of E₂ samples given prior thermal treatment as in *Table 3*, involving slow approach (4°C/min and 0.5°C/min) to maximum temperature

a more detailed study of the effect of rate of heating to the holding temperature, the holding temperature itself, and the cooling rate, upon the overall crystallinity and amount of γ developed and on the melt distribution on reheating. *Figures 5 and 6* show DSC traces of E_2 copolymer film which had undergone different prior thermal treatments as indicated in *Table 3*. *Table 3* also gives data on the crystallization exotherms recorded during the cooling process.

Melting point distributions

It will be observed that, irrespective of holding time or cooling rate, the only samples displaying appreciable melting at $\sim 170^\circ\text{C}$ are those which had been heated fairly fast to a temperature where melting was not complete and then at the slowest possible rate available ($0.5^\circ\text{C}/\text{min}$) to 160°C . This effect can be explained as follows. During heating, crystallites formed from chains of short isotactic polypropylene sequences will melt and those with longer sequences can recrystallize to form more perfect thick crystallites. The extent of this 'morphological rearrangement' will be very dependent upon the heating rate. Only at slow rates will there be enough time for crystallites to be developed which are sufficiently perfect to be stable at 160°C . These crystallites will act as nucleating agents during subsequent crystallization on cooling.

The rate of cooling also has an effect on the subsequent melting behaviour. As seen in *Figure 6b*, immediate cooling at the fast rate of $64^\circ\text{C}/\text{min}$ gave a smaller peak at a slightly lower temperature than cooling at $0.5^\circ\text{C}/\text{min}$. The latter gave a melt distribution resembling most closely that obtained after the standard slow cooling in the oil bath (*Figure 3*). Longer holding times, up to 16 h, increased the size of the upper peak slightly and increased its temperature. All chains potentially able to produce crystallinity with melting point $> 170^\circ\text{C}$ appear to now have done so.

The effect of higher holding temperature was also examined. E_2 was heated to 162.5 , 165 and 170°C at $0.5^\circ\text{C}/\text{min}$ and then cooled immediately at the same rate. The DSC curves are shown in *Figures 6e, f, g*. Up to 165°C the upper melting peak increases in temperature but decreases in size. After heating to 170°C it is no longer observable; crystallization has occurred with considerable supercooling as shown by the exothermic peak at 124°C . The DSC traces obtained while cooling from the lower temperatures show no such exotherm although the crystallinity developed is higher. This is consistent with crystallization starting immediately on cooling and continuing gradually. There is no sudden change in dH/dt to be recorded as a distinct exothermic process.

Nevertheless complete order cannot have been destroyed at 170°C because on cooling from 230°C at $0.5^\circ\text{C}/\text{min}$ the peak temperature of crystallization is lower still at 112°C . This is reflected in the peak melting points on reheating of 155°C and 148°C respectively (*Figures 6g and 5e*).

Figure 5 shows that, at the faster initial heating rate of $16^\circ\text{C}/\text{min}$, all but a very small amount of crystallinity in the E_2 copolymer film is melted at 160°C and only small peaks of melting point $> 170^\circ\text{C}$ are recorded after subsequent cooling. It is also noticeable that more crystallites of higher melting point (i.e. in the approximate melting range 150 – 170°C) are developed on cooling immediately $0.5^\circ\text{C}/\text{min}$ from 160°C than after holding for longer

times. In other words the balance between growth on nuclei present and their dispersion due to thermal motions is in favour of the latter, in spite of 160°C being well below the maximum melting point of an appreciable proportion of the polymer. The destruction of nuclei with increased holding time is also shown by the lower temperature of crystallization on cooling at 16°C/min.

The above results explain why the particular thermal pre-treatment we have adopted as our standard procedure involving slow approach to 160°C was effective as a chain structure fractionation procedure. *Figures 6b* and *6f* show that for E₂ the upper peak is related in temperature and size to the temperature from which slow cooling is started. For copolymers more highly modified than those discussed here, melting may be complete at 160°C and cooling would then have to be started from a lower temperature to prevent supercooling. We have found that 160°C is normally the best compromise when comparing different polymers.

In a later section it will be shown that annealing at a temperature below 160°C causes some recrystallization to polymer of higher melting point. Clearly a slower rate of cooling would produce a more perfect fractionation but for routine analysis we have found that the procedure described provides the best compromise.

Development of γ -form: morphology of mixed α - and γ -forms

The results given in *Table 3* show that after heating fast (16°C/min) to the holding temperature:

- (a) The proportion of γ developed decreases as the rate of cooling increases: fast cooling from 230°C gave α -form only. This is consistent with earlier observations on the homopolymer stereoblock fractions¹ which gave α -form only on quenching from the melt.
- (b) At corresponding cooling rates more γ is formed on cooling from 160°C than from 230°C.
- (c) Longer holding times at 160°C decrease the amount of γ -form on cooling.

Development of γ -form is therefore favoured by slow cooling but more particularly when some crystallinity or order is left in the melt as discussed in the previous section.

Fractionation studies described in a later section show that the high melting peaks at ~170°C represent melting of α -form crystallites. On cooling at 0.5°C/min from 160°C a smaller proportion of γ -form is produced after approaching this temperature slowly (0.5°C/min) than at the faster rate (16°C/min). Comparison of the relevant DSC traces shows that this can be attributed to the development of the large α -form peak of *Figure 6b* which is not present in *Figure 5b*, i.e. to the preferential crystallization into the α -form and γ -form, respectively, of chains containing only a small proportion of ethylene units. Similarly more γ forms on cooling at 0.5°C/min from 165°C because no large α peak is developed, (*Figure 6f*). It appears that the maximum amount of γ is formed when a high proportion of crystallites melting in the range 150–170°C are present, as in *Figures 5b* and *6f* (thick lines), but no large α -form peak. The proportion of γ -form decreases again on cooling from

170°C because more order in the melt is destroyed and fewer crystallites in this melting range are developed (*Figure 6g*).

At this stage it is only possible to provide a speculative explanation for the above results. Crystal growth into α - or γ -form may occur by direct nucleation into either α - or γ -forms and by growth on to existing α -form crystallites, either in α -form or in the γ -form by epitaxial growth.

Evidence for epitaxial growth between the α - and γ -forms has been provided by Morrow⁴ who showed that individual single crystals made from very low molecular weight propylene homopolymers by solution crystallization can consist of regions of α - and γ -forms. This is attributed to the close relationship between the packing of the left and right handed helices of the α - and γ -forms^{1,2,4}. The crystal lamellae are formed from extended chains so that the question of chain folding does not arise.

Kardos³ has shown that normal highly isotactic polypropylene crystallized in the γ -form under high pressure, converts to α -form on heating by a solid-solid crystal phase transition. As high pressure crystallized γ -form has been shown to consist of folded chains^{3,14,15} and not extended chains as in polythene, it follows that the fold planes of the two forms must be closely related. Evidence has been provided that the fold plane of the α -form is the ac plane^{16,17} so that the fold plane of the γ -form is likely to be the crystallographically closely related ac plane (see figure 10 of reference 1). Epitaxial growth of γ on α and vice versa is therefore extremely probable in high molecular weight polymers even where chain folding is involved.

In particular we have to explain why the maximum amount of γ -form is developed when a small proportion of α -form crystallites melting above 170°C are left in the melt before cooling, and when cooling is carried out under conditions which yield the maximum amount of crystallites melting in the range 150–170°C (see *Figures 5b* and *6f*).

On slow cooling from a melt in which a little α crystallinity is retained, crystallization can start immediately on these crystallites. As the temperature drops chains of progressively shorter sequence length can crystallize by lateral addition to the folded chain lamellae but with progressively shorter fold lengths. This type of overgrowth has been observed in single crystals grown from solution as the temperature is lowered¹⁸. These overgrowths are likely to be initially in the α -form from chains of the longest isotactic polypropylene sequence but may be epitaxial growths in the γ -form as more highly modified chains crystallize. Meanwhile more nuclei will form which will be more likely to be γ -nuclei as the chains forming the nuclei have progressively shorter average sequence lengths. It is known that stereoblock fractions with isotactic sequence lengths below a certain (unknown) average give γ -form only on slow cooling from the melt¹. It is also possible that order remaining in the melt, as opposed to true α -form crystallites, may predispose to the formation of γ -nuclei by chains modified by copolymer units to only a low degree.

It seems possible that if all the most highly isotactic chains which will nucleate or grow on existing crystallites in the α -form only are first crystallized, and therefore removed from crystallizing phase, then further new nucleation may now occur preferentially in the γ -form. This might also favour γ -form epitaxial growth on existing α -crystallites. In this way the maximum amount

of γ -form can develop with the minimum interference from new α -form nuclei.

If, however, crystallization by slow cooling is carried out under conditions which ensure that nuclei or order are first destroyed, then crystallization develops from nuclei formed at a much higher degree of supercooling as discussed in the previous section. At this temperature both chains with the longest polypropylene sequences and the more modified chains nucleate and grow simultaneously. A large number of α -nuclei might then be formed from the former, favouring further overgrowths in the α -form and therefore decreasing the γ content, as observed.

As crystallization proceeds, and since the sequence lengths even within one chain are likely to vary, parts of chains with the shortest sequences may be excluded from the growing crystallites and be incorporated at lower temperatures into other crystals of shorter fold length and lower degree of perfection or as fringed micelle growth.

Fast cooling complicates the picture still more because development of α -form is now favoured even in the more highly modified chains. It is possible that there is a temperature above and below which direct nucleation occurs preferentially into γ and α respectively.

Crystallites of the same melting point may be formed from chains of different sequence length in either the α - or γ -forms depending whether growth occurs on existing crystallites or by direct nucleation. Hence we should not expect to find a clear temperature demarcation in the DSC remelt endotherms below and above which all the melting crystallites are γ or α respectively. At low temperatures γ -form melting predominates. We have attempted to follow the melting of the two forms by running x-ray diffractometer scans at different temperatures. In a sample of E_2 slow cooled from 160°C, γ -form started to melt first as expected but in the middle melting range recrystallization to polymer of higher melting point occurs because the rate of scanning is necessarily slow. This complicated the observations because some conversion of γ -form to α -form was also involved as described in the next section. The γ -form had completely disappeared by 145°C but the α -crystallinity increased slightly over this range. Conversion to α -form of γ -form made from homopolymer by high pressure crystallization has been discussed by several authors^{2,11,14,19}. The mechanism of conversion will be discussed by the author in relation to these copolymers in a sequel to this paper.

FRACTIONATION OF PROPYLENE-ETHYLENE COPOLYMER E_2

None of the copolymers so far described has been crystallized entirely in the γ -form free of α -form. The solvent fractionation of propylene homopolymers¹ only yielded very small quantities of stereoblock polymer crystallizing entirely in the γ -form. Solvent fractionation of the copolymer E_2 , the one yielding the highest proportion of γ -form, was undertaken with a view to obtaining larger quantities of polymer which could be crystallized in the γ -form only, to permit a more detailed investigation of the γ -form crystalline morphology and to provide material for attempts to grow single crystals which would help to confirm the unit cell postulated¹. This work was carried

out before the publication of the electron diffraction photographs from γ -form single crystals obtained from very low molecular weight polymer⁴. These photographs did, in fact, confirm the originally proposed unit cell in c -axis projection except that doubling of the b -axis was proposed. The possibility that either a or b axes might be doubled had been suggested¹ but could not be established from x-ray photographs of unoriented polymer.

As γ -form is developed most readily in the chains with shorter polypropylene sequences, it was desirable to separate these from chains containing less comonomer which have been shown to crystallize either α or γ depending upon thermal treatment.

It was found that after applying the standard slow cooling procedure to E_2 , further annealing at various temperatures below 160°C caused recrystallization of these less modified chains to crystallites of higher melting point and therefore lower solubility. Subsequent rapid cooling to room temperature crystallized the short sequence chains to a low degree and hence rendered them as soluble as possible, thus providing optimum conditions for their separation by solvent extraction. Annealing for one hour at 150°C, followed by rapid cooling, was found to give good separation as shown by the remelt distribution of *Figure 7*, curve B. A subsidiary upper melting peak has developed at 165°C while the broad low temperature endotherm, well separated from the upper peak, results from the short sequence chains which were melted at 150°C and recrystallized on cooling. The proportion of γ -form was reduced from 50% to 25% during this treatment.

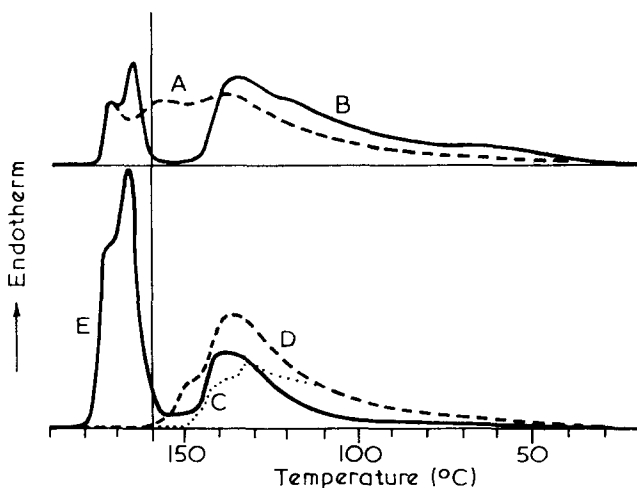


Figure 7 DSC reheat endotherms from copolymer E_2 and its fractions as described in *Table 4* (10 mg samples used for each scan)

The resulting polymer was first extracted with boiling hexane and then boiling heptane and the soluble polymer recovered. *Table 4* gives data on the soluble fractions and the residue. *Figure 7* shows the DSC heating curves of the two soluble extracts (C) and (D) after slow-cooling from 160°C and of the residue after extraction (E). It will be seen that the greater part of the lower melting crystallites of curve B had been extracted. The residue now showed

only a trace of γ -crystallinity while, as expected, the degree of crystallinity had been increased. The absence of γ -form from the residue shows that the melting peak at 172°C (curve A) which remained unchanged after annealing at 150°C was originally in the α -form.

The reduction in the proportion of γ -form during annealing is probably primarily due to conversion of γ to α of higher melting point but may partly be due to the subsequent fast cooling from 150°C which favours development

Table 4 Data on fractions from copolymer E₂

DSC Curve (Figure 7)	Crystal- linity (%)	γ -form (%)	Weight (mg)	Ethylene (wt %)	(mol %)
A, E ₂ unextracted sc* from 160°C †	58.5	50	1000	4.5	6.5
B, A held at 150°C for 16h then rapidly cooled	53.5	25			
C, hexane sol. fract. from B — as recovered		0	166	~13	18.5
— sc from 160°C †	42.5	90			
D, heptane sol. fract. from B — as recovered		0	475	~4.2 ‡	6 ‡
— sc from 160°C †	51	92			
E, residue after heptane extraction	72.5	trace	355	~1.0	1.5
— sc from 160°C	68	25			

* sc—slow cooled † at 6 C°/h ‡ by difference

of α -form as previously discussed. Both the hexane and heptane soluble polymers were found to be in the α -form after recovery from solvent, but showed over 90% γ after slow cooling from 160°C. The heptane soluble fraction was still well crystalline (52.5%) so that the object of obtaining polymer capable of forming well crystalline γ -form only had been substantially achieved. The infra-red spectrum of this fraction was obscured by aromatic substances present in the heptane used, but by difference contained about 6 mol% ethylene compared with about 18.5 mol% in the hexane soluble fraction and 1.5% in the residue, both largely present as $-(CH_2)_n-$ sequences where $n = 5$ or 7. The heptane soluble fraction was of high molecular weight because highly oriented crystalline fibres in the α -form were obtained from it.

Twenty five percent of γ -form was developed in the residue after slow-cooling, again from 160°C, thus providing additional evidence that this fraction contained chains capable of crystallizing in either α - or γ -form.

ATTEMPTS TO GROW SINGLE CRYSTALS AND MORPHOLOGY OF BULK POLYMER

Attempts were made to grow single crystals in the γ -form from the hot heptane soluble fractions described in the last section and also from the

unfractionated copolymer E₂. With heptane as solvent α -form only was obtained on slow cooling and by isothermal crystallization. Similar experiments with 5% solutions in polyethylene wax²⁰ and an ester wax were also unsuccessful; even 50/50 mixtures developed no γ -form on slow cooling.

Five percent mixtures with a practically amorphous polypropylene wax made at 170°C and cooled at 6°C/h and 1°C/h yielded 40% γ and 50% γ , respectively, in the residue left after extraction with cold hexane. Isothermal crystallization at temperatures between 120°C and 130°C also yielded some 50–55% γ -form. The hexane insoluble residues were dispersed ultrasonically and then examined in the electron microscope. No evidence of single lamellar crystals was obtained although γ -form electron diffraction powder patterns were obtained from some fragments which were therefore aggregates of small crystals.

Specimens for examination of free surface and fracture surface morphology were made by isothermal crystallization of E₂ under the conditions given above. The best textural detail was obtained by crystallization at 125°C (51% γ). Replication of the free surface revealed a mat-like array of 'ropes', ~ 200 Å in width with a longitudinal periodicity of ~ 200 Å. Fractured surface replication indicated a 'pebbled' structure 500–1000 Å in diameter, possibly made up of smaller units ~ 200 Å in extent, but no clear lamellar structure was seen. Further heating of this specimen at 125°C for 5 h with a view to improving the lamellar structure resulted in no change in the fracture surface morphology.

The bulk crystallized specimen was disintegrated using the nitric acid selective oxidation procedure²¹. Electron diffraction studies of the debris again only gave γ -form powder patterns. For comparison, similar disintegration was carried out on a propylene homopolymer crystallized into α -form isothermally at 125°C under the same conditions. This gave sufficiently large fragments to enable well defined single crystal electron diffraction photographs to be obtained.

All evidence suggests that these propylene copolymers crystallized in the γ -form are composed of very small crystallites, the lateral dimensions of which are much less than 500 Å.

As the heptane soluble fraction contains ~ 6 mol% ethylene present mainly as $-(\text{CH}_2)_5-$ and $-(\text{CH}_2)_7-$ sequences, then the propylene sequences will on average be 50 monomer units long, capable of forming ~ 17 helical turns in a 3_1 helix corresponding to 110 Å. Such short sequences are not likely to give well formed lamellae, even if of uniform length and the ethylene units are located at the folds. It also appears that the chains with longer polypropylene sequences present in E₂ (only 1.5 mol% ethylene was present in the residue after fractionation) are also unable to develop good lamellae even after annealing. It is not yet possible to say whether the crystal morphology involves chain folding or is of the fringe micelle type or a mixture of both.

SPHERULITIC TEXTURE

The spherulitic morphology developed in the various fractions after slow cooling from 160°C at 6°C/h is complicated. The texture varied considerably

in different regions of individual samples and sometimes spherulites were of mixed type and showed changes in birefringence during growth. Further investigations, which will be the subject of a later communication, are being undertaken to establish the distribution of α - and γ -crystallinity within the textural entities when both types are present simultaneously. The principal features are described below:

The heptane soluble fraction D showed well formed spherulites of positive birefringence which must be γ -form spherulites since 92% of the crystallinity is γ . The hexane soluble fraction C showed poorly formed sheaf spherulites of positive birefringence, varying in size considerably in different regions which must also be γ -form. The residue, after slow cooling from 160°C, showed well-formed positive and well-formed negative spherulites, both presumably α -form as described by Keith²², together with some regions of poorly formed positive spherulites which might possibly be produced from the 25% γ -form present (Table 4), but may be α since it is not known how the γ -form is distributed. The γ -form may consist of very fine textural entities embedded in or between α -form spherulites. The whole copolymer A (50% γ) showed small areas of well-formed negative spherulites which are likely to be α -form corresponding to the high melting peak at $\sim 170^\circ\text{C}$. The bulk of the material showed a very fine texture of small sheaf spherulites of positive birefringence, which by analogy with heptane and hexane soluble fractions are presumably mainly γ -form.

CONCLUSIONS

Random copolymers of propylene with minor amounts of ethylene and butene and other comonomers made with stereospecific catalysts develop mixed α and γ crystal forms on crystallization by slow cooling from temperatures near the melting point. The proportion of γ -form increases with increasing comonomer content; its development is ascribed to the interruptions in the isotactic polypropylene sequences caused by the comonomer units.

The observation by DSC of the melting point distributions produced after slow cooling from 160°C under carefully controlled conditions, together with measurements of the degrees of crystallinity and proportion of γ -form by x-ray diffraction on samples similarly prepared, offer a means at least qualitatively of characterizing the chain distribution present in these copolymers without fractionation. The two series of copolymers examined in this paper proved not to be truly random but to contain chains with widely varying comonomer contents.

The method of analysis is also applicable to mixtures of homopolymer and copolymer, to block polymers and blends of homopolymers with minor amounts of polyethylene, and also to homopolymers containing appreciable stereoblock polymer capable of forming γ -form on crystallization from the melt. These methods have been in use for many years in our laboratories for examining our own copolymers and those of unknown origin in conjunction with infra-red analysis.

The ratio of γ - to α -form developed in any one copolymer varies with

pretreatment and is a complicated balance of several factors — time and temperature in the melt and rate of approach to this temperature, which involves the proportion of crystallinity or 'order' retained before cooling, and the cooling rate itself.

No evidence of γ -form lamellar morphology has yet been found in the 6.5 mol% ethylene copolymer selected for special study, either in whole polymer or in lower melting (but still high molecular weight) fractions which crystallized almost entirely in the γ -form, and attempts to grow single crystals in the γ -form failed. The fractions have been shown to possess isotactic polypropylene sequences too short for regular chain folding and may contain crystallites primarily of the fringed micelle type. It is probable that in the whole polymer variation in sequence length, both between chains and within each chain, results in a complicated morphology involving very small crystals with chain folds of irregular length and fold surface, together with fringed micelle type growth.

The relative stabilities of the α - and γ -forms and the conversion of γ - to α -form in the copolymers in relation to their crystal structures will be discussed in a later paper.

ACKNOWLEDGEMENTS

The author's thanks are due to Dr T. G. Heggs and Dr C. N. Turton who made the copolymers, Messrs M. E. A. Cudby, D. A. Hemsley and A. J. Cobbold for infra-red, optical and electron microscope data, respectively, Dr P. J. Holdsworth for criticism of the manuscript, and to Mr D. R. Beckett and Mr A. B. Wootton for the experimental work.

*ICI Plastics Division,
Welwyn Garden City, Herts, UK*

*(Received 4 January 1971)
(Revised 18 March 1971)*

REFERENCES

- 1 Turner-Jones, A., Aizlewood, J. M. and Beckett, D. R. *Makromol. Chem.* 1964, **75**, 134
- 2 Kardos, J. L., Christiansen, A. W. and Baer, E. *J. Polym. Sci. (A-2)* 1966, **4**, 777
- 3 Pae, K. D., Morrow, D. R. and Sauer, J. A. *Nature* 1966, **211**, 514
- 4 Morrow, D. R. and Newman, B. A. *J. Appl. Phys.* 1968, **39**, 4944
- 5 Kojima, M. *J. Polym. Sci. (B)* 1967, **5**, 245
- 6 Kojima, M. *J. Polym. Sci. (A-2)* 1968, **6**, 1255
- 7 Turner-Jones, A. *Polymer, Lond.* 1966, **7**, 23
- 8 Coover, H. W., McConnell, R. L., Joyner, F. B., Slonaker, D. F. and Combs, R. L. *J. Polym. Sci. (A-1)* 1966, **4**, 2563
- 9 Barrall, E. M., Porter, R. G. and Johnson, J. F. *J. Appl. Polym. Sci.* 1965, **9**, 3061
- 10 Natta, G., Corradini, P. and Cesari, M. *Rend. Accad. Naz. Lincei* 1957, **22**, 11
- 11 Pae, K. D. *J. Polym. Sci. (A-2)* 1968, **6**, 657
- 12 Ke, B. (Ed.) 'Newer methods of polymer characterisation,' Interscience, New York, 1964, Chap. IX
- 13 Beck, H. N. *J. Polym. Sci. (A-2)* 1966, **4**, 631
- 14 Sauer, J. A., Morrow, D. R. and Richardson, G. C. *J. Appl. Phys.* 1965, **36**, 3017
- 15 Kojima, M. *J. Polym. Sci. (A-2)* 1967, **5**, 597

- 16 Sauer, J. A. and Pae, K. D. *J. Appl. Phys.* 1968, **39**, 4959
- 17 Kardos, J. L., Baer, E. and Morrow, D. *J. Polym. Sci. (B)* 1966, **4**, 453
- 18 Bassett, D. C. and Keller, A. *Phil. Mag.* 1962, **7**, 1553
- 19 Morrow, D. R. *J. Macromol. Sci. (B)* 1969, **3**, 53
- 20 Turner-Jones, A. and Cobbold, A. J. *J. Polym. Sci. (B)* 1968, **6**, 539
- 21 Palmer, R. P. and Cobbold, A. J. *Macromol. Chem.* 1964, **74**, 174
- 22 Keith, H. D. and Padden F. J. *J. Appl. Phys.* 1959, **30**, 1485

Absolute reactivity in the cationic polymerization of N-vinylcarbazole

P. M. BOWYER, A. LEDWITH and D. C. SHERRINGTON

The cationic polymerization of N-vinylcarbazole initiated by tropylium hexachloroantimonate and tropylium perchlorate has been studied in detail. Initiation was rapid and complete and conversion to polymer was quantitative in all cases. Reaction rates were measured by an adiabatic calorimetric technique and half lives were of the order of 1–2 s. Catalyst concentrations employed were sufficiently low ($<10^{-5}$ M) for essentially complete dissociation into free ions, as indicated by the ion-pair dissociation constants. The rate coefficient for propagation by free cations in dichloromethane at 0°C is estimated as $\sim 3 \times 10^{+5} \text{ M}^{-1} \text{ s}^{-1}$, approximately five orders of magnitude greater than that for the corresponding free radical polymerization. Molecular weights were higher when SbCl_6^- was the counter-ion than with ClO_4^- and it is suggested that monomer transfer reactions occur more readily with the small equilibrium concentrations of ion pairs (allowing an effect of counter-ion), whereas propagation occurs predominantly via free cations. Initiation is shown to occur by addition of tropylium ion to the monomer double bond and detailed mechanisms for this, together with propagation and transfer reactions, are considered.

N-VINYLCARBAZOLE (NVC) is a useful crystalline monomer, easily purified, and readily polymerized by free radical^{1,2} cationic³⁻⁷ and organometallic⁸ induced polymerization processes. Ionizing radiation has also been used to initiate polymerization of NVC particularly in the solid state⁹. The radical or ionic nature of the propagating species was readily demonstrated in most cases by copolymerization studies and/or the effect of suitable additives¹⁻⁹. Some years ago we embarked on a study of reactivity and mechanism in cationic polymerization¹⁰ and designed catalyst systems¹¹ and reaction conditions which permit ready evaluation of absolute rate coefficients for propagation processes. A central feature of these studies was the use of stable carbonium ion salts as initiators^{11,12}, notably hexachloroantimonate salts of cycloheptatrienyl (tropylium) and triphenyl methyl cations. The very stability of the initiator salts meant that only reactive monomers could be initiated and this has been confirmed by polymerization of alkyl vinyl ethers, *p*-methoxy styrene, indene, NVC and certain cyclic ethers such as tetrahydrofuran. Full details of the kinetics and mechanism of cationic polymerization of isobutyl vinyl ether have been published¹³ as part of a series¹⁴; the present paper reports in detail similar studies of the cationic polymerization of NVC.

For any ionic process (including polymerization) in solvents of low dielectric constant, reaction rates and products will be seriously affected by the nature of the ionic reactant, especially its degree of association or aggregation with counter-ions (gegen-ions) and other ion-pair species. The effects of

ion-pair dissociation equilibria on organic reactions in solvents of low polarity were first characterized by Winstein and his collaborators¹⁵ and for anionic polymerization, elegant work by Szwarc and his associates as well as other groups¹⁶, has dramatized the vast differences in reactivity between propagating free ions and corresponding ion-pairs. Effects of ion-pair equilibria in cationic polymerizations have been discussed by Plesch¹⁷, and characterized recently by Pepper and collaborators¹⁸ for the perchloric acid initiated polymerization of styrene. As noted previously, determination of absolute reactivity in the polymerization systems under study, requires knowledge of the ion-pair dissociation equilibria for both initiating and propagating species. Consequently a full study of the initiators was made using conductance measurements, and details have now been published^{12,19}.

EXPERIMENTAL

Materials

Methylene dichloride was purified and stored as described¹³; solvent remaining on the vacuum line after three days was discarded and replaced by a freshly purified batch. Acetonitrile was purified²⁰ by passage over a column of molecular sieves followed by fractionation from phosphorus pentoxide (b.p. 82.5°C at 760 mmHg). It was stored, under vacuum, over fresh calcium hydride and transferred using normal vacuum techniques. Tropylium hexachloroantimonate was prepared and purified as previously described¹³. Tropylium perchlorate²¹ was made by oxidation of cycloheptatriene using 2,3-dichloro-5,6-dicyano-*p*-benzoquinone in the presence of perchloric acid. The crude product was washed several times with dry ether, dissolved in the minimum volume of acetonitrile and reprecipitated by addition of ether. It was dried and finally stored under vacuum. The compound exploded during elemental analysis. N-Vinylcarbazole was recrystallized three times from A.R. methanol. In each case the flasks and solutions were flushed with dry nitrogen so that crystallization occurred in the absence of oxygen. The crystals were dried by pumping on a high vacuum line for two days, and stored *in vacuo* in the dark, m.p. 64.0°C. Analysis: found, C, 86.88, H, 5.75, N, 7.56%; required for C₁₄H₁₁N, C, 87.04, H, 5.70, N, 7.25%.

Kinetic technique

Polymerizations were investigated using the adiabatic calorimetric technique previously described in detail¹³. A slightly modified calorimeter was used in which the lower section¹³ was made longer so as to reduce heat losses, the stirrer now being mounted in a Teflon bush in the calorimeter base in order to improve the efficiency of mixing. The solvent metering system¹³ was changed to a conventional cold distillation arrangement, and the Biddulph-Plesch tap discarded. With these modifications, the previously described procedure¹³ for solvent scavenging was found to be superfluous.

Catalyst solution was introduced into the polymerization mixture by the use of the vacuum phial technique¹³. In the case of the hexachloroantimonate salt the solvent for catalyst phials was methylene dichloride but for tropylium

perchlorate it was found necessary to use acetonitrile in order to attain the required catalyst solubility. It should be stressed however that during polymerization the solvent was still $\sim 99\%$ methylene dichloride.

Polymer was recovered by addition of excess filtered methanol to the reaction mixture, previously reduced in volume to ~ 25 ml. Samples were collected in pre-weighed glass sinter crucibles and after drying overnight in a vacuum oven were reweighed to determine polymer yields. Molecular weights were determined by viscometry on benzene solutions and intrinsic viscosities, $[\eta]$, were converted to molecular weights, M , using the expression²²

$$[\eta] = 3.35 \times 10^{-4} M^{0.58}$$

This relationship has been confirmed by more recent work²³ and differs substantially from the equation derived by North and Hughes¹.

Preliminary investigations showed that NVC has a substantial enthalpy of polymerization; polymerizations were extremely rapid and thus introduced considerable limitations on the concentration ranges employed. Polymer yields were invariably quantitative even at the lowest initiator concentrations employed ($< 10^{-5}$ M).

Recorder traces from kinetic runs showed a general similarity to those obtained¹³ in the parallel study of isobutyl vinyl ether (IBVE) polymerization. One major difference however is that initiation in the present case appears to be virtually instantaneous since, even at -25°C , recorder traces were found to rise sharply as soon as the initiator phial was broken (see *Figure 1*). Rapid

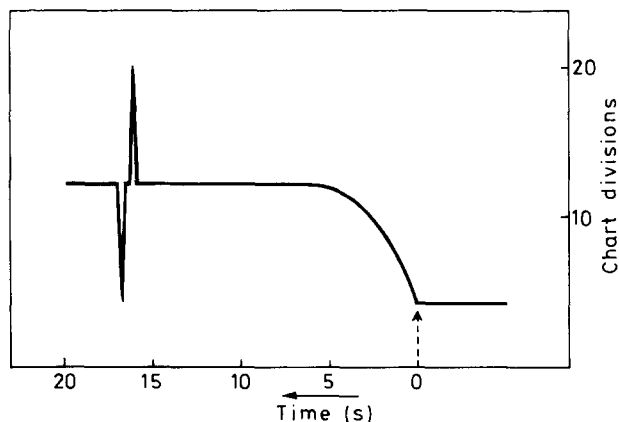


Figure 1 Typical recorder trace for polymerization of NVC by $\text{C}_7\text{H}_7^+\text{SbCl}_6^-$ in CH_2Cl_2 at 0°C

initiation and the apparent absence of termination permitted direct evaluation of the polymerization rates R_p from the maximum slopes (essentially the initial slopes) of recorder traces. Propagation rate coefficients (k_p) were then obtained from the expression $R_p = k_p [\text{C}_7\text{H}_7^+]_0 [\text{NVC}]_0$ as indicated below.

Typical kinetic run for polymerization of NVC in methylene dichloride at 0°C

$$[\text{C}_7\text{H}_7^+\text{SbCl}_6^-]_0 = 0.987 \times 10^{-6} \text{ M}; [\text{NVC}]_0 = 5.39 \times 10^{-2} \text{ M}$$

$$\text{Polymer yield} = 1.026\text{g} \equiv 5.31 \times 10^{-3} \text{ mol (99.8\%)}$$

$$\text{Initial slope of recorder trace} = 1.85/0.60 \text{ chart divisions per second.}$$

$$\text{Total rise of trace corrected for breaker contribution} = 6.30 \text{ chart divisions}$$

Equating the total rise to the polymer yield,

$$6.30 \text{ chart divisions} \equiv 5.31 \times 10^{-2} \text{ M}$$

$$\therefore \text{initial rate} = \frac{1.85}{0.60} \text{ chart divisions/second}$$

$$= 2.60 \times 10^{-2} \text{ M s}^{-1}.$$

$$\text{thus } k_p = 4.9 \times 10^5 \text{ M}^{-1} \text{ s}^{-1}$$

Molar heats of polymerization, ΔH_p , were calculated as outlined previously and in this example $\Delta H_p = -22.9 \text{ kcal mol}^{-1}$.

RESULTS

Details of the kinetic and molecular weight data obtained for tropylium salt initiated polymerization of NVC are shown in *Tables 1* and *2*.

Averaged values for the enthalpy of polymerization of NVC were $-22.7 \pm 1.5 \text{ kcal mol}^{-1}$ and $-25.0 \pm 1.5 \text{ kcal mol}^{-1}$ at 0°C and -25°C respectively. Conceivably this difference may represent experimental error but it is now apparent that enthalpies of solution for poly(N-vinyl carbazole) in CH_2Cl_2 show a similar variation with temperature²⁴. A full discussion of these

Table 1 Polymerization of NVC by $\text{C}_7\text{H}_7^+ \text{SbCl}_6^-$ in CH_2Cl_2

Temp. (°C)	[NVC] ₀ (10 ² M)	[C] ₀ (10 ⁶ M)	10 ² R _p (M s ⁻¹)	10 ⁻⁵ k _p (M ⁻¹ s ⁻¹)	10 ⁻⁵ Mol. Wt.
0	5.39	0.987	2.60	4.9	2.58
0	5.40	0.987	2.42	4.5	1.68
0	5.40	0.987	2.39	4.5	1.49
0	5.40	0.750	1.97	4.9	1.92
0	2.70	1.00	1.15	4.3	1.38
0	4.04	1.00	1.87	4.6	1.84
average 4.6					
-25	5.40	2.00	1.42	1.3	10.2
-25	5.39	1.75	1.90	2.0	9.00
-25	5.40	.. 1.50	1.09	1.4	8.83
-25	5.39	.. 1.00	0.703	1.3	8.57
-25	2.69	.. 1.50	0.577	1.4	7.59
-25	4.05	.. 1.25	0.951	1.8	8.77
-25	4.05	.. 1.75	1.48	2.1	11.3
average 1.6					

CATIONIC POLYMERIZATION OF N-VINYLCARBAZOLE

 Table 2 Polymerization of NVC by $C_7H_7^+ClO_4^-$ in CH_2Cl_2 *

Temp. (°C)	[NVC] (10^2M)	[C] ₀ (10^6M)	$10^2 R_p$ ($M s^{-1}$)	$10^{-5} k_p$ ($M^{-1} s^{-1}$)	$10^{-5} Mol. Wt.$
0	5.52	2.64	3.64	2.5	0.893
0	5.51	2.79	2.34	1.5	0.908
0	5.50	3.30	5.06	2.8	0.743
0	5.53	3.96	3.25	1.5	0.710
0	5.52	4.18	5.40	2.3	1.14
0	5.53	4.62	4.75	1.9	0.715
0	5.52	5.57	3.60	1.2	0.632
0	2.76	2.79	2.21	2.9	0.640
0	4.07	2.79	3.32	2.9	0.719
<i>average 2.2</i>					
-25	5.70	3.40	1.35	0.70	1.52
-25	5.70	4.08	1.72	0.74	1.12
-25	5.71	5.45	1.84	0.59	1.16
-25	5.69	5.74	2.54	0.78	0.830
-25	5.70	8.62	2.12	0.43	0.820
-25	5.70	11.5	2.50	0.38	0.726
-25	2.98	5.74	1.47	0.86	0.849
-25	4.13	5.74	1.89	0.79	0.860
<i>average 0.66</i>					

*Catalyst added as solution in CH_3CN giving a polymerization solvent composition, approx. 99% CH_2Cl_2 , 1% CH_3CN .

anomalies, and their possible significance, will be presented separately. Values of ΔH_p at the appropriate reaction temperatures are needed for evaluation of k_p but any errors introduced by apparent variation in ΔH_s for the polymer would be comparatively small, with little effect on the order of magnitude of k_p .

Polymer yields and molecular weights were invariably high but, because the carbazole rings in alkyl carbazoles [including poly(N-vinylcarbazole)] are highly reactive towards electrophilic reagents²⁵, it is at least possible that propagating cations alkylate carbazole rings of monomeric segments. Accordingly N-ethylcarbazole (NEC) was chosen as a model for monomer segments in poly(NVC), without the steric hindrance of polymeric substituents, and its effect on polymerization studied as indicated in Table 3.

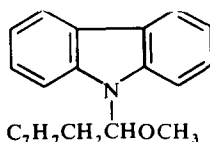
 Table 3 Polymerization of NVC in CH_2Cl_2 at 20°C in the presence of NEC

[NVC] (M)	[NEC] (M)	[$C_7H_7^+SbCl_6^-$] (10^5M)	Polymer yield (%)	$10^{-4} Mol. Wt.$
0.102	0	1.58	93	1.54
0.102	0.417	1.58	97	1.54

Reaction of NVC with tropylium hexachloroantimonate in methanol

NVC (0.63 g) was dissolved in methanol (50 ml) and added to a solution of tropylium hexachloroantimonate (1.17 g) in methylene dichloride (200 ml). A

transient red colour was formed before the solution became clear, whereupon the solution was extracted with aqueous alkali and twice with distilled water. The methylene dichloride layer was separated and dried over anhydrous sodium sulphate. Removal of the solvent on a rotary evaporator yielded a tacky product (0.95 g, 95%). I.r. analysis of this showed the presence of cycloheptatrienyl (702 cm^{-1}) and methoxy groups (1120 cm^{-1}). The crude product was separated into five fractions by dissolving in hot methanol and adding successive amounts of distilled water. The fraction most soluble in methanol (0.26 g, 25%) gave a very sharp, well resolved, i.r. spectrum with the cycloheptatriene absorption at 702 cm^{-1} more intense than the carbazole peaks (720 and 760 cm^{-1}). This material was a white crystalline solid, m.p. 112°C . Analysis: found, C, 83.22, H, 6.66, N, 4.61%; required for $\text{C}_{22}\text{H}_{21}\text{ON}$, C, 83.75, H, 6.71, N, 4.41%, which is entirely consistent with the anticipated structure:



The other fractions gave broader but similar i.r. spectra with the cycloheptatriene absorption becoming progressively weaker relative to the carbazole ring absorbances as solubility in methanol decreased. Melting points also tended to increase in the range 113 – 116°C in the same sequence. Presumably these materials consist of similar oligomeric adducts containing more than one NVC segment per cycloheptatrienyl unit.

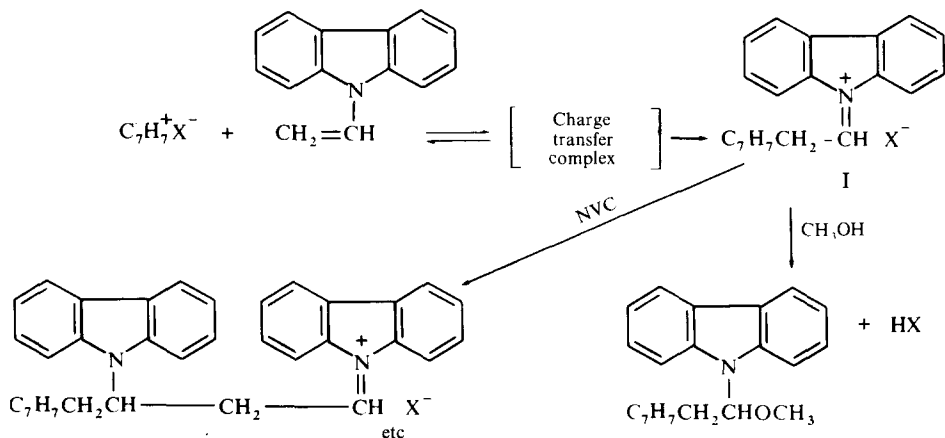
DISCUSSION

Polymerizations of NVC initiated by tropylium hexachloroantimonate and tropylium perchlorate showed identical features. For both catalysts there was a virtually instantaneous initiation reaction followed by very rapid propagation. Yields of polymer were invariably quantitative and, as in the case of the polymerization of isobutyl vinyl ether¹³, the evidence points to absence of termination during the kinetic lifetimes. Molecular weights of poly(N-vinylcarbazole) from the perchlorate initiation were slightly lower than those from the hexachloroantimonate catalysis and did not show the same temperature variation. From both catalysts however the molecular weight data showed clear evidence of a transfer reaction, characteristic of homogeneous cationic systems^{17,26,27}, though the degree of transfer is significantly less than in the case of isobutyl vinyl ether polymerization¹³. Mechanistic features of the initiation, propagation and transfer processes will now be considered in detail.

Initiation

Although reactions between tropylium salts and NVC were instantaneous under most conditions, at temperatures below -50°C the two reagents

reacted to form only a pink coloured solution from which polymer could not be precipitated on addition of methanol. However, if the solutions were allowed to warm to around -30°C before addition of methanol, polymer formed rapidly. It seems likely therefore that initiation involves pre-equilibrium formation of a charge transfer complex which, at temperatures above -50°C , collapses rapidly to yield a propagating cation such as I:

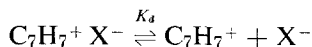


Charge transfer complexes between tropylium ion and non-polymerizable carbazole derivatives, e.g. N-alkyl carbazoles, have been recorded previously²⁸ and the reaction of tertiary amines with tropylium salts studied by McGeachin²⁹ provides independent evidence for the addition process with enamines.

In the present work overwhelming evidence for the proposed addition mechanism was provided by the isolation and characterisation of the cycloheptatrienyl derivative II, from reactions carried out in the presence of methanol. Ion-pair equilibria for the initiation reaction are considered in the next section.

Propagation reactions

Ion-pair dissociation equilibria for both tropylium salts have been investigated by conductance measurements, i.e.,



Data for the hexachloroantimonate salt in methylene dichloride have been reported previously^{12,19} and the data for the perchlorate salt in $\sim 99\%$ v/v $\text{CH}_2\text{Cl}_2/\text{CH}_3\text{CN}$ are very similar; values of K_d were 0.33×10^{-4} and 0.50×10^{-4} M at 0°C and -45°C respectively. It follows that, at the catalyst concentrations employed in the present work, the initiating salts will be predominantly dissociated into their free ions and initiation, in both cases, will involve addition of free organic cation to monomer.

Arguments in support of the assumption that the propagating species will be similarly dissociated at these low concentrations have already been presented¹³ and, since conditions in the present work are very similar, the discussion need not be repeated. Values of k_p obtained therefore represent

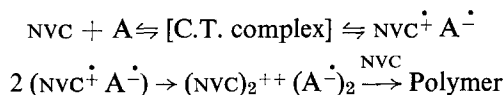
estimates of the rate coefficient for the reaction of free propagating cation with monomer, i.e. they are a measure of the absolute reactivity of the cation derived from NVC. The data should be independent of the initiating salt used and should correlate with values of rate constants for similar fundamental processes. Average values of k_p obtained are summarized in *Table 4* together with estimated activation enthalpies.

Table 4 Polymerization of NVC by tropylium salts in CH_2Cl_2

Counter-ion	Temperature (°C)	$10^{-5} k_p$ ($\text{M}^{-1} \text{s}^{-1}$)	Activation enthalpy (kcal/mol)
ClO_4^-	0	2.2	6.5
	-25	0.66	
SbCl_6^-	0	4.6	5.7
	-25	1.6	

Data for the two catalysts are in good agreement, although it is not possible to decide whether the variations are due to slightly different ion-pair dissociation equilibria, arising because of different counter-ions, or merely represent the experimental limitations of the fast reaction technique. Nevertheless the agreement is such as to provide adequate support for the assumptions made, in the computation of k_p , and, that largely free ions are involved in these systems.

In recent years the polymerization of NVC initiated by electron transfer reactions to organic molecules has been widely reported and the literature reviewed by Ellinger³⁰. Much of this work is qualitative in nature although it is clear that cationic polymerization results in almost every case, e.g. (A = acceptor molecule)



Suitable acceptor molecules include aromatic and aliphatic polynitro compounds, quinones and tetracyanoethylene³⁰. Pac and Plesch³ and Szwarc and his collaborators⁴ independently studied polymerization of NVC in nitrobenzene initiated by tetranitromethane. Both groups found the overall rate of polymerization to be represented by an expression of the form:

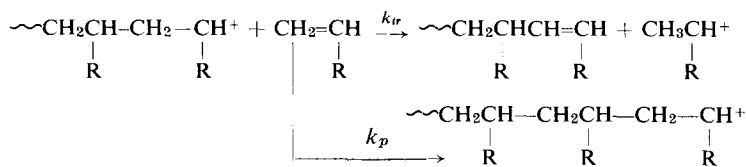
$$\frac{-d[\text{NVC}]}{dt} = k [\text{C}]_0 [\text{NVC}]$$

where $[\text{C}]_0$ is the initial concentration of added initiator. A similar expression was derived for the polymerization of NVC in CH_2Cl_2 initiated by tetracyanoethylene⁵ and for all these systems, estimated values of k were similar ($k = 11 \text{ M}^{-1} \text{ s}^{-1}$ at 34°C ³, $4.3 \text{ M}^{-1} \text{ s}^{-1}$ at 10°C ⁴ and $13 \text{ M}^{-1} \text{ s}^{-1}$ at 30°C ⁵). It follows therefore that cationic polymerizations of NVC initiated by these

organic electron acceptors do not involve free cations as propagating species. This is not too surprising since the nature of counter-ions derived from organic electron acceptors is uncertain and, in many cases, complex ion-pairs may well be involved. It is interesting to compare data from the free radical polymerization of NVC in tetrahydrofuran reported by North and Hughes with the present results. Values of the free radical propagation rate constant, k_p , were 6.0, 2.2 and 0.84 M⁻¹ s⁻¹ at +10, -10 and -30°C, respectively, many orders of magnitude below the reactivity of free NVC cation now reported. Data for the absolute reactivity of free styryl ($3.5 \times 10^{+6}$ M⁻¹ s⁻¹ at 15°C) and α -methyl styryl ($4.0 \times 10^{+6}$ M⁻¹ s⁻¹ at 0°C) cations in their respective bulk monomers is also available³¹ and in the light of these the present value for NVC is very reasonable. For NVC the activation enthalpy is slightly larger than that determined for the propagation of free styryl cation³¹ but very similar to that obtained for isobutyl vinyl ether^{12,13}.

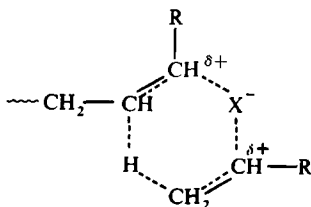
Transfer reactions

Tables 1 and 2 show that molecular weights of poly(N-vinylcarbazole) are limited by transfer reactions though the degree of transfer is considerably less than that found in many cationic systems. The slightly lower molecular weights of polymers prepared using the perchlorate salt and the relatively small dependence on temperature compared with polymers from the hexachloroantimonate salt catalysis indicate a definite molecular weight dependence on counter-ion*. Therefore, despite propagation occurring largely by the reaction of free ions, the small equilibrium fractions of ion-pairs appear to affect the transfer step. Apparently the activation energy for transfer from a perchlorate ion pair is lower than that from a hexachloroantimonate ion-pair. Recent work by Tazuke³² provides evidence for the effect of ion-pairs containing perchlorate ion, in facilitating chain transfer by methanol, during polymerization of NVC initiated by protic acids. However these systems are not so well characterized as in the present work and it may be that the apparent common effect of perchlorate ion arises from quite different phenomena. Transfer to monomer is the most common molecular weight controlling process in cationic polymerization^{17,26,27} although mechanistic details are not clear, and may vary for different monomers¹³. For a polymerizable olefin, RCH=CH₂, transfer to monomer may be represented as a simple proton equilibrium between the double bond of the monomer and that of the terminal olefinic linkage formed in the polymer chain i.e.:



*Since the systems containing perchlorate ion also contain a small amount of CH₃CN, transfer by the latter cannot be completely ruled out. However data (unpublished) from perchlorate salts in other solvents makes this possibility less likely.

Clearly, the transition state for transfer to monomer will be similar to that for propagation, and in many systems^{13,18} values of k_p and k_{tr} do not differ greatly at room temperature and above. The relative importance of free ions and ion pairs in transfer to monomer has not previously been discussed, but it is at least plausible that the enthalpy of activation (and hence the rate) for monomer transfer may be lowered, relative to the propagation step, by participation of certain counter-ions. A possible transition state, showing the counter-ion having a stabilizing effect on both leaving and developing charges, for monomer transfer, is indicated below:



A preferential effect of certain counter-ions on proton transfer between carbanions has been noted in several systems³³ and the structurally related hydride ion transfer between tetrahydrofuran and triphenyl methyl cation occurs more rapidly with $\text{Ph}_3\text{C}^+\text{SbCl}_6^-$ ion-pairs than with the free cation¹². In the present work it seems clear that transfer (presumably to monomer) is favoured for the systems having perchlorate counter-ions and a highly plausible explanation would be that ion-pairs present, in low equilibrium concentrations, dominate the monomer transfer reactions — the effect being greatest for ion-pairs containing perchlorate ions. The possibility that ion-pairs are mainly responsible for monomer transfer reactions in cationic polymerization would be of much wider significance, if established, and further work is now in progress to test the idea.

In cationic polymerization of olefins having aromatic substituents there is always the possibility of transfer occurring via intra- or intermolecular electrophilic aromatic substitution by the growing polymeric cations. Such effects would be expected to be manifest in the case of NVC polymerization, on account of the enormously high reactivity of carbazole derivatives in this type of reaction^{25,34}. However polymerizations carried out in the presence of excessive amounts of N-ethylcarbazole (NEC) — used as a model for poly-(NVC) — showed no effect on molecular weight, or yield, of poly(NVC) (Table 3). It may be concluded therefore that alkylation of aromatic rings is not an important transfer process for cationic polymerization of NVC at the low concentrations of active sites used in the present work. It must be noted however that polymerization of NVC by cationic initiators at significantly higher active site concentrations leads to crosslinked polymers, especially in chlorinated hydrocarbon solvents⁴⁴.

Termination reactions

True termination processes are difficult to envisage for polymerizations of a monomer like NVC, having a propensity for reaction with both protic and Lewis acids. No evidence of significant termination during kinetic lifetimes

was obtained in the present work, but previously we have shown^{6,13} that side reactions of SbCl_6^- ions may lead to chloride termination, especially at higher temperatures. Covalent bond formation with ClO_4^- counter-ions is an apparent termination process in cationic polymerization of styrene^{17,18} but does not appear to be significant with NVC. For the latter however there is the additional, remote, possibility that loss of active centres might result from quaternization of the carbazole nitrogen atoms of segmental units. The unshared pair of electrons on the nitrogen atom of a carbazole ring comprise part of a 14 π -electron aromatic system, isoelectronic with anthracene. This undoubtedly accounts for the comparative acidity of the N-H bond in carbazole and makes quaternization of alkyl carbazoles unlikely. Recently Hellwinkel and Seifert have synthesized salts of the N,N-dimethyl carbazole cation by an indirect method and the great reactivity of this quaternary salt alkylating agent makes it likely that any similar species, formed during cationic polymerization of NVC, would react immediately with monomer to initiate further chains. Finally it should be noted that the effects of added NEC referred to above (see *Table 3*) clearly argue against termination by quaternization.

ACKNOWLEDGEMENT

We wish to thank Professor C. E. H. Bawn for his constant interest and encouragement, and British Petroleum (P.M.B.) and SRC (D.C.S.) for maintenance awards.

*Donnan Laboratories,
University of Liverpool,
Liverpool, UK*

(Received 1 March 1971)

REFERENCES

- 1 Hughes, J. and North, A. M. *Trans. Faraday Soc.* 1966, **66**, 62
- 2 Ellinger, L. P. *J. Appl. Polym. Sci.* 1965, **9**, 3939
- 3 Pac, J. and Plesch, P. H. *Polymer, Lond.* 1967, **8**, 237
- 4 Gumbs, R., Penczek, S., Jagur-Grodzinski, J. and Szwarc, M. *Macromolecules* 1969, **2**, 77
- 5 Bawn, C. E. H., Ledwith, A. and Sambhi, M. *Polymer, Lond.* 1971, **12**, 209
see also Nakamura, T., Soma, M., Onishi, T., and Tamaru, K. *Makromol. Chem.* 1970, **135**, 241
- 6 Cowell, G. W., Kocharyan, K., Ledwith, A. and Woods, H. J. *European Polymer J.* 1970, **6**, 561
- 7 Barrales-Rienda, J. M., Brown, G. R. and Pepper, D. C. *Polymer, Lond.* 1969, **10**, 327
- 8 Heller, J., Tieszin, D. O. and Parkinson, D. B. *J. Polym. Sci. (A)* 1963, **1**, 125
- 9 Chapiro, A. and Hardy, G. *J. Chim. Phys.* 1962, **59**, 993
- 10 Bawn, C. E. H., Fitzsimmons, C. and Ledwith, A. *Proc. Chem. Soc.* 1964, p 391;
Bawn, C. E. H., Bell, R. M. and Ledwith, A. *Polymer, Lond.* 1965, **6**, 95
- 11 Ledwith, A. *J. Appl. Chem.* 1967, **17**, 344
- 12 Ledwith, A. *Amer. Chem. Soc. Advances in Chemistry Series*, 1969, **91**, 317
- 13 Bawn, C. E. H., Fitzsimmons, C., Ledwith, A., Penfold, J., Sherrington, D. C. and Weightman, J. A. *Polymer, Lond.* 1971, **12**, 119
- 14 Ledwith, A. and Sherrington, D. C. *Polymer, Lond.* 1971, **12**, 344;
Eckard, A., Ledwith, A. and Sherrington, D. C. *Polymer, Lond.* 1971, **12**, 444

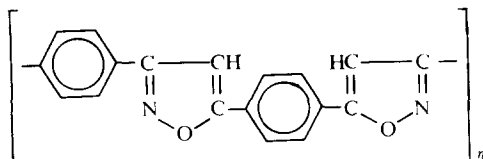
- 15 For a review see Winstein, S., Appel, B., Baker, R. and Diaz, A. *Chem. Soc. (London), Spec. Publ.* 1965, **19**, 109
- 16 For an excellent and comprehensive review, see Szwarc, M. 'Carbanions, living polymers and electron-transfer processes,' Interscience, New York, 1968
- 17 Plesch, P. H. *Progress in High Polymers* 1968, **2**, 137
- 18 Darcy, L. E., Millrine, W. P. and Pepper, D. C. *Chem. Comm.* 1968, p 1441
McCarthy, B., Millrine, W. P. and Pepper, D. C. *ibid.* 1968, p 1442
- 19 Bowyer, P. M., Ledwith, A. and Sherrington, D. C. *J. Chem. Soc. (B)* 1971, in press.
- 20 Coetzee, J. F., Cunningham, G. P., McGuire, D. K. and Padmanabhan, G. R. *Analyt. Chem.* 1962, **34**, 1139
- 21 Reid, D. H., Frazer, M., Molloy, B. B. and Payne, H. A. S. *Tetrahedron Letters* 1961, **15**, 530
- 22 Ueberrieter, K. and Springer, J. Z. *Phys. Chem. (Frankfurt)* 1963, **36**, 299
- 23 Sitaramaiah, G. and Jacobs, D. *Polymer, Lond.* 1970, **11**, 165
- 24 Eckard, A., unpublished work
- 25 Bruck, P., Ledwith, A. and White, A. C. *J. Chem. Soc. (B)* 1970, p 205;
Bruck, P. *J. Org. Chem.* 1970, **35**, 2222;
Iles, D. H. and Ledwith, A. *Chem. Comm.* 1969, p 364;
Sumpter, W. C. and Miller, F. M. 'The chemistry of heterocyclic compounds', Vol. 8 (A. Weissberger, Ed.), Interscience, New York, 1954
- 26 Eley, D. D., 'The chemistry of cationic polymerisation', (P. H. Plesch, Ed.) Pergamon, Oxford, 1963, p 375
- 27 Zlamal, Z. in 'Vinyl Polymerisation', Vol. 1, Pt. II (G. Ham, Ed.) Dekker, New York, 1970, p. 231
- 28 Sambhi, M., PhD Thesis, Univ. of Liverpool, 1966
- 29 McGeachin, S. G. *Canad. J. Chem.* 1969, **47**, 151
- 30 Ellinger, L. P. *Advances in Makromol. Chem.* 1968, **1**, 169
- 31 Williams, F., Hayashi, K., Ueno, K., Hayashi, K. and Okamura, S. *Trans. Faraday Soc.* 1967, **63**, 1501;
Ueno, K., Hayashi, K. and Okamura, S. *J. Macromol. Sci.* 1968, **2**, 209;
Metz, D. J. *Amer. Chem. Soc. Advances in Chemistry Series* 1961, **91**, 202
- 32 Tazuke, S. *Chem. Comm.* 1970, p 1277
- 33 Hogan-Esch T. E. and Smid, J. J. *Amer. Chem. Soc.* 1967, **98**, 2764;
Hunter, D. H. and Lin, Y-T. *J. Amer. Chem. Soc.* 1968, **90**, 5921
- 34 Ledwith, A., North, A. M. and Whitelock, K. E. *European Polymer J.* 1968, **4**, 133
- 35 Hellwinkel, D. and Seifert, H. *Chem. Comm.* 1968, p 1683

Notes to the Editor

ESR and crystallinity of polyphenyleneisoxazole

S. J. HONG*, Y. IWAKURA and K. UNO

We have already reported the synthesis of a polyphenyleneisoxazole with high crystallinity by the direct condensation of terephthalohydroxamoyl chloride with 1,4-diethynylbenzene in refluxing toluene¹. In the present communication, we describe further experimental findings on the e.s.r. and the crystallinity of polyphenyleneisoxazole at low temperature. The polymer used was prepared and purified by extracting in hot methanol as previously described¹.



$\eta_{sp}/c = 0.24$ in 0.5 g/dl of 98% sulphuric acid.
 $\nu(C=C) = 1610 \text{ cm}^{-1}$. N: found, 9.5% (calculated, 9.5%)

The e.s.r. signal of polyphenyleneisoxazole observed in the solid state showed asymmetric multiplet absorption lines at room temperature. The shape of the shoulder varied with power from 4 to 20 to 40 mW, at -10°C , as indicated in *Figure 1*. This clearly demonstrates the occurrences of at least two kinds of stable free radicals in the polymer. If only one single radical were present, the shape of the shoulder part of the absorption line should be reduced or enlarged regularly with power.

The g -factor of the spectra of polyphenyleneisoxazole was 2.0035 ± 0.0001 at room temperature and no change of g -factor was observed at -196°C . TCNQ-Li complex was used as a standard (g -factor, 2.0026 ± 0.0001 from reference 2).

The x-ray diffraction diagrams were obtained by the powder method using nickel-filtered $\text{Cu-K}\alpha$ radiation at 40 kV, 20 mA, and at $2^\circ/\text{min}$ of scanning speed, at 25, -10 , -60 , -100 , and -180°C . *Figure 2* shows the XRD pattern at 25°C . The change in the 2θ values with lowering temperature is shown in *Figure 3*. The value of 2θ of polyphenyleneisoxazole increased on lowering the temperature. However, the 2θ value of 7.1° measured at 25°C did not change, and this can only be attributed to the polymer chain. On the other hand, shifting of 2θ to higher values is due to the narrowing of interplanar spacing of crystalline polymer.

The isoxazole ring is known to release electrons less readily than the phenyl group^{3,4}. This idea about phenylisoxazole can also be applied to

*All correspondence should be sent to this author at the following address: Dept. of Chemical Engineering, Kon-kuk University, Seoul, Korea

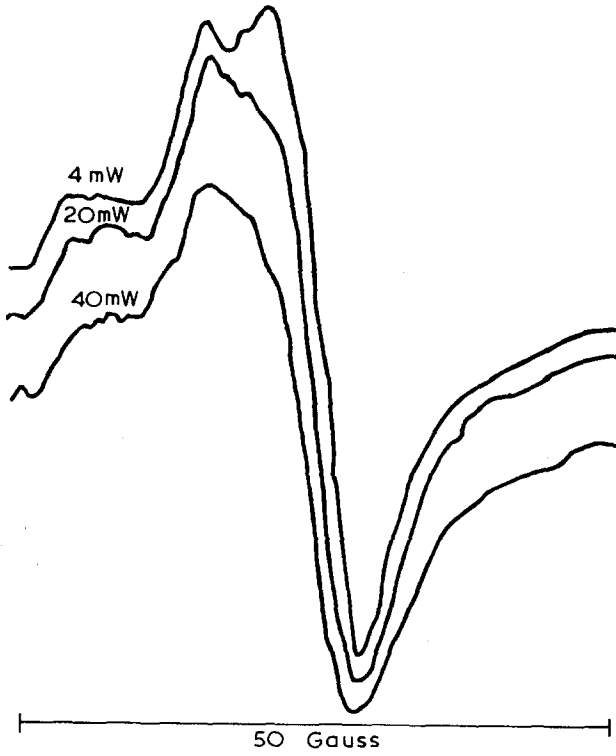


Figure 1 Change in the e.s.r. spectrum of polyphenyleneisoxazole on variation of power, at -10°C

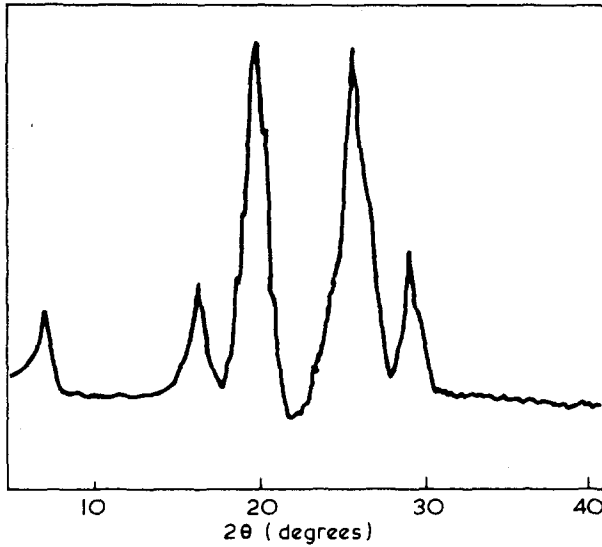


Figure 2 The XRD pattern of polyphenyleneisoxazole at 25°C

polyphenyleneisoxazole. The phenylene group would act as the electron donor, and the isoxazole ring as the electron acceptor. If the polyphenyleneisoxazole is considered to form a band structure, the phenylene group would interact with isoxazole rings between the bands. Thus charge transfer would occur. This interaction between bands would get stronger as the

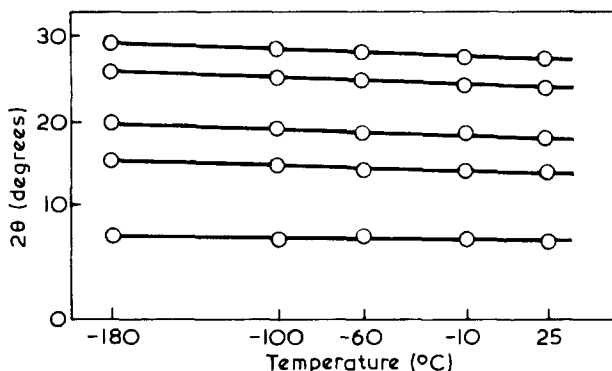


Figure 3 Values of 2θ for polyphenyleneisoxazole plotted against temperature. A linear relationship is obtained

temperature is lowered and the interplanar spacing of crystalline structure and the distance between the bands would become less. Also, the absorption intensity of the e.s.r. spectra increases as the temperature is lowered.

The possibility of charge transfer interaction between the crystalline bands deserves consideration. Further investigations are in progress, to characterize the radical species and crystalline structure.

ACKNOWLEDGEMENTS

The authors acknowledge Dr M. Sukigara for his helpful discussion. We are also indebted to the Rigaku-Denki Company for the measurement of the x-ray diffraction, and the Japan Electron Optics Laboratory Company Ltd, for the e.s.r. measurements.

*Department of Synthetic Chemistry,
Faculty of Engineering,
The University, Tokyo, Japan*

(Received 26 April 1971)

REFERENCES

- 1 Iwakura, Y., Uno, K., Hong, S. J. and Hongu, T., *Polymer Journal, Japan*, 1971, 2, 36
- 2 Determined by Japan Electron Optics Laboratory Co., Ltd
- 3 Katritzky, A. R., and Boulton, A. J. *Spectro chim. Acta* 1961, 17, 238
- 4 Boulton, A. J., and Katritzky, A. R. *Tetrahedron* 1961, 12, 51

The far infra-red spectrum and skeletal vibrations of syndiotactic poly(methyl methacrylate)

T. R. MANLEY and C. G. MARTIN

Samples of poly(methyl methacrylate) (PMMA) were polymerized with u.v. radiation at room temperature. Cast film (0.001 in, 0.025 mm), microtomed sections (0.003–0.005 in) and rod (0.5 in diameter) were obtained. Comparison of their spectra in the 4000–650 cm^{-1} region (Grubb Parsons GS3) with a spectrum of syndiotactic PMMA showed that predominantly syndiotactic species (*s*-PMMA) were present.

The far infra-red spectra were obtained using a Grubb Parsons DM4 double beam grating spectrophotometer (500–200 cm^{-1}) and a Grubb Parsons IS3 Fourier Transform Spectrometer (480–10 cm^{-1}) with 0.00025 in, 0.0005 in and 0.001 in beam splitters. Raman spectra were obtained by courtesy of Professor D. A. Long on a Spex spectrometer using an argon arc laser with an exciting line of 20 493 cm^{-1} and power of approximately 1.5

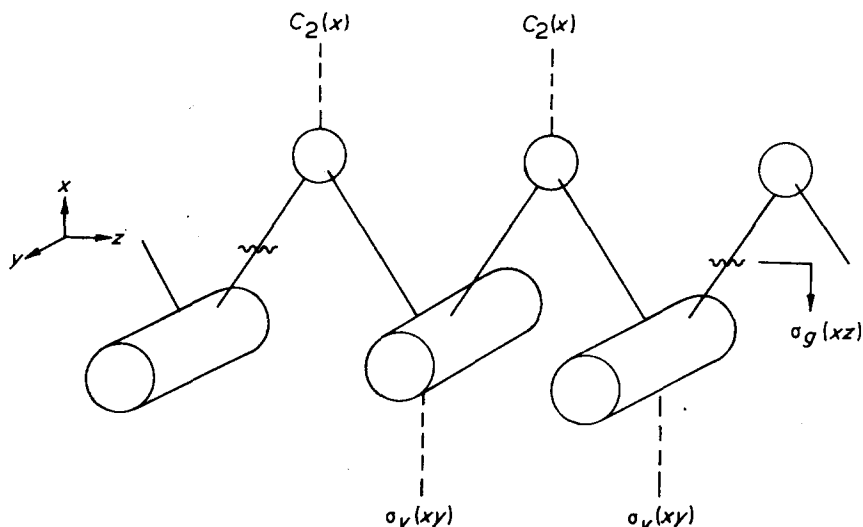


Figure 1 Schematic diagram of model used in treatment of skeletal modes of syndiotactic poly(methyl methacrylate)

watts. The Raman spectra and infra-red spectra between 4000 and 250 cm^{-1} were in substantial agreement with those of Willis *et al*¹.

Several bands were observed in the longer wavelength region which have not been reported previously, namely:

35 cm^{-1} , 58 cm^{-1} , 95 cm^{-1} , 225 cm^{-1} (216 cm^{-1} Raman)

Since skeletal vibrations are known to occur in the far infra-red region, a study of the skeletal modes of syndiotactic PMMA was undertaken. A schematic model (Figure 1) for the treatment of the skeletal modes can be obtained

$$\left[\begin{array}{l}
 M_2\omega^2 - G - 2F\sin^2\frac{dK}{2} \quad G\cos\frac{dK}{2} \quad iP\sin dK \quad i(N - 2P)\sin\frac{dK}{2} \\
 G\cos\frac{dK}{2} \quad M_1\omega^2 - G - 2F\sin^2\frac{dK}{2} \quad i(2P - N)\sin\frac{dK}{2} \quad -iP\sin dK \\
 -iP\sin dK \quad i(N - 2P)\sin\frac{dK}{2} \quad M_2\omega^2 - R - Q(\cos dK + 3) \quad (4Q + R)\cos\frac{dK}{2} \\
 i(2P - N)\sin\frac{dK}{2} \quad iP\sin dK \quad (4Q + R)\cos\frac{dK}{2} \quad M_1\omega^2 - R - Q(\cos dK + 3)
 \end{array} \right] = 0$$

where $G = 2k_s\cos^2\alpha$
 $F = 2k_b\sin^2\alpha$
 $N = 2k_s\cos\alpha\sin\alpha$
 $d =$ repeat distance
 $k_b =$ bending force constant of the C-C-C angle
 $M_2 =$ mass of (CH₃-C-COOCH₃) group
 (force constant data taken from reference 5)

$P = 2k_b\cos\alpha\sin\alpha$
 $Q = 2k_b\cos^2\alpha$
 $R = 2k_s\sin^2\alpha$

$k_s =$ stretching force constant of the C-C bond
 $M_1 =$ mass of a CH₂ group
 $\alpha =$ angle between any C-C bond and the chain direction

(Equation 1)

by considering a single *s*-PMMA chain in which the backbone carbon atoms form an extended planar zig-zag arrangement² and with the CH₂ group and the ester and α -methyl group treated as structureless masses in a plane perpendicular to the backbone axis.

The symmetry elements of this model show that the line group of the polymer chain has a factor group isomorphous with the point group *C*_{2v}. Due to the alternate nature of the syndiotactic chain there are four 'masses' in the repeat unit and hence there will be 3*N* = 12 skeletal normal vibrations of which four will be non-genuine, i.e. three translations and one rotation about the chain axis. Of the remaining eight genuine vibrations, six will be infra-red active and all are Raman active.

The symmetry species, characters, number of skeletal normal modes and selection rules for *s*-PMMA are given in *Table 1*.

Table 1 Symmetry species, number of skeletal normal modes (*n*) and selection rules for extended syndiotactic poly(methyl methacrylate)

<i>C</i> _{2v}	<i>E</i>	<i>C</i> ₂ (<i>x</i>)	$\sigma_v(xy)$	$\sigma_v(xz)$	<i>n</i>	T.R.	I.R.	R.
A ₁	1	1	1	1	2	<i>T_x</i>	a	a
A ₂	1	1	-1	-1	2	—	i	a
B ₁	1	-1	1	-1	2	<i>T_y, R_z</i>	a	a
B ₂	1	-1	-1	1	2	<i>T_z</i>	a	a

a = active, i = inactive

As an aid to the assignment of the skeletal modes the expected frequencies were calculated. For this purpose the model in *Figure 1* was considered as an infinite planar zig-zag chain of point masses *M*₁ and *M*₂, where *M*₁ is the mass of a (CH₂) group and *M*₂ is the mass of the (CH₃-C-COOCH₃) group.

From Kirkwood's equations³ for the in-plane vibrations, Zbinden^{4a} obtained the secular equation, shown opposite as equation (1), for an infinite chain of unequal point masses.

In equation (1) *K* is the 'wave number vector' and is related to the phase difference ϕ between successive masses by

$$\phi = \frac{dK}{2} \quad (2)$$

Since the only potentially active vibrations are those in which each unit cell is vibrating in phase then if the repeat unit of the chain contains *q* chemical units these frequencies must satisfy the condition⁵:

$$\phi = \frac{2r}{q} \text{ where } r = 0, 1, \dots, (q - 1) \quad (3a)$$

or

$$K = \frac{4r}{dq} \text{ where } r = 0, 1, \dots, (q - 1) \quad (3b)$$

Hence for *s*-PMMA where $q = 4$, the only allowable values of phase difference for potentially active vibrations are:

$$\phi = 0, \frac{\pi}{2}, \pi, \frac{3\pi}{2}, K = 0, \frac{\pi}{d}, \frac{2\pi}{d}, \frac{3\pi}{d}$$

and thus equation (1) reduces to

$$\begin{bmatrix} (M_2\omega^2 - G) & G & 0 & 0 \\ G & (M_1\omega^2 - G) & 0 & 0 \\ 0 & 0 & (M_2\omega^2 - R - 4Q) & (4Q + R) \\ 0 & 0 & (4Q + R) & (M_1\omega^2 - R - 4Q) \end{bmatrix} = 0 \quad (4)$$

for $\phi = 0, \pi, K = 0, 2\pi/d$

which factorizes into two quadratic equations in ω^2 giving $\nu_1 = 0, \nu_2 = 803 \text{ cm}^{-1}, \nu_3 = 0, \nu_4 = 761 \text{ cm}^{-1}$, ($\omega = 2\pi c\nu$, where c is the velocity of light) and

$$\begin{bmatrix} (M_2\omega^2 - G - 2F) & 0 & 0 & i(N - 2P) \\ 0 & (M_1\omega^2 - G - 2F) & i(2P - N) & 0 \\ 0 & i(N - 2P) & (M_2\omega^2 - R - 2Q) & 0 \\ i(2P - N) & 0 & 0 & (M_1\omega^2 - R - 2Q) \end{bmatrix} = 0 \quad (5)$$

for $\phi = \pi/2, K = \pi/d$

and the same result after expansion for $\phi = 3\pi/2, K = 3\pi/d$. Expansion of equation (5) results in a biquadratic equation in ω^2 with four real roots,

$$\nu_5 = 796 \text{ cm}^{-1}, \nu_6 = 370 \text{ cm}^{-1}, \nu_7 = 591 \text{ cm}^{-1}, \nu_8 = 201 \text{ cm}^{-1}.$$

Thus vibrations $\nu_1-\nu_8$ are the in-plane vibrations and include two null vibrations.

The solution for the out-of-plane normal vibrations of a zig-zag chain is given by Zbinden^{4b} following Pitzer⁶, as:

$$\omega^2 = \frac{4K_t \sin^2\left(\frac{dK}{2}\right)}{M_1 M_2} \left[M_1 + M_2 \pm \sqrt{M_1^2 + M_2^2 + 2M_1 M_2 \cos dK} \right] \quad (6)$$

where K_t is the torsional force constant for the C-C-C-C chain. It is seen that for $\phi = 0, \pi, K = 0, 2\pi/d$ the potentially active vibrations are zero vibrations. However for

$$\phi = \frac{\pi}{2}, \frac{3\pi}{2}, K = \frac{\pi}{d}, \frac{3\pi}{d} \quad (7a)$$

$$\omega_+^2 = \frac{8K_t}{M_2} \text{ and } \omega_-^2 = \frac{8K_t}{M_1} \quad (7b)$$

Therefore for the out-of-plane vibrations we obtain

$$\nu_9 = 0, \nu_{10} = 182 \text{ cm}^{-1}, \nu_{11} = 0, \nu_{12} = 73 \text{ cm}^{-1}.$$

Thus the calculations give eight genuine frequencies and four zero frequencies as predicted by the group symmetry analysis (Table 1).

The calculated frequencies are compared with the observed frequencies and their assignments given in *Table 2*.

Table 2 Skeletal modes and assignments of syndiotactic poly(methyl methacrylate)

Observed frequency		Calculated frequency		Assignment
Infra-red (cm^{-1})	Raman $\Delta\nu(\text{cm}^{-1})$			
807 vw	786 w ^(a)	ν_2 803	$\nu(\text{C}-\text{C}) \parallel$	(B ₂) $\nu_+(\pi)$ ^(c)
749 m	732 w	ν_4 761	$\nu(\text{C}-\text{C}) \perp$	(A ₁) $\nu_+(0)$
—	786 w ^(a)	ν_5 796	$\nu(\text{C}-\text{C})$	(A ₂) $\nu_+(\frac{\pi}{2})$ & $\nu_+(\frac{3\pi}{2})$
552 vw	552 w	ν_7 591	$\nu(\text{C}-\text{C})$	(B ₁) $\nu_+(\frac{\pi}{2})$ & $\nu_+(\frac{3\pi}{2})$
320 sh	296 w	ν_6 370	$\delta(\text{C}-\text{C}-\text{C})$ in-plane	(B ₁) $\nu_-(\frac{\pi}{2})$ & $\nu_-(\frac{3\pi}{2})$
—	216 ^(b)	ν_8 201	$\delta(\text{C}-\text{C}-\text{C})$ in-plane	(A ₂) $\nu_-(\frac{\pi}{2})$ & $\nu_-(\frac{3\pi}{2})$
225 w,br	216 ^(b) w	ν_{10} 182	$\delta(\text{C}-\text{C}-\text{C})$ out-of-plane	(B ₂) $\nu(\frac{\pi}{2})$ & $\nu(\frac{3\pi}{2})$
95 w	— ^(d)	ν_{12} 73	$\delta(\text{C}-\text{C}-\text{C})$ out-of-plane	(A ₁) $\nu(\frac{\pi}{2})$ & $\nu(\frac{3\pi}{2})$
58vww	—	—	hindered rotation	
34vww	—	—	or translation	

(a) observed as broad weak shoulder on strong band $\Delta\nu = 810 \text{ cm}^{-1}$

(b) very broad band $\approx 186\text{--}246 \text{ cm}^{-1}$

(c) notation of reference 5

(d) outside range of instrument without special filters

Abbreviations: w = weak, v = very, m = medium, sh = shoulder, br = broad, ν = stretching, δ = bending

In the calculations we have replaced the (CH_2) and $(\text{CH}_3\text{--C--COOCH}_3)$ groups by point masses. However, this approximation applies only where there is strong coupling between the chain carbon atoms and the substituents, for weaker coupling the mass M_2 must be replaced by a point mass somewhere between the mass of a C atom and the mass of the $(\text{CH}_3\text{--C--COOCH}_3)$ group. Hence the calculated frequencies will be higher for lesser degrees of coupling. Also since the results are affected by choice of force constants the calculated frequencies may only be used as guides to assignments.

The force constants used in the methacrylate calculations are those for polythene⁵. Re-calculation of the skeletal frequencies of polythene using these values in the above equations give the same results for $\nu_+(0)$, $\nu_+(\pi)$ and the degenerate modes $\nu_+(\pi/2)$, $\nu_+(3\pi/2)$, $\nu_-(\pi/2)$, $\nu_-(3\pi/2)$ and $\nu(\pi/2)$, $\nu(3\pi/2)$.

The degeneracy of these modes arises because the repeat distance was considered to contain two identical monomer units, i.e. four CH_2 groups.

The values for polythene have been used in the assignment of the skeletal modes of syndiotactic poly(vinyl chloride)⁷. However, in the case of *s*-PVC the repeat distance no longer contains two identical monomer units and hence the degeneracy is split, e.g. $\nu_+(\pi/2)$ and $\nu_+(3\pi/2)$ modes will be of different frequencies as shown in *Table 3*.

The use of the assignments based on polythene is supported by the close agreement between the results obtained. Thus the degree of coupling of the backbone chain and the H and Cl atoms in *s*-PVC must be small since the observed values are quite close to those calculated for the carbon chain in polythene.

Table 3 Comparison of the skeletal vibrations and assignments of polythene, *s*-PVC and *s*-PMMA

Assignment ^(a)	Polythene ^(a)	<i>s</i> -PVC ^(b)	<i>s</i> -PMMA ^(c)	
	Calculated frequency (cm ⁻¹)	Observed frequency (cm ⁻¹)	Calculated frequency (cm ⁻¹)	Observed frequency (cm ⁻¹)
$\nu_+(0)$	1070	1096	761	749
$\nu_+(\pi)$	1137	1125	803	807
$\nu_+(\frac{\pi}{2})$ & $\nu_+(\frac{3\pi}{2})$	980	{ 963 833	{ 796 591	{ 786 ^(d) 552
$\nu_-(\frac{\pi}{2})$ & $\nu_-(\frac{3\pi}{2})$	438	{ 487 430	{ 370 201	{ 320 216 ^(d)
$\nu(\frac{\pi}{2})$ & $\nu(\frac{3\pi}{2})$	198	{ 182 160	{ 182 73	{ 225 95

(a) reference 5, (b) reference 7, (c) see Table 2, (d) from Raman spectrum

A similar splitting is expected for *s*-PMMA due to the alternation in position of the ester and α -methyl groups. However, it is not possible to assign the skeletal modes of *s*-PMMA by analogy with the polythene results. The bands observed in *s*-PMMA in the regions of the calculated skeletal modes of polythene are all accounted for by α -methyl and ester group vibrations¹. Also, the methacrylate calculations performed in this work give assignments at much lower frequencies than those calculated for polythene.

The Raman bands observed in *s*-PMMA at 1060 cm⁻¹ (i.r. 1063 cm⁻¹) and 1125 cm⁻¹ have been attributed to skeletal vibrations^{1,2,8}. They coincide with the calculated values for $\nu_+(0)$ and $\nu_+(\pi)$ in polythene but are much higher than our calculated values for those modes in *s*-PMMA. These bands are now assigned therefore as either uncoupled carbon backbone stretching modes⁵ or a combination of CH₃ (rock), CH₂ (wag) and C-C stretch for the 1125 cm⁻¹ band and a combination of C-C stretch, C-CH₃ stretch and C-(COOCH₃) bending for the 1060 cm⁻¹ (i.r. 1063 cm⁻¹) band. This agrees with bands observed⁹ at 1130 cm⁻¹ and 1095 cm⁻¹ respectively for the *trans* form of syndiotactic polypropylene, C-H bending of course being involved in the latter.

The observed frequencies for *s*-PMMA are in fair agreement with those now calculated (see Table 3), indicating that the degree of coupling is higher than that of *s*-PVC.

The parallel and perpendicular chain stretching modes $\nu_+(\pi)$ and $\nu_+(0)$ are assigned to $\nu_2(B_2)$ and $\nu_4(A_1)$ observed at 807 cm⁻¹ ($\Delta\nu \approx 786$ cm⁻¹) and 749 cm⁻¹ ($\Delta\nu = 732$ cm⁻¹).

The out-of-plane bending modes $\nu_{10}(B_2)$ and $\nu_{12}A(1)$ are assigned to the bands observed at 225 cm⁻¹ and 95 cm⁻¹, respectively. Part of the very broad weak band observed at $\Delta\nu = 216$ cm⁻¹ in the Raman is attributed to ν_{10} ; ν_{12} observed at 95 cm⁻¹ could not be resolved in the Raman because of its nearness to the exciting line.

This will be examined at a later date using filtering techniques to remove the Rayleigh line.

Out of the four remaining bands ν_5 - ν_8 , two are of A_2 species and two of B_1 species.

Since the A_2 species are infra-red inactive the B_1 species are assigned to the bands observed at 320 cm^{-1} ($\Delta\nu = 296\text{ cm}^{-1}$) and 552 cm^{-1} ($\Delta\nu = 552\text{ cm}^{-1}$) which are in fair agreement with the calculated frequencies ν_6 and ν_7 , respectively.

The two remaining infra-red inactive bands are thus assigned to $\nu_5(A_2)$ which is observed at $\Delta\nu \approx 786\text{ cm}^{-1}$ along with ν_2 (i.r. 807 cm^{-1}) as a broad weak shoulder on the strong band observed at $\Delta\nu = 810\text{ cm}^{-1}$, and to $\nu_1(A_2)$ which is observed as part of the very broad band at $\Delta\nu = 216\text{ cm}^{-1}$ along with $\nu_{10}(B_2)$ (i.r. 225 cm^{-1}).

The weak shoulder observed at 400 cm^{-1} has been assigned¹ to $\delta(\overset{\parallel}{\text{COC}})$ of the ester group. Examination of spectra of poly(ethylene terephthalate), poly(cyclohexane 1,4-dimethyleneterephthalate) and related model compounds^{10,11} show that the $\delta(\overset{\parallel}{\text{COC}})$ mode appears as an out-of-plane component at 400 cm^{-1} and an in-plane component at 190 cm^{-1} . Similarly in poly(ethylene glycol) contributions from $\delta(\overset{\parallel}{\text{COC}})$ appear at 209 cm^{-1} and 392 cm^{-1} ¹². Therefore, the weak band at 400 cm^{-1} is probably $\delta(\overset{\parallel}{\text{COC}})$ out of the plane of the ester group with $\delta(\overset{\parallel}{\text{COC}})$ in the plane of the ester group, adding to the out of plane and in-plane skeletal bending modes ν_{10} and ν_8 resulting in the broad weak band observed at 225 cm^{-1} in the infra-red and the very broad weak band ($\Delta\nu = 216\text{ cm}^{-1}$) in the Raman.

The two bands for $\delta(\overset{\parallel}{\text{COC}})$ parallel and perpendicular to the plane of the ester group should exhibit σ and π polarization respectively with respect to the polymer chain axis.

Finally, the two very weak bands observed at 34 cm^{-1} and 58 cm^{-1} are tentatively assigned to hindered rotation and translation modes in the more ordered parts of the polymer.

ACKNOWLEDGEMENT

We thank the Science Research Council for a studentship to C. G. Martin.

*Department of Materials Science,
Newcastle upon Tyne Polytechnic,
Ellison Building, Ellison Place,
Newcastle upon Tyne, NE1 8ST, UK*

(Received 29 March 1971)

REFERENCES

- 1 Willis, H. A., Zichy, V. J. I. and Hendra, P. J. *Polymer, Lond.* 1969, **10**, 737
- 2 Havriliak, S. and Roman, N. *Polymer, Lond.* 1966, **7**, 387
- 3 Kirkwood, J. G. *J. Chem. Phys.* 1939, **7**, 506

- 4 Zbinden, R., 'Infrared Spectroscopy of High Polymers', Academic Press, London, 1964, (a) p 111, (b) p 118
- 5 Krimm, S., Liang, C. Y. and Sutherland, C. B. B. M. *J. Chem. Phys.* 1956, **25**, 543
- 6 Pitzer, S. *J. Chem. Phys.* 1940, **8**, 711
- 7 Krimm, S. and Liang, C. Y. *J. Polym. Sci.* 1956, **22**, 95
- 8 Nagai, H. *J. Appl. Polym. Sci.* 1963, **7**, 1697
- 9 Schachtschneider, J. H. and Snyder, R. G. *Spectrochim. Acta* 1965, **21**, 1527
- 10 Manley, T. R. and Williams, D. A. *Polymer, Lond.* 1969, **10**, 339
- 11 Manley, T. R. and Williams, D. A. *Polymer, Lond.* 1971, **12**, 2
- 12 Miyazawa, T., Fukushima, K. and Ideguchi, Y. *J. Chem. Phys.* 1962, **37**, 2764

Book review

Ring-forming polymerizations, Vol. 13A

Carbocyclic and metallorganic rings

by R. J. COTTER and M. MATZNER

Academic Press, New York and London, 1969, 395 pp., \$19.50

In their preface to this book, one of the Academic Press series of monographs on organic chemistry, the authors state their objective of 'attempting to collect and classify . . . the formation of linear polymers containing a new ring structure', i.e., where the polymerization reaction results in the introduction of cyclic units within the polymer chain. The present work is the first part of a two-volume project on the literature of such ring-forming polymerizations and provides a comprehensive and up-to-date review of synthetic methods leading to polymers with carbocyclic or organometallic rings.

Discussing linear polymer formation from polyfunctional rather than from strictly difunctional precursors, the authors refer to Carothers' classical papers and suggest that progress may have been 'delayed by the functionality laws of polymer science'. Be that as it may, the many reactions reviewed here would show the extensive researches carried out in many directions so as to provide ring-containing linear and ladder polymers rather than uncontrolled networks.

The first four chapters deal with polymerizing systems whereby homocyclic carbon rings are introduced and cover polymers containing double bonds (regarded as two-membered rings), intra-intermolecular processes, and Diels-Alder and other reactions in which polymers are formed. Chapters 5-10 relate to polymers from metals and unsaturated carbon compounds and to organometallic polymers produced by chelation processes involving ring formation. The final chapter (11) deals with the formation of polysiloxanes, polysilazanes and some polymetalloxanes.

The book extensively catalogues the relevant reactions and polymers falling within the scope of the classification adopted, each chapter providing information on the methods employed, together with clear formulae for the reactions involved and, where appropriate, an indication of the properties of the materials. Within the individual chapters there are comprehensive tables which index the monomers and derived polymers, properties, and comments on structure, together with relevant references which are then listed in full. A supplementary reference list provided at the end of the book brings the literature up to 1968.

Although few of the very many polymers reviewed are likely to have industrial applications, much important information on polymer formation and structure is collected, and this comprehensive compilation undertaken by the authors will be of value to those concerned with many aspects of polymer synthesis and properties. It provides a useful first source for reference purposes, more detailed information then being available by recourse to the original papers. In addition, the book will be of value to those having a more general interest in organic and organometallic syntheses in indicating the scope and applications of the individual reactions. The book is well produced and provided with a multitude of clearly presented formulae, together with a numbering and indexing system which contributes much to the ease with which the text and tables can be consulted.

R. J. W. REYNOLDS

Ductile crack growth in poly(ethylene terephthalate) film

P. I. VINCENT

A study of crack growth in a poly(ethylene terephthalate) film has been made to check the applicability of fracture mechanics and to devise a suitable technique for assessing the fracture toughness of ductile thermoplastics. A combination of mechanical tests and microscopic examination has shown that fracture mechanics, in a simple single-parameter form, cannot be applied to this material. It is concluded that, because careful tensile tests on unnotched specimens can give so much useful information, it is worth considering whether tests on sharply notched specimens are desirable.

INTRODUCTION

SINCE THE pioneering work by Berry¹ in 1961 some of the fundamental studies of fracture in thermoplastics have followed the Griffith–Orowan–Irwin approach known as fracture mechanics². Sharply notched or cracked specimens have been used, stress distributions and fracture toughness being calculated by assuming linear elasticity. For the more brittle polymers, such as polystyrene and poly(methyl methacrylate), this approach has unified the behaviour of sharply notched specimens with different shapes³ and has demonstrated the overwhelming contribution to fracture toughness of high but localized strains^{1,4}. However, the majority of commercial thermoplastics are less brittle than these two materials; in standard tensile tests at room temperature it is common to observe load-extension relations which are far from linear. It appears unlikely that the fracture behaviour of such ductile materials can be treated satisfactorily by theories which assume linear elasticity. Nevertheless, because of the increasing popularity of this approach, it seemed desirable to make a detailed examination of crack propagation in a ductile thermoplastic in order to discover more about the uses and limitations of linear elastic fracture mechanics for this important class of materials. This paper describes the results. Some of the work summarized here has been published in more detail in two reports with limited circulation^{5,6} which are available on application to the author.

TEST MATERIAL

The material selected for this work was a commercial biaxially drawn and thermally crystallized poly(ethylene terephthalate) film about 25 μm thick. This material is both mechanically and optically anisotropic. It has three different principal refractive indices γ , β and α where $\gamma > \beta > \alpha$. The particular sample used was specially selected so that β was in the extrusion direction, γ was in the transverse direction and α was perpendicular to the film plane.

Figure 1 shows the non-linear tensile stress/strain curve obtained when a parallel-sided strip was extended at room temperature; the specimen was 1 cm wide, 10 cm between the clamps and was stretched in the γ direction at 5 mm per minute. No crazes, deformation bands or necks were observed in the specimen during extension; this is thought to be a consequence of the fact that there is no drop in load before fracture.

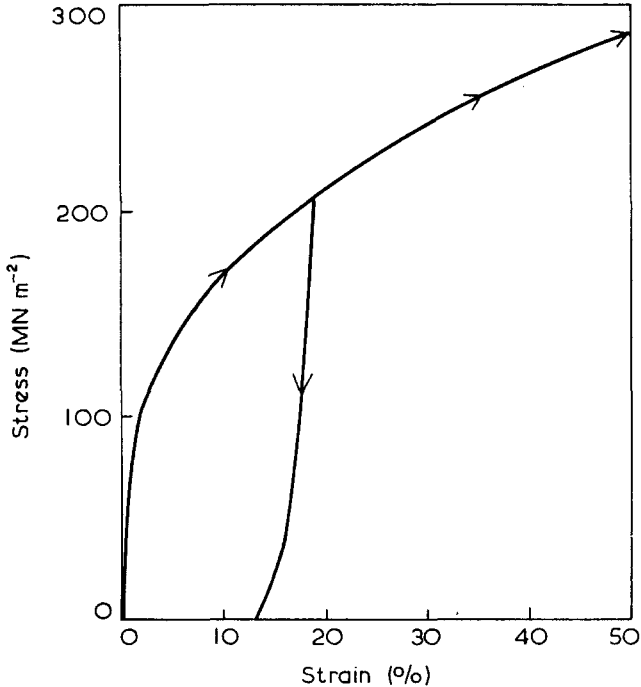


Figure 1 Tensile stress/strain curve for the test material in the γ direction with the recovery curve from 19% strain. The elongation to break is between 57% and 62%

NOTCHING TECHNIQUE

The actual point on the load/extension curve at which fracture occurs, when a parallel-sided strip is stretched, depends to some extent on accidental defects in the specimen which are difficult to control or quantify. In the fracture mechanics approach a sharp notch or crack is inserted in the specimen; this controlled defect is so severe that it overrides the accidental defects, and its length can be measured. To obtain reliable results it is necessary to ensure that the tip of the notch is clean and sharp and that the material adjacent to the notch has not been permanently deformed. For the 25 μm thick film used in this study parallel-sided strips were notched with a new razor blade while the specimen was held under a tensile strain of about 1%. The tip radius of a notch produced in this way was found to be too small to measure in an optical microscope and there was no evidence of residual deformation.

Equally good results were not obtained when notching other materials in the same way. In a thicker film of the same material the crack front tilted sideways as it advanced ahead of the razor blade. In films from several other polymers it was difficult to avoid permanent deformation in front of the notch tip.

CRACK GROWTH PHENOMENA AND MACROSCOPIC STRESSES

When a notched specimen of the test material is extended, the crack grows in a controllable manner in the sense that the growth can be halted by removing the applied deformation. A previous report⁵ has shown that the results of tests on notched strips extended in the β direction cannot be accounted for by theories based on average stresses or on the linear elastic assumption. *Table 1*

Table 1 Tests on single-edge-notched strips extended in the γ direction

Initial notch depth (mm)	Net stress (MN m ⁻²)	Stress intensity factor (MN m ^{-3/2})	Crack growth (μ m)
4.42	60	9.40	147
4.34	56.6	8.71	75
4.40	50	7.72	31
4.63	45	7.35	9.5
1.67	85	6.71	63
1.81	75	6.16	32
1.78	65	5.33	21
1.41	61.2	4.43	14
1.38	55	3.93	7.6
1.87	50	4.16	4.2
0.36	79.2	2.89	13.2
0.39	71.1	2.70	6.9
0.37	60.4	2.24	5.2

summarizes some further tests on single-edge-notched strips extended in the γ direction. The specimens were extended at constant speed until the required load was reached; the specimen was then unloaded and the crack growth was measured with a microscope. *Figure 2* shows the amount of crack growth as a function of the net stress on the reduced section. The results fall into three groups depending on the initial depth of the notch. It is obvious that these measurements cannot be unified by considering only the net stress; there is, however, an indication that the amount of crack growth is unmeasurably small when the net stress is less than 40 MN/m² over the whole range of notch depths used. *Figure 3* shows the amount of crack growth as a function of the stress intensity factor calculated using the correction factors given by Paris and Sih⁷. As before⁵ it is clear that these results cannot be accounted for by considering the stress intensity factor calculated by linear elastic fracture mechanics. Furthermore, a comparison of *Figures 2* and *3* suggests that the

net stress is a more useful parameter than the stress intensity factor; the curves of *Figure 3* do not suggest that the initiation of observable crack growth occurs at a single value of the stress intensity factor.

Rice⁸ has stated that linear elastic stress intensity factors are useful when 'the yielded zone at the tip is small compared to characteristic geometric dimensions'. He goes on to say that such 'small-scale yielding solutions have been found to be highly accurate approximations to available complete

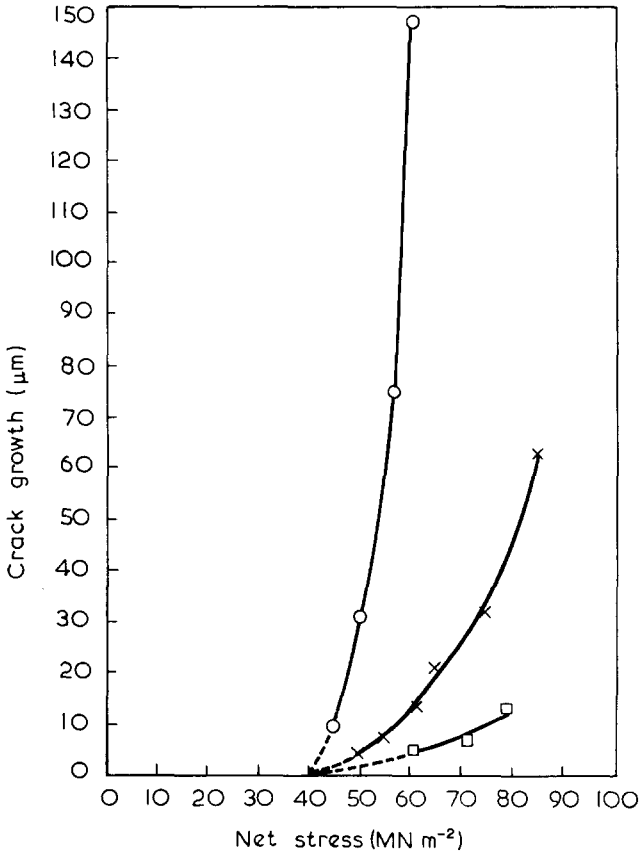


Figure 2 Crack growth as a function of average net stress on the reduced section for various initial notch depths: ○, 4.34–4.63 mm; ×, 1.38–1.87 mm; □, 0.36–0.39 mm

solutions up to substantial fractions (typically, one-half) of general yielding loads'. From *Figure 1* the stress/strain relation becomes grossly non-linear at a stress around 100 MN/m² which may be taken as the yield stress in the γ direction. From *Table 1* and *Figure 2* it can be concluded that the small-scale yielding solution is not an adequately accurate approximation when the net stress is over 40% of the yield stress. Evidently there is only observable crack growth when the average stress is so large, relative to the yield stress, that the

yielded zone is large and the linear elastic stress intensity factor is no longer a useful measure of the stress field.

It is possible to obtain some appreciation of the size of the yielded zone by stretching a notched specimen and observing it between crossed polars. *Figure 4* is a micrograph of such a specimen taken by monochromatic green light. At this stage the crack had grown forward about 30 μm . By the methods to be discussed in the next section, it can be shown that the outer isochromatic fringe corresponds to a local strain of 5% and is therefore inside the yielded

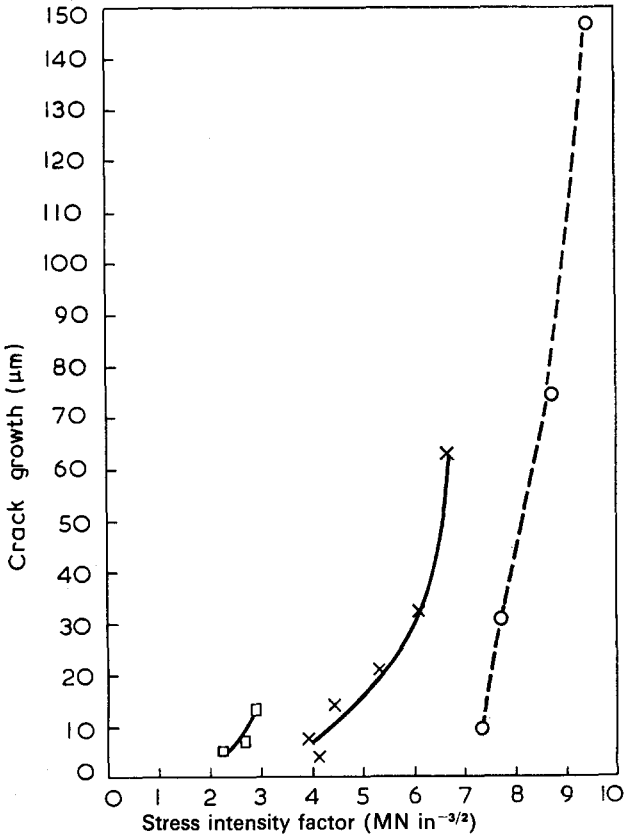


Figure 3 Crack growth as a function of stress intensity factor: initial notch depths—
 ○, 4.34–4.63 mm; ×, 1.38–1.87 mm; □, 0.36–0.39 mm

zone. It is about 17 μm ahead of the crack tip and this figure gives a measure, though an underestimate, of the size of the yielded zone. *Figure 5* is a micrograph of the same specimen taken after the crack growth was about 150 μm ; at this stage the centre of the isochromatic fringe is about 98 μm ahead of the crack tip. As the crack grows, the yielded zone expands.

Because the dominant contribution to the fracture toughness comes from the strain energy in the yielded zone, the expansion of this zone implies that the fracture toughness increases as the crack grows. This is also evident from

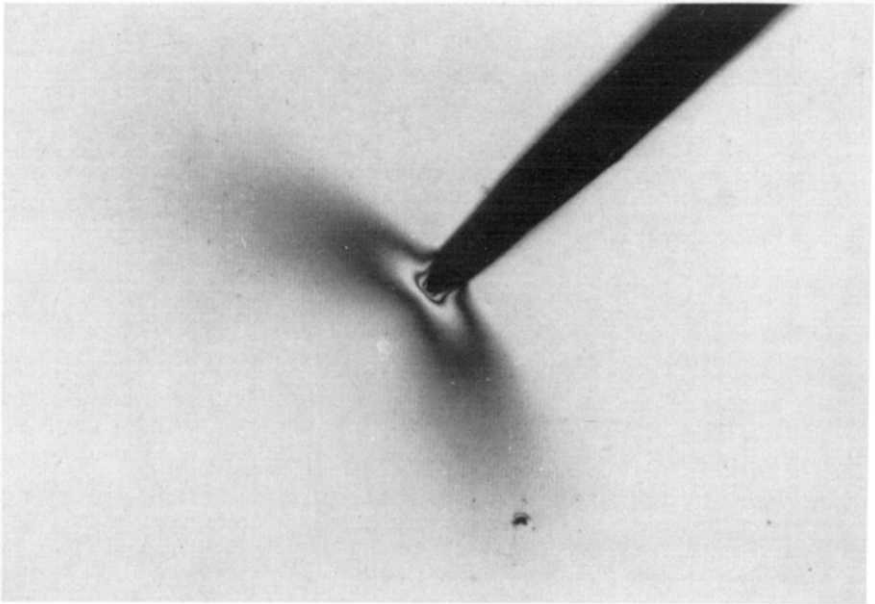


Figure 4 Isochromatic fringes for a crack growth of $30\ \mu\text{m}$ ($\times 153$)

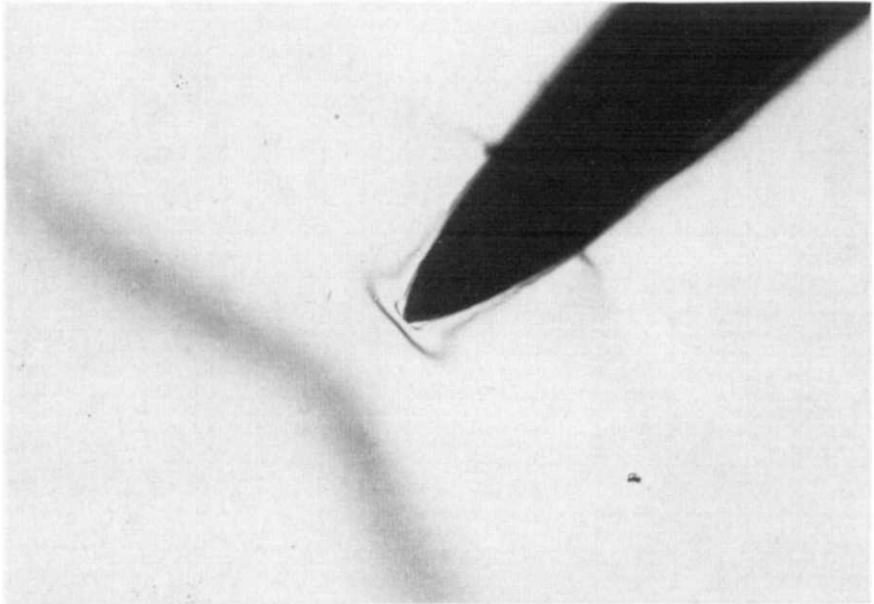


Figure 5 Isochromatic fringes for a crack growth of $150\ \mu\text{m}$ ($\times 153$)

macroscopic tests⁵ and from *Figures 2* and *3*. The fracture toughness of a sharply notched specimen of a ductile thermoplastic cannot be characterized by a single number. Rice⁸ has explained that such:

'growth effects occur because of the advance of a crack into plastically deformed material. The effect is most easily seen in the fully plastic deformation of a rigid-plastic (or nearly so) material under imposed boundary displacements. This may be contrasted with a non-linear elastic material having similar uniaxial monotonic tension behaviour, for which the advance of a crack would cause the strain field to re-adjust so that a large concentration remains at the tip'.

Figure 1 shows the recovery curve obtained when a parallel-sided strip was stretched by 19% before the machine was reversed at the same speed. The material is neither rigid-plastic nor non-linear elastic but, from the large size of the hysteresis loop, it seems sufficiently plastic to account for the occurrence of growth effects.

Close examination of the notch tip in *Figure 5* shows that the tip has tilted sideways during growth. This suggests the possibility that the crack is growing in the tearing mode (anti-plane strain) rather than in the opening mode (plane strain or plane stress)^{7,9}. (The author is indebted to Professor K. E. Puttick for pointing out this possibility.) With due care in the preparation of the original notch, no crack tilting is observed before the crack growth reaches about 60 μm , before which all the other effects described in this paper may be measured. There is, therefore, no evidence that the conclusions of this work are affected by the presence of additional shear stresses near the notch tip.

STRAIN ANALYSIS

Because the amount of crack growth is not determined by either the average net stress or the linear elastic stress intensity factor, it is necessary to find some technique for determining the actual stress or strain distribution during crack growth. It was shown previously⁵ that this can be achieved by photo-analysis. Tests made on unnotched specimens under strain showed that the change in optical path difference was proportional to the axial strain and was independent of the time under load and whether the measurements were made during extension or recovery. *Figure 6* shows the relation between axial strain in the γ direction and the optical path difference, which is proportional to the birefringence ($\gamma - \beta$). Comparing *Figures 1* and *6* it is obvious that the relation between optical path difference and stress is non-linear and multi-valued.

This finding suggests that changes in optical path difference in notched specimens under stress can be used to measure strain distributions. First, however, it is necessary to consider two points of detail.

(1) When the direction of the strain at any point is neither the local γ direction nor the local β direction, there is a tendency for the γ direction to rotate towards the applied strain. This rotation complicates the strain analysis unduly and it is therefore necessary to use this photo-analysis of

strain only where it is clear from symmetry that the local strain is always along either the γ or β direction. Measurements were therefore made only on specimens cut in the γ or β direction, notched at right angles to the axis of the specimen and only at points on the line of symmetry between the notch tip and the opposite edge of the specimen.

(2) The calibration is obtained on a specimen subjected to a uniaxial tensile stress whereas it is known¹⁰ that in a tension test on a notched specimen of an isotropic elastic material the state of stress near the notch tip is biaxial (or even triaxial for a thick specimen). An experiment was performed to check the significance of this possible complication. If the extension ratios are

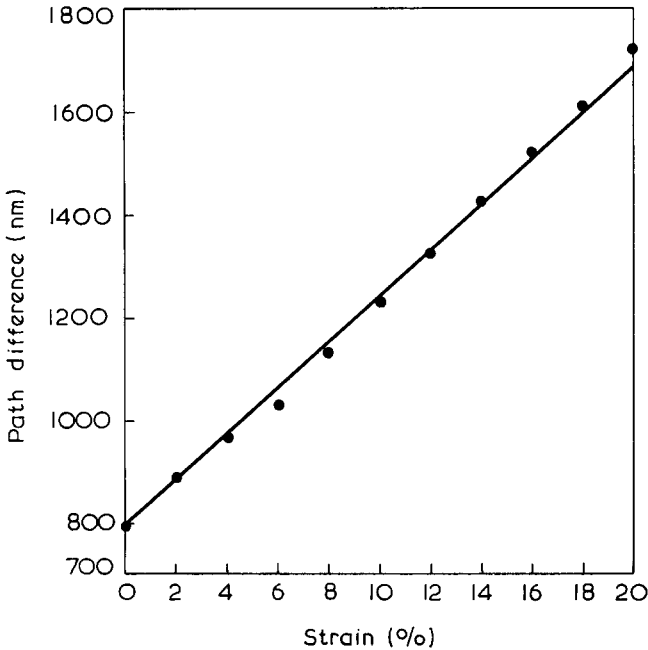


Figure 6 A calibration curve of optical path difference against axial strain in the γ direction

denoted by λ_1 in the extension direction, λ_2 in the film plane, perpendicular to the extension direction, and λ_3 perpendicular to the film plane; then λ_1 , λ_2 and the change in optical path difference were measured directly on an unnotched specimen stretched in the γ direction. A notched specimen was also stretched in the γ direction and held at constant extension. The change in optical path difference was measured as a function of x (the distance from the notch tip). Then the transmission interference pattern was used to measure λ_3 as a function of x . λ_1 as a function of x could then be estimated in two different ways:

(a) Assuming that the relation between λ_1 and change in optical path difference is the same in the unnotched and notched specimens.

(b) Assuming that the change in optical path difference is proportional to $(\lambda_1 - \lambda_2)$ and that $\lambda_1\lambda_2\lambda_3 = 1$.

Figure 7 is a graph of λ_1 deduced by method (a) against λ_1 deduced by method (b) at the same point in the notched specimen. It can be seen that there is no evidence of systematic deviation between the two methods.

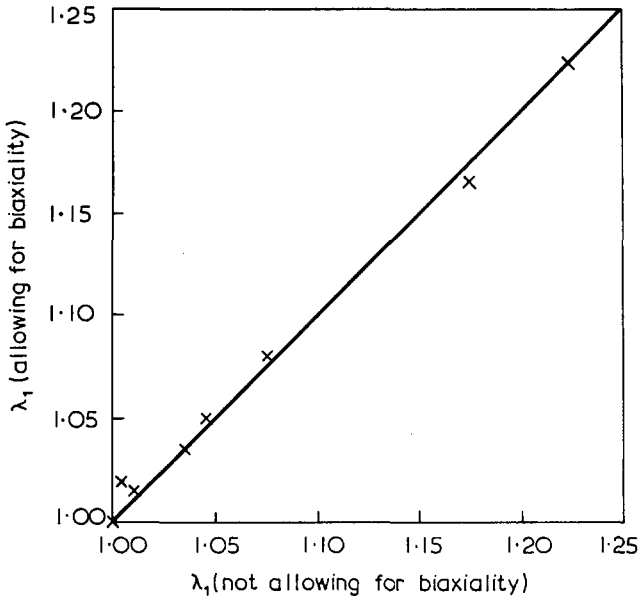


Figure 7 A graph showing that it is not necessary to allow for biaxiality of strain (see text for details)

Accordingly, it seems reasonable to use only the far simpler method (a). Of course this is not generally true in photo-elasticity but there is a special reason why it is permissible in this case: the material is anisotropic and the thickness change under stress is not more than a few per cent. Thus the strain state at a point in a notched specimen is similar to that in an unnotched specimen though the stress state may be different.

If a notched specimen is held under strain and viewed between crossed polars through a microscope, it is possible to measure the optical path difference as a function of distance from the crack tip to within about $1 \mu\text{m}$ of the tip. Using the calibration graph (Figure 6) this can be converted into a graph of axial strain (ϵ) against distance from the crack tip (x) along the line of symmetry. For a material which obeys the linear elastic theory, a graph of $1/\epsilon^2$ against x should be a straight line passing through the origin. It was shown in reference 5 that, for notched specimens extended in the β direction, the graph of $1/\epsilon^2$ against x was approximately straight but that, when extrapolated, it did not pass through the origin; ϵ was found to have a finite value, denoted by ϵ_{max} , at $x = 0$. Also, because of the expansion of the yielded zone, the strain at a given x increases as the crack grows. Figure 8 illustrates this

DUCTILE CRACK GROWTH IN PET FILM

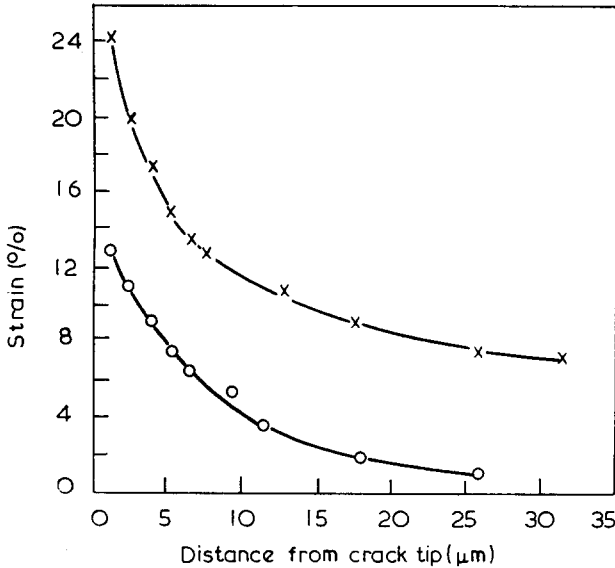


Figure 8 Curves showing the distributions of strain near the crack tip for specimens stretched in the γ direction. Two different amounts of crack growth: \circ , 10 μm ; \times , 97 μm

Table 2 Changes in strain distribution for four specimens stretched in the γ direction

Specimen width (mm)	20	20	1.07	10
Notch depth (mm)	9.21	0.47	0.10	2.36
Crack growth (μm)	102	100	101	97

Distance from crack tip (μm)	Strain (%)			
1.3	25.4	26.1	26.2	24.2
2.6	17.9	20.2	18.1	19.7
3.9	15.8	18.3	17.3	17.2
5.2	14.3	15.2	15.1	14.6
6.5	13.4	14.3	14.7	13.4
13.0	10.4	11.3	11.4	10.6
18.0	9.1	9.7	9.9	9.1
26.0	6.9	8.4	8.6	7.4
33.0	6.2	6.5	8.4	7.0
39.0	5.8	5.0	7.3	5.8

point for two specimens stretched in the γ direction. It was also stated in reference 5 that the strain distribution was not affected by certain changes in initial notch and specimen dimensions. Table 2 illustrates this point for four specimens stretched in the γ direction. The specimen width was varied by a factor of 20 and the notch depth was varied by a factor of 90 but the amount of crack growth was held constant at about 0.10 mm. Differences between the tabulated strains can be seen to be relatively insignificant.

The basic principle of fracture mechanics is that fracture occurs at a given

stress (or strain) distribution near the crack tip; this critical distribution can be represented by a single parameter which is independent of specimen dimensions. A similar principle appears applicable to this ductile thermoplastic but in a more complex form. One has to say that a certain amount of crack growth is related to a given strain distribution which is independent of dimensions but which cannot be represented by only one parameter.

FRACTURE CRITERION

In reference 5 it was suggested that ϵ_{\max} , being independent of specimen and notch dimensions, and of crack growth above $60 \mu\text{m}$, was a possible fracture criterion. The fact that ϵ_{\max} was less than the breaking strain of unnotched specimens was attributed to the different stress state. It now seems preferable to consider the fracture criterion suggested by McClintock and Irwin⁹ that the strain reaches a critical value at a distance ρ_s from the crack tip. ρ_s is regarded as a structural size or the limit at which 'one can no longer regard the material as a homogeneous plastic continuum'. The work of Yeh and Geil¹¹ suggests that the value of ρ_s for drawn poly(ethylene terephthalate) is of the order of 10^{-8} m. If this is so, then the extrapolation suggested in reference 5, though appearing small, in fact covers two orders of magnitude in x and so the values of ϵ_{\max} are unlikely to be accurate. This point is made clear in *Figure 9* where strain is plotted against x (on a log scale) for two

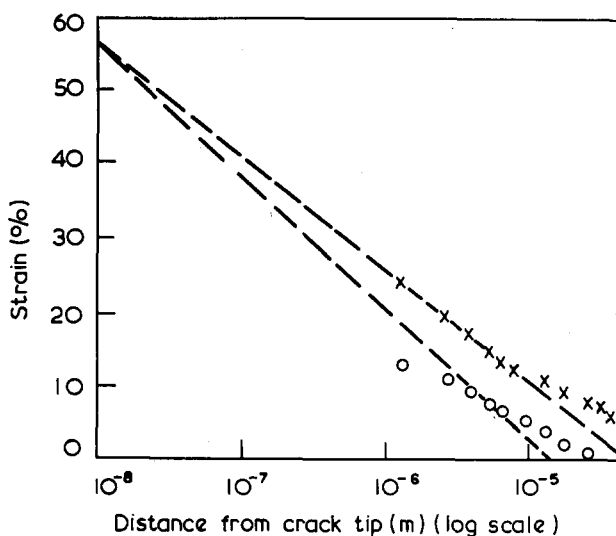


Figure 9 Strain as a function of distance from the crack tip on a log scale

different amounts of crack growth. Straight lines are drawn from the point 57% (taken as the break point of unnotched specimens) and 10^{-8} m (taken as ρ_s) through the points representing the experimental results. It can be seen

that these results are not adequate to verify the suggested criterion. It would be necessary to develop a technique for measuring strains at between 10^{-6} and 10^{-8} m from the crack tip.

DISCUSSION

The original object of this work was to find a satisfactory technique for assessing the resistance to fracture of a ductile thermoplastic film which could be used both for the prediction of service performance and for the relation of mechanical properties to micro-structure. Tests on sharply notched specimens were selected for study on the grounds that they would provide reproducible results, that any real material contains defects at which fractures originate and that satisfactory theories were available for deducing useful parameters from the results of such tests. In fact, the main product of the work has been a better understanding of the limitations of this type of approach. In order to obtain reproducible results it is necessary to spend a good deal of time on careful notching and refined measurements. Although it is true that real materials contain defects, they are quite different from artificial notches in size, shape and resultant stress field; consequently, the results of tests on sharply notched specimens cannot readily be used for predicting service performance or for understanding the effect of changes in microstructure. Although a satisfactory theory is available for brittle fracture, when the net stress is below half the yield stress and the yielded zone is negligibly small, the theoretical problem is much less tractable when it becomes necessary to consider higher stresses, larger yield zones, non-linear stress/strain relations, partial and time-dependent recovery and anisotropy.

An essential part of the analysis of the stress field near a notch or crack in a ductile material is a knowledge of the details of the stress/strain relations obtained on unnotched specimens. At the very least, therefore, it is necessary to measure tensile load/extension curves for test materials. Careful tensile tests can also provide the elongation to break which is a measure of fracture in the presence of real, rather than artificial, defects. Much useful information about service performance and the effects of micro-structural variables can be obtained from careful tensile tests and it is worth considering whether tests on sharply notched specimens, with their many additional complications, are really justifiable.

CONCLUSIONS

- (1) Measurements of crack growth in a ductile thermoplastic cannot be unified by considering average stresses or by linear elastic fracture mechanics.
- (2) The size of the yielded zone and the fracture toughness are not constant but increase as the crack grows. This seems to be a consequence of hysteresis.
- (3) The actual strain distribution can be measured to within about $1 \mu\text{m}$ of the crack tip by a photo-analytical technique. It differs significantly from the distribution assumed in linear elastic fracture mechanics.

- (4) The measured strains are independent of specimen and notch dimensions, within the range examined.
- (5) It would be necessary to measure strains much closer to the crack tip in order to discover the true fracture criterion.
- (6) So much useful information can be obtained from careful tensile tests that it is doubtful whether tests on sharply notched specimens are of much value.

ACKNOWLEDGEMENT

The experimental work in this final stage was carried out by Mr P. White.

*Imperial Chemical Industries Limited,
Plastics Division,
Welwyn Garden City, Hertfordshire, UK*

(Received 10 March 1971)

REFERENCES

- 1 Berry, J. P. J. *Polym. Sci.* 1961, **50**, 107
- 2 Sih, G. C. and Liebowitz, H. 'Fracture', (Ed. H. Liebowitz), Academic Press, New York and London, 1968, Vol II, pp 67-190
- 3 Marshall, G. P., Culver, L. E. and Williams, J. G. *Plastics and Polymers* 1969, **37**, 75
- 4 Berry, J. P. J. *Polym. Sci. (A)* 1965, **3**, 2027
- 5 Vincent, P. I., Picknell, S. and Harding, G. F., Technical report 73 from Division of Polymer Science, Case Western Reserve University, Cleveland, Ohio, 1967
- 6 Vincent, P. I., Technical Report 97 from Division of Polymer Science, Case Western University, Cleveland, Ohio, 1968
- 7 Paris, P. C. and Sih, G. C. 'Fracture toughness testing and its applications', *ASTM Special Technical Publication No. 381*, 1965, p 44
- 8 Rice, J. R. 'Fracture', (Ed. H. Liebowitz), Academic Press, New York and London, 1968, Vol II, pp 191-311
- 9 McClintock, F. A. and Irwin, G. R. 'Fracture toughness testing and its applications', *ASTM Special Technical Publication No. 381*, 1965, p 95
- 10 Coker, E. G. and Filon, L. N. G. 'A treatise on photo-elasticity', Cambridge University Press, 1957
- 11 Yeh, G. S. Y. and Geil, P. H. *Macromol. Sci.* 1967, **B1**, 251

Polystyrenes of known structure: Part 1. The reaction of polystyryl potassium with $^{14}\text{CO}_2$ and the viscosity– molecular weight correlations for linear polymers

J. PANNELL

The reaction between potassium polystyryl and gaseous labelled carbon dioxide ($^{14}\text{CO}_2$) in tetrahydrofuran was investigated as a means of determining the absolute molecular weights of a series of polystyrenes by measurements of the radioactivity of the labelled carboxyl end-groups. In most cases, the number average molecular weights obtained by the tracer method show good agreement with the osmotic values obtained using the Schleicher and Schuell 08 membrane ('feinst'), and it is concluded that the complicating side reactions which occur when lithium polystyryl is carboxylated, to give higher molecular weight products, probably do not occur with potassium polystyryl.

The low shear melt viscosities and the intrinsic viscosities of the linear polymers prepared in this and in subsequent work on the synthesis of branched polystyrenes have been measured and their dependence on molecular weight found to be given by

$$\begin{aligned} \log \eta_0 &= 3.4 \log \bar{M}_n - 12.72 \text{ at } 460 \text{ K} && \text{for } 10^6 \geq \bar{M}_n > M_c \\ \log [\eta] &= 0.65 \log \bar{M}_n - 3.58 \text{ in tetrahydrofuran at } 298 \text{ K} && \text{for } 10^6 \geq \bar{M}_n \geq 2.8 \times 10^4 \end{aligned}$$

where M_c ($\approx 33\,000$) is the critical molecular weight for the onset of chain entanglements.

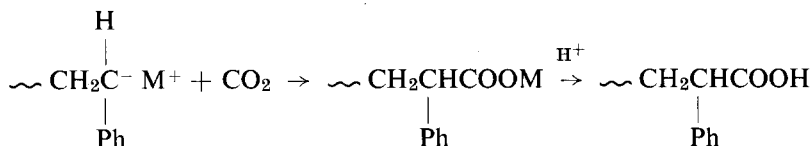
INTRODUCTION

THE ANIONIC polymerization of styrene and a few other monomers is characterized by the absence of a termination step, when impurities such as oxygen, water and other proton donating species are excluded and under ideal conditions it is possible to obtain polymers with very narrow molecular weight distributions. As well as being intrinsically interesting kinetically and mechanistically, living polymers have great potential in synthetic work. For example, the reactive anionic end-groups on living polymers are capable not only of further polymerization on addition of the same monomer, but also of initiating polymerization of a second monomer, in some cases, to form a block copolymer. They will also react with certain groups, such as $-\text{CH}_2\text{Cl}$ or $-\text{CO}(\text{OMe})$ on dead, pre-formed polymer chains to form graft copolymers or branched polymers of known structure, or will react with suitable low-molecular weight reagents to give (1) polymers with a variety of end-groups or (2) tri- and tetra-branched star-shaped polymers. A review article by Fetters and Morton¹ summarizes much of the work which has

been carried out on systems involving living polymers and references to some of the more recently published work are given at the end of this paper²⁻¹⁴.

For several years we have been working in these laboratories on the use of living polymers in the synthesis of branched polymers of known structure, with the object of correlating polymer properties and polymer structure, and some of the results obtained on comb-shaped branched polystyrenes appear in Part 2³². In considering the properties of branched polymers it is obviously important to compare them with linear polymers and one of the objects of the present paper is, therefore, to establish the melt viscosity- and intrinsic viscosity-molecular weight relationships for linear polystyrenes which in turn depends on establishing a reliable molecular weight scale. The other purpose of this paper is to describe our experiments on the carboxylation of potassium polystyryl with ¹⁴C-labelled CO₂ and the use of this reaction in determining the molecular weights of living polymers.

Trotman and Szwarc¹⁵ were the first to use the property of living polymers to react with various reagents to determine the molecular weights of the polymers. Treatment of the living polymers with Michler's ketone [C₆H₄.N(CH₃)₂]₂CO, followed by acidification produces a polymer with an intensely blue colour and this was used in the colorimetric determination of the end-groups. Carbon dioxide also reacts with living polymers to place a carboxyl group on the end of the chain:



where M is an alkali metal atom. By using radioactive ¹⁴C-labelled CO₂ and sodium as the alkali metal, Trotman and Szwarc showed that this reaction could be used in the determination of the molecular weight of living polymers, the value so obtained agreeing with that determined by the colorimetric method and by viscometry. On the other hand Wyman *et al*¹⁶ have shown that when lithium is the alkali metal the extent of the above reaction depends on the relative amounts of CO₂ and living polymer. When a solution of lithium polystyryl in benzene was reacted slowly with gaseous CO₂, the carboxylated polymer was found to undergo further reaction with unchanged living polymer to produce dipolystyryl ketone:



The ultracentrifuge sedimentation pattern (and fractionation) of the product showed the presence of three species, with molecular weights in the ratio 1:2:3, indicating that a second side reaction also takes place. The extent of the side reactions involving the carboxylate-ended polymer was reduced, though these were not eliminated completely, by using a large excess of CO₂

(dry ice). Similar attempts by Glusker *et al*¹⁷ to make use of the reaction of CO₂ with living poly(methyl methacrylate) to determine molecular weights were not successful because of spontaneous decarboxylation of the polymers in solution.

EXPERIMENTAL

Preparation of potassium polystyryl

The high vacuum apparatus used in the preparation of living polymers is based on those already described in the literature. All reagents, including the initiator (α -phenyl isopropyl potassium), styrene, methanol and gaseous labelled CO₂ were contained in break-seal ampoules on the apparatus. Reactive impurities in the apparatus were removed prior to the preparation by purging with a solution of α -phenyl isopropyl potassium in tetrahydrofuran (THF), followed by rinsing with condensed THF. The initiator solution was transferred to the reaction vessel containing about 500 cm³ THF and a small amount of styrene added to it at room temperature to complete the initiation step. The bulk of the styrene (50–60 cm³) was added dropwise to the reaction vessel after this had been cooled to 195 K, the rate of addition being controlled by an all-metal bellows valve¹⁸. Vigorous stirring was maintained throughout these operations. On completion of the polymerization the contents of the reaction vessel were warmed to room temperature and part of the living polymer solution transferred and isolated in that part of the apparatus containing the ampoule of labelled CO₂, which was subsequently opened to terminate this quantity of living polymer. The remainder of the living polymer in the reaction vessel was terminated with methanol.

Handling of labelled CO₂ and determination of its activity

In the preparation and handling of the labelled CO₂ it was essential to ensure that traces of moisture and oxygen were not present to terminate the living polymer. The radioactive CO₂, with a total activity of about 1 millicurie/millimole was obtained from the Radiochemical Centre, Amersham. This was diluted to about 10³ cm³ with inactive CO₂ at about one atmosphere pressure on a conventional high vacuum apparatus to give CO₂ with an activity of just over 0.02 millicurie/millimole. The inactive CO₂ was prepared on the vacuum line from degassed BaCO₃ and a large excess of concentrated H₂SO₄ and was freed of traces of moisture by several trap-to-trap distillations. Known volumes of the labelled CO₂ at a known pressure were then transferred to break-seal ampoules which had previously been flamed to remove adsorbed oxygen and water from the internal surfaces. The ampoules were sealed off after freezing the contents and removed from the vacuum line. The activity of the CO₂ was determined by carboxylating 9-fluorenyl sodium to produce fluorene 9-carboxylic acid. The 9-fluorenyl sodium was prepared in two ways, (1) by adding a solution of sodium naphthalene in THF to a solution of fluorene in THF at 333 K¹⁹ in an atmosphere of argon and (2) by allowing a solution of fluorene to stand in contact with metallic sodium for several weeks. The fluorene 9-carboxylic acid was extracted by the procedure

described by Calvin *et al*²⁰ after evaporating the THF and its activity determined by scintillation counting in solution. (A solution of fluorene 9-carboxylic acid in a 50–50 mixture of toluene and peroxide-free dioxan was added to a known volume of scintillator solution, which consisted of 0.5% PPO in a 1:1:1 mixture of dioxan, ethancl and xylene.) The average activity of three samples of fluorene 9-carboxylic acid prepared, and hence of the CO₂ also, was 0.023 ± 0.0016 millicurie/millimole (98 966 dpm per 100 mg carboxylic acid). Each ampoule of CO₂ contained about 4×10^{-5} mole with an activity of approximately 1 microcurie.

Treatment of carboxylated polymers

Adequate purification of the main bulk of the polymer produced by methanol termination of the living polymer was achieved by one precipitation into water and one into methanol, followed by drying. With the radioactive carboxylated polymer, on the other hand, it was necessary to find the best procedure for purification, that is the removal of radioactive impurities if present. The effect of the precipitation procedure on the disintegration rate of the polymer is shown in *Table 1*. The first precipitation into HCl was always carried out, to remove basic inorganic impurities, and this was followed by washing with water and methanol and the polymer dried. Between 100 and 300 mg, depending on the expected molecular weight, of the polymer was weighed out accurately and dissolved in 10 cm³ toluene containing the scintillator (PPO) and counted.

Table 1 Effect of precipitation procedure on the disintegration rate of labelled carboxylated polymer

<i>Polymer</i>	1 <i>Precipitation into dil HCl</i>	2 <i>1st precipitation into methanol</i>	3 <i>2nd precipitation into methanol</i>	4 <i>2nd precipitation into dil HCl</i>
U 21	4 320 dpm	2 780	2 757	–
U 22	27 800	27 830	27 710	–
U 23	11 710	11 000	10 890	–
U 24	6 400	5 470	5 420	–
U 27	1 + 2 → 34 900		–	34 200

Subsequent precipitations into methanol or HCl were also carried out and the disintegration rates measured after each. It is seen from *Table 1* that the count rate is sometimes lower after one precipitation into methanol than after precipitation into HCl alone, especially when the molecular weight is high, i.e. at low counts, but that further precipitations whether into methanol or into HCl have little effect on the disintegration rate. Thus one precipitation into dilute HCl followed by one into methanol seems to be sufficient to remove radioactive impurities.

The molecular weight of the polymer as determined by the tracer method is given by:

$$\bar{M}_n = 210.08 d_F/d_P$$

where 210.08 is the molecular weight of the fluorene carboxylic acid, d_F is the

disintegration rate/ 10^{-3} kg of the acid, and d_P the disintegration rate/ 10^{-3} kg of the polymer. Using the known activity of fluorene carboxylic acid

$$\bar{M}_n = 5197 \times 10^7 \times (\text{wt. of polymer, } x \text{ kg}) / (\text{dpm of } x \text{ kg polymer})$$

Molecular weights by osmometry

Osmotic pressure measurements were made in a Mechrolab Membrane Osmometer, Model 501. In the original measurements, the membrane used was the Schleicher Schuell 08 membrane ('feinst') and the solvent toluene at 310 K. Measurements on a number of linear polymers prepared in this work, and in later work on branched polystyrenes showed that another membrane, referred to here as the Sylvania membrane²² gave similar results to the Schleicher and Schuell membrane. Measurements on some of the polymers were also made using the Sartorius membrane ('allerfeinst') at room temperature, the solvent being tetrahydrofuran.

Molecular weights were calculated from the intercept of a plot of π/C against C or from a plot of $(\pi/C)^{1/2}$ against C .

Molecular weights by light scattering

Light scattering data were obtained in tetrahydrofuran at room temperature using vertically polarized light of wavelength 546 nm after the solutions had been filtered through Whatman G.F.C. filters (pore size $0.5 \mu\text{m}$). The photometer used was designed and made in these laboratories and was calibrated using Ludox sols of known turbidity. The data obtained at various angles and concentrations were extrapolated to zero angle and zero concentration, using the usual Zimm plot. In most cases the Zimm plots were satisfactory, but on occasions a sudden curvature was apparent at low angles ($20\text{--}30^\circ$), possibly indicating the presence of a small amount of very large molecules. To have used these data would have given a molecular weight too heavily weighted in favour of these large species so it was discarded in favour of the data at higher angles.

Melt viscosities and intrinsic viscosities

The low shear melt viscosities were measured at 460 K in a melt penetrometer²³ and the solution viscosities were measured in toluene and in tetrahydrofuran at 298 K in an Ubbelohde dilution viscometer. The kinetic energy corrections were negligible.

RESULTS AND DISCUSSION

The results of all measurements on carboxylated polymers are summarized in *Table 2*. In assessing the molecular weights determined by the tracer method one is faced with the difficulty of choosing between the two values obtained by osmometry using two different membranes. The results of measurements on the first nine samples listed in *Table 2* clearly show that the tracer method gives best agreement with the osmotic values obtained with

the Schleicher and Schuell ('feinst') membrane. We are inclined to accept the value obtained with this membrane as being more realistic than that obtained using the Sartorius ('allerfeinst') membrane, not only because of this agreement with the tracer method (which is, of course, not subject to membrane phenomena) but also because it has been shown recently²¹ that, although the densest membrane ('allerfeinst') is desirable for measurements on low molecular weight polymers, it does appear to underestimate increasingly the molecular weight as this increases.

For those three samples where the tracer method gives apparent molecular weights which are very much higher than the values from osmometry,

Table 2 Comparison of molecular weights determined by different methods

Sample	Tracer* method (\bar{M}_n)	Osmometry (\bar{M}_n)		\bar{M}_w (light scattering)
		Fienst mem ^t rane (S & S)	Allerfeinst membrane	
U 18	79 600	82 400	60 900	86 000
U 20	80 600	86 400	—	100 000
U 14	108 000	117 100	108 700	110 000
U 19	113 400	117 900	—	150 000
U 29	117 850	121 600	87 900	≈ 140 000
U 27	152 000	155 000	—	210 000
U 17	420 000	403 000	394 300	450 000
U 23	478 000	477 000	336 600	440 000
U 24	958 200	891 000	≈ 500 000	—
U 36	127 800	107 200	95 200	108 000
U 28	298 900	386 200	345 000	338 000
U 22	185 200	224 400	—	270 000
U 25	> 10 ⁶	382 000	276 000	400 000
U 21	> 10 ⁶	659 000	726 300	660 000
U 31	≥ 10 ⁶	932 000	—	990 000
U 26	—	36 000	31 900	41 000
NBS705	—	182 500	178 000	179 300†
U 38	—	147 400	129 000	149 000

* The error in the molecular weights determined by the tracer method are directly attributable to variation in the activity of the fluorene carboxylic acid samples prepared is about 7%. Osmotic pressures measured with the Schleicher and Schuell membrane were found to give molecular weights reproducible to about 5%.

† This value of \bar{M}_w is that quoted by the National Bureau of Standards.

The value of \bar{M}_n quoted by N.B.S. is 170 900

(U 21, U 25 and U 31) it is thought that air entered the CO₂ ampoules at some stage, probably as a result of faulty break seals, and only a fraction of the living polymer was terminated by CO₂. It is more difficult to account for the discrepancy between the two methods for the three samples U 36, U 28 and U 22, although for U 28 and U 22 the presence of a small quantity of a low molecular weight material which is not removable by our precipitation procedure, would affect the tracer method to give somewhat low values for

\bar{M}_n . In the osmometer this low molecular weight material might permeate the membrane unnoticed and have little effect on the final molecular weight. Unfortunately insufficient of these samples was available to check this possibility.

Apart from the three experiments in which air was thought to have entered the CO₂ ampoules, there is only one other case in which the tracer method gives a molecular weight in excess of the osmotic value. From this we conclude that potassium polystyryl probably reacts with CO₂ to form carboxylate-ended polymer without the complicating side reactions which take place with lithium polystyryl¹⁶.

The results in *Table 2* also show that most of the polymer samples prepared in the manner described have relatively narrow molecular weight distributions as judged from the ratio of the weight to number average molecular weights, and this has since been confirmed by gel permeation chromatography.

Viscosity molecular weight correlations

The melt viscosity- and intrinsic viscosity-molecular weight correlations for the linear polystyrenes prepared in the work on the carboxylation of potassium polystyryl and throughout the course of the work on the synthesis of branched polymers are shown graphically in *Figures 1* and *2* respectively. The data used for these plots are given in *Table 3*. Since the molecular weights of all the linear polystyrenes prepared were measured by osmometry (using the Schleicher and Schuell or Sylvania membranes), whereas the tracer method was used on only a limited number of these samples, the molecular weights used in *Figures 1* and *2* are the osmotic values. The straight lines drawn through the experimental points in *Figures 1* and *2* were obtained by a least squares analysis of the results obtained in these laboratories and are given by

$$\log \eta_0 = 3.4 \log \bar{M}_n - 12.72 \text{ at } 460 \text{ K} \quad \text{for } 10^6 \geq \bar{M}_n > M_c$$

and

$$\log [\eta] = 0.65 \log \bar{M}_n - 3.58 \text{ in THF at } 298 \text{ K} \\ \text{for } 10^6 \geq \bar{M}_n \geq 2.8 \times 10^4$$

and

$$\log [\eta] = 0.675 \log \bar{M}_n - 3.69 \text{ in toluene at } 298 \text{ K} \\ \text{for } 4 \times 10^5 \geq \bar{M}_n \geq 4.6 \times 10^4$$

where M_c ($= 33\,000$) is the critical molecular weight for the onset of chain entanglements. (The actual slopes given by the least squares analysis of the data are 3.396 ± 0.072 , 0.650 ± 0.014 and 0.675 ± 0.024 , respectively.) The scatter in *Figures 1* and *2* is due partly to the variation in the molecular weight distributions of the polymers and partly to experimental error. The ratio \bar{M}_w/\bar{M}_n from the light scattering and osmotic pressure, and from gel permeation chromatography, shows that the majority of the samples prepared possess relatively narrow molecular weight distributions ($\bar{M}_w/\bar{M}_n \leq 1.2$ in most cases).

Also shown in *Figures 1* and *2* are some results of measurements of melt

Table 3 Intrinsic viscosities, melt viscosities and number average molecular weights of linear polystyrenes

Sample	Intrinsic viscosities* at 298 K (dm ³ kg ⁻¹)		Melt viscosity† at 460 K (N s m ⁻²)	$\bar{M}_n \times 10^{-5}$
	$[\eta]_{\text{THF}}$	$[\eta]_{\text{TOL}}$	η_0	
U26	21.2	—	—	0.36
B114.L	28.4	28.2	1.15×10^2	0.465
B111.L	31.5	29.7	1.15×10^2	0.496
B112.L	29.0	29.8‡	1.70×10^2	0.498
B110.L	31.8	35.6	3.47×10^2	0.567
B118.L	35.7	34.0	2.43×10^2	0.603
B107.L	45.3	41.8	5.05×10^2	0.783
B116.L	36.9	34.5	2.88×10^2	0.801
U18	38.1	—	—	0.824
B105.L	45.9	48.4	1.40×10^3	0.946
B121.L	55.5	54.1	6.80×10^3	1.11
B123.L	53.3	52.0	5.03×10^3	1.14
U14	55.4	—	3.18×10^3	1.17
U19	59.0	—	—	1.18
U29	44.6	48.1	2.02×10^3	1.22
B108.L	65.4	63.0	1.20×10^4	1.36
B137.L	58.3	—	3.99×10^3	1.42
U27	61.4	—	9.55×10^3	1.55
B120.L	69.4	66.3	1.01×10^4	1.57
B130.L	70.7	69.4	1.88×10^4	1.75
U34	70.2	68.6	1.63×10^4	1.81
B131.L	69.7	69.8	2.51×10^4	1.96
B103.L	79.6	78.4	2.73×10^4	2.06
U33	73.2	72.8	2.39×10^4	2.12
B124.L	86.6	81.6	6.17×10^4	2.13
B122.L	94.1	104.7	6.57×10^4	2.42
B115.L	96.3	93.6‡	7.19×10^4	2.66
B106.L	122	118	3.30×10^5	3.67
U25	108	—	1.29×10^5	3.82
U28	108	—	1.16×10^5	3.86
U17	116	—	2.76×10^5	4.03
B104.L	114	117	2.58×10^5	4.18
U23	124	—	3.16×10^5	4.77
U21	158	—	1.07×10^6	6.59
U31	197	—	2.91×10^6	8.20
U24	188	—	1.62×10^6	8.91
25170¶	28.9	—	8.86×10^2	0.49
41995¶	46.8	—	—	0.962
41984¶	67.2	—	—	1.64
4190037¶	127.6	—	4.76×10^5	3.92
4190038¶	219	—	5.83×10^6	7.73
NBS 705	70.1	—	1.41×10^4	1.82

* 100 dm³ kg⁻¹ \equiv 1 dl g⁻¹ (pre-SI unit for intrinsic viscosity)† 0.1 N s m⁻² = 0.1 kg m⁻¹s⁻² \equiv poise (pre-SI unit for melt viscosity)‡ Intrinsic viscosities estimated from $[\eta]_{\text{THF}}$ vs. $[\eta]_{\text{TOL}}$ plot

¶ These samples were prepared by the Pressure Chemical Co. in USA. Molecular weights given here are those quoted by P.C.C. Intrinsic viscosities were measured in our own laboratories

and intrinsic viscosities on some of the narrow distribution polystyrenes prepared by the Pressure Chemical Company, Pittsburgh, USA, and supplied by Waters Associates as calibration samples in gel permeation chromatography. The molecular weights used for these samples were those quoted by the makers. The slopes of the lines obtained for these samples are 4.14 and 0.72 for the $\log \eta_0 - \log M$ and $\log [\eta]_{\text{THF}} - \log M$ plots respectively, which are

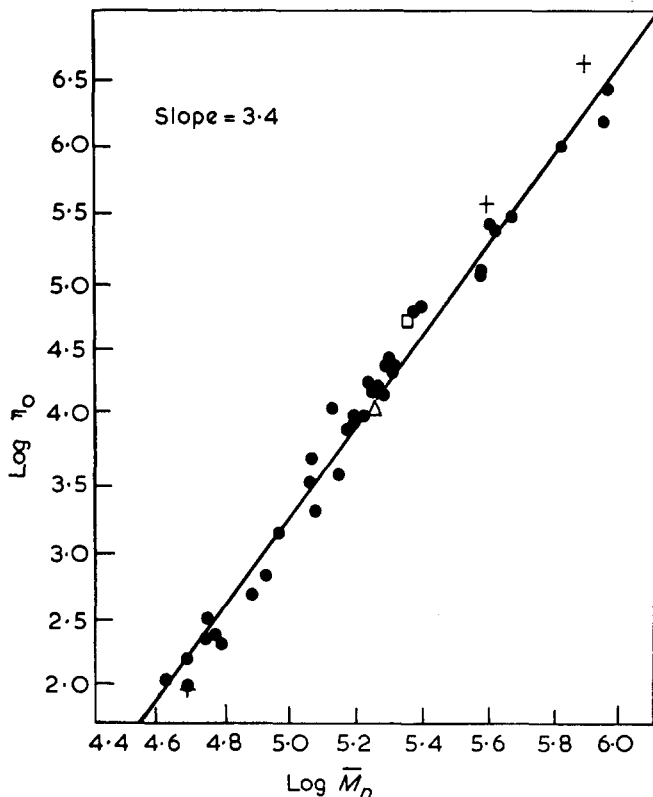


Figure 1 Dependence of the low shear melt viscosity on molecular weight for linear polystyrene at 460 K. The straight line shown is obtained by least squares analysis of the data on the polymers in this work (●). +, Pressure Chemical Company samples; Δ, sample NBS 705; □, linear backbone for comb-shaped polymers (ref. 32).

appreciably higher than the values obtained for the samples prepared in these laboratories. There is some variation in the published figures for the slope of the $\log \eta_0 - \log M$ plot for linear polystyrenes, these ranging from 3.14 given by Rudd²⁴ through 3.4 by Fox and Flory²⁵ and 3.75 by Akovali²⁶ to 4.0 by Tobolsky, Aklonis and Akovali²⁷. (Although these figures were obtained at different temperatures by different workers, the slope is independent of temperature.) However, the slope of 3.4 obtained in the present work is the same as that found recently by Carraher²⁸ and obtained by measurements on concentrated solutions of polystyrene obtained from the Pressure Chemical Company.

The slopes of the $\log [\eta]$ against $\log M$ plots in both tetrahydrofuran and in toluene at 298 K are close to that of 0.644 obtained by Berry²⁹ for measurements in toluene over the same range of molecular weights.

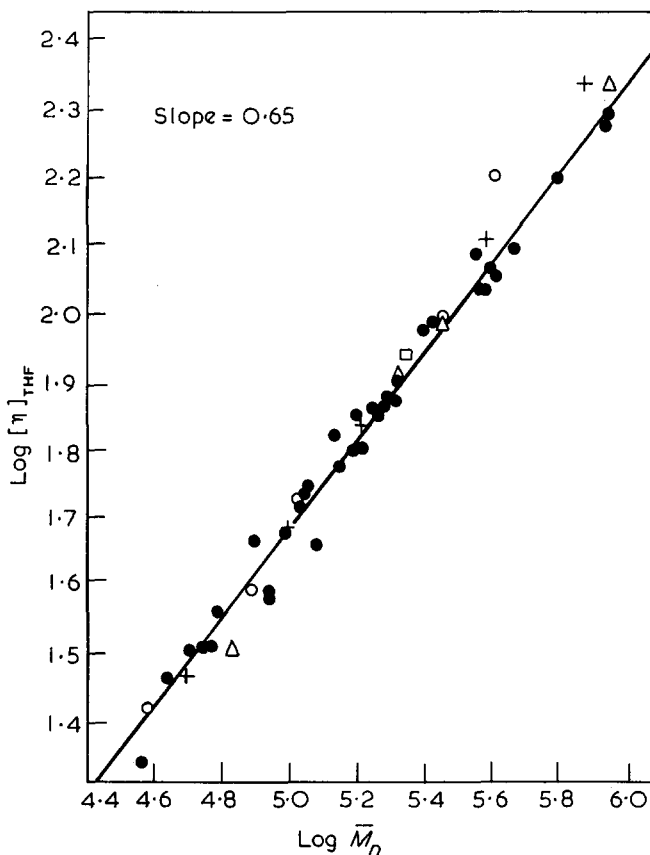


Figure 2 Dependence of the intrinsic viscosity in THF at 298 K on molecular weight for linear polystyrene. The straight line shown is obtained by least squares analysis of the data on the polymers in this work (●). +, Pressure Chemical Company samples; ○, Papazian's data (ref. 31); △, Benoit's data (ref. 30); □, see Figure 1.

ACKNOWLEDGEMENTS

I should like to thank Mr F. Yearsley for the light scattering measurements, Mr D. R. Mosely for osmotic pressure measurements with the Sartorius membrane, and Mr A. Titterton whose skill contributed largely to the success of this work.

*Imperial Chemical Industries Limited,
Plastics Division, Research Department,
Welwyn Garden City,
Hertfordshire, UK*

(Received 3 March 1971)
(Revised 17 May 1971)

REFERENCES

- 1 Morton, M. and Fetters, L. J. *Macromol. Rev.* 1967, **2**, 71
- 2 Koenig, R., Reiss, G. and Banderet, A. *European Polym. J.* 1967, **3**, 723
- 3 Nobutoki, K. and Sumitomo, H. *Bull. Chem. Soc., Japan* 1967, **40**, 1741, 2725
- 4 Yamazaki, N., Sharakuwa, H. and Kambara, S. *J. Polym. Sci., (C)* 1967, **16**, 1685
- 5 Iwakura, Y., Toda, F., Katsuki, H. and Watanabe, H. *J. Polym. Sci. (B)* 1968, **6**, 329
- 6 Worsfold, D. M., Rempp, P. and Franta, E. *Comp. Rend. Acad. Sci., Paris* 1968, **267C**, 374
- 7 Candau, F. and Rempp, P. *Comp. Rend. Acad. Sci., Paris* 1968, **267C**, 601
- 8 Candau, F. and Rempp, P. *Makromol. Chem.*, 1969, **122**, 15
- 9 Kraus, G., Gruver, J. T., and Childers, C. W. *J. Appl. Polym. Sci.* 1967, **11**, 1581
- 10 Kraus, G. and Gruver, J. T. *Amer. Chem Soc., Polymer Preprints* 1969, **10**, 111
- 11 Andreeva, G. A., Mitsengendler, S. P. and Korotkov, A. A. *Vys. Soed. Krat. Soobschch.* 1969, **11B**, 182
- 12 Heller, J., Schimscheimer, J. F., Pasternak, R. A. and Kingsley, C. B. *J. Polym. Sci. (A-1)* 1969, **7**, 73
- 13 Lazarewska, V. and Rempp, P. *Comp. Rend. Acad. Sci., Paris* 1969, **268C**, 1841
- 14 Decker, D. *Makromol. Chem.* 1969, **125**, 136
- 15 Trotman, J. and Szwarc, M. *Makromol. Chem.*, 1960, **37**, 39
- 16 Wyman, D. P., Allen, V. R. and Altares, T. *J. Polym. Sci. (A)* 1964, **2**, 4545
- 17 Glusker, D. L., Stiles, E. and Yoncoskie, B. *J. Polym. Sci.* 1961, **49**, 297
- 18 Manufactured by Scientific Instrument and Model Co Ltd., Ross-on-Wye, Herefordshire, England
- 19 Normant, H. and Angelo, B. *Bull. Chem. Soc., France* 1960, p 354
- 20 Calvin, M., Heidelberger, C., Reid, J. C., Tolbert, B. M. and Yankwich, P. F., 'Isotopic Carbon', John Wiley, New York, 1949, p 188
- 21 Ghosh, K. K. and Swenson, H. A. *J. Appl. Polym. Sci.* 1968, **12**, 1531
- 22 Moistened membrane obtained in sheet from FMC Corporation, American Viscose Division, Fredericksburg, Virginia 22401, USA
- 23 Small, P. A. *J. Polym. Sci.* 1958, **28**, 223
- 24 Rudd, J. F. *J. Polym. Sci.* 1960, **44**, 459
- 25 Fox, T. G. and Flory, P. J. *J. Polym. Sci.* 1954, **14**, 315
- 26 Akovali, G. *J. Polym. Sci. (A-2)* 1967, **5**, 875
- 27 Tobolsky, A. V., Aklonis, J. J. and Akovali, G. *J. Chem. Phys.* 1965, **42**, 723
- 28 Carraher, C. E. *Macromolecules* 1969, **2**, 304
- 29 Berry, G. C. *J. Chem. Phys.* 1967, **46**, 1338
- 30 Benoit, H., Grubisic, Z. and Rempp, P. *J. Polym. Sci. (B)* 1967, **5**, 753
- 31 Papazian, L. A. *Polymer, Lond.* 1969, **10**, 399
- 32 Pannell, J. *Polymer, Lond.* 1971, **12**, 558

Polystyrenes of known structure: Part 2. Comb-shaped molecules

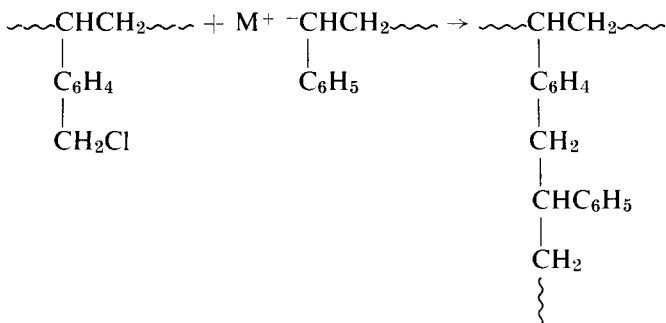
J. PANNELL

The preparation of some comb-shaped polystyrenes by reaction of lithium polystyryl with chloromethylated polystyrene in benzene is described. In all cases the branches are considerably shorter in length than the backbone, with number average molecular weights below 46 000. The low-shear melt viscosities of all the comb-shaped polymers prepared here are lower than those of linear polymers of comparable molecular weights and, with the exception of only two polymers, are also lower than the melt viscosity of the backbone. Where the mol. wt. of the branches is fixed (at $\bar{M}_n = 5200$ and $\bar{M}_n = 6600$ in two series), the melt viscosity decreases as the branching frequency increases (from 10 to 475 branches per backbone). For the series in which the branching frequency is fixed (at 33 and 71 branches per backbone in two series), the melt viscosity at first decreases with increase in branch length, reaches a minimum and then increases with further increase in branch length. An empirical equation is given, relating the melt viscosity with the molecular weights of the branches, the backbone and the branched polymer. The intrinsic viscosities, both in cyclohexane at 308 K and in tetrahydrofuran at 298 K, show a much slower and more complex variation with molecular weight than linear polymers. The results presented here are consistent with those of Decker, who showed that the θ -temperature of comb-shaped polystyrenes in cyclohexane depends on the length of the branches but is below 308 K, the θ -temperature for linear polystyrenes in cyclohexane.

INTRODUCTION

IN SPITE of the fact that a method of synthesizing branched polymers of known structure, using well-characterized living polymers, has been available for some years now, only a few systematic studies of the effect of varying the branch length and branching frequency on the properties of branched polymers have so far been published. As far as comb-shaped branched polymer molecules are concerned, the earliest work reported is that of Berry *et al*¹⁻⁴ who studied the intrinsic- and melt-viscosity behaviour of some comb-shaped poly(vinyl acetates), which were prepared by free radical methods. More recently Decker⁵ has described the solution behaviour of some comb-shaped polystyrenes and showed that the θ -temperature of these polymers in cyclohexane is below that of linear polystyrenes and depends on the length of the branches but is apparently independent of the branching frequency. The excellent work described by Fujimoto *et al*⁶ shows how the melt viscosity of some branched polystyrenes varies with branch length and branching frequency over a limited range of each of these variables. As explained below, however, the branched polymers studied by Fujimoto *et al* are considered here as polymers with long-chain branching rather than comb-shaped polymers, so discussion of them will be left to our paper dealing with polymers with long-chain branching⁸.

The present paper describes our attempts to study the effect of varying the branch length and branching frequency on the intrinsic viscosity and low-shear melt viscosity behaviour of some comb-shaped branched polystyrenes. For convenience, comb-shaped polymers are arbitrarily defined here as those branched polymers in which the number average molecular weight of the branches, all attached to a common linear backbone, is less than 46 000. The branch length in the majority of these polymers is also, incidentally, below the critical chain length for entanglements for linear polymers ($\bar{M}_c = 33\,000$)¹⁷. The branched polystyrenes described here and in the next paper in this series⁸ were prepared by reacting a linear backbone molecule containing pendant chloromethyl groups with living polymer:



where M^+ is an alkali metal ion.

The behaviour of these comb-shaped polystyrenes, both in solution and in the melt, is both unusual and unexpected.

EXPERIMENTAL

Polymerization

The living polystyrene used in the coupling reaction was prepared in benzene solution using *n*-butyl lithium as initiator. According to the kinetic studies of the benzene/*n*-butyl-lithium/styrene system by Cubbon and Margerison⁹, complete consumption of the initiator occurs only if:

$$M_0^{6/5}/a_0 \geq 45 \text{ mol}^{1/5} \text{ cm}^{3/5} \text{ at } 288 \text{ K} \quad (1)$$

where M_0 is the initial monomer concentration and a_0 the *n*-butyl lithium concentration. In this case the degree of polymerization \bar{P}_n is given by $\bar{P}_n = M_0/a_0$. It was important to ensure the complete consumption of *n*-butyl lithium in the polymerization step for the reason that *n*-butyl lithium and the chloromethyl group undergo lithium-halogen interchange. That this interchange reaction results in crosslinking was all too clearly shown by the formation of gel in the early attempts at coupling. In all subsequent runs where the above ratio of monomer and initiator was satisfied, and where the molecular weight was greater than 5000, there was no evidence of gel in the branched product after coupling. Where the polymer molecular weight was less than 5000, in which region the above ratio of monomer and initiator cannot be satisfied, it was necessary to add a small amount of tetrahydrofuran

to the system to accelerate initiation and ensure the complete consumption of *n*-butyl lithium^{10,11}.

All operations were carried out in an atmosphere of argon. The benzene, previously dried and stored over calcium hydride, was distilled from *n*-butyl lithium into the reaction vessel. The styrene was freed of inhibitor, vacuum distilled and dried and stored over calcium hydride at 258 K. It was deoxygenated just prior to polymerization with a stream of argon. The initiator was prepared initially in diethyl ether from *n*-butyl chloride and lithium metal¹². After allowing the lithium chloride to settle, the ethereal solution was decanted and the ether replaced by dry benzene. Its concentration was determined by the double titration procedure of Gilman and Haubein¹³.

Polymerization was carried out in a 500 cm³ graduated cylindrical vessel fitted with a B19 socket at its upper end and a greaseless tap at its lower end. After distilling the benzene into the reaction vessel a serum cap was quickly fitted in the B19 socket and the *n*-butyl lithium solution injected from a hypodermic syringe fitted with a stainless-steel needle. The styrene was then added in a similar way, followed by a little THF where necessary. Because heat was evolved during polymerization it was necessary to vent the reaction vessel and this was done by flushing a stream of argon across the solution using syringe needles passing through the serum cap for the inlet and outlet. The reaction vessel was gently shaken for about half an hour and the stream of argon removed when polymerization was complete and the solution had cooled to room temperature. Using this simple technique it was possible to prepare living polystyrenes, the measured molecular weights of which were generally in good agreement with the calculated values ($\bar{P}_n = M_n/a_0$). Furthermore, the higher molecular weight polymers which were examined by gel permeation chromatography were shown to possess fairly narrow molecular weight distributions (i.e. $\bar{M}_w/\bar{M}_n < 1.2$).

Chloromethylation of polystyrene

The backbone polymer used throughout this work was a commercial polystyrene and was purified by several precipitations from tetrahydrofuran into water and into methanol and dried in a vacuum oven at 333 K. It was chloromethylated by dissolving it in a large excess of chloromethyl methyl ether and adding anhydrous zinc chloride¹⁴ at room temperature. The reaction was quenched by chilling the solution and adding a mixture of THF and ice-water. On occasions aliquots were withdrawn at various intervals of time and separately quenched in order to prepare samples with a range of chloromethyl group contents. The polymer solution was then precipitated into a large volume of ice-cold water. (It was essential to keep the polymer cold since the heat produced in the hydrolysis of the excess chloromethyl methyl ether was otherwise sufficient to induce crosslinking at this stage.) The resulting polymer was dried and precipitated into water twice more in order to remove soluble zinc compounds and finally precipitated into methanol and dried. Infra-red examination of the products showed that even in the most heavily chloromethylated polymers the chloromethyl group was exclusively in the *para* position of the benzene rings. There was no evidence of *ortho*- or *meta*-substitution. The oxygen flask combustion method was used to

determine the chlorine content where this was sufficiently high (i.e. $> 1\%$). Where the chlorine content was lower, x-ray fluorescence spectroscopy was used, the polymer being dissolved in THF. In this case a calibration curve was first obtained using a series of solutions containing known concentrations of *p*-chlorobenzoic acid in THF.

Coupling reaction between polystyryl lithium and chloromethylated polystyrene

Before carrying out the coupling reactions tetrahydrofuran was distilled from sodium naphthalene in a stream of argon onto weighed amounts of the chloromethylated polymers. The air originally adsorbed on the polymer dissolved in the THF and was removed by bubbling argon through the solution for 30 minutes. The solution was then stoppered until required. The coupling reaction was carried out by slowly running the living polymer solution in the polymerization vessel into the chloromethylated polymer solution. Knowing the weight and chlorine content of the chloromethylated polymer and the calculated molecular weight of the living polymer, the minimum quantity of the latter required for complete coupling was calculated. In general, however, because of impurities present more than the calculated quantity of living polystyrene was required and sufficient of this was added to give a permanent orange colour in the coupling reaction vessel. After coupling, the excess lithium polystyryl was terminated by the addition of methanol. Part of the living polymer was separately terminated with methanol and its molecular weight subsequently measured by ebulliometry, vapour pressure osmometry or membrane osmometry, as appropriate. Branched polymers were prepared in sets from a given living polymer. They differed only in the number of branches attached to the same backbone.

Separation of linear and branched polystyrenes

Since some of the living polymer was terminated by impurities and since an excess was added to ensure complete reaction with the chloromethyl groups in the backbone, the product obtained after coupling was a mixture of branched and linear polystyrenes. It was possible to effect a separation of the linear and branched polymers by a simple fractional precipitation by ensuring that the difference in the molecular weights of the two components was sufficiently large so that the respective molecular weight distributions did not overlap. This was done by keeping the branch length shorter than the backbone and by attaching a sufficient number of branches to it. In practice the separation was carried out by first determining the volume of methanol required just to begin to precipitate the linear precursor from a 1% solution of this in methyl ethyl ketone (MEK). A 1% solution of the mixture of linear and branched polymers in MEK was then prepared and sufficient methanol added slowly with stirring to completely precipitate the branched component but insufficient to precipitate the linear component. The branched polymer separated as a very viscous second phase which settled to the bottom. Usually the MEK-methanol mixture was cloudy due to small globules of the polymer-rich phase in suspension. That the branched polymer had

been completely precipitated was checked by centrifuging the MEK-methanol phase to produce a clear liquid and then adding a drop or two of methanol to it. This remained clear if the branched polymer had been completely removed and the precipitation point of the linear polymer had not been reached. The viscous polymer was redissolved in THF, precipitated into methanol and dried. For the polymers described here the volume of methanol required to completely precipitate the branched component was in all cases less than the volume required to precipitate the linear component, but the difference became smaller as the molecular weight of the linear precursor was increased and the number of branches decreased.

The fractional precipitation procedure was repeated at least once after the branched polymer had been redissolved in MEK (to give a 1% solution), to reduce the amount of linear polymer present to negligible proportions. The effectiveness of the separation was demonstrated by gel permeation chromatography. *Figure 1* shows the chromatograms before and after a single

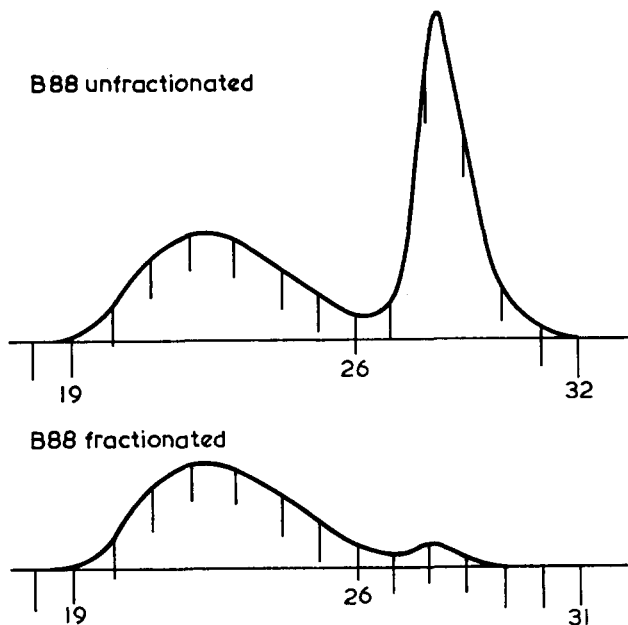


Figure 1 GPC traces of a typical product obtained after the reaction of chloromethylated polystyrene with lithium polystyryl. In this example a large fraction of the linear precursor polymer ($\bar{M}_n = 35\,000$), formed by termination of lithium polystyryl by impurities, is removed from the branched polymer ($\bar{M}_n = 1.28 \times 10^6$) by just one fractional precipitation

fractional precipitation for sample B88, which contains 33 branches, the molecular weight (\bar{M}_n) of which is 35 200. Osmotic pressure measurements on some of the branched polymers also proved useful in detecting the presence of low molecular weight linear polymer after fractionation.

Molecular weight, intrinsic viscosity and melt viscosity measurements

Number average molecular weights were measured by ebulliometry, vapour pressure osmometry or membrane osmometry, as appropriate and light scattering was used to measure the weight average molecular weights. Intrinsic viscosities were measured at 298 K in tetrahydrofuran and at 308 K in cyclohexane, and the low shear melt viscosities were measured at 460 K in a melt penetrometer. Details are given in Part 1⁷.

RESULTS AND DISCUSSION

Molecular weight measurements

The most extensive molecular weight measurements carried out on the branched polystyrenes after removal of the linear homopolymer were done by light scattering, although for some of the polymers it was possible to measure the number average molecular weights by osmometry also. The latter are recorded in *Table 1*, in which the calculated value of M_n^B for the branched polymer is given by

$$M_n^B = M_n^L + \bar{p}M_n^b \quad (2)$$

where M_n^L is number average molecular weight of backbone (= 114 000)

M_n^b is number average molecular weight of branches

and \bar{p} is the average number of branches per backbone molecule

Table 1 Number average data for some branched polymers and their branches

Sample	Branch M_n^b	Number of branches \bar{p}^*	M_n^B of branched polymer $\times 10^{-5}$		Number of fractional precipit- ations
			Calculated	Measured	
B50	5380	26	2.49	2.37	2
B51	5380	71	4.83	4.89	2
B63	5100	9-10	1.60	1.86	2
B64	5100	33	2.82	2.31	3
B71	6500	9-10	1.76	1.72	2

* The number of branches is calculated from the chlorine content of the chloromethylated backbone

The polymer samples shown in *Table 1* in which the molecular weights, M_n^b , of the branches are 5380 and 5100 are members of two series of polymers in which the branching frequency, p , varies from about 10 to 475 branches per backbone. Because the branch length does not differ greatly in these two series, they are conveniently considered throughout this paper as a single series in which $M_n^b = 5200$. Similarly, where reference is made to a series of polymers in which $M_n^b = 6600$, in reality this consists of polymers in which $M_n^b = 6500$ and 6800 respectively. In the two series of polymers referred to, in which the branching frequency is constant at 33 and 71 branches per backbone respectively, the molecular weight of the branches ranges from 5200 to 45 000.

Because of extrapolation difficulties in the Zimm plots for many of the samples, the weight average molecular weights are recorded as \bar{M}_{90} , obtained from the 90° scatter corrected for dissymmetry and assuming the polymer molecules to be random coils. In *Figure 2* the results obtained in this way are plotted against the values of M_n^B calculated on the assumption that coupling between the living polymer and the chloromethylated backbone has taken place as expected. M_n^B was calculated from an equation given by Orofino¹⁵ for branched polymers in which the branches are randomly attached to a common linear backbone (see Appendix). If coupling has taken place as expected then the results should fall on a line with a slope of unity in *Figure 2*. Although it is clear from *Figure 2* that there is considerable scatter in the

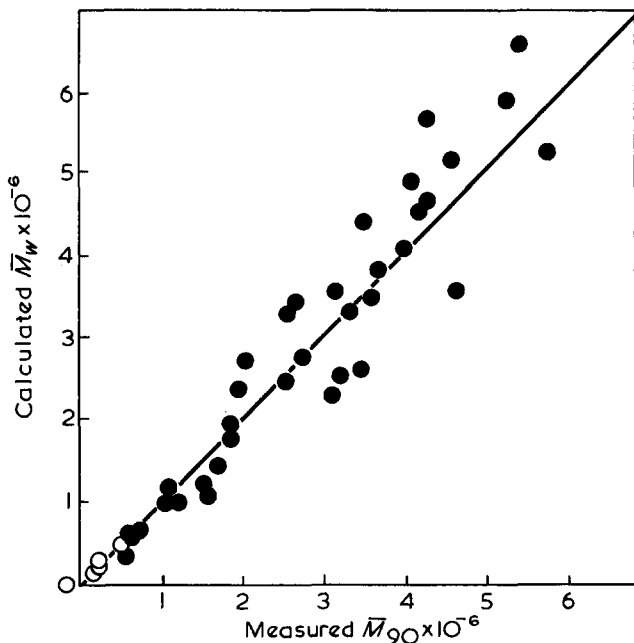


Figure 2 A plot of the molecular weight \bar{M}_{90} , obtained by light scattering measurements (●), against the expected molecular weight \bar{M}_w (see equation A2). A few measurements were possible by osmometry (○)

results, it can none the less be seen that up to a molecular weight of about 2×10^6 the values of \bar{M}_{90} fall close to or are higher than the expected values whereas above 2×10^6 values of \bar{M}_{90} are in most cases lower. Since it is by no means certain whether the model chosen to represent the configuration of these comb-shaped polymers in solution is appropriate, some uncertainty attaches to the values of \bar{M}_{90} obtained from light scattering measurements for these molecules. However, the results shown in *Figure 2* do show that high molecular weight (branched) polymers have been prepared.

The curvature noted in the Zimm plots at low angles, which prevented

reliable values of \bar{M}_w being obtained, is indicative of the presence of a soluble, very high molecular weight component presumably formed by crosslinking, and this need be present only in very small amounts to adversely affect the intensity of the scattered light at low angles to give unreliable values of \bar{M}_w . Crosslinking would be the outcome of lithium-halogen interchange between the lithium polystyryl (or other lithium compound present) and the chloromethylated backbone polymer. Where the molecular weight of the branches exceeded 5000 none of the branched polymers showed any sign of the presence of gel and it is thought that the lithium-halogen interchange reaction occurred only to a very small extent in their preparation. However, in several coupling reactions carried out in which the molecular weight of the lithium polystyryl, M_n^b , was less than 5000 (not described in the experimental section) it was clear that crosslinking was becoming more extensive. For example, when $M_n^b = 500$, gel formation actually occurred when the lithium polystyryl solution reacted with the chloromethylated polymer. Also, when $M_n^b = 2300$ and 1300, the molecular weights obtained by light scattering measurements on the soluble products were considerably higher than the values expected of a simple coupling reaction. It may be significant that the formation of living polymers with molecular weights below 5000, using *n*-butyl lithium as initiator in benzene, required the addition of THF to ensure rapid initiation and complete consumption of initiator (see experimental section). The occurrence of lithium-halogen interchange, leading to crosslinking, when $M_n^b < 5000$, is possibly caused by a lithium compound formed by cleavage of THF by *n*-butyl lithium which is known to occur above 238 K¹⁶, rather than by the lithium polystyryl.

A further comment may be made regarding the values of the molecular weights \bar{M}_{90} above 2×10^6 . The values of \bar{M}_{90} in this region, which are lower than expected, could be attributed to incomplete coupling between the chloromethylated polymer and the living polymer rather than to an incorrect model used to treat the light scattering data. The extent of coupling in a number of the branched polymers, in which both high and low branching frequencies were covered, was therefore checked by analysing for residual chlorine. In all cases the residual chlorine was no higher (< 50 p.p.m.) than the background level found in an un-chloromethylated polymer, showing that all the chloromethyl groups had probably reacted in the coupling reaction. This conclusion is also supported by the fact that none of the branched polymers described here crosslinked when their melt viscosities were measured. It has been found that the presence of just a few chloromethyl groups in polystyrene makes the polymer very susceptible to crosslinking when heated to 460 K, the temperature at which the melt viscosities were measured.

The molecular weights used in discussing the properties of the comb-shaped polymers in the following sections are those obtained from equation (2) and equation (A1) given in the Appendix, rather than those obtained from light scattering.

Low-shear melt viscosities of comb-shaped polymers

The effect on the low-shear melt viscosity, η_0 , of altering the frequency of branching while keeping the average backbone and branch lengths fixed, is

shown in *Figure 3* for two series of polymers. This shows that at all levels of branching, ranging from an average of 10 to 475 branches per backbone, the polymers have lower melt viscosities than linear polymers of corresponding molecular weights, and that the melt viscosities decrease progressively as the frequency of branching increases. For all polymers except those with the lowest branching frequency (10 branches per backbone) the melt viscosities are lower than that of the backbone in spite of their higher molecular weights.

Figure 4 shows how the melt viscosity varies with molecular weight when the average branch length is increased (from $\bar{M}_n = 2300$ to 46 000) but the number of branches and the backbone remain unchanged. As the average branch length increases the low-shear melt viscosity decreases at first, reaches a minimum and then increases again. Even when the average branch length is nearly as long as half that of the backbone the viscosities of the branched

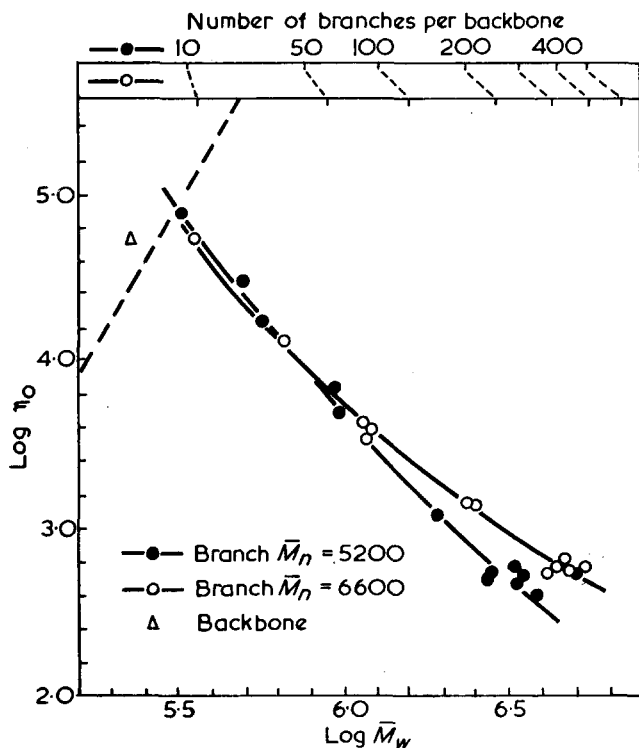


Figure 3 Dependence of the melt viscosity on molecular weight for the series of comb-shaped polymers with a fixed branch length and variable branching frequency. The dependence of η_0 on \bar{M}_w for narrow distribution linear polystyrenes is shown by the broken line. Melt viscosities are in N s m^{-2}

polymers are still below that of the backbone. The molecular weight of the branched polymer at which the minimum occurs is lower for the series of polymers with 33 branches than for the series with 71 branches per backbone.

Thus, above a certain minimum number of branches, the presence of

short and intermediate length branches has the effect of lowering the low-shear melt viscosity, η_0 , below the value for the backbone to which they are attached. This effect is similar to, though less marked than, that which is observed by blending a linear polymer of the same (low) molecular weight as the branches with the backbone polymer in the same proportions as in the branched polymers. The fluidizing effect of these branches increases as their number increases. While there are no results for comb-shaped polystyrenes with very low branching frequencies the results for the two polymers with 10 branches per backbone suggest that polymers with fewer branches per

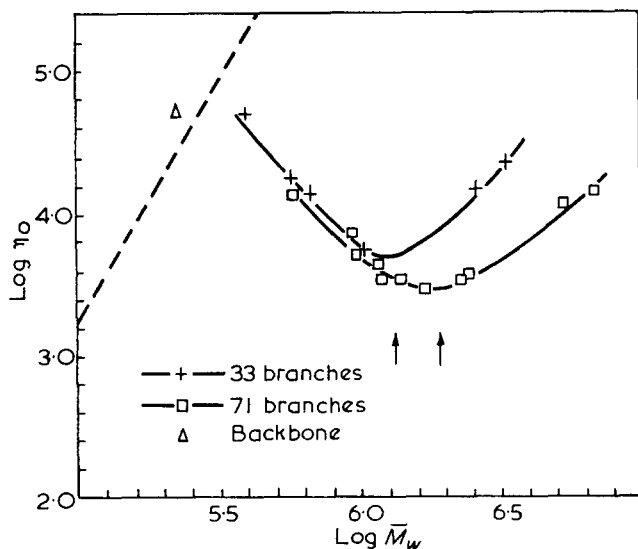


Figure 4 Dependence of the melt viscosity on molecular weight for the series of comb-shaped polymers with fixed branching frequency and variable branch length

backbone will have melt viscosities which are higher than that of the backbone. That this is so for comb-shaped poly(vinyl acetates) is shown by the results of Berry *et al*⁴ who succeeded in making some reasonably well-characterized polymers by a free-radical method. A comparison of the two polymer species (see Table 2) shows that the comb-shaped poly(vinyl acetates) have lower branching frequencies than the polystyrenes (the branching frequency is inversely proportional to λ , see below). Examination of the results on comb-shaped poly(vinyl acetates) also reveals that those polymers which have branch lengths in excess of the critical chain length for entanglements in linear polymers have melt viscosities higher than those of linear polymers of comparable molecular weights, and *vice versa*. The melt viscosities of the comb-shaped polystyrenes are lower than those of linear polymers of the same molecular weights irrespective of whether the branch length is greater or less than the critical chain length, suggesting that the length of the branches relative to the critical chain length for linear polymers is not necessarily significant in the melt viscosity behaviour of comb-shaped polymers.

In *Table 2* the inverse branching frequency (λ) is used to compare the two species of polymer and this is defined here as the number of backbone repeat units per branch:

$$\lambda = M_n^L / \bar{p} M_0 = \text{degree of polymerization of backbone} / \bar{p} \quad (3)$$

where M_n^L and \bar{p} have already been defined and M_0 is the monomer molecular weight. The usefulness of the parameter λ is that a direct comparison of

Table 2 Comparison of some data for comb-shaped polystyrenes and comb-shaped poly(vinyl acetates)

	Polystyrenes	Poly(vinyl acetates)
Inverse branching frequency, λ	110–2	3590–425
Molecular weight of backbone, M_n^L	1.14×10^5	1.5×10^6 – 2.54×10^6
Molecular weight of branches, M_n^b	5.2×10^3 – 4.6×10^4	1.8×10^4 – 7.5×10^5
Critical chain length for linear polymers, M_c^*	3.3×10^4	2.2×10^4

* The critical chain lengths for these two polymers are taken from the review by Porter and Johnson¹⁷

the extent of branching in different species of polymer is possible, notwithstanding differences in the molecular weights of the backbone or monomer.

Empirically it has been found that the low shear melt viscosity of the comb-shaped polystyrenes is given by

$$\log \eta_0 = a \log [M_n^b + M_n^L (M_n^L - M_n^b) / M_n^b] + b \quad (4)$$

where the coefficient a and the constant b differ for each series of polymers.

A plot of $\log \eta_0$ against $\log [M_n^b + M_n^L (M_n^L - M_n^b) / M_n^b]$ is shown in *Figure 5* for one of the series of polymers with a fixed branching frequency and for one series with a fixed branch length; the other two series of polymers studied gave similar straight line plots but these are not shown in *Figure 5*. By substituting equation (2) into equation (4) and differentiating with respect to M_n^b , it may be shown that equation (4) exhibits a minimum when

$$M_n^b = M_n^L (\sqrt{1 + \bar{p}} - 1) / \bar{p} \text{ at constant } \bar{p}$$

For $M_n^L = 114\,000$ as in the branched polymers prepared here

$$\begin{aligned} M_n^b &= 16\,700 \text{ when } \bar{p} = 33 \\ \text{and } M_n^b &= 11\,900 \text{ when } \bar{p} = 71 \end{aligned}$$

These calculated values for the branch length at the minima lie close to the observed minima and this is shown in *Figure 4*.

In attempting to understand the melt viscosity behaviour of these comb-shaped polystyrenes, it is informative to consider first the behaviour of linear polymers. It has been shown by Fox and Allen¹⁸ that the zero shear melt viscosities of narrow distribution linear polystyrenes are related to the mean square radii of gyration of the polymer molecules in a θ -solvent by

$$\eta_0 \sim \langle S_0^2 \rangle^{1.0} \text{ in the absence of interchain entanglements,} \\ \text{i.e. for } M < M_c$$

and $\eta_0 \sim \langle S_0^2 \rangle^{3.4}$ in the region of interchain entanglements, i.e. for $M > M_c$

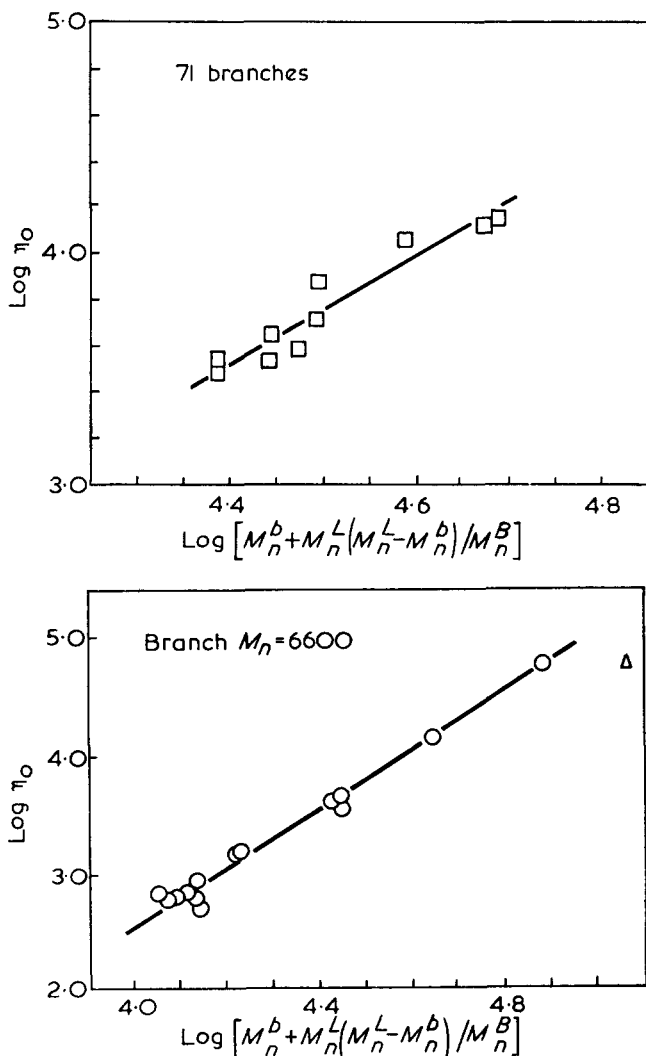


Figure 5 Plot showing the linear dependence of $\log \eta_0$ on $\log [M_n^b + M_n^L(M_n^L - M_n^b)/M_n^B]$. Similar plots are obtained for the other series of polymers studied

where M_c is the so-called critical molecular weight for entanglements and the exponents are also the slopes of the $\log \eta_0$ against $\log M$ plot in the two regions, respectively. A similar correlation between η_0 and $\langle S_0^2 \rangle$ has been found for polystyrenes with long-chain branching (see Part 3, reference 8), although the exponent of $\langle S_0^2 \rangle$ is 4.8 for these polymers. Although no measurements of the θ -point dimensions of the comb-shaped polymers were made, it is possible to calculate the mean square unperturbed radius of gyration, $\langle S_0^2 \rangle$, assuming the molecules take on a random coil configuration, from an equation by Orofino¹⁹. The results of these calculations may be summarized as follows:

- (1) For the series of polymers in which the branches are short and fixed in length and the branching frequency is varied, the calculated value of $\langle S_0^2 \rangle$ remains very nearly constant irrespective of the branching frequency; the total increase in size throughout each series is less than 5% of the size of the backbone. The corollary to this is that the average segment density within the coil increases continuously as the number of branches increases. Hence, if the configuration and size of these comb-shaped molecules in the melt are related to the calculated θ -point dimensions, as is apparently the case for linear polystyrenes, then the observed decrease in melt viscosity as the number of branches increases occurs in spite of the fact that the size of the molecules remains virtually constant. In fact, the decrease in melt viscosity accompanies the increase in average segment density.
- (2) For the two series of comb-shaped polystyrenes with a fixed branching frequency and variable branch length, there is a steady increase in both the calculated value of $\langle S_0^2 \rangle$ and the segment density as the branch length increases. The total increase in $\langle S_0^2 \rangle$, calculated from Orofino's equation,

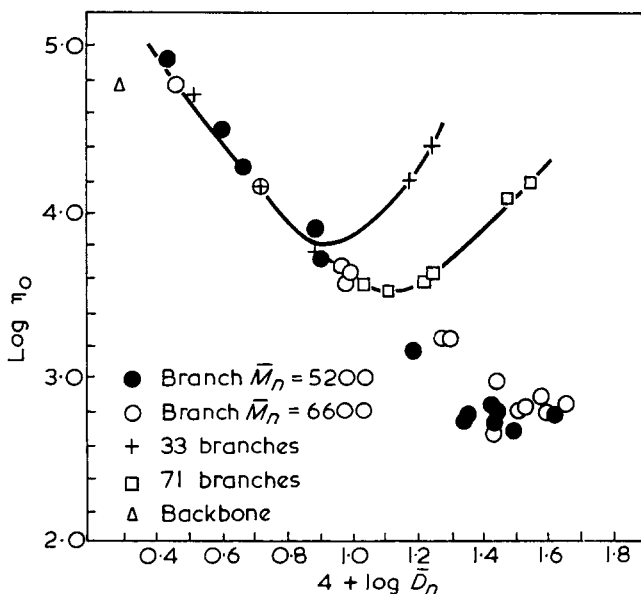


Figure 6 Dependence of the low-shear melt viscosity on the segment density calculated from the theoretical θ -point dimensions (see Appendix)

is about the same (38% of the size of the backbone) for both series of polymers, whereas the increase in segment density over that of the backbone for the polymers with 71 branches per backbone is about twice that for the series with 33 branches per backbone, for a given branch length. It is apparent from Figure 6, in which $\log \eta_0$ is plotted against $\log \bar{D}_n$, where \bar{D}_n is the average segment density (see Appendix), that

the curve describing the initial decrease in the melt viscosity for these comb-shaped polymers with fixed branching frequency coincides with that for the other polymers with variable branching frequency. In other words, in the region of decreasing melt viscosity for comb-shaped polymers, the melt viscosity (and the probability of interchain entanglements) decreases with increasing segment density and is independent of the theoretical size of the molecule. Beyond a certain branch length, however, the melt viscosity increases as the size (i.e. $\langle S_0^2 \rangle$) increases, although there is also an increase in the average segment density.

In studying the solution properties of some comb-shaped polystyrenes, Decker⁵ found that the actual dimensions of these molecules at their measured θ -points are appreciably higher than the dimensions calculated from Orofino's equation, which assumes a Gaussian distribution of chain segments. The converse therefore applies to the average segment density, though this is still higher for comb-shaped polymers than that of linear polymers of the same molecular weight. This result has been taken to imply that the actual distribution of chain segments in the molecular coil is non-Gaussian for these comb-shaped polymers, though the actual distribution still remains unknown. The results obtained by Decker are not sufficiently extensive to show how, for example, the actual θ -point dimensions vary in a series of polymers in which the branch length varies at a fixed frequency of branching so it is not possible at present to see how far the melt viscosity behaviour described here can be related to the dimensions and configuration of the molecules at their actual θ -points. In reality, however, the region of decreasing melt viscosity exhibited by comb-shaped polystyrenes might still be a result of a steadily increasing segment density. Where, after a certain branch length, the melt viscosity rises again with further increase in branch length, the actual distribution of chain segments might be such that a sheath of low segment density forms around the core of high segment density. The presence of such a region of low segment density would make it possible for neighbouring molecules to interpenetrate to some extent thereby giving rise to an increased resistance to flow. Alternatively, beyond a certain branch length the actual average segment density throughout the molecular domain might decrease with further increase in branch length, thereby increasing the probability of interchain entanglements.

Intrinsic viscosities of comb-shaped polymers

The intrinsic viscosities of these branched polymers were measured in cyclohexane (CH) at 308 K and in tetrahydrofuran (THF) at 298 K and the results are presented in *Figures 7* and *8* as plots of $\log [\eta]$ against $\log M_w^B$. The variation of the intrinsic viscosity of narrow distribution polymers (see Part 17) is shown by a broken line. Variation of the intrinsic viscosity with molecular weight for the comb-shaped polymers is both much slower and more complex than for linear polymers, and this is true in both solvents. For the series of polymers in which the branching frequency is varied at a fixed branch length, the most surprising finding is that the overall increase in $[\eta]$ in cyclohexane is greater than that in THF over the same range of molecular weights. It is surprising because the opposite is found for linear poly-

mers, for which THF at 298 K is a good solvent and cyclohexane at 308 K is a θ -solvent. Figures 7 and 8 also show that a change in the molecular weight of the branches (from 5200 to 6600) produces a noticeable shift of the $\log [\eta]$ against $\log M_w^B$ curve in cyclohexane but has no effect on the variation of $[\eta]$ in THF.

For the two series of polymers in which the branching frequency is constant, the intrinsic viscosity in THF increases with increasing branch length, the rate of increase being greater for the series with the fewest branches, whereas the variation in the intrinsic viscosity in cyclohexane is smaller and

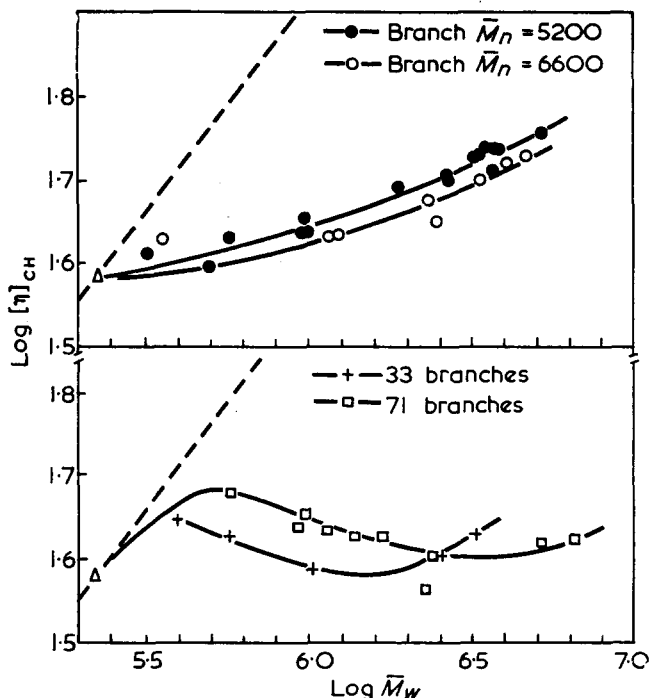


Figure 7 Variation of the intrinsic viscosity in cyclohexane at 308 K with molecular weight for comb-shaped polystyrenes. The broken line shows the variation for linear polystyrenes (ref. 7). Intrinsic viscosities are in $\text{dm}^3 \text{kg}^{-1}$.

more complex. It is interesting to note that these series of polymers also exhibit a more complex melt viscosity behaviour than the series in which the branch length is fixed, i.e. a minimum is observed in the $\log \eta_0$ against $\log M_w^B$ plot.

Since this work was carried out, Decker⁵ has published the results of his studies of the solution properties of comb-shaped polystyrenes. In his work, which was referred to in the previous section on melt viscosity, the range of branch lengths covered was similar to that in the work described here. Probably the most significant result obtained by Decker was that which shows that the θ -temperature in cyclohexane is lower than that of linear

polymers (for which $T_\theta = 308$ K), increases with the length of the branches and is insensitive to changes in the length of the backbone polymer or changes in the branching frequency. From this it follows that for the comb-shaped polystyrenes studied here, the intrinsic viscosity measurements in cyclohexane at 308 K were made above the θ -temperature in all cases. It also follows that in the series of polymers in which the branch length varies, each polymer is, thermodynamically, in a different solvent when dissolved in cyclohexane at 308 K, i.e. cyclohexane approaches nearer to a θ -solvent for the comb-shaped polymers as the length of the branches increases. This could account for the descending portion of the $\log [\eta]_{\text{CH}}$ against $\log \bar{M}_w$ plot shown in *Figure 7*(lower) since the actual size of the comb-shaped polymers might decrease in this region as the branch length increases.

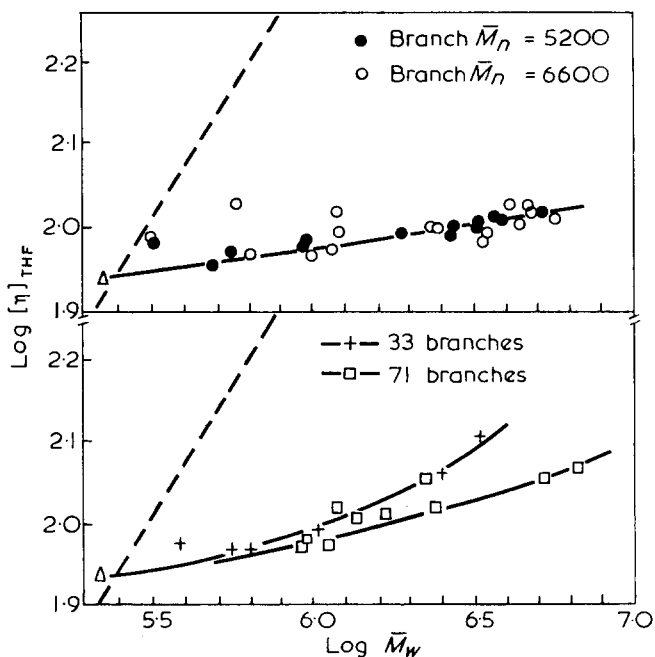


Figure 8 Variation of the intrinsic viscosity in tetrahydrofuran at 298 K with molecular weight for comb-shaped polystyrenes. The broken line shows the variation for linear polystyrenes (ref. 7)

For the two series of polymers with a variable branching frequency it follows from a consideration of Decker's results that the polymers for which the molecular weight of the branches, M_n^b , is 5200 are in a somewhat better solvent, i.e. are more expanded, when dissolved in cyclohexane at 308 K than are those for which $M_n^b = 6600$. This factor alone is sufficient to explain the occurrence of two separate curves in the plot of $\log [\eta]_{\text{CH}}$ against $\log \bar{M}_w$ in this solvent for the two series of polymers [*Figure 7*(upper)].

The variation of the θ -temperature of comb-shaped polystyrenes with branch length in cyclohexane and the peculiar intrinsic viscosity behaviour of these polymers in this solvent at 308 K raises the question as to whether or

not THF at 298 K, for example, can be regarded as the same solvent, thermodynamically, for all the comb-shaped polymers studied. The intuitive answer is that it cannot since the amount by which a branched polymer will expand in a good solvent to minimize segment-segment interactions is expected to depend on both the length and the number of branches. However, in an environment in which the polymer coil is able to expand, small changes in, for example, the length of the branches, may not give rise to changes in the intrinsic viscosity behaviour as pronounced as they do in poorer solvents. This is confirmed by the fact that, in *Figure 8*(upper), only a single intrinsic viscosity/molecular-weight plot is obtained in THF at 298 K for the two series of polymers in which the molecular weight of the branches is 5200 and 6600 respectively; in cyclohexane at 308 K two curves are obtained [*Figure 7*(upper)] for the two series.

The behaviour of the comb-shaped polystyrenes in THF is also usefully discussed with reference to the behaviour of linear polystyrenes in the same solvent. According to the Fox-Flory treatment of the solution viscosity of linear polymers

$$[\eta] = \phi \alpha^3 \langle S_0^2 \rangle^{3/2} / M \quad (5)$$

where ϕ is a universal constant and α^3 is the expansion factor, that is it is a measure of the amount by which the polymer coil expands above its θ -point dimensions when dissolved in a good solvent i.e.

$$\alpha^3 = \langle S^2 \rangle^{3/2} / \langle S_0^2 \rangle^{3/2} \text{ and } \alpha^3 > 1 \text{ in a good solvent} \quad (6)$$

where $\langle S^2 \rangle$ and $\langle S_0^2 \rangle$ are the mean square radii of gyration in a good and a θ -solvent, respectively. Flory has also shown that

$$\langle S_0^2 \rangle \sim M \text{ and } \alpha^3 \sim M^{(a - 0.5)} \quad (7)$$

where a is the exponent in the Mark-Houwink relationship, and it may be deduced from equations (5), (6) and (7) that

$$[\eta] \sim \langle S_0^2 \rangle^a \quad (8)$$

for linear polymers. For the comb-shaped polymers studied here the relationship, if any, between the intrinsic viscosity and the actual θ -point dimensions of the molecules cannot be checked since measurements of the latter were not made. However, it has been found that for the series of polymers with 33 branches (of varying length) the intrinsic viscosity in THF is related to the calculated mean square unperturbed radius of gyration by

$$[\eta] \sim \langle S_0^2 \rangle^{1.15}$$

which is of the same form as equation (8) except that the exponent for these branched polymers is greater than that for linear polymers in THF (0.65, see Part 1, ref. 7). The calculated mean square unperturbed radius of gyration used is that obtained from the equation by Orofino (see Appendix) which assumes that comb-shaped polymers obey random flight statistics. It has not been possible to show whether or not a similar dependence of $[\eta]$ on $\langle S_0^2 \rangle$ holds for the series of polymers with 71 branches, because of the large scatter in the results, but it is shown in Part 3⁸, that the polystyrenes with long-chain

branching obey a similar relationship to equation (8), although the exponent shows some dependence on the branching frequency. In the case of the series of polymers with a fixed branch length and variable branching frequency, there is very little increase in the calculated unperturbed dimensions (see Appendix) with increasing molecular weight, and as may be seen from *Figure 8*(upper) only a small increase in the intrinsic viscosity in THF.

The dependence of the intrinsic viscosity in a good solvent, such as THF, on the actual θ -point dimensions of a series of comb-shaped polymers with a fixed branching frequency and variable branch length remains to be investigated. This would be particularly interesting since Decker⁵ has found that the actual mean square radii of gyration of some comb-shaped polystyrenes at the measured θ -point in cyclohexane are greater than those calculated from Orfino's equation, implying that these molecules do not obey random flight statistics.

The sizes of the comb-shaped molecules in THF at 25°C determined from light scattering measurements are subject to some uncertainty, as are the molecular weights M_{90} , since they are obtained from the 90° scatter corrected for dissymmetry and depend on the model chosen to represent the configuration of the molecules in solution. However, in *Figure 9* is shown how the

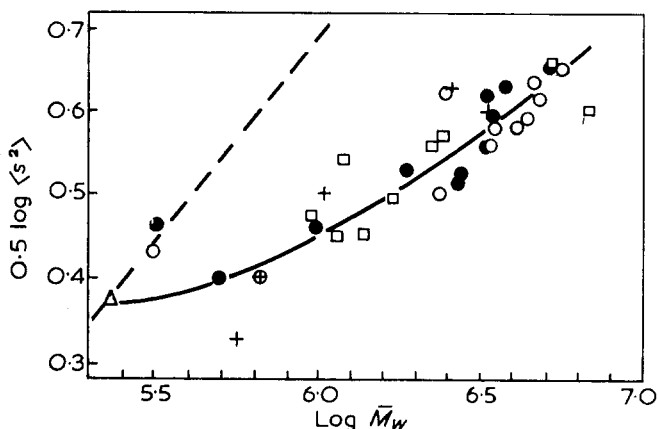


Figure 9 Dependence of the r.m.s. radius of gyration of comb-shaped polystyrenes in tetrahydrofuran on molecular weight, Variable branching frequency: ●, $M_n^b = 5200$, ○, $M_n^b = 6600$. Variable branch length: □, $\bar{p} = 71$, +, $\bar{p} = 33$ (narrow distribution linear polymers, - - - -)

root mean square radius of gyration in THF determined in this way varies with molecular weight for comb-shaped polystyrenes. Also shown is a straight line of slope 0.55 expected for linear polystyrenes, since it may be shown from the Fox-Flory theory that for linear polymers in a good solvent the r.m.s. radius of gyration is given by

$$\langle S^2 \rangle^{\frac{1}{2}} \sim M^{(a+1)/3}$$

where $a = 0.65$ for polystyrene in THF at 298 K in the molecular weight range $2.8 \times 10^4 - 1 \times 10^6$. It is apparent from *Figure 9* that at a given

molecular weight the comb-shaped polymer is smaller than a linear one and the rate of increase in size with molecular weight is also smaller for the branched molecules.

CONCLUSION

In this work we have prepared and studied some properties of a group of branched polystyrenes with a limited range of branch lengths but a fairly wide range of branching frequencies. The range of polymers that could be prepared were limited by the techniques used. Although these comb-shaped polymers are of great interest in themselves and show unusual and largely unexpected behaviour, it is recognized that they do not closely resemble the type of branched polymer likely to be produced by transfer reactions in conventional free-radical polymerizations. This situation is partially remedied in Part 3^B where an account is given of a group of branched polymers with lower branching frequencies and longer branches than the comb-shaped polymers described here. Some attempt is also made in Part 3 to provide a framework in which the properties of these polymers and other branched polymers, e.g. star-shaped polymers and branched polymers formed in free-radical processes, may be related.

ACKNOWLEDGEMENTS

The author is grateful to Drs J. C. Greaves, P. P. Manning and P. A. Small for their encouragement and useful discussions in this work. Thanks are due to Mr F. Yearsley for the light scattering measurements and to Mr A. Titterton for his able assistance in the experimental work.

*Imperial Chemical Industries Ltd,
Plastics Division, Research Department,
Welwyn Garden City,
Hertfordshire, UK*

*(Received 3 March 1971)
(Revised 17 May 1971)*

REFERENCES

- 1 Hobbs, L. M. and Long, V. C. *Polymer, Lond.* 1963, **4**, 479
- 2 Berry, G. C. and Craig, R. G. *Polymer, Lond.* 1964, **5**, 19
- 3 Berry, G. C., Hobbs, L. M. and Long, V. C. *Polymer, Lond.* 1964, **5**, 31
- 4 Berry, G. C., Hobbs, L. M. and Long, V. C. *Polymer, Lond.* 1964, **5**, 517
- 5 Decker, D. *Makromol. Chem.* 1969, **125**, 136
- 6 Fujimoto, T., Narukawa, H. and Nagasawa, M. *Macromolecules* 1970, **3**, 57
- 7 Pannell, J. *Polymer, Lond.* 1971, **12**, 547
- 8 Pannell, J. *Polymer, Lond.* in the press
- 9 Cubbon, R. C. P. and Margerison, D. *Proc. Roy. Soc.* 1962, **A268**, 260; *Polymer, Lond.* 1965, **6**, 102
- 10 Altares, T., Wyman, D. P. and Allen, V. R. *J. Polym. Sci. (A-2)* 1964, **2**, 4533
- 11 Worsfold, D. J. and Bywater, S. *Can. J. Chem.* 1962, **40**, 1564

- 12 Shirley, D. A. 'Preparation of Organic Intermediates', p 65, John Wiley and Sons Inc., New York, 1951
 13 Gilman, H. and Haubein, A. H. *J. Amer. Chem. Soc.* 1944, **66**, 1515
 14 Jones, G. D. *Ind. & Eng. Chem.* 1952, **44**, 2686
 15 Orofino, T. A. *Polymer, Lond.* 1961, **2**, 295
 16 Gilman, H. and Gaj, B. J. *J. Org. Chem.* 1957, **22**, 1165
 17 Porter, R. S. and Johnson, J. F. *Chem. Rev.* 1966, **66**, 1
 18 Fox, T. G. and Allen, V. R. *J. Chem. Phys.* 1964, **41**, 344
 19 Orofino, T. A. *Polymer, Lond.* 1961, **2**, 305

APPENDIX

Molecular weights and molecular weight distributions of comb-shaped polymers

Orofino¹⁵ has shown that the ratio M_w^B/M_n^B for branched polymers in which the branches are randomly attached to a common linear backbone is given by

$$M_w^B/M_n^B = x_w/x_n + \bar{p} \bar{y}_n^2 [(\bar{x}_n - \bar{p})/\bar{x}_n + \bar{y}_w/\bar{y}_n - 1]/(\bar{x}_n + \bar{p} \bar{y}_n)^2 \quad (A1)$$

where M_n^B is given by equation (2) (see the section on molecular weight measurements).

\bar{x} is the degree of polymerization of the backbone ($\bar{x}_n = M_n^L/104$)

\bar{y} is the degree of polymerization of the branches ($\bar{y}_n = M_n^b/104$)

and the subscripts n and w denote the usual averages.

Substitution of values of the parameters characterizing the backbone, the branches and the branching frequency in equations (2) and (3) shows that $M_w^B/M_n^B \approx 2$, to better than 5% for all the branched polymers described here, i.e.

$$M_w^B \approx 2(M_n^L + \bar{p}M_n^b) = 2M_n^B \quad (A2)$$

This means that the molecular weight distributions in these comb-shaped polymers are determined almost exclusively by that of the backbone polymer (for which $\bar{x}_w/\bar{x}_n \approx 2$).

Theoretical random flight dimensions of comb-shaped polystyrenes

An expression for the random flight dimensions of branched polymers in which the branches are randomly attached to a common linear backbone has been derived by Orofino¹⁹:

$$\langle S_0^2 \rangle = (b^2/6Z_w Z_n \bar{x}_n) \{Z_n^2 \bar{x}_w \bar{x}_z + \bar{p} y_n^2 [3\bar{x}_w Z_n + y_n (\bar{x}_n - 3\bar{p})]\} \quad (A3)$$

where $\langle S_0^2 \rangle$ is the Z-average mean square radius of gyration, \bar{p} is the average number of branches per backbone and b is the length of one freely jointed chain element. Z , \bar{x} and y are the degrees of polymerization of the branched polymer, backbone and branches respectively and the subscripts z , w and n denote the usual averages. The branches are assumed in this expression to be homogeneous in chain length.

For the comb-shaped polymers discussed in this paper, the backbone polymer was a free-radical polymer and is assumed to possess a most probable distribution of molecular weights i.e. $\bar{x}_z:\bar{x}_w:\bar{x}_n = 3:2:1$. Number and weight average molecular weight measurements on the backbone polymer

confirmed that $\bar{x}_w/\bar{x}_n \approx 2$. It was shown in the previous section that the molecular weight distribution in these comb-shaped polymers is the same as that of the backbone polymer, i.e. $Z_w/Z_n = M_w^B/M_n^B \approx 2$. Equation (A3) now simplifies to

$$\langle S_0^2 \rangle = (b^2/6) \{3\bar{x}_n + (\bar{p}y_n^2/2\bar{x}_n Z_n^2) [6\bar{x}_n Z_n + y_n (\bar{x}_n - 3\bar{p})]\} \quad (\text{A4})$$

$Z_n (= M_n^B/104)$ is calculated from equation (2).

The average segment density \bar{D}_n is defined here as the average number of segments per unit volume in a sphere of radius $\langle S_0^2 \rangle^{1/2}$:

$$\bar{D}_n = (Z_n/M_0)/(4\pi\langle S_0^2 \rangle^{3/2}/3) = (3Z_n/4\pi M_0)/\langle S_0^2 \rangle^{3/2} \quad (\text{A5})$$

where M_0 is the monomer molecular weight. This definition of \bar{D}_n implies that there is a uniform distribution of segments throughout the sphere, although the values so obtained are related, by a numerical constant, to the segment density, ρ_{max} , at the peak of a Gaussian distribution with the same mean square radius of gyration:

$$\rho_{\text{max}} = n(3/2\pi)^{3/2}/\langle S_0^2 \rangle^{3/2} \quad (\text{A6})$$

where n is the number of segments per chain.

Polyacrylonitrile degradation kinetics studied by the micropyrolysis–g.l.c. technique

F. A. BELL*, R. S. LEHRLE and J. C. ROBB

The thermal degradation of thin films of polyacrylonitrile (thickness ~ 750 Å) has been studied in the temperature range 200–850°C by the micropyrolysis–g.l.c. technique. Throughout the temperature range 300–850°C the following products were characterized: ammonia, hydrogen cyanide, monomer, acetonitrile and methacrylonitrile. From studies of (a) the limiting yields of products, (b) the conversion curves and kinetics of the evolution of some of the products, (c) the influence of water on the degradation and (d) stoichiometric considerations, it is concluded that three independent processes occur: (1) ammonia evolution, possibly by a stepwise process leaving a ladder polymer containing some five-membered rings, (2) hydrogen cyanide evolution, either from head-to-head linkages or by a chain reaction, leaving double bonds randomly within the polymer molecules, and (3) monomer evolution by a depropagation process, involving intermolecular and intramolecular transfer steps leading to acetonitrile and methacrylonitrile production. A fourth independent process is the only one observed at 200°C; this is probably a laddering process which leads to the stabilization of the polymer towards subsequent degradation at higher temperatures. High-temperature kinetic studies of polymer samples which had been pre-heated at 200°C have indicated the limitations of this stabilization process and have shown that the parts of the polymer which are not ladderized degrade in the same way as normal polymer.

1. INTRODUCTION

THE MICROPYROLYSIS–GLC technique¹ is a convenient and quantitative method of studying polymer degradation; the experimental requirements for studying the kinetics of the pyrolysis process itself by this method have been discussed^{2a}. The technique has been applied to elucidate the changes in mechanism with temperature in the thermal degradation of poly(methyl methacrylate)^{2b}, in which the sole volatile pyrolysis product is monomer. In the present work the method has been used to study the more complex thermal degradation of polyacrylonitrile.

Several aspects of the thermal behaviour of polyacrylonitrile have been reported during the last twenty years. The coloration of the polymer occurring below 200°C has been extensively studied and discussed^{3–20}; this phenomenon has been generally attributed to the development of conjugated sequences of C=N groups (leading to ladder formation), and is not associated with the evolution of volatile products. At higher temperatures the coloration is accompanied by the evolution of degradation products, and a number of

* Present address: ICI Fibres, Ltd, Harrogate, Yorkshire, England.

these have been characterized^{3,5,8,21-25}. In thermal analysis studies^{5,7,14,15,21,25-30} there has been much discussion about the exotherm observed in the 200–300°C temperature region; it has been attributed to an increase in the rate of formation of conjugated C=N sequences^{14,27}, and also to the evolution of volatiles²⁶, such as ammonia³⁰. Several authors have examined the weight loss of samples during degradation^{5,7,14,15,21,26,27}, and there have been various attempts to measure the limiting yields or rates of evolution of some of the volatile products^{3,5,8,18,19,22,31}, but only the products HCN and NH₃ have been examined quantitatively from this point of view.

This paper describes a method of separating the different volatile products, which are analysed as they are formed. In addition to the fact that this approach provides data for kinetic analysis, it has an important advantage over some alternative methods. This advantage is that the present one-stage method eliminates the necessity of condensing and storing the products prior to subsequent analysis; in two-stage methods it is probable that some interaction of the primary products occurs during storage, in which case the subsequent analysis is not representative of the degradation process itself.

2. MATERIALS

Acrylonitrile monomer was first washed with 5% sulphuric acid, then with 5% sodium hydroxide, and finally washed twice with distilled water. It was then fractionally distilled under nitrogen through a 5 ft (1.5 m) (1 in, 2.5 cm, diameter) column packed with Fenske helices. No impurities could be detected in the middle fraction by infra-red analysis. The purified monomer was stored over calcium hydride, and all subsequent operations (e.g. the charging of dilatometers) were performed by distillation in a high vacuum apparatus.

Dimethyl formamide was first washed with potassium hydroxide solution and then distilled under an atmosphere of nitrogen; the middle fraction, boiling at 153°C, was collected and stored over anhydrous calcium chloride.

Azo-bis-isobutyronitrile was twice recrystallized from ethanol, the solution being filtered hot to remove insoluble materials derived from the decomposition of this initiator. The pure crystals were filtered off and dried under high vacuum.

Polyacrylonitrile. Solutions of acrylonitrile in dimethylformamide were polymerized in vacuum dilatometers thermostatted at 30°C. *Azo-bis-isobutyronitrile* was used as the initiator, and the conversion/time plots were (surprisingly) linear up to about 40% conversion. The systems were observed to be homogeneous throughout, provided monomer concentrations less than 3 molar were used. The polymerization order with respect to initiator concentration was found to be 0.60 ± 0.04 , which compares favourably with the value 0.59 published by Thomas³². (The fact that this order slightly exceeds 0.5 may imply the participation of some degradative chain transfer or geminate termination process.) Polymer samples were precipitated by slow addition of the dilatometer contents to methanol, and then dried under high vacuum at 100°C.

3. DEGRADATION APPARATUS AND TECHNIQUE

A boosted-filament pyrolysis unit¹, coupled to a capillary column/flame-ionization detector g.l.c. apparatus, has been used throughout this work. Constructional and operational details are discussed in reference 2a.

Thin films of polymer were deposited in the central region of the ribbon filament by using a 1 μ l Hamilton microsyringe to deliver a 0.1% solution of polyacrylonitrile in dimethylformamide, and then allowing the residual solvent to evaporate off in the g.l.c. carrier-gas stream. Any carbonaceous residue remaining on the filament after pyrolysis was removed by first gently scraping with a sharp blade and then heating the filament in air to $\sim 1000^\circ\text{C}$ for one minute.

The mass spectrometer used in characterizing the volatile degradation products was an AEI type MS9.

4. RESULTS

(4.1) *Characterization of pyrolysis products*

Throughout the temperature range of interest in the present work (up to 850°C), pyrolysis chromatograms display the same set of peaks; the pyrolysis temperature influences only the relative proportions of these peaks and the rate of degradation. Six distinct peaks can be seen on the chromatogram shown in *Figure 1*, which actually corresponds to a 30-sec pyrolysis of polyacrylonitrile at 350°C .

The peaks were identified by trapping the individual components from the g.l.c. effluent gas and subjecting the samples to mass spectrometric analysis. In order to obtain larger samples for analysis, the pyrolyses were performed on samples of larger size (~ 1 mg) in a pyrolysis-g.l.c. (katharometer)

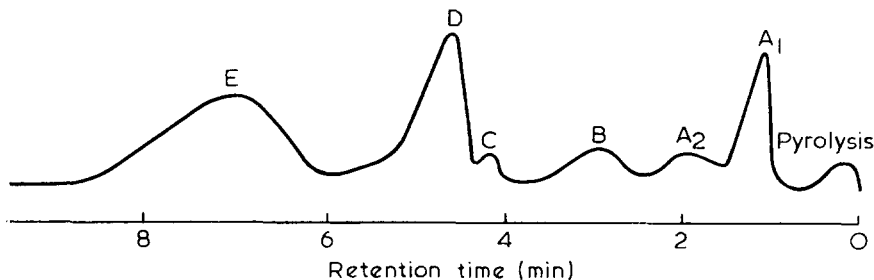


Figure 1 Chromatogram of the pyrolysis products of polyacrylonitrile. Degradation temperature: 350°C ; degradation time: 30 seconds; g.l.c. column coating: tricresyl phosphate

apparatus previously described³³. The chromatographic column was 4 ft long (0.2 inches diameter) and packed with 60–80 mesh acid-washed Chromosorb W containing 10% dinonyl phthalate as stationary liquid phase.

Peaks B, C, and D were identified in this way as hydrogen cyanide, acetonitrile and acrylonitrile, respectively. These assignments were confirmed by the correspondence of the retention times of these compounds when they were directly injected into the g.l.c. apparatus.

Mass spectrometric analysis of the condensate corresponding to peak E indicated an m/e ratio of 67 for the parent in the cracking pattern; it was therefore initially considered that E could correspond to vinyl acetonitrile, since this compound had earlier been reported by Madorsky⁵ and Monahan⁸ as a product from polyacrylonitrile pyrolysis. However, it was found that the retention time of vinyl acetonitrile was approximately twice that recorded for peak E. An investigation of the retention times of the isomeric nitriles crotonitrile and methacrylonitrile indicated that E corresponds to methacrylonitrile, and the mass spectrum is consistent with this interpretation. Confirmation was obtained by degrading a sample of polymethacrylonitrile (which is known^{34,35} to degrade to its monomer); the degradation product was shown to have the same retention time as peak E. Methacrylonitrile, rather than vinyl acetonitrile is therefore one of the principal products of polyacrylonitrile pyrolysis. This conclusion is supported by the work of Takayama²³ and Ming²¹ who also report methacrylonitrile as a significant degradation product.

Peak A₁ was not observed in the chromatograms from the larger-scale degradations, and it has not yet been identified. Peak A₂ was shown to correspond to ammonia; its retention time in both the flame-ionization and katharometer apparatus was the same as that for an injected sample.

(4.2) 'Limiting yields' of volatile products

When polyacrylonitrile is degraded at a specified temperature under nitrogen, the yields of the volatile products initially increase with time but tend asymptotically to limiting values corresponding to rather small total yields of volatiles (see section 4.3 and below).

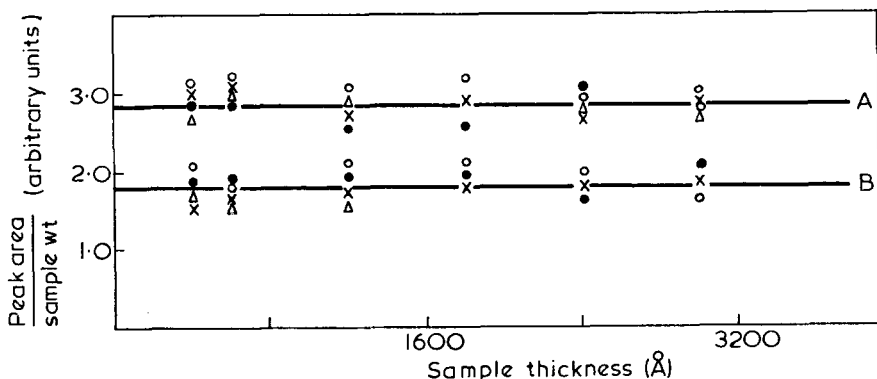


Figure 2 Variation of the quantities of volatile products with sample thickness. A, acrylonitrile; B, methacrylonitrile

The results shown in Figure 2 demonstrate that this phenomenon is not a function of the thickness of the samples used (400–3000 Å), and suggest that the effect might be utilized to obtain information about the chemistry of the degradation processes.

The variation with temperature of the limiting yields of three of the principal products, monomer, methacrylonitrile and hydrogen cyanide, is

shown in *Figure 3*. (The yields of acetonitrile were much too small to provide significant results; the yield of ammonia increased by about 60% over the same temperature range.) These results suggest the processes leading to methacrylonitrile formation and HCN formation share some limiting factor which is independent of temperature (above $\sim 400^\circ\text{C}$), whereas the total available monomer (and, to a lesser extent, the ammonia) increases with temperature.

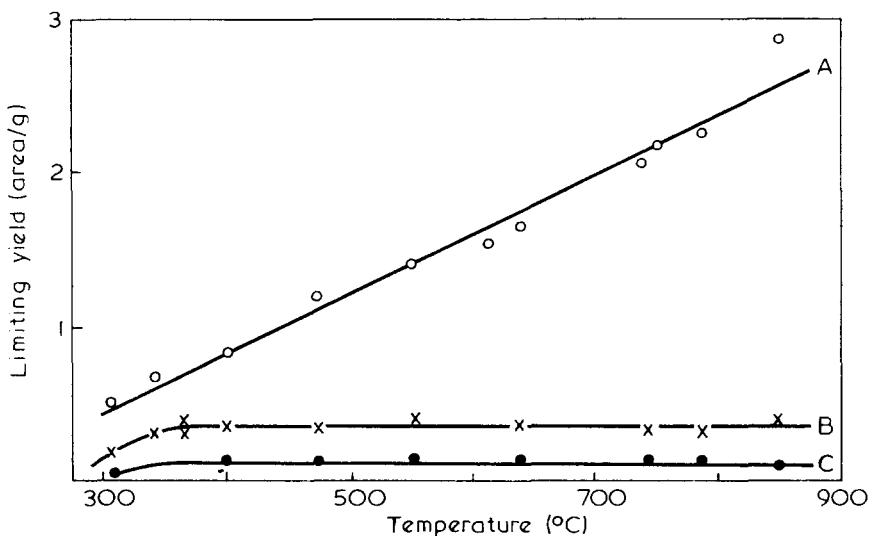


Figure 3 Dependence of the limiting yield of the volatile products on degradation temperature: A, acrylonitrile; B, methacrylonitrile; C, hydrogen cyanide

In order to obtain absolute figures for the limiting yields of volatiles, the flame-ionization detector response factors must be known for the conditions used. These factors were determined for different sample sizes; the results are shown in *Table 1*. No reliable value for hydrogen cyanide could be obtained since injections of dilute aqueous hydrogen cyanide (4%) gave inconclusive results. The factor for HCN was therefore arbitrarily assumed to be similar to that for ammonia. Bearing in mind this assumption, the total limiting yield

Table 1 Response factors of degradation products

Compound	Response of different sample sizes (g per unit area)			
	0.05 μl	0.1 μl	0.2 μl	0.5 μl
Acrylonitrile	3.0×10^{-8}	2.9×10^{-8}	3.3×10^{-8}	2.7×10^{-8}
Acetonitrile	3.7×10^{-8}	3.3×10^{-8}	3.8×10^{-8}	4.0×10^{-8}
Methacrylonitrile	2.8×10^{-8}	2.7×10^{-8}	2.6×10^{-8}	2.4×10^{-8}
Ammonia	2.0×10^{-7}	2.1×10^{-7}	2.3×10^{-7}	2.0×10^{-7}

at degradation temperatures of 300°C, 460°C and 850°C corresponded to about 10%, 18% and 25% total weight loss. These results suggest that some concurrent process is occurring which stabilizes the residue, at least at temperatures up to 850°C. A direct investigation of a controlled stabilization reaction is presented in a later section (4.6).

Similar experiments were performed on polymethacrylonitrile for comparison. Over the temperature range 275–340°C the sole volatile product is monomer, and the limiting yield is 90–95%. Clearly the concurrent stabilization process is less efficient for this polymer.

(4.3) Rate of evolution of volatiles

The pyrolysis–g.l.c. technique may be applied in two ways to obtain conversion curves for the evolution of volatiles:

(1) A single polymer sample is degraded at a specified temperature for a short specified time and the chromatogram of volatile products obtained. The residue is then further degraded under the specified conditions and a second

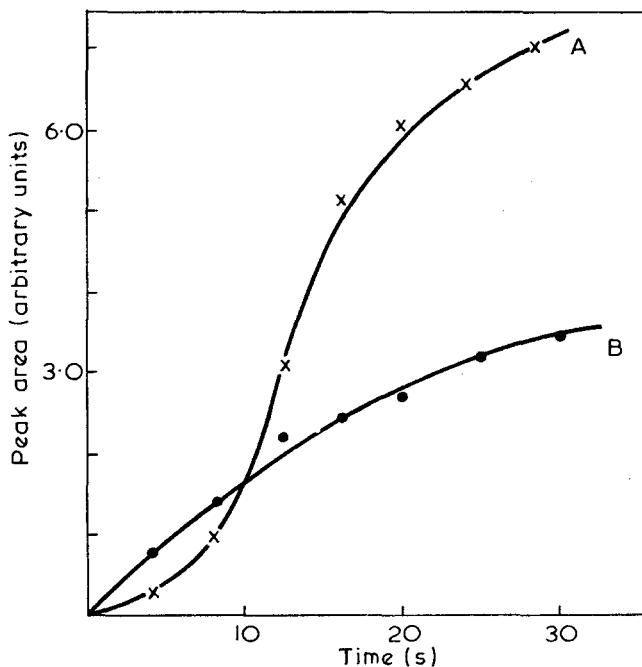


Figure 4 Effect of sample thickness on the conversion curves for acrylonitrile formation. Sample thickness: A, 3000 Å; B, 750 Å

chromatogram recorded. Further degradations provide a complete sequence of data from which a cumulative graph of conversion against reaction time can be plotted.

(2) In this method the conversion curve is obtained by plotting the results from a series of identical samples degraded for different times at the specified temperature.

Initial results obtained using method (1) are shown in *Figure 4(A)*. The first few degradations were of 4-sec duration and the durations were later increased to 10 sec and 30 sec as the yields became smaller. Because the individual yields were small for each degradation, rather large samples (10^{-6} g, thickness ~ 3000 Å) were used in the experiment. The conversion curve has a sigmoid shape, quite different from those obtained in parallel experiments using method (2), described below. In order to check whether diffusion effects or

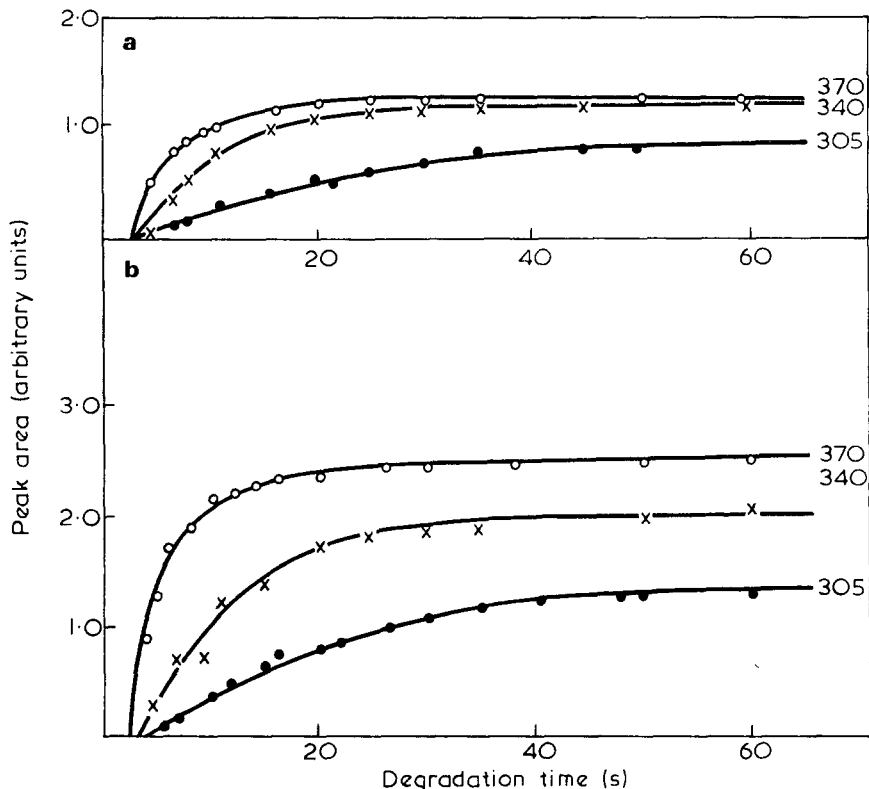


Figure 5 Conversion curves for the formation of volatile products from polyacrylonitrile: (a), acrylonitrile; (b), methacrylonitrile

thermal conductivity effects were responsible for the unusual shape, the experiment was repeated using samples of decreasing thickness. The initial curvature eventually disappeared when the sample thickness had been reduced to about 750 Å; the curve obtained for a sample of this size is shown in *Figure 4(B)*. No detailed explanation of the original initial curvature can be offered, though temperature gradients and diffusion effects in thick samples may be responsible¹. These results, however, underline the importance of investigating sample thickness effects at all stages in the work. Because of the sensitivity problems arising from the use of small samples and short degradation periods when this method is used, and because of the dangers of cumulative error (i.e. summation of all pre- and after-effects of the sequence of heating cycles), method (2) has been employed for all quantitative measure-

ments of the rate of evolution of volatiles, and samples of 750 Å or less have been used throughout.

Conversion curves for monomer and methacrylonitrile evolution, obtained by method (2), are shown in *Figure 5*. The ordinate axes are in arbitrary area units, but the approximate scale can be deduced from the fact that at 300°C the limiting yields of monomer and methacrylonitrile were calculated to be

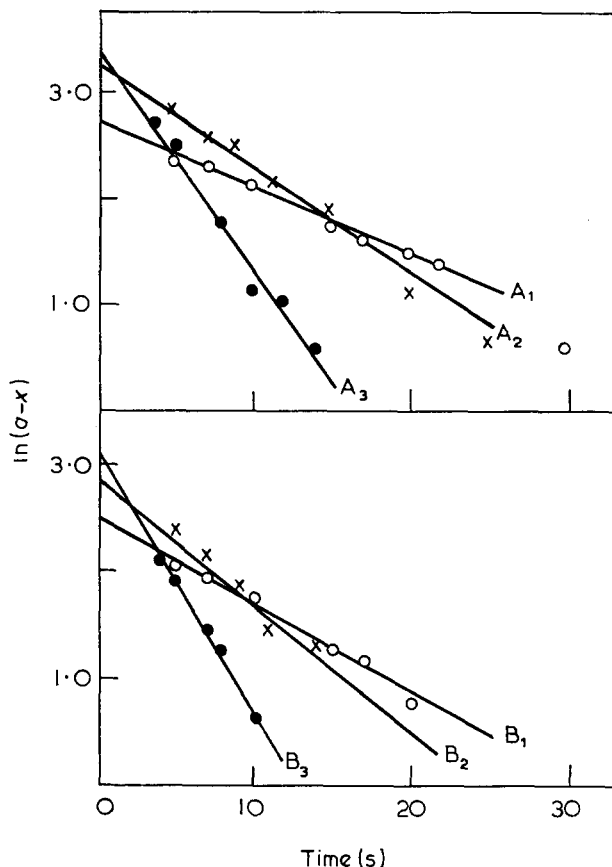


Figure 6 Graphs of $\ln(a-x)$ against time. Plots for acrylonitrile formation at temperatures of 305°C, 340°C, 370°C, are given by lines A₁, A₂ and A₃ respectively; plots for methacrylonitrile formation at the corresponding temperatures are given by B₁, B₂, B₃

about 3% and 1.5% according to the corresponding detector response factors. In the present work the kinetics of volatilization have been considered from the point of view of growth of volatiles to the limiting yields rather than from weight loss from the total sample. Thus, a first order process here is one in which $\ln(a-x)$ plots linearly against time t , where x is the area of the chromatographic peak corresponding to a degradation time of t seconds, and a is the limiting value of the peak area, i.e. the asymptote of the conversion curve. Plots of this kind for monomer and methacrylonitrile evolution are

shown in *Figure 6*, and the corresponding rate constants listed in *Table 2*. These results indicate not only that the processes are probably first order, but also that the rate constants for the two processes are identical (within experimental error) at each temperature, despite the fact that the two products attain different limiting yields. Results of similar accuracy could not be obtained for the evolution of acetonitrile, ammonia and hydrogen cyanide. However, it was observed in all cases that the limiting yields of ammonia and hydrogen cyanide had been evolved before 50% of the limiting yields of monomer and methacrylonitrile had been obtained; it thus appears that the rate constants for HCN and NH₃ evolution are significantly larger than those for monomer and methacrylonitrile. Acetonitrile was obtained in such small yields that no definite conclusions could be drawn, though the possibility that the rate constant could be comparable with that for monomer could not be excluded. From these results it therefore appears that the processes leading to the formation of monomer and methacrylonitrile (and possibly acetonitrile) involve some common mechanism, whereas HCN and ammonia are evolved by more rapid processes. A reconciliation of these findings with those in section 4.2 is presented in a later section (5).

Table 2 Rate constants for polyacrylonitrile degradation (s⁻¹)

<i>Temperature</i> (°C)	<i>Acrylonitrile formation</i>	<i>Methacrylonitrile formation</i>
305	0.060 ± 0.008	0.074 ± 0.008
340	0.11 ± 0.01	0.13 ± 0.01
370	0.22 ± 0.02	0.21 ± 0.02

[An Arrhenius plot of the data in *Table 2* indicated an overall activation energy of about 14 kcal/mol. This figure may be compared with those obtained by Madorsky⁵ and Davydov⁷ (31 kcal/mol and 61 kcal/mol, respectively) by measuring the rate of weight loss from the polymer, and with the figure obtained by Monahan⁸ (16 kcal/mol) by measuring the rate of evolution of HCN. However, it would be premature to draw any conclusions from these figures at the present stage because of the differences in experimental approach and the lack of knowledge of detailed mechanisms.]

(4.4) *Stoichiometric considerations*

With the exception of monomer, the volatile products obtained from polyacrylonitrile degradation are all hydrogen-rich with respect to the original polymer. If, for example, we consider the degradation at 300°C, the total available volatiles correspond to only 10% by weight of sample; this 10% is composed of monomer (3.2%), HCN (3.0%), NH₃ (2.2%), methacrylonitrile (1.6%) and acetonitrile (trace). From these figures can be calculated the relative molar yields of the products and thereby the relative numbers of atoms. Summation of these numbers gives the total relative number of atoms in the volatiles, which may be compared with the corresponding figures

relating to the same weight of bulk polymer. The results are shown in *Table 3*, in which the number of carbon atoms in the polymer is arbitrarily put at 100. These results show quantitatively that the total volatiles are considerably poorer in carbon content, and richer in nitrogen and hydrogen content, than

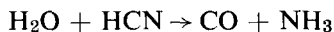
Table 3 Polyacrylonitrile degradation at 300°C: comparison of relative numbers of atoms in the 10% limiting yield of volatiles and in a corresponding weight of polymer

	<i>Relative number of atoms</i>		
	C	N	H
Polymer	100	33.3	100
Total available volatiles	68	57	140

the polymer. Conversely, the residue is correspondingly rich in carbon, but it may be noted that it will be less so if the degradations are performed at higher temperatures, because of relative increase in the limiting yield of monomer with temperature (section 4.2).

(4.5) *Influence of water on the degradations*

The white-spot nitrogen, used as the carrier gas, was passed through a column of molecular sieve (BDH No. 5A) in order to remove any traces of water. Nevertheless, it was thought possible that water might become adsorbed on the sample or degradation chamber during the deposition of the sample and its insertion into the chamber. To test for any chemical effects of traces of water which could be present for that reason, water was deliberately introduced by three different methods. In the first method, water was deposited on the polymer surface from a syringe and the excess allowed to evaporate off to leave an adsorbed film. The next method involved adding water to the polymer solution so that water would be trapped within the polymer film. The final method involved saturation of the carrier gas with water by bubbling the nitrogen through water before it reached the degradation chamber. No significant change in the product ratios was observed when any of the above methods was used. In particular, the ratio of NH₃ to HCN yield was not detectably affected; this is of interest because it indicates that the mechanism proposed by Monahan⁸ for the formation of ammonia



cannot be responsible for the bulk of the yield of ammonia. Ammonia must therefore be regarded as a primary product of the degradation.

(4.6) *The stabilization of polyacrylonitrile at low temperature*

The possibility of a concurrent stabilization reaction was mentioned in section 4.2. It has in fact been known for some time (e.g. references 4, 6, 7) that polyacrylonitrile can be stabilized to thermal degradation by pre-heating the polymer at low temperature (e.g. 150–200°C) for several hours. However,

there has been no detailed work published on the subsequent degradation behaviour of polymer pre-treated in this way; an examination of the evolution of individual volatile products during high-temperature degradation of pre-treated polymer has therefore been carried out in the present study.

Polymer samples were pre-treated by coating the pyrolysis filament with sample and then passing an appropriate current through the filament to maintain it at 200°C for the chosen duration. Unless otherwise stated, the pre-treatment was carried out in an atmosphere of nitrogen. This method has the advantage of pre-treating the sample *in situ* so that no further handling or exposure to air occurs prior to any subsequent investigation of the high-temperature degradation behaviour.

In order to check whether volatile material was evolved during the long periods of pre-treatment (over 20 h), a large sample (50 mg) was given the same treatment for 24 h and the total weight loss was measured. The decrease in weight of sample was found to be less than 0.3%, which was attributed to the loss of adsorbed solvent, since solvent peaks corresponding to a fractional weight loss of this order are normally observed when samples deposited from solution are initially heated on the filament.

Pre-treated samples were degraded by the previously described method of repeatedly heating the single sample for short time intervals, and the chromatograms were examined to detect the extent to which the pre-treatment had caused changes in (a) the nature of the volatile degradation products, (b) the limiting yields of the volatile products, and (c) the rates of evolution of the volatile products:

(a) *The nature of the degradation products.* Each of the products evolved from conventional samples was evolved from pre-treated samples; moreover, no new degradation products could be detected from the pre-treated samples. Samples pre-treated in air again yielded the same products.

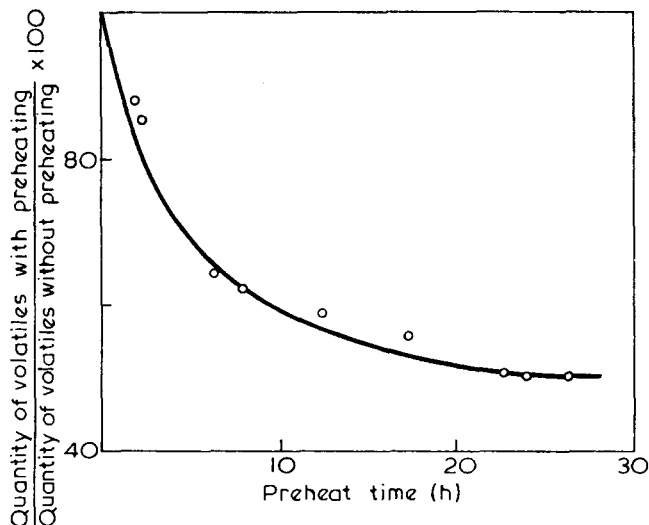


Figure 7 Effect of pre-heating on the available yield of volatile products. (Pre-heat temperature 200°C; degradation temperature 310°C)

(b) *The limiting yields of the degradation products.* Pre-treatment causes a decrease in the total available volatiles at a specified degradation temperature. This is illustrated in Figure 7, in which for degradations performed at 310°C the ratio of the total limiting yield of volatiles for a pre-treated sample to that for an untreated sample is plotted against the duration of pre-treatment. From the figure it is evident that whilst short periods of pre-treatment cause large reductions in available volatiles, after 20 h pre-treatment the stabilization effect appears to be approaching a limit corresponding to about 50% of the volatiles available from an untreated sample. No significant changes in the relative yields of the various products with pre-treatment could be detected, from which it can be inferred that the stabilization process is not specifically inhibiting one of the degradation processes, but is effectively causing sections of the polymer to be inert to thermal degradation at moderate temperatures.

(c) *The rates of evolution of the volatile products.* Because of the smaller yields of volatiles obtained from pre-treated samples, it has been possible to obtain

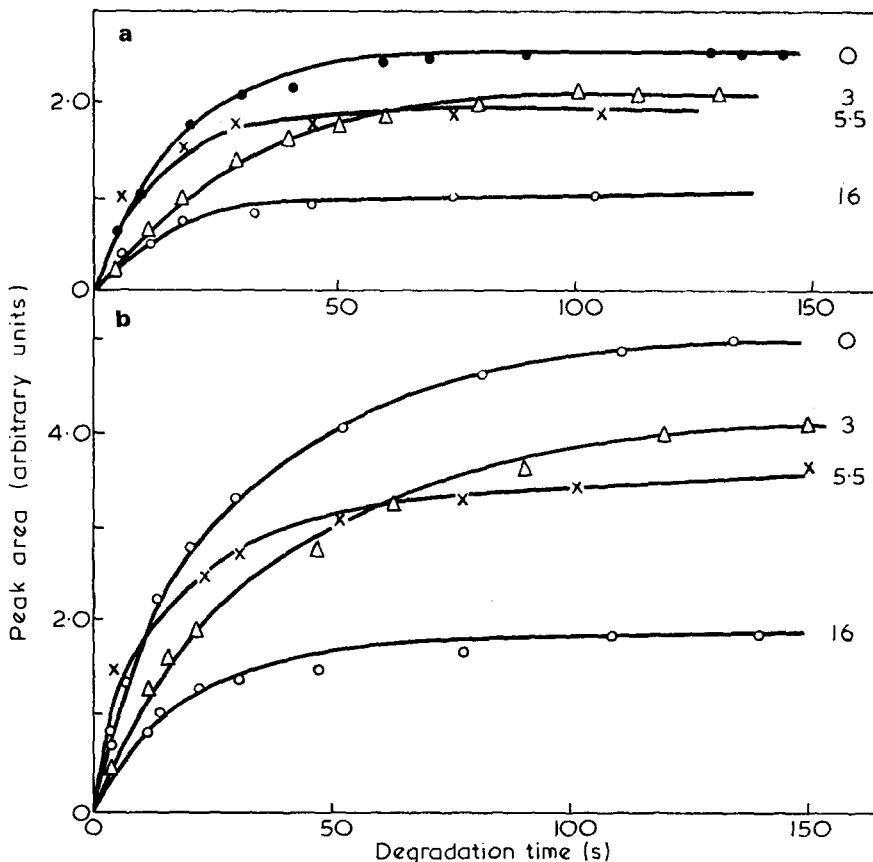


Figure 8 Effect of pre-heating on degradation rates; (a) methacrylonitrile, (b) acrylonitrile. Pre-heat time (hours) indicated beside each line

conversion curves which are quantitatively reliable only for the products monomer and methacrylonitrile. These are shown in *Figure 8*, where the pre-heating time (200°C) of each sample is shown alongside the corresponding curve. As before, first order plots of these curves were drawn by plotting $\ln(a - x)$ against degradation time t , and these are shown in *Figure 9*. (Note that the value of 'a', as previously defined, is different for samples which have been pre-treated for different times, since 'a' corresponds to the limiting yield of product for the specified sample.) With the possible exception of the

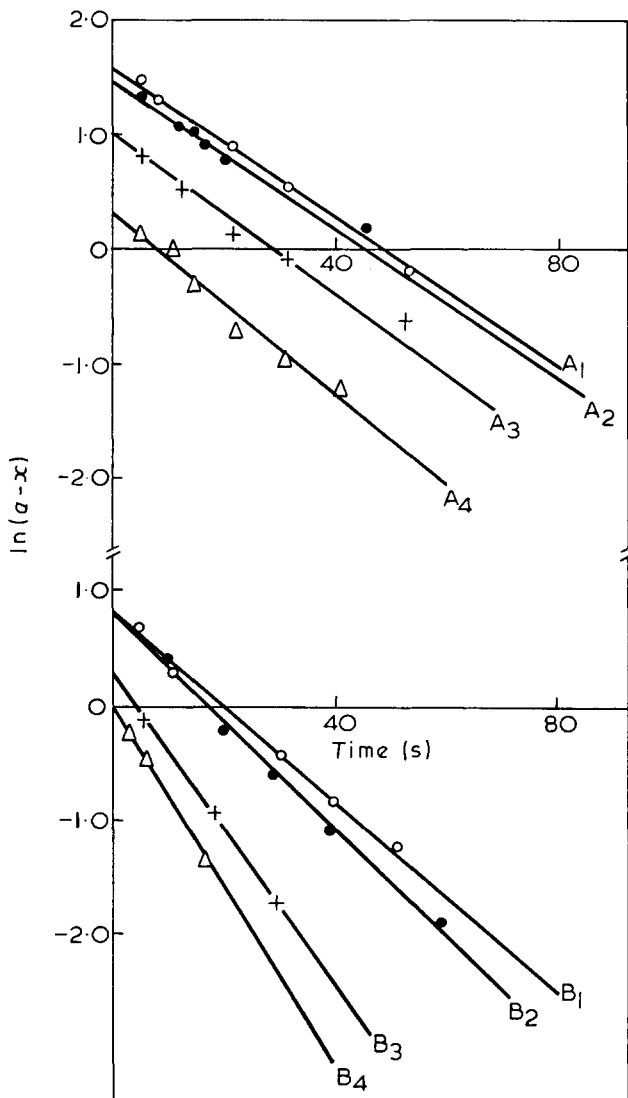


Figure 9 Graphs of $\ln(a - x)$ against time for pre-heated samples. Graphs A₁, A₂, A₃ and A₄ are for acrylonitrile pre-heated for 0, 3, 5½ and 16 hours respectively. Corresponding graphs for methacrylonitrile are given by B₁, B₂, B₃ and B₄

sample pre-heated for 3 h, the rate constants (i.e. gradients of the log plots) are identical, within experimental error, for all the pre-treated samples, and indistinguishable from that of the untreated sample (i.e. that with zero hours pre-treatment). These findings are in accord with the conclusion at the end of paragraph (b) above.

Spectroscopic examination of pre-treated polymer films. Films of polyacrylonitrile, 0.02 mm thick, were pre-heated at 200°C in the absence of air, and mounted in a Perkin-Elmer Model 21 IR spectrophotometer or a Unicam SP 800 ultra-violet spectrophotometer. The infra-red spectra of the pre-heated polymers showed changes consistent with the development of cyclic (ladder) structures of the type proposed by Grassie, Hay and McNeill³⁶. The ultra-violet spectra suggested, from comparison with Takata's u.v. spectra of model compounds³⁷, that the length of the ladder structures does not exceed about five monomer units, and that increasing the duration of pre-heating does not increase the ladder length. Full details of these spectroscopic studies are presented elsewhere³⁸.

5. DISCUSSION

Any discussion about mechanisms must be consistent with the following results and conclusions from section 4 above:

(1) At low temperatures (200°C and below) there are no volatile degradation products evolved from polyacrylonitrile; in this temperature range structural modifications occur which lead to sections of the polymer becoming inert to degradation at higher temperatures. These sections are probably ladders up to 5 monomer units long, and do not increase in length if the heating is prolonged at 200°C. The unstabilized parts of the polymer degrade at higher temperatures to yield the same products, at the same rate, as polymer which has not been pre-heated at 200°C.

(2) At higher temperatures (up to 850°C) a number of volatile products are evolved: ammonia, hydrogen cyanide, acrylonitrile and methacrylonitrile are the major products, and acetonitrile is evolved in trace amounts. Ammonia is a primary degradation product and does not result from any reaction of HCN with traces of water.

(3) At any specified pyrolysis temperature the yields of the volatile products tend asymptotically to limiting values as the degradation time is increased. The total limiting yield of volatiles is rather small (~ 10% at 300°C, 25% at 850°C).

(4) The limiting yield of monomer increases with temperature, whilst the limiting yields of HCN and methacrylonitrile do not. (Over the same temperature range the limiting yield of NH₃ showed a small increase).

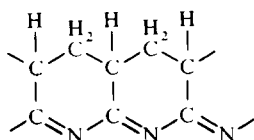
(5) The evolution of monomer and methacrylonitrile (expressed as a fraction of the limiting yield of monomer or methacrylonitrile) is first order, and the rate constants for the two processes are identical at each temperature studied. Whilst it is possible that the evolution of acetonitrile may also have the same rate constant, the rate constants for the evolution of HCN and ammonia are certainly larger.

(6) The total volatiles are considerably richer in nitrogen and hydrogen content, and poorer in carbon content, than the original polymer. The residue is correspondingly richer in carbon content, but this effect is less marked at higher degradation temperatures.

On the basis of the above we tentatively postulate that four independent processes occur when polyacrylonitrile is pyrolysed:

I *The stabilization reaction*

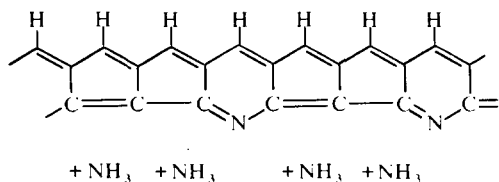
This is the only process occurring at low temperatures and probably corresponds to the formation of short ladders with the structure



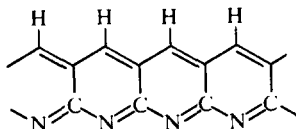
The absence of conjugation along the main chain has been demonstrated³⁹. Possible mechanisms for the process have been reviewed by Beevers¹⁶ and Reich.¹⁵ The reaction has been studied in detail by Kirby, Brandrup, and Peebles⁹⁻¹³, and further studies are in progress (e.g. ref. 14).

II *The ammonia reaction*

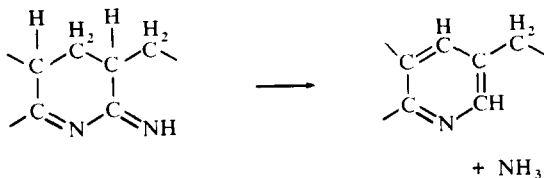
Ammonia is one of the major products of the reaction ($\sim 70\%$ of the monomer yield at 300°C), and its evolution does not appear to be linked kinetically with the formation of the other degradation products (i.e. the variation of its limiting yield with temperature is unique, and its specific rate of evolution is greater than that for monomer and methacrylonitrile). No satisfactory mechanism can be postulated which would be consistent with large yields of ammonia evolved at high rates, but it is tempting to propose a stepwise elimination reaction along the chain to give a residue structure of the type



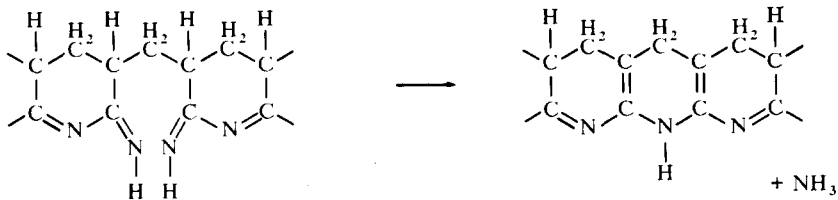
Such a residue is of course carbon-rich with respect to the original polymer and its structure would be consistent with the spectroscopic data previously published⁴ and attributed to structures of the type



Hay³⁰ has suggested that ammonia may be produced by aromatization of a 'ladder-end', i.e.



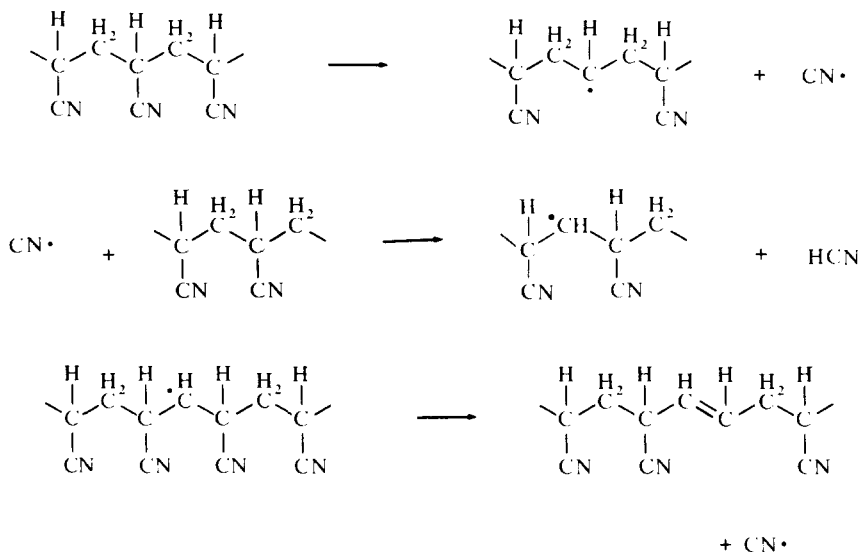
or the chance interaction of two 'ladder-ends', (see also ref. 18), i.e.



If either of these reactions were predominantly responsible for the ammonia evolution, it would be expected that higher ammonia yields would be obtained by degrading pre-treated samples, but no evidence for this effect has been obtained in the present work. We therefore propose that ammonia evolution occurs as suggested earlier, i.e. during the propagation of a ladder, to give a different type of stabilized residue containing five-membered rings.

III The hydrogen cyanide reaction

Hydrogen cyanide is evolved in large yield by a rapid process not kinetically linked to monomer formation. It is possible that a random elimination reaction of the type proposed by Stromberg⁴⁰ for the elimination of HCl from poly(vinyl chloride) is responsible:



This reaction would thus result in the formation of isolated double bonds throughout the chains. The fact that the limiting yield of HCN does not increase with temperature suggests that there may be only a small number of initiation centres in the polymer for the first step in the elimination, and that these are rapidly consumed. The loss of HCN (to yield isolated double bonds in the chains) by this mechanism can be related to the similar temperature dependence of the limiting yield of methacrylonitrile. This will be considered in section IV below.

The above mechanism leaves two important questions open: (a) what are the initiation centres responsible, and (b) why is HCN not evolved by a similar process during the pyrolysis of polymethacrylonitrile? If it is proposed that HCN is lost only at *head-to-head sites* in the polymer chain, plausible answers to these questions may be given. First of all, it is clear that number of such sites is limited, and this would determine the yield of HCN without the necessity of proposing a small number of initiation centres. Secondly, it is probable that the number of head-to-head sites formed during the synthesis of polymethacrylonitrile will be very small, due to steric reasons. Hence the yield of HCN on pyrolysis could be negligible. Further consequences of the head-to-head mechanism will be considered in the next section.

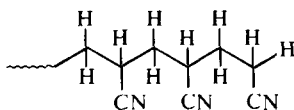
Watt's original intermolecular mechanism³¹ for HCN evolution was later withdrawn after studies of the fibre modulus.¹⁹

IV The chain reaction and chain transfer reactions

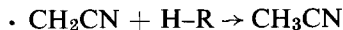
The high yields of methacrylonitrile monomer obtained when polymethacrylonitrile is thermally degraded suggest the occurrence of an unzipping chain reaction, in which transfer is discouraged because of the methyl substitution at the α -carbon atom. In polyacrylonitrile there is no such substitution and chain transfer is therefore more probable. The fact that monomer

is evolved at the same specific rate from polyacrylonitrile whether the polymer is extensively laddered or not, indicates that the sections of polymer between the ladders are available to continue the depropagation; this would be the case if intermolecular chain transfer were a frequently-occurring process. Our studies do not provide any information about possible initiation mechanisms for the depropagation reaction, though the fact that the limiting yield of monomer increases with pyrolysis temperature may indicate that different initiating centres, with different activation energies, are present. Possible sites would be ends of molecules (either 'normal' ones or those resulting from transfer to solvent during the synthesis), double-bonded ends (created during a transfer process followed by scission during the degradation, see below), or chain scission centres. The latter could be head-to-head sites in the polymer chains, or double bond sites formed by loss of HCN. It is unlikely that 'ladder ends' within the chain provide initiation centres, since if this were the case the rate of monomer evolution would be greater for pre-heated polymer, and this effect is not observed.

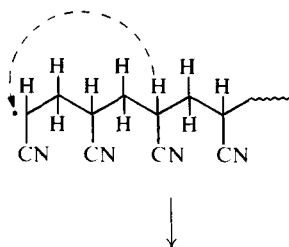
Accepting that chain transfer is very probable in polyacrylonitrile degradation, one can speculate that the products acetonitrile and methacrylonitrile might be formed indirectly as a result of intermolecular and intramolecular transfer processes. Thus, an intermolecular transfer process will convert the unzipping polymeric radical into a dead molecule with the transferred hydrogen at the end:

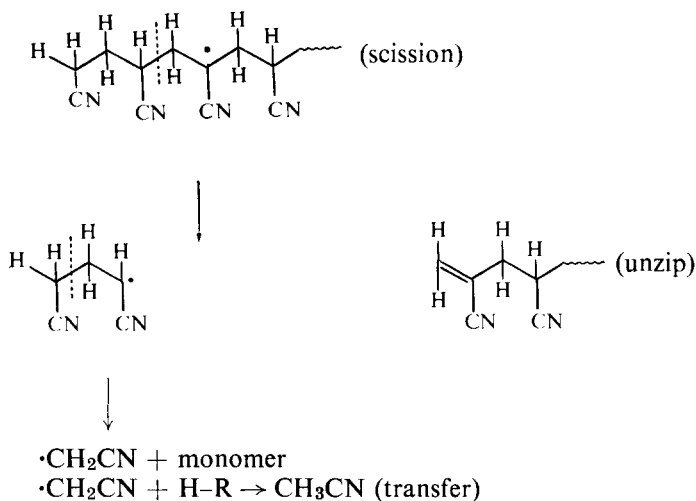


If a second initiation occurs such that this molecule unzips from the left, the free electron at all stages will most probably be sited on the α -carbon atoms, and the ultimate fragment will be a cyanomethyl radical. This will be an extremely reactive entity and will probably collect a hydrogen atom very quickly from any polymer chain by a transfer process, giving acetonitrile:

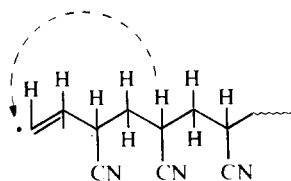


The fact that two distinct unzips are required to produce one molecule of acetonitrile would be consistent with the observed very low yields of this product. Acetonitrile could also be formed as a result of intramolecular transfer during the unzip (or immediately following scission):

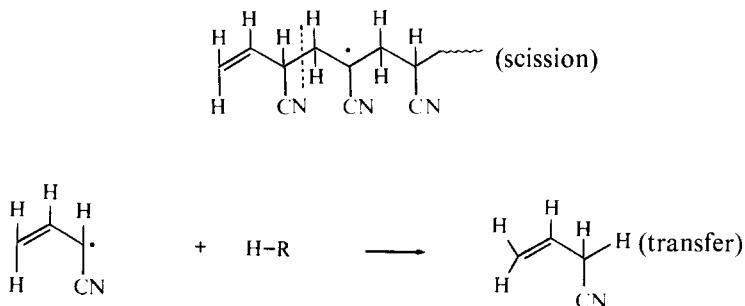




Intramolecular transfer may be favoured when the depropagation reaches a double bond produced by previous loss of HCN:

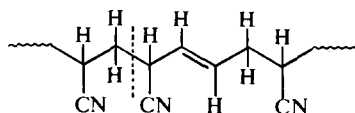


The following sequence could then result in the formation of methacrylonitrile:

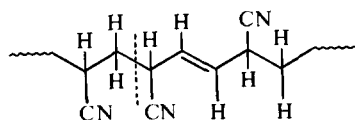


It is assumed that the vinyl acetonitrile product isomerizes at the high temperatures to methacrylonitrile. (The presence of ammonia as an independent degradation product may catalyse this rearrangement.)

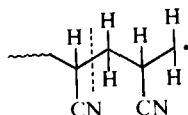
An alternative mechanism for methacrylonitrile formation involves scission adjacent to a double bond resulting from HCN loss. Thus, we can write



if the HCN has been evolved from normal sites, and



if the HCN has been evolved from a head-to-head site. In either case a possible product of the scission is the radical



which at the first stage of unzip will tend to form



Methacrylonitrile may well be the most stable form of the entity in parentheses. These mechanisms, in which methacrylonitrile production is linked to HCN evolution, are consistent with the experimental results on limiting yields, i.e. we suggest that the rapid evolution of HCN has determined the number of methacrylonitrile molecules formed by reactions occurring at the resulting double bonds.

ACKNOWLEDGEMENTS

The authors wish to thank the Science Research Council for a research award to F.A.B. during 1963–66, (during the tenure of which this work was carried out), and Mr J. Suggate for contributions to the discussions.

*Chemistry Department,
The University of Birmingham,
PO Box 363, Birmingham B15 2TT, UK*

*(Received 7 January 1971)
(Revised 20 May 1971)*

REFERENCES

- 1 Lehrle, R. S. *Lab. Pract.* 1968, **17**, 696
- 2 (a) Barlow, A., Lehrle, R. S., Robb, J. C. and Sunderland, D. *Polymer, Lond.* 1967, **8**, 523;
(b) *ibid.* 1967, **8**, 537; Bagby, G., Lehrle, R. S. and Robb, J. C. *Polymer, Lond.* 1969, **10**, 683
- 3 Kern, L. W. and Gernow, H. *Rubber Chemistry Technology* 1944, **17**, 356
- 4 Houtz, R. C. *Textile Research Journal* 1950, **20**, 786
- 5 Madorsky, S. L. and Strauss, G. *J. Res. Nat. Bur. Standards* 1958, **61**, 77
- 6 Grassie, N. and Hay, J. N. *J. Polym. Sci.* 1962, **56**, 189
- 7 Davydov, B. E., Geiderikh, M. A. and Krentzel, B. A. *Izvestia Akad. Nauk. S.S.S.R., (Khim)* 1965, **4**, 636
- 8 Monahan, A. R. *J. Polym. Sci. (A-1)* 1966, **1**, 2391
- 9 Kirby, J. R., Brandrup, J. and Peebles, L. H. *Macromolecules* 1968, **1**, 53
- 10 Brandrup, J., Kirby, J. R. and Peebles, L. H. *Macromolecules* 1968, **1**, 59
- 11 Brandrup, J. and Peebles, L. H. *Macromolecules* 1968, **1**, 64
- 12 Brandrup, J. *Macromolecules* 1968, **1**, 72
- 13 Friedlander, H. N., Peebles, L. H., Brandrup, J. and Kirby, J. R. *Macromolecules* 1968, **1**, 79
- 14 Grassie, N. and McGuchan, R. *Europ. Polym. J.* 1970, **6**, 1277
- 15 Reich, L. *Makromolec. Rev.* 1968, **3**, 49
- 16 Beevers, R. B. *Makromolec. Rev.* 1968, **3**, 113
- 17 Noh, I. and Yu, H. *J. Polym. Sci. (B)* 1966, **4**, 721
- 18 Watt, W. and Green, J. Paper presented at the Plastics Institute Conference on Carbon Fibres, February, 1971
- 19 Watt, W. '3rd Conf. Industrial Carbons and Graphite, 1970,' Soc. Chem. Ind., London, 1971, p 431
- 20 Watt, W. *Proc. Roy. Soc., Lond.* 1970, **A319**, 5
- 21 Ming Tao Tong, Koo Hueh Ch'u Pon She, 1963, p 266 (*Chem. Abs.* 1966, p 2186)
- 22 Nagao, H., Uchida, M. and Yamaguchi, T. *Kogyo Kagaku Zasshi* 1958, **59**, 698
- 23 Takayama, Y. *Kogyo Kagaku Zasshi* 1958, **61**, 1021
- 24 Burlant, W. J. and Parsons, J. C. *J. Polym. Sci.* 1956, **22**, 249
- 25 Kennedy, J. P. and Fontana, C. M. *J. Polym. Sci.* 1959, **39**, 501
- 26 Thomson, E. V. *J. Polym. Sci. (B)* 1966, **4**, 361
- 27 Turner, W. N. and Johnson, F. C. *J. Appl. Polym. Sci.* 1969, **13**, 2073
- 28 Gillham, J. K. and Schwenker, R. F. 'Thermoanalysis of fibres and fibre-forming polymers' (*Applied Polymer Symposia*, 2), R. F. Schwenker, Ed., Interscience, New York, 1966, p 59
- 29 Kaesche-Krischer, B. *Chem.-Ingr. Tech.* 1965, **37**, 944
- 30 Hay, J. N. *J. Polym. Sci.* 1968, **6**, 2127
- 31 Watt, W. *Nature* 1969, **222**, 265
- 32 Thomas, W. M., Gleeson, E. H. and Pellon, J. J. *J. Polym. Sci.* 1955, **17**, 275
- 33 Barlow, A., Lehrle, R. S. and Robb, J. C. *Polymer, Lond.* 1961, **2**, 27
- 34 Grassie, N. and McNeill, I. C. *J. Chem. Soc.* 1956, p 3929
- 35 Kern, L. W. and Fernow, H. *J. Prakt. Chem.* 1942, **160**, 296
- 36 Grassie, N., Hay, J. N. and McNeill, I. C. *J. Polym. Sci.* 1958, **31**, 205
- 37 Takata, T. *J. Polym. Sci.* 1962, **39**, 211
- 38 Bell, F. A. Thesis, 1966, Birmingham University
- 39 Braun, V. D. and Sayed, I. A. A. El. *Angew. Makromolek. Chem.* 1969, **6**, 136
- 40 Stromberg, R. R. and Strauss, S. *J. Polym. Sci.* 1959, **35**, 355

Book Reviews

Thermal stability of polymers, Vol. 1

Edited by R. T. CONLEY

Marcel Dekker, New York, 1970, 644 pp., £21.75

This is the first of two volumes on the subject of polymer stability and is devoted principally to the thermal and oxidative degradation of polymers. On page 17 it is mentioned that solvolysis and degradation by radiation and mechanical means will be treated in detail in the second volume but no further information is given. The contributors are all recognised experts in the field and Professor Conley himself is either the sole or joint author of six of the fourteen chapters.

After an introductory chapter in which polymer degradation processes and the effect on them of some structural features are briefly reviewed, the whole question of the relationships between structure and stability is considered. Three further chapters on the Mechanism and Kinetics of Thermal Depolymerization, Random Scission Processes, and The Fundamental Reactions in Oxidation Chemistry, complete what may be regarded as a broad, general and very effective introduction to the thermal and oxidative degradation of polymers. Thereafter individual classes of polymers are considered in separate chapters.

Chapters 6-8 are devoted by and large to the common high tonnage thermoplastics under the titles: Thermal and Oxidative Degradation of Polyethylene, Polypropylene and Related Olefin Polymers; Thermal and Oxidative Degradation of Natural Rubber and Allied Substances; Vinyl and Vinylidene Polymers. Thereafter there are chapters on the following topics: Fluorocarbon Polymers; Thermal and Thermo-Oxidative Degradation of Polyamides, Polyesters, Polyethers and Related Polymers; Thermosetting Resins; Thermal and Thermo-Oxidative Degradation of Cellulosic Polymers; Heterocyclic Polymers; Degradation of Inorganic Polymers.

In his preface Professor Conley states that, owing to the nature of the field and the interests of the contributors, a number of polymer types are omitted, some treated in cursory fashion and some in great detail. Nevertheless the present reviewer finds the book comprehensive, comprehensible and remarkably uniform in style. Detailed descriptions of a great deal of the earlier pioneering work is often omitted but adequate references are given to allow a more complete survey of the literature to be made.

It is to be expected that a book of this kind should be accepted as authoritative and reliable and workers in the field will wish to use it as a source of basic facts in order to obviate prolonged perusal of original papers. This places a heavy responsibility on authors of this kind of review to report accurately. Factual inaccuracies in the text will inevitably be perpetuated because the great majority of readers will not consult original papers. It is therefore with considerable misgivings that the reviewer finds on pages 225 and 226, where a topic in which he has special knowledge is discussed, that a succession of completely wrong facts are given, adding up to a completely erroneous picture of the thermal degradation of poly(methyl methacrylate). This seriously marred the otherwise pleasurable experience of reading this book.

On the assumption that this is an isolated aberration on the part of the authors, this book is recommended to all with academic, commercial or industrial interests in the stability or degradation of polymers as a pleasantly readable, up-to-date and fairly comprehensive account of the present state of the subject. One suspects that it will be largely confined to libraries, however, since its price will severely inhibit purchase by individuals.

N. GRASSIE

Studies in heterocyclic polymers: Part 2. The thermal degradation of some macrocyclic polymers

R. J. GAYMANS, K. A. HODD and W. A. HOLMES-WALKER

Isothermal weight loss and thermogravimetric studies have been made of macrocyclic polymers derived from pyromellitic tetranitrile and a number of aromatic diamines and compared with polyimide. The results have been used to calculate the apparent activation energies and Arrhenius factors of thermal degradation of these polymers. An analysis of the results showed that macrocyclic polymers have a lower resistance to thermal degradation than has polyimide. The thermo-oxidative degradation of the macrocyclic polymer derived from pyromellitic tetranitrile and 4,4'-diaminodiphenyl ether has been studied using differential thermal analysis (d.t.a.) combined with mass spectrometric analysis of the gases evolved.

INTRODUCTION

MACROCYCLIC POLYMERS have a ladder structure of the type shown in *Figure 1*. Part 1 of this study¹ reported the results of thermogravimetric analyses of macrocyclic polymers in terms of the 10% weight loss temperatures. The polymers were derived from pyromellitic tetranitrile and a number of aromatic diamines. These results and those reported elsewhere^{2,3} suggest that macrocyclic polymer is a system of high thermal stability.

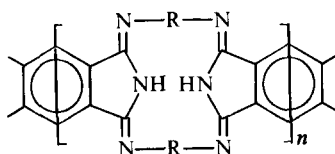


Figure 1 Structure of macrocyclic polymers

To confirm this conclusion and to obtain an indication of the maximum service temperature of this type of polymer a series of isothermal weight loss studies were conducted on macrocyclic polymer, where R (*Figure 1*) is derived from 4,4'-diaminodiphenyl ether (MP1), using both powder and moulded samples.

The thermograms of some other macrocyclic polymers were analysed to obtain degradation rates using Doyle's method⁴.

For the purpose of comparison some isothermal and thermogravimetric weight loss measurements were also made on polyimide.

In an attempt to gain a fuller understanding of the mode of thermal oxidative breakdown of macrocyclic polymer the volatiles generated when polymer MPI is heated were analysed mass spectroscopically.

EXPERIMENTAL

Preparation of macrocyclic polymers

Macrocyclic polymers were prepared by the methods reported previously¹.

Moulding of macrocyclic polymers

Macrocyclic polymer powder was moulded into simple bar forms using a platen temperature of 370°C and a pressure of 6.89×10^7 N m⁻² and a heating period of 5 min. The specimens were allowed to cool to ambient temperature under pressure.

Polyimide

Polyimide derived from pyrometallic dianhydride and 4,4'-diaminodiphenyl ether was provided by Dr J. Idris Jones of the National Physical Laboratory.

Weight loss studies

Thermogravimetric analyses. These were conducted on a Stanton Thermobalance TR01 in air and nitrogen using a heating rate of 4°C/min.

Isothermal analyses. These studies were made in air using a Stanton Thermobalance TR01 controlled by a Stanton-Redcroft LVP CA10 programmer on a 60 mg 100-mesh samples of the macrocyclic polymers and polyimide.

Differential thermal analyses (d.t.a.)

All the d.t.a. studies were made using a Stanton LDTA in air or helium at a heating rate of 8°C/min.

Mass spectrometry (m.s.)

Effluent gas analyses were made using an AEI MS 10 mass spectrometer linked by a stainless-steel capillary tube, 2 m long \times 0.32 mm i.d., to the head of the Stanton LDTA. The capillary was heated to about 150°C to prevent the condensation of volatile products.

The MS10 was fitted with a 4.1 kg magnet which gives it a mass limit of 220. Runs were made with the voltage set for a limited number of *m/e* ratios, so that d.t.a. runs were made for seven mass ranges between *m/e* 16 and *m/e* 205.

The d.t.a./m.s. combination was calibrated for H₂O as follows. Samples of CuSO₄.5H₂O of increasing weight were heated on the d.t.a./m.s. to

250°C under the same conditions as were used for the polymer studies. The peak area for m/e 18 was plotted against the calculated content of sample weight to give a correlation between mass spectrometric signal and the calculated weight of water evolved.

Using samples of NaHCO_3 and the same procedure, a similar correlation was obtained between m/e 44 peak area and the calculated weight of CO_2 evolved.

The correlations for both H_2O and CO_2 were found to be linear, within the sample weight ranges measured and the peak signals used for the analyses.

Using an AEI MS 902 mass spectrometer, analyses were made of the breakdown products generated by the polymer when it was heated at fixed temperatures within the range 285–315°C in high vacuum.

Infra-red spectra

All i.r. spectra were recorded on a Hilger and Watts Infragraph using KBr discs.

RESULTS AND DISCUSSION

The isothermal studies on the powder samples of polymer MP1 and polyimide revealed that the former loses weight faster than polyimide in the temperature range 300–375°C (*Figure 2*). From these data the degradation processes were found to be first order.

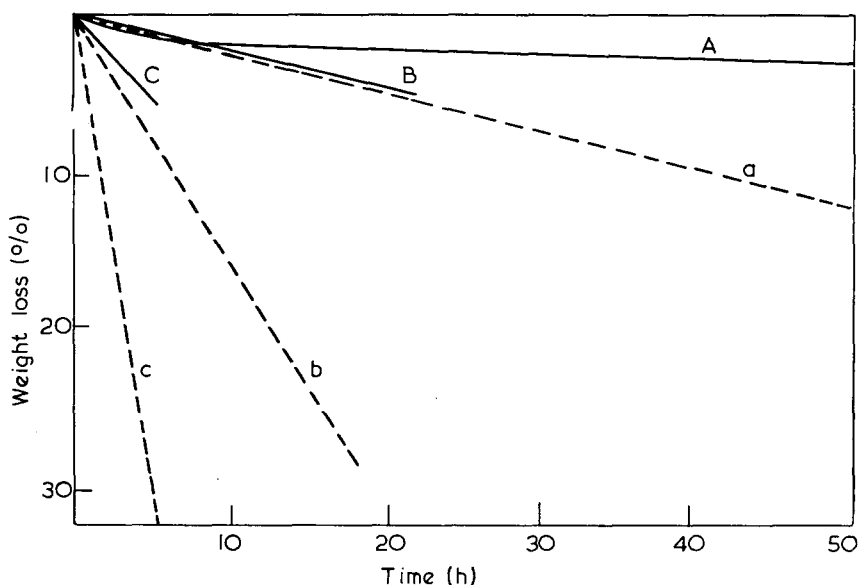


Figure 2 Isothermal weight losses in air of MP1 (---) and polyimide (—). A, a, 300°C; B, b, 343°C; C, c, 375°C

The Arrhenius equation expresses the relation:

$$\log k = \log A - \frac{E}{2.303 RT} \quad (1)$$

where k is the apparent rate constant of degradation, E the apparent activation energy and A the apparent frequency factor. Figure 3 shows a plot of $\log k$ vs. $1/T$ derived from the isothermal data for MPI and polyimide.

Because of the time-consuming nature of isothermal studies, complete analyses of the other macrocyclic polymers were not made by this technique. Instead their thermograms were analysed, to obtain rates of degradation using Doyle's method⁴.

Each point on a thermogram is an expression of the relation between T and k . According to Doyle⁴ k can be expressed as:

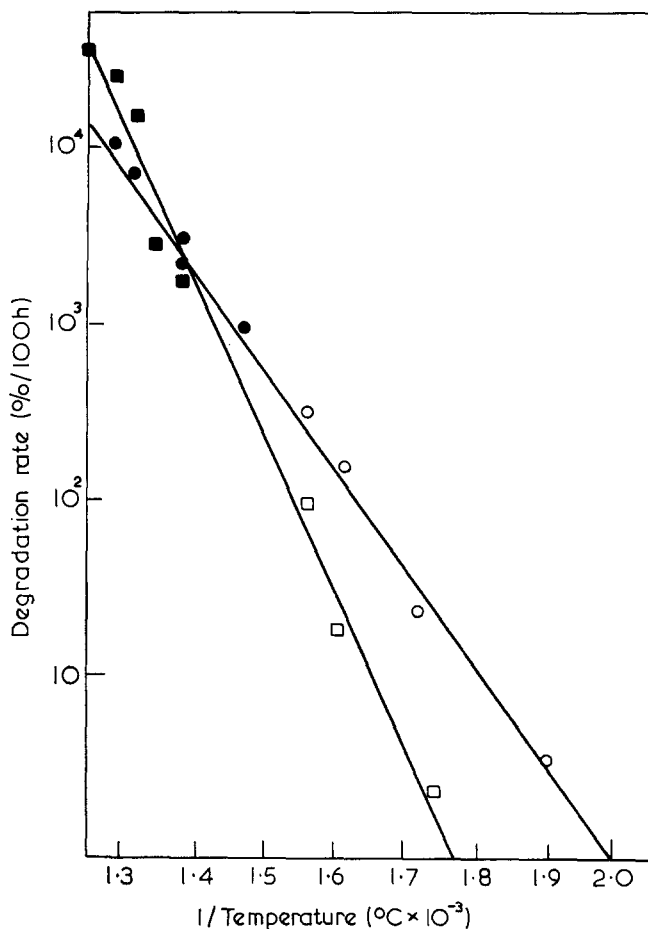


Figure 3 Log k against $1/T$ for MPI and for polyimide. ○ MPI, isothermal data; ● MPI, t.g.a. data; □ polyimide, isothermal data; ■ polyimide, t.g.a. data

Table 1 Degradation data (k) for macrocyclic polymers and polyimide ($\%/100 \text{ h} \times 10^2$)

Macrocyclic polymers (R^*)	673	693	713	733	753	773	793	813	Apparent activation energy (E) (kJ mol^{-1})	Apparent frequency factor (A) (sec^{-1})
4,4'-Diphenylene ether (MP1)	0.42	0.83	1.55	2.1	4.2	5.0	6.6	12.5	108	5.2×10^3
4,4'-Diphenylene methane (MP2)	0.39	0.78	1.42	1.8	2.5	3.1	4.7	6.9	85	4×10
1,3-Phenylene (MP3)	—	—	0.6	1.4	2.6	3.2	3.9	7.4	85	3×10
2,6-Tolyleno (MP4)	—	1.25	1.76	2.1	3.2	3.6	5.0	6.3	57	2.5×10^{-2}
2,4-Tolyleno (MP5)	1.08	1.55	2.24	2.5	3.7	4.1	5.6	5.9	63	5.2×10^{-2}
1,4-Phenylene (MP6)	0.8	1.4	2.3	3.6	5.2	8.7	14	—	107	3×10^3
Polyimide	—	—	0.8	2.0	8.2	16	25	33	142	4×10^5

*For macrocyclic polymers derived from pyromellitic tetranitrile (see Figure 1)

$$k = \frac{B}{f(h)} \left(-\frac{dh}{dt} \right) \quad (2)$$

where B is the heating rate in $^{\circ}\text{C}/\text{min}$ and h is the active weight.

Using equation (2) and the data obtained from the thermograms of MPI and polyimide, values of k at different temperatures were obtained for each polymer. These values, included in *Figure 3*, can be seen to fall upon the same lines as the results from the isothermal studies. From this we conclude that this method has an accuracy comparable with the isothermal technique.

This analysis was also applied to thermograms obtained for other macrocyclic polymers derived from pyromellitic tetranitrile and the diamines listed in *Table 1*. The values of k obtained for different values of T are presented in *Table 1*, and plotted in *Figure 4* as $\log k$ vs. $1/T$. The values of A and E were calculated from *Figures 3* and *4* using the Arrhenius equation.

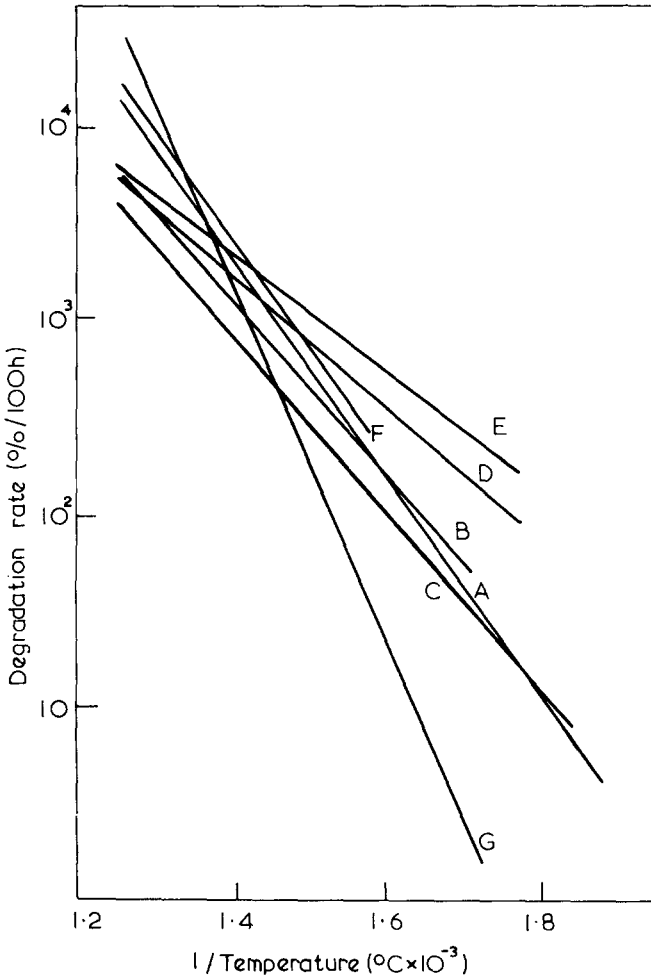


Figure 4 $\log k$ against $1/T$ for macrocyclic polymers and polyimide. A, MPI; B, MP2; C, MP3; D, MP4; E, MP5; F, MP6; G, polyimide (see *Table 1*)

Figure 4 shows that all the macrocyclic polymers lose weight faster than polyimide in air at temperatures below 420°C. All have lower apparent activation energies of degradation than polyimide so that despite the greater stiffness conferred upon them by their ladder structure the net result is a reduction in their thermal stability. The lower apparent activation energies of these polymers may be attributable to the strained macrocycles which form part of the macromolecules.

The apparent activation energy of degradation for polyimide derived from Figure 3 is 1.42×10^2 kJ mol⁻¹. This figure compares closely with values reported elsewhere in the literature for polyimide, e.g. Bruck reports 1.38×10^2 kJ mol⁻¹ for kapton H film⁵ and Kolesnikov 1.42×10^2 kJ mol⁻¹.⁶

MPI has the highest apparent activation of the macrocyclic polymers but in comparison with polyimide (Figure 2) its performance is inferior and not consistent with that required of a thermally stable polymer. In order to confirm this impression and to assess the influence that exposed surface area and the possible presence of unreacted functional groups, e.g. amino groups, might have on isothermal weight loss, studies were made on moulded samples of MPI in air at 300°C (Figure 5). During the course of heating the samples lost weight, also cracked and crazed very badly.

D.t.a. studies of macrocyclic polymers in air suggest the development of degradative exotherms at relatively low temperatures¹. A closer study of this exotherm was made for MPI using a mass spectrometer linked to the d.t.a. apparatus which enabled volatiles produced during the exotherm to be analysed. The volatile species giving the strongest signals were water and

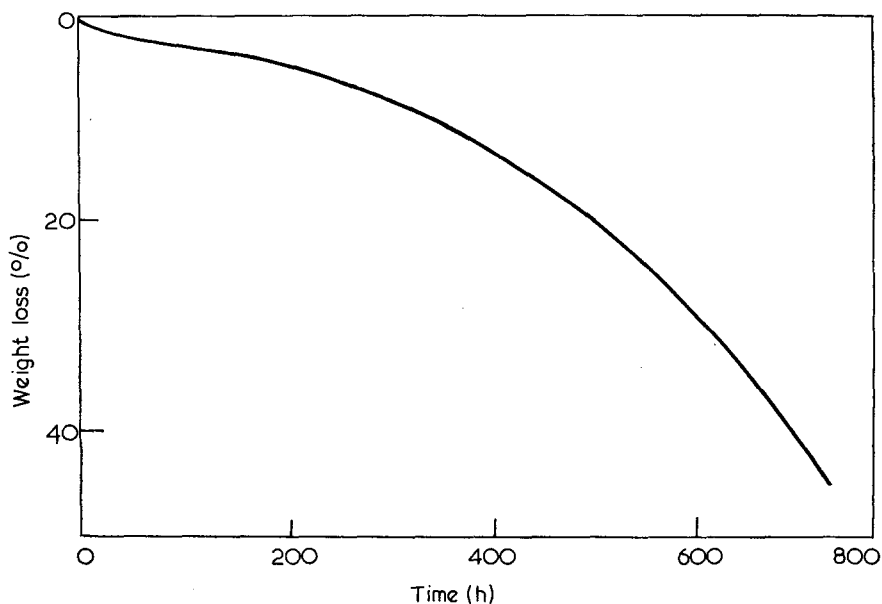


Figure 5 Isothermal weight losses at $300^\circ\text{C} \pm 2^\circ\text{C}$ in air of a moulded sample ($10 \times 5 \times 3$ mm) of MPI

carbon dioxide (m/e 18 and 44 respectively). *Figure 6* shows graphs of their profiles in conjunction with the d.t.a. trace. The small peak in the water trace at about 100°C corresponds precisely to a d.t.a. endotherm. This is due to the evolution of absorbed water, since MPI is hygroscopic¹. Other mass species detected included m/e 30, 58, 78 and 91 but their peak strengths were very weak.

Of especial interest is the absence of m/e ratios attributable to nitrogen-bearing molecules. The ratio m/e 17 to m/e 18 peak heights remained constant over the temperature range 20 – 450°C and hence no ammonia was evolved. Further, no m/e 30 NO^+ was detected and so the possibility that N_2O^+ was formed was discounted and the m/e 44 peak attributed solely to CO_2 . The peak height of m/e 32 O_2 fell during the d.t.a. exotherm from 250°C onwards, and is evidence of oxidation occurring. The level of m/e 28

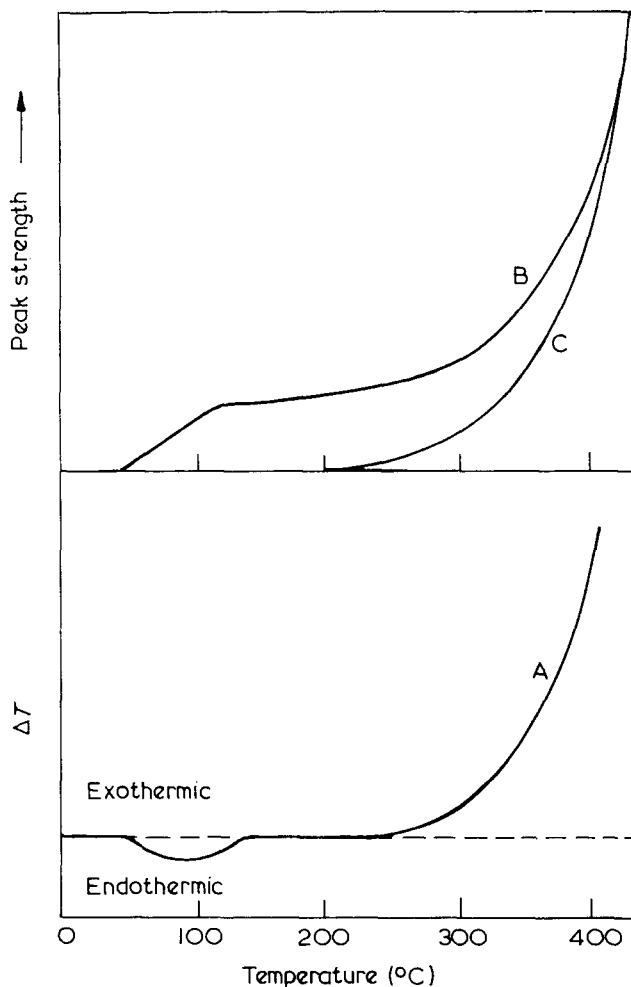


Figure 6 Combined d.t.a., m/e 18 and m/e 44 curves for MPI heated in air. A, d.t.a.; B, m/e 18; C, m/e 44

(N₂) was so high as to make it impossible to detect m/e 27 (HCN) reliably.

A quantitative estimate of the mass spectrometric analyses of m/e water and carbon dioxide was made having first calibrated the d.t.a./m.s. apparatus with CuSO₄·5H₂O as a water source and NaHCO₃ as a source of carbon dioxide (Figure 7).

From Figure 7 it may be seen that the hydrogen is lost from the polymer at a lower temperature than the carbon. Most of the hydrogen in the macrocyclic structure is attached to the diphenyl ether groupings. Kolesnikov⁶ has pointed out that in the thermo-oxidative degradation of a series of polyimides having increasing diphenyl ether content, at least 50% of the observable weight loss can be ascribed to the breakdown of the aryl ether moiety. Thus in the case of macrocyclic polymer it seems reasonable to assume that the oxidative degradation of the diphenyl ether segments occurs in the early stages of the breakdown of the polymer.

Studies of the breakdown products liberated by macrocyclic polymer heated in helium were also made using the coupled d.t.a./m.s. equipment. When the polymer was heated to 500°C in helium the degradation exotherm observed in air did not develop and neither water nor carbon dioxide was detected in significant amounts mass spectrometrically.

However, macrocyclic polymer does degrade when heated in an inert atmosphere as can be judged from Figure 8 which compares the polymer's thermograms in air and in nitrogen. From these it may be seen that about

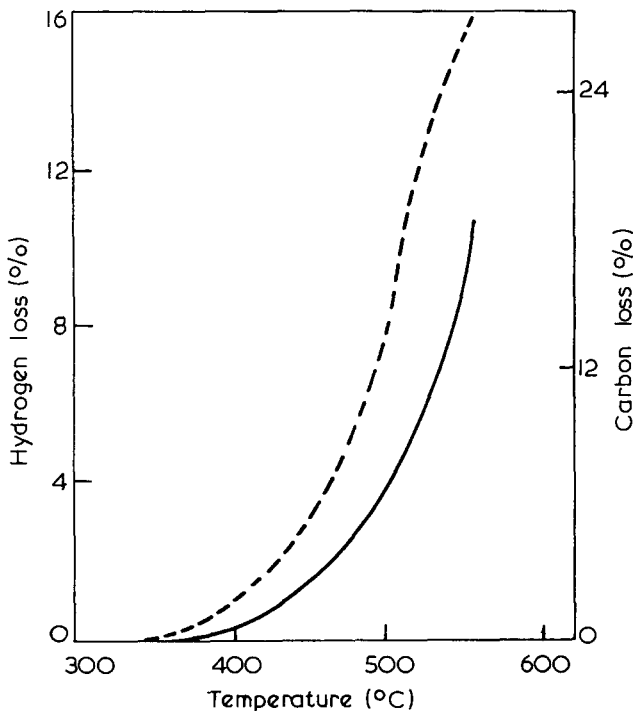


Figure 7 Carbon (—) and hydrogen (----) losses from MPI heated at 10°C/min in air

HETEROCYCLIC POLYMERS (2)

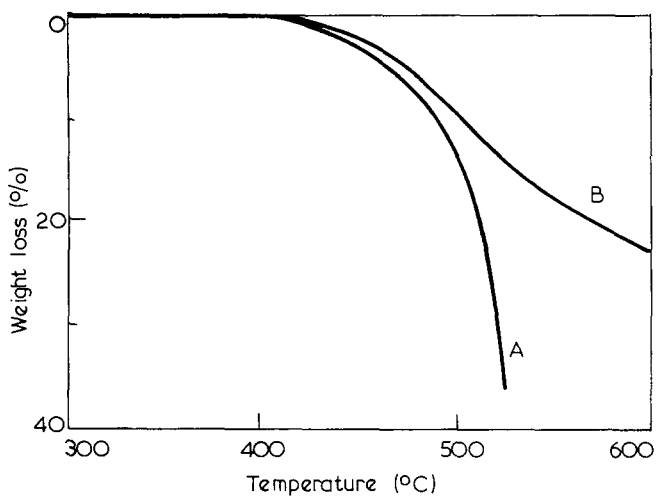


Figure 8 Thermograms of MPI in (A) air and (B) nitrogen

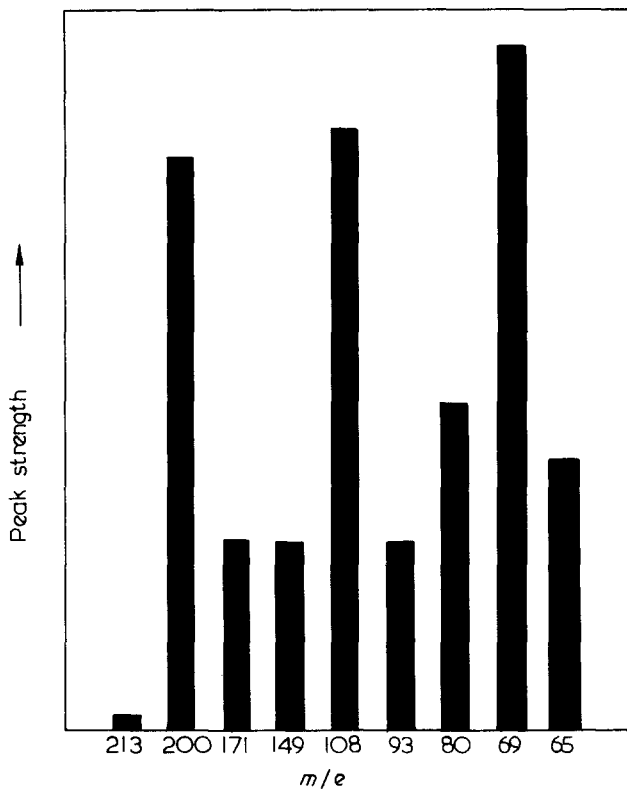



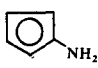
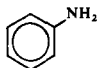
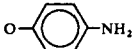
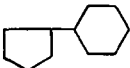
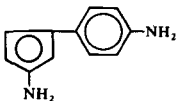
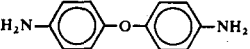
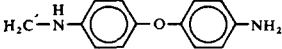


Figure 9 A typical mass distribution obtained by heating MPI at 310°C in MS 902

10% of the polymer's weight is lost below 515°C in either case. Studies made, using the MS 902, of the volatiles produced *in vacuo* in the range 285–315°C are reported in Figure 9 as *m/e* peak values. The majority of these peaks can be related to the 4,4'-diaminodiphenyl ether moiety of the structure (Table 2). From these studies it is concluded that the breakdown of macrocyclic polymer at high temperature in an inert atmosphere liberates the constituent diamine. This may be generated by a completion of the macrocyclization process (Figure 10). Alternatively, Elvidge⁷ has reported the formation of 1,1-dimethylbis(isoindigo) from 1,3-dimethyldiiminoisoindolene (Figure 11), and it is possible that derivatives of aromatic amines and diiminoisoindolene undergo this rearrangement at higher temperatures.

Table 2 Composition of the breakdown products derived by heating MPI *in vacuo* at 310°C

Mass	Formula	Structure
65	C ₅ H ₅	
69	C ₅ H ₉	
78	C ₆ H ₆	
80	C ₅ H ₆ N	
93	C ₆ H ₇ N	
108	C ₆ H ₆ NO	
149	C ₁₁ H ₁₇	
171	C ₁₁ H ₁₁ N ₂	
200	C ₁₂ H ₁₂ N ₂ O	
213	C ₁₃ H ₁₃ N ₂ O	

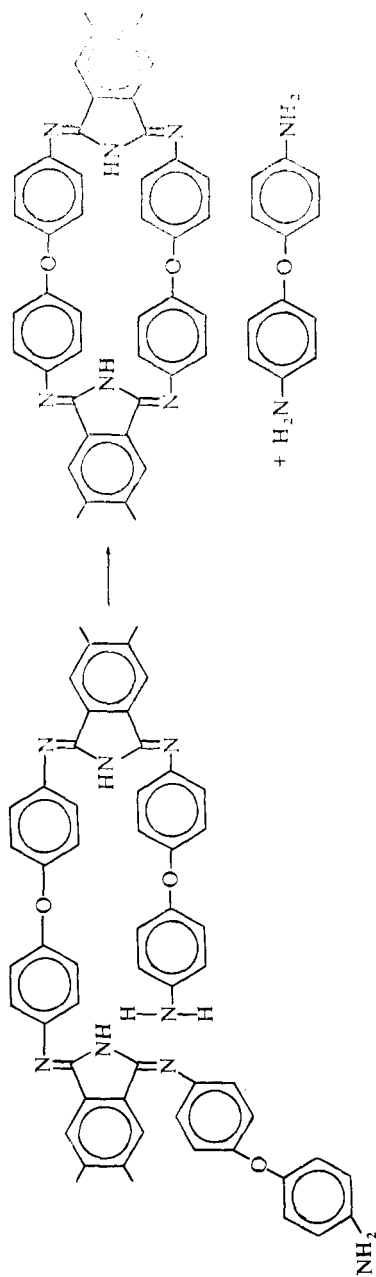


Figure 10 A diamine elimination step

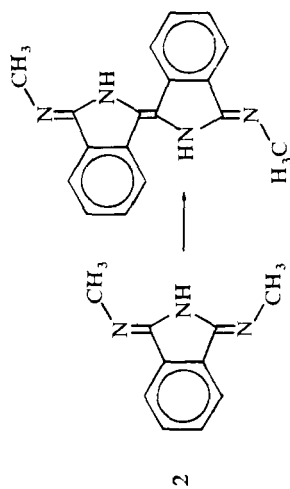


Figure 11 The rearrangement of 1,3-dimethylimidisoindole to 1,1-dimethylbis(isoindigo)

Such a rearrangement involving macrocyclic polymer can be expected to generate a poly(isoindigo) structure (*Figure 12*) in the residue, together with diaminodiphenyl ether.

The changes observed in the i.r. spectrum of MPI when it is heated in air or nitrogen are in agreement with the proposed rearrangement although the spectra exhibit the progressive broadening of absorption bands usually encountered when degrading a polymer. In particular the spectra of polymer heated up to 500°C in air or in nitrogen are closely similar. In each case there is no absorption attributable to carbonyl (1720 cm^{-1}) and the imino absorption ($>C=N-$) at 1640 cm^{-1} weakens as the temperature of degradation is increased.

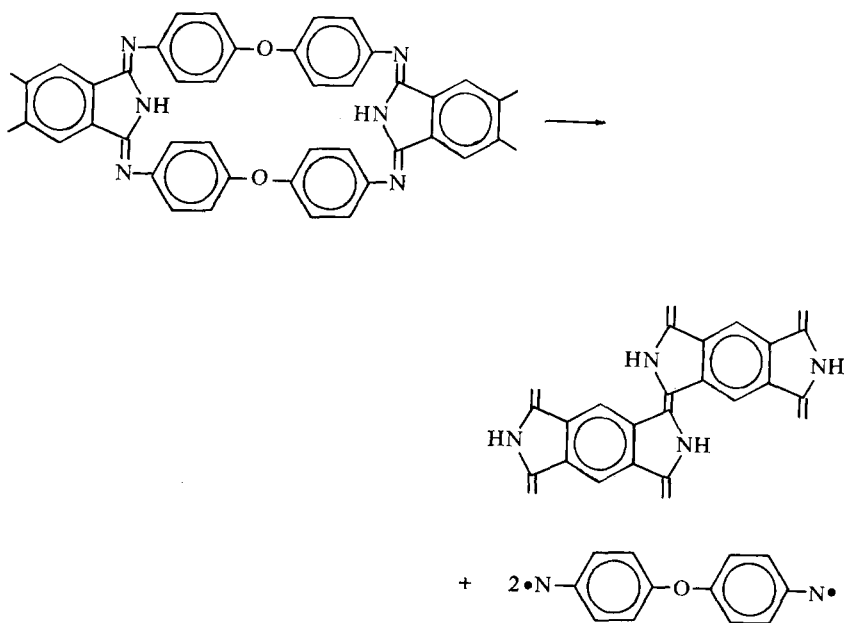


Figure 12 The rearrangement of MPI to an isoindigoid structure

CONCLUSIONS

The thermogravimetric analyses show that macrocyclic polymers degrade faster in air than polyimide at temperatures up to 420°C. The use of d.t./m.s. analysis confirms that macrocyclic polymer undergoes an exothermic breakdown in air at temperatures above 250°C and suggests that in the early stages of this breakdown the diamine component suffers oxidation. When macrocyclic polymer is heated in an inert atmosphere the diamine is liberated which may result in the formation of an 'isoindigoid' structure.

ACKNOWLEDGEMENTS

One of us (R.J.G.) acknowledges with thanks the financial assistance of the NRDC. Our thanks are also due to Dr J. Idris Jones, National Physical Laboratory, Teddington, Middlesex, for supplying a sample of polyimide. We are indebted to AEI Scientific Instruments, Manchester, for the use of their mass spectrometric equipment.

*Department of Polymer Science and Technology,
Brunel University,
Woodlands Avenue, London W3 9BX*

(Received 1 March 1971)

(Revised 7 July 1971)

REFERENCES

- 1 Gaymans, R. J., Hodd, K. A. and Holmes-Walker, W. A. *Polymer, Lond.* 1971, **12**, 400
- 2 Packham, D. I. and Rackley, F. A. *Chem. and Ind.* 1967, p 1254
- 3 Packham, D. I. Davies, J. D. and Paisley, H. M. *Polymer, Lond.* 1969, **10**, 923
- 4 Slade, P. E. and Jenkins, L. T. 'Techniques of Polymer Analysis and Evaluation,' Dekker, London, 1966, Vol 1, p 163
- 5 Bruck, S. D. *Polymer, Lond.* 1964, **5**, 435
- 6 Kolesnikov, G. S. *et al. Soviet Plastics* 1969, pp 38-40
- 7 Elvidge, J. A. and Golden, J. H. *J. Chem. Soc.* 1956, p 4144

Study on crystallization of nylon-6 (polycapramide): Part 1. Isothermal crystallization

E. TURSKA and S. GOGOLEWSKI

The kinetics of primary isothermal crystallization of nylon-6 have been studied dilatometrically over the temperature range 201–213°C. Below 200°C the kinetics were impossible to measure because of the high rate of crystallization from the melt. Investigations were made with polydispersive samples of various origins. The different samples crystallized at different rates in the same temperature conditions. Exponent n in the Avrami equation (except BASF sample) was constant and equal to 4 at temperatures of 210–213°C, and changed below 210°C. It was ascertained for all samples, assuming that $n = 4$, and that the melting point rises with crystallization temperature, that there are linear relations for $\log K$ against both $T_m/T(\Delta T)$ and $T_m^2/T(\Delta T)^2$.

INTRODUCTION

SEVERAL IMPORTANT technological properties of polymers used in manufacturing processes depend to a considerable extent not only on the crystalline phase content but also on the type of morphological forms occurring in polymers during crystallization from the melt. Nylon-6 is such a polymer and many workers have examined crystallization kinetics with a view to determining rate and growth constants at different temperatures, the mechanism of nucleation and growth, and the effect of various factors on the crystallization process. Such investigations have been carried out by various methods; the following are the most common: the dilatometric method of measuring the changes in relative volume¹⁻⁶, the methods of measuring the changes in density taking place during crystallization^{7,8}, the microscope method of measuring the growth rate of spherulite radius and light-depolarization method⁹⁻¹¹.

Most of the published data have been interpreted with the aid of the well-known Avrami equation^{12,13}:

$$\theta = \exp [-Kt^n] \quad (1)$$

where θ is the fraction not yet transformed, K contains the nucleation and growth constants, and n has integral values between 1 and 4 depending on the nature of the nucleation and of the growth processes. The equation, developed for metals, may be used for examining the crystallization of polymers provided that several restrictions are made according to the assumptions which are the basis for the equation.

In the present work results of dilatometric examination of the crystallization kinetics of nylon-6 samples from various manufacturers are given. Experiments were performed to find out whether different origins of samples and consequently differences in amount of residual impurities affect the

kinetic parameters. Investigations were also carried out at temperatures close to the melting point of the polymer, when it was possible to obtain programmed supercooling in the samples. Small quantities of samples (50–100 mg) ensured uniform temperature distribution throughout the samples. Examination of the crystallization from the melt instead of from the glassy state enabled the less-known effect of supercooling of the melt on crystallization mechanism to be avoided.

EXPERIMENTAL

Materials

For the investigations fibre-forming polycapramide samples from the following firms were used: Toyo Rayon (Japan), Du Pont (USA), Steelon (Poland) and BASF (Germany). The samples from Toyo Rayon, Du Pont and BASF were unstabilized; the sample from Steelon was stabilized with acetic acid. The characteristics of the samples, which contained no titanium dioxide, are given in *Table 1*.

Measurements of viscosity were carried out in 98% sulphuric acid at 25°C using solutions of the polymer (0.25 and 0.35 g/100 ml). Intrinsic viscosity, viscosity-average degree of polymerization \bar{P}_v and viscosity-average molecular weight were calculated from the Matthes equations¹⁴. The ratio \bar{M}_w/\bar{M}_n was calculated from the gel permeation chromatography data provided by Waters Associates, Inc., Framingham, Mass., USA.

Table 1 Materials used for the experiments

<i>Manufacturers</i>	$[\eta]$	\bar{P}_v	\bar{M}_v	$\frac{\bar{M}_w}{\bar{M}_n}$ (g.p.c.)	T_m (°C)
Steelon	1.10	242	27 400	1.64	220
BASF	1.14	258	29 200	1.52	223
Toyo Rayon	1.16	264	29 800	1.48	221
Du Pont	1.30	306	35 000	1.76	225

Examination of thermal degradation

Unextracted samples were put into glass ampoules and dried at 100°C in a vacuum of 10^{-6} mmHg (1 mmHg \equiv 133.3 N/m²) and then annealed at 160°C for periods from 1 to 7 h.

To determine the resistance of samples to the action of various media used for treatment and crystallization, melting was carried out in sealed ampoules under vacuum, nitrogen and silicone oil. The samples were melted for 30 min at 261°C. The results of annealing and melting on \bar{P}_v , under various conditions, are shown in *Figure 1*. The values of \bar{P}_v for all samples after all crystallization runs have also been determined, in order to find whether

maintaining the samples at temperatures above 200°C under mercury for prolonged periods had any effect on molecular weight. The results are presented in *Figure 1* as the mercury points.

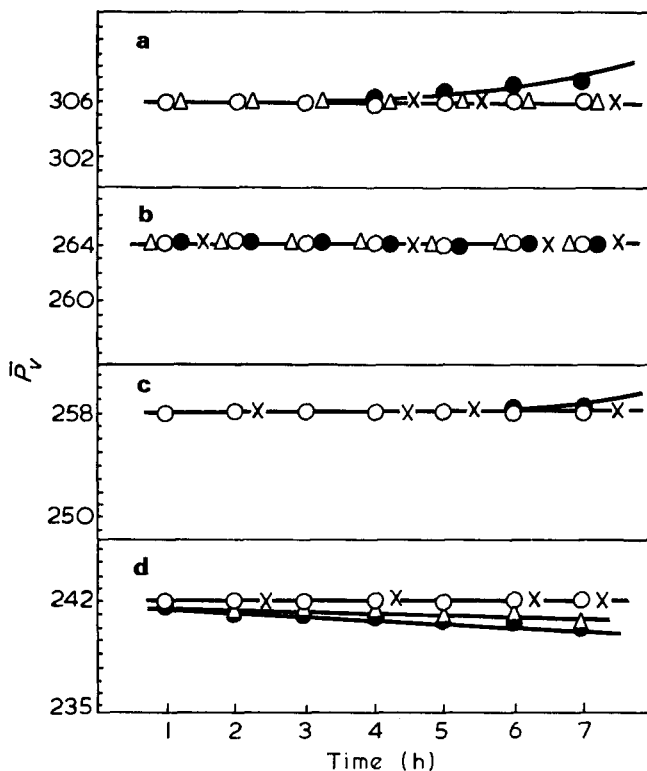


Figure 1 Effect of thermal exposure on viscosity-average degree of polymerization for samples listed in *Table I*. (a) Du Pont, (b) Toyo Rayon, (c) BASF, (d) Steelon. ●, nitrogen; ○, silicone oil; △, vacuum; ×, mercury

Crystallization conditions

For kinetic investigations samples of cylindrical shape having no empty spaces were used; they were formed by extruding melted polymer under vacuum. The samples were put into a dilatometer of special construction^{15,16} with precision bore measuring capillary of 0.50 mm diameter. For control purposes the measurements were carried out in two dilatometers simultaneously in thermostats containing silicone oil DC-F-6-7024, maintaining a constant temperature within $\pm 0.02^\circ\text{C}$. The construction of the thermostats allowed the process of crystallization to be observed in dilatometers immersed fully under the surface of silicone oil. Further details regarding the sample extruding, filling the dilatometers and construction of thermostats have been given previously¹⁶.

Choice of temperature and duration of melting and temperature of crystallization

To select the temperature and time for melting the samples before crystallization, the data of Magill¹⁰ were used. Magill has found that after having melted nylon-6 at 260°C or above for 30 min, the 'melting' is substantially completed. Below 260°C there is definite dependence of the nucleation rate on melt conditions. These results have been confirmed in this work and therefore, all the samples were melted at 261°C for 30 min. Crystallization temperatures of 201, 204, 206, 210 and 213°C were chosen, the range being slightly below the melting point of polymer and that allowed to carry out the dilatometric measurements under conditions of programmed supercooling. At temperatures lower than 200°C, crystallization of samples begin before they are cooled to the proper temperature. These observations are in agreement with the results of Inoue⁴.

Calculation of the kinetic data

The Avrami equation for the dilatometric measurements may be represented as⁴:

$$\frac{h_t - h_\infty}{h_0 - h_\infty} = \exp [-Kt^n] \quad (2)$$

where h_t represents the mercury height at time t , h_0 the height during the induction period and h_∞ the height after the isotherm has levelled off. The parameter n was calculated from the differentiated form of equation (2), according to the method proposed by Hay¹⁷. Values for the constant K were determined from values of half-times of crystallization ($t_{1/2}$) both for variables n found experimentally and for constant $n = 4$:

$$K = \frac{\ln 2}{t_{1/2}^n} \quad (3)$$

RESULTS

Examination of the thermal degradation

The results of examining the effect of thermal treatment on viscosity-average degree of polymerization \bar{P}_v are given in *Figure 1*. No polymer was found to anneal and melt under silicone oil nor did mercury change its molecular weight.

The sample of Toyc Rayon did not undergo any changes under the conditions studied. The polymer of BASF showed a slight increase in \bar{P}_v , on annealing under nitrogen. The polymer of Du Pont like that of BASF showed an increase in \bar{P}_v which is in agreement with the data of Valko and Chiklis¹⁸. The polymer of Steelon was degraded under nitrogen and vacuum. The reason for the different behaviour of samples annealed under the same conditions of temperature seems to be in differences in quantity and type of impurities.

Isothermal crystallization

The exemplary relationship between $\theta = h_t - h_\infty / h_0 - h_\infty$ and $\log t$ is illustrated in *Figure 2*, for the Toyo Rayon sample.

The relationship between $\log(-\log \theta)$ and $\log t$ for these samples is illustrated in *Figure 3*.

The effect of temperature on the crystallization rate is shown in *Figures 4 and 5*.

The relationship between exponent n and temperature of crystallization for various samples is given in *Figure 6*.

Temperature dependence of rate for all samples is shown in *Figures 7-10*.

The relationship between the crystallization temperature and calculated melting points is illustrated by small diagrams within *Figures 7-10*.

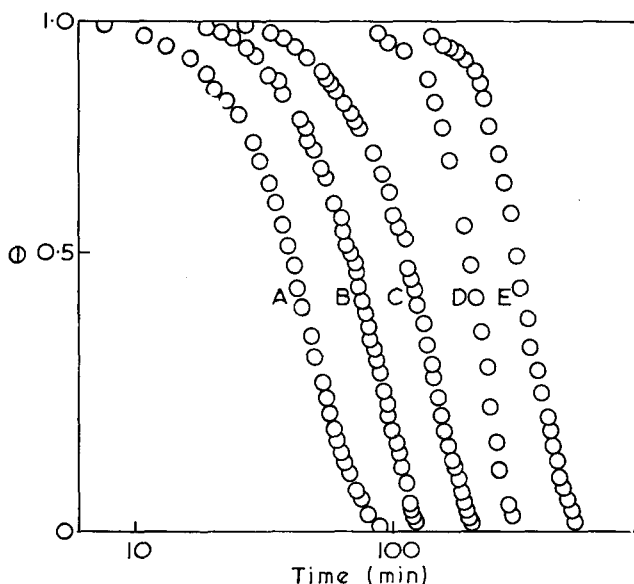


Figure 2 Crystallization isotherms of θ vs. $\log(\text{time})$ at various crystallization temperatures for Toyo Rayon sample: A, 201°C; B, 204°C; C, 206°C; D, 210°C; E, 213°C

DISCUSSION

Rate of crystallization

It is clear from calculated values of constant K and half-times of crystallization for various samples at different temperatures that, within the range of temperatures close to the melting point of polymer, the crystallization rate increases with decrease of temperature. The order of magnitude of the constant K is slightly different from the data of Inoue⁴ and Rybníkář¹⁹ for the crystallization of polycapramide under similar conditions of supercooling. The differences may result from the differences in procedure of

CRYSTALLIZATION OF NYLON-6 (1)

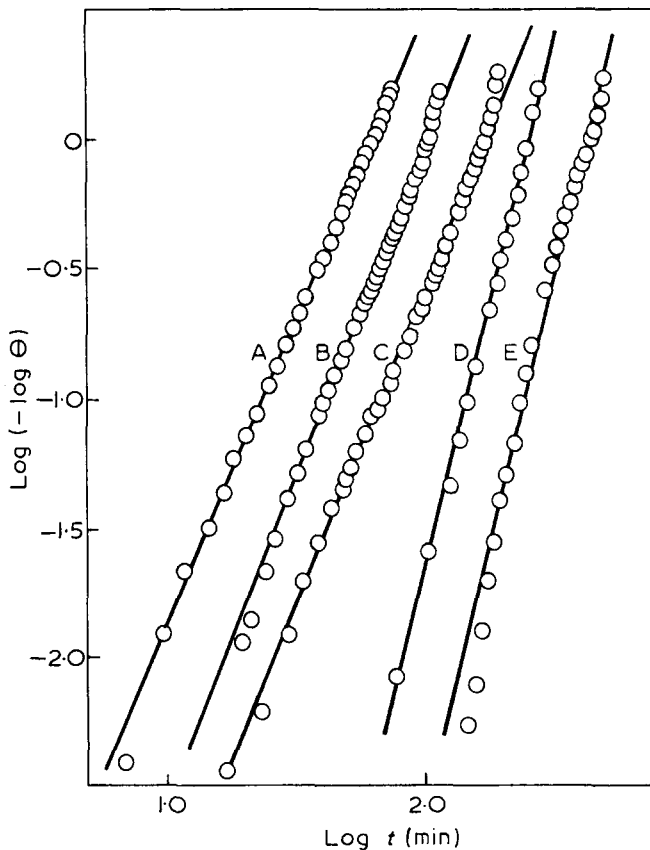


Figure 3 Dependence of $\log(-\log \theta)$ vs. $\log(\text{time})$ at various crystallization temperatures for Toyo Rayon sample. A, 201°C; B, 204°C; C, 206°C; D, 210°C; E, 213°C.

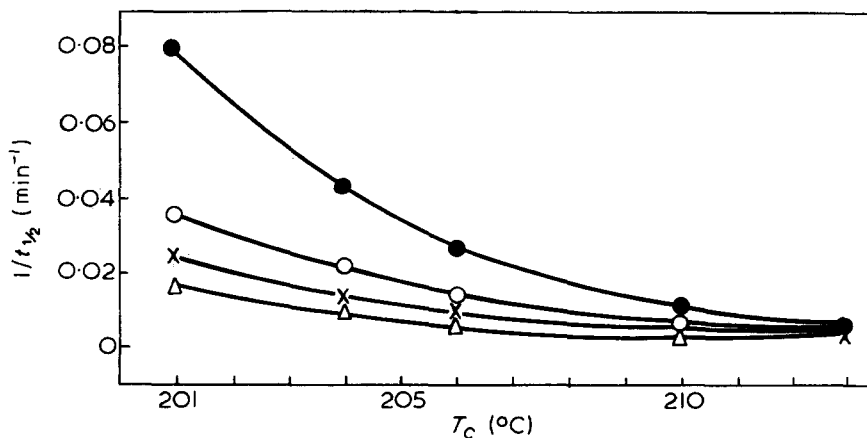


Figure 4 Half-times of crystallization vs. temperature for samples of nylon-6 from different sources: ●, Steelon; ○, BASF; ×, Toyo Rayon; △, Du Pont

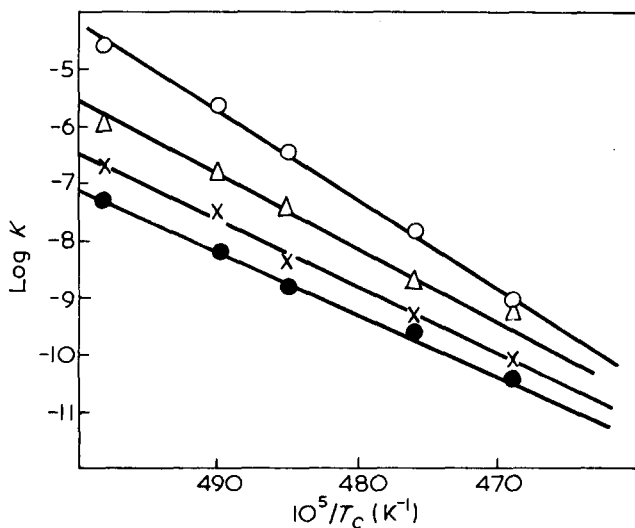


Figure 5 Arrhenius plots for nylon-6 using rate constants as a function of temperature: ○, Steelon; △, BASF; ●, Du Pont; ×, Toyo Rayon

thermal treatment before melting, temperature and duration of melting as well as from differences in the values of molecular weight of samples. Comparison of the results obtained by us with the data of other authors was not possible because they used a different method for kinetic measurements^{9,10}.

It is seen from *Figures 4* and *5* that the crystallization rate of the samples examined under the same conditions of supercooling is highest in the case of Steelon polymer and is decreasing successively for samples of BASF, Toyo Rayon and Du Pont. The differences in rate may be due to differences in molecular weight and polydispersity of samples and to differences in the preparation method. Such a possibility has been pointed out by Sheldon²⁰ and McLaren²¹ in the case of poly(ethylene terephthalate) and nylon-6,6.

The differences in rate may then result from type and concentration of industrial impurities left in the sample during the production process, from their melting point, size, molecular weight, resistance to the action of heat at the temperature of melting before crystallization, etc. Ability of rejection of impurities into intercrystalline spaces by the growing crystallization fronts may also affect the crystallization rate²².

Mechanism of crystallization

It can be seen from the values of the exponent n that the mechanism of nucleation and growth of crystals in polycapramide samples under investigation depends on temperature which is shown by different values of n for various crystallization temperatures.

It was found that there is an interval of temperature which demarcates two different nucleation mechanisms. That interval includes temperatures

CRYSTALLIZATION OF NYLON-6 (1)

from 209°C to 210°C. At temperatures lower than the limiting one, including the range 201–209°C, variable values of 2.3–3 were obtained which corresponds to three-dimensional growth and heterogeneous or instantaneous nucleation.

At temperatures of 210–213°C, these being higher than the limiting ones, constant values of $n = 4$ were obtained, which corresponds to three-dimensional growth from sporadic nuclei. An exception is the sample of BASF, for which $n = 3$ at 210°C, the growth being three-dimensional from instantaneous nuclei.

The reason for different behaviour in the BASF sample under identical conditions of crystallization may be the result of differences in the type of

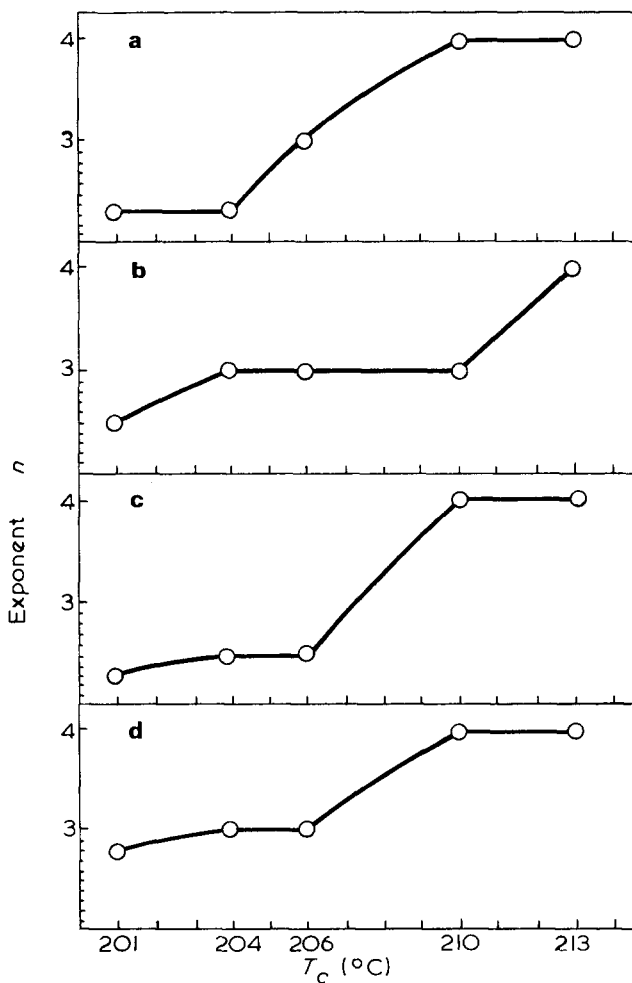


Figure 6 Dependence of Avrami exponent n vs. crystallization temperatures for various samples. (a) Steelon, (b) BASF, (c) Toyo Rayon, (d) Du Pont

impurities in the samples being used. These impurities probably cause lowering of the extent of supercooling with simultaneous rise of the melting temperature of the polymer connected with an increase in volume of 'crystalline' region and more perfect configuration of crystalline forms of higher resistance to the melting conditions^{23,24}.

The obtained values of exponent n for samples of Steelon, Toyo Rayon and Du Pont are in agreement with the data of Inoue⁴ who has obtained similar values for n , and has observed the occurrence of limiting temperature of changes in the nucleation mechanism from sporadic to instantaneous one, in polycapramide of Toyo Rayon crystallized from the melt. On the other hand, the results are different from those of Rybníkář¹⁹ who has obtained constant $n = 4$ at crystallization temperatures of 194 to 214°C.

Different values of exponent n given in the literature for the chemically identical polymer may be due to differences in thermal treatment of samples and inaccuracy of the measurement methods used.

Differences in the n values, particularly in the case of measurements of crystallization kinetics from the glassy state^{10,11} may result from a less-known effect of freezing of the melt on crystallization mechanism which is revealed by generation of internal stress, nuclei and ordered regions²⁵.

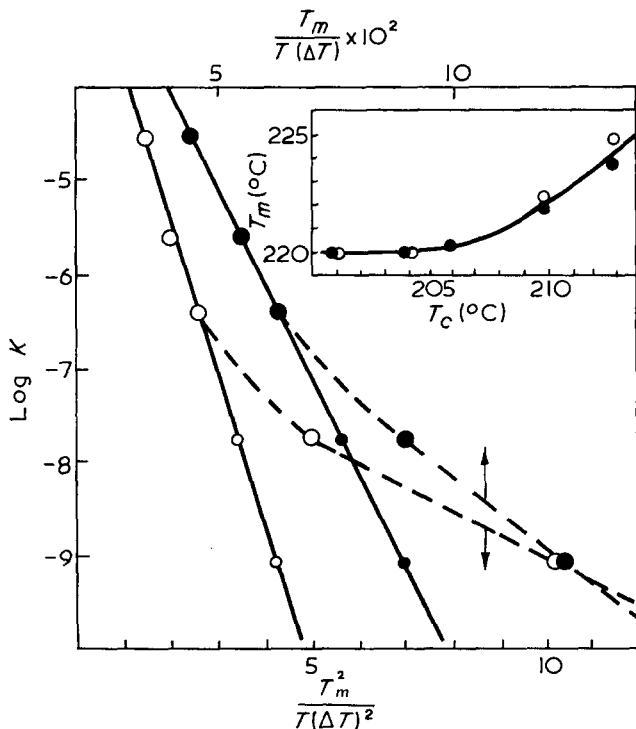


Figure 7 Temperature dependence of rate constant K for Steelon sample

CRYSTALLIZATION OF NYLON-6 (1)

Fractional values of exponent n obtained at 201–206°C may be a result of either simultaneous or successive crystallization processes each of which has a different mechanism²⁶, simultaneous formation of crystals from sporadic and heterogeneous nuclei²⁶ or superimposition of effects of primary and secondary crystallization³.

Temperature dependence of rate

According to the theoretical assumptions²⁷ the relations between the crystallization rate and temperature shown in *Figures 7–10* should have a linear course. For the crystal growth from secondary two-dimensional nuclei, the dependence of $\log K$ on $T_m/T(\Delta T)$ should be a straight line. Accordingly, for the growth from secondary three-dimensional nuclei the dependence of $\log K$ on $T_m^2/T(\Delta T)^2$ should be linear in character. However, in all the cases at $n = 4$ and at constant T_m , the straight lines obtained have characteristic bends (dotted lines). This is due to the fact that the value of melting temperature accepted for calculation does not correspond to the value of equilibrium melting point T_m^0 . The bends may also be a reflection of changes

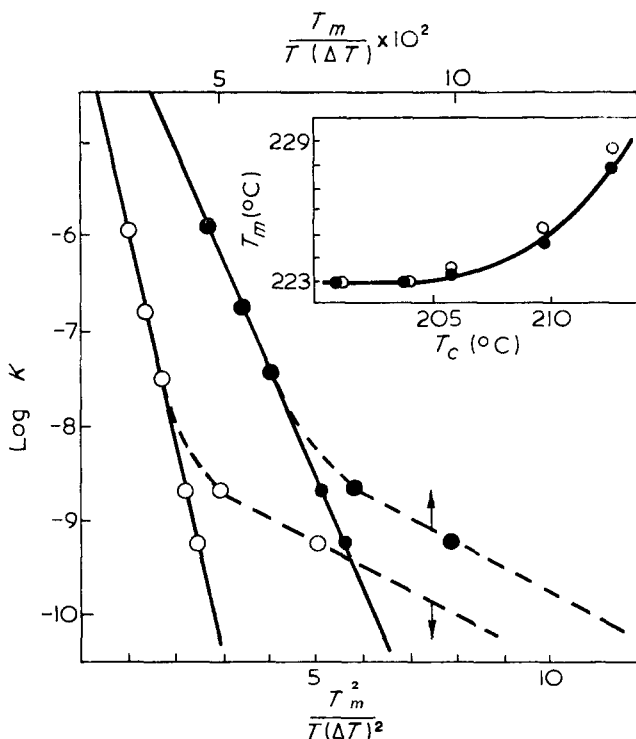


Figure 8 Temperature dependence of rate constant K for BASF sample

in the surface free energies involved in forming the critical secondary nuclei of two different forms of crystals with different densities²⁸. The calculated values of melting point necessary to obtain a linear shape of the above-mentioned relations within the whole range of investigated crystallization temperatures, illustrated by the plots of dependence between T_m and T_c , increases with crystallization temperature. The increment is particularly clear within the range of temperatures at which was observed change of crystallization mechanism from instantaneous to sporadic.

Similar phenomena have been found for polycapramide⁴, polypropylene and polycarbonates²⁹, polypropylene and polybutene²⁸ and for poly(decamethylene terephthalate)³⁰.

ACKNOWLEDGEMENTS

The authors wish to thank Dr S. Wakano of the Plastics Laboratory, Toyo Rayon Co., Ltd, Japan; Mr L. G. Seebach of Plastics Department, Du Pont de

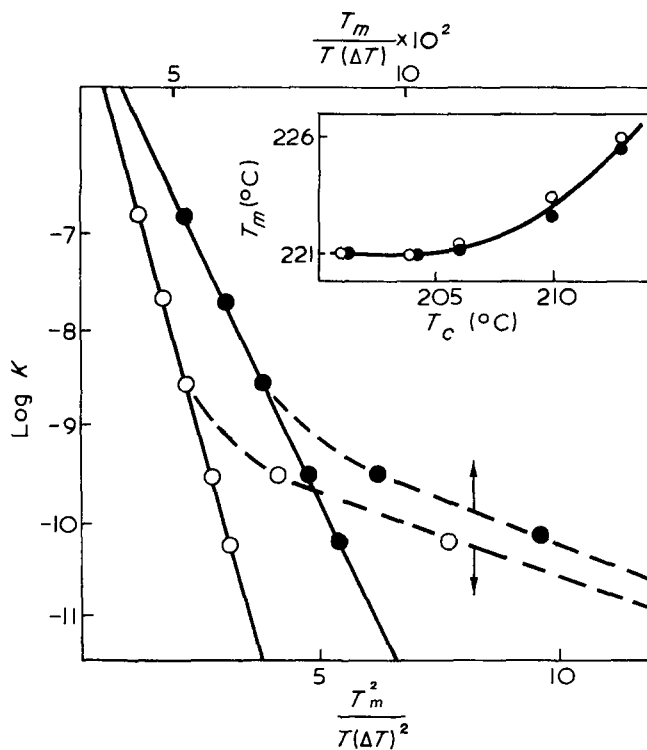


Figure 9 Temperature dependence of rate constant K for Toyo Rayon sample

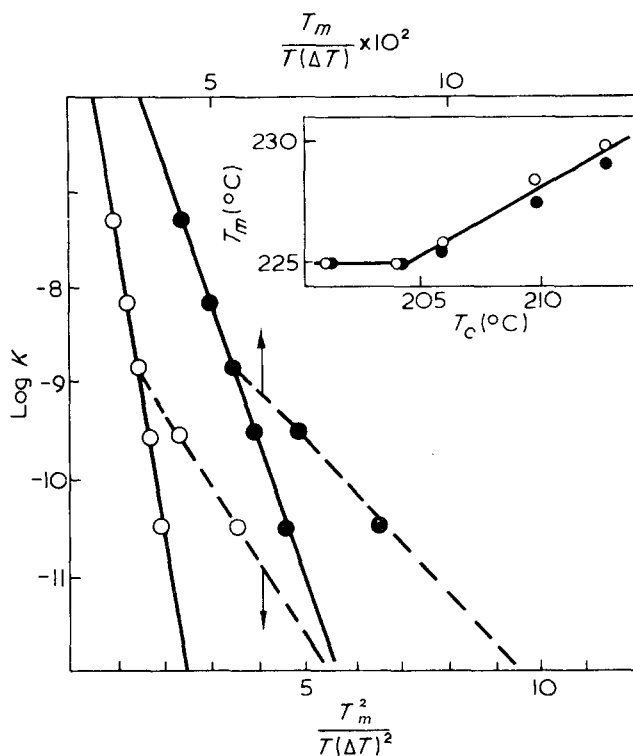


Figure 10 Temperature dependence of rate constant K for Du Pont sample

Nemours & Co., USA, and H. F. Peglar of ICI Fibres Ltd, UK, who kindly supplied us with the samples of polycapamide used in this work. The authors are grateful to Mr B. A. Denenberg from Waters Associates Inc., Switzerland and Mr K. H. Duellke from Waters Messtechnik G.m.b.H.-DBR, for g.p.c. analysis of polycapamide samples and the permission to use these results for publication.

Technical University of Łódź,
Dept of Physical Chemistry of Polymers,
Łódź 40, Poland

E. Turcka

Institute of Polymers,
Ministry of High Education and Polish Academy of Sciences,
Dept of Physical Chemistry of Polymers,
Łódź 40, Poland

S. Gogolewski

(Received 10 June 1970)
(Revised 18 January 1971)

REFERENCES

- 1 Kanamaru, K., Uematsu, I. and Fakuda, K. *Chem. High Polymers (Japan)* 1950, **7**, 1
- 2 Čefelin, P., Chmelir, M. and Wichterle, O. *Coll. Czech. Chem. Comm.* 1960, **25**, 1267
- 3 Inoue, M., and Takayanagi, T. *J. Polym. Sci.* 1960, **47**, 498
- 4 Inoue, M. *J. Polym. Sci.* 1961, **55**, 753
- 5 Rybníkář, F. *Chem. průmysl* 1961, **11** (36), 157
- 6 Tomka, J., Šebenda, J. and Wichterle, O. *J. Polym. Sci. (C)* 1966, **16**, 53
- 7 Rybníkář, F. *Chem. průmysl* 1961, **11** (36), 217
- 8 Ueda, N. and Nukushina, Y. *Chem. High Polymers (Japan)* 1966, **23**, 769
- 9 Burnett, B. B. and McDevit, W. F. *J. Appl. Phys.* 1957, **88**, 1101
- 10 Magill, J. H. *Polymer, Lond.* 1962, **3**, 43, 655; 1965, **6**, 367
- 11 Ishibashi, T., Tani, Y. Yoshizaki, O. and Nagai, E. *Chem. High Polymers (Japan)* 1966, **23**, 177, 205, 208
- 12 Avrami, M. *J. Chem. Phys.* 1939, **7**, 1103; 1940, **8**, 212; 1941, **9**, 177
- 13 Evans, U. R. *Trans. Faraday Soc.* 1945, **41**, 365
- 14 Matthes, A. *J. prakt. Chem.* 1943, **162**, 245; *Makromol. Chem.* 1950, **5**, 165
- 15 Gordon, M. and Hillier, I. H. *Trans. Faraday Soc.* 1964, **60**, 763 and personal communication
- 16 Gogolewski, S. *Polimery* 1971, **16**, 130
- 17 Hay J. N., *J. Polym. Sci. (A)* 1965, **3**, 433
- 18 Valko, E. I. and Chiklis, Ch. K. *J. Appl. Polym. Sci.* 1965, **9**, 2855
- 19 Rybníkář, F. *Coll. Czech. Chem. Comm.* 1961, **26**, 106
- 20 Sheldon, R. P. *Polymer, Lond.* 1963, **4**, 213
- 21 McLaren, J. V. *Polymer, Lond.* 1963, **4**, 175
- 22 Keith, H. D., Padden, F. J. Jr *J. Appl. Phys.* 1963, **34**, 2409; 1964, **35**, 1270
- 23 Beck, H. N. and Ledbetter, H. D. *J. Appl. Polym. Sci.* 1965, **9**, 2131
- 24 Beck, H. N. *J. Polym. Sci. (A-2)*, 1966, **4**, 631
- 25 Ziabicki, A. in 'Poliamidy', PWT, Warszawa, 1964
- 26 Banks, W. and Sharples, A. *Makromol. Chem.* 1965, **59**, 233
- 27 Mandelkern, L. 'Crystallization of Polymers', McGraw-Hill, New York, 1964
- 28 Gordon, M. and Hillier, I. H. *Polymer, Lond.* 1965, **6**, 213
- 29 von Falkai, B. and Rellensman, W. *Makromol. Chem.* 1965, **88**, 38
- 30 Sharples, A. and Swinton, F. L. *Polymer, Lond.* 1963, **4**, 119

Study on crystallization of nylon-6 (polycapramide): Part 2. Effect of molecular weight on isothermal crystallization kinetics

E. TURSKA and S. GOGOLEWSKI

Further studies of the kinetics of primary isothermal crystallization of fractions of nylon-6 with viscosity-average molecular weights ranging from 17 000 to 49 000 are reported. The results were analysed in terms of the Avrami equation to give rate constants and the mechanism of crystallization. In accordance with theoretical assumptions the crystallization rate decreased as molecular weight and temperature increased within the investigated range of molecular weight and crystallization temperature. The relation between the logarithm of half-time of crystallization and the molecular weight is linear. The Avrami exponent n depends on the crystallization temperature and molecular weight of the fractions. Above 210°C the Avrami exponent n was constant and equal to 4–6 for various fractions, corresponding to spherical and sheaf-like growth from sporadic nucleation. Below 210°C, n was equal to 2.8–5, corresponding to spherical and sheaf-like growth from pre-determined nuclei. It has been found that the Avrami exponent n depends on the molecular weight starting from the limiting value of 32 500. For fractions with a lower molecular weight, the exponent n was not dependent on that parameter. Above that value exponent n decreased as the molecular weight increased for all crystallization temperatures. For all samples, assuming $n = 4$ and rise of crystallization temperature is accompanied by rise of melting temperature, linear relations for $\log K$ against $T_m/T(\Delta T)$ and $T_m^2/T(\Delta T)^2$ were obtained.

INTRODUCTION

DURING RECENT years much attention has been paid to the problem of crystalline region formation in polymers and to the effect of various factors on the crystallization processes. Many of the published papers are concerned with investigations of the isothermal crystallization kinetics of polymers including also polyamides. Results obtained are interpreted with the aid of the Avrami equation^{1,2}:

$$\theta = \exp [- Kt^n] \quad (1)$$

where θ is the fraction not yet transformed, K contains nucleation and growth constants, and n has integral values between 1 and 4 depending on the nature of the nucleation and the growth processes.

One of the important factors affecting the crystallization process of polymers is their molecular weight. Only a few reports have dealt with this in detail. The more important of these are on polyethylene³⁻⁷, poly(ethylene adipate)⁸⁻¹⁰, poly(tetramethyl-*p*-silphenylene)siloxane¹¹, poly(ethylene terephthalate) and polycarbonates¹². Some authors have discussed the effect of

molecular weight on the crystallization kinetics of polyamides^{13-19,31}. However, except for the work of McLaren¹⁶ on nylon-6,6, the data in these papers are only fragmentary. There is also a lack of data in the literature on the crystallization kinetics of fractionated samples of polyamides, although it is known that both the polydispersity and the nature of molecular weight distribution have an effect on the course of crystallization.

The aim of the present work was to verify the application of the Avrami equation for fractions of nylon-6 of varying molecular weight, and to determine the relation between molecular weight and the parameters K and n in this equation. The melting time and temperature and crystallization temperature of samples were so selected as to eliminate the effect of 'thermal history' on the crystallization process and to make possible measurements under conditions of programmed supercooling. The use of the dilatometric method allowed a high reproducibility of the results to be obtained.

EXPERIMENTAL

Materials

Nylon-6 (without titanium dioxide) from Toyo Rayon was used for fractionation; it was obtained by hydrolytic polycondensation of caprolactam. As found out previously²⁰, the polymer has the highest resistance to the thermal treatment used. The fractionation was carried out by the method of distribution between two liquid phases^{21,22} in the system phenol-tetrachloroethane as solvent and *n*-heptane as non-solvent.

From sixteen fractions obtained by this method, five were selected with viscosity-average molecular weights of 17 000, 23 000, 32 500, 37 000 and 49 000. Characteristics of the original polymer and selected fractions used for kinetic measurements of crystallization are given in *Table 1*.

Table 1 Characteristics of samples used for investigations

Viscosity-average molecular weight	$[\eta]$	\bar{P}_v	\bar{M}_v	$\frac{\bar{M}_w}{\bar{M}_n}$	$T_m(^{\circ}\text{C})$
17 000	0.80	151	17 070	1.35	220
23 000	0.98	203	22 980	1.33	221
32 500	1.23	288	32 585	1.30	222
37 000	1.34	326	36 815	1.30	222
49 000	1.62	432	48 850	1.31	225
Whole polymer	1.16	264	29 800	1.48	221

Viscosity measurements were carried out in 98% sulphuric acid at 25°C using polymer solutions containing 0.25 and 0.35 g/100 ml. Intrinsic viscosity, viscosity-average degree of polymerization \bar{P}_v , and viscosity-average molecular weight \bar{M}_v were calculated from the Matthes equations²³, and the ratio \bar{M}_w/\bar{M}_n from the gel permeation chromatography data.

The obtained fractions were extracted with water, dried to constant weight

and dissolved in 85% formic acid. From this solution the films were obtained at 25°C. It was found that the above procedure did not cause any degradation of the samples.

Thermal degradation

The fractions were annealed at 160°C under a vacuum of 10^{-6} mm Hg (1 mmHg \equiv 133.3 N/m²) for periods from 1 to 7 h, then mercury or silicone oil was distilled in and the samples were melted for 30 min at 261°C.

Crystallization conditions

Kinetic measurements were carried out in dilatometers containing about 70 mg of the polymer. The diameter of precision bore capillary tubing was 0.48 mm. The dilatometers were placed in thermostats maintaining constant temperature to within $\pm 0.02^\circ\text{C}$. More details on the sample moulding, construction of the dilatometers and thermostats have been given previously²⁴.

Melting conditions and crystallization temperatures

The fractions were melted at 261°C for 30 min. These conditions, as stated previously for the case of polydisperse samples²⁰, destroy 'the crystalline memory'. The crystallization was carried out isothermally at 201, 205, 206, 207, 209, 210 and 213°C. At temperatures below 200°C, the crystallization occurred before reaching the state of programmed supercooling.

Constant in the Avrami equation

The Avrami equation is commonly used for interpretation of the crystallization isotherms. For dilatometric measurements⁴:

$$\frac{h_t - h_\infty}{h_0 - h_\infty} = \exp[-Kt^n] \quad (2)$$

where h_t represents the mercury height at time t , h_0 the height during the induction period and h_∞ the height after the isotherm has levelled off. The exponent n was calculated from equation (2) after differentiation against n :

$$n = \frac{-t dh_t/dt}{(h_t - h_\infty) \ln(h_0 - h_\infty)/(h_t - h_\infty)} \quad (3)$$

The values of constant K were calculated from values of half-time of crystallization for variable n obtained from measurements and for constant $n = 4$.

$$K = \frac{\ln 2}{t_{\frac{1}{2}}^n} \quad (4)$$

RESULTS

Thermal degradation

The annealed and melted samples treated under the conditions described

and the samples taken from the dilatometers after the crystallization run did not show any change in molecular weight.

Isothermal crystallization

Dilatometric measurements provided data for calculating the values of $\theta = h_t - h_\infty / h_0 - h_\infty$ needed to draw plots of θ against $\log t$ and $\log(-\log \theta)$ against $\log t$. Examples of typical crystallization isotherms for fractions $\bar{M}_v = 23\ 000$ and $37\ 000$ are shown in *Figures 1-4*. Calculated values of

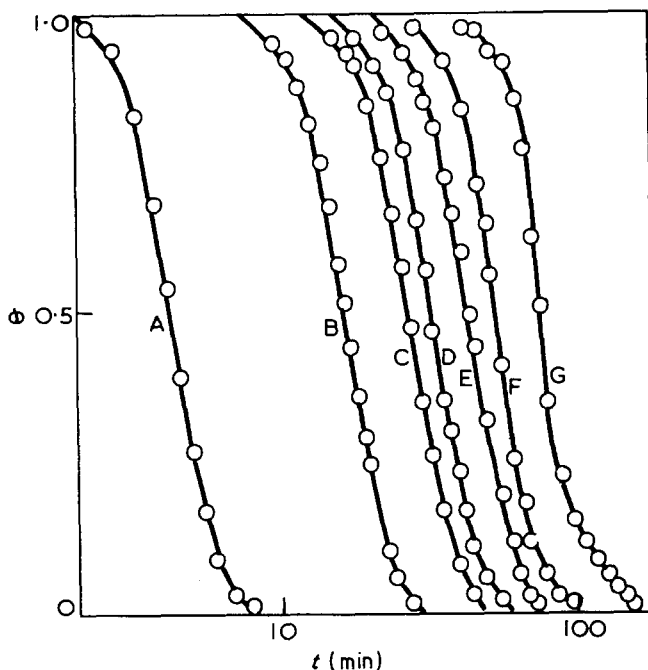


Figure 1 Crystallization isotherms of θ vs. $\log(\text{time})$ at various temperatures for the 23 000 fraction: A, 201°C; B, 205°C; C, 206°C; D, 207°C; E, 209°C; F, 210°C; G, 213°C

kinetic parameters for all the samples are given in *Table 2*.

The effect of temperature on the crystallization rate is illustrated in *Figure 5* which shows the dependence of reciprocal half-time of crystallization on temperature. The relationship between the logarithm of half-time of crystallization and molecular weight is shown in *Figure 6*.

The dependence of exponent n on temperature and molecular weight is illustrated in *Figures 7 and 8*. Exemplary temperature dependence of rate for fractions 23 000 and 37 000 are shown in *Figures 9 and 10*. Small plots within *Figures 9 and 10* illustrate the dependence of melting temperature on temperature of crystallization.

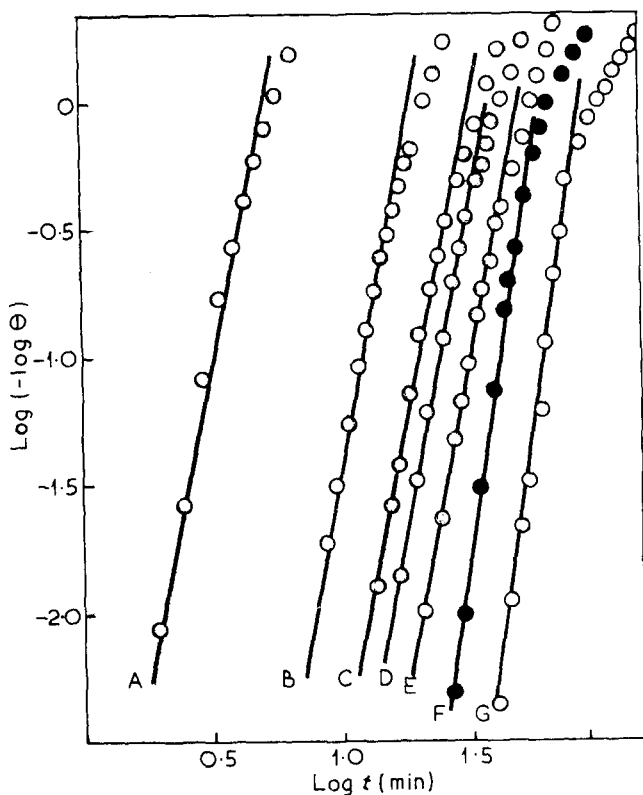


Figure 2 Dependence of $\log(-\log \theta)$ vs. $\log(\text{time})$ at various temperatures for the 23 000 fraction: A, 201°C; B, 205°C; C, 206°C; D, 207°C; E, 209°C; F, 210°C; G, 213°C

DISCUSSION

Crystallization rate

The crystallization rate of the nylon-6 fractions decreased with rise in temperature and increased with molecular weight (Figure 5). These results, being in agreement with theoretical assumptions²⁹ may be explained by an increase in viscosity of the polymer melt owing to increase in molecular weight and accompanying decrease in mobility of crystallizing macromolecules, thus, by reducing the transport of macromolecules to and from the crystal surface. The relationship shown in Figure 6 has a rectilinear character within the whole investigated range of crystallization temperatures and molecular weights. The straight lines for crystallization temperatures of 210°C to 213°C are parallel to each other, similar to those for temperatures of 205°C to 209°C. However, these groups of lines have different angle coefficients. The line for 201°C has the greatest slope and is the most remote

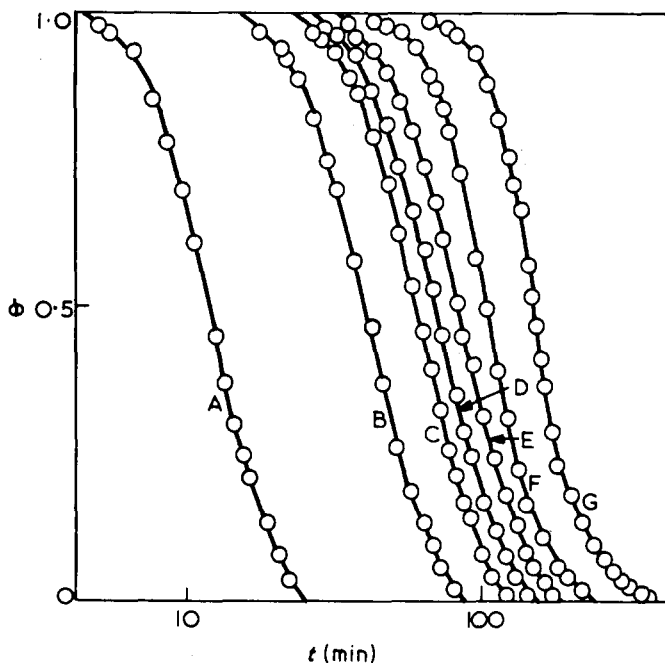


Figure 3 Crystallization isotherms of θ vs. $\log(\text{time})$ at various temperatures for the 37 000 fraction. A, 201°C; B, 205°C; C, 206°C; D, 207°C; E, 209°C; F, 210°C; G, 213°C

from the other lines, which may be evidence that unlike the case of polydispersive samples²⁰ the crystallization of the fractions may occur at the initial stage under non-isothermal conditions. Because of the increase in the homogeneity of the fractions, the crystallization rate is so high at 201°C that the crystallization takes place in the sample before attaining the temperature of the crystallization bath. The dilatometric variations observed under these conditions are due to overlap of crystallization and cooling processes of the samples.

A linear relation between the half-time of crystallization and molecular weight of polypropylene has been found by Chiu²⁵, while Magill¹¹ has obtained a rectilinear relation between the growth rate of spherulites and the logarithm of molecular weight of TPMS fractions.

The values of constant K obtained for the nylon-6 fractions are considerably higher than those for polydispersive samples of similar molecular weight²⁰ crystallized under the same conditions of supercooling. This is due to higher homogeneity of fractionated samples, the reason being in agreement with the Keith and Padden theory²⁶.

Crystallization mechanism

It was found that exponent n varies with the crystallization temperature and molecular weight of the samples. For fractions 17 000, 23 000 and 32 500

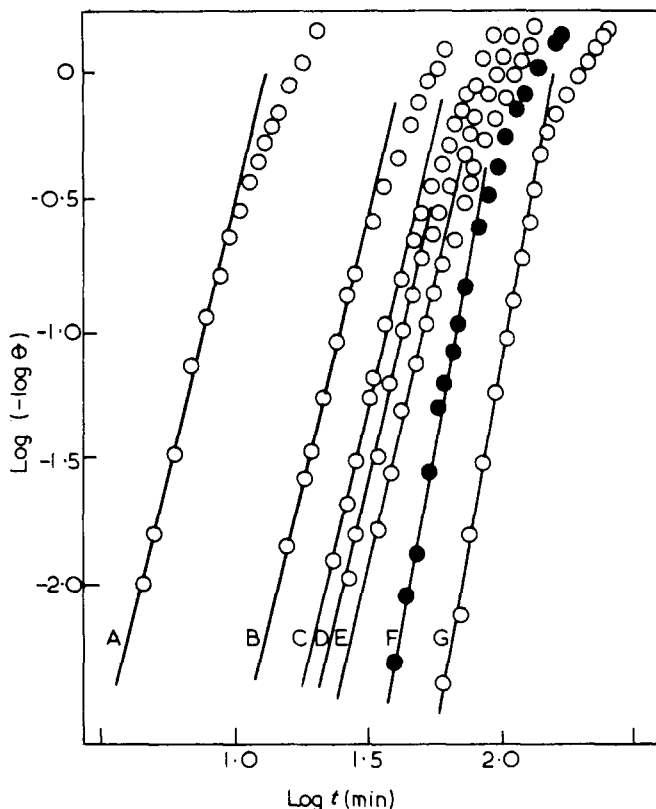


Figure 4 Dependence of $\log(-\log \theta)$ vs. $\log(\text{time})$ at various temperatures for the 37 000 fraction. A, 201°C; B, 205°C; C, 206°C; D, 207°C; E, 209°C; F, 210°C; G, 213°C

constant values of $n = 6$ were obtained at 210–213°C, and $n = 5$ at 201–209°C. Such values of n , according to the theory of Avrami^{1,2} and Morgan²⁷ correspond to sheaf-like growth from sporadic and instantaneous nucleation, respectively. This growth is a result of completion of primary crystallization at the initial stage of sheaf-like aggregation without growing further into spherulites. The improvement of homogeneity of samples due to fractionation may increase the mobility of macromolecules under conditions of crystallization from the melt and facilitate their penetration into clusters of super-critical dimensions. This causes an acceleration of nuclei formation; and, particularly in the case of lower molecular weight fractions, such a considerable increase in their concentration in the melt occurs that the crystals formed cannot attain such perfect shapes as those of spherulites, owing to mutual interaction.

For fraction 37 000 $n = 5$ was obtained at 210–213°C, corresponding to sheaf-like growth from instantaneous nuclei. At 201–209°C n was equal to 3.9 which corresponds to spherical growth from sporadic nucleation within the limits of calculation error.

Table 2 Kinetic parameters for the crystallization of fractions of varying molecular weight

Molecular weight of samples	Kinetic parameters	Temperatures of crystallization (°C)							
		201	205	206	207	209	210	213	
17 000	$t_{1/2}$ (min)	3.0	16.8	20.1	23.1	35.3	38.3	69.5	
	n	5.0	5.0	5.0	5.0	5.0	6.0	6.0	
23 000	K (min^{-4})	8.84×10^{-3}	7.95×10^{-6}	4.33×10^{-6}	2.44×10^{-6}	4.46×10^{-7}	3.07×10^{-7}	2.97×10^{-8}	
	$t_{1/2}$ (min)	4.2	22.3	26.6	29.1	42.9	47.4	74.8	
32 500	n	5.0	5.0	5.0	5.0	5.0	6.0	6.0	
	K (min^{-4})	2.33×10^{-3}	2.81×10^{-6}	1.38×10^{-6}	9.73×10^{-7}	2.04×10^{-7}	1.37×10^{-7}	2.21×10^{-8}	
37 000	$t_{1/2}$ (min)	6.6	38.5	43.5	48.8	68.5	72.0	102.0	
	n	5.0	5.0	5.0	5.0	5.0	6.0	6.0	
49 000	K (min^{-4})	3.65×10^{-4}	3.15×10^{-7}	1.94×10^{-7}	1.22×10^{-7}	3.14×10^{-8}	2.58×10^{-8}	6.40×10^{-9}	
	$t_{1/2}$ (min)	9.2	45.7	52.5	66.8	80.4	87.7	126.0	
49 000	n	3.9	3.9	3.9	3.9	3.9	5.0	5.0	
	K (min^{-4})	9.66×10^{-5}	1.26×10^{-7}	9.11×10^{-8}	3.48×10^{-8}	1.66×10^{-8}	1.17×10^{-8}	2.74×10^{-9}	
49 000	$t_{1/2}$ (min)	23.5	96.6	109.9	120.0	146.0	155.0	212.0	
	n	2.8	2.8	2.8	2.8	2.8	4.0	4.0	
49 000	K (min^{-4})	2.27×10^{-9}	7.79×10^{-6}	4.90×10^{-6}	3.34×10^{-9}	1.52×10^{-9}	1.20×10^{-9}	3.45×10^{-10}	

CRYSTALLIZATION OF NYLON-6 (2)

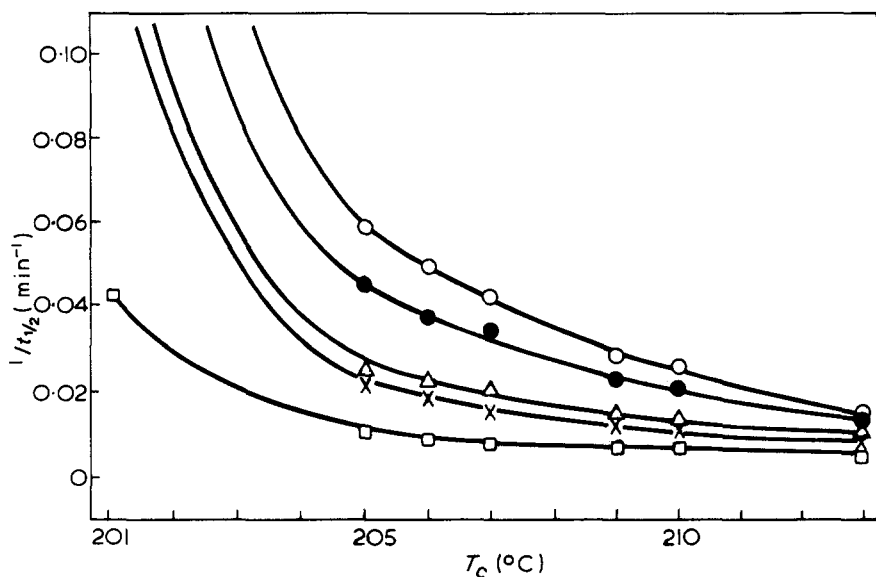


Figure 5 Half-times of crystallization vs. temperature for various fractions: ○, 17 000; ●, 23 000; △, 32 500; ×, 37 000; □, 49 000

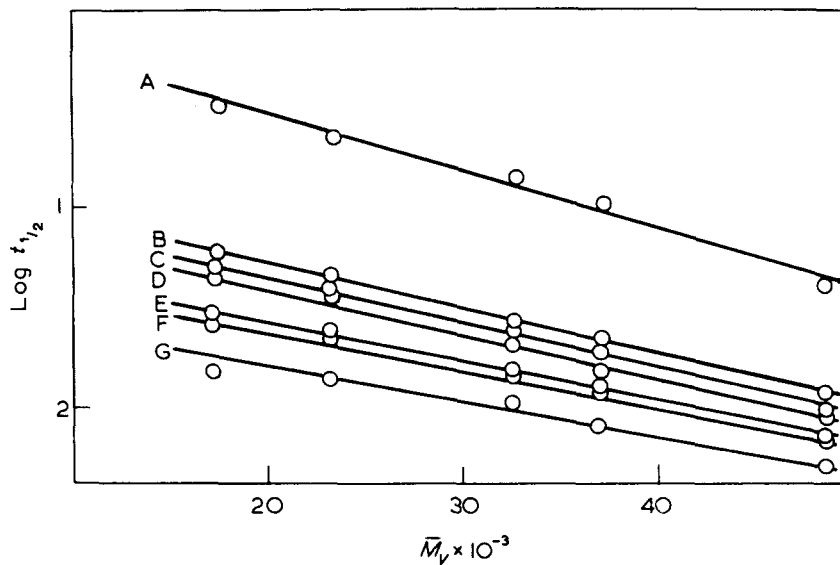


Figure 6 Dependence of log(half-times of crystallization) vs. viscosity-average molecular weight: A, 201°C; B, 205°C; C, 206°C; D, 207°C; E, 209°C; F, 210°C; G, 213°C

The values of n for fraction 49 000 were equal to 4 at 210–213°C which corresponds to spherical growth from sporadic nuclei, and equal to 3 at 210–213°C which corresponds to spherical growth from instantaneous nuclei.

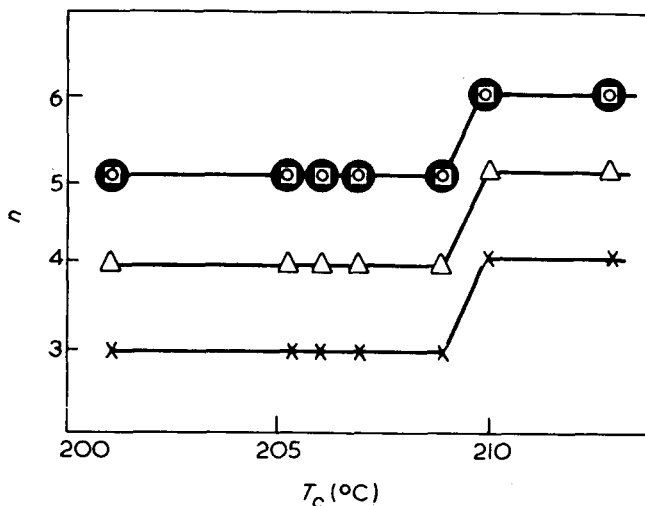


Figure 7 Dependence of Avrami exponent n vs. crystallization temperatures for various fractions. \bar{M}_v : ●, 17 000; □, 23 000; ○, 32 500; △, 37 000; ×, 49 000

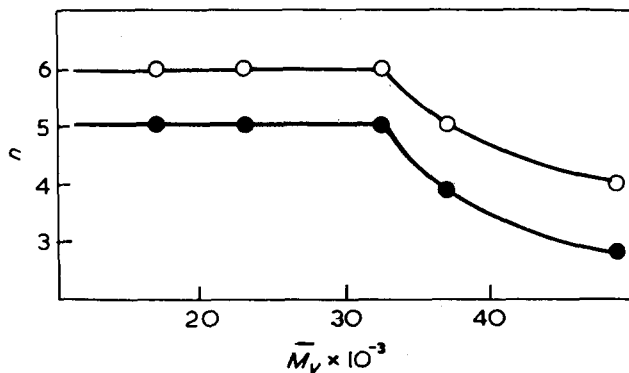


Figure 8 Dependence of Avrami exponent n vs. viscosity-average molecular weight for various fractions. ○, T_c 210–213°C; ●, T_c 201–209°C

It is clear that exponent n for fractionated samples varies within the given range of crystallization temperatures of 209–210°C, as in the case of poly-dispersive samples²⁰. Above that range the growth of crystals occurs from sporadic nuclei, and below the range from instantaneous nuclei. The change in the crystallization mechanism may be due to the nucleation rate and critical dimensions of nuclei being highly sensitive to the supercooling conditions. A slight drop in the crystallization temperature causes such a considerable rise in the formation rate of nuclei that they are formed simultaneously and growth of crystals occurs from instantaneous nuclei.

The fraction of molecular weight 37 000 is exceptional, in that at temperatures higher than the limiting one the sheaf-like growth occurs from instantaneous nuclei, and at lower temperatures the spherical growth occurs

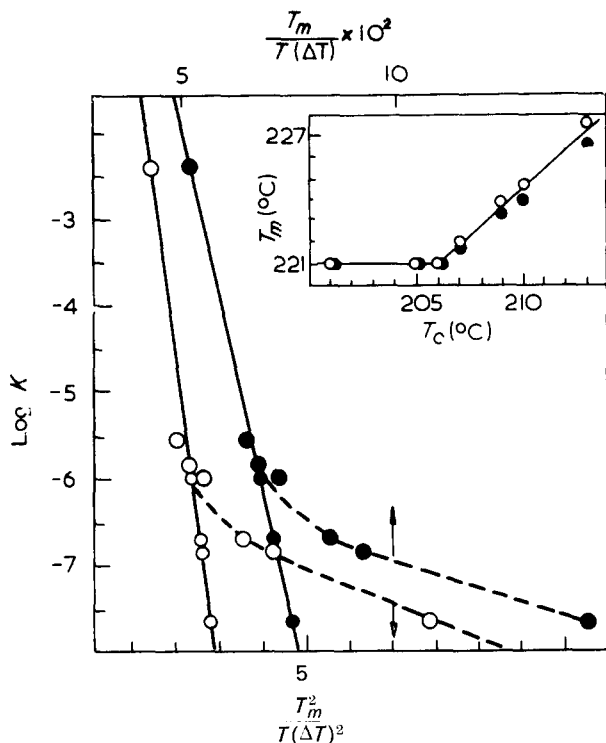


Figure 9 Temperature dependence of rate constant, K , for the 23 000 fraction

from sporadic nuclei. It is possible that in the fraction 37 000 a higher degree of crystalline order was created, which is not completely destroyed even by prolonged treatment of the melt at 261°C. It may be assumed that the regions of the highest order may remain in the melt and cause either sporadic or instantaneous nucleation depending on the crystallization temperature.

At higher crystallization temperatures the dimensions of critical nuclei are relatively large and need a relatively long time for their formation. Under these conditions the remaining nuclei of sub-critical dimensions grow in size and become nuclei of instantaneous nucleation.

At slightly lower temperatures the critical dimensions of nuclei are smaller and the rate of their formation much higher. The number of them quickly exceeds that remaining in the melt and the nucleation proceeds as sporadic.

It is clear from Figure 8 that the value of n rises with decrease in molecular weight from the value of 2.8 for the fraction 49 000 to the value of 5 for the fraction of 32 500 at 201–209°C, and from 4 to 6 respectively for the same fractions crystallized at 210–213°C.

On the basis of the results it may be concluded that for the samples under investigation, a molecular weight equal to about 32 500 is a limiting value below which there is no distinct effect of molecular weight on the crystallization mechanism determined by the exponent n .

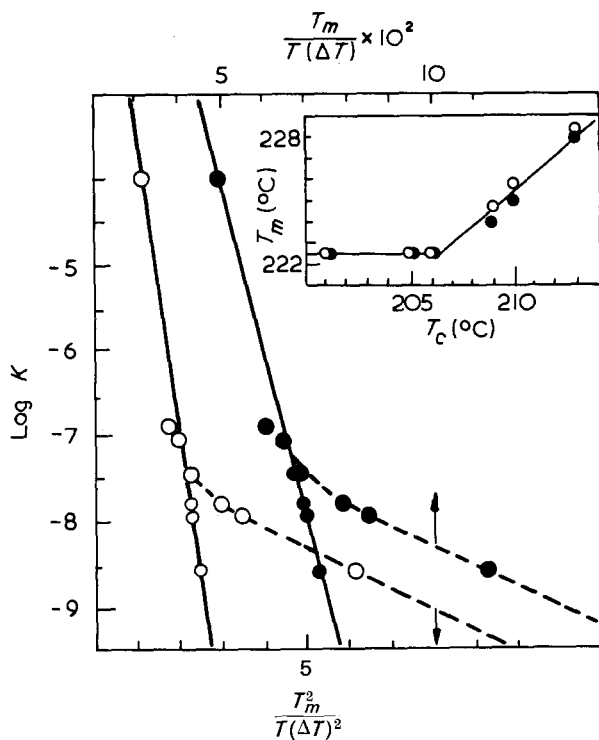


Figure 10 Temperature dependence of rate constant, K , for the 37 000 fraction

An increase in the value of n with decrease in molecular weight has been observed by Banks and co-workers^{4,5} in the case of polyethylene and by Parrini and Corrieri¹⁹ in polypropylene.

Temperature dependence of rate

Figures 9 and 10 illustrate the dependence of $\log K$ on $T_m/T(\Delta T)$ and $T_m^2/T(\Delta T)^2$, where T_m is constant or higher than the determined one.

In both cases for all the fractions, similar to the case of polydisperse samples²⁰, rectilinear relations were obtained, taking into account in the calculation that the rise of the crystallization temperature was accompanied by rise of the melting temperature and that $n = 4$. The character of changes in the calculated values of melting temperature to get rectilinear plots of the change of crystallization temperature is illustrated by the inset graphs in Figures 9 and 10.

The acceptance of constant value of T_m for calculations results in characteristic curves (broken line) in plots of $\log K$ against $T_m/T(\Delta T)$ and $T_m^2/T(\Delta T)^2$.

Similar relations have been found for polypropylene and polycarbonates²⁸, polypropylene and polybutene²⁹, poly(decamethylene terephthalate)³⁰ and polycapramide^{14,20}.

Technical University of Łódź,
Dept of Physical Chemistry of Polymers,
Łódź 40, Poland

E. Turska

Institute of Polymers,
Ministry of High Education and Polish Academy of Sciences,
Dept of Physical Chemistry of Polymers,
Łódź 40, Poland

S. Gogolewski

(Received 6 July 1971)

(Revised 16 March 1971)

REFERENCES

- 1 Avrami, M. *J. Chem. Phys.* 1939, **7**, 1103; 1940, **8**, 212; 1941, **9**, 177
- 2 Evans, U. R. *Trans. Faraday Soc.* 1945, **41**, 365
- 3 Buckser, S. and Tung, L. H. *J. Phys. Chem.* 1959, **63**, 763
- 4 Banks, W., Gordon, M., Roe, R. J. and Sharples, A. *Polymer, Lond.* 1963, **4**, 61
- 5 Banks, W., Hay, J. N., Sharples, A. and Thomson, G. *Polymer, Lond.* 1964, **5**, 193
- 6 Mandelkern, L. *J. Polym. Sci. (C)* 1966, **15**, 129
- 7 Fatou, J. G. and Mandelkern, L. *J. Phys. Chem.* 1965, **64**, 417
- 8 Hoshino, S., Meinecke, E., Powers, J. and Stein, R. S. *J. Polym. Sci. (A-2)* 1965, **3**, 3041
- 9 Parrini, P. and Corrieri, G. *Makromol. Chem.* 1963, **62**, 83
- 10 Kamide, K., Inamoto, Y. and Ohno, K. *Chem. High Polymer (Japan)* 1965, **22**, 597
- 11 Magill, J. H. *J. Appl. Phys.* 1964, **35**, 3249; *J. Polym. Sci. (A-2)* 1967, **5**, 89; *J. Polym. Sci. (B)* 1968, **6**, 853
- 12 Turska, E. and Przygocki, W. *Faserforsch. Textiltech.* 1964, **11**, 732; *Bull. Acad. polon. Sci., Sér. Sci. chem.* 1965, **13**, 183; *J. Polym. Sci. (C)* 1968, **16**, 3373
- 13 Burnett, B. B. and McDevit, W. F. *J. Appl. Phys.* 1957, **88**, 1101
- 14 Inoue, M. *J. Polym. Sci.* 1961, **55**, 753
- 15 Magill, J. H. *Polymer, Lond.* 1962, **3**, 43
- 16 McLaren, J. V. *Polymer, Lond.* 1963, **4**, 175
- 17 Ueda, N. and Nukushina, Y. *Chem. High Polymers (Japan)* 1966, **23**, 769
- 18 Lindengren, C. R. *J. Polym. Sci.* 1961, **50**, 180
- 19 Hartley, F. D., Lord, F. W. and Morgan L. B., *Ricerca. Sci. (Suppl.)* 1954, **25A**, 577
- 20 Turska, E. and Gogolewski, S. *Polymer, Lond.* 1971, **12**, 616
- 21 Turska, E. and Matuszewska-Czerwik, J. *Polimery* 1963, **8**, 13
- 22 Gogolewski, S. *Polimery* 1966, **11**, 98
- 23 Matthes, A. *J. prakt. Chem.* 1943, **162**, 245; *Makromol. Chem.* 1950, **5**, 165
- 24 Gogolewski, S. *Polimery* 1971, **16**, 130
- 25 Chiu Jen, *Analyt. Chem.* 1964, **36**, 2048
- 26 Keith, H. D. and Padden, F. J. Jr *J. Appl. Phys.* 1963, **34**, 2409; 1964, **35**, 1270
- 27 Morgan, L. B. *Phil. Trans.* 1954, **A247**, 13; *J. Appl. Phys. Chem.* 1954, **4**, 160
- 28 Falkai, B. and Rellensman, W. *Makromol. Chem.* 1965, **28**, 38
- 29 Gordon, M. and Hillier, I. H. *Polymer, Lond.* 1965, **6**, 213
- 30 Sharples, A. and Swinton, F. L. *Polymer, Lond.* 1963, **4**, 119
- 31 Ishibashi, T. and Tani, Y. *Chem. High Polymers (Japan)* 1969, **26**, 199

Oligomers in polytetrahydrofuran

J. M. ANDREWS and J. A. SEMLYEN

The oligomeric content of samples of polytetrahydrofuran has been investigated. The polymers were prepared by monomer-polymer equilibrations in the bulk, and in solution in toluene, using boron trifluoride diethyl etherate and epichlorohydrin. Two series of oligomers were found to be present in the polymers. Both series are believed to consist of linear chain molecules. Their concentrations were far higher than those predicted for polymers with a most probable distribution of chain lengths. Cyclic oligomers $(\text{CH}_2\text{CH}_2\text{CH}_2\text{CH}_2\text{O})_x$ were not found to be present in the equilibrated polymers, and it is concluded that macrocyclic oxonium ions were not formed during the polymerization reactions.

INTRODUCTION

TETRAHYDROFURAN polymerizes under the influence of a wide range of Lewis acids and their salts to give polytetrahydrofuran, with the repeat unit $-\text{CH}_2\text{CH}_2\text{CH}_2\text{CH}_2\text{O}-$ ¹⁻⁴. The polymer is also called poly(tetramethylene oxide). The polymerization process is reversible and an equilibrium between monomer and polymer may be established in the undiluted polymer⁵⁻⁸ or in solution^{9,10}. There have been a number of studies of the kinetics of the polymerization process and detailed reaction mechanisms have been suggested⁴. The polymer has been characterized by conventional polymer techniques and it is generally accepted that polytetrahydrofuran is a linear polymer, although there have been no reports of the analysis and characterization of individual molecular species.

In this paper, we report the results of an investigation into the nature and concentrations of oligomers in undiluted and solution equilibrates of polytetrahydrofuran. At present, we are investigating the concentrations of cyclic molecules in a number of polymeric systems including polyethers, and this study of polytetrahydrofuran was directed primarily at investigating whether or not cyclic oligomers are present in the equilibrated polymer.

EXPERIMENTAL

Materials

Tetrahydrofuran and toluene were dried over sodium wire and calcium hydride respectively, and fractionally distilled before use. Boron trifluoride diethyl etherate, epichlorohydrin and diethylamine were obtained from B.D.H. and they were used as supplied.

All operations involving tetrahydrofuran, including its purification, were carried out in an atmosphere of dry, oxygen-free nitrogen.

Polymerizations

Undiluted and solution polymerizations were carried out on a 200–250 ml scale. Boron trifluoride diethyl etherate and epichlorohydrin were added to flasks containing tetrahydrofuran in toluene. The flasks were shaken to ensure homogeneity and maintained at constant temperature. All the polymerization reactions were quenched by the addition of small amounts of diethylamine.

Extraction of oligomers

Oligomers were extracted from the polymers using the following procedure. Each quenched polymeric product was dissolved in a solution of methanol and acetone (2 : 1 v/v) at a polytetrahydrofuran concentration of ~12% (w/w) by warming the mixture. The solution was allowed to stand at 273 K overnight, so that the polymer precipitated slowly. The supernatant solution was then decanted off and the solvent was removed on a rotary evaporator to yield ~2% (w/w) of the polytetrahydrofuran in the form of oligomers. The procedure was repeated several times, successively smaller quantities of oligomers being obtained. After five precipitations, the total material extracted amounted to less than 0.2% (w/w) of the polymer. The oligomeric content of each extract was investigated by gas-liquid chromatography; and the polymer, before and after extraction, was analysed by gel permeation chromatography. The chromatograms showed that after five extractions, effectively all the low molecular weight oligomers had been removed from each polymer.

After extraction of the oligomers, the residual polymers were dried in a vacuum oven at 313 K. The amounts of monomer converted to polymers in the polymerization processes were calculated from the weights of residual polymers together with the weights of extracted oligomers. The results were in good agreement with the values published for monomer-polymer equilibria of polytetrahydrofuran in the bulk and in solution⁵⁻¹⁰. The intrinsic viscosities of the polymers were measured, and their molecular weights were estimated using the Mark-Houwink equation for polytetrahydrofuran in toluene at 301 K published by Ali and Huglin¹¹.

Molecular distillation of oligomers

The first four oligomeric extracts from a sample of polytetrahydrofuran polymerized in the bulk at 273 K were combined and dissolved in a methanol and acetone mixture by warming. The solution was cooled to 273 K. About half the material precipitated. A 1g sample of the oligomers which were recovered from the supernatant solution was separated into fractions by distillation at 10^{-2} mm Hg using a molecular still with a cooled glass probe. The still was maintained at successively higher temperatures in the range 373–511 K for periods of 24–72 h. Five fractions (each weighing 0.05–0.11 g) were obtained, together with a residue weighing 0.6 g. Each fraction was analysed separately by gas-liquid chromatography and in some cases by gel permeation chromatography. No detectable decomposition of the oligomers occurred during the molecular distillation.

Gas-liquid chromatography

A Pye- Unicam (Series 104) gas-liquid chromatograph fitted with a heated dual flame-ionisation detector was used to analyse the oligomers. The sample and reference columns were 4 ft \times 3 mm i.d. glass tubing packed with Embacel (treated beforehand for the removal of polar groups by the method of Bohemen *et al.*¹²) and coated with 6% (w/w) OV17 (supplied by the Field Instrument Co.). Injections were made with a 10 μ l hypodermic syringe through a serum cap into a flash heater.

The oligomers of polytetrahydrofuran were found to be thermally stable, and a comparison of gas-liquid chromatograms at elevated temperatures with gel permeation chromatograms (obtained at 303 K) showed that the main oligomeric components did not decompose in the gas-liquid chromatographic columns. In addition, the thermal stabilities of oligomeric mixtures were tested by adding weighed amounts of a thermally stable standard, and carrying out the gas-liquid chromatographic analyses at different rates of temperature programming. Response factors for the oligomers were estimated by using the fractions obtained by the molecular distillation described above.

Gel permeation chromatography

A gel permeation chromatograph¹³ fitted with a Waters Model R4 differential refractometer detector was used to examine the molecular weight distributions of some of the polymeric and oligomeric samples.

Mass spectrometry

A combined A.E.I. MS12 mass spectrometer/Pye- Unicam (Series 104) gas-liquid chromatograph was used to produce mass spectra of some of the individual oligomers.

RESULTS

Gas-liquid chromatograms of the extracts from bulk and solution equilibrates of polytetrahydrofuran, prepared as described above, showed two series of thermally stable oligomers. These oligomers had retention times characteristic of two separate homologous series. A combined extract from a bulk equilibrate of polytetrahydrofuran at 273 K was fractionated and distilled into a number of fractions as described above. Gas-liquid chromatograms of the first four fractions are shown in *Figure 1*. The weight fractions of the two series of oligomers in a bulk equilibrate and a solution equilibrate of polytetrahydrofuran at 273 K are shown in *Figures 2* and *3*.^{*} Both series of

* Other oligomers were also observed in small amounts in the gas-liquid chromatograms of extracts from the polymers. Their elution times were all greater than those of the species c and C shown in *Figure 1*. Their concentrations were very small in all the oligomeric extracts and they will not be discussed in detail here. Attention will be confined to the two oligomeric series present in the highest concentrations.

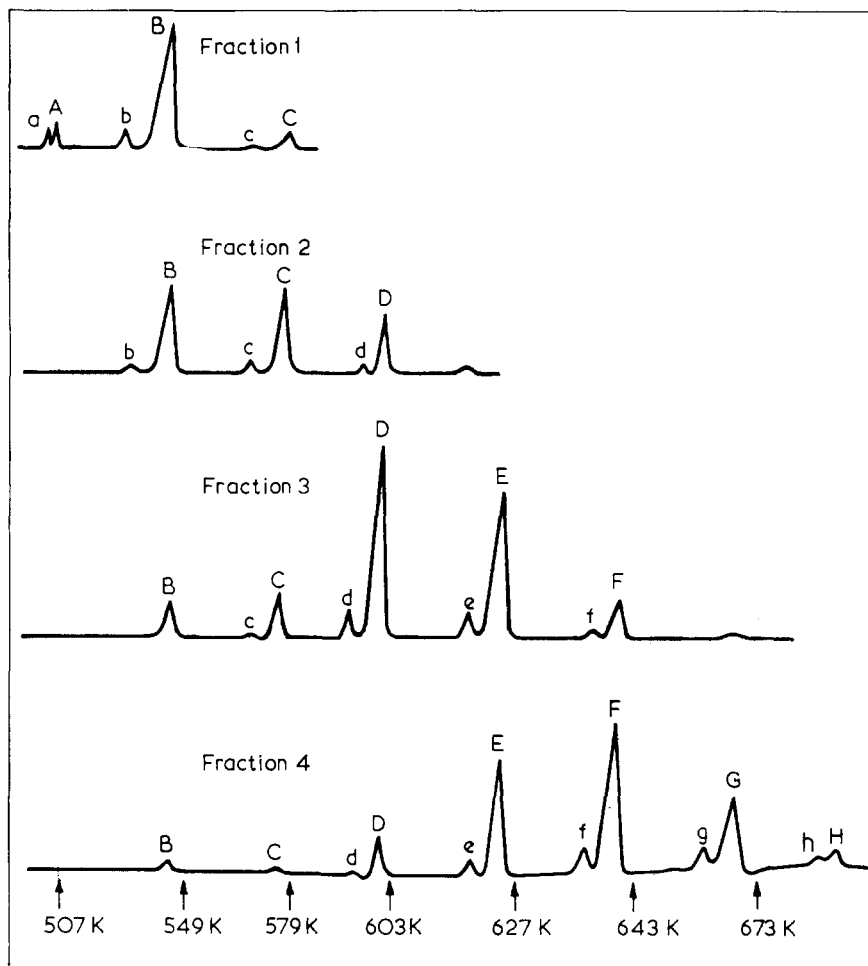


Figure 1 Gas-liquid chromatograms of fractions obtained by the molecular distillation of a combined oligomeric extract from polytetrahydrofuran polymerized in the bulk at 273 K. Oligomers are labelled A, B, C, . . . and a, b, c, . . . The column temperature was increased at intervals as shown

oligomers are believed to be chain molecules of the type $X-(CH_2CH_2CH_2-CH_2O)_y-X'$ where X, X' denote terminal groups and $y = 1, 2, 3, \dots$. Their weight fractions are considerably in excess of those calculated for a most probable distribution of chain lengths^{14,15}.

The conclusion that the oligomers are chains, and not the cyclics $(CH_2-CH_2CH_2CH_2O)_x$, is based on the following evidence:

(1) The mass spectra of the first four oligomers (termed a, A, b, B, in Figure 1) did not correspond to those expected for the cyclics $(CH_2CH_2CH_2CH_2O)_x$, but they were compatible with the spectra expected for the linear molecules

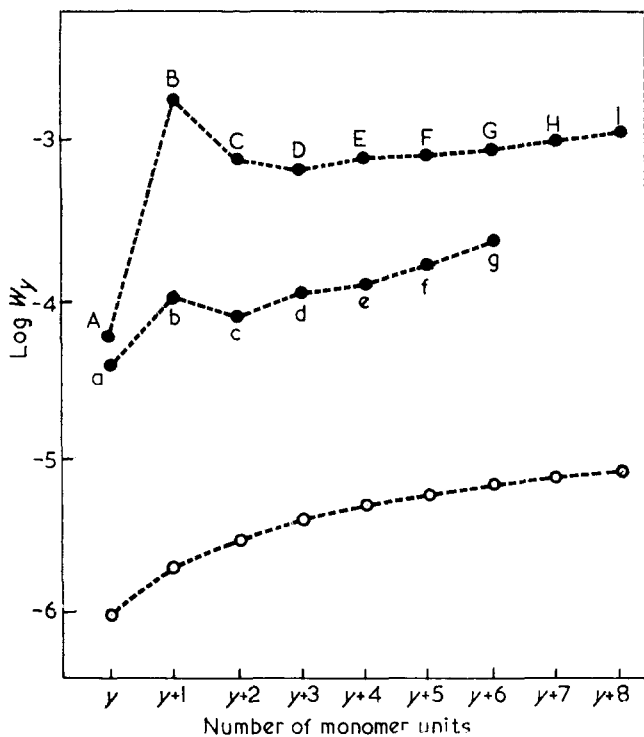


Figure 2 Weight fractions of oligomers in polytetrahydrofuran polymerized in the bulk at 273 K shown as a function of the number of monomeric units. The oligomers are labelled as in Figure 1, and experimental weight fractions are denoted ●. The weight fractions of linear chains calculated from the average molecular weight of the polymer by assuming a most probable distribution of chain lengths, and taking $y = 1$, are denoted ○.

$X-(CH_2CH_2CH_2CH_2O)_y-X'$. The spectra showed that all four oligomers contain chlorine, and A and B probably contain nitrogen as well.

(2) The weight fractions of all the higher molecular weight oligomers are considerably lower than those predicted for macrocyclics by the Jacobson and Stockmayer¹⁶ equilibrium theory of cyclization. Furthermore, there is no decrease in the weight fractions of the oligomers with increase in their molecular weights as would be expected for a macrocyclic series (see Figures 2 and 3).

(3) The relative amounts of the two series of oligomers were found to be the same within experimental error for undiluted equilibrates at 273 and 323 K, and for concentrated solution and dilute solution equilibrates at 273 K. The molecular weights of all these polymer samples were high. If one of the series of oligomers were the cyclics $(CH_2CH_2CH_2CH_2O)_x$, raising the temperature of equilibration above the melting point of the polymer or diluting with solvent would have been expected to have increased their weight fractions relative to the chains.

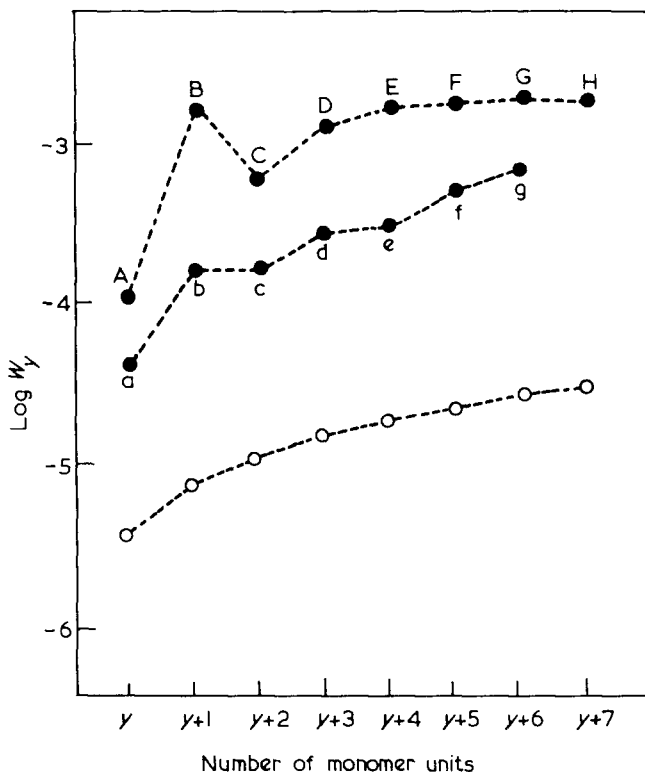
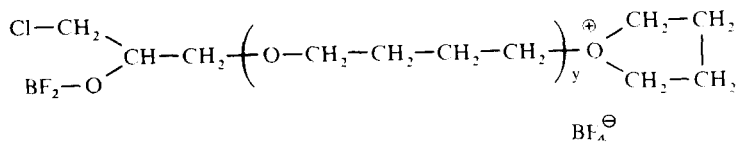


Figure 3 Weight fractions of oligomers in a polytetrahydrofuran equilibrated by polymerizing tetrahydrofuran in toluene (in a ratio of 1.4 : 1) at 273 K. The experimental and calculated values, denoted ● and ○ respectively, are defined as in the legend to Figure 2

DISCUSSION

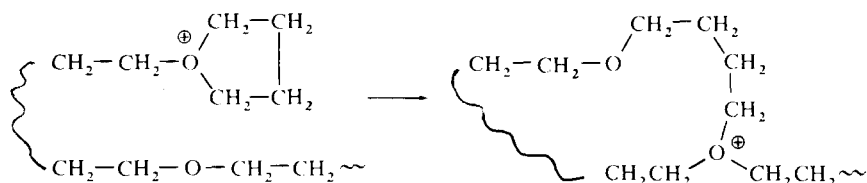
Dreyfuss and Dreyfuss⁴ have reviewed investigations into the mechanism of the polymerization of tetrahydrofuran in some detail. The propagating species in the polymerization of tetrahydrofuran by boron trifluoride diethyl etherate in the presence of epichlorohydrin are believed to be trialkyl oxonium ions associated with BF_4^- gegenions



Propagation is thought to occur by step-wise addition of monomer, and depropagation by step-wise removal of monomer. When polytetrahydrofuran

equilibrates are quenched by diethylamine, inactive chains containing both chlorine and nitrogen would be expected to result and these primary chains could be the oligomers denoted A, B, C, . . . in *Figure 1*. Now, Meerwein¹ has suggested that termination could also proceed by reaction of the BF_4^- gegenion with the growing oxonium ion to produce chains terminated with fluorine. Furthermore, termination by traces of moisture could result in hydroxyl end groups, and epichlorohydrin may be involved in a termination reaction. Hence, it is possible to rationalize the presence of two series of chain oligomers in the polytetrahydrofuran samples, as well as the small amounts of the other oligomers that were observed.

The absence of cyclics $(\text{CH}_2\text{CH}_2\text{CH}_2\text{CH}_2\text{O})_x$ in the polytetrahydrofuran samples is surprising. Dreyfuss and Dreyfuss^{4,17} have carried out detailed investigations into chain transfer reactions in polytetrahydrofuran polymerizations involving acyclic ethers; and in related studies^{14,15} they have concluded that polymer oxygen atoms can react with trialkyl oxonium ions to produce broad molecular weight distributions. These authors have pointed out that polymer oxygen would be expected to react intramolecularly as well as intermolecularly and so produce macrocyclic oxonium ions, thus⁴



Attack by tetrahydrofuran at the carbon atom (attached to the charged oxygen atom), that is not involved in the cyclic part of the oxonium ion, would then result in the formation of the cyclics $(\text{CH}_2\text{CH}_2\text{CH}_2\text{CH}_2\text{O})_x$. Such cyclics were not found to be present in the polytetrahydrofuran samples investigated. Evidently, macrocyclic oxonium ions were not formed in the polymerization reactions.

ACKNOWLEDGEMENTS

We are indebted to the Courtaulds' Educational Trust Fund for a Research Scholarship (to J. M. A.). We thank Dr C. B. Thomas for help in the interpretation of the mass spectra.

*Department of Chemistry,
University of York,
Heslington, York YO1 5DD, UK*

(Received 15 March 1971)

REFERENCES

- 1 Meerwein, H., Delfs, D. and Morshel, H. *Angew. Chem.* 1960, **72**, 927
- 2 'The Chemistry of Cationic Polymerisation', Plesch, P. H. (Ed.) Pergamon, Oxford, 1963
- 3 Furukawa, J. and Saegusa, T. 'Polymerisation of Aldehydes and Oxides', Interscience, New York, 1963
- 4 Dreyfuss, P. and Dreyfuss, M. P. *Adv. Polym. Sci.* 1967, **4**, 528
- 5 Sims, D. *J. Chem. Soc.* 1964, p864
- 6 Bawn, C. E. H., Bell, R. M. and Ledwith, A. *Polymer, Lond.* 1965, **6**, 95
- 7 Rozenberg, B. A., Chekhuta, O. M., Lyudvig, Ye. B., Gantmakher, A. R. and Medvedev, S. S. *Polym. Sci. (U.S.S.R.)* 1964, **6**, 2246
- 8 Ivin, K. J. and Leonard, J. *Polymer, Lond.* 1965, **6**, 621
- 9 Vofsi, D. and Tobolsky, A. V. *J. Polym. Sci. (A)* 1965, **3**, 2361
- 10 Sims, D. *Makromol. Chem.* 1966, **98**, 235
- 11 Ali, S. M. and Huglin, M. B. *Makromol. Chem.* 1965, **84**, 117
- 12 Bohemen, J., Langer, S. H., Perrett, R. H. and Purnell, J. H. *J. Chem. Soc.* 1960, p2444
- 13 Wright, P. V., D.Phil. Thesis, Univ. York, 1970
- 14 Dreyfuss, M. P. and Dreyfuss, P., 159th Meeting of Amer. Chem. Soc., Houston, Texas, February 1970
- 15 Dreyfuss, P. and Dreyfuss, M. P. *Adv. Chem. Ser.* 1969, **91**, 335
- 16 Jacobson, H. and Stockmayer, W. H. *J. Chem. Phys.* 1950, **18**, 1600
- 17 Dreyfuss, M. P. and Dreyfuss, P. *J. Polym. Sci. (A-1)*, 1966, **4**, 2179

Notes to the Editor

Studies on cyclic tris(ethylene terephthalate)

EIKO ITO and SABURO OKAJIMA

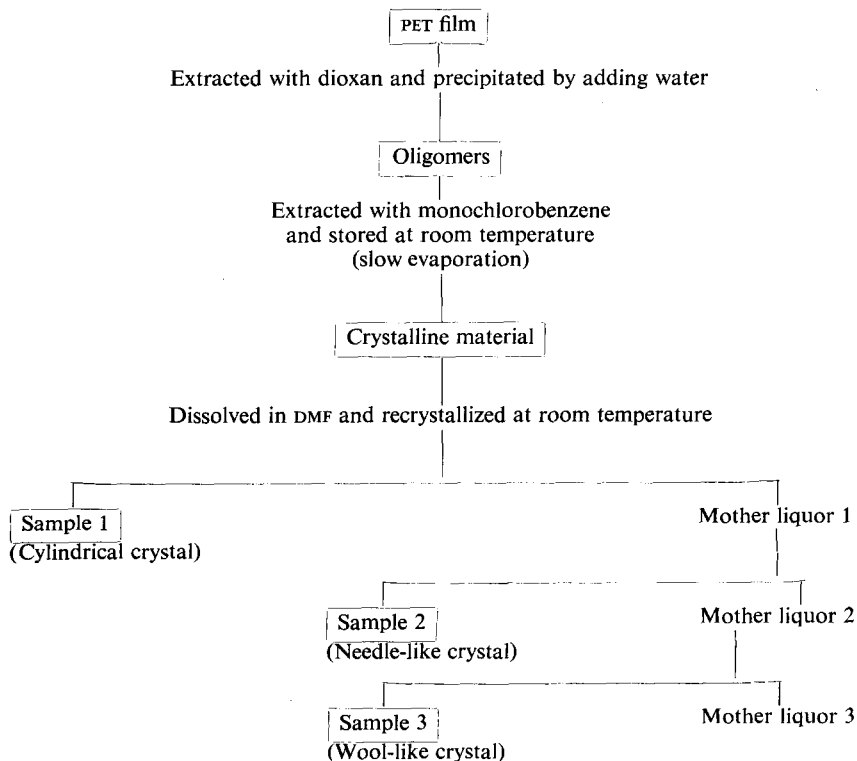
Lattice spacings of tris(ethylene terephthalate) have been reported by a few authors¹⁻⁴ but the results obtained are not all consistent. The reason may be insufficient purity of the samples and/or polymorphic behaviour of the trimer, because the crystalline form changes according to the condition of crystallization.

EXPERIMENTAL

Sample preparation

Oligomers were extracted from a piece of commercial poly(ethylene terephthalate) (PET) film with dioxan, and recrystallized repeatedly as shown in *Table 1* to give samples 1-3. Crystallization from DMF solution continued

Table 1 Recrystallization scheme



for several days at room temperature, hence the three samples were gathered at three stages. When a part of this material (samples 1-3 were the same material, as mentioned later) was crystallized from monochlorobenzene solution, two kinds of crystals—platelet and needle-like—developed in the same mother liquor.

Thin-layer chromatography

The thin-layer chromatography was carried out on a plate of silica gel G sprayed with a chloroform solution of antimony chloride, using chloroform/ethyl-acetate (9:1 v/v) and benzene/ethyl-acetate (8:2 v/v) as developing solvent.

Gas chromatography

The gas chromatography was performed using the mixed column 1% OV-17 + 1% SE-30 Chromosorb W-AW-DMCS at 325°C.

High resolution nuclear magnetic resonance (n.m.r.)

High resolution n.m.r. spectrum (100 MHz) was obtained with a 4H-100 spectrometer of the Japan Electron Optics Laboratory Co. Ltd, tetramethylsilane being used as an internal standard in deuteriochloroform solution.

Infra-red spectrum measurement

The infra-red spectrum of the sample was obtained by means of a potassium bromide disc method on a Hitachi EPI-2 infra-red spectrometer.

X-ray diffraction measurement

The x-ray diffraction measurements were carried out using a Weissenberg camera of Rigakudenki Co. Ltd.

RESULTS

Thin-layer chromatography exhibited only one spot corresponding to $R_f = 0.65$ for any of these three samples 1-3 irrespective of the developing solvents - benzene/ethyl-acetate and chloroform/ethyl-acetate.

The gas chromatogram also showed only one peak for any sample. The i.r. spectra of samples 1-3 agreed exactly with one another. Hence the three samples are considered to be the same substance.

Also the result of high resolution n.m.r. study showed that the intensity of the peak at $\tau = 1.82$ of aromatic protons was equal to that at $\tau = 5.29$ of $-\text{O}-\text{CH}_2-\text{CH}_2-\text{O}-$ protons. At low magnetic field, no peak was observed suggesting the existence of a COOH group or a free OH group.

The molecular weight, determined by the Rast method, was 600 and the elementary analysis 62.3% C and 3.74% H. This compares with the calculated value of 576 for the molecular weight of tris(ethylene terephthalate) and a calculated composition of 62.5% C and 4.17% H. Further, the i.r. absorption bands characteristic of the trimer such as 1458, 1364, 1167, 1094, 1036, 899 and 877 cm^{-1} are clearly observed. These results afford evidence

that the samples are tris(ethylene terephthalate) and are satisfactorily pure.

When a solution of needle-like crystals⁴ of sample 2 in DMF was placed at room temperature and evaporated very slowly, many cylindrical crystals (shown in *Figure 1*) were obtained, which were similar to sample 1. The unit cell of this crystal from the Weissenberg photograph is monoclinic: $a = 16.84 \text{ \AA}$, $b = 19.41 \text{ \AA}$, $c = 8.31 \text{ \AA}$, $\beta = 98^\circ 36'$ and space group Cc . The determined density in an aqueous solution of zinc chloride was 1.372 g/cm^3 at 24°C . Accordingly, in the unit cell, four trimer molecules lie in general positions. These results agree well with those obtained by Farrow⁵: $a = 17.13 \text{ \AA}$, $b = 19.52 \text{ \AA}$, $c = 8.288 \text{ \AA}$, $\beta = 96.8^\circ$ and density 1.363 g/cm^3 .

When a dilute monochlorobenzene solution of samples 1–3 was evaporated very slowly at room temperature two kinds of crystals, platelet as shown in *Figure 2* and the needle-like crystals described in a previous paper⁴, developed in the same mother liquor. The two forms of crystals were separated.



Figure 1 Optical micrograph of single crystal obtained from DMF solution ($\times 100$)

In *Table 2*, the first and second lines indicate the indexing and the lattice spacings calculated from the present authors' unit cell mentioned above and the lattice spacings of needle-like crystal from DMF solution. It is noted further that the patterns ($0k0$) do not appear when k are odd numbers; therefore, the unit cell may have a screw axis along the b axis and the space group is concluded to be $Cc/2$.

Table 3 shows that the lattice spacings of needle-like crystals obtained from monochlorobenzene solution do not agree with those of the platelet crystal obtained from the same solution but are in good accordance with the one previously obtained in a similar way from monochlorobenzene solution⁴. Hence the trimer seems to crystallize in two different crystal structures, although the precise conditions for this polymorphism are not clear at present. Thus the previous conclusion⁴ that the needle-like crystal from monochloro-

Table 2 Comparison of the lattice spacings of variously obtained sample (values in Å)

1. Index	020	200	111	220	310	040	330	420	222	202	060	440	530
2. Calculation	9.70	8.31	6.55	6.31	5.33	4.85	4.20	3.82	3.65	3.48	3.23	3.15	2.95
3. Crystal from DMF	9.72	8.35	6.53	6.26	5.33	4.84	4.24	3.83	3.65	3.47	3.25	3.12	2.93
4. Platelet crystal from monochlorobenzene	—	—	6.61	6.33	5.31	4.84	4.23	3.86	3.66	3.48	3.22	3.14	2.91
5. A-type of Binns <i>et al.</i> ²	9.88	8.60	6.67	6.37	5.28	4.84	4.24	3.87	3.65	3.44	—	3.10	2.92
1. Index	080	043	602	063	750	010 0	533	083	733	970	10 02	555	
	133		333										
2. Calculation	2.42	2.38	2.15	2.08	2.02	1.94	1.88	1.81	1.62	1.53	1.46	1.34	
	2.44		2.18										
3. Crystal from DMF	2.44	2.34	2.14	2.08	2.02	1.94	1.89	1.84	1.63	1.50	1.46	1.34	
4. Platelet crystal from monochlorobenzene	2.43	2.39	2.14	2.07	2.01	—	—	1.83	—	—	—	—	
5. A-type of Binns <i>et al.</i> ²	—	—	—	—	—	—	—	—	—	—	—	—	

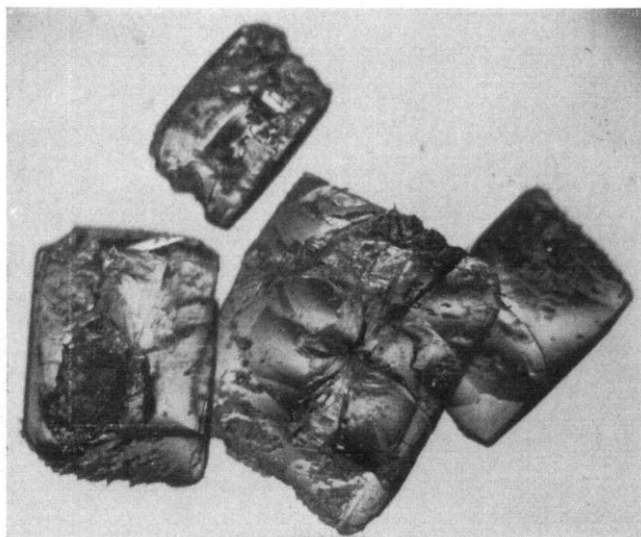


Figure 2 Optical micrograph of the platelet crystal obtained from monochlorobenzene solution ($\times 100$)

Table 3 Comparison between the lattice spacings of two kinds of crystal obtained from monochlorobenzene (MCB) solution (values in Å)

<i>Platelet crystal</i>	<i>Needle-like crystal</i>	<i>Crystal from MCB</i>	<i>Platelet crystal</i>	<i>Needle-like crystal</i>	<i>Crystal from MCB</i>
6.61	--	--	3.48	--	--
6.33	--	--	--	3.42	3.42
5.31	--	--	--	3.25	3.25
--	5.21	5.18	3.14	--	--
4.48	--	--	--	3.01	3.03
--	4.60	4.60	2.91	--	--
--	4.31	4.32	--	2.87	2.87
--	--	4.09	2.43	--	--
4.23	--	--	2.14	--	--
--	3.96	3.96	2.07	--	--
3.86	--	--	2.01	--	--
--	3.70	3.70	1.83	--	--
3.66	--	--	--	--	--

benzene solution is identical with the *A*-type crystal of Binns *et al.*² is not correct; there may be a new crystalline form.

ACKNOWLEDGEMENT

We are pleased to acknowledge the considerable assistance rendered to us by Professor T. Seto of Tokyo Metropolitan University and Associate Professor Y. Hirose of Tokyo University.

*Faculty of Technology,
Tokyo Metropolitan University,
1-1 Fukazawa, 2-chome, Setagaya-ku,
Tokyo, Japan*

*(Received 7 December 1970)
(Revised 18 May 1971)*

REFERENCES

- 1 Goodman, I. *et al. Polymer, Lond.* 1960, **1**, 384
- 2 Binns, G. L. *et al. Polymer, Lond.* 1966, **7**, 583
- 3 Miyake, A. *J. Polym. Sci.* 1959, **38**, 479
- 4 Ito, E. and Okajima, S. *J. Polym. Sci. (B)* 1969, **7**, 483
- 5 Farrow, G. *Makromol. Chem.* 1960, **38**, 147

*Simple preparation of solvent cast films
for infra-red spectroscopy*

V. ROSSBACH AND D. NISSEN

For the characterization of man-made fibres from poly(ethylene terephthalate) (PET), nylon-6 and nylon-6,6, a rapid technique for substance preparation for the purpose of IR spectroscopy was needed. For this reason the already known methods for preparing polymer-films¹, requiring a lot of time and equipment, were improved as follows.

PET was dissolved in trifluoroacetic acid, polyamide in trifluoroethanol or formic acid at room temperature. In addition, PET could be dissolved in 1,1,2,2-tetrachloroethane at 120°C. Owing to the relatively high vapour pressure of the fluorinated solvents (CF₃COOH: 37.0°C at 191 mm Hg²; CF₃CH₂OH: 37.8°C at 84 mm Hg³) it was possible to remove them almost completely by drying in vacuum (see *Table 1*).

By casting the solutions on polyethylene-foil, previously soaked with the corresponding solvent, films were obtained which could be peeled off very easily, even when they were very thin or brittle. A preparation of the surface

benzene solution is identical with the *A*-type crystal of Binns *et al.*² is not correct; there may be a new crystalline form.

ACKNOWLEDGEMENT

We are pleased to acknowledge the considerable assistance rendered to us by Professor T. Seto of Tokyo Metropolitan University and Associate Professor Y. Hirose of Tokyo University.

*Faculty of Technology,
Tokyo Metropolitan University,
1-1 Fukazawa, 2-chome, Setagaya-ku,
Tokyo, Japan*

*(Received 7 December 1970)
(Revised 18 May 1971)*

REFERENCES

- 1 Goodman, I. *et al. Polymer, Lond.* 1960, **1**, 384
- 2 Binns, G. L. *et al. Polymer, Lond.* 1966, **7**, 583
- 3 Miyake, A. *J. Polym. Sci.* 1959, **38**, 479
- 4 Ito, E. and Okajima, S. *J. Polym. Sci. (B)* 1969, **7**, 483
- 5 Farrow, G. *Makromol. Chem.* 1960, **38**, 147

*Simple preparation of solvent cast films
for infra-red spectroscopy*

V. ROSSBACH AND D. NISSEN

For the characterization of man-made fibres from poly(ethylene terephthalate) (PET), nylon-6 and nylon-6,6, a rapid technique for substance preparation for the purpose of IR spectroscopy was needed. For this reason the already known methods for preparing polymer-films¹, requiring a lot of time and equipment, were improved as follows.

PET was dissolved in trifluoroacetic acid, polyamide in trifluoroethanol or formic acid at room temperature. In addition, PET could be dissolved in 1,1,2,2-tetrachloroethane at 120°C. Owing to the relatively high vapour pressure of the fluorinated solvents (CF₃COOH: 37.0°C at 191 mm Hg²; CF₃CH₂OH: 37.8°C at 84 mm Hg³) it was possible to remove them almost completely by drying in vacuum (see *Table 1*).

By casting the solutions on polyethylene-foil, previously soaked with the corresponding solvent, films were obtained which could be peeled off very easily, even when they were very thin or brittle. A preparation of the surface

Table 1 Content of solvent in polymer films

Compound	Thickness of film (μm)		% F	% Cl
	(A)	(B)		
Poly(ethylene terephthalate)	5	5.9-6.2	0.14	0.30
Nylon-6	10	12.2-14.0	0.33	-

(A) Mechanically determined; (B) determined by density

of the polyethylene-foil, as described for glass-plates (moistening with water, impregnation with a detergent or silicone fluid⁴), was unnecessary in view of the smaller surface adhesion.

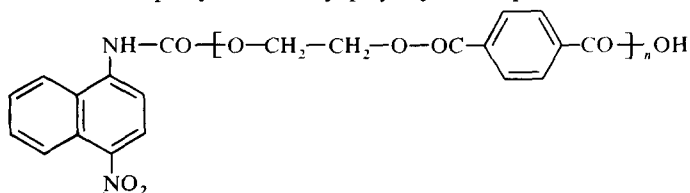
Since alcohols and organic acids cause polyethylene to swell, smooth films were not obtained due to the surface alteration. Therefore, inter-ferral effects were reduced.

With the technique described it was possible to rapidly produce clear films, free of wrinkles and solvents from polyamide- and PET-fibres and the corresponding end-group-modified-derivatives (see Table 2).

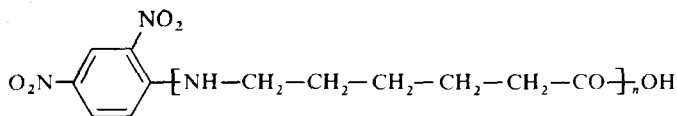
All spectra are characterized by excellent resolution and reproducibility.

Table 2 End-group-modified-derivatives of polyamides and PET (unpublished results)

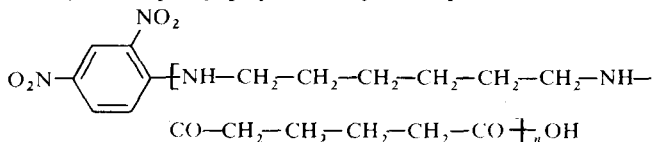
1. O-4-nitro-naphthyl-1-carbamoyl-polyethylene terephthalate



2. N-2,4-dinitrophenyl-polycapronamide



3. N-2,4-dinitrophenyl-polyhexamethylene adipamide



4. N-acetyl-polycapronamide-hydrazide resp.-hydroxamate

5. N-acetyl-polyhexamethylene adipamide-hydrazide

6. Nylon-6 and nylon-6,6 reactive dyed with Remazolbrilliantblau

EXPERIMENTAL

A polyethylene-foil (Lupolen 1810 D, without any additives, thickness of the foil 0.18–0.20 mm) is stretched over a glass-plate and then cleaned with chloroform and soaked with the corresponding solvent, being removed afterwards (for PET: 1,1,2,2-tetrachloroethane and trifluoroacetic acid; for polyamide and derivatives: trifluoroethanol and formic acid). The polymer solution (5–10%) is then cast and spread out with a glass-rod. After careful evaporation of the solvent in a stream of warm air the formed films are scratched with a razor-blade and then taken off with a small, elastic, self-adhesive IR-frame made from Hostalen. Thus the film adheres without any wrinkles before the hole (see *Figure 1*). A self-adhering layer on the Hostalen-frame could be obtained with double-adhesive Tesa-film.

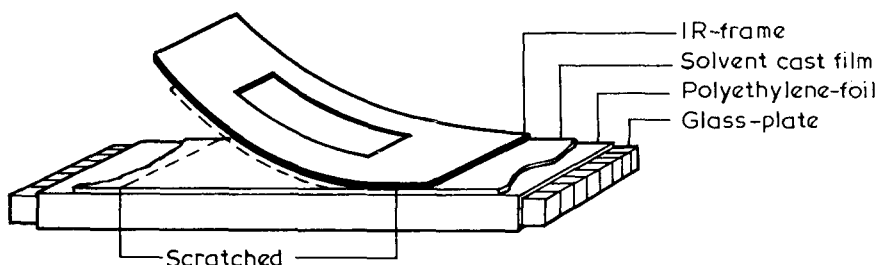


Figure 1 Removal of the film from the polyethylene foil

Removal of residual solvents, CF_3COOH , HCOOH , $\text{CF}_3\text{CH}_2\text{OH}$, CHCl_2 - CHCl_2 is then achieved by drying at 50°C (1 mm Hg) over potassium hydroxide, calcium chloride and paraffin, respectively. As the analyses of fluorine and chlorine show, the films are nearly free of solvents.

ACKNOWLEDGEMENTS

We wish to express our thanks to the 'Landesamt für Forschung beim Ministerium für Bildung und Wissenschaft des Landes Nordrhein-Westfalen' and the 'Verband der Chemischen Industrie' for their support of this work.

*Deutsches Wollforschungsinstitut an der
RWTH-Aachen,
Veltmanplatz 8,
51 Aachen, Germany*

(Received 13 April 1971)

REFERENCES

- 1 'Laboratory Methods in IR Spectroscopy' (Miller, R. G. -G. J., Ed.) Heyden, 1965, pp 43, 113.
- 2 Kauk, E. A. and Diesslin, A. R. *Ind. and Eng. Chem.* 1951, **43**, 2332
- 3 Private information from Th. Schuchardt G.m.b.H., Munich
- 4 Kemmer, G. 'I.r. Spektroskopie', Franckh'sche Verlagshandl., Stuttgart, 1969, p 96

*The temperature dependence of the optical anisotropy
of swollen polydimethylsiloxane rubber*

N. J. MILLS

In a previous publication¹ it was shown that the temperature dependence of the optical anisotropy of unswollen polydimethylsiloxane rubber is strong, and could not be satisfactorily explained in terms of the rotational isomeric chain model for this polymer². Recently it has become apparent that in bulk rubbers there is local ordering of polymer chains because of the high chain packing density³. In crosslinked polyethylene the measured optical anisotropy of Kuhn and Grün's⁴ statistical segment falls when the rubber is swollen with decalin, and the anomalously high temperature dependence of this quantity disappears⁵. Similarly in *cis*- and *trans*-1,4-polyisoprenes⁶ the optical anisotropy of the statistical segment falls on swelling with a solvent having geometrically isotropic molecules.

Samples of polydimethylsiloxane rubbers previously described¹ were swollen with tetrachloromethane (optically and geometrically isotropic). This has a refractive index $n_D^{20} = 1.466$ close to that of the polymer so that form birefringence is minimized. Isothermal stress-birefringence measurements were made on rubber strips in an oven through which passed a thermostatically controlled nitrogen stream. The optical anisotropy of a statistical segment γ_s was calculated from the birefringence Δn , the tensile stress t , the mean refractive index \bar{n} , and the absolute temperature T by

$$\gamma_s = \frac{\Delta n}{t} \frac{45}{2\pi kT} \frac{\bar{n}}{(\bar{n}^2 + 2)^2}$$

where k is Boltzmann's constant.

Figure 1 shows the data of segment anisotropy plotted against temperature

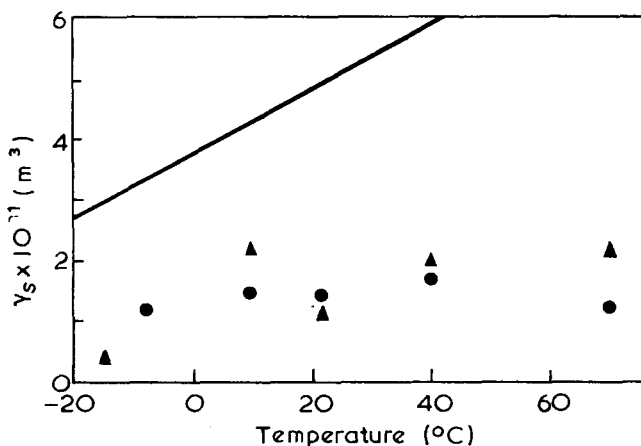


Figure 1 Segment optical anisotropy versus temperature for polydimethylsiloxane swollen with tetrachloromethane. \blacktriangle , 5% EP 5687 hydride crosslinked, \bullet , 10% EP 5687. The line represents data for slightly crosslinked unswollen polydimethylsiloxane

for two swollen polydimethylsiloxane rubbers prepared by silicon hydride crosslinking¹, the volume fraction rubber being 0.35 when the amount of the hydride containing component is 5%, and 0.71 when it is 10%. These data are compared with the marked temperature dependence for unswollen slightly crosslinked rubber. The segment optical anisotropy has decreased on swelling with tetrachloromethane (as noted by Tsvetkov⁷) and its temperature dependence has also decreased. A single result at 20°C for a lightly peroxide crosslinked sample with $V_f = 0.19$ was $\gamma_s = 1.0 \times 10^{-25} \text{ cm}^3$, so it must be concluded that the dependence of γ_s on the degree of crosslinking noticed for the unswollen rubber does not occur in the swollen rubber.

Given that the optical anisotropy of the monomer unit is not known, then the rotational isomeric model² of polydimethylsiloxane will now be capable of explaining the temperature dependence of the optical anisotropy of the swollen rubber. The ratio of *gauche* to *trans* rotational isomers increases with increasing temperature, causing both the chain dimensions and optical anisotropy to increase slowly. If this gradual uncoiling of the chains increases the short range orientational order in the unswollen rubber, this would explain the greater temperature dependence of optical anisotropy.

Increased crosslinking in the unswollen rubber decreases γ_s and its temperature dependence¹, presumably by destroying short range order rather than through non-Gaussian behaviour as previously suggested.

*Department of Physical Metallurgy
and Science of Materials,
University of Birmingham,
Birmingham 15, UK.*

(Received 19 May 1971)

REFERENCES

- 1 Mills, N. J. and Saunders, D. W. *J. Macromol. Sci.* 1968, **B2**, 369
- 2 Nagai, K. and Ishikawa, T. *J. Chem. Phys.* 1966, **45**, 3128
- 3 Robertson, R. E. *J. Phys. Chem.* 1965, **69**, 1575
- 4 Kuhn, W. and Grün, F. *Kolloid-Z.* 1942, **101**, 243
- 5 Gent, A. N. and Vickroy, V. V. *J. Polym. Sci. (A-2)* 1967, **5**, 47
- 6 Gent, A. N. *Macromolecules* 1969, **2**, 262
- 7 Tsvetkov, V. N. and Ye, A. *Grishchenko Polym. Sci. U.S.S.R.* 1965, **7**, 902

Book reviews

Reviews in macromolecular chemistry Vol. 5, Part 2

Edited by G. B. BUTLER, K. F. O'DRISCOLL and M. SHEN

Marcel Dekker, New York, 1970, 236 pp., £8.35

This volume, as was the case with those which preceded it, contains a survey of a number of interesting areas of research in macromolecular chemistry and physics. The particular subjects covered are ring-chain equilibria (H. R. Allcock), occupied volume of liquids and polymers (R. N. Haward), application of electron spin resonance techniques to high polymer fracture (H. H. Kausch-Blecken von Schmeling), science of determining copolymerization reactivity ratios (P. W. Tidwell and G. A. Mortimer) and block copolymers and related heterophase elastomers (G. M. Estes, S. L. Cooper and A. V. Tobolsky).

The first chapter draws attention to the wide-spread occurrence of ring-chain equilibria in polymer chemistry. The subject has become intimately associated with the practical problems of the stability of high polymers and particularly the high temperature behaviour of inorganic and heteroatom backbone polymers. Most of the important known examples are discussed and general observations are formulated. In recent years a number of theories have been proposed to describe the properties of polymers in the liquid state which make use of the concept of 'free volume'. The chapter on this subject describes the useful definitions of free volume and how this is related to the types of free volume theories being currently developed.

A new tool for the investigation of polymer fracture has been added with the development of microwave resonance absorption techniques and Chapter 3 reviews the identification of e.s.r. spectra obtained from ground polymers and fibres, the theory of thermo-mechanical activation of chain fracture and the influence of chain scission on crack initiation and growth on the surface energy and strength of fibres.

In spite of the wide usage of the concept of reactivity ratios in copolymerization studies much of the published data is only of qualitative significance. This review examines the correctness of published data, the reasons for inconsistencies in the published literature, and the best procedures for obtaining quantitative data.

Recently there has been considerable interest in heterophase systems which possess enhanced physical properties in the elastomeric state. This article reviews that part of the subject dealing with block polymers and deals with the morphological, mechanical and viscoelastic properties which arise from chemical composition, physical modification and deformation history. The review is a valuable critical summary of the growing literature in this new field.

The book as a whole is a valuable source of information on many new and important aspects of polymer science.

C. E. H. BAWN

Plastics and synthetic rubbers

by A. J. GAIT and E. G. HANCOCK

Pergamon Press, Oxford, 1970, 302 pp., £3.25

This book forms part of the Chemical Industry series published by Pergamon Press in their International Library of Science, Technology, Engineering and Liberal Studies and intended as teaching manuals.

An industrial bias appears intentional in the layout and presentation of material, the book commencing with a description of the more important polymer industrial companies and institutions together with a glossary explaining the industry's jargon.

High polymer synthesis mechanisms, their processing and fabrication methods, are explained in clear, simple terms together with an outline of the commoner techniques used to characterize the molecular weight and mechanical properties of these materials. A series of chapters cover phenolic, amino, unsaturated polyester, epoxy resins, and the polyurethanes each with respect to their basic chemistry, fabrication techniques, and product

outlets. This section forms a short, easily read description of the principal thermosetting plastics in common usage. In the same manner are covered the thermoplastics namely polyolefins, styrene-containing polymers, poly(vinyl chloride) and its copolymers, nylon, poly(vinyl acetate) and the like. Cellulose and casein are used as examples of natural plastics in commercial production and brief mention is made of natural resins such as shellac, rosin, bitumen, and lignin.

Elastomers are described in terms of their chemical structure and one common manufacturing polymerization process, some indication being given of the compounding and crosslinking systems necessary to transform them into useful rubbers. A brief glimpse of the future emerges at the end of the book when speciality polymers such as polyimides, poly(phenylene oxide), polysulphones and others are mentioned through the media of their chemical structure and one or two outstanding properties.

This book should fulfill its purpose in providing a simple, easily read text for the general reader whose objective is an introduction to plastic and rubber materials with their related technology. Each chapter contains a selected reading list, unfortunately older text books predominate and no references are made to the many standard works of polymer science and technology which would enable this field to be pursued in greater depth by readers wishing to specialize.

C. HEPBURN

Epoxide resins

by W. G. POTTER

Liffé Books, for the Plastics Institute, London, 1970, 248 pp., £4.50

Thermosets continue to receive much less attention than thermoplastics in the scientific literature, despite their great industrial importance. For that reason, an up-to-date survey of epoxide resins is welcome, and Dr Potter, who was for some years concerned with the marketing and development of these materials, is well qualified to write on this subject.

This monograph aims to cover both the science and technology of epoxide resins, primarily written for those studying for the professional examinations of the Plastics Institute. This may seem to be a limited target, but in fact, the book will be of interest to all those connected with this department of polymer technology, either as manufacturers, intermediaries or users. This represents a very wide sector of industry, as a glance at the contents of this book will show.

The treatment of the chemistry (so often the least satisfactory feature of this sort of book) is excellent, and provides most of the background information that the average reader will require. Generally speaking, the references stop short at 1968, but this is not a serious fault. One aspect of this sort of book is the extensive use of abbreviations. This is almost inevitable (and by no means to be deprecated) but it can lead to rather peculiar sentences such as the following (p 181): '... the aromatic amines such as DDM and the anhydrides HPA and NMA are systems needing elevated temperature curing, but providing higher HDT's ...' This is concise, and crystal clear to the expert, but the less knowledgeable reader may find it a bit forbidding. Dr Potter introduces in full each chemical which is described by an abbreviation, but after this has been done a few times the reader is left on his own. This is fair enough, and my only criticism is that the index is not fully cross-referenced for these compounds. For example, 'polyazelaic polyanhydride (PAPA)' is listed thus in the index, but there is no separate glossary in which to find PAPA, nor is PAPA indexed in its own right.

One problem in a book such as this on materials, is to maintain the correct balance between the chemistry, properties and applications. The chemistry, as I have said is well taken care of, as are the applications. This has led to some sacrifices of the treatment of properties, so that this is not the book to refer to for a detailed treatment of the mechanical or electrical properties of epoxide resins—such topics are beyond its scope. However, the various chemical and physical methods of modifying properties are given a separate chapter.

Nearly half the book is devoted to applications, with which Dr Potter has had a great deal of first-hand experience. He provides an excellent survey of what is a very wide field.

Book reviews

Reviews in macromolecular chemistry Vol. 5, Part 2

Edited by G. B. BUTLER, K. F. O'DRISCOLL and M. SHEN

Marcel Dekker, New York, 1970, 236 pp., £8.35

This volume, as was the case with those which preceded it, contains a survey of a number of interesting areas of research in macromolecular chemistry and physics. The particular subjects covered are ring-chain equilibria (H. R. Allcock), occupied volume of liquids and polymers (R. N. Haward), application of electron spin resonance techniques to high polymer fracture (H. H. Kausch-Blecken von Schmeling), science of determining copolymerization reactivity ratios (P. W. Tidwell and G. A. Mortimer) and block copolymers and related heterophase elastomers (G. M. Estes, S. L. Cooper and A. V. Tobolsky).

The first chapter draws attention to the wide-spread occurrence of ring-chain equilibria in polymer chemistry. The subject has become intimately associated with the practical problems of the stability of high polymers and particularly the high temperature behaviour of inorganic and heteroatom backbone polymers. Most of the important known examples are discussed and general observations are formulated. In recent years a number of theories have been proposed to describe the properties of polymers in the liquid state which make use of the concept of 'free volume'. The chapter on this subject describes the useful definitions of free volume and how this is related to the types of free volume theories being currently developed.

A new tool for the investigation of polymer fracture has been added with the development of microwave resonance absorption techniques and Chapter 3 reviews the identification of e.s.r. spectra obtained from ground polymers and fibres, the theory of thermo-mechanical activation of chain fracture and the influence of chain scission on crack initiation and growth on the surface energy and strength of fibres.

In spite of the wide usage of the concept of reactivity ratios in copolymerization studies much of the published data is only of qualitative significance. This review examines the correctness of published data, the reasons for inconsistencies in the published literature, and the best procedures for obtaining quantitative data.

Recently there has been considerable interest in heterophase systems which possess enhanced physical properties in the elastomeric state. This article reviews that part of the subject dealing with block polymers and deals with the morphological, mechanical and viscoelastic properties which arise from chemical composition, physical modification and deformation history. The review is a valuable critical summary of the growing literature in this new field.

The book as a whole is a valuable source of information on many new and important aspects of polymer science.

C. E. H. BAWN

Plastics and synthetic rubbers

by A. J. GAIT and E. G. HANCOCK

Pergamon Press, Oxford, 1970, 302 pp., £3.25

This book forms part of the Chemical Industry series published by Pergamon Press in their International Library of Science, Technology, Engineering and Liberal Studies and intended as teaching manuals.

An industrial bias appears intentional in the layout and presentation of material, the book commencing with a description of the more important polymer industrial companies and institutions together with a glossary explaining the industry's jargon.

High polymer synthesis mechanisms, their processing and fabrication methods, are explained in clear, simple terms together with an outline of the commoner techniques used to characterize the molecular weight and mechanical properties of these materials. A series of chapters cover phenolic, amino, unsaturated polyester, epoxy resins, and the polyurethanes each with respect to their basic chemistry, fabrication techniques, and product

outlets. This section forms a short, easily read description of the principal thermosetting plastics in common usage. In the same manner are covered the thermoplastics namely polyolefins, styrene-containing polymers, poly(vinyl chloride) and its copolymers, nylon, poly(vinyl acetate) and the like. Cellulose and casein are used as examples of natural plastics in commercial production and brief mention is made of natural resins such as shellac, rosin, bitumen, and lignin.

Elastomers are described in terms of their chemical structure and one common manufacturing polymerization process, some indication being given of the compounding and crosslinking systems necessary to transform them into useful rubbers. A brief glimpse of the future emerges at the end of the book when speciality polymers such as polyimides, poly(phenylene oxide), polysulphones and others are mentioned through the media of their chemical structure and one or two outstanding properties.

This book should fulfill its purpose in providing a simple, easily read text for the general reader whose objective is an introduction to plastic and rubber materials with their related technology. Each chapter contains a selected reading list, unfortunately older text books predominate and no references are made to the many standard works of polymer science and technology which would enable this field to be pursued in greater depth by readers wishing to specialize.

C. HEPBURN

Epoxide resins

by W. G. POTTER

Liffé Books, for the Plastics Institute, London, 1970, 248 pp., £4.50

Thermosets continue to receive much less attention than thermoplastics in the scientific literature, despite their great industrial importance. For that reason, an up-to-date survey of epoxide resins is welcome, and Dr Potter, who was for some years concerned with the marketing and development of these materials, is well qualified to write on this subject.

This monograph aims to cover both the science and technology of epoxide resins, primarily written for those studying for the professional examinations of the Plastics Institute. This may seem to be a limited target, but in fact, the book will be of interest to all those connected with this department of polymer technology, either as manufacturers, intermediaries or users. This represents a very wide sector of industry, as a glance at the contents of this book will show.

The treatment of the chemistry (so often the least satisfactory feature of this sort of book) is excellent, and provides most of the background information that the average reader will require. Generally speaking, the references stop short at 1968, but this is not a serious fault. One aspect of this sort of book is the extensive use of abbreviations. This is almost inevitable (and by no means to be deprecated) but it can lead to rather peculiar sentences such as the following (p 181): '... the aromatic amines such as DDM and the anhydrides HPA and NMA are systems needing elevated temperature curing, but providing higher HDT's ...' This is concise, and crystal clear to the expert, but the less knowledgeable reader may find it a bit forbidding. Dr Potter introduces in full each chemical which is described by an abbreviation, but after this has been done a few times the reader is left on his own. This is fair enough, and my only criticism is that the index is not fully cross-referenced for these compounds. For example, 'polyazelaic polyanhydride (PAPA)' is listed thus in the index, but there is no separate glossary in which to find PAPA, nor is PAPA indexed in its own right.

One problem in a book such as this on materials, is to maintain the correct balance between the chemistry, properties and applications. The chemistry, as I have said is well taken care of, as are the applications. This has led to some sacrifices of the treatment of properties, so that this is not the book to refer to for a detailed treatment of the mechanical or electrical properties of epoxide resins—such topics are beyond its scope. However, the various chemical and physical methods of modifying properties are given a separate chapter.

Nearly half the book is devoted to applications, with which Dr Potter has had a great deal of first-hand experience. He provides an excellent survey of what is a very wide field.

It is not a serious criticism to suggest that the chapter entitled 'Laminates' would better be described 'Composites'. In the field of materials science, it is preferable to confine the word laminates to two-dimensional arrangements of phases such as Formica.

The book is well produced and has been carefully edited. Bearing in mind today's inflated prices, it is good value for money at £4.50.

L. HOLLIDAY

Progress in polymer science, Vol. II

Edited by A. D. JENKINS

Pergamon Press, Oxford, 1970, 279 pp., £5.50. \$14.75

The second volume of this series comprises four articles. The first of these, by C. G. Eastmond, which reviews solid-state polymerizations, is not intended to be comprehensive and omits solid-state polymerization of aldehydes and solid-state polycondensations. The review is concerned mainly with the important aspects of solid-state polymerization and in particular the principles of the reaction mechanisms. In recent years there has been a significant advance in the preparation of heat-resistant polymers. One of the more important groups of these polymers is the polyazoles and the chemistry and properties of these materials (up to the end of 1965) is thoroughly reviewed in the second chapter (J. P. Critchley). The following article by L. Mandelkern discusses the thermodynamics and physical properties of polymer crystals formed from dilute solution. The special properties reviewed include density, enthalpy of fusion, infra-red absorption spectra, selective oxidation, crystallite size and thermodynamic stability. The experimental basis on which the major features of crystallite properties rest is clearly summarized and the chapter critically examines the origin of the properties and the need for further study. The final contribution by Johnson and Porter on gel permeation chromatography is largely devoted to the theory of the mechanism of separation and instrumentation and does not review the scope or application of the method to specific systems. This book is clearly written for the specialist reader. Each of the contributions deals with a recent advance in polymer science but the presentation is uneven in that some of the articles review only certain aspects of the subject under consideration.

C. E. H. BAWN

Polymer solutions

General Discussions of the Faraday Society, No. 49

Faraday Society, London, 1971, 290 pp., £7.00

This latest Discussion of the Faraday Society is a compilation of papers presented to a meeting of the Society held recently at the University of Manchester. This volume follows closely the usual format of the majority of previously published Faraday Society Discussions. There is an introductory lecture followed by presented papers on various aspects of the topic of the meeting, together with reported general discussion. It is axiomatic that this particular volume on polymer solutions is only likely to be of interest to the researcher in this or closely allied fields, and that the book is in general neither an introductory nor a comprehensive text on the subject of polymer solutions.

An exception to these remarks is the introductory lecture, the fifteenth Spiers memorial lecture given by Professor Flory on thermodynamics of polymer solutions. Here we have a very lucid, instructive and thought provoking dissertation on a topic by one of the great experts. I found the lecture made fascinating reading and I recommend all those who aspire to, or are concerned with polymer science to read this lecture.

There follows three sections labelled 'introductory', 'static properties of solutions' and 'dynamic properties of solutions' in which twenty-one individual papers on a number of allied topics are presented. The introductory section is concerned largely with theoretical models. Each section is followed by a reported general discussion which has the merit for the reader of highlighting difficult and/or controversial aspects of the presented papers.

It is not a serious criticism to suggest that the chapter entitled 'Laminates' would better be described 'Composites'. In the field of materials science, it is preferable to confine the word laminates to two-dimensional arrangements of phases such as Formica.

The book is well produced and has been carefully edited. Bearing in mind today's inflated prices, it is good value for money at £4.50.

L. HOLLIDAY

Progress in polymer science, Vol. II

Edited by A. D. JENKINS

Pergamon Press, Oxford, 1970, 279 pp., £5.50. \$14.75

The second volume of this series comprises four articles. The first of these, by C. G. Eastmond, which reviews solid-state polymerizations, is not intended to be comprehensive and omits solid-state polymerization of aldehydes and solid-state polycondensations. The review is concerned mainly with the important aspects of solid-state polymerization and in particular the principles of the reaction mechanisms. In recent years there has been a significant advance in the preparation of heat-resistant polymers. One of the more important groups of these polymers is the polyazoles and the chemistry and properties of these materials (up to the end of 1965) is thoroughly reviewed in the second chapter (J. P. Critchley). The following article by L. Mandelkern discusses the thermodynamics and physical properties of polymer crystals formed from dilute solution. The special properties reviewed include density, enthalpy of fusion, infra-red absorption spectra, selective oxidation, crystallite size and thermodynamic stability. The experimental basis on which the major features of crystallite properties rest is clearly summarized and the chapter critically examines the origin of the properties and the need for further study. The final contribution by Johnson and Porter on gel permeation chromatography is largely devoted to the theory of the mechanism of separation and instrumentation and does not review the scope or application of the method to specific systems. This book is clearly written for the specialist reader. Each of the contributions deals with a recent advance in polymer science but the presentation is uneven in that some of the articles review only certain aspects of the subject under consideration.

C. E. H. BAWN

Polymer solutions

General Discussions of the Faraday Society, No. 49

Faraday Society, London, 1971, 290 pp., £7.00

This latest Discussion of the Faraday Society is a compilation of papers presented to a meeting of the Society held recently at the University of Manchester. This volume follows closely the usual format of the majority of previously published Faraday Society Discussions. There is an introductory lecture followed by presented papers on various aspects of the topic of the meeting, together with reported general discussion. It is axiomatic that this particular volume on polymer solutions is only likely to be of interest to the researcher in this or closely allied fields, and that the book is in general neither an introductory nor a comprehensive text on the subject of polymer solutions.

An exception to these remarks is the introductory lecture, the fifteenth Spiers memorial lecture given by Professor Flory on thermodynamics of polymer solutions. Here we have a very lucid, instructive and thought provoking dissertation on a topic by one of the great experts. I found the lecture made fascinating reading and I recommend all those who aspire to, or are concerned with polymer science to read this lecture.

There follows three sections labelled 'introductory', 'static properties of solutions' and 'dynamic properties of solutions' in which twenty-one individual papers on a number of allied topics are presented. The introductory section is concerned largely with theoretical models. Each section is followed by a reported general discussion which has the merit for the reader of highlighting difficult and/or controversial aspects of the presented papers.

BOOK REVIEWS

All these sections require of the reader a not unconsiderable knowledge of the latest theoretical treatments of polymer behaviour in solution.

As a collection of papers which represent the latest trends in understanding polymer solution behaviour this volume priced at £7 will only be of interest to the researcher involved with polymers in solution. The introductory lecture, as is so often the case in Faraday Society Discussions, will interest a much larger scientific public. Perhaps at some future date the Faraday Society will publish a collection of such past general lectures. Such a volume would interest many of us

H. BLOCK

Heat transfer and vulcanization of rubber

by D. A. HILLS

Elsevier, London, 1971, 133 pp., £3.80

The Institution of the Rubber Industry encourages the preparation of specialist monographs and this book extends the series being designed to serve the needs of industrial rubber technologists by presenting in collected form various techniques found useful in determining heat transfer and vulcanization characteristics of rubber. Simple equations and graphical techniques requiring only the assistance of a slide rule are employed, it being assumed that, as yet, few technologists have computer facilities readily available.

A historical introduction to rubber vulcanization is followed by definitions and explanations of optimum cure, scorch, heat history, and the time-temperature dependence of chemical reactions occurring during cure. Most of the book (38 pages) concerns the manipulation of various equations and techniques suitable for the calculation of heat transfer and state of cure. Worked examples of specific heat transfer problems are detailed for the benefit of readers unfamiliar with these techniques. It would have extended the usefulness of this section if specific reference data had been quoted in the forms of tables giving thermal conductivity and diffusivity, specific heat, and density. A series of appendices of this nature would have been valuable in a book specifically concerned with heat transfer in this specialized application field.

Interpretation of vulcanization characteristics is discussed for Mooney, Curometer and Oscillating Disc Rheometers together with descriptions of other curemeters now finding application in industrial laboratories namely the Viscurometer, Cepar Apparatus and Agfa Vulcameter. These newer instruments have caused a quiet revolution over the past five years in the measurement and control of vulcanization parameters and especially useful is the description of all commonly available instruments in the one book.

Chapter 5 deals with practical curing processes relating the basic heat transfer theory and cure assessment techniques of earlier chapters to plant operational practice. All classical techniques are described as exemplified by stress-strain properties, porosity, free sulphur contents, swelling characteristics together with methods of calculating shrinkage, temperature gradients in thick-walled products, and similar.

This book is very readable being clearly and concisely written with good illustrations and logical layout. Binding and printing are of good quality but the index is poor. It is well worth the attention of practising rubber technologists both as a text book and simple reference work.

C. HEPBURN

Introduction to polymer chemistry

by RAYMOND B. SEYMOUR

McGraw-Hill, New York, 1971, 437 pp., £7.90

This book is intended as a text for final year undergraduate students majoring in chemistry or chemical engineering. We are told by the author that it has been classroom-tested in manuscript form for four successive years, and that many industrial chemists have also found it to be a useful reference work. It is the reviewer's impression that the author

It is not a serious criticism to suggest that the chapter entitled 'Laminates' would better be described 'Composites'. In the field of materials science, it is preferable to confine the word laminates to two-dimensional arrangements of phases such as Formica.

The book is well produced and has been carefully edited. Bearing in mind today's inflated prices, it is good value for money at £4.50.

L. HOLLIDAY

Progress in polymer science, Vol. II

Edited by A. D. JENKINS

Pergamon Press, Oxford, 1970, 279 pp., £5.50. \$14.75

The second volume of this series comprises four articles. The first of these, by C. G. Eastmond, which reviews solid-state polymerizations, is not intended to be comprehensive and omits solid-state polymerization of aldehydes and solid-state polycondensations. The review is concerned mainly with the important aspects of solid-state polymerization and in particular the principles of the reaction mechanisms. In recent years there has been a significant advance in the preparation of heat-resistant polymers. One of the more important groups of these polymers is the polyazoles and the chemistry and properties of these materials (up to the end of 1965) is thoroughly reviewed in the second chapter (J. P. Critchley). The following article by L. Mandelkern discusses the thermodynamics and physical properties of polymer crystals formed from dilute solution. The special properties reviewed include density, enthalpy of fusion, infra-red absorption spectra, selective oxidation, crystallite size and thermodynamic stability. The experimental basis on which the major features of crystallite properties rest is clearly summarized and the chapter critically examines the origin of the properties and the need for further study. The final contribution by Johnson and Porter on gel permeation chromatography is largely devoted to the theory of the mechanism of separation and instrumentation and does not review the scope or application of the method to specific systems. This book is clearly written for the specialist reader. Each of the contributions deals with a recent advance in polymer science but the presentation is uneven in that some of the articles review only certain aspects of the subject under consideration.

C. E. H. BAWN

Polymer solutions

General Discussions of the Faraday Society, No. 49

Faraday Society, London, 1971, 290 pp., £7.00

This latest Discussion of the Faraday Society is a compilation of papers presented to a meeting of the Society held recently at the University of Manchester. This volume follows closely the usual format of the majority of previously published Faraday Society Discussions. There is an introductory lecture followed by presented papers on various aspects of the topic of the meeting, together with reported general discussion. It is axiomatic that this particular volume on polymer solutions is only likely to be of interest to the researcher in this or closely allied fields, and that the book is in general neither an introductory nor a comprehensive text on the subject of polymer solutions.

An exception to these remarks is the introductory lecture, the fifteenth Spiers memorial lecture given by Professor Flory on thermodynamics of polymer solutions. Here we have a very lucid, instructive and thought provoking dissertation on a topic by one of the great experts. I found the lecture made fascinating reading and I recommend all those who aspire to, or are concerned with polymer science to read this lecture.

There follows three sections labelled 'introductory', 'static properties of solutions' and 'dynamic properties of solutions' in which twenty-one individual papers on a number of allied topics are presented. The introductory section is concerned largely with theoretical models. Each section is followed by a reported general discussion which has the merit for the reader of highlighting difficult and/or controversial aspects of the presented papers.

BOOK REVIEWS

All these sections require of the reader a not unconsiderable knowledge of the latest theoretical treatments of polymer behaviour in solution.

As a collection of papers which represent the latest trends in understanding polymer solution behaviour this volume priced at £7 will only be of interest to the researcher involved with polymers in solution. The introductory lecture, as is so often the case in Faraday Society Discussions, will interest a much larger scientific public. Perhaps at some future date the Faraday Society will publish a collection of such past general lectures. Such a volume would interest many of us

H. BLOCK

Heat transfer and vulcanization of rubber

by D. A. HILLS

Elsevier, London, 1971, 133 pp., £3.80

The Institution of the Rubber Industry encourages the preparation of specialist monographs and this book extends the series being designed to serve the needs of industrial rubber technologists by presenting in collected form various techniques found useful in determining heat transfer and vulcanization characteristics of rubber. Simple equations and graphical techniques requiring only the assistance of a slide rule are employed, it being assumed that, as yet, few technologists have computer facilities readily available.

A historical introduction to rubber vulcanization is followed by definitions and explanations of optimum cure, scorch, heat history, and the time-temperature dependence of chemical reactions occurring during cure. Most of the book (38 pages) concerns the manipulation of various equations and techniques suitable for the calculation of heat transfer and state of cure. Worked examples of specific heat transfer problems are detailed for the benefit of readers unfamiliar with these techniques. It would have extended the usefulness of this section if specific reference data had been quoted in the forms of tables giving thermal conductivity and diffusivity, specific heat, and density. A series of appendices of this nature would have been valuable in a book specifically concerned with heat transfer in this specialized application field.

Interpretation of vulcanization characteristics is discussed for Mooney, Curometer and Oscillating Disc Rheometers together with descriptions of other curemeters now finding application in industrial laboratories namely the Viscurometer, Cepar Apparatus and Agfa Vulcameter. These newer instruments have caused a quiet revolution over the past five years in the measurement and control of vulcanization parameters and especially useful is the description of all commonly available instruments in the one book.

Chapter 5 deals with practical curing processes relating the basic heat transfer theory and cure assessment techniques of earlier chapters to plant operational practice. All classical techniques are described as exemplified by stress-strain properties, porosity, free sulphur contents, swelling characteristics together with methods of calculating shrinkage, temperature gradients in thick-walled products, and similar.

This book is very readable being clearly and concisely written with good illustrations and logical layout. Binding and printing are of good quality but the index is poor. It is well worth the attention of practising rubber technologists both as a text book and simple reference work.

C. HEPBURN

Introduction to polymer chemistry

by RAYMOND B. SEYMOUR

McGraw-Hill, New York, 1971, 437 pp., £7.90

This book is intended as a text for final year undergraduate students majoring in chemistry or chemical engineering. We are told by the author that it has been classroom-tested in manuscript form for four successive years, and that many industrial chemists have also found it to be a useful reference work. It is the reviewer's impression that the author

has attempted, not entirely successfully, to serve the rather incompatible needs of both types of reader simultaneously.

Undeniably, a large amount of information has been packed into this book. The preparation, properties, characterization, processing and applications of polymers are covered in 16 chapters and two appendices, including chapters on natural and inorganic polymers, additives, test methods, historical and economic aspects. There are also several useful tables, approximately 1400 references (mainly to U.S. sources) and a good subject index.

High information content is generally achieved at the expense of readability, and the style in this case is, to say the least, terse and demanding, though the persevering reader is occasionally rewarded by the discovery of unusual or little known facts embedded in an otherwise dense and uniform matrix. In view of the range of topics treated there are relatively few (approximately 50) diagrams, and the fact that some of the graphical plots lack numerical labelling of axes diminishes their utility. The displays of chemical formulae are generally so encumbered with unnecessary hydrogen atoms as to obscure their essential significance. A more irritating feature is the absence of any numerical coupling between the text and the references listed at the end of each section. The latter provide the chief source of minor misprints, though some serious ones were noted in the rather inadequate chapter on Rheology and Solubility.

The author's treatment of certain important topics (e.g. the choice of interfacial polymerization to introduce the subject of polycondensation kinetics) may tend to confuse, rather than enlighten, some students. Elsewhere in the text occasional examples of misleading or disputable statements can be found. The more mathematical areas of polymer chemistry receive scant attention, a deficiency which some (though surely not chemical engineering students) may regard as a virtue.

As a reference text for those working outside the field of polymer chemistry, or used as a basis for supplementing student's notes, this book will undoubtedly find a place in many libraries, but one would hesitate to recommend it to undergraduates here as a suitable introduction to the subject.

The number of good general textbooks on polymer chemistry is exceedingly small; the reviewer reluctantly concludes that it remains essentially unchanged by the publication of this volume.

P. F. ONYON

BOOK REVIEWS

All these sections require of the reader a not unconsiderable knowledge of the latest theoretical treatments of polymer behaviour in solution.

As a collection of papers which represent the latest trends in understanding polymer solution behaviour this volume priced at £7 will only be of interest to the researcher involved with polymers in solution. The introductory lecture, as is so often the case in Faraday Society Discussions, will interest a much larger scientific public. Perhaps at some future date the Faraday Society will publish a collection of such past general lectures. Such a volume would interest many of us

H. BLOCK

Heat transfer and vulcanization of rubber

by D. A. HILLS

Elsevier, London, 1971, 133 pp., £3.80

The Institution of the Rubber Industry encourages the preparation of specialist monographs and this book extends the series being designed to serve the needs of industrial rubber technologists by presenting in collected form various techniques found useful in determining heat transfer and vulcanization characteristics of rubber. Simple equations and graphical techniques requiring only the assistance of a slide rule are employed, it being assumed that, as yet, few technologists have computer facilities readily available.

A historical introduction to rubber vulcanization is followed by definitions and explanations of optimum cure, scorch, heat history, and the time-temperature dependence of chemical reactions occurring during cure. Most of the book (38 pages) concerns the manipulation of various equations and techniques suitable for the calculation of heat transfer and state of cure. Worked examples of specific heat transfer problems are detailed for the benefit of readers unfamiliar with these techniques. It would have extended the usefulness of this section if specific reference data had been quoted in the forms of tables giving thermal conductivity and diffusivity, specific heat, and density. A series of appendices of this nature would have been valuable in a book specifically concerned with heat transfer in this specialized application field.

Interpretation of vulcanization characteristics is discussed for Mooney, Curometer and Oscillating Disc Rheometers together with descriptions of other curemeters now finding application in industrial laboratories namely the Viscurometer, Cepar Apparatus and Agfa Vulcameter. These newer instruments have caused a quiet revolution over the past five years in the measurement and control of vulcanization parameters and especially useful is the description of all commonly available instruments in the one book.

Chapter 5 deals with practical curing processes relating the basic heat transfer theory and cure assessment techniques of earlier chapters to plant operational practice. All classical techniques are described as exemplified by stress-strain properties, porosity, free sulphur contents, swelling characteristics together with methods of calculating shrinkage, temperature gradients in thick-walled products, and similar.

This book is very readable being clearly and concisely written with good illustrations and logical layout. Binding and printing are of good quality but the index is poor. It is well worth the attention of practising rubber technologists both as a text book and simple reference work.

C. HEPBURN

Introduction to polymer chemistry

by RAYMOND B. SEYMOUR

McGraw-Hill, New York, 1971, 437 pp., £7.90

This book is intended as a text for final year undergraduate students majoring in chemistry or chemical engineering. We are told by the author that it has been classroom-tested in manuscript form for four successive years, and that many industrial chemists have also found it to be a useful reference work. It is the reviewer's impression that the author

The geometry of twinning and phase transformations in crystalline polyethylene

M. BEVIS and E. B. CRELLIN

New theories of the crystallography of deformation twinning and phase transformations have been used to examine in detail for the first time the crystallography of twinning and phase transformation processes which have been reported to occur in crystalline polyethylene. Details of the analysis used for the prediction of the shear modes, the results of the application of the analysis and a detailed comparison of theoretical and published experimental results are presented.

1. INTRODUCTION

DEFORMATION TWINNING and stress-induced phase transformations are considered to be important modes of deformation in single crystal and bulk crystalline forms of polyethylene. Stress-induced phase transformations of the orthorhombic (D_{2h}^{16} - $Pnma$) form of polyethylene to the monoclinic (C_{2h}^3 - $C2/m$) form and $\{310\}$ and $\{110\}$ deformation twinning have been reported for both bulk and single crystal forms of polyethylene¹⁻⁶.

Kiho *et al*¹ have carried out the most detailed experimental study of the phase transformations and twinning processes which occur as a result of the deformation of polyethylene single crystals. In addition to some new shear modes Kiho *et al*¹ incorporated in their paper the shear modes published by Frank *et al*⁴ and Tanaka *et al*² to describe the operative phase transformations and twins which occur in crystalline polyethylene. In a more recent paper Seto *et al*³ presented the results of a more detailed examination of the transformation processes in the bulk form of polyethylene. The volumes of the unit cells of the orthorhombic and monoclinic forms of polyethylene are equal or very nearly equal and it was assumed in the papers by Kiho *et al*¹ and Tanaka *et al*³ that the shape deformation associated with the phase transformation process is a simple shear. At the time of publication of the results of the four investigations of the geometry of deformation modes in polyethylene¹⁻⁴ there were no procedures available for the systematic determination of shear modes which describe both deformation twinning and phase transformation shear processes which are most likely to be operative in a particular structure.

The recent publication of new theories of the crystallography of deformation twinning and phase transformations by Bevis and Crocker and co-workers⁷⁻¹⁰ now enables a systematic investigation of these shear systems to be made, and in this paper the theories are applied in detail for crystalline polyethylene.

In addition to being of value in relation to the classification of twinning and transformation systems in polyethylene this application serves as an example of the procedure which has to be used for investigating the crystallography of shear-like processes in any crystalline material.

In section 2 of the paper we describe the essential features of the analysis used for the prediction of the shear modes. In section 3 the analysis is applied to the stress-induced phase transformations which transform the orthorhombic structure illustrated in *Figure 1a* into the monoclinic structure illustrated in *Figure 1b*. The analysis is applied to deformation twinning in polyethylene in section 4, and in section 5 the results presented in sections 3 and 4 are compared with those obtained in previous investigations^{1,3,4} and with the available experimental observations.

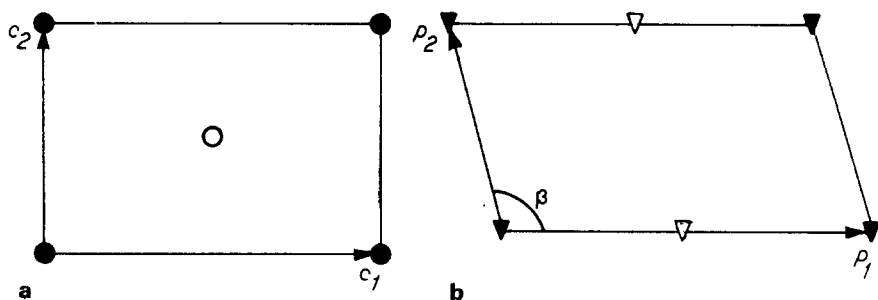


Figure 1 A projection of the primitive unit cell of polyethylene:

(a) Orthorhombic structure. The molecular chains are parallel to c_3 which is the lattice basis vector normal to the plane of the paper. \circ and \bullet each represent a $(\text{CH}_2-\text{CH}_2)$ molecular unit which differ only in orientation. The dimensions of the unit cell as determined by Bunn are given by the magnitudes of the lattice basis vectors c_1 , c_2 and c_3 which are 7.41 Å, 4.94 Å and 2.53 Å, respectively.

(b) Monoclinic structure (after Seto *et al*³). \triangle and \blacktriangle represent differently orientated $(\text{CH}_2-\text{CH}_2)$ molecular units. The basis vector p_3 is normal to the plane of the diagram. The dimensions of the unit cell are given by $p_1 = 8.09$ Å, $p_2 = 4.79$ Å, $p_3 = 2.53$ Å and $\beta = 107.9^\circ$

2. THE PREDICTION OF TWINNING AND TRANSFORMATION SHEAR MODES

It is convenient to categorize into six types the product lattices which can result when a lattice (the parent lattice) undergoes a simple shear. The six types are as follows:

- (1) A lattice identical with the parent lattice but with an orientation relation with the parent lattice of reflection in the shear plane or a rotation of π about the shear direction. The two types of orientation relation describe type I and type II twinning shears, respectively.
- (2) A lattice identical with the parent lattice but with an orientation relation different from those described in (1). This type of shear is termed a non-conventional twinning shear⁷.
- (3) A superlattice of the product lattice produced by the shear is identical to

a superlattice of the parent lattice and related to it by one of the orientation relations described in (1). If a primitive cell of the superlattice has a volume which is n times that of a primitive cell of the parent lattice then the shear is termed an $m = n$ twinning shear.

- (4) As for (3) but with an orientation relation of the type described in (2).
 (5) The parent lattice is sheared into a product lattice of the required lattice parameters which are different from that of the parent lattice.
 (6) The parent lattice is sheared to produce a lattice with a superlattice which is identical to a superlattice of the product lattice with the required lattice parameters. This type of transformation shear has an m value not equal to one.

The $\{310\}$ and $\{110\}$ twinning shear modes given by Frank *et al*⁴ to describe twinning in polyethylene are of category (2) and the transformation shear mode given by Tanaka *et al*² to describe the stress-induced phase transformation in polyethylene belongs to category (6). Examples of the six categories of shear systems described above are illustrated schematically in *Figure 2* for the case of two-dimensional square lattices. For shears of categories (3), (4) and (6) some lattice shuffles¹¹ are required to restore the sheared structure to the desired product structure. In the examples shown in *Figure 2* the modes of categories (3), (4) and (6) are $m = 2$ modes and the

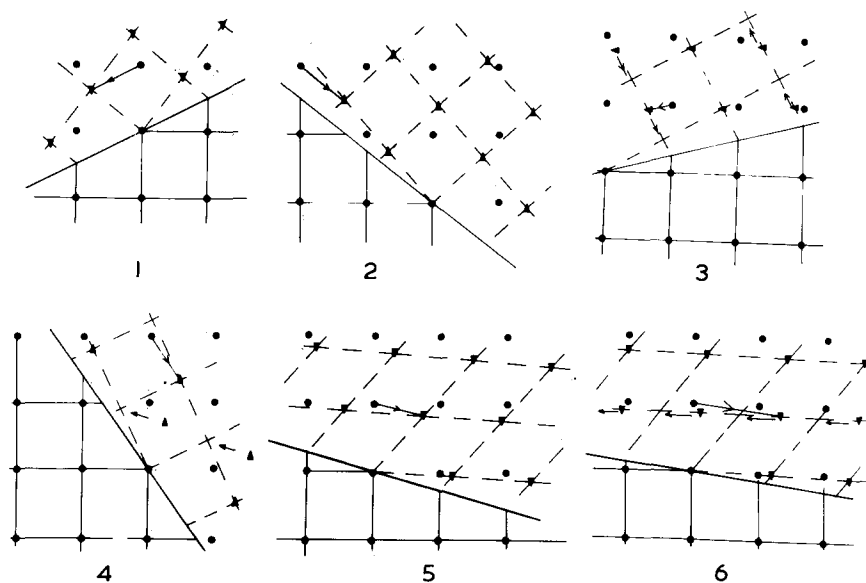


Figure 2 Plane of shear plots representing the six categories of product lattice which can result when a parent lattice undergoes a simple shear. The parent lattice in these examples is taken to be a square lattice of side a and is represented by \bullet . The product lattice is represented by \blacktriangle . The lattice shuffles which are required to restore the lattice for shears belonging to categories (3), (4) and (6) are indicated by arrows. The unit cell of the product lattice in (5) and (6) has edges of lengths $1.1a$ and $1.2a$ which describe an included angle of 63°

lattice shuffles are indicated by arrows. In assigning the term 'twinning shear' to a shear mode we have used the general definition of a twin given by Bilby and Crocker¹¹, that is, a deformation twin is a region of a crystalline body, which has undergone a homogeneous shape deformation in such a way that the product structure is identical with that of the parent, but oriented differently. Shear modes in categories (5) and (6) will be referred to as martensitic transformations^{10,12,13}. The shape change associated with a martensitic transformation is in general an invariant plane strain which in the case of no volume change reduces to a simple shear.

In a simple shear process the shear plane is both undistorted and unrotated and is therefore an invariant plane of the process. The shear plane is called the K_1 plane¹² and the shear direction is called the η_1 direction. The other undistorted but rotated plane of the shear process is called the K_2 plane, and the plane which is defined by the normals to the K_1 and K_2 planes is called the plane of shear. The η_2 direction is defined by the direction of intersection of the plane of shear and the K_2 plane. The collection of shear elements K_1 , K_2 , η_1 and η_2 is called a shear mode. The magnitude of the shear strain of the twinning shear is equal to $s = 2 \cot \phi$ where ϕ is the angle between the K_1 and K_2 planes. The parameters K_1 , K_2 , η_1 , η_2 , s and the plane of shear S are illustrated in Figure 3. The reciprocal shear mode has shear elements $K_1' = K_2$, $K_2' = K_1$, $\eta_1' = \eta_2$ and $\eta_2' = \eta_1$ with magnitude of the shear strain equal to that of the mode K_1 , K_2 , η_1 , η_2 .

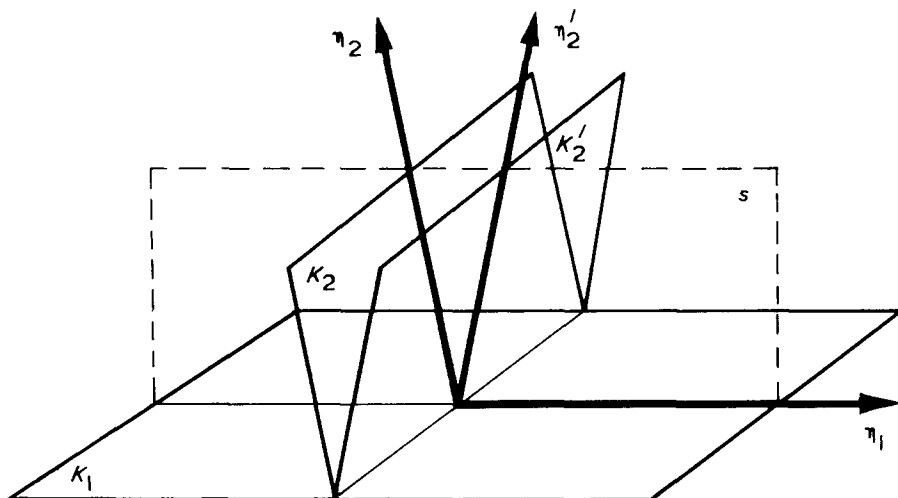


Figure 3 Schematic diagram illustrating the relative orientations of the parameters K_1 , K_2 , η_1 , η_2 , s and ϕ which define a shear mode

In this paper we describe a two-dimensional analysis which may be used for the determination of the shear modes giving rise to the six product lattice types described above. The analysis has been restricted to two dimen-

sions for the following reasons. The two-fold symmetry axis of the parent and product lattices of the phase transformation in polyethylene is invariant under the transformation. Further, the interplanar spacings of the planes normal to the two-fold axis are the same for both structures. Although in principle it is possible to shear the parent lattice to obtain the required product lattice by shearing in a direction other than in a plane normal to the two-fold axis and satisfy the requirements stated above, the severe restrictions placed on the form of the shear mode make this unlikely¹⁰. For convenience, contrary to the usual convention, the two-fold axis of the monoclinic structure has been labelled p_3 and the axis parallel to p_3 in the orthorhombic structure has been labelled c_3 . Thus $(001)_c$ is invariant under the transformation and the shear plane and shear direction must be of the forms $(hko)_c$ and $[kho]$, respectively. The $(001)_c$ and $(001)_p$ lattice planes have a one-fold stacking sequence so that the problem of considering ways of shearing the orthorhombic lattice into the monoclinic lattice within the requirements mentioned above is essentially two dimensional in character. The plane of shear of the transformation modes will always be the $(001)_c$ plane.

In crystalline polyethylene the chain molecules are parallel to c_3 and p_3 and it is unlikely that the covalently bonded chain axes will be extended by a transformation or twinning strain. Thus it is reasonable to restrict the investigation to those shear modes which leave the $[001]_c$ direction undistorted. This restriction is satisfied for transformation modes of the type discussed above. The general form of the elements of a shear mode which result from this requirement are that either K_1 or K_2 be of the form $(hko)_c$. There is no restriction on the form of η_1 and η_2 . In the case of twinning the restrictions placed on the shear modes are not as restrictive as in the case of transformations because the lattice bases of parent and product are identical except for their difference in orientation. Three-dimensional twinning modes have been determined using the Bevis-Crocker theory^{7,8} to investigate the possibility of twinning shears being operative in single crystals of polymers that could result in dimensional changes in the thickness of the crystal. These modes are presented in section 4 of this paper.

The form of the analysis used for studying the phase transformation follows closely that given by Crocker and Ross⁹ and described in detail by Acton *et al*¹⁰. The analysis is a generalization of the theory of the crystallography of deformation twinning due to Bevis and Crocker^{7,8}. Basically, the problem is as follows. In what ways is it possible to shear a parent two-dimensional lattice C defined by the vectors c_1 and c_2 with included angle α to become the product lattice P defined by p_1 and p_2 with included angle β . Let the lattice P be deformed into itself so that a lattice vector p of P will become Up where the deformation U when referred to the basis p_1, p_2 has components which are integers. If P is to be obtained from C by a simple shear and there is a 1:1 relationship between the lattice points of P and C , then the shear of a vector c given by Sc must be equal to RU_p where R represents a rigid body rotation. For a shear mode of type (6) it is clear that all of the components of U when U is referred to p_1, p_2 will not be integers. The exact form of the components for modes of a particular m value have been discussed previously⁷. If the components of U with respect to p_1, p_2 are

$$u_{ij} = \begin{pmatrix} u_{11} & u_{12} \\ u_{21} & u_{22} \end{pmatrix}$$

then it follows that the vector $[1, 0]_c$ is sheared to become the vector $[u_{11}, u_{21}]_p$, and the vector $[0, 1]_c$ becomes the vector $[u_{12}, u_{22}]_p$ after shear. Expressed in this way the matrix $U = (u_{ij})$ is the correspondence matrix of the transformation. Given the lattice parameters of the parent and product lattices, and the correspondence matrix U then the indices of the shear plane K_1 , shear direction η_1 and the magnitude of the shear strain s for the shear mode which will take the polyethylene orthorhombic lattice into the polyethylene monoclinic lattice are given by the following equations which are a particular two-dimensional form of equations given previously¹⁰. The indices of K_1 and η_1 are taken to be $(h_1, h_2, o)_c$ and $[u_1, u_2, o]_c$ respectively and in terms of u_{ij} are given by the solution of the following equation:

$$\begin{aligned} & \{(c_1)^2 - (p_1 u_{11})^2 - 2p_1 p_2 u_{11} u_{21} \cos \beta - (p_2 u_{21})^2\} (h_2/h_1)^2 - \\ & 2\{c_1 c_2 \cos \alpha - (p_1)^2 u_{11} u_{12} - p_1 p_2 (u_{21} u_{12} + u_{11} u_{22}) \cos \beta - \\ & (p_2)^2 u_{21} u_{22}\} (h_2/h_1) + \{(c_2)^2 - (p_1 u_{12})^2 - \\ & 2p_1 p_2 u_{12} u_{22} \cos \beta - (p_2 u_{22})^2\} = 0 \end{aligned} \quad (1)$$

There are two solutions to this quadratic equation which will be represented by $(h_1^+ h_2^+ o)$ and $(h_1^- h_2^- o)$. These two planes correspond to K_1 and K_2 so that the same correspondence matrix defines a twinning mode and the corresponding reciprocal mode. The full twinning elements for the twinning mode K_1, K_2, η_1, η_2 are

$$(h_1^+, h_2^+, o), (h_1^-, h_2^-, o), [\bar{h}_2^+, h_1^-, o], [\bar{h}_2^-, h_1^-, o]$$

where the relative signs of h_1^+, h_2^+, h_1^- and h_2^- are such that the angles $\phi, \angle K_1 \eta_2$ and $\angle K_2 \eta_1$ are all acute. There is a restriction on the correspondence matrices which can define a shear mode. The two dimensional form of this restriction called the shear criterion¹⁰ is given by¹⁰

$$\begin{aligned} & (c_2)^2 \{(p_1 u_{11})^2 + 2p_1 p_2 u_{11} u_{21} \cos \beta + (p_2 u_{21})^2\} + \\ & (c_1)^2 \{(p_1 u_{12})^2 + 2p_1 p_2 u_{12} u_{22} \cos \beta + (p_2 u_{22})^2\} \\ & = (c_1)^2 \{(p_2 u_{11}^{-1})^2 - 2p_1 p_2 u_{11}^{-1} u_{12}^{-1} \cos \beta + (p_1 u_{12}^{-1})^2\} + \\ & (c_2)^2 \{(p_2 u_{21}^{-1})^2 - 2p_1 p_2 u_{21}^{-1} u_{22}^{-1} \cos \beta + (p_1 u_{22}^{-1})^2\} \end{aligned} \quad (2)$$

where the elements u_{ij}^{-1} are the elements of the matrix U^{-1} which is the inverse of the matrix U . It may be readily shown that all two-dimensional correspondence matrices satisfy equation (2), so that there are an infinite number of ways of shearing one two-dimensional lattice into another. Equations (1) and (2) also apply for the case of twinning where $c_1 = p_1$, $c_2 = p_2$ and $\alpha = \beta$. The magnitude of the shear strain associated with the shear process is given by:

$$\begin{aligned} s^2 = & (c_1)^{-2} \{(p_1 u_{11})^2 + 2p_1 p_2 u_{11} u_{21} \cos \beta + (p_2 u_{21})^2\} + \\ & (c_2)^{-2} \{(p_1 u_{12})^2 + 2p_1 p_2 u_{12} u_{22} \cos \beta + (p_2 u_{22})^2\} - 2 \end{aligned} \quad (3)$$

Equation (3) provides a way of systematically investigating transformation and twinning shears because it relates the elements of the correspondence matrix to the magnitude of the shear strain. For example, for a square lattice the magnitude of shear of a twinning mode is given by $s^2 = (u_{11})^2 + (u_{12})^2 + (u_{21})^2 + (u_{22})^2 - 2$. Operative twinning and transformation modes have

always been observed to be associated with relatively small magnitudes of shear strain so that the operative modes are those to be predicted from matrices whose sum of the squares of elements is relatively small. A list of two-dimensional matrices which will predict all $m = 1$ square lattice shear modes with shears less than $(46)^{\frac{1}{2}}$ are given in *Table 1*. This table of matrices

Table 1 The two-dimensional unimodular correspondence matrices which define twinning shears in a square lattice with magnitude of shear $s < (46)^{\frac{1}{2}}$. When applied to a simple lattice basis the resulting shear modes will be $m = 1$ modes because the elements u_{ij} are integers

u_{11}	u_{12}	u_{21}	u_{22}
1	0	0	1
0	1	1	0
1	1	0	1
1	0	2	1
1	1	2	1
1	3	0	1
1	1	2	3
3	-1	-2	1
1	2	2	3
1	4	0	1
4	3	1	1
1	-3	-1	4
1	5	0	1
5	2	2	1
1	6	0	1
3	4	2	3
3	5	1	2
2	-5	-1	3
5	4	1	1
1	-4	-1	5

may also be used as the basic data for investigating shear modes in less symmetric lattices. It is necessary in such cases, however, to ensure that the range of matrices considered is sufficiently large to be sure of predicting all shear modes with magnitudes of shear less than the desired limiting value. The matrix variants obtained from each matrix in *Table 1* by interchanging matrix columns, matrix rows and the signs of rows and columns will give rise to crystallographically equivalent twinning modes in a square lattice. For lattices of less symmetry these operations give rise to correspondences

Table 2 Variants of a given correspondence for two-dimensional point lattices ($a \neq \beta$)

Lattice type	Notation	Variants
parallelogram	$u_{ij} (\alpha \beta) \pm \alpha, \pm \beta = 1, 2$	16
rectangular	$u_{ij} (\alpha \beta) \alpha, \beta = 1, 2$	4
diamond	$u_{ij} (\alpha \beta) \pm \alpha, \pm \beta = 1$	4
120° rhombus		
square	u_{ij}	1

which define shear modes which are not crystallographically equivalent. The non-crystallographically equivalent variants of a two-dimensional correspondence matrix are given in Table 2. α and β represent the column and row of the original matrix which constitute the first column and row respectively of the correspondence matrix which results from interchanging rows and columns.

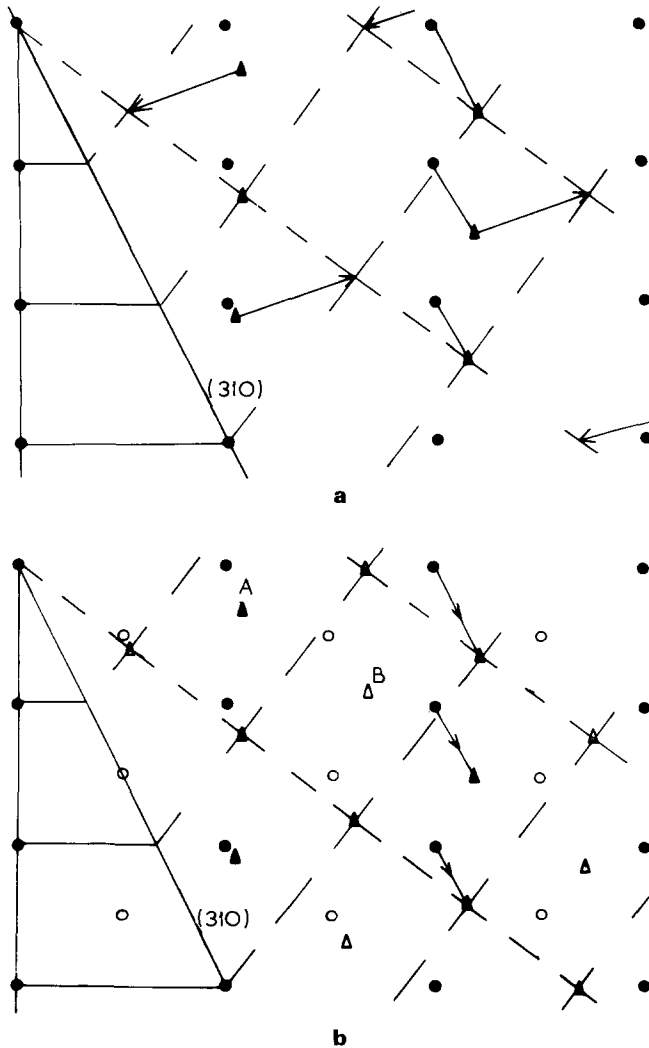


Figure 4 Plane of shear plot of the $\{310\}$ twinning mode:
 (a) As used by Frank *et al.*⁴ to describe $\{310\}$ twinning in polyethylene. Shuffles which are indicated by arrows are required to restore the lattice in a twin orientation.
 (b) When all $(\text{CH}_2-\text{CH}_2)$ molecular units are considered to shear individually. Lattice shuffles are not required to restore the lattice in this case if the molecular units undergo rotations

The above treatment of twinning and phase transformations only takes into account the space lattices of the parent and product structures. In geometrical treatments of the type described above which were developed initially to predict twinning and transformation modes in metal structures it is assumed that the motif unit shears as a whole and the structure is restored by atomic shuffles. The complexity of the shuffles will be determined to a large extent by the m value of the shear mode. As stated above the $\{310\}$ and $\{110\}$ twinning modes assigned by Frank *et al*⁴ to deformation twinning in polyethylene both have $m = 2$. The plane of shear plot of the $\{310\}$ mode is shown in *Figure 4a*. Lattice shuffles are required to restore the lattice in the orientation relationship of reflection in $\{310\}$ observed experimentally. However, if one considers each of the molecular units per lattice point to shear individually as shown in *Figure 4b* and as considered by Frank *et al*⁴ then the shuffles are quite simple. However, it must be stressed that like molecules do not all shuffle in the same way because the twinning mode is an $m = 2$ mode. To describe the twinning process in terms of dislocations it is necessary for unit twinning dislocations to propagate in pairs to ensure that the correct orientation relation results from the twinning process, i.e. it is necessary to introduce the concept of the zonal twinning dislocation. The

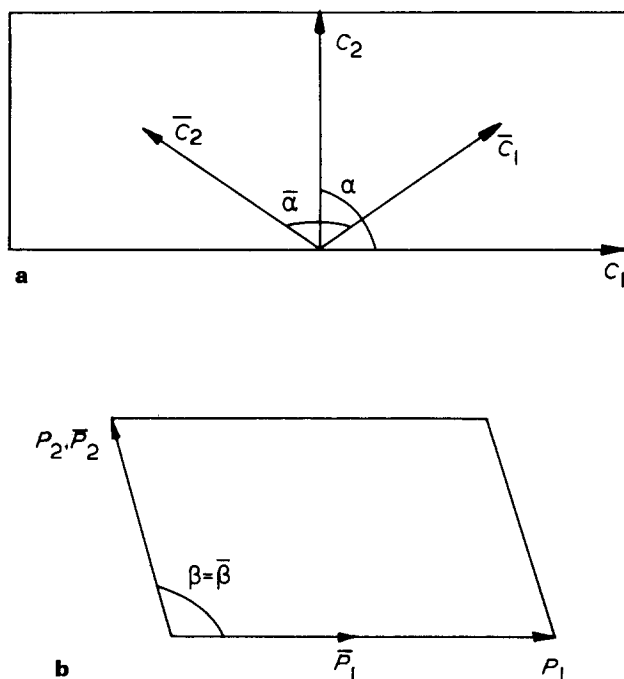


Figure 5 (a) Parent lattice basis vectors for both twinning and phase transformations. In the case of twinning the product lattice basis vectors are the same as for the parent lattice but differ in orientation: $c_1 = 7.41 \text{ \AA}$; $c_2 = 4.94 \text{ \AA}$; $\alpha = 90^\circ$; $\bar{c}_1 = \bar{c}_2 = 4.45 \text{ \AA}$; $\bar{\alpha} = 112.6^\circ$
 (b) The product lattice basis vectors for phase transformations:
 $p_1 = 2\bar{p}_1 = 8.09 \text{ \AA}$; $p_2 = \bar{p}_2 = 4.79 \text{ \AA}$; $\beta = \bar{\beta} = 107.9^\circ$

simplicity of the shuffle mechanism in *Figure 4b* indicates that it is valuable to consider in addition to the $m = 1$ modes for the simple orthorhombic lattice to also consider the $m = 1$ modes in the base-centred orthorhombic lattice which results if the difference in orientation of the molecular units A and B in *Figure 4b* is ignored. If all pairs of the (CH₂-CH₂) molecular units in *Figure 4b* are replaced by points then the resulting lattice of points is completely restored in a twin orientation relation by the {310} shear. The {310} twinning mode in this case may be compared directly with the operative {310} twinning mode in α -uranium which has a base-centred orthorhombic Bravais lattice. The same considerations also apply to the shear mode proposed by Tanaka *et al*² to account for the stress-induced phase transformation. In sections 3 and 4 the $m = 1$ shear modes are determined for the space lattice of the structure being considered and also for the lattice obtained when each of the (CH₂-CH₂) molecular units is replaced by a point. The sets of basis vectors used for the study of twinning and transformation shears are shown in *Figures 5a* and *5b* respectively. The pseudo-space lattice bases are indicated by \bar{c}_1, \bar{c}_2 and \bar{p}_1, \bar{p}_2 respectively. The transformation of correspondence from the lattice basis (U) to the pseudo-lattice basis (\bar{U}) may be shown to be:

$$\begin{pmatrix} \bar{u}_{11} & \bar{u}_{12} & 0 \\ \bar{u}_{21} & \bar{u}_{22} & 0 \\ 0 & 0 & 1 \end{pmatrix} = \begin{pmatrix} 1 & 1 & 0 \\ -1 & 1 & 0 \\ 0 & 0 & 1 \end{pmatrix} \begin{pmatrix} u_{11} & u_{12} & 0 \\ u_{21} & u_{22} & 0 \\ 0 & 0 & 1 \end{pmatrix} \begin{pmatrix} \frac{1}{2} & -\frac{1}{2} & 0 \\ \frac{1}{2} & \frac{1}{2} & 0 \\ 0 & 0 & 1 \end{pmatrix} \quad (4)$$

and

$$\begin{pmatrix} \bar{u}_{11} & \bar{u}_{12} & 0 \\ \bar{u}_{21} & \bar{u}_{22} & 0 \\ 0 & 0 & 1 \end{pmatrix} = \begin{pmatrix} 2 & 0 & 0 \\ 0 & 1 & 0 \\ 0 & 0 & 1 \end{pmatrix} \begin{pmatrix} u_{11} & u_{12} & 0 \\ u_{21} & u_{22} & 0 \\ 0 & 0 & 1 \end{pmatrix} \begin{pmatrix} \frac{1}{2} & -\frac{1}{2} & 0 \\ \frac{1}{2} & \frac{1}{2} & 0 \\ 0 & 0 & 1 \end{pmatrix} \quad (5)$$

for twinning and phase transformation respectively.

3. APPLICATION TO THE STRESS INDUCED PHASE TRANSFORMATIONS

The correspondence matrices listed in *Table 1* and the variants represented in *Table 2* have been used in equations (1), (2) and (4) to determine the $m = 1$ shear modes which generate the lattices P and \bar{P} from C and \bar{C} respectively. The correspondence matrices, the indices of the corresponding shear planes K_1 and K_2 with respect to the basis c_1, c_2 and the magnitudes of shears for those modes with magnitude of shear $s < 1$ are listed in *Table 3*. The shear mode will be referred to by the form given in the first column in the table where T indicates a transformation mode and the numerals 1-10 represent the place of the shear mode in the table. Subscripts 1 and 2 will be used in the text to distinguish between the mode listed and the reciprocal mode with elements $K'_1 = K_2, K'_2 = K_1$ etc. The correspondence matrices in columns 2 and 3 in *Table 3* are related by equation (5). A space in column 2 indicates that all molecular units are sheared to their correct positions but that the lattice is not restored by the shear. The true m value of the shear mode is

Table 3 Transformation shear modes with $s \leq 1$

N	U	\bar{U}	m	K_1	K_2	s
T1		1 0 0 1	2	1, 3.86, 0	-4.62, 1, 0	0.24
T2	1 0 1 1	-1 1 -1 0	1	1, 2.34, 0	16.66, -1, 0	0.35
T3	1 0 0 1		1	1, -2.34, 0	16.75, 1, 0	0.36
T4		0 1 -1 1	2	2.48, 1, 0	1.44, -1, 0	0.46
T5		-1 0 0 1	2	-1, 1.26, 0	1.28, 1, 0	0.78
T6	1 0 2 1		1	1, 1.264, 0	47.33, -1, 0	0.97
T7	1 0 -1 1	1 -1 0 1	1	48.6, 1, 0	1, -1.237, 0	0.99
T8	0 1 -1 1	1 1 0 1	1	-1.21, 1, 0	1, 1.52, 0	1.03
T9		1 0 -1 1	2	1.17, 1, 0	8.246, -1, 0	1.04
T10	0 1 1 0		1	1.22, 1, 0	-1, 1.566, 0	1.05

given in column 4 of *Table 3*. A space in column 3 indicates that the shear mode takes all lattice points to their correct positions, but that all molecular units are not sheared to their correct positions. A matrix in both columns 3 and 4 indicates that lattice points and molecular units are restored to their correct positions. The $(001)_c$ plane of shear plots of the transformation shear modes T1_{1,2}-T10_{1,2} are shown in *Figure 6*.

4. APPLICATION TO TWINNING

The correspondence matrices listed in *Table 1* and the variants listed in *Table 2* have been used to determine the $m = 1$ shear modes which generate twinned lattices from C and \bar{C} respectively. The deformation twinning shears D1_{1,2}-D6_{1,2} with magnitude of shear less than 1.5 are listed in *Table 4* in the

Table 4 Two-dimensional twinning shear modes with $s < 1.33$. D2₂, D4₁ and D6₂ restore the lattice to the identity

N	U	\bar{U}	m	K_1	K_2	η_1	η_2	s
D1		-1 1 0 1	2	310	$\bar{1}\bar{1}0$	$\bar{1}\bar{3}0$	110	0.25
D2	1 0 1 1		1	120	100	210	010	0.67
D3	0 1 1 0	-1 0 0 1	1	110	110	110	$\bar{1}10$	0.83
D4		1 1 0 1	2	$\bar{1}10$	1, 1.26, 0	110	$\bar{1}.26, 1, 0$	1.08
D5	-1 -1 1 0		1	1, 4.2, 0	3.37, 1, 0	$\bar{4}.2, 1, 0$	$\bar{1}, 3.37, 0$	1.3
D6	1 0 2 1	2 -1 1 0	1	110	100	$\bar{1}\bar{1}0$	010	1.33

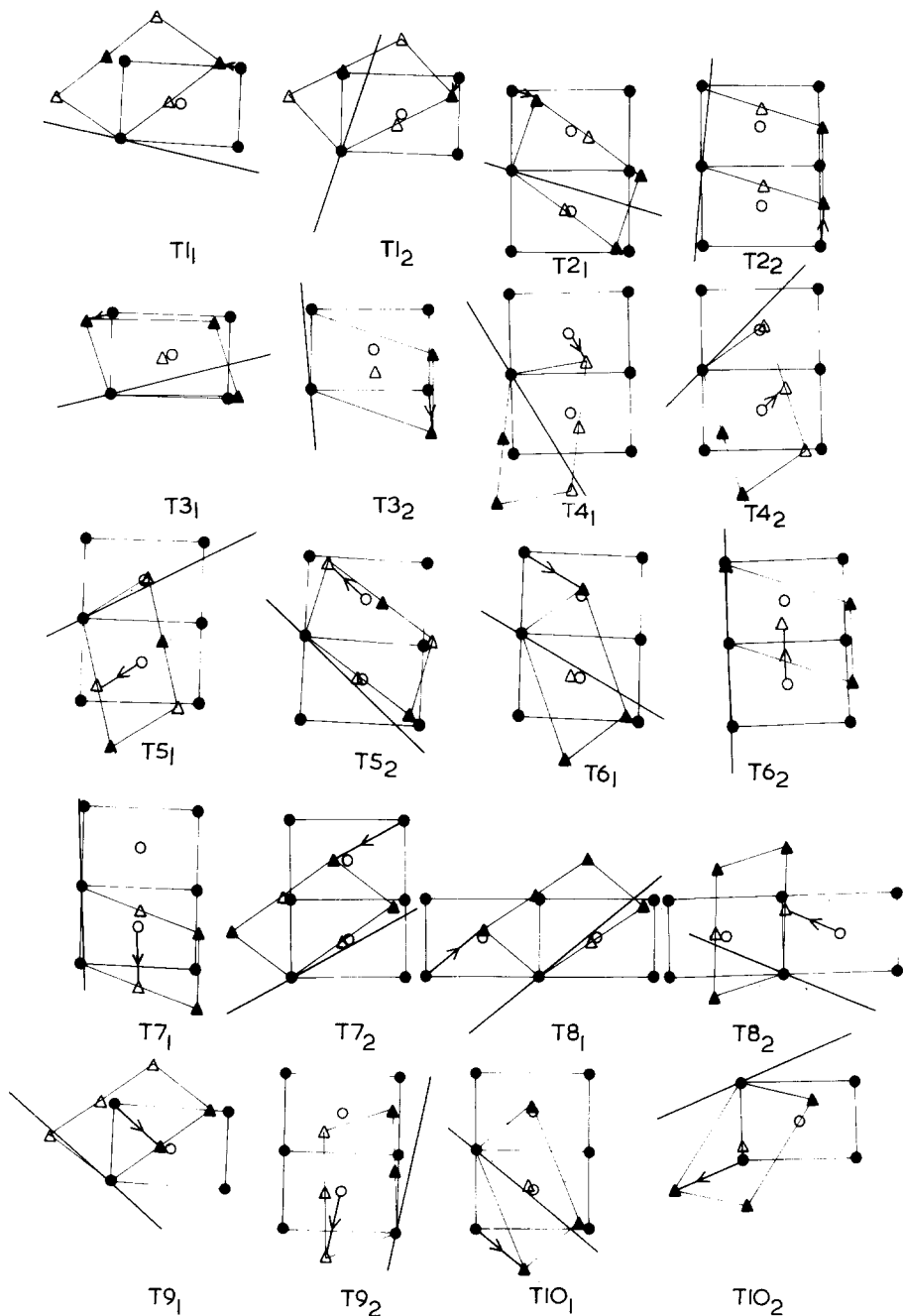


Figure 6 Plane of shear plots for the transformation modes $T_{11,2}$ - $T_{101,2}$. The (CH_2-CH_2) molecular units of the product structure are represented by \triangle and \blacktriangle . \bullet and \circ shear to \blacktriangle and \triangle respectively. In cases where the final distribution of triangles is different from that in either Figure 1b or when the \blacktriangle and \triangle in Figure 1b are interchanged, then the shear mode is an $m = 2$ mode. Lattice shuffles are required to restore the structure in such cases. This can occur if like molecules do not all shuffle in the same way

same way as the transformation shears are listed in *Table 3*. The $(001)_c$ plane of shear plots for the modes $D1_{1,2}$ – $D6_{1,2}$ are shown in *Figure 7*.

In addition to the two-dimensional twinning modes listed in *Table 4* the

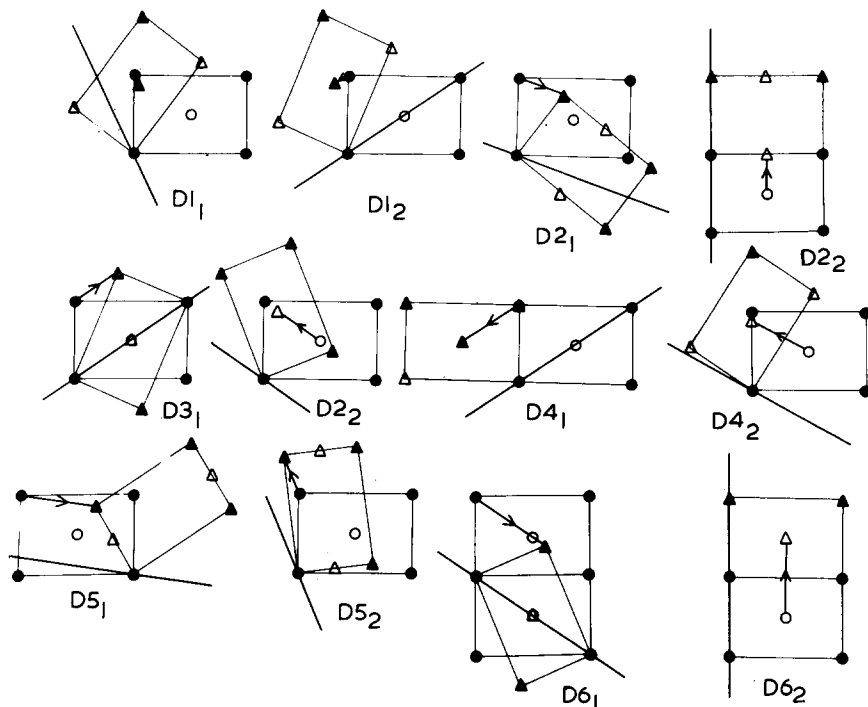


Figure 7 Plane of shear plots for the twinning modes $D1_{1,2}$ – $D6_{1,2}$. The $(\text{CH}_2\text{--CH}_2)$ molecular units of the product structure are represented by \triangle and \blacktriangle . \bullet and \circ shear to \blacktriangle and \triangle , respectively. In cases where the final distribution of triangles is different from that either *Figure 1a* or when the \blacktriangle and \triangle in *Figure 1a* are interchanged, then the shear mode is an $m = 2$ mode. Lattice shuffles are required to restore the structure in such cases.

This can occur if like molecules do not all shuffle in the same way

$m = 1$ three-dimensional twinning modes which leave $[001]_c$ undistorted have also been determined using the analysis described by Bevis and Crocker^{7,8}. The correspondence matrices which define such modes must be of the form

$$\begin{pmatrix} u_{11} & u_{12} & 0 \\ u_{21} & u_{22} & 0 \\ u_{31} & u_{32} & 1 \end{pmatrix}$$

and the resulting shear elements of the $m = 1$ modes with magnitude of shear $s < 1$ are listed in *Table 5*. The irrational twinning elements have been approximated to rational elements. Irrational elements are enclosed in

Table 5 Three-dimensional twinning shear modes with $s \leq 1.0$ and which leave $[001]_c$ undistorted

<i>N</i>	<i>U</i>	<i>K</i> ₁	<i>K</i> ₂	η_1	η_2	<i>s</i>	<i>Type</i>
1	100 010 101	102	100	$20\bar{1}$	001	0.34	compound (compound)
2	100 010 011	010	012	001	021	0.52	(compound) compound
3	100 010 111	110	112	001	'18, 44, $3\bar{1}$ '	0.62	(<i>II</i>), <i>I</i>
4	$\frac{1}{2}$ $-\frac{1}{2}$ 0* $-\frac{3}{2}$ $-\frac{1}{2}$ 0 $-\frac{1}{2}$ $-\frac{1}{2}$ 1	110	$51\bar{4}$	'31, $3\bar{1}$, 28'	132	0.67	<i>I</i> , <i>II</i>
5	100 010 201	101	100	$10\bar{1}$	001	0.69	compound (compound)
6	100† 110 101	001	'7, 11, 3'	110	$2\bar{1}1$	0.75	(<i>I</i>), <i>II</i>
7	100 010 211	210	212	001	'18, 22, $2\bar{9}$ '	0.86	(<i>II</i>), <i>I</i>
8	100† 110 201	100	'19, 18, 10'	012	$2\bar{1}\bar{2}$	0.96	(\bar{I}) $\bar{I}\bar{I}$
9	100 010 021	010	011	001	01 $\bar{1}$	1.03	(compound) compound
10	010 100 111	110	' $2\bar{3}1$ '	' $3\bar{3}7$ '	$11\bar{1}$	1.04	<i>I</i> , <i>II</i>

**m* = 2 mode

†*m* = 1 mode

inverted commas. The *m* = 1 mode also shears all molecular units to twin positions. For *m* = 2 mode all molecular units are sheared to correct twin positions. No symbol indicates an *m* = 1 mode in which only one-half of the molecular units are sheared to their correct twin positions. The twinning modes will be referred to by the letter and number given in the first column of the table together with a subscript 1 or 2 as for the modes listed in Tables 3 and 4. The orientation relation associated with a twinning mode is determined by the distribution of rational and irrational shear elements. In type *I* modes *K*₁ and η_2 are rational, and *K*₂ or η_1 , or both *K*₂ and η_1 are irrational. The orientation relation in this case is reflection in *K*₁ or rotation of π about the normal to *K*₁. In type *II* modes *K*₂ and η_1 are rational and *K*₁ or η_2 , or both *K*₁ and η_2 are irrational. The orientation relationship in this case is a rotation of π about η_1 or reflection in the plane normal to η_1 . The type of a twinning mode is given in the last column of Table 5, the first is the type for the mode indicated, and the second is the type of the reciprocal mode.

When all twinning elements are rational the mode is termed compound. Other distributions of rational and irrational twinning elements can arise^{7,8}. When all of the twinning elements are irrational the mode is termed non-conventional. Non-conventional twinning modes with K_1 and η_1 or K_2 and η_2 as irrational elements and with the remaining elements being rational can also arise. Examples of both types of non-conventional mode have been presented in *Table 4*. When the twin type in the last column of *Table 5* is enclosed in parentheses the shear process restores the lattice to the identity and is not therefore a possible operative mode.

5. COMPARISON OF PREDICTED MODES WITH EXPERIMENTAL RESULTS

The lattice parameters of the martensitic phase in polyethylene have been determined by Tanaka *et al*³, and they have been quoted in section 1 of this paper. The dimensions of the electron diffraction patterns obtained from deformed single crystals of polyethylene correspond closely to the lattice parameters determined from bulk polyethylene³. It is reasonable therefore to assume that the structures of the product phases of the two-phase transformations reported by Kiho *et al*¹ are the same as those determined for the phase transformation observed by Tanaka *et al*³ in bulk polyethylene. The orientation relations between the parent orthorhombic and product monoclinic phases as determined by Kiho *et al*¹ and measured from diffraction patterns in their paper are as follows:

Transformation

$$\begin{aligned} \text{Type } I: \quad \angle(0\bar{1}0)_p(1\bar{1}0)_c &= I_1 = 0^\circ \pm 1^\circ \\ \angle(200)_p(110)_c &= I_2 = 3^\circ \pm 1^\circ \\ \angle(2\bar{1}0)_p(200)_c &= I_3 = 5^\circ \pm 1^\circ \end{aligned}$$

$$\begin{aligned} \text{Type } III: \quad \angle(010)_p(110)_c &= III_1 = 0^\circ \pm 1^\circ \\ \angle(220)_p(0\bar{2}0)_c &= III_2 = 0^\circ \pm 1^\circ \\ \angle(2\bar{1}0)_p(1\bar{1}0)_c &= III_3 = 7^\circ \pm 1^\circ \end{aligned}$$

Kiho *et al*¹ called the phase transformations in polyethylene type *I* and type *III* following the occurrence of each phase for particular directions of applied stress in the single crystal deformation experiments. We have adopted this notation here and have also used it to identify the angles which specify the observed orientation relations. The shear modes which were predicted in section 3 may be readily compared with the experimental results on noting that for phases *I* and *III* the planes $(010)_p$ and $(1\bar{1}0)_c$ and $(110)_c$ respectively, are parallel.

Tanaka *et al*² used* only transformation mode $T1_1$ in the form of a plane of shear plot to explain the crystallography of the phase transformation *I*. There is no relation between the mode $T1_1$ and a $\{310\}$ shear process as

*It is to be noted, however, that Seto *et al* in their later paper³ did consider mode $T1_2$ as a possible explanation of the phase transformation

implied by Tanaka *et al*². The correspondence matrix which defines the mode T1₁ is, for example, not related in any way to the correspondence which defined the {310} twinning mode described by Frank *et al*⁴. The orientation relation, between the parent and product phase for mode T1₁ is given by $I_1 = 7^\circ$, $I_2 = 2.5^\circ$, $I_3 = 12.5^\circ$ and does not correspond very closely with that observed experimentally. The mode T1₁ which has also been used by Kiho *et al*¹ to explain transformation *I* is open to question if the shape deformation associated with the transformation process is a simple shear. The following transformation modes correspond more closely to transformation *I* than mode T1₁

	I_1	I_2	I_3
T7 ₂	1°	3°	5°
T8 ₁	1°	5.5°	3°
T9 ₁	5°	1°	8.5°

The modes T7₂ and T8₁ correspond very closely to the observed experimental relations and are probably within experimental error of the results reported by Kiho *et al*¹. The modes T7₂ and T8₁ are more favourable as operative modes if restoration of the product lattice is an important factor. Both T7₂ and T8₁ are $m = 1$ modes and in addition all (CH₂—CH₂) units are sheared to their correct positions by the shear. The modes T7 and T8 have large magnitudes of shear strain compared with mode T1 and if either of these modes are operative they could account for the change in single crystal dimensions far more readily than T1 and therefore reduce the requirement for other modes of deformation to be operative. Operative deformation twinning modes in general have a small magnitude of shear and a small value of m and it is therefore rather surprising that such high magnitudes of shear strain be operative in the formation of the monoclinic phase.

A comparison of the orientation relations associated with transformation *III* and the orientation relations associated with the transformation modes predicted in section 3 shows that the following modes correspond very closely with the experimental results:

	III_1	III_2	III_3
T2 ₁	2°	2°	9°
T5 ₂	1°	2°	7°

Kiho *et al*¹ did not give the magnitude of the shear strain or the shear elements of the transformation mode they used to describe transformation *III*. However, the diagrams they used to explain the transformation could correspond to mode T2₁.

Transformation mode T2₁ is an $m = 1$ mode and all (CH₂—CH₂) units are sheared to their correct positions. This mode differs from the mode T1₁ which was used by Kiho *et al*¹ and Tanaka *et al*² to explain transformation *I* in that in the case of T2₁ the space lattice is restored by the shear. Thus all like (CH₂—CH₂) units undergo the same displacements which would appear to be more acceptable than the case where they do not.

The orientation relations between the two phases is best described by mode T_{5_2} . Although all lattice points are restored to their correct positions by the shear some molecular-unit shuffles are required to restore the structure as in the case of mode T_{1_1} used by Tanaka *et al*² to explain transformation *I*. It is not possible to uniquely assign shear modes to the transformations *I* and *III* because of the multiplicity of modes which are consistent with the experimentally determined orientation relations. This problem of assignment of shear modes to the transformations is discussed further in section 6.

Deformation twinning has been reported to occur in single crystals, see, for example, Kiho *et al*¹ and more recently Geil⁶, and is associated with the orientation relations of reflection in $\{110\}$ and $\{310\}$. $\{110\}$ twinning is the predominant form of twinning in single crystals of polyethylene. A detailed discussion of the shear elements which are consistent with the observed orientation relationships has been given by Kiho *et al*¹. However, these authors did not determine all of the possible twinning modes which are consistent with a small shear, and considered only the modes D_1 , D_2 and D_6 of Table 4.

The twinning modes D_{1_1} and D_{1_2} were introduced by Frank *et al*⁴ to explain twinning in bulk polyethylene for which both twin orientation relations have been observed, see for example Tanaka *et al*¹⁴. These modes do not restore the orthorhombic lattice in a new orientation but do restore all (CH_2-CH_2) units to their correct positions, and are associated with the smallest magnitude of twinning shear strain of all the modes that we have determined. If the $\{110\}$ fold plane is to remain undistorted as a result of a twinning shear then both D_{1_1} and D_{1_2} satisfy this criterion as in the case of D_{1_1} the K_2 (undistorted but rotated) plane of the shear process is a $\{110\}$ plane. Thus (110) and (310) twinning could be operative in the (110) sectors of a crystal and leave the fold plane undistorted. Modes D_{3_1} and D_{3_2} were not considered by Kiho *et al*¹ yet satisfy completely the requirements for restoring the lattice and the (CH_2-CH_2) molecular units correctly and also leave both (110) and $(1\bar{1}0)$ folds undistorted as K_1 and K_2 are of the form $\{110\}$. The modes D_{3_1} and D_{3_2} which are crystallographically equivalent would therefore be expected to be able to propagate from one $\{110\}$ sector to another. Kiho *et al*¹ considered modes D_6 to also be likely operative modes. Although the magnitudes of the shear strains for these modes are large it is to be noted that mode D_{6_1} could propagate in both (110) and (100) type sectors, without distorting the fold plane. The (100) fold plane would be rotated by the (110) shear. It is to be noted that D_{6_2} restores the lattice to the identity and is therefore a degenerate form of twinning which can be related to simple slip shear. Modes D_4 and D_5 are of interest in that they are not compound modes. It should be noted that modes D_{4_1} , D_{4_2} , D_{5_1} and D_{5_2} are non-conventional in that they are associated with orientation relations which are not equivalent to a rotation of π about η_1 or reflection in K_1 yet both shears restore the original lattice in a new orientation. Mode D_4 has a $\{110\}$ shear plane and would appear to be a possible description of $\{110\}$ twinning. However, mode D_{4_1} is a degenerate type of non-conventional twinning shear which restores the lattice to the identity. As stated in section 2 it is possible to shear a polyethylene crystal in a direction other than that contained in the $(001)_c$ plane and to leave $[001]_c$ undistorted. The three-

dimensional twinning modes which satisfy this restriction are listed in *Table 5*. Twinning modes 4_1 and 10_1 of *Table 5* are consistent with an orientation relation of reflection in $\{110\}$. However, the most likely descriptions of $\{110\}$ twinning in polyethylene, which is the predominant twinning mode, are given by $D1_2$ and $D3_1$ – $D3_2$ when consideration of such variables as magnitude of shear strain, complexity of shuffles and fold plane requirements are taken into account. As in the case of phase transformations it is not possible to assign a unique shear mode to the $\{110\}$ twinning process.

6. CONCLUDING REMARKS

The results of a detailed investigation of the crystallography of shear-like processes in the polyethylene crystal structure have been presented. A description of the procedure used for predicting the shear modes which describe twinning and transformation processes has also been presented. The procedure could be applied to any crystal structure. It must be stressed that both the parent and product lattice parameters have been used as data and all that has been determined are the ways of shearing the parent lattice into the product lattice. The orientation relations between parent and product lattices which are given for any predicted mode may be compared with the orientation relations determined experimentally. When there is correspondence between experiment and theory then the predicted shear mode is a possible macroscopic description of the shear process. In section 5 it was shown that for transformations *I* and *III* and for $\{110\}$ deformation twinning there is a multiplicity of shear modes which describe each of the observed orientation relations. To uniquely assign a shear mode to a transformation or twinning shear process it is necessary to obtain in addition to agreement between the experimentally and theoretically determined orientation relations, agreement between the experimentally and theoretically determined magnitude of shear strain and shear plane.

It is not possible to compare experiment and theory in this way for the previously published experimental results. Detailed electron microscopy studies of deformed polyethylene single crystals which are currently in progress¹⁵ should enable a more definitive comparison of experimental results and the shear modes predicted in this paper to be carried out. The aim of the transmission electron microscopy investigation is to establish that the shape change associated with the transformation and twinning processes which result from the deformation of crystalline polyethylene is a simple shear or more generally in the case of transformations an invariant plane strain. An attempt will also be made to determine the shear planes and magnitude of the shear strains associated with the shear processes. In addition it is hoped that the investigation will indicate whether or not a transformation microstructure is associated with the transformation process in polyethylene. Such microstructures are often operative in transformations in metallic materials¹⁶ and a consequence of this is that any theory of the crystallography of transformation processes must make allowance for the presence of the microstructure. Theories which take into account a multiplicity of microstructures as well as the volume change associated with the trans-

formation process are now well established^{10,12,13,17,18}. Only when the characteristics of phase transformations discussed above have been established will it then be realistic to consider a more detailed mechanistic model for the transformation processes in polyethylene.

ACKNOWLEDGEMENTS

Financial support from the Science Research Council is acknowledged by the authors. E.B.C. is indebted to the University of Liverpool for the award of a research studentship. The authors would like to take the opportunity of thanking Drs A. G. Crocker and N. D. H. Ross for some past co-operative studies and discussions, which have contributed considerably to the investigation reported in this paper.

*Department of Metallurgy and Materials Science,
University of Liverpool,
Liverpool L69 3BX, UK*

(Received 24 March 1971)

(Revised 21 April 1971)

REFERENCES

- 1 Kiho, H., Peterlin, A. and Geil, P. H. *J. Appl. Phys.* 1964, **35**, 1599.
- 2 Tanaka, K., Seto, T. and Hara, T. *Reports Prog. Polym. Phys. Japan* 1963, **6**, 293
- 3 Seto, T., Hara, T. and Tanaka, K. *Japan J. Appl. Phys.* 1968, **7**, 31
- 4 Frank, F. C., Keller, A. and O'Connor A. *Phil. Mag.* 1958, **3**, 64
- 5 Geil, P. H. *J. Polym. Sci. (A-2)* 1964, **2**, 3813
- 6 Geil, P. H. and Haas, K. *J. Polym. Sci. (A-2)* 1966, **4**, 289
- 7 Bevis, M. and Crocker, A. G. *Proc. Roy. Soc. (A)* 1968, **304**, 123
- 8 Bevis, M. and Crocker, A. G. *Proc. Roy. Soc. (A)* 1969, **313**, 509
9. Crocker, A. G. and Ross, N. D. H. in 'The Mechanism of phase transformations in crystalline solids', Institute of Metals, London, 1969, p. 176
- 10 Acton, A. F., Bevis, M., Crocker, A. G. and Ross, N. D. H. *Proc. Roy. Soc. (A)* 1970, **320**, 101
- 11 Bilby, B. A. and Crocker, A. G. *Proc. Roy. Soc. (A)* 1965, **228**, 240.
- 12 Christian, J. W. 'The theory of transformations in metals and alloys', Pergamon Press, Oxford, 1965
- 13 Wayman, C. M. 'Introduction to the crystallography of martensitic transformations', Macmillan, New York, 1964
- 14 Tanaka, K., Seto, T., Hara, T. and Tajima, Y. *Reports Prog. Polym. Phys. Japan* 1964, **7**, 63
- 15 Allan, P. and Bevis, M. (work in progress)
- 16 Rowlands, P. C., Fearon, E. O. and Bevis, M. *J. Materials Sci.* 1970, **5**, 769

Molecular-weight distribution and long-chain branching of low-density polyethylene

JOSEPH MILTZ and ARIE RAM

The molecular-weight distribution curves, indices and frequencies of long-chain branching for some samples of low-density polyethylenes were obtained. The study was based on intrinsic viscosity data of the whole polymer and on gel permeation chromatography distribution curves, both for 1,2,4-trichlorobenzene solutions at 130°C. A correlation between the index of long-chain branching and the first molecular-weight dispersion index (ratio between weight and number average molecular weights) has been postulated. Results are limited to two models for branching used in this work.

INTRODUCTION

LOW-DENSITY polyethylene (LDPE) has been extensively studied with a view to determining its molecular structure—in particular the molecular-weight distribution (MWD) and the degree of long-chain branching (LCB), two parameters apparently of major importance in determining flow properties and physical behaviour. Efforts were devoted either to the measurement of various molecular-weight averages and to the calculation of branching indices of the whole polymers¹⁻⁴ or to similar studies based on fractions⁵⁻¹². Since the advent of the gel permeation chromatograph (g.p.c.), the MWD analysis of polyethylene has been extended and refined¹³⁻¹⁶.

The difficulty in exact characterization of LDPE is due to the influence of the LCB on the experimental distribution curve of the g.p.c., the elution volume being related to the hydrodynamic apparent volume of the polymer chain (V) rather than to its mass (M).

The modified Einstein equation:

$$[\eta] = \frac{KV}{M} \quad (1)$$

(where $[\eta]$ = intrinsic viscosity) leads to the conclusion that the product $[\eta]M$ should be uniquely related to the volume of any polymer chain, linear or branched. The concept of universal calibration of the g.p.c. by correlating the product $[\eta]M$ with the elution volume (V_e) has recently been adopted by several workers¹⁷⁻¹⁹. This correlation is valid only for the given system, namely the number and type of the columns, the solvent and the temperature. In the case of linear polymers there is usually no need for measuring the intrinsic viscosity, provided a reliable equation of the Mark-Houwink type (equation 2) is available for conditions (temperature and solvent) identical to those of the g.p.c.:

$$[\eta] = K M^a \quad (2)$$

Thus for linear polymers the universal curve yields the molecular weight

directly. For polymers with long-chain branching (such as LDPE), however, there is no single Mark-Houwink equation owing to the decrease of the hydrodynamic chain volume with the degree of LCB. The effect of the latter is allowed for through the factor g , defined as the ratio of the mean square radius of gyration of a branched chain and that of a linear one of the same molecular weight:

$$g = \frac{\bar{S}^2_b}{\bar{S}^2_l} \quad (g < 1) \quad (3)$$

The factor g was related by Zimm and Stockmayer²⁰ to the weight-average number of trifunctional LCB, n_w (the index of branching), by the following expression:

$$g = \frac{6}{n_w} \left[\frac{1}{2} \left(\frac{n_w + 2}{n_w} \right)^{0.5} \ln \frac{(n_w + 2)^{0.5} + n_w^{0.5}}{(n_w + 2)^{0.5} - n_w^{0.5}} - 1 \right] \quad (4)$$

The problem now is to find g by simple measurement, presumably through the intrinsic viscosity.

According to Flory²¹:

$$[\eta] = \phi \frac{\bar{R}^3}{M} \quad (5)$$

where \bar{R} denotes the end-to-end mean length of the polymer chain and ϕ is an universal constant. If the ratio of radii of gyration is replaced, albeit as an approximation, by the equivalent ratio of end-to-end lengths, g may be expressed through intrinsic viscosities as follows:

$$g = \frac{\bar{R}^2_b}{\bar{R}^2_l} = \left(\frac{[\eta]_b}{[\eta]_l} \right)^{2/3} \quad (6)$$

In addition to this simple model, alternative relations have been proposed. In general,

$$\frac{[\eta]_b}{[\eta]_l} = g' = g^x \quad (7)$$

By equation (6), x should equal $3/2$, and this value was initially adopted²². Stockmayer and Fixman²³ proposed $g' = h^3$, with the latter graphically related to the branching factor g . More recent analysis of the branched model²⁴ showed that x is very close to $1/2$. The discrepancies between the branching indices obtained by the three approaches are quite considerable (cf. *Figure 1*). In spite of this controversy, there is good evidence^{16, 25} of the validity of $x = 1/2$ in equation (7). Accordingly, equations (2) and (7) are combined in the form:

$$[\eta]_b = K M^a g^{1/2} \quad (8)$$

Finally, an assumption regarding the frequency of branching is called for. The simplest would be that the index of LCB (number of long branches per molecule) is proportional to the chain length (molecular weight),

$$n = \alpha M \quad (9)$$

Thus the branching frequency (α) should be constant for the same polymer species (produced at similar conditions) independent of chain length. This

assumption was fairly well verified in studies on fractions^{5,12,16}. Combined equations (4) and (8) yield:

$$[\eta]_i = K M_i^a \left\{ \frac{6}{\alpha M_i} \left[\frac{1}{2} \frac{(\alpha M_i + 2)^{0.5}}{(\alpha M_i)^{0.5}} \ln \frac{(\alpha M_i + 2)^{0.5} + (\alpha M_i)^{0.5}}{(\alpha M_i + 2)^{0.5} - (\alpha M_i)^{0.5}} - 1 \right] \right\}^{0.5} \quad (10)$$

The universal curve is related to individual polymer chains of molecular weight M_i , by:

$$[\eta]_i M_i = K M_i^{a+1} \left\{ \frac{6}{\alpha M_i} \left[\frac{1}{2} \frac{(\alpha M_i + 2)^{0.5}}{(\alpha M_i)^{0.5}} \ln \frac{(\alpha M_i + 2)^{0.5} + (\alpha M_i)^{0.5}}{(\alpha M_i + 2)^{0.5} - (\alpha M_i)^{0.5}} - 1 \right] \right\}^{0.5} \quad (11)$$

The intrinsic viscosity of the whole polymer is taken as the sum of the contributions of the individual chains:

$$[\eta] = \sum W_i [\eta]_i \quad (12)$$

where W_i is the weight fraction of species i in the polymer. Equations (10), (11) and (12) provide a working tool for determining, simultaneously, both the LCB and the MWD curve for whole (unfractionated) branched polymers from the predetermined g.p.c. universal curve.

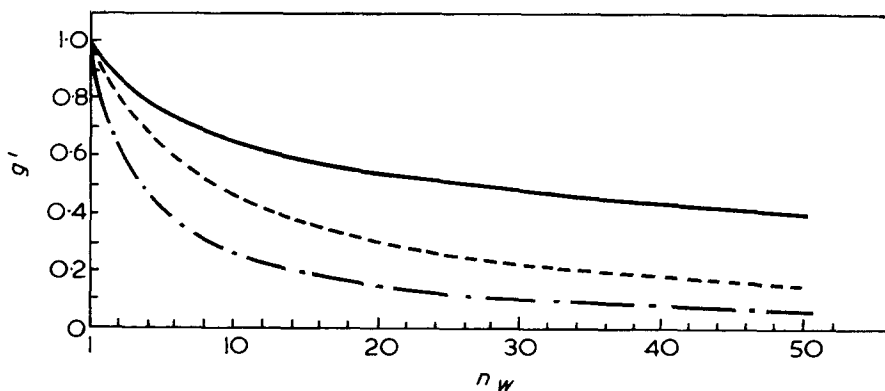


Figure 1 Variation of the branching index, n_w , with parameter g' . — $g' = g'^{1/2}$, --- $g' = h^3$, - · - $g' = g'^{3/2}$.

The procedure for determining the characterization of LDPE is as follows. The chromatogram is obtained from the g.p.c. apparatus, and the intrinsic viscosity of the whole polymer is measured for the same temperature and solvent

In order to derive the MWD, the heights of the chromatogram, h_i , at intervals of 0.5 counts (2.5 ml) of the elution volume, V_e , are measured. At each V_e , the weight fraction of the polymer is calculated by the ratio of h_i

to the sum of all the h_i values. The first guess of the molecular weight at each V_e is found from the curve relating the molecular weight of linear polyethylene with V_e (Figure 3). Combining equations (10) and (12) gives:

$$[\eta]_{br} = \sum W_i K M_i^a \left\{ \frac{6}{\alpha M_i} \left[\frac{1}{2} \frac{(\alpha M_i + 2)^{0.5}}{(\alpha M_i)^{0.5}} \ln \frac{(\alpha M_i + 2)^{0.5} + (\alpha M_i)^{0.5}}{(\alpha M_i + 2)^{0.5} - (\alpha M_i)^{0.5}} - 1 \right] \right\}^{0.5} \quad (12a)$$

Having a set of preliminary values of M_i for each W_i , the first value of α is calculated by trial and error from equation (12a). Using this α and having the set of the products $[\eta]_i M_i$ for each V_e from the universal calibration curve, a new series of M_i values is calculated from equation (11). The corrected M_i values are used in order to calculate a new value of α from equation (12a). This procedure is repeated until two successive distribution curves differ by less than 1%.

EXPERIMENTAL

Gel permeation chromatography

A 'Waters' model 200 g.p.c. apparatus was used, with four columns packed with polystyrene gel in the following pore sizes: 700–2000 Å, 1.5×10^4 – 5×10^4 Å, 1.5×10^5 – 7×10^5 Å and 7×10^5 – 5×10^6 Å.

The apparatus was run at 130°C, with 1,2,4-trichlorobenzene (TCB) as solvent, and calibrated with the aid of eight narrow distributed polystyrene standards under the same conditions. To avoid solvent evaporation in the syphon box, a Teflon tube was passed from the outlet of the sample line into the syphon, which was plugged by a suitable stopper.

Intrinsic viscosity

The intrinsic viscosity of a series of high-density polyethylene (HDPE) was measured in TCB and tetralin both at 130°C, using a Cannon-Ubbelohde viscometer. Three well-characterized samples of LDPE, designated PE-75, PE-76 and PE-77 (kindly donated by F. W. Billmeyer, Jr) were also tested at 130°C and their MWD values were determined. The characterization of these three samples is discussed here; further analysis of other commercial grades will be dealt with in a subsequent paper.

RESULTS AND DISCUSSION

Polystyrene standards were used in constructing the calibration curve, described as the extended chain length Å (on a logarithmic scale) vs. the elution volume at the peak V_e . The molecular weights of these standards being known (their dispersion index, $D_n = \bar{M}_w/\bar{M}_n$ is less than 1.1) and using

the following relationship for intrinsic viscosity of polystyrene in TCB at 130°C ¹⁸,

$$[\eta]_{\text{TCB}}^{130^{\circ}\text{C}} = 8.95 \times 10^{-5} M^{0.727} \quad (13)$$

the universal curve, $[\eta]M$ vs. V_e was first constructed. As regards the correlation of linear polyethylene under the same conditions, the only equation found in the literature²⁶:

$$[\eta]_{\text{TCB}}^{130^{\circ}\text{C}} = 1.5 \times 10^{-3} M^{0.6} \quad (14)$$

appeared unreliable (its exponent being suspiciously too low) and the authors determined their own constants from the intrinsic viscosities of the HDPE samples mentioned earlier. The correlation between the intrinsic viscosity

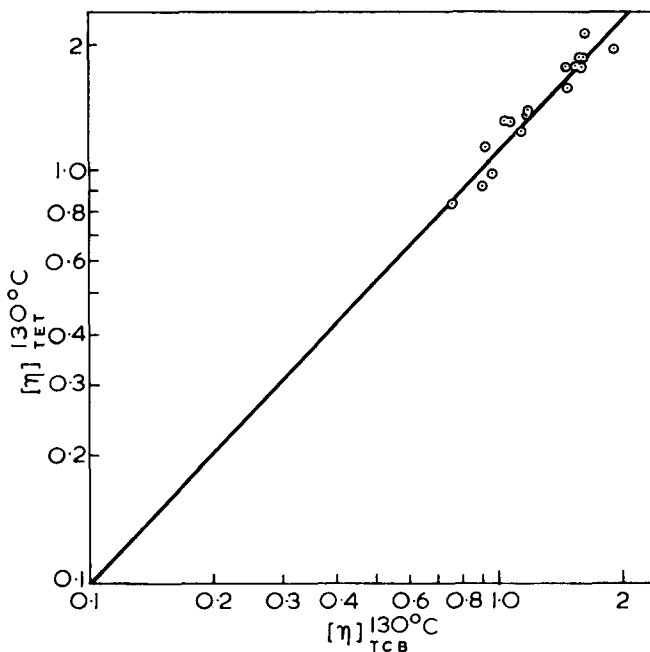


Figure 2 Correlation between intrinsic viscosities of HDPE

in two different solvents (tetralin and TCB) is shown in *Figure 2*. The least-square equation is obtained as

$$\log [\eta]_{\text{tet}}^{130^{\circ}\text{C}} = 1.035 \log [\eta]_{\text{TCB}}^{130^{\circ}\text{C}} \quad (15)$$

Tung²⁷ proposed, for the intrinsic viscosity of HDPE in tetralin at 130°C , a relation later confirmed by other workers:

$$[\eta]_{\text{tet}}^{130^{\circ}\text{C}} = 4.6 \times 10^{-4} \bar{M}_w^{0.725} \quad (16)$$

Equations (15) and (16) yield the following correlation for HDPE in TCB:

$$[\eta]_{\text{TCB}}^{130^{\circ}\text{C}} = 5.96 \times 10^{-4} \bar{M}_w^{0.70} \quad (17)$$

Recent data of Drott and Mendelson²⁸ fit equation (17) fairly well. Using equation (17) and the universal curve, a direct calibration curve for HDPE was plotted (Figure 3). A similar curve is obtainable by multiplying the extended chain length by a Q factor of 11.4 (suggested for HDPE) but in view of the obvious discrepancy between the two curves, the use of a Q factor is not recommended.

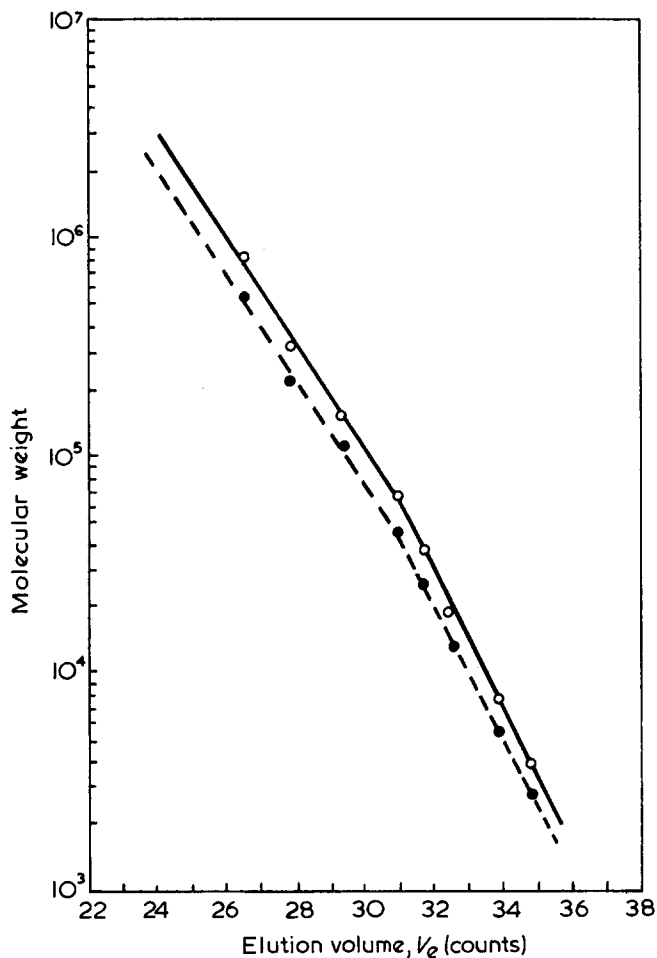


Figure 3 Calibration curves for HDPE. O from the universal curve; ● from Q factor = 11.4

The intrinsic viscosities of the three LDPE samples, as measured in TCB at 130°C, are given in Table 1, and compared with Billmeyer's original data in another solvent (α -CIN at 125°C). Figures 4, 5 and 6 describe the actual MWD of the three polymer samples, respectively, calculated according to the above-mentioned model and using a special Algol programme in an Elliott 503 digital computer. The dotted lines in Figures 4, 5 and 6 describe the

distribution curves obtained by postulating a fictitious linear chain (either by using $\alpha = 0$ or employing a Q factor of 11.4). The calculated values of the major molecular weight averages, \bar{M}_w and \bar{M}_n , the index of LCB, n_w , and its frequency α are given in Table 2. Table 3 lists some dispersion indices, the

Table 1 Intrinsic viscosity of LDPE

Polymer	Intrinsic viscosity (dl/g)	
	TCB at 130°C	α -Chloronaphthalene at 125°C ³
PE-75	0.800	0.795
PE-76	0.730	0.757
PE-77	0.985	0.961

Table 2 Molecular weight averages and indices of LCB

Polymer	Present study				Billmeyer's data ³		
	\bar{M}_w	\bar{M}_n	n_w	$\alpha \times 10^1$	\bar{M}_w	\bar{M}_n	n_w
PE-75	427 000	14 100	229	5.38	500 000	10 700	23
PE-76	239 000	15 100	110	4.61	300 000	13 300	16
PE-77	456 000	19 800	148	3.25	550 000	19 100	19

Table 3 Distribution indices (dispersions)

Polymer	\bar{M}_w/\bar{M}_n	\bar{M}_z/\bar{M}_w	\bar{M}_{z+1}/\bar{M}_z
	D_n	D_w	D_z
PE-75	30.2	7.62	1.98
PE-76	15.8	9.91	2.60
PE-77	23.1	8.81	2.04

most useful of which being represented by $D_n = \bar{M}_w/\bar{M}_n$. Billmeyer's molecular weight averages (included in Table 2) were obtained by light scattering (\bar{M}_w) and cryoscopy (\bar{M}_n). His osmometric data yielded excessively high values. Our own data were obtained from the chromatograms with the aid of a simplified LCB model and intrinsic viscosity correlations, and the close fit of the molecular weight averages (within 20%) is quite satisfactory. One of our samples (PE-76) was previously fractionated by Schneider *et al*¹¹. These workers claim that it is almost impossible to obtain sharp fractions from LDPE by a single fractionation process because solubility is affected by LCB as well as by molecular weight. Therefore, they have represented two curves in their MWD description, one representing \bar{M}_n and the other \bar{M}_w . We have replotted their results of integral MWD and added our data for comparison (Figure 7). Taking into account that the osmotic \bar{M}_n values for the lower fractions are artificially too high, there seems to be a fair agreement for the same polymer derived by the two different methods.

We have refined the LCB model by postulating a lower bound for molecular weight below which no essential long-chain branching occurs. This new model may be described as:

$$n = \alpha' (M - M_0) \quad \text{for } M > M_0 \quad (18)$$

Typical values for M_0 were taken in the range of 8000–12 000 (received by extrapolating existing data). Moreover from the fractionation data of Guillet⁵ it seems that below this range of molecular weight, the curves of intrinsic viscosity against molecular weight for linear and branched polyethylenes

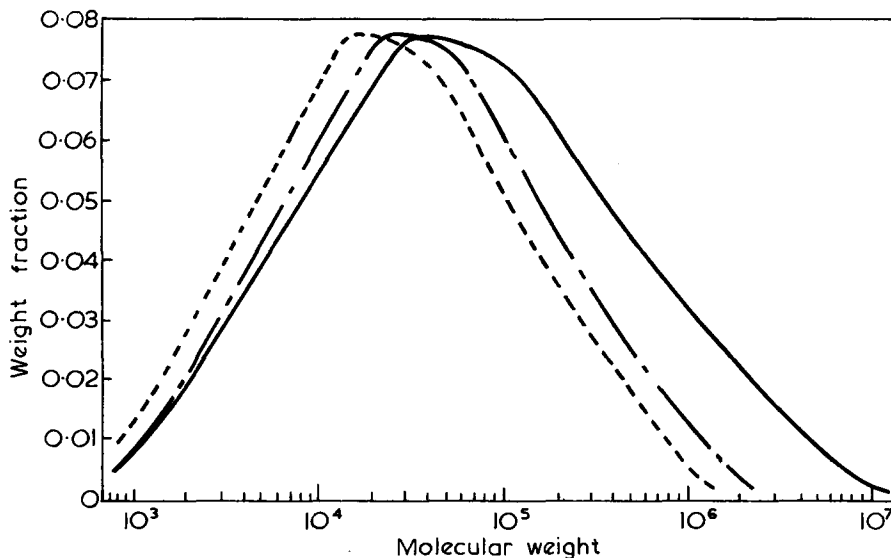


Figure 4 MWD of PE-75. — true curve; - · - · - assuming $\alpha = 0$ (linear); - - - - using $Q = 11.4$ (linear)

coincide which shows that our model is a more realistic one. It seems that this new model provides a better fit between the calculated molecular weight averages and Billmeyer's measured ones. This is shown in Table 4.

Table 4 Molecular weight averages and indices of LCB for a modified branching model (equation 18)

Polymer	M_w	M_n	n_w	$\alpha' \times 10^4$
PE-75 A	431 000	13 300	238	5.5
B	432 000	13 100	241	5.6
PE-76 A	241 000	14 400	114	4.7
B	242 000	14 200	115	4.8
PE-77 A	457 000	19 000	148	3.2
B	459 000	18 800	150	3.3

A: $M_0 = 8000$; B: $M_0 = 12\ 000$

The main discrepancy concerning the LCB indices (which differ by one order of magnitude), has at least two reasons. The first reason stems from the fact that this model permits calculation of the branching index, \bar{n}_w , averaged over all chains in a whole polymer (i.e. taking into account the true MWD).

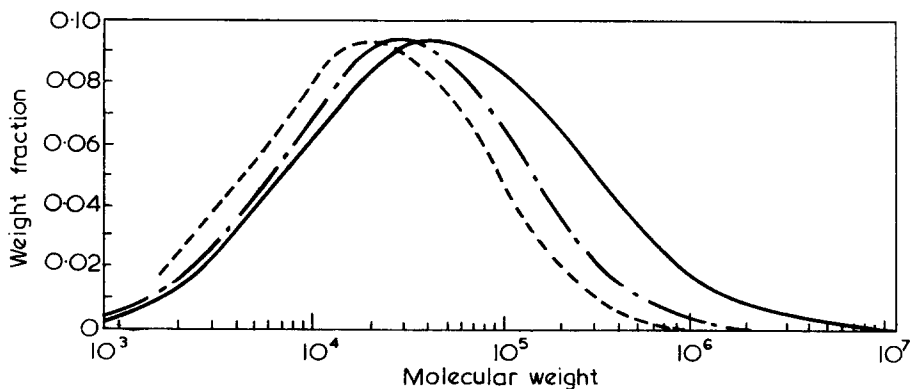


Figure 5 MWD of PE-76. — true curve; - · - · - assuming $\alpha = 0$ (linear); - - - - using $Q = 11.4$ (linear)

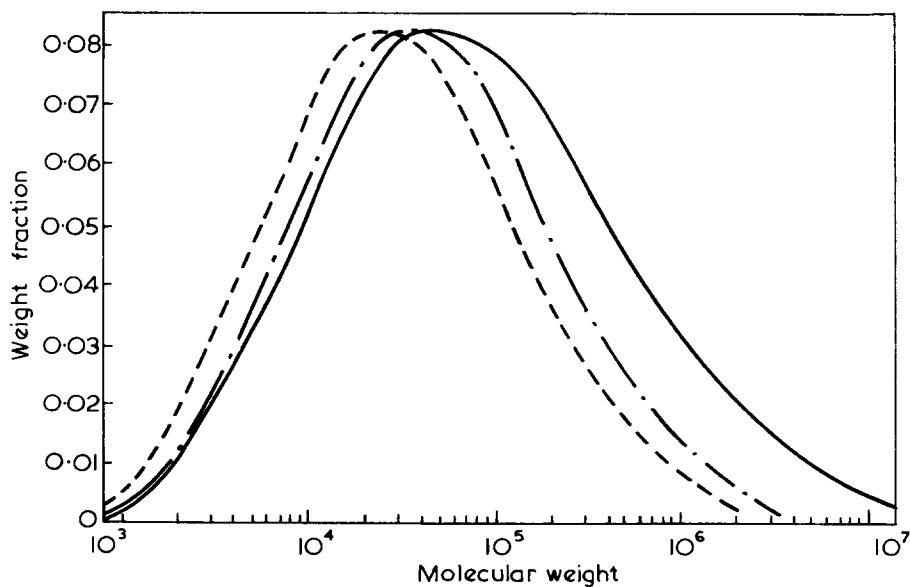


Figure 6 MWD of PE-77. — true curve; - · - · - assuming $\alpha = 0$ (linear); - - - - using $Q = 11.4$ (linear)

while Billmeyer¹, who used molecular weight averages, states that his branching indices are 'unspecified lower averages dependent upon MWD'. The second reason is the exponent $x = 1/2$ in equation (7) as against Billmeyer's $g' = h^3$. An attempt to use $g' = g^{3/2}$ yielded molecular weight averages

(\bar{M}_w) about 3 to 5 times higher than those measured by Billmeyer. Figure 1 shows that the branching index for $g' = h^3$ is quite close to that obtained by $g^{3/2}$. However, it is reassuring to note that our branching frequencies are of the same order of magnitude as those obtained by Mendelson and Drott¹² for LDPE fractions, and recently also for whole polymers²⁸.

Both LCB models used in the present work assume a nearly constant branching frequency for the same polymer. In order to prove this model it

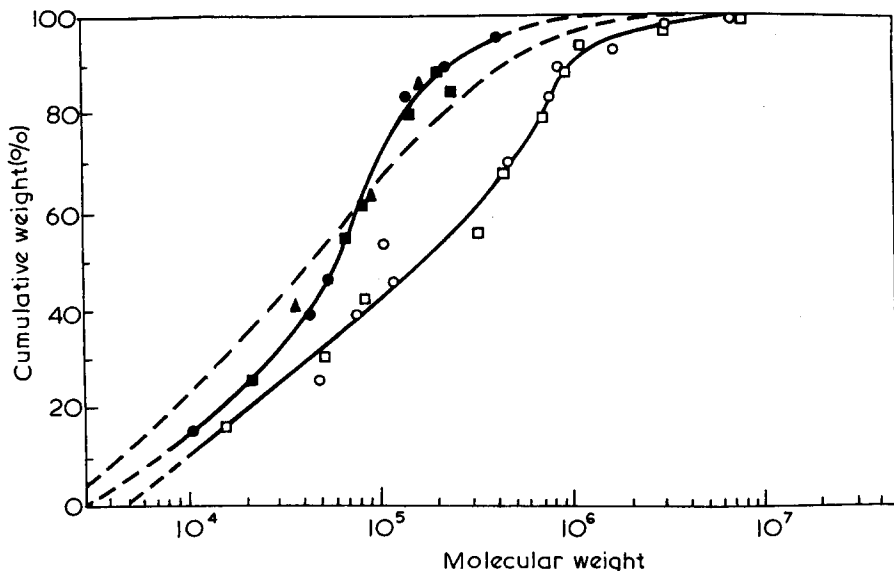


Figure 7 Integral MWD of PE-76. — data from ref. 11 (black symbols \bar{M}_n , white symbol \bar{M}_w); - - - our results

is proposed to develop a new independent tool for LCB estimation by controlled pyrolysis-gas-chromatography (p.g.c.) and separating the short and long-chain derivatives from the pyrolytic products. It is hoped that this further data would confirm the results described in this paper. Lastly, some relation between the MWD and LCB is called for. It has been claimed²⁹ that MWD widens as the index of branching increases. For low frequencies they actually calculated a linear relationship between the LCB index and the first dispersion index ($D_n = \bar{M}_w/\bar{M}_n$). The latter is the most popular representative of MWD, though more exact parameters (derived by adopting a mathematical model that fits the corrected distribution curves) should be preferred. Such distribution parameters for our data will be discussed in a further publication. As yet it is worthwhile to stress that a simple correlation between the LCB index and the dispersion index, D_n , is exhibited in Figure 8, wherein additional data from recent literature²⁸ fit quite well.

This relationship may be expressed as:

$$D_n = \bar{M}_w/\bar{M}_n = A + B \log n_w \quad (19)$$

The significance of equation (19) will be analysed in view of additional studies.

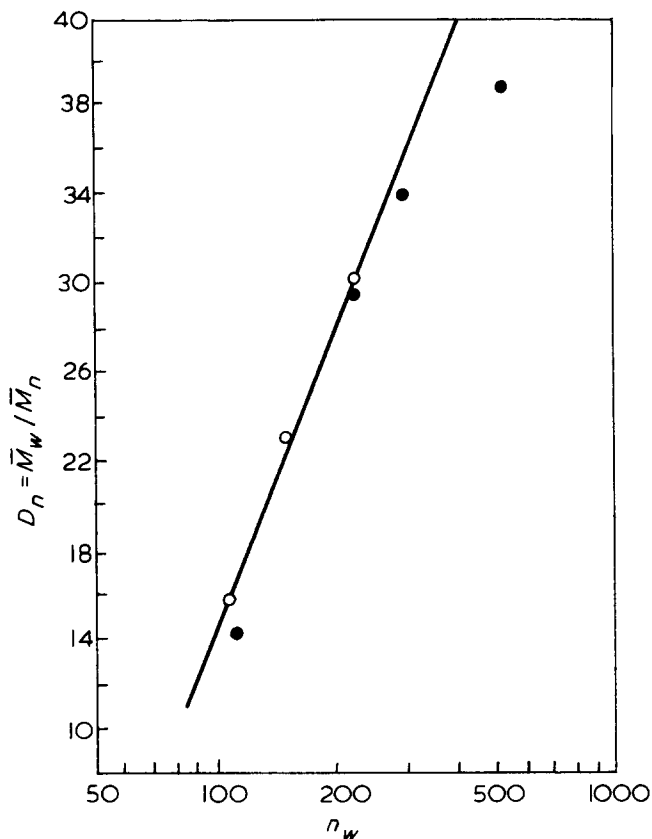


Figure 8 Correlation between branching index, n_w , and molecular weight dispersion index ($D_n = \bar{M}_w / \bar{M}_n$). ○ our data; ● data from ref. 28.

ACKNOWLEDGEMENT

The authors wish to thank Professor F. W. Billmeyer, Jr, for kindly supplying the polymer samples mentioned in this work. This paper is partly based on the Sc.D. work of J. M.

Department of Chemical Engineering,
Technion-Israel Institute of Technology,
Haifa,
Israel

(Received 23 November 1970)
(Revised 16 March 1971)

REFERENCES

- 1 Billmeyer, F. W. *J. Amer. Chem. Soc.* 1953, **75**, 6118
- 2 Muus, L. T. and Billmeyer, F. W. *J. Amer. Chem. Soc.* 1957, **79**, 5079
- 3 Kokle, V., Billmeyer, F. W., Muus, L. T. and Newitt, E. J. *J. Polym. Sci.* 1962, **62**, 251
- 4 Mendelson, R. A. *J. Polym. Sci.* 1960, **46**, 493

- 5 Guillet, J. E. *J. Polym. Sci. (A)* 1963, **1**, 2869
- 6 Guillet, J. E., Combs, R. L., Slonaker, D. F. and Coover, H. W. *J. Polym. Sci.* 1960, **47**, 307
- 7 Mussa, C. *J. Polym. Sci.* 1958, **28**, 587
- 8 Wesslau, H. *Makromol. Chem.* 1958, **26**, 102
- 9 Tung, L. H. *J. Polym. Sci.* 1962, **61**, 449
- 10 Traskos, R. T., Schneider, N. S. and Hoffman, A. S. *J. Appl. Polym. Sci.* 1968, **12**, 509
- 11 Schneider, N. S., Traskos, R. T. and Hoffman, A. S. *J. Appl. Polym. Sci.* 1968, **12**, 1567
- 12 Mendelsohn, R. A. and Drott, E. E. *J. Polym. Sci. (B)* 1968, **6**, 795
- 13 Salovey, R. and Hellman, M. Y. *J. Polym. Sci. (A-2)* 1967, **5**, 333
- 14 Wild, L. and Guliana, R. *J. Polym. Sci. (A-2)*, 1967, **5**, 1087
- 15 Drott, E. E. Fourth International GPC Seminar, Miami Beach, 1967
- 16 Drott, E. E. and Mendelson, R. A. Fifth International GPC Seminar, London, 1968
- 17 Grubisic, Z., Rempp, P. and Benoit, H. *J. Polym. Sci. (B)* 1967, **5**, 753
- 18 Boni, K. A., Sliemers, F. A. and Stickney, P. B. *J. Polym. Sci. (c) (A-2)* 1968, **6**, 1579
- 19 Le Page, M., Beau, R. and De Varies, A. J. *J. Polym. Sci.* 1968, **21**, 119
- 20 Zimm, B. H. and Stockmayer, W. H. *J. Chem. Phys.* 1949, **17**, 1301
- 21 Flory, P. J., 'Principles of polymer chemistry', Cornell University Press, Ithaca, N.Y., 1953
- 22 Thurmond, C. D. and Zimm, B. H. *J. Polym. Sci.* 1952, **8**, 477
- 23 Stockmayer, W. H. and Fixman, M. *Ann. New York Acad. Sci.* 1953, **57**, 334
- 24 Zimm, B. H. and Kilb, R. W. *J. Polym. Sci.* 1959, **37**, 19
- 25 Spiro, J. G., Goring, D. A. I. and Winkler, C. A. *J. Phys. Chem.* 1964, **68**, 323
- 26 Thiery, M. and Cousin, C. 'GPC on polyethylenes-calibration', Waters Assoc. Inc.
- 27 Tung, L. H. *J. Polym. Sci.* 1959, **36**, 287
- 28 Drott, E. E. and Mendelson, R. A. *J. Polym. Sci. (A-2)* 1970, **8**, 1361, 1373
- 29 Graessley, W. W. and Mittelhauser, H. M. *J. Polym. Sci. (A-2)* 1967, **5**, 431

The measurement of molecular orientation in drawn poly(methyl methacrylate) by broad line nuclear magnetic resonance

M. KASHIWAGI*, M. J. FOLKES and I. M. WARD

Measurements have been made of the anisotropy of the proton magnetic resonance second moment at room temperature for a series of drawn non-crystalline poly(methyl methacrylate) samples. These data have been used to calculate orientation functions, which characterize the molecular orientation. This was carried out on the basis of a model in which the polymer is regarded as an aggregate of transversely isotropic units. The structure of these units is based on considerations derived from the crystal structure of crystalline poly(methyl methacrylates). Orientation functions $\overline{P}_2(\cos \Delta)$ and $\overline{P}_4(\cos \Delta)$ for all samples are shown to be close to those derived from a pseudo-affine deformation for re-orientation of the aggregate units in the drawing process. It is found that an excellent correlation exists between the measured birefringence and $\overline{P}_2(\cos \Delta)$ as expected from the aggregate theory. The pattern of mechanical anisotropy is shown to be completely explicable using the aggregate model.

INTRODUCTION

IN A NUMBER of recent publications^{1,2}, attempts have been made to predict the mechanical anisotropy in drawn semi-crystalline polymers on the basis of a model in which the polymer is regarded as an aggregate of anisotropic units which become progressively aligned during the drawing process. It has been shown that the mechanical anisotropy in drawn low-density polyethylene can be predicted to a good approximation using orientation functions [derived from either nuclear magnetic resonance (n.m.r.) or x-ray diffraction studies] characterizing the distribution of units about the draw direction. In this particular polymer it appears that the mechanical anisotropy relates to the orientation of the crystalline regions.

Considerable interest exists, however, in the possibility of extending such considerations to polymers which do not crystallize. In this case the x-ray diffraction methods cannot be used. The present work concerned with poly(methyl methacrylate) (PMMA) was therefore undertaken with a view to establishing the application of the n.m.r. technique to amorphous polymers.

EXPERIMENTAL

Preparation of drawn material

The drawn PMMA specimens were in the form of sheets, 3 mm thick, and were prepared by drawing a commercial type of isotropic material (Perspex)

*On leave from Toray Industries, Inc., Basic Research Laboratory, Tebiri, Kamakura, 248 Japan

in a tensometer at a variety of temperatures to a fixed draw ratio. The specifications of the specimens in terms of birefringence and drawing temperature are shown in *Table 1*.

Table 1 Specifications of the oriented poly(methyl methacrylate) samples. The birefringence values are of negative sign with respect to the draw direction

Sample	Drawing temperature (°C)	Birefringence $\times 10^4$
O	—	0
AA	160	-2.2
AE	140	-3.5
BF	123	-5.7
AG	130	-8.8
AN	95	-13.2
AI	120	-14.0

Apparatus and second moment measurements

All of the n.m.r. measurements were carried out using a Varian DP60 spectrometer and the procedure was very similar to that described in an earlier publication¹. In the present work, measurements were made at room temperature only.

As will be shown later, the anisotropy of the second moment in PMMA is very much smaller than in polyethylene. As a result, additional care was necessary in order to enable accurate second moment values to be obtained.

The probe head modified previously¹ was reconstructed to enable the sample to be set more exactly at the correct orientation in the magnetic field. A Teflon sample holder was attached to the rotating part of the goniometer, the rotating axis being perpendicular to the magnetic field. The specimens were punched from the plates in the form of a rectangle, the larger side of which was perpendicular to the draw direction. The rectangular specimens were then mounted on the holder with their longer edge parallel to the rotating axis.

The n.m.r. spectrometer was operated under two conditions. First, to examine the fine structure of the n.m.r. signal a modulation field of small amplitude (peak-to-peak amplitude 0.4 gauss) was applied. Secondly, to obtain accurate second moment values a modulation field of large amplitude (peak-to-peak amplitude 1.90 gauss) was applied. Although the n.m.r. signal was considerably distorted by such a large modulation field, the trace so obtained contains sufficient information and has a greatly improved signal: noise ratio. An accurate second moment value may therefore be obtained by using the Andrew correction for large modulation amplitude. In all cases a Time Averaging Computer was used to store successive sweeps enabling the signal: noise ratio to be improved by a factor $(N)^{\frac{1}{2}}$ where N = number of scans.

The second moment was calculated for each spectrum by measuring the derivative absorption intensity at small intervals from the centre of the resonance, the data being programmed for computer calculation. The second moment thus calculated had an estimated accuracy of ± 0.1 gauss². Since the modulation field amplitude could be measured to ± 0.1 gauss, the total accuracy of the second moment values after the Andrew correction³, was

estimated to be ± 0.2 gauss². This is adequate for determining the orientation distribution functions as shown later.

The second moment was measured for each sample at seven orientation angles γ ranging from 0° to 90° in 15° steps, where γ is the angle between the sample draw direction and the magnetic field direction.

THEORY

A previous paper¹ contains a full account of the theory of the second moment anisotropy for a uniaxially oriented polymer regarded as an aggregate of units of structure and for this reason only the results of this theory will be presented here.

The value of the second moment $\langle \Delta H^2 \rangle$ for a drawn polymer when the steady magnetic field makes an angle γ with the draw direction of the sample is given by equation (12) in the previous paper¹:

$$\langle \Delta H^2 \rangle = \frac{4G}{N} \sum_{l=0,2,4} a_l S_l P_l(\cos \gamma) \overline{P_l(\cos \Delta)} \quad (1)$$

where $G = 3/2[I(I+1)g^2\mu_n^2]$, I is the nuclear spin number, g the nuclear g -factor, μ_n the nuclear magneton, N the number of magnetic nuclei over which the sum is taken and a_0, a_2, a_4 are numerical coefficients with values $1/5, 2/7$ and $18/35$ respectively. The quantities P_l are Legendre polynomials and Δ is the angle between the symmetry axis of the units and the draw direction. The orientation functions, defining the distribution of units about the draw direction, are given by $\overline{P_l(\cos \Delta)}$, the bar indicating that an average has been taken over the aggregate of units.

The quantities S_l are defined by the equation:

$$S_l = \sum_{j>k} P_l(\cos \theta_{jk}) r_{jk}^{-6}$$

and are the lattice sums. θ_{jk} and r_{jk} are respectively the orientation (with respect to the symmetry axis of the unit) and length of the particular inter-nuclear pair. S_l can therefore be evaluated from a knowledge of the spatial coordinates of the resonant nuclei.

For a crystalline material, the lattice sums can be calculated directly from the crystal structure as determined by x-ray diffraction methods. Since our PMMA specimens are non-crystalline we must adopt a different approach.

The second moment interactions consist of two parts: first the intramolecular interactions, and secondly the intermolecular interactions. In the crystalline regions of crystalline polymers, although the intermolecular interactions are smaller than the intramolecular interactions, both interactions are anisotropic. This is because in the crystalline regions all the nuclei have definite spatial coordinates and produce anisotropic magnetic interactions. On the other hand, in an amorphous polymer even when it is oriented there is no exact correlation between molecules. We will therefore assume that the intermolecular interactions in an amorphous polymer are always isotropic and that the magnetic anisotropy arises from the intramolecular interactions only.

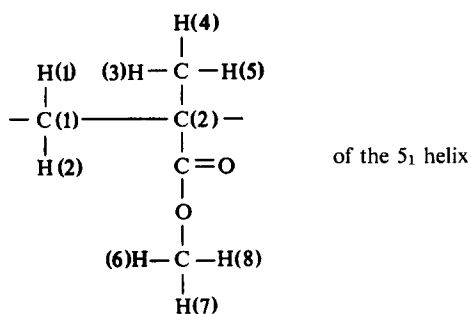
To calculate the intramolecular interactions we will furthermore assume

that the local conformation of the molecule in the amorphous specimens which we have examined is identical to that in the crystalline regions of crystalline PMMA. There is, however, a further complication. There are two forms of crystalline PMMA: the isotactic and the syndiotactic form. Fortunately, it seems reasonable to assume that from the view point of second moment values at room temperature, the intramolecular interactions of the isotactic and syndiotactic configuration will be almost identical. This is because at room temperature, both the chain and ester methyl groups in the polymer are undergoing rotation, and by motional narrowing of the line width⁴, their contributions to the second moment are small.

At the moment only the isotactic structure has been determined by x-ray diffraction methods^{5,6}. We have therefore used the chain configuration of the isotactic PMMA as the basic anisotropic unit of structure.

The isotactic PMMA chain has a 5_1 helix structure⁶, (see *Figure 1*) from which the positions of the hydrogen atoms were calculated assuming that the C-C bond length is 1.54 Å, the C-H bond length is 1.094 Å and the

Table 2 Atomic coordinates in the monomer unit:



of isotactic poly(methyl methacrylate)

Atom	X (Å)*	Y (Å)*	Z (Å)*
C(1)	0.3760	1.1574	0.5700
H(1)	0.7913	2.1051	0.2152
H(2)	-0.6537	1.0553	0.2152
C(2)	1.2169	0.0000	0.0000
H(3)	3.2637	-0.6906	0.1300
H(4)	3.0881	1.0794	0.1300
H(5)	2.6767	0.1449	1.5931
Average position of H(3), H(4) and H(5)	3.0095	0.1779	0.6177
H(6)	-2.2883	-2.7133	0.7897
H(7)	-0.6591	-3.4273	0.7897
H(8)	-1.2724	-2.6108	2.2520
Average position of H(6), H(7) and H(8)	-1.4066	-2.9171	1.2771
Direction of rotation axis of chain methyl†	-1.6811	-0.1667	-0.5792
Direction of rotation axis of ester methyl†	0.6781	1.5471	-0.5792

* Coordinates referred to the orthogonal coordinate system X-Y-Z

† This direction is not normalized. For the convenience of calculation of the lattice sums, the vector length is taken to be 1.786 Å equivalent to the proton-proton distance in a methyl group

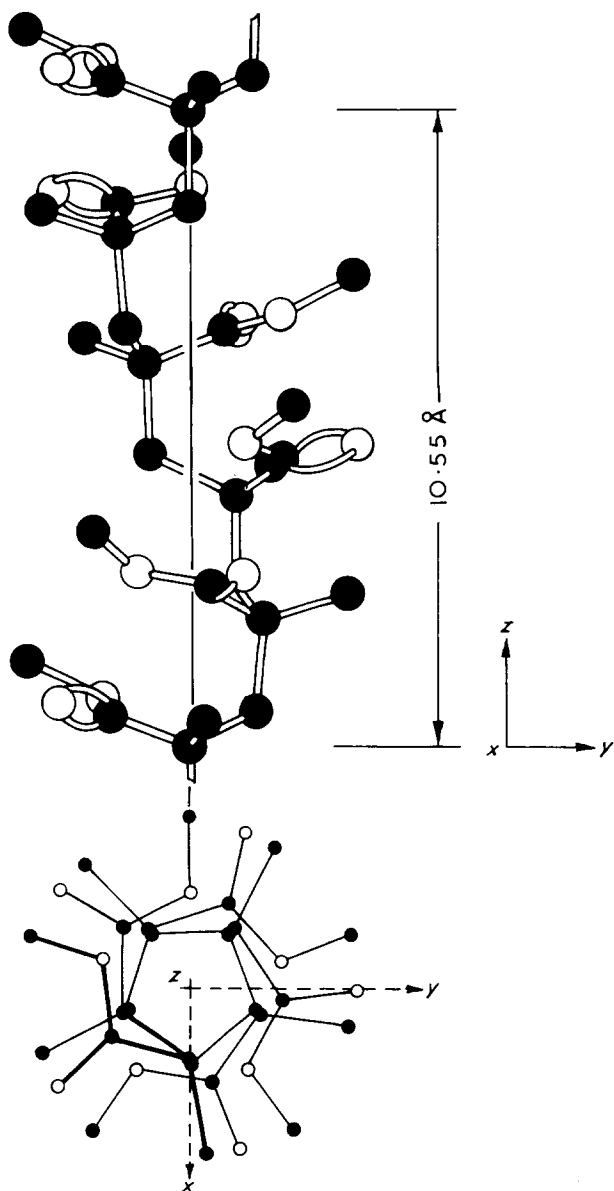


Figure 1 5_1 helix of isotactic poly(methyl methacrylate)

H-C-H angle is $109^\circ 28'$, and by using the data for the ester group shown in Figure 2. On the basis of steric considerations it was assumed that the direction perpendicular to the O-CH₃ bond in the plane of the ester group is perpendicular to the axis of the helix, and the methyl groups are arranged with two protons perpendicular to this axis. The positions of the hydrogen atoms obtained from these calculations are shown in Table 2. In the Table

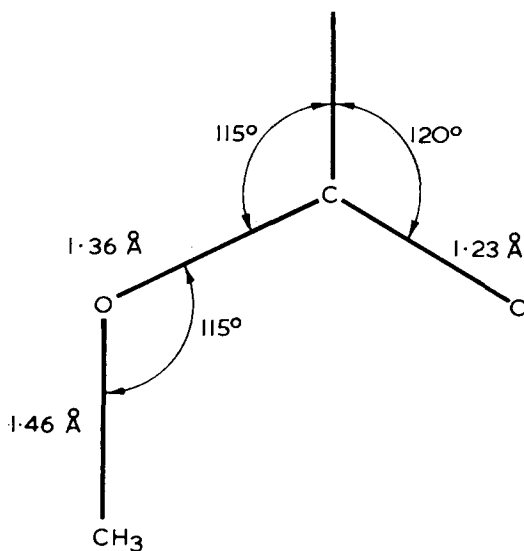


Figure 2 Atomic data for the ester group

the average proton positions of each methyl group are listed, together with the directions of the axis of rotation of the methyl groups, which is perpendicular to the plane containing the three methyl protons.

The intramolecular lattice sum is divided into two parts: (i) the contribution of isolated rotating methyl groups; and (ii) all other contributions.

The first part was calculated by using the directions of the axis of rotation of methyl groups on the basis of reference 4. The second part was calculated by assuming a structure in which a nucleus with three times the magnetic moment of a proton occupies the average position of the methyl protons.

Table 3 Intramolecular lattice sums for isotactic poly(methyl methacrylate)

S_0	S_2	S_4
0.11896	-0.02042	0.01597

The final computed lattice sums are given in Table 3. These are computed on the basis of the intramolecular interactions only. We assume that the intermolecular interactions are isotropic. This gives rise to an additional term in the S_0 lattice sum. This extra part of S_0 will be found from the experimental data, as described in the next section.

RESULTS AND DISCUSSION

Evaluation of the orientation distribution functions from the n.m.r. data

The orientation distribution functions were calculated from the computed lattice sums and the n.m.r. second moment data by the least squares method. In principle $\overline{P}_2(\cos \Delta)$ and $\overline{P}_4(\cos \Delta)$ can be obtained as two independent parameters by solution of equation (1) for any pair of orientation angles γ ,

MOLECULAR ORIENTATION IN DRAWN PMMA

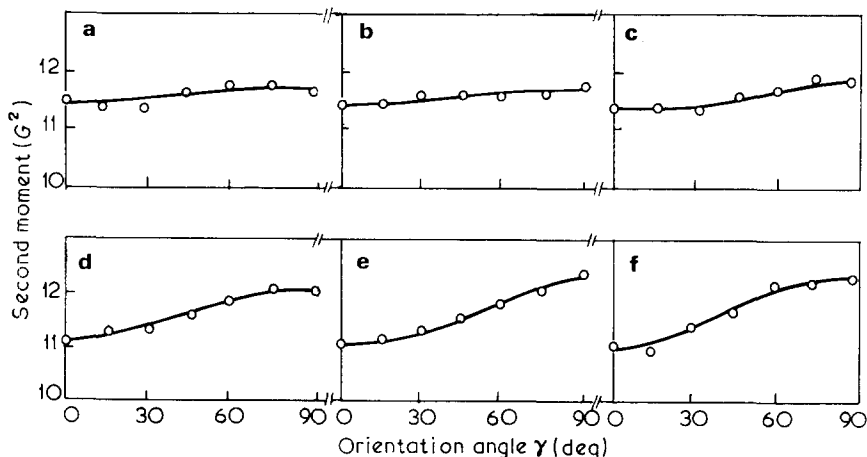


Figure 3 Variation of second moment with orientation angle γ for various samples of PMMA. The lines represent the least squares fit to the experimental data—shown as circles. (a) AA; (b) AE; (c) BF; (d) AG; (e) AN; (f) AI

as described previously¹. In the present work, because of the much smaller degree of magnetic anisotropy in PMMA as compared with polyethylene and the comparative inaccuracy of the lattice sums calculation it was not possible to obtain a good fit to the present data in this way.

The experimental dependence of second moment with orientation angle γ for the six samples of PMMA investigated is shown in Figure 3. It can be seen that there is a progressive increase in the measured anisotropy from sample AA to AI which is expected from the birefringence results listed in Table 1. However, the maximum anisotropy recorded is still only ~ 1 gauss² which again emphasizes the need for great accuracy in the second moment values.

As previously mentioned, the evaluation of S_0 which fixes the magnitude of the isotropic second moment is subject to error. In view of this we write:

$$S_0 = S'_0 + \delta$$

where S'_0 is our approximate value based on intramolecular interactions only and δ is a correction term. We now define a quantity ξ where:

$$\xi = \sum_{\gamma=0^\circ}^{90^\circ} \left\{ \frac{4G}{N} \sum_{l=0,2,4} a_l S_l P_l(\cos \gamma) P_l(\cos \Delta) - \langle \Delta H^2 \rangle_{\text{exp}} \right\}^2$$

and regard $\overline{P_2(\cos \Delta)}$, $\overline{P_4(\cos \Delta)}$ and δ as independent parameters which are chosen, by a computer programme, so as to minimize ξ . It was found that the value of S_0 obtained using this method was constant to within 1% for all the samples investigated, justifying our procedure of adjusting the computed lattice sum S'_0 in this way. The measured n.m.r. anisotropy of each sample together with the fit obtained by the least squares method is shown in Figure 3.

Table 4 shows the values of $\overline{P_2(\cos \Delta)}$ and $\overline{P_4(\cos \Delta)}$ obtained using the least squares method together with the isotropic second moment obtained from S_0 by means of our adjustment method. Also listed are the values of $\overline{\cos^2 \Delta}$ and $\overline{\cos^4 \Delta}$ calculated from $\overline{P_2(\cos \Delta)}$ and $\overline{P_4(\cos \Delta)}$ and the root mean

Table 4 Orientation distribution functions obtained from n.m.r. measurements

Sample	$\overline{P_2(\cos \Delta)}$	$\overline{P_4(\cos \Delta)}$	$\overline{\cos^2 \Delta}$	$\overline{\cos^4 \Delta}$	Isotropic second moment G^2	Root mean square deviation G^2
AA	0.0518	-0.0079	0.3679	0.2278	11.61	0.12
AE	0.0546	-0.0306	0.3698	0.2242	11.63	0.08
BF	0.1674	0.0266	0.4449	0.3017	11.69	0.07
AG	0.2350	-0.0065	0.4900	0.3328	11.76	0.06
AN	0.3070	0.0486	0.5380	0.3865	11.75	0.06
AI	0.3134	-0.0184	0.5422	0.3749	11.82	0.10

square deviation of the experimental points from the curve obtained by the least squares method. It is seen that the isotropic second moment is constant within experimental error for all the samples and is coincident with the measured second moment of 11.80 gauss² of isotropic PMMA (sample O).

Comparison of second moment anisotropy with optical and mechanical measurements

On the basis of the aggregate model, the birefringence Δn of a uniaxially oriented polymer is given by:

$$\Delta n = \Delta n_{\max} \frac{1}{2} (3 \overline{\cos^2 \Delta} - 1) = \Delta n_{\max} \overline{P_2(\cos \Delta)}$$

where Δn_{\max} is the maximum birefringence for a completely oriented polymer and Δ is the angle between the draw direction and the symmetry axis of the polarizable unit of structure. Thus, if the optical and magnetic anisotropy arise from the progressive alignment of similar units of structure, we would expect to obtain a good correlation between the measured birefringence and the values of $\overline{P_2(\cos \Delta)}$ obtained from the n.m.r. measurements.

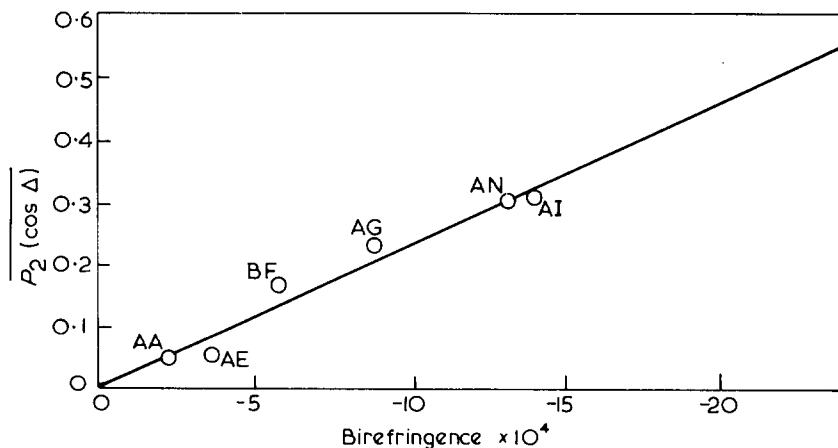


Figure 4 Variation of $\overline{P_2(\cos \Delta)}$, obtained from n.m.r. measurements, with the birefringence. Circles are experimental results while line is predicted from the aggregate theory

Figure 4 shows a plot of $\overline{P_2(\cos \Delta)}$ against measured birefringence from which it is seen that there is a good correlation. Extrapolation to full orien-

tation gives a value Δn_{\max} of 43×10^{-4} , which may be of value in further structural studies of PMMA.

Next, the values of $\overline{\cos^2 \Delta}$ and $\overline{\cos^4 \Delta}$ obtained from the n.m.r. data were compared with values for these parameters predicted on the basis of a pseudo-affine deformation scheme⁷, in which, during the orientation process the unique axes of the units of structure undergo the same changes of direction as lines connecting pairs of material points in a body undergoing uniaxial deformation, without change of volume. Usually a knowledge of the draw ratio of the material is required in evaluating $\overline{\cos^2 \Delta}$ and $\overline{\cos^4 \Delta}$ using the pseudo-affine model. Our samples were drawn at a number of temperatures to a fixed draw ratio and so this information is not known. However, we can predict the dependence of $\overline{\cos^4 \Delta}$ on $\overline{\cos^2 \Delta}$ and compare this with our experimentally determined values thus avoiding a knowledge of the effective draw ratio for each sample. This is illustrated in *Figure 5* where it can be

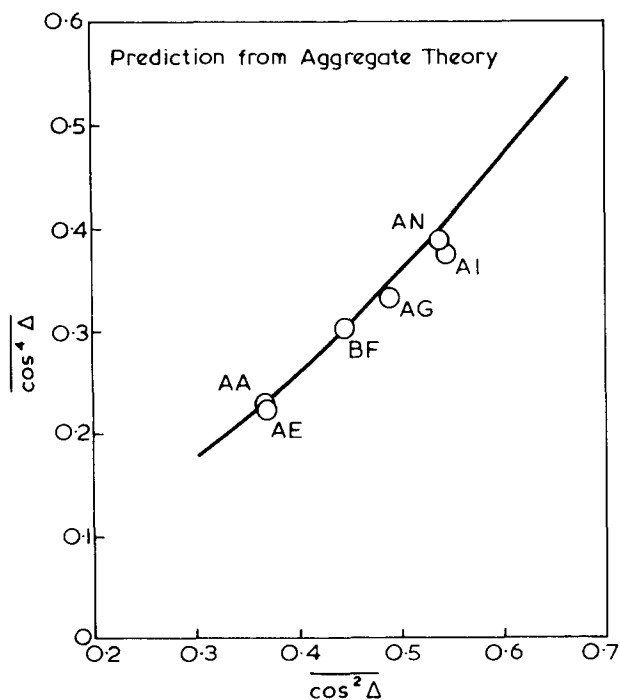


Figure 5 Comparison between the measured and theoretical variation of $\overline{\cos^4 \Delta}$ with $\overline{\cos^2 \Delta}$

seen that the experimentally determined values of $\overline{\cos^4 \Delta}$ and $\overline{\cos^2 \Delta}$ are very similar to those expected from the pseudo-affine deformation scheme, although it may well be that the re-orientation processes are more complex than are envisaged by this scheme.

We have finally attempted to predict the mechanical anisotropy of the samples using the n.m.r. orientation functions, on the basis of the aggregate

model. The elastic constants for the aggregate can be obtained in two ways: either by considering compliances or stiffnesses. One may assume that either we have a uniform stress throughout the aggregate, in which case the strains are not continuous or a uniform strain which gives rise to discontinuity of stress. The uniform stress approach implies a summation of compliance constants, and gives rise to the Reuss average⁸; uniform strain implies a summation of stiffnesses and gives the Voigt average⁹. It has been shown by Bishop and Hill¹⁰ that these two averages represent upper and lower bounds respectively for the true compliances of the aggregate.

The elastic constants of a partly drawn polymer regarded as an aggregate of units of structure are given by equations (5.3)–(5.12) of a previous paper⁷. If the five independent elastic constants (either the compliance constants S_{11} , S_{12} , S_{13} , S_{33} and S_{44} or the corresponding stiffness constants) of the transversely isotropic unit of structure are given, the elastic constants (S'_{11} , S'_{12} , . . . etc.) of the partly oriented polymer can be calculated provided that the orientation functions are known.

To obtain the stiffness constants C_{11} , C_{12} , C_{13} , C_{33} and C_{44} in the present study, we used the results shown in *Figure 6* for the measured behaviour of the stiffness constants C'_{11} , C'_{12} , C'_{13} , C'_{33} and C'_{44} for the partly oriented

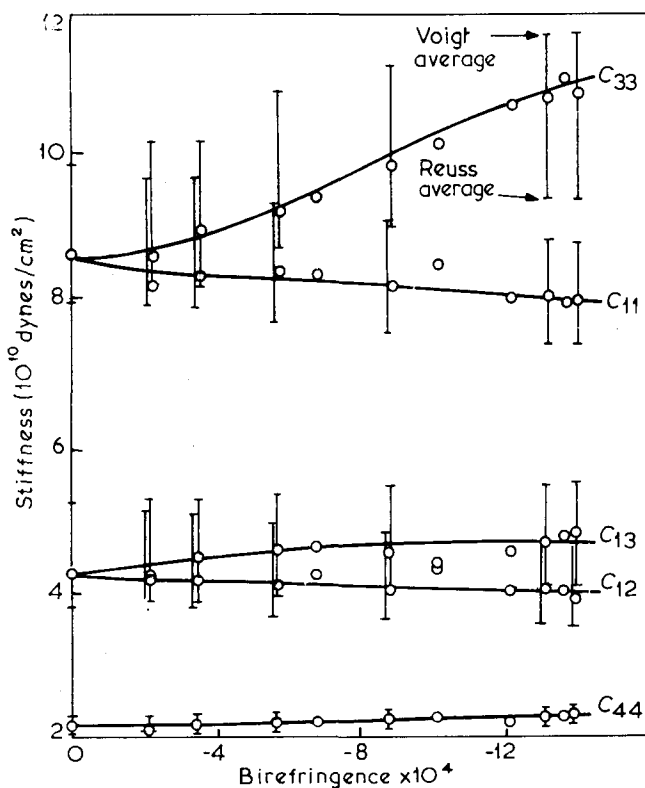


Figure 6 Stiffness constants of PMMA as a function of the birefringence

polymer as a function of the birefringence. We previously estimated the maximum birefringence to be -43×10^{-4} . Linear extrapolation of the measured stiffness constants to this value of birefringence gave:

$$\begin{aligned} C_{11} &= 7 \times 10^{10} \text{ dynes cm}^{-2} \\ C_{12} &= 3.5 \times 10^{10} \text{ dynes cm}^{-2} \\ C_{13} &= 5.9 \times 10^{10} \text{ dynes cm}^{-2} \\ C_{33} &= 16.6 \times 10^{10} \text{ dynes cm}^{-2} \\ C_{44} &= 2.3 \times 10^{10} \text{ dynes cm}^{-2} \end{aligned}$$

while the corresponding compliance constants were calculated as:

$$\begin{aligned} S_{11} &= 2.22 \times 10^{-11} \text{ dynes}^{-1} \text{ cm}^2 \\ S_{12} &= 6.36 \times 10^{-12} \text{ dynes}^{-1} \text{ cm}^2 \\ S_{13} &= 5.64 \times 10^{-12} \text{ dynes}^{-1} \text{ cm}^2 \\ S_{33} &= 1.00 \times 10^{-11} \text{ dynes}^{-1} \text{ cm}^2 \\ S_{44} &= 9.35 \times 10^{-11} \text{ dynes}^{-1} \text{ cm}^2 \end{aligned}$$

by inverting the stiffness matrix.

These values for the elastic constants were used together with the orientation functions obtained by n.m.r. to calculate the Reuss and Voigt averages for the stiffness constants. The results are shown in *Figure 6*, from which it can be seen that all the experimental data lie between the predicted Reuss and Voigt average values.

Intuitively it is difficult to interpret the magnitude of each of the elastic constants for a single unit of structure in terms of the detailed morphology of the unit. However, one would expect a significant difference in either C_{11} and C_{33} or S_{11} and S_{33} since the former principally arises from weak van der Waals forces linking neighbouring chains while the latter is due to much stronger covalent forces directed along the chain axes. Indeed this simple physical reasoning is reflected by the values we obtain for these two elastic constants. A complete assessment of this problem must await further work.

It can be concluded from this work that the application of the aggregate model in amorphous PMMA is reasonable and that we have obtained satisfactory extrapolated values, first for the maximum birefringence and secondly for the stiffness constants.

It should, however, perhaps be emphasized that we have had to make a somewhat arbitrary choice of the molecular conformation of the aggregate unit, in order to undertake the quantitative calculations. Although the choice of the helical unit is reasonable in view of the considerations discussed in detail above, it must be accepted that structural studies (e.g. infra-red and n.m.r. spectroscopy) show that commercial PMMA contains substantial proportions of syndiotactic and atactic material. Fortunately, it is likely that the present calculations are not very sensitive to the finer details of the structure for the following reason. At room temperature, where both the chain and ester methyl groups are undergoing rotation the proton-proton interactions within a sphere of interaction of radius 5 \AA would be expected to be similar for helical structures which are not as regular as that assumed here. Interactions at distances greater than 5 \AA do not make a significant contribution to the lattice sums, and this indeed justifies our treatment of the anisotropy

of the second moment in terms of intramolecular interactions only. In the absence of other data, the isotactic model had to be chosen as a basis for the calculations, but it does seem likely that if further structural information can be obtained in future, it would then be worthwhile to generalize the model to allow for a range of re-orientating units of structure.

The shape of the distribution function

The polar plots of the distribution function for samples AA, BF and AI are shown in *Figure 7(a)*. These plots were calculated from equation (17) of a previous paper¹:

$$f(\Delta) = \sum_{l=0,2,4} (1 + \frac{1}{2}) \overline{P_l(\cos \Delta)} P_l(\cos \Delta)$$

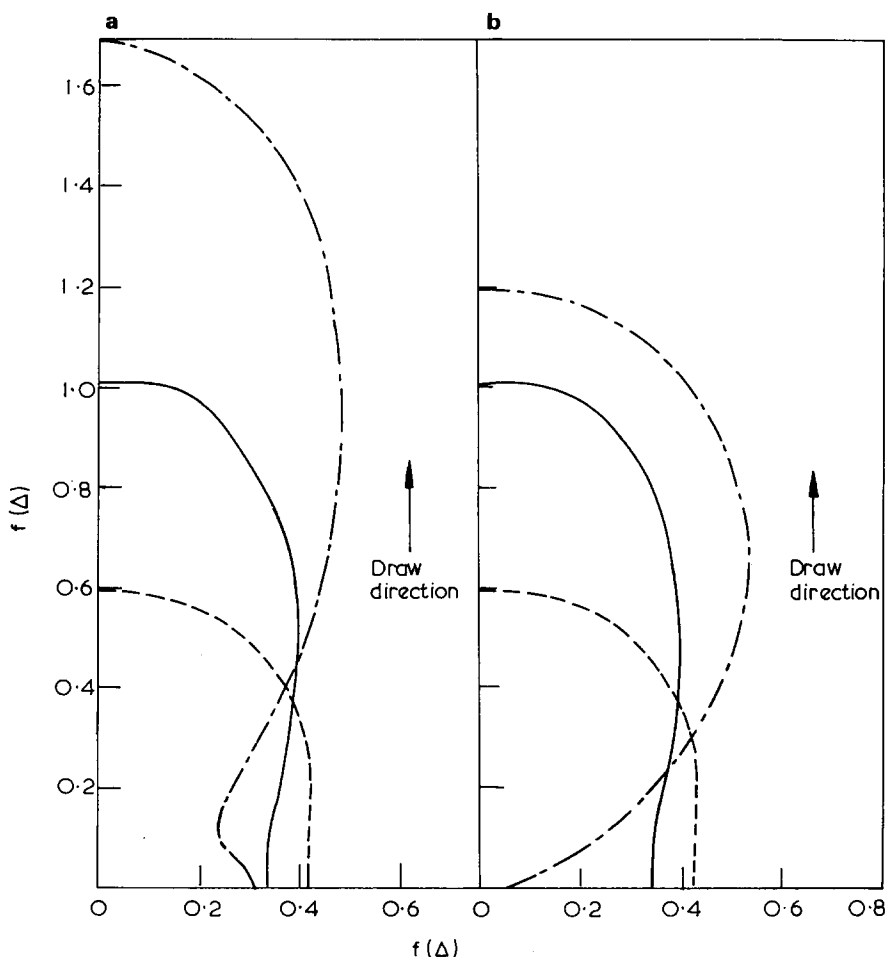


Figure 7 Polar plots of the distribution function for various samples of PMMA. (a) Experimental; (b) theoretical—based on pseudo-affine model. — — — AI; — BF; - - - - AA

These can be compared with the plots shown in *Figure 7(b)* based on the orientation functions derived from the pseudo-affine deformation scheme. The shape of the distribution functions based on this model differs significantly at the highest drawn ratio (sample AI) from that predicted on the pseudo-affine deformation scheme. It is to be noted that quite small deviations from the values of $\overline{P_2(\cos \Delta)}$ and $\overline{P_4(\cos \Delta)}$ from those predicted on this scheme give rise to very appreciable changes in the distribution function.

The shape of the n.m.r. spectra for orientated PMMA

Figure 8 shows the changes in the n.m.r. spectrum of highly oriented PMMA (sample AI) that occur when the orientation of the sample in the

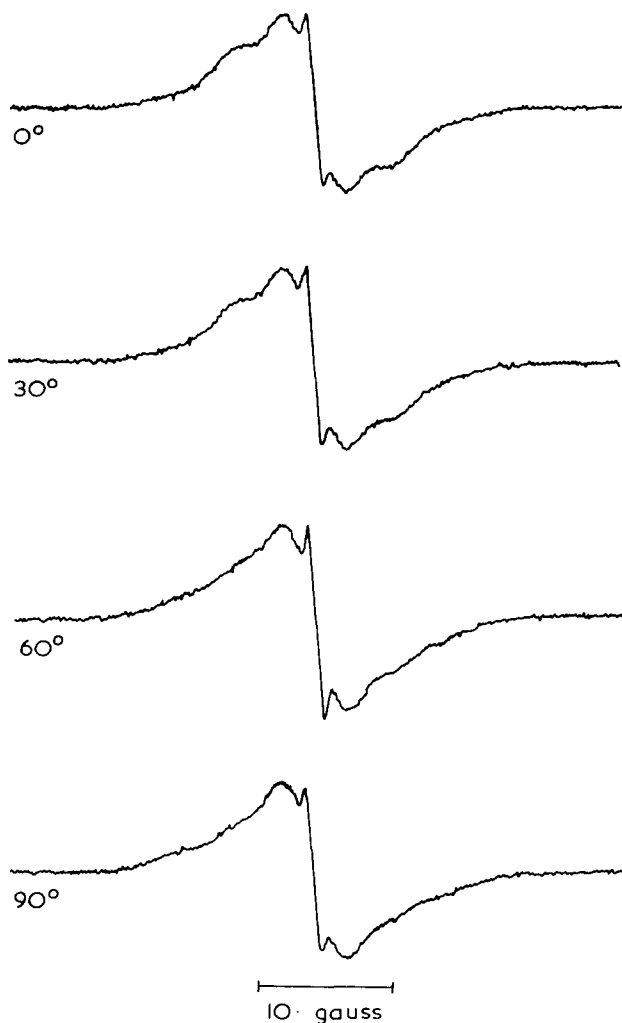


Figure 8 Change of the n.m.r. spectrum of oriented PMMA with angle γ between the magnetic field and draw direction

magnetic field is changed. In the present work, it is confirmed from the magnitude of the measured second moment that both the chain and ester methyl groups undertake rotation at room temperature. This is in agreement with results obtained from studies of the temperature dependence of the molecular motion in isotropic PMMA^{11,12}.

Further studies of molecular motion in oriented PMMA will be undertaken in the future.

ACKNOWLEDGEMENTS

The drawn poly(methyl methacrylate) specimens were prepared by the Department of Polymer and Fibre Science, U.M.I.S.T. and were made available to us by the courtesy of Professor L. R. G. Treloar and Dr E. F. T. White. The experimental dependence of the stiffness constants against birefringence shown in *Figure 6* is the work of Mr H. Wright to whom we are most grateful.

We are indebted to Dr A. J. Manuel for his advice on the accurate measurement of second moments.

One of us (M.K.) was supported by Toray Industries, Inc.

*Department of Physics,
University of Leeds,
Leeds 2, UK*

M. Kashiwagi and I. M. Ward

*H. H. Wills Physics Laboratory,
University of Bristol,
Royal Fort,
Tyndall Avenue,
Bristol BS8 1TL, UK*

*M. J. Folkes
(Received 4 January 1971)*

REFERENCES

- 1 McBrierty, V. J. and Ward, I. M. *Brit. J. Appl. Phys.* 1968, **1**, 1529
- 2 Gupta, V. B., Keller, A. and Ward, I. M. *J. Macromol. Sci. (Phys.)* 1968, **1** (2), 139
- 3 Andrew, E. R. *Phys. Rev.* 1953, **91**, 425
- 4 Gutowsky, H. S. and Pake, G. E. *J. Chem. Phys.* 1950, **18**, 162
- 5 Stroupe, J. D. and Hughes, R. E. *J. Amer. Chem. Soc.* 1958, **80**, 2341
- 6 Liquori, A. M. *et al. Nature*, 1965, **206**, 358
- 7 Ward, I. M. *Proc. Phys. Soc.* 1962, **80**, 1176
- 8 Reuss, A. Z. *Angew. Math. Mech.* 1929, **9**, 49
- 9 Voigt, W. 'Lehrbuch der Kristallphysik', Leipzig, Teubner, 1928, p 410
- 10 Bishop, J. and Hill, R. *Phil. Mag.* 1951, **42**, 414, 1298
- 11 Sinnott, K. M. *J. Polym. Sci.* 1960, **42**, 3
- 12 Odajima, A., Sohma, J. and Koike, M. *J. Phys. Soc. Japan* 1957, **12**, 272

The melting and crystallization of copolymers of nylon-6,6 and nylon-6,10 with poly(hexamethylene terephthalamide) (nylon-6T)

E. D. HARVEY* and F. J. HYBART

Rates of crystallization of copolyamides of nylon-6,6 and nylon-6,10 containing up to 20 and 15% nylon-6T [poly(hexamethylene terephthalamide)] have been measured by a photometric technique, using a hot stage microscope. Co-crystallization is confirmed for the nylon-6,6/6T copolymers and leads to an increase in the melting points from the melting point of nylon-6,6; there is a reduction in the extents of crystallization as shown by heats of fusion, and kinetic measurements show that the copolymers crystallize more slowly. In nylon-6,10/6T copolymers, the behaviour is similar to that already reported, when co-crystallization is not occurring; the nylon-6T units act as a diluent in the nylon-6,10 crystalline areas.

INTRODUCTION

IN MOST COPOLYMER systems, the copolymers show lower melting and crystallization temperatures than the homopolymers^{1,2}. An exception is the nylon-6,6/nylon-6T copolyamide system which shows isomorphous crystallization³, because the distance separation of the amide groups in the two copolymer constituents are nearly identical.

EXPERIMENTAL AND RESULTS

Melting behaviour

The melting points of nylon-6,6/6T copolyamides and nylon-6,10/6T copolyamides containing up to 20% nylon-6T [poly(hexamethylene terephthalamide)] are shown in *Figure 1*. Two techniques were used for these measurements; for maximum observable melting points, the sample in thin film form was heated on the stage of a hot stage microscope at 2°C/min, and the temperature of the disappearance of the last trace of birefringence was observed; for average melting points, a DuPont 900 Thermal Analyzer fitted with the D.S.C. cell was used, and the sample was heated in nitrogen at 5°C/min. In the nylon-6,6/6T copolymers, as the amount of nylon-6T comonomer is increased, the difference between these melting point values is increased, showing a wider range of melting. In the nylon-6,10/6T copolymers, a steady drop in melting point is observed as the comonomer is introduced.

* Present address: Department of Mechanical and Production Engineering, Trent Polytechnic, Nottingham.

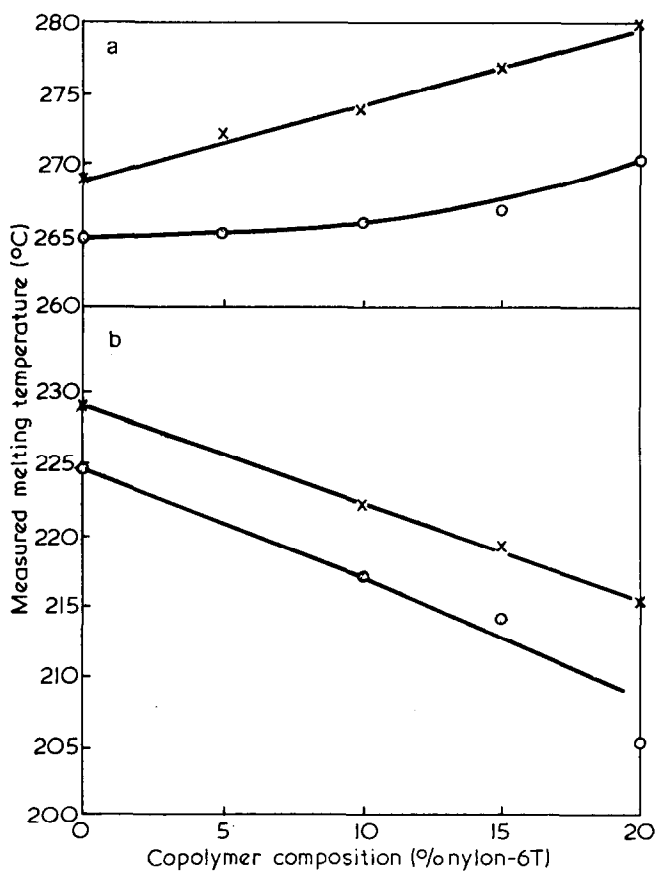


Figure 1 Melting points of (a) nylon-6,6/6T copolymers and (b) nylon-6,10/6T copolymers as a function of copolymer composition.

×, hot-stage microscopy; ○, differential thermal analysis

Table 1 Heats of fusion of nylon copolymers

Copolymer composition		Un-annealed heat of fusion (J/kg)	Annealed heat of fusion (J/kg)
Nylon-6T (%)	Other component		
0	nylon-6,6	80 800	105 200
5		74 100	94 000
10		52 700	84 300
15		39 700	76 500
20		29 300	64 800
0	nylon-6,10	79 000	95 600
10		50 600	63 100
15		33 100	45 100
20		19 200	

The heats of fusion of the copolymers were measured using the DuPont Thermal Analyzer and the results are shown in *Table 1*. Measurements were also made using samples which had been annealed in nitrogen for 5 hours at either 245°C (for nylon-6,6/6T copolyamides) or 200°C (for nylon-6,10/6T copolyamides). The reduction observed in the heats of fusion of the nylon-6,6/6T copolymers suggests a reduced level of crystallinity in these copolymers, by comparison with nylon-6,6 homopolymer. Isomorphous replacement of nylon-6T within the homopolymer is not completely effective. A substantial recovery of the lost crystallinity occurs during the annealing process.

Rates of crystallization

The rates of crystallization of the copolymers have been compared by using the time for one half of the crystallization, $t_{1/2}$, including the secondary process. The supercooling temperatures, ΔT , represent the difference between the crystallization temperature and the melting point from hot stage microscopy. Rates of crystallization were measured using a hot stage microscope

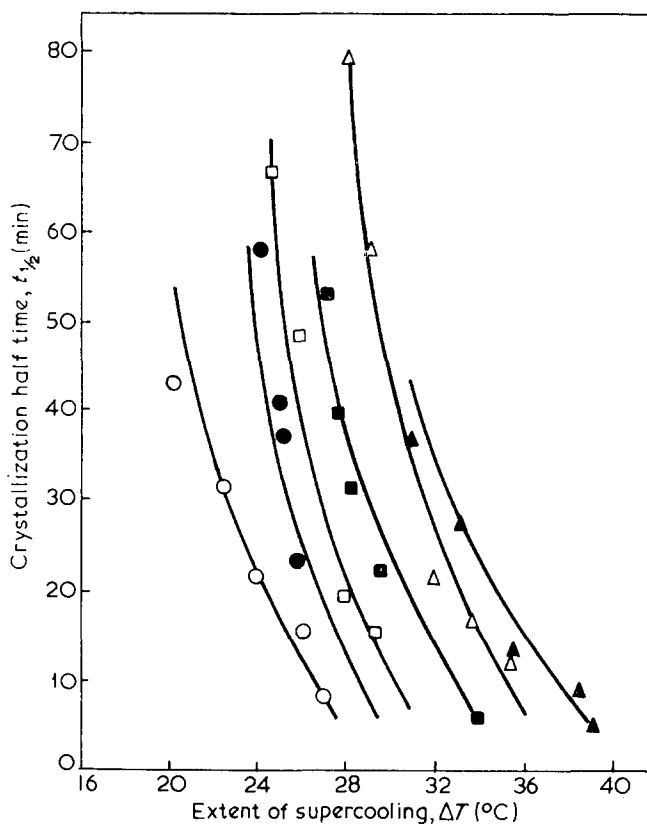


Figure 2 Rates of crystallization of nylon-6,6 and nylon-6,6/6T copolymers. The effect of supercooling temperature on the crystallization half-time: ○, nylon-6,6; ●, 2% copolymer; □, 5% copolymer; ■, 10% copolymer; △, 15% copolymer; ▲, 20% copolymer

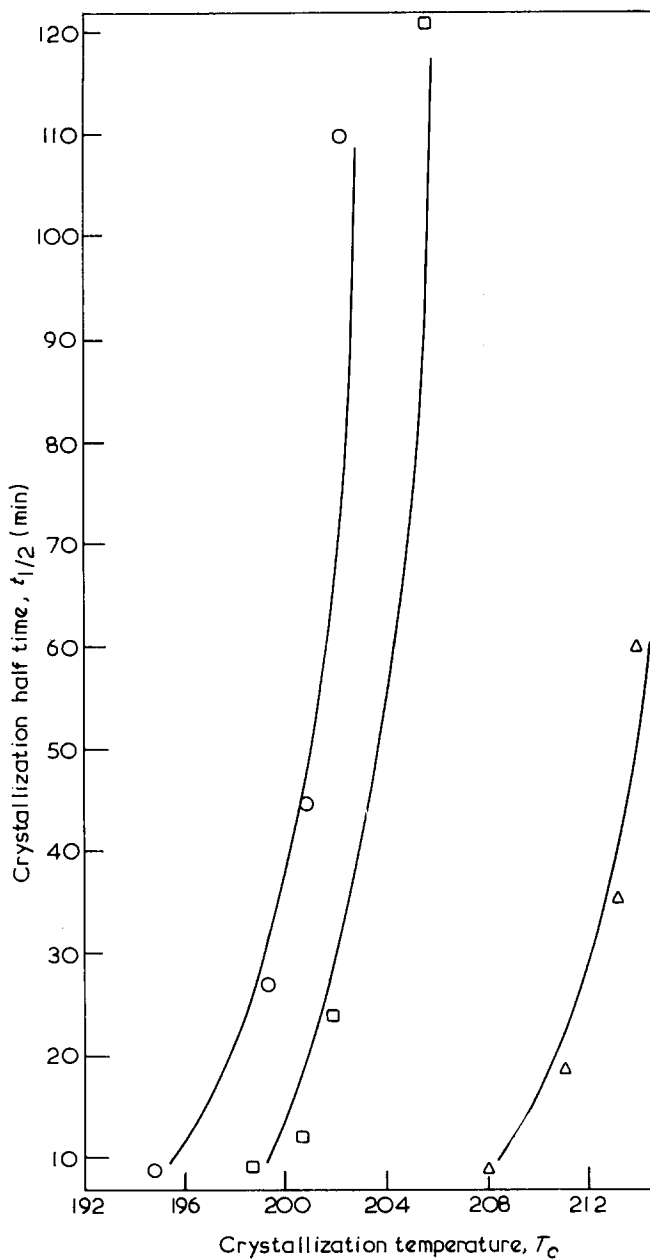


Figure 3 Rates of crystallization of nylon-6,10 and nylon-6,10/6T copolymers. Temperature dependence of half crystallization times: Δ , nylon-6,10; \square , 10% copolymer; \circ , 15% copolymer

fitted with a recording photoresistor eyepiece attachment⁴. *Figure 2* shows the $t_{\frac{1}{2}}$ values for nylon-6,6 and nylon-6,6/6T copolymers for various amounts of supercooling. As the crystallization temperatures giving $t_{\frac{1}{2}}$ values of 20 min for the 0–15% copolymers only ranged from 243.5 to 245°C, the rates of crystallization of these copolymers are nearly identical with the nylon-6,6 homopolymer rate measurements. For the 20% copolymer, a 20 min $t_{\frac{1}{2}}$ value was obtained at a crystallization temperature of 247°C. The crystallization behaviour of the nylon-6,10/6T copolymers is comparable with nylon-6,6/6 copolymers², and ΔT is noticed to be approximately constant for a certain $t_{\frac{1}{2}}$ value. In *Figure 3* the observed $t_{\frac{1}{2}}$ values are shown for various crystallization temperatures.

Plots of $\log 1/t_{\frac{1}{2}}$ against $T_m^2/T(\Delta T)^2$ are normally found to be linear for homopolymers, providing that the thermodynamic melting temperature is taken for T_m ⁵. We have found that we may consider copolyamides using this treatment². The melting points which must be taken in order to obtain linear graphs may be considered as the copolymer thermodynamic melting points. With nylon-6,6/6T copolymers, we again find curves for the measured melting points which become linear at a temperature 2–6°C above these values. *Figure 4*

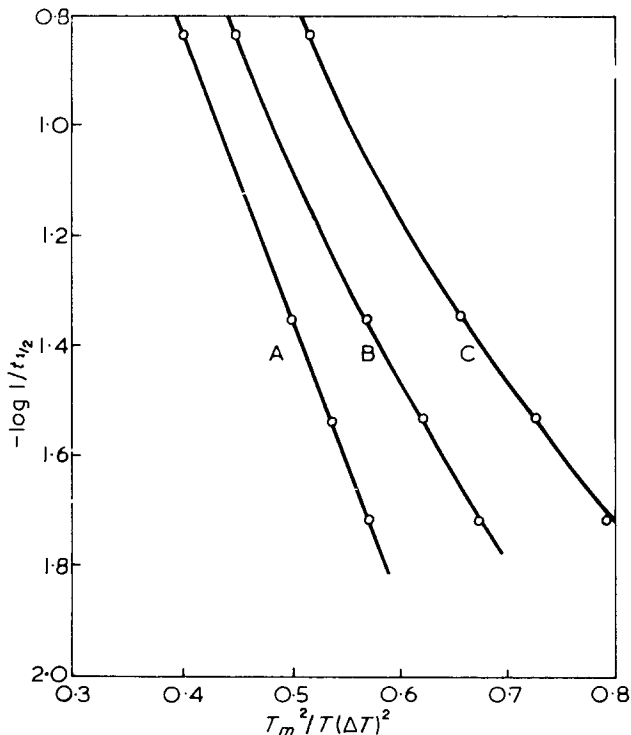


Figure 4 Temperature dependence of crystallization rates for a copolymer of 10% nylon-6T/90% nylon-6,6. Graph showing $-\log 1/t_{\frac{1}{2}}$ against $T_m^2/T(\Delta T)^2$ for three values of the melting temperature, T_m . A linear graph is obtained if the melting temperature is taken as 279°C. A, $T_m = 279^\circ\text{C}$; B, $T_m = 276.5^\circ\text{C}$; C, $T_m = 274^\circ\text{C}$

illustrates this for the copolymer of 10% nylon-6T in nylon-6,6, which has an optical melting point of 274°C and an estimated thermodynamic melting point of 279°C. Using this method, the thermodynamic melting points for the copolymers were obtained, and the results are shown in *Table 2*.

Table 2 Thermodynamic melting points^a of copolyamides

<i>Nylon-6T/6,6 copolymers:</i>						
Nylon-6T(%)	0	2	5	10	15	20
Measured melting point (hot stage microscopy) (°C)	268	270.5	272	274	277	281
Thermodynamic melting point (°C)	274	275	277	279	281	284
<i>Nylon-6T/6,10 copolymers:</i>						
Nylon-6T (%)	0	10	15	20		
Measured melting point (°C)	229	222	219	215		
Thermodynamic melting point (°C)	231	224	221	217		

ACKNOWLEDGEMENTS

The authors are grateful to the Science Research Council and the University of Aston in Birmingham for the award of research studentships to E. D. H. The polymers were prepared using materials which were donated by Imperial Chemical Industries Ltd.

*Chemistry Department,
The University of Aston in Birmingham,
Birmingham B4 7ET, UK*

*(Received 22 March 1971)
(Revised 17 June 1971)*

REFERENCES

- 1 Hybart, F. J. and Pepper, B. *J. Appl. Polym. Sci.* 1969, **13**, 2643
- 2 Harvey, E. D. and Hybart, F. J. *J. Appl. Polym. Sci.* 1970, **14**, 2133
- 3 Edgar, O. B. and Hill, R. *J. Polym. Sci.* 1952, **8**, 1
- 4 Magill, J. H. *Polymer, Lond.* 1961, **2**, 221
- 5 Mandelkern, L. 'Crystallization of Polymers', McGraw-Hill, New York, 1964

Properties of piperazine homopolyamide films

LINO CREDALI and PAOLO PARRINI

Properties of films prepared from the following poly(piperazine amides) were examined: poly(2-methylpiperazine fumaramide); poly(*trans*-2,5-dimethylpiperazine fumaramide); poly(*trans*-2,5-dimethylpiperazine mesaconamide); poly(*trans*-2,5-dimethylpiperazine terephthalamide); poly(*trans*-2,5-dimethylpiperazine isophthalamide); poly(*trans*-2,5-dimethylpiperazine adipamide). Mechanical properties of these films are good; they have in fact a high tensile strength and in accordance with the rigidity of the polymer chain, low elongations and a high modulus of elasticity. Optical properties are very good. Since the films have a high water absorption, permeability to water vapour is very high while treatment of the films in water causes lowering of mechanical properties. Resistance to thermal ageing in an atmosphere of nitrogen is good. Among the various films considered those obtained from polymers with an unsaturated acid (fumaric and mesaconic) seem to show the best properties.

INTRODUCTION

POLYAMIDES of piperazine and substituted piperazine are of interest because of the general ease with which they may be transformed into films, and of some properties such as a high melting or degradation temperature, high water absorption, and high water permeability.

These properties, deriving from the lack of a H atom at the amide nitrogen and from the rigidity given to the polymer chain by the presence of the piperazine ring, may be influenced by the nature of the dicarboxylic acid, and by the degree of substitution of piperazine.

Bruck¹⁻³, and Bruck and Levi⁴ studied the thermal decay of homopolyamides and copolyamides derived from piperazine and from substituted piperazine. More recently Bruck⁵ stressed the possibility of the potential use of piperazine-derived copolyamides in medical implant applications, particularly as a possible substitute for the cornea.

In a previous study⁶ we dealt with the properties of piperazine-derived polyfumaramides with different degrees of substitution; some properties of films prepared from poly(2-methylpiperazine fumaramide) and from poly(*trans*-2,5-dimethylpiperazine fumaramide) have been considered in particular. The properties of films prepared from homopoly-piperazineamides deriving from fumaric, mesaconic, isophthalic and terephthalic acids are reported in the present study. The properties of the films are considered in relation to the polymer nature and to their preparation process.

EXPERIMENTAL

Preparation of polymers

Poly(2-methylpiperazine fumaramide) (2-MPF) and poly(*trans*-2,5-dimethylpiperazine fumaramide) (*t*-2,5-DMPF) were prepared by condensing fumaroyl dichloride and respectively 2-methylpiperazine and *trans*-2,5-dimethylpiperazine according to a method previously described⁷.

Poly(*trans*-2,5-dimethylpiperazine mesaconamide) (*t*-2,5-DMPM) was prepared by condensing mesaconyl dichloride and *trans*-2,5-dimethylpiperazine, according to a method previously described⁸.

Poly(*trans*-2,5-dimethylpiperazine terephthalamide) (*t*-2,5-DMPT), poly(*trans*-2,5-dimethylpiperazine isophthalamide) (*t*-2,5-DMPI) and poly(*trans*-2,5-dimethylpiperazine adipamide) (*t*-2,5-DMP-6) were prepared by condensing the respective acid dichlorides with *trans*-2,5-dimethylpiperazine according to a method indicated by Morgan⁹.

Polymers used in the preparation of films showed the following inherent viscosity values:

2-MPF	(at 30°C in H ₂ SO ₄ , 0.5%)	= 1.2
<i>t</i> -2,5-DMPF	(at 30°C in H ₂ SO ₄ , 0.5%)	= 2.2
<i>t</i> -2,5-DMPM	(at 30°C in H ₂ SO ₄ , 0.5%)	= 1.1
<i>t</i> -2,5-DMPT	(at 30°C in H ₂ SO ₄ , 0.5%)	= 1.6
<i>t</i> -2,5-DMPI	(at 30°C in <i>m</i> -cresol, 0.5%)	= 3.1
<i>t</i> -2,5-DMP-6	(at 30°C in H ₂ SO ₄ , 0.5%)	= 1.5

Film preparation

Films were prepared by dry casting from polymer solutions. Before preparing the solution, polymers were dried at 105°C to constant weight to eliminate the moisture which had been absorbed.

Films from formic acid (Carlo Erba RS) were obtained from a 10 wt. % solution. The solution was prepared at room temperature and filtered under pressure through a G-3 type glass filter. The solution was spread on a glass sheet and the solvent was allowed to evaporate at 30°C.

The films from the chloroform-methanol mixture (88:12) (Carlo Erba RS) were obtained by the same procedure from 5–6 wt. % solutions. During the evaporation of the solvent, particular care must be taken to avoid absorption of moisture which might cause polymer precipitation. The last traces of solvent were eliminated by a long treatment at 105°C under vacuum.

Films with a thickness varying between 10 and 100 μm may be obtained easily by controlling the polymer concentrations and the thickness of the casting knife spreading.

The film properties have been determined on films of 25 μm thickness.

Mechanical properties

The tensile properties were determined by means of an Instron apparatus according to the ASTM-D-882 method.

The resistance to bursting (Mullen) was determined according to the ASTM-D-774-63 T method and the tear resistance by the ASTM-D-1922-67 method. The folding endurance was determined according to the ASTM-D-2176-63 T method.

Density

Densities of films were determined by flotation in a mixture of toluene-carbon tetrachloride at 25°C.

Optical properties

Optical properties have been determined by means of a Gardner spectrophotometer following the ASTM-D-1003 method.

Electrical properties

The electrical resistivity was measured by a Teraohmmeter Ihare following the ASTM method D-257. The dielectric constant ϵ and the dissipation factor $tg\delta$ were measured by a General Radio apparatus (Schering Bridge) following the ASTM method D-150 and the dielectric strength by an apparatus following the ASTM method (short-time test) D-149.

Moisture regain

Moisture regain was determined by exposing a dry sample to 65% and 98% relative humidity atmospheres at 23°C for 24 h. Water absorption was determined by difference in weight.

Water vapour permeability

Water vapour permeability was determined by following the cup method in accordance with the ASTM-E-96 specifications, procedure B.

Water resistance

Water resistance was determined by dipping the film test sample in water and determining the loss of tensile properties with time. The film test sample dipped in water was taken out after successive intervals and wiped quickly between two sheets of filter paper, after which the properties were determined.

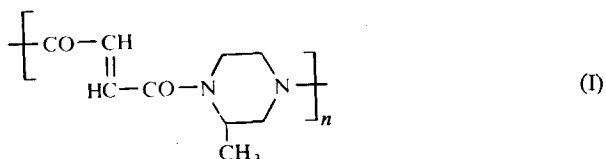
Temperature resistance

Thermal ageing was measured by treating the films at 150, 200 and 250°C in nitrogen in a closed system and determining the tensile properties after successive intervals.

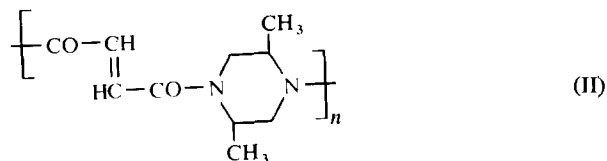
RESULTS AND DISCUSSION

The films we considered have been prepared respectively from the following polymers:

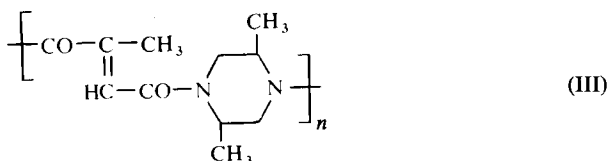
poly(2-methylpiperazine fumaramide) (2-MPF)



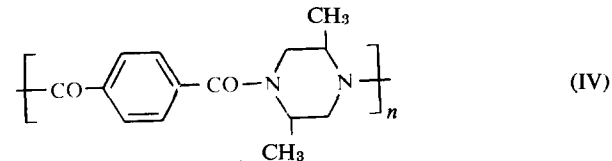
poly(*trans*-2,5-dimethylpiperazine fumaramide) (*t*-2,5-DMPF)



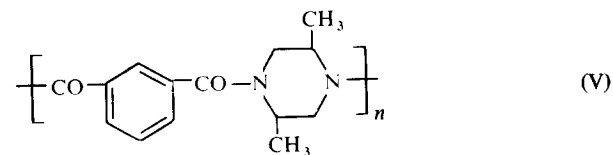
poly(*trans*-2,5-dimethylpiperazine mesaconamide) (*t*-2,5-DMPM)



poly(*trans*-2,5-dimethylpiperazine terephthalamide) (*t*-2,5-DMPT)

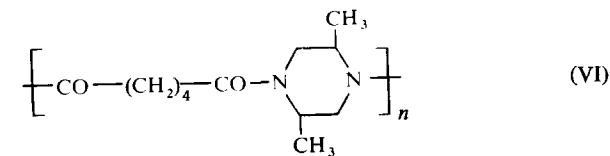


poly(*trans*-2,5-dimethylpiperazine isophthalamide) (*t*-2,5-DMPI)



Some properties have also been determined on a piperazine polyamide derived from a saturated aliphatic acid:

poly(*trans*-2,5-dimethylpiperazine adipamide) (*t*-2,5-DMP-6)



Polymers (I) and (II) cannot be melted and have decomposition temperatures in nitrogen ranging from 350 to 380°C⁷.

Polymer (III) decomposes in nitrogen at 380°C⁸.

Polymer (V) melts at 320°C while polymer (IV) does not melt until 420°C, and decomposes at 450–475°C⁴. For polymer (VI) a softening temperature of 290°C has been reported⁹.

While polyamides (IV) and (V) are amorphous on x-ray analysis⁴, polyamides derived from fumaric acid, (I) and (II), are partly crystalline and for (II) an identity period of $8.4 \pm 0.15 \text{ \AA}$ has been determined along the polymer chain⁷.

Generally, films of the above-mentioned polymers may be prepared from solutions in formic acid but for *t*-2,5-DMPM and *t*-2,5-DMP-6 a chloroform-methanol mixture was preferred. *t*-2,5-DMPF has been cast as film from several solvents or couples of solvents; reported data about this polymer generally refer to films prepared from formic acid and from chloroform-methanol mixtures.

Mechanical properties

Mechanical properties of films prepared from formic acid and from chloroform-methanol mixture are given in *Tables 1* and *2* respectively. Values for 2-MPF and *t*-2,5-DMPF are taken from a previous paper⁶.

Table 1 Tensile properties of piperazine polyamide films cast from formic acid solutions

Polyamide	Conditioning*	Water content (wt. %)	Yield strength (kg/cm ²)	Tensile strength at break (kg/cm ²)	Elongation at yield (%)	Elongation at break (%)	Tensile modulus (kg/cm ² $\times 10^{-3}$)
2-MPF	dry	0	—	1193	—	6.5	32.10
2-MPF	conditioned	8.3	—	729	—	3.0	29.60
<i>t</i> -2,5-DMPF	dry	0	—	1220	—	6.8	28.10
<i>t</i> -2,5-DMPF	conditioned	6.1	890	810	3.5	5.0	31.00
<i>t</i> -2,5-DMPT	dry	0	†	†	†	†	†
<i>t</i> -2,5-DMPT	conditioned	6.5	—	853	—	6.4	33.40
<i>t</i> -2,5-DMPI	dry	0	—	848	—	5.7	26.20
<i>t</i> -2,5-DMPI	conditioned	7.6	—	629	—	2.4	30.40

*Conditioned at 23°C, 65% r.h., for 24 h

†Too brittle, no measurement was possible

Measurements of mechanical properties have been made on samples of completely dry films as well as on conditioned samples. In each case there is a general reduction in toughness on passing from a dry to a conditioned sample, i.e. to one having a water content varying from 5 to 10%.

Values given in *Tables 1* and *2* confirm the excellent mechanical properties of polyamides derived from fumaric acid, in comparison to the corresponding isophthalic acid and adipic acid polyamides. The greater toughness should, in fact, belong to the dry film of *t*-2,5-DMPT but, in actual fact under these conditions, the films are so brittle that it becomes practically impossible to perform measurements on them.

The influence of the casting solvent on the mechanical properties was examined for *t*-2,5-DMPF. The solvents used were: *m*-cresol; phenol-tetra-chloroethane mixture; *m*-cresol-chloroform mixture; methanol-chloroform mixture and methanol-methylene chloride mixture. In all cases the tensile

Table 2 Tensile properties of piperazine polyamide films cast from methanol-chloroform mixture (12:88)

Polyamide	Conditioning*	Water content (wt. %)	Yield strength (kg/cm ²)	Tensile strength at break (kg/cm ²)	Elongation at yield (%)	Elongation at break (%)	Tensile modulus (kg/cm ² × 10 ⁻³)
<i>t</i> -2,5-DMPF	dry	0	—	1203	—	9.8	26.00
<i>t</i> -2,5-DMPF	conditioned	5.5	870	835	3.8	7.8	28.00
<i>t</i> -2,5-DMPM	dry	0	709	667	1.3	11.7	24.40
<i>t</i> -2,5-DMPM	conditioned	8.7	737	637	3.4	23.7	35.60
<i>t</i> -2,5-DMP-6	dry	0	—	855	—	3.2	26.80
<i>t</i> -2,5-DMP-6	conditioned	6.4	—	810	—	3.8	27.10

*Conditioned at 23°C, 65% r.h., for 24 h

strength values of films conditioned at 65% relative humidity, at 23°C for 24 h fell between 800 and 850 kg/cm².

The resistance to bursting, tear strength and folding endurance are given in Table 3. The values of resistance to bursting and tear are very interesting as they are generally of the same order of magnitude as those of the best known commercial films; *t*-2,5-DMPM gave the best results.

The stiff character of films is shown by the folding endurance values; the use of chloroform-methanol mixture as casting solvent enhances the values of this property.

Table 3 Bursting strength, tear resistance and folding endurance properties. Samples conditioned at 23°C, 65% r.h. for 24 h

Polyamide	Casting solvent	Bursting strength (Mullen test) (kg/cm ²)	Tear resistance (Elmendorf) (g/25 μm)	Folding endurance (No.)
2-MPF	HCOOH	1.2	12	200
<i>t</i> -2,5-DMPF	HCOOH	2.0	16	1 000
<i>t</i> -2,5-DMPF	CHCl ₃ /CH ₃ OH	2.8	15	20 000
<i>t</i> -2,5-DMPM	CHCl ₃ /CH ₃ OH	4.5-7.3	20	1 100
<i>t</i> -2,5-DMPT	HCOOH	*	*	*
<i>t</i> -2,5-DMPI	HCOOH	2.8	15	450

*Too brittle, no measurement was possible

Density, optical and electrical properties

Table 4 gives the values of densities determined on dry samples at 25°C. The density values of the various films do not show any important variations. The value for 2-MPF is slightly higher.

Density measurements have not been made for films with different water contents or for heat-treated films as we believe their trend to be the same as that already determined for *t*-2,5-DMPF and previously reported⁶. For this polymer, we have already found that a water content of nearly 5 wt. %

Table 4 Densities at 25°C of piperazine polyamide dried films

<i>Polyamide</i>	<i>Density</i> (g/cm ³)
2-MPF	1.285
<i>t</i> -2,5-DMPF	1.217
<i>t</i> -2,5-DMPM	1.221
<i>t</i> -2,5-DMPT	1.233
<i>t</i> -2,5-DMPI	1.212

increases the density value, but at higher water content density decreases.

Optical properties are given in Table 5. Properties of *t*-2,5-DMPT films are not given in Table 5 because such films are generally opaque and milky. The films given in Table 5, prepared with formic acid as casting solvent appear perfectly transparent and brilliant. Films prepared with a methanol-chloro-

Table 5 Optical properties of piperazine polyamide films. Samples conditioned at 23°C, 65% r.h., for 24 h

<i>Polyamide</i>	<i>Casting solvent</i>	<i>Haze</i> (%)	<i>Luminous transmittance</i> (%)	<i>Gloss</i> (%)
2-MPF	HCOOH	0.8	95-96	187
<i>t</i> -2,5-DMPF	HCOOH	1.6	94-96	160
<i>t</i> -2,5-DMPM	CHCl ₃ /CH ₃ OH	9	90-94	135
<i>t</i> -2,5-DMPI	HCOOH	1	94-96	181

form mixture generally have poorer optical properties, which are influenced more by the casting conditions.

Gloss values for 2-MPF and *t*-2,5-DMPI are very good and higher than those of cellulose acetate or polyester films.

Optical properties of *t*-2,5-DMPM are of poorer quality as the film is obtained using a methanol-chloroform mixture as solvent.

Electrical properties are given in Table 6 and are not very good as could easily be foreseen, given the hydrophilic nature of these polymers. They may be improved for films in the dry state, but this fact is not of practical interest.

Resistivity is rather poor, and the polymers' polar character is revealed particularly by the rather high *tgδ* value. The dielectric constant varies between 3.5 and 4.5. The dielectric strength values are of the same order as those of traditional polyamides.

Table 6 Electrical properties of piperazine polyamide films. Samples conditioned at 23°C, 65% r.h., for 24 h

Polyamide	Casting solvent	Resistivity ($\Omega \cdot \text{cm}$)	Dissipation factor* ($\text{tg}\delta$)	Dielectric constant* (ϵ)	Dielectric strength† (kV/25 μm)
2-MPF	HCOOH	9×10^{12}	0.4×10^{-2}	3.5	2.5
<i>t</i> -2,5-DMPF	HCOOH	2×10^{12}	2×10^{-2}	3.7	1.0
<i>t</i> -2,5-DMPM	CHCl ₃ /CH ₃ OH	3×10^{12}	1.5×10^{-2}	3.9	2.5
<i>t</i> -2,5-DMPI	HCOOH	2×10^{12}	1.8×10^{-2}	4.5	2.5

*10⁶ Cycles

†50 Cycles

Behaviour to water

One of the most interesting properties of piperazine homopolyamide films is their behaviour to water. This behaviour, which may be remarkably important for applications of these films, mainly derives from their high water absorption.

Table 7 gives the moisture regain of film with 65% and 98% relative humidity. As can be seen from these values the regain of moisture by

Table 7 Moisture regain of piperazine polyamide films at 65% and 98% r.h., after 24 h at 23°C

Polyamide	Casting solvent	Moisture regain (% by weight)	
		65% r.h.	98% r.h.
2-MPF	HCOOH	8.3	23.4
<i>t</i> -2,5-DMPF	HCOOH	6.1	16.6
<i>t</i> -2,5-DMPF	CHCl ₃ /CH ₃ OH	5.5	16.5
<i>t</i> -2,5-DMPM	CHCl ₃ /CH ₃ OH	8.7	21.9
<i>t</i> -2,5-DMPT	HCOOH	6.5	19.8
<i>t</i> -2,5-DMPI	HCOOH	7.6	23.6

piperazine homopolyamide films is generally very high. Under the same conditions a cellulose acetate film with 39.8% acetyl contents gave the following moisture absorption values: 4.3% in weight at 65% r.h. and 13.4% in weight at 98% r.h.

The higher moisture regain shown by piperazine homopolyamides, in comparison with polyamides from primary diamines, may be related to the lack of a hydrogen atom at the amide nitrogen, which prevents hydrogen interchain formation links.

Films derived from 2-MPF and *t*-2,5-DMPI have the highest moisture absorption values; *t*-2,5-DMPM has a higher value than *t*-2,5-DMPF, while we could expect the opposite given the greater number of methyl substituent groups of *t*-2,5-DMPM.

Permeabilities to water vapour of the various kinds of films are given in

Table 8. These values show that permeabilities to water vapour of piperazine-amide films are rather high. Under the same conditions a cellulose acetate film with an acetylation degree of 39.8% gave a value of:

$$0.154 \frac{\text{g} \times \text{cm}}{\text{m}^2 \times \text{mmHg} \times 24 \text{ h}}$$

Among the various films 2-MPF has the highest permeability value. On the contrary *t*-2,5-DMPI and *t*-2,5-DMPT give a lower value.

A comparison between the values of Tables 7 and 8 show that, for every

Table 8 Water vapour permeability at 25°C of piperazine polyamide films

Polyamide	Casting solvent	Water vapour permeability
		$\left(\frac{\text{g} \times \text{cm}}{\text{m}^2 \times \text{mmHg} \times 24 \text{ h}} \right)$
2-MPF	HCOOH	0.350
<i>t</i> -2,5-DMPF	HCOOH	0.347
<i>t</i> -2,5-DMPF	CHCl ₃ /CH ₃ OH	0.238
<i>t</i> -2,5-DMPM	CHCl ₃ /CH ₃ OH	0.270
<i>t</i> -2,5-DMPT	HCOOH	0.140
<i>t</i> -2,5-DMPI	HCOOH	0.177

film, there is no correspondence between water absorption and permeability. In particular the high water absorption of *t*-2,5-DMPI and *t*-2,5-DMPT compared with *t*-2,5-DMPF does not correspond to a higher permeability. In first approximation such behaviour can be explained qualitatively, by considering that permeability depends on the solubility and rate of diffusion of the molecules of the diffusing substance in the medium in which it diffuses. The chemical structure of the polymers considered may influence these two parameters differently leading to different relations between solubility and permeability values. A study of the relation between water permeability and polymer structure is under investigation and will be reported later.

Values obtained for *t*-2,5-DMPF also show a considerable influence of the casting solvent on permeability. It is probable, in fact, that acid residues derived from formic acid used as casting solvent, considerably alter the permeability values.

A special property of piperazine polyamide films is their mechanical behaviour after dipping in water; in fact, after water treatment these films become partly elastic and their mechanical properties tend to be lowered considerably.

A series of test samples was dipped into water for a certain period; after the samples were taken out of the water, and quickly wiped at their surface between two sheets of filter paper, their mechanical properties were then determined. The results are given in Table 9. As may be observed from the values obtained after treatment of 24 and 720 h a general decrease of the tensile strength occurred. At best this was only 30% of the initial value for the dry sample. There was also a remarkable decrease in the modulus of elasticity and an increase in elongation. In agreement with the structure of

Table 9 Tensile properties* of piperazine polyamide films after immersion in water

Polyamide	Casting solvent	Immersion time						% Tensile strength retained on the original one of the dried samples	
		24 h			720 h			24 h immersion	720 h immersion
		TS	E	TM	TS	E	TM		
2-MPF	HCOOH	140	48	30	136	46	41	11.7	11.4
<i>t</i> -2,5-DMPF	HCOOH	256	63	34	143	23	56	21.0	11.7
<i>t</i> -2,5-DMPF	CHCl ₃ /CH ₃ OH	375	54	213	236	61	67	31.2	19.7
<i>t</i> -2,5-DMPM	CHCl ₃ /CH ₃ OH	210	18	102	205	120	65	31.5	30.8
<i>t</i> -2,5-DMPI	HCOOH	107	11	140	107	35	174	12.4	12.4
<i>t</i> -2,5-DMPT	HCOOH		Brittle			Brittle		—	—

*TS = tensile strength at break (kg/cm²); E = elongation at break (%); TM = tensile modulus (kg/cm² × 10⁻³)

the polymer chain with a larger number of methyl substituent groups, *t*-2,5-DMPM has the highest residual load, while there are no changes in passing from polyamides based on fumaric to those containing isophthalic acid.

Mechanical tests have not been carried out on the *t*-2,5-DMPT film because the samples proved exceedingly brittle after dipping in water. A certain influence of the casting solvent may be found for the first 24 h of water treatment. After 24 h treatment, *t*-2,5-DMPF film, prepared from the methanol-chloroform mixture, shows better mechanical properties than that prepared from formic acid. For subsequent times, however, samples left in water tend to behave in the same way.

Behaviour to temperature

It has been shown in a previous paper⁶ that 2-MPF and *t*-2,5-DMPF films have a poor resistance to temperature when heated in the presence of oxygen, while temperature resistance properties are excellent when these films are heated in non-oxidizing conditions. *Table 10* gives the tensile strength half-time breakdown of piperazine polyamide films, under non-oxidizing conditions, so that the influence of the chemical structure on this property can be examined.

Table 10 Thermal ageing of piperazine polyamide films in nitrogen at different temperatures

<i>Polyamide*</i>	<i>Half time tensile strength breakdown at</i>		
	<i>150°C</i>	<i>200°C</i>	<i>250°C</i>
2-MPF	> 3 months	> 3 months	72 h
<i>t</i> -2,5-DMPF	> 3 months	> 3 months	1 month
<i>t</i> -2,5-DMPM	2 months	480 h	12 h
<i>t</i> -2,5-DMP-6	1 month	48 h	< 6 h
<i>t</i> -2,5-DMPI	240 h	48 h	24 h
<i>t</i> -2,5-DMPT	2 months	156 h	48 h

*Casting solvent formic acid

It may be observed from these data that poly(piperazine amides) based on fumaric and mesaconic acids are more resistant than the corresponding polyamides based on adipic, terephthalic and isophthalic acids. Poly(piperazine fumaramides) are also more resistant than poly(piperazine mesaconamides) and this may be linked to the different structure of the two acids, in which an extra methylene substituent group leads to poorer resistance to temperature.

In the course of these tests solvent residue (formic acid) as well as water absorbed by the polymer were found to have a remarkable influence on thermal resistance. For this reason samples tested on thermal ageing have been dried for a long time before being measured.

CONCLUSIONS

Films prepared from piperazine polyamides generally show good mechanical properties; in fact films with high tensile strength, low elongation and a high elastic modulus were obtained. Considering that these films did not undergo any stretching treatment, they can be ranked among the best for their mechanical properties. It has been previously shown⁶, moreover, for *t*-2,5-DMPF, that stretching brings the tensile strength to very high values of 2550 kg/cm² with an elastic modulus of 72 400 kg/cm²; a similar course is also foreseeable for the other polyamides described in this paper.

The films have very good optical properties. In fact, piperazine polyamide films are highly transparent, with low haze and high gloss value. Such properties give to the films an even better aspect than that of polyester or cellulose acetate films.

A detrimental property of the films considered is the loss of tensile strength when they are wet. This involves several difficulties in the eventual application of these polymers. Steam permeability properties are, on the contrary, very good.

Among the various poly(piperazine amides) which have been examined, *t*-2,5-DMPF has the best properties, within the above indicated limits, with regard to the ease of obtaining films, as well as to the mechanical, optical and thermal ageing resistance properties. Loss of mechanical properties of *t*-2,5-DPM film after water treatment is slightly less.

From the related properties taken as a whole, it may be inferred that the presence of an unsaturated acid, as a component of the poly(piperazine amides) leads to better properties in the preparation of the films as well as in their intrinsic properties. As for the preparation, use of formic acid as a casting solvent leads to films having excellent optical properties, while the use, when possible, of a chloroform-methanol mixture results in films generally having inferior optical properties. The use of formic acid, however, leads to considerable difficulty in eliminating acid residues remaining in the film, which might give rise to large variations in the properties of the films themselves.

ACKNOWLEDGEMENTS

Thanks are due to Prof. L. Mortillaro and Prof. M. Russo for supplying us with the polymers, and to Prof. P. Manaresi for his kind interest in this work.

*Montecatini Edison SpA,
Centro Ricerche Ferrara,
44100 Ferrara, Italy*

(Received 11 March 1971)

REFERENCES

- 1 Bruck, S. *Polymer, Lond.* 1965, 6, 483
- 2 Bruck, S. *Polymer, Lond.* 1966, 7, 231
- 3 Bruck, S. *Polymer, Lond.* 1966, 7, 321

- 4 Bruck, S. and Levi, A. A. *J. Macromol. Sci. (A1)* 1967, **6**, 1096
- 5 Bruck, S. *Polymer, Lond.* 1969, **10**, 939
- 6 Credali, L., Parrini, P., Mortillaro, L., Russo, M. and Simonazzi, T. *Angew. makromol. Chem.* 1971, (in press).
- 7 Mortillaro, L., Russo, M., Guidotti, V. and Credali, L. *Makromol. Chem.* 1970, **138**, 151
- 8 Guidotti, V., Russo, M., and Mortillaro, L. *Makromol. Chem.* 1971, **147**, 111
- 9 Morgan, P. W. 'Condensation polymers: by interfacial and solution methods'. Interscience, New York, 1965

Analogies between chain-folded and extended-chain crystallization of polyethylene

D. C. BASSETT and JANET M. PHILLIPS

Polyethylene lamellae grown from the melt under vacuum and at 5 kbar (1 bar = 10^5 N m^{-2}) have been compared. Molecules in them persist in folding even at intervals close to their own length. The temperature dependence of layer thickness is identical in both cases. All data are fitted by the same expression, which coincides at lower supercoolings with that developed in kinetic theories of chain-folding. Only at low pressure, however, are the parameters sensible. Pursuit of the analogy between low and high pressure crystallization suggests that theories of chain-folded growth from the melt are inadequate if they neglect lamellar thickening behind the growth front.

INTRODUCTION

RECENT INVESTIGATIONS in this laboratory have revealed a qualitative similarity between the thicknesses of polyethylene lamellae grown at low and high pressures. So-called 'extended-chain' crystallization of fractionated polymer gives layers whose average thickness increases with temperature and time¹. Because this is the same trend of behaviour as reported for chain-folded crystallization at atmospheric pressure, it becomes increasingly of interest to compare the two cases in more detail. This has been attempted in the present paper which reports a preliminary examination of the relative effect of crystallization temperature on lamellar thickness at 5 kbar (1 bar = 10^5 N m^{-2}) and under vacuum.

Particular importance was attached in the first instance to making a comparison with very short molecules at low pressure in order to have a ratio of molecular length to crystal thickness similar to that for the high pressure data. This was because whereas kinetic theories of chain-folding predict observed crystal thicknesses reasonably well for typical molecular lengths, their applicability is not strictly justified unless the actual crystallization approximates to that of the infinite molecule, i.e. where the molecular length is much greater than the fold length². In the event, however, this caution proved unwarranted. At least to a first approximation, the observed thickness at a particular supercooling under vacuum showed no change with molecular weight for chain lengths as short as 500 Å. Moreover, all high and low pressure data fit surprisingly well to the same reduced curve, implying that a single unified formalism is capable of describing crystal thicknesses throughout the pressure range to 5 kbar including what are usually known as chain-folded and extended-chain crystals.

EXPERIMENTAL

Materials

Three linear polyethylenes have been used, which are listed in *Table 1*. Samples 1 and 2, obtained by column fractionation, both had a weight- to number-average molecular weight ratio of 1.14 when characterized by gel permeation chromatography¹. Sample 3, in contrast, was a crude fraction of low molecular weight obtained by selective dissolution from a sample of Rigidex 50. The homopolymer was subjected to boiling amyl acetate in a Soxhlet extractor, giving a soluble product which after cooling, filtration and drying then had the lowest molecular weights similarly removed by boiling 2-butoxyethanol. The dried residue was sample 3. Viscosity measurements and the use of Chiang's relation³

$$[\eta] = 6.2 \times 10^{-4} \bar{M}_v^{0.7}$$

gave its molecular weight as $\bar{M}_v = 5270 \pm 300$.

Table 1. Molecular weights of samples used

Sample	Molecular weight		
	Number average	Weight average	Viscosity average
1	50 100	57 200	
2	21 600	24 700	
3			5270

Lamellar thickness

Measurements of lamellar thickness came from two sources. Values to about 500 Å produced by low pressure crystallization were determined primarily by low-angle x-ray diffraction. For the most part only first-order diffraction peaks were detected, whose position was converted to a long spacing using Bragg's law and without correcting for slit collimation. On occasion, however, data were reinforced by electron microscopy of fracture surfaces.

For the higher thicknesses found in 'extended-chain' samples this is the only technique yet available, despite its well-known disadvantages. In this case dimensions were measured parallel to *c*, i.e. along the striations produced by fracture. Random sampling of a large number of lamellae was used and led to a number-average figure, as has been described previously¹. The identical treatment used for vacuum-grown polymer gave fair agreement with x-ray values. *Figure 1*, for example, is a histogram compiled in 200 Å intervals of measurements made on the fracture surface of *Figure 2*. The material is sample 3 crystallized at 125°C. *Figure 1* gives a mean value of 555 Å with a probable error of 25 Å, which compares with an x-ray value of 433 ± 45 Å and an estimated viscosity average molecular length of 480 Å.

The microscopic measure, which is of fold length should be higher by a factor $\sec \theta$ (θ being the angle between *c* and the lamellar normal) than the layer thickness determined by x-rays. From observation and also model

systems^{4,5}, θ appears to be about 35° . This essentially accounts for the difference between the two lengths as their direct ratio gives $\theta = 39^\circ$ with a probable error of $+9, -13^\circ$. However, there are in addition other factors which are difficult to quantify. Chief among these are the representative nature of a fracture surface and the conversion of a single diffraction peak

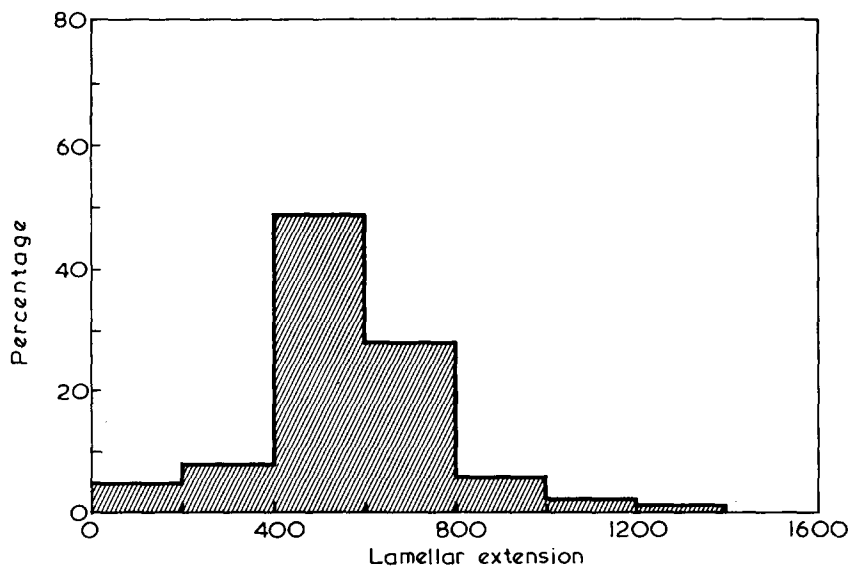


Figure 1 Histogram of molecular extensions measured on the fracture surface of Figure 2 for 89 lamellae. The number average mean length is $555 \pm 25 \text{ \AA}$; $\Delta T = 12^\circ\text{C}$ period

using Bragg's law. Regarding the former, one knows that the brittle character of fracture increases with greater relative molecular extension¹. One might, therefore, anticipate that a propagating crack would reveal the more-extended chain regions in a sample preferentially.

Nevertheless, generally one can state that these (and other) uncertainties are partly mitigated when one compares only values obtained with the same technique, as is effectively the case throughout this work. In Figure 3 it is achieved by reduction to a relative change in spacing. An arbitrary reference value of 16 K of supercooling was taken, falling conveniently as it did within the range of all three sets of data. Some diffuseness, greater than may appear at first sight must, nevertheless, remain in Figure 3, if only because spacings are time dependent and should, therefore, be compared at equivalent times. The experimental basis for so doing is not yet available. We have, accordingly, for the rapidly changing sizes found at 5 kbar, used figures measured at the shortest times. The time dependence is less marked at low pressure and then we have been content with values recorded after longer intervals required effectively to complete growth at the higher temperatures.

Determination of supercooling

The various crystallization temperatures, T_c , used have been reduced to a common basis of supercooling defined as $\Delta T = T_m^0 - T_c$ where T_m^0 is the

directly observed melting temperature of a highly-extended-chain sample of the fraction. At 5 kbar, T_m^0 was determined as that temperature of annealing at which samples close to full molecular extension were first able to be quenched to low-melting polymer¹. All other melting points were recorded as the peak of the melting endotherm recorded by a Perkin-Elmer DSC1B instrument, using a scanning rate of 8 K/min and calibrated against indium.

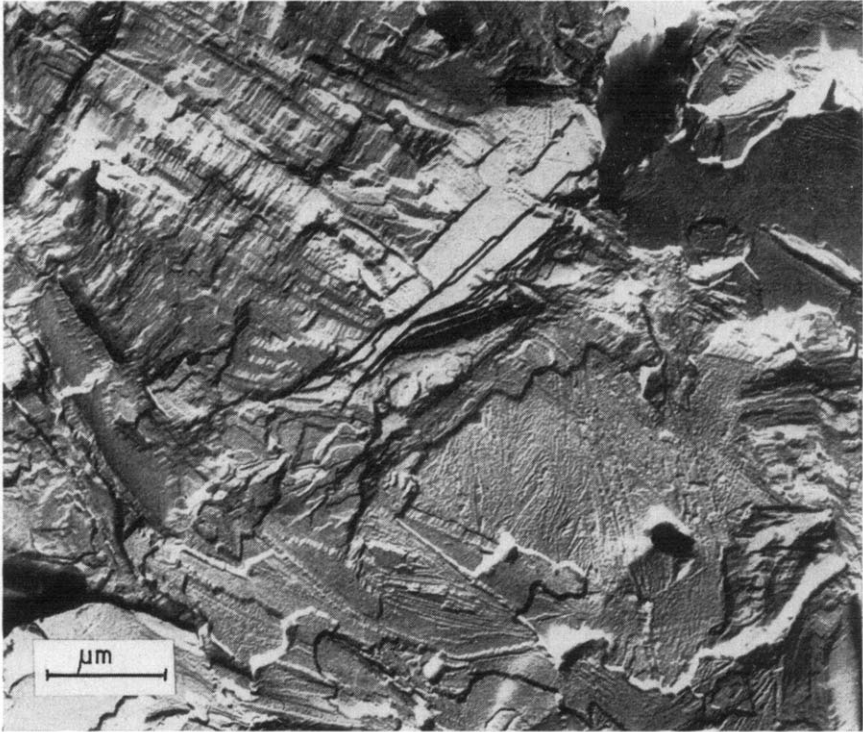


Figure 2 Portion of a fracture surface of sample 3 crystallized at 125°C for 24 h under vacuum

RESULTS

Data are collected in *Table 2* and *Figure 3*. They include high pressure data taken from earlier work¹ and combine chain-folded (*Figures 2* and *4*) and 'extended-chain' (*Figures 2* and *5*) morphologies. At low pressure, samples were sealed in glass ampoules while being evacuated with a diffusion pump, and crystallized after holding for 3 min at 150°C. The procedure at 5 kbar (4.9 ± 0.25 kbar) has been described elsewhere¹.

DISCUSSION

Although polyethylene fractions of 20 000 and 5000 molecular weight give slightly different spacings at the same crystallization temperature under

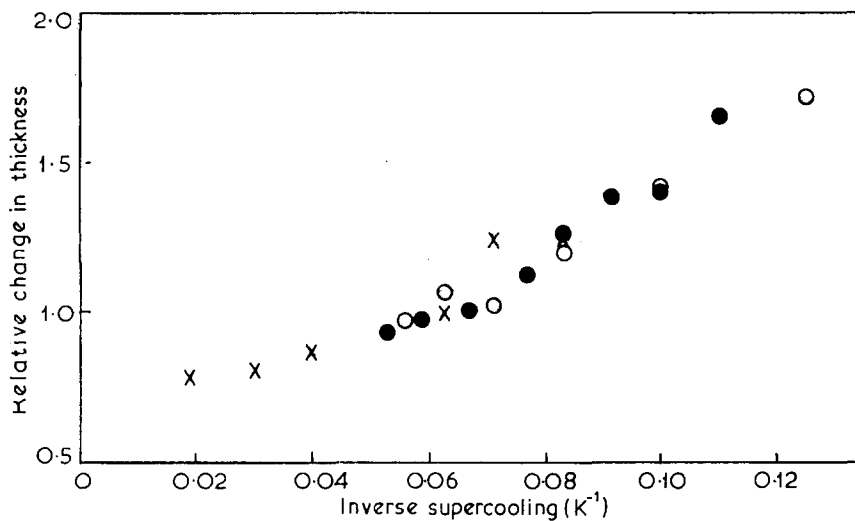


Figure 3 Reduced curve of relative spacing change against inverse supercooling for all data (see text). \times Sample 1 (5 kbar); \circ sample 2 (0 bar); \bullet sample 3 (0 bar)



Figure 4 Chain-folded morphology in sample 2 crystallized at 127°C under vacuum for 24 h

Table 2 Combined data for samples tested

Sample	Pressure (bar)	Crystallization temperature (T_c) (°C)	Measured T_m^0 (°C)	Supercooling ($T_m^0 - T_c$)(°C)	Time (h)	Mean crystal thickness (Å)	Atmospheric $m.p.$ (°C)
1	4900	229	243	13	0.5	3271	140
		227		16	0.5	2623	141.5
		218		24	0.5	2285	141
		210		32	0.5	2104	139
2	0	190	137	52	0.5	2033	129
		129		8	96	520	140
		127		10	22	433	127
		125		12	21	360	136.5
		123		14	22	307	136
		121		16	24	322	134.5
		119		18	23	293	134
		126		9	66	500	133.5
		125		10	24	433	132.5
		124		11	24	460	133.5
3	0	123	135	12	22	361	123
		122		13	24	325	122.5
		120		15	65	286	131.5
		118		17	24	260	130.5
		116		19	24	278	118
					24		117.5

vacuum, values become the same when expressed in terms of supercooling using the experimentally determined values of T_m^0 . This parallels growth from solution where the insensitivity of crystal thickness to molecular length is well known. Of particular interest, however, is that this behaviour should hold to molecular lengths little longer than the crystal size. The implication

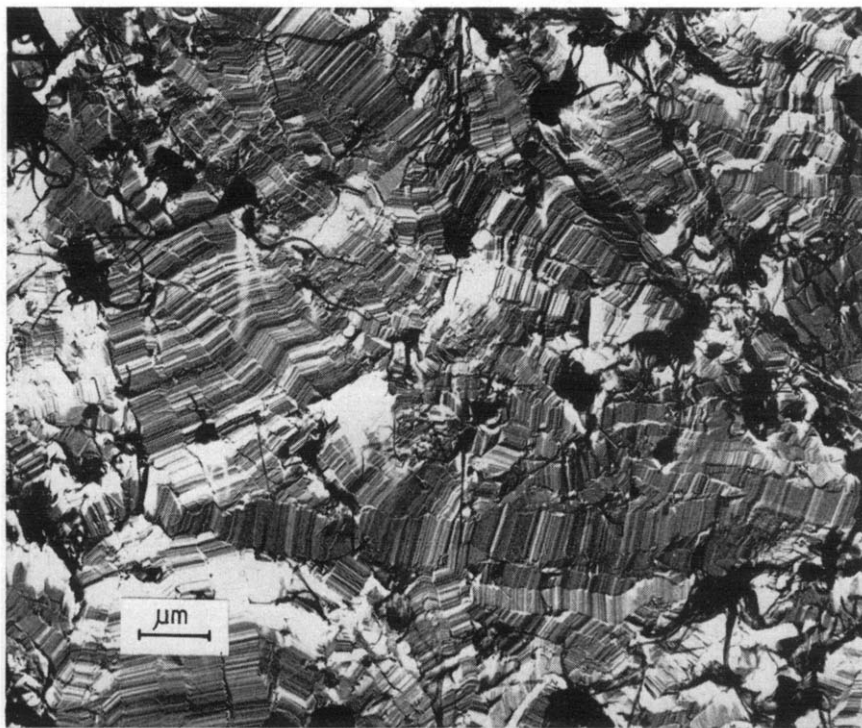


Figure 5 'Extended-chain' crystals of sample 1 prepared at 4.9 kbar by crystallizing at 218°C for 30 min (Courtesy of D. V. Rees)

appears to be that for sample 3 and also sample 1 at 5 kbar, molecules will fold once into a walking stick configuration rather than crystallize fully extended. This is a somewhat controversial point which needs further consideration.

If a single molecular species is being considered and is found to give lamellae thinner than its length, then it must be concluded either that fully extended molecules are tilted within the layer (i.e. the basal plane is not perpendicular to c) or that there is molecular folding. Interpretation of experiments with both oligomeric amides and polyoxyethylenes in this way⁶ has favoured folding. With polydisperse samples, however, one must consider a third alternative which involves fractionation. This is that molecules always crystallize fully extended and increases of x-ray long period with crystallization temperature reflect merely the progressive inability of the shorter molecules to crystallize⁷. One could presumably argue further that

even when all the sample crystallized, the longest molecules could form separate extended-chain crystals of their own, which would not be directly represented in an x-ray value, taken from the peak of a distribution. Such a procedure must lead to an average length.

Although this scheme has points of similarity to the present data, it does not appear to provide a sufficient explanation of them. Segregation of low molecular weight polymer does occur in certain circumstances and may be recognised by the appearance of a second, lower temperature, melting peak which is sensitive to cooling conditions and whose proportion becomes constant in time. This is not always the case, however, and considerable variation in spacing can occur with a single melting peak as in samples 1 and 2 (*Table 2*). Secondly, even when there is progressive separation of shorter molecules with temperature, there is no correlation with changes in spacing. Furthermore samples 2 and 3, of which the former crystallizes as a whole, give equivalent spacings. For all these reasons, fractionation appears to be irrelevant to the point in question and we are forced to conclude that molecular folding persists from the melt until fold and molecular lengths are very nearly equal.

When one considers crystals grown from solution for comparison, there is direct support for folding of very short molecules by the persistence of sectorization in crystals of low molecular weight polyethylene. This phenomenon is a consequence of each region containing a sufficient proportion of molecules folded along a preferred plane (which is no doubt usually the growth plane). Its study in low molecular weight polyethylene has shown that not just folding itself, but even the particular asymmetric shapes of folds are preserved down to very low molecular weights^{8,9}. With sharp gel permeation chromatography fractions sectors (and thus chain-folds) have been revealed in crystals of polyethylene as low as 2300 in molecular weight¹⁰.

The finding that x-ray long period is little dependent on molecular weight at a given supercooling may be expressed alternatively by the consideration that crystal thickness is unaffected by cutting an infinite molecule into short lengths. In other words the cut ends must in some way be paired in the crystal. This might be by being physically adjacent or perhaps, as has recently been suggested¹¹, by end-groups tending, on the whole, either to start or finish neighbouring segments in the crystal. Such a scheme does not necessarily imply total exclusion of chain-ends from lamellae but is rather a means of accounting for their accessibility to chemical attack¹². Indeed, a proportion of both folds and end-groups lie buried within a layer to some extent on this model. Moreover, it has been shown that there is sufficient flexibility of interchange between full molecular extension and singly folded, approximately hairpin configurations, in even moderately polydisperse samples to allow a quasi-continuous increase in crystal thickness with crystallization temperature. With monodisperse polymer, however the long period can only take discrete values such as have been observed for polyoxethylene¹³.

The translation of this latter proposal to the analogous situation of molecules crystallized at high extension under pressure is not entirely straightforward. One may, of course, draw the same pictorial molecular configurations, merely changing the relative scale, but this would leave the crystal density unaltered, whereas in practice densities of around 0.995 result in

pressure-crystallized samples, much higher than the 0.97 recorded for crystals of short chain polyethylene¹¹. Moreover one has not only the continuous increase of lamellar thickness with temperature to account for, but also that with time and this, too, in lamellae whose molecular weight range has been sharpened by fractional crystallization¹. For present purposes, however, this problem is a side issue. Our concern is more with the demonstration of chain-folding persisting in melt growth to high molecular extensions and with the comparison of high and low pressure behaviour.

The comparison of melt crystallization at high and low pressures is contained in *Figure 3*. No parameters are adjustable. They have all been measured. The observations are evidently compatible with a single reduced curve, the strict meaning of which is that crystal thickness has the same shape of temperature dependence in both cases. The effect of pressure is hidden in reducing the spacings to a relative change, but the formal implication is that a single magnification factor is sufficient to represent the pressure dependence in a unified description of melt crystallization.

The particular plot of *Figure 3* was chosen bearing in mind that kinetic theories of chain-folding predict a fold length:

$$l = \frac{2\sigma_e}{\Delta S_f \Delta T} + \delta l \quad (1)$$

ΔS_f being the entropy of fusion per unit volume and δl a constant. This relation is obeyed well for solution growth at 1 bar¹⁴ where spacing is observed to be linear in inverse supercooling¹⁵. The reduced plot becomes linear with decreasing supercooling when it may be said to be represented by an expression of the type of equation (1). Use of equation (1) itself, however, though giving a reasonable value for σ_e , the end surface free energy of ~ 100 erg/cm² from the slope at 1 bar, leads to the unacceptable conclusion that σ_e is proportional to reference length. There is no experimental support for this. Our unpublished measurements confirm that polyethylene crystals have practically the same thickness when grown at 5 kbar as at 1 bar¹⁶. One cannot look, therefore, to sufficient increase in σ_e to account for extended-chain thicknesses. Thus although kinetic theory formalism may fit the results, it does not do so with sensible parameters. Moreover, one can go further and criticize the relevance of current kinetic theories of chain-folding to the experimental observations at high pressure, because they take no account of lamellar thickening.

The theoretical solutions for chain-folded thicknesses are independent of time, molecular configurations remaining as they were laid down on the growth face except for minor readjustments such as fold smoothing. They lead to a difficulty, however, in predicting melting points of lamellae to be closer to their growth temperatures than is observed. A possible explanation was postulated to be isothermal lamellar thickening during crystallization¹⁷, but a better may be decreasing σ_e due to improved fold packing¹⁸. This would be in agreement with observations on solution-grown crystals where there is independent evidence for the latter¹⁹ but not the former. With melt growth, however, the situation is apparently different. For polyethylene the L_2 x-ray peak moves to smaller diffraction angles with time²⁰, (although L_1 , which

some interpret as the overall layer thickness²¹, remains constant). In addition there is a quantity of evidence (Rybnikar, F., personal communication) on samples quenched during crystallization showing both L_1 and L_2 increasing with time. We found a similar modest increase with the present samples at low pressure. At high pressure there is microscopic evidence of substantial increases with time¹. However, the relative change in layer thickness is about the same as that at atmospheric pressure¹. Evidently there is a further qualitative similarity here between high and low pressure crystallization whose study should usefully clarify both. The present results on temperature dependence, are not so much concerned with longer term thickening as with that occurring early in the establishment of the measured lamellar size. In a theory by Peterlin²², the two are related but our results are not in agreement with its predictions as we found no evidence for a strong dependence on molecular weight for molecules only slightly longer than the layer thickness.

It appears from high pressure observations that the large 'extended-chain' dimensions are attained behind a much thinner growing edge¹. The effect is most evident for very long molecules which seem to slow it down. Whilst this would allow one to interpret the measured thickness as a multiple of that initially laid down (which would not only be consistent with *Figure 3* if the multiple were constant, but could thereby avoid unreasonable parameters in the use of equation (1)) it leaves the reason for the large thickness unexplained. Nevertheless, if the phenomenon happens at high pressure then it must also occur under vacuum insofar as crystallization is analogous. Thus the work in this paper by supporting the analogy between low and high pressure crystallization carries with it the implication that theories of chain-folded growth from the melt are inadequate if they fail to take into account substantial lamellar thickening behind the growth front.

*J. J. Thomson Physical Laboratory,
University of Reading,
Reading RG6 2AF, UK*

*(Received 11 March 1971)
(Revised 27 April 1971)*

REFERENCES

- 1 Rees, D. V. and Bassett, D. C., *J. Polym. Sci. (A-2)* 1971, **9**, 385
- 2 Hoffman, J. D., *Kolloid Z.* 1969, **231**, 590
- 3 Chiang, R., *J. Phys. Chem.* 1965, **69**, 1645
- 4 Keith, H. D., *J. Appl. Phys.* 1964, **35**, 3115
- 5 Kawai, T. and Keller, A. *Phil. Mag.* 1965, **11**, 1165
- 6 Balta Calleja, F. J. and Keller, A. *J. Polym. Sci. (A)*. 1964, **2**, 2151, 2171
- 7 Arlie, J. P., Spegt, P. A. and Skoulios, A. E., *Makromol. Chem.* 1966, **99**, 160
- 8 Bassett, D. C., *Phil. Mag.* 1965, **12**, 119
- 9 Bassett, D. C., *Phil. Mag.* 1968, **17**, 37
- 10 Sadler, D. M. and Keller, A., *Kolloid Z.* 1970, **242**, 641
- 11 Sadler, D. M. and Keller, A., *Kolloid Z.* 1970, **242**, 1081
- 12 Keller, A. and Priest, D. J., *J. Macromol. Sci. (B)* 1968, **2**, 479
- 13 Arlie, J. P., Spegt, P. and Skoulios, A., *Compte rend.* 1965, **260**, 5774
- 14 Miller, R. L., *Kolloid Z.* 1968, **225**, 62
- 15 Peterlin, A. and Reinhold, C., *J. Polym. Sci. (A)* 1965, **3**, 2801
- 16 Wunderlich, B., *J. Polym. Sci. (A)* 1963, **1**, 1245
- 17 Hoffman, J. D., *SPE Trans.* 1964, **4**, 1

- 18 Lauritzen, J. I. and Passaglia, E., *J. Res. Nat. Bur. Stand. (A)* 1967, **71**, 261
19 Bassett, D. C., Frank, F. C. and Keller, A., *Phil. Mag.* 1963, **8**, 1739, 1753
20 Hoffman, J. D. and Weeks, J. J., *J. Chem. Phys.* 1965, **42**, 4301
21 Illers, K-H. and Hendus, H., *Makromol. Chem.* 1968, **113**, 1
22 Peterlin, A., *Polymer, Lond.* 1965, **6**, 25

ERRATUM

'The relationship between volume and elasticity in polymer glasses', by R. N. Haward and J. R. MacCallum, *Polymer* 1971, **12**, 189-194.

In *Figure 1* (page 191), the caption on the vertical scale should be $\times 10^{-10}$ and the caption on the horizontal scale should be $15 (V_0/V)^5 - 9 (V_0/V)^3$. We apologise for these errors.

- 18 Lauritzen, J. I. and Passaglia, E., *J. Res. Nat. Bur. Stand. (A)* 1967, **71**, 261
19 Bassett, D. C., Frank, F. C. and Keller, A., *Phil. Mag.* 1963, **8**, 1739, 1753
20 Hoffman, J. D. and Weeks, J. J., *J. Chem. Phys.* 1965, **42**, 4301
21 Illers, K-H. and Hendus, H., *Makromol. Chem.* 1968, **113**, 1
22 Peterlin, A., *Polymer, Lond.* 1965, **6**, 25

ERRATUM

'The relationship between volume and elasticity in polymer glasses', by R. N. Haward and J. R. MacCallum, *Polymer* 1971, **12**, 189-194.

In *Figure 1* (page 191), the caption on the vertical scale should be $\times 10^{-10}$ and the caption on the horizontal scale should be $15 (V_0/V)^5 - 9 (V_0/V)^3$. We apologise for these errors.

The fracture of polystyrene: some observations on strength and cracking phenomena

R. J. BIRD, G. ROONEY and J. MANN

Tensile tests have shown that crazes formed in stressed polystyrene are regions of unimpaired strength. The study of fracture surfaces with the aid of carbon replicas in the transmission electron microscope has revealed that at the onset of fracture the material has a sponge-like character and a great deal of fibrous structure. Investigation of the changing surface detail produced as the crack propagates has given new information, particularly on slow secondary fracture features.

INTRODUCTION

IN POLYSTYRENE and a number of other glassy polymers, fracture is preceded by the formation of planar crazes. These features are regions of optical discontinuity, oriented at right angles to the stress field, which look like cracks but Spurr and Niegisch¹ and others have shown them to be filled with coherent material. Craze material is thought to be deformed and to contain small voids, which, in polycarbonate, were reported by Kambour² to be in the size region 20–100 Å and to constitute 40–65% of the volume of the craze.

When fracture occurs it is initiated within a craze, by coalescence of voids, and propagates as far as it can in the craze, as shown by Murray and Hull³. These workers traced the progress of the crack through the craze and described its interaction with some secondary fractures.

We have carried out some work on the tensile fracture of polystyrene, using injection-moulded samples, which has confirmed the load-bearing nature of craze material and produced fresh evidence on the initiation and propagation of cracks in this material.

EXPERIMENTAL

Specimens were made from Shell Carinex HR polystyrene to the standard ASTM 0.19 m (7.5 in) dumb-bell shape by injection moulding.

Strength of craze material

To assess the strength of craze material, six of these specimens were stressed to fracture. As is usual with such injection-moulded samples, these showed crazes extending over the greater part of the cross-sectional area but not into the outer skin of material. From suitably large pieces of these specimens,

this clear outer skin was removed by filing and polishing to provide small dumb-bell specimens crazed over their whole cross-sectional area. These were then tested to fracture. Whereas the mean fracture stress of the original samples was 41.8 MN/m^2 , that of eight small crazed samples made from them was 43.5 MN/m^2 ; thus the formation of craze material is certainly not accompanied by a reduction of strength.

RESULTS

The main part of the work was an examination of the two faces produced by the very slow fracture of one of the ASTM-type specimens. It was fractured as slowly as possible in a Dennison testing machine, the duration of stress application to failure being about 1 h.

Normal appearance

A low-magnification photograph of one of the surfaces is shown in *Figure 1*. The main feature on the surface is a large dumb-bell-shaped mirror-like area corresponding to the area occupied by the craze through which the fracture

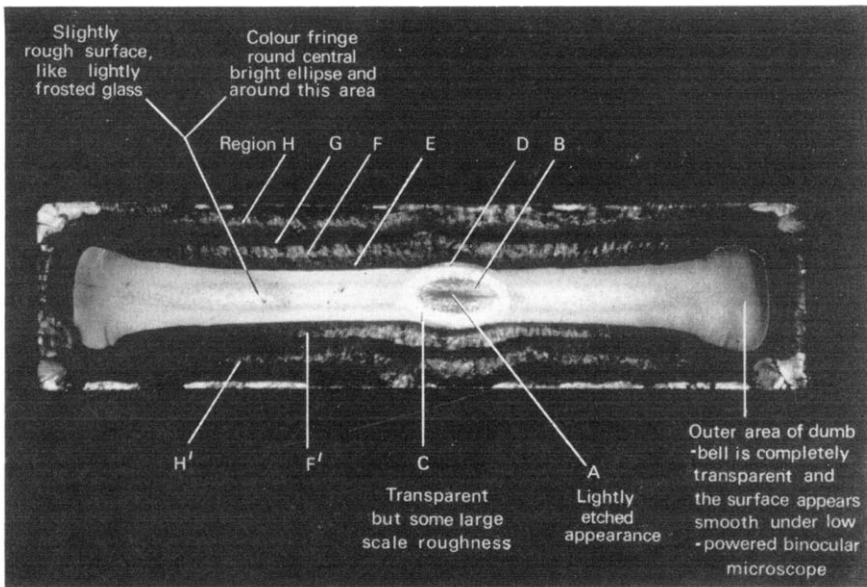


Figure 1 Visual appearance of fracture surface ($\times 8$)

occurred. At the centre of the mirror area there are some dark lines (A) oriented approximately parallel to the major axis of the section, and surrounding these an elliptical area B, surrounded in turn by a bright elliptical band C. Beyond C the remaining part of the mirror area (D) extends only a

short distance along the direction of the minor axis of the ellipse, but a considerable distance in the direction at right angles. Outside the dumb-bell there are four broad bright lines F and H above and 2 corresponding features F' and H' below, which extend the length of the fracture face and reflect the shape of the ellipse. Such lines have been termed 'hesitation' lines⁴, and they are probably explicable in terms of subsidiary crazes forming ahead of a main craze as observed by Hull⁵. The other fracture surface was of exactly corresponding appearance.

Microscopic examination

Both fracture surfaces were examined in the electron microscope by the carbon-replica technique. Initially, low-magnification composite micrographs were made of each, to cover the greater part of the elliptical regions B and C and a little beyond. On these the bars of the specimen grids provided a convenient system of reference co-ordinates which facilitated relocation of interesting detail.

Fracture-initiation region. A wealth of asymmetric secondary fracture features, such as we have studied previously⁶, could be seen in area B, and from these we could deduce the direction of crack propagation; it was clear that failure had initiated at the lines A and had travelled out radially. This is broadly in accord with the findings of Murray and Hull³ working with Carinex GP; they consider the crack-initiation region in this material to be a cavity formed by coalescence of voids, and extending the whole depth of the craze, but they do not show or discuss the fine detail of these parts of the fracture surfaces.

Figure 2 shows a relatively low-power view of region A. It shows a considerable amount of drawn material and in the area of finest detail there seems to be a three-dimensional mesh, a sponge-like structure. In *Figure 3*, a stereo pair of images of another part of this region at higher magnification, the sponge-like appearance is less pronounced but the drawn material is better revealed. It appears to have a distinctly fibrous nature, not only in the upstanding walls of the sponge where the fibres tend to be somewhat coarser, often with thickened retracted ends*, but everywhere over the hollow surfaces of the cavities where there seems to be a fairly uniform basic fibril diameter of 100–500 Å. This fine fibrillar detail is further illustrated at higher magnification in *Figure 4*. The surfaces of these cavities appear to be collapsed masses of fibrils, sometimes in tangled random array and sometimes more orderly. The uniformity of the widths of these fibrils suggests they are governed by some basic property of the polymer, perhaps indirectly by the molecular weight. The directionally grained surface discussed previously⁶ as characteristic of slow fracture has a grain-width dimension of similar magnitude and may therefore be another manifestation of the same structure. Fibrils of about 100 Å width have been shown in rubber by Andrews⁷ but

* The thickening of upstanding broken ends suggests recovery or plastic flow but these signs should be viewed with some caution because of the possibility of heat damage during the making of the surface replicas.

THE FRACTURE OF POLYSTYRENE

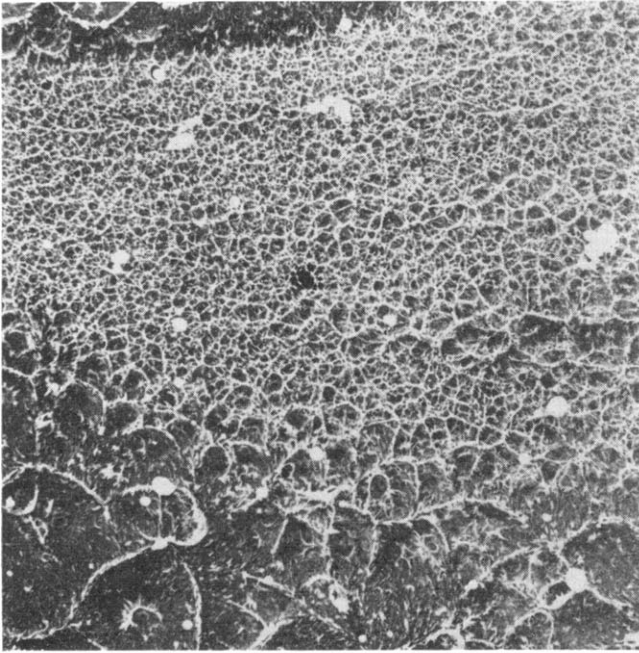


Figure 2 Ductile fracture of centre of specimen (region A) ($\times 2100$)

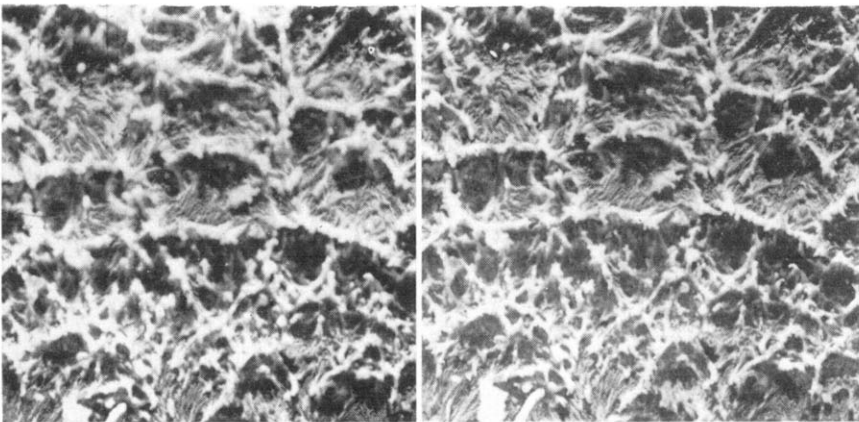


Figure 3 Region A, stereoscopic pair ($\times 8750$)

only at extensions approaching 700%, and Walters⁸ found evidence of fibres 100–1000 Å thick in rubber stretched from 100 to 450% extension and torn along the stressing direction. Our observations suggest that although Kam-bour showed the mean extension of craze material to be about 60%, considerably higher extensions occur locally in the process of fracture initiation.

Slow secondary fractures. The secondary fracture features occurring in region B, the region of slow crack growth, appear to be of two characteristically different types. These are readily recognizable from their foci which are either neatly rounded or of a ragged multipoint star shape (see R and S in

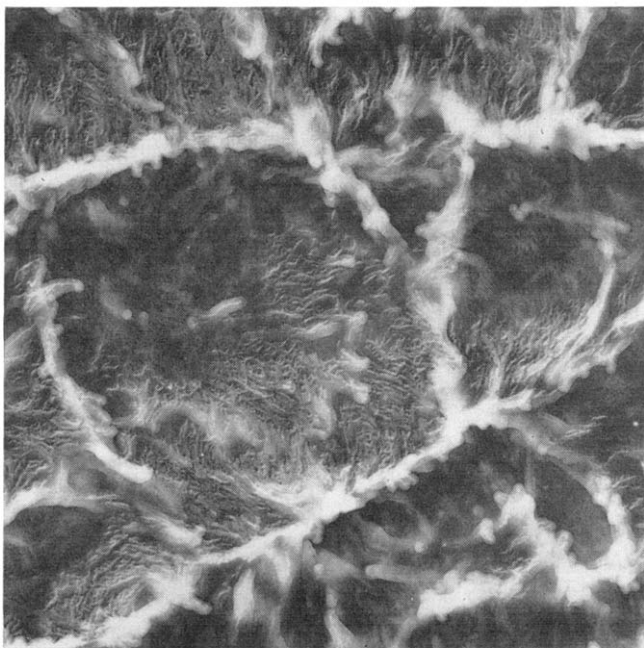


Figure 4 Ductile fracture at centre of specimen (region A) ($\times 21\,000$)

Figure 5). There is a difference also in the direction of the drawn fringe of material in the two cases. That of R with the plain focus is outwards, whilst that of S with the star-like focus is inwards.

Murray and Hull, working with Shell Carinex GP polystyrene, deduced from optical interference microscopy that hollows in one fracture face corresponded with hillocks on the other. In the present work the greater resolution of the electron microscope has given a clearer impression of these features as they occur in the Carinex HP grade. In a number of instances stereoscopic pairs of images were obtained of corresponding features in the two fracture faces. Of these Figure 6 is typical. (The shadowing direction in replica making, and the orientation of the resulting specimens in the

electron microscope were not controllable and this has led to difficulty in presentation.) The main interest in *Figure 6* is the closely spaced pair of secondary fractures. There is a substantial size difference in these features as seen on the two faces, and the drawn fringes are clearly seen. Three-dimensional viewing facilitates the sketching of the shape of these fracture faces

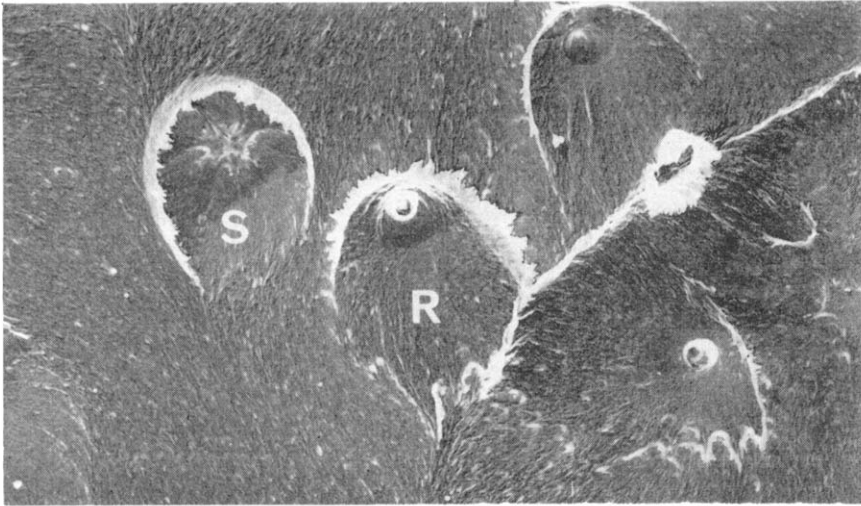


Figure 5 Slow secondary fractures in region B ($\times 3200$)

in normal section along a line through their centres. The result is shown in *Figure 7a* in which the direction left to right corresponds to top to bottom in *Figure 6*, the direction of main crack propagation. This sketch suggests that both fractures were initiated at a level (in the sketch) above the plane of the advancing main crack; they then propagated down towards that plane along conical paths. The two surfaces generated by each of these secondary fractures suffered considerable distortion owing to plastic deformation during fracture, particularly those in the lower half of the sketch which have broadened and collapsed to such an extent as to produce hollows containing only small remnants of the original cone tips. Other secondary fractures in the region B have been similarly examined and found to be essentially similar (*Figures 7b* and *7c*) except that the deep hollow cones occur sometimes on the one face and sometimes on the other, with equal probability.

Crack propagation over the whole of the area B may be loosely described as slow, and the secondary fracture features have everywhere the same essential characteristics. There is, however, a tendency for the appearance of these features to change somewhat towards the outside of this region where they are generally broader and flatter and more nearly alike on the two fracture faces, except for the foci which are almost always distinctive.

The essentially similar appearances of the two faces generated by the fracture indicate that fracture occurred not only at a craze but within it. The secondary fractures must initiate at points of weakness in the region of

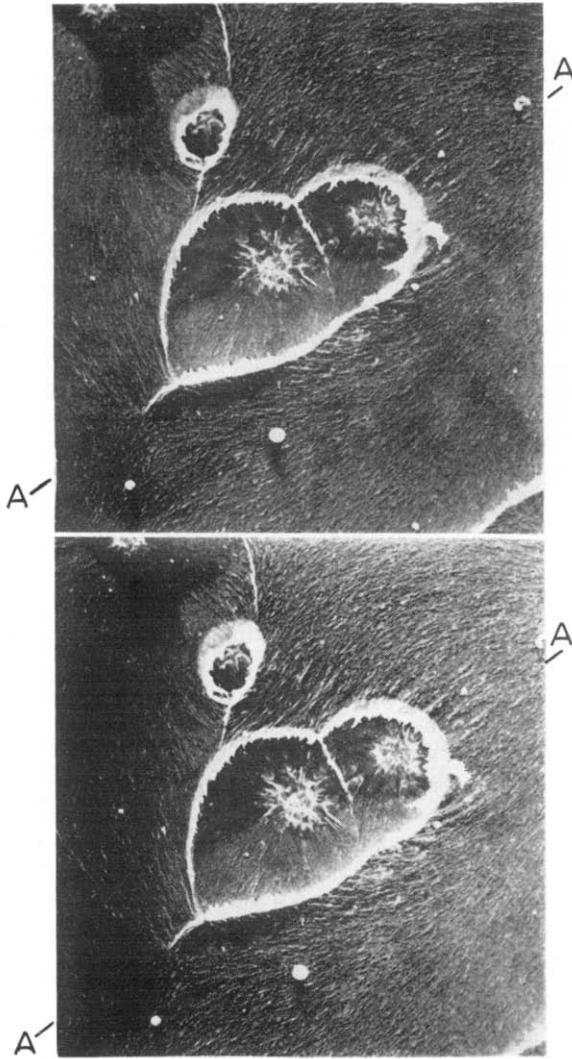


Figure 6 Secondary fractures in region B—stereoscopic pairs of corresponding features on the two fracture faces ($\times 1500$). The replicas of the two fracture halves were not similarly oriented in the microscope. The lines AA indicate a common reference direction.

THE FRACTURE OF POLYSTYRENE

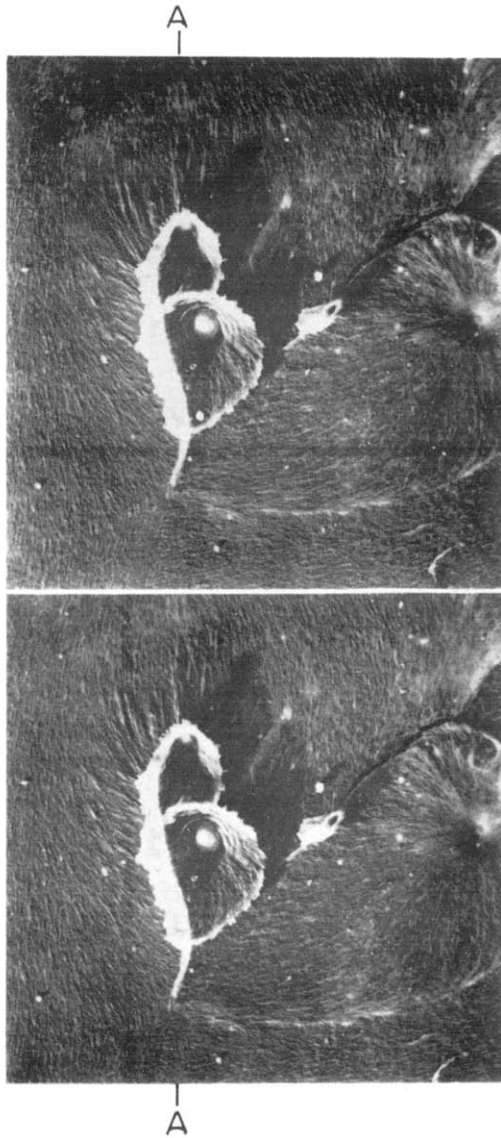


Figure 6 (continued).

stress concentration just ahead of the main crack, close to the plane of the latter. Murray and Hull suggested they occur on the craze boundaries. After initiation they do not run away as plane cracks parallel to the main crack, but follow conical paths suggestive of shear failure.

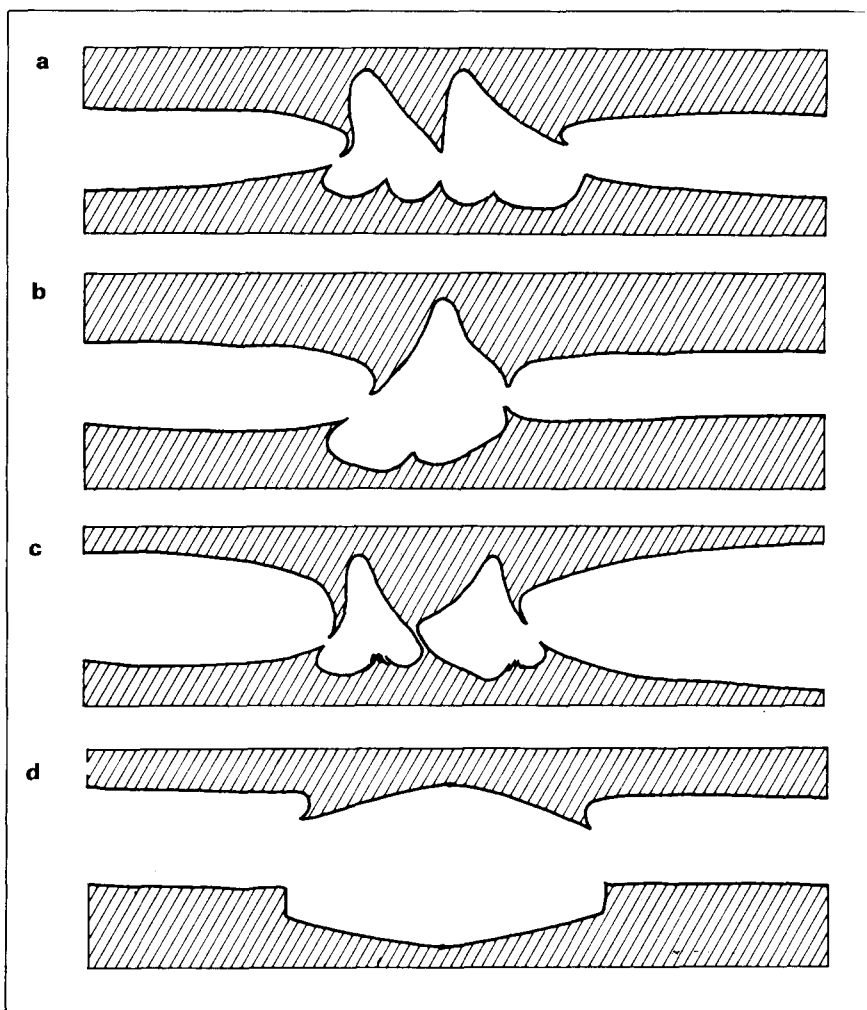


Figure 7 Shapes in section of corresponding secondary features in the two fracture surfaces—as deduced from stereoscopic electron micrographs. (a) Closely spaced pair of secondary fractures; (b) single secondary fracture; (c) another closely spaced pair of secondary fractures; (d) idealized slow secondary fracture in the beginning of the fast cracking region

No detailed explanation will be offered here for this phenomenon, occurring as it does in a rather complicated stress field⁹; but some qualitative comment may be relevant. A certain amount of drawing and orientation will occur before failure everywhere within the craze and this may lead to lateral weakness as in the 'fibrillation' changes resulting from the drawing of other

polymers such as polypropylene. Failure of a cluster of fibrils just off the plane of the advancing crack, above or below, might well then be followed by rupture of the lateral bonds between these and the unbroken fibrils, from the initiation point down to the main crack plane, the plane of maximum stress. The deep hole and the upstanding cone of material would suffer further deformation and the latter might even show some elastic recovery at its centre as fracture continued, so that it finally presented the only modestly raised, starred appearance seen in the micrographs. The idea of a fibre texture in craze material is supported to some extent by a micrograph of a cross-section of a polystyrene craze published by Spurr and Niegisch¹. The amount of drawing existing generally in the craze immediately before fracture must however be well short of the limits to which polystyrene can be taken, about 250 % extension¹⁰, as evidenced by the much greater extension shown by the drawn fringes round the secondary features that are produced in the final separation.

Fast cracking region. At the outer limit of the central elliptical area B, there is a change from directional grain-like surface texture to a non-directional stipple texture, which, as discussed in an earlier paper⁶, we take to indicate a transition from slow to fast fracture. Unfortunately, a fair amount of this boundary region is obscured by specimen grid bars, but where the boundary is visible the transition is seen to be abrupt. In some places the change from grained to stippled appearance is not on an unbroken front. *Figure 8* shows the transition, but it extends only from X to Y in that field

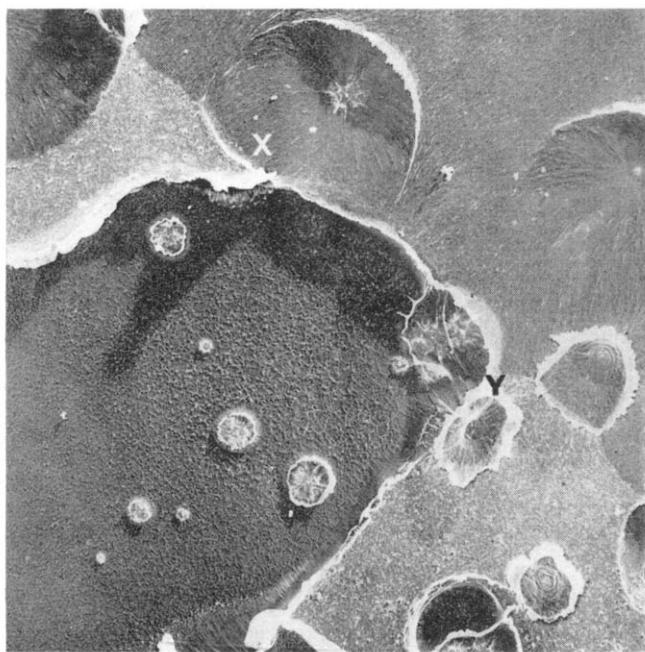


Figure 8 Boundary between slow and fast cracking, i.e. between regions B and C ($\times 2250$)

of view. It seems a reasonable assumption that when normal fast cracking starts it may run on and spread out sometimes failing to join up completely with the slow cracked region. This would leave islands of material which might subsequently fracture in a somewhat different manner and provide an explanation of the regions of different surface appearance that flank the line XY in *Figure 8*. A clearer example of this coarser non-directional stippled

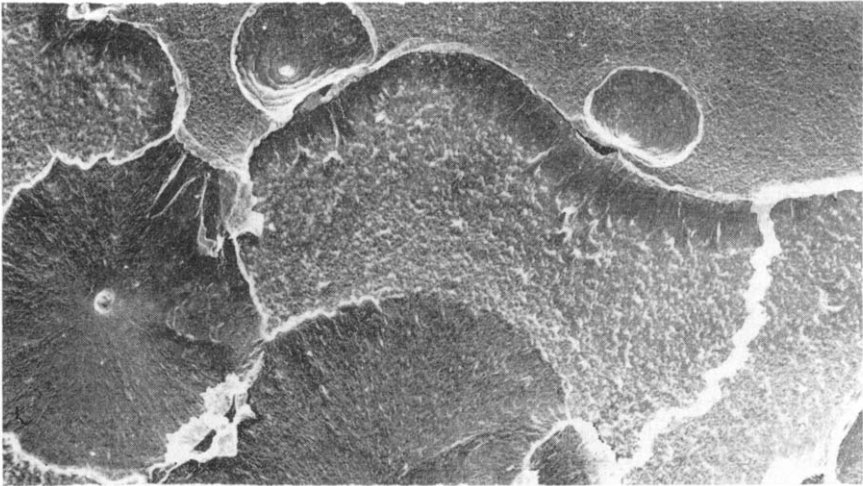


Figure 9 Boundary between slow and fast cracking, i.e. between regions B and C ($\times 3250$)

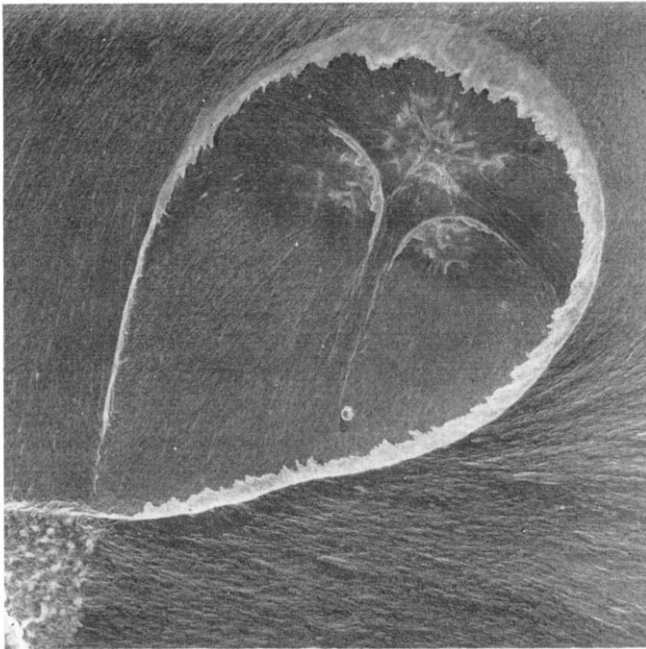


Figure 10 Secondary fracture in region B ($\times 6150$)

surface is visible in *Figure 9*. It exists as patches between more normal fast-cracking surfaces (visible along the top and the left-hand side) and the slow secondary fractures. This type of coarse stipple appears to be associated usually with a change of level, supporting the view that it is the result of the fracture of islands of material left between two cracks propagating on different levels. Islands of this texture occur frequently round the boundary of the central ellipse, and occasionally entirely within the slow-cracking region, as may be seen in *Figure 10* (bottom left).

Spurr and Niegisch published a micrograph of a polycarbonate fracture surface showing a transition from a directional grain to a stipple rather like that discussed here. They attributed the stipple to fracture at the craze wall and the grained surface to fracture outside the craze. In *Figure 10* adjoining the stippled area there are three regions of grained surface, all of which, we maintain, were generated by fracture within the craze; and these are disposed below, on the same level as, and above, the plane of the stippled surface. Again in *Figure 9* the finer texture at top and left, characteristic of fast cracking within a craze, is disposed respectively above and below the coarser stipple. The latter cannot therefore be associated with a craze boundary plane.

For a very short distance after the change to fast cracking, i.e. after the disappearance of directional, grained surface texture, it is possible to find secondary features approximating to the normal slow cracking. They have a radially grained surface texture and usually contain foci of one or other of the types discussed above. They are always roughly circular in outline, consistent with their having been united with a main crack travelling at a much greater speed. In one instance we have studied the corresponding halves of such a fracture by the stereoscopic method, and the shapes in section, somewhat idealized, are indicated in *Figure 7d*. This feature is unusual for a secondary fracture in that the two halves are of similar general appearance and the foci, which are very small, are not characteristically different. These observations suggest that the fracture was originally initiated on the median plane of the advancing crack or, more strictly, on the plane of symmetry of the stress system ahead of the crack, and thus propagated as a planar crack. The fast crack which finally united with it approached on a slightly different level and the usual drawn fringes were not very pronounced. Drawn fringes seem less in evidence on slow secondary features in this region.

In this region also we see what must be a fast-cracking version of a steep conical fracture. The hollow cone feature is fairly well preserved during the fracture process and shows relatively little drawing round its open end, as can be seen at the top of *Figure 9*, but the final form of the corresponding other half of the fracture bears no resemblance to a cone. Good examples of this can be seen in *Figure 8* (lower left). They take the form of rough surface protuberances of rounded general shape. A corresponding pair of features on opposite fracture faces has been studied as stereo pairs, confirming this description of their structure.

The transition region we have been discussing is the inner edge of the bright ellipse C (*Figure 1*). Moving outwards through this bright band, the replica first shows fewer secondary fractures and larger unbroken areas of stippled fast-fractured surface. In terms of the microscopic appearance there is no clearly defined outer boundary to the region C, the bright ellipse. In

this vicinity, the size of the relatively featureless areas again diminishes, the change being continuous and fairly rapid. The surface is divided up into very irregular indented areas by rambling upstanding lines of drawn material. The scale of the effect continues to diminish right out to the sharply defined

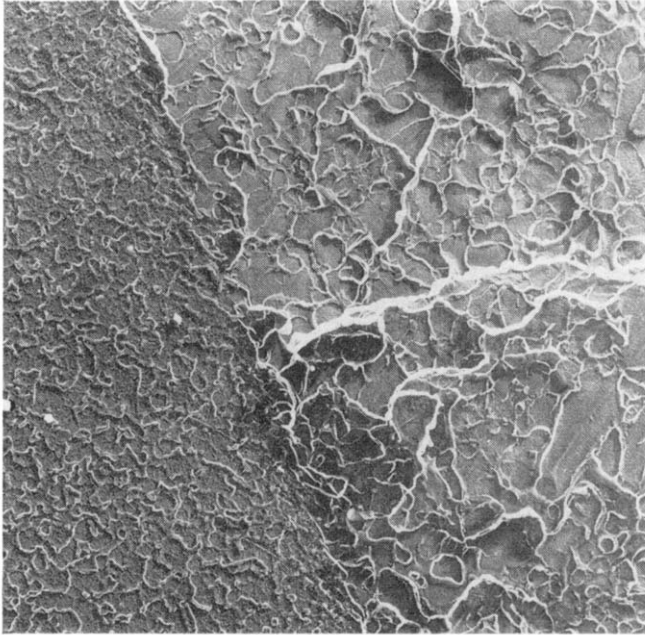


Figure 11 Boundary between regions D and E ($\times 2150$)

outer boundary of the region D. This is the outer edge of the mirror area and it is thought also to be the outer limit of the craze through which the fracture occurred (see *Figure 11*).

The lines dividing up this type of surface are seen from stereo pairs to coincide with slight changes of level. Fracture has occurred on two closely spaced planes (about $1\ \mu\text{m}$ apart at one position examined), jumping back and forth between them. Murray and Hull^{3,11} reported this appearance and attributed it to separation along the craze boundary surfaces, the separation of which diminishes progressively out to the mirror boundary craze tip.

At the boundary of the mirror area there is an abrupt change in the nature of the fracture surface, as seen in *Figure 11*, and this is true at all points on the mirror boundary that have been examined. The nature of the detail found in this further region E seems, however, to vary with the distance out along the dumb-bell. *Figure 11* refers to a position close to the central ellipse. So far as can be judged without stereoscopic assistance, it shows the crack continuing roughly on the same plane with still some evidence of biplanar splitting, and probably in this area there is an increase in the amount of

THE FRACTURE OF POLYSTYRENE

drawn material. Stereo pairs, *Figures 12a* and *12b* relate respectively to positions half way along the dumb-bell and at its end. They show that in those positions the fracture surface is no longer planar across the mirror boundary. There has been a sudden change in the cracking direction at the boundary. Furthermore, the new type of surface is seen to be rugged and largely devoid of drawn material.

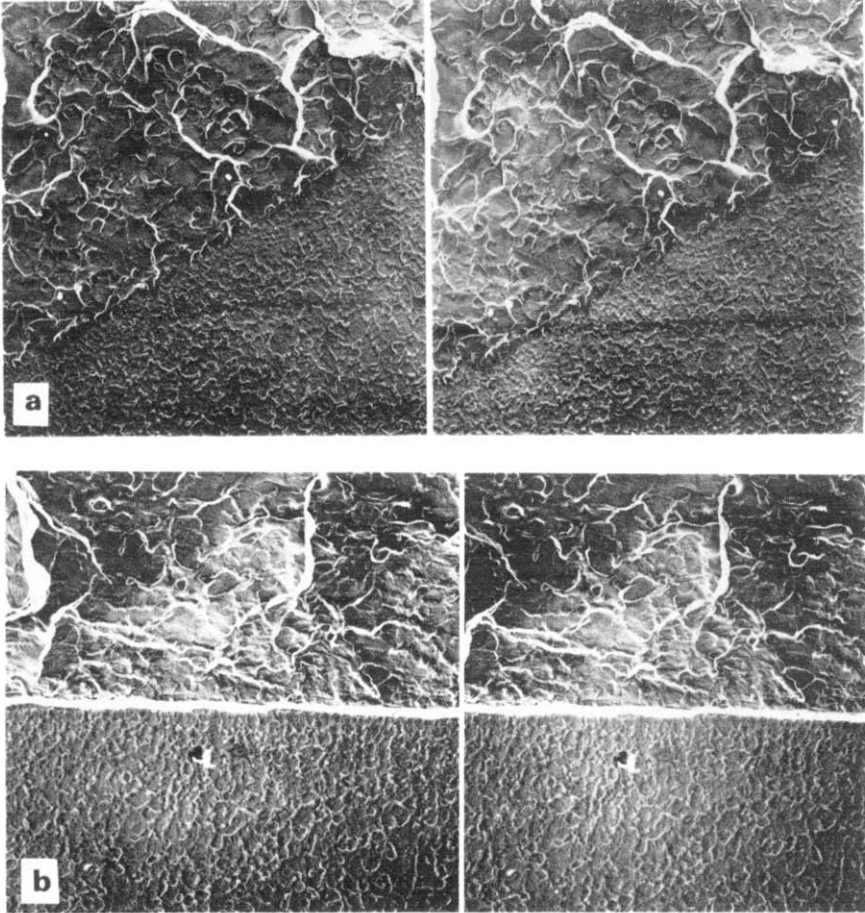


Figure 12 Biplanar splitting at boundary of mirror area. (a) Halfway from specimen centre to mirror extremity (stereo pair $\times 2200$); (b) at an extremity of the mirror area (stereo pair $\times 2200$)

Beyond the regions E and E' above and below the mirror area which appear dark, there are moderately bright bands, F and F' being the first of two each side. Parallel bands such as F, F' have been alluded to as 'hesitation' bands and it has been suggested that the main crack front is slowed down in these regions. To the eye all four of these bands have a rather mottled appear-

ance suggestive of a relatively rough surface, and micrographs show relatively large features again. In places there are some signs of the two-plane type of fracture as found in areas C and D (*Figure 13*) where it is particularly well shown. This fits in with the idea of these bands being due to the fracture running through a system of subsidiary crazes formed ahead of the propagating crack⁵. Much of the surface has a texture corresponding to that seen in



Figure 13 Fracture surface showing biplanar splitting in region F (hesitation line) ($\times 2150$)

areas C and D but there are also patches of a much finer surface texture such as was seen in places in the inner parts of the bright elliptical zone C, i.e. just after the transition from slow to fast cracking. It is possible that the finer surface texture corresponds to secondary fracture.

The study of this fracture was terminated with a brief examination of the dark band G, where we assume the crack was travelling faster again, perhaps as in E. The type of surface found was indeed indistinguishable from that in E.

DISCUSSION

These observations on fracture may be summarized as follows:

1. Crazes in polystyrene are regions of unimpaired strength. Although they must have suffered some elongation, the amount is much less than that which polystyrene is capable of undergoing.

2. The observations support the findings of Murray and Hull³ that fracture is initiated near the centre of the craze, where voids grow and coalesce to form a flat hole of sufficient Griffith size to propagate outwards and lead to failure of the sample. Observations at higher magnifications than those of Murray and Hull have revealed additional detail in this region which indicates that at the onset of failure the material has a sponge-like character and a great deal of fibrous structure.
3. The changing surface detail produced as the crack propagates has been investigated. In particular, slow secondary fracture features have been studied and their form found to be rather different from that deduced by Murray and Hull from optical interference microscopy of rather coarser features.
4. The biplanar splitting described by Murray and Hull has been seen not only in the outer part of the mirror regions of the fracture faces but also further out, supporting the idea of the crack propagating through subsidiary crazes forming ahead of it.
5. At the boundary of the mirror area there is an abrupt change of surface character, the ensuing type of surface varying with the distance from the specimen centre.
6. The amount of evidence of drawn material varies over the fracture face, there being very little of it in the outer regions away from the centre of the specimen, i.e. where the crack was travelling fastest.

Kambour² working with thin sections reported on the structure of craze material in polycarbonate and postulated that it contains spherical voids in the size range 20–1000 Å. This work depended on producing in the voids metallic silver introduced initially as silver nitrate solution, and was not a good guide to size and shape. More recently, Kambour and Holik¹² experimented with a higher melting polymer, poly(2,6-dimethyl-1,4-phenylene oxide), infused with liquid sulphur, thought to be much more capable of revealing the true nature of the voids. Their results still showed spherical voids rather than a simple fibre structure, but the voids did tend to be interconnected and lie in lines along the stressing direction, giving rise to a kind of fibrillar structure corresponding in size to that reported here for polystyrene. Kambour and Holik noticed additionally that there was often a thin layer of craze material adjacent to the interface that was much less oriented. Such layers would probably be relatively weak and favour the biplanar splitting type of fracture.

The micrograph published by Spurr and Niegisch of a vertical fracture through a polystyrene craze suggests a fibre structure (as did some of our preliminary results). Our results as discussed above would also be consistent with a measure of fibre structure within crazes; and in the fracture initiation region we see copious evidence of fibres in the region of 100–500 Å thick. It would seem at least as likely, therefore, that the voids in crazes are elongated and oriented, and this would be important in considering their behaviour. In the fracture initiation region we see rounded cavities formed within the fibrous structure but these are much larger, ranging up to 20 000 Å in size (about the same size as seen in fractured ductile metals^{13,14}).

Whatever the shape of the voids the instability of crazes is to be expected since the stress on the load-bearing material must be close to the bulk yield stress of polystyrene. Thus the bulk yield stress is about 100 MN/m^2 ($15\,000 \text{ lbf/in}^2$), the fracture stress is about 50 MN/m^2 ($7\,500 \text{ lbf/in}^2$) and the craze contains about 40 % voids. When the craze has filled the cross-section of the sample, the stress in the craze must therefore be close to the bulk yield stress. The stress distribution within the void-containing craze will not be uniform and there will be points at which the stress is greater than average. The polystyrene at these points will extend more rapidly than elsewhere and this will lead eventually to fracture. The reason why this process starts near the centre of the craze in the injection-moulded sample is probably because the material is under the greatest hydrostatic tension. Increasing hydrostatic tension is known to lower the yield stress of polystyrene¹⁵. Once fracture has occurred the stress on adjacent material will increase and the fracture process will spread, producing a multitude of small cavities which coalesce. When these cavities meet, the material between them will be free to compensate for longitudinal extension by a reduction in lateral dimensions, thus giving rise to the walls of the sponge which have clearly undergone large extensions.

It is now clear that the tensile strength of polystyrene depends on the inhomogeneous response to the applied stress which creates craze matter and leads on to the growth of a void large enough to promote failure by the Griffith mechanism. The theory for craze formation must involve cavitation in a plastically deformable material, and since the yield stress is greater than the stress at which crazes form, the theory must postulate the existence of stress concentrations or regions of low yield stress. When the fracture of the craze is considered there may be help from theories which are being developed¹⁶ for the ductile fracture of metals, where void coalescence is operative; but, of course, simple metal structures do not exhibit the same propensity to form fibrous texture when drawn as do many polymers, and in the case of polystyrene we shall have to take into account the present evidence of a 100–500 Å fibrillar structure generated during failure in the region of crack initiation.

*Shell Research Ltd,
Thornton Research Centre,
Chester CH1 3SH, UK*

R. J. Bird and G. Rooney

*Shell Research Ltd,
Carrington Plastics Laboratory,
Urmston,
Manchester, UK*

*J. Mann
(Received 18 January 1971)*

REFERENCES

- 1 Spurr, O. K. and Niegisch, W. D. N., *J. Appl. Polym. Sci.* 1962, **6**, 585
- 2 Kambour, R. P., *Polymer, Lond.* 1964, **5**, 143
- 3 Murray, J. and Hull, D., *Polymer, Lond.* 1969, **10**, 451
- 4 Schardin, H., 'Fracture', (Ed. B. L. Averbach), John Wiley, New York, 1959, pp 250, 227
- 5 Hull, D., *J. Material Sci.*, 1970, **5**, 357

THE FRACTURE OF POLYSTYRENE

- 6 Bird, R. J., Mann, J., Pogany, G. and Rooney, G., *Polymer, Lond.*, 1966, **7**, 307
- 7 Andrews, E. H., *J. Polym. Sci.*, 1966, **4**, 668
- 8 Walters, M. H., *J. Polym. Sci.*, 1963, **1**, 3091
- 9 Cook, J. and Gordon, J. E., *Proc. Roy. Soc.* 1964, **A282**, 508
- 10 Holliday, L., Mann, J., Pogany, G., Pugh, H. Ll. D. and Gunn, D. A., *Nature*, 1964, **202**, 382
- 11 Murray, J. and Hull, D. *J. Polym. Sci. (A-2)* 1970, **8**, 583
- 12 Kampour, R. P. and Holik, A. S., *J. Polym. Sci. (A-2)* 1969, **7**, 1393
- 13 Puttick, K. E., *Phil. Mag.*, 1959, **4**, Ser. 8, 964
- 14 Beachem, C. D., *J. Basic Eng.* 1965, **87**, 299
- 15 Pugh, H. Ll. D., Holliday, L. and Mann, J., *J. Material Sci.* in press
- 16 McClintock, F. A., *J. Appl. Mechanics ASME.*, 1968, **35**, 363

The electroinitiated polymerization of styrene: Part 2

B. M. TIDSWELL and A. G. DOUGHTY*

Electrolysis of a solution of styrene and sodium borofluoride in dimethyl acetamide gives rise to polystyrene at the cathode. The polymerization occurs by an anionic mechanism initiated by solvated electrons produced during electrolysis. Kinetics in a single compartment cell and a divided compartment cell show differences. Acceleration occurs in the cathode compartment of the divided cell giving rise to high current efficiencies. Evidence is given for the presence of an electrolytic termination reaction occurring in the single cell.

INTRODUCTION

IN Part 1¹ we described the cationic polymerization of styrene initiated by BF_3 liberated at the anode during the electrolysis of NaBF_4 dissolved in sulpholane. It was then pointed out that the locus of polymerization could be changed by merely changing the solvent, giving rise to polymerization occurring by a totally different mechanism. The present paper describes this work and attempts to interpret the results obtained when using *N,N*-dimethyl acetamide (DMA) as solvent.

EXPERIMENTAL

Materials

The materials used were purified according to methods described in Part 1.

Equipment and technique

The equipment and techniques used are identical to those outlined in Part 1 with the addition of a direct reading conductivity bridge (Portland Electronics Ltd.). In all cases the initial electrolyte concentration was 0.05 M. All polymerization experiments were carried out at 25°C.

RESULTS AND DISCUSSION

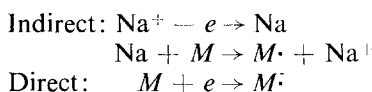
In order to elucidate the mechanism of the electropolymerization, copolymers of styrene and acrylonitrile were produced in the cathode compartment of the divided cell. From the nitrogen content of the copolymers and by applying the Finemann-Ross² equation, monomer reactivity ratios of $r_1 = 0.4$ and $r_2 = 14.2$ were obtained. These values are in relatively good agreement with those of Zutty and Welch³ who, using the known anionic catalyst *n*-butyl lithium in iso-octane at -12°C , reported $r_1 = 0.2$ and $r_2 = 14.0$.

* Present address: University of Southampton

ELECTROINITIATED POLYMERIZATION OF STYRENE (2)

The addition of proton donors such as methanol or water retard the reaction (*Figure 1*). Radical scavengers such as *p*-benzoquinone and diphenyl pycryl hydrazyl give no inhibition period but do alter the overall rate of polymerization due, possibly, to electrolytic reduction at the cathode.

It is possible that initiation may be due either to indirect or direct electron transfer to monomer:



Sodium discharged at the cathode may also react with the solvent. Electrolysis was carried out using dimethyl sulphoxide (DMSO), sulpholane, N,N-dimethyl formamide (DMF) and DMA, in the absence of monomer; the

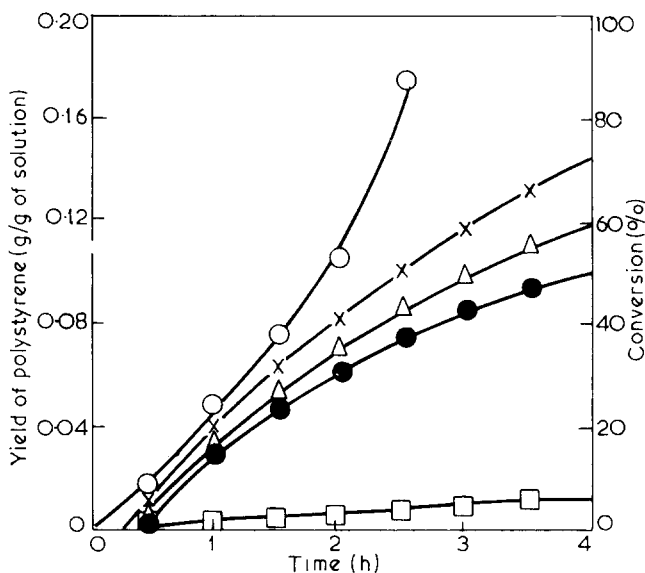


Figure 1 Effect of addition of methanol and water on the formation of polystyrene at the cathode of the divided cell at 30 mA in DMA/NaBF₄. ○, no additive; ×, 3.83×10^{-2} mol/l methanol; ●, 7.93×10^{-2} mol/l methanol; △, 3.01×10^{-2} mol/l water; □, 18.35×10^{-2} mol/l water

u.v. spectra of the catholytes were compared with those of solutions of sodium metal in the respective solvents. In all cases, except that of the electrolysis of sodium borofluoride in DMA, the spectra simply consisted of two absorption peaks (*Table 1*), which suggests that DMA has the least tendency to react with added sodium or electrodeposited sodium metal. In the case of the other solvents reaction products may inhibit anionic polymerization. It has been shown^{4,5} that metallic sodium reacts with DMSO to produce sodium dimsyl (methyl sulphanyl carbanion) together with mixed gases (62% hydrogen and 38% dimethyl sulphide); NaOH and H₂O must also be produced during the reaction, which will act as inhibitors. Sodium dimsyl produced by the reaction

of DMSO with sodium hydride does initiate the polymerization of styrene⁶, thus no inhibiting by-products must be present. Bawn⁷ observed that potassium dimethylsilyl, produced by reaction of potassium *t*-butoxide and DMSO will only initiate the polymerization of styrene if the ratio styrene:DMSO is greater than unity. Lower monomer concentrations yield only a complex mixture of unsaturated molecules similar to those reported by Walling and Bollyky⁸. During the electrolysis of 1 M styrene in DMSO only a small quantity of the polymer was produced at the cathode which may be due to a low styrene:DMSO ratio. It has recently been reported⁹ that electrolysis of sodium chloride in DMSO gives products different to those obtained by the addition of sodium to DMSO⁴. Similar considerations may apply in the case of sulpholane and DMF, thus limiting the yields of polystyrene. In the case of DMA a blue transient species is observed at the cathode during the passage of current in the

Table 1 Interaction of sodium and solvents

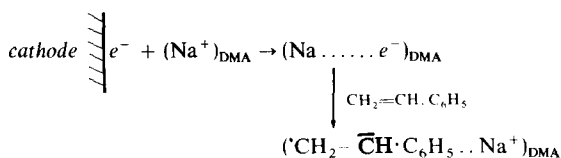
Solvent	Reaction time (min)	Peak 1		Peak 2	
		λ_{\max} (nm)	Absorbance	λ_{\max} (nm)	Absorbance
<i>Addition of sodium metal:</i>					
DMA	18	285	0.65	365	0.08
DMF	3	270	1.85	365	1.75
DMSO	3	266	1.68	340	0.20
Sulpholane	6	319	0.68	350	0.35
<i>Electrolysis NaBF₄ (0.05 M) at 10 mA:</i>					
DMA	10	299	0.88	nil	nil
DMF	10	270	1.88	352	0.70
DMSO	10	270	1.80	350	0.20
Sulpholane	10	320	1.40	358	0.24

absence of monomer; this was not observed on the addition of sodium metal to DMA. The formation of the blue colour at the cathode in DMA is possibly characteristic of the presence of solvated electrons. Szwarc¹⁰ has reported that electrolysis of alkali metal solutions produces an accumulation of blue coloured species at the cathode. Dainton *et al.*¹¹ successfully polymerized styrene by the addition of blue solutions of potassium in either tetrahydrofuran or dimethoxy ethane; these blue solutions are considered to contain solvated electrons.

Kaneko¹² has postulated that the electropolymerization of acrylonitrile occurs by virtue of the solvated electrons formed on the electrolysis of monomer, hexamethyl phosphonamide and lithium chloride. Similarly, Laurin and Parravano¹³ describe the electropolymerization of 4-vinyl pyridine initiated by solvated electrons.

It is possible, therefore, that electropolymerization of styrene in DMA/NaBF₄ may take place at the cathode by a reaction involving a solvated electron:

ELECTROINITIATED POLYMERIZATION OF STYRENE (2)



(where solvation by the solvent is denoted by the subscript DMA).

Anionic propagation then follows by dimerization of the styrene radical anion. The red colour, typical of the 'living' styrene dianion is observed at the cathode. Subsequent nitrogen analysis of the polymer indicates that no initiating species are formed by electrolytic decomposition of the solvent.

Figures 2 and 3 illustrate yield/time curves for the formation of polystyrene in both single and divided cells when the current is varied between 5 and 50 mA at 25°C. In the divided cell polymerization, occurring in the cathode compartment, accelerates with time, the acceleration increasing with the current. In the single cell there is no such acceleration. Applying steady state conditions, Figure 4 shows that a linear relationship occurs in both cases between current and rate indicating a first-order dependence on current.

Similar experiments maintaining the current constant and varying the monomer concentration (Figures 5 and 6) again show acceleration in the case of polymerization in the divided cell, the acceleration increasing with monomer concentration but giving rise to sigmoidal shaped curves at higher conversions at the higher concentrations. In the single cell a perfectly linear

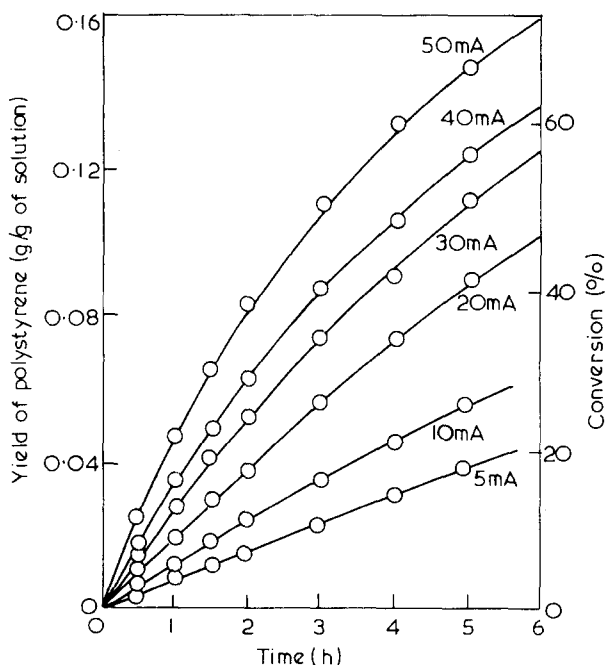


Figure 2 Formation of polystyrene with time at various currents for 2 M styrene in DMA/NaBF₄ in the single cell

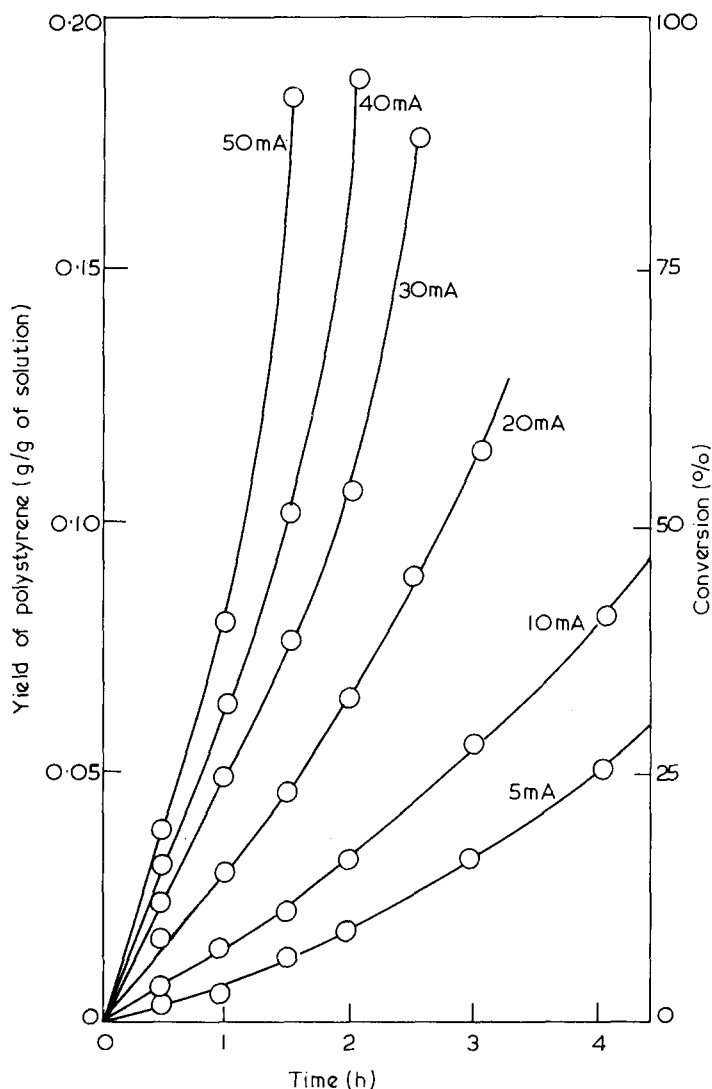


Figure 3 Formation of polystyrene with time at various currents for 2 M styrene in DMA/NaBF₄ at the cathode of the divided cell

relationship exists between yield and time over the range of conditions considered. Again, from the slopes of these curves the initial rate of polymerization can be seen to be first order with respect to monomer concentration (Figure 7). This conclusion is substantiated, in the case of the single cell, by studies under protracted electrolysis. Thus rate of polymerization $\propto [M_0]I$ during the initial stages of the polymerization before any acceleration occurs, where $[M_0]$ is the initial styrene concentration.

It may be assumed, therefore, that during the initial period of polymerization the number of active species which initiate polymerization is

ELECTROINITIATED POLYMERIZATION OF STYRENE (2)

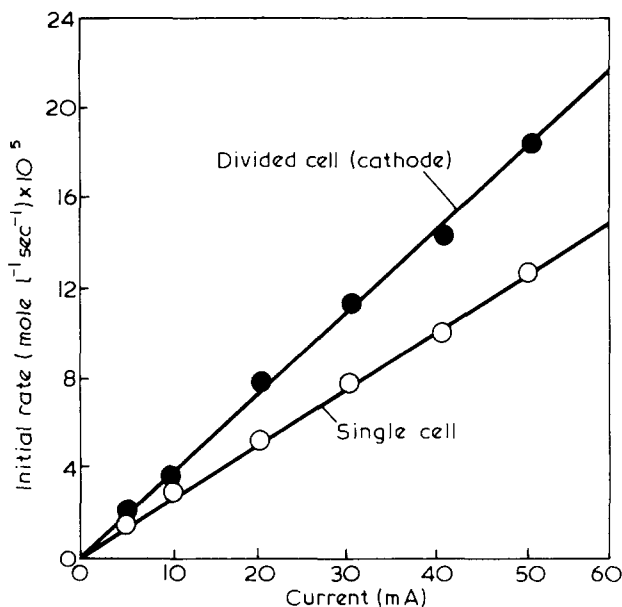
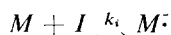


Figure 4 Dependence of initial rate of electropolymerization on the current for 2 M styrene in DMA/NaBF₄

proportional to the applied current, I . In the divided cell, as polymerization proceeds, non-steady state conditions apply as the number of active species increases, which, in turn, may be due either to the absence of a termination step or the presence of a slow termination step. Attempts to interpret the sigmoidal shaped curves using a treatment similar to that of Funt¹⁴ proved unsuccessful. From the evidence accumulated, it would appear that initiation occurs at the cathode by means of a solvated electron, the number of which will be proportional to the applied current.

The overall process may be considered as:



followed by dimerization and propagation with rate constants k_2 and k_p respectively.

In both cells the initial rate of electropolymerization of styrene in DMA/NaBF₄ is found to be first order with respect to both monomer concentration and applied current. Two hypotheses may be considered to explain these results. Firstly, the assumption that the rate-determining step is the dimerization of the radical ion. On this premise the overall rate of polymerization is given by:

$$\text{Rate} = \frac{1}{2}k_2[M\cdot]^2$$

assuming steady state conditions

$$\frac{dM\cdot}{dt} = k_i[M]I - \frac{1}{2}k_2[M\cdot]^2 = 0$$

thus the rate of polymerization = $k_i[M]I$.

This hypothesis was proposed by Funt and Williams¹⁵ in order to explain their results obtained during the electropolymerization of acrylonitrile in DMF using NaNO_3 as electrolyte. No evidence was obtained to justify the belief that the radical anion of acrylonitrile was suitably resonance stabilized to give it finite existence.

The second approach results from the work of Szwarc^{16,17} who suggests that the styrene radical anions have only a transient existence and dimerize almost instantaneously. For a truly living polymer the rate of polymerization depends only on the rate of propagation, termination being absent. In the

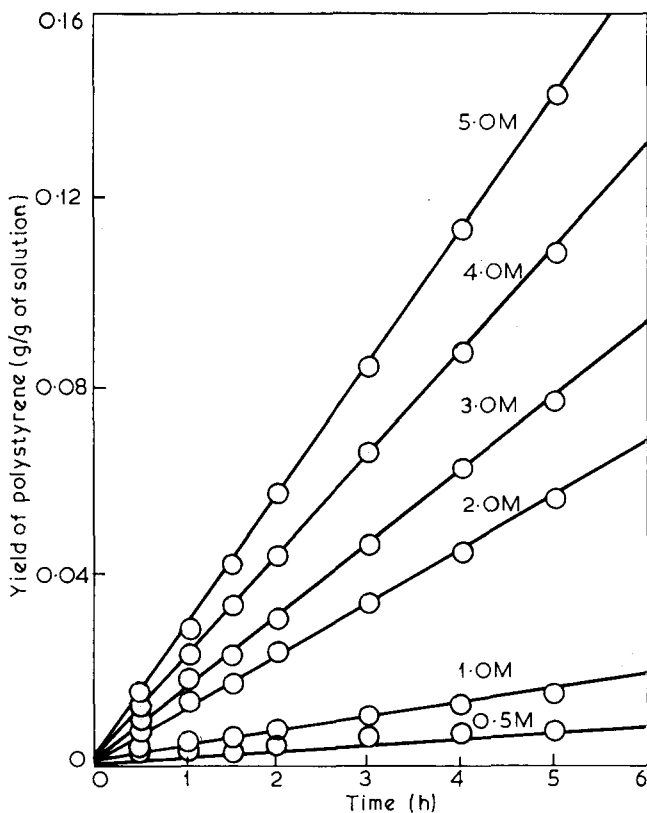


Figure 5 Formation of polystyrene with time at various initial monomer concentrations at 10 mA in DMA/ NaBF_4 in the single cell

present system, as will be seen, some termination does apparently occur by reaction with solvent or, in the case of the single cell only, by reaction with other species. Despite the destruction of anion centres by these various processes the continuous electrolytic process produces new active centres.

The rate of polymerization may be expressed as:

$$R_p = k_p[\text{anion centre}]M$$

where [anion centre] is the concentration of polymeric carbanions, assuming that the dianion affords two centres and the mono-ion one. The concentra-

ELECTROINITIATED POLYMERIZATION OF STYRENE (2)

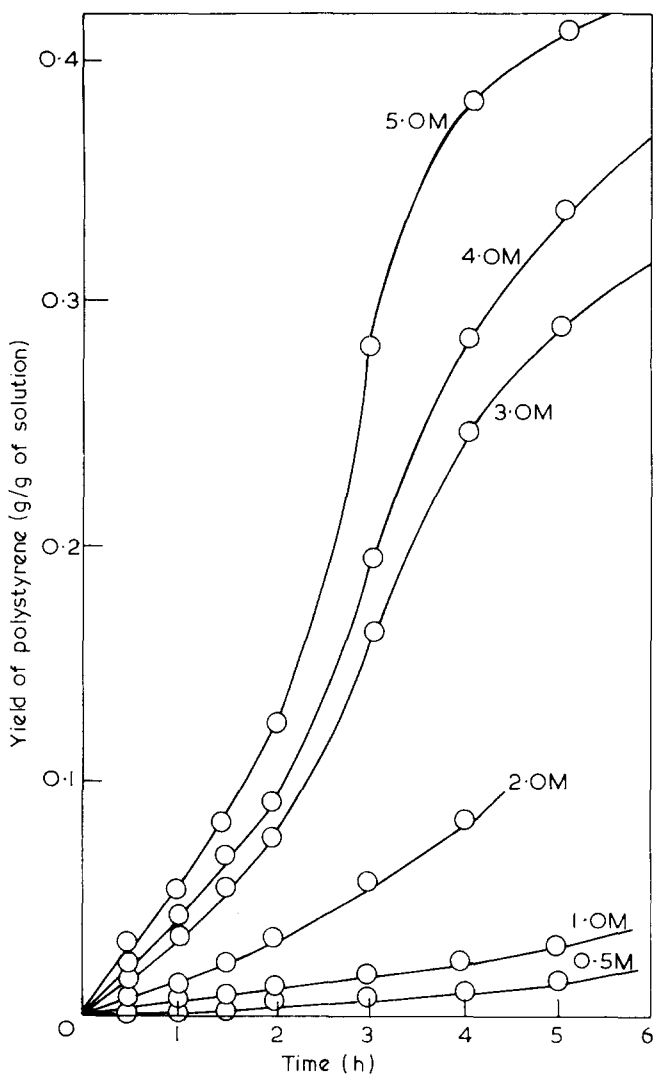


Figure 6 Formation of polystyrene with time at various initial monomer concentrations at 10 mA in DMA/NaBF₄ at the cathode of the divided cell

tion of the anion centre will, therefore, be proportional to the applied current. Hence the rate of polymerization in both cells will be expressed as:

$$\text{Polymerization rate} \propto [M_0]I$$

The results of investigations of chain transfer reactions using several monomer/solvent ratios and taking conversions to less than 10% are shown in Figure 8, indicating chain transfer to solvent occurring in both cases. Application of the equation:

$$\frac{1}{(\overline{DP}_n)} = \frac{1}{(\overline{DP}_n)_0} + C_s \frac{[\text{DMA}]}{[\text{Styrene}]} \quad (1)$$

ELECTROINITIATED POLYMERIZATION OF STYRENE (2)

account for low molecular weight products obtained during the anionic polymerization of styrene initiated by sodium dimsyl.

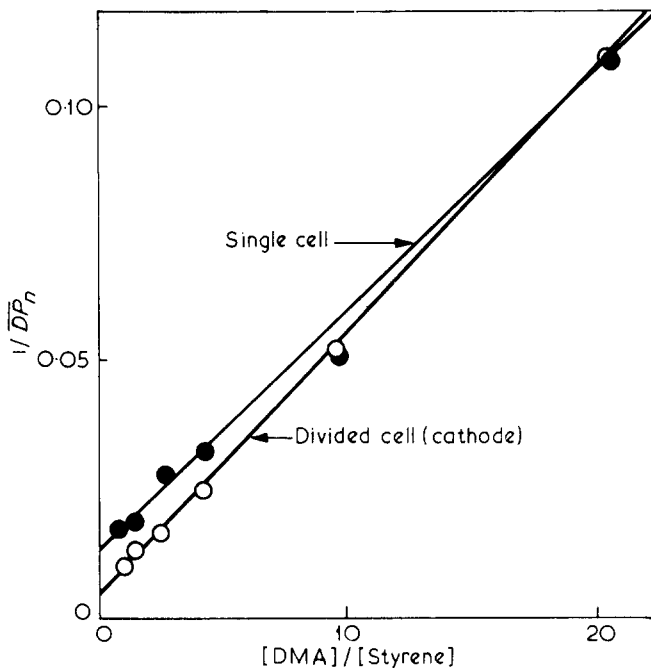


Figure 8 Transfer to solvent during electropolymerization of styrene in DMA/ NaBF_4 at 40 mA and 25°C

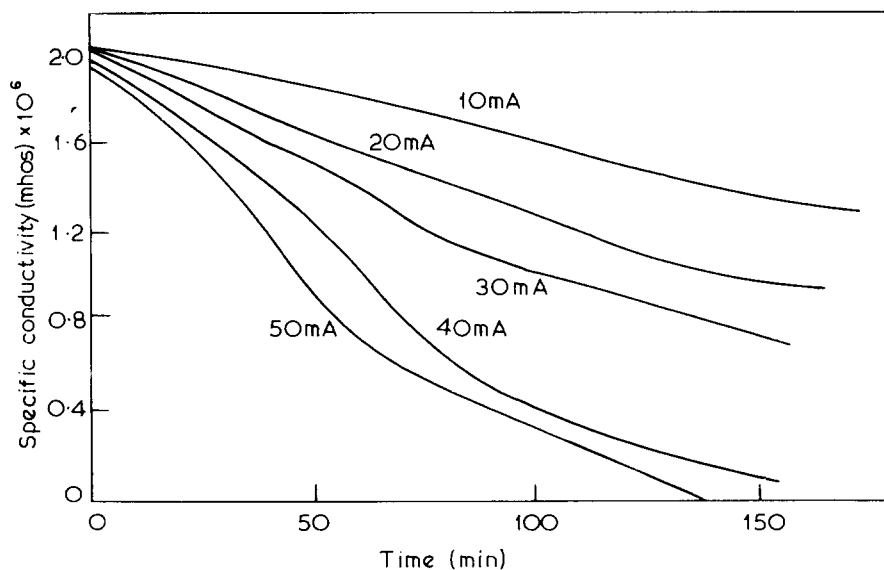


Figure 9 Variation of specific conductivity at the cathode of the divided cell with time for various currents during electrolysis of 2 M styrene in DMA/ NaBF_4 at 25°C

From *Figure 7* the values of the intercepts are: $1/(\overline{DP}_n)_0 = 0.0125$ (single cell) and $1/(\overline{DP}_n)_0 = 0.0050$ (divided cell), which implies that, in the single cell, further chain termination processes are occurring, possibly due to the presence of the anode electrode in the same locality as the cathode. A growing carbanion may be terminated either by direct discharge at the anode or by reaction with anodically produced positive ions.

In the case of the single cell the rate of electrolytic termination will be proportional to the active anion centre concentration and the applied current measured as Faraday/litre.

The rate of electrolytic termination $R_e = k_e[\text{anion centre}]I$. Equation (1) may be rewritten as:

$$\frac{1}{(\overline{DP}_n)} = \left\{ \frac{1}{(\overline{DP}_n)_0} \right\}' + \frac{k_e I}{k_p} + C_s \frac{[\text{DMA}]}{[\text{Styrene}]}$$

$$\frac{1}{(\overline{DP}_n)_0} = \left\{ \frac{1}{(\overline{DP}_n)_0} \right\}' + \frac{k_e I}{k_p}$$

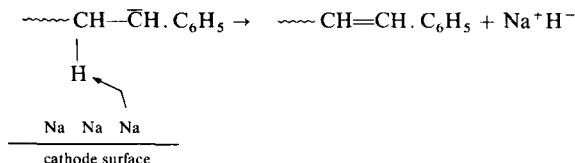
For a current of 40 mA passing for 1 h and assuming $\{1/(\overline{DP}_n)_0\}' = 0.005$, obtained above, k_e/k_p is given at 50×10^{-2} indicating considerable electrolytic termination in the single cell but which is absent in the divided cell. This is substantiated by the fact that in the divided cell the red colour typical of the styryl anion appears immediately on the surface of the cathode eventually pervading the whole of the cathode compartment. The colour is instantaneously removed on mixing anolyte with catholyte. In the case of the divided cell, although polymerization does occur, the solution remains a pale yellow throughout the reaction.

The current efficiency, i.e. the number of moles monomer polymerized per Faraday, and the % conversion are shown in *Table 2* for both the single and divided cells over a range of monomer concentrations when 40 mA current is

Table 2 Electropolymerization of styrene in DMA/NaBF₄

[Styrene] (mol/l)	Yield (g)	Conversion (%)	DP_n	Current efficiency (mol/Farad)	Molecules polymer/primary electrochem. act
0.5	1.2901	24.8	9	2.1	0.23
1.0	3.6985	35.5	19	6.0	0.31
2.0	9.9499	45.6	31	16.0	0.52
3.0	14.3970	46.1	37	23.0	0.63
4.0	18.7635	45.1	55	30.2	0.55
5.0	22.6320	43.5	58	36.4	0.63
<i>Cathode of divided cell (40 mA 100 ml electrolysed)</i>					
0.5	1.6138	62.0	7	5.2	0.74
1.0	3.8163	73.3	19	12.3	0.65
2.0	8.8183	84.7	39	28.4	0.73
3.0	14.0626	90.1	62	45.3	0.73
4.0	19.6215	94.3	79	63.1	0.80
5.0	24.9031	95.7	96	80.1	0.84

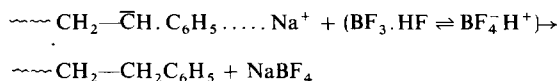
observed¹⁸. Such absorption is also observed in the infra-red spectra of polymer produced in the cathode of the divided cell. It is possible that at the cathode metallic sodium is deposited as a result of the discharge of sodium ions which may catalyse the reaction in a manner analogous to that suggested by Szwarc¹⁹.



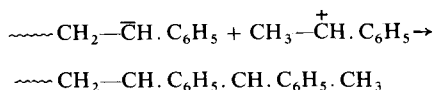
This reaction could also occur at the cathode of the single cell and would therefore appear to be relatively unimportant in view of the different rates of polymerization observed in the two cells.

In reaction (b), a polymeric carbanion discharged at the anode as a macro-radical may either react with an anodically generated F^\cdot , dimerize or propagate by a free radical mechanism. It would appear from elemental analysis and kinetic studies that again these reactions are relatively unimportant.

A totally different type of termination possibly occurring in the single cell involves reaction of the polymeric carbanions with positively charged species liberated at the anode. The instant decolorization observed on mixing catholyte and anolyte suggests that this type of reaction is more favourable. Possible species which could act in this way are protons which may be produced by BF_3 and HF :



and styrene cations which are incapable of cationic propagation due to strong solvation by DMA.



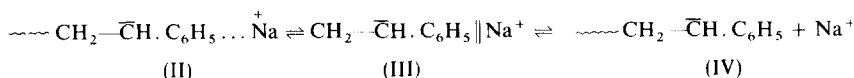
In the divided cell termination of a growing carbanion at either the anode or by anodically generated positively charged species is apparently eliminated by the presence of a physical barrier, i.e. a sintered glass frit. Thus, as electrolysis progresses there is a continuous build up of active centres which give rise to an acceleration in the rate of polymerization.

Monitoring the change in specific conductivity in the cathode compartment during electrolysis (*Figure 9*) indicates that, in the case of styrene (2 M) in DMA at 25°C, there is initially a linear decrease with time at several currents which could be due to the removal of sodium ions by electrolysis of NaBF_4 . At the higher currents a more rapid decrease in conductivity follows, the time when this occurs decreasing with increasing current and coincides roughly with the acceleration and the time to complete formation of the red colour of living polystyryl anions.

ELECTROINITIATED POLYMERIZATION OF STYRENE (2)

In addition to the rapid decrease in conductivity a notable increase in viscosity also occurs at this stage which could possibly account for the decrease in conductivity as being the direct result of decreased ionic mobility. Application of Walden's rule suggests that this effect could indeed be quite large, although it is difficult to give a quantitative estimation of the effect. When polymerization is virtually complete the conductivity continues to decrease, at a rate slower than that initially observed, due to further electrolysis of electrolyte.

Because of the relatively high salt concentrations used in the electropolymerization intimate or contact ion pairs (II) and solvent separated ion pairs (III) are more probably present in the system than are free ions (IV).



and so the equilibrium will be shifted to the left. As electrolysis proceeds the concentration of salt will decrease, tending to push the equilibrium to the right. In addition, the high dielectric constant (37.8 at 25°C) will tend to favour free ion formation (IV). It is difficult, therefore, to estimate the ratio II:III:IV in this system.

Thus, as in the cationic case previously described, the introduction of a porous barrier between the two electrodes effects the elimination of an electrolytic termination reaction and allows for the build up of a concentration of active species giving rise to acceleration of polymerization. It is interesting to note that by merely changing the solvent the entire locus of polymerization is changed.

ACKNOWLEDGEMENT

The authors wish to thank the University of Bradford for the grant of a research scholarship to one of them (A. G. D.).

*School of Polymer Science,
University of Bradford,
Bradford, Yorkshire BD7 1DP, UK*

*(Received 9 December 1970)
(Revised 20 July 1971)*

REFERENCES

- 1 Tidswell, B. M. and Doughty, A. G. *Polymer, Lond.* 1971, **12**, 431
- 2 Finemann, M. and Ross, S. D. *J. Polym. Sci.* 1950, **5**, 269
- 3 Zutty, N. L. and Welch, F. T. *J. Polym. Sci.* 1960, **43**, 445
- 4 Price, G. G. and Whiting, M. C. *Chem. and Ind.* 1963, p 775
- 5 Ledwith, A. and McFarlane, N. R. *Proc. Chem. Soc.* 1964, p 108
- 6 Molau, G. E. and Mason, J. E. *J. Polym. Sci. (A-1)* 1966, **4**, 2336
- 7 Bawn, C. E. H., Ledwith, A. and McFarlane, N. R. *Polymer, Lond.* 1967, **8**, 484
- 8 Walling, C. and Bollyky, L. *J. Org. Chem.* 1964, **29**, 2699

- 9 Giodana, M. S., Barzan, J. C. and Arvia, A. J. *Electrochim. Acta* 1966, **11**, 741
- 10 Szwarc, M. 'Carbanions, Living Polymers and Electron Transfer Processes', p 349, Wiley, Interscience, New York, 1968
- 11 Dainton, F. S., Wiles, D. M. and Wright, A. N. *J. Polym. Sci.* 1960, **45**, 127
- 12 Kaneko, H., *J. Metal Finish. Soc. Japan* 1970, **21**, 93
- 13 Laurin, D. and Parravano, G., *J. Polym. Sci. (C)* 1968, **1**, 103
- 14 Funt, B. L., Blain, T. J. and Young, R. A. *Polym. Preprints* 1970, **11**, 2
- 15 Funt, B. L. and Williams, F. B. *J. Polym. Sci. (A)* 1964, **2**, 865
- 16 Szwarc, M. *Nature* 1956, **178**, 1169
- 17 Milkovich, R. M., Levy, M. and Szwarc, M. *J. Amer. Chem. Soc.* 1956, **78**, 2656
- 18 Rao, C. N. R. 'Chemical Applications of Infra-Red spectroscopy', p 147, Academic Press, New York, 1963
- 19 Spach, G., Levy, M. and Szwarc, M. *J. Chem. Soc.* 1962, p 355

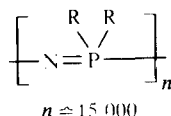
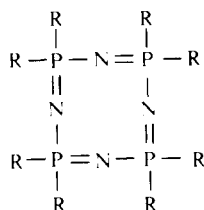
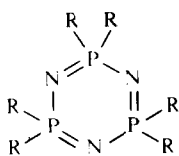
The elastic modulus of the poly-(phosphonitrilic chloride) crystal

T. R. MANLEY and C. G. MARTIN

The Young's modulus for a crystal of poly(phosphonitrilic chloride) (polydichlorophosphazene) $(\text{NPCl}_2)_n$ has been calculated using force constants derived from spectroscopy. Assuming that the molecule is a uniform helix the value of the modulus is 1.38×10^9 dyne cm^{-2} [dyne $\text{cm}^{-2} = 0.1 \text{ N m}^{-2}$]; the result is 1.66×10^{10} dyne cm^{-2} if a *cis*-planar structure is assumed for the molecule. Neither value is close to those obtained experimentally (1.8×10^6 to 6.5×10^6 dyne cm^{-2}). This is because experimental values relate to the amorphous polymer whereas the calculated values are those for the crystal. There is good agreement between the values calculated for the $(\text{NPCl}_2)_n$ crystal and those for other polymer crystals.

INTRODUCTION

THE PHOSPHAZENES are ring or chain compounds with alternating phosphorus and nitrogen atoms in the skeleton and two substituents on each phosphorus atom. Representative structures are the cyclic trimer, the cyclic tetramer, and the high polymer:



R can be halogen, pseudo-halogen, amino, azido or a wide variety of organic groups.

The phosphonitrilic halides (NPX_2) are the nitrogen analogues of the phosphoryl halides (POX_3) and like the latter are acid halides and susceptible to a wide variety of solution reactions. They differ from their oxygen analogues in their ability to form high molecular weight elastomers. Polydichlorophosphazene [or poly(phosphonitrilic chloride)] $(\text{NPCl}_2)_n$ is prepared by heating the cyclic trimer¹, but neither monomer nor dimer has been isolated. The trimer $(\text{NPCl}_2)_3$ is of fundamental interest being an inorganic analogue of benzene.

The phosphazenes display an unusual form of skeletal bonding. This bonding differs uniquely from both the σ -*p*- π double bonding of organic chemistry and the co-ordination bonding of many inorganic compounds. Phosphorus 3*d* orbitals overlap with nitrogen 2*p* orbitals to give *dπ*-*pπ* bonds^{2,3}.

The phosphorus–nitrogen bond in high molecular weight polyphosphazenes has an unusually high degree of torsional mobility. This is consistent with the expected behaviour of $d\pi-p\pi$ bonds where there is no appreciable barrier for successive involvement of alternate d -orbitals as the phosphorus–nitrogen bond is rotated. This is in marked contrast to $p\pi-p\pi$ systems. The torsional mobility of the (P=N) chain is comparable to that of the siloxane chain $(R_2SiO)_n$, since they are based on the isoelectronic repeat units SiO and PN.

Polydichlorophosphazene is elastomeric down to -63°C , it exhibits almost ideal rubber elasticity and does not melt below 300°C . It has one serious disadvantage, the phosphorus–chlorine bonds are hydrolytically unstable and cause the polymer to degrade slowly in contact with atmospheric moisture. This can be mitigated by replacing the chlorine atoms by stable organic groups.

Poly(phosphonitrilic chloride) $(NPCI_2)_n$ has been proposed as a radiation resistant rubber for use in nuclear reactors by Manley⁴ and other exotic uses may well be seen. In conjunction with phenolic resins and in other ways the material has found use as a flame retardant and proofing agent.

The polymerization of chlorophosphazenes was originally postulated as a free radical reaction⁵. This was shown to be erroneous^{6,7} and it is generally held that an ionic polymerization is involved⁸. The detailed mechanism has not been fully elucidated⁹.

Results from x-ray diffraction and infra-red spectroscopy with data from inter-atomic forces, make possible the calculation of the theoretical elastic modulus for a perfect polymer crystal. The modulus of elasticity in the principal chain direction of a polymer crystal of known structure may be calculated from the force constants of the chemical bonds of the chain derived from vibration frequencies of molecules. From the cellulose crystal values were obtained for the longitudinal modulus of 7.7×10^{11} and 12.1×10^{11} dyne cm^{-2} corresponding to two different estimates of the force constants¹⁰.

Lyons¹¹ extended the treatment to crystals of nylon-6,6 and poly(ethylene terephthalate) and obtained moduli of 15.7×10^{11} and 14.6×10^{11} dyne cm^{-2} respectively. By determining the change in lattice spacing from x-ray measurements whilst stressing a crystal of poly(ethylene terephthalate) Dulmage and Contois¹² obtained a longitudinal modulus of 14.0×10^{11} dyne cm^{-2} . Treloar¹³ calculated the longitudinal elastic moduli of polythene, nylon-6,6, poly(ethylene terephthalate) and cellulose as 1.82×10^{12} , 1.96×10^{12} , 14.6×10^{11} , and 5.65×10^{11} dyne cm^{-2} respectively, using a modified treatment.

Jaswon *et al*¹⁴ calculated the elastic constants for cellulose with respect to its principal axes of elasticity and also considered the effects of secondary bonds both intra- and inter-molecular on the calculated values.

They obtained the same value as Treloar for the Young's modulus in the chain direction before correcting for secondary bonds.

Up to this point the polymers mentioned have been linear and planar or with only very slight deviation from a planar structure. The elastic constants of helical polymers were calculated by Shimanouchi *et al*¹⁵ and also Asahina and Enomoto^{16,17} who derived a general formula for helical polymers based on a Urey–Bradley force field.

In this paper, the energy method of Jaswon *et al*¹⁴ is applied to a crystal

ELASTIC MODULUS OF POLY(PHOSPHONITRILIC CHLORIDE) CRYSTAL

of the simple helical polymer poly(phosphonitrilic chloride). The simplicity of the helix (two monomer units per turn) makes this polymer an ideal starting point for the application of an analysis involving systematic Cartesian coordinate specification.

STRUCTURE OF THE LINEAR POLY(PHOSPHONITRILIC CHLORIDE)

The x-ray pattern of the polymer crystal was first investigated by Meyer *et al*¹⁸ who deduced an orthorhombic unit cell containing four chains with the following dimensions: $a_0 = 11.07 \text{ \AA}$, $b_0 = 4.92 \text{ \AA}$ (fibre axis) and $c_0 = 12.72 \text{ \AA}$. They proposed a regular backbone chain with two monomer units in the repeat distance of 4.92 \AA assuming bond lengths and angles based on other phosphonitrilic compounds. No chain azimuthal angles were given.

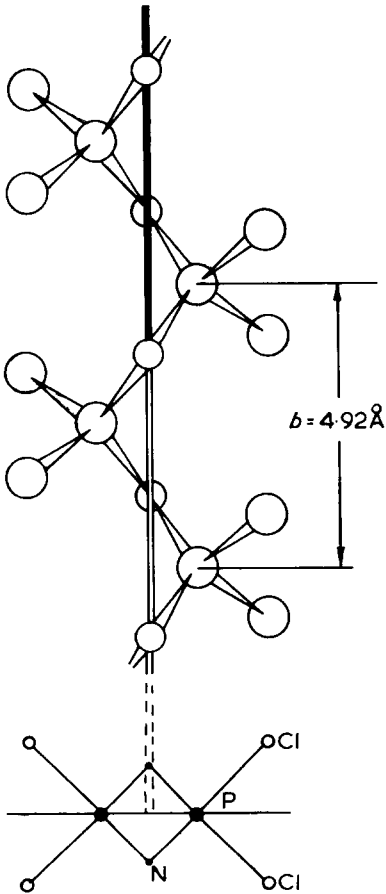


Figure 1 Uniform helical model of linear $(NPCl_2)_n$

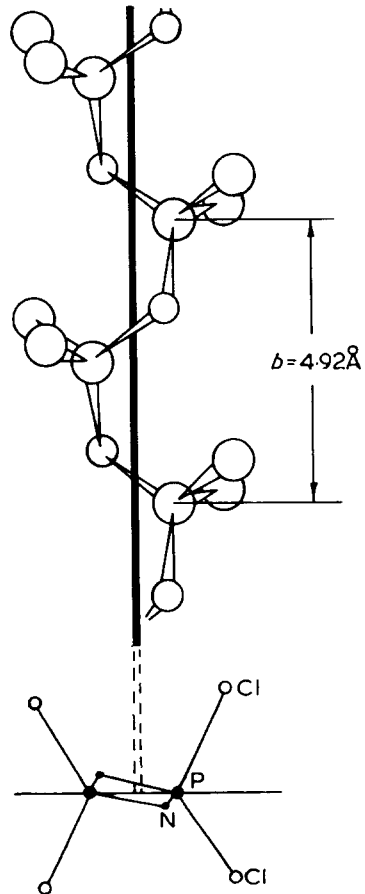


Figure 2 Distorted 'cis-planar' helical model of linear $(NPCl_2)_n$

Using data¹⁹ on the trimer Huggins²⁰ proposed a uniform helical structure with two monomer units per turn and an azimuthal bond angle of 90° assuming equivalent bond lengths and angles in the chain of 1.65 \AA and 124° respectively.

Giglio *et al*²¹ showed that the identity period was not sufficient to define chain conformation and used optical fourier transform methods to compare model structures with the observed x-ray diffraction photograph. Their preliminary investigation gave the two most likely structures as: (1) uniform helix structure (*Figure 1*) with $P-N = 1.74 \text{ \AA}$, $PNP = NPN = 120^\circ$; and (2) *cis*-planar structure (*Figure 2*) with $P-N = 1.60 \text{ \AA}$, $PNP = 127^\circ$, $NPN = 119^\circ$ and azimuthal angles round the $P-N$ and $N-P$ bonds as 156° and 14° respectively. Further analysis of the x-ray photograph showed that the molecular conformation is closer to the *cis*-planar than to the uniform helical model. This was also shown by infra-red spectroscopy²². However, both structures will be used in the calculation of the elastic modulus.

GENERAL GEOMETRICAL DESCRIPTION

The two proposed structural forms may be represented by the general helical model shown in *Figure 3* for one repeating unit of length 4.92 \AA . The chlorine atoms are omitted for clarity.

P_1, P_2 and P_3 and N_1, N_2 and N_3 represent phosphorus and nitrogen atoms

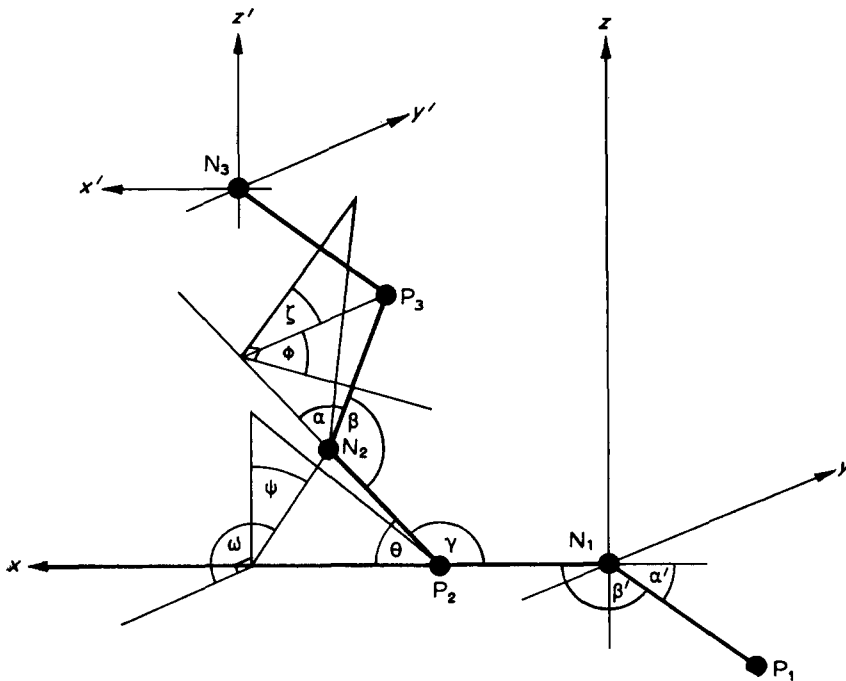


Figure 3 Designation of bond lengths and angles showing Cartesian reference frame

respectively. The repeat distance between P_1 and P_3 and between N_1 and N_3 is 4.92 Å. Therefore the bonds P_1N_1 and P_3N_3 are parallel.

In order to characterize this model it is convenient to introduce a rectangular Cartesian reference frame by taking N_1 as the origin and N_1P_2 as the direction of the x axis. The y axis lies perpendicular to N_1P_2 and is in the plane of $P_1N_1P_2$. The z axis is then perpendicular to this plane $P_1N_1P_2$.

The repeat unit P_1P_3 can then be characterized by five geometrical quantities, independent of the choice of axes, namely the bond length l where $P_1N_1 = N_1P_2 = P_2N_2 = N_2P_3 = l$, the interbond angles β and γ which are related to the auxiliary angles α and θ by $P_1N_1P_2 = P_2N_2P_3 = \beta = (\pi - \alpha)$ and $N_1P_2N_2 = \gamma = (\pi - \theta)$, the angle ζ which is the bond rotation angle between planes $N_1P_2N_2$ and $P_2N_2P_3$ taken in a clockwise sense, also giving the auxiliary angle ϕ , where $\zeta + \phi = \pi/2$, i.e. ϕ is the rotation angle from the plane perpendicular to $P_2N_2P_3$ and passing through P_2N_2 .

Finally the angle ω which is the bond rotation angle between the $P_1N_1P_2$ plane (xy) and the plane $N_1P_2N_2$ taken in a clockwise sense, also giving the auxiliary angle ψ which is the angle between the xz plane and the plane $N_1P_2N_2$ taken in a clockwise sense and where

$$\psi = (\omega - \pi/2)$$

We can now assign vector components as follows referring to *Figure 3*.

$$P_1N_1 = (-\cos\alpha', \sin\alpha', 0)l$$

$$N_1P_2 = (1, 0, 0)l$$

$$P_2N_2 = (\cos\theta, \sin\theta\sin\psi, \sin\theta\cos\psi)l$$

$$N_2P_3 = [\cos\alpha\cos\theta - \sin\alpha\sin\theta\cos\phi, \sin\psi(\cos\alpha\sin\theta + \sin\alpha\cos\theta\cos\phi) - \sin\alpha\sin\phi\cos\psi, \cos\psi(\cos\alpha\sin\theta + \sin\alpha\cos\theta\cos\phi) + \sin\alpha\sin\phi\sin\psi]l$$

$$P_3N_3 = (\cos\alpha, \sin\alpha, 0)l$$

We can now write down systematically the coordinates of every atom in the system with respect to the origin at N_1 .

$$P_1 = (-l\cos\alpha', -l\sin\alpha', 0)$$

$$N_1 = (0, 0, 0)$$

$$P_2 = (l, 0, 0)$$

$$N_2 = (l + l\cos\theta, l\sin\theta\sin\psi, l\sin\theta\cos\psi)$$

$$P_3 = [l + l\cos\theta + l\cos\alpha\cos\theta - l\sin\alpha\sin\theta\cos\phi, l\sin\theta\sin\psi - l\sin\alpha\sin\phi\cos\psi + l\sin\psi(\cos\alpha\sin\theta + \sin\alpha\cos\theta\cos\phi), l\sin\theta\cos\psi + l\cos\psi(\cos\alpha\sin\theta + \sin\alpha\cos\theta\cos\phi) + l\sin\alpha\sin\phi\sin\psi]$$

$$N_3 = [l + l\cos\theta + l\cos\alpha\cos\theta - l\sin\alpha\sin\theta\cos\phi + l\cos\alpha, l\sin\theta\sin\psi - l\sin\alpha\sin\phi\cos\psi + l\sin\psi(\cos\alpha\sin\theta + \sin\alpha\cos\theta\cos\phi) + l\sin\alpha, l\sin\theta\cos\psi + l\cos\psi(\cos\alpha\sin\theta + \sin\alpha\cos\theta\cos\phi) + l\sin\alpha\sin\phi\sin\psi]$$

or $N_3 = (0, 0, 0)$ with respect to the axes X', Y', Z' in *Figure 4*.

The distance N_1N_3 can be written as:

$$N_1N_3 = (\cos\Omega\cos\chi, \cos\Omega\sin\chi, \sin\Omega)L \quad (1)$$

where Ω is the inclination of N_1N_3 to the xy plane and χ is the inclination of the projection of N_1N_3 on the xy plane to the x axis, and L is the repeat distance.

Equating the components in the z direction we get:

$$L\sin\Omega = l\sin\theta\cos\psi + l\cos\psi(\cos a\sin\theta + \sin a\cos\theta\cos\phi) + l\sin a\sin\theta\sin\psi \quad (2)$$

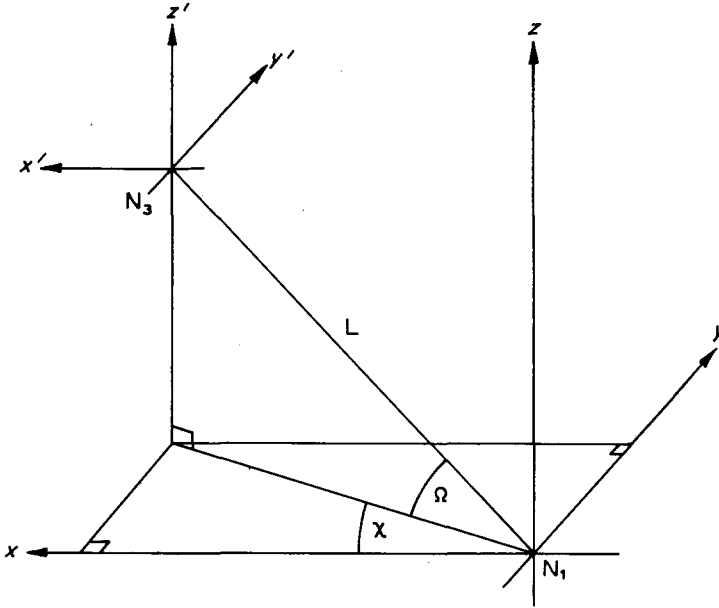


Figure 4 Designation of overall length and direction of the repeat distance of $(NPCl_2)_n$

Similarly for the x direction:

$$L\cos\Omega\cos\chi = l + l\cos\theta + l\cos a\cos\theta - l\sin a\sin\theta\cos\phi + l\cos a \quad (3)$$

and hence Ω and χ can be calculated from l, L, a, θ, ϕ and ψ .

CALCULATION OF ELASTIC CONSTANTS

Since the values of the extra coupling constants are small compared with c_{12}, c_{23} and c_{31} and also the off diagonal components are generally small compared with c_{11}, c_{22}, c_{33} , the approximation

$$\begin{aligned} c_{11} &= s_{11}^{-1} \\ c_{22} &= s_{22}^{-1} \\ c_{33} &= s_{33}^{-1} \end{aligned}$$

may be used for the Young's moduli in the three axial directions.

The largest and most important modulus is c_{22} , which can be obtained by

considering a uniform strain e_2 in the direction of the main fibre axis, no other strain component being allowed.

The stress components necessary to maintain this strain are then given by

$$\begin{aligned}\sigma_1 &= c_{12}e_2 \\ \sigma_2 &= c_{22}e_2 \\ \sigma_3 &= c_{32}e_2 \\ \sigma_4 &= \sigma_5 = \sigma_6 = 0\end{aligned}$$

This holds both for D_2 and C_2 symmetries. It is not necessary, however, to calculate these stress components as c_{22} can be obtained from the strain energy function since

$$\begin{aligned}e_1 = e_3 = e_4 = e_5 = e_6 &= 0 \\ \therefore \frac{W}{V} &= \frac{1}{2}c_{22}e_2^2\end{aligned}\quad (4)$$

This equation represents the strain energy per unit volume when an isolated chain is deformed along its own direction, introducing a strain e_2 . The symmetry of the chain is not changed by the deformation and therefore it can still be described by the five geometrical quantities introduced earlier, i.e. $l, \beta, \gamma, \zeta, \omega$.

These can be considered as five degrees of freedom which can be varied independently of one another, and which contribute separately to the extension of the chain along its fibre axis.

If dl_i is the small change in a degree of freedom describing a particular bond then the increase in strain energy will be given by the expression:

$$w_i = \frac{1}{2}c_i(dl_i)^2 \quad (5)$$

where c_i is the force constant for deformation of the i th degree of freedom. Therefore the strain energy of the repeat unit as a whole may be written in general form as

$$W = \frac{1}{2} \sum_{i=1}^9 C_i(dl_i)^2 \quad (6)$$

(i changes to nine degrees of freedom from five, since although bonds $P_1N_1, N_1P_2, P_2N_2, N_2P_3$ have the same bond length l , they are in different directions. Similarly although $P_1N_1P_2 = P_2N_2P_3 = (\pi - \alpha)$ each deformation contributes a different amount in the chain direction N_1N_3).

If the repeat length L is extended by a length $dL = Le_2$ then dL is made up as the sum of the small changes dL_i in the chain direction due to variations in the degrees of freedom

$$\therefore dL = Le_2 = \sum_{i=1}^9 dL_i. \quad (7)$$

The contributions (dL_i) in the chain direction may be determined as follows.

$$dL_1 = \bar{n}(-\cos\alpha', -\sin\alpha', 0)dl_1$$

where \bar{n} represents the unit vector given in equation (1)

$$N_1N_3 = (\cos\Omega\cos\chi, \cos\Omega\sin\chi, \sin\Omega)L = \bar{n}L \quad (8)$$

$$\therefore dL_1 = (-\cos\Omega\cos\chi\cos\alpha' - \cos\Omega\sin\chi\sin\alpha')dl_1 \quad (9)$$

similarly

$$dL_2 = \cos\Omega\cos\chi dl_2 \quad (10)$$

$$dL_3 = (\cos\Omega\cos\chi\cos\theta + \cos\Omega\sin\chi\sin\theta\sin\psi + \sin\Omega\sin\theta\cos\psi)dl_3 \quad (11)$$

$$dL_4 = \{\cos\Omega\cos\chi(\cos\alpha\cos\theta - \sin\alpha\sin\theta\cos\phi) + \cos\Omega\sin\chi[\sin\psi(\cos\alpha\sin\theta + \sin\alpha\cos\theta\cos\phi) - \sin\alpha\sin\phi\cos\psi] + \sin\Omega[\cos\psi(\cos\alpha\sin\theta + \sin\alpha\cos\theta\cos\phi) + \sin\alpha\sin\phi\sin\psi]\}dl_4 \quad (12)$$

These are the contributions to dL due to small changes dl_i ($i = 1$ to 4) in the bond lengths P_1N_1 , N_1P_2 , P_2N_2 , N_2P_3 (see *Figure 3*).

We must now consider the contribution to dL of small changes in the inter-bond angles and bond rotation angles taking into account the inter-relation between them.

The relations between α , θ , ϕ , and ψ and their differentials with respect to β , γ , ζ and ω , may be determined by differentiation of the following equations:

$$\cos\eta = 1 - 2\sin^2\gamma\sin^2\psi \quad (13)$$

$$\cos\eta = 1 - 2\sin^2\theta\cos^2\omega \quad (14)$$

$$\begin{aligned} \cos\eta' = & \cos^2\beta\cos^2\theta + \sin^2\beta\sin^2\theta\cos^2\phi + \\ & \cos 2\psi[\sin^2\beta\cos^2\theta\cos^2\phi - \sin^2\beta\sin^2\phi + \cos^2\beta\sin^2\theta] + \\ & \frac{1}{2}\sin 2\beta\sin 2\theta\cos\phi(1 - \cos 2\psi) + \\ & \sin 2\psi[\sin 2\phi\sin^2\beta\cos\theta - \sin 2\beta\sin\theta\sin\phi] \end{aligned} \quad (15)$$

$$\begin{aligned} \cos\eta' = & \cos^2\theta\cos^2\alpha + \sin^2\alpha\sin^2\theta\sin^2\zeta + \\ & \cos 2\psi[\sin^2\alpha\cos^2\theta\sin^2\zeta - \sin^2\alpha\cos^2\zeta + \cos^2\alpha\sin^2\theta] - \\ & \frac{1}{2}\sin 2\alpha\sin 2\theta\sin\zeta(1 - \cos 2\psi) + \\ & \sin 2\psi[\sin 2\alpha\sin\theta\cos\zeta + \sin 2\zeta\sin^2\alpha\cos\theta] \end{aligned} \quad (16)$$

where η and η' are the hypothetical angles between bonds, P_2N_2 and its mirror image in the xz plane, and direction N_2P_3 and its mirror image in the xz plane respectively.

The derivation and differentiation of these equations are given fully in the Appendix.

The subscripts 5, 6, 7, 8 and 9 refer to β' , γ , ω , β ($P_1N_1P_2$ and $P_2N_2P_3$ are in different positions with respect to the x , y and z axes), and ζ .

$$dL_5 = \bar{n}l \frac{\partial}{\partial\beta'} [-\cos\alpha', -\sin\alpha', 0] d\beta'$$

where $\beta' = \pi - \alpha'$ and $d\beta' = -d\alpha'$

$$\therefore dL_5 = (-l\cos\Omega\cos\chi\sin\alpha' + l\cos\Omega\sin\chi\cos\alpha') d\beta' \quad (17)$$

Similarly:

$$dL_6 = l \left[\cos\Omega\cos\chi\sin\theta - \cos\Omega\sin\chi \left(\sin\theta\cos\psi \frac{d\psi}{d\gamma} - \sin\psi\cos\theta \right) - \sin\Omega \left(\cos\psi\cos\theta + \sin\theta\sin\psi \frac{d\psi}{d\gamma} \right) \right] d\gamma \quad (18)$$

$$\begin{aligned}
 dL_7 = l \left[-\cos\Omega\cos\chi\sin\theta \frac{d\theta}{d\omega} + \right. \\
 \left. \cos\Omega\sin\chi \left(\sin\theta\cos\psi + \sin\psi\cos\theta \frac{d\theta}{d\omega} \right) + \right. \\
 \left. \sin\Omega \left(\cos\psi\cos\theta \frac{d\theta}{d\omega} - \sin\theta\sin\psi \right) \right] d\omega \quad (19)
 \end{aligned}$$

$$\begin{aligned}
 dL_8 = l \left\{ \cos\Omega\cos\chi \left[\sin\alpha\sin\theta\sin\phi \frac{d\phi}{d\beta} + \right. \right. \\
 \left. \left[\cos\theta\sin\alpha + \cos\alpha\sin\theta\cos\phi \right] - \right. \\
 \left. \left[\cos\alpha\sin\theta + \sin\alpha\cos\theta\cos\phi \right] \frac{d\theta}{d\beta} \right] + \\
 \cos\Omega\sin\chi \left[\left[(\cos\alpha\sin\theta + \sin\alpha\cos\theta\cos\phi)\cos\psi + \right. \right. \\
 \left. \left. \sin\alpha\sin\phi\sin\psi \right] \frac{d\psi}{d\beta} + \right. \\
 \left. \left[\sin\psi(\cos\alpha\cos\theta - \sin\alpha\sin\theta\cos\phi) \right] \frac{d\theta}{d\beta} - \right. \\
 \left. \left[\sin\psi(\cos\alpha\cos\theta\cos\phi - \sin\alpha\sin\theta) - \cos\alpha\sin\phi\cos\psi \right] - \right. \\
 \left. \left[\sin\alpha\cos\phi\cos\psi + \sin\psi\sin\alpha\cos\theta\sin\phi \right] \frac{d\phi}{d\beta} \right] + \\
 \sin\Omega \left[\left[\cos\psi(\cos\alpha\cos\theta - \sin\alpha\sin\theta\cos\phi) \right] \frac{d\theta}{d\beta} - \right. \\
 \left. \left[\cos\psi(\cos\alpha\cos\theta\cos\phi - \sin\theta\sin\alpha) + \cos\alpha\sin\phi\sin\psi \right] + \right. \\
 \left. \left[\sin\alpha\sin\psi\cos\phi - \cos\psi\sin\alpha\cos\theta\sin\phi \right] \frac{d\phi}{d\beta} + \right. \\
 \left. \left[\sin\alpha\sin\phi\cos\psi - \sin\psi(\cos\alpha\sin\theta + \right. \right. \\
 \left. \left. \sin\alpha\cos\theta\cos\phi) \right] \frac{d\psi}{d\beta} \right] \quad \left. d\beta \right\} \quad (20)
 \end{aligned}$$

$$\begin{aligned}
 dL_9 = l \left\{ \cos\Omega\cos\chi \left[-\sin\alpha\sin\theta\sin\phi - \right. \right. \\
 \left. \left[\cos\theta\sin\alpha + \cos\alpha\sin\theta\cos\phi \right] \frac{d\alpha}{d\zeta} - \right. \\
 \left. \left[\cos\alpha\sin\theta + \sin\alpha\cos\theta\cos\phi \right] \frac{d\theta}{d\zeta} \right] + \\
 \cos\Omega\sin\chi \left[\left[(\cos\alpha\sin\theta + \sin\alpha\cos\theta\cos\phi)\cos\psi + \right. \right. \\
 \left. \left. \sin\alpha\sin\phi\sin\psi \right] \frac{d\psi}{d\zeta} + \right. \\
 \left. \left[\sin\psi(\cos\alpha\cos\theta - \sin\alpha\sin\theta\cos\phi) \right] \frac{d\theta}{d\zeta} + \right. \\
 \left. \left[\sin\psi(\cos\alpha\cos\theta\cos\phi - \sin\alpha\sin\theta) - \right. \right. \\
 \left. \left. \cos\alpha\sin\phi\cos\psi \right] \frac{d\alpha}{d\zeta} + \right.
 \end{aligned}$$

$$\begin{aligned} & [\sin\alpha\cos\phi\cos\psi + \sin\psi\sin\alpha\cos\theta\sin\phi] + \\ \sin\Omega & \left[\cos\psi(\cos\alpha\cos\theta - \sin\alpha\sin\theta\cos\phi) \frac{d\theta}{d\zeta} + \right. \\ & \left. [\cos\psi(\cos\alpha\cos\theta\cos\phi - \sin\theta\sin\alpha) + \right. \\ & \left. \cos\alpha\sin\phi\sin\psi] \frac{d\alpha}{d\zeta} - \right. \\ & \left. [\sin\alpha\sin\psi\cos\phi - \cos\psi\sin\alpha\cos\theta\sin\phi] + \right. \\ & \left. [\sin\alpha\sin\phi\cos\psi - \sin\psi(\cos\alpha\sin\theta + \right. \\ & \left. \sin\alpha\cos\theta\cos\phi)] \frac{d\psi}{d\zeta} \right] d\zeta \quad (21) \end{aligned}$$

Superposing the quantities dL_i as previously

$$dL = \sum_{i=1}^9 dL_i$$

which can be written preferably as:

$$dL = \sum \left(\frac{\partial L}{\partial l_i} \right) dl_i \quad (22)$$

For a prescribed dL the above equation can be regarded as a constraint upon the dl_i which must be chosen so as to minimize W in the strain energy function.

$$W = \frac{1}{2} \sum C_i (dl_i)^2 \quad (23)$$

Minimization by the method of Lagrangian multipliers yields:

$$\frac{\partial W}{\partial (dl_i)} = \lambda \frac{\partial (dL)}{\partial (dl_i)} \quad \text{for } i = (1, 2, \dots, 9) \quad (24)$$

where λ is to be determined.

Differentiation of equation (22) yields

$$\begin{aligned} \frac{\partial (dL)}{\partial (dl_i)} &= \frac{(\partial L)}{(\partial l_i)} \\ \therefore \frac{\partial^2 W}{\partial (dl_i)} &= \lambda \left(\frac{\partial L}{\partial l_i} \right) \end{aligned}$$

Also from equation (23)

$$\frac{\partial W}{\partial (dl_i)} = C_i (dl_i)$$

and

$$\begin{aligned} \frac{\partial W}{\partial (dl_i)^2} &= C_i \\ \therefore C_i (dl_i) &= \lambda \left(\frac{\partial L}{\partial l_i} \right) \end{aligned}$$

and

$$dl_i = \lambda \left(\frac{\partial L}{\partial l_i} \right) / \frac{\partial^2 W}{\partial (dl_i)^2}$$

Substituting in equation (22):

$$dL = \lambda \sum \left(\frac{\partial L}{\partial l_i} \right)^2 \bigg/ \frac{\partial^2 W}{\partial (dl_i)^2}$$

$$\therefore \lambda = \frac{dL}{A} \quad \text{where } A = \sum \left(\frac{\partial L}{\partial l_i} \right)^2 \bigg/ \frac{\partial^2 W}{\partial (dl_i)^2}$$

Substituting for λ :

$$dl_i = \frac{dL}{A} \left(\frac{\partial L}{\partial l_i} \right) \bigg/ \frac{\partial^2 W}{\partial (dl_i)^2}$$

Hence

$$W = \frac{1}{2} \sum \left[\frac{\partial^2 W}{\partial (dl_i)^2} \right] \left(\frac{dL}{A} \right)^2 \left(\frac{\partial L}{\partial l_i} \right)^2 \bigg/ \left[\frac{\partial^2 W}{\partial (dl_i)^2} \right]^2$$

$$= \frac{1}{2} \left(\frac{dL}{A} \right)^2 \left(\frac{\partial L}{\partial l_i} \right)^2 \bigg/ \frac{\partial^2 W}{\partial (dl_i)^2} = \frac{1}{2} \left(\frac{dL}{A} \right)^2 A$$

$$\therefore W = \frac{1}{2} A^{-1} (dL)^2 \quad (25)$$

where A^{-1} is the gross elastic constant for the repeating unit. Denoting the gross constant by C^{-1} we obtain¹⁴:

$$C^{-1} = A = \sum \left(\frac{\partial L}{\partial l_i} \right)^2 \bigg/ \frac{\partial^2 W}{\partial (dl_i)^2} \quad (26)$$

$$\therefore C^{-1} = \left(\frac{dL_1}{dl_1} \right)^2 \bigg/ C_1 + \left(\frac{dL_2}{dl_2} \right)^2 \bigg/ C_2 + \dots + \left(\frac{dL_i}{dl_i} \right)^2 \bigg/ C_i + \dots \quad (27)$$

to $i = (1, 2, 3, \dots, 9)$.

C^{-1} can then be related to c_{22} by the energy balance

$$W = \frac{1}{2} c_{22} e_2^2 V' = \frac{1}{2} C (dL)^2 = \frac{1}{2} C (L e_2)^2$$

$$\therefore c_{22} = \frac{CL^2}{V'} \quad (28)$$

where L is the repeat distance and V' is the volume of the repeating unit. (In this case V' equals $V/4$ where V is the volume of the unit cell which contains four chains.)

NUMERICAL SOLUTION FOR YOUNG'S MODULUS (c_{22})

In order to calculate the elastic constant c_{22} we need suitable values for substitution in equations (2), (3), (9) to (21), (27) and (28). These values are obtained from the geometric parameters of the polymer helix given below.

Cis-planar helical structure:

$$l = 1.60 \times 10^{-8} \text{ cm}$$

$$L = 4.92 \times 10^{-8} \text{ cm}$$

$$V = 6.901 \times 10^{-22} \text{ cm}^3$$

$$\beta = 127^\circ = (\pi - \alpha)$$

$$\gamma = 119^\circ = (\pi - \theta)$$

$$\zeta = 14^\circ = \left(\frac{\pi}{2} - \phi \right)$$

$$\omega = 156^\circ = \left(\psi + \frac{\pi}{2} \right)$$

hence: $\alpha = 53^\circ$; $\theta = 61^\circ$; $\phi = 76^\circ$; $\psi = 66^\circ$.

Uniform helical structure:

$$\begin{aligned} l &= 1.74 \times 10^{-8} \text{ cm} \\ L &= 4.92 \times 10^{-8} \text{ cm} \\ V &= 6.901 \times 10^{-22} \text{ cm}^3 \\ \beta &= \gamma = 120^\circ \\ \zeta &= \omega = 90^\circ \end{aligned}$$

hence: $\theta = \alpha = 60^\circ$; $\phi = \psi = 0^\circ$.

Force constant data were taken from the work of Manley and Williams²² on the cyclic phosphonitrilic halides and were as follows:

$$\begin{aligned} C_1 &= C_2 = C_3 = C_4 = 7.08 \times 10^5 \text{ dyne cm}^{-1} \\ C_5 &= C_8 = 1.32 \times 10^{11} \text{ dyne cm rad}^{-1} \\ C_6 &= 9.09 \times 10^{-11} \text{ dyne cm rad}^{-1} \\ C_7 &= C_9 = 0.408 \times 10^{-11} \text{ dyne cm rad}^{-1} \end{aligned}$$

The above equations were computed (IBM 1620) (using the above data) and the results obtained are given below.

Cis-planar structure: $c_{22} = 1.66 \times 10^{10} \text{ dyne cm}^{-2}$.

Uniform helix structure: $c_{22} = 1.38 \times 10^9 \text{ dyne cm}^{-2}$.

In the uniform helix, $\sin\psi$ and $\sin\phi$ ($\psi = 0^\circ$, $\phi = 0^\circ$) are zero, therefore some of the quotients become indeterminate. To overcome this the program was rewritten so as to approach 0° in small increments. Values of the c_{22} were calculated and the value at 0° obtained by extrapolation.

DISCUSSION

The Young's modulus of poly(phosphonitrilic chloride) is reported as 2.0 to $3.14 \times 10^6 \text{ dyne cm}^{-2}$ over the range $20\text{--}50^\circ\text{C}$ ²³ and as 1.8 to $6.5 \times 10^6 \text{ dyne cm}^{-2}$ for polymer of molecular weight 38 000 to 173 400 at 20°C and 70% relative humidity²⁴.

The difference between the experimental figures and the calculated value is too large to be accounted for by considerations of hydrolytic instability, 'flaws' in the polymer, or errors in using force constants derived from trimeric phosphonitrilic chloride.

Our calculations relate to the deformation of an isolated chain in a crystal of poly(phosphonitrilic chloride). Under normal conditions the deformation of the non-crystalline material present will be much greater than that in the crystallites resulting in a much lower modulus. Thus the observed moduli^{23, 24} cannot be compared with the calculated values.

x-Ray techniques such as those of Dulmage and Contois¹² measuring changes in crystal lattice spacing with stress should give values suitable for comparison but no data are available for $(\text{NPCl}_2)_n$.

The calculated values for $(\text{NPCl}_2)_n$ and for other polymers are given in Table 1. The values for the $(\text{NPCl}_2)_n$ crystal are considerably lower than those for polyethylene and nylon but are of similar order of magnitude to

ELASTIC MODULUS OF POLY(PHOSPHONITRILIC CHLORIDE) CRYSTAL

those of poly(ethylene glycol) and polypropylene which also possess helical structures.

Poly(phosphonitrilic chloride) has a polymer chain of high torsional mobility and, as in poly(ethylene glycol), large changes in internal rotation angles occur on stretching resulting in the low values for those polymers.

Table 1 Young's moduli of polymer crystals

<i>Polymer</i>	<i>Calculated value</i> (dyne cm ⁻²)
Nylon-6,6 ^a	1.96 × 10 ^{12d}
Polyethylene ^a	1.82 × 10 ^{12d}
Poly(ethylene terephthalate) ^a	1.46 × 10 ^{12d}
PTFE ^b	1.66 × 10 ^{12e}
Poly(isobutylene) ^c	7-8 × 10 ^{11f}
isotactic Polypropylene ^c	4.9 × 10 ^{11f}
Poly(ethylene glycol) ^c	4.8 × 10 ^{10f}
(NPCl ₂) _n <i>cis</i> -planar	1.66 × 10 ^{10g}
(NPCl ₂) _n uniform helix	1.38 × 10 ^{9g}

^aPlanar zig-zag structure. ^bHelical but can be considered as distorted planar zig-zag. ^cHelical structure. ^dRef. 13. ^eRef. 15. ^fRefs. 16 and 17. ^gThis work.

Owing to the absence of suitable experimental values for the modulus of the (NPCl₂)_n crystal no confirmation of structure can be made on the basis of the calculated values for each model.

ACKNOWLEDGEMENT

We thank the Science Research Council for a scholarship to C.G.M.

*Department of Materials Science,
Newcastle-upon-Tyne Polytechnic,
Ellison Building, Ellison Place,
Newcastle-upon-Tyne NE1 8ST, UK*

*(Received 30 December 1970)
(Revised 17 May 1971)*

REFERENCES

- 1 Stokes, H. N. *J. Amer. Chem. Soc.* 1897, **19**, 43
- 2 Craig, D. P. *Chem. and Ind.* 1958, p 3
- 3 Craig, D. P. and Paddock, N. L. *Nature* 1958, **181**, 1052
- 4 Brit. Pat. Appln 17336/59
- 5 Patat, F. and Kallinsky, F. *Makromol. Chem.* 1951, **6**, 292
- 6 Manley, T. R. *Nature* 1959, **184**, 899
- 7 Spindler, M. W. and Vale, R. L. *Makromol. Chem.* 1961, **43**, 231
- 8 Eley, D. D. and Willis, M. R. *J. Chem. Soc.* 1963, p 1534
- 9 Colclough, R. O. and Gee, G. *J. Polym. Sci. (C)* 1968, **16**, 3639
- 10 Meyer, K. H. and Lotmar, W. *Helv. Chim. Acta* 1936, **19**, 68
- 11 Lyons, W. J. *J. Appl. Phys.* 1958, **29**, 1429
- 12 Dulmage, W. J. and Contois, L. E. *J. Polym. Sci.* 1958, **28**, 275

- 13 Treloar, L. R. G. *Polymer, Lond.* 1960, **1**, 95, 279, 290
- 14 Jaswon, M. A., Gillis, P. P. and Mark, R. E. *Proc. Roy. Soc.* 1968, **A306**, 389
- 15 Shimanouchi, T., Asahina, M. and Enomoto, S. *J. Polym. Sci.* 1962, **59**, 93
- 16 Asahina, M. A. and Enomoto, S. *J. Polym. Sci.* 1962, **59**, 101
- 17 Asahina, M. A. and Enomoto, S. *J. Polym. Sci.* 1962, **59**, 113
- 18 Meyer, K. H., Lotmar, W. and Pankow, G. W. *Helv. Chim. Acta* 1936, **19**, 930
- 19 Brockway, L. O. and Bright, W. M. *J. Amer. Chem. Soc.* 1943, **65**, 1551
- 20 Huggins, M. L. *J. Chem. Phys.* 1945, **13**, 37
- 21 Giglio, E., Pompa, F. and Ripamonti, A. *J. Polym. Sci.* 1962, **59**, 293
- 22 Manley, T. R. and Williams, D. A. *Polymer, Lond.* 1969, **10**, 307
- 23 Specker, H. *Angew. Chem.* 1953, **65**, 299
- 24 Yokoyama, M. *Chem. High Polymers (Japan)* 1960, **17**, 651

APPENDIX

Relationship of the auxiliary angles α, θ, ϕ and ψ to the degrees of freedom β, γ, ζ and ω

Let η be the angle between P_2N_2 and P_2N_2' where P_2N_2' is the mirror image of P_2N_2 in the XZ plane i.e. a rotation of $-\psi$ about the X axis. (See *Figure A1*).

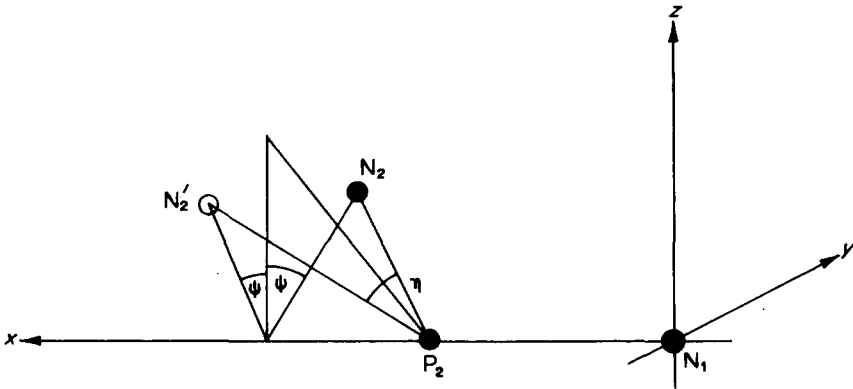


Figure A1 Designation of angles used in deriving equations (A1) to (A5)

Then $\cos\eta = (\text{Direction cosine } P_2N_2) (\text{Direction cosine } P_2N_2')$ i.e.
 $\cos\eta = (\cos\theta, \sin\theta\sin\psi, \sin\theta\cos\psi)(\cos\theta, -\sin\theta\sin\psi, \sin\theta\cos\psi)$
 $\therefore \cos\eta = \cos^2\theta - \sin^2\theta\sin^2\psi + \sin^2\theta\cos^2\psi$

which can be reduced to

$$\cos\eta = 1 - 2\sin^2\theta\sin^2\psi \tag{A1}$$

Now since $\gamma = \pi - \theta$, $\sin\gamma = \sin\theta$

$$\therefore \cos\eta = 1 - 2\sin^2\gamma\sin^2\psi \quad (\text{A2})$$

$d\psi$ can now be related to $d\gamma$ by differentiating equation (A2) keeping η constant

$$\begin{aligned} 0 &= \sin\gamma\cos\psi d\psi + \sin\psi\cos\gamma d\gamma \\ \therefore \frac{d\psi}{d\gamma} &= -\frac{\sin\psi\cos\gamma}{\sin\gamma\cos\psi} \end{aligned} \quad (\text{A3})$$

Also since $\psi = \omega - \pi/2$, $\sin\psi = -\cos\omega$
Substitution in equation (A1) gives

$$\cos\eta = 1 - 2\sin^2\theta\cos^2\omega \quad (\text{A4})$$

Differentiating with respect to θ and ω and keeping η constant we get

$$\begin{aligned} 0 &= \cos\omega\cos\theta d\theta - \sin\theta\sin\omega d\omega \\ \therefore \frac{d\theta}{d\omega} &= \frac{\sin\theta\sin\omega}{\cos\omega\cos\theta} \end{aligned} \quad (\text{A5})$$

Equations (A2) to (A5) give the relationships of the auxiliary angles θ and ψ to the corresponding degrees of freedom γ and ω .

Similarly let η' be the angle between directions N_2P_3 and N_2P_3' where N_2P_3' is the mirror image of N_2P_3 in the plane xz .

Then $\cos\eta' = (\text{Direction cosine } N_2P_3)(\text{Direction cosine } N_2P_3')$
i.e.

$$\begin{aligned} \cos\eta' &= (\cos a \cos \theta - \sin a \sin \theta \cos \phi)^2 - \\ & \quad [(\cos a \sin \theta + \sin a \cos \theta \cos \phi) \sin \psi - \sin a \sin \theta \cos \phi]^2 + \\ & \quad [(\cos a \sin \theta + \sin a \cos \theta \cos \phi) \cos \psi + \sin a \sin \theta \sin \psi]^2 \end{aligned}$$

$$\begin{aligned} \cos\eta' &= \cos^2\theta\cos^2a - \frac{1}{2}\sin 2\theta\sin 2a\cos\phi + \sin^2a\sin^2\theta\cos^2\phi - \\ & \quad \cos^2a\sin^2\theta\sin^2\psi - \sin^2a\cos^2\psi\sin^2\phi - \\ & \quad \sin^2a\sin^2\psi\cos^2\theta\cos^2\phi + \cos^2a\cos^2\psi\sin^2\theta + \\ & \quad \sin^2a\sin^2\psi\sin^2\phi + \sin^2a\cos^2\psi\cos^2\theta\cos^2\phi + \\ & \quad \sin 2a\sin 2\psi\sin\theta\sin\phi - \\ & \quad \frac{1}{2}\sin 2\theta\sin 2a\cos\phi(\cos^2\psi - \sin^2\psi) + \\ & \quad \sin 2\psi\sin 2\phi\sin^2a\cos\theta \end{aligned}$$

$$\begin{aligned} \cos\eta' &= \cos^2\theta\cos^2a + \sin^2a\sin^2\theta\cos^2\phi + \cos^2a\sin^2\theta\cos 2\psi - \\ & \quad \sin^2a\sin^2\phi\cos 2\psi + \sin^2a\cos^2\theta\cos^2\phi\cos 2\psi - \\ & \quad \frac{1}{2}\sin 2a\sin 2\theta\cos\phi(1 - \cos 2\psi) + \\ & \quad \sin 2\psi[\sin 2a\sin\theta\sin\phi + \sin 2\phi\sin^2a\cos\theta] \end{aligned}$$

$$\begin{aligned} \therefore \cos\eta' &= \cos^2\theta\cos^2a + \sin^2a\sin^2\theta\cos^2\phi + \\ & \quad \cos 2\psi[\sin^2a\cos^2\theta\cos^2\phi - \sin^2a\sin^2\phi + \cos^2a\sin^2\theta] - \\ & \quad \frac{1}{2}\sin 2a\sin 2\theta\cos\phi(1 - \cos 2\psi) + \\ & \quad \sin 2\psi[\sin 2a\sin\theta\sin\phi + \sin 2\phi\sin^2a\cos\theta] \end{aligned} \quad (\text{A6})$$

Using $\alpha = \pi - \beta$ we can write equation (A6) in terms of β , θ , ϕ and ψ .

$$\begin{aligned} \therefore \cos\eta' &= \cos^2\beta\cos^2\theta + \sin^2\beta\sin^2\theta\cos^2\phi + \\ &\quad \cos 2\psi[\sin^2\beta\cos^2\theta\cos^2\phi - \sin^2\beta\sin^2\phi + \cos^2\beta\sin^2\theta] + \\ &\quad \frac{1}{2}\sin 2\beta\sin 2\theta\cos\phi(1 - \cos 2\psi) + \\ &\quad \sin 2\psi[\sin 2\phi\sin^2\beta\cos\theta - \sin 2\beta\sin\theta\sin\phi] \end{aligned} \quad (A7)$$

$d\beta$ may now be related to $d\theta$ by differentiating equation (A7) with respect to β and θ , keeping η' , ϕ and ψ constant

$$\begin{aligned} 0 &= -\cos^2\theta\sin 2\beta d\beta - \cos^2\beta\sin 2\theta d\theta + \\ &\quad \cos^2\phi(\sin^2\beta\sin 2\theta d\theta + \sin^2\theta\sin 2\beta d\beta) + \\ &\quad \cos 2\psi[\cos^2\phi(\cos^2\theta\sin 2\beta d\beta - \sin^2\beta\sin 2\theta d\theta) - \\ &\quad \sin^2\phi\sin 2\beta d\beta - \sin^2\theta\sin 2\beta d\beta + \cos^2\beta\sin 2\theta d\theta] + \\ &\quad \frac{1}{2}\cos\phi(1 - \cos 2\psi)[2\sin 2\beta\cos 2\theta d\theta + 2\sin 2\theta\cos 2\beta d\beta] + \\ &\quad \sin 2\psi[\sin 2\phi(\cos\theta\sin 2\beta d\beta - \sin^2\beta\sin\theta d\theta) - \\ &\quad \sin\phi(\sin 2\beta\cos\theta d\theta + 2\sin\theta\cos 2\beta d\beta)] \\ \therefore \frac{d\theta}{d\beta} &= \frac{\left[\begin{aligned} &\sin 2\beta(\cos^2\phi\cos^2\theta - \sin^2\theta)(1 - \cos 2\psi) + \\ &\sin 2\beta\sin^2\phi(1 + \cos 2\psi) - \\ &\sin 2\theta\cos 2\beta\cos\phi(1 - \cos 2\psi) - \\ &\sin 2\psi(\sin 2\beta\sin 2\phi\cos\theta - 2\cos 2\beta\sin\theta\sin\phi) \end{aligned} \right]}{\left[\begin{aligned} &\sin 2\theta(\cos^2\phi\sin^2\beta - \cos^2\beta)(1 - \cos 2\psi) + \\ &\sin 2\beta\cos 2\theta\cos\phi(1 - \cos 2\psi) - \\ &\sin 2\psi(\sin 2\phi\sin^2\beta\sin\theta + \sin\phi\cos\theta\sin 2\beta) \end{aligned} \right]} \end{aligned} \quad (A8)$$

Continuing we differentiate equation (A7) with respect to β and ϕ ; θ , ψ and η' being kept constant.

$$\begin{aligned} 0 &= -\cos^2\theta\sin 2\beta d\beta + \sin^2\theta(\cos^2\phi\sin 2\beta d\beta - \sin^2\beta\sin 2\phi d\phi) + \\ &\quad \cos 2\psi[\cos^2\theta(\cos^2\phi\sin 2\beta d\beta - \sin^2\beta\sin 2\phi d\phi) - \\ &\quad (\sin^2\beta\sin 2\phi d\phi + \sin^2\phi\sin 2\beta d\beta) - \sin^2\theta\sin 2\beta d\beta] + \\ &\quad \frac{1}{2}\sin\theta(1 - \cos 2\psi)[2\cos\phi\cos 2\beta d\beta - \sin 2\beta\sin\phi d\phi] + \\ &\quad \sin 2\psi[\cos\theta(\sin 2\phi\sin 2\beta d\beta + \sin^2\beta 2\cos 2\phi d\phi) - \\ &\quad \sin\theta(\sin 2\beta\cos\phi d\phi + 2\sin\phi\cos 2\beta d\beta)] \\ \therefore \frac{d\phi}{d\beta} &= \frac{\left[\begin{aligned} &\sin 2\beta(\cos^2\phi\cos^2\theta - \sin^2\theta)(1 - \cos 2\psi) + \\ &\sin 2\beta\sin^2\phi(1 + \cos 2\psi) - \\ &\sin 2\theta\cos 2\beta\cos\phi(1 - \cos 2\psi) - \\ &\sin 2\psi(\sin 2\beta\sin 2\phi\cos\theta - 2\cos 2\beta\sin\theta\sin\phi) \end{aligned} \right]}{\left[\begin{aligned} &\sin 2\phi\sin^2\beta\cos^2\theta(1 - \cos 2\psi) - \\ &\sin 2\phi\sin^2\beta(1 + \cos 2\psi) + \\ &\frac{1}{2}\sin 2\theta\sin 2\beta\sin\phi(1 - \cos 2\psi) - \\ &\sin 2\psi(2\cos\theta\sin^2\beta\cos 2\phi - \sin\theta\cos\phi\sin 2\beta) \end{aligned} \right]} \end{aligned} \quad (A9)$$

Similarly we can obtain the relation between $d\beta$ and $d\psi$ by differentiating equation (A7) keeping η' , θ and ϕ constant.

$$\begin{aligned}
 0 = & -\cos^2\theta\sin 2\beta d\beta + \sin^2\theta\cos^2\phi\sin 2\beta d\beta + \\
 & \cos 2\psi(\cos^2\theta\cos^2\phi\sin 2\beta - \sin^2\phi\sin 2\beta - \sin^2\theta\sin 2\beta)d\beta - \\
 & 2\sin 2\psi(\sin^2\beta\cos^2\theta\cos^2\phi - \sin^2\beta\sin^2\phi + \cos^2\beta\sin^2\theta)d\psi + \\
 & \frac{1}{2}\sin 2\theta\cos\phi[2\sin 2\beta\sin 2\psi d\psi + 2(1 - \cos 2\psi)\cos 2\beta d\beta] + \\
 & \sin 2\psi(\sin 2\phi\cos\theta\sin 2\beta - 2\sin\theta\sin\phi\cos 2\beta)d\beta + \\
 & 2\cos 2\psi(\sin 2\phi\sin^2\beta\cos\theta - \sin 2\beta\sin\theta\sin\phi)d\psi \\
 \therefore \frac{d\psi}{d\beta} = & \frac{\left[\begin{aligned} & \sin 2\beta(\cos^2\phi\cos^2\theta - \sin^2\theta)(1 - \cos 2\psi) + \\ & \sin 2\beta\sin^2\phi(1 + \cos 2\psi) - \\ & \sin 2\theta\cos 2\beta\cos\phi(1 - \cos 2\psi) - \\ & \sin 2\psi(\sin 2\beta\sin 2\phi\cos\theta - 2\cos 2\beta\sin\theta\sin\phi) \end{aligned} \right]}{\left[\begin{aligned} & 2\cos 2\psi(\sin 2\phi\sin^2\beta\cos\theta - \sin 2\beta\sin\theta\sin\phi) - \\ & 2\sin 2\psi[\sin^2\beta(\cos^2\theta\cos^2\phi - \sin^2\phi) + \cos^2\beta\sin^2\theta] + \\ & \sin 2\theta\sin 2\beta\sin 2\psi\cos\phi \end{aligned} \right]} \quad (A10)
 \end{aligned}$$

Returning now to equation (A6) and substituting for ϕ using $\phi + \zeta = \pi/2$ we obtain:

$$\begin{aligned}
 \cos\eta' = & \cos^2\theta\cos^2\alpha + \sin^2\alpha\sin^2\theta\sin^2\zeta + \\
 & \cos 2\psi(\sin^2\alpha\cos^2\theta\sin^2\zeta - \sin^2\alpha\cos^2\zeta + \cos^2\alpha\sin^2\theta) - \\
 & \frac{1}{2}\sin 2\alpha\sin 2\theta\sin\zeta(1 - \cos 2\psi) + \\
 & \sin 2\psi(\sin 2\alpha\sin\theta\cos\zeta + \sin 2\zeta\sin^2\alpha\cos\theta) \quad (A11)
 \end{aligned}$$

$d\alpha$ may now be related to $d\zeta$ by differentiating equation (A11) keeping η' , θ and ψ constant.

$$\begin{aligned}
 0 = & -\cos^2\theta\sin 2\alpha d\alpha + \sin^2\theta(\sin^2\alpha\sin 2\zeta d\zeta + \sin^2\zeta\sin 2\alpha d\alpha) + \\
 & \cos 2\psi[\cos^2\theta(\sin^2\alpha\sin 2\zeta d\zeta + \sin^2\zeta\sin 2\alpha d\alpha) - \\
 & (\cos^2\zeta\sin 2\alpha d\alpha - \sin^2\alpha\sin 2\zeta d\zeta) - \sin^2\theta\sin 2\alpha d\alpha] - \\
 & \frac{1}{2}\sin 2\theta(1 - \cos 2\psi)[\sin 2\alpha\cos\zeta d\zeta + 2\sin\zeta\cos 2\alpha d\alpha] + \\
 & \sin 2\psi[\sin\theta(2\cos\zeta\cos 2\alpha d\alpha - \sin 2\alpha\sin\zeta d\zeta) + \\
 & \cos\theta(\sin 2\zeta\sin 2\alpha d\alpha + \sin^2\alpha 2\cos 2\zeta d\zeta)] \\
 \therefore \frac{d\alpha}{d\zeta} = & \frac{\left[\begin{aligned} & \sin 2\zeta[\sin^2\alpha(1 + \cos 2\psi) - \cos^2\theta\sin^2\alpha(1 - \cos 2\psi)] - \\ & \frac{1}{2}\sin 2\alpha\sin 2\theta\cos\zeta(1 - \cos 2\psi) + \\ & \sin 2\psi(2\cos 2\zeta\cos\theta\sin^2\alpha - \sin 2\alpha\sin\theta\sin\zeta) \end{aligned} \right]}{\left[\begin{aligned} & \sin 2\alpha(\cos^2\theta\sin^2\zeta - \sin^2\theta)(1 - \cos 2\psi) + \\ & \sin 2\alpha\cos^2\zeta(1 + \cos 2\psi) + \\ & \sin 2\theta\cos 2\alpha\sin\zeta(1 - \cos 2\psi) - \\ & \sin 2\psi(2\cos 2\alpha\sin\theta\cos\zeta + \sin 2\alpha\sin 2\zeta\cos\theta) \end{aligned} \right]} \quad (A12)
 \end{aligned}$$

Similarly $d\theta$ may be related to $d\zeta$ by differentiating equation (A11) keeping η' , α and ψ constant.

$$\begin{aligned}
 0 = & -\cos^2\alpha\sin 2\theta d\theta + \sin^2\alpha(\sin^2\theta\sin 2\zeta d\zeta + \sin^2\zeta\sin 2\theta d\theta) + \\
 & \cos 2\psi[\sin^2\alpha(\cos^2\theta\sin 2\zeta d\zeta - \sin^2\zeta\sin 2\theta d\theta) + \\
 & \sin^2\alpha\sin 2\zeta d\zeta + \cos^2\alpha\sin 2\theta d\theta] - \\
 & \frac{1}{2}\sin 2\alpha(1 - \cos 2\psi)(2\sin\zeta\cos 2\theta d\theta + \sin 2\theta\cos\zeta d\zeta) +
 \end{aligned}$$

$$\begin{aligned} & \sin 2\psi [\sin 2\alpha (\cos \zeta \cos \theta d\theta - \sin \theta \sin \zeta d\zeta) + \\ & \sin^2 \alpha (\cos \theta 2 \cos 2\zeta d\zeta - \sin 2\zeta \sin \theta d\theta)] \\ \therefore \frac{d\theta}{d\zeta} = & \frac{\left[\begin{aligned} & \sin 2\zeta [\sin^2 \alpha (1 + \cos 2\psi) - \sin^2 \alpha \cos^2 \theta (1 - \cos 2\psi)] - \\ & \frac{1}{2} \sin 2\alpha \sin 2\theta \cos \zeta (1 - \cos 2\psi) + \\ & \sin 2\psi (2 \sin^2 \alpha \cos 2\zeta \cos \theta - \sin 2\alpha \sin \theta \sin \zeta) \end{aligned} \right]}{\left[\begin{aligned} & \sin 2\theta (1 - \cos 2\psi) (\cos^2 \alpha - \sin^2 \alpha \sin^2 \zeta) + \\ & \sin 2\alpha \cos 2\theta \sin \zeta (1 - \cos 2\psi) - \\ & \sin 2\psi (\sin 2\alpha \cos \theta \cos \zeta - \sin^2 \alpha \sin 2\zeta \sin \theta) \end{aligned} \right]} \quad (A13) \end{aligned}$$

Finally differentiating equation (A11) with respect to ψ and ζ , keeping η' , α and θ constant:

$$\begin{aligned} 0 = & \sin^2 \alpha \sin^2 \theta \sin 2\zeta d\zeta + \\ & \cos 2\psi (\sin^2 \alpha \cos^2 \theta \sin 2\zeta + \sin^2 \alpha \sin 2\zeta) d\zeta - \\ & 2 \sin 2\psi (\sin^2 \alpha \cos^2 \theta \sin^2 \zeta - \sin^2 \alpha \cos^2 \zeta + \cos^2 \alpha \sin^2 \theta) d\psi - \\ & \frac{1}{2} \sin 2\alpha \sin 2\theta [2 \sin \zeta \sin 2\psi d\psi + (1 - \cos 2\psi) \cos \zeta d\zeta] + \\ & \sin 2\psi (2 \cos 2\zeta \sin^2 \alpha \cos \theta - \sin 2\alpha \sin \theta \sin \zeta) d\zeta + \\ & 2 \cos 2\psi (\sin 2\alpha \sin \theta \cos \zeta + \sin 2\zeta \sin^2 \alpha \cos \theta) d\psi \\ \therefore \frac{d\psi}{d\zeta} = & \frac{\left[\begin{aligned} & \sin 2\zeta [\sin^2 \alpha (1 + \cos 2\psi) - \sin^2 \alpha \cos^2 \theta (1 - \cos 2\psi)] - \\ & \frac{1}{2} \sin 2\alpha \sin 2\theta \cos \zeta (1 - \cos 2\psi) + \\ & \sin 2\psi (2 \sin^2 \alpha \cos 2\zeta \cos \theta - \sin 2\alpha \sin \theta \sin \zeta) \end{aligned} \right]}{\left[\begin{aligned} & 2 \sin 2\psi [\sin^2 \alpha (\cos^2 \theta \sin^2 \zeta - \cos^2 \zeta) + \cos^2 \alpha \sin^2 \theta] + \\ & \sin 2\alpha \sin 2\theta \sin 2\psi \sin \zeta - \\ & 2 \cos 2\psi (\sin 2\alpha \sin \theta \cos \zeta + \sin 2\zeta \sin^2 \alpha \cos \theta) \end{aligned} \right]} \quad (A14) \end{aligned}$$

A test for molecular orientation in a 'single crystal' of SBS three-block copolymer by infra-red spectroscopy

M. J. FOLKES, A. KELLER and F. P. SCALISI*

A sample of a polystyrene-polybutadiene-polystyrene (SBS) three-block copolymer with the characteristics of a macroscopic single crystal constituted by a regular lattice of polystyrene (S) cylinders in a polybutadiene (B) matrix was examined as regards infra-red dichroism. No dichroism for either phase could be detected implying molecular isotropy over a 'unit cell' of the macrocrystal within specified limits. The implications of this are discussed.

WE HAVE REPORTED previously¹⁻³ that the three-block copolymer Kraton 102 consisting of a sequence of polystyrene-polybutadiene-polystyrene blocks (SBS) with 25% (wt.) polystyrene content (20% vol.) can be obtained in the form of a macroscopic 'single crystal'. Here the polystyrene phase (atactic) is in the form of cylinders of 150 Å diameter arranged in a crystallographically defined hexagonal array with a lattice parameter of 300 Å within a continuous polybutadiene matrix^{1,2}, both phases being amorphous. The samples exhibiting this property are in the form of extruded plugs with the cylinder axes along the extrusion direction. In studies which followed⁴ the optical and mechanical anisotropy was investigated. Complete agreement with theory was obtained on the basis that the molecular orientation in both S and B phases is random. The optical studies in particular revealed a weak positive birefringence with respect to the extrusion direction which could be quantitatively accounted for by form birefringence alone. It was stated that this agreement implies either that there is no molecular birefringence or that the molecular birefringence within the two phases fortuitously cancel. The need was felt to obtain information on the molecular orientation, or absence of it, by a method which is specific to the molecular orientation alone and individually so for the two different phases. Clearly infra-red dichroism satisfies these requirements.

Since the work in reference 4 was reported, we have investigated thin sections of such samples using i.r. radiation. 60 μm samples were cut from the extruded plug parallel to the extrusion direction. This was carried out by first glueing the copolymer sample to a block of Tufnol by means of Araldite. The samples were then sliced using a microtome blade while liquid air was sprayed continually over the sample area during the cutting process. In this way very satisfactory samples were produced possessing a uniform thickness.

Infra-red spectra were recorded using a Perkin-Elmer Model 225 spectrometer equipped with a multiple-plate silver chloride polarizer. Spectra were

* Present address: SIR, Sesto S. Giovanni, Milano, Italy

taken with the plane of polarization of the i.r. radiation parallel and perpendicular to the extrusion direction of the sample.

Typical absorption spectra recorded in the range 600–1800 cm^{-1} are shown in *Figure 1*. In fact the spectra corresponding to the plane of polarization parallel and perpendicular to the extrusion direction are identical within experimental error and thus appear as almost a single trace in *Figure 1*.

The observed spectra are of course a superposition of spectra from the S and B regions separately with any additional bands which may arise from interfacial layers between the two phases. Both phases possess characteristic

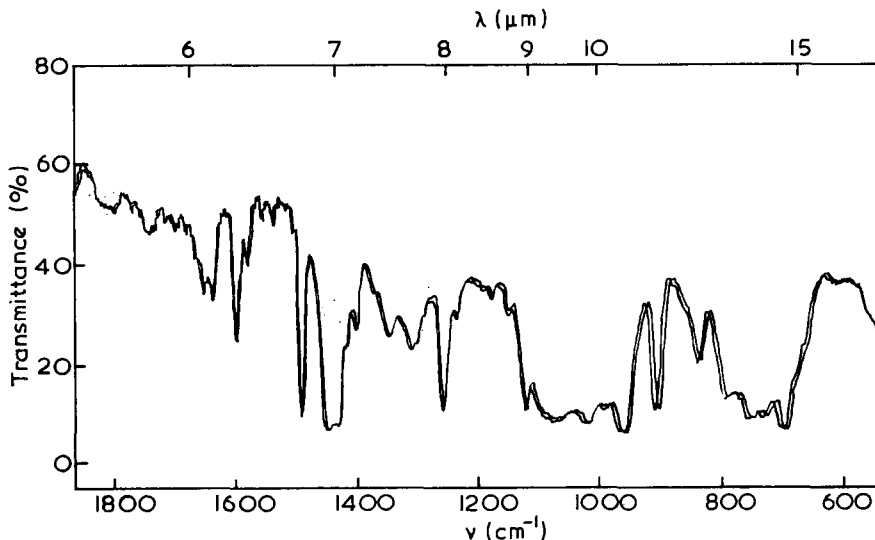


Figure 1 Infra-red spectra of single crystal sbs block copolymer with plane of polarization parallel and perpendicular to the extrusion direction. (The relative shift of the two spectra below 1000 cm^{-1} occurred due to a prism change and was left deliberately uncorrected so as to show each trace separately as an illustration of the practical identity of the two curves.)

absorption bands in the range 600–1800 cm^{-1} which can be highly dichroic in an oriented single phase sample (e.g. the 1027 cm^{-1} , 1350 cm^{-1} and 1495 cm^{-1} bands for S and the 967 cm^{-1} , 1646 cm^{-1} and 1667 cm^{-1} bands for B. These are all vibrations associated with main chain atoms). It can be seen from *Figure 1* that none of the absorption bands appear dichroic within the estimated accuracy of measurement of 1%. By choosing bands associated with the S and B phases separately which are known to be highly dichroic, as listed above, a corresponding value for the minimum dichroic ratio can be estimated which is just detectable with our measurements. This is in the range of 1.05–1.08. Experiments now in progress in which the dichroism of Kraton 102 is being studied in the course of stretching enables us to estimate that the minimum dichroic ratio which can be detected within our accuracy corresponds to 7% uniaxial strain referred to the macroscopic sample. Using the measured dichroic ratios of stretched bulk polystyrene as reported by other workers a similar limiting figure can be placed on the S regions. It

follows that the maximum molecular anisotropy in our unstressed Kraton single crystal sample, as measured on a macroscopic specimen, cannot exceed to what corresponds to a 7% sample extension and may well be less. Thus sizeable anisotropy over the sample as a whole, hence in view of the single crystal nature of our specimen, over regions comprising a 'unit cell' repeat is excluded. If such anisotropic regions exist within a cell, e.g. at the microphase interfaces, the magnitude of this anisotropy and the region over which it extends must be sufficiently small so as not to have any detectable effect within the limits just specified. All this confirms our previous conclusions⁴. In particular, it does full justice to our assignment of the observed birefringence to form birefringence alone and furthermore justifies our mechanical treatment of the rubbery phase in terms of an isotropic matrix material⁴.

Two alternative conclusions may be drawn about the molecules from this result. Firstly, that the molecular conformation within both S and B phases is essentially random throughout. Secondly, if there are molecules which are stressed or compressed, i. e. with end-to-end distances different from the unperturbed random chain, such deformation on the molecular scale would be sufficiently averaged in respect of direction so as not to lead to a macroscopic resultant beyond the limits specified. For both cases, possible departures at interfaces are subject to the same qualification as stated in the preceding paragraph. Departures from the unperturbed end-to-end distances of chains in particular feature in recent theories on microphase separation^{5,6} and hence may become central to the understanding of the subject. All we can state here is that thanks to our special samples we are in a position to assess such departures in case they have a resultant when averaged over the 'unit cell' dimension of our macrocrystal. We can state that at least within our limits no such resultant has been found.

We feel that this result has further reaching implications concerning speculations on possible localized order, subcrystalline block structure or even a microcrystalline structure, such as escapes detection by diffraction methods, within polymers which are conventionally defined as amorphous⁷⁻⁹. The fact that the molecules are random even within cylinders of 150 Å diameter and in spaces of comparable dimensions in between, implies that regions of molecular parallelization, as far as present, can only extend over distances much smaller than this dimension. Only in this case can an ensemble of such regions when confined to within boundaries spaced at 150 Å exhibit complete isotropy. (The maximum possible size of such regions cannot be readily specified as this will depend on the shape of the ordered regions and will have to take into consideration the requirements set by the molecular continuity at the phase boundary.) Our present observations therefore set stringent limits to the spatial extent of pre-existing order in amorphous polymers, as far as such is present, and affects the scope of models or theories based on such ordering accordingly.

ACKNOWLEDGEMENTS

The authors would like to thank Dr P. L. Goggin, Chemistry Department, University of Bristol for making the Perkin-Elmer I.R. Spectrometer available.

*H. H. Wills Physics Laboratory,
University of Bristol,
Royal Fort,
Tyndall Avenue,
Bristol BS8 1TL, UK*

(Received 15 March 1971)

REFERENCES

- 1 Keller, A., Pedemonte, E. and Willmouth, F. M. *Nature* 1970, **225**, 538
- 2 Keller, A., Pedemonte, E. and Willmouth, F. M. *Kolloid Z.* 1970, **238**, 385
- 3 Dlugosz, J., Keller, A. and Pedemonte, E. *Kolloid Z.* 1970, **242**, 1125
- 4 Folkles, M. J. and Keller, A. *Polymer, Lond.* 1971, **12**, 222
- 5 Krömer, H., Hoffman, M. and Kämpf, G. *Ber. Bunsengesellschaft Phys. Chem.* 1970, **74**, 859
- 6 Meier, D. J. *Polymer Preprints* 1970, **11**, 400
- 7 Yeh, G. S. and Geil, P. H. *J. Macromol. Sci.* 1967, **B1**, 235
- 8 Discussion contributions by Keith, H. D., Bonart, R. and Stuart, H. A. *Kolloid Z.* 1969, **231**, 430
- 9 Pechhold, W. and Blasenbrey, S. *Kolloid Z.* 1970, **241**, 955

*The influence of stretching on tensile strength and solubility of poly(vinyl alcohol) fibres**

D. HEIKENS, A. C. A. M. BLEIJENBERG, J. J. M. HOPPENBROUWERS and
W. M. BARENTSEN

The strength of wet-spun poly(vinyl alcohol) (PVA) fibres is given as function of bath-stretching, wet-stretching and hot-stretching. In the two equations derived for strength of wet-stretching and hot-stretching the complex influence of the bath-stretching and hot-stretching is demonstrated. The bath-stretching is connected with a pure orientation effect and the residence time in the coagulating bath which is a measure for the 'freshness' of the fibre. The hot-stretching can be separated in a pure orientation effect and a crystallization effect. Fibres of the PVA, used in the experiments, were soluble in boiling water. After shrinkage of the fibres at temperatures near the temperature of hot-stretching, the dissolution temperature can be raised. Insoluble PVA fibres were prepared after removing most of the bulky residual ester groups.

INTRODUCTION

MUCH WORK has already been done on high strength poly(vinyl alcohol) (PVA) fibres. As there are many variable factors involved in the wet-spinning process there are empirical rules that correlate the strength of the fibres and the process conditions. It is known that an increase of stretching increases the strength and the modulus of elasticity and decreases the elongation at break.

In this paper a mathematical relation between the strength of wet-spun PVA fibres and the three stretch factors (bath-stretching, wet-stretching and hot-stretching) is presented. The commercially available atactic Elvanol 71/30 (DuPont) was used in the experiments. This PVA is believed to have a degree of polymerization of 1800, 0.65 mol % residual acetate groups and 1.2 mol % glycol units¹. The spinning was carried out in a conventional laboratory spinning unit (*Figure 1*).

EXPERIMENTAL

The spinning solution was made by dissolving PVA in water. One percent boric acid was added to the 16% PVA solution to prevent gelling. The solution was stirred for at least 14 h at 90°C and poured into the spinning vessel. Spinning was carried out by pressing the solution with the aid of a gearpump through a spinneret with 40 holes of 80 μm diameter (Baker 40/80 Au/Pt).

* Paper presented at IUPAC Symposium, Leiden, The Netherlands (1970)

The temperature of spinning solution and the bath were kept at 50°C. At the end of the spinning bath the coagulated fibres were pulled out of the bath by means of the first of four stretching rollers, with a linear velocity of v_1 also called f_b . This factor can be interpreted as the reciprocal residence time but due to the bath resistance there is also a stretching effect on the

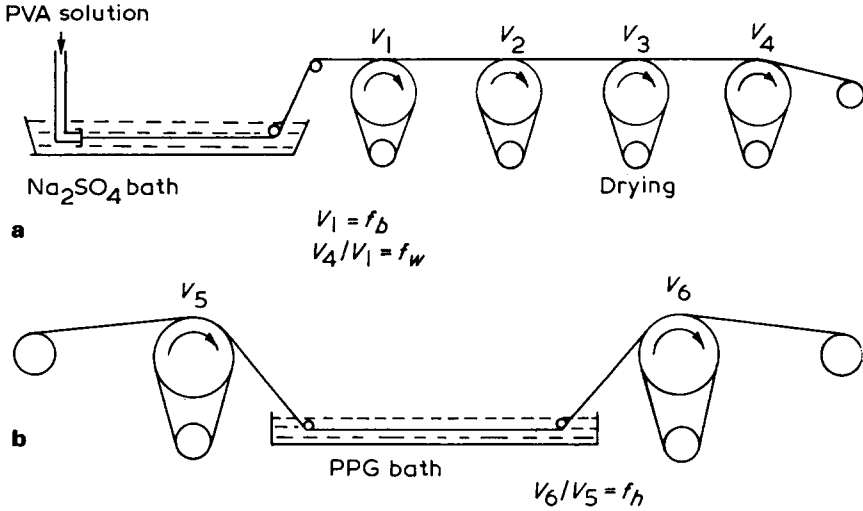


Figure 1 (a) Springing and wet-stretching and (b) hot-stretching of PVA fibres

coagulating fibre. The factor f_b had a lower limit of 3 m/min and an upper limit of 25 m/min. However, breaking of filaments at the spinneret occurred already at $f_b = 15$ m/min. At $f_b \geq 25$ m/min no fibres could be spun. Between the first and second roller the fibres are stretched. The third roller was kept at 90°C and served as drying roller. The fourth roller was used to cool down the fibre to room temperature. Its speed was so adjusted that there was zero tension on the fibres between rollers 3 and 4.

The wet-stretch factor f_w is defined as v_4/v_1 . The upper limit for $f_w = 3$ and gives the stretching factor at which breaking occurred for fibres with lowest values for f_b .

The hot-stretching was carried out by passing the fibres through a poly(propylene glycol) (PPG) bath at 220°C. This temperature is about 8°C below the theoretical melting point of PVA². After stretching, the fibres were washed with acetone to remove the adhering PPG (Figure 1). The hot-stretch factor f_h is defined as v_6/v_5 . The upper limit for f_h was 25 for fibres with the lowest value of f_b .

The fibres were conditioned at 20°C and 45% r.h. prior to testing. Stress-strain curves of twined fibres were recorded with an Instron Tensile Tester at a speed of 66% elongation/min.

RESULTS

The results of the measurements are given in Figures 2 and 3. The relation

TENSILE STRENGTH AND SOLUBILITY OF PVA FIBRES

between the wet strength (σ_w) of the fibres and the variable process parameters f_b and f_w was found to be

$$\sigma_w = [0.20(f_w - 1) + 0.13]f_b \quad \begin{matrix} 3 \text{ m/min} < f_b < 15 \text{ m/min} \\ 1 < f_w < 3 \end{matrix} \quad (1)$$

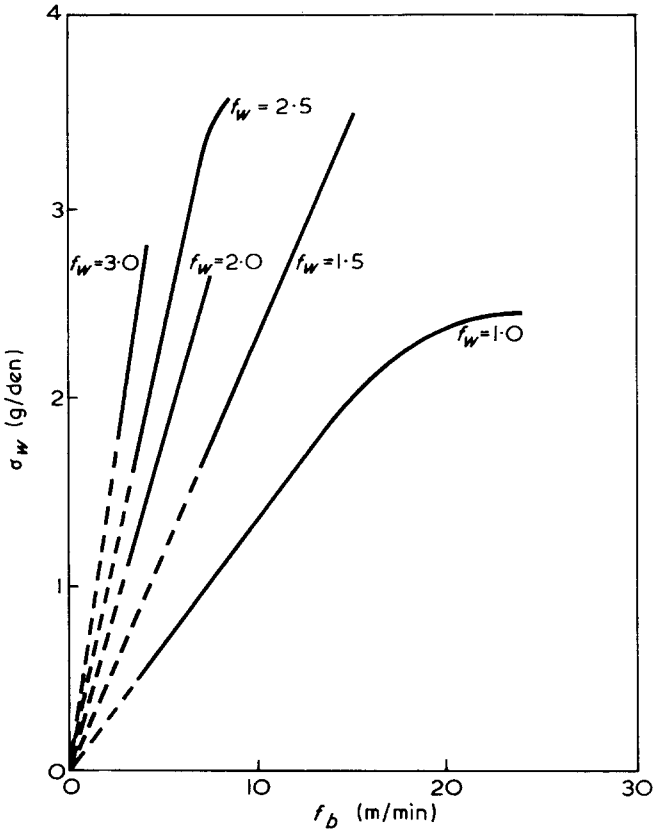


Figure 2 Strength of PVA fibres after wet-stretching
 $\sigma_w = [0.20(f_w - 1) + 0.13]f_b$

The measurements on fibres which were also hot-stretched, gave the following relation:

$$\sigma_h = [0.20(f_w f_h - 1) + 0.13]f_b + 0.33(f_w f_h - 1) \quad \begin{matrix} 3 < f_b < 13 \\ 1 < f_w < 3 \\ 1.4 < f_h < 2.5 \end{matrix} \quad (2)$$

DISCUSSION

Equation (1) can be separated in two terms, the first depending on $f_w f_b$, the second only on f_b . The strength of fibres without wet-stretching ($f_w = 1$) can be varied between 0.4 and 2.6 g/den. The strength $0.13 f_b$ is believed to

be partly the result of the bath orientation as pulling the coagulating fibre through the bath will cause friction. During wet-stretching the fibres are still in the swollen state and it could be expected that an increase in orientation by stretching would result in an increase in strength. If f_b was a factor of

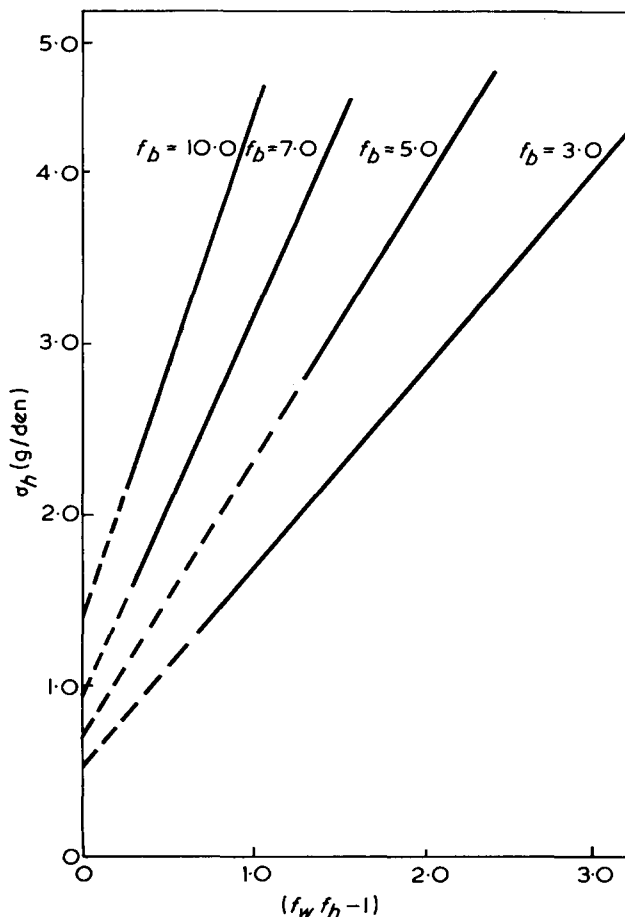


Figure 3 Strength of PVA fibres after hot-stretching
 $\sigma_h = [0.20(f_w f_h - 1) + 0.13]f_b + 0.33(f_w f_h - 1)$

stretching only it could be expected that the strength of the fibres could be sufficiently described by a single term of $c f_b (f_w - 1)$. Therefore f_b includes an effect depending on the reciprocal residence time in the coagulating bath as well. The higher f_b the shorter the residence time the more swollen the fibre and the larger the effect on strength by orientation in wet-stretching.

The first part of equation (2) for the strength of hot-stretched fibres is equivalent to equation (1) if $f_h = 1$. If f_h would contribute to the orientation only then the first part of equation (2) would suffice to describe the generally known increase in strength by orientation. But equation (2) has a second term which is not zero for $f_h = 1$. That means that a heat treatment only will increase the strength. The effect is larger if the pre-orientation described

by f_w is larger. This term can be interpreted as a crystallization effect which is larger for larger pre-orientation. Evidence for this assumption was given by Sakurada who found that the crystallinity of PVA films increased after heat treatment³. The increase in modulus of elasticity after a heat treatment of the fibres, can also be explained in terms of crystallization.

If f_b is kept constant it shows that σ_h of the fibres is not dependent on the way of stretching as f_w and f_h are interchangeable. This suggests that the molecular mechanism that responds to the stretching is essentially the same.

As pointed out by several authors the solubility of PVA fibres in water was a limiting factor for application of PVA in textiles. Although an increase in crystallinity diminishes the solubility of PVA fibres, they are soluble in boiling water. Some experiments on the solubility of the PVA fibres were made. All the fibres dissolved in water at 70°C. If hot-stretching was carried out in air at 210°C, the dissolution temperature was raised to about 90°C. In applying a controlled shrinkage (10%) at 200°C to the fibres this temperature was raised slightly. We found as a result of other experiments that PVA fibres derived from poly(vinyl trifluoroacetate) did not dissolve in boiling water. This PVA has no residual ester groups and no 1,2 glycol units could be detected. As this PVA is reported to be atactic⁴ it is possible that the solubility of Elvanol 71/30 is caused by irregularities along the main chain. We tried to remove the residual acetate group in this PVA by alkaline hydrolysis which resulted in PVA with less than 0.2 mol % ester groups. After spinning, wet-stretching and hot-stretching followed by 10% shrinkage, the fibres did not dissolve in boiling water.

*Dept. of Chemical Engineering,
Eindhoven University of Technology,
The Netherlands*

(Received 17 March 1971)

REFERENCES

- 1 Zwick, M. M. and van Bochove, C. *Textile Res. J.* 1964, **34**, 417
- 2 Tubbes, R. K. *J. Polym. Sci.* 1965, **A3**, 4181
- 3 Sakurada, I., Nukushina, Y. and Sone, Y., Paper presented at Int. Symp. on Macromolecular Chemistry (1954), Milan, Turin, Italy
- 4 Murahashi, S., Nozakura, S., Sumi, M. and Matsumura, K. *J. Polym. Sci.* 1966, **B4**, 59

Note to the Editor

Dielectric relaxation in polydimethylsiloxane

M. E. BAIRD and C. R. SENGUPTA

Studies of the dielectric behaviour of silicone polymers at low temperatures, where loss peaks due to segmental motion will occur in the audio-frequency region are limited^{1,2}. Polydimethylsiloxane fluids ranging in viscosity from 100 cSt to 10⁵ cSt (1 cSt $\equiv 10^{-6}$ m²/s) at room temperature have been examined with a GR 1615 A Capacitance Bridge using a three-terminal electrode assembly mounted in a cryostat so that the guarded upper electrode follows the contraction of the polymer specimen as the temperature is lowered. Temperature control to $\pm 0.5^\circ\text{C}$ was achieved through a heat balance between a refrigerant vessel containing liquid nitrogen and heaters surrounding the electrode assembly and measured with a chromel-alumel thermocouple with one junction inserted in a hole in a metal block surrounding the electrode assembly. The fluids solidified at about -50°C and gradually became more opaque at lower temperatures due to crystallization and growth of spherulites³.

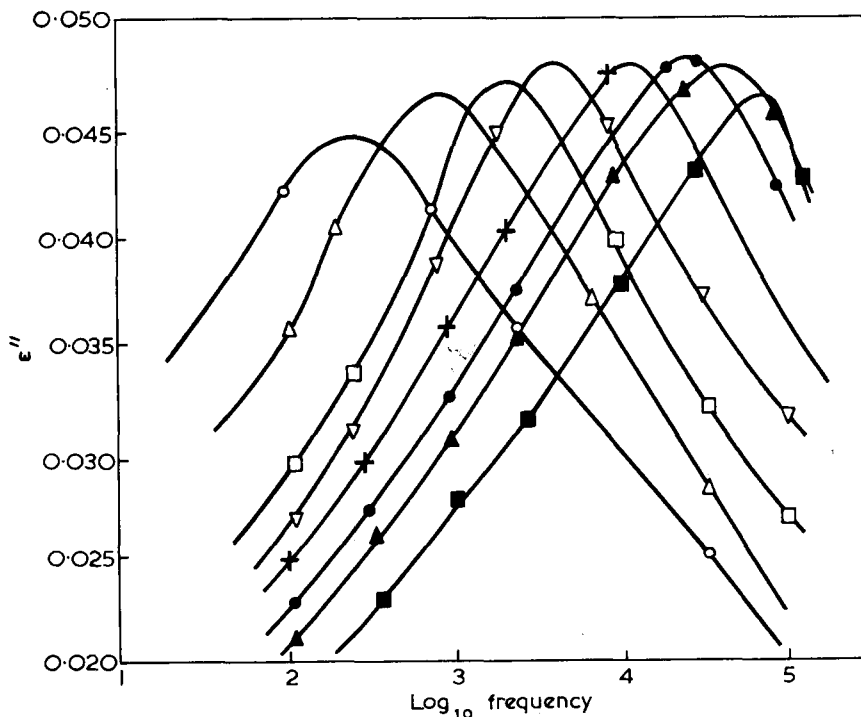


Figure 1 Plots of dielectric loss factor ϵ'' against log frequency for polydimethylsiloxane (of viscosity about 1568 cSt at room temperature) at various temperatures. \circ -118°C ; \triangle -116°C ; \square -114°C ; ∇ -112°C ; $+$ -110°C ; \bullet -108°C ; \blacktriangle -106°C ; \blacksquare -104°C

Broad loss peaks in the audio-frequency region were observed in the temperature range -120°C to -100°C as shown in *Figure 1*. The maximum loss factor was in the range $4.5\text{--}4.9 \times 10^{-2}$, corresponding to a dielectric increment $\epsilon_s - \epsilon_{\infty}$ in the range $0.3\text{--}0.45$. The plots of log frequency of maximum loss against reciprocal of absolute temperature were approximately linear corresponding to an experimental activation energy of about 1.0×10^5 joule mol^{-1} . Variations in cooling rate were found to affect the dielectric behaviour and a standard rate of cooling and specimens of similar thickness were used. The effect of incorporating fillers on segmental motion was also investigated because little is known about this despite the wide and important use of fillers for reinforcement in silicone compounds. These fillers consisted of untreated silica of large surface area ($100\text{--}300 \text{ m}^2/\text{g}$) and were dispersed in the fluid at normal temperature. A marked broadening of the loss peaks associated with segmental motion was observed, particularly on the low frequency side, as illustrated in *Figure 2* for dimethyl siloxane fluid containing 2% of

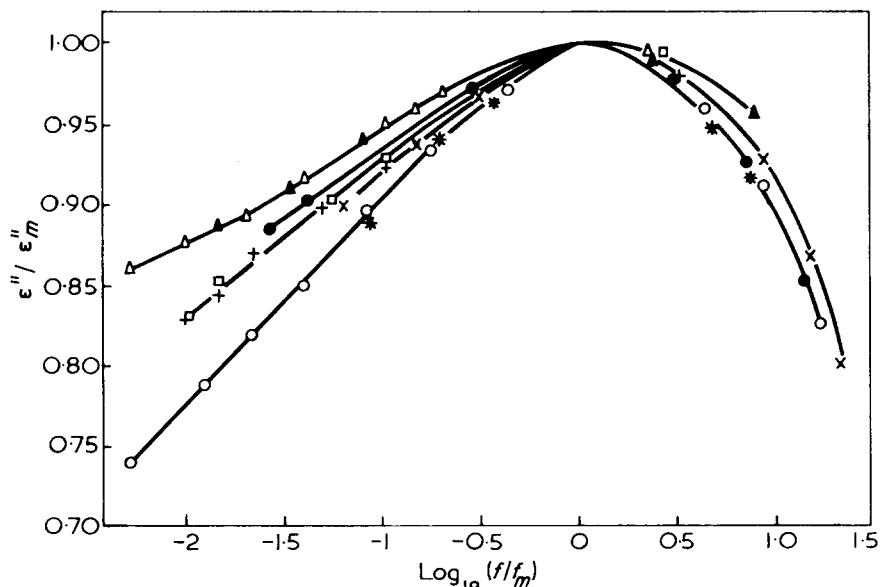


Figure 2 Plots of the ratio of loss factor ϵ'' to the maximum loss factor ϵ''_m against log ratio of frequency f to frequency f_m giving maximum loss factor for polydimethylsiloxane (of viscosity $\sim 10^5$ cSt at room temperature) without filler and for a single sample containing 2% of untreated silica filler of surface area about $110 \text{ m}^2/\text{g}$. * Fluid alone; \circ fluid + 2% filler after standing for about 1 year; \triangle filled sample immediately after applying ultrasonic vibration; \square filled sample 3 days after applying ultrasonic vibration; $+$ filled sample 4 days after applying ultrasonic vibration; \times filled sample 13 days after applying ultrasonic vibration; \blacktriangle filled sample immediately after applying further ultrasonic vibration; \bullet filled sample 4 days after applying further ultrasonic vibration.

silica filler with a surface area of $110 \text{ m}^2/\text{g}$. This effect is similar to that produced on the comparable relaxation in organic polymers by increasing crystallinity⁴. On standing, the broadening effect gradually diminishes but by subjecting the compound to the action of ultrasonic vibrations it is restored. On further standing it diminishes again. This can be explained by a

clustering of the filler particles (each of diameter 15×10^{-9} m), the action of ultrasonics being to break up the clusters to a certain extent. This clustering and the effect of ultrasonics has been confirmed by electron micrographs taken with a magnification of about 35 000.

The broadening of the loss curves can be explained by a reduction of the mobility of the Si-O dipoles near filler particles as compared with that for those further away along the molecule. Thus the distribution of retardation times is widened. Further studies are being made to explain the effects in detail.

ACKNOWLEDGEMENTS

We are indebted to Midland Silicones, Ltd., Barry, Glam. for a grant to C. R. S., and to Mr T. Kendrick, Dr D. Thomas and Dr D. Pocknell for general helpful discussion and preparation of samples.

*Department of Applied Physics,
University of Wales Institute of Science and Technology,
Cathays Park,
Cardiff, CF1 3NU, UK*

(Received 5 July 1971)

REFERENCES

- 1 Andrianov, K. A. and Golubkov, G. E. *Zhur. Tekh. Fiz.* 1956, **26**, 1689; *Soviet Phys. Tech. Phys.* 1956, **26**, 1642
- 2 Huggins, C. M., St. Pierre, L. E. and Bueche, A. M. *J. Phys. Chem.* 1960, **64**, 1304
- 3 Slonimskii, G. L., Andrianov, K. A., Zhadanov, A. A., Levin, V. Yu and Manucharova, I. F. *Vysokomol. Soedineniya B* 1968, **10**, 773
- 4 Ishida, Y., Yamafuji, K., Ito, H. and Takayanagi, M., *Kolloid-Z. Z. Polym.* 1962, **184**, 97

Classified Contents

- Absolute reactivity in the cationic polymerization of N-vinylcarbazole, 509
- Alkyl vinyl ethers, mechanism of initiation of cationic polymerization by molecular iodine, 344
- Amylose: a non-helical biopolymer in aqueous solution, 141
- Amylose in aqueous solution—a viscometric study, 452
- Aromatic polymers, relaxation phenomena, 85
- Benzene and poly(ethylene oxide), thermodynamics of mixtures, 309
- Benzene and poly(propylene oxide), thermodynamics of mixtures, 320
- Benzophenones, polymerization of methyl methacrylate photosensitized by, 271
- Biopolymer, non-helical, amylose in aqueous solution, 141
- Birefringence and mechanical properties of a 'single crystal' from a three-block copolymer, 222
- Bisphenol-A diglycidyl ether/*m*-phenylene diamine system, 335
- Block copolymers, morphology of (styrene)_x(butadiene)_y (styrene)_x, 258
- Branching, long-chain, and molecular weight distribution in low-density polyethylene, 685
- Bulk crystallized *trans*-1,4-polybutadiene, morphology, 27
- Cationic polymerization of indene, 444
- Cationic polymerization of isobutyl vinyl ether, reactivity and mechanism, 119
- Cationic polymerization of N-vinylcarbazole, absolute reactivity, 509
- Chain extension, polymer, produced by impinging jets and its effect on polyethylene solution, 467
- Copolymerization of trioxan with 1,3-dioxolan, 358
- Copolymer, three-block, birefringence and mechanical properties of a 'single crystal', 222
- Copolymers, ethylene-propylene, investigation of a sequence length distribution by pyrolysis and reaction gas chromatography, 70
- Copolymers of propylene, analysis of the γ -crystal form by DSC and X-ray methods, 487
- Crystalline polyethylene, geometry of twinning and phase transformations, 666
- Crystallinity and ESR of polyphenyleneisoxazole, 521
- Crystallization, non-isothermal, kinetics, 150
- Crystallization of nylon-6(polycapramide): (1) isothermal crystallization, 616 (2) effect of molecular weight on isothermal crystallization kinetics, 629
- Crystallization of polyethylene, analogies between chain-folded and extended-chain, 730
- Crystallization of polyethylene, kinetics, 365
- Cyclic tris(ethylene terephthalate), studies on, 650
- Dielectric behaviour of polyamides, low frequency, 159
- Dielectric relaxation in polydimethylsiloxane, 802
- 1,3-Dioxolan, copolymerization of trioxan with, 358
- Ditonic solutions, polymer solutions considered as, 389
- DSC and X-ray methods, analysis of the γ -crystal form in random copolymers of propylene, 487
- Ductile crack growth in poly(ethylene terephthalate) film, 534
- Elasticity and volume, relationship in polymer glasses, 189
- Elastic modulus of the poly(phosphonitrilic chloride) crystal, 775
- Electroinitiated polymerization of styrene: Part (1), 431 Part (2), 760
- Electron microscope study of the microstructure of some rubber-reinforced polystyrenes, 478
- Electron microscopy of crazes in polystyrene and rubber modified polystyrene use of iodine-sulphur eutectic as a craze-reinforcing impregnant, 237
- Epoxy cure, kinetics of: (1), 335
- Equilibrium ring concentrations and the statistical conformations of polymer chains: Part 5, Stereoisomeric cyclics in poly(phenylmethylsiloxane) equilibrates, 373 Part 6, Freezing point of liquid sulphur, 383
- ESR and crystallinity of polyphenyleneisoxazole, 521

- Ethylene-propylene copolymers, investigation of sequence length distribution by pyrolysis and reaction gas chromatography, 70
- Feather keratin, structure, 35
- Fracture of polystyrene: some observations on strength and cracking phenomena, 742
- Heat of fusion of isotactic poly(propylene oxide), 327
- Heterocyclic polymers: (1) Synthesis and structure of macrocyclic polymers, 400
(2) Thermal degradation of some macrocyclic polymers, 602
- Homodisperse fractions, application of Lagrange's expansion, 57
- Hydrostatic pressure, effect on the viscoelastic properties of polymers, 101
- Impinging jets, polymer chain extension produced by, and its effect on polyethylene solution, 467
- Indene, cationic polymerization, 444
- Infra-red spectroscopy, simple preparation of solvent cast films for, 655
- Infra-red spectroscopy, test for molecular orientation in a 'single crystal' of SBS three-block copolymer, 793
- Infra-red spectrum and molecular structure of poly(cyclohexane 1,4-dimethylene terephthalate), 2
- Infra-red spectrum and skeletal vibrations of syndiotactic poly(methyl methacrylate), 524
- Initiation of cationic polymerization of alkyl vinyl ethers by molecular iodine, 344
- Iodine-sulphur eutectic as a craze-reinforcing impregnant; electron microscopy of crazes in polystyrene and rubber modified polystyrene, 237
- Isobutyl vinyl ether, reactivity and mechanism in the cationic polymerization, 119
- Isotactic poly(propylene oxide), heat of fusion, 327
- Kinetics of crystallization of polyethylene, 365
- Kinetics of epoxy cure: (1), 335
- Kinetics of non-isothermal crystallization, 150
- Kinetics of polyacrylonitrile degradation studied by the micro-pyrolysis-g.l.c. technique, 579
- Lagrange's expansion method, application to homodisperse fractions, 57
- Liquids, including solutions, thermodynamic properties of: Part 2, Polymer solutions considered as ditonic systems, 389
- Liquid sulphur, freezing point of, 383
- Low temperature relaxation, effect of water content in some aromatic polymers, 85
- Macrocyclic polymers, synthesis and structure, 400
- Macrocyclic polymers, thermal degradation, 602
- Mechanical properties and birefringence of a 'single crystal' from a three-block copolymer, 222
- Mechanism and reactivity in the cationic polymerization of isobutyl vinyl ether, 119
- Melting and crystallization of copolymers of nylon-6,6 and nylon-6,10 with poly-(hexamethylene terephthalamide) (nylon-6T), 711
- Melting behaviour of heat crystallized poly(ethylene terephthalate), 195
- Metallocenes, polymerization of methyl methacrylate by, 422
- Methyl methacrylate photosensitized by benzophenones, polymerization of, 271
- Methyl methacrylate, polymerization by metallocenes, 422
- Micropyrolysis-g.l.c., polyacrylonitrile degradation kinetics studied by, 579
- Molecular orientation in a 'single crystal' of SBS three-block copolymer by infra-red spectroscopy, 793
- Molecular orientation in drawn poly(methyl methacrylate) by broad line nuclear magnetic resonance, 697
- Molecular structure and infra-red spectrum of poly(cyclohexane 1,4-dimethylene terephthalate), 2
- Molecular weight distribution and long-chain branching of low-density polyethylene, 685
- Molecular weight on isothermal crystallization kinetics, effect of, 629
- Morphology of bulk crystallized *trans*-1,4-polybutadiene, 27
- Morphology of (styrene)_x(butadiene)_y (styrene)_x block copolymers, 258
- Multiple glass transitions, network properties (1), 247
- Network properties: (1) Multiple glass transitions, 247

- Non-helical biopolymer, amylose, in aqueous solution, 141
- Non-isothermal crystallization, kinetics, 150
- Nuclear magnetic resonance, broad line, measurement of molecular orientation in drawn poly(methyl methacrylate), 697
- Nylon-6(polycapramide), studies on crystallization; (1) isothermal crystallization, 616
(2) effect of molecular weight on isothermal crystallization kinetics, 629
- Nylon-6,6 and nylon-6,10, melting and crystallization of copolymers with poly-(hexamethylene terephthalamide) (nylon-6T), 711
- Oligomers in poly(tetrahydrofuran), 642
- Optical anisotropy of swollen polydimethylsiloxane rubber, temperature dependence, 658
- Peroxide concentration in crosslinked linear polyethylene, effects of varying, 176
- Piperazine homopolyamide films, properties of, 717
- Polyacrylonitrile degradation kinetics studied by the micropyrolysis-g.l.c. technique, 579
- Polyamides, low frequency dielectric behaviour, 159
- trans*-1,4-Polybutadiene, bulk crystallized, morphology, 27
- Polycondensates, randomly branched, statistics, 57
- Poly(cyclohexane 1,4-dimethylene terephthalate), infra-red spectrum and molecular structure, 2
- Polydimethylsiloxane, dielectric relaxation, 802
- Polydimethylsiloxane rubber, temperature dependence of the optical anisotropy, 658
- Polyethylene, analogies between chain-folded and extended-chain crystallization, 730
- Polyethylene, crosslinked linear, the effects of varying peroxide concentration, 176
- Polyethylene, crystalline, geometry of twinning and phase transformations, 666
- Polyethylene, kinetics of crystallization, 365
- Polyethylene, low-density, molecular weight distribution and long-chain branching, 685
- Polyethylene solution, effect of polymer chain extension produced by impinging jets, 467
- Poly(ethylene oxide) and benzene, thermodynamics of mixtures, 309
- Poly(ethylene terephthalate) film, ductile crack growth, 534
- Poly(ethylene terephthalate), heat crystallized, melting behaviour, 195
- Poly(hexamethylene terephthalate) (nylon-6T), melting and crystallization of copolymers of nylon-6,6 and nylon-6,10 with, 711
- Polymerization and 2+2 cycloaddition in the system N-vinyl-carbazole-tetracyanoethylene, 209
- Polymerization of methyl methacrylate by metallocenes, 422
- Polymerization of methyl methacrylate photosensitized by benzophenones, 271
- Polymerization, cationic, initiation of alkyl vinyl ethers by molecular iodine, 344
- Polymers, aromatic, relaxation phenomena, 85
- Polymers, effect of hydrostatic pressure on the viscoelastic properties, 101
- Polymers glasses, the relationship between volume and elasticity, 189
- Poly(methyl methacrylate), far infra-red spectrum and skeletal vibrations, 524
- Poly(methyl methacrylate), measurement of molecular orientation by broad line nuclear magnetic resonance, 697
- Polyphenyleneisoxazole, ESR and crystallinity, 521
- Poly(phenylmethylsiloxane) equilibrates, stereoisomeric cyclics in, 373
- Poly(phosphonitrilic chloride), elastic modulus, 775
- Poly(propylene oxide) and benzene, thermodynamics of mixtures, 320
- Poly(propylene oxide), isotactic, heat of fusion, 327
- Polystyrene and rubber modified polystyrene, electron microscopy of crazes: use of iodine-sulphur eutectic as a craze-reinforcing impregnant, 237
- Polystyrene, fracture: some observations on strength and cracking phenomena, 742
- Polystyrenes of known structure: Part (1) The reaction of polystyryl potassium with $^{14}\text{CO}_2$ and the viscosity-molecular weight correlations for linear polymers, 547
Part (2) Comb-shaped molecules, 558
- Polystyrenes, rubber-reinforced, electron microscope study of microstructure, 478
- Polystyryl potassium, reaction with $^{14}\text{CO}_2$ and the viscosity-molecular weight correlations for linear molecules, 547
- Poly(tetrahydrofuran), oligomers in, 642
- Poly(vinyl alcohol) fibres, tensile strength and solubility, influence of stretching on, 797

- Properties of piperazine homopolyamide films, 717
- Propylene copolymers, analysis of the γ -crystal form by DSC and X-ray methods, 487
- Pyrolysis and reaction gas chromatography, investigation of the sequence length distribution in ethylene-propylene copolymers, 70
- Randomly branched polycondensates, statistics, 57
- Reaction gas chromatography and pyrolysis, investigation of the sequence length distribution in ethylene-propylene copolymers, 70
- Reactivity and mechanism in the cationic polymerization of isobutyl vinyl ether, 119
- Relaxation phenomena in some aromatic polymers, 85
- Rubber-reinforced polystyrenes, electron microscope study of microstructure, 478
- SBS three-block copolymer, molecular orientation in a 'single-crystal' by infra-red spectroscopy, 793
- Sequence length distribution in ethylene-propylene copolymers by pyrolysis and reaction gas chromatography, 70
- Skeletal vibrations and far infra-red spectrum of syndiotactic poly(methyl methacrylate), 524
- Solid state transitions in zinc (II) di-*n*-alkylphosphinate polymers, 409
- Solvent cast films for infra-red spectroscopy, simple preparation of, 655
- Solvents, mixed, statistical thermodynamics of polymers in, 290
- Statistical conformations of polymer chains and equilibrium ring concentrations: Part 5, Stereoisomeric cyclics in poly-(phenylmethylsiloxane) equilibrates, 373 Part 6, Freezing point of liquid sulphur, 383
- Statistical thermodynamics of solutions of polymers in mixed solvents, 290
- Strength and cracking phenomena: fracture of polystyrene, 742
- Stretching, influence on tensile strength and solubility of poly(vinyl alcohol) fibres, 797
- (Styrene)_x (butadiene)_y (styrene)_x block copolymers, morphology of, 258
- Styrene, electroinitiated polymerization Part (1), 431 Part (2), 760
- Temperature dependence of the optical anisotropy of swollen polydimethylsiloxane rubber, 658
- Temperature dependence of the thermal diffusivity, 146
- Thermal degradation of some macrocyclic polymers, 602
- Thermal diffusivity, measurement of, 145
- Thermal diffusivity, temperature dependence of, 146
- Thermodynamic properties of liquids, including solutions: Part 2, Polymer solutions as ditonic systems, 389
- Thermodynamics of mixtures of poly(ethylene oxide) and benzene, 309
- Thermodynamics of mixtures of, poly-(propylene oxide) and benzene, 320
- Thermodynamics, statistical, of solutions of polymers in mixed solvents, 290
- Trioxan, copolymerization of, with 1,3-dioxolan, 358
- Twinning and phase transformations, geometry in crystalline polyethylene, 666
- N-Vinylcarbazole, absolute reactivity in cationic polymerization, 509
- N-Vinylcarbazole-tetracyanoethylene, polymerization and 2+2 cycloaddition, 209
- Viscoelastic properties of polymers, effect of hydrostatic pressure, 101
- Viscosity-molecular weight correlations, reaction of polystyryl potassium with ¹⁴CO₂, 547
- Volume and elasticity, relationship in polymer glasses, 189
- Water content, effect on the low temperature relaxation in some aromatic polymers, 85
- X-ray and DSC methods, analysis of the γ -crystal form in random copolymers of propylene, 487
- Zinc (II) di-*n*-alkylphosphinate polymers, solid state transitions, 409

Author Index

- ACITELLI, M. A., PRIME, R. B. and SACHER, E.: Kinetics of epoxy cure: (1) The system bisphenol-A diglycidyl ether/*m*-phenylene diamine, 335
- ALLEN, G., MCAINSH, J. and JEFFS, G. M.: Relaxation phenomena in some aromatic polymers: effect of water content on the low temperature relaxation, 85
- ANDREWS, J. M. and SEMLYEN, J. A.: Oligomers in poly(tetrahydrofuran), 642
- BAIRD, M. E., GOLDSWORTHY, G. T. and CREASEY, C. J.: Low frequency dielectric behaviour of polyamides, 159
- BAIRD, M. E. and SENGUPTA, C. R.: Dielectric relaxation in polydimethylsiloxane, 802
- BAMFORD, C. H., EASTMOND, G. C. and WHITTLE, D.: Network properties: (1) Multiple glass transitions, 247
- BANKS, W. and GREENWOOD, C. T.: Amylose: a non-helical biopolymer in aqueous solution, 141
- BANKS, W., GREENWOOD, C. T., HOURSTON, D. J. and PROCTER, A. R.: Amylose in aqueous solution—a viscometric study, 452
- BARENTSEN, W. M.: *See* HEIKENS, D., BLEIJENBERG, A. C. A. M., HOPPENBROUWERS, J. J. M. and BARENTSEN, W. M.
- BASSETT, D. C. and PHILLIPS, JANET M.: Analogies between chain-folded and extended-chain crystallization of polyethylene, 730
- BAWN, C. E. H., FITZSIMMONS, C., LEDWITH, A., PENFOLD, J., SHERRINGTON, D. C. and WEIGHTMAN, J. A.: Reactivity and mechanism in the cationic polymerization of isobutyl vinyl ether, 119
- BAWN, C. E. H., LEDWITH, A. and SAMBHI, M.: Polymerization and 2+2 cycloaddition in the system N-vinyl-carbazole-tetracyanoethylene, 209
- BEEVERS, M. S. and SEMLYEN, J. A.: Equilibrium ring concentrations and the statistical conformations of polymer chains: Part 5. Stereoisomeric cyclics in poly(phenylmethylsiloxane) equilibrates, 373
- BELL, F. A., LEHRLE, R. S. and ROBB, J. C.: Polyacrylonitrile degradation kinetics studied by the micropyrolysis-g.l.c. technique, 579
- BEVIS, M. and CRELLIN, E. B.: The geometry of twinning and phase transformations in crystalline polyethylene, 666
- BILLINGHURST, P. R. and TABOR, D.: The effect of hydrostatic pressure on the viscoelastic properties of polymers, 101
- BIRD, R. J., ROONEY, G. and MANN, J.: The fracture of polystyrene: some observations on strength and cracking phenomena, 742
- BLEIJENBERG, A. C. A. M.: *See* HEIKENS, D., BLEIJENBERG, A. C. A. M., HOPPENBROUWERS, J. J. M. and BARENTSEN, W. M.
- BLOCK, H., LEDWITH, A. and TAYLOR, A. R.: Polymerization of methyl methacrylate photosensitized by benzophenones, 271
- BOOTH, A. and HAY, J. N.: The kinetics of crystallization of polyethylene, 365
- BOOTH, C. and DEVOY, C. J.: Thermodynamics of mixtures of poly(ethylene oxide) and benzene, 309
- BOOTH, C. and DEVOY, C. J.: Thermodynamics of mixtures of poly(propylene oxide) and benzene, 320
- BOOTH, C., DEVOY, C. J. and GEE, G.: Heat of fusion of isotactic poly(propylene oxide), 327
- BOWYER, P. M., LEDWITH, A. and SHERRINGTON, D. C.: Absolute reactivity in the cationic polymerization of N-vinylcarbazole, 509
- CANTOW, L.: *See* MICHAJLOV, L., CANTOW, H.-J. and ZUGENMAIER, P.
- CATALINA, F.: *See* FERNÁNDEZ BERMÚDEZ, S., FATOU, J. M^a G. and CATALINA, F.
- CREASEY, C. J.: *See* BAIRD, M. E., GOLDSWORTHY, G. T. and CREASEY, C. J.
- CREDALI, LINO and PARRINI, PAOLO: Properties of piperazine homopolyamide films, 717
- CRELLIN, E. B.: *See* BEVIS, M. and CRELLIN, E. B.
- DEVOY, C. J. *See* BOOTH, C. and DEVOY, C. J.
- DEVOY, C. J.: *See* BOOTH, C., DEVOY, C. J. and GEE, G.
- DOUGHTY, A. G.: *See* TIDSWELL, B. M. and DOUGHTY, A. G.

- EASTMOND, G. C.: *See* BAMFORD, C. H., EASTMOND, G. C. and WHITTLE, D.
- ECKARD, A. D., LEDWITH, A. and SHERRINGTON, D. C.: Cationic polymerization of indene, 444
- FATOU, J. M^a G.: *See* FERNÁNDEZ BERMÚDEZ, S., FATOU, J. M^a G. and CATALINA, F.
- FERNÁNDEZ BERMÚDEZ, S., FATOU, J. M^a G. and CATALINA, F.: Morphology of bulk crystallized *trans*-1,4-polybutadiene, 27
- FITZSIMMONS, C.: *See* BAWN, C. E. H., FITZSIMMONS, C., LEDWITH, A., PENFOLD, J., SHERRINGTON, D. C. and WEIGHTMAN, J. A.
- FOLKES, M. J.: *See* KASHIWAGI, M., FOLKES, M. J. and WARD, I. M.
- FOLKES, M. J. and KELLER, A.: The birefringence and mechanical properties of a 'single crystal' from a three-block copolymer, 222
- FOLKES, M. J., KELLER, A. and SCALISI, F. P.: A test for molecular orientation in a 'single crystal' of SBS three-block copolymer by infra-red spectroscopy, 793
- FRANK, F. C., KELLER, A. and MACKLEY, M. R.: Polymer chain extension produced by impinging jets and its effects on polyethylene solution, 467
- FRASER, R. D. B., MACRAE, T. P., PARRY, D. A. D. and SUZUKI, E.: The structure of feather keratin, 35
- GAYMANS, R. J., HODD, K. A. and HOLMES-WALKER, W. A.: Studies of heterocyclic polymers: Part 1. The synthesis and structure of macrocyclic polymers, 400
- GAYMANS, R. J., HODD, K. A. and HOLMES-WALKER, W. A.: Studies in heterocyclic polymers: Part 2. The thermal degradation of some macrocyclic polymers, 602
- GEE, G.: *See* BOOTH, C., DEVOY, C. J. and GEE, G.
- GIANCOTTI, V., RIPAMONTI, A. and TEMUSSI, P. A.: Solid state transitions in zinc (II) di-*n*-alkyl-phosphinate polymers, 409
- GOGOLEWSKI, G.: *See* TURSKA, E. and GOGOLEWSKI, G.
- GOLDSWORTHY, G. T.: *See* BAIRD, M. E., GOLDSWORTHY, G. T. and CREASEY, C. J.
- GREENWOOD, C. T.: *See* BANKS, W. and GREENWOOD, C. T.
- GREENWOOD, C. T.: *See* BANKS, W., GREENWOOD, C. T., HOURSTON, D. J. and PROCTER, A. R.
- HANDS, D. and HORSFALL, F.: On the measurement of thermal diffusivity, 145
- HARVEY, E. D. and HYBART, F. J.: The melting and crystallization of copolymers of nylon-6,6 and nylon-6,10 with poly-(hexamethylene terephthalamide) (nylon-6T), 711
- HAWARD, R. N. and MACCALLUM, J. R.: The relationship between volume and elasticity in polymer glasses, 189
- HAY, J. N.: *See* BOOTH, A. and HAY, N. J.
- HEIKENS, D., BLEIJENBERG, A. C. A. M., HOPPENBROUWERS, J. J. M. and BARENTSEN W. M.: The influence of stretching on tensile strength and solubility of poly-(vinyl alcohol) fibres, 797
- HODD, K. A.: *See* GAYMANS, R. J., HODD, K. A. and HOLMES-WALKER, W. A.
- HOLDSWORTH, P. J. and TURNER-JONES, A.: The melting behaviour of heat crystallized poly(ethylene terephthalate), 195
- HOLMES-WALKER, W. A.: *See* GAYMANS, R. J., HODD, K. A. and HOLMES-WALKER, W. A.
- HONG, S. J., IWAKURA, Y. and UNO, K.: ESR and crystallinity of polyphenyleneisoxazole, 521
- HOPPENBROUWERS, J. J. M.: *See* HEIKENS, D., BLEIJENBERG, A. C. A. M., HOPPENBROUWERS, J. J. M. and BARENTSEN, W. M.
- HORSFALL, F.: *See* HANDS, D. and HORSFALL, F.
- HOUSTON, D. J.: *See* BANKS, W., GREENWOOD, C. T., HOUSTON, D. J. and PROCTER, A. R.
- HUGGINS, M. L.: The thermodynamic properties of liquids, including solutions: Part 2. Polymer solutions considered as ditonic systems, 389
- HYBART, F. J.: *See* HARVEY, E. D. and HYBART, F. J.
- ITO, EIKO and OKAJIMA, SABURO: Studies on cyclic tris(ethylene terephthalate), 650
- IWAKURA, Y.: *See* HONG, S. J., IWAKURA, Y. and UNO, K.
- JEFFS, G. M.: *See* ALLEN, G., MCAINSH, J. and JEFFS, G. M.
- KABAIVANOV, V.: *See* KONSTANTINOV, CH. and KABAIVANOV, V.
- KAERIYAMA, K.: Polymerization of methyl methacrylate by metallocenes, 422

- KAJIWARA, K.: Statistics of randomly branched polycondensates: (2) The application of Lagrange's expansion method to homodisperse fractions, 57
- KAMBOUR, R. P. and RUSSELL, R. R.: Electron microscopy of crazes in polystyrene and rubber modified polystyrene: use of iodine-sulphur eutectic as a craze-reinforcing impregnant, 237
- KASHIWAGI, M., FOLKES, M. J. and WARD, I. M.: The measurement of molecular orientation in drawn poly(methyl methacrylate) by board line nuclear magnetic resonance, 697
- KELLER, A.: *See* FOLKES, M. J. and KELLER, A.
- KELLER, A.: *See* FOLKES, M. J., KELLER, A. and SCALISI, F. P.
- KELLER, A.: *See* FRANK, F. C., KELLER, A. and MACKLEY, M. R.
- KONSTANTINOV, CH. and KABAIVANOV, V.: Studies on the copolymerization of trioxan with 1,3-dioxolan, 358
- LEDWITH, A.: *See* BAWN, C. E. H., FITZSIMMONS, C., LEDWITH, A., PENFOLD, J., SHERRINGTON, D. C. and WEIGHTMAN, J. A.
- LEDWITH, A.: *See* BAWN, C. E. H., LEDWITH, A. and SAMBHI, M.
- LEDWITH, A.: *See* BLOCK, H., LEDWITH, A. and TAYLOR, A. R.
- LEDWITH, A.: *See* BOWYER, P. M., LEDWITH A. and SHERRINGTON, D. C.
- LEDWITH, A.: *See* ECKARD, A. D., LEDWITH A. and SHERRINGTON, D. C.
- LEDWITH, A. and SHERRINGTON, D. C.: The mechanism of initiation of cationic polymerization of alkyl vinyl ethers by molecular iodine, 344
- LEHRLE, R. S.: *See* BELL, F. A., LEHRLE, R. S. and ROBB, J. C.
- LEWIS, P. R. and PRICE, C.: The morphology of (styrene)_x (butadiene)_y (styrene)_x block copolymers, 258
- MCAINSH, J.: *See* ALLEN, G., MCAINSH, J. and JEFFS, G. M.
- MACCALLUM, J. R.: *See* HAWARD, R. N. and MACCALLUM, J. R.
- MACKLEY, M. R.: *See* FRANK, F. C., KELLER, A. and MACKLEY, M. R.
- MACLEAN, D. L.: *See* YAMAMOTO, M., WHITE, J. L. and MACLEAN, D. L.
- MACRAE, T. P.: *See* FRASER, R. D. B., MACRAE, T. P., PARRY, D. A. D. and SUZUKI, E.
- MANLEY, T. R. and MARTIN, C. G.: The elastic modulus of the poly(phosphonitric chloride) crystal, 775
- MANLEY, T. R. and MARTIN, C. G.: The far infra-red spectrum and skeletal vibrations of syndiotactic poly(methyl methacrylate), 524
- MANLEY, T. R. and QAYYUM, M. M.: The effects of varying peroxide concentration in crosslinked linear polyethylene, 176
- MANLEY, T. R. and WILLIAMS, D. A.: The infra-red spectrum and molecular structure of poly(cyclohexane 1,4-dimethylene terephthalate), 2
- MANN, J.: *See* BIRD, R. J., ROONEY, G. and MANN, J.
- MARTIN, C. G.: *See* MANLEY, T. R. and MARTIN, C. G.
- MICHAJLOV, L., CANTOW, H.-J. and ZUGENMAIER, P.: Investigation of the sequence length distribution in ethylene-propylene copolymers by pyrolysis and reaction gas chromatography, 70
- MILLS, N. J.: The temperature dependence of the optical anisotropy of swollen polydimethylsiloxane rubber, 658
- MILTZ, JOSEPH and RAM, ARIE: Molecular-weight distribution and long-chain distribution of low-density polyethylene, 685
- MOORE, J. D.: An electron microscope study of the microstructure of some rubber-reinforced polystyrenes, 478
- NISSEN, D.: *See* ROSSBACH, V. and NISSEN, D.
- OKAJIMA, SABURO: *See* ITO, EIKO and OKAJIMA, SABURO
- OZAWA, T.: Kinetics of non-isothermal crystallization, 150
- PANNELL, J.: Polystyrenes of known structure: Part 1. The reaction of polystyryl potassium with ¹⁴CO₂ and the viscosity-molecular weight correlations for linear polymers, 547
- PANNELL, J.: Polystyrenes of known structure: Part 2. Comb-shaped molecules, 558
- PARRINI, PAOLO: *See* CREDALI, LINO and PARRINI, PAOLO
- PARRY, D. A. D.: *See* FRASER, R. D. B., MACRAE, R. P., PARRY, D. A. D. and SUZUKI, E.
- PENFOLD, J.: *See* BAWN, C. E. H., FITZSIMMONS, C., LEDWITH, A., PENFOLD, J. SHERRINGTON, D. C. and WEIGHTMAN, J. A.

- PHILLIPS, JANET M.: *See* BASSETT, D. C. and PHILLIPS, JANET M.
- PRICE, C.: *See* LEWIS, P. R. and PRICE, C.
- PRIME, R. B.: *See* ACITELLI, M. A., PRIME, R. B. and SACHER, E.
- PROCTER, A. R.: *See* BANKS, W., GREENWOOD, C. T., HOURSTON, D. J. and PROCTER, A. R.
- QAYYUM, M. M.: *See* MANLEY, T. R. and QAYYUM, M. M.
- RAM, ARIE: *See* MILTZ, JOSEPH and RAM, ARIE
- RIDDIFORD, A. W.: On the temperature dependence of the thermal diffusivity, 146
- RIPAMONTI, A.: *See* GIANCOTTI, V., RIPAMONTI, A. and TEMUSSI, P. A.
- ROBB, J. C.: *See* BELL, F. A., LEHRLE, R. S. and ROBB, J. C.
- ROONEY, G.: *See* BIRD, R. J., ROONEY, G. and MANN, J.
- ROSSBACH, V. and NISSEN, D.: Simple preparation of solvent cast films for infra-red spectroscopy, 655
- RUSSELL, R. R.: *See* KAMBOUR, R. P. and RUSSELL, R. R.
- SACHER, E.: *See* ACITELLI, M. A., PRIME, R. B. and SACHER, E.
- SAMBHI, M.: *See* BAWN, C. E. H., LEDWITH, A. and SAMBHI, M.
- SCALISI, F. P.: *See* FOLKES, M. J., KELLER, A. and SCALISI, F. P.
- SEMLYEN, J. A.: Equilibrium ring concentrations and the statistical conformations of polymer chains: Part 6. Freezing point of liquid sulphur, 383
- SEMLYEN, J. A.: *See* Andrews, J. M. and SEMLYEN, J. A.
- SEMLYEN, J. A.: *See* BEEVERS, M. S. and SEMLYEN, J. A.
- SENGUPTA, C. R.: *See* BAIRD, M. E. and SENGUPTA, C. R.
- SHERRINGTON, D. C.: *See* BAWN, C. E. H., FITZSIMMONS, C., LEDWITH, A., PENFOLD, J., SHERRINGTON, D. C. and WEIGHTMAN, J. A.
- SHERRINGTON, D. C.: *See* BOWYER, P. M., LEDWITH, A., and SHERRINGTON, D. C.
- SHERRINGTON, D. C.: *See* ECKARD, A. D., LEDWITH, A. and SHERRINGTON, D. C.
- SHERRINGTON, D. C.: *See* LEDWITH, A. and SHERRINGTON, D. C.
- SUZUKI, E.: *See* FRASER, R. D. B., MACRAE, R. P., PARRY, D. A. D. and SUZUKI, E.
- TABOR, D.: *See* BILLINGSHURST, P. R. and TABOR, D.
- TAYLOR, A. R.: *See* BLOCK, H., LEDWITH, A. and TAYLOR, A. R.
- TEMUSSI, P. A.: *See* GIANCOTTI, V., RIPAMONTI, A. and TEMUSSI, P. A.
- TIDSWELL, B. M. and DOUGHTY, A. G.: The electroinitiated polymerization of styrene: Part I, 431
- TIDSWELL, B. M. and DOUGHTY, A. G.: The electroinitiated polymerization of styrene: Part II, 760
- TURNER-JONES, A.: Development of the γ -crystal form in random copolymers of propylene and their analysis by DSC and X-ray methods, 487
- TURNER-JONES, A.: *See* HOLDSWORTH, P. J. and TURNER-JONES, A.
- TURSKA, E. and GOGOLEWSKI, G.: Study on crystallization of nylon-6(polycapramide) Part I. Isothermal crystallization, 616
- TURSKA, E. and GOGOLEWSKI, G.: Study on crystallization of nylon-6(polycapramide): Part 2. Effect of molecular weight on isothermal crystallization kinetics, 629
- UNO, K.: *See* HONG, S. J., IWAKURA, Y. and UNO, K.
- VINCENT, P. I.: Ductile crack growth in poly(ethylene terephthalate) film, 534
- WARD, I. M.: *See* KASHIWAGI, M., FOLKES, M. J. and WARD, I. M.
- WHITE, J. L.: *See* YAMAMOTO, M., WHITE, J. L. and MACLEAN, D. L.
- WHITTLE, D.: *See* BAMFORD, C. H., EASTMOND, G. C. and WHITTLE, D.
- WILLIAMS, D. A.: *See* MANLEY, T. R. and WILLIAMS, D. A.
- YAMAMOTO, M., WHITE, J. L. and MACLEAN, D. L.: Statistical thermodynamics of solutions of polymers in mixed solvents, 290
- ZUGENMAIER, P.: *See* MICHAJLOV, L., CANTOW, H. -J. and ZUGENMAIER, P.

UK Editors

C. H. Bamford PhD, ScD, FRS
Campbell Brown Professor of Industrial
Chemistry, University of Liverpool

C. E. H. Bawn CBE, FRS
Grant Brunner Professor of Inorganic
and Physical Chemistry, University of
Liverpool

E. M. Bradbury PhD
Head of Biophysics Section,
Portsmouth Polytechnic

Geoffrey Gee CBE, FRS
Sir Samuel Hall Professor of
Chemistry, University of Manchester

R. J. W. Reynolds PhD, FPI
Professor and Director, Institute of
Polymer Technology, Loughborough
University of Technology

Annual subscription including postage

UK £15; USA \$37.50 (surface mail)
Airmail USA \$55.00; Japan £23
Rates for other countries available on request

Published monthly by IPC Science
and Technology Press Ltd,
IPC House, 32 High Street, Guildford,
Surrey, England.
Telephone: Guildford 71661

American Representatives: IPC
(America) Inc., 300 East 42nd Street,
New York, NY 10017, USA.

Overseas Editors

H. C. Benoit PhD
Professor, Faculty of Science,
University of Strasbourg
Director, Centre de Recherche sur
les Macromolécules, 6, Rue
Boussingault, 67 Strasbourg, France

S. Bywater PhD
Head, Polymer Section,
National Research Council,
Ottawa 7, Canada

F. Danusso PhD
Professor of Macromolecular
Chemistry
Istituto Chimica Industriale del
Politecnico, Piazza Leonardo da Vinci
32—20133 Milano, Italy

M. Szwarc FRS
State University Polymer Research
Center, Syracuse University, Syracuse,
New York, 13210, USA

Managing Editor
M. I. Dawes

Assistant Editor
J. A. G. Thomas PhD

Editorial Assistant
J. R. Ross BSc